MESOSCALE CHARACTERISTICS OF THE TEXAS HIPLEX AREA DURING SUMMER 1978

LP-123

TDWR CONTRACTS NO. 14-90026 AND 14-00003

Prepared by:

DEPARTMENT OF METEOROLOGY
COLLEGE OF GEOSCIENCES
TEXAS A&M UNIVERSITY
COLLEGE STATION, TEXAS

Prepared for:

TEXAS DEPARTMENT OF WATER RESOURCES
AUSTIN, TEXAS

Funded by:

DEPARTMENT OF THE INTERIOR, WATER AND POWER RESOURCES SERVICE
TEXAS DEPARTMENT OF WATER RESOURCES

MS-280 (3-78)
Bureau of Reclamation

TECHNICAL REPORT STANDARD TITLE PAGE

1. REPORT NO.	2. GOVERNMENT ACCESSION NO.	3. RECIPIENT'S CATALOG NO.

4. TITLE AND SUBTITLE

Mesoscale Characteristics of the Texas HIPLEX Area During Summer 1978

5. REPORT DATE
March, 1980

6. PERFORMING ORGANIZATION CODE
330

7. AUTHOR(S)
Meta E. Sienkiewicz, James R. Scoggins, Steven F. Williams, Myron L. Gerhard

8. PERFORMING ORGANIZATION REPORT NO.
LP-123

9. PERFORMING ORGANIZATION NAME AND ADDRESS
Texas Department of Water Resources
P.O. Box 13087, Capitol Station
Austin, TX 78711

10. WORK UNIT NO.

11. CONTRACT OR GRANT NO.
14-06-D-7587

13. TYPE OF REPORT AND PERIOD COVERED
Technical

12. SPONSORING AGENCY NAME AND ADDRESS
Office of Atmospheric Resources Management
Water and Power Resources Service
Building 67, Denver Federal Center
Denver, Colorado 80225

14. SPONSORING AGENCY CODE

15. SUPPLEMENTARY NOTES Subcontractor:
Texas A&M University; Department of Meteorology; College Station, TX 77843

16. ABSTRACT

Mesoscale surface and upper air data were obtained for the Texas HIPLEX area on 26 days between June 1 and July 26, 1978. Rawinsonde soundings were made at 3-h intervals between 1500 and 0300 GMT on 17 of the 26 days at four sites, while surface data consisting of 10-min average values of temperature, humidity, pressure, and wind direction and speed were available from 20 stations for all 26 days.

The data were analyzed and results are presented for each day separately. Composite analyses of surface variables, and upper level kinematic, moisture, atmospheric and energy processes associated with convective activity are presented. Pronounced cloud-environment interaction is evident due to convective activity. Temporal and spatial changes in horizontal and vertical flux of moisture proximate to convective activity are shown to be indicative of surface processes important to the development and maintenance of convective activity.

17. KEY WORDS AND DOCUMENT ANALYSIS

a. DESCRIPTORS--
mesoscale analysis; moisture divergence; vertical motion; vorticity; energy budget; moisture budget; surface analysis; kinematic parameters; energetics; time changes; meteorological data; winds

b. IDENTIFIERS-- Texas HIPLEX area/Big Spring, Texas/High Plains Cooperative Program (HIPLEX)

c. COSATI Field/Group COWRR:

18. DISTRIBUTION STATEMENT
Available from the National Technical Information Service, Operations Division, Springfield, Virginia 22161.

19. SECURITY CLASS (THIS REPORT)	21. NO. OF PAGES
UNCLASSIFIED	
20. SECURITY CLASS (THIS PAGE)	22. PRICE
UNCLASSIFIED	

GPO 845-630

MESOSCALE CHARACTERISTICS OF THE TEXAS HIPLEX AREA DURING SUMMER 1978
LP-123

Meta E. Sienkiewicz, James R. Scoggins, Steven F. Williams, and
Myron L. Gerhard
Department of Meteorology
College of Geosciences
Texas A&M University
College Station, Texas 77843

April 1980

Final Report
TDWR Contract Nos. 14-90026 and 14-00003

Availability Unlimited

Prepared for
Texas Department of Water Resources
Austin, Texas

Funded by
Department of the Interior, Water and Power Resources Service, and the
State of Texas through the Texas Department of Water Resources

MESOSCALE CHARACTERISTICS OF THE TEXAS HIPLEX AREA DURING SUMMER 1978

by

Meta E. Sienkiewicz, James R. Scoggins, Steven F. Williams,
and Myron L. Gerhard
Department of Meteorology
College of Geosciences
Texas A&M University
College Station, Texas 77843

ABSTRACT

This report contains an analysis for 26 days on which mesoscale meteorological data were obtained in the Texas HIPLEX area during the period June 1 to July 26, 1978. Rawinsonde soundings were made at 3-h intervals between 1500 and 0300 GMT on 17 of the 26 days at Midland, Robert Lee, Post, and Big Spring. Surface data consisting of 10-min average values of temperature, humidity, pressure, and wind direction and speed were available from 20 stations for all 26 days. In addition, data were available from the National Weather Service radar at Midland.

The data were analyzed and results presented for each day separately. In addition, composite analyses of surface variables, and upper level kinematic, moisture, atmospheric and energy processes associated with convective activity are presented. Variables considered in the surface analysis for each day include temperature, dew point depression, mixing ratio, velocity divergence, vertical motion, vertical flux of moisture, moisture divergence, equivalent potential temperature, vorticity, pressure change, and relative wind fields. Charts of analyzed fields determined from data placed on a 15-km grid are compared with radar data coded on a similar grid. Variables considered in the upper-air analysis include mass divergence, vertical motion, moisture divergence, and budgets of latent heat energy, kinetic energy, and water vapor. Composite analyses are presented for the surface and upper-air variables as a function of convective activity.

The results show pronounced interactions between the environment and convective activity. Marked changes in nearly all surface and upper-air variables occur in association with convective activity. The analysis of individual days as well as the composite analyses suggest that surface processes indicated by moisture divergence, vertical flux of moisture, and vertical motion are important in the formation and maintenance of convective clouds. The importance of these same variables also is reflected in the upper-air analyses as well as energy processes and time changes.

The results presented in this report are consistent with and support similar analyses for 1976 and 1977. Results for all three years show the importance of the lower atmosphere, including the surface layer, as the source region for initiating and maintaining convective activity. The convective activity derives much of its energy through horizontal convergence of moisture in the lower 3 km above the ground which is then transported aloft by vertical motion where condensation takes place. The results show variations in these processes as function of the intensity and other characteristics of the convective activity, but their importance is demonstrated beyond doubt.

Key Words

Mesoscale analysis
Moisture divergence
Vertical motion
Vorticity
Energy budget
Moisture budget
Surface analysis
Kinematic parameters
Energetics
Time changes
Meteorological data
Winds

ACKNOWLEDGMENTS

The authors gratefully acknowledge the assistance of Mr. John Rod for preparation of the figures, and Mrs. Karen Hood and Ms. Susan Callander for typing and assembling the manuscript. Also, the guidance and council provided by Mr. Robert Riggio, Mr. John Carr, and Dr. Herbert Grubb of the Texas Department of Water Resources during this research is greatly appreciated.

This research was funded by the Water and Power Resources Service, Department of the Interior, and the State of Texas through the Texas Department of Water Resources under TDWR Contract Nos. 14-90026 and 14-00003.

TABLE OF CONTENTS

TABLE OF CONTENTS (CONTINUED)

TABLE OF CONTENTS (CONTINUED)

TABLE OF CONTENTS (CONTINUED)

TABLE OF CONTENTS (CONTINUED)

LIST OF FIGURES

LIST OF FIGURES (CONTINUED)

LIST OF FIGURES (CONTINUED)

LIST OF FIGURES (CONTINUED)

LIST OF FIGURES (CONTINUED)

LIST OF FIGURES (CONTINUED)

LIST OF FIGURES (CONTINUED)

LIST OF FIGURES (CONTINUED)

1. INTRODUCTION

Convective activity is perhaps one of the least understood phenomena today because of the complex relationship between convective clouds and their environment. A basic understanding of these interactions both at the surface and aloft is essential in the development of rainfall enhancement technology.

Mesoscale experiments have been conducted during the summers of 1976, 1977, 1978, and 1979 as part of the Texas HIPLEX program. The primary objective of these experiments is to investigate interactions between convective clouds and their environment to determine factors and environmental conditions responsible for the initiation, growth, maintenance, and dissipation of convective clouds. A report was prepared (Scoggins et al., 1978) which presented a case study analysis of 15 days including a composite surface analysis and average atmospheric energetics for times with and without convective activity using data collected during the summer of 1976. A similar report analyzing mesoscale data on 19 case study days during the summer of 1977 also was prepared (Scoggins et al., 1979), which included an extended surface analysis of pressure and pressure change, and average moisture processes as a function of convective activity. The present report contains a mesoscale analysis for 26 case study days from data collected during June 1 through July 26, 1978. An expanded surface station network and surface fields of dew point depression were added to the analysis of 1978 data. A complete listing of the data used in this analysis can be found in the document prepared by Reynolds, et al., (1979). Computational procedures for the analysis of surface and upper air are identical to those used in the analysis of 1977 data and are presented in Section 4.

This report contains a description of the mesoscale experiment for 1978, a brief discussion of the data used and processing procedures, methods of data analysis, results for each case study, a composite analysis of surface data, average conditions of upper-level moisture processes, and kinematic and atmospheric energetics as a function of convective activity. A standard format was used in the presentation of the results to facilitate the retrieval of information for any case study day as well as for making comparisons between case study days.

It is not the purpose of this report to present a comprehensive interpretation of the results, but rather to present an analysis and

description of the results with sufficient depth to permit the interpretation and integration of mesoscale conditions with other phases of scientific research such as radar, satellite, and aircraft data analysis. Also the similar presentation of mesoscale data to previous analysis reports provides an addition to the data set for use in stratification of results by convective regime, the development of models, and comparisons of various years, all of which lead to the establishment of environmental conditions associated with convective activity.

2. THE MESOSCALE EXPERIMENT

The 1978 mesoscale experiment was bounded approximately by Midland-Robert Lee-Clairemont-Tahoka-Seminole-Midland, an area larger than the 1976 and 1977 experiments covered. All data for both surface and atmospheric soundings were taken within this area.

2.1 Surface Measurements

A network of fifteen special surface stations was in operation during the entire period of the 1978 mesoscale experiment. The locations of the stations are shown in Fig. 2.1.1. The instrumentation at each station consisted of a hygrothermograph for measurements of temperature and relative humidity, a microbarograph for measuring pressure, and an MRI automatic weather station for measuring wind direction and speed as well as temperature. A standard-type instrument shelter was used at each station

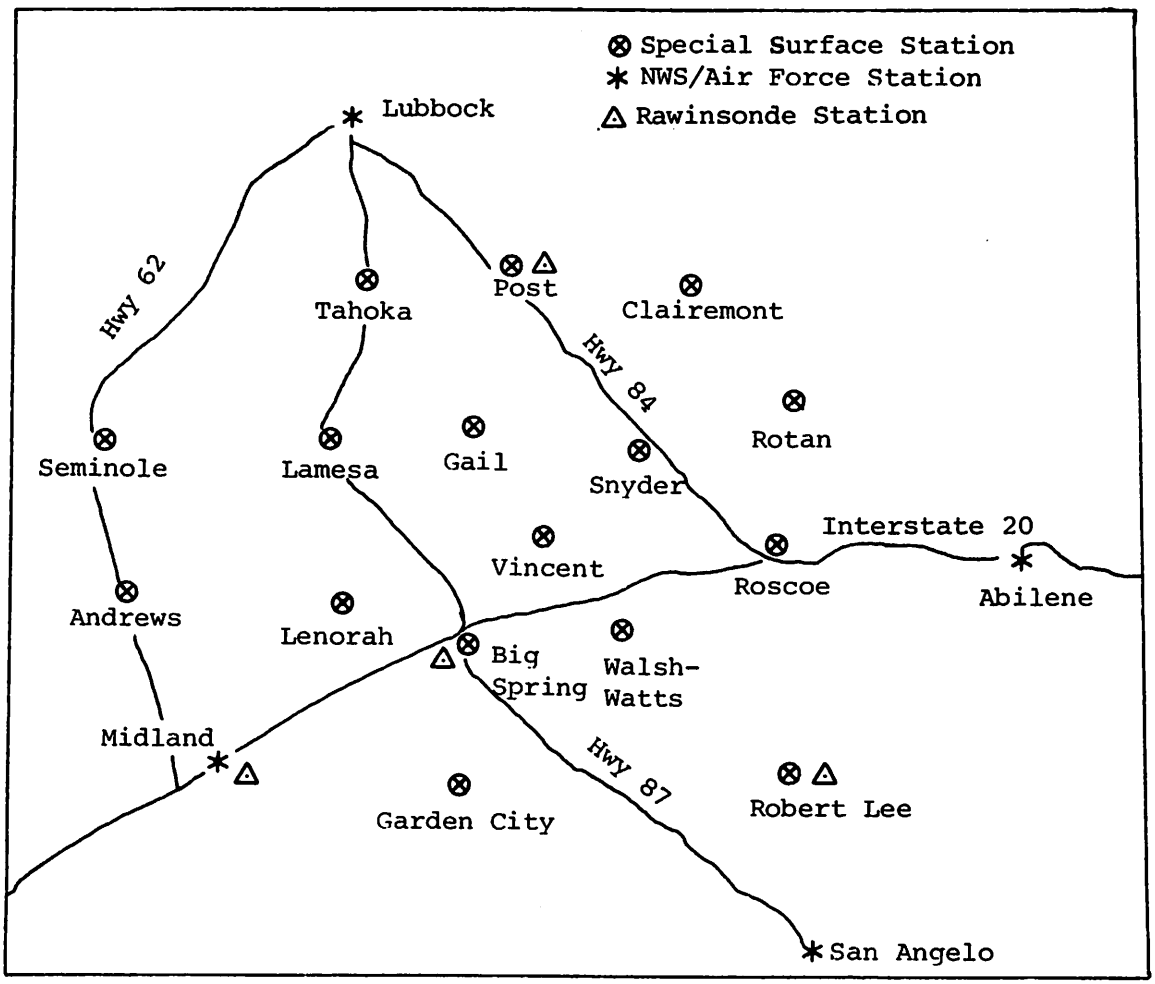

Fig. 2.1.1 Target area and locations of special surface and rawinsonde stations.

to house the hygrothermograph and microbarograph. The instruments were calibrated routinely at 3-day intervals during the entire experimental period. The hygrothermograph data were checked by use of an aspirated psychrometer, and the microbarograph data by use of an aneroid barometer that was checked against a fortin-type barometer each day at Big Spring. The accuracy of the wind data could not be checked to the same extent that the thermodynamic data were checked, but estimates of wind speed and direction were made to determine whether or not the equipment was functioning properly.

2.2 Upper Air Measurements

Atmospheric soundings were made at four locations including Midland, Post, Robert Lee, and Big Spring. These locations are shown in Fig. 2.1.1. Arrangements were made with the National Weather Service for the purchase of soundings for Midland. The Colorado River Municipal Water District operated the sounding station at Big Spring, and Texas A&M University operated those at Post and Robert Lee. Soundings were made on 19 selected days at 3-h intervals beginning at 1500 GMT (1000 CDT) and ending at 0300 GMT (2200 CDT).

All stations used the same type of radiosonde. An RD-65 rawinsonde set was used at Big Spring, while GMD-1b units were used at the other locations. All sounding stations provided comparable data although the tracking equipment was somewhat different.

2.3 Radar

An M-33 radar located at Snyder, Texas, and operated by Meteorology Research Inc., was dedicated to the task of obtaining radar data for all convective echoes over the Texas HIPLEX area during the mesoscale experiment. Excellent data were obtained in digital form for all mesoscale days.

The National Weather Service (NWS) radar at Midland was operated continuously by NWS personnel during the experiment, and a copy of PPI (Plan Position Indicator) overlays and the radar operator logs were made available for our use. The data were coded and used in this report to locate convective echoes.

Additional radar data were collected by the FPS-77 radar located at the Big Spring Municipal Airport (formerly Webb Air Force Base). This radar was used primarily for aircraft operations and photographic documentation.

2.4 Rainfall

Rainfall measurements were made at approximately 162 locations during the experimental period. There were approximately 81 recording raingages, and the same number of fencepost gages. Since these data are not used in this report no further discussion of the data will be provided.

2.5 Other

Surface data were obtained from four locations in addition to the fifteen special surface stations discussed in Section 2.1 above. The four stations included Lubbock (Reese AFB), Midland (NWS), San Angelo (NWS), and Big Spring (Texas Agricultural Experiment Station). Hourly data from Big Spring were extracted from strip charts and treated as a special surface station. All other surface data collected from Midland, Lubbock, and San Angelo were obtained from teletype data for each hour on the hour which coincides with the measurement schedule for the fifteen special surface stations. All teletype and facsimile data consisting of routine observations and charts prepared by the National Weather Service were obtained from the Texas A&M University Weather Station and archived for future reference and use. In addition, complete surface observations and regularly scheduled rawinsonde releases made by National Weather Service personnel at Midland were obtained. Cloud observations at time of balloon release also were recorded at all stations.

3. DATA

3.1 Processing Procedures

3.1.1 Surface

All data collected at the fifteen special surface stations as well as Big Spring were recorded on strip charts continuously as a function of time. Ten-minute average values of temperature, relative humidity, pressure, wind speed, and direction were extracted from the charts each hour on the hour. These data were keypunched, checked and cross-checked for errors, and appropriate corrections made as necessary. The final data set was placed on magnetic tape for subsequent analysis.

3.1.2 Soundings

All atmospheric soundings made as part of the mesoscale program were processed by two methods. The method developed by the Water and Power resources Service (WPRS) is based on criteria for determining significant points in a sounding. The soundings including baseline data were coded and placed on magnetic tape, and processed on the WPRS computer in Denver following the field program.

The second method used to process the soundings was a method developed at Texas A&M University as part of NASA's Atmospheric Variability Experiments in which data are extracted from the sounding records for every pressure contact and later interpolated to 25-mb intervals. The contact data provides the greatest accuracy and resolution possible for the rawinsonde system, while the 25-mb data generally provides more resolution than the significant point data provided by the WPRS method. The significant point method is essentially the same as used by the National Weather Service and is adequate for most purposes.

Data for the soundings processed at Texas A&M University were placed on magnetic tape and a data report prepared (Reynolds, et al., 1979). The 25-mb data were used in the analysis presented in this report.

3.1.3 National Weather Service Radar

Radar data obtained from the National Weather Service station at Midland consisted of the operators log and PPI overlays at approximately 20-min intervals during periods when significant convective activity existed. Information was provided on areal extent of the echoes, movement,

intensity, and height. The PPI charts were digitized by overlaying a grid and coding the echoes for each grid point as a function of height. If an echo appeared within one half a grid distance from a grid point, a code was assigned to that grid point of either 1, 2, or 3. A code of 1 represents an echo whose height did not exceed 6.1 km (20,000 ft), a 2 was used for echoes whose height was between 6.1 and 9.1 km (20,000 and 30,000 ft), while a 3 was used to denote an echo exceeding an altitude of 9.1 km (30,000 ft). These data were keypunched, checked, and used in this report to locate convective echoes.

3.2 Data Inventory for 1978

Surface data were collected each day during the period June 1-July 26, 1978, while sounding data were collected on 19 days during this period. Some instrumentation difficulties were encountered which resulted in the loss of some surface and sounding data. A complete description and presentation of all surface and sounding data were presented by Reynolds et al., (1979). Results are presented in the present report for all days on which consecutive soundings were made at all four stations as well as a number of days when only surface data were obtained.

4. METHODS OF DATA ANALYSIS

4.1 Gridding of Data

An objective analysis scheme developed by Barnes (1964) was used to interpolate the HIPLEX surface data to an 18 x 18 grid (Fig. 4.1.1) with approximately a 16-km spacing between grid points. The analysis scheme operates by making successive corrections to a "first guess field" (usually a constant value over the network) and results in a Fourier representation of the variables after gridding. Each grid point in the array was also assigned a terrain height from a standard topographic map and an analysis of the terrain (hundreds of feet) is also shown in Fig. 4.1.1.

In addition to the HIPLEX mesoscale surface stations (two letter station identifiers), data from surrounding National Weather Service and Air Force stations (three letter station identifiers) were used in the surface analyses (stations shown in Fig. 4.1.1). Only the four rawinsondes (Midland, Big Spring, Robert Lee, and Post) were used in the upper air analyses but these data were not gridded. The five basic variables objectively analyzed onto the grid surface were temperature, mixing ratio, pressure, and the "u" and "v" wind components. All other surface parameters were computed from these basic fields.

The "scanning radius" of influence around each input station was specified for the objective analysis program based upon the station spacing at the surface. The final gridded fields contained features and systems consistent with the spatial and temporal resolution of the input data. A comparison between these fields and carefully hand analyzed fields was used to "fine tune" the gridding program.

4.2 Surface

The basic meteorological variables were objectively gridded onto the 18 x 18 array each hour of every day for 56 consecutive days starting June 1, 1978 and ending July 26, 1978. These gridded variables were used to approximate the parameters that follow by using centered difference computations over two grid distances and applied to the center point.

4.2.1 Velocity Divergence

Surface wind velocity divergence was calculated using the expression

$$\vec{\nabla}_2 \cdot \vec{V}_2 = \frac{\partial u}{\partial x} + \frac{\partial v}{\partial y} \simeq \frac{u_2 - u_1}{2\Delta x} + \frac{v_2 - v_1}{2\Delta y}$$

where it is understood that all expressions refer to surface variables and

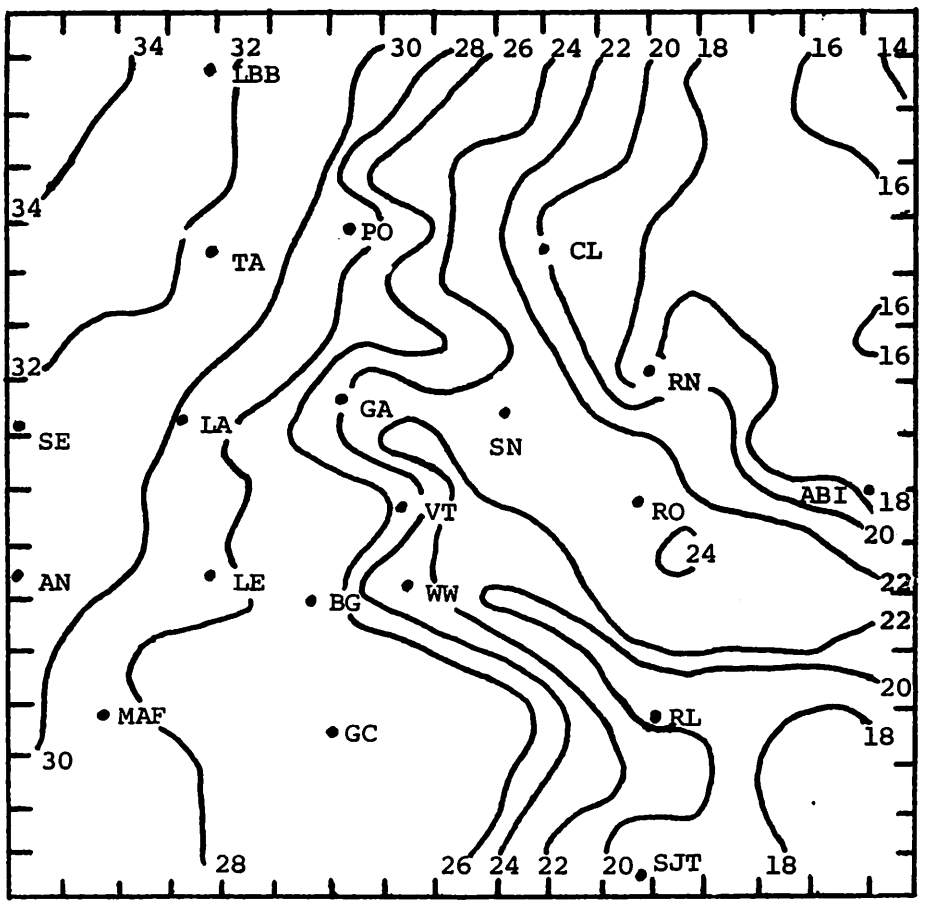

Fig. 4.1.1 Analysis of terrain heights (hundreds of feet) drawn from computer-gridded data. The grid is indicated by tick marks.

have their usual meteorological meanings. The subscripts "1" and "2" are grid point values surrounding the "center point" and in the positive direction, respectively, and $\Delta x=\Delta y=16$ km.

4.2.2 Moisture Divergence

Surface moisture divergence was computed by use of the expression

$$\vec{\nabla}_2 \cdot q\vec{v}_2 = \frac{\partial(qu)}{\partial x} + \frac{\partial(qv)}{\partial y} \simeq \frac{q_2u_2 - q_1u_1}{2\Delta x} + \frac{q_2v_2 - q_1v_1}{2\Delta y} .$$

The subscripts have the same meaning as above, and all computed values were applied to the center point.

4.2.3 Vertical Motion

In computing vertical motion 50 mb above the surface, both terrain-induced vertical motion and velocity divergence of the surface wind were considered. By assuming the surface wind field as representative of the

mean wind through a 50-mb deep layer above the surface, the equation of continuity in pressure coordinates

$$\vec{\nabla}_2 \cdot \vec{v}_2 = - \frac{\partial \omega}{\partial p}$$

can be integrated from the surface to the top of the 50-mb layer to give the vertical motion through the top of the layer. Thus,

$$\omega_{(P_s - 50\ mb)} = \omega_{P_s} + \int_{(P_s - 50\ mb)}^{P_s} (\vec{\nabla}_2 \cdot \vec{v}_2)\, dp$$

where $\omega = \frac{dp}{dt}$ and P_s is the surface pressure. The magnitude of ω_{P_s} can be approximated by the terrain-induced vertical motion

$$w_T = u\left(\frac{\partial h}{\partial x}\right) + v\left(\frac{\partial h}{\partial y}\right) \simeq \frac{u(h_2 - h_1)}{2\Delta x} + \frac{v(h_2 - h_1)}{2\Delta y}$$

where h is the terrain height. For the range of surface temperatures and pressures in the Texas HIPLEX area

$$w_T (cm\ s^{-1}) = -\omega_{P_s} (\mu b\ s^{-1}).$$

Therefore, the resultant vertical motion at 50 mb above the surface was calculated using the expression

$$\omega_{(P_s - 50\ mb)} = -w_T + (\vec{\nabla}_2 \cdot \vec{v}_2)\Delta p$$

where Δp = 50 mb.

4.2.4 Vertical Flux of Moisture

The vertical flux of moisture is given by the product of the vertical velocity 50 mb above the ground (cm s^{-1}), the surface mixing ratio, and air density. Units are g $cm^{-2} s^{-1}$.

4.2.5 Vorticity

The vorticity of the surface wind was calculated using the expression

$$\vec{\nabla}_2 \times \vec{v}_2 = \frac{\partial v}{\partial x} - \frac{\partial u}{\partial y} \simeq \frac{v_2 - v_1}{2\Delta x} - \frac{u_2 - u_1}{2\Delta y}$$

where subscripts have the same meaning as before.

4.3 Upper-Level Kinematic Parameters

The data analysis procedures used for the 1978 data are identical to those used to analyze 1977 data.

4.3.1 Horizontal Velocity Divergence

For a given time period and pressure surface, the horizontal velocity divergence was computed by use of the expression

$$\vec{\nabla}_p \cdot \vec{v}_2 = \frac{1}{A}\frac{dA}{dt} \simeq \frac{1}{\bar{A}}\frac{\Delta A}{\Delta t}$$

where A is the horizontal triangular area determined from the three rawinsonde balloon locations (MAF, PO, and RL) projected onto a constant pressure surface, $\bar{A}$ is the average area of the triangle between two pressure surfaces 50 mb apart, and ΔA is the change of triangular area that occurs as the balloons move through a pressure layer 50 mb thick in time Δt.

4.3.2 Horizontal Moisture and Mass Divergence

Horizontal moisture and mass divergence were determined using the vector identity

$$\vec{\nabla}_p \cdot C\vec{v}_2 = \vec{v}_2 \cdot \vec{\nabla}_p C + C\vec{\nabla}_p \cdot \vec{v}_2$$

(1) (2) (3)

where C is any scalar. For moisture and mass divergence, q (mixing ratio) and ρ (air density) were used in place of C. Then term 2 was computed by the centered finite difference formula

$$\vec{v}_2 \cdot \vec{\nabla}_p C = u\frac{\partial C}{\partial x} + v\frac{\partial C}{\partial y} \simeq \bar{u}\frac{(C_2 - C_1)}{2\Delta x} + \bar{v}\frac{(C_2 - C_1)}{2\Delta y}$$

where $\bar{u}$ and $\bar{v}$ are the average wind components over the network along a pressure surface, and $\frac{C_2 - C_1}{2\Delta x}$ and $\frac{C_2 - C_1}{2\Delta y}$ are the horizontal vector components of the gradient of C in the "x" and "y" directions, respectively. Term 3 was calculated by multiplying C (an average for the pressure surface) by the horizontal velocity divergence computed previously. Since the velocity divergence represents a 50-mb layer mean value, term 2 was actually computed as a mean horizontal advection by averaging data from three 25-mb data levels constituting the 50-mb layer used in the velocity divergence calculation.

4.3.3 Vertical Motion

Vertical motion was computed on constant pressure surfaces using the formula

$$(\omega_p)_k = \omega_s + \sum^{k} \overline{(\vec{\nabla}_p \cdot \vec{v}_2)_k}(\Delta p)$$

where $(\omega_p)_k$ is vertical velocity on a constant pressure surface k, ω_s is the

vertical velocity at the ground, $\overline{(\vec{\nabla}_p \cdot \vec{v}_2)}_k$ is the 50-mb layer mean divergence below layer k, and Δp = 50 mb.

4.4 Energetics

4.4.1 Total Energy Budget

The budget of total energy (kinetic, internal, and gravitational potential) per unit volume is given by

$$\rho \frac{dQ}{dt} = \frac{\partial}{\partial t} \rho\left(\frac{V^2}{2} + gz + c_v T\right) + \vec{\nabla} \cdot \rho \vec{V}\left(\frac{V^2}{2} + gz + c_p T\right) + \frac{\partial}{\partial p} \rho\omega\left(\frac{V^2}{2} + gz + c_p T\right) - \rho \vec{V} \cdot \vec{F}.$$

In this equation $\frac{V^2}{2}$ is kinetic energy, gz the gravitational potential energy, $c_v T$ the internal energy, $c_p T$ the enthalpy or sensible heat, $\vec{F}$ the frictional force, all per unit mass, and Q the heat added by diabatic processes. Other symbols have the standard meteorological meanings.

The above equation written in integral form in the x, y, p, t system is

$$\frac{1}{g} \int \frac{dQ}{dt} dV = \frac{1}{g} \int \frac{\partial}{\partial t}\left(\frac{v^2}{2} + gz + c_v T\right) dV + \frac{1}{g} \int \vec{\nabla} \cdot \left(\frac{v^2}{2} + gz + c_p T\right) \vec{V}\, dV + \frac{1}{g} \int \frac{\partial}{\partial p}\left(\frac{v^2}{2} + gz + c_p T\right) \omega\, dV - \frac{1}{g} \int \vec{V} \cdot \vec{F}\, dV.$$

This is the form of the equation evaluated in this research.

Diabatic heating can be evaluated from the first law of thermodynamics in the form

$$\frac{dQ}{dt} = c_p \frac{\partial T}{\partial t} + c_p \vec{V} \cdot \vec{\nabla} T + \left(c_p \frac{\partial T}{\partial p} - \alpha\right) \omega.$$

The net effect of the various forms of diabatic heating such as evaporation/condensation, radiation, and sensible heat transfer is obtained from this equation in integral form.

4.4.2 Latent Heat Energy Budget

The budget of latent heat energy is given by

$$\frac{\partial}{\partial t}(\rho L q) + \vec{\nabla} \cdot (\rho L q \vec{V}) + \frac{\partial}{\partial p}(\rho L q \omega) = R$$

where L is the latent heat of vaporization and q is specific humidity. All other symbols have their usual meaning. The term on the right of this equation represents evaporation and/or condensation and energy processes that cannot be resolved in time and/or space using the available input data and computational procedures. Since this term is computed as a residual, some error from the remaining terms is included as well.

The integral form of the latent heat energy budget in the x, y, p, t system is

$$\frac{1}{g}\int \frac{\partial}{\partial t}(Lq)\,dV + \frac{1}{g}\int \vec{\nabla}\cdot(Lq)\vec{V}dV + \frac{1}{g}\int \frac{\partial}{\partial p}(Lq\omega) = \int R dV$$

which is the form of the equation evaluated in this research.

4.4.3 Computational Procedures

The above equations were integrated vertically to obtain the energy balance of each atmospheric layer. The friction term in the first equation was not evaluated in this study. Values of all other terms were computed as averages per unit volume through a depth of 50 mb and horizontally covering the area bounded by the MAF-PO-RL triangle. A description of the method of computing vertical motion has been given earlier in this report. Terms were evaluated at the surface and at 50-mb intervals from 850 mb to 100 mb. Vertical integration was performed over 50-mb intervals except in the lowest layer which extended from the surface (about 920 mb) to 850 mb. The trapezoidal rule was used for integration purposes.

4.4.4 Interpretation of Results

Accuracy of the energy budget terms is an important consideration. Again, it is difficult to estimate accuracy without introducing errors in the input data and observing the results. While this has not been done so far, values of the energy budget terms show reasonable vertical consistency and time continuity. Recent results by Vincent and Chang (1975) and Kornegay and Vincent (1976) indicated that random errors in input data do not affect seriously the results of synoptic-scale kinetic energy studies.

Kung and Tsui (1975) described the interpretation which should be given to energy budgets obtained from subsynoptic-scale data. They noted that energy processes can be strongly influenced by the presence of nearby convective cells but that features due to the larger scales of motion are not filtered out. They suggested that the type of energy budgets computed

in this study "should be taken as the energy budget computed with sub-synoptic-scale network data."

The hydrostatic assumption, used in computing radiosonde data, is a potential source of distortion during times of convective activity. A few sondes are thought to have entered severe updrafts or downdrafts during the Texas HIPLEX 1978 program and have been identified for use in data analysis and interpretation.

4.5 Water Vapor Budget

The equation for the continuity of water substance can be expressed as

$$\int_V \frac{\partial(q\rho a)}{\partial t}\,dV + \int_S (q\rho_a V_n)\,dS + \int_A (q\rho_a \omega)\,dA - R = 0$$

where:

q is mixing ratio,

ρ_a is density of the air,

V_n is the component of the horizontal velocity that is normal to the surface S,

ω is vertical velocity,

V is volume,

A is the horizontal area,

R is a residual representing the sources and sinks of moisture (evaporation, condensation, precipitation, and turbulent flux of moisture through the boundaries), and

S is the lateral surface area.

The terms in this equation from left to right represent: the local rate-of-change or the net gain or loss of water vapor within the volume; the transport of water vapor through the lateral boundaries; the transport of water vapor through the vertical boundaries; and the residual. All terms in this equation except the residual were evaluated at 50-mb intervals from 850 to 300 mb over the triangle formed by Robert Lee-Post-Midland. The residual represents the sum of all other terms in the equation.

4.5.1 Net Horizontal Transport of Water Vapor

The net horizontal transport of water vapor was computed as the algebraic sum of the transport of water vapor through all lateral boundaries

of the volume. This value represents the transport of water vapor out of the volume minus the transport of water vapor into the volume through lateral boundaries of a 50-mb layer.

4.5.2 Net Vertical Transport of Water Vapor

The net vertical transport of water vapor was computed for each 50-mb layer as the difference in the transport of water vapor between the top and bottom boundaries of the layer. This value represents the transport of water vapor out of the volume minus the transport of water vapor into the volume through vertical boundaries of 50-mb layers.

4.5.3 Vertical Transport of Water Vapor Through Constant Pressure Surfaces

The vertical transport of water vapor through constant pressure surfaces was computed directly from Term 3 of the equation for the continuity of water substance at each pressure level. This value represents the vertical transport of water vapor through vertical boundaries at 50-mb intervals.

4.5.4 Combined Net Horizontal and Vertical Transport of Water Vapor

The combined net horizontal and vertical transport of water vapor was computed as the algebraic sum of the net transport of water vapor through lateral and vertical boundaries of a 50-mb layer. This value represents the total net transport of water vapor leaving the volume minus the transport of water vapor entering the volume through all the boundaries of a 50-mb layer.

4.5.5 Total Mass of Water Vapor

The total mass of water vapor was computed as the total precipitable water in each 50-mb layer.

4.5.6 Local Rate-of-Change in the Total Mass of Water Vapor

The local rate-of-change term was computed for each 50-mb layer applying a 3-h forward time difference at 1500 GMT, a 6-h centered time difference at 1800, 2100, and 0000 GMT, and a 3-h backward time difference at 0300 GMT.

4.6 Composite Surface Analysis

The analysis of surface parameters for each day and hour were stratified by several criteria to determine relationships between each parameter and radar echoes. Parameters considered were velocity divergence, moisture divergence, vertical motion 50-mb above the surface, and the vertical flux of moisture 50-mb above the surface. Contingency tables and frequency distributions were prepared for various categories of convective echoes.

4.7 Average Conditions of Upper-Level Kinematics and Atmospheric Energetics During Times With and Without Convective Activity

The analysis of upper-level kinematics and atmospheric energetics for each sounding time were stratified and averaged according to "convective" or "non-convective" conditions to summarize the case studies from 1978 data. Parameters averaged included mass divergence, vertical motion, moisture divergence, horizontal and vertical flux divergence of latent heat energy, local change of latent heat energy, residual of the latent heat energy equation, diabatic heating, horizontal and vertical flux divergence of energy, local change of kinetic energy, horizontal and vertical flux divergence of sensible heat energy, local change of internal energy, horizontal and vertical flux divergence of potential energy, and local change of potential energy. Average vertical profiles for each of these parameters were prepared and are presented in Section 5.28 with a description of the stratification criteria used.

4.8 Average Moisture Processes as a Function of Convective Activity

The analysis of the water budget from each sounding time was stratified and averaged according to "convective" or "nonconvective" conditions to summarize the case studies from 1978 data. Average vertical profiles for net horizontal transport of water vapor, net vertical transport of water vapor, vertical transport of water vapor through constant pressure surfaces, combined net horizontal and vertical transport of water vapor, local rate-of-change in the total mass of water vapor, and the residual of the water budget equation were prepared and are presented in Section 5.29 with a description of the stratification criteria used.

5. RESULTS

In this section, figures are labeled in either Central Daylight Time (CDT) or Greenwich Mean Time (GMT), although GMT is used in the text. GMT is obtained by adding five hours to CDT.

5.1 1 June 1978

5.1.1 Radar

There were no radar echoes observed on this day.

5.1.2 Surface

Patterns of surface temperature (Fig. 5.1.2.1) changed constantly through the day. Lowest temperatures were in the west and northwest. Some warm and cool centers formed but did not last more than two hours.

Dewpoint depressions (Fig. 5.1.2.2) increased with the general temperature increase through the day and decreased after 0000 GMT. Minimum depressions were located near Roscoe with maximums near Garden City.

Surface mixing ratios (Fig. 5.1.2.3) and equivalent potential temperatures (Fig. 5.1.2.4) were similar in pattern throughout the day. Maximum values were near Roscoe before 0000 GMT. The mixing ratios and equivalent potential temperatures were moderate in value.

Terrain-induced vertical motion (Fig. 5.1.2.5) was small throughout the day and patterns were variable.

Figure 5.1.2.6 shows the surface velocity divergence. Divergence predominates up to 1800 GMT when moderate convergence formed near Walsh-Watts. At 2300 GMT a center of convergence formed near Midland and persisted throughout the remainder of the day. This center was strongest at 2300 GMT.

The vertical motion 50 mb above the surface (Fig. 5.1.2.7), surface moisture divergence (Fig. 5.1.2.8), and vertical flux of moisture 50 mb above the surface (Fig. 5.1.2.9), all exhibited patterns similar to those of the surface divergence. Values of these parameters were moderate. The strongest upward motion and moisture convergence took place at 2300 GMT near Midland.

Surface vorticity (Fig. 5.1.2.10) also shows moderate values. A center of positive vorticity was present near Big Spring and Garden City between 1800 and 2300 GMT.

Surface pressure changes (Fig. 5.1.2.11) were mostly small. At 0100 GMT a strong pressure rise is indicated at Lenorah. This shows the difference between an interpolated value of pressure for that station before 0100 GMT and the actual station pressure at 0100 GMT.

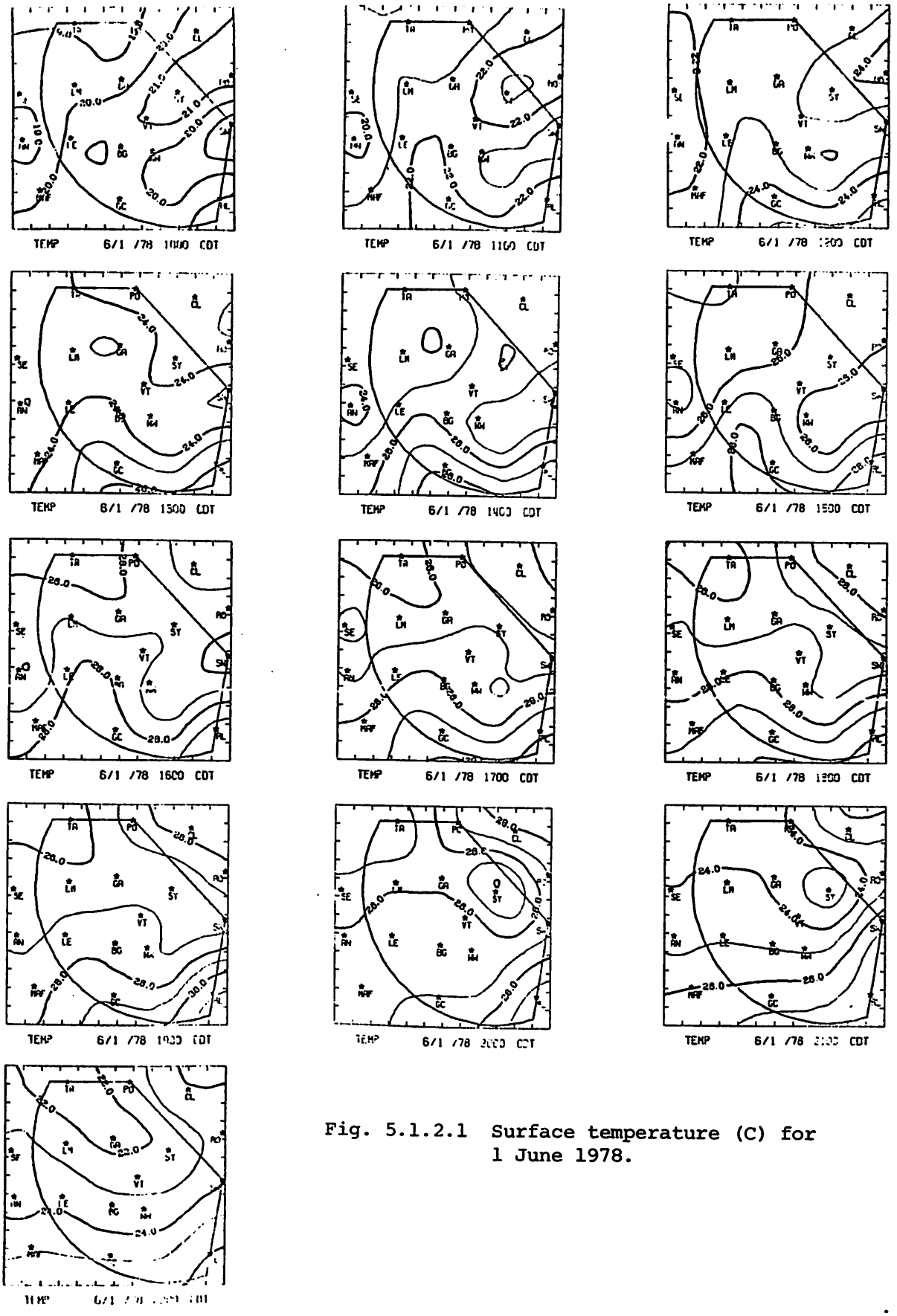

Fig. 5.1.2.1 Surface temperature (C) for 1 June 1978.

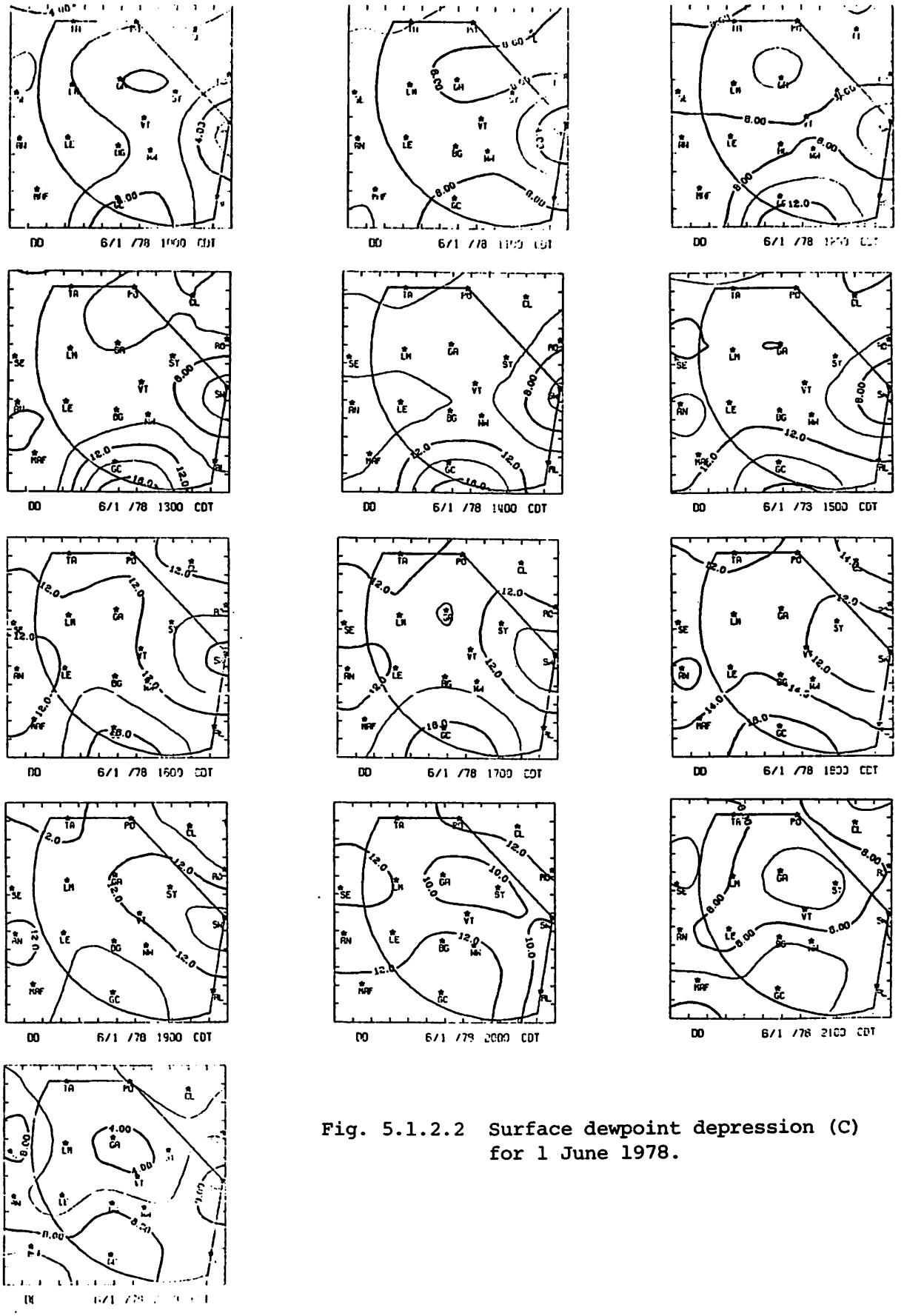

Fig. 5.1.2.2 Surface dewpoint depression (C) for 1 June 1978.

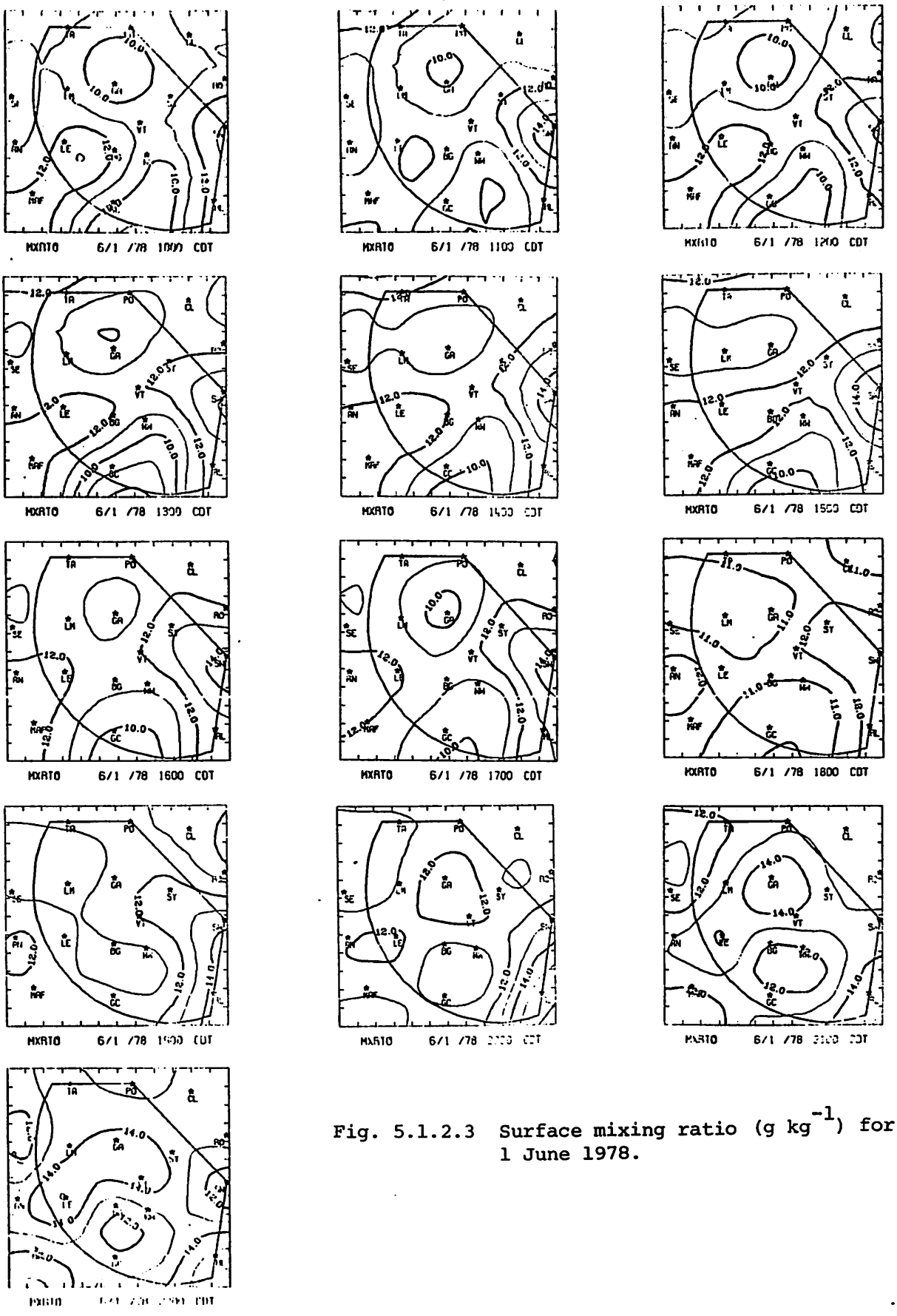

Fig. 5.1.2.3 Surface mixing ratio (g kg^{-1}) for 1 June 1978.

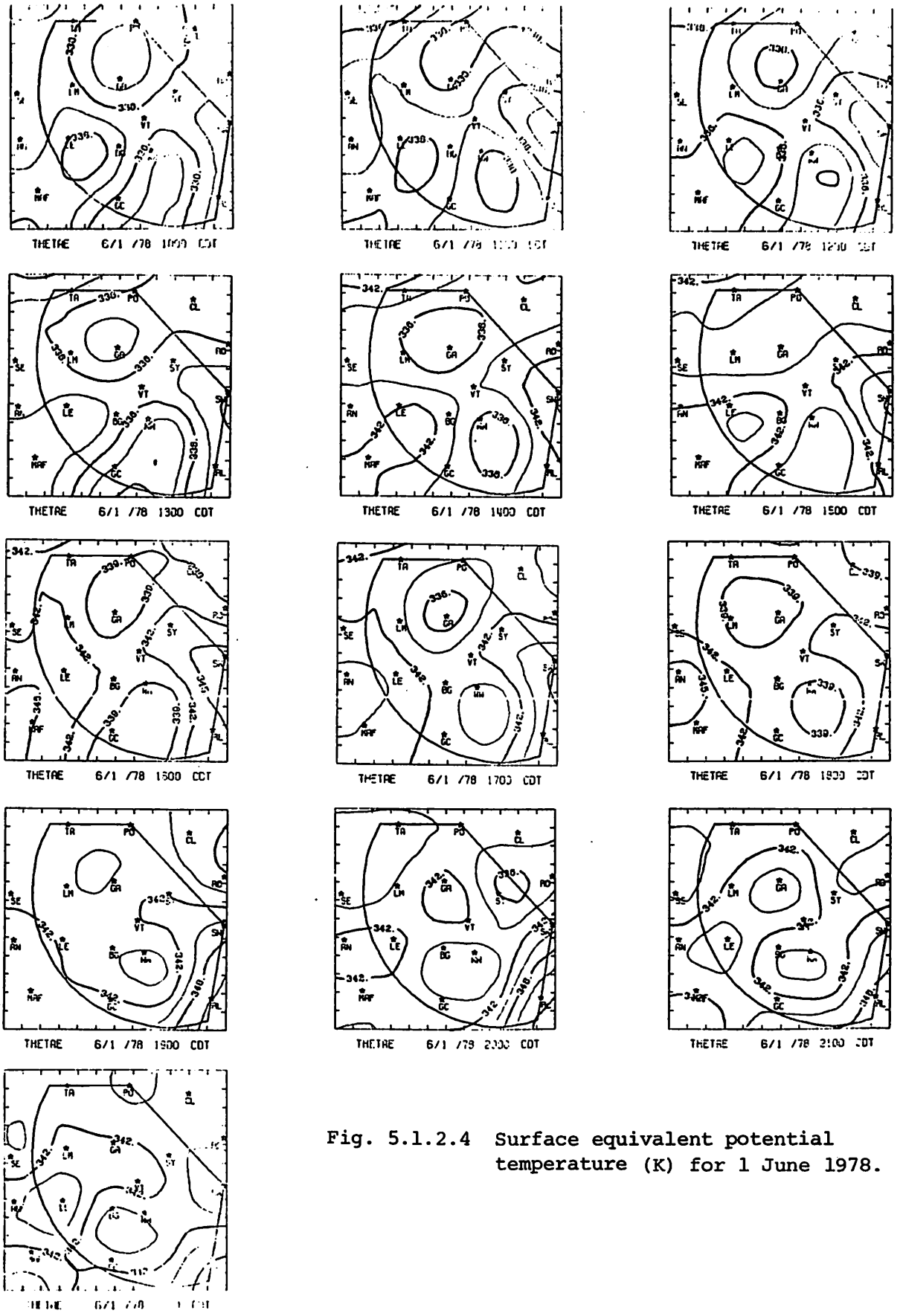

Fig. 5.1.2.4 Surface equivalent potential temperature (K) for 1 June 1978.

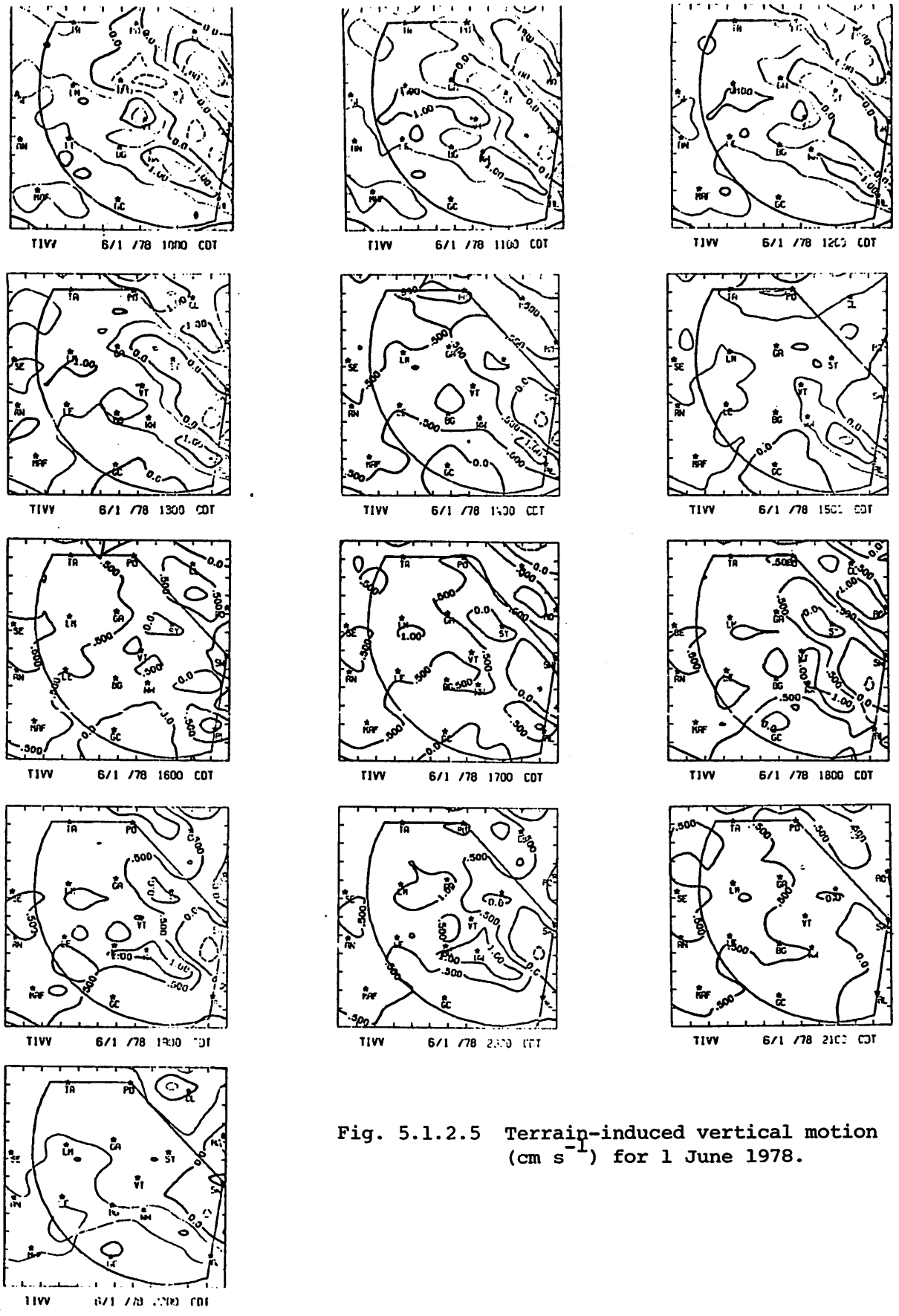

Fig. 5.1.2.5 Terrain-induced vertical motion (cm s^{-1}) for 1 June 1978.

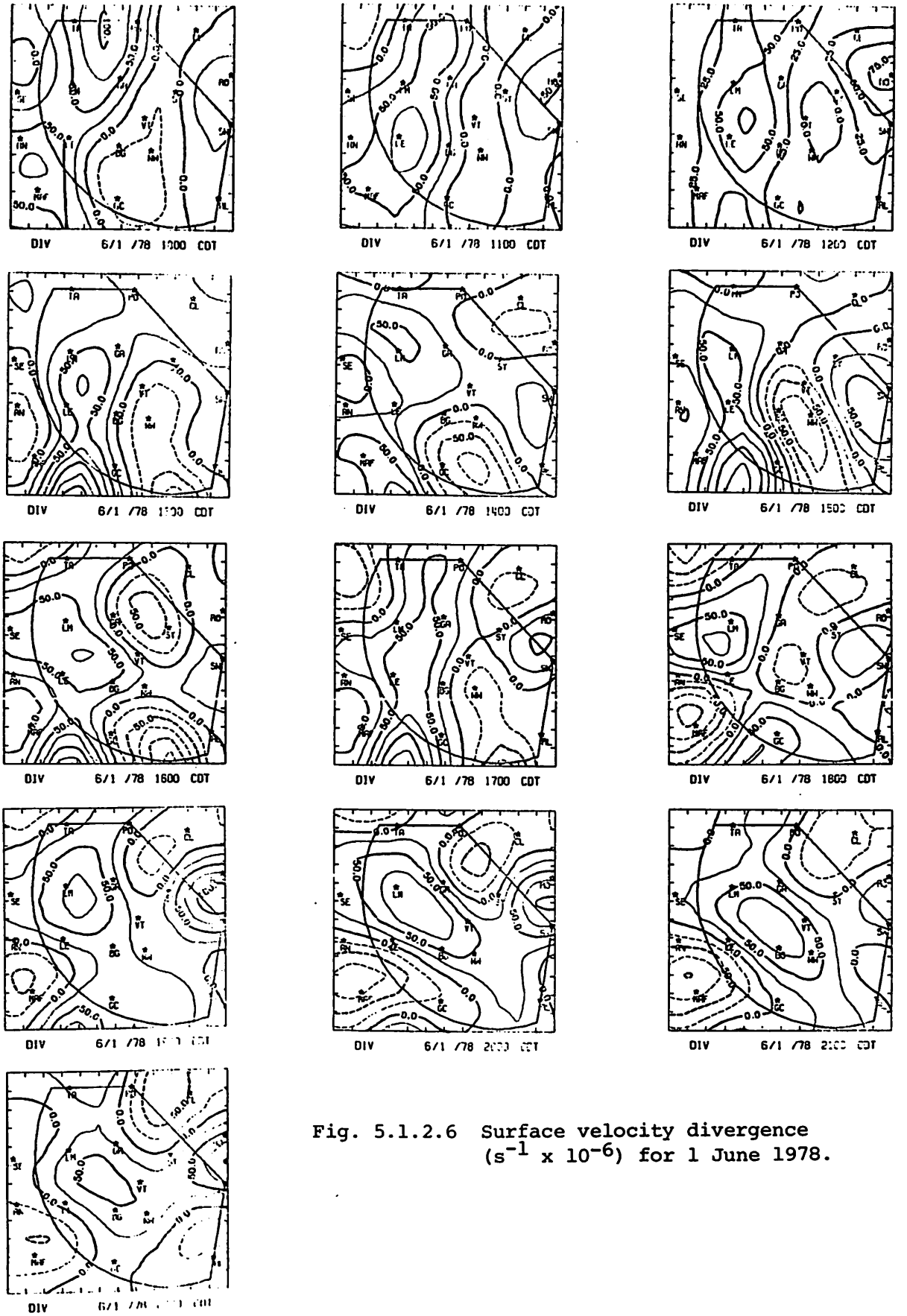

Fig. 5.1.2.6 Surface velocity divergence (s^{-1} x 10^{-6}) for 1 June 1978.

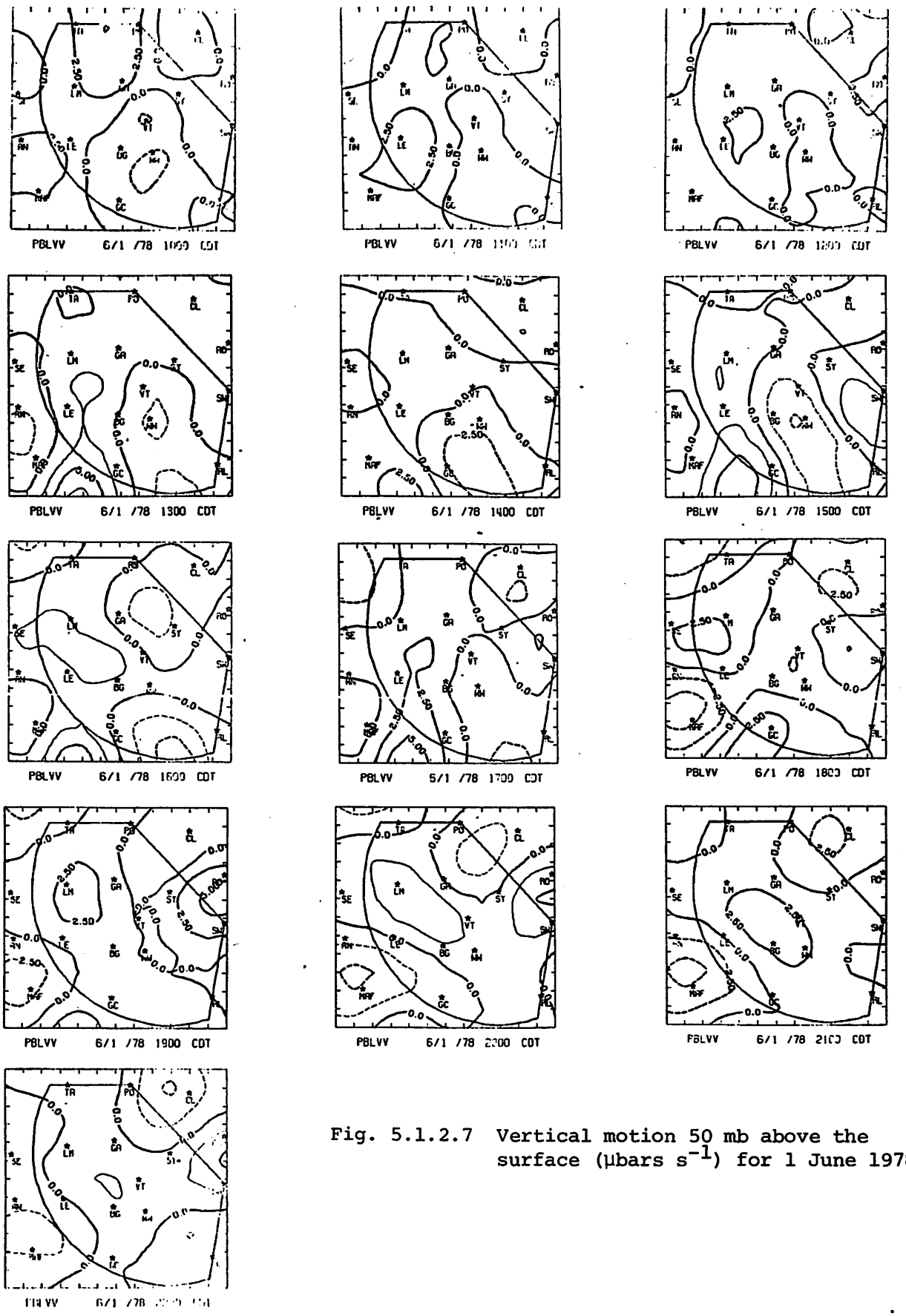

Fig. 5.1.2.7 Vertical motion 50 mb above the surface (μbars s^{-1}) for 1 June 1978.

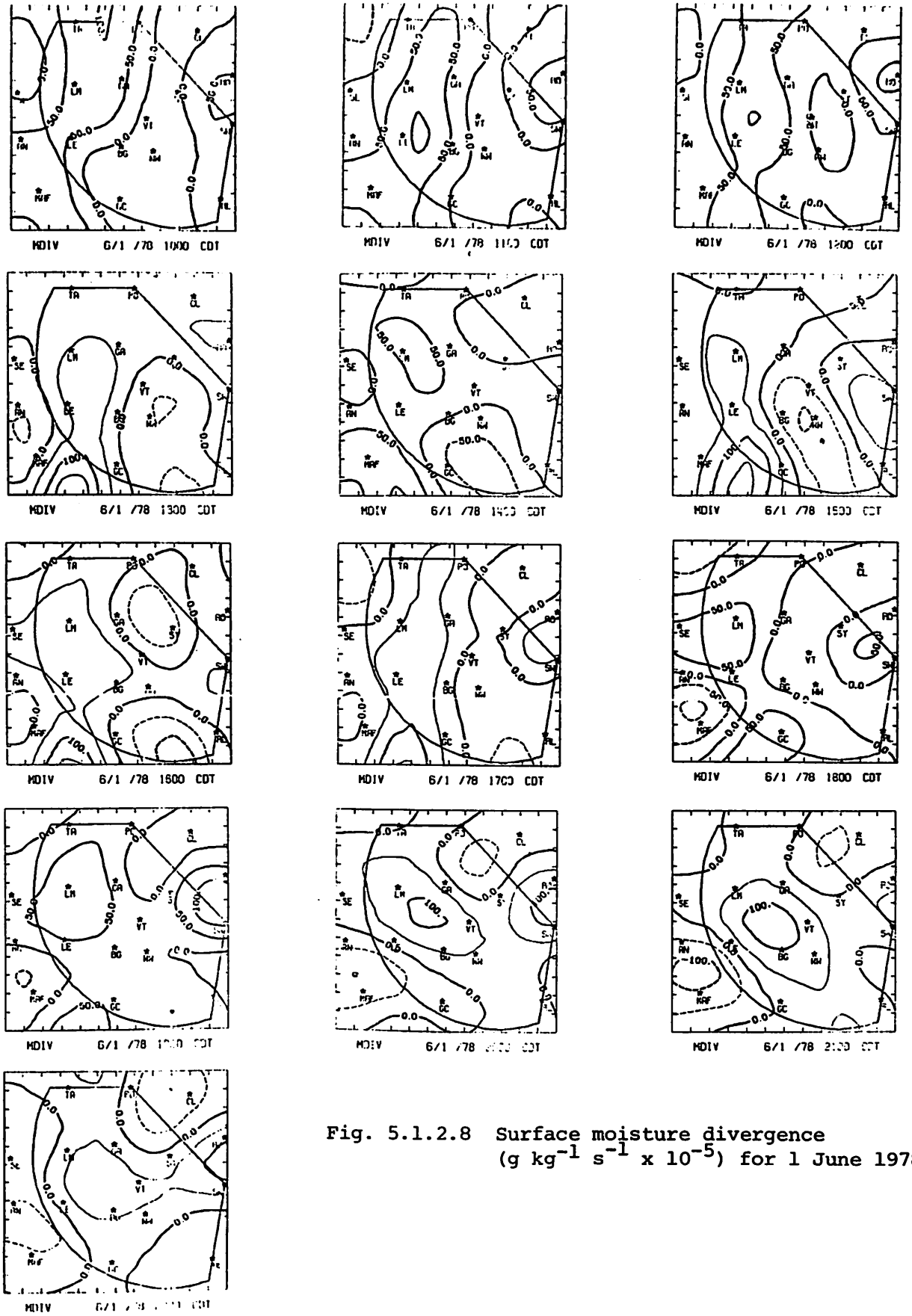

Fig. 5.1.2.8 Surface moisture divergence (g kg^{-1} s^{-1} x 10^{-5}) for 1 June 1978.

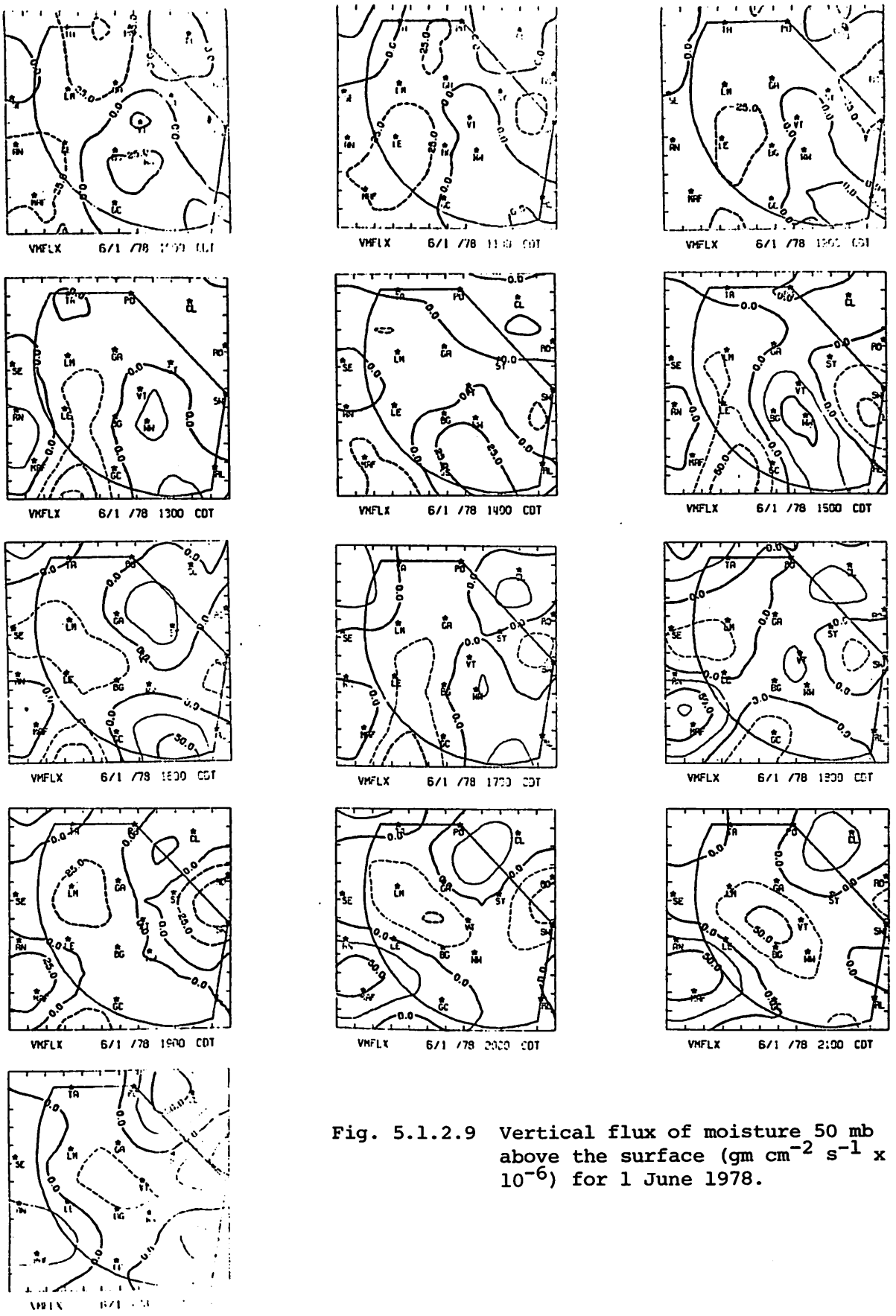

Fig. 5.1.2.9 Vertical flux of moisture 50 mb above the surface (gm cm^{-2} s^{-1} x 10^{-6}) for 1 June 1978.

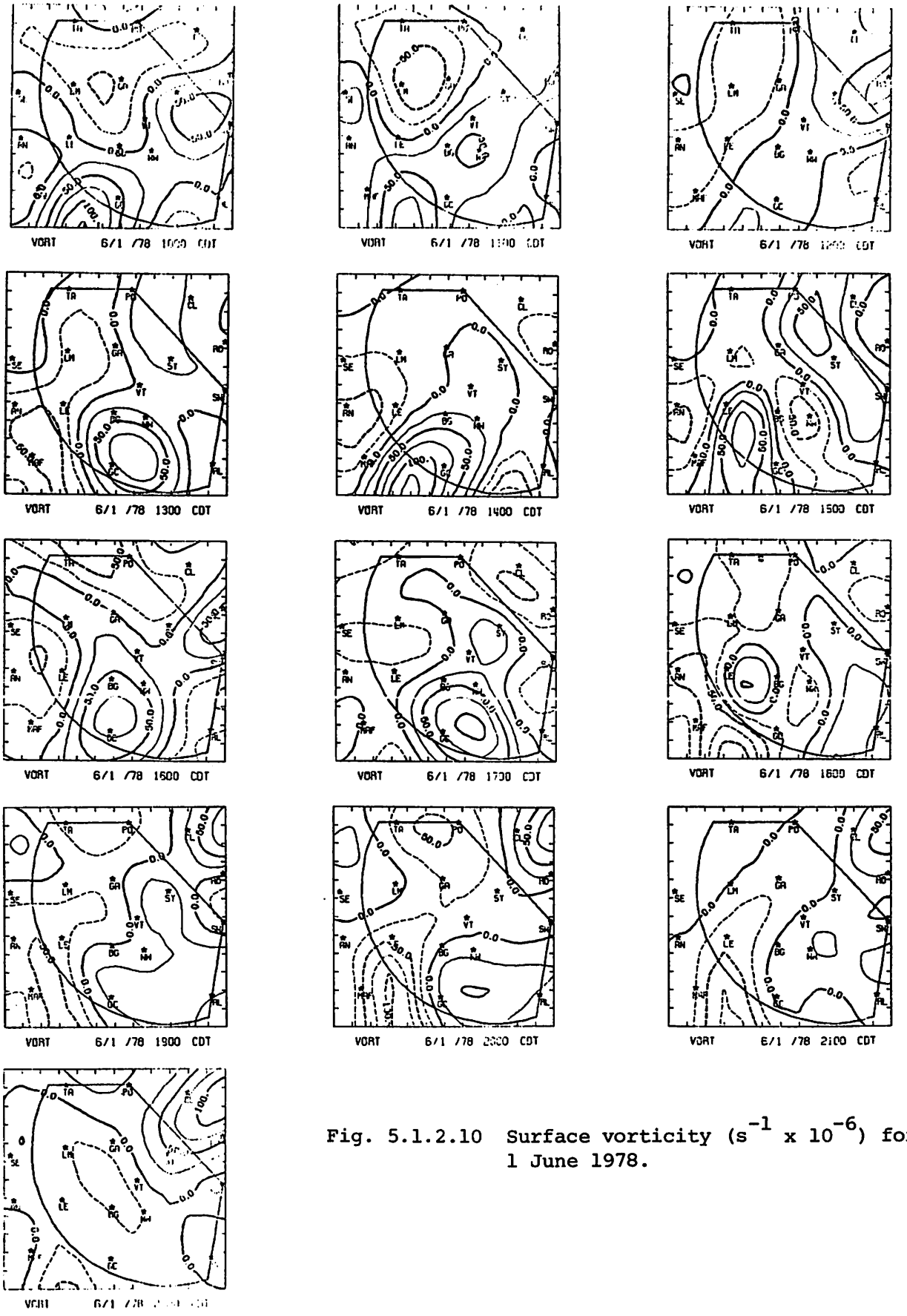

Fig. 5.1.2.10 Surface vorticity (s^{-1} x 10^{-6}) for 1 June 1978.

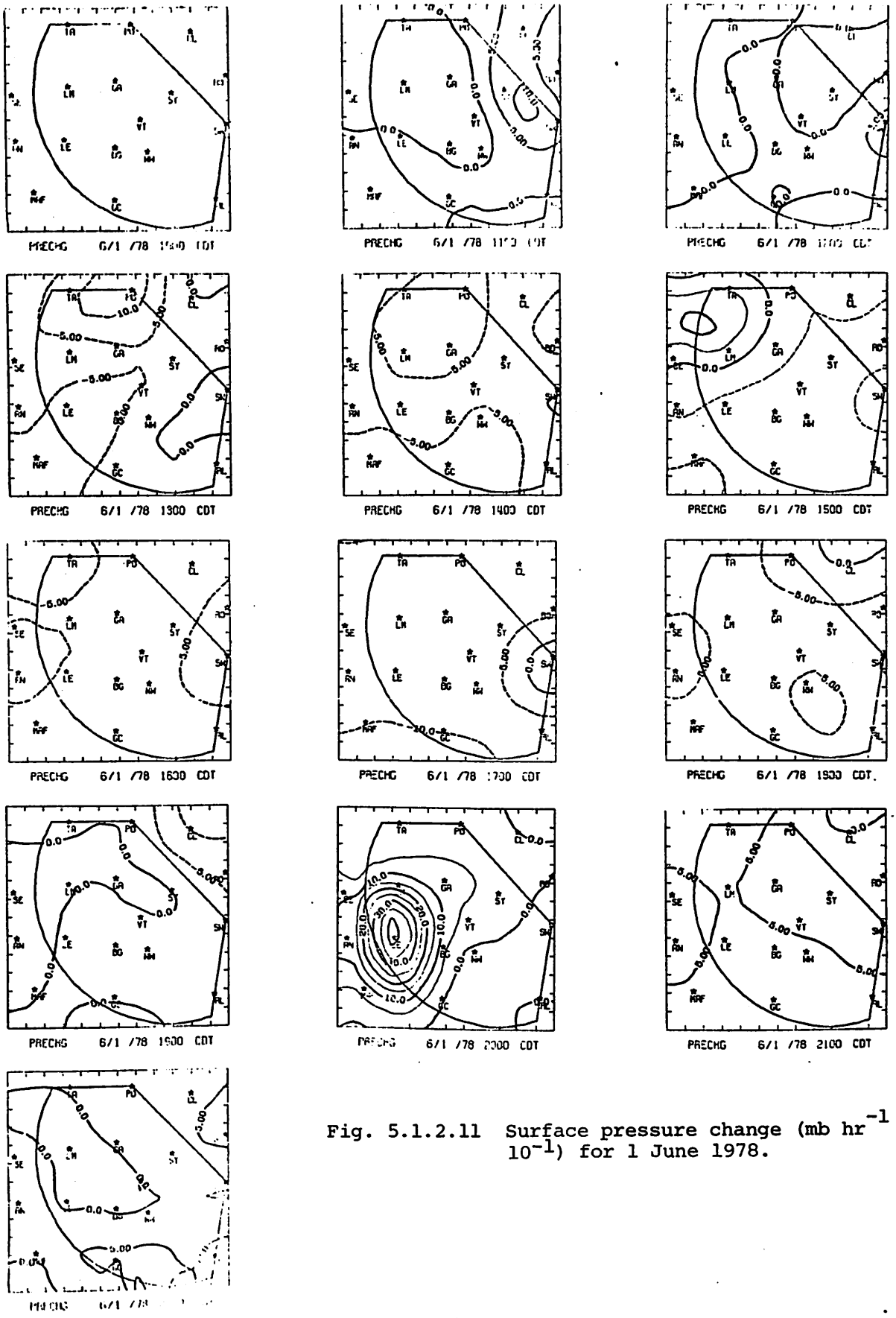

Fig. 5.1.2.11 Surface pressure change (mb hr^{-1} x 10^{-1}) for 1 June 1978.

Relative surface winds (Fig. 5.1.2.12) were from the northeast at 1500 GMT but shifted to the east by 1900 GMT. Winds were generally easterly after that time.

5.1.3 Upper Level Kinematic Parameters

For these figures only the 1500 GMT profile was available because wind data were missing at the other hours.

At 1500 GMT mass divergence extends to 350 mb (Fig. 5.1.3.1). Convergence is present near 300 mb below the level of highest winds. Vertical motion (Fig. 5.1.3.2) at 1500 GMT was downward at all levels though small in the lowest levels. Also, moisture divergence (Fig. 5.1.3.3) was present in most levels though it is near zero above 500 mb. The presence of a deep layer of mass divergence, downward vertical motion, and moisture divergence is characteristic of a day with no echo activity.

5.1.4 Energetics

For all figures except Fig. 5.1.4.3, only the 1500 GMT profile is available. In Fig. 5.1.4.3, dealing with local change of latent heat, only the 0300 GMT profile is shown.

Figure 5.1.4.1 shows that the horizontal flux of latent heat at 1500 GMT was outward at most levels. The largest outflow occurred at low levels and values were near zero in upper levels.

The profiles of vertical transport of latent heat (Fig. 5.1.4.2) at 1500 GMT indicate transport downward from upper levels into lower levels. Layers into which heat is transported are near 650 mb and below 750 mb.

The profile of local change of latent heat energy (Fig. 5.1.4.3) for 0300 GMT indicates small losses in low levels and somewhat larger gains in upper levels.

It was not possible to compute profiles of the residual of the latent heat energy equation and of diabatic heating for this day.

Horizontal transport of kinetic energy (Fig. 5.1.4.4) was outward in lower and middle layers at 1500 GMT. In upper layers near the jet stream level there was strong inflow. The profile of vertical transport of kinetic energy (Fig. 5.1.4.5) shows transport into nearly all layers. The maximum value was near 300 mb.

5.1.5 Water Vapor Budget

The profile of net horizontal moisture transport (Fig. 5.1.5.1) at 1500 GMT shows moisture outflow in lower layers with small inflow aloft.

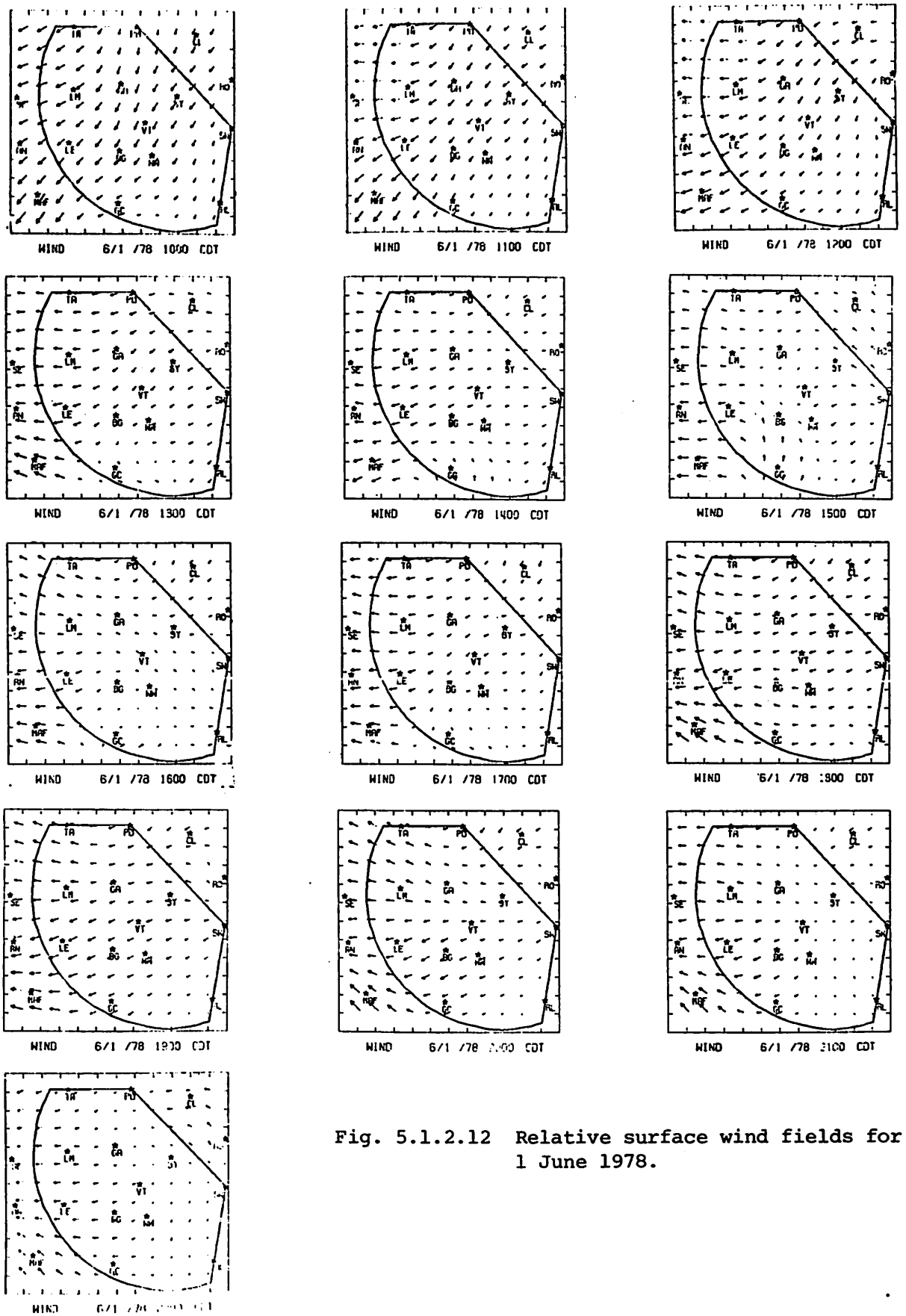

Fig. 5.1.2.12 Relative surface wind fields for 1 June 1978.

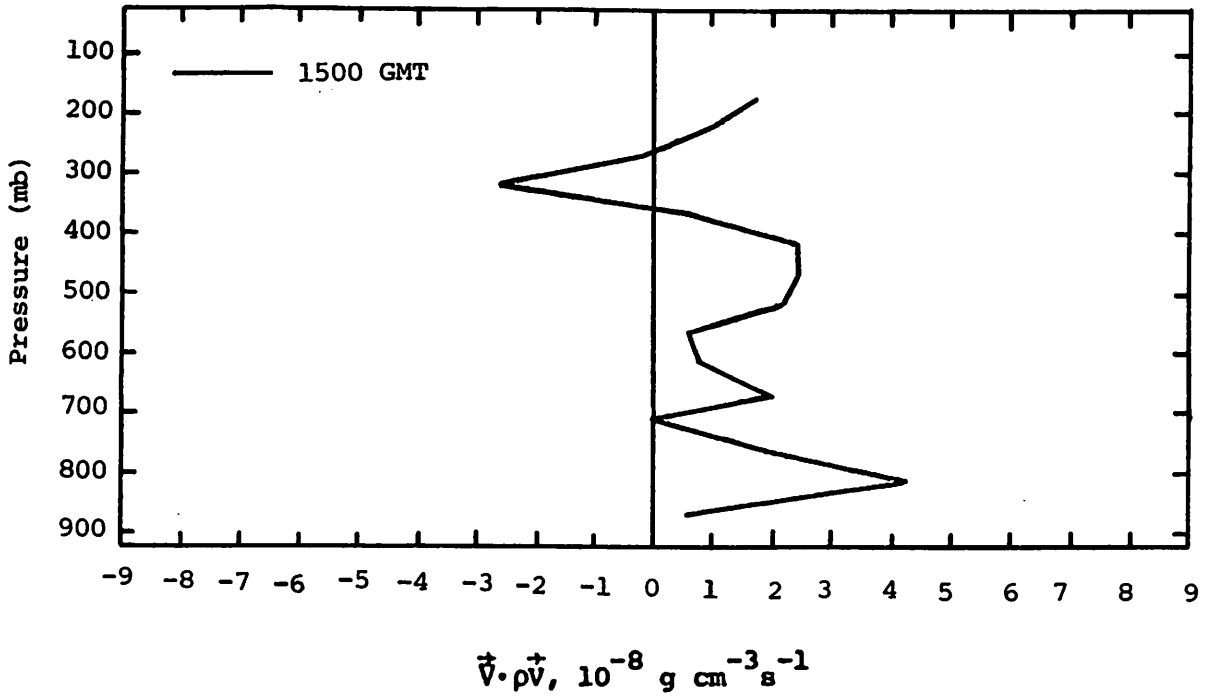

Fig. 5.1.3.1 Vertical profiles of mass divergence on 1 June 1978.

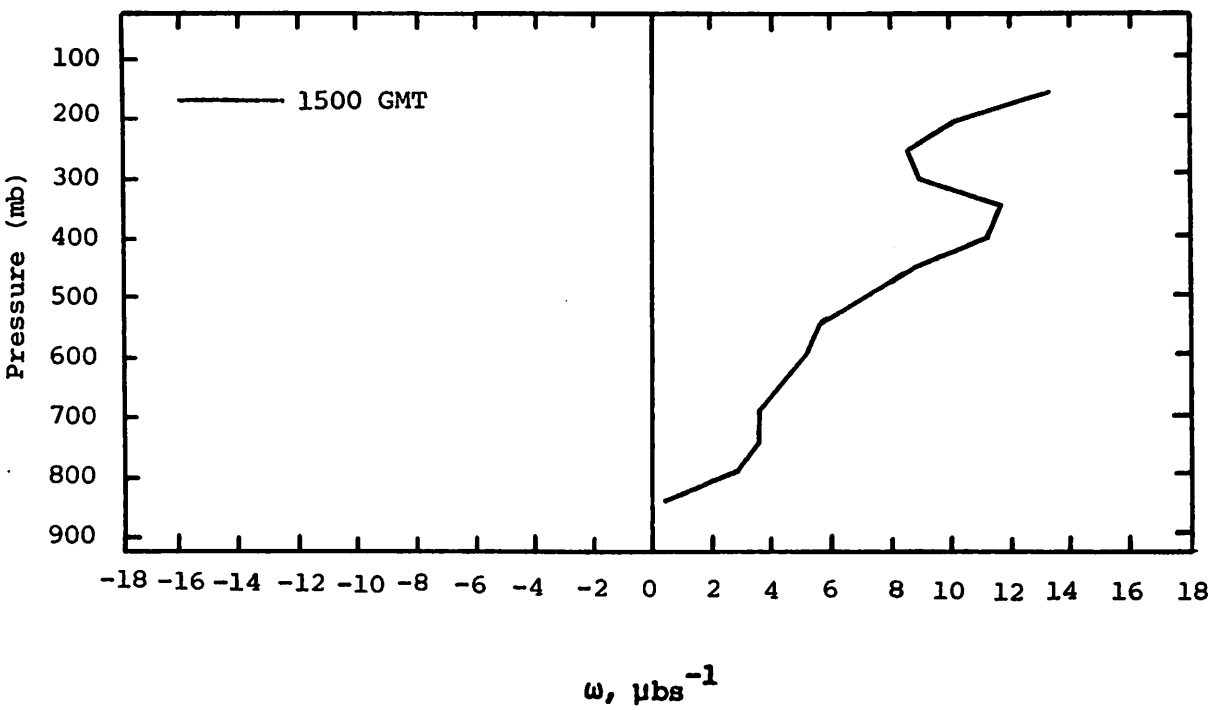

Fig. 5.1.3.2 Vertical profiles of vertical motion on 1 June 1978.

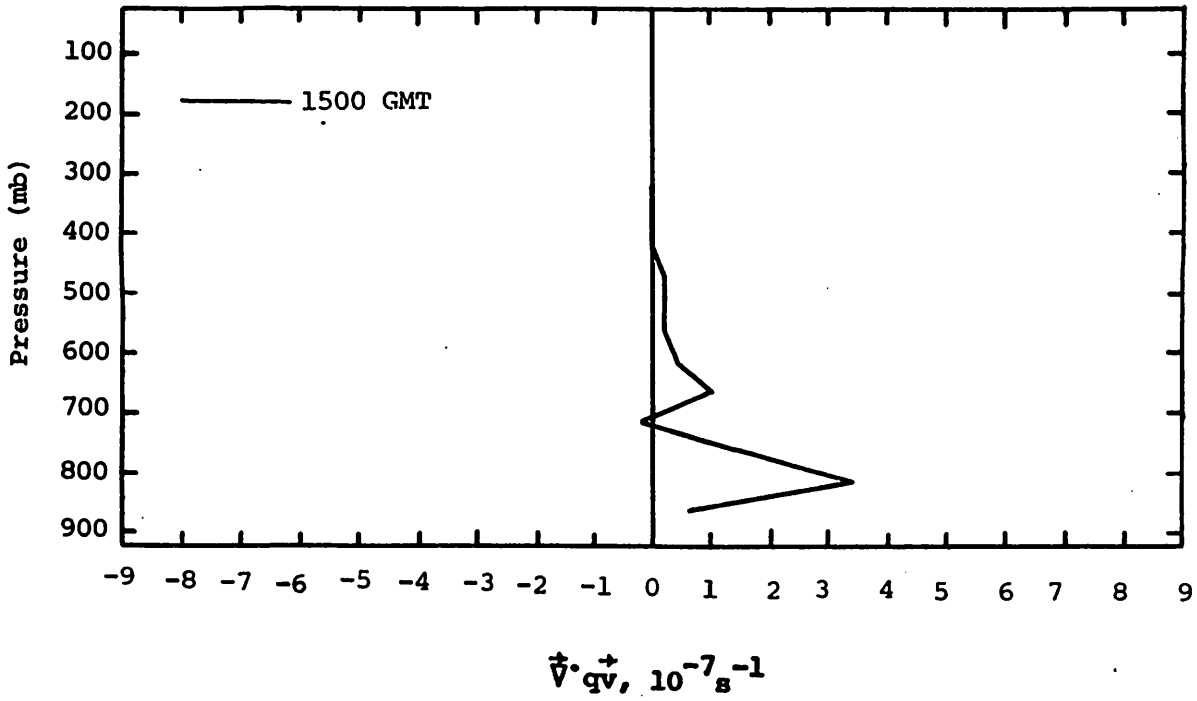

Fig. 5.1.3.3 Vertical profiles of moisture divergence on 1 June 1978.

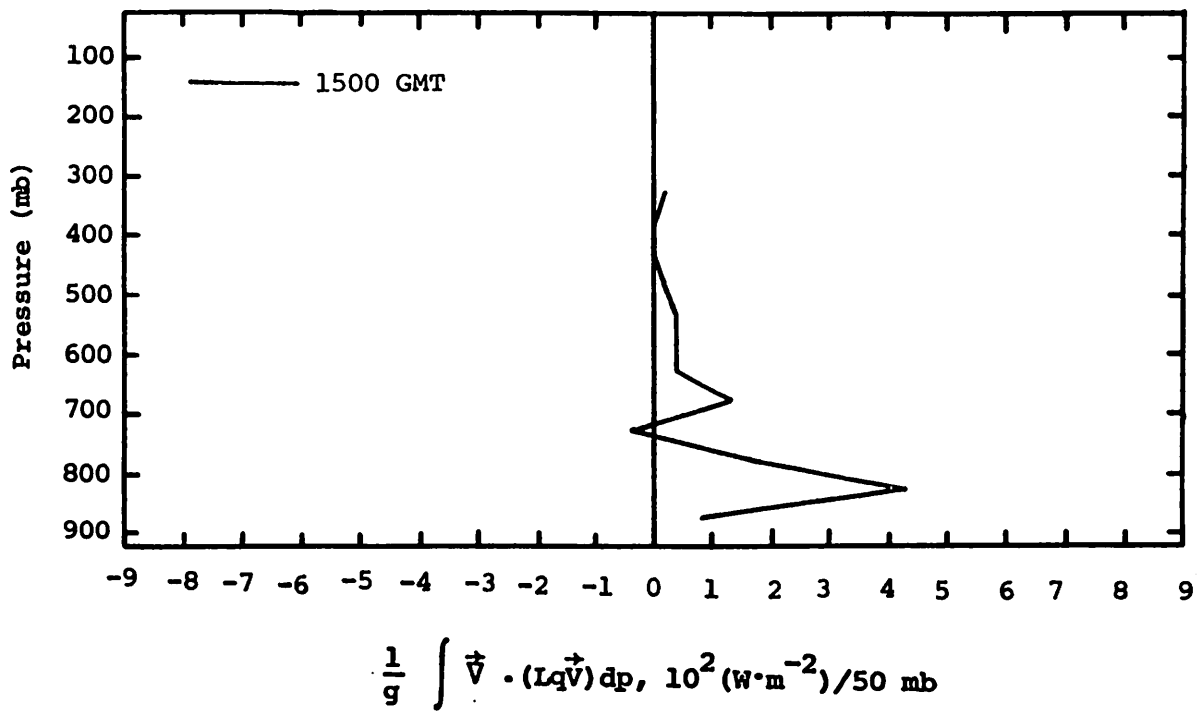

Fig. 5.1.4.1 Vertical profiles of the horizontal flux of latent heat energy on 1 June 1978.

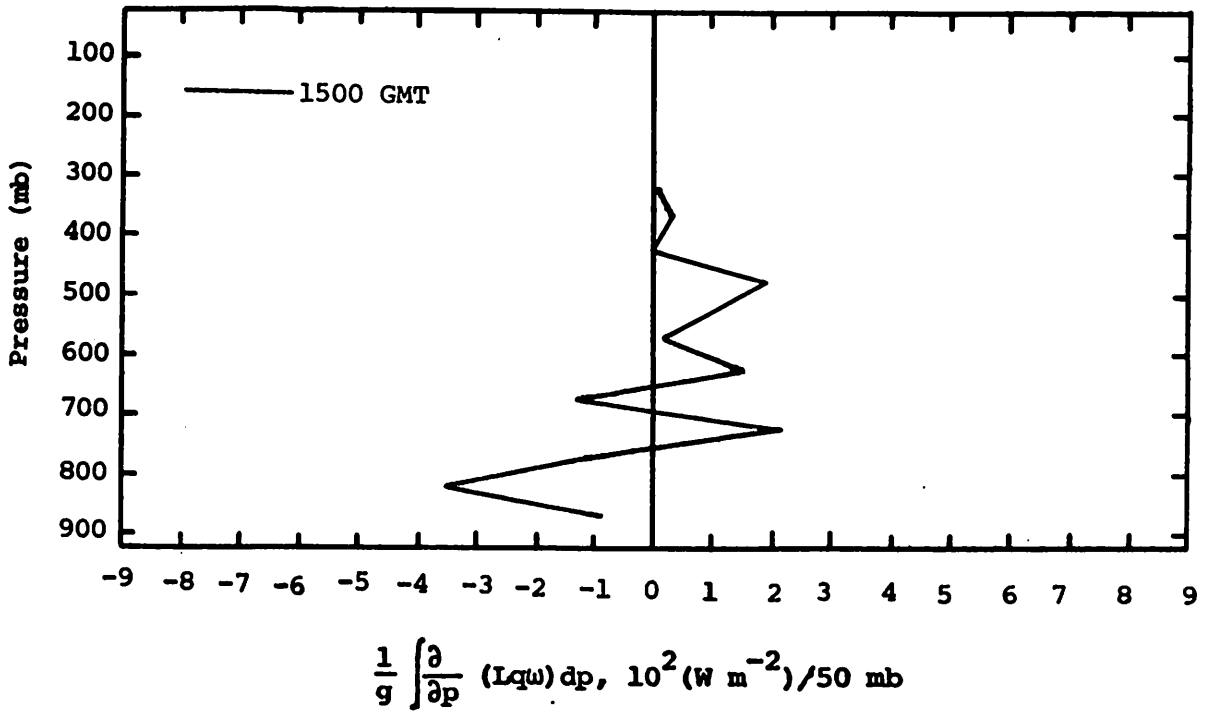

Fig. 5.1.4.2 Vertical profiles of the vertical flux of latent heat energy on 1 June 1978.

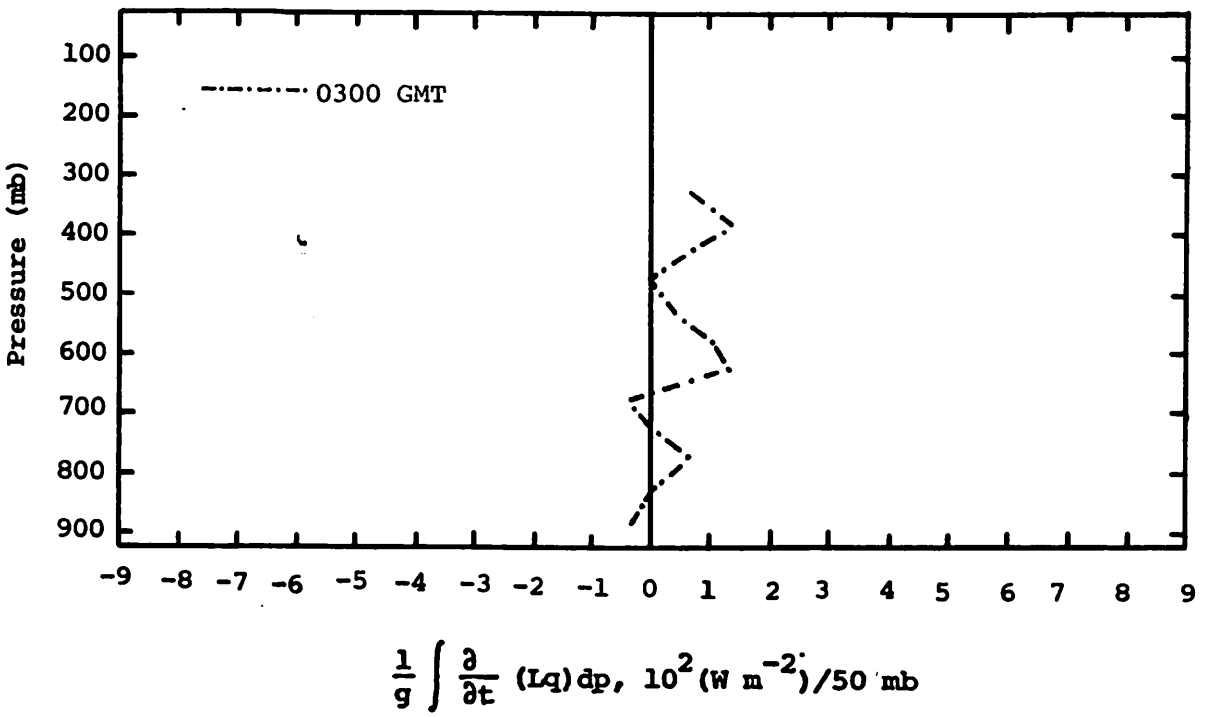

Fig. 5.1.4.3 Vertical profiles of the local change of latent heat energy on 1 June 1978.

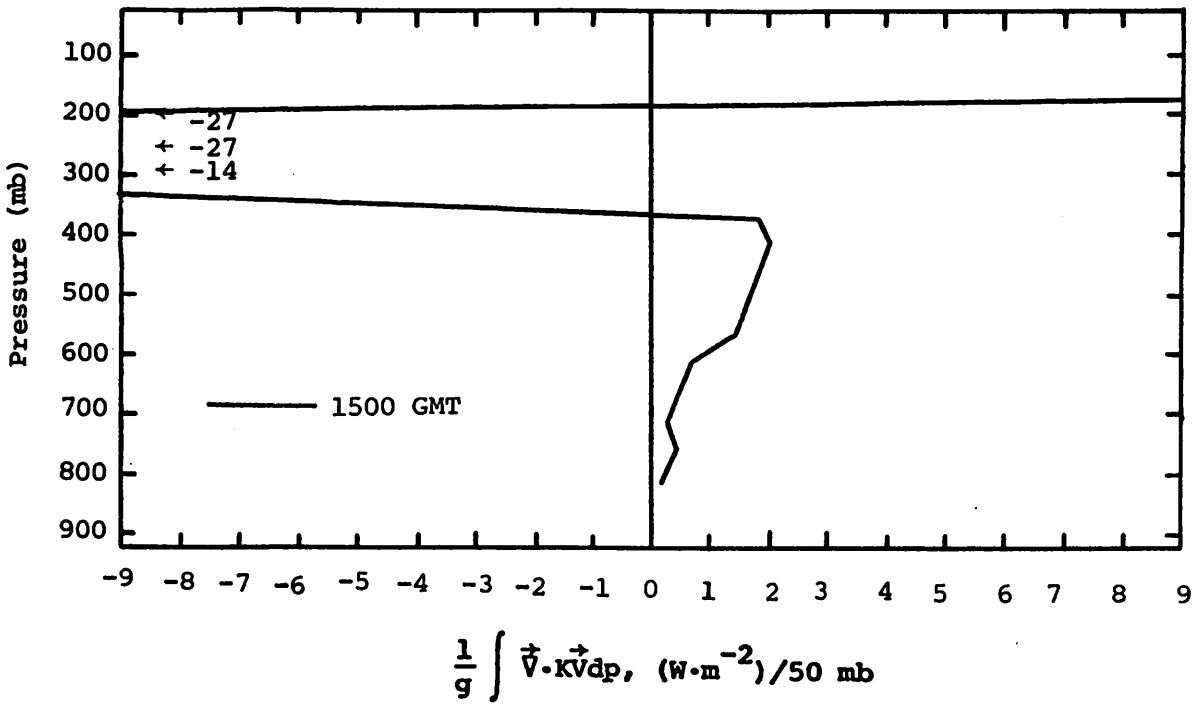

Fig. 5.1.4.4 Vertical profiles of the horizontal flux of kinetic energy on 1 June 1978.

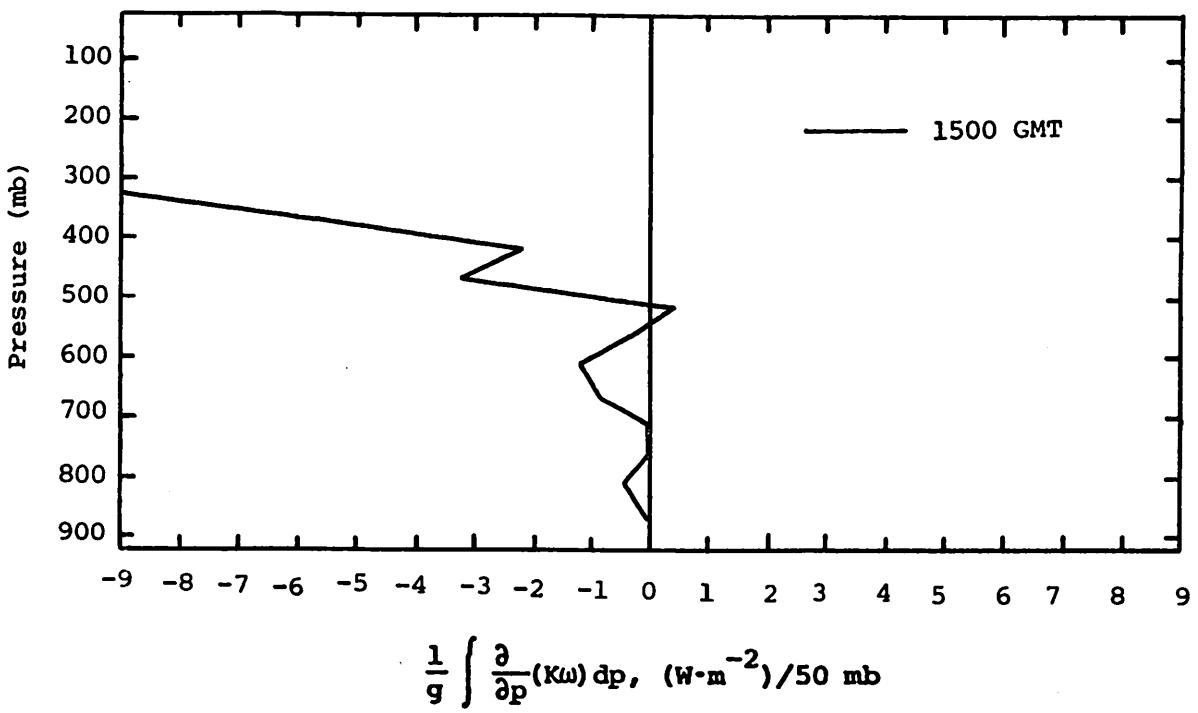

Fig. 5.1.4.5 Vertical profiles of the vertical flux of kinetic energy on 1 June 1978.

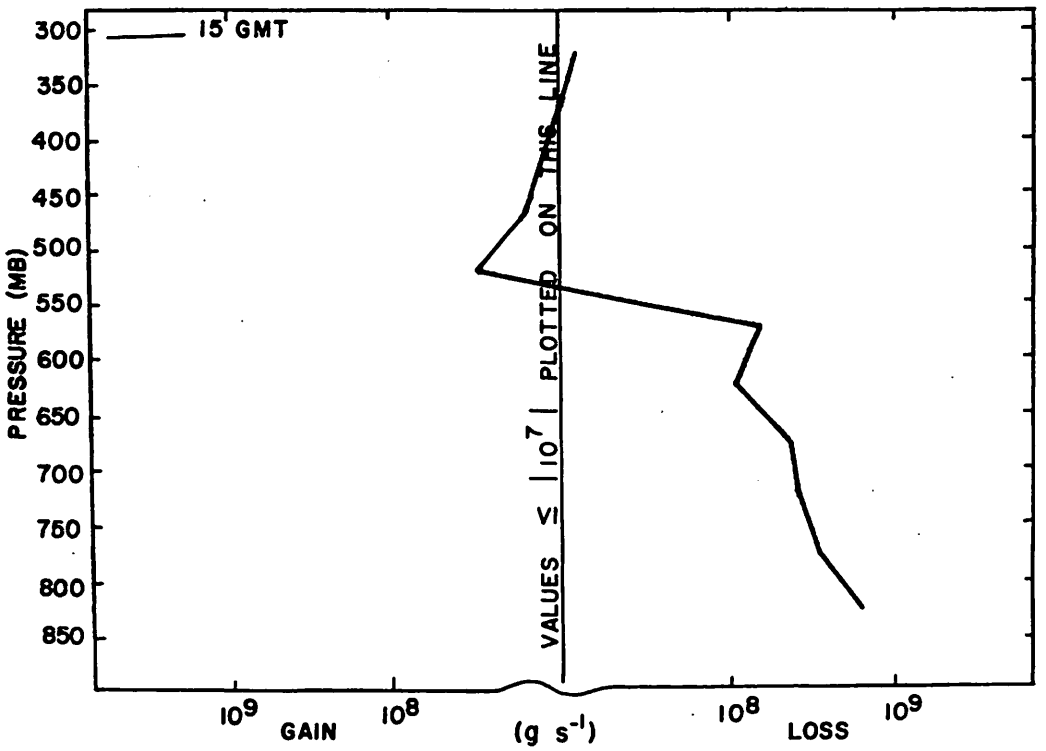

Fig. 5.1.5.1 Net horizontal transport of water vapor through boundaries of 50-mb layers (gm s^{-1}) over the Texas HIPLEX area for 1 June 1978.

This is consistent with the lack of echoes noted on this day.

The net vertical transport profile (Fig. 5.1.5.2) at 1500 GMT shows gains near the surface and also near 650 mb and losses in other layers. This is similar to Fig. 5.1.4.2, the profile of vertical transport of latent heat.

Vertical transport of moisture through constant pressure surfaces (Fig. 5.1.5.3) is downward at all levels at 1500 GMT. The profile of combined net horizontal and vertical transport of moisture (Fig. 5.1.5.4) shows net losses at all levels above 800 mb with gains only near the surface. The resemblance of this profile to Fig. 5.1.5.2 shows that vertical transport predominated on this day.

Figure 5.1.5.5, the profile of total mass of water vapor, does not show any exceptionally dry or moist layers at 1500 GMT. Since only the 1500 GMT profile was available, the local rate-of-change profile could not be computed.

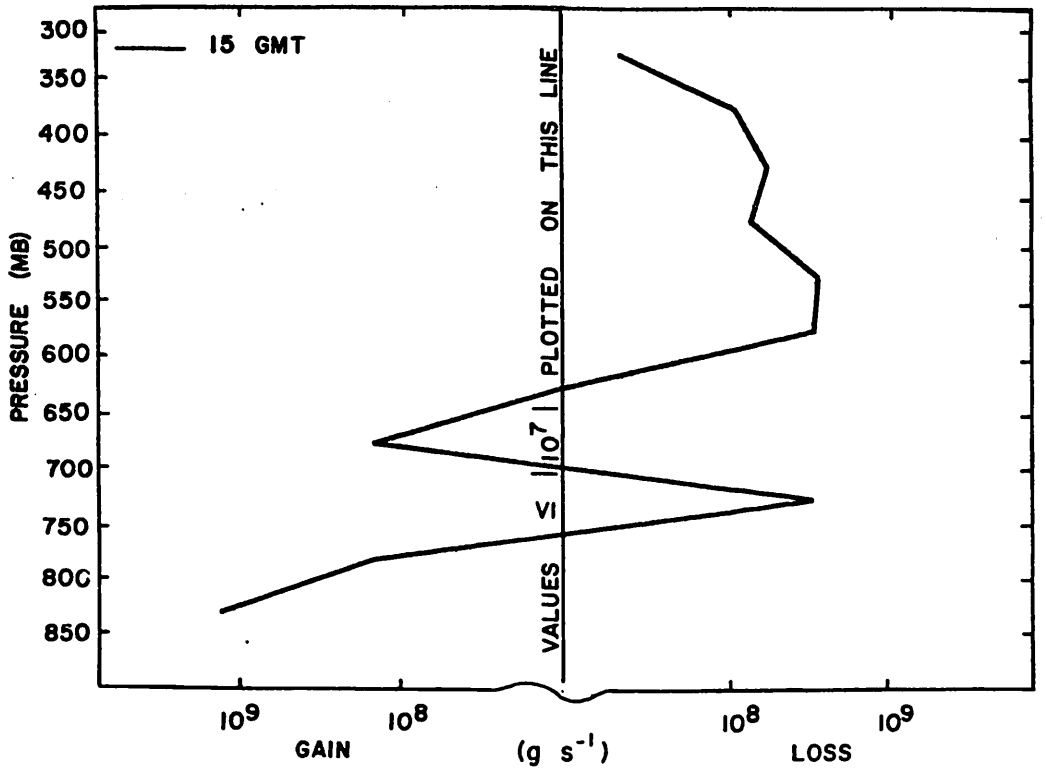

Fig. 5.1.5.2 Net vertical transport of water vapor through boundaries of 50-mb layers (gm s^{-1}) over the Texas HIPLEX area for 1 June 1978.

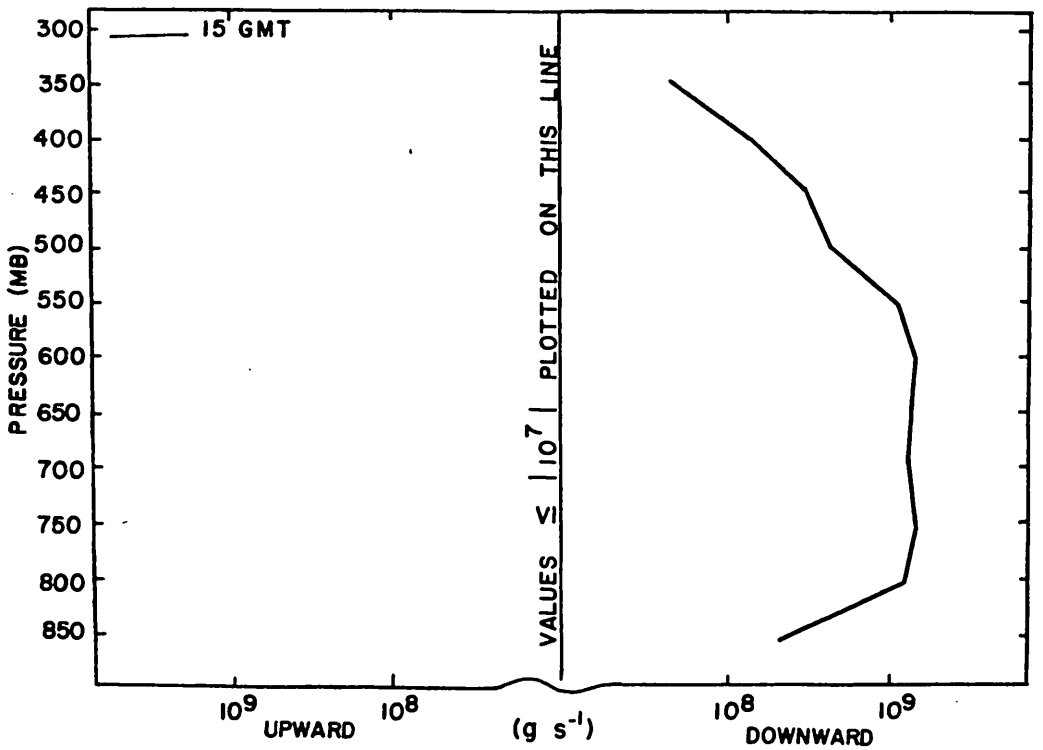

Fig. 5.1.5.3 Vertical transport of water vapor through constant pressure surfaces (g s^{-1}) over the Texas HIPLEX area for 1 June 1978.

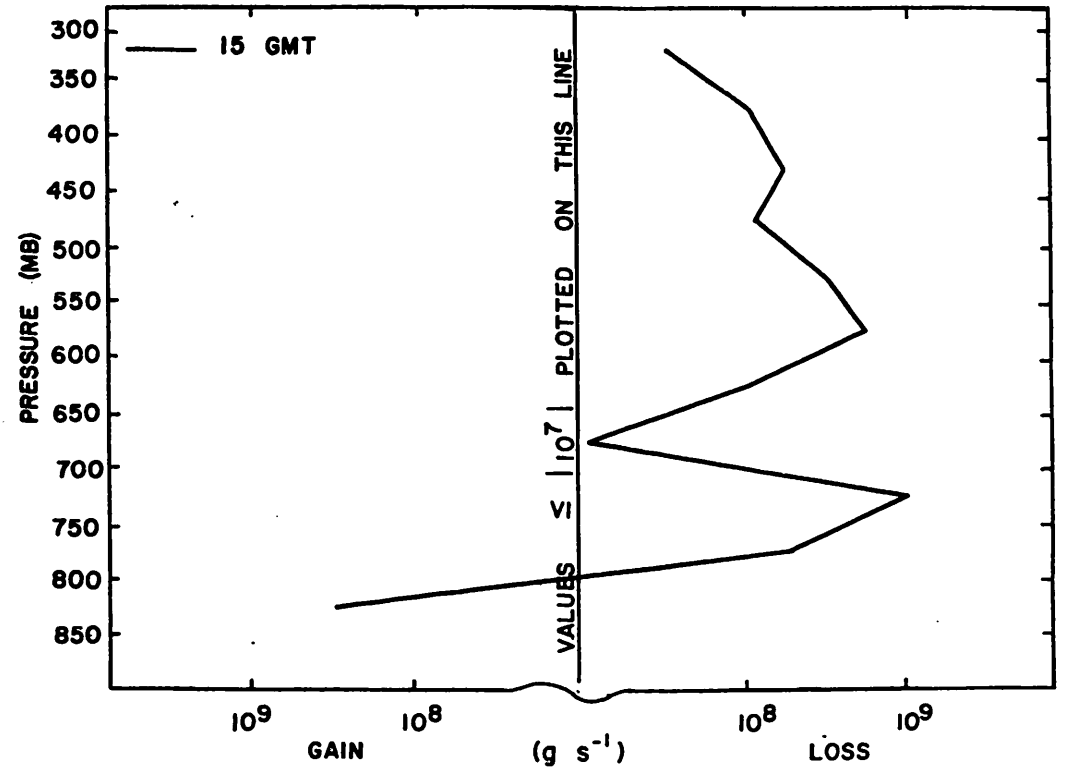

Fig. 5.1.5.4 Combined net horizontal and vertical transport of water vapor through boundaries of 50-mb layers (gm s^{-1}) over the Texas HIPLEX area for 1 June 1978.

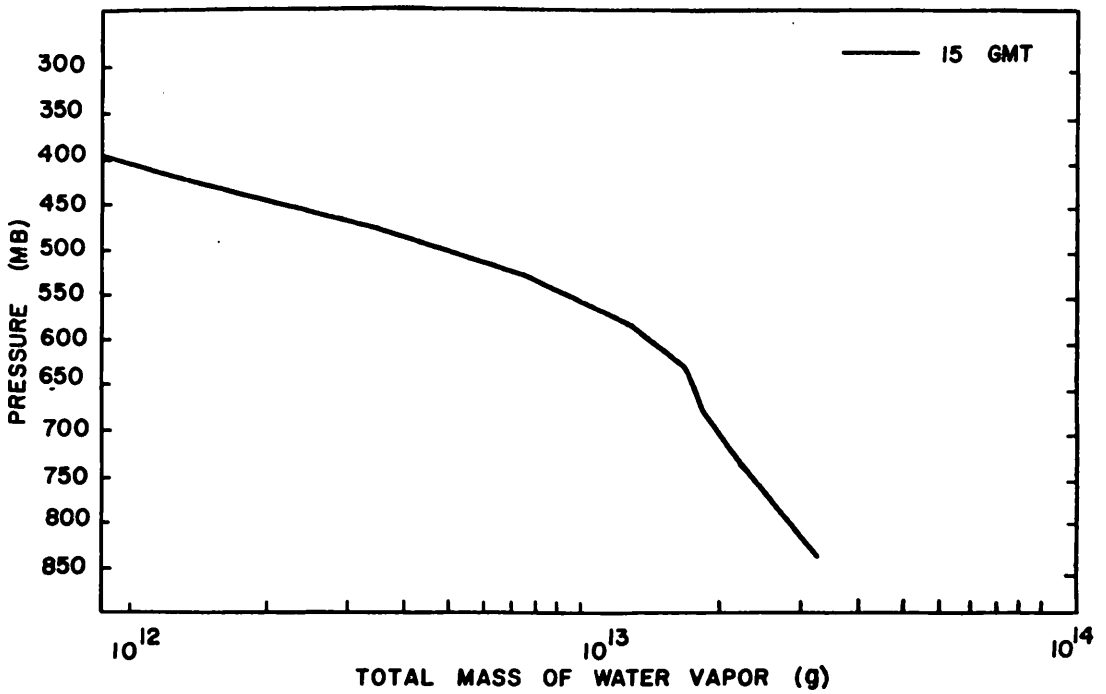

Fig. 5.1.5.5 Total mass of water vapor in layers 50 mb deep (gm) over the Texas HIPLEX area on 1 June 1978.

5.2 2 June 1978

5.2.1 Radar

Showers and thundershowers were present over the area throughout the day (Fig. 5.2.1.1). At 1500 GMT there were two strong cells present and at 1600 GMT another strong cell moved into the area. The cell between Walsh-Watts and Robert Lee had an echo top of 13.1 km (43K ft). All the strong cells moved out of the area by 1900 GMT. The shower activity covered a limited area between 1900 and 2100 GMT but was again widespread by 2200 GMT. At 0200 GMT a strong cell with height of 12.8 km (42K ft) was indicated near Midland but this was gone by 0300 GMT.

5.2.2 Surface

The surface temperature fields (Fig. 5.2.2.1) had a minimum in the northwest throughout the day with maximums generally in the south. At 1500 and 1600 GMT minimum temperatures were present near Garden City and Walsh-Watts associated with the downdraft of the large thunderstorm that was located between Walsh-Watts and Robert Lee. At 1700 GMT the temperature minimum was in the east between Roscoe and Robert Lee and temperatures in that part of the area were lower than nearby until 2300 GMT. A maximum formed near Gail at 2000 GMT and remained in the central part of the HIPLEX area until 0000 GMT when showers moved over that area and temperatures dropped.

Dewpoint depressions (Fig. 5.2.2.2) were small at 1500 GMT but increased in the southwest at 1600 GMT where there were no showers. Dewpoint depressions increased over the area by 2000 GMT as shower activity diminished and temperatures increased. Maximum dewpoint depressions coincided with the temperature maximums in the central part of the area between 2000 and 2300 GMT. As cooling took place between 0000 and 0300 GMT, dewpoint depressions decreased again.

Surface mixing ratios (Fig. 5.2.2.3) were moderate with a maximum near Lenorah and Big Spring between 1500 and 2100 GMT. A minimum was in the central part of the area between 2100 and 0000 GMT, and in the north central part of the area after that. Between 0100 and 0300 GMT there was a general decrease in mixing ratio across the area.

The surface equivalent potential temperature (Fig. 5.2.2.4) at 1500 GMT shows a maximum near Lenorah, where no showers were present, and a minimum near Walsh-Watts in the vicinity of a strong storm cell. As the showers

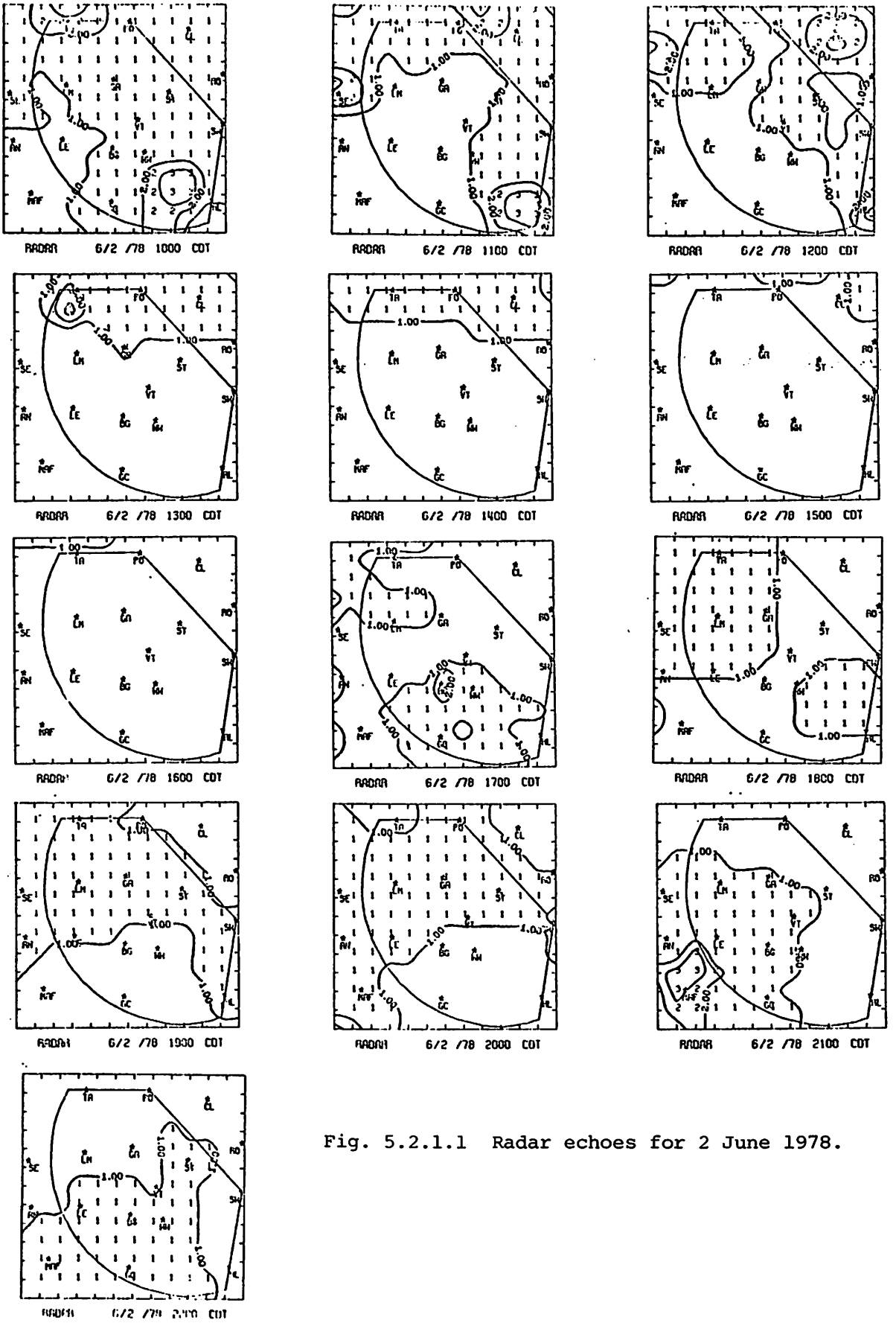

Fig. 5.2.1.1 Radar echoes for 2 June 1978.

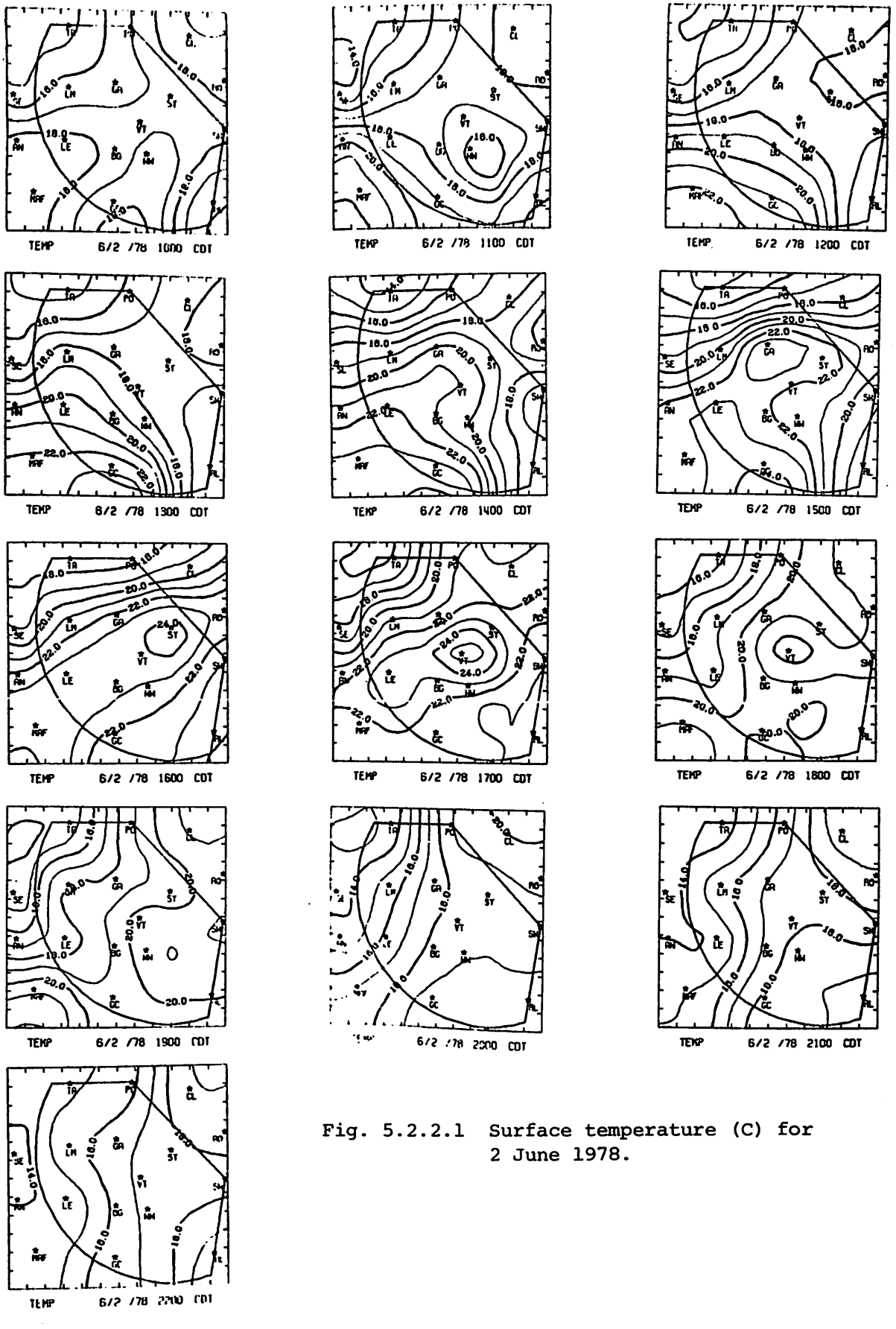

Fig. 5.2.2.1 Surface temperature (C) for 2 June 1978.

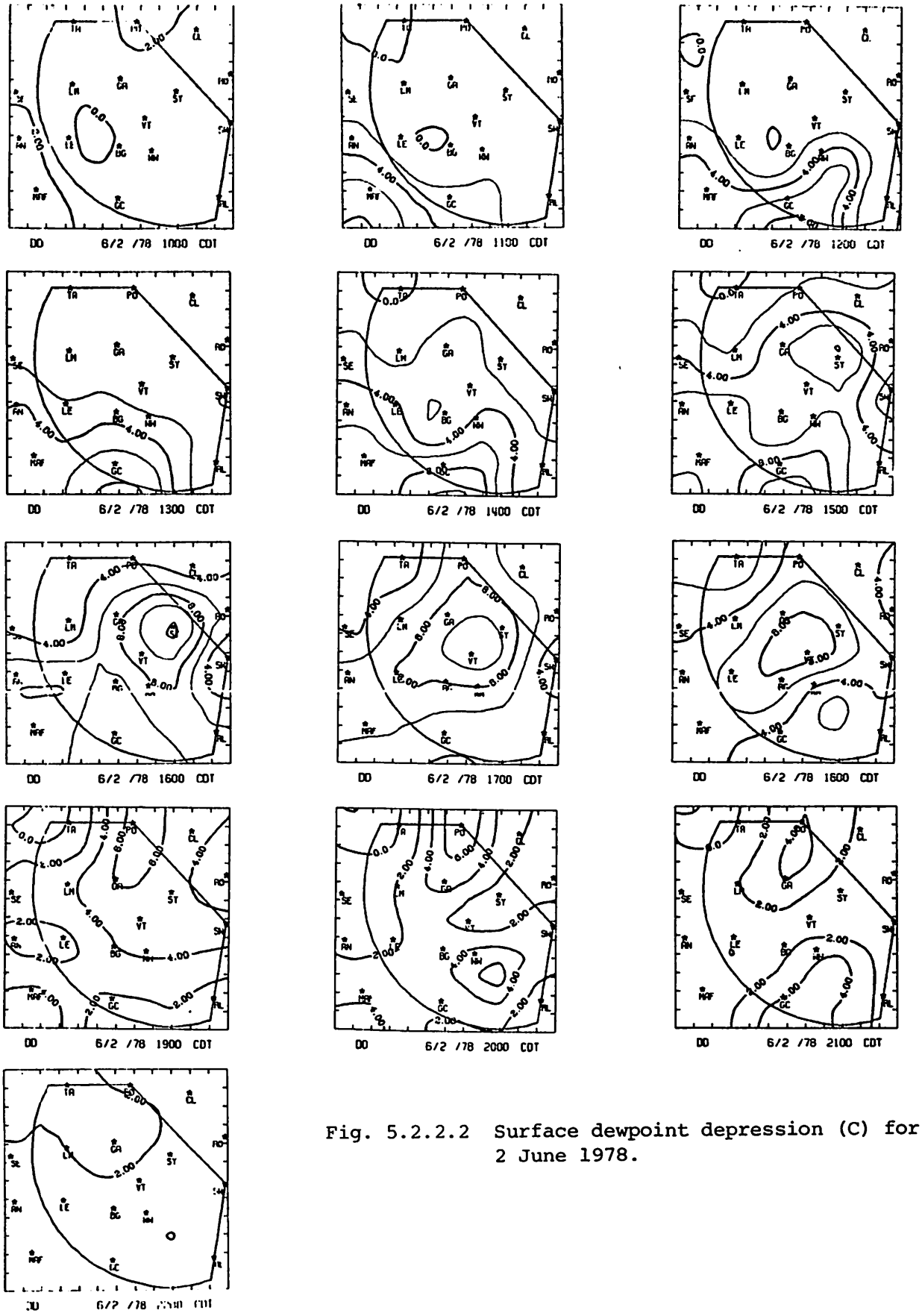

Fig. 5.2.2.2 Surface dewpoint depression (C) for 2 June 1978.

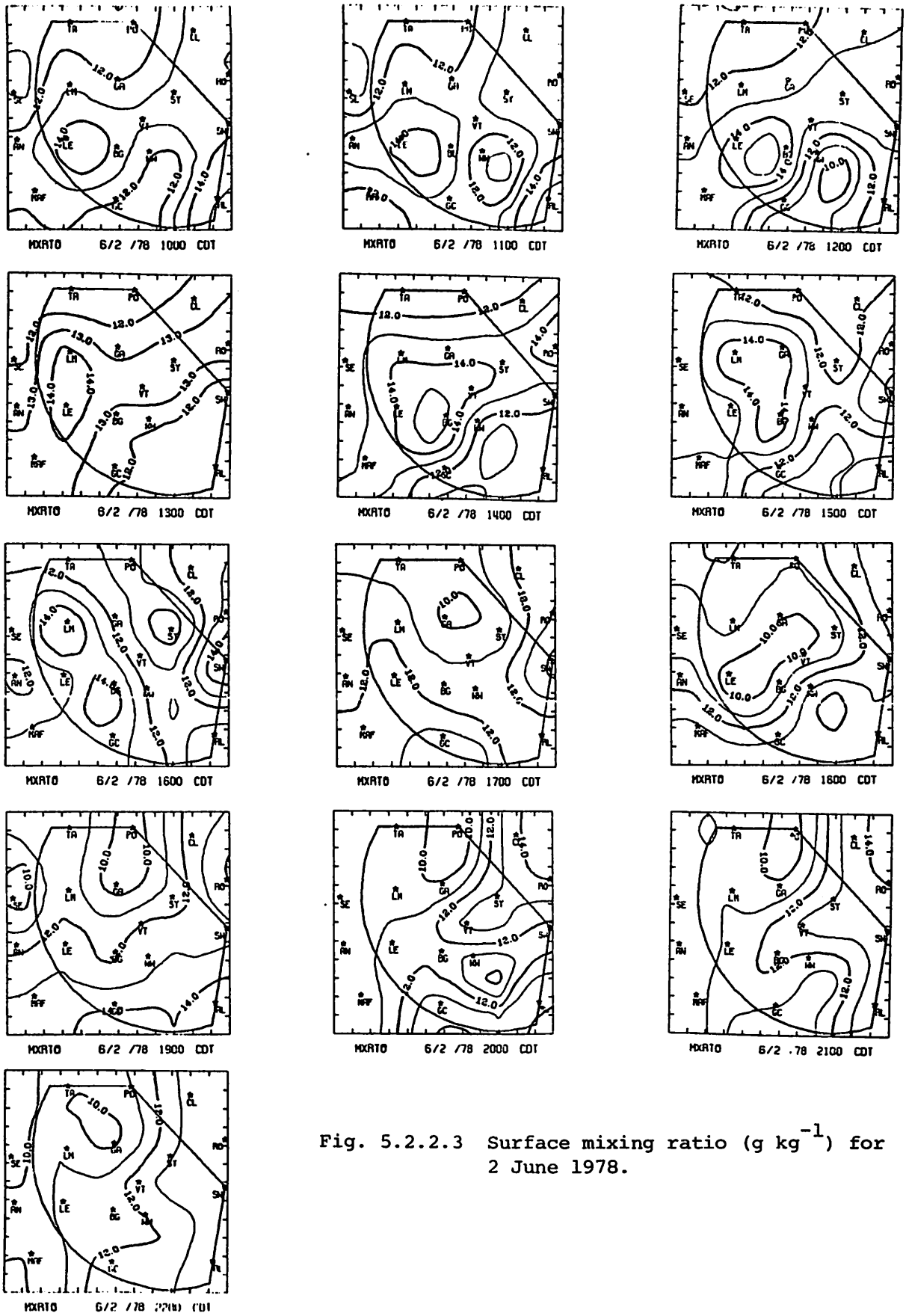

Fig. 5.2.2.3 Surface mixing ratio (g kg^{-1}) for 2 June 1978.

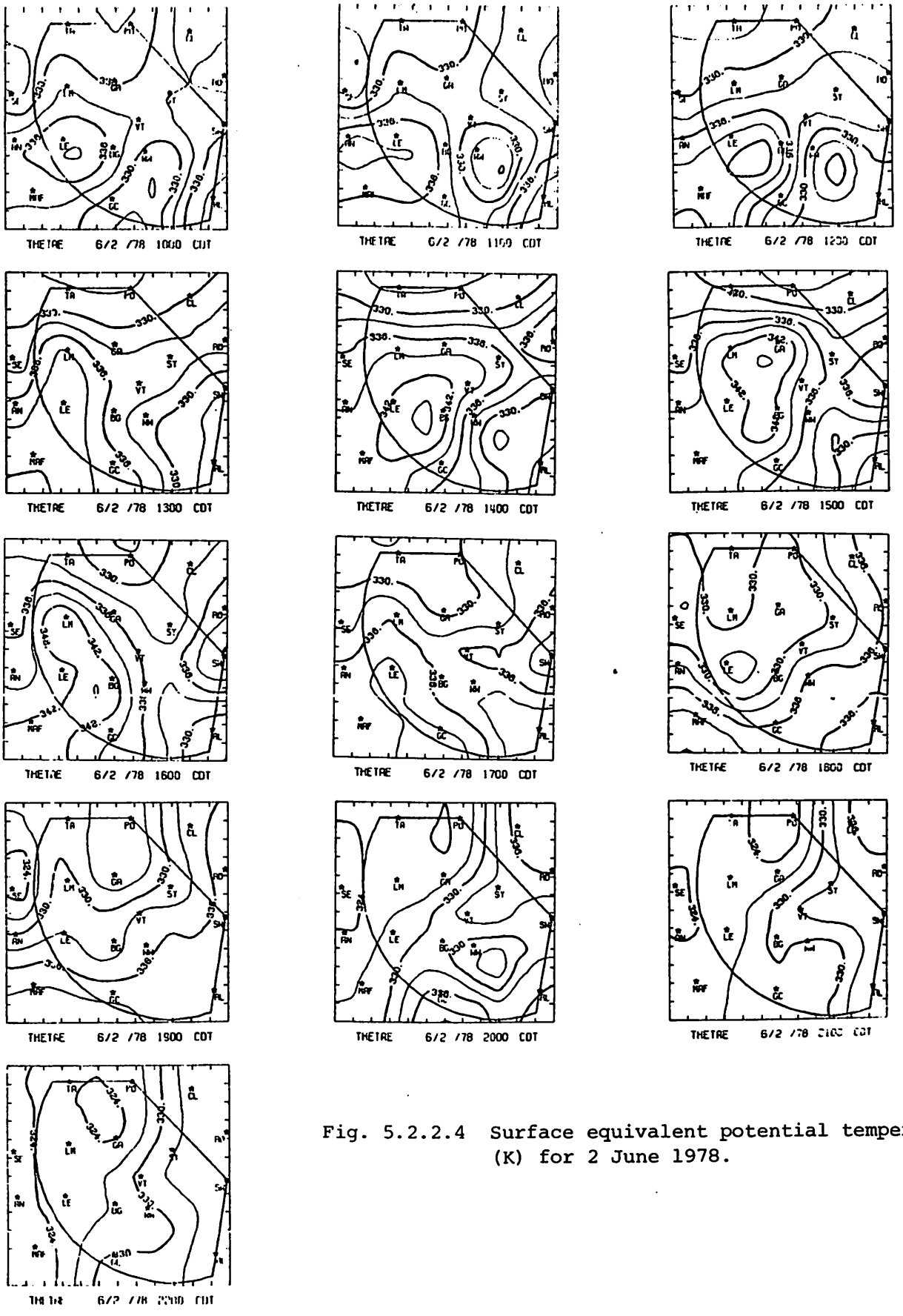

Fig. 5.2.2.4 Surface equivalent potential temperature (K) for 2 June 1978.

moved out of the HIPLEX area, the maximum near Lenorah increased in size, When the strong storm moved out of the area, the minimum near Walsh-Watts disappeared, but generally lower potential temperatures were present in the southeast. As showers moved into the area, potential temperatures decreased, first in the northwest and then across the area.

Terrain-induced vertical motion (Fig. 5.2.2.5) was generally small. A prominent negative motion center was near Walsh-Watts at 1500 GMT under the strong cell but the center was gone at 1600 GMT. Another center of downward motion was present between Gail and Snyder from 1700 to 0000 GMT, and a center of upward motion was present between Walsh-Watts and Robert Lee.

Surface divergence fields (Fig. 5.2.2.6) were strong throughout the day although patterns shifted from hour to hour. A center of divergence was present at 1500 GMT near the cell southeast of Walsh-Watts. This divergence became quite strong at 1700 GMT as the storm cell left the area. At 1800 and 1900 GMT divergence was strong throughout the central part of the area as shower activity decreased. The magnitudes of the convergence and divergence decreased between 2000 and 2100 GMT but increased again when the shower activity began again at 2200 GMT. A strong center of divergence was present north of Midland at 0200 GMT associated with a strong cell. Convergence was present just to the southeast of that storm.

The fields of vertical motion 50 mb above the surface (Fig. 5.2.2.7) showed similar patterns to the divergence. A downdraft area was south of Walsh-Watts in the vicinity of the strong cell at 1500 GMT. Another downdraft area was between Lamesa and Gail at that time. Upward vertical motion was present to the north of the strong cell. A center of upward vertical motion was present near Vincent and Walsh-Watts between 1700 and 1800 GMT but did not seem to be associated with any particular storm. Strong downward motion was present near Gail at 1800 and 1900 GMT as showers moved out of the area. At 2200 GMT when showers resumed, a band of upward motion extended across the center of the area and remained through 2300 GMT. By 0100 GMT vertical motion was small. At 0200 GMT a strong downdraft formed north of Midland with the strong cell there, and an updraft area was located to the southeast of the cell. This persisted until 0300 GMT.

The surface moisture divergence (Fig. 5.2.2.8) and vertical flux of moisture 50 mb above the surface (Fig. 5.2.2.9) had patterns similar to the velocity divergence and vertical motion patterns. Moisture divergence and

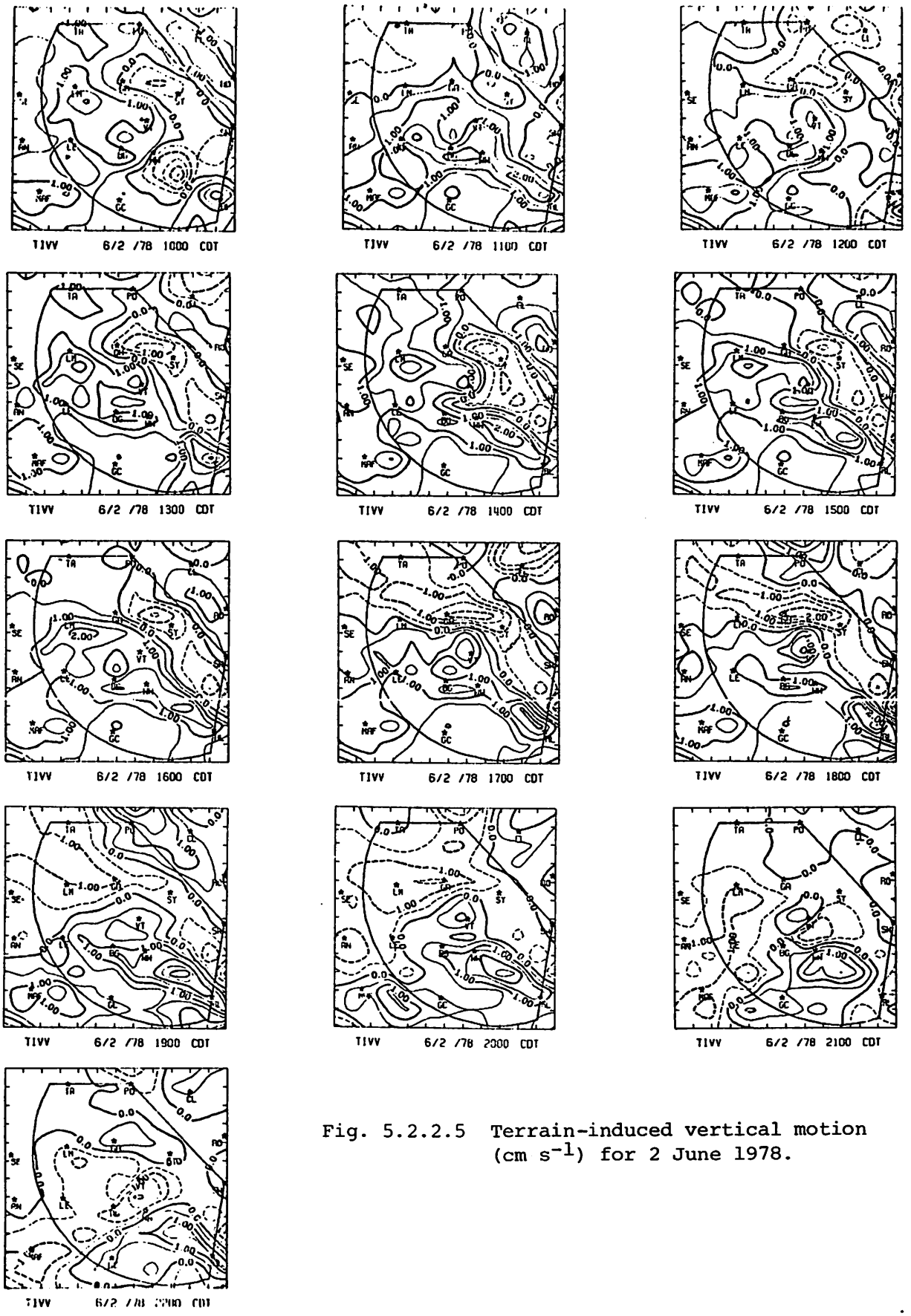

Fig. 5.2.2.5 Terrain-induced vertical motion (cm s^{-1}) for 2 June 1978.

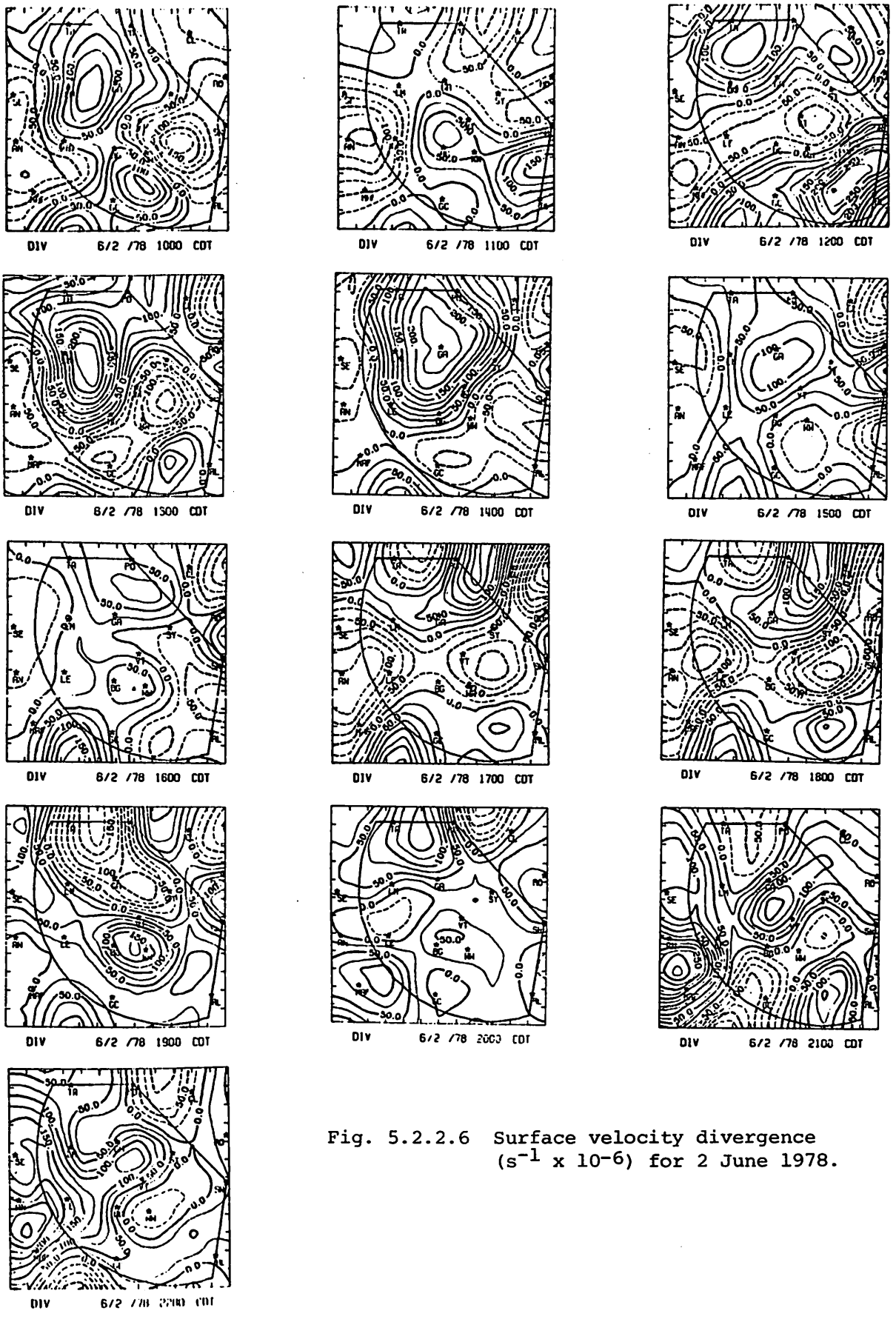

Fig. 5.2.2.6 Surface velocity divergence (s^{-1} x 10^{-6}) for 2 June 1978.

Fig. 5.2.2.7 Vertical motion 50 mb above the surface (μbars s^{-1}) for 2 June 1978.

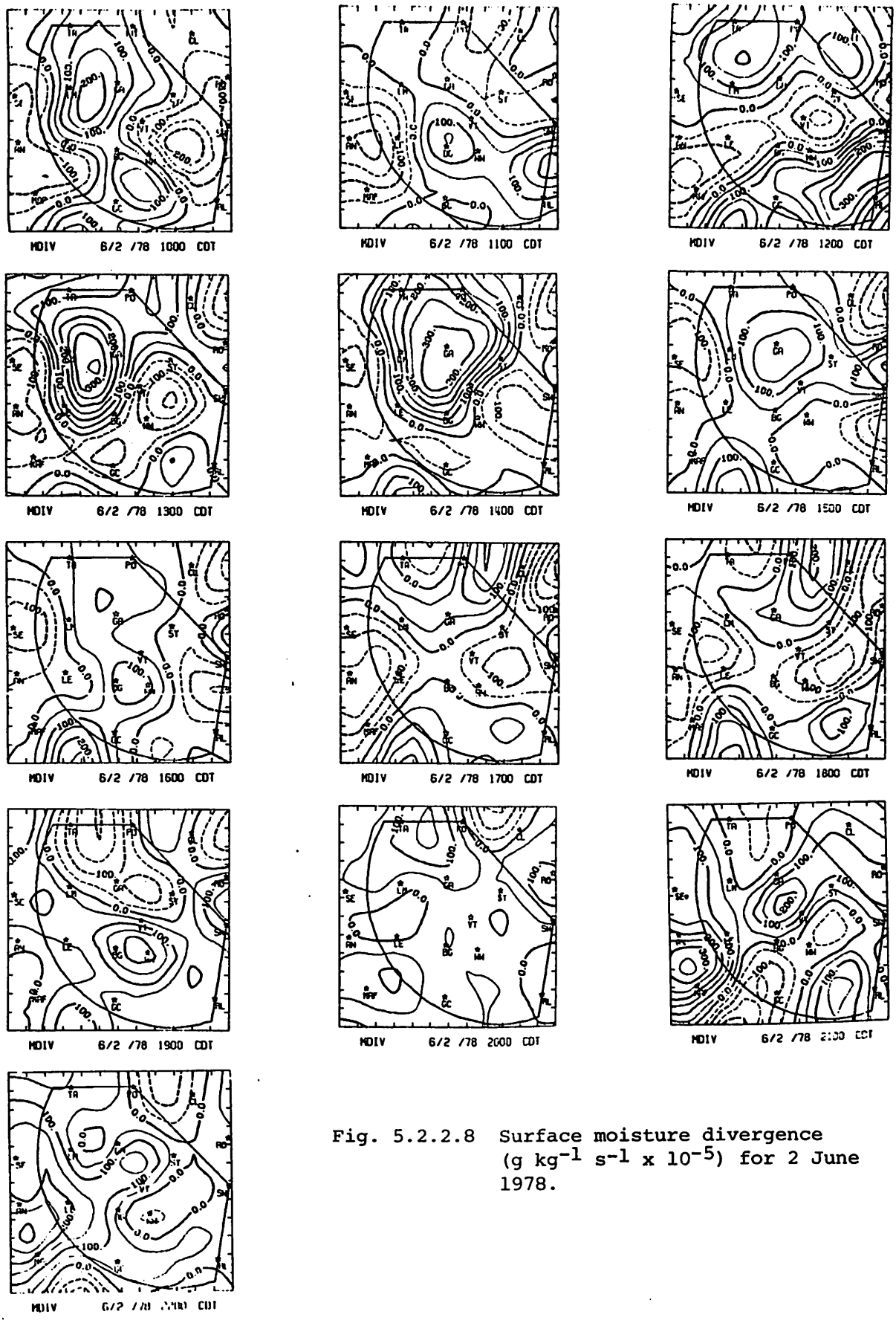

Fig. 5.2.2.8 Surface moisture divergence ($g\ kg^{-1}\ s^{-1} \times 10^{-5}$) for 2 June 1978.

Fig. 5.2.2.9 Vertical flux of moisture 50 mb above the surface (g cm^{-2} s^{-1} x 10^{-6}) for 2 June 1978.

downward flux of moisture was just to the southwest of the strong cell near Walsh-Watts at 1500 GMT, and strong convergence and upward flux was to the northeast of the cell. Strong divergence and downward flux was present near Gail at 1800 and 1900 GMT as showers moved out of the area. Moisture convergence and upward flux of moisture was present in the central part of the area at 2200 and 2300 GMT as showers again moved into the area. By 0100 GMT there was mainly weak divergence and downward flux of moisture. At 0200 GMT, however, strong moisture divergence formed near Midland in association with the storm cell there, and this divergence and downward flux of moisture remained through 0300 GMT.

Figure 5.2.2.10 shows surface vorticity fields. Values were fairly high during most of the day. Strong centers of negative and positive vorticity were just to the east and west, respectively, of the strong storm near Walsh-Watts at 1500 GMT. Negative vorticity was present in the central portion near Vincent throughout the day. Positive vorticity was present in the south near Garden City. A center of negative vorticity remained near Andrews and Midland until 0200 GMT when the strong storm was in that area. At 0300 GMT strong positive vorticity had formed in that area.

Surface pressure change (Fig. 5.2.2.11) was large at some places. Large pressure rises were shown at Seminole and Clairemont at 1700 GMT as showers moved through those areas. A moderate pressure drop occurred at Tahoka during the same time period. Pressure dropped 3.1 mb at Post between 1800 and 1900 GMT, when shower activity was diminishing. A 2.0 mb drop was recorded at Clairemont between 2000 and 2100 GMT. Andrews had some interesting pressure changes between 0000 and 0300 GMT. Between 2300 and 0000 GMT the pressure change was +1.3, and between 0000 and 0100 GMT there was an additional 2.0 mb rise. At 0200 GMT a strong cell had formed to the south of Andrews and there was a 2.7 mb pressure drop there, along with a 2.0 mb rise at Midland at the same time. By 0300 GMT the storm was gone and pressures increased again at Midland.

Figure 5.2.2.12 shows relative surface wind fields. Between 1500 and 2300 GMT winds were mostly easterly in the southern part of the area and northerly to northeasterly in the northern part. At 0000 GMT northwest winds began near Tahoka and Lamesa. At 0200 GMT in most areas the winds have a westerly component and near Tahoka winds were shifting to the southwest. By 0300 GMT winds were southerly and southwesterly in the northern part of the area, and northerly and northwesterly in the southern part.

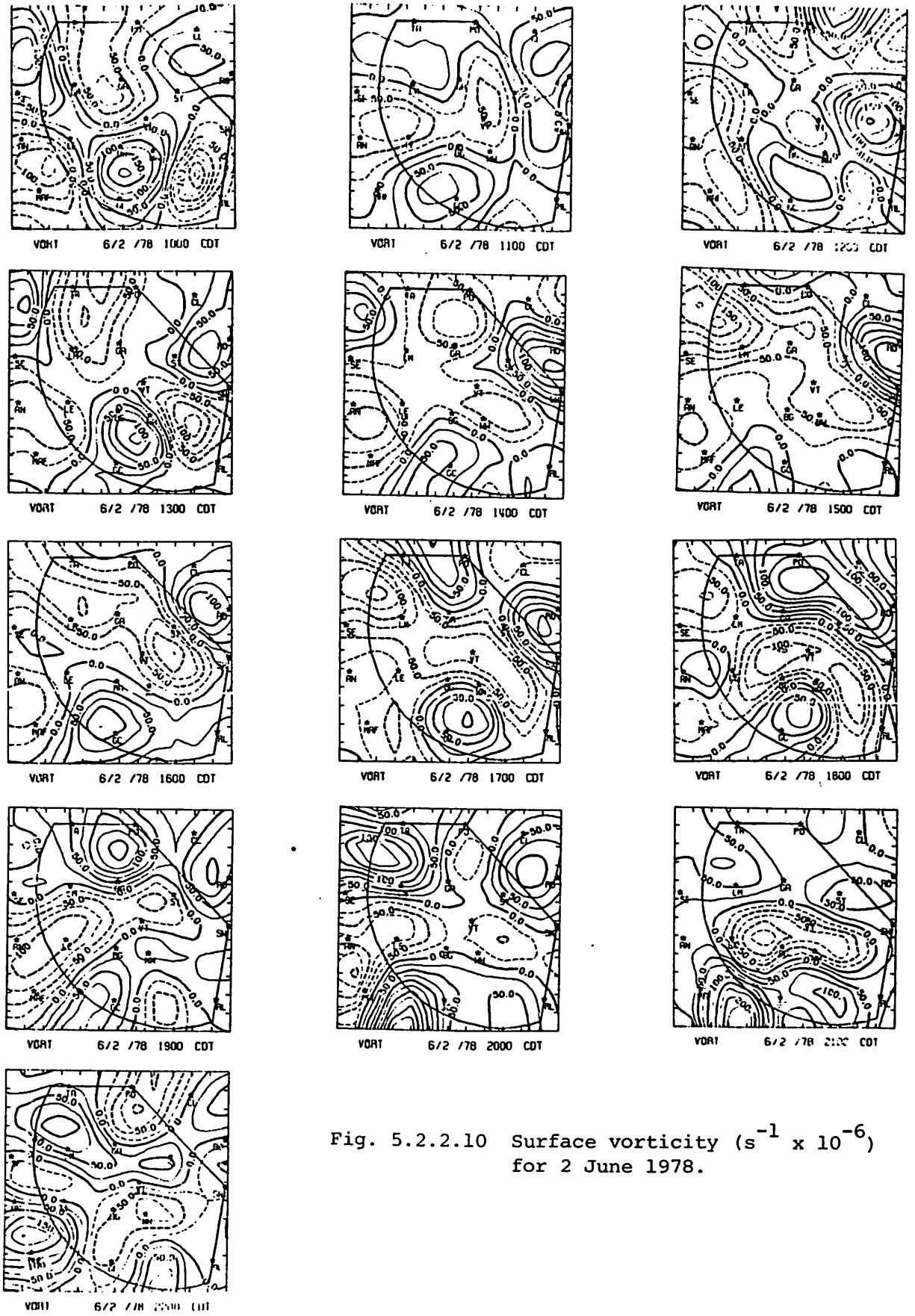

Fig. 5.2.2.10 Surface vorticity ($s^{-1} \times 10^{-6}$) for 2 June 1978.

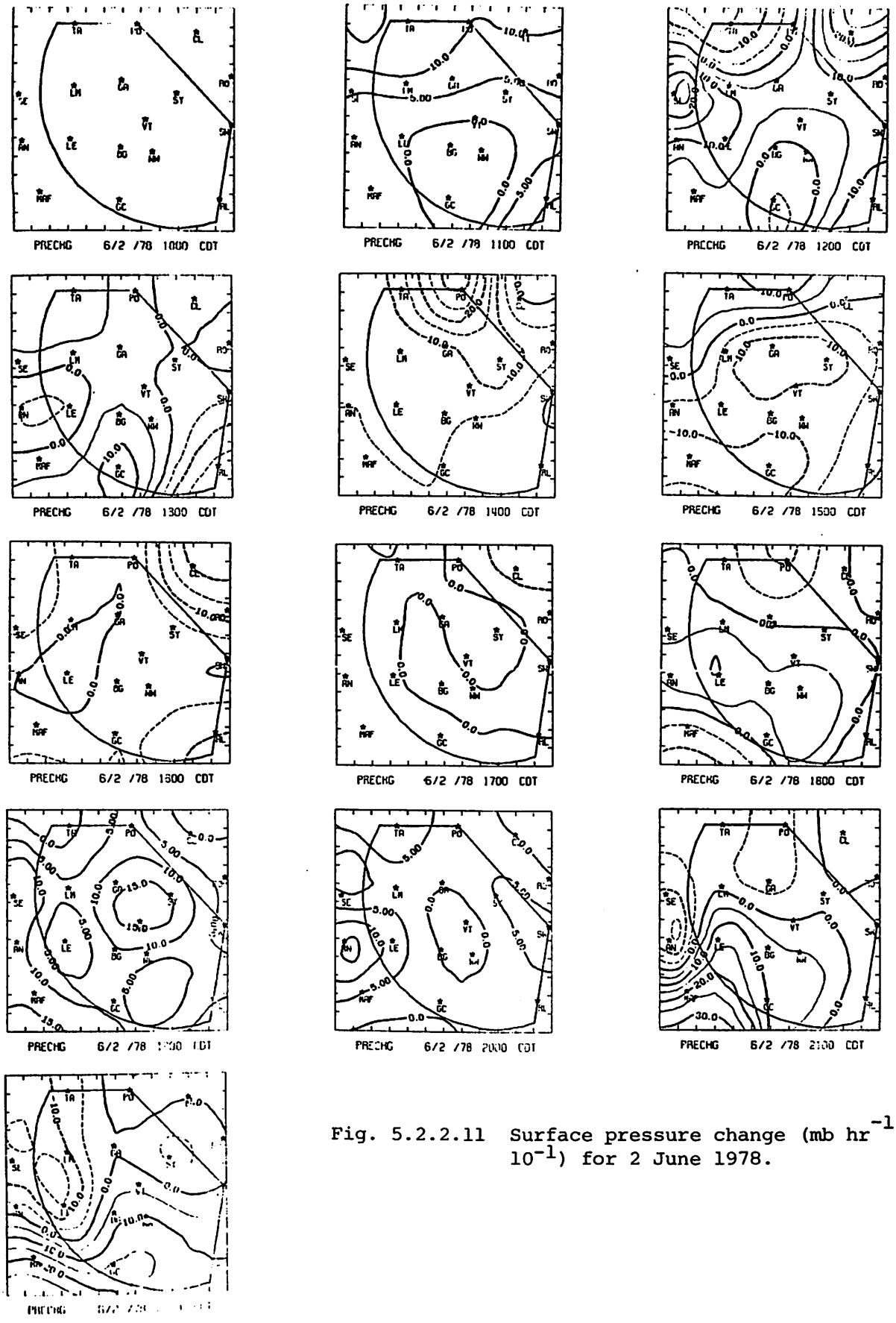

Fig. 5.2.2.11 Surface pressure change (mb hr^{-1} x 10^{-1}) for 2 June 1978.

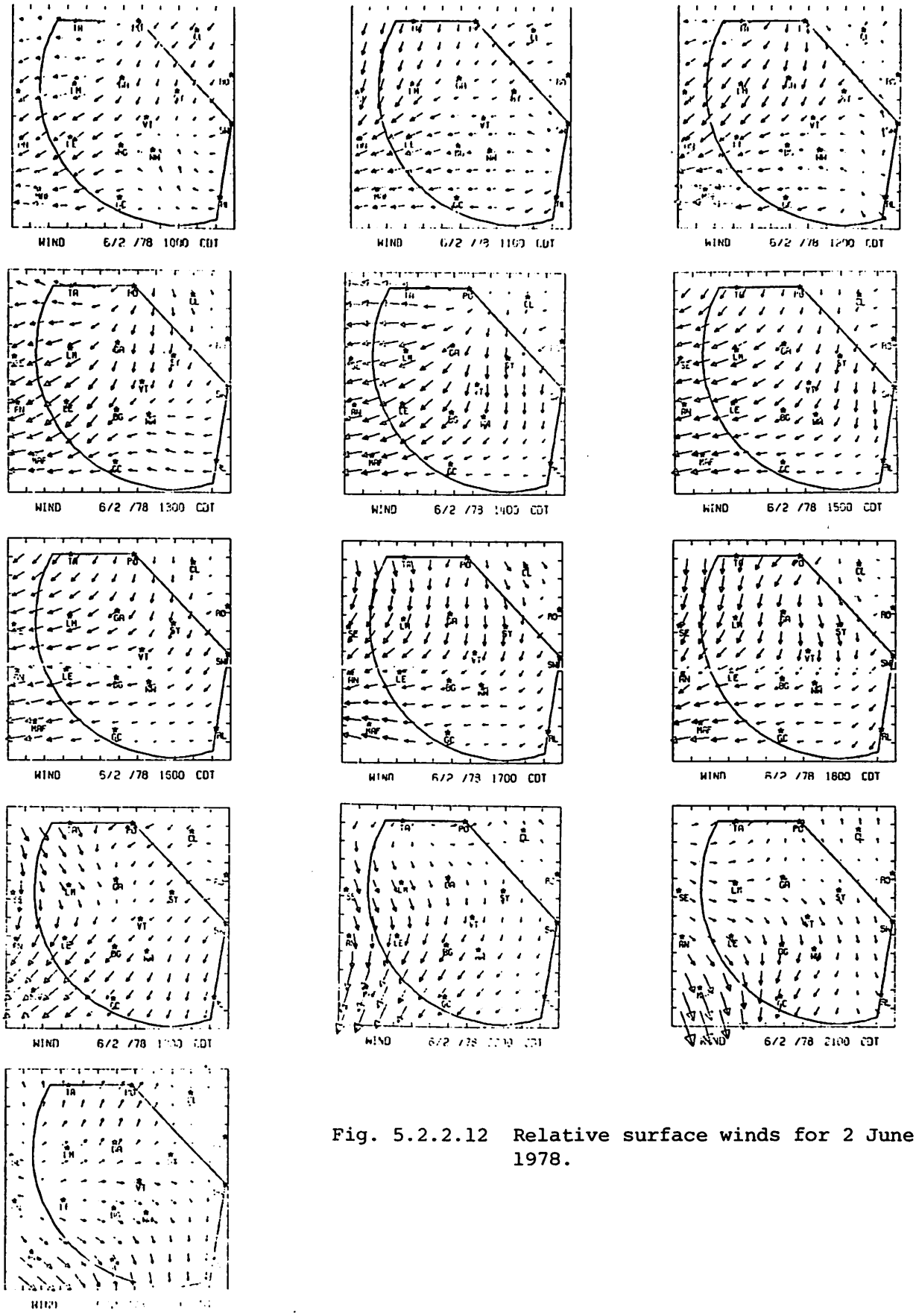

Fig. 5.2.2.12 Relative surface winds for 2 June 1978.

5.3 4 June 1978

5.3.1 Radar

No echoes were recorded on this day until 0300 GMT when a shower approached the HIPLEX area from the northwest (Fig. 5.3.1.1).

5.3.2 Surface

Patterns of surface variables showed no unusual features on this day of little activity. Surface temperature (Fig. 5.3.2.1) was moderate with minimum values in the northwest and southeast. Temperatures increased with daytime heating and decreased after 0000 GMT.

Surface dewpoint depressions (Fig. 5.3.2.2) were low at 1500 GMT and increased with the daytime heating to moderately high values. A maximum was located near Snyder that persisted until 0000 GMT.

Surface mixing ratios (Fig. 5.3.2.3) were moderate. A minimum was present near Snyder that corresponded to the maximum dewpoint depression there. A maximum in mixing ratio occurred near Clairemont after 1800 GMT.

Figure 5.3.2.4 shows fields of surface equivalent potential temperature. A maximum was present near Clairemont after 1700 GMT but the patterns were otherwise variable.

Terrain-induced vertical motion (Fig. 5.3.2.5) was small and no strong centers persisted more than one hour.

Figure 5.3.2.6, surface velocity divergence, shows a variable pattern with maximum convergence between Gail and Snyder at most times. A center of convergence was near Rotan throughout the day, but exhibited only moderate values prior to 0300 GMT. At that time, when showers started to move into the area, convergence exceeded $10^{-4} s^{-1}$ near Rotan.

Similar patterns are shown in Figs. 5.3.2.7 to 5.3.2.9. Vertical motion 50 mb above the surface (Fig. 5.3.2.7) was predominantly downward except near Roscoe. The area and the magnitude of the upward motion increased steadily after 2300 GMT, four hours prior to the appearance of radar echoes in the HIPLEX area.

Figure 5.3.2.8 shows fields of surface moisture divergence. As with the surface velocity divergence there is a center of moisture divergence between Gail and Snyder during much of the day, and moisture convergence near Rotan. The strongest convergence occurred at 0300 GMT.

The vertical flux of moisture (Fig. 5.3.2.9) was generally upward except for downward flux in the vicinity of Gail and Snyder during part of the day.

MISSING DATA

RADAR 6/4 /78 1000 CDT

MISSING DATA

RADAR 6/4 /78 1100 CDT

NO ECHOES

RADAR 6/4 /78 1200 CDT

NO ECHOES

RADAR 6/4 /78 1300 CDT

NO ECHOES

RADAR 6/4 /78 1400 CDT

NO ECHOES

RADAR 6/4 /78 1500 CDT

NO ECHOES

RADAR 6/4 /78 1600 CDT

NO ECHOES

RADAR 6/4 /78 1700 CDT

NO ECHOES

RADAR 6/4 /78 1800 CDT

NO ECHOES

RADAR 6/4 /78 1900 CDT

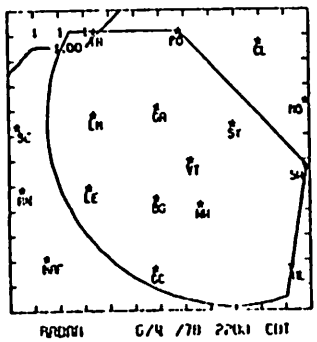

NO ECHOES

RADAR 6/4 /78 2000 CDT

NO ECHOES

RADAR 6/4 /78 2100 CDT

Fig. 5.3.1.1 Radar echoes for 4 June 1978.

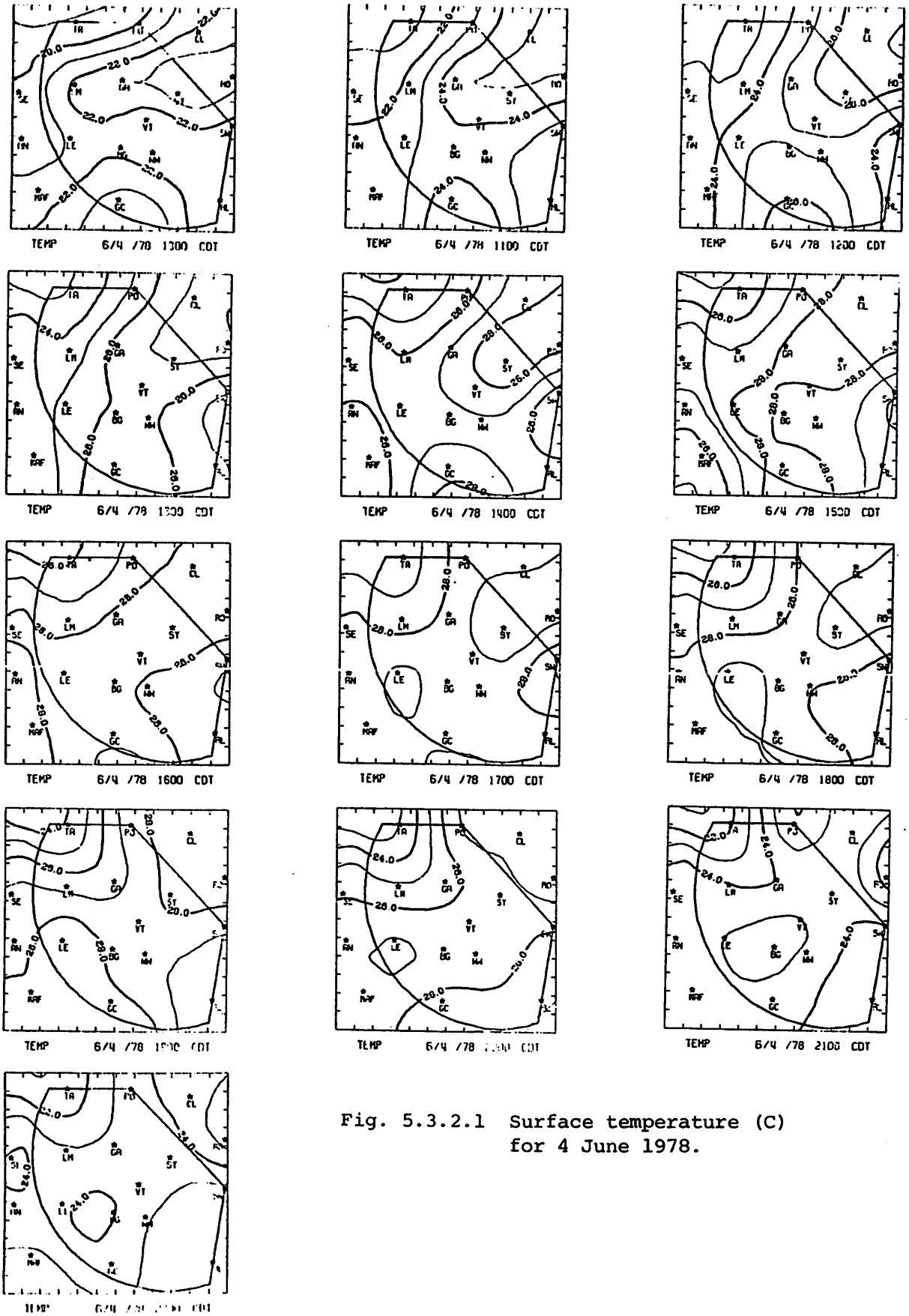

Fig. 5.3.2.1 Surface temperature (C) for 4 June 1978.

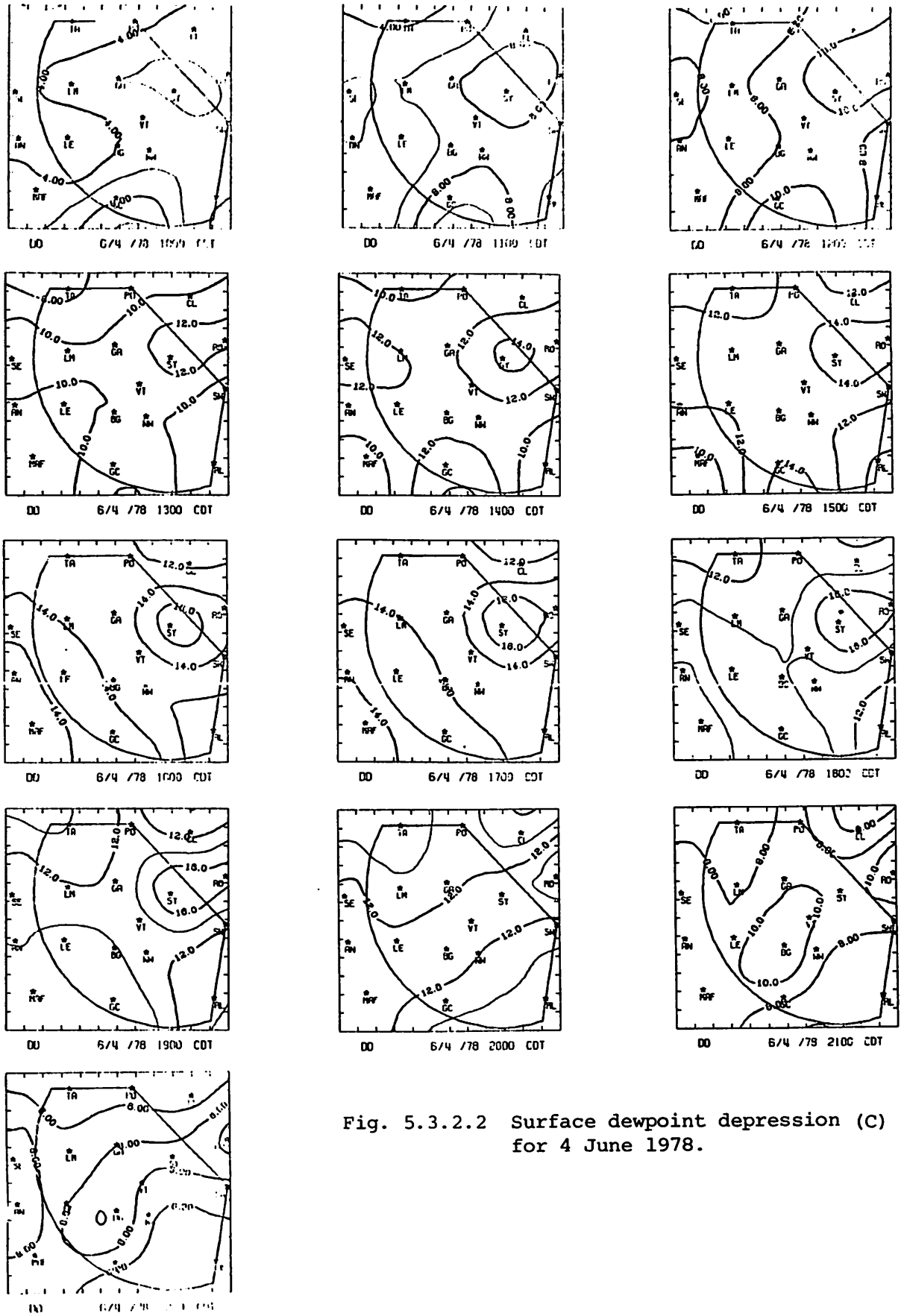

Fig. 5.3.2.2 Surface dewpoint depression (C) for 4 June 1978.

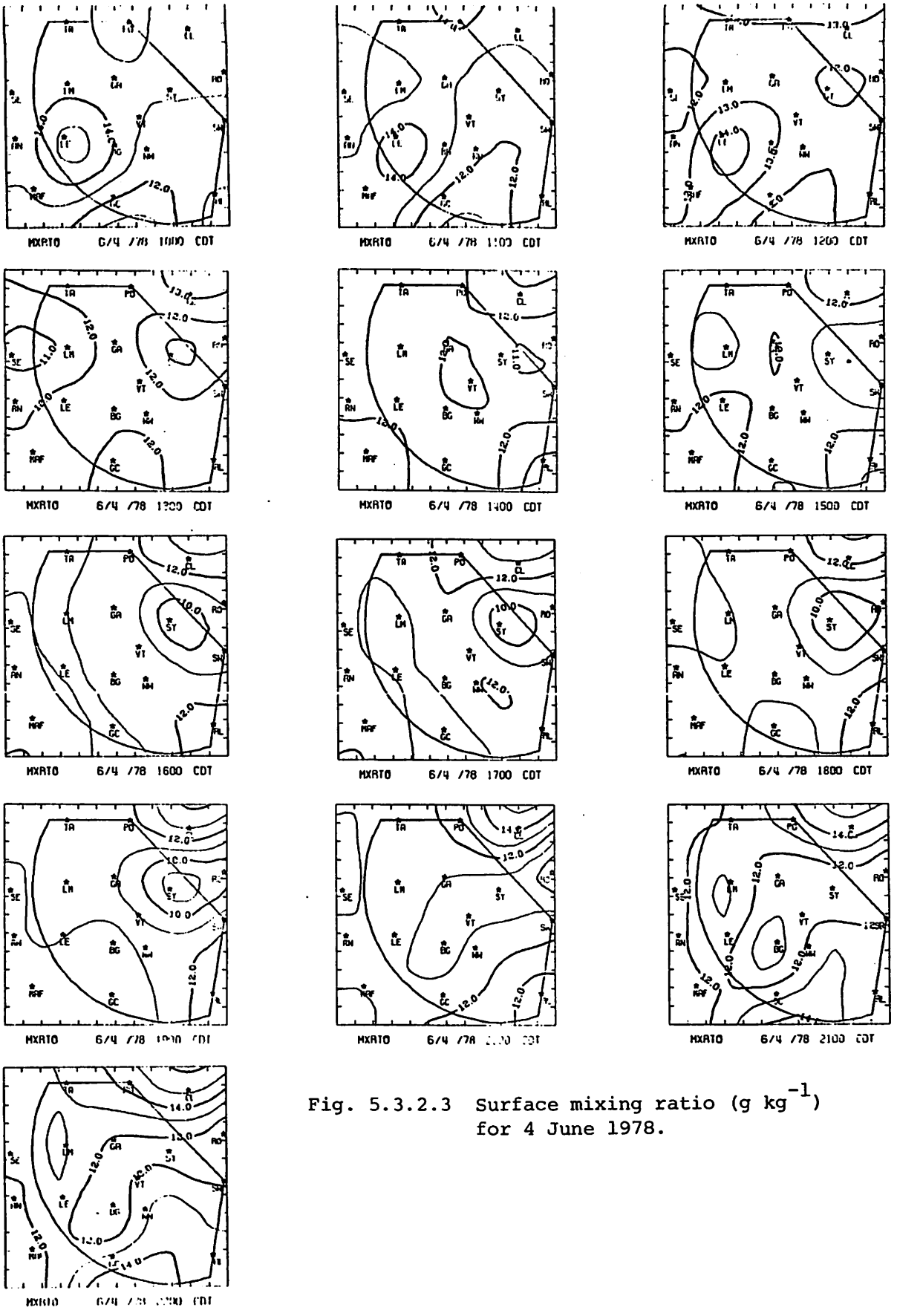

Fig. 5.3.2.3 Surface mixing ratio (g kg^{-1}) for 4 June 1978.

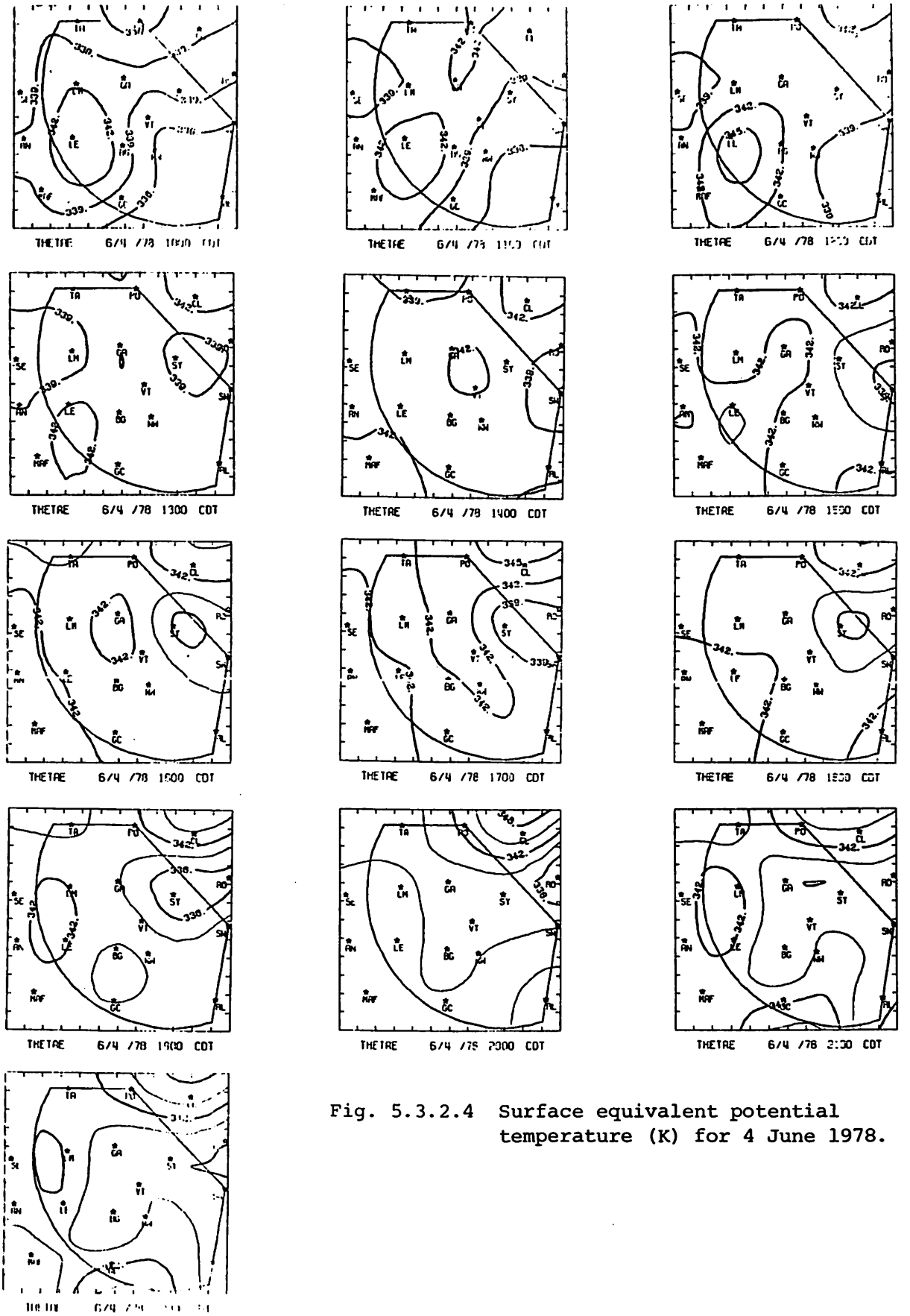

Fig. 5.3.2.4 Surface equivalent potential temperature (K) for 4 June 1978.

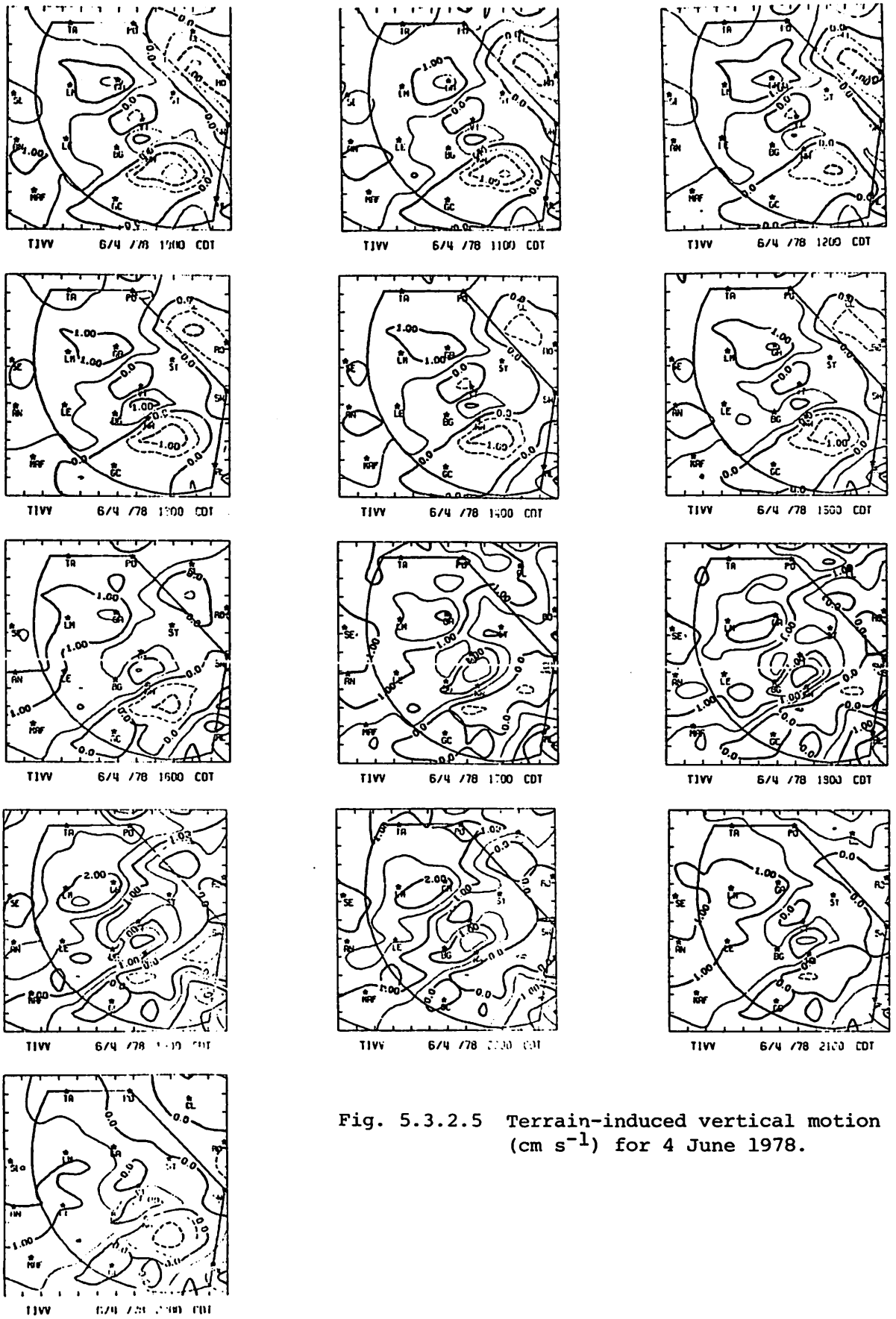

Fig. 5.3.2.5 Terrain-induced vertical motion (cm s^{-1}) for 4 June 1978.

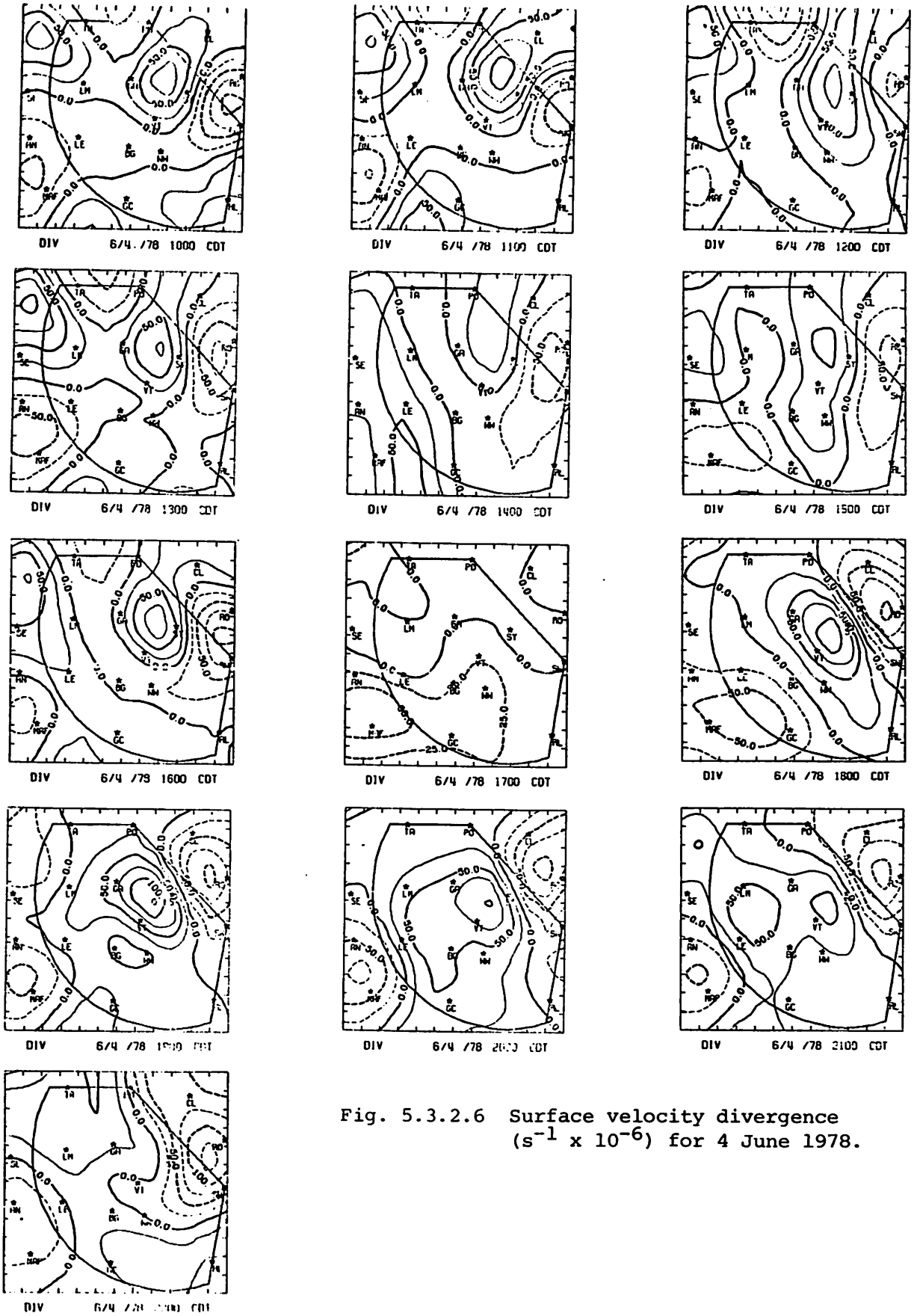

Fig. 5.3.2.6 Surface velocity divergence (s^{-1} x 10^{-6}) for 4 June 1978.

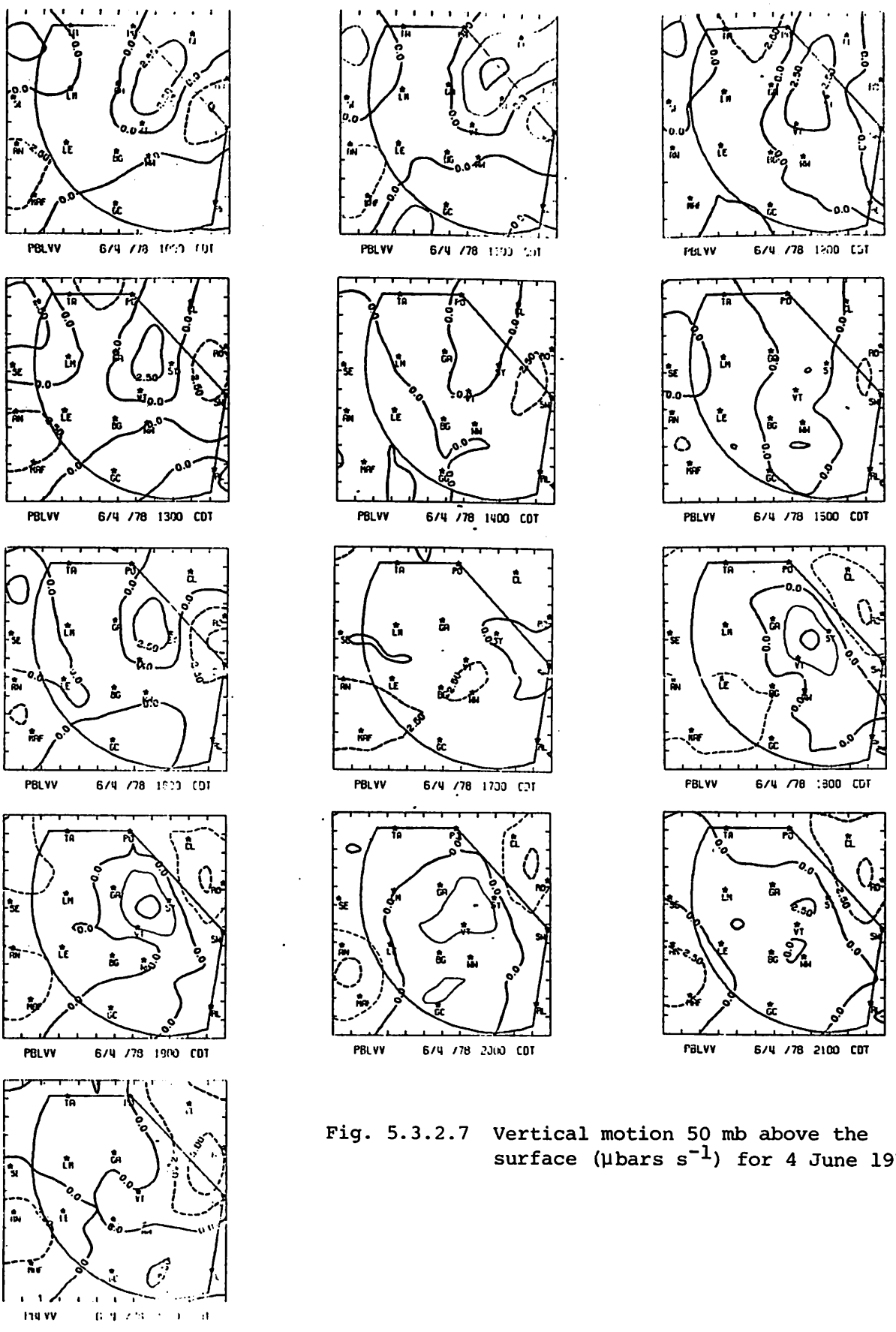

Fig. 5.3.2.7 Vertical motion 50 mb above the surface (μbars s^{-1}) for 4 June 1978.

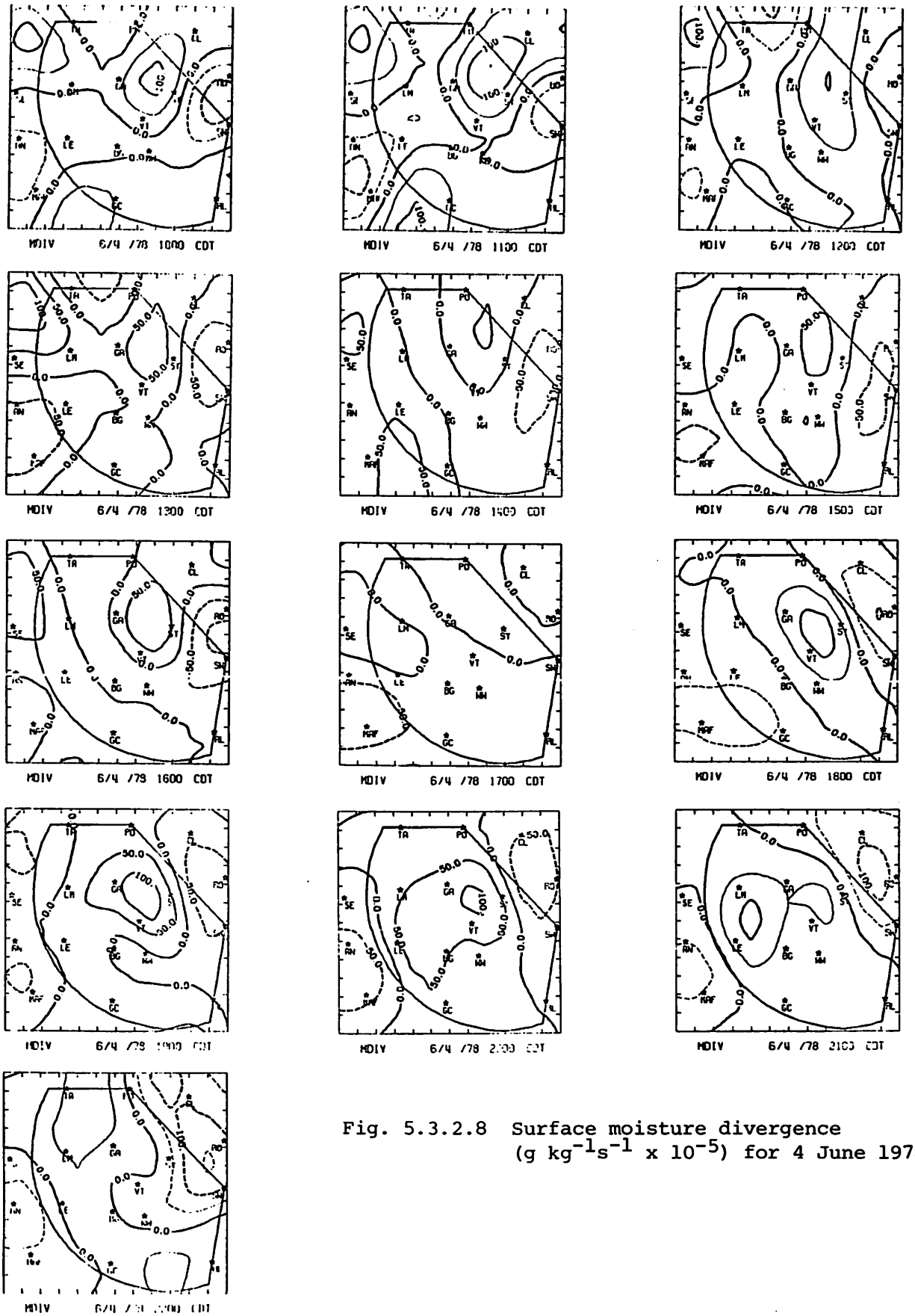

Fig. 5.3.2.8 Surface moisture divergence ($g\ kg^{-1}s^{-1} \times 10^{-5}$) for 4 June 1978.

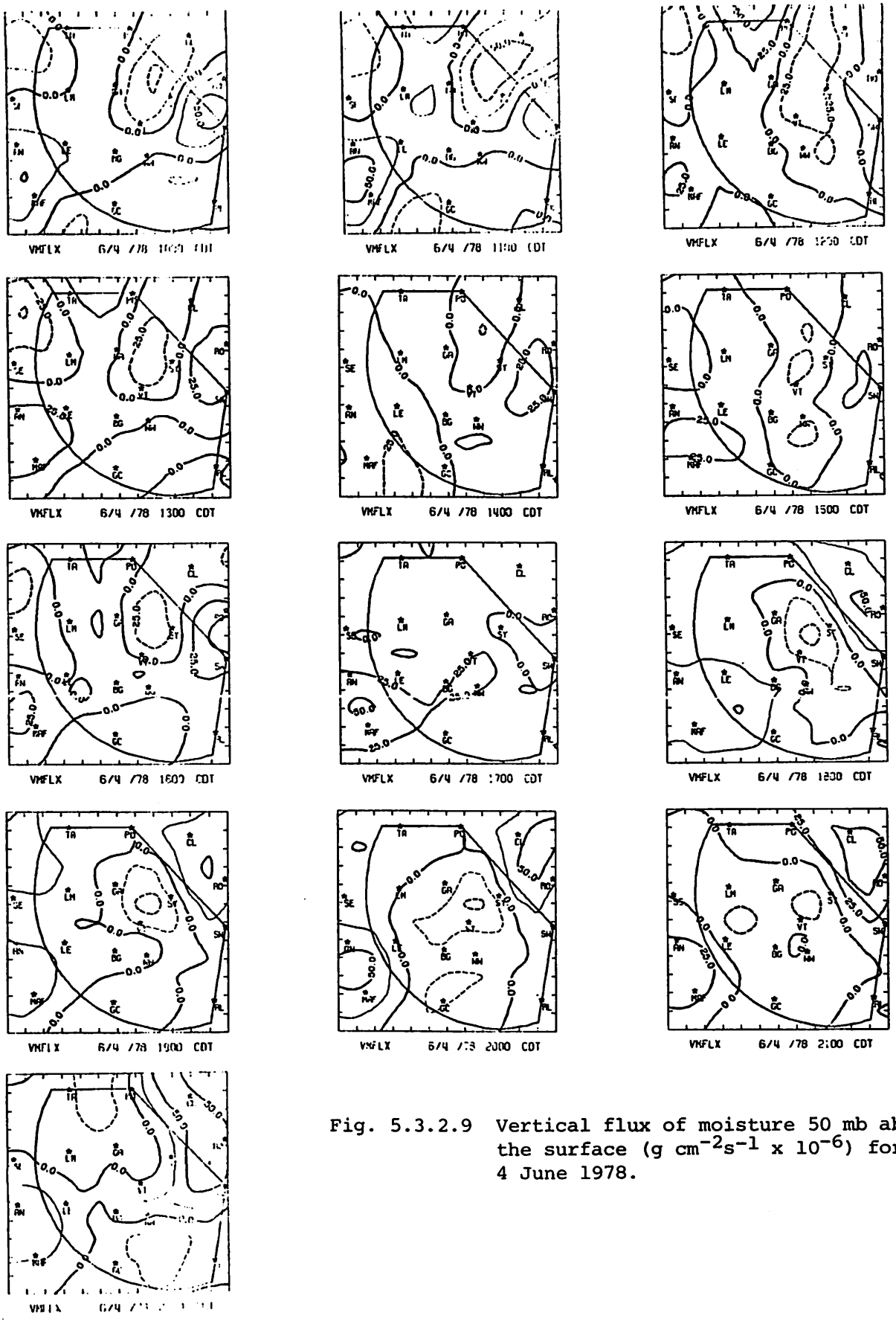

Fig. 5.3.2.9 Vertical flux of moisture 50 mb above the surface (g $cm^{-2}s^{-1}$ x 10^{-6}) for 4 June 1978.

The area where upward vertical flux exceeded 5 x 10^{-5} g $cm^{-2}s^{-1}$ was fairly small until after 0100 GMT.

Surface vorticity (Fig. 5.3.2.10) showed several centers of positive and negative values. Negative vorticity centers were south of Tahoka and southeast of Snyder during most of the day, while positive centers remained near Clairemont and Walsh-Watts.

Surface pressure changes (Fig. 5.3.2.11) were generally small. Pressure was decreasing or remaining stable over the area until 0200 GMT when rises occurred in the northwest just before showers moved into that area.

Surface winds (Fig. 5.3.2.12) were mostly southerly during the first part of the day but shifted to generally southeast by 2100 GMT. The winds remained southerly near Rotan, however.

5.3.3 Upper Level Kinematic Parameters

The profiles of mass divergence (Fig. 5.3.3.1) were variable throughout the day. Profiles for 1500 and 0300 GMT are similar with a layered structure of alternating convergence and divergence. The peaks in the 0300 GMT profile are stronger and located at lower levels than in the 1500 GMT profile. At 0300 GMT when showers moved into the area the low level convergence was much stronger than at any other time. The profile at 1800 GMT shows slight divergence at most levels. At 2100 and 0000 GMT divergence was present in lower levels with strong convergence above.

Figure 5.3.3.2 shows profiles of vertical motion. At 1500 GMT upward motion prevailed although small in magnitude. By 1800 GMT vertical motion was downward and largest in upper levels. At 2100 and 0000 GMT profiles are similar with downward motion in lower levels and strong upward motion above 500 mb. At 0300 GMT, the beginning of shower activity, the situation reversed with lower levels having upward motion and upper levels having downward motion.

The profiles of moisture divergence (Fig. 5.3.3.3) indicate that moisture divergence prevailed at most levels throughout the day. The only strong moisture convergence was below 800 mb at 0300 GMT.

5.3.4 Energetics

Profiles of horizontal flux of latent heat (Fig. 5.3.4.1) show moderate outflow of latent heat at most levels throughout the day. Only at 1500 and 0300 GMT was there any appreciable inflow of latent heat.

Figure 5.3.4.2 shows profiles of the vertical flux of latent heat. The vertical flux is small for layers above 600 mb. At 1500 and 1800 GMT the

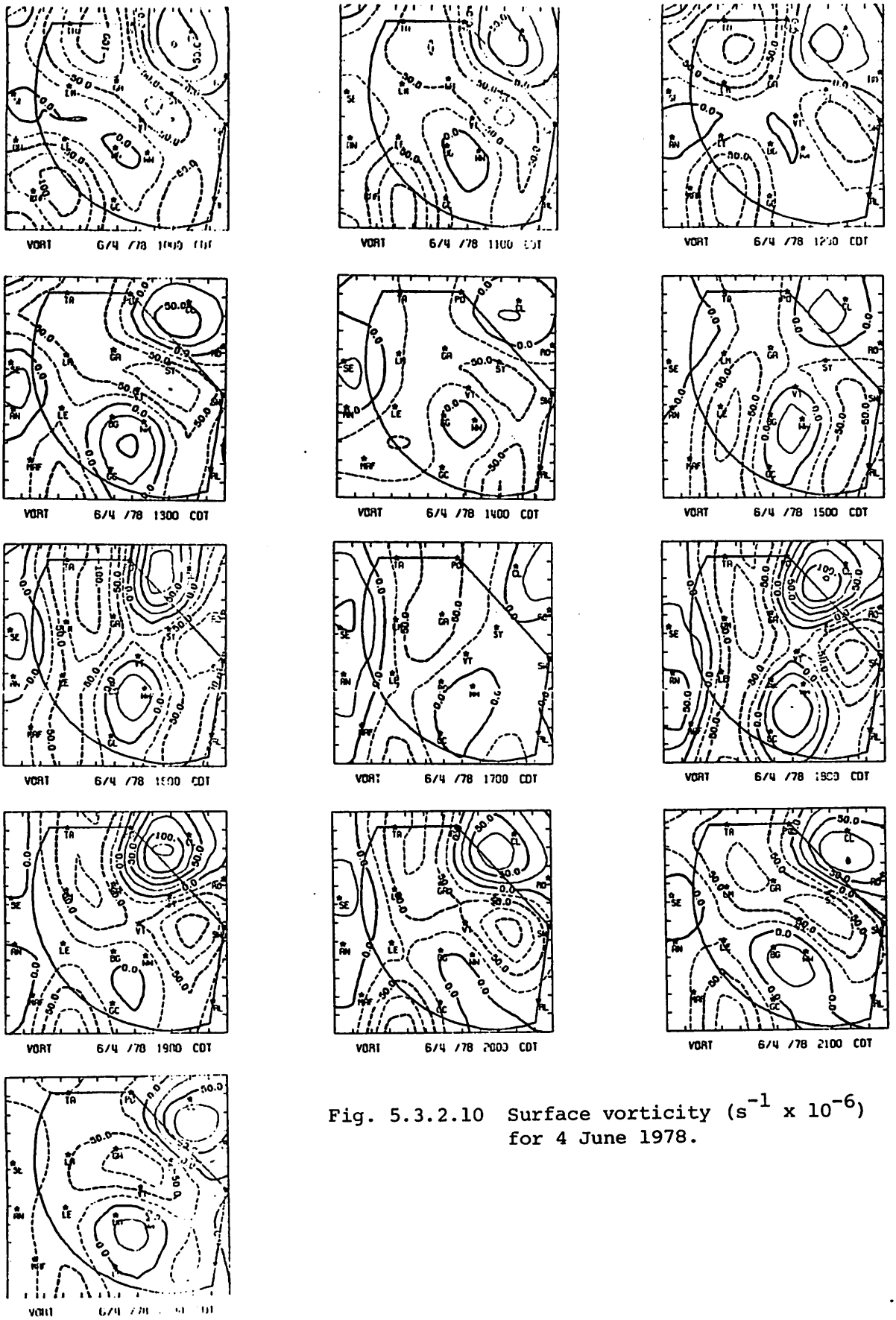

Fig. 5.3.2.10 Surface vorticity (s^{-1} x 10^{-6}) for 4 June 1978.

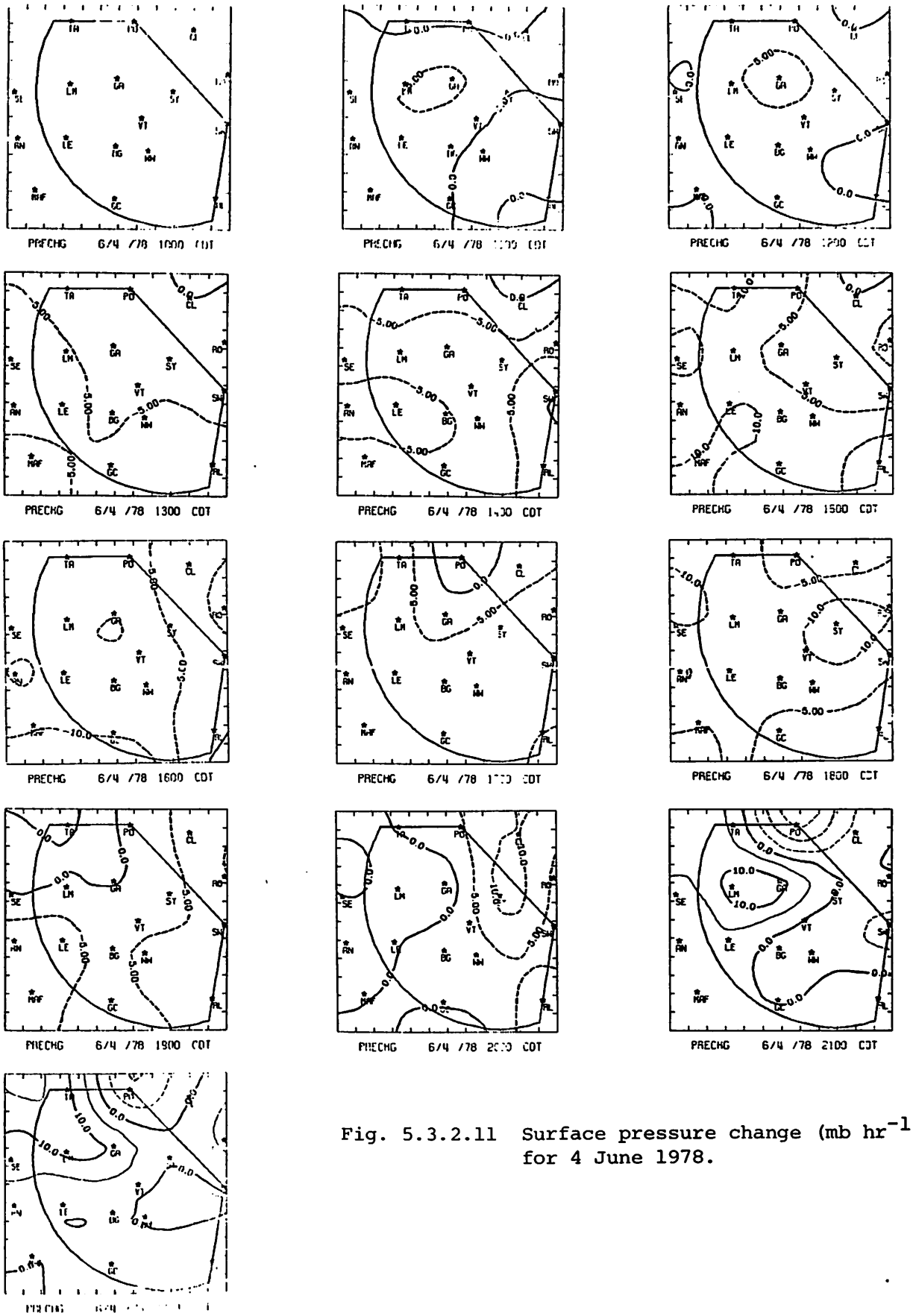

Fig. 5.3.2.11 Surface pressure change (mb hr^{-1} x 10^{-1}) for 4 June 1978.

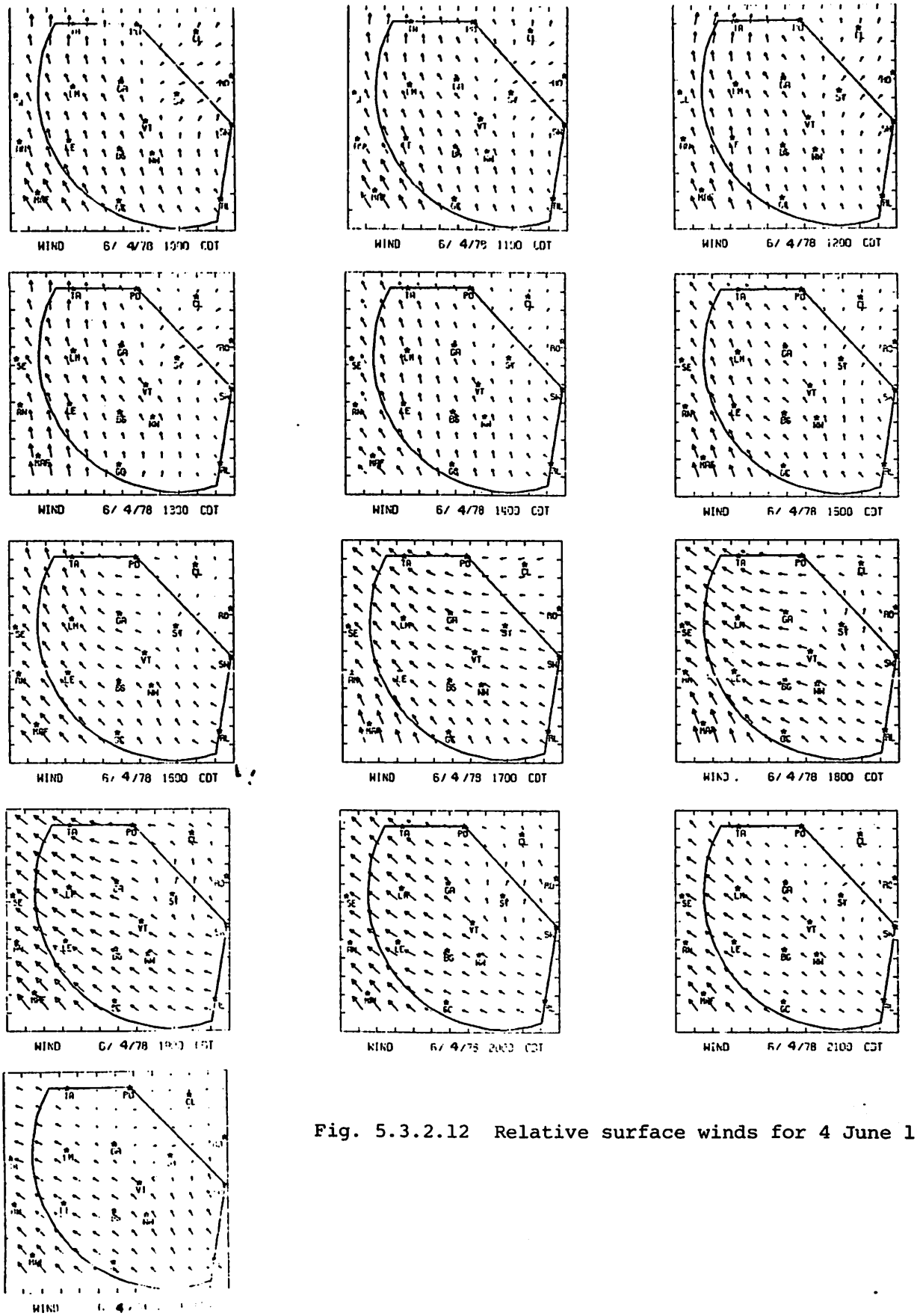

Fig. 5.3.2.12 Relative surface winds for 4 June 1978.

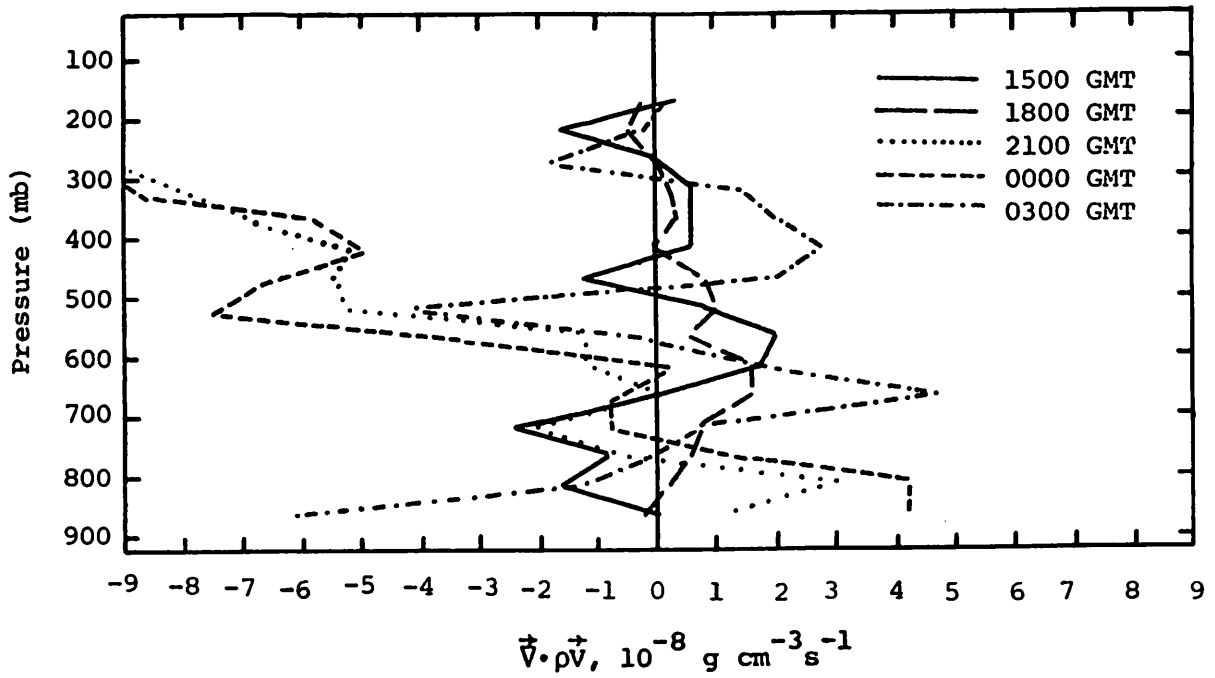

Fig. 5.3.3.1 Vertical profiles of mass divergence on 4 June 1978.

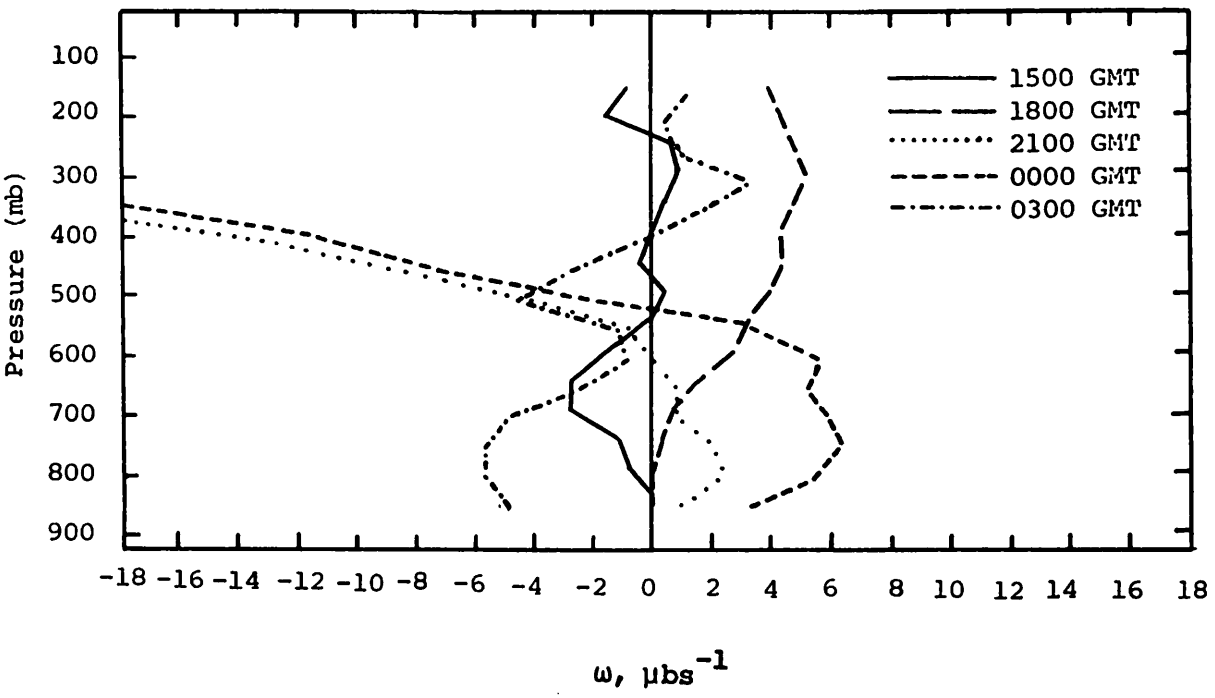

Fig. 5.3.3.2 Vertical profiles of vertical motion on 4 June 1978.

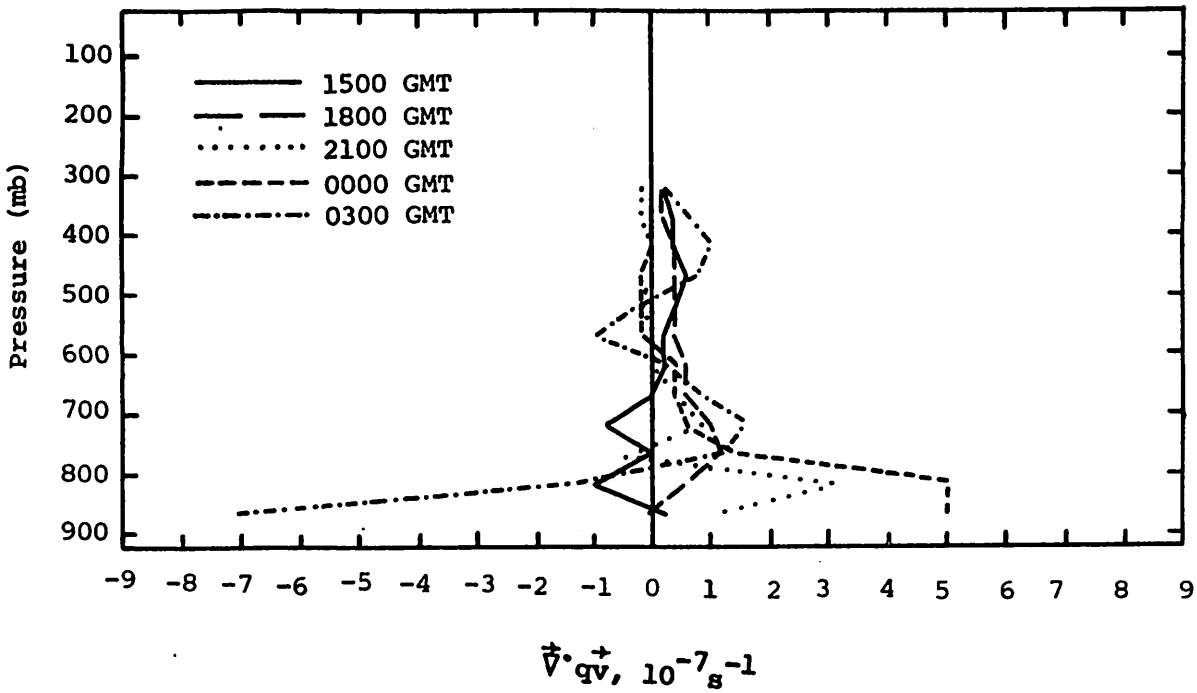

Fig. 5.3.3.3 Vertical profiles of moisture divergence on 4 June 1978.

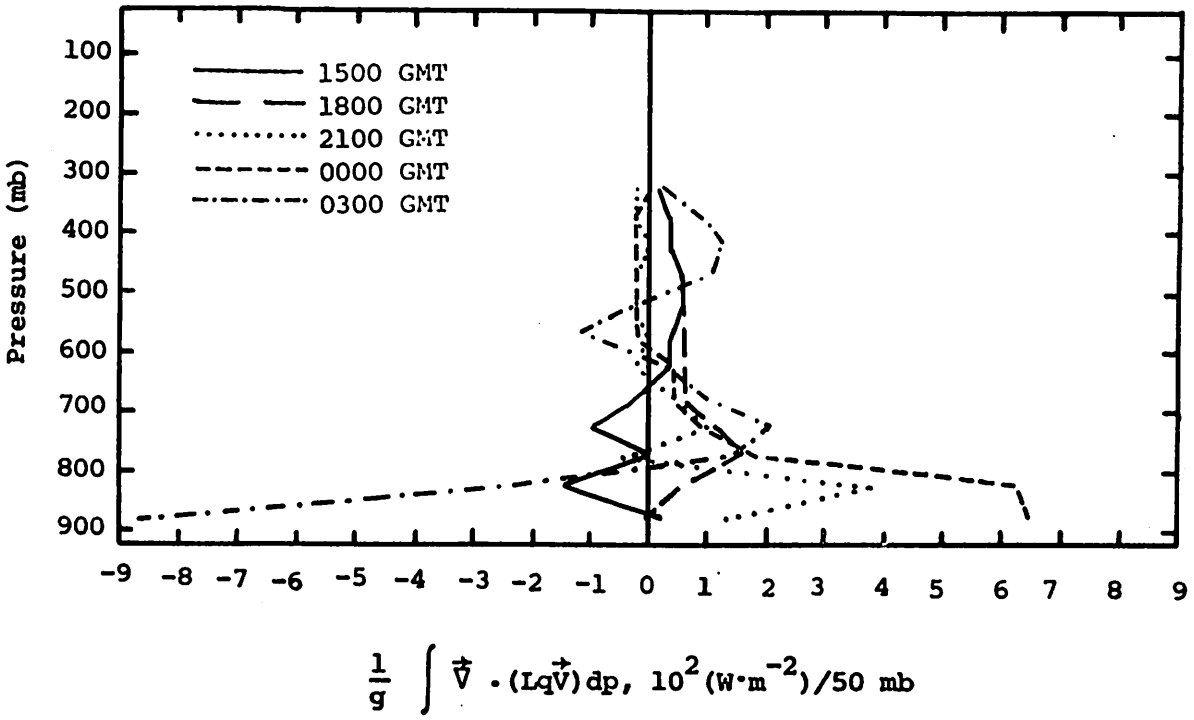

Fig. 5.3.4.1 Vertical profiles of the horizontal flux of latent heat energy on 4 June 1978.

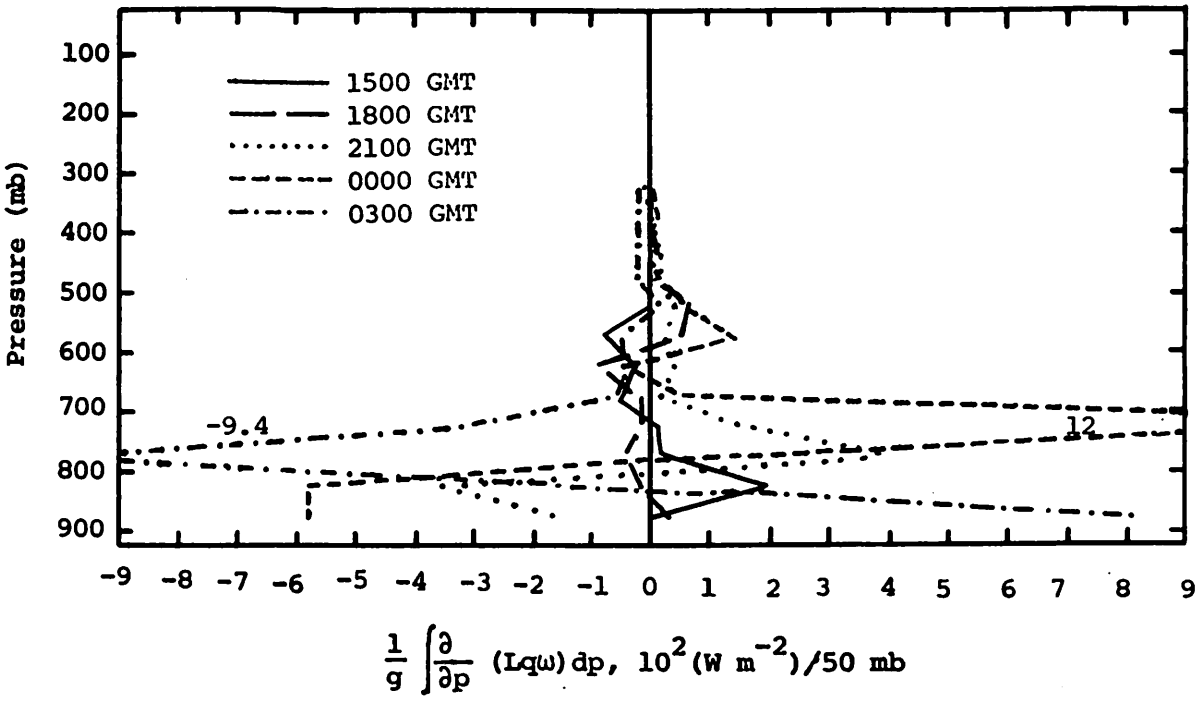

Fig. 5.3.4.2 Vertical profiles of the vertical flux of latent heat energy on 4 June 1978.

vertical flux was small at lower levels also. Transport downward from middle levels began at 2100 GMT and was strong at 0000 GMT. At 0300 GMT the situation reversed and transport was upward from the surface to 800 mb.

The profiles of local change of latent heat (Fig. 5.3.4.3) show slight decreases at most times. Latent heat increases were indicated in lower levels at 2100 GMT, prior to the beginning of activity. At 0300 GMT when showers were present there were gains in middle levels near 500 mb and moderate losses in lower levels.

The residual of the latent heat equation is shown in Fig. 5.3.4.4. At 1500 GMT values were positive which could indicate condensation taking place or some turbulent transfer that could not be resolved. The profiles for 1800 through 0000 GMT indicate negative values which suggest evaporation. The largest value occurred at 0000 GMT below 700 mb. At 0300 GMT large positive values are shown which indicate that condensation may be taking place. This fits well with radar indications of shower activity.

The profiles of diabatic heating (Fig. 5.3.4.5) indicate cooling at most levels at 1500 and 1800 GMT. At 2100 and 0000 GMT diabatic heating

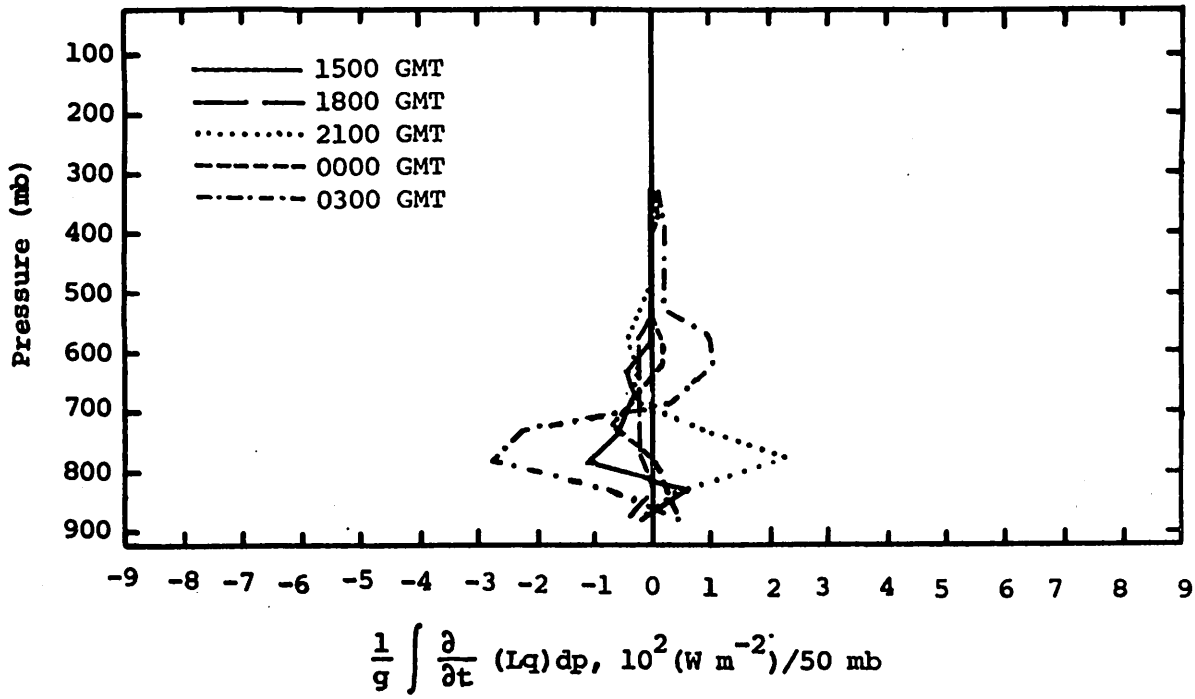

Fig. 5.3.4.3 Vertical profiles of the local change of latent heat energy on 4 June 1978.

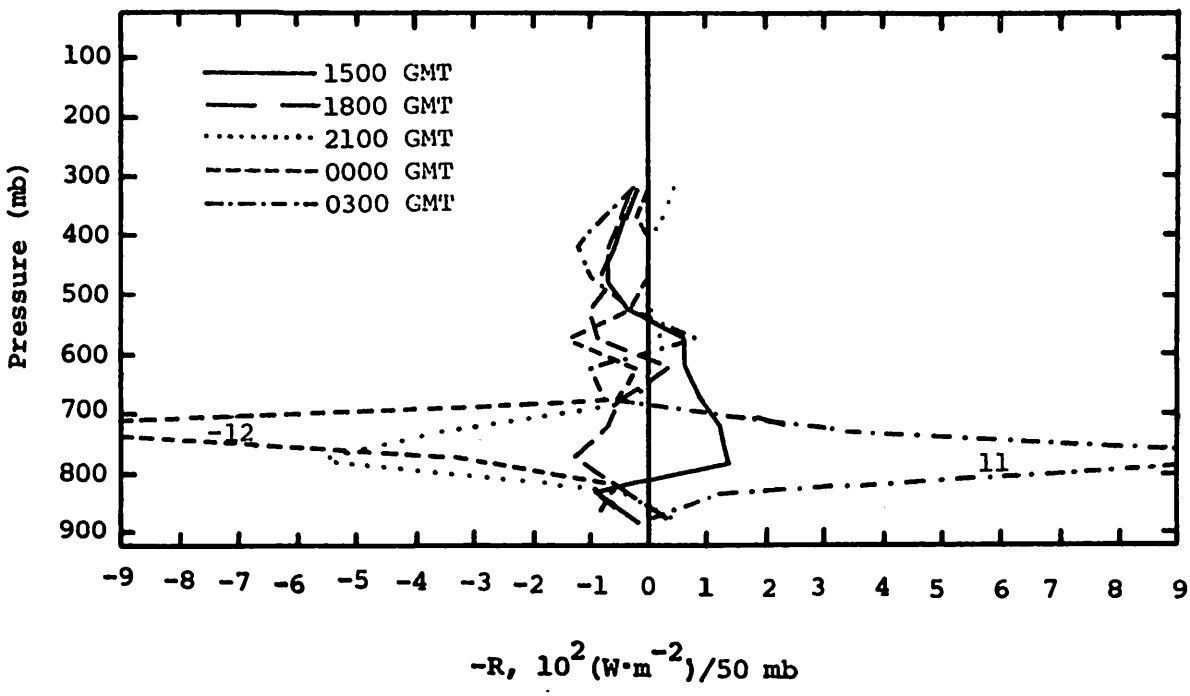

Fig. 5.3.4.4 Vertical profiles of the residual of the latent heat energy equation on 4 June 1978.

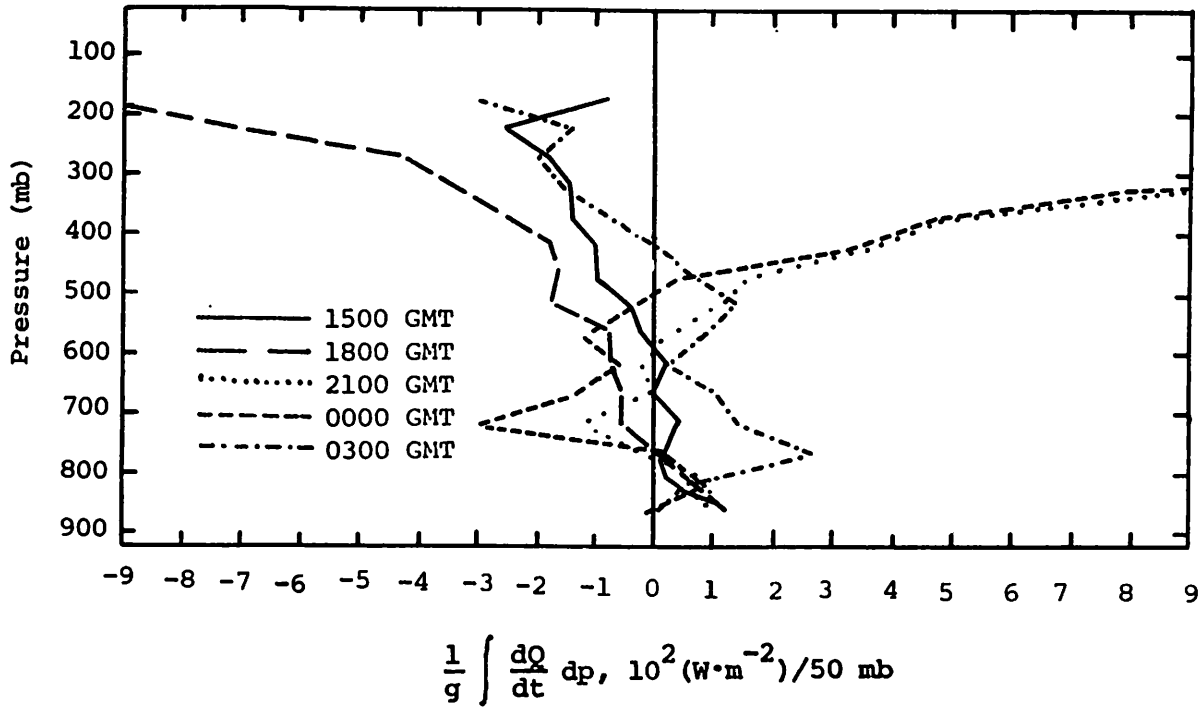

Fig. 5.3.4.5 Vertical profiles of diabatic heating computed from the first law of thermodynamics on 4 June 1978

occurred in upper levels with cooling below 500 mb. At 0300 GMT this changed to heating below 400 mb and cooling in upper layers. The peaks near 750 mb at 2100, 0000, and 0300 GMT correspond to peaks in the profiles of the residual of the latent heat equation (Fig. 5.3.4.4). This suggests that those peaks resulted from heating and cooling due to condensation and evaporation. The large values in upper levels are not explained by evaporation/condensation and so they must be due to radiation or other diabatic processes.

The profiles of horizontal flux of kinetic energy (Fig. 5.3.4.6) indicate inflow at lower levels for most time periods and large outflow at upper levels. At 0300 GMT there are layers of inflow and outflow at middle levels as well.

Figure 5.3.4.7 shows profiles of vertical flux of kinetic energy. At 1500 GMT the vertical flux below 500 mb was near zero. Vertical flux at this time was out of upper layers into a layer near 400 mb. At 1800 GMT vertical flux of kinetic energy was negative at levels above 600 mb and near zero below. This indicates flux into the upper layers and, since vertical motions were downward at this time (Fig. 5.3.3.2), the flux was downward

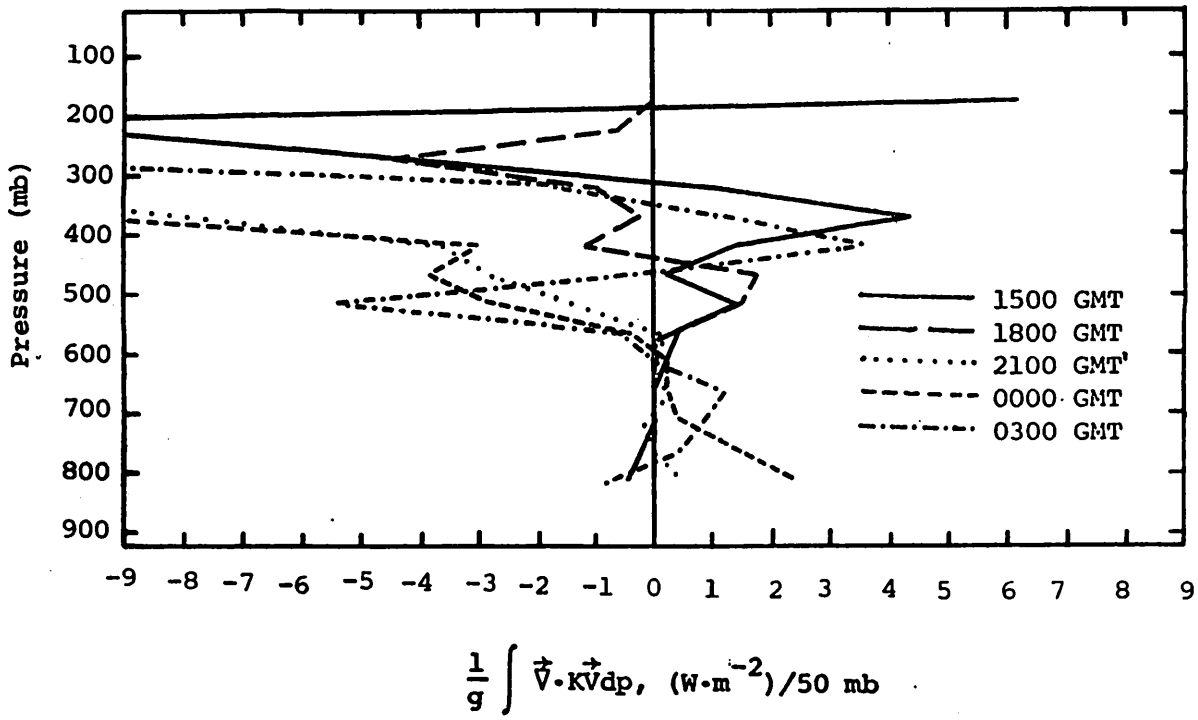

Fig. 5.3.4.6 Vertical profiles of the horizontal flux of kinetic energy on 4 June 1978.

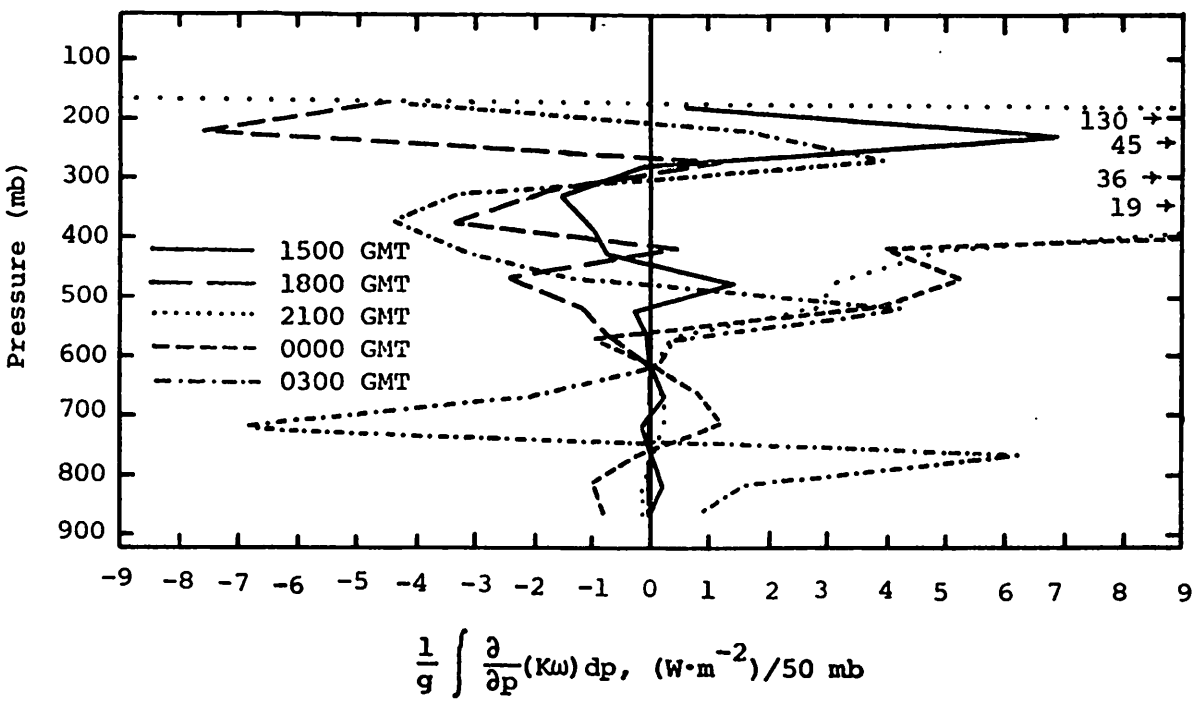

Fig. 5.3.4.7 Vertical profiles of the vertical flux of kinetic energy on 4 June 1978.

from very high levels. Profiles at 1800 and 2100 GMT are similar with large fluxes of kinetic energy out of the upper layers. The lower layers at these times show smaller values. At 0300 GMT there was a moderate amount of vertical transport of kinetic energy out of layers near the surface, and at 500 and 250 mb. Layers gaining kinetic energy by vertical transport were near 700, 450, and above 200 mb.

5.3.5 Water Vapor Budget

Figure 5.3.5.1 shows profiles of net horizontal transport of water vapor over the HIPLEX area. At 1500 GMT gains are shown in lower levels with losses above 650 mb. At 1800 GMT there were losses at all levels. By 2100 GMT horizontal inflow of water vapor was taking place above 700 mb with outflow below. The 0000 GMT profile is similar to the one at 2100 GMT, however, by 0300 GMT changes had taken place in the highest and lowest levels. Inflow was present below 750 mb at 0300 GMT and horizontal outflow of water vapor developed above 500 mb. This was when showers began to move into the HIPLEX area.

Figure 5.3.5.2 shows profiles of net vertical transport of water vapor. The 1500 GMT profile shows gains in water vapor between 500 and 700 mb, and between 750 and 800 mb with losses in other layers. At 1800 GMT mostly gains were present in lower layers and losses above 600 mb. Profiles at 2100 and 0000 GMT show mostly losses except in the lowest layer. At 0300 GMT this changed to losses in the lowest layer and between 500 and 550 mb, and gains in all other layers.

Profiles of net vertical transport through constant pressure surfaces are shown in Fig. 5.3.5.3. Upward transport prevailed at 1500 and 0300 GMT and downward transport at 1800 GMT. The profiles at 2100 and 0000 GMT show large downward transport below 500 mb with upward transport above.

The profiles of combined net horizontal and vertical transport (Fig. 5.3.5.4) are similar at 1500 and 0300 GMT. Gains in water vapor are shown in layers below 500 mb at these two times, with mostly losses below 500 mb shown in the other three profiles. Losses occurred above 500 mb except at 1800 and 0000 GMT which showed slight gains.

Profiles of the total mass of water vapor (Fig. 5.3.5.5) show that at 1500 GMT there were no layers that were especially dry or moist. At 1800 GMT drying between 700 and 500 mb created a dry layer there. This layer, although modified by the addition of moisture, persisted throughout the

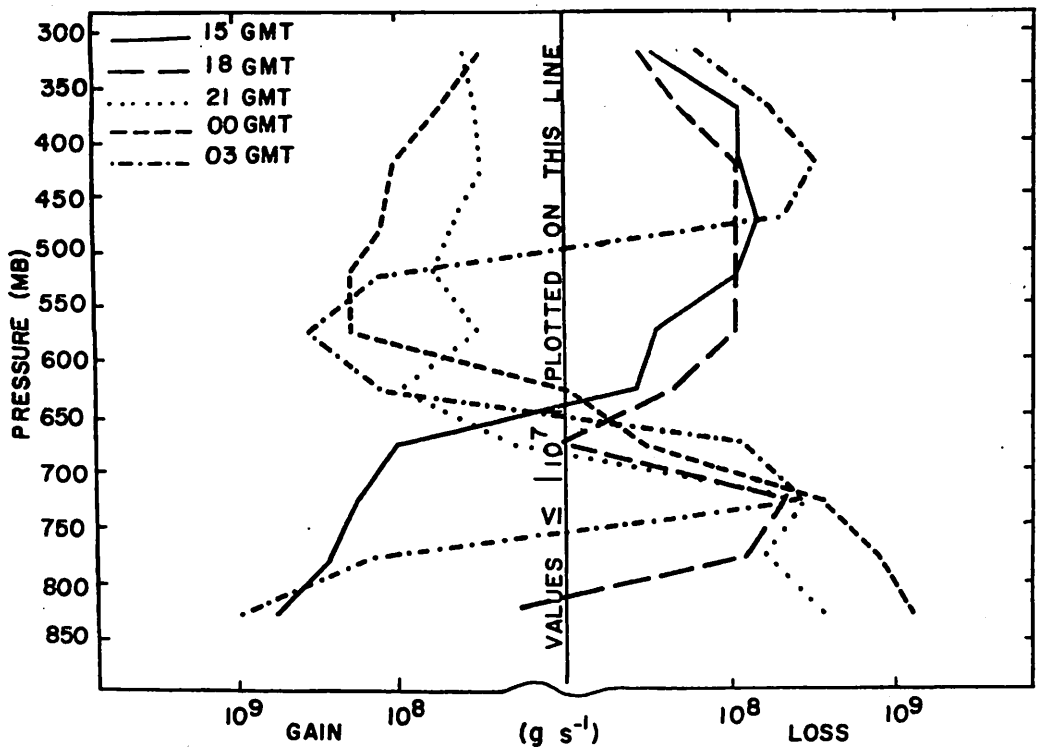

Fig. 5.3.5.1 Net horizontal transport of water vapor through boundaries of 50-mb layers (gm s^{-1}) over the Texas HIPLEX area for 4 June 1978.

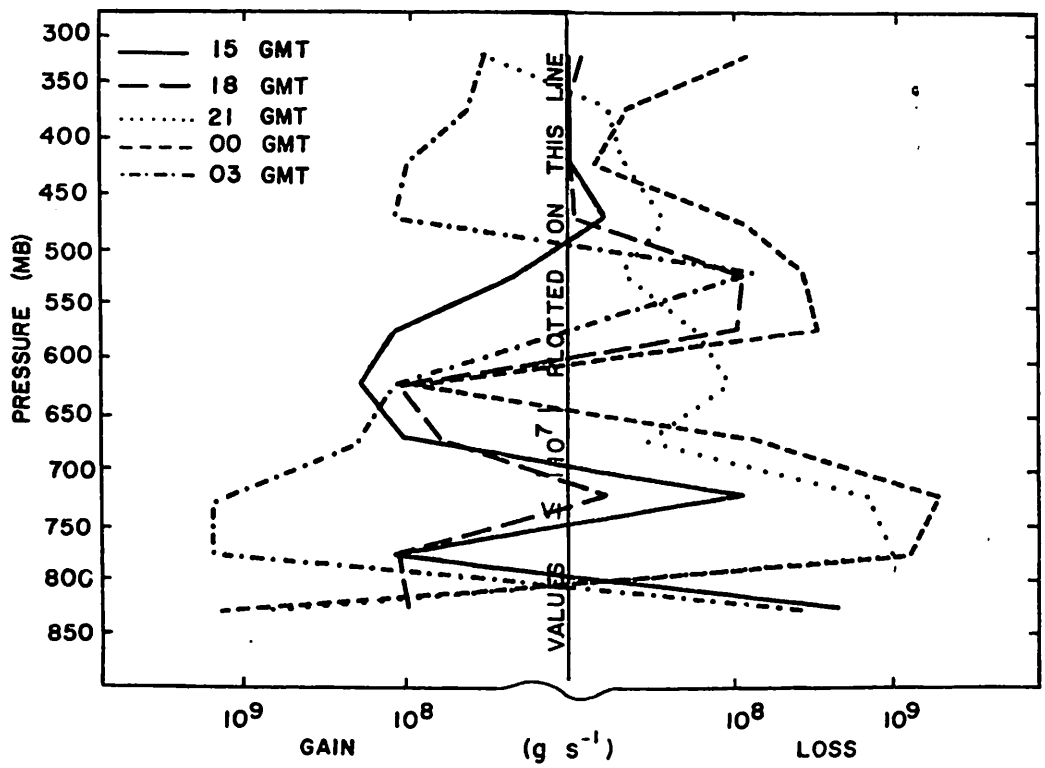

Fig. 5.3.5.2 Net vertical transport of water vapor through boundaries of 50-mb layers (gm s^{-1}) over the Texas HIPLEX area for 4 June 1978.

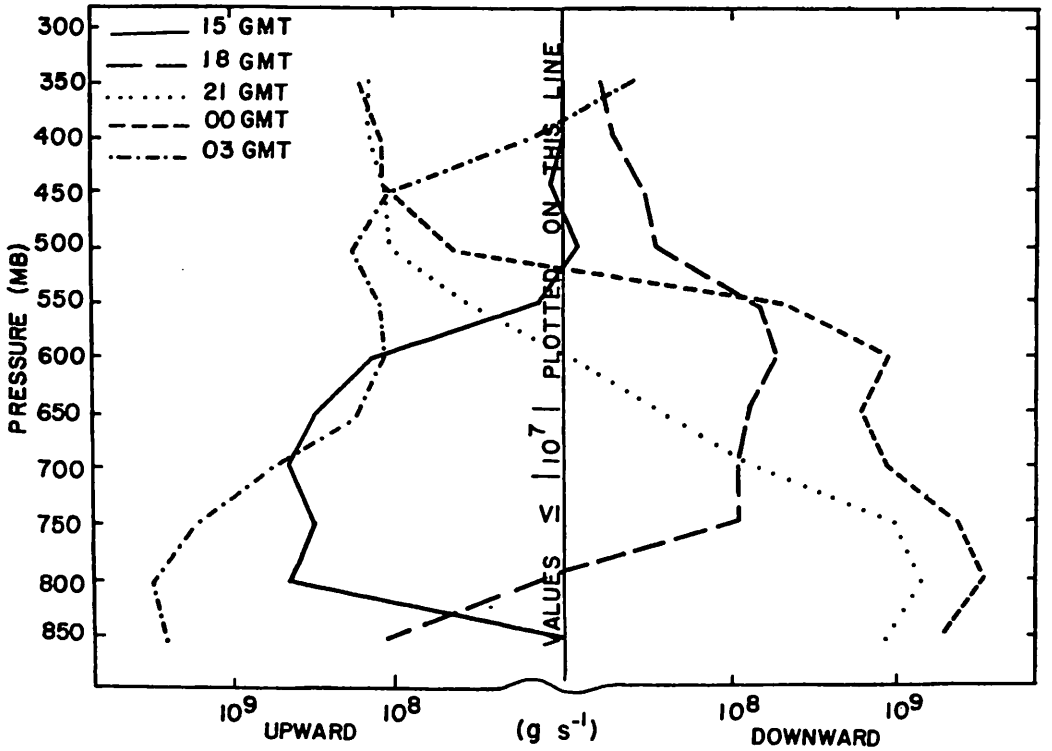

Fig. 5.3.5.3 Net vertical transport of water vapor through constant pressure surfaces (gm s^{-1}) over the Texas HIPLEX area for 4 June 1978.

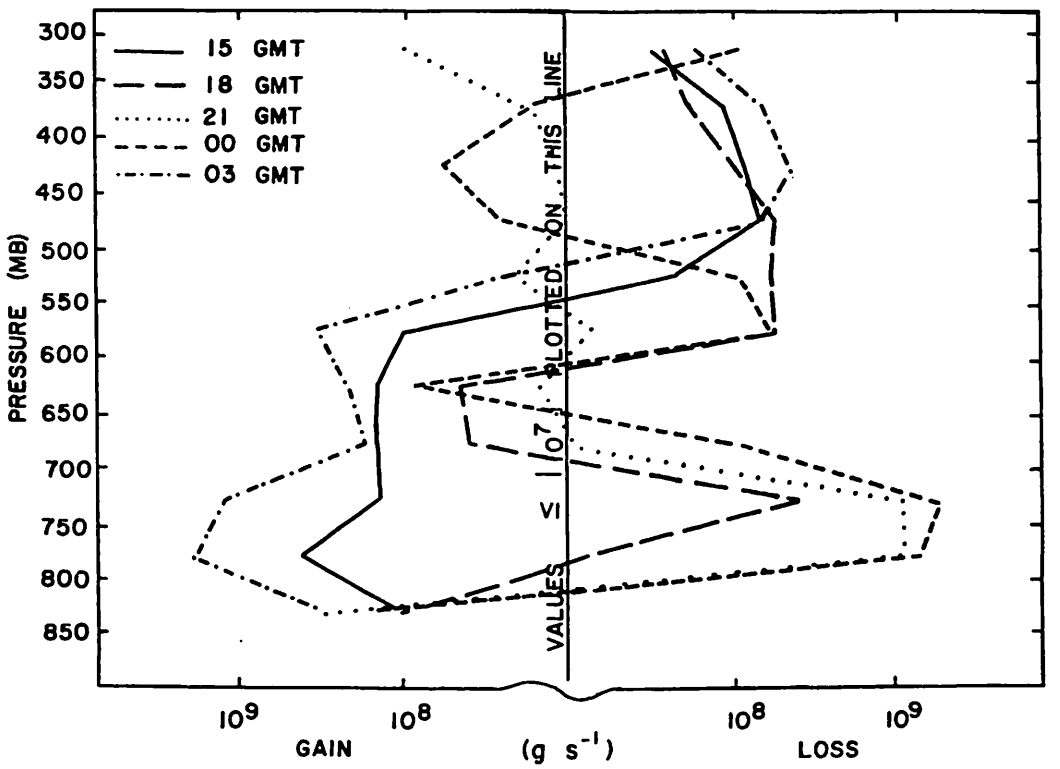

Fig. 5.3.5.4 Combined net horizontal and vertical transport of water vapor through boundaries of 50-mb layers (gm s^{-1}) over the Texas HIPLEX area for 4 June 1978.

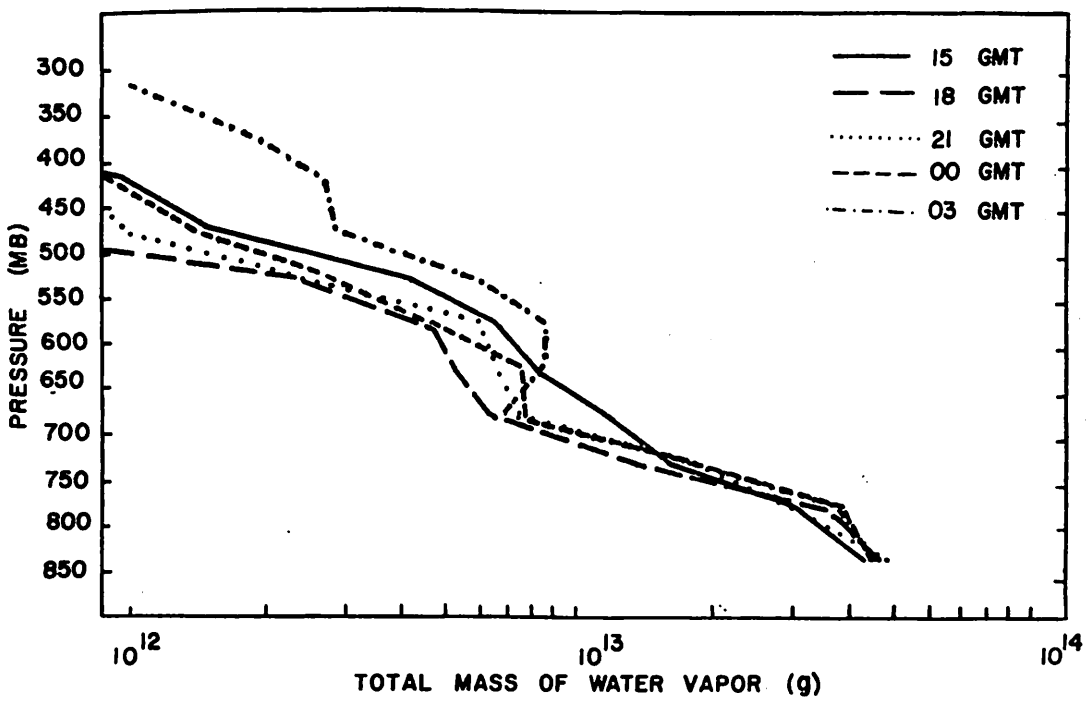

Fig. 5.3.5.5 Total mass of water vapor in layers 50 mb deep (g) over the Texas HIPLEX area on 4 June 1978.

remainder of the day. The addition of moisture created a relatively moist layer above 600 mb at 0300 GMT.

Profiles of the local rate-of-change of the total mass of water vapor (Fig. 5.3.5.6) reflect the changes in the total mass profiles. Between 1500 and 1800 GMT losses occurred above 800 mb. For the other profiles mainly gains were shown, except in the lower layers.

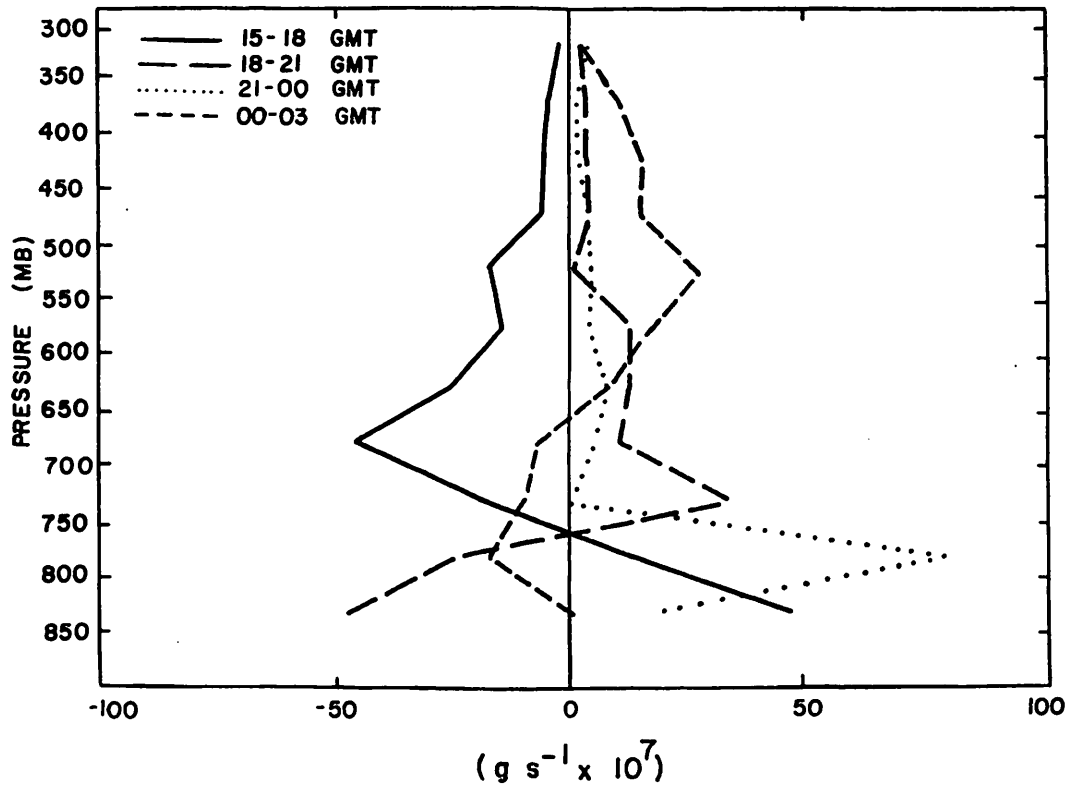

Fig. 5.3.5.6 Local rate-of-change in total mass of water vapor ($g\ s^{-1} \times 10^7$) for the Texas HIPLEX area for 4 June 1978.

5.4 5 June 1978

5.4.1 Radar

Scattered showers and thundershowers were over the HIPLEX area between 1600 GMT and 0300 GMT (Fig. 5.4.1.1). A cell of Code 3 moved from near Seminole to near Lamesa between 1900 GMT and 2000 GMT. Cells of Code 3 were also near Lenorah and Gail at 2200 GMT. These cells moved westward and were followed by two other Code 3 cells near Tahoka and Post at 0000 GMT. This activity moved out of the area by 0300 GMT. Cells with heights over 9.1 km (30K ft) were over the area for five consecutive hours - 2200 GMT to 0200 GMT.

5.4.2 Surface

The surface temperature pattern (Fig. 5.4.2.1) was fairly stable up to 2200 GMT with the temperature gradient northwest to southeast. The thunderstorm present between 1900 GMT and 2000 GMT did not show a noticeable effect on the temperature pattern. This cell was less intense than those that followed later in the day.

At 2200 GMT, downdraft-induced cooling associated with the thunderstorms resulted in the formation of a cold center near Lamesa. As the storms moved through the area the position of the cold center shifted so that by 0100 GMT the lowest temperatures were located near Vincent. This cold center remained near Vincent even after the storms moved out of the area at 0300 GMT. Between 2300 GMT and 0000 GMT the temperature dropped by 11°C at Vincent.

The patterns of surface dewpoint depression (Fig. 5.4.2.2) were variable but there was a general increase in dewpoint depressions between 1500 GMT and 2100 GMT. The lowest depressions were generally in the northwest. At 2200 GMT a center of low dewpoint depression appeared near Lamesa. This was associated with the downdraft mentioned earlier. While there was some increase in surface moisture (see Fig. 5.4.2.3) the main reason for the decrease in surface dewpoint depression was the cooling that took place.

The surface mixing ratios (Fig. 5.4.2.3) were variable during the day. No definite maxima or minima that persisted for more than an hour appeared until 2200 GMT. Maximum surface mixing ratios, indicating an increase in moisture content, were along a line from Lamesa to Lenorah. This increase in moisture was associated with the thunderstorm in the area. Mixing ratios did not increase all through the area with storm passage since the cooling in the area would limit increases in the mixing ratio. A minimum remained near Snyder and Vincent

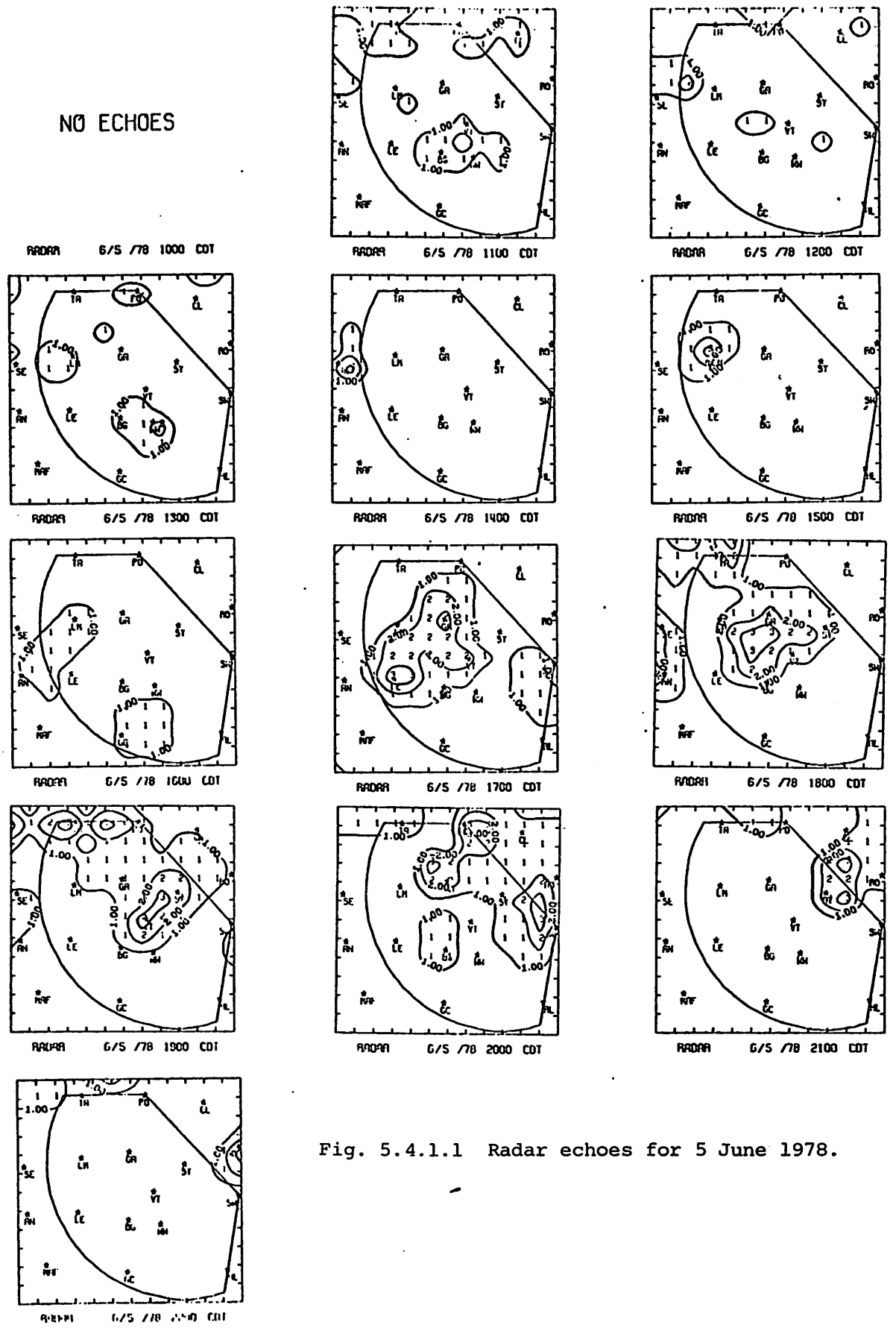

Fig. 5.4.1.1 Radar echoes for 5 June 1978.

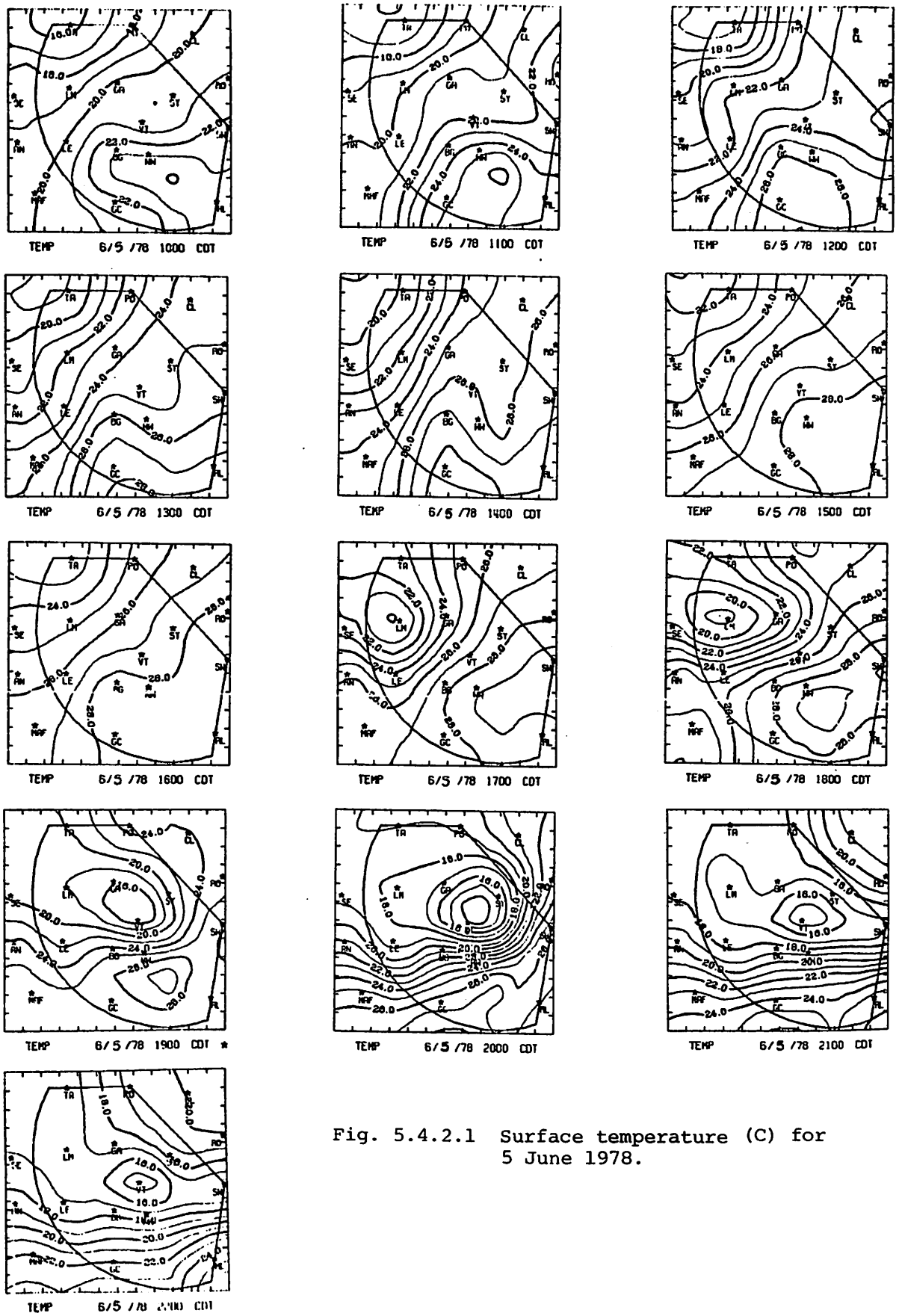

Fig. 5.4.2.1 Surface temperature (C) for 5 June 1978.

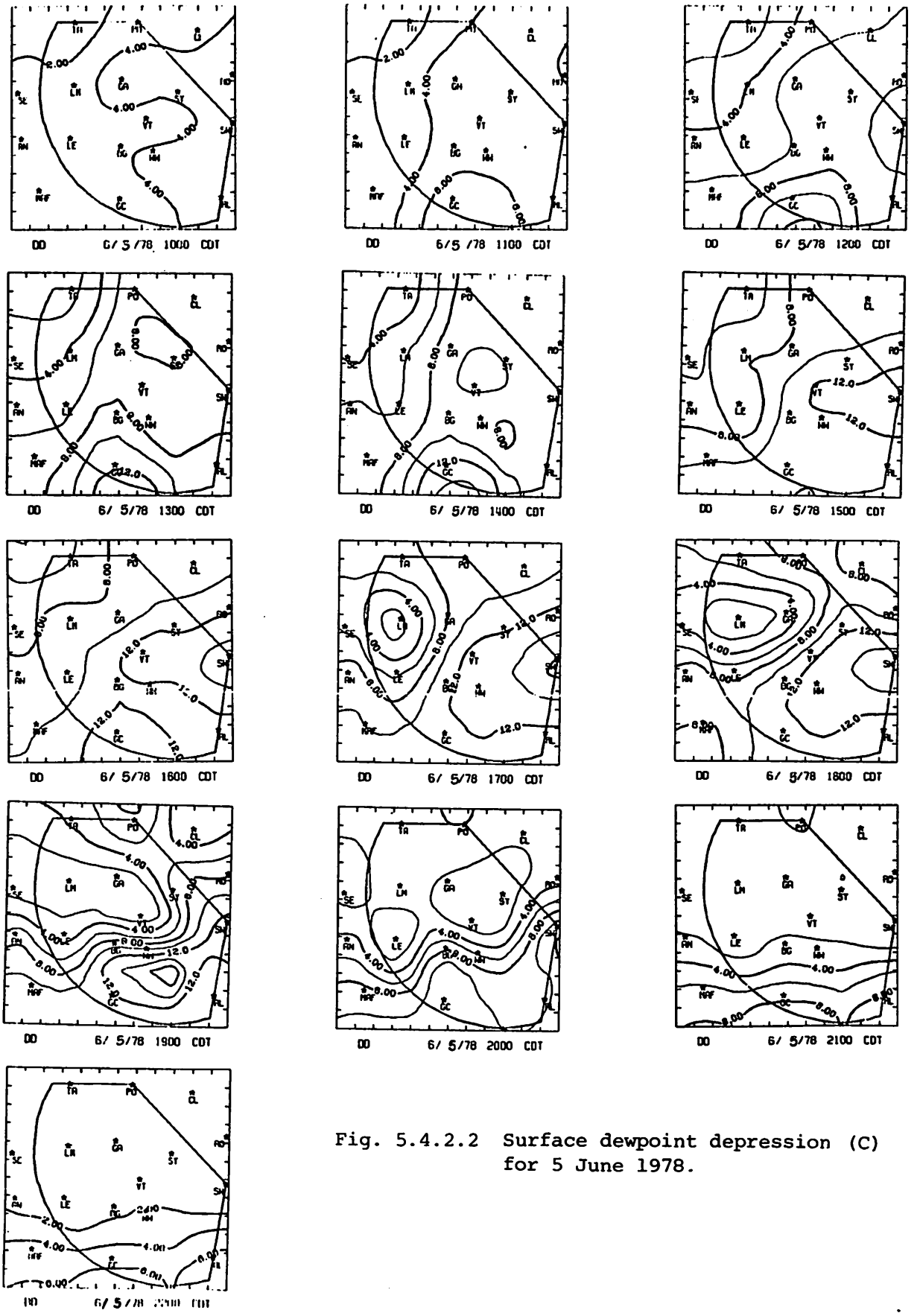

Fig. 5.4.2.2 Surface dewpoint depression (C) for 5 June 1978.

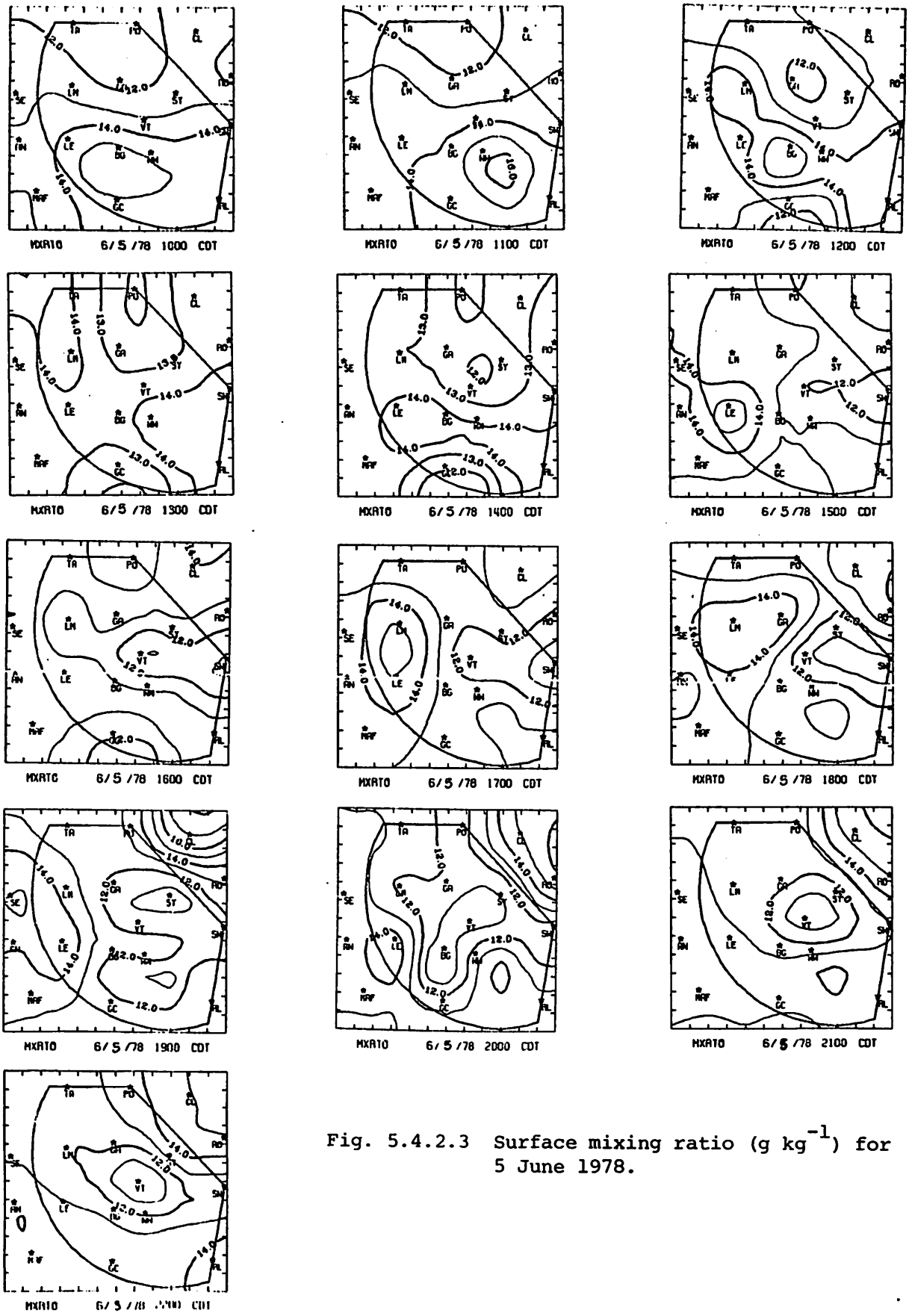

Fig. 5.4.2.3 Surface mixing ratio (g kg^{-1}) for 5 June 1978.

after 0000 GMT associated with a minimum in the temperature field. Increases in mixing ratio took place at Clairemont and Rotan where the storm-induced cooling was not as great.

Surface equivalent potential temperature (Fig. 5.4.2.4) increased from north to south. Maximum potential temperatures were present near Big Spring and Lenorah during the first part of the day before the passage of the storms. At 2200 GMT the equivalent potential temperature decreased over much of the northwest along with the temperature decrease in that area. The relatively higher equivalent potential temperatures between Lamesa and Lenorah reflect the maximum moisture present there. A minimum formed near Vincent at 2300 GMT along with a minimum surface mixing ratio (Fig. 5.4.2.3). This center intensified at 0000 GMT when downdraft-induced cooling occurred and was present there through 0300 GMT.

The terrain-induced vertical motion field (Fig. 5.4.2.5) had some centers of moderate value. Negative values indicating downward motions were near Walsh-Watts early in the day. Positive motion was between Walsh-Watts and Vincent between 2000 GMT and 2200 GMT.

Fields of surface velocity divergence (Fig. 5.4.2.6), vertical motion 50 mb above the surface (Fig. 5.4.2.7), surface moisture divergence (Fig. 5.4.2.8), and vertical moisture flux 50 mb above the surface (Fig. 5.4.2.9) begin with moderate convergence and upward motion centered north of Vincent. This center diminishes at 1800 GMT as another center of convergence forms south of Clairemont. The center remains south of Clairemont until 2100 GMT, and the thunderstorm present between 1900 GMT and 2000 GMT does not change the divergence and vertical motion patterns much. The patterns change considerably at 2200 GMT when two cells of Code 3 are present. Convergence and upward vertical motion develops near Lenorah with divergence and downward motion between Lamesa and Tahoka. The area of convergence stayed generally to the south and east of the storms. The fields were strong up to 0300 GMT when the storms had moved out of the area.

The surface vorticity fields (Fig. 5.4.2.10) show an axis of positive (cyclonic) vorticity persisting until 2100 GMT generally north-south through Vincent and Walsh-Watts. After 2200 GMT the patterns shift each hour and some strong centers of cyclonic and anticyclonic vorticity form and move in association with the thunderstorm activity in the area. By 0200 GMT with diminished activity the centers had weakened.

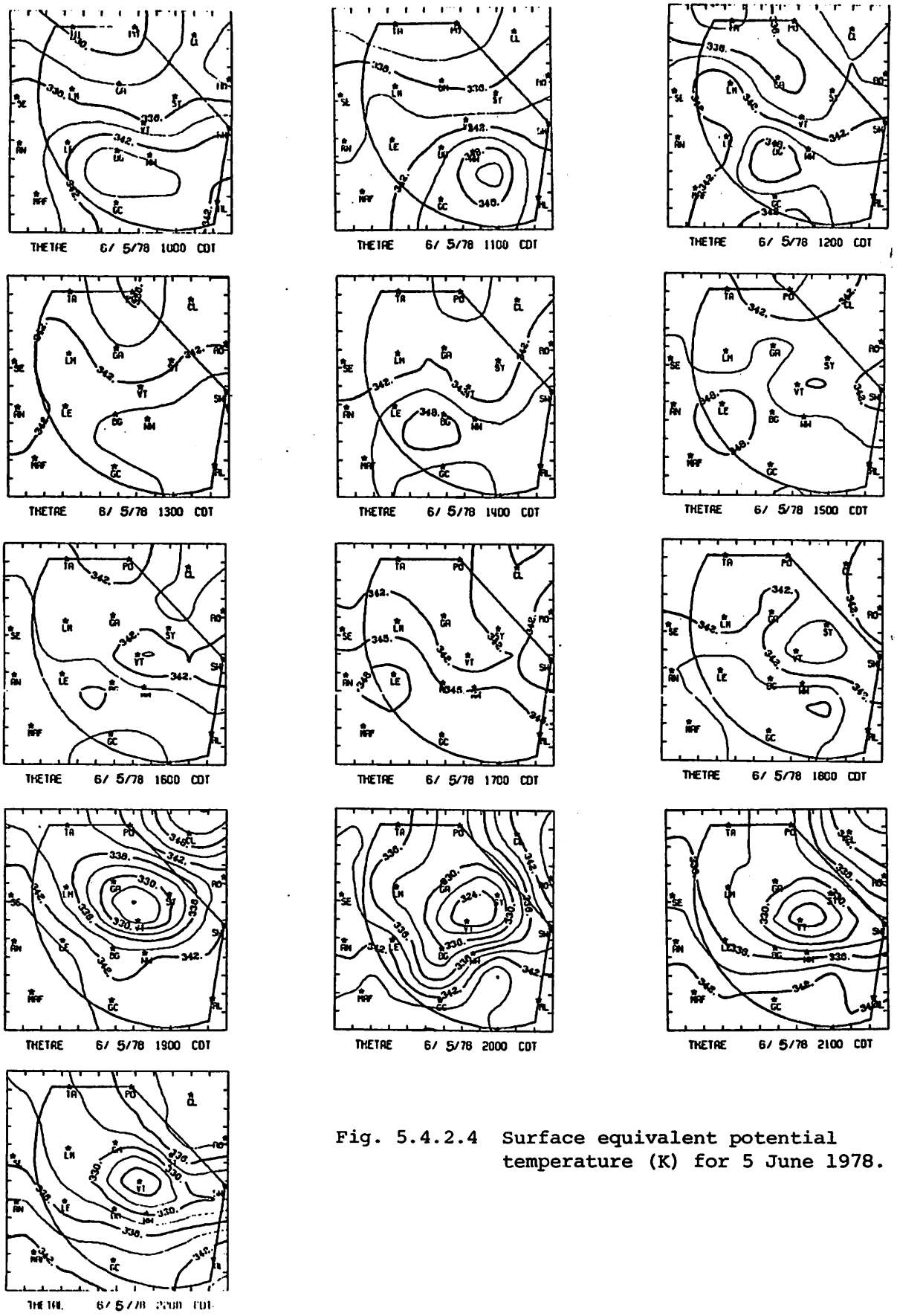

Fig. 5.4.2.4 Surface equivalent potential temperature (K) for 5 June 1978.

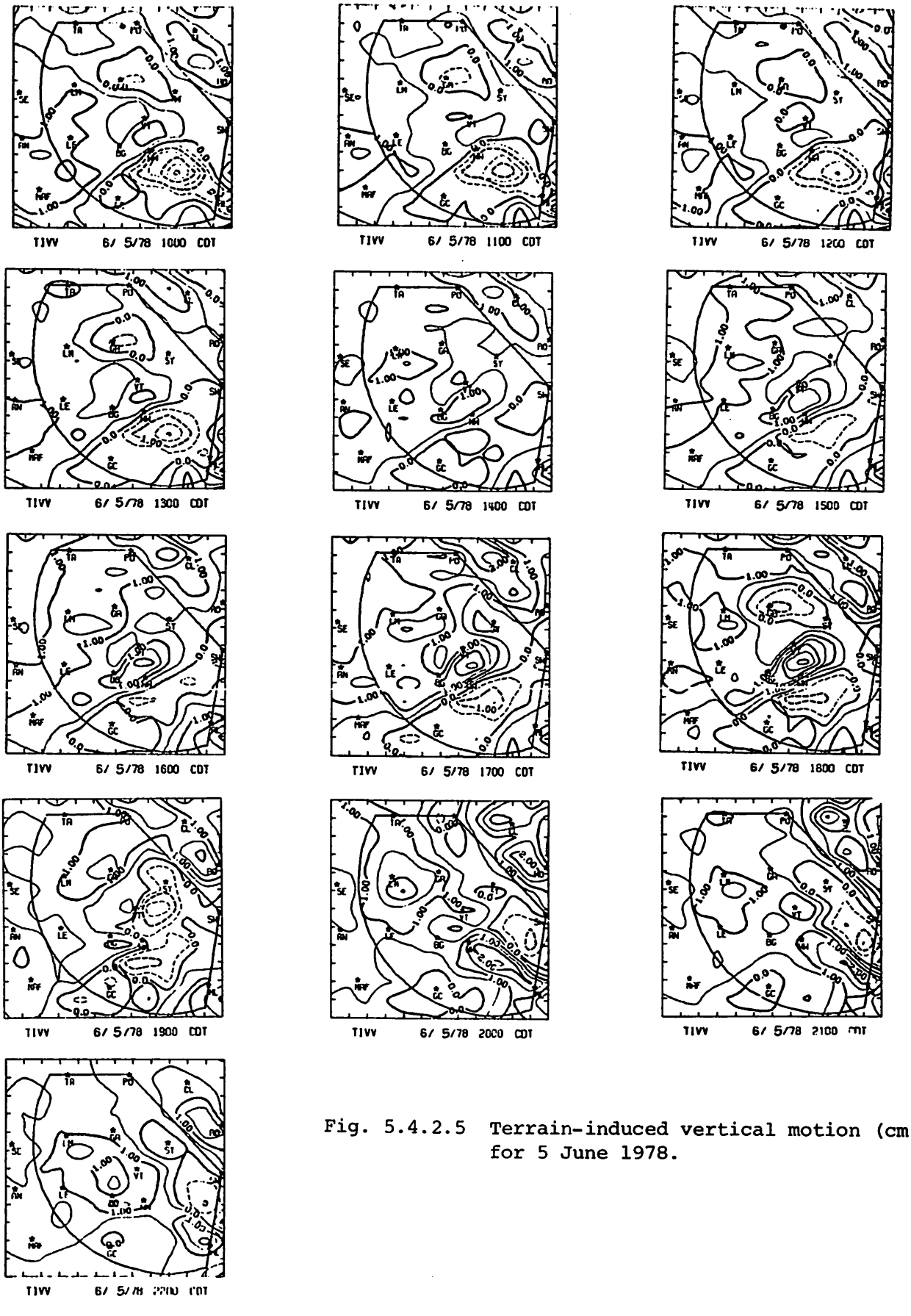

Fig. 5.4.2.5 Terrain-induced vertical motion (cm s^{-1}) for 5 June 1978.

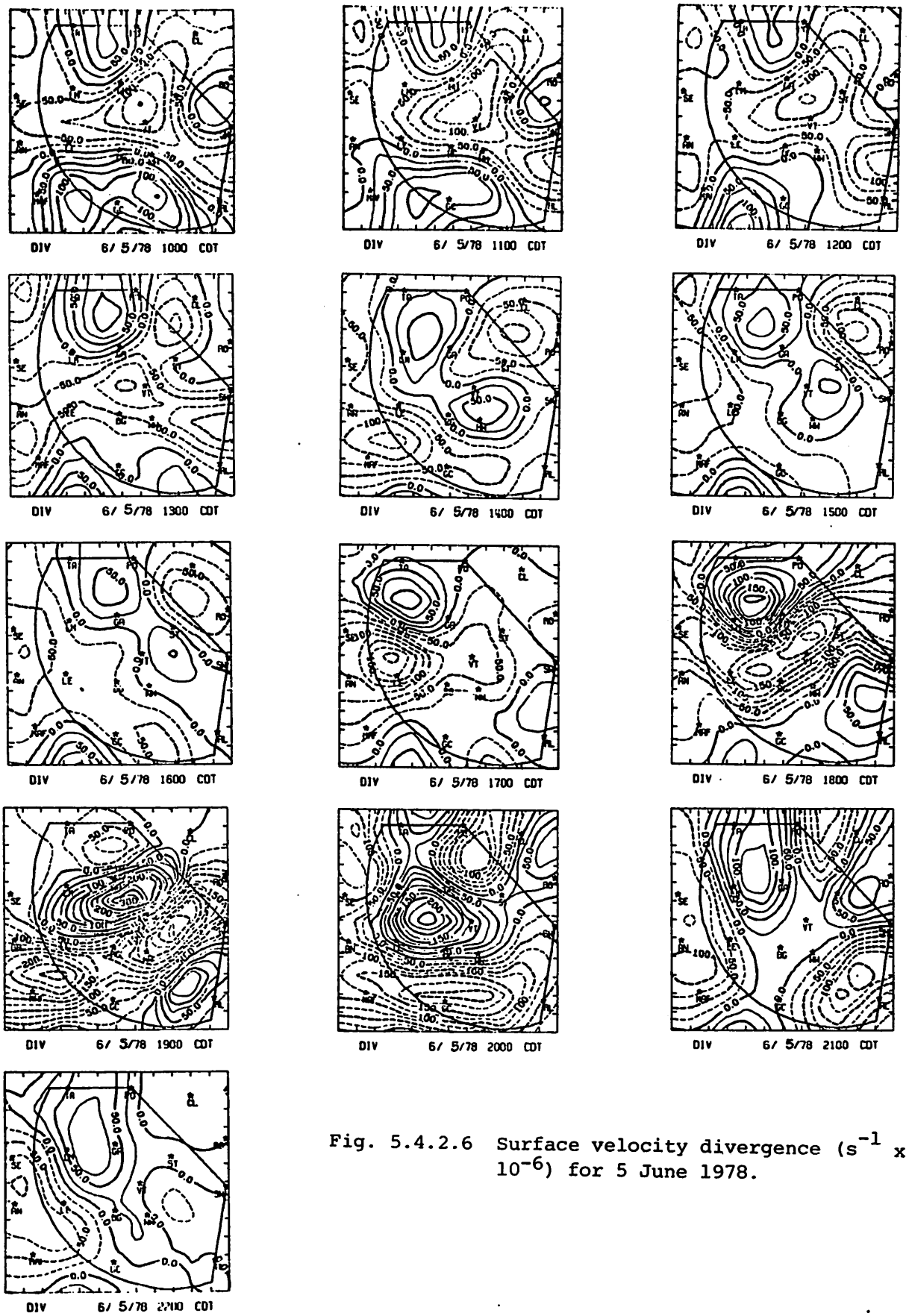

Fig. 5.4.2.6 Surface velocity divergence (s^{-1} x 10^{-6}) for 5 June 1978.

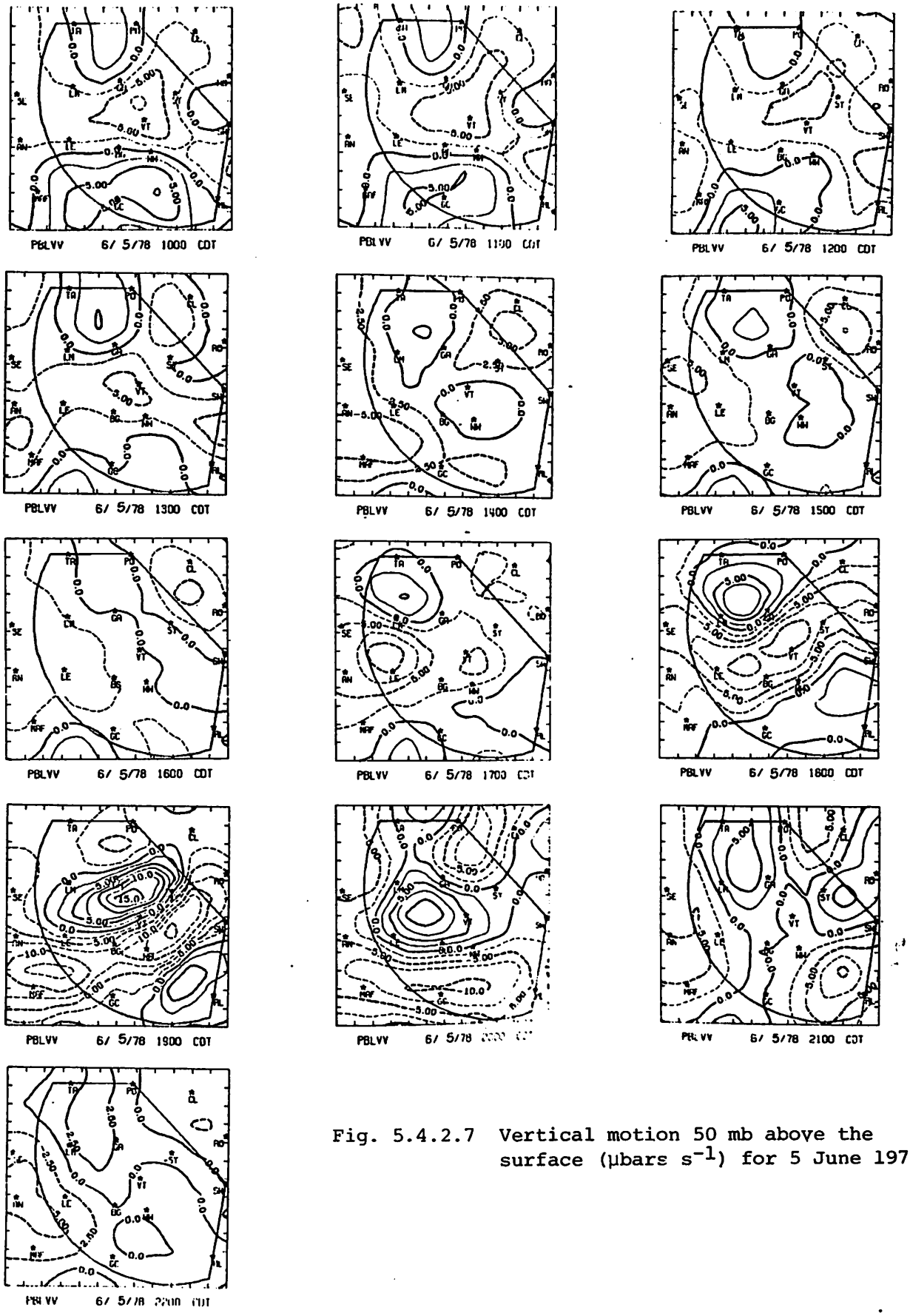

Fig. 5.4.2.7 Vertical motion 50 mb above the surface (μbars s^{-1}) for 5 June 1978.

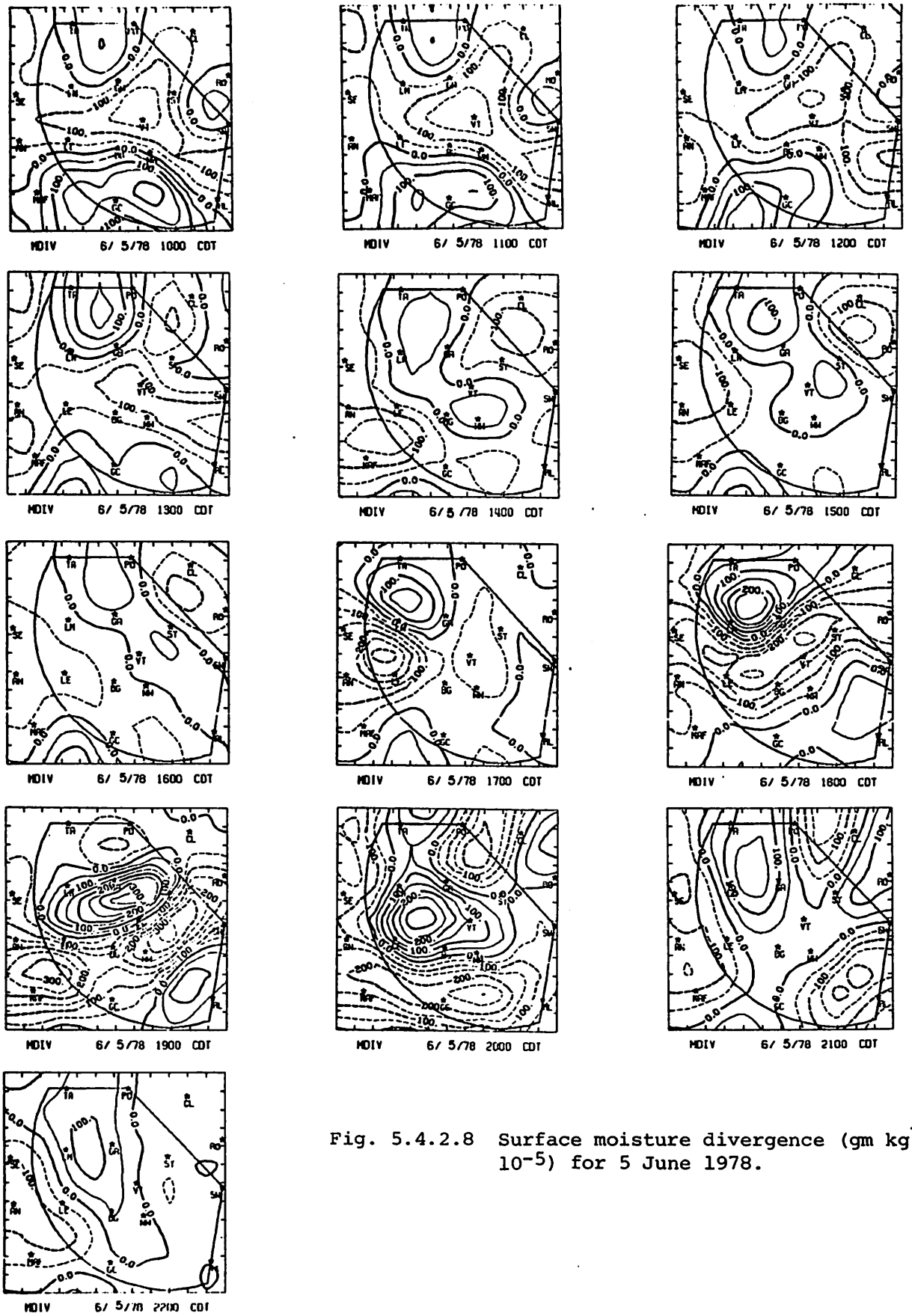

Fig. 5.4.2.8 Surface moisture divergence (gm kg^{-1} s^{-1} x 10^{-5}) for 5 June 1978.

Fig. 5.4.2.9 Vertical flux of moisture 50 mb above the surface (gm cm^{-2} s^{-1} x 10^{-6}) for 5 June 1978.

Fig. 5.4.2.10 Surface vorticity (s^{-1} x 10^{-6}) for 5 June 1978.

Surface pressure changes (Fig. 5.4.2.11) were moderate during much of the day prior to 2300 GMT. Pressure rose 1.7 mb between 2200 and 2300 GMT at Gail and also between 2300 and 0000 GMT at Vincent. These rises were in the areas of the downdraft-induced cooling caused by the storms. Pressure drops were present just ahead of the storms at 2300 GMT between Walsh-Watts and Snyder, and at 0000 GMT southeast of Walsh-Watts. These drops were small, however.

Relative surface wind patterns (Fig. 5.4.2.12) were generally similar for the first few hours of the day. Winds were from the east and northeast in the northern part of the area, and from the south and southeast in the southern part. Thus, there was confluence midway through the area along a line from Seminole to Snyder. At 2300 GMT the influence of the thunderstorms is indicated by very light winds. Wind patterns shift and change with the passage of the storms. At 0300 GMT when the storms moved out of the area generally easterly flow was present over the area.

5.4.3 Upper Level Kinematic Parameters

Profiles of horizontal mass divergence (Fig. 5.4.3.1) show a deep layer of mass convergence at 1500 GMT, before any radar echoes were recorded. The layer of low level convergence was shallower at the other times. The profiles for 1800 and 2100 GMT are much the same with strong convergence near the surface, moderate to strong divergence in mid-levels, and moderate convergence in upper levels. At 0000 GMT, the time of maximum activity, the profiles also are similar except the layer of mid-level convergence is much stronger and deeper. By 0300 GMT, when activity decreased, the layer of mid-level convergence became shallower and was overlain by a deep layer of upper-level divergence.

The profiles of vertical motion (Fig. 5.4.3.2) exhibit mainly upward motion. Downward motion was present only above 300 mb at 0300 GMT. The largest values of upward motion were at 0000 GMT.

Moisture convergence was present at low levels for all times (Fig. 5.4.3.3). At 1500 GMT, before echoes were present, convergence was present to 600 mb. At the other time periods this was replaced by a layer of moisture divergence. At 0000 GMT when activity was greatest a layer of moderate convergence was present near 600 mb which decreased in intensity and depth by 0300 GMT.

5.4.4 Energetics

Low level horizontal inflow of latent heat was present at all times (Fig. 5.4.4.1). A deep layer of latent heat inflow was present in low levels at 1500 GMT. Strong latent heat outflow replaced the inflow layer at both 1800

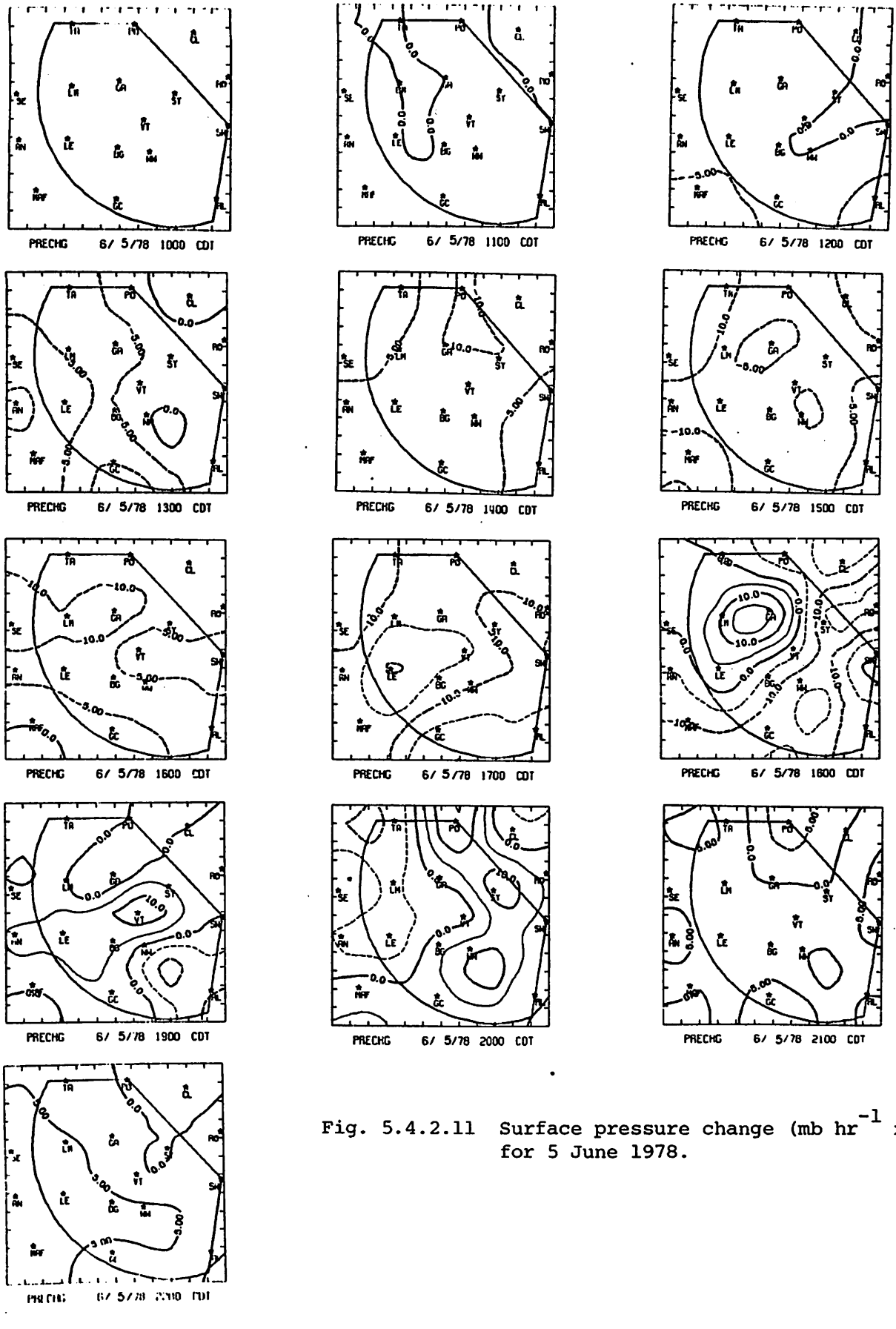

Fig. 5.4.2.11 Surface pressure change (mb hr^{-1} x 10^{-1}) for 5 June 1978.

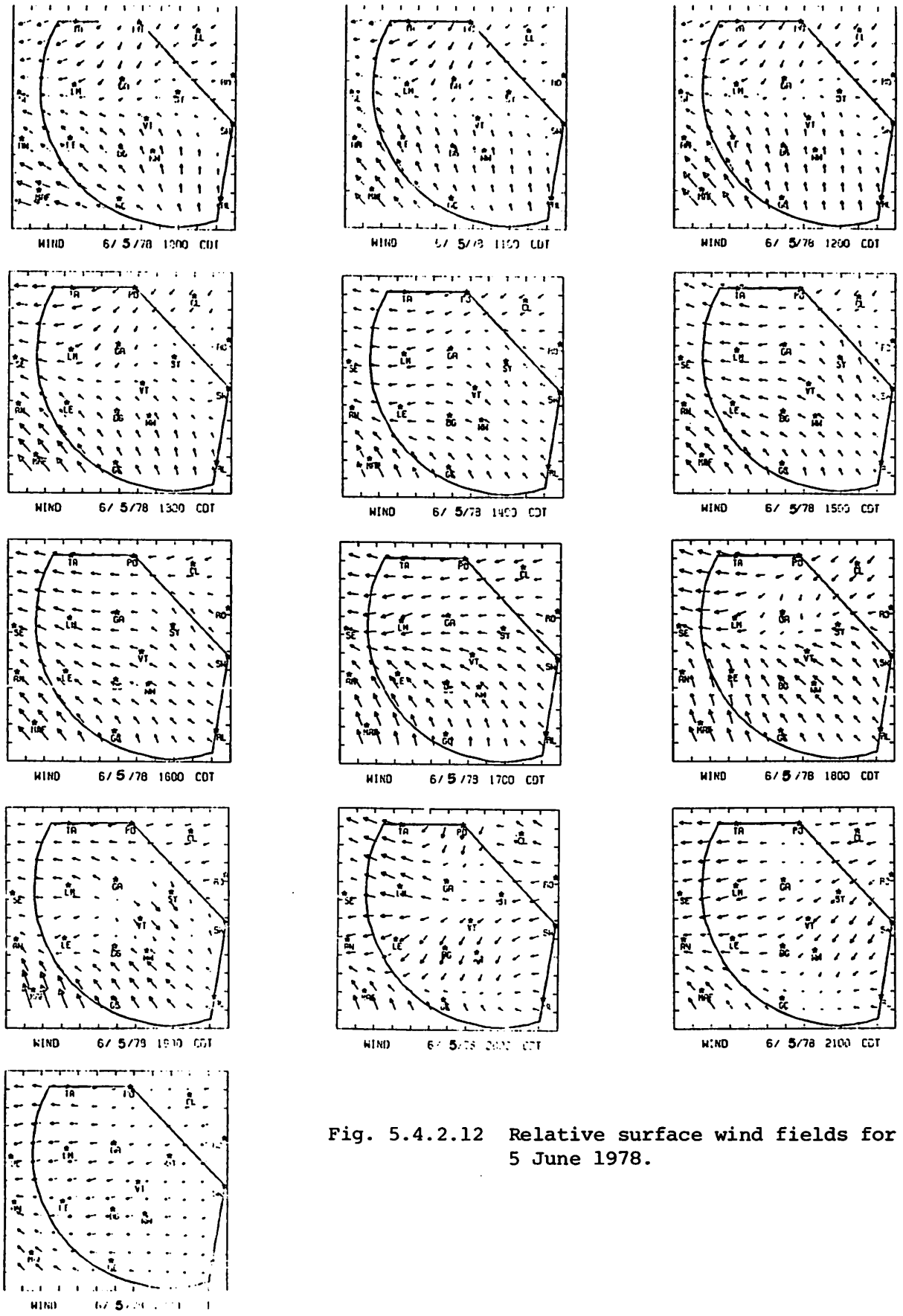

Fig. 5.4.2.12 Relative surface wind fields for 5 June 1978.

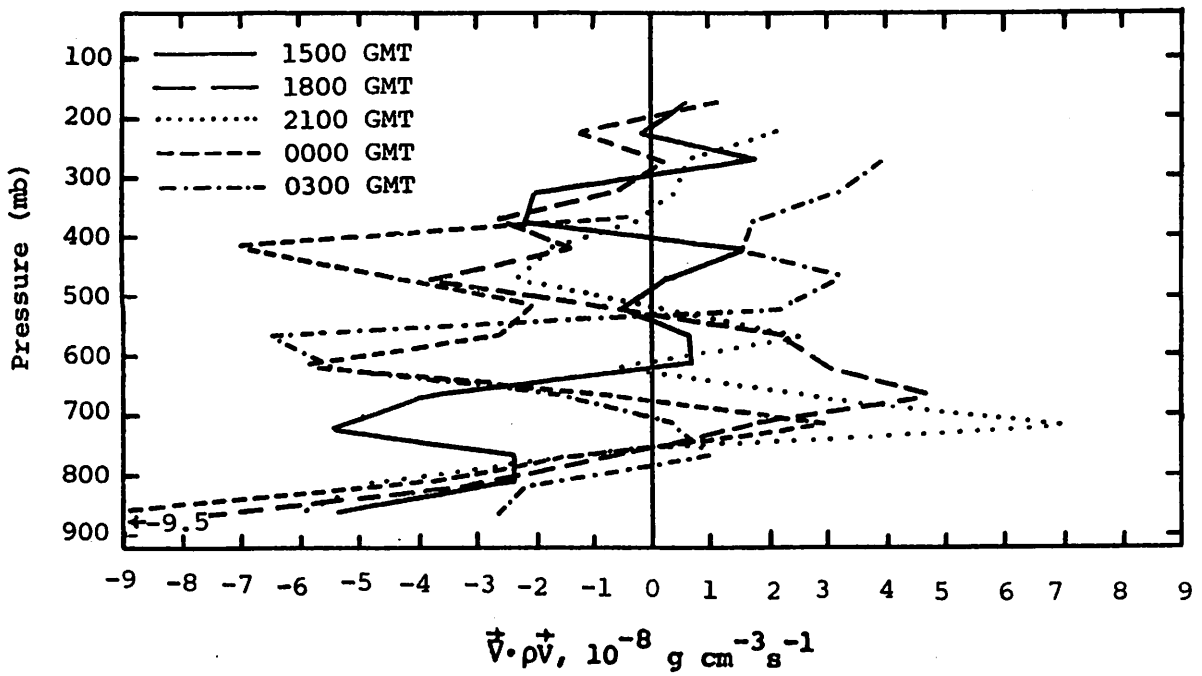

Fig. 5.4.3.1 Vertical profiles of mass divergence on 5 June 1978.

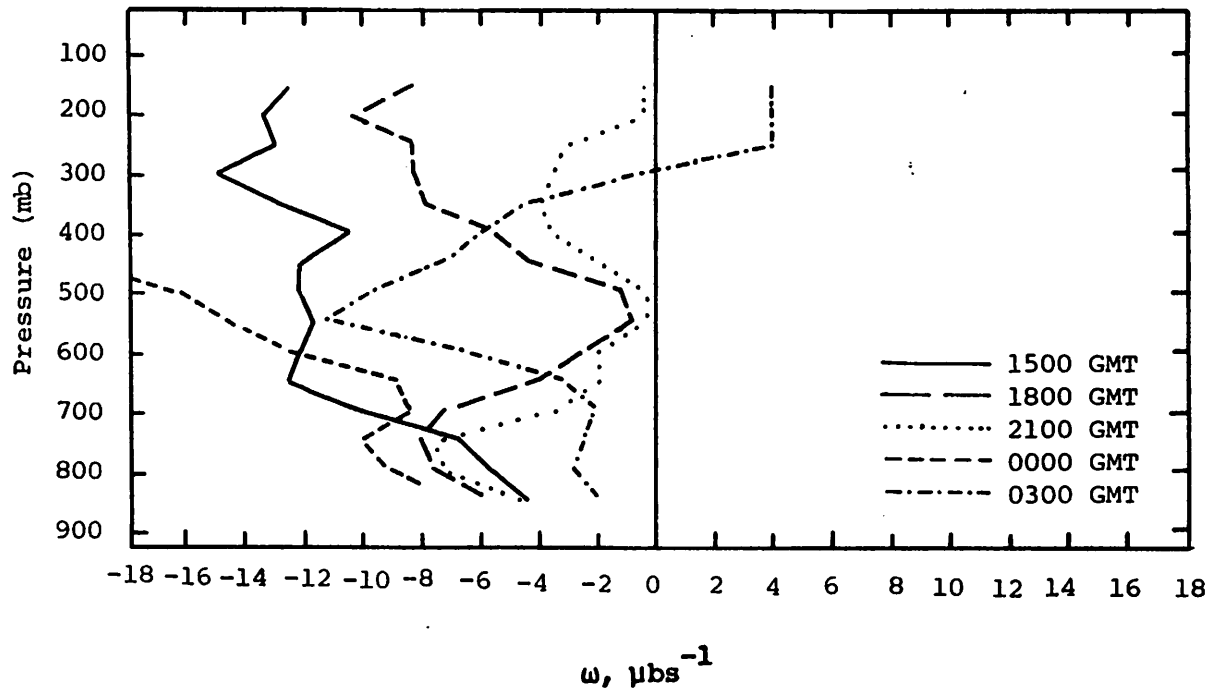

Fig. 5.4.3.2 Vertical profiles of vertical motion on 5 June 1978.

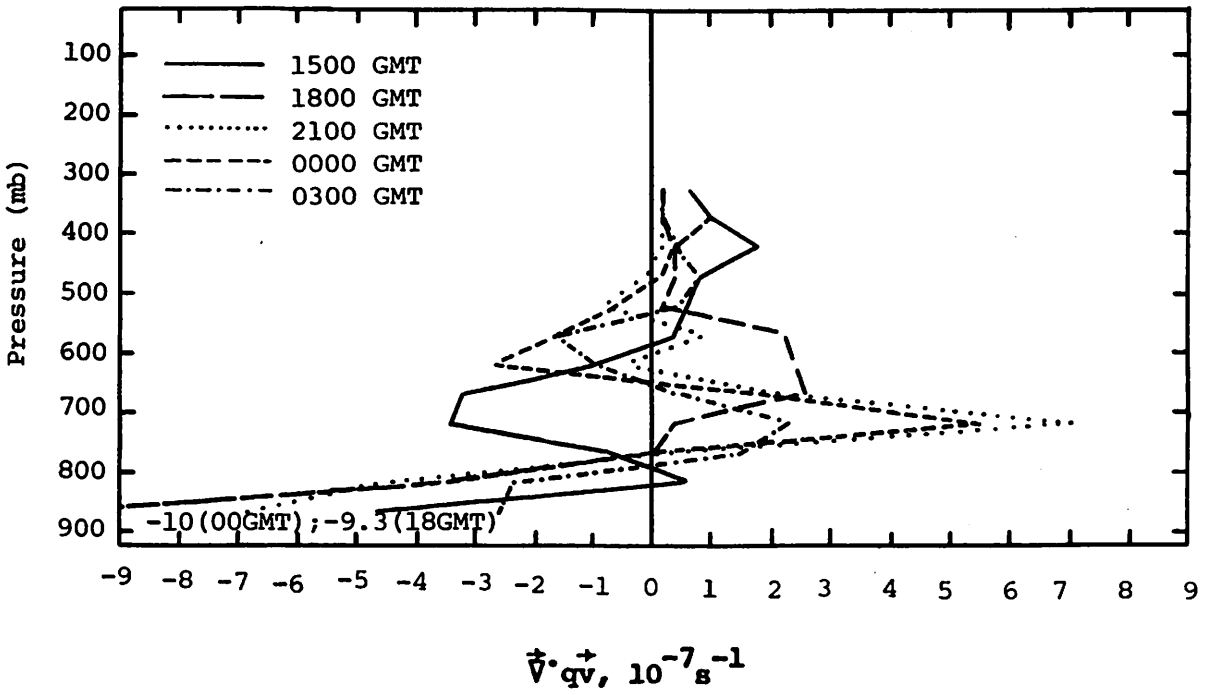

Fig. 5.4.3.3 Vertical profiles of moisture divergence on 5 June 1978.

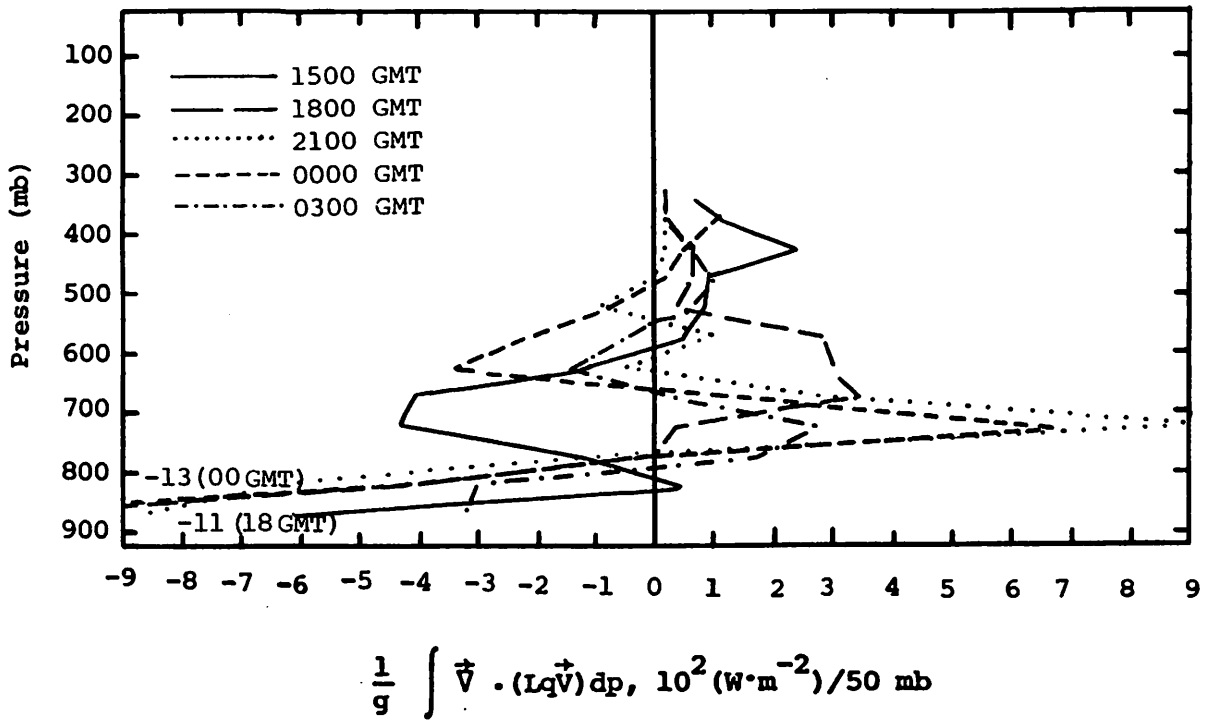

Fig. 5.4.4.1 Vertical profiles of the horizontal flux of latent heat energy on 5 June 1978.

and 2100 GMT, with weaker outflow in the higher levels. By 0000 GMT latent heat inflow was present at mid levels but decreased by 0300 GMT. The magnitude of the low-level inflow was greatest at 0000 GMT when several strong echoes were present.

The profiles of vertical flux of latent heat (Fig. 5.4.4.2) show transport out of lower levels into middle and upper layers. The source of the latent heat in the lower layers is provided by the strong horizontal inflow.

The local change of latent heat (Fig. 5.4.4.3) was, for the most part, negative except in lower levels and at 2100 GMT. The profile was negative or near zero at all levels at 0000 GMT when echo coverage was a maximum.

The graph of the residual of the latent heat (Fig. 5.4.4.4) shows mainly positive values. Negative values were present only above 500 mb and at low levels. These profiles show the effect of sources and sinks of latent heat energy. The positive values (increases in -R) show decreases in latent heat due to condensation. The negative values at upper levels could result from evaporation or some unresolved horizontal or vertical transport.

The profiles of the residual in the sensible heat equation show the effects of the condensation as increases in sensible heat at most levels (Fig. 5.4.4.5).

The horizontal flux of kinetic energy (Fig. 5.4.4.6) is mainly outward at lower levels. A layer of inflow, generally strong, is present at some middle levels at all times, with outflow in the upper layers near the jet stream. At 0300 GMT, outflow of kinetic energy occurs at all levels above 500 mb while at other times the outflow layer is above 300 mb.

The profiles of vertical transport of kinetic energy (Fig. 5.4.4.7) and of vertical motion (Fig. 5.4.3.2) show that kinetic energy transport was mainly out of the lower levels into levels above 450 mb.

5.4.5 Water Vapor Budget

Between 1600 and 0300 GMT convective activity was present over the area. The strongest activity occurred between 2200 and 0300 GMT when several cells of Code 3 moved across the area.

The profile for net horizontal transport of water vapor at 1500 GMT, prior to the convective activity, shows moisture convergence up to 500 mb with divergence above. At 1800 GMT a layer of middle-level outflow centered near 600 mb had formed. This layer remained during the rest of the day but was located near 700 mb in the last three profiles (Fig. 5.4.5.1).

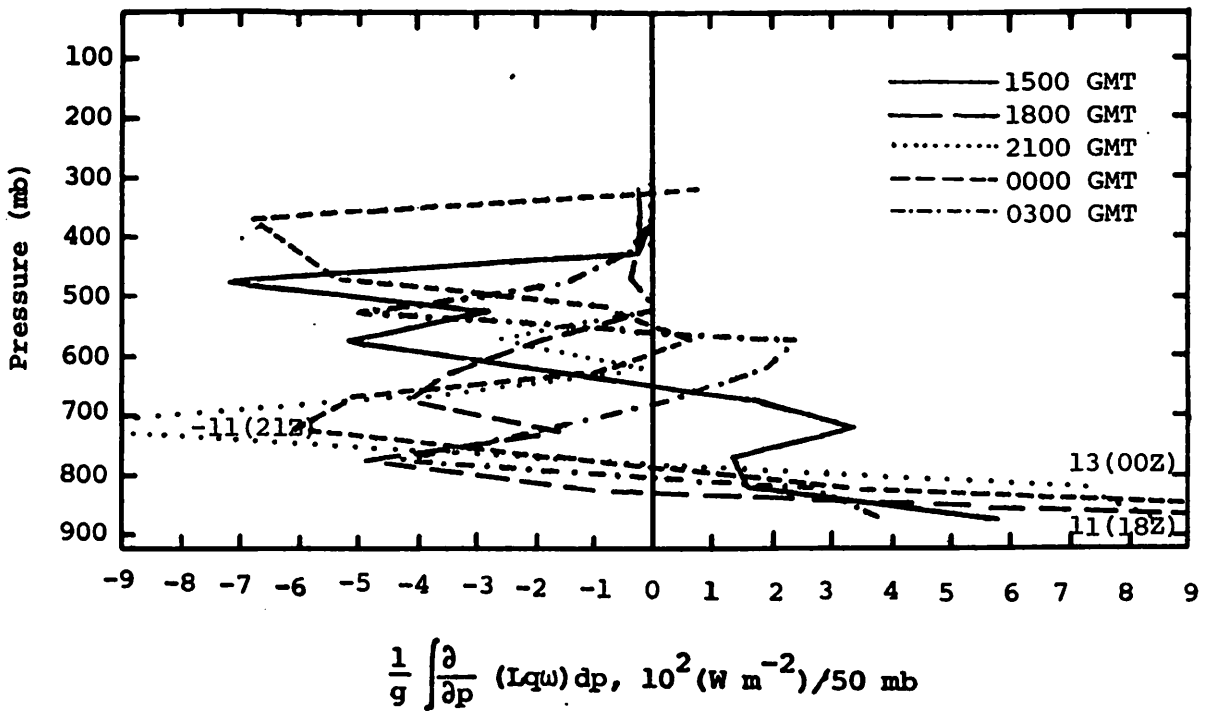

Fig. 5.4.4.2 Vertical profiles of the vertical flux of latent heat on 5 June 1978.

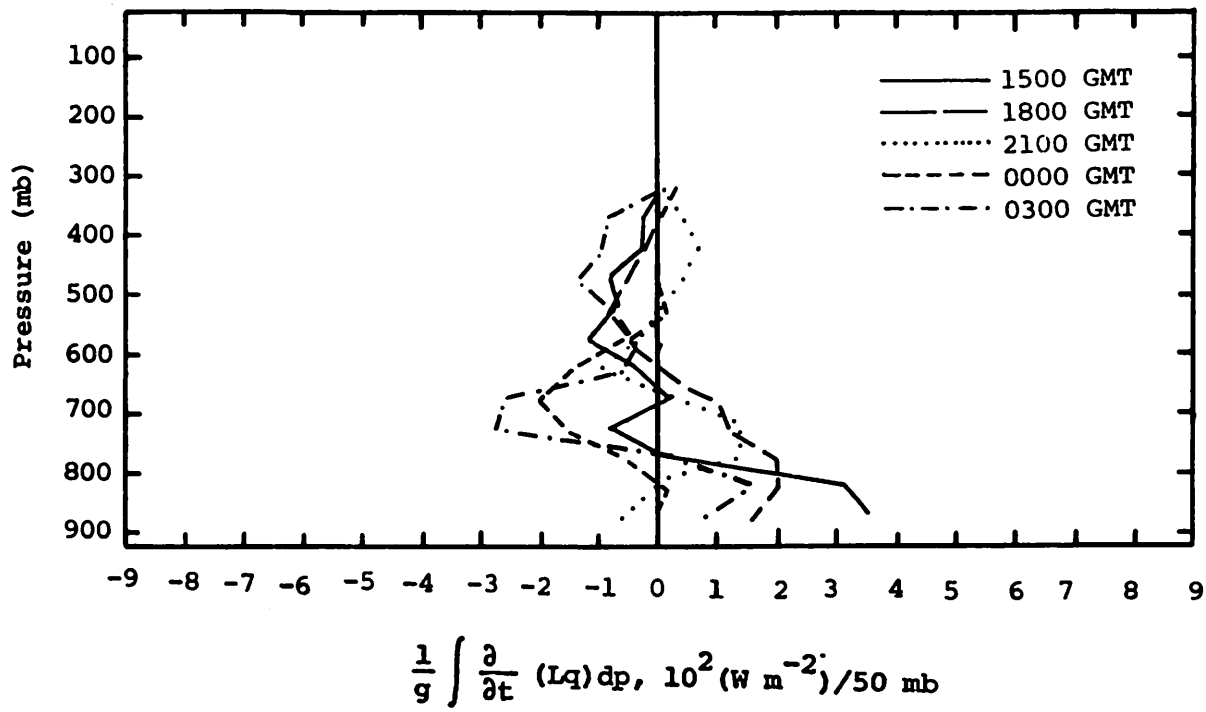

Fig. 5.4.4.3 Vertical profiles of the local change of latent heat energy on 5 June 1978.

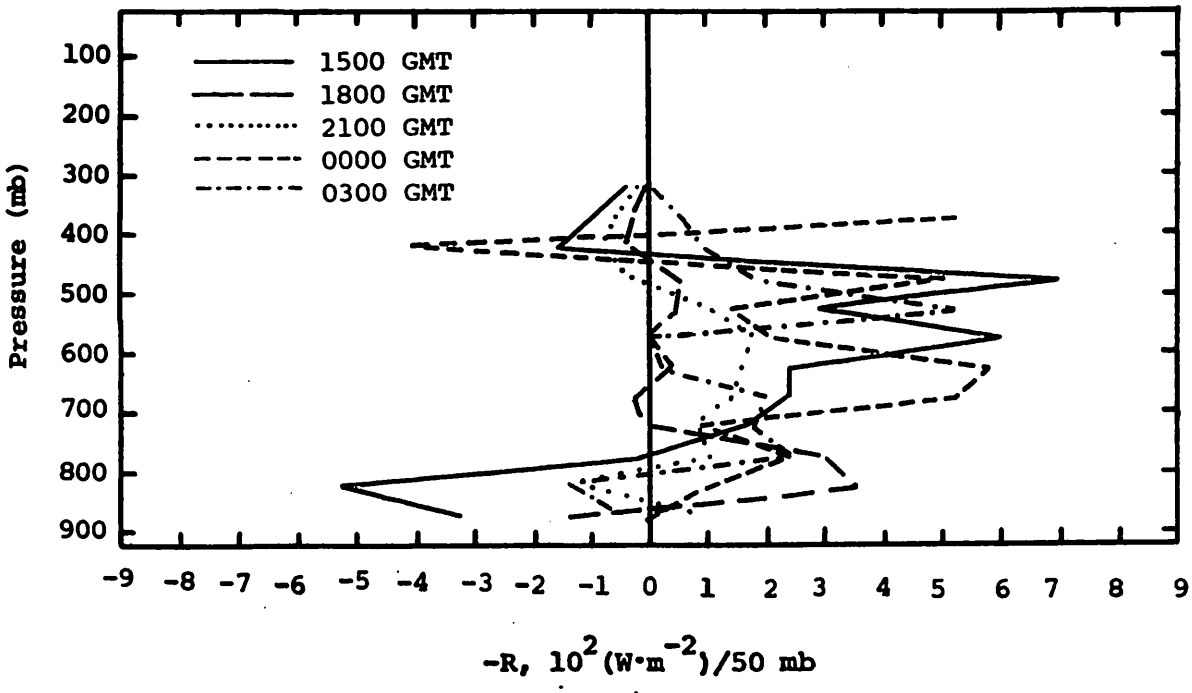

Fig. 5.4.4.4 Vertical profiles of the residual of the latent heat energy equation on 5 June 1978.

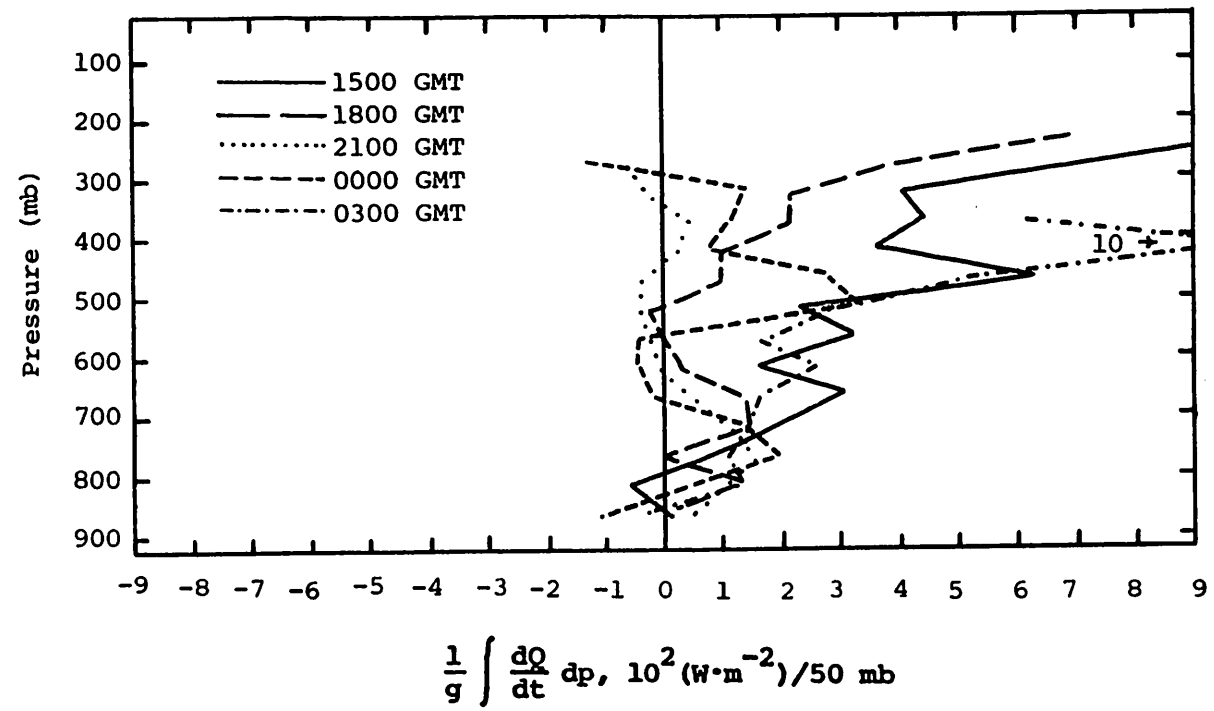

Fig. 5.4.4.5 Vertical profiles of diabatic heating computed from the first law of thermodynamics on 5 June 1978.

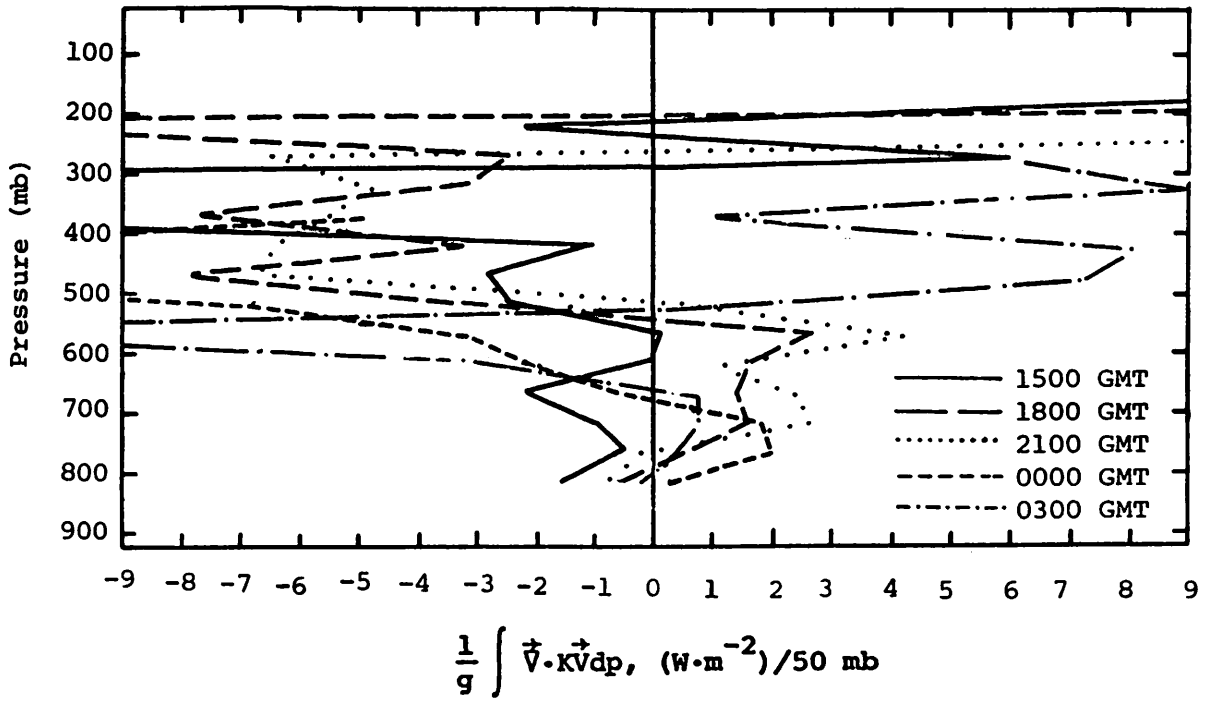

Fig. 5.4.4.6 Vertical profiles of the horizontal flux of kinetic energy on 5 June 1978.

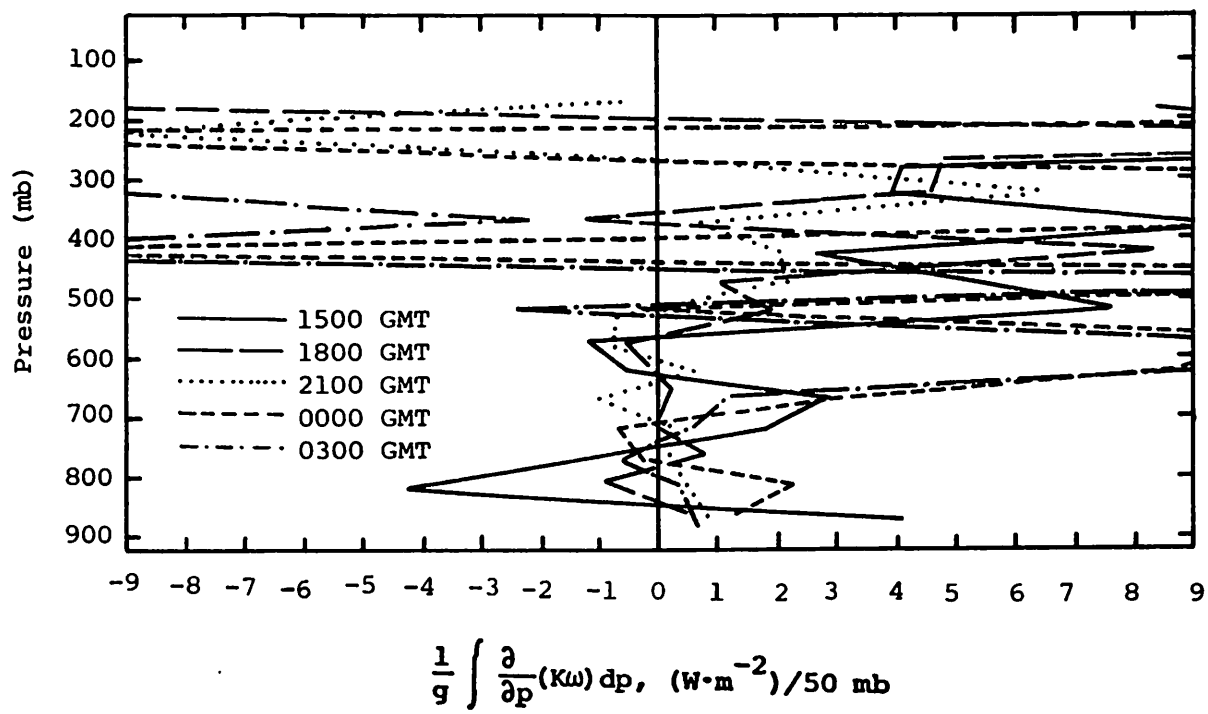

Fig. 5.4.4.7 Vertical profiles of the vertical flux of kinetic energy on 5 June 1978.

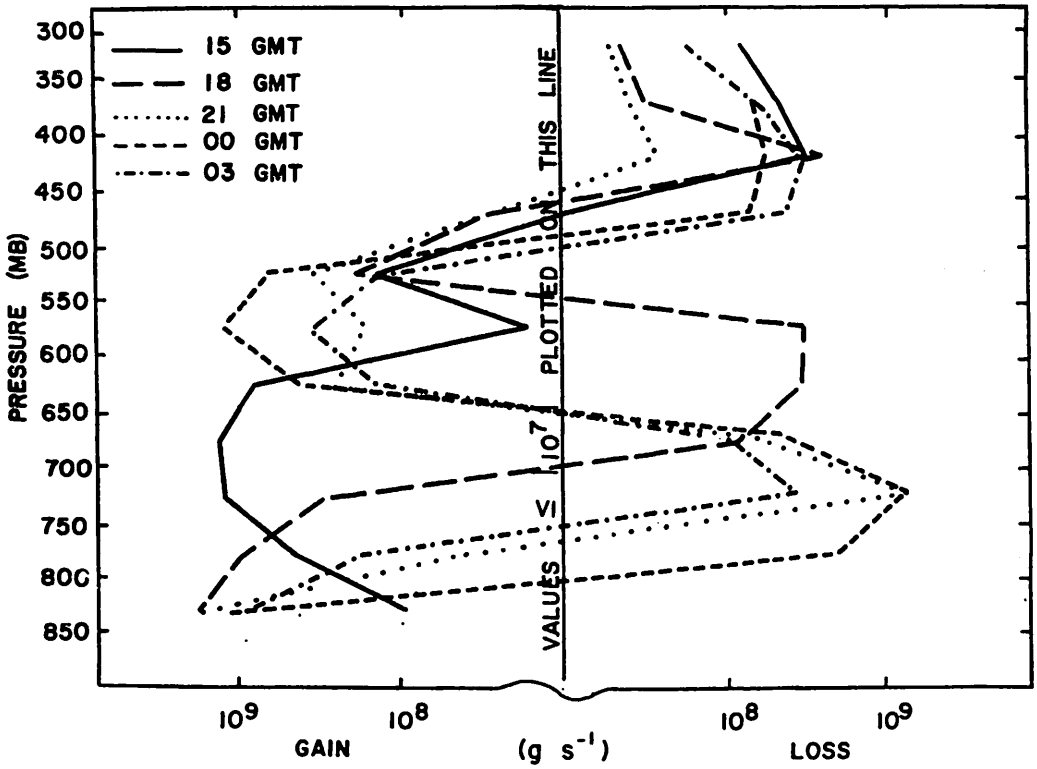

Fig. 5.4.5.1 Net horizontal transport of water vapor through boundaries of 50-mb layers (gm s^{-1}) over the Texas HIPLEX area for 5 June 1978.

Profiles of net vertical transport of water vapor (Fig. 5.4.5.2) show mostly gains above 800 mb. At 1500 GMT there was transport out of a layer near 650 mb. The profiles for 0000 and 0300 GMT show another slightly higher layer that experienced losses due to vertical transport.

The vertical transport of moisture through constant pressure surfaces (Fig. 5.4.5.3) was upward for all times this day. The largest values of this transport were at 0000 GMT when the echoes were strongest.

The profiles of combined net horizontal and vertical transport of water vapor (Fig. 5.4.5.4) show gains at nearly all levels below 500 mb with losses above. There are losses near the surface at 1500 GMT and at 625 mb at 0000 GMT. These losses are due to vertical transports of water vapor when horizontal convergence is not large enough to compensate for the vertical losses.

The profiles of total mass of water vapor (Fig. 5.4.5.5) reveal a dry layer near 650 mb at 1500 GMT. This dry layer weakens at 1800 GMT and is completely gone at 2100 GMT when low-level moisture is at a maximum.

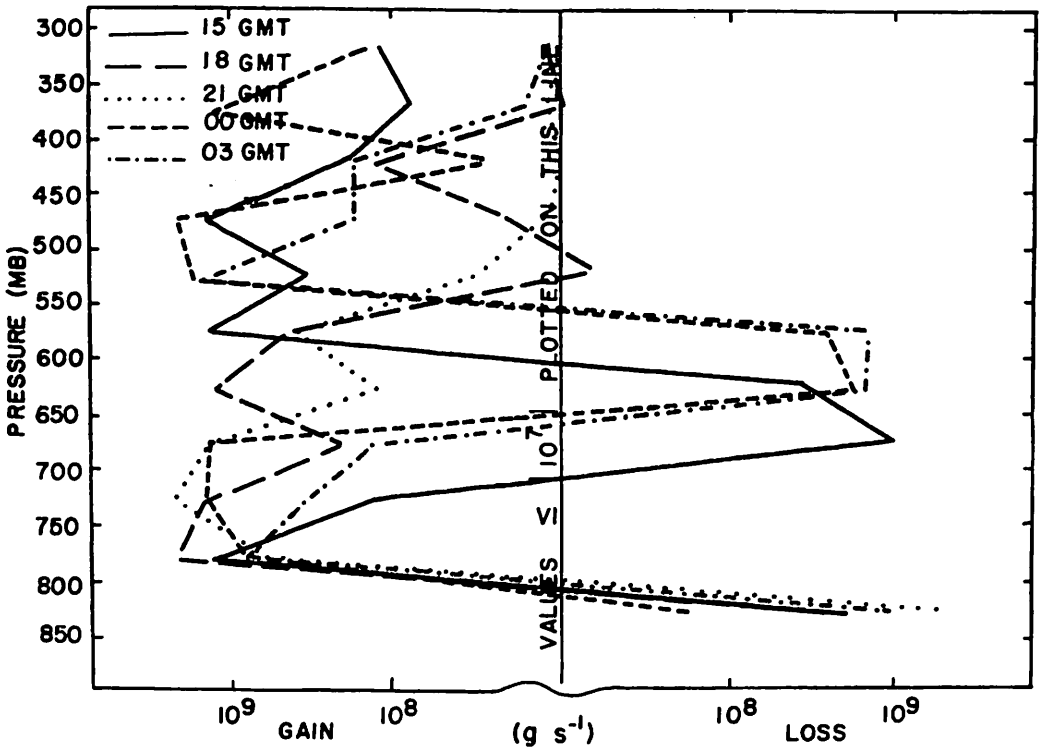

Fig. 5.4.5.2 Net vertical transport of water vapor through boundaries of 50-mb layers (gm s^{-1}) over the Texas HIPLEX area for 5 June 1978.

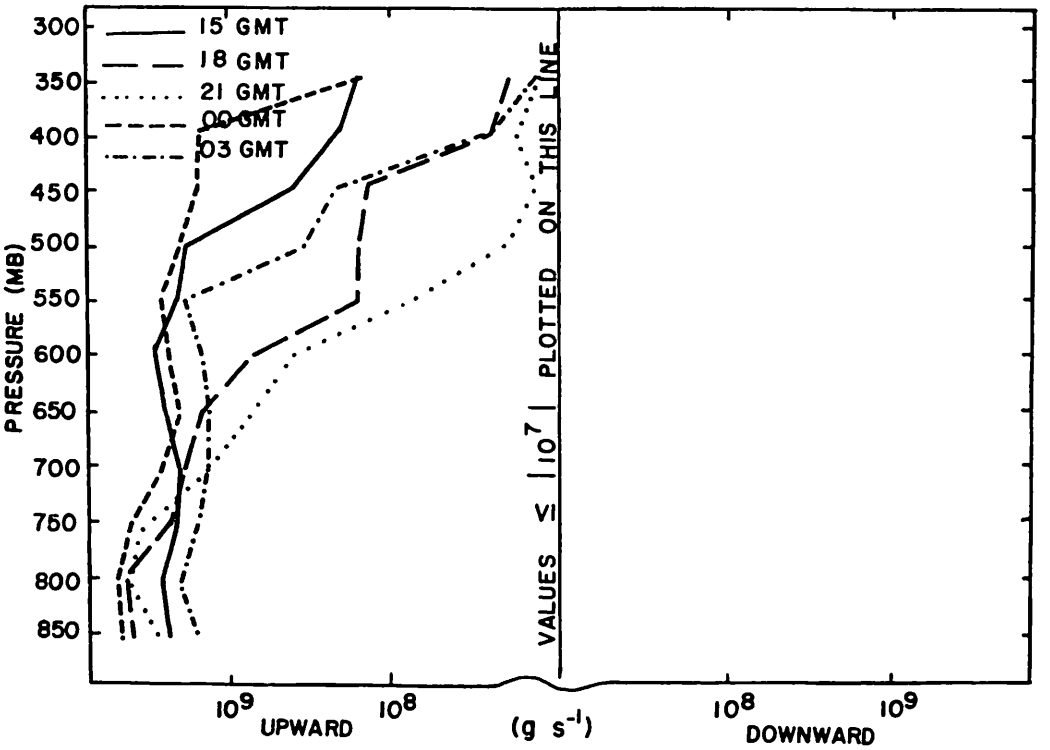

Fig. 5.4.5.3 Vertical transport of water vapor through constant pressure surfaces (gm s^{-1}) over the Texas HIPLEX area for 5 June 1978.

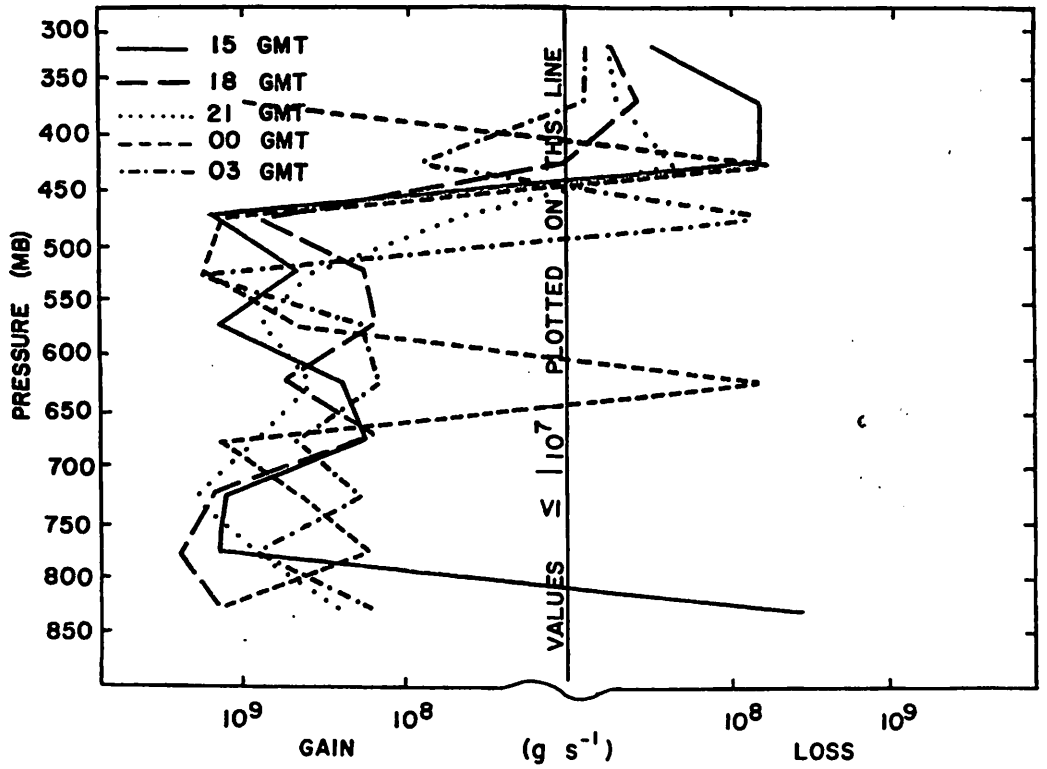

Fig. 5.4.5.4 Combined net horizontal and vertical transport of water vapor through boundaries of 50-mb layers (gm s^{-1}) over the Texas HIPLEX area for 5 June 1978.

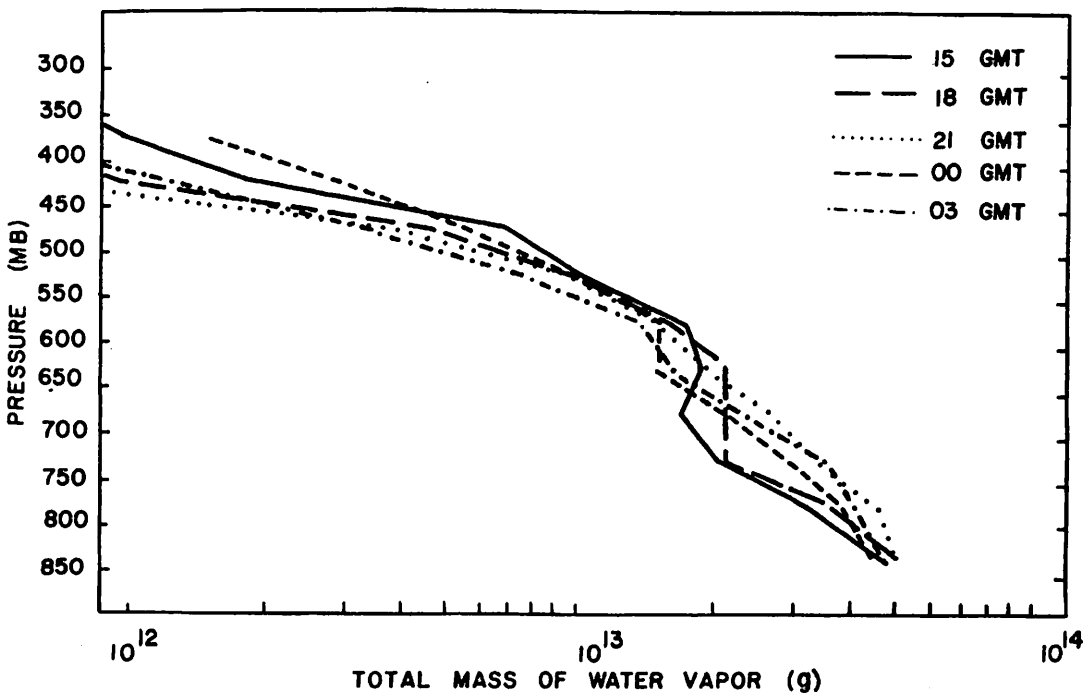

Fig. 5.4.5.5 Total mass of water vapor in layers 50 mb deep (gm) over the Texas HIPLEX area on 5 June 1978.

Profiles of the local rate-of-change of water vapor are shown in Fig. 5.4.5.6. Prior to 2100 GMT the mass of water vapor in lower levels increased and that in upper levels decreased. Between 2100 GMT and 0000 GMT, when some of the strongest activity took place, losses were present in lower layers with gains in upper layers. Between 0000 and 0300 GMT the activity moved out of the HIPLEX area and the lower layers again experienced gains and the upper layers losses.

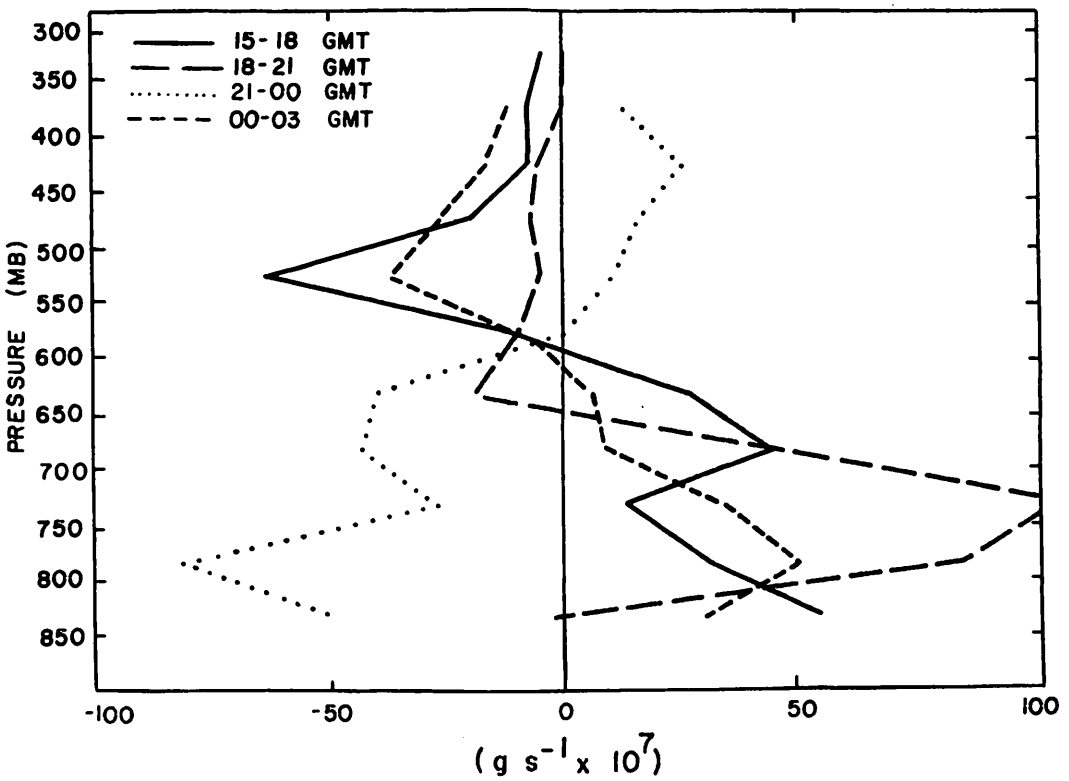

Fig. 5.4.5.6 Local rate-of-change in total mass of water vapor (g s^{-1} x 10^7) for the Texas HIPLEX area for 5 June 1978.

5.5 6 June 1978

5.5.1 Radar

At 1500 GMT most of the area was covered by showers (Fig. 5.5.1.1). There were two cells with heights in excess of 9.1 km (30K ft) at 1500 GMT; one south of Andrews, the other near Walsh-Watts. These cells either moved out of the area or dissipated by 1800 GMT. There was no significant activity after this until 0000 GMT, when a thunderstorm approached from the west and moved across the area. This storm also had heights in excess of 9.1 km.

5.5.2 Surface

The thundershowers early in the day were associated with low temperatures in the northwest at 1500 GMT and widespread cooling by 1700 GMT (Fig. 5.5.2.1). Temperatures rose after the storms moved out of the area, and a center of maximum temperature persisted near Walsh-Watts until 0300 GMT. At 0000 GMT cooling occurred in the western part of the area in association with the downdraft of the storms moving into the area at that time. The cooling had spread all across the area by 0300 GMT.

Dewpoint depressions (Fig. 5.5.2.2) were quite small early in the day when showers were in the area. The depressions increased during the day with the increase in temperature. The depressions decreased when showers again moved into the area at 0000 GMT.

Mixing ratios (Fig. 5.5.2.3) showed moderate values at the start of the day. As the showers moved out of the area, a maximum formed near Big Spring and remained there until 0000 GMT. A minimum was associated with the downdraft-induced cooling in the west at that time.

Patterns of surface equivalent potential temperature (Fig. 5.5.2.4) were similar to those of mixing ratio. A maximum was near Big Spring until 0000 GMT. A minimum associated with the storm formed in the west at 0000 GMT. Equivalent potential temperatures dropped all across the area as the storms moved through after 0000 GMT.

The terrain-induced vertical motions (Fig. 5.5.2.5) were of moderate values. They showed no persistent patterns throughout the day.

The surface velocity divergence (Fig. 5.5.2.6) showed large values at 1500 GMT. Strong convergence associated with a strong thunderstorm cell was present between Walsh-Watts and Tahoka. Strong divergence was located to the northwest of the cell. Patterns of divergence shifted as the cells moved across the area.

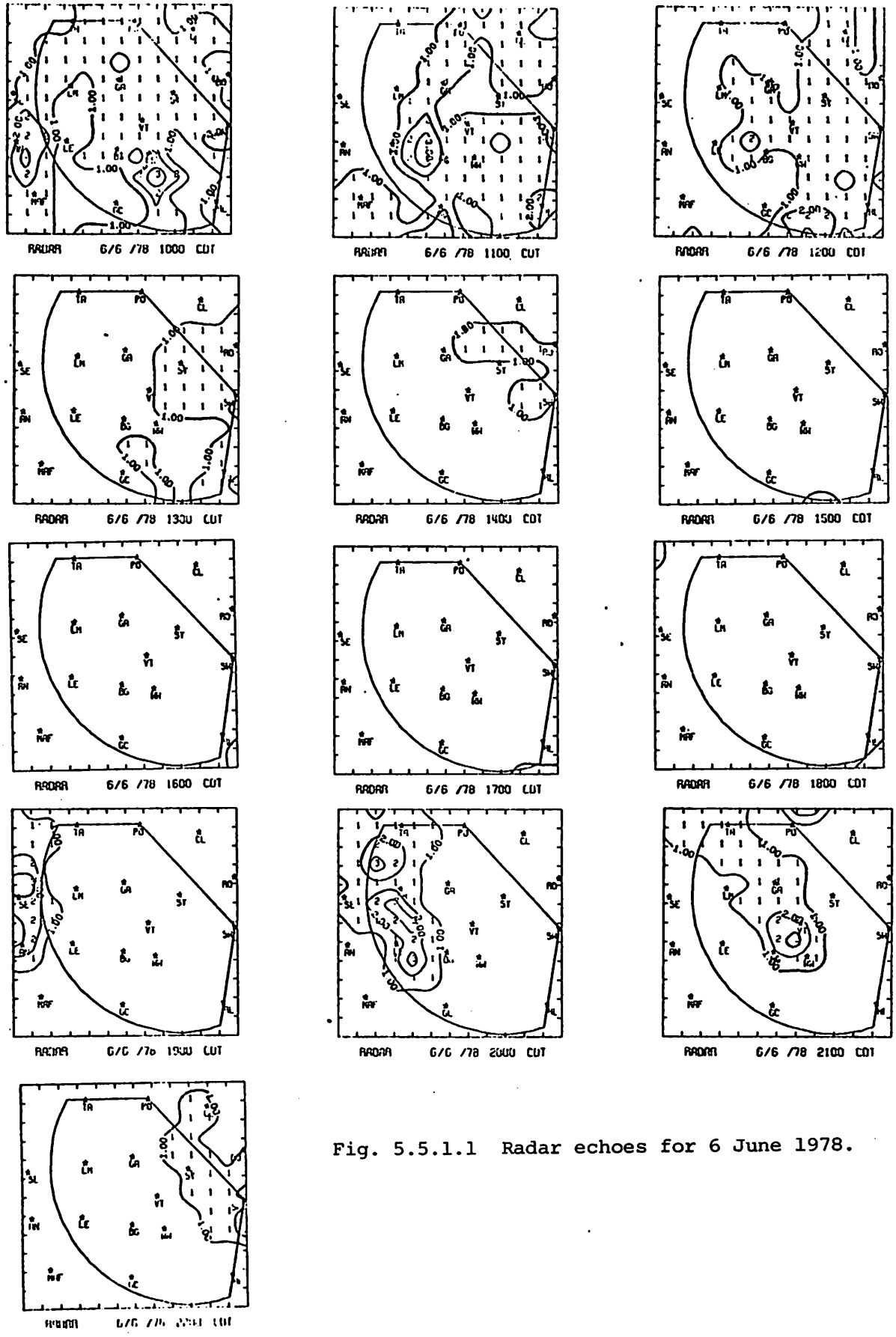

Fig. 5.5.1.1 Radar echoes for 6 June 1978.

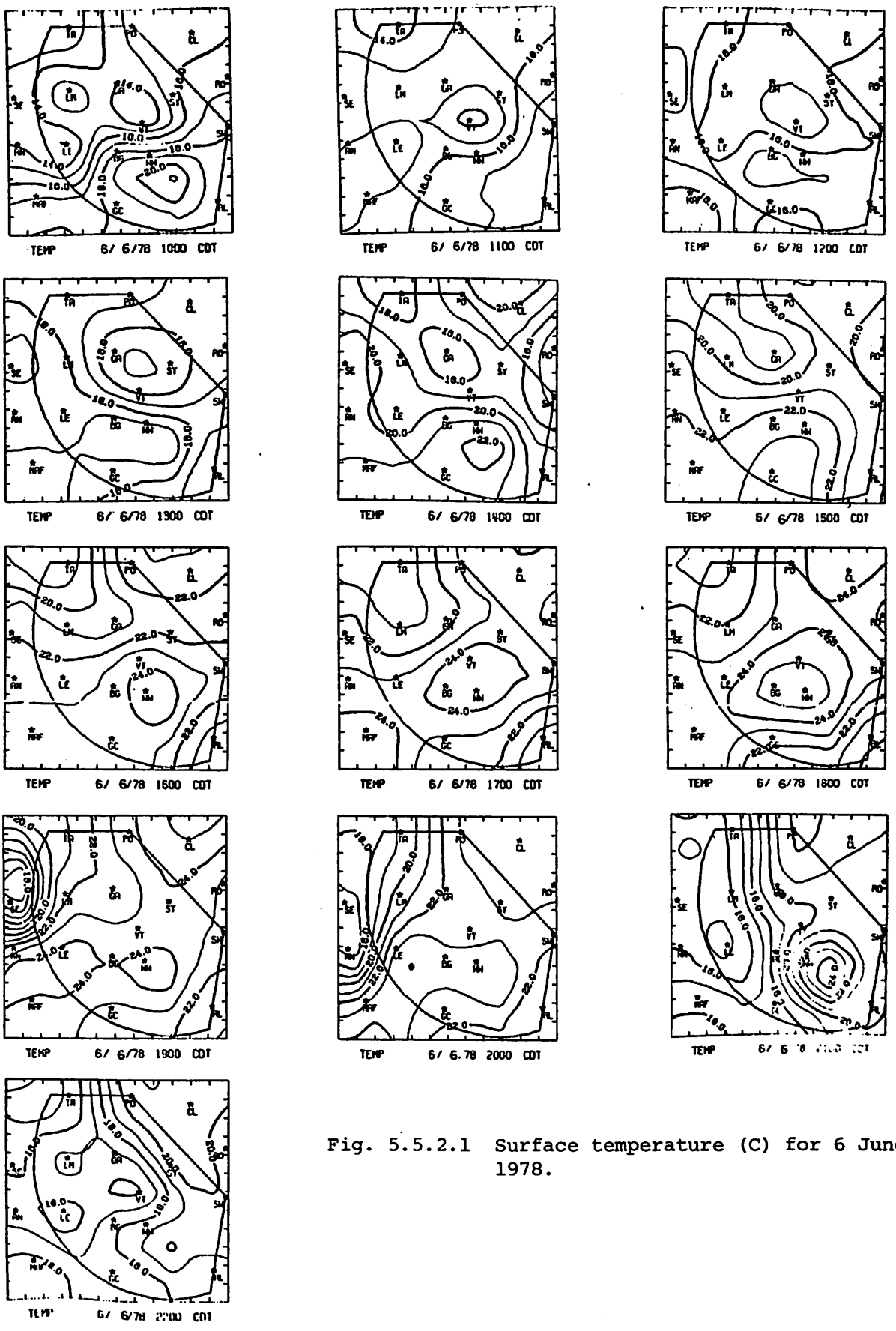

Fig. 5.5.2.1 Surface temperature (C) for 6 June 1978.

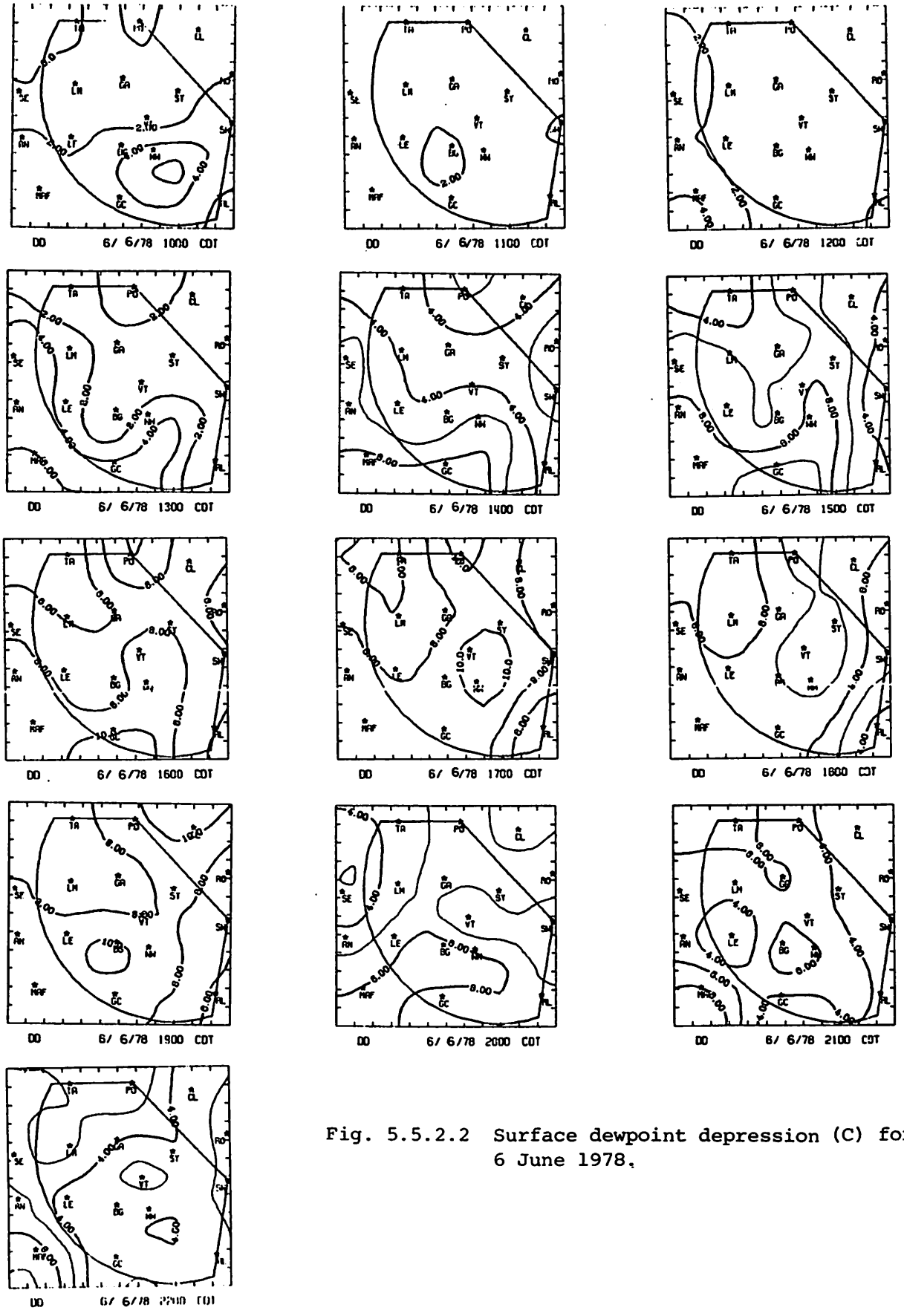

Fig. 5.5.2.2 Surface dewpoint depression (C) for 6 June 1978.

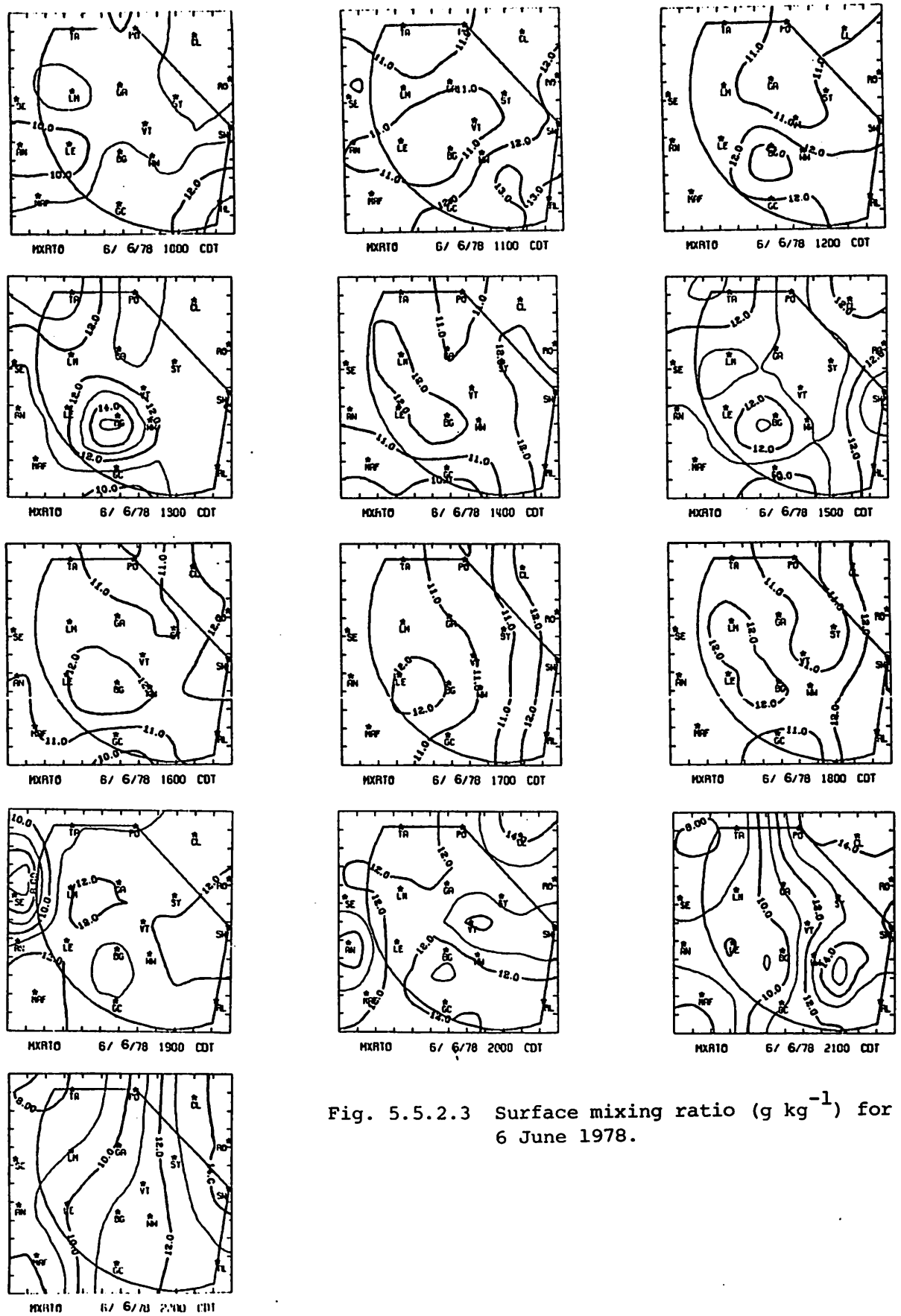

Fig. 5.5.2.3 Surface mixing ratio (g kg^{-1}) for 6 June 1978.

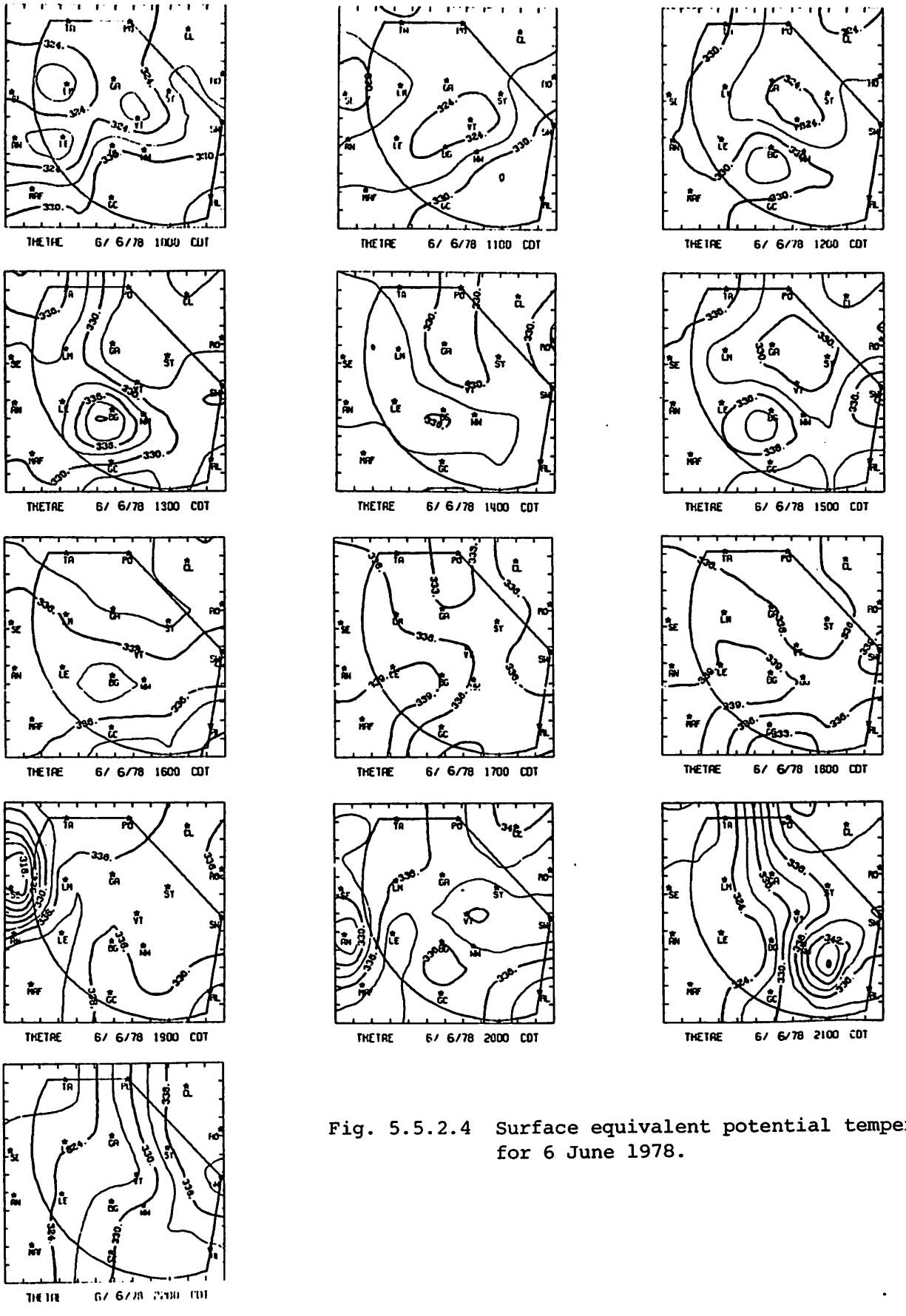

Fig. 5.5.2.4 Surface equivalent potential temperature (K) for 6 June 1978.

Fig. 5.5.2.5 Terrain-induced vertical motion (cm s^{-1}) for 6 June 1978.

Fig. 5.5.2.6 Surface velocity divergence (s^{-1} x 10^{-6}) for 6 June 1978.

At 1800 GMT when the cells were moving out of the area the magnitudes at the centers had decreased. Convergence developed along and south of a line from Midland to Clairemont at 2300 GMT and persisted until 0200 GMT. The convergence was along the eastern edge of a strong thunderstorm at 0200 GMT, and there was strong divergence just to the west of the storm.

Vertical motion 50 mb above the surface (Fig. 5.5.2.7) showed patterns similar to those of the divergence. Strongest upward motions were just to the west of the cell near Walsh-Watts at 1500 GMT, and strong downward motions were to the northwest. Upward motion was present between Andrews and Midland for three hours before a storm moved into that area at 0000 GMT. As the storm moved across the HIPLEX area, downward motion was present to the west of the storm and was strongest at 0200 GMT. Strong upward motion was present in the eastern part of the storm along the leading edge at 0200 GMT.

Surface moisture divergence (Fig. 5.5.2.8) was strong at 1500 GMT between Vincent and Gail. Strong convergence was present between Garden City and Walsh-Watts. The moisture divergence centers remained fairly strong between 1500 GMT and 1800 GMT, when showers were moving out of the area. There was some strong moisture convergence between 0000 GMT and 0300 GMT associated with the storm passing through at that time but this was not as strong as at 1500 GMT.

Vertical flux of moisture 50 mb above the surface (Fig. 5.5.2.9) was strongest at 1500 GMT. A strong center of upward flux was associated with a strong cell south of Walsh-Watts and strong downward flux was present to the northwest of the cell. The magnitude of the vertical flux decreased after this though strong downward flux was present at 1700 GMT and 1800 GMT as showers left the area. Moderate values prevailed over the area until 2200 GMT, when a strong center of upward flux was present between Andrews and Midland two hours before storms moved into that area. An axis of upward moisture flux formed between Midland and Clairemont. At 2300 GMT, this axis remained in the central part of the area until 0200 GMT when the upward flux was generally along the eastern edge of the storm with strong downward flux to the west.

The surface vorticity fields (Fig. 5.5.2.10) show a strong center of negative vorticity at 1500 GMT to the northwest of the large cell located near Walsh-Watts. Another negative center was south of Andrews where another strong storm cell was located. The magnitude of the vorticity decreased at 1600 and 1700 GMT but the magnitudes increased again at 1800 GMT. Strong centers of

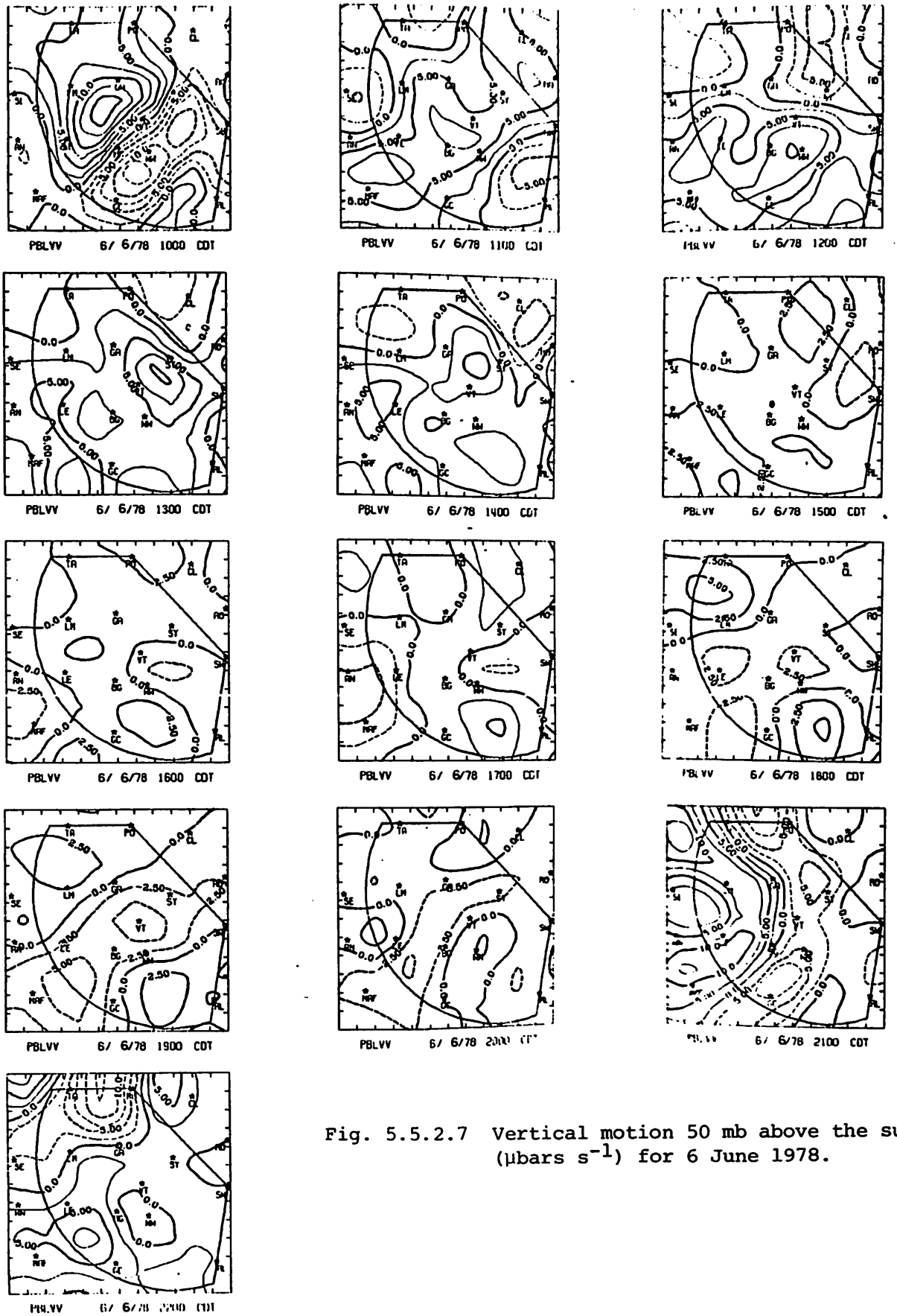

Fig. 5.5.2.7 Vertical motion 50 mb above the surface (μbars s^{-1}) for 6 June 1978.

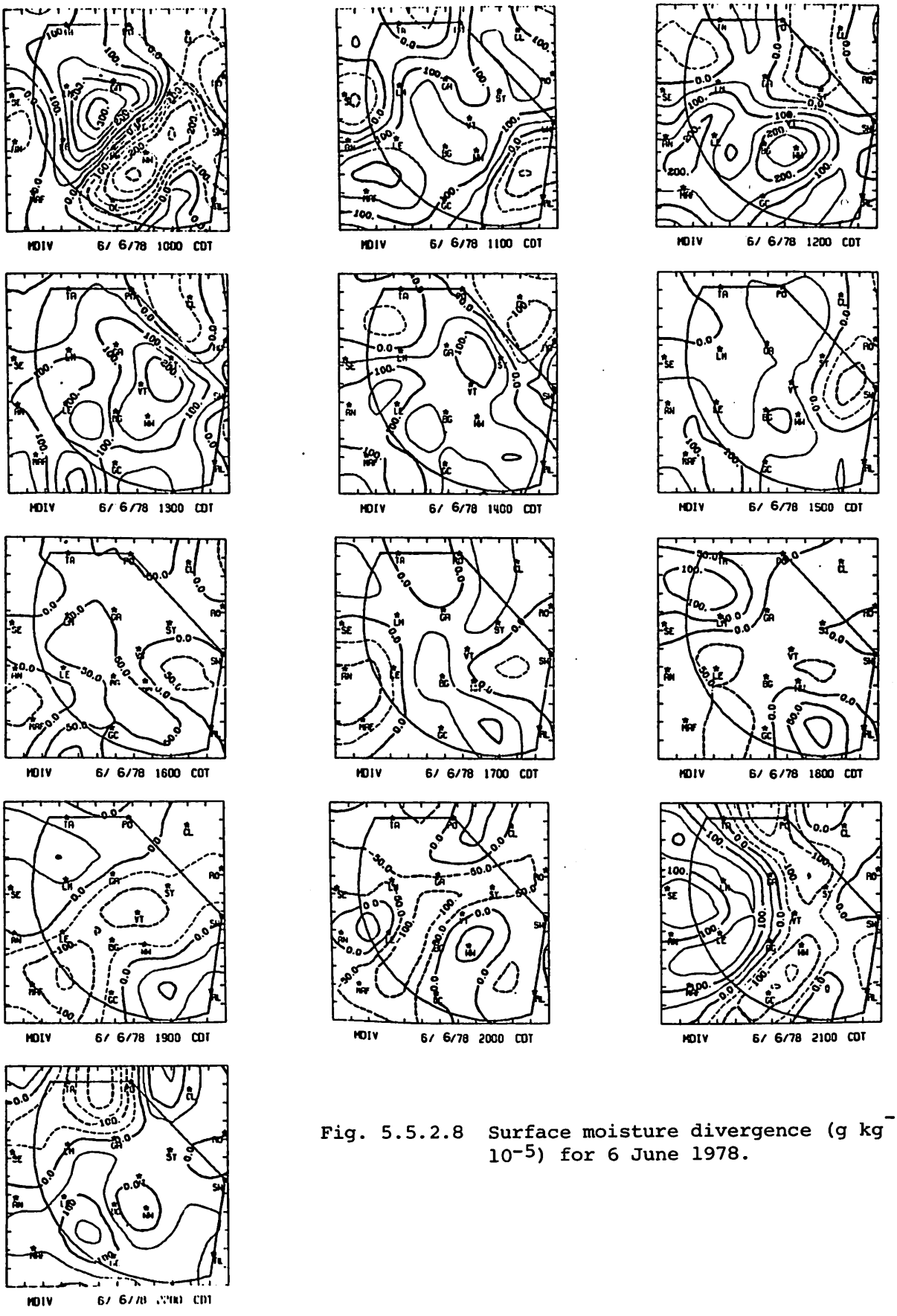

Fig. 5.5.2.8 Surface moisture divergence (g kg^{-1} s^{-1} x 10^{-5}) for 6 June 1978.

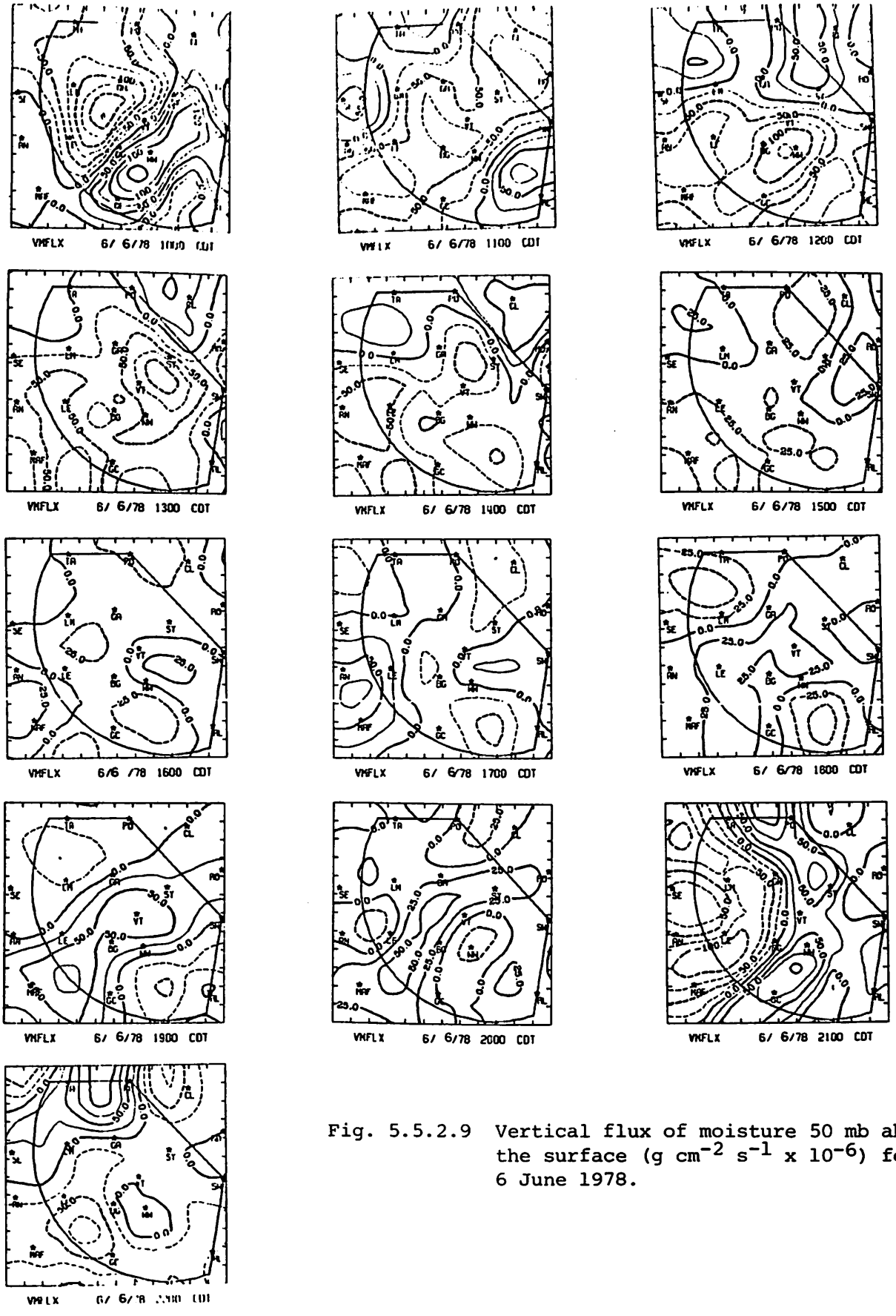

Fig. 5.5.2.9 Vertical flux of moisture 50 mb above the surface (g cm^{-2} s^{-1} x 10^{-6}) for 6 June 1978.

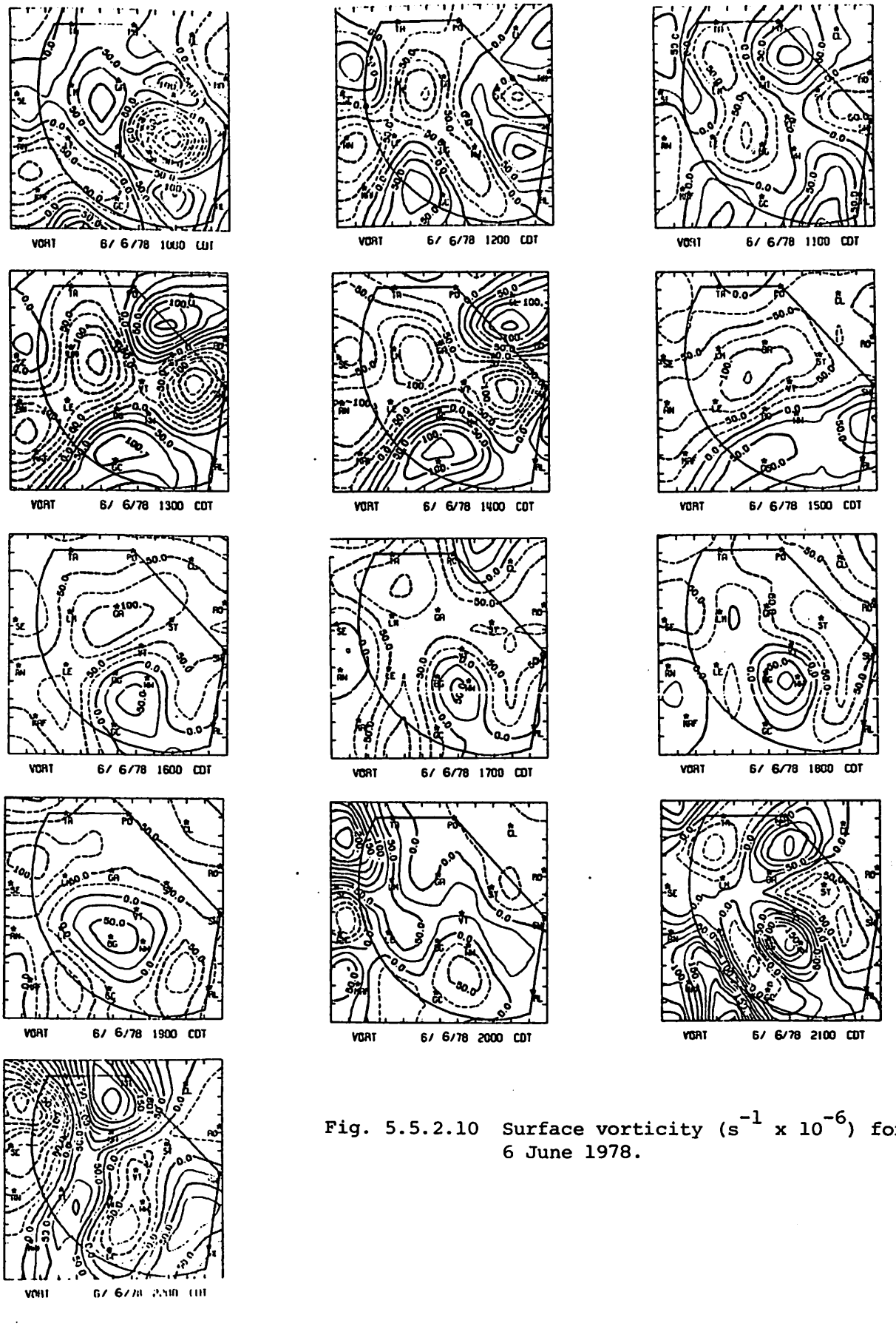

Fig. 5.5.2.10 Surface vorticity (s^{-1} x 10^{-6}) for 6 June 1978.

anticyclonic vorticity were present at 1800 and 1900 GMT as storms were leaving the area. The vorticity remained moderate between 2000 and 0000 GMT. At 0100 GMT strong centers developed in the west in association with the storms moving in at that time.

Figure 5.5.2.11 shows charts of surface pressure change. At 1600 GMT there was a pressure drop of 1.7 mb at Post as showers were leaving that area. Rises occurred in the eastern part of the area with the strong rise of 2.4 mb at Rotan. At 1900 GMT there was a strong pressure drop of 2.8 mb at Rotan. Showers were leaving the HIPLEX area at that time. Pressure falls took place over most of the area from 2000 GMT to 2300 GMT. At 0000 GMT pressure rises began in the west as storms moved into that area. Pressure rises took place all through the area after that time, except at 0200 GMT to the west of the storm where small pressure drops were noted.

Surface winds (Fig. 5.5.2.12) were generally northerly at 1500 GMT, except for east winds near Clairemont and south winds near Robert Lee. As the storms moved out of the area, the winds shifted to easterlies in the southern part of the area and to southerly in the northern part at 1800 GMT. By 2200 GMT winds were mostly southeasterly and generally light. At 0100 GMT strong westerly winds followed the passage of the storm cell, and by 0300 GMT winds were mostly from the west and northwest.

5.5.3 Upper Level Kinematic Parameters

At 1500 GMT although only part of the profile is shown, strong convergence was present to 700 mb (Fig. 5.5.3.1). This occurred at the time of greatest convective activity. The echo coverage was decreasing at 1800 GMT to almost nothing at 2100 GMT. At these times there was considerable divergence to 650 mb and convergence above to 500 mb. Generally weak divergence was present in the upper layers. At 0000 GMT, with shower activity again moving into the HIPLEX area, there was convergence below 800 mb and above 400 mb. Most of the profiles for 0300 GMT were not available.

The vertical motion profiles (Fig. 5.5.3.2) for 1800 GMT and 2100 GMT show mainly downward motion. The largest values were present at 1800 GMT when the storms were leaving the area or dissipating. Profiles for 1500, 0000, and 0300 GMT are not shown.

Strong moisture convergence (Fig. 5.5.3.3) was present below 700 mb at 1500 GMT, but this was replaced by moisture divergence through most levels at

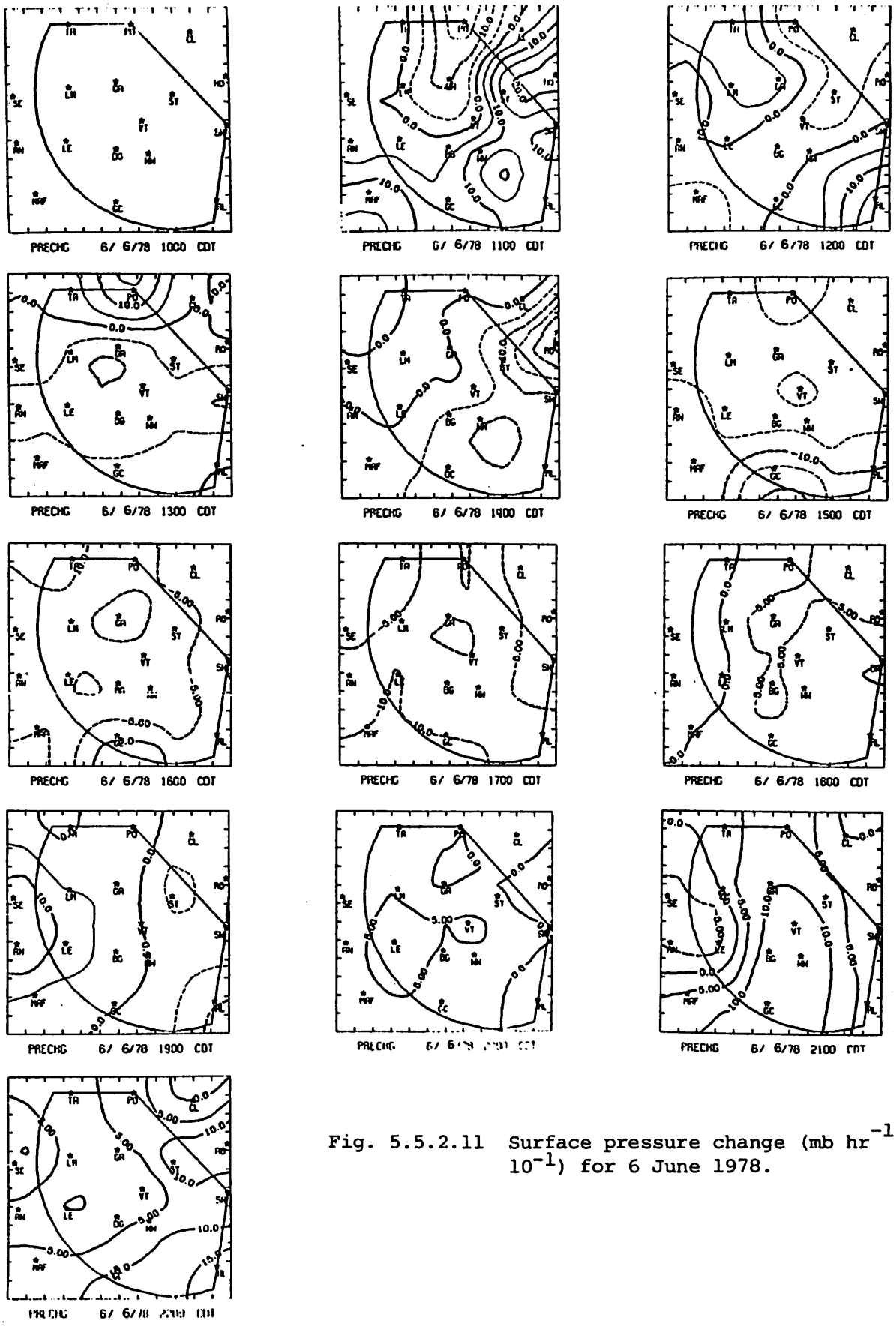

Fig. 5.5.2.11 Surface pressure change (mb hr^{-1} x 10^{-1}) for 6 June 1978.

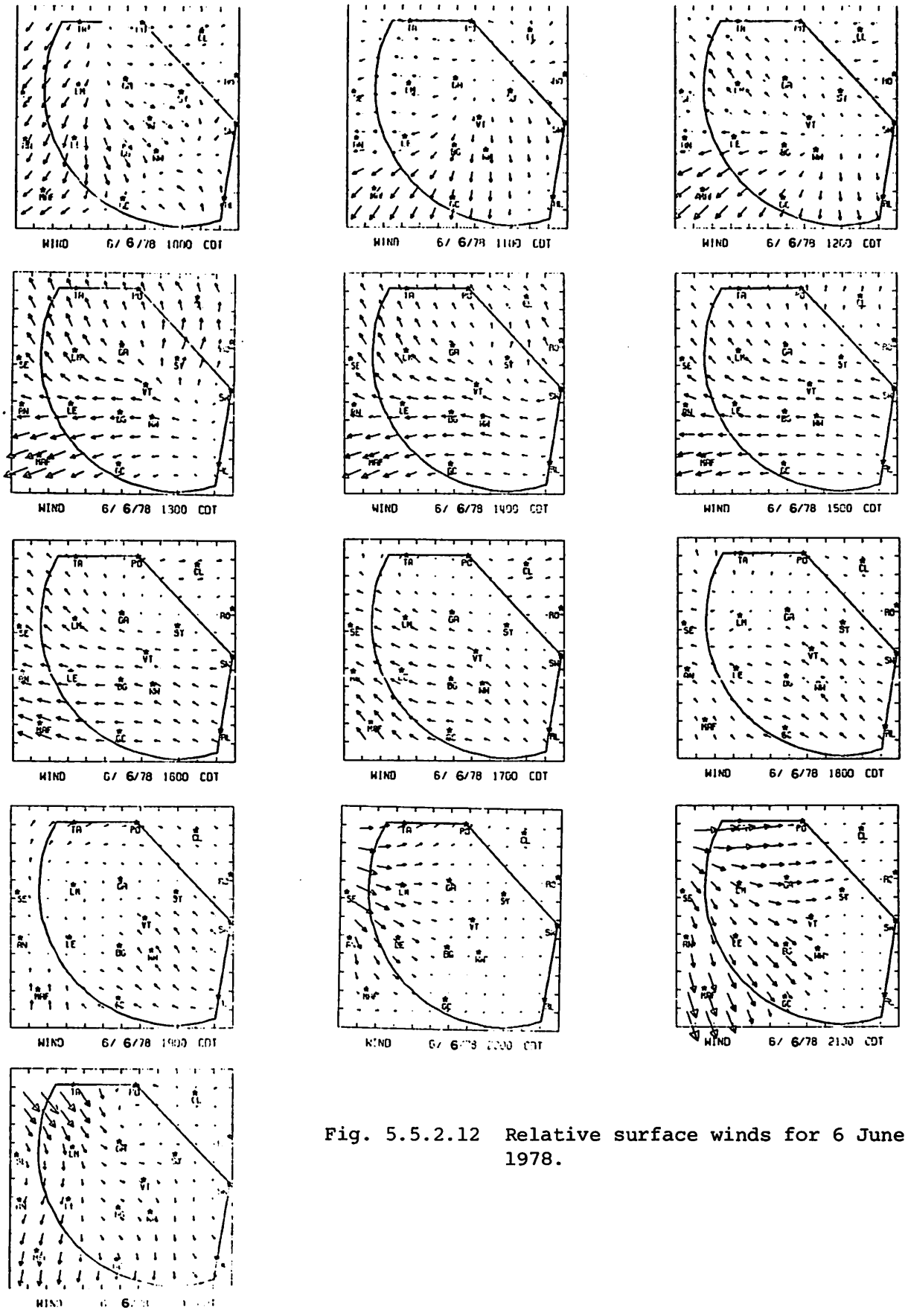

Fig. 5.5.2.12 Relative surface winds for 6 June 1978.

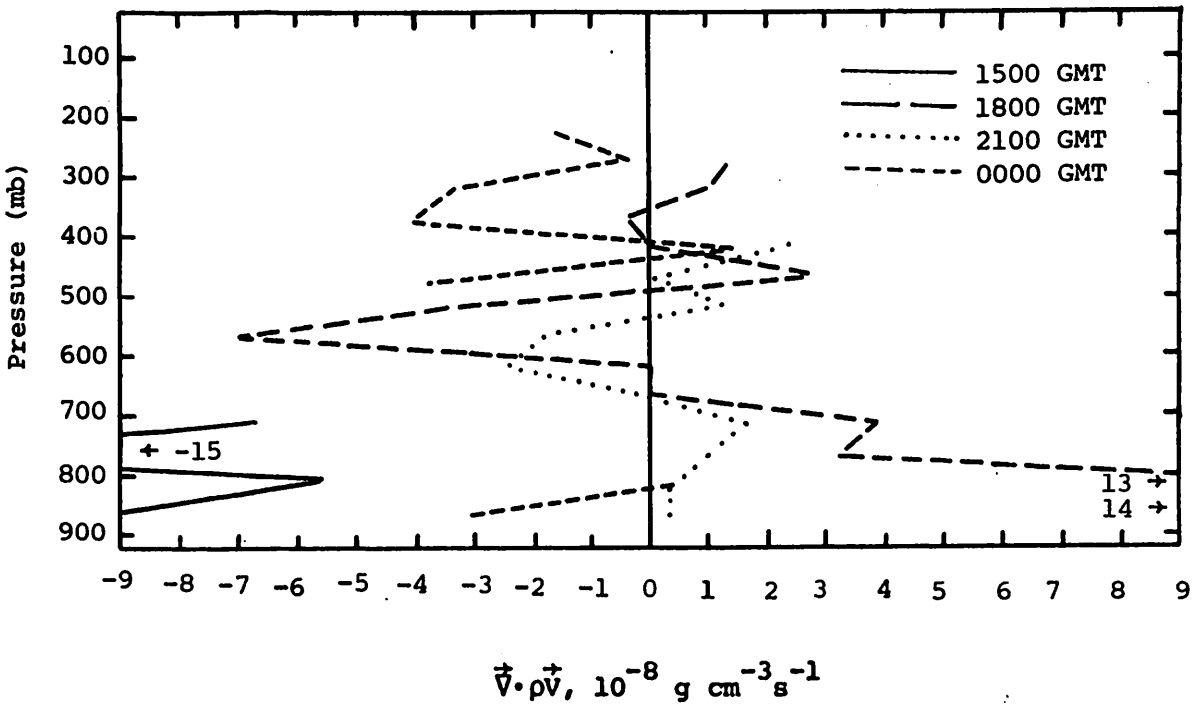

Fig. 5.5.3.1 Vertical profiles of mass divergence on 6 June 1978.

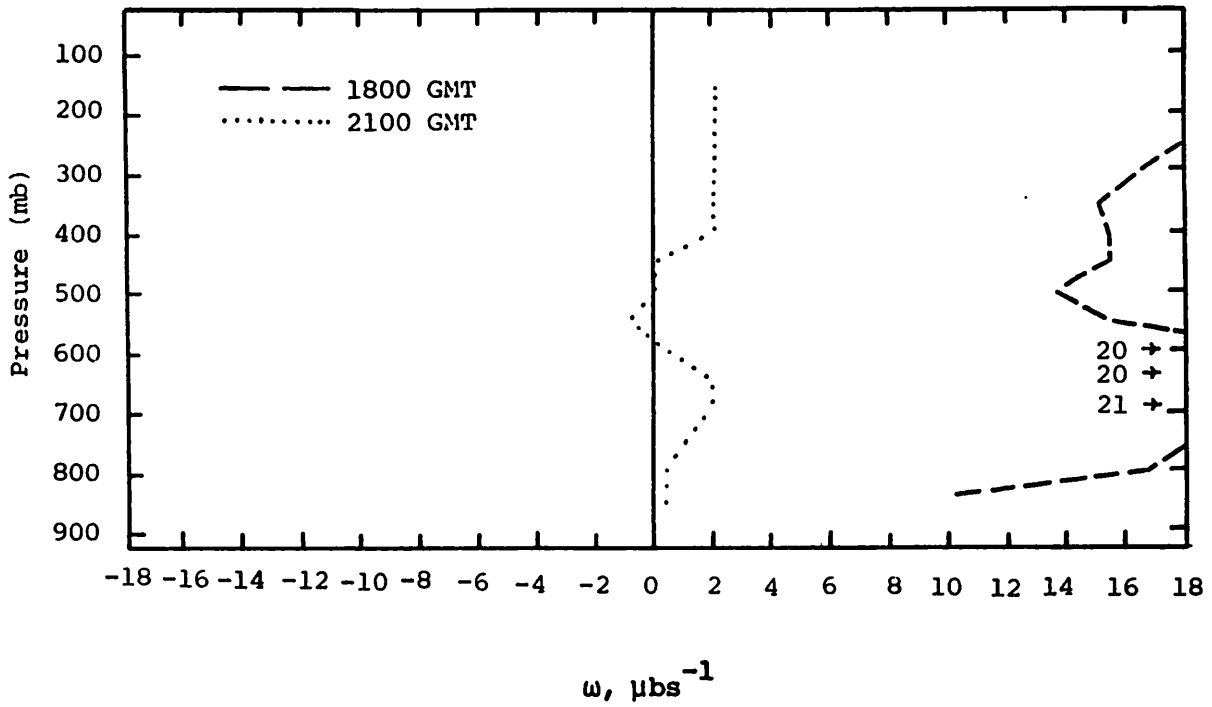

Fig. 5.5.3.2 Vertical profiles of vertical motion on 6 June 1978.

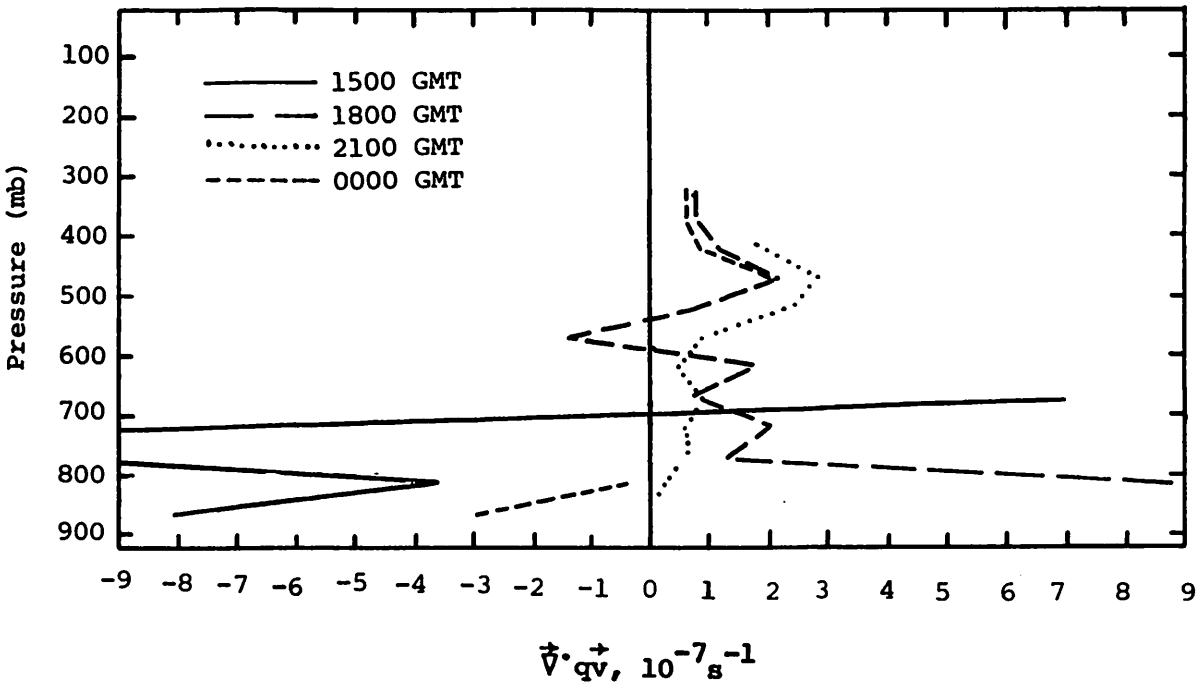

Fig. 5.5.3.3 Vertical profiles of moisture divergence on 6 June 1978.

1800 GMT. The magnitude of the divergence decreased below 600 mb at 2100 GMT. At 0000 GMT with the return of showers to the area, moisture convergence resumed at low levels.

5.5.4 Energetics

Horizontal inflow of latent heat energy below 700 mb was present at 1500 GMT with outflow above (Fig. 5.5.4.1). This profile was not complete above 700 mb. At 1800 and 2100 GMT, with shower activity at a minimum, there was outflow of latent heat at most levels. By 0000 GMT latent heat inflow resumed near the surface.

The profiles of vertical flux of latent heat (Fig. 5.5.4.2) together with profiles of vertical motion (Fig. 5.5.3.2) show latent heat transport from middle layers to lower layers of the atmosphere at 1800 and 2100 GMT. The effect was greatest at 1800 GMT, a time when the radar echoes were disappearing. Other profiles were unavailable.

Profiles of the local rate-of-change of latent heat (Fig. 5.5.4.3) show increases below 700 mb and decreases above that level at the first three time periods. At 0000 GMT latent heat energy was decreasing at all levels, while at 0300 GMT latent heat was decreasing at all levels except near 650 mb.

The profiles of the residual term of latent heat (Fig. 5.5.4.4) show large negative values at 1800 and 2100 GMT. These may correspond to the evaporation

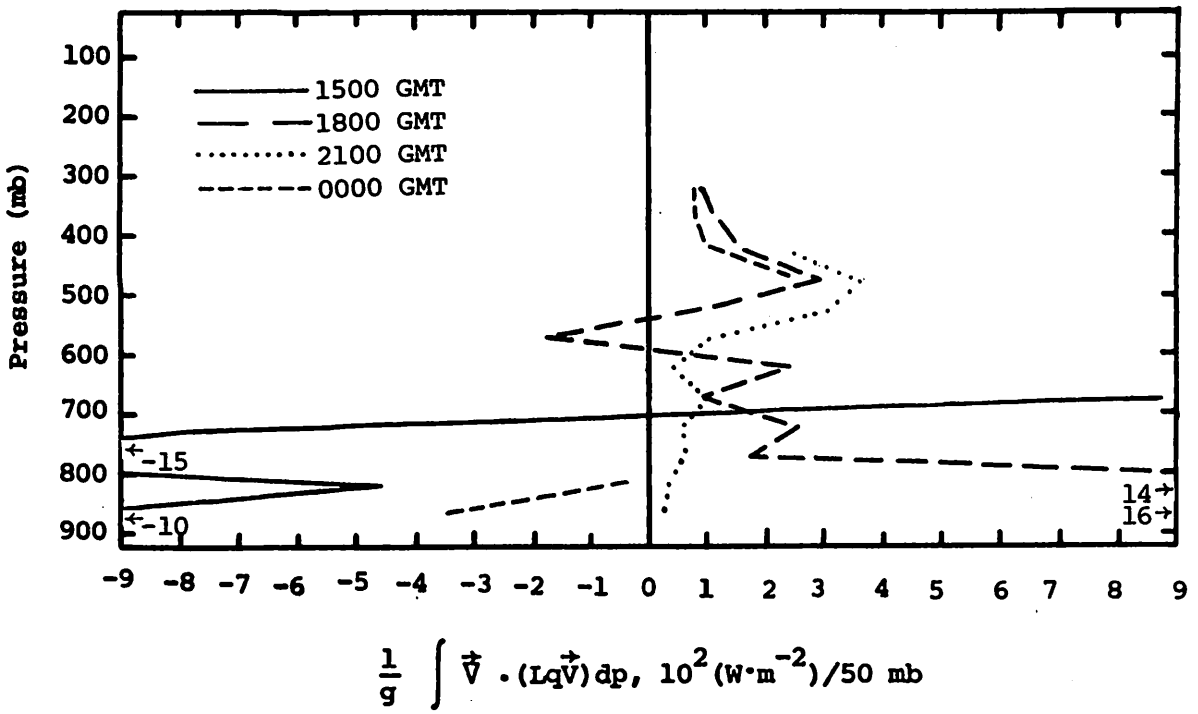

Fig. 5.5.4.1 Vertical profiles of the horizontal flux of latent heat on 6 June 1978.

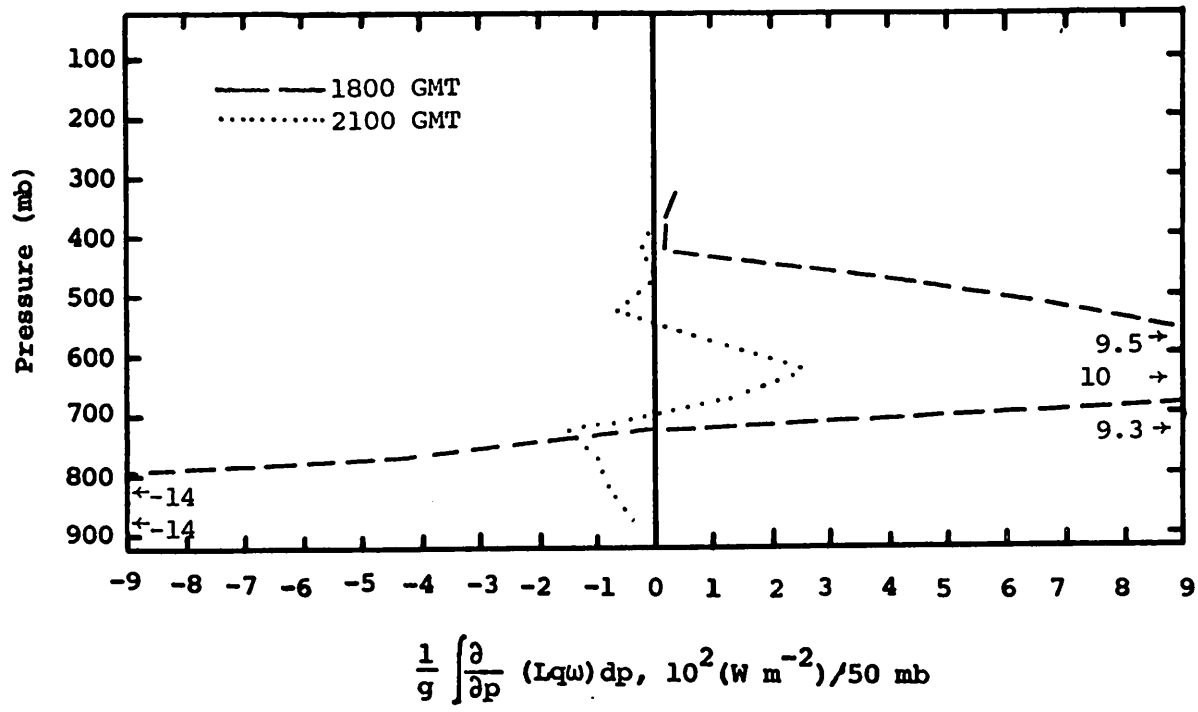

Fig. 5.5.4.2 Vertical profiles of the vertical flux of latent heat on 6 June 1978.

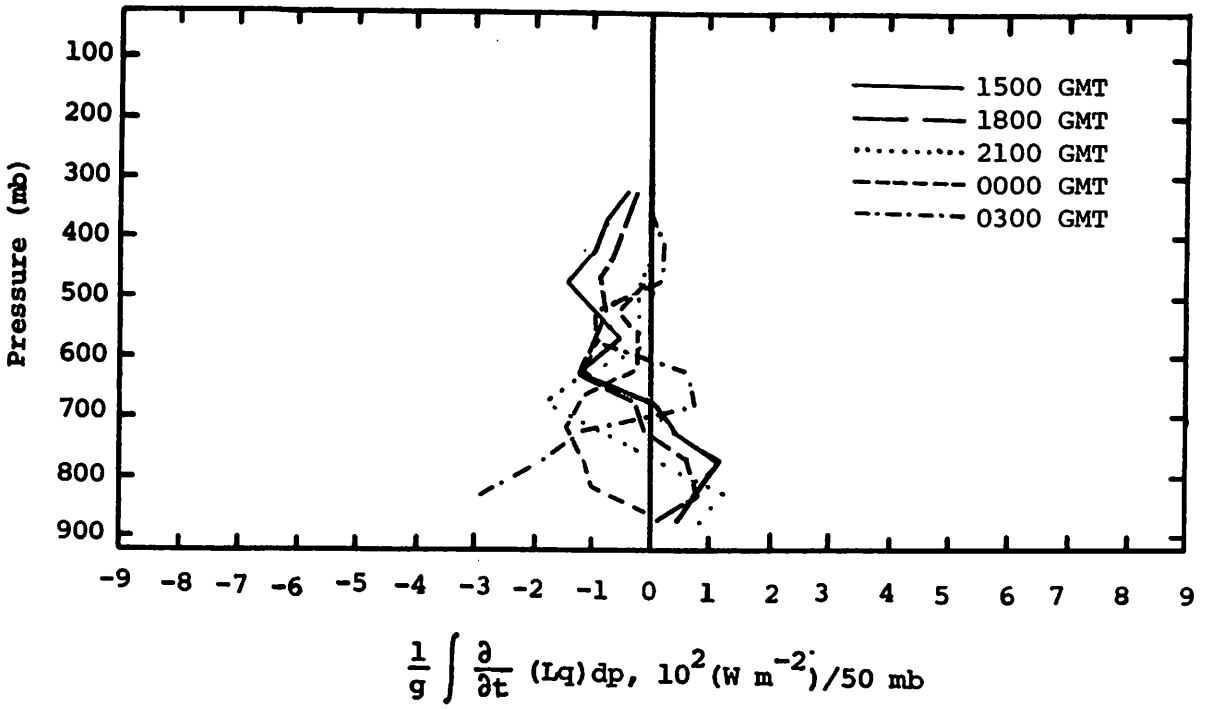

Fig. 5.5.4.3 Vertical profiles of the local change of latent heat on 6 June 1978.

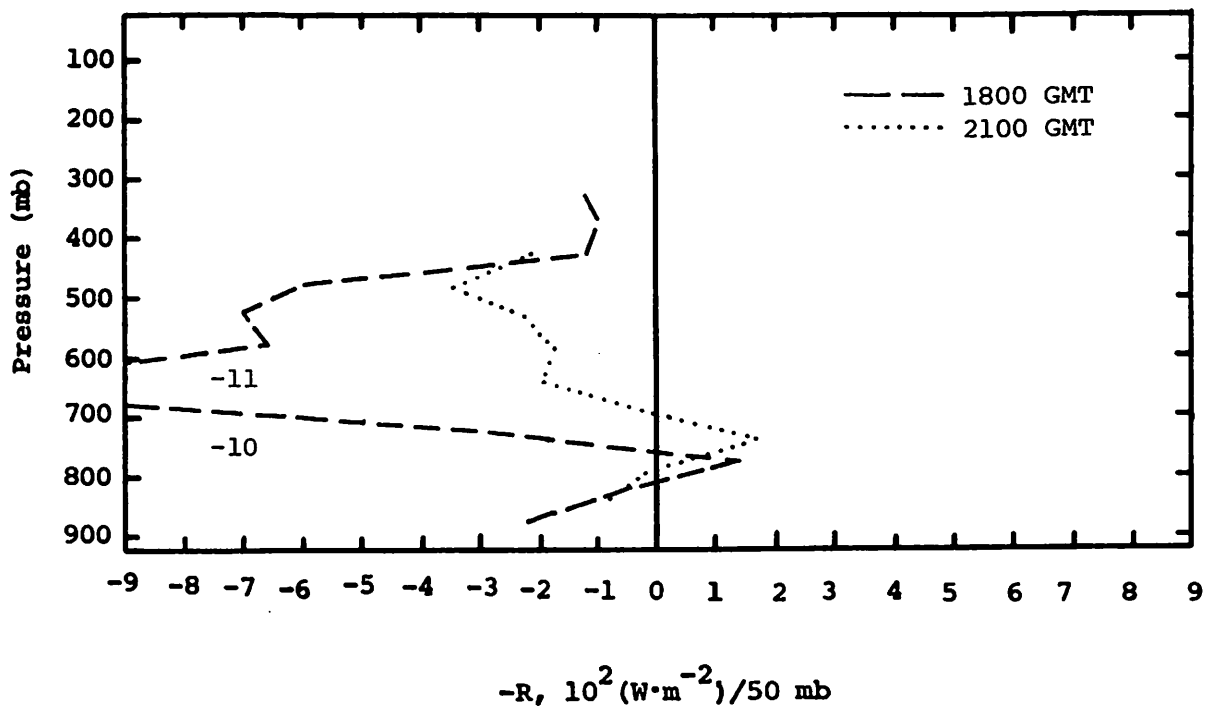

Fig. 5.5.4.4 Vertical profiles of the residual of the latent heat energy equation on 6 June 1978.

of cloud droplets taking place at these times.

The negative values shown in the profiles of diabatic heating (Fig. 5.5.4.5) at 1800 and 2100 GMT could result from cooling by the evaporation indicated in the residual of the latent heat budget.

Figure 5.5.4.6 shows profiles of horizontal flux of kinetic energy. The incomplete profile for 1500 GMT shows inflow below 700 mb which corresponds to the convergence shown in Figure 5.5.3.1. The profiles at 1800 and 2100 GMT are similar except the magnitudes of the terms are much less at 2100 GMT. These profiles indicate low-level outflow of kinetic energy and layers of inflow near 550 and 300 mb.

The profiles of vertical flux of kinetic energy (Fig. 5.5.4.7) show that, at 1800 GMT with downward vertical motion prevailing, there was transport of kinetic energy downward from the upper layers near the jet stream to below 200 mb. Also, there were large values of transport from a layer near 500 mb into layers below. Values of transport were small at 2100 GMT in lower levels but became large above 450 mb. Other profiles are not shown.

5.5.5 Water Vapor Budget

In this section, profiles were only available for 1800 and 2100 GMT. Figure 5.5.5.1 shows profiles of the net horizontal transport of water vapor. At 1800 GMT there were losses in upper and lower levels and gains in middle levels. The profile at 2100 GMT is similar except for gains in water vapor in the lowest levels.

The profiles of net vertical transport (Fig. 5.5.5.2) show gains in lower layers and mostly losses in upper layers at 1800 and 2100 GMT. The gain just below 500 mb at 2100 GMT seems to fit with the upward transport through constant pressure surfaces at 550 mb indicated in Fig. 5.5.5.3. Downward transport of water vapor was present at all other levels.

The profiles of combined net horizontal and vertical transport at 1800 and 2100 GMT (Fig. 5.5.5.4) show gains only in lower layers with losses above. The water vapor gains at 2100 GMT took place through a thicker layer than at 1800 GMT.

The profiles of total mass of water vapor (Fig. 5.5.5.5) show no exceptionally dry layers at either time. The drying in middle layers is also shown in the profile of the local rate-of-change (Fig. 5.5.5.6).

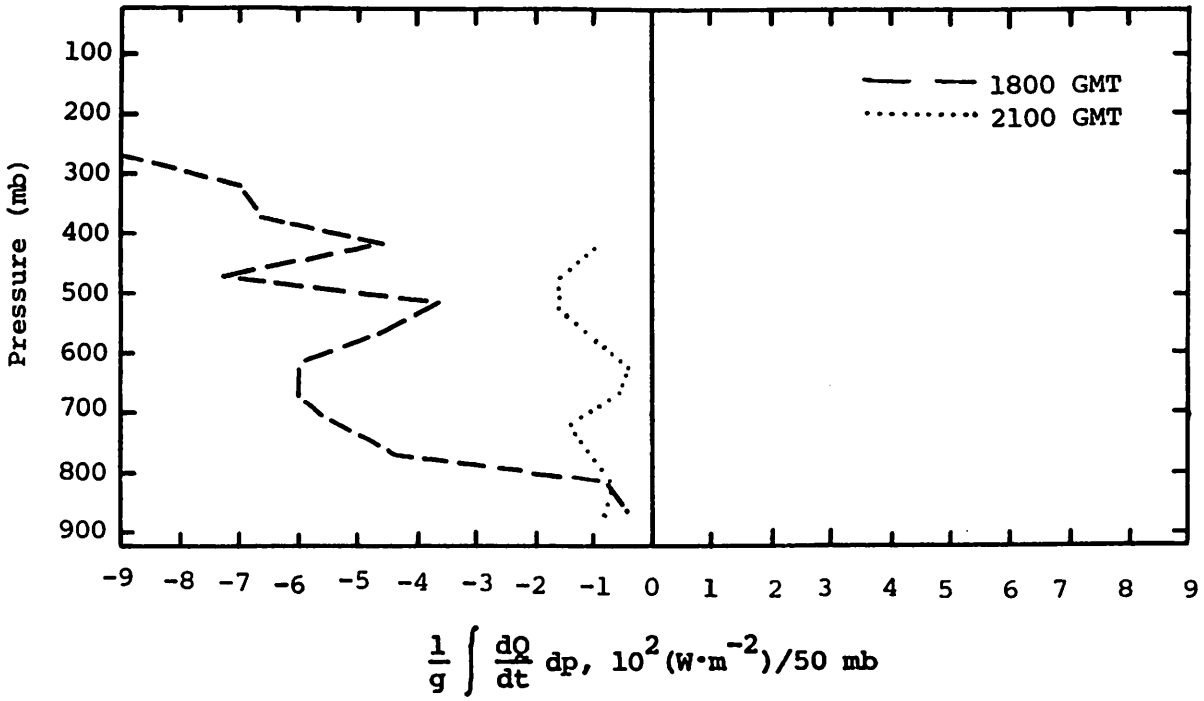

Fig. 5.5.4.5 Vertical profiles of diabatic heating computed from the first law of thermodynamics on 6 June 1978.

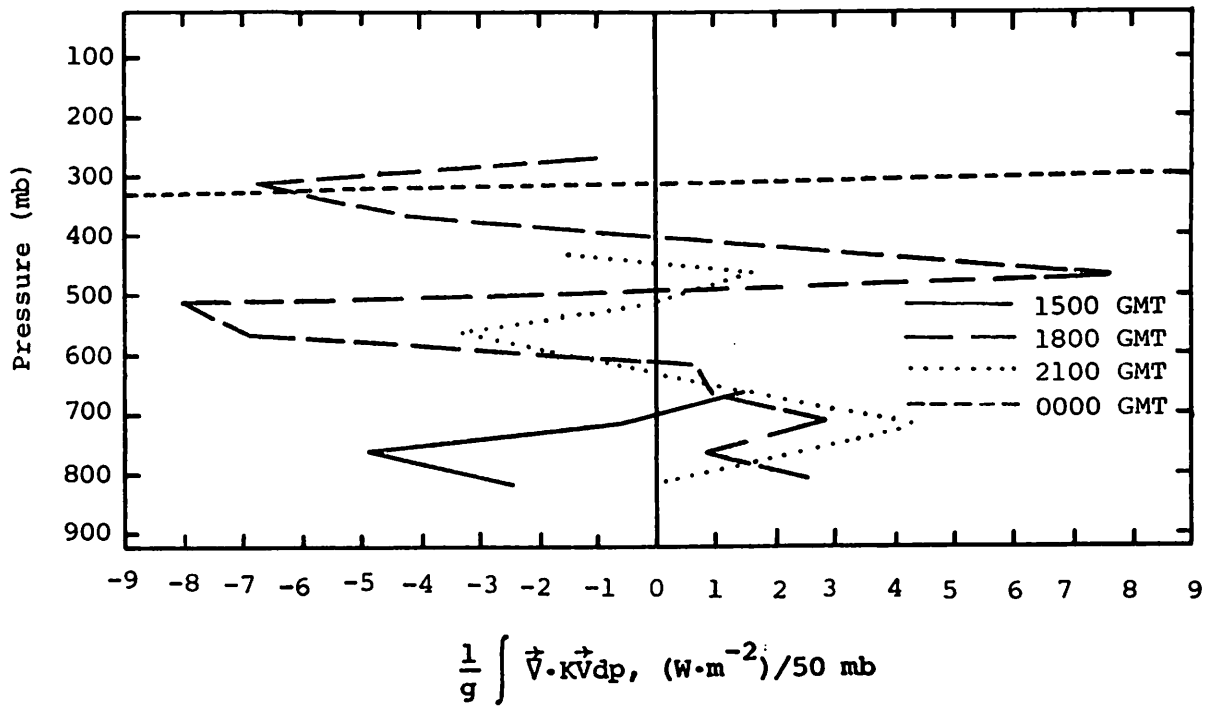

Fig. 5.5.4.6 Vertical profiles of the horizontal flux of kinetic energy on 6 June 1978.

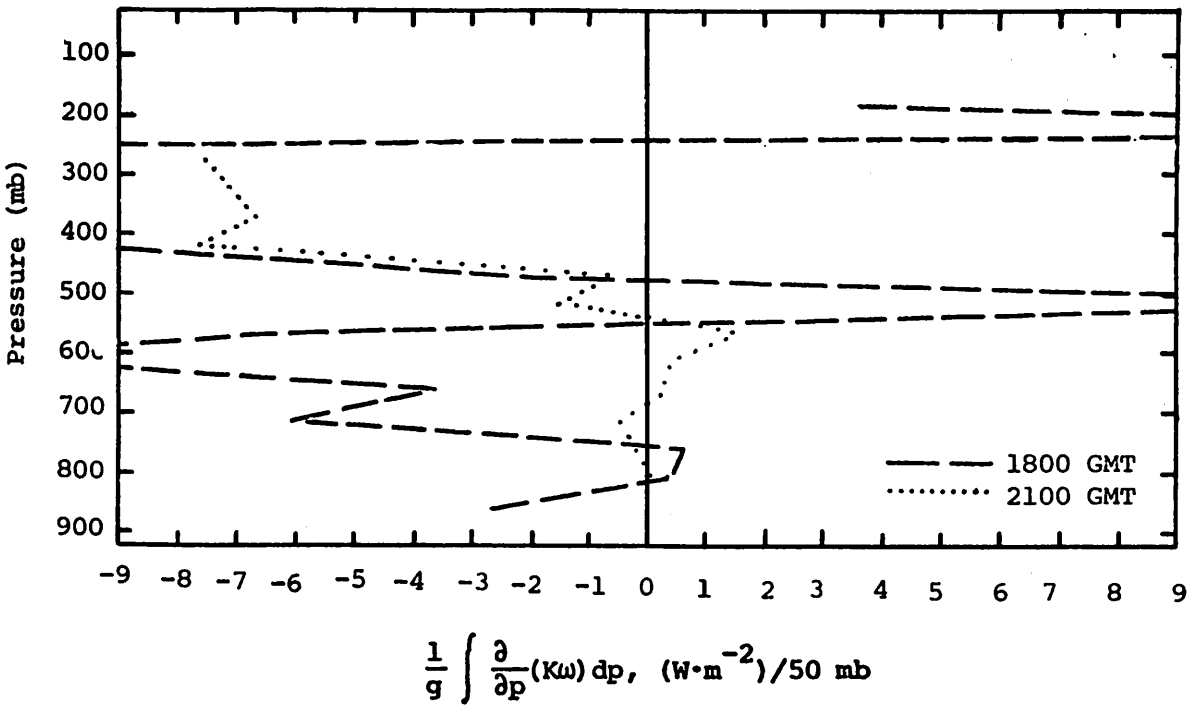

Fig. 5.5.4.7 Vertical profiles of the vertical flux of kinetic energy on 6 June 1978.

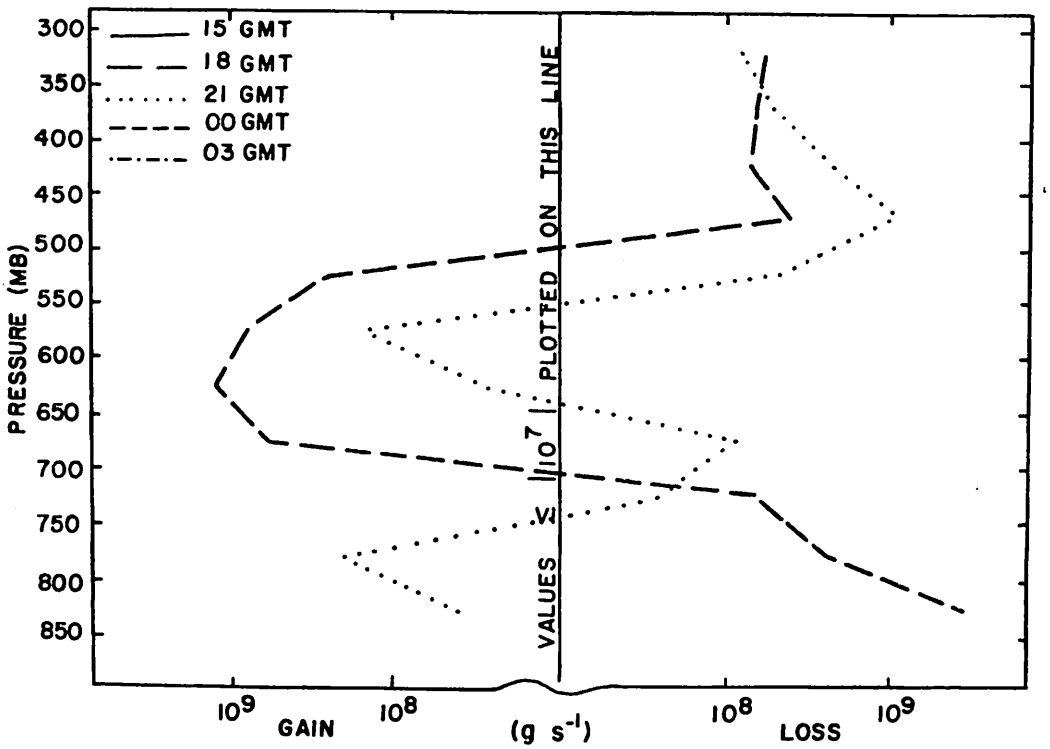

Fig. 5.5.5.1 Net horizontal transport of water vapor through boundaries of 50-mb layers (gm s^{-1}) over the Texas HIPLEX area for 6 June 1978.

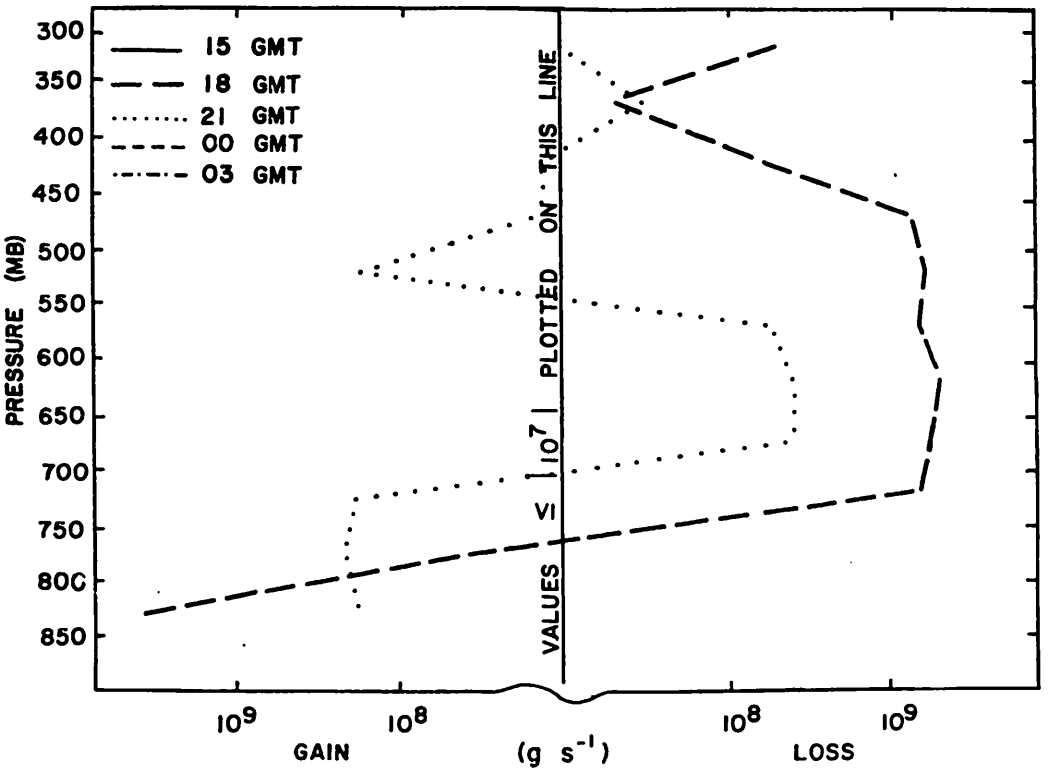

Fig. 5.5.5.2 Net vertical transport of water vapor through boundaries of 50-mb layers (gm s^{-1}) over the Texas HIPLEX area for 6 June 1978.

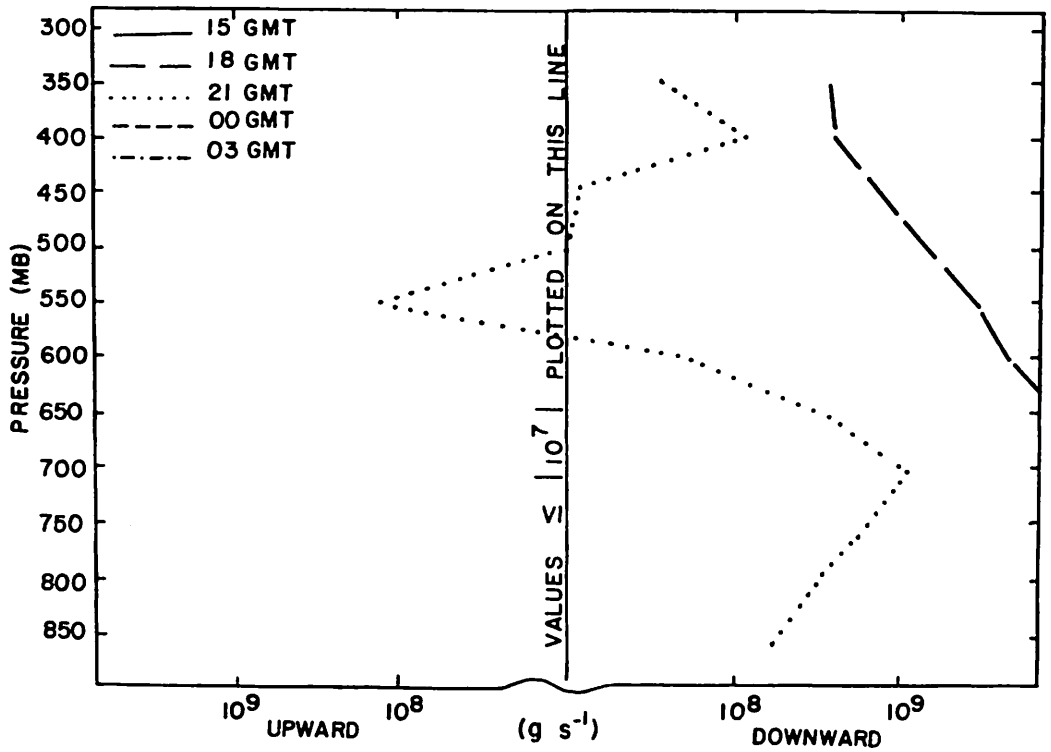

Fig. 5.5.5.3 Vertical transport of water vapor through constant pressure surfaces (gm s^{-1}) over the Texas HIPLEX area for 6 June 1978.

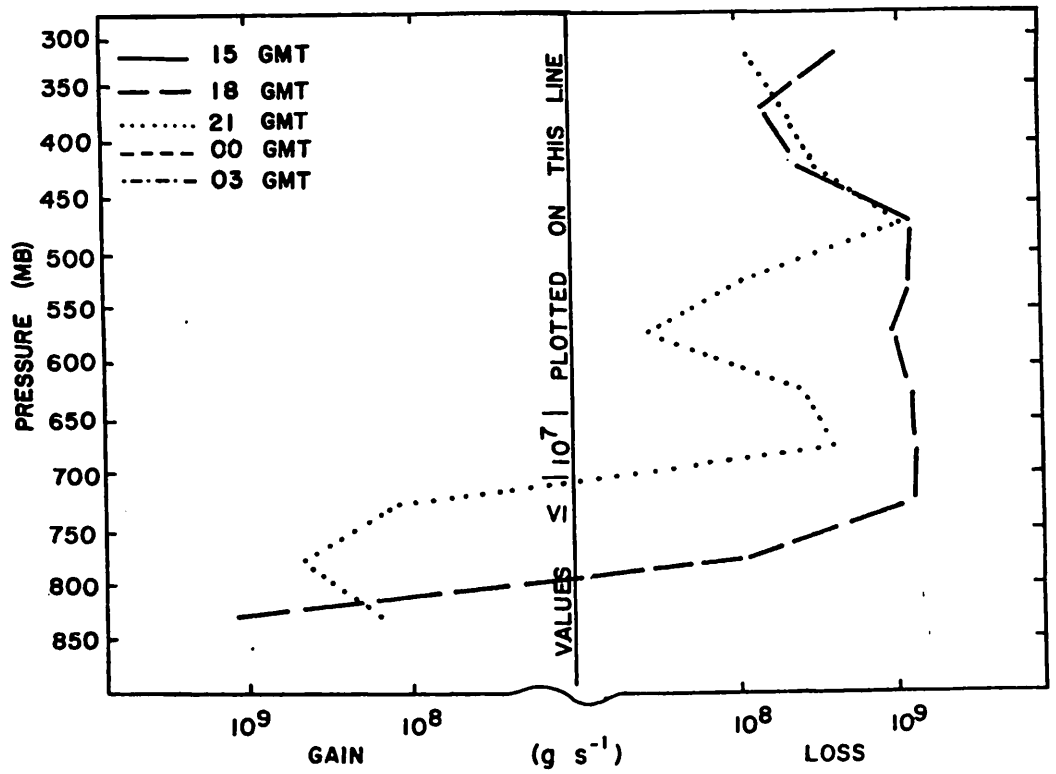

Fig. 5.5.5.4 Combined net horizontal and vertical transport through boundaries of 50-mb layers (gm s^{-1}) over the Texas HIPLEX area for 6 June 1978.

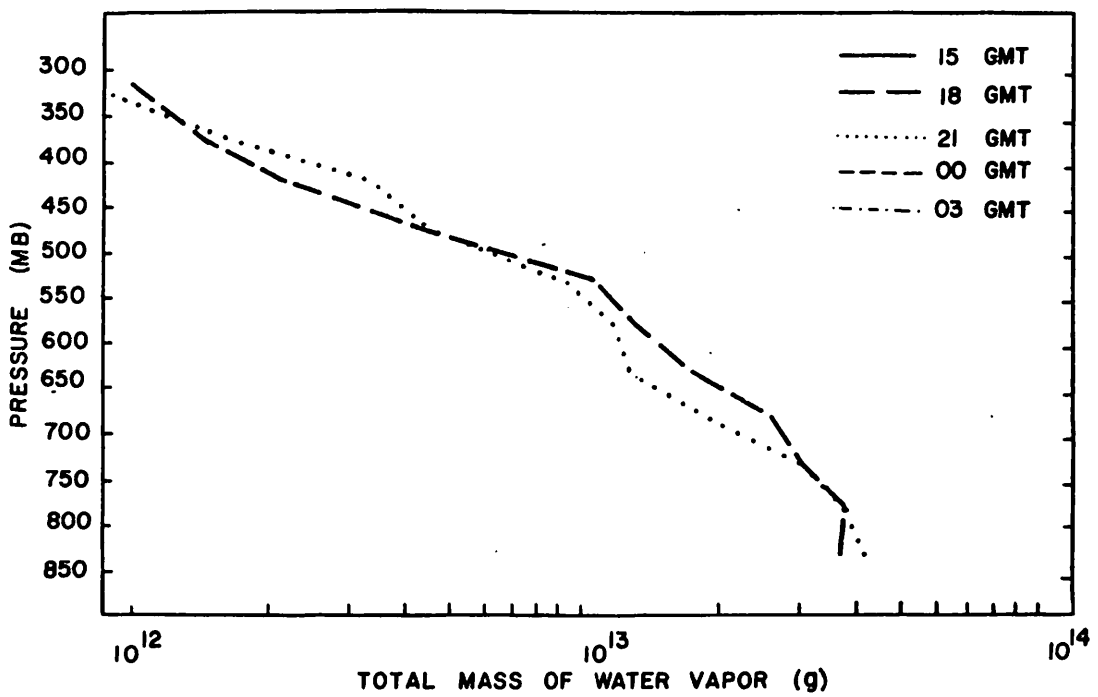

Fig. 5.5.5.5 Total mass of water vapor in layers 50 mb deep (g) over the Texas HIPLEX area on 6 June 1978.

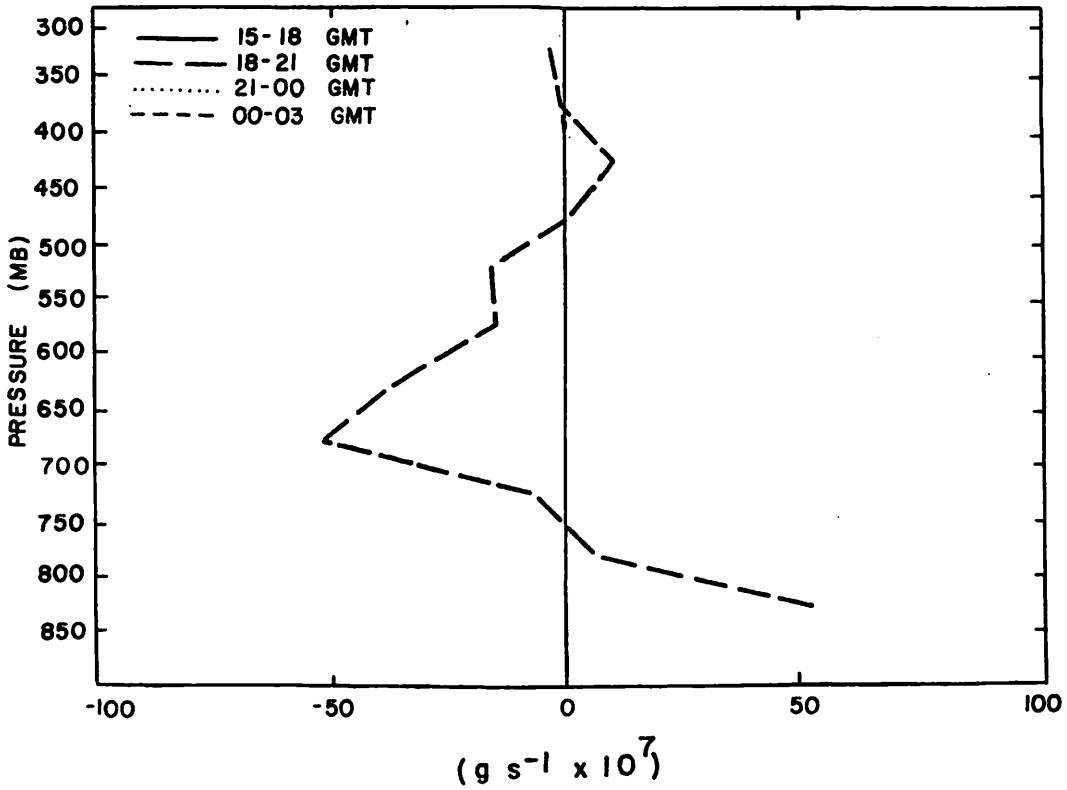

Fig. 5.5.5.6 Local rate of change in total mass of water vapor (g s^{-1} x 10^7) for the Texas HIPLEX area for 6 June 1978.

5.6 7 June 1978

5.6.1 Radar

There were two cells with heights above 5.1 km (20K ft) present at 2100 GMT. One was located between Tahoka and Post; the other was northwest of Robert Lee. Both echoes left the area or dissipated by 0000 GMT (Fig. 5.6.1.1).

5.6.2 Surface Parameters

The surface temperature pattern (Fig. 5.6.2.1) was fairly stable prior to 2200 GMT. Minimum temperatures existed toward the northwest with maximums toward the southern part of the area. After 2200 GMT the patterns were more irregular and variable than before this time. Cooling occurred near Clairemont at 2300 GMT and near Gail at 0000 GMT. This may have been due to the storms that were in the area just before these times.

The pattern of surface dewpoint depression (Fig. 5.6.2.2) also was stable during much of the day. Maximum dewpoint depressions were in the southwest, with minimums in the northwest. At 2200 GMT the minimum shifted to the northwest due to the cooling and moistening effect of the showers.

This addition of moisture was shown very clearly by the surface mixing ratio patterns (Fig. 5.6.2.3). Mixing ratio had been fairly low, about 9-10 g kg^{-1} prior to 2200 GMT. Following 2200 GMT mixing ratios in the northwest increased to 12-14 g kg^{-1} while the rest of the area remained dry.

Surface equivalent potential temperature (Fig. 5.6.2.4) was variable throughout the day. A maximum developed near Clairemont at 2200 GMT. This was a result of the large amount of moisture present. This maximum persisted even with the temperature drop at 2300 GMT. A secondary maximum developed near Lamesa at 2300 GMT. This maximum also persisted throughout the remainder of the day. A minimum developed near Lenorah at 0000 GMT and moved to Big Spring where it remained for the remainder of the day. This minimum was associated with a minimum mixing ratio during the same time period.

Terrain-induced vertical motion (Fig. 5.6.2.5) was small and variable. A center of downward vertical motion was observed near Vincent most of the day but it was not strong and did not have much effect.

Surface velocity divergence (Fig. 5.6.2.6), vertical motion 50 mb above the surface (Fig. 5.6.2.7), surface moisture divergence (Fig. 5.6.2.8), and vertical moisture flux 50 mb above the surface (Fig. 5.6.2.9) had centers

MISSING DATA

RADAR 6/7 /78 1000 CDT

MISSING DATA

RADAR 6/7 /78 1300 CDT

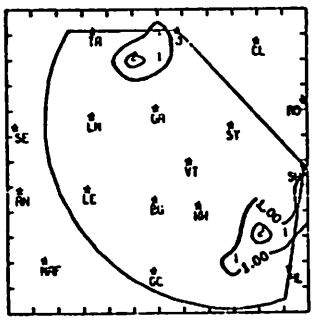

RADAR 6/7 /78 1600 CDT

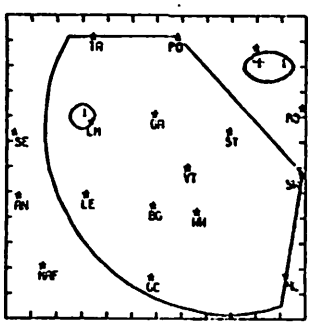

RADAR 6/7 /78 1900 CDT

NO ECHOES

RADAR 6/7 /78 2200 CDT

MISSING DATA

RADAR 6/7 /78 1100 CDT

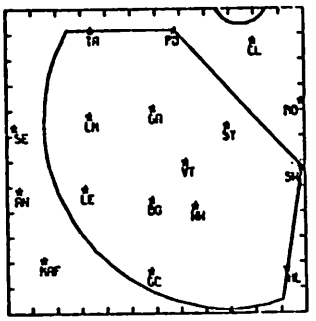

RADAR 6/7 /78 1400 CDT

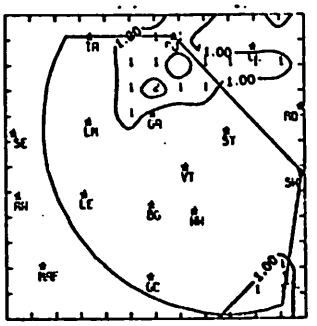

RADAR 6/7 /78 1700 CDT

NO ECHOES

RADAR 6/7 /78 2000 CDT

MISSING DATA

RADAR 6/7 /78 1200 CDT

NO ECHOES

RADAR 6/7 /78 1500 CDT

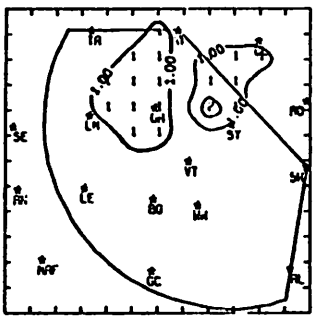

RADAR 6/7 /78 1800 CDT

NO ECHOES

RADAR 6/7 /78 2100 CDT

Fig. 5.6.1.1 Radar echoes for 7 June 1978.

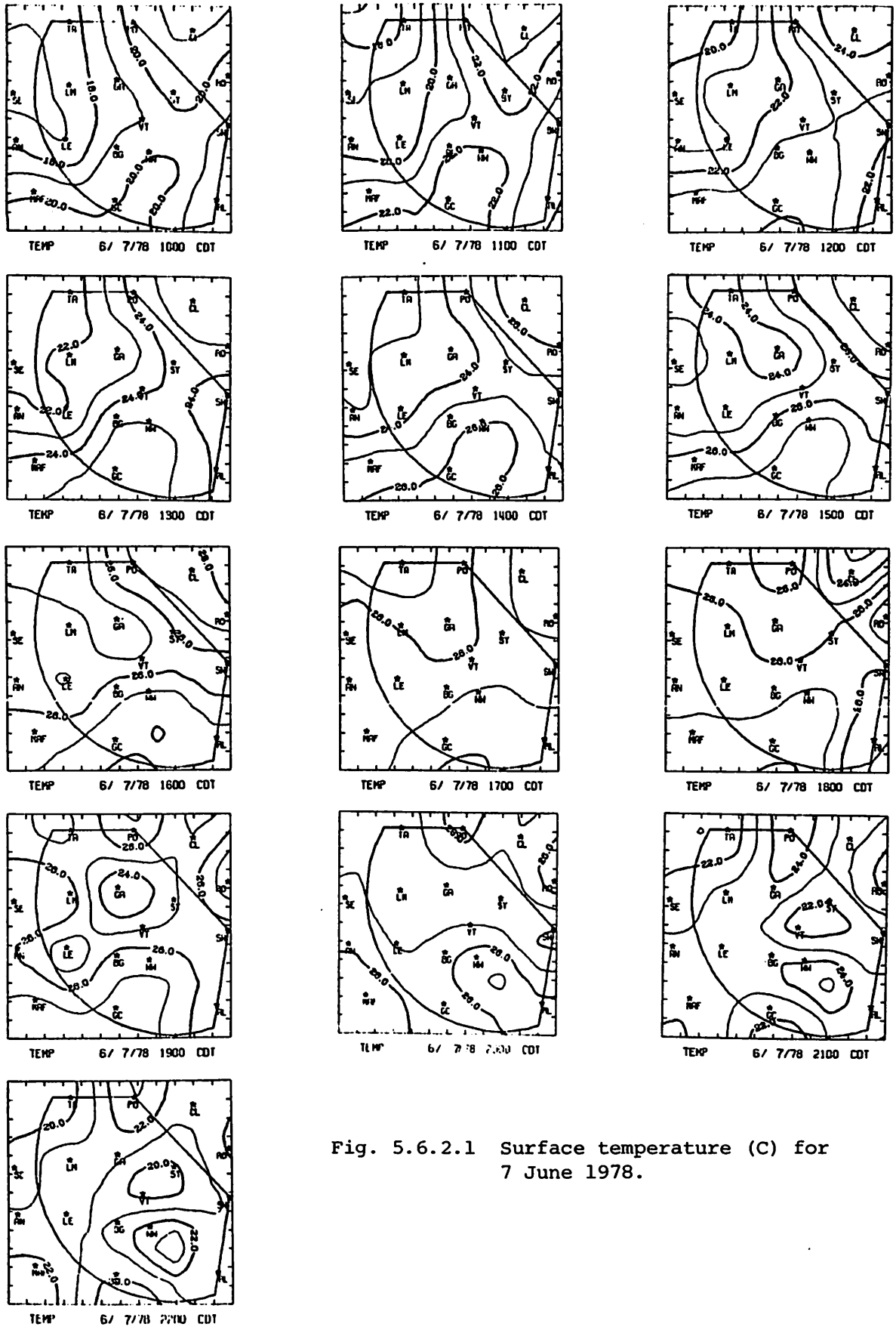

Fig. 5.6.2.1 Surface temperature (C) for 7 June 1978.

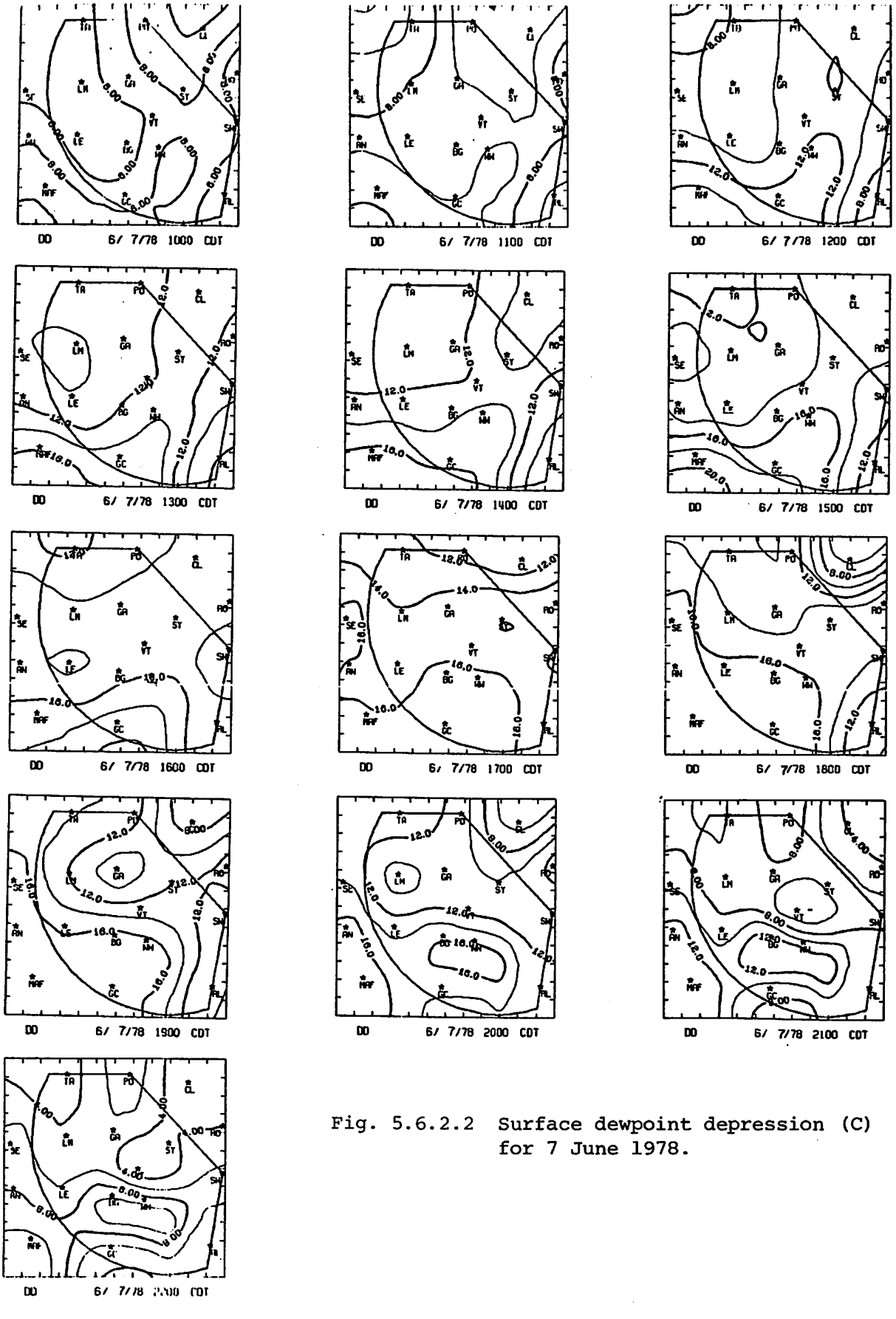

Fig. 5.6.2.2 Surface dewpoint depression (C) for 7 June 1978.

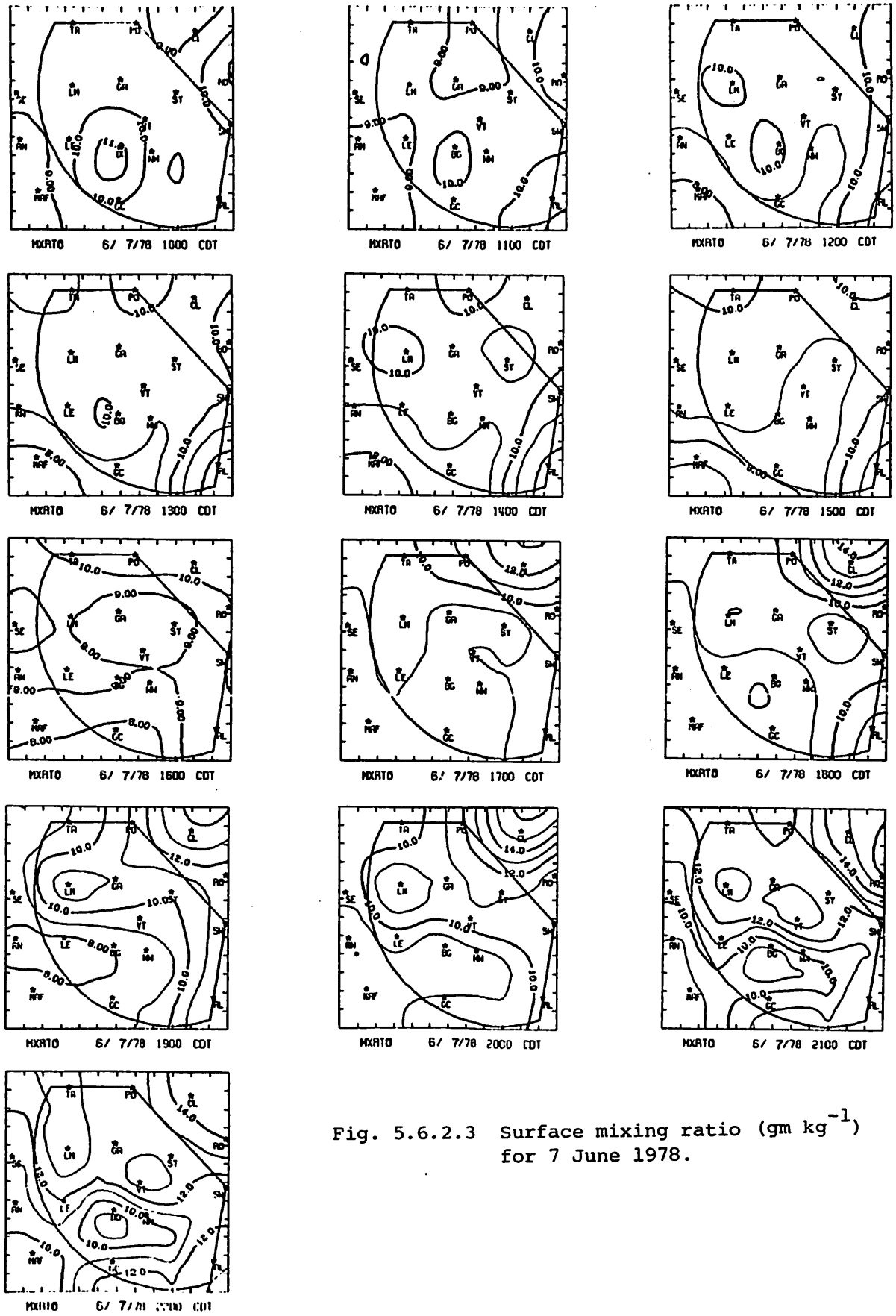

Fig. 5.6.2.3 Surface mixing ratio (gm kg^{-1}) for 7 June 1978.

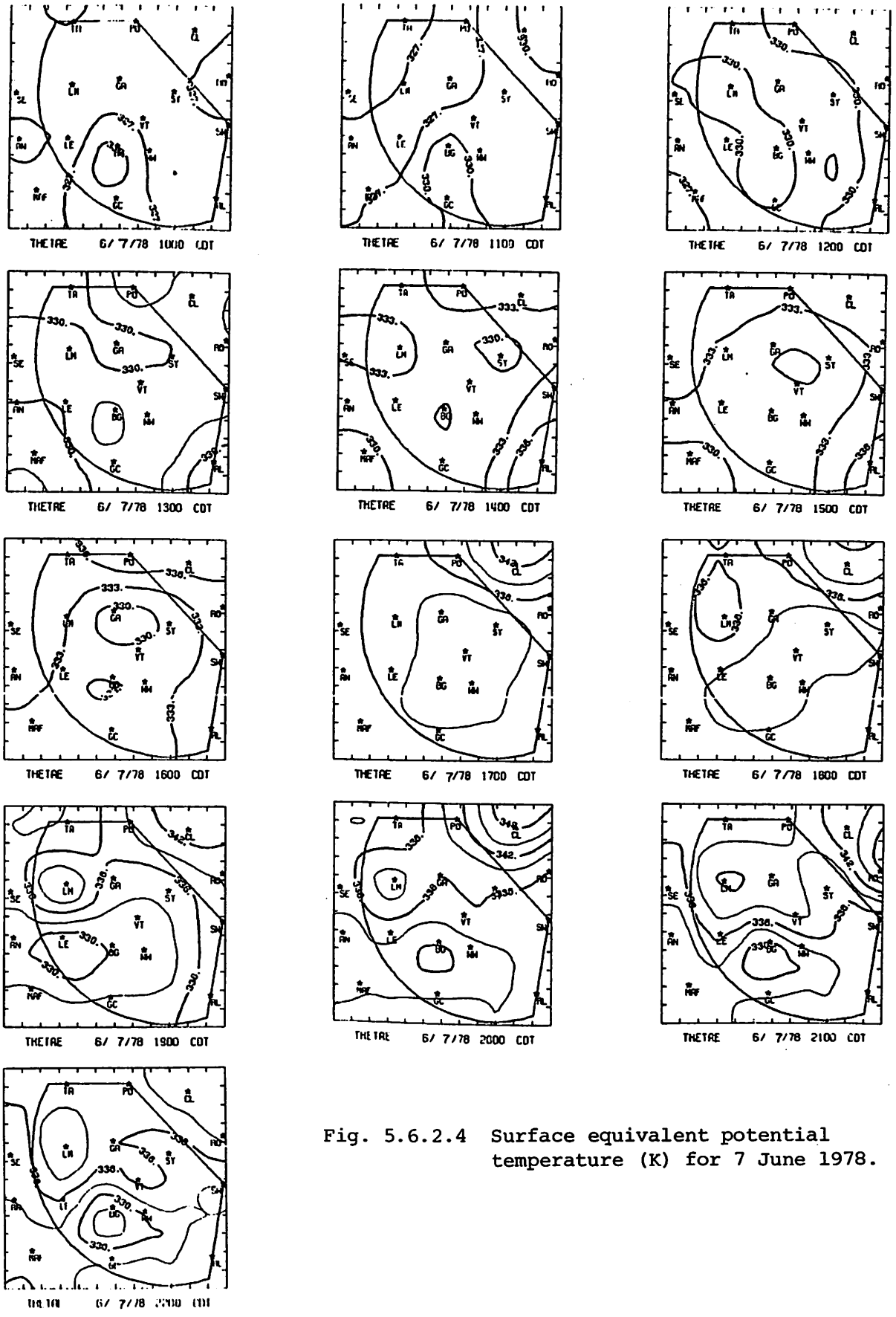

Fig. 5.6.2.4 Surface equivalent potential temperature (K) for 7 June 1978.

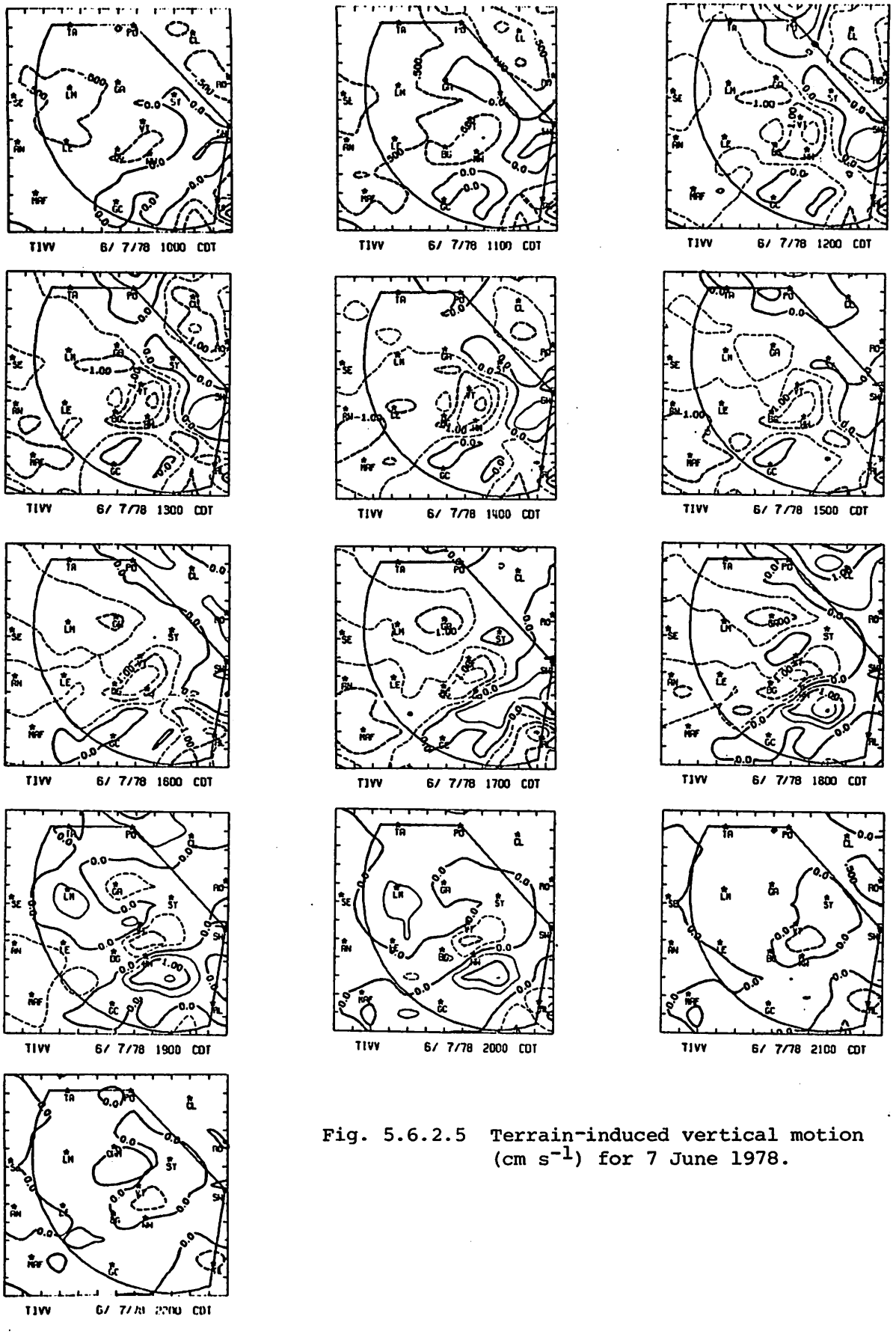

Fig. 5.6.2.5 Terrain-induced vertical motion (cm s^{-1}) for 7 June 1978.

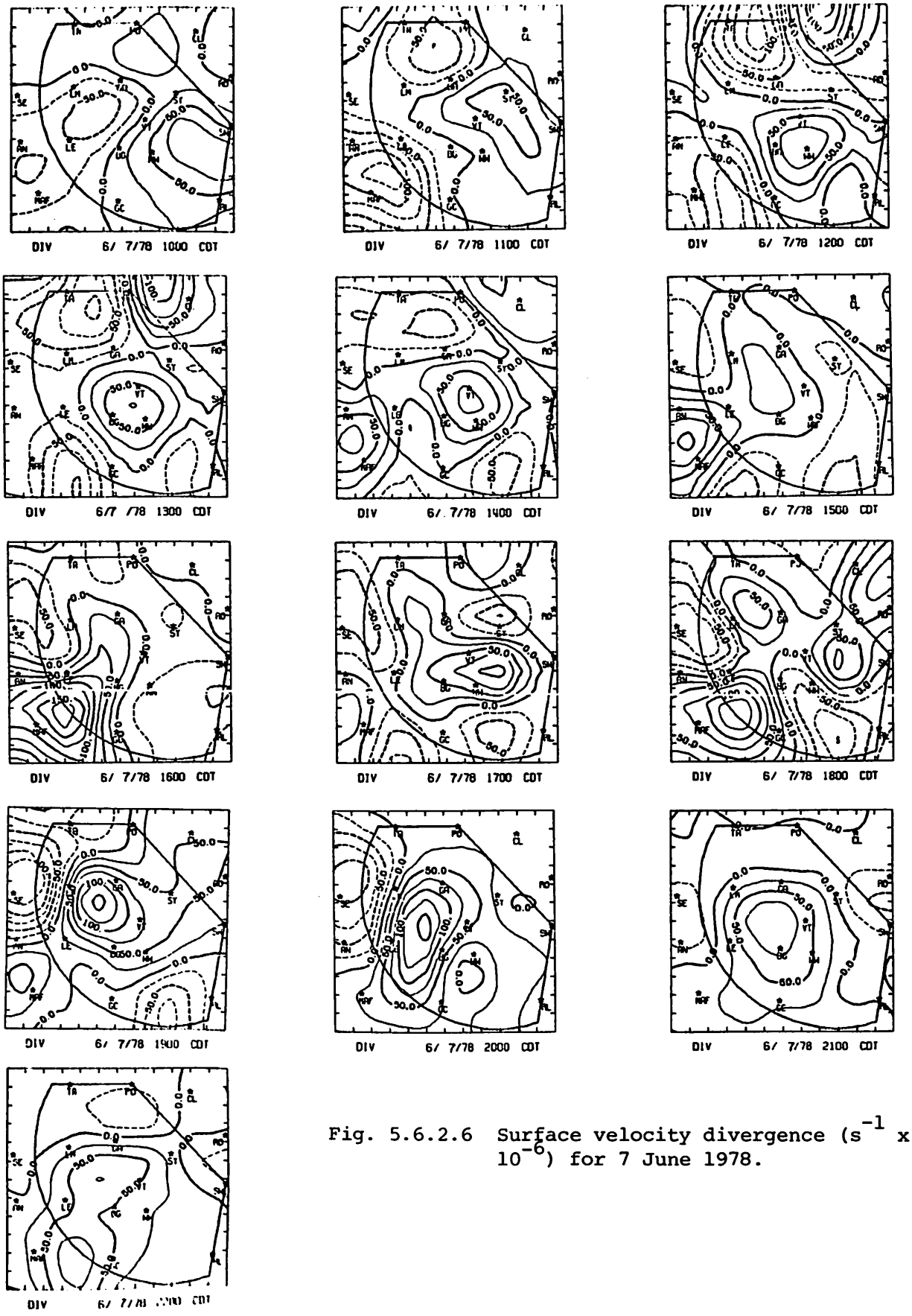

Fig. 5.6.2.6 Surface velocity divergence (s^{-1} x 10^{-6}) for 7 June 1978.

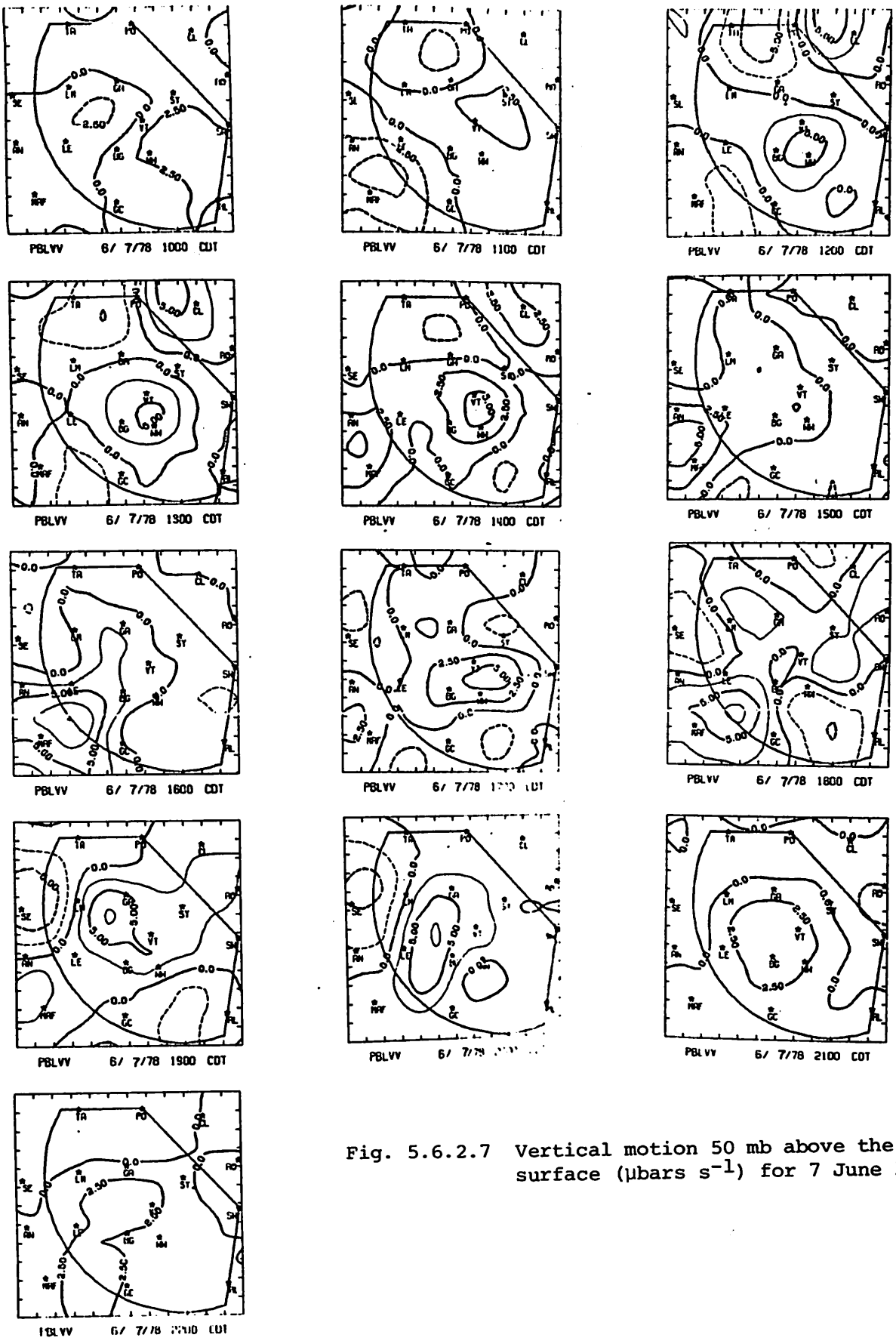

Fig. 5.6.2.7 Vertical motion 50 mb above the surface (μbars s^{-1}) for 7 June 1978.

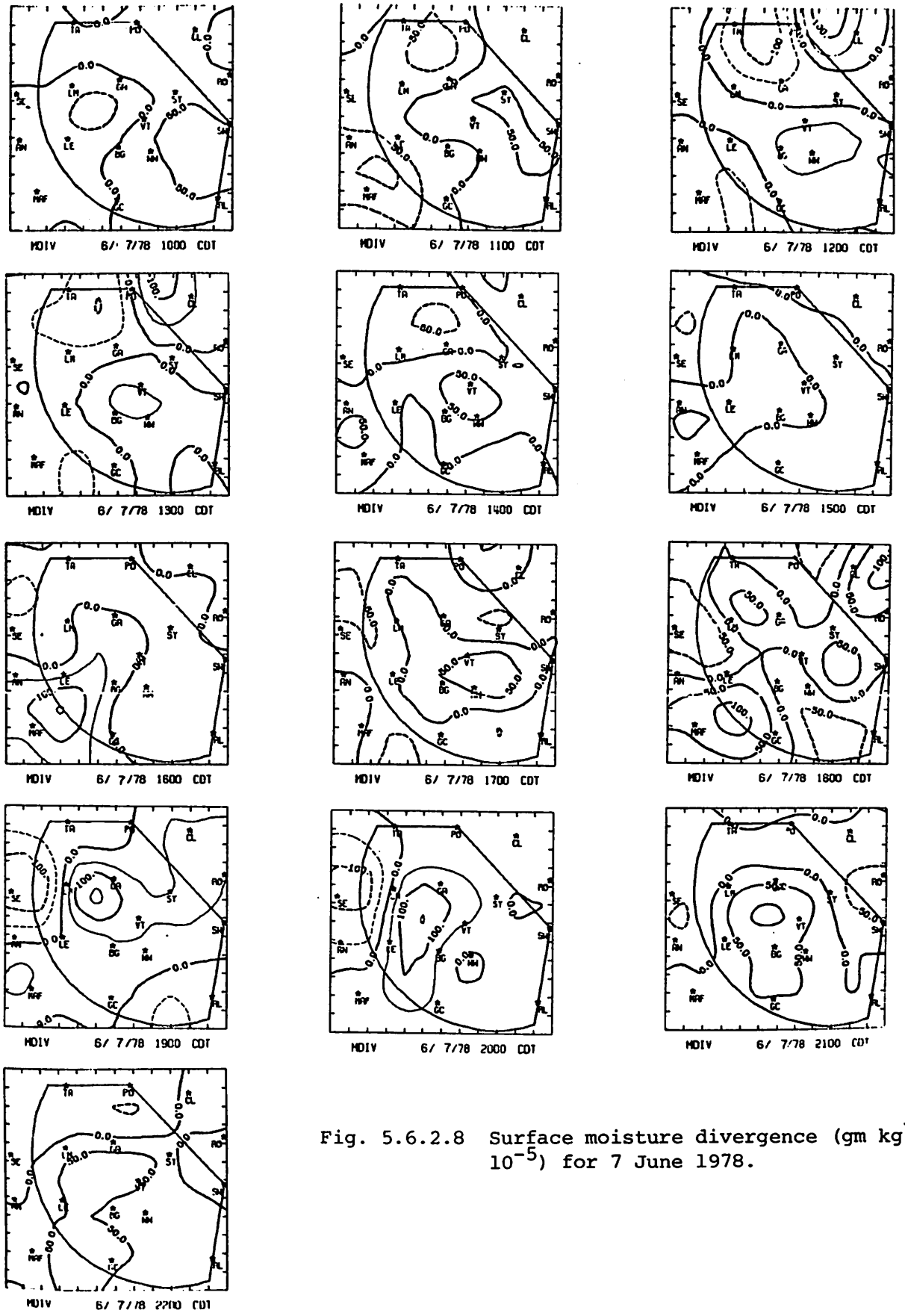

Fig. 5.6.2.8 Surface moisture divergence (gm kg^{-1} s^{-1} x 10^{-5}) for 7 June 1978.

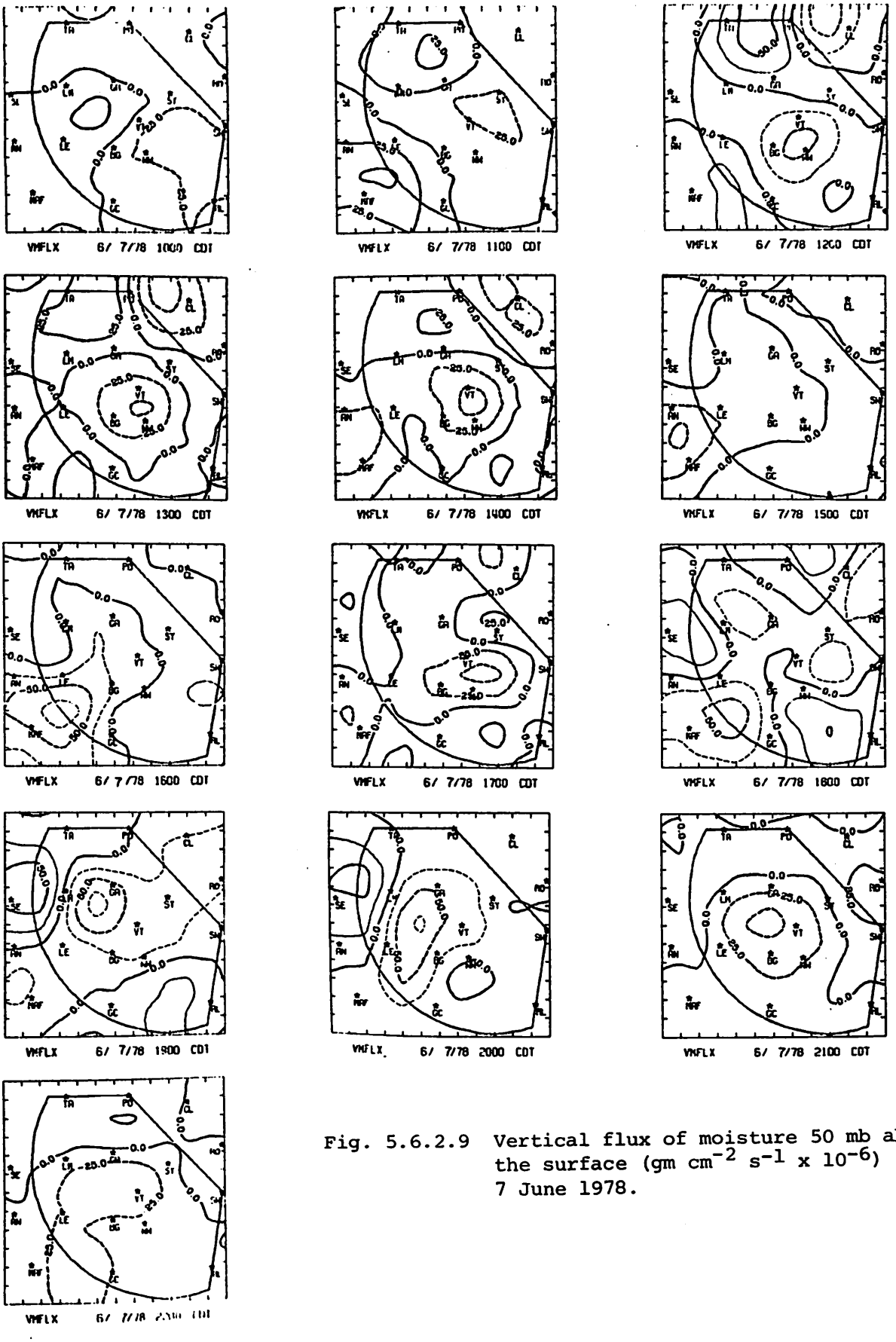

Fig. 5.6.2.9 Vertical flux of moisture 50 mb above the surface (gm cm^{-2} s^{-1} x 10^{-6}) for 7 June 1978.

of moderate value throughout the day. The stronger centers in the north, near Post, suggest that convective activity was taking place but radar data were missing at these times. A center of surface velocity convergence, upward vertical motion, surface moisture convergence, and upward vertical moisture flux developed near Seminole at 2100 GMT. These centers along with centers of strong downward motion and divergence, were associated with the showers that took place between 2100 and 0000 GMT. The center of convergence produced an inflow of energy as evidenced by the formation of the secondary maximum in equivalent potential temperature near Lamesa. The values of the centers of convergence and vertical motion were not as great as those of 5 June 1978 but the storms this day were not as intense.

Surface vorticity patterns are shown in Fig. 5.6.2.10. A maximum axis of cyclonic vorticity was along a Gail-to-Lenorah line from 1600 to 0200 GMT. After this time, when showers had dissipated, the vorticity pattern became disorganized and the magnitude of vorticity decreased.

Surface pressure change (Fig. 5.6.2.11) remained small throughout the day. The largest changes were 1 mb rises between 0000 and 0300 GMT near Gail and Snyder.

Surface winds (Fig. 5.6.2.12) were generally from the west and northwest at 1500 GMT. These shifted to northerly by 2300 GMT. After 0200 GMT winds were light and northerly.

5.6.3 Upper Level Kinematic Parameters

Mass convergence dominates the profiles in Fig. 5.6.3.1. Convergence was present at all levels at 1800 and 2100 GMT. At 0000 GMT when activity in the area had decreased there was strong divergence near the surface and strong convergence near 400 mb. At 1500 GMT divergence was present at nearly all levels below 400 mb.

Downward vertical motion (Fig. 5.6.3.2) was present at all levels at 1500 GMT with a maximum near 450 mb. At 1800 and 2100 GMT vertical motion was upward.*

Moisture convergence (Fig. 5.6.3.3) was present at most levels after 1800 GMT. At 1500 GMT there were layers of divergence near the surface and

---

*NOTE: The large values of vertical velocity at 1800 and 2100 GMT are questionable and may cause errors in other computations as well.

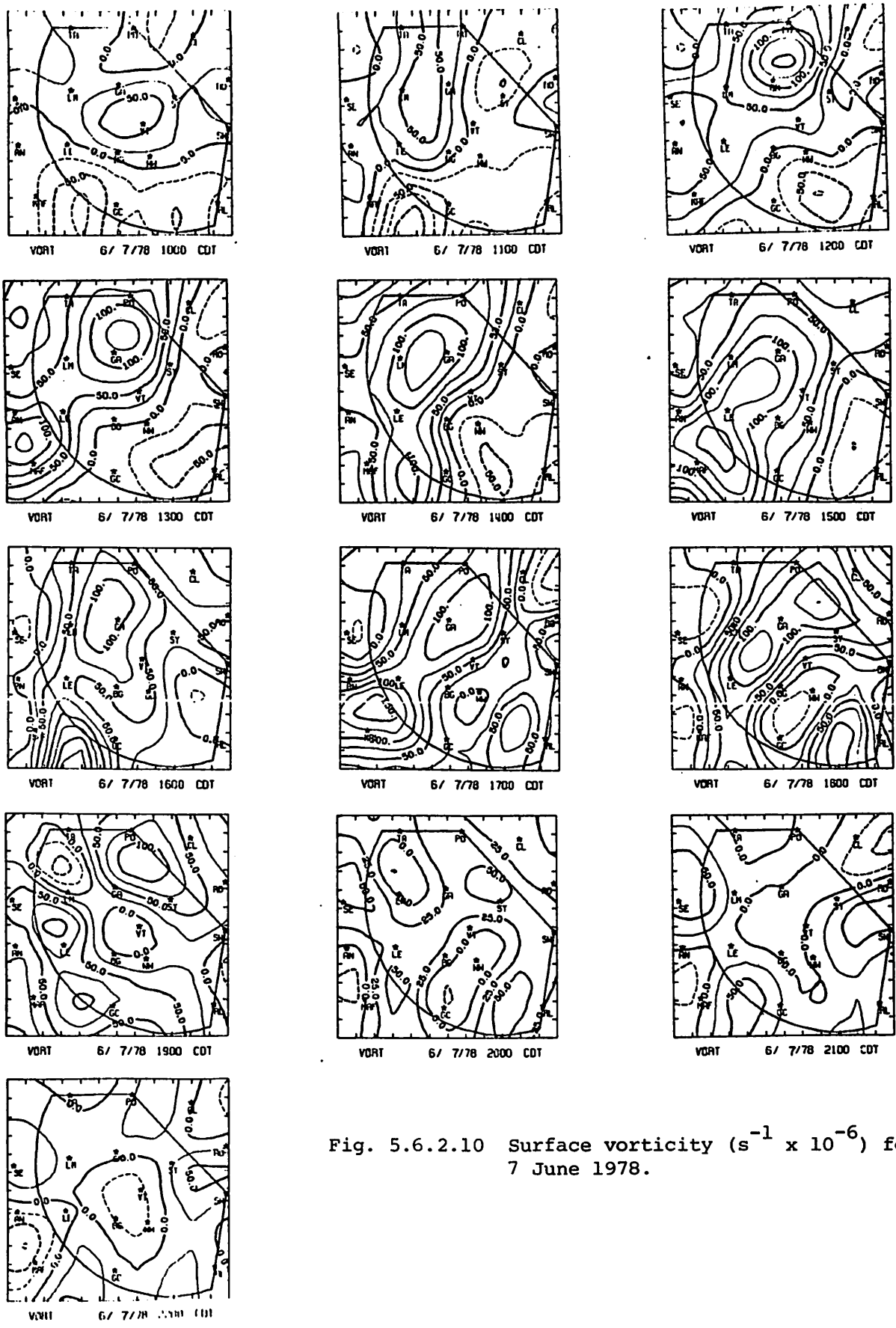

Fig. 5.6.2.10 Surface vorticity (s^{-1} x 10^{-6}) for 7 June 1978.

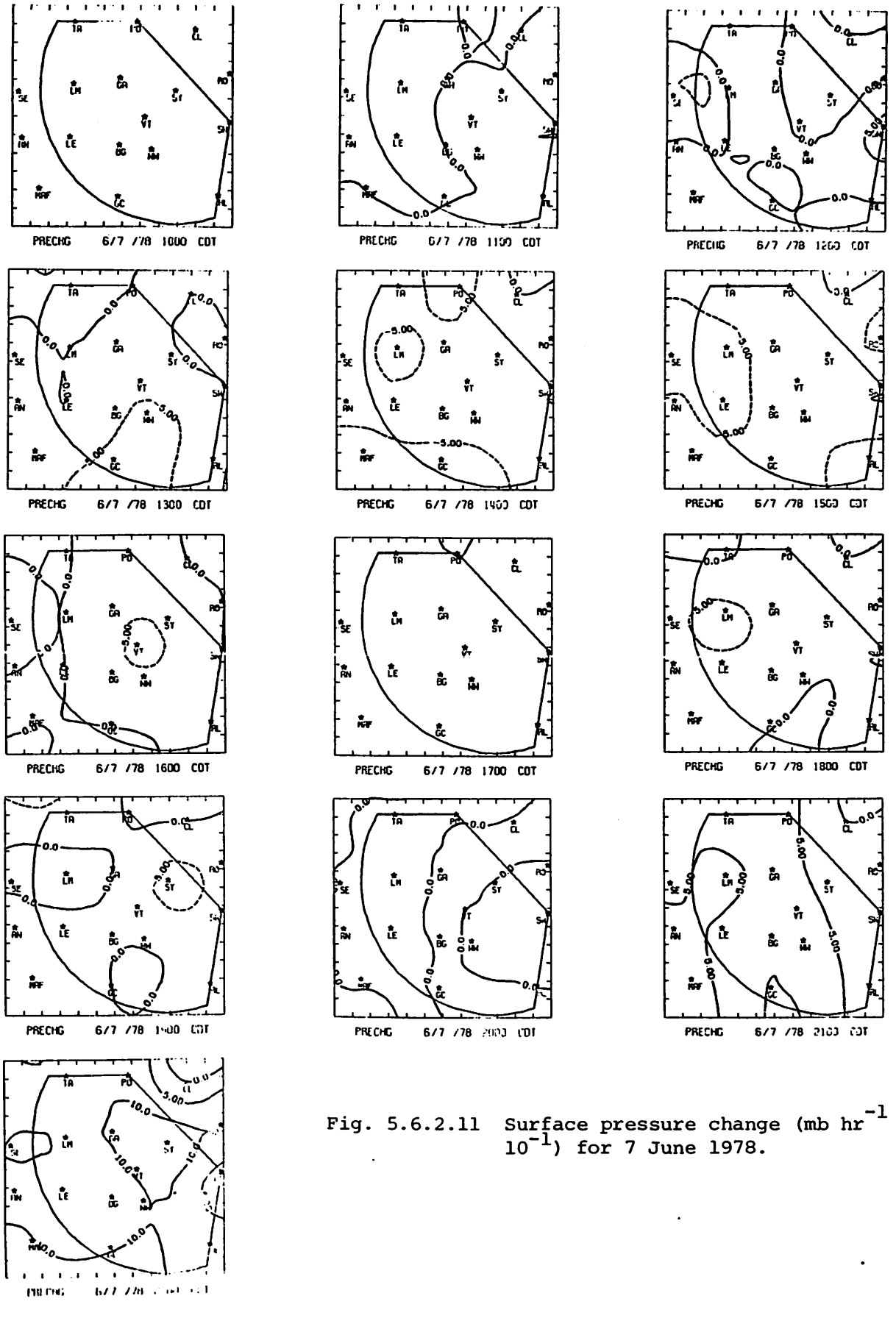

Fig. 5.6.2.11 Surface pressure change (mb hr^{-1} x 10^{-1}) for 7 June 1978.

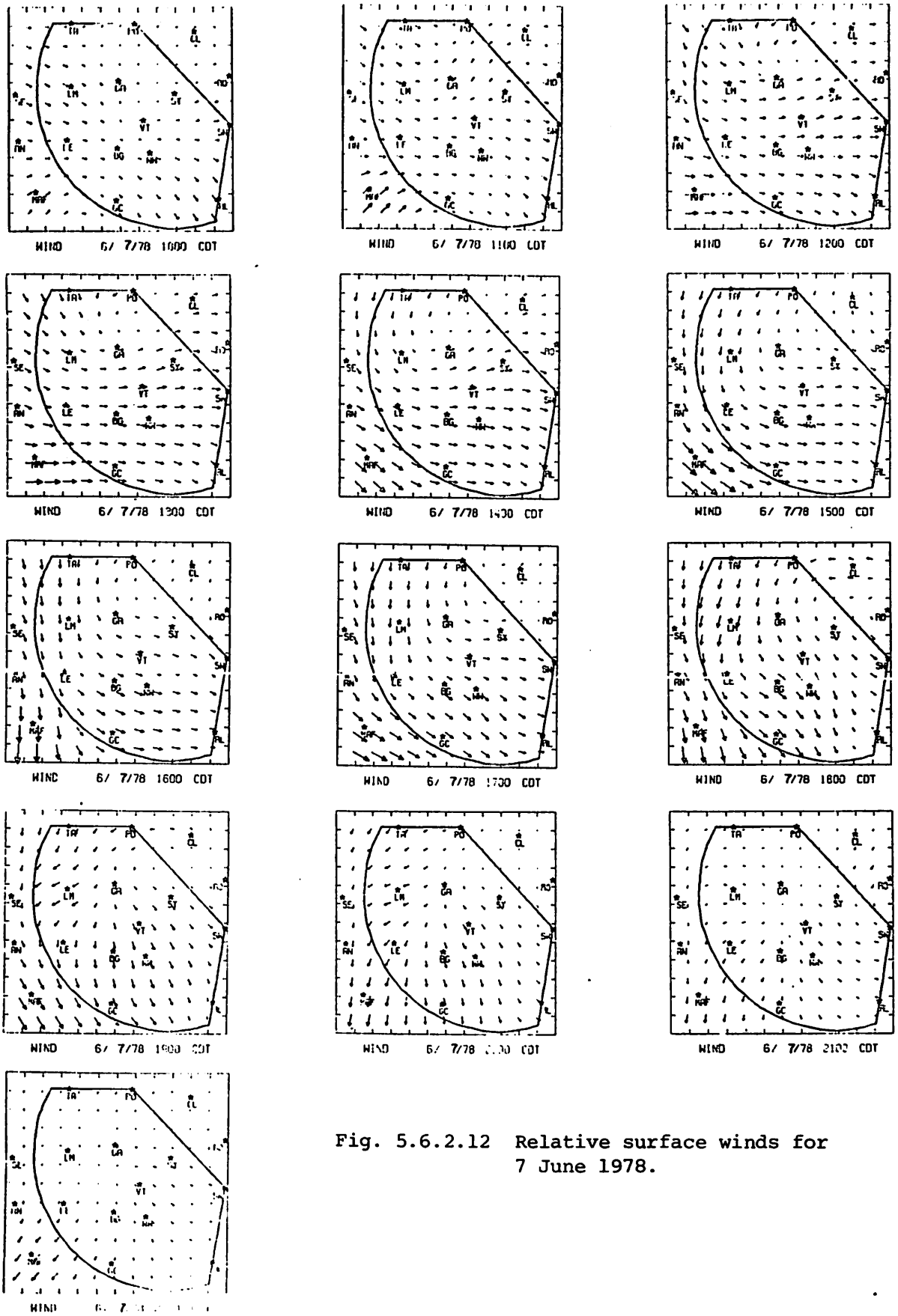

Fig. 5.6.2.12 Relative surface winds for 7 June 1978.

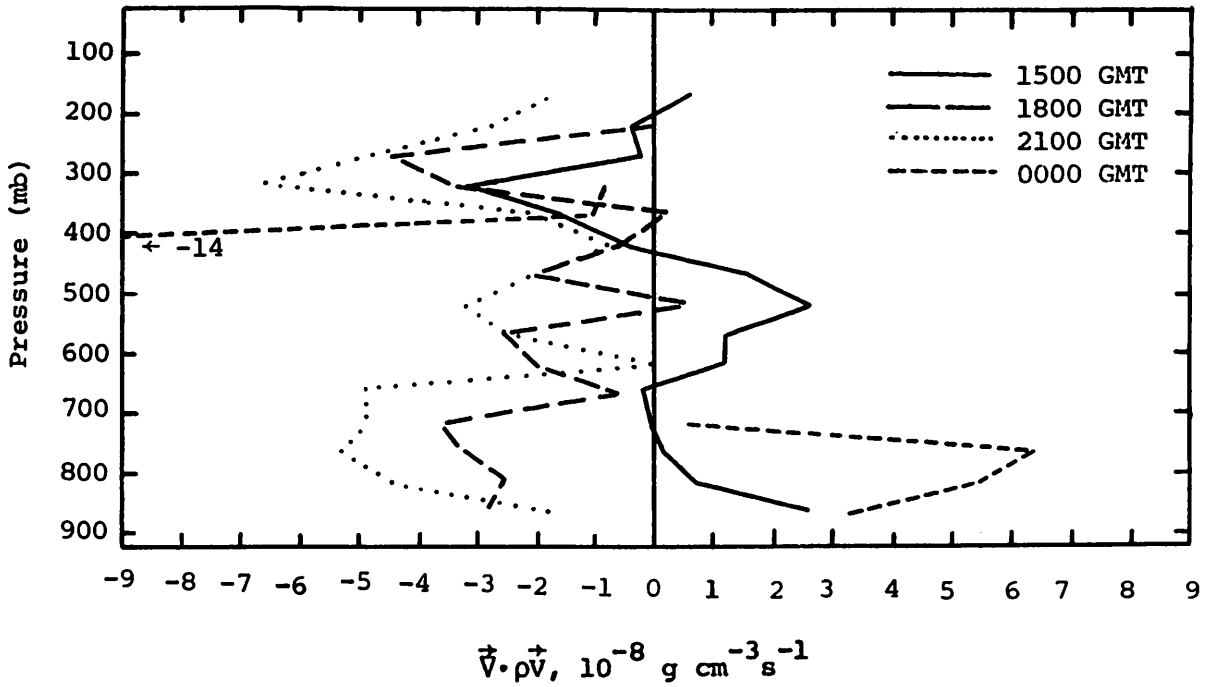

Fig. 5.6.3.1 Vertical profiles of horizontal mass divergence on 7 June 1978.

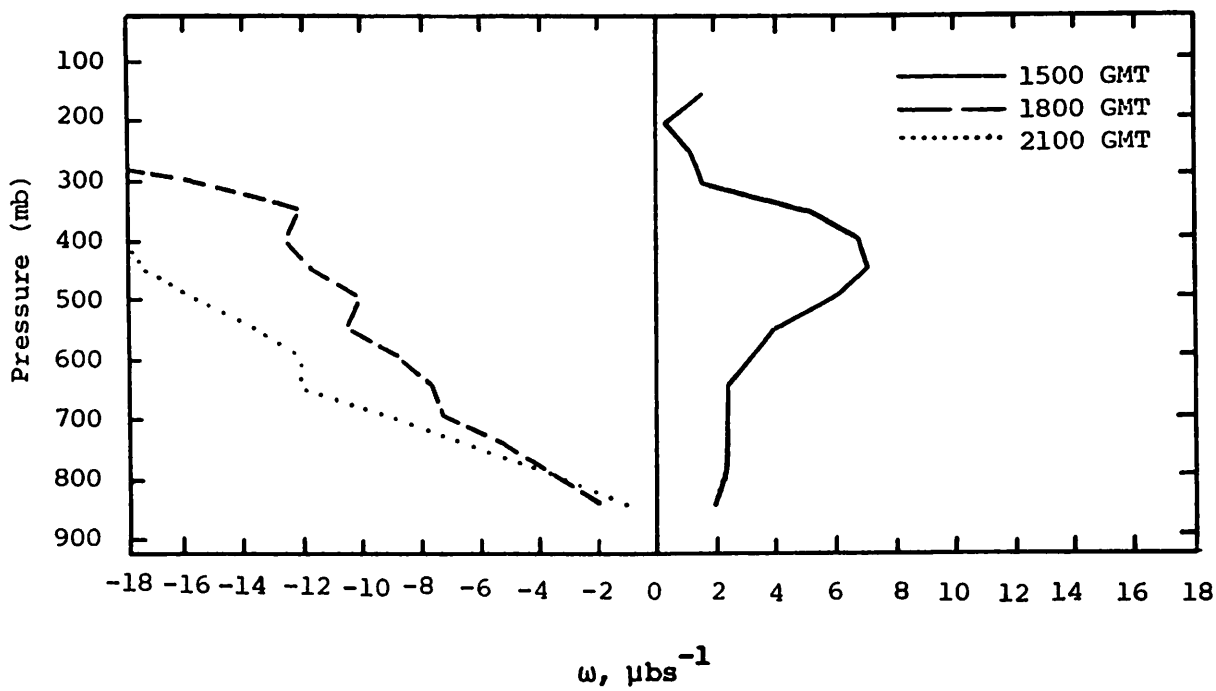

Fig. 5.6.3.2 Vertical profiles of vertical motion on 7 June 1978.

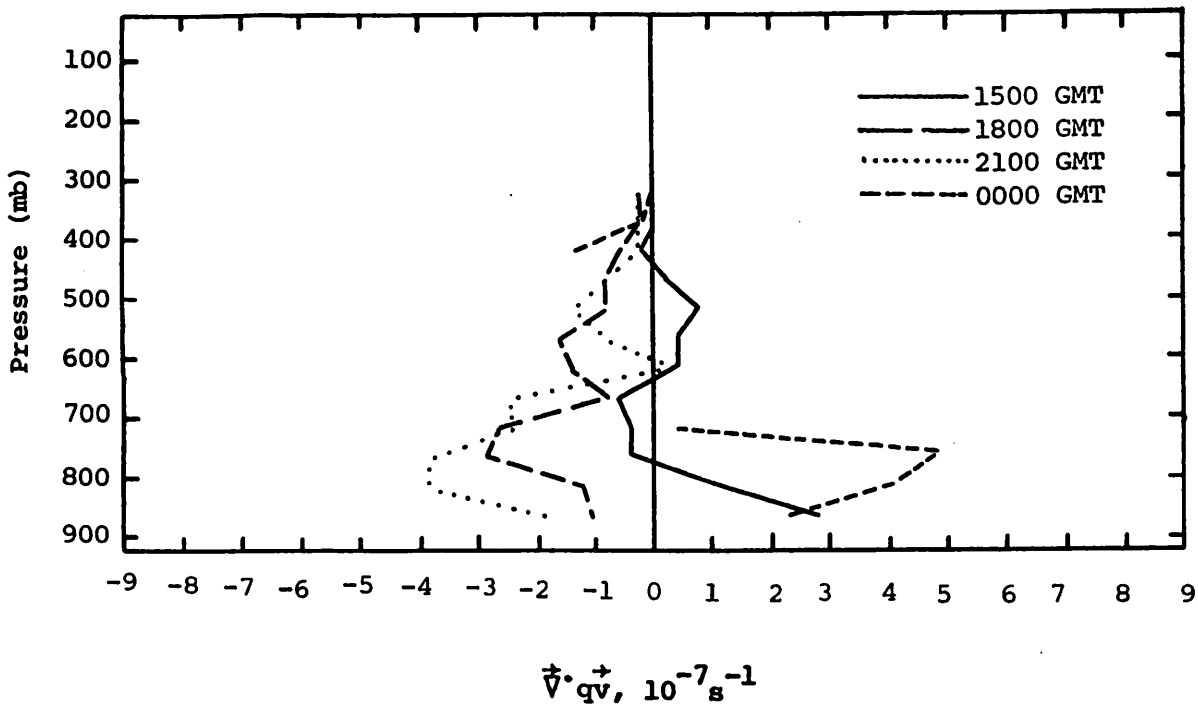

Fig. 5.6.3.3 Vertical profiles of moisture divergence on 7 June 1978.

in middle levels. At 1800 and 2100 GMT inflow of moisture was maximum near 800 mb and decreased upward. By 0000 GMT when echoes were disappearing there was a strong layer of moisture divergence near the surface with convergence above.

5.6.4 Energetics

The initiation of a layer of inflow of latent heat near 850 mb at 1500 GMT is indicated in Fig. 5.6.4.1. The horizontal inflow increased at 1800 and 2100 GMT and extended into all levels during the time when echoes were present. By 0000 GMT when the echoes were disappearing, the strong convergence of latent heat was replaced by divergence near the surface but convergence continued at upper levels.

The vertical flux of latent heat energy (Fig. 5.6.4.2) indicates downward transport from levels above 800 mb to near the surface at 1500 GMT. When convective activity was present, as at 1800 and 2100 GMT, the pattern shifted to upward transport from lower levels to layers above 700 mb.

The local rate-of-change of latent heat (Fig. 5.6.4.3) was near zero during much of the day. Values were positive before 0000 GMT when the

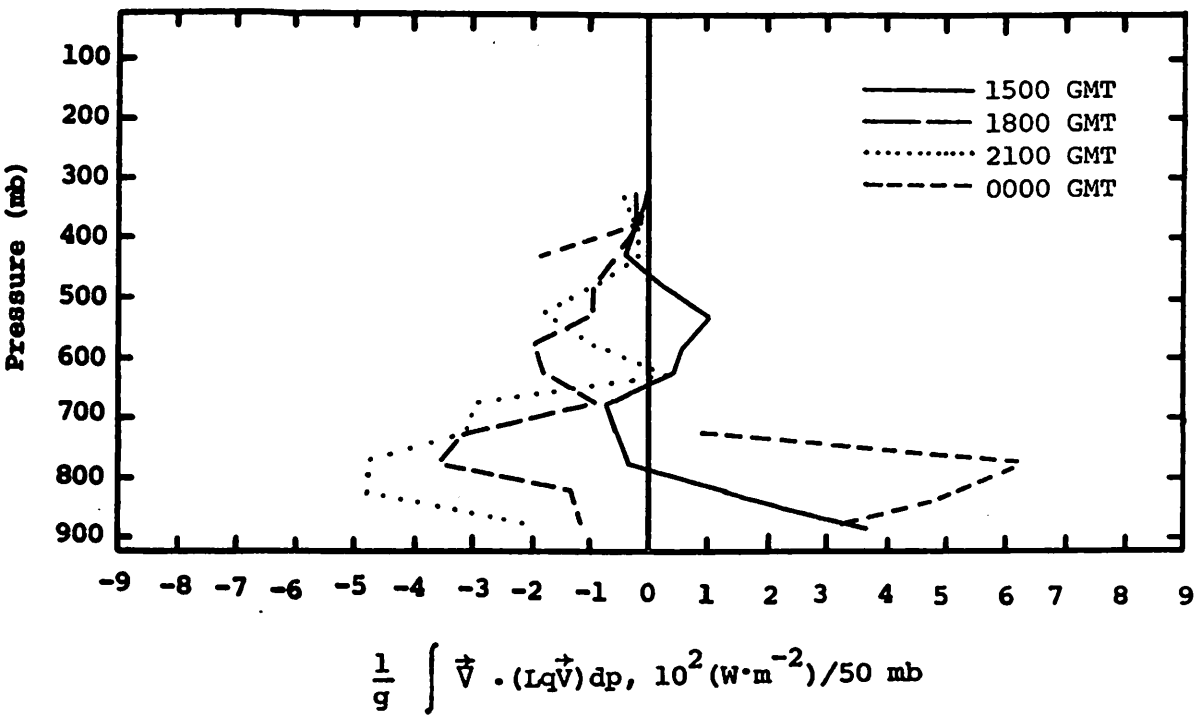

Fig. 5.6.4.1 Vertical profiles of the horizontal flux of latent heat energy on 7 June 1978.

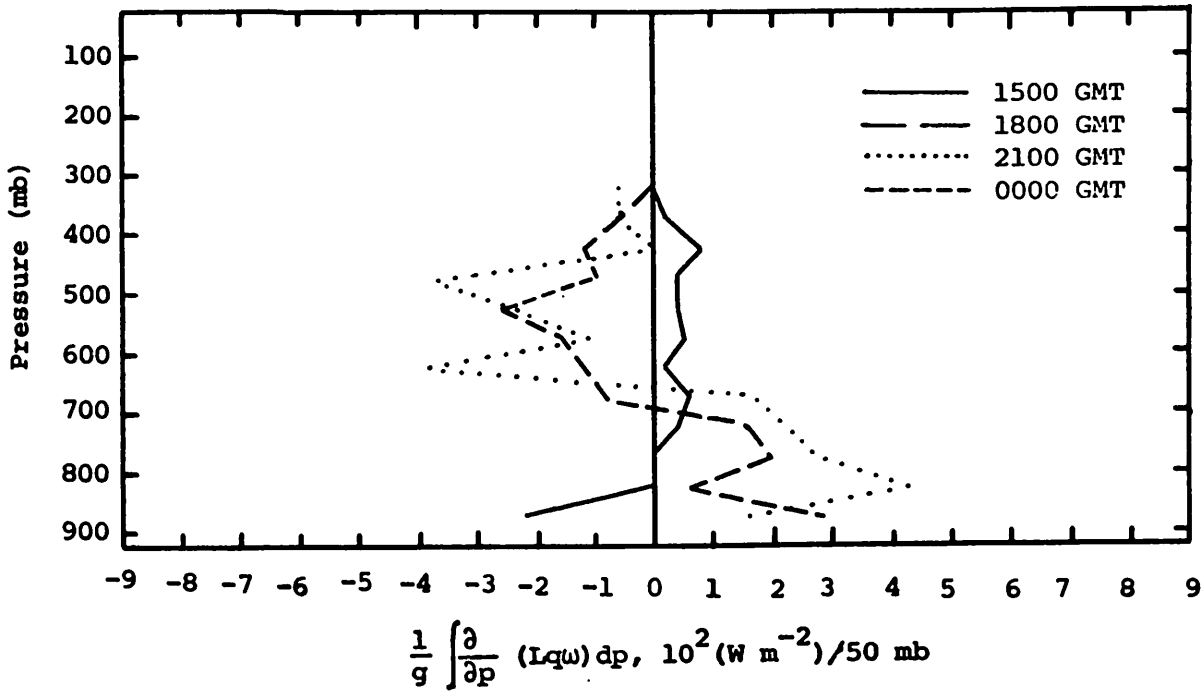

Fig. 5.6.4.2 Vertical profiles of the vertical flux of latent heat energy on 7 June 1978.

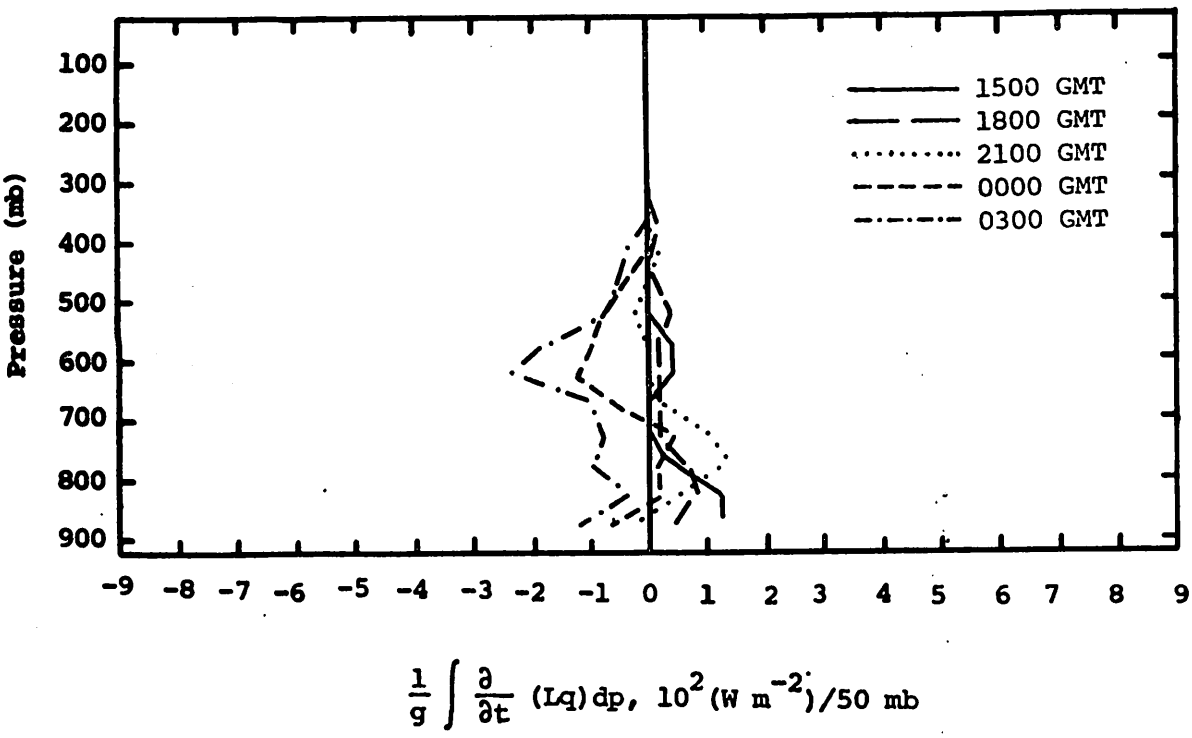

Fig. 5.6.4.3 Vertical profiles of the local change of latent heat energy on 7 June 1978.

local rate-of-change became negative above 700 mb. The losses were greatest at 0300 GMT.

The profile of the residual of the latent heat equation (Fig. 5.6.4.4) showed generally negative values at 1500 GMT which indicates that evaporation may have been taking place. At 1800 and 2100 GMT the profiles were positive which suggests the presence of condensation.

The residual of the sensible heat equation (Fig. 5.6.4.5) was negative at most levels at 1500 GMT from the evaporative cooling taking place. The positive values at 1800 and 2100 GMT are in agreement with the condensation taking place at these times. The large values shown above 400 mb are related to the large vertical velocities.

Profiles of horizontal transport of kinetic energy (Fig. 5.6.4.6) are similar for the first three times. Small values of kinetic energy inflow were present near the surface. Outflow occurred near 500 mb at 1500 GMT and at higher levels at the later times. Strong inflow was present just below the level of the jet stream, and at 1500 GMT there was outflow above 200 mb.

The profiles of vertical flux of kinetic energy (Fig. 5.6.4.7) show

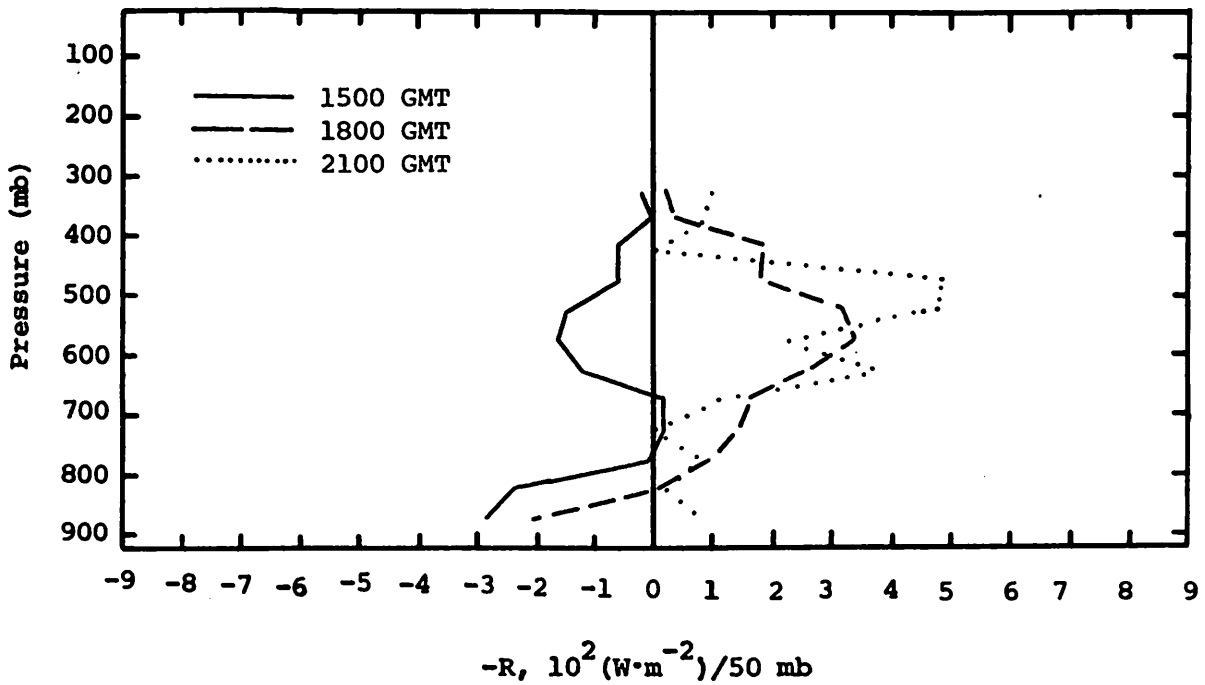

Fig. 5.6.4.4 Vertical profiles of the residual of the latent heat energy equation on 7 June 1978.

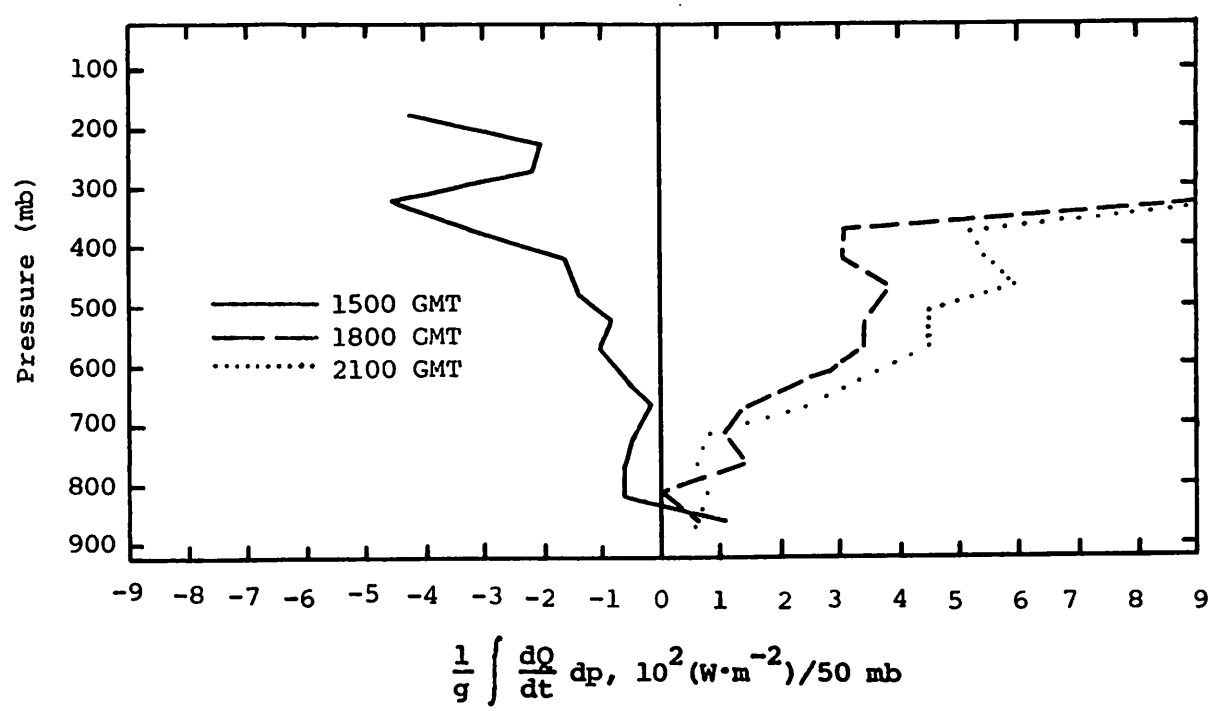

Fig. 5.6.4.5 Vertical profiles of diabatic heating computed from the first law of thermodynamics on 7 June 1978.

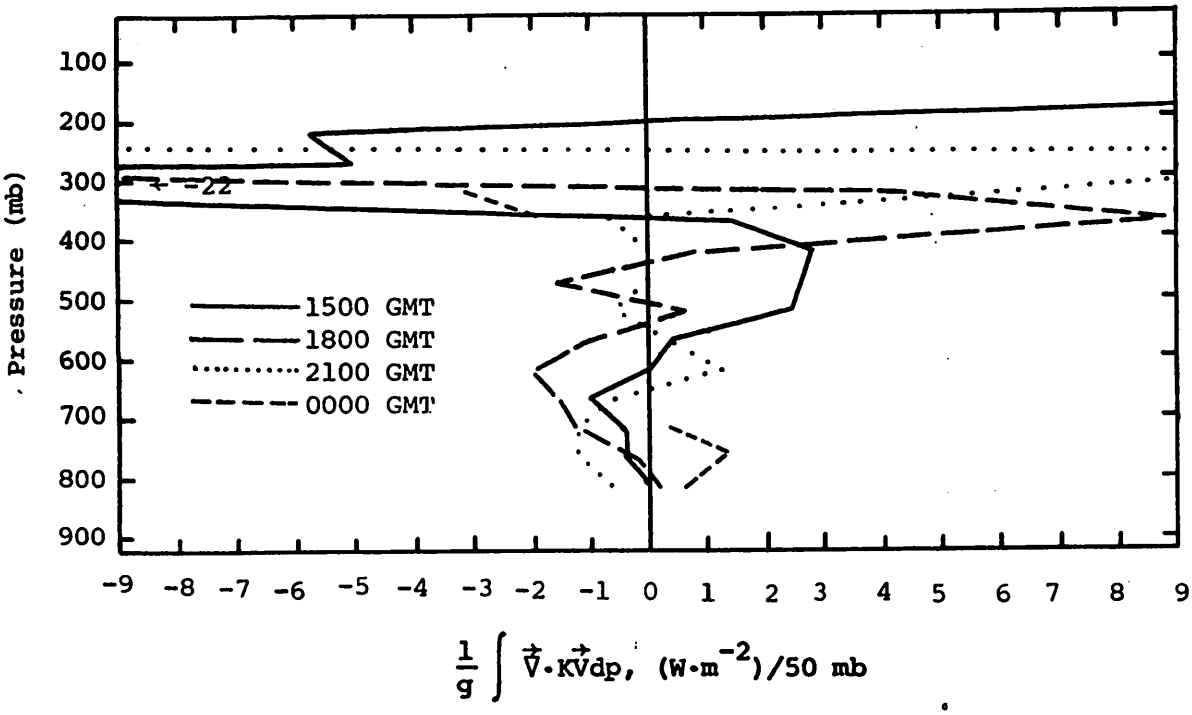

Fig. 5.6.4.6 Vertical profiles of the horizontal flux of kinetic energy for 7 June 1978.

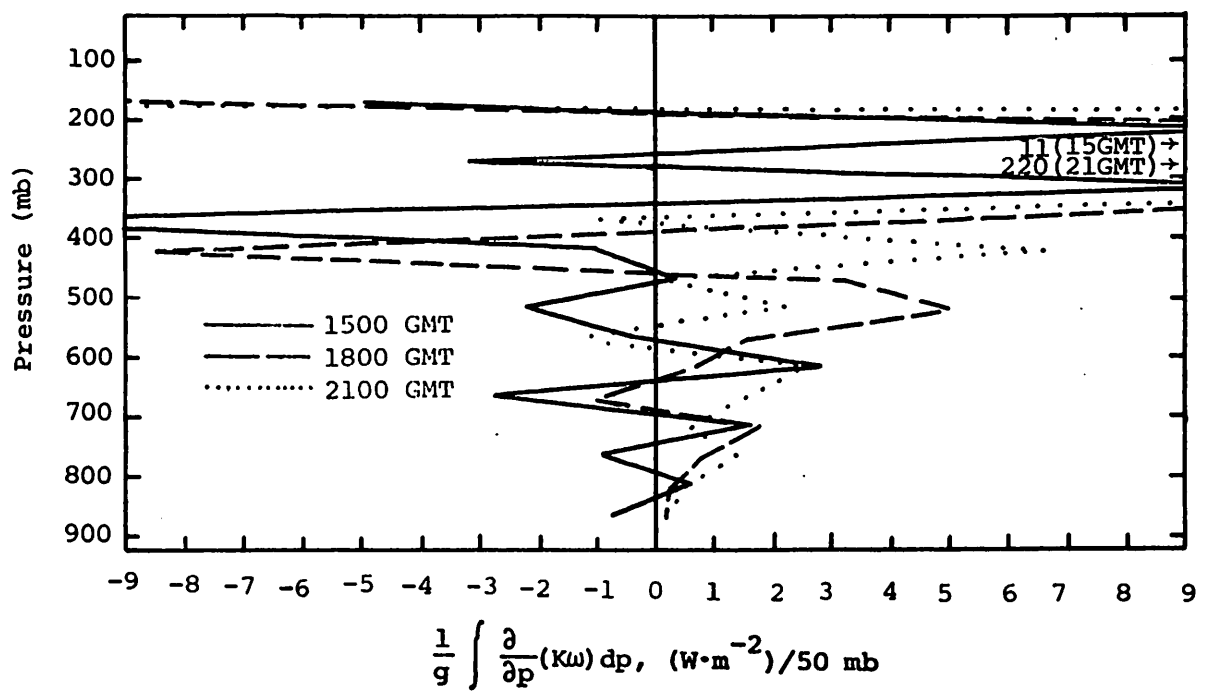

Fig. 5.6.4.7 Vertical profiles of the vertical flux of kinetic energy for 7 June 1978.

mainly transport out of layers below 500 mb. This transport was downward at 1500 GMT and upward at the other time periods. Above 500 mb there was a layer with vertical inflow at 1500 and 1800 GMT. Large values of transport out of layers between 350 and 200 mb were present with increases above 200 mb. The profiles at 1800 and 2100 GMT, together with profiles of horizontal transport, suggest a pattern of inflow of kinetic energy at low layers and vertical transport to upper layers where outflow occurred.

5.6.5 Water Vapor Budget

Figure 5.6.5.1 shows the net horizontal transport of water vapor. Outflow of water vapor was present at 1500 GMT at middle levels. Inflow of water vapor was present at all levels for the other two times.

The profiles of net vertical transport of water vapor show losses at all levels at 1500 GMT (Fig. 5.6.5.2). At 1800 and 2100 GMT losses occurred at lower levels with net gains above 700 mb.

The vertical transport of water vapor through constant pressure surfaces was downward at 1500 GMT. This is consistent with the downward vertical motion (Fig. 5.6.3.2) at this time and suggests that no activity was taking place. At 1800 and 2100 GMT transport of water vapor through constant pressure surfaces was upward at all levels (Fig. 5.6.5.3). This upward transport fits well with Fig. 5.6.5.2 with water vapor transported out of lower layers into upper layers.

The profiles of combined net horizontal and vertical transport show losses in the upper layers at 1500 GMT (Fig. 5.6.5.4). Gains were present in all levels at 1800 GMT, but there were net losses near the surface at 2100 GMT. This is because more water vapor was transported upward from this layer than was brought in horizontally.

Figure 5.6.5.5 shows profiles of the total mass of water vapor. The profiles are nearly identical at 1500 and 1800 GMT, but the water vapor content at all levels increased at 2100 GMT. This also is shown in Fig. 5.6.5.6 for the local rate-of-change of water vapor. The largest gains were near 800 mb.

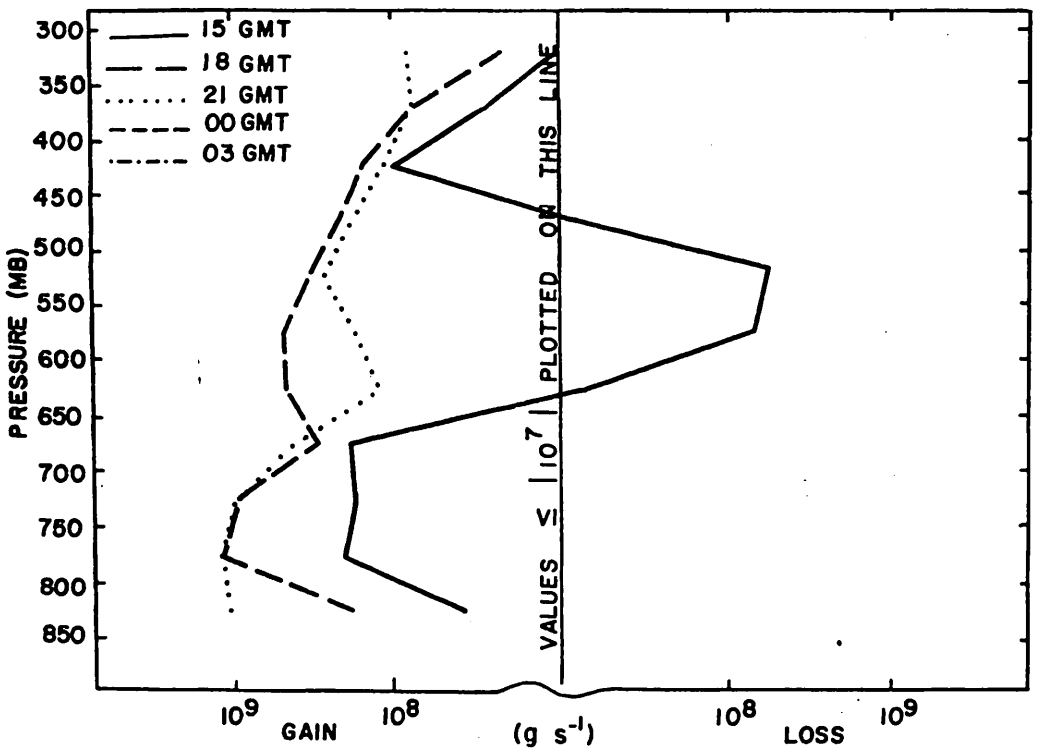

Fig. 5.6.5.1 Net horizontal transport of water vapor through boundaries of 50-mb layers (gm s^{-1}) over the Texas HIPLEX area for 7 June 1978.

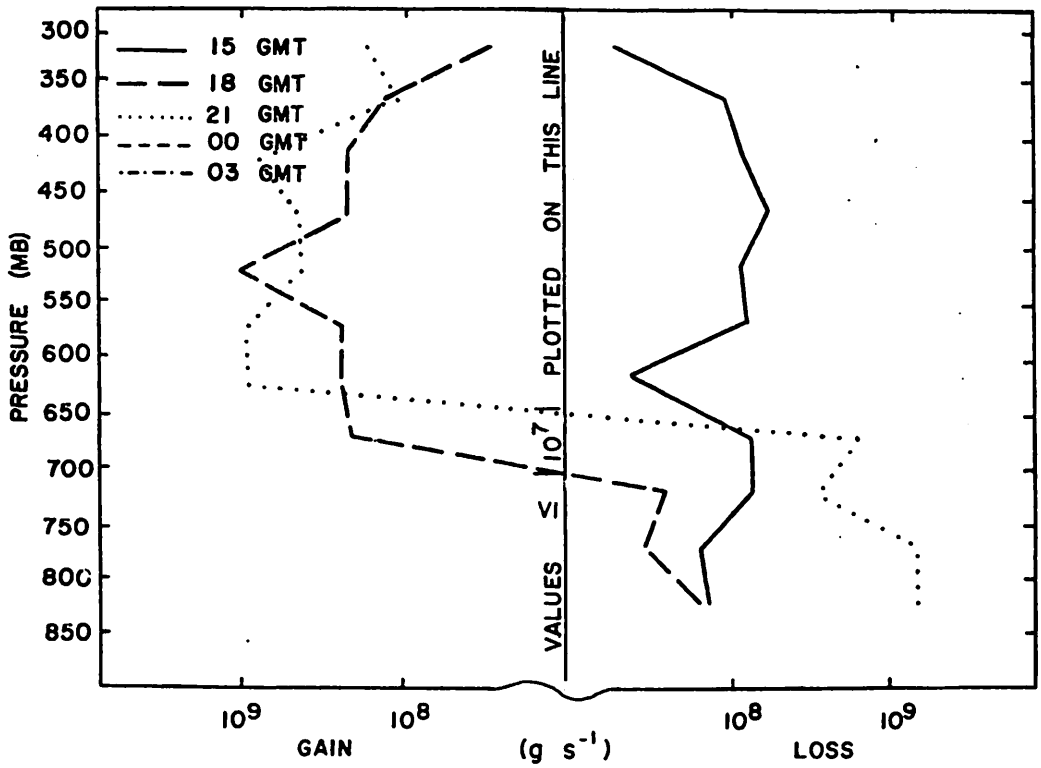

Fig. 5.6.5.2 Net vertical transport of water vapor through boundaries of 50-mb layers (gm s^{-1}) over the Texas HIPLEX area for 7 June 1978.

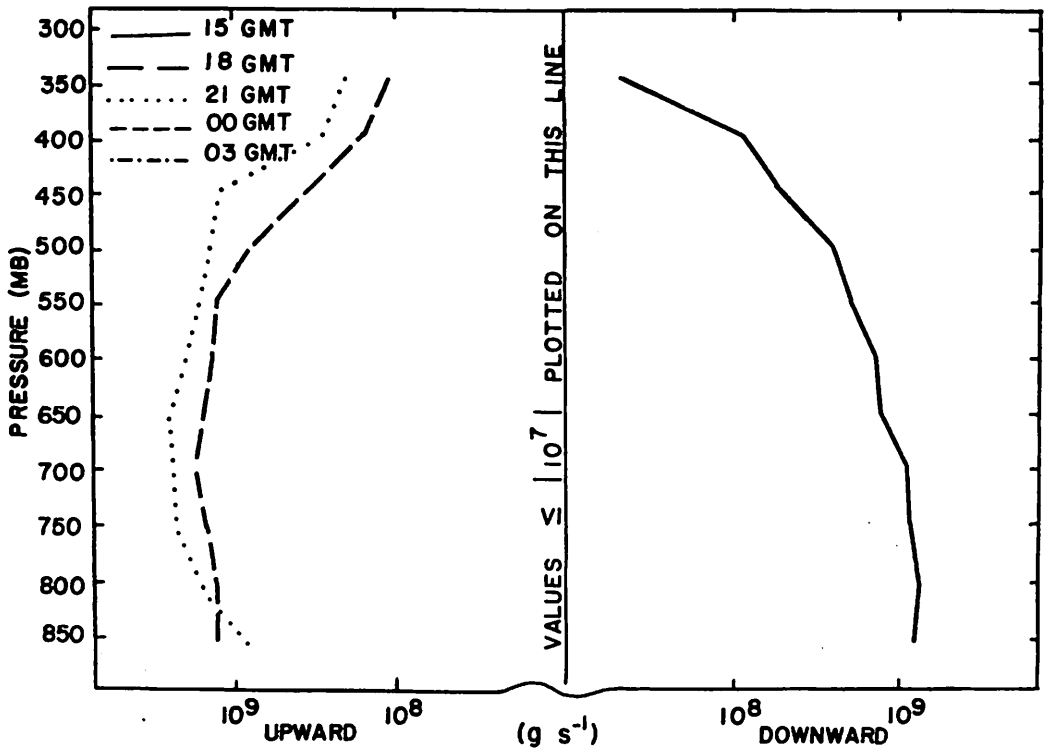

Fig. 5.6.5.3 Vertical transport of water vapor through constant pressure surfaces (gm s^{-1}) over the Texas HIPLEX area for 7 June 1978.

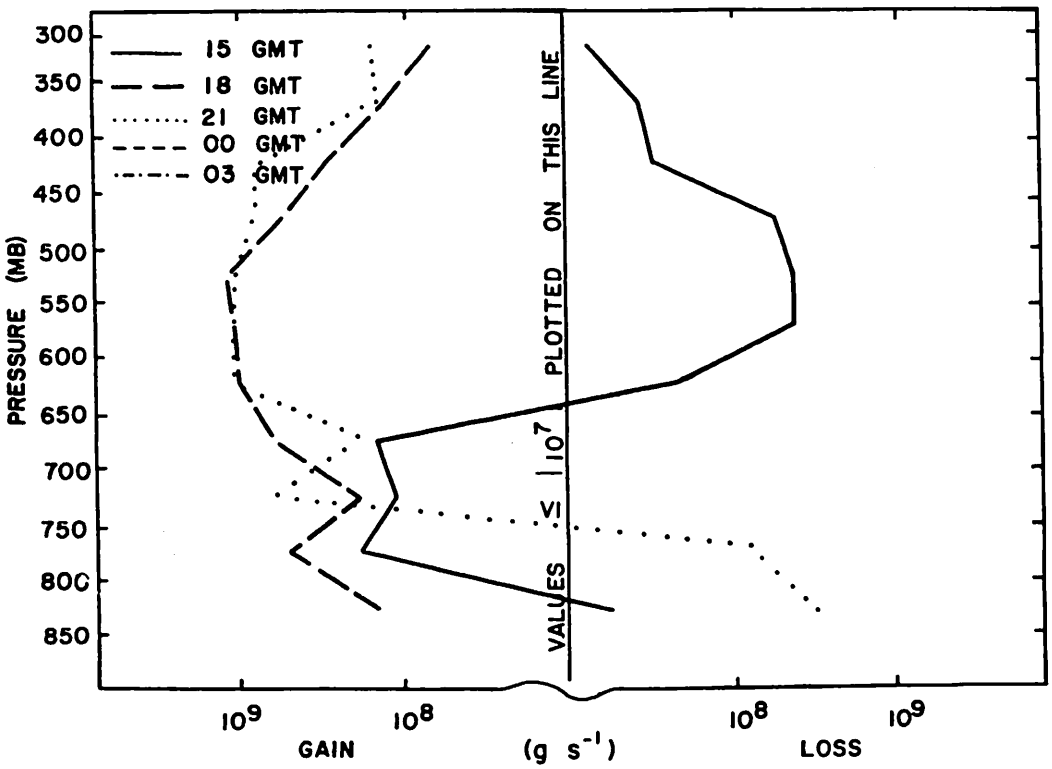

Fig. 5.6.5.4 Combined net horizontal and vertical transport of water vapor through boundaries of 50-mb layers (gm s^{-1}) over the Texas HIPLEX area for 7 June 1978.

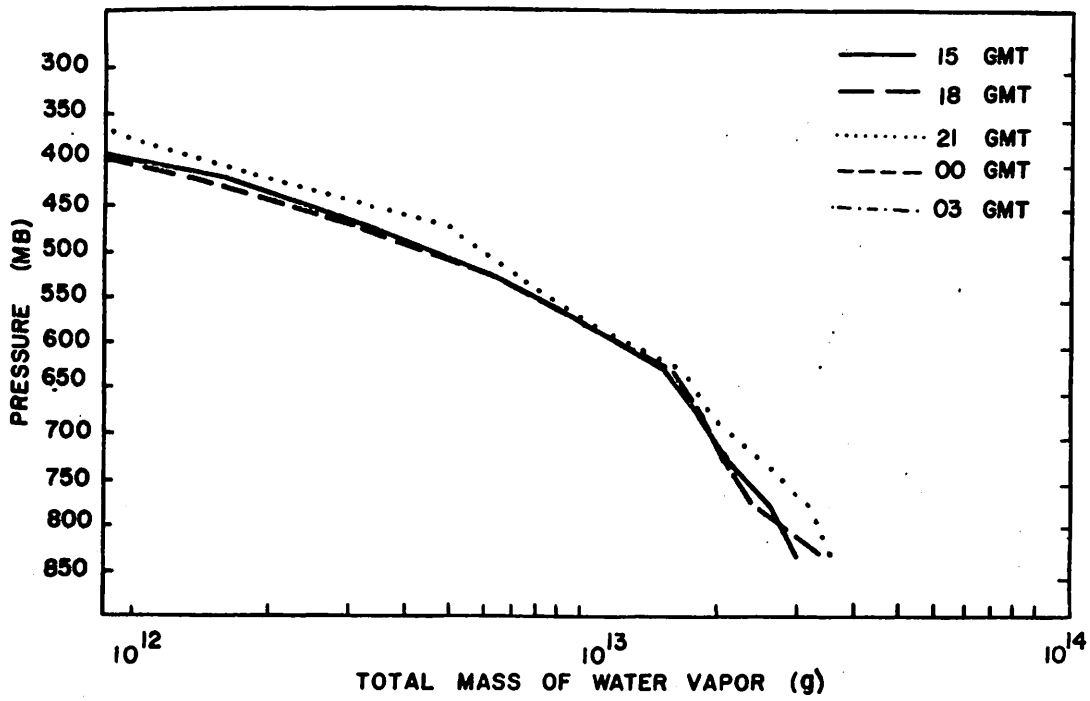

Fig. 5.6.5.5 Total mass of water vapor in layers 50 mb deep (gm) over the Texas HIPLEX area on 7 June 1978.

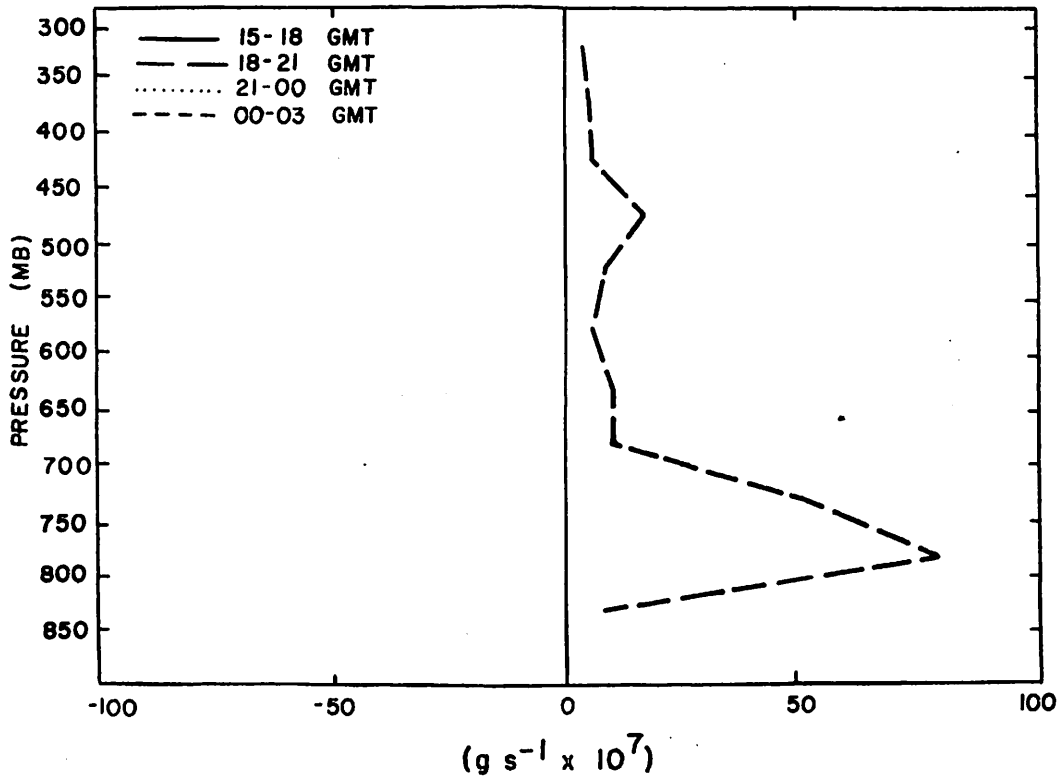

Fig. 5.6.5.6 Local rate-of-change in total mass of water vapor (g s^{-1} x 10^7) for the Texas HIPLEX area for 7 June 1978.

5.7 12 June 1978

5.7.1 Radar

Radar echoes were in the area at only three times (Fig. 5.7.1.1). At 0100 GMT, an echo top reached 14 km (46K ft), and at 0200 GMT the top was 8.5 km (28K ft). A line of well developed thunderstorms occurred 60 km west of Seminole, but did not enter the area.

5.7.2 Surface

Most features observed in the surface analysis on this day resulted from local moisture or wind fluctuations which were not associated with echoes. The temperature field was fairly flat (Fig. 5.7.2.1), but dewpoint depression (Fig. 5.7.2.2), mixing ratio (Fig. 5.7.2.3), and equivalent potential temperature (Fig. 5.7.2.4) fields show a moist area over Big Spring from 1500 to 2100 GMT. This resulted from the persistence of high relative humidity values at Big Spring which were not associated with any known convective elements.

At 0100 GMT, when a radar echo was adjacent to Clairemont, mixing ratios increased in that vicinity. Moisture associated with the echo spread toward the west to Post which recorded a mixing ratio of 17 gm/kg at 0300 GMT.

Although the echo observed at 0100 GMT did not affect surface kinematic fields, some local features persisted in those fields throughout the day. Terrain-induced vertical motion (Fig. 5.7.2.5) exhibited the effect of fairly strong and persistent surface winds. Values reached 2 cm/sec between Vincent and Walsh-Watts where a substantial terrain height gradient exists.

An area of convergence (Fig. 5.7.2.6) persisted close to Snyder throughout the day. This was caused by wind directions at Snyder which deviated from those of adjacent stations. Values of vertical motion 50 mb above the surface (Fig. 5.7.2.7), moisture divergence (Fig. 5.7.2.8), and vertical moisture flux (Fig. 5.7.2.9) also reflect that feature.

The vorticity analysis shows little organization and values were generally low (Fig. 5.7.2.10). The exception occurred near Snyder where the same wind direction deviation that resulted in large values of divergence also caused vorticity centers.

The pressure change charts (Fig. 5.7.2.11) reveal a quiescent pressure field which was unaffected by the echoes at 0100 and 0200 GMT.

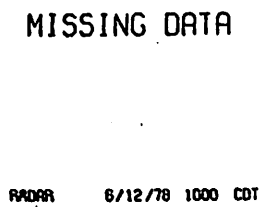

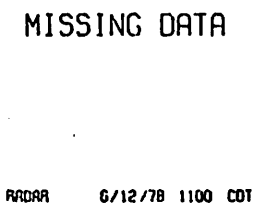

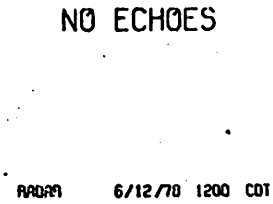

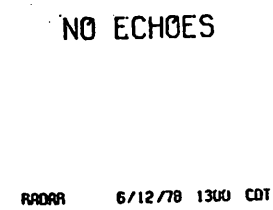

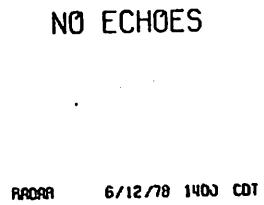

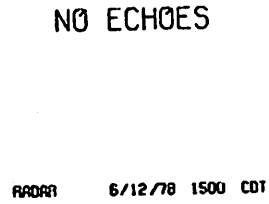

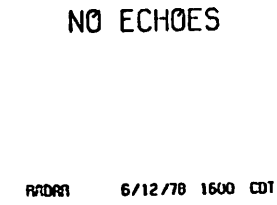

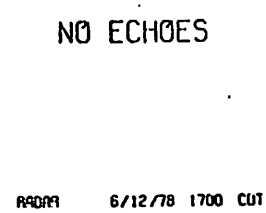

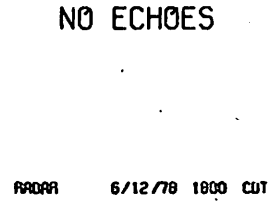

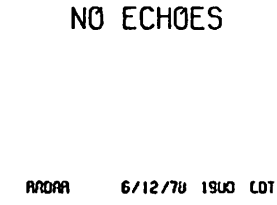

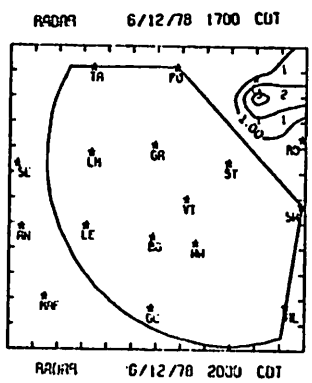

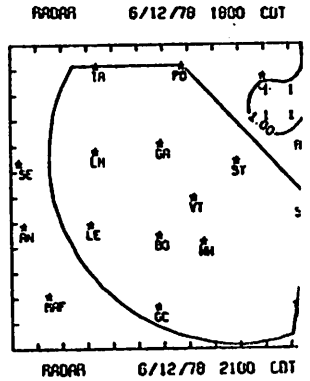

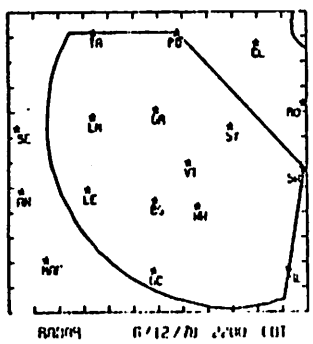

Fig. 5.7.1.1 Radar echoes for 12 June 1978.

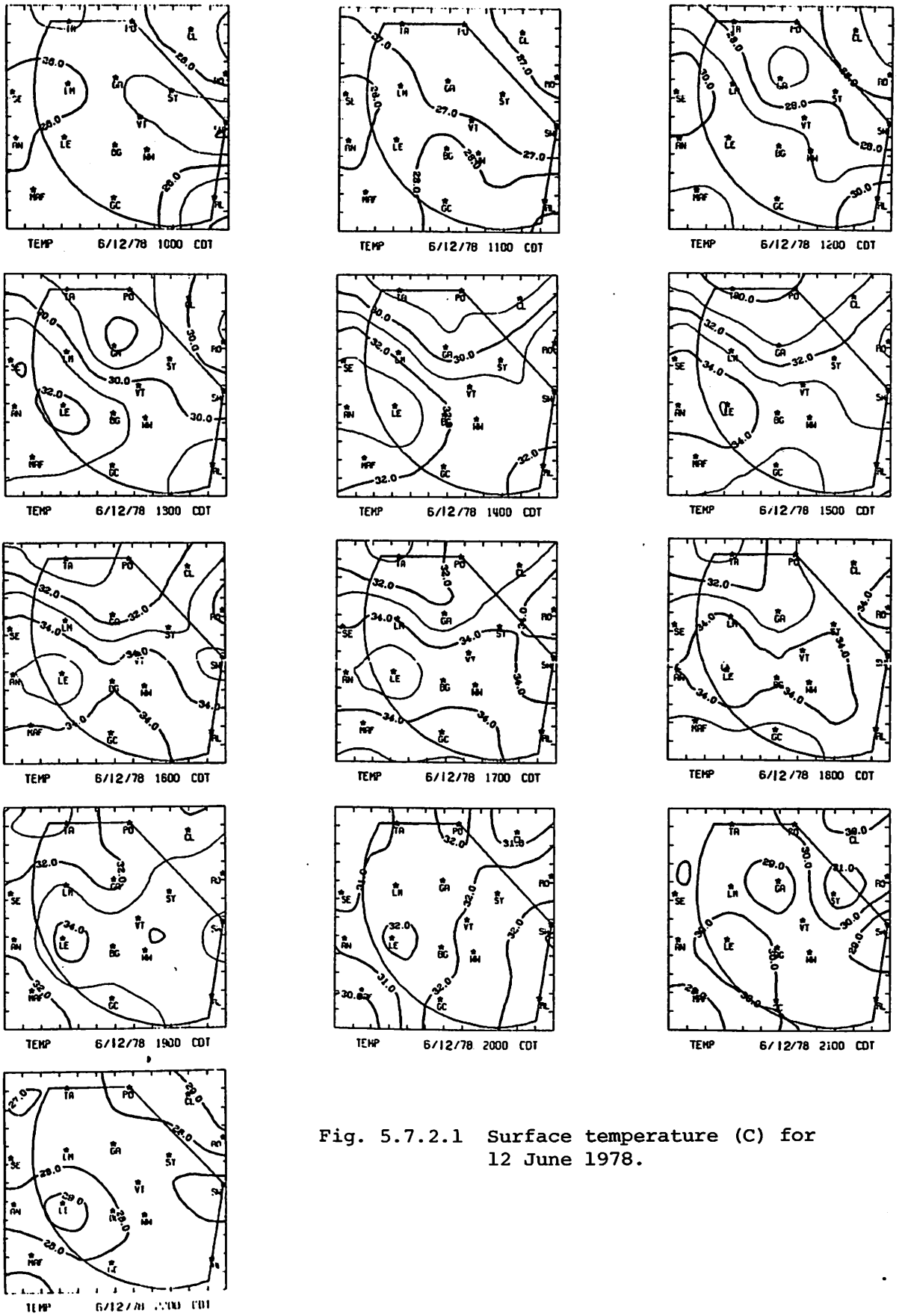

Fig. 5.7.2.1 Surface temperature (C) for 12 June 1978.

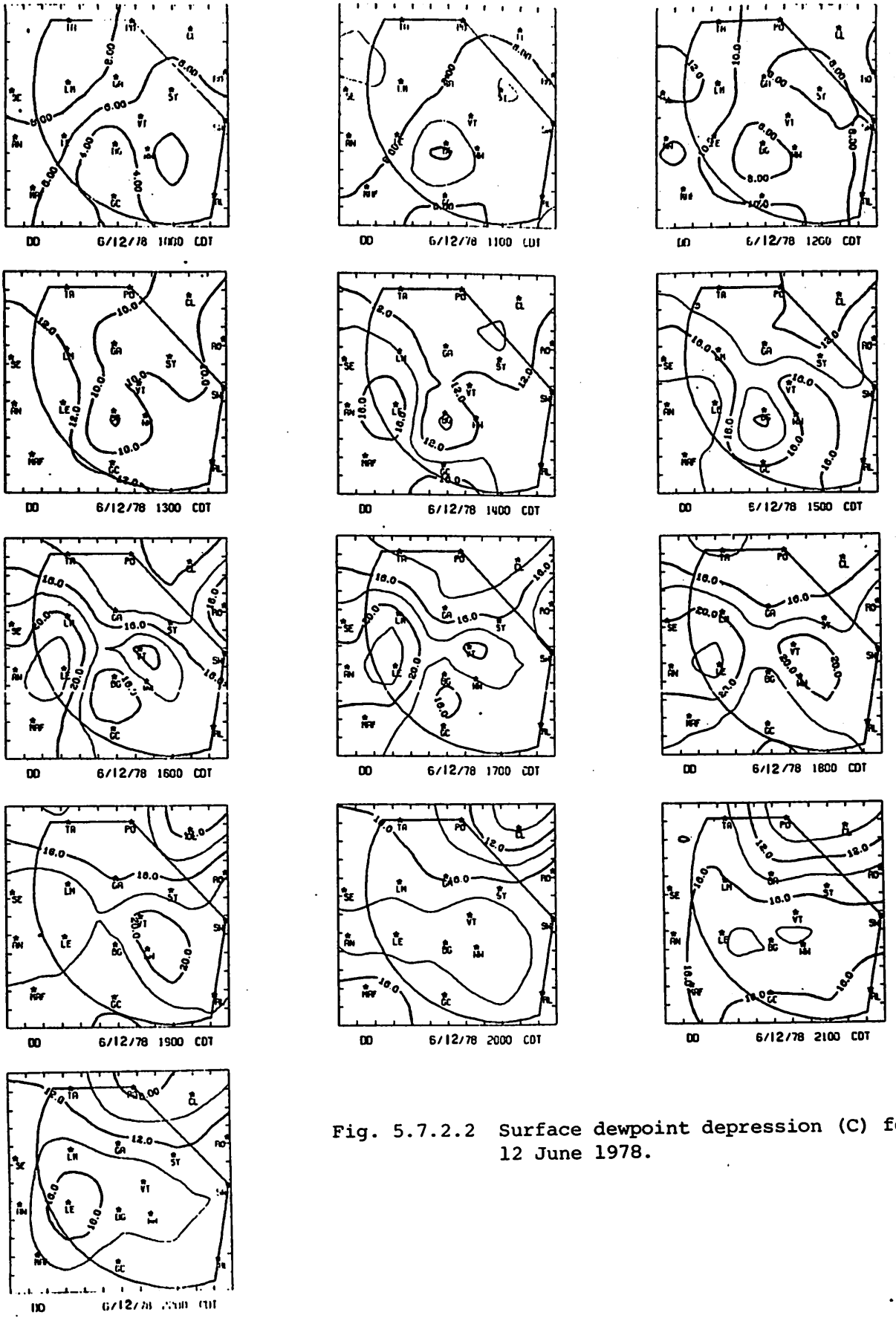

Fig. 5.7.2.2 Surface dewpoint depression (C) for 12 June 1978.

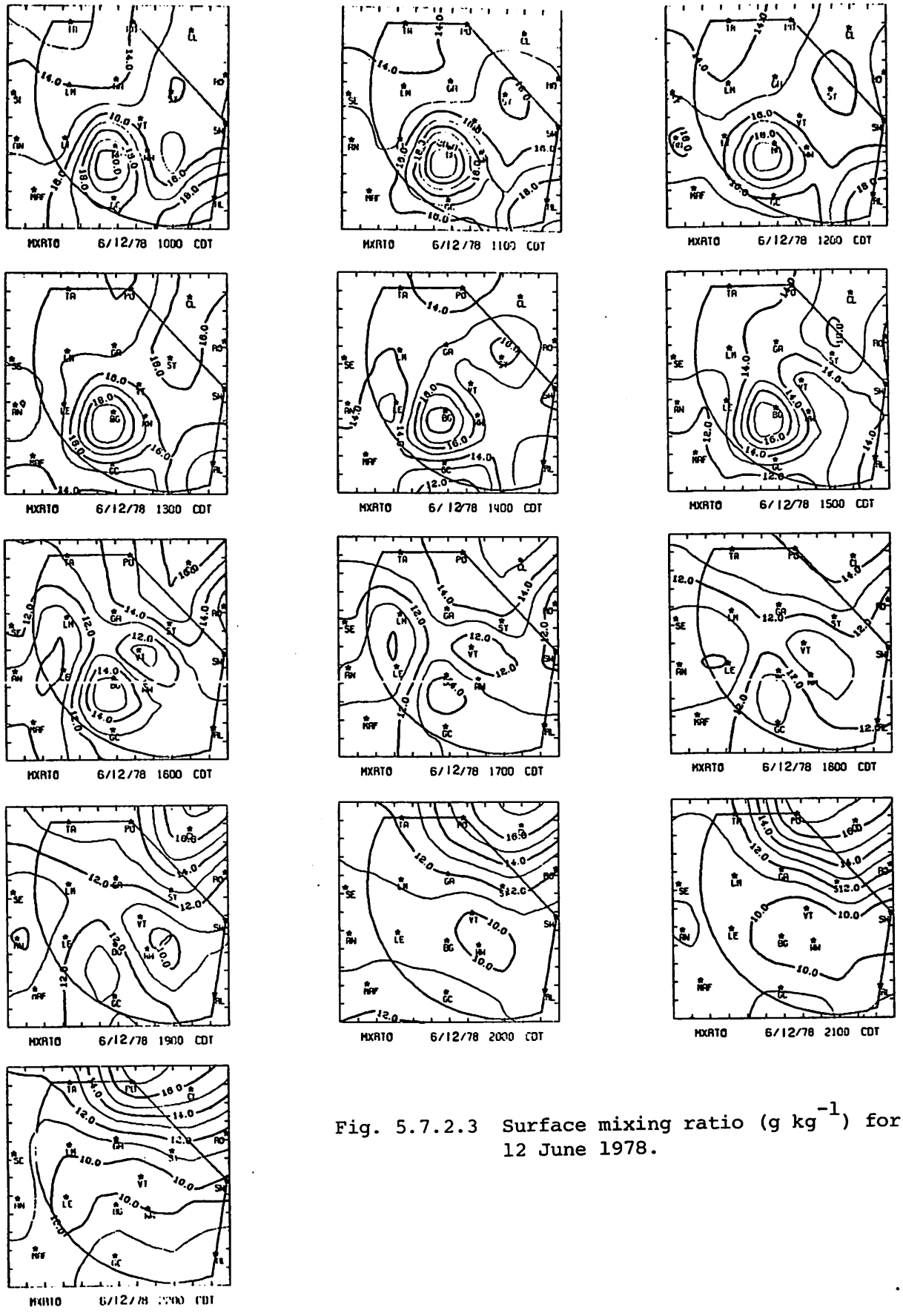

Fig. 5.7.2.3 Surface mixing ratio (g kg^{-1}) for 12 June 1978.

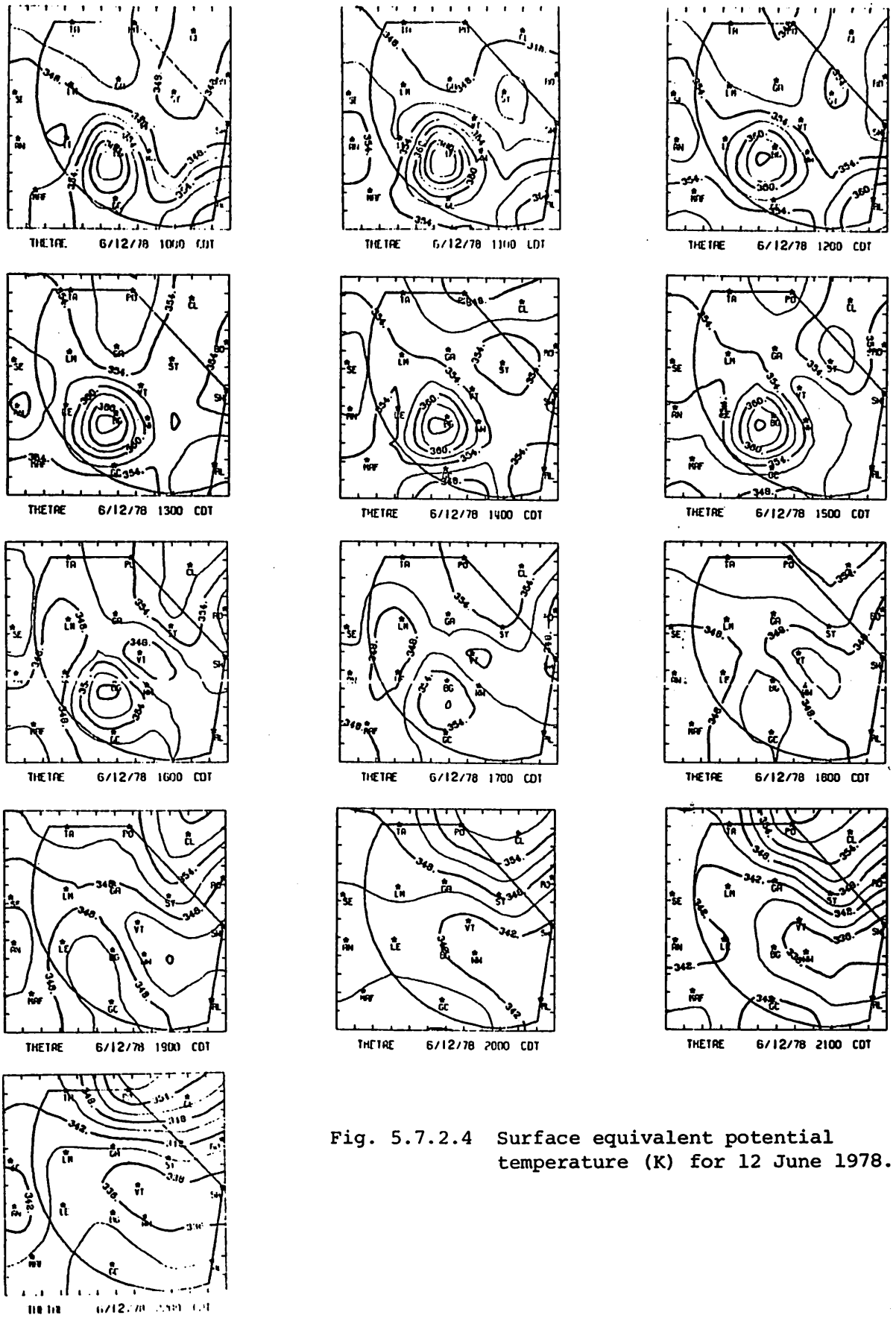

Fig. 5.7.2.4 Surface equivalent potential temperature (K) for 12 June 1978.

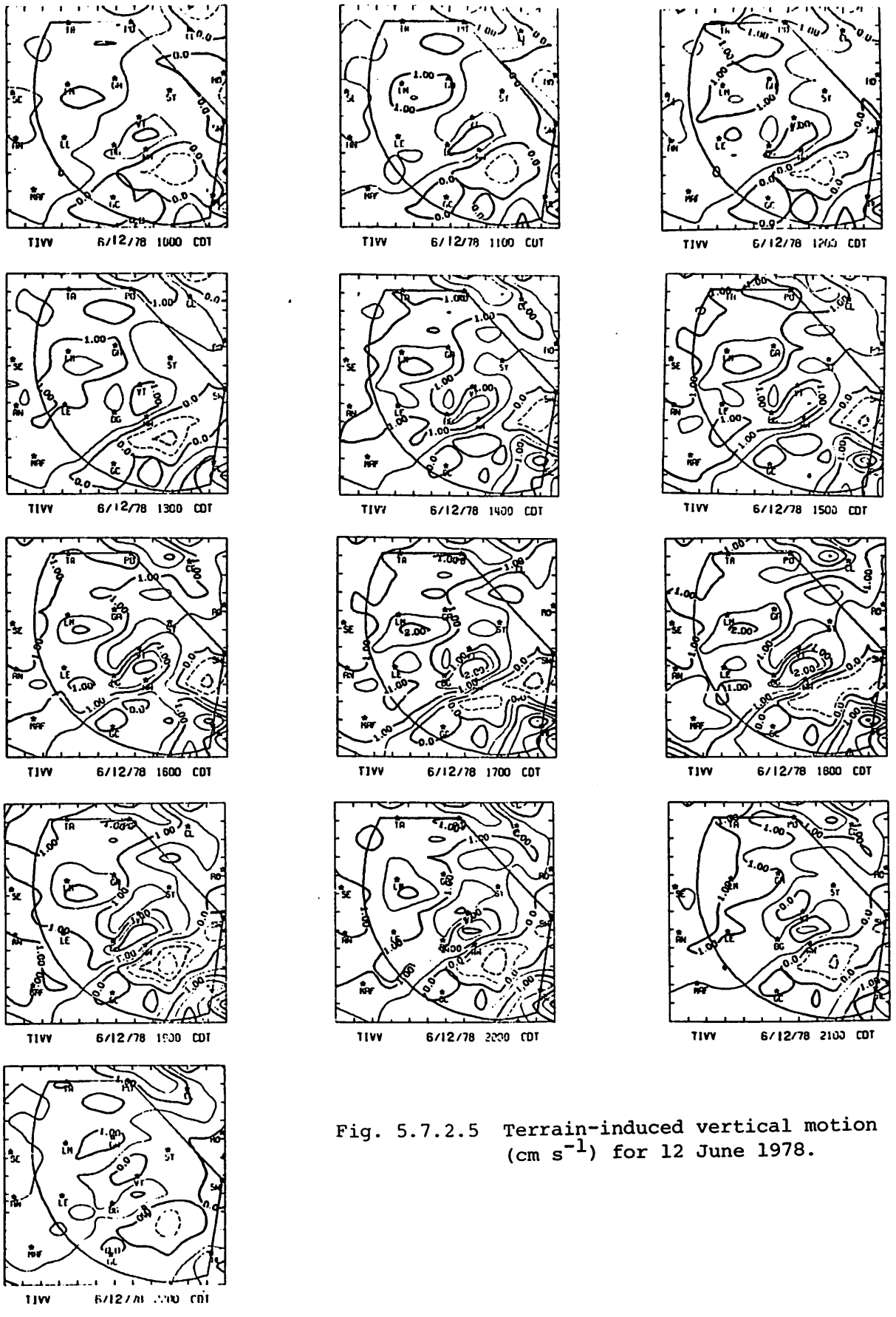

Fig. 5.7.2.5 Terrain-induced vertical motion (cm s^{-1}) for 12 June 1978.

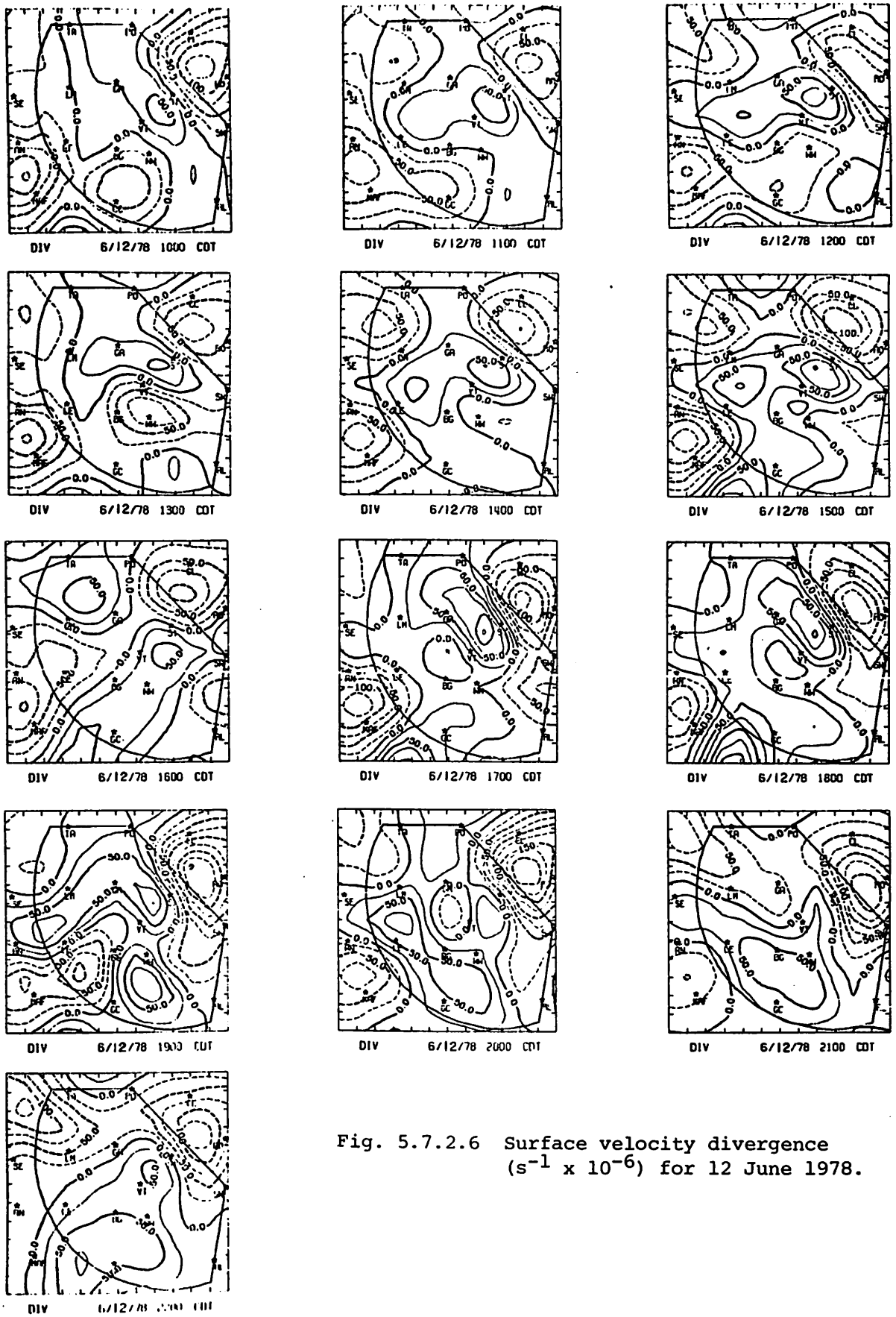

Fig. 5.7.2.6 Surface velocity divergence (s^{-1} x 10^{-6}) for 12 June 1978.

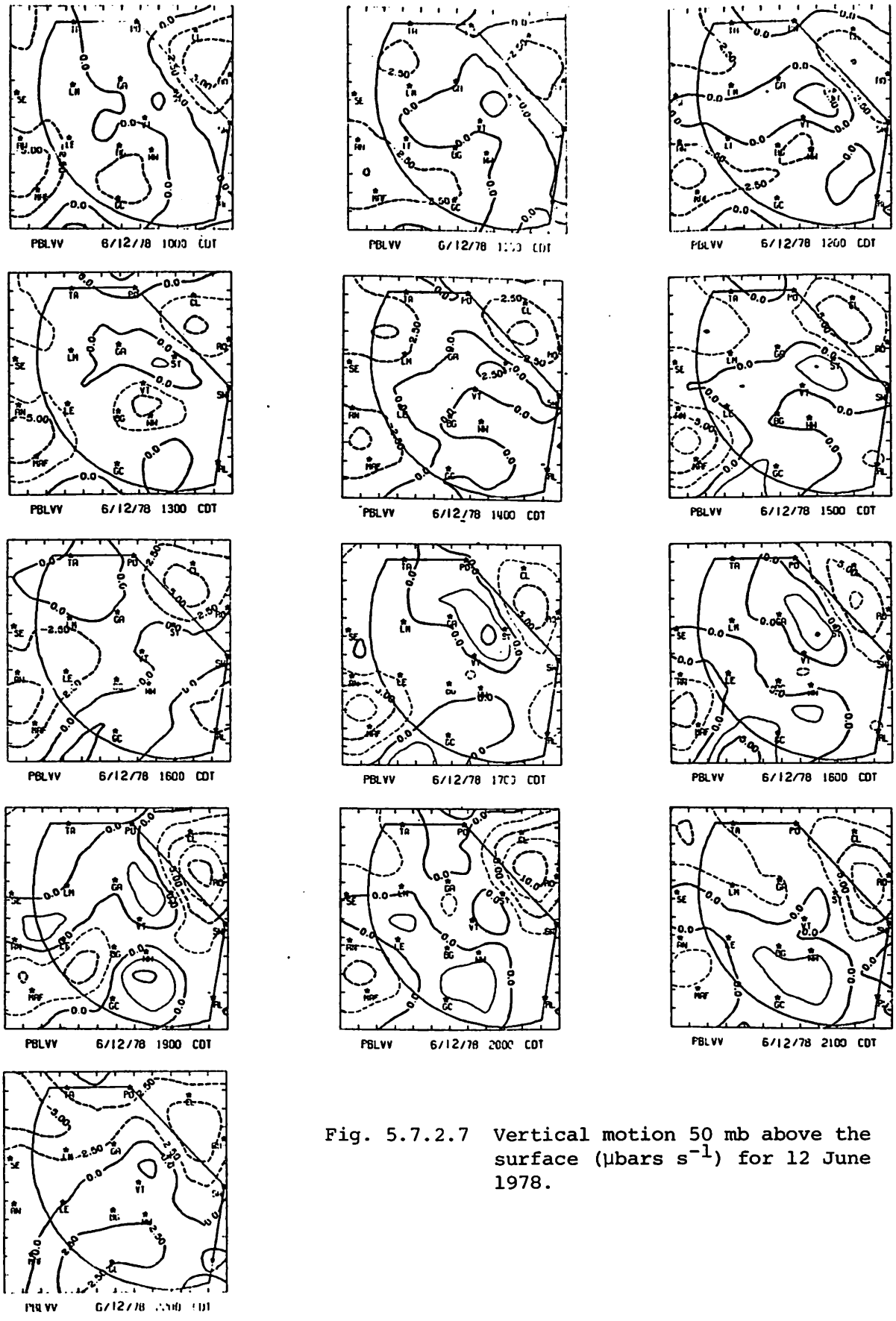

Fig. 5.7.2.7 Vertical motion 50 mb above the surface (μbars s^{-1}) for 12 June 1978.

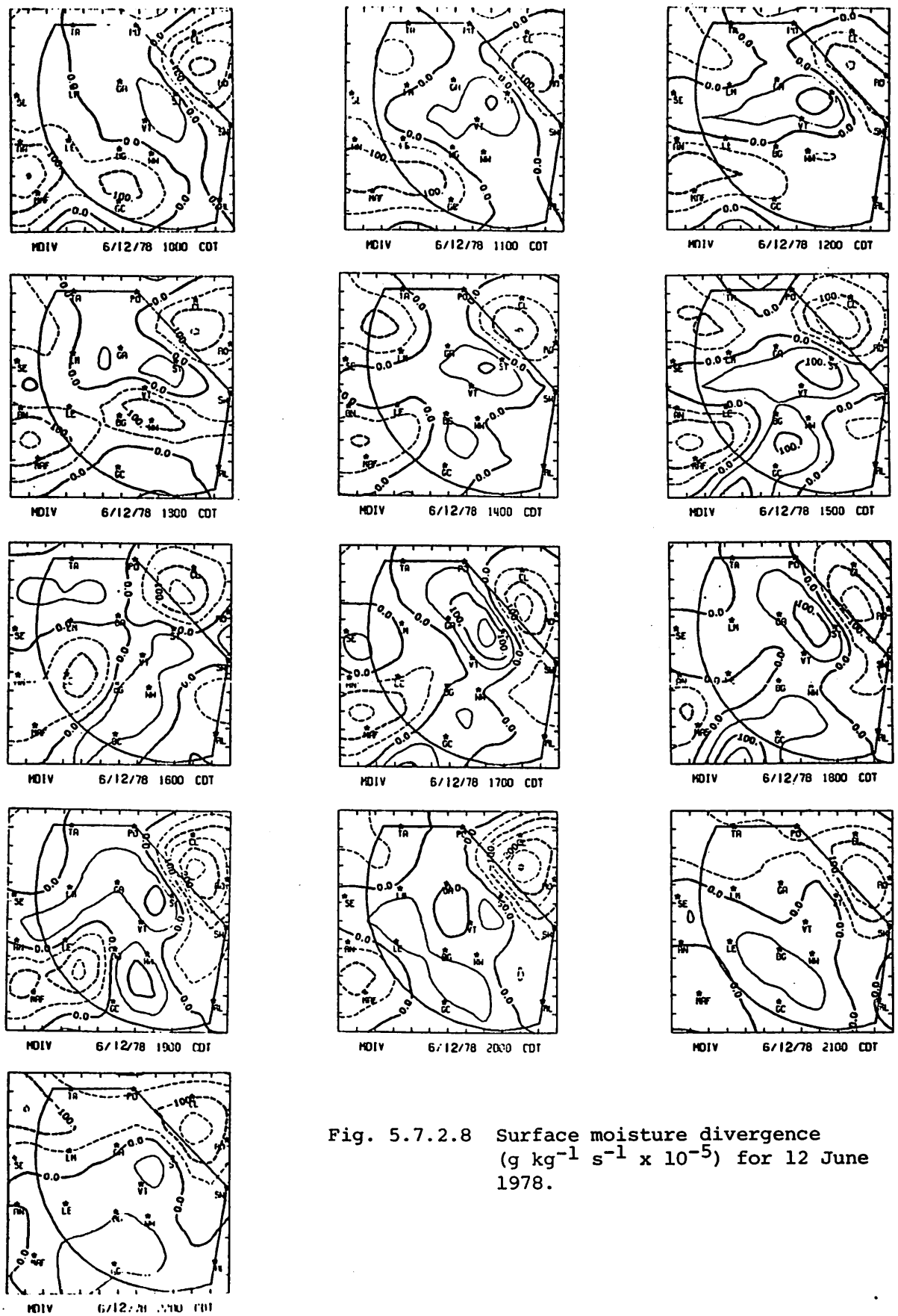

Fig. 5.7.2.8 Surface moisture divergence ($g\ kg^{-1}\ s^{-1} \times 10^{-5}$) for 12 June 1978.

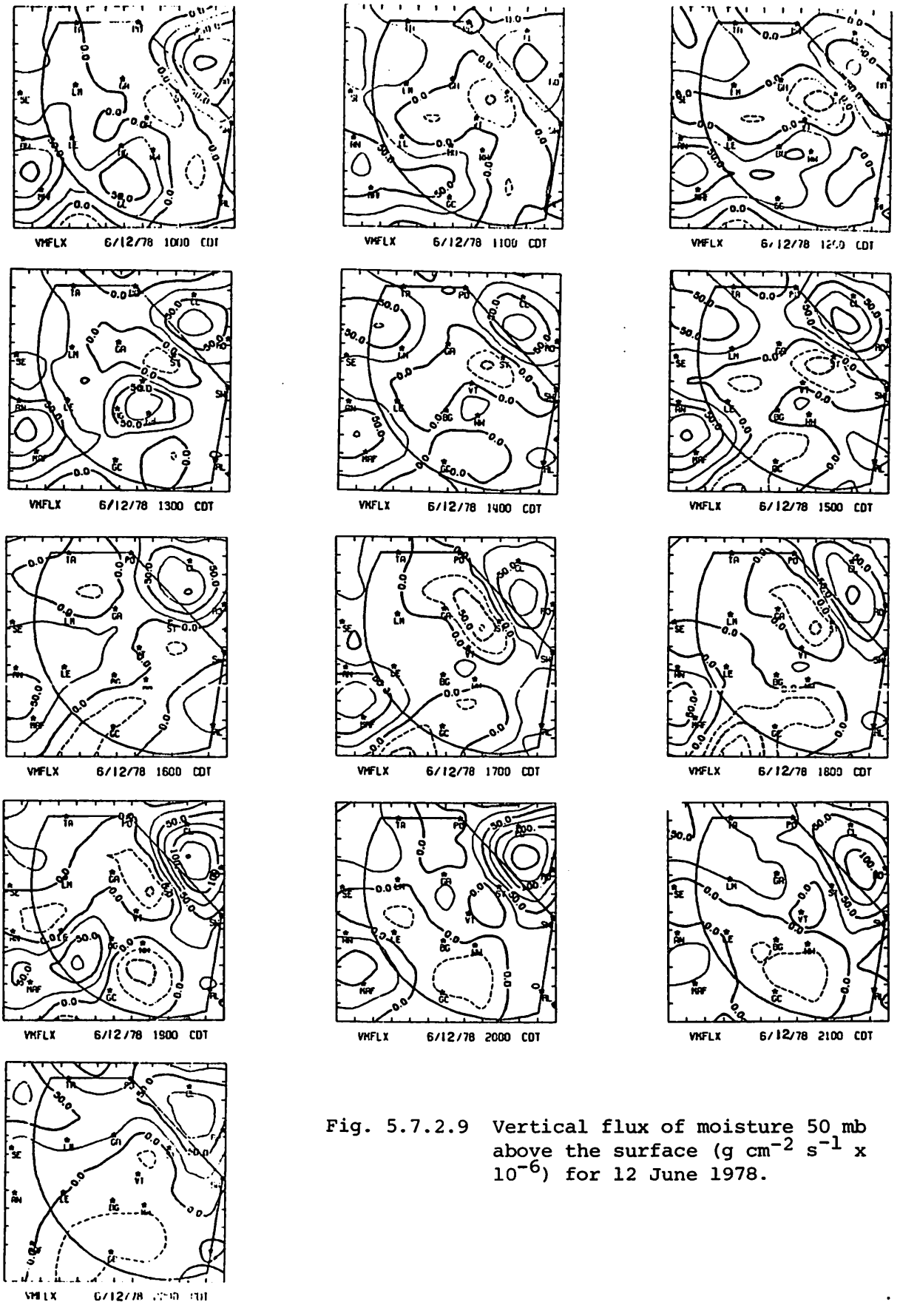

Fig. 5.7.2.9 Vertical flux of moisture 50 mb above the surface (g cm^{-2} s^{-1} x 10^{-6}) for 12 June 1978.

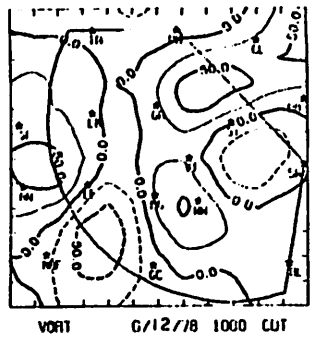

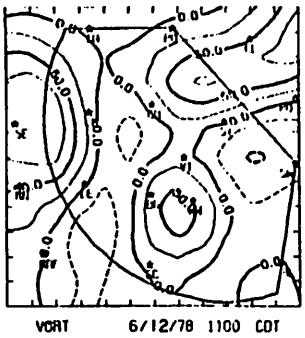

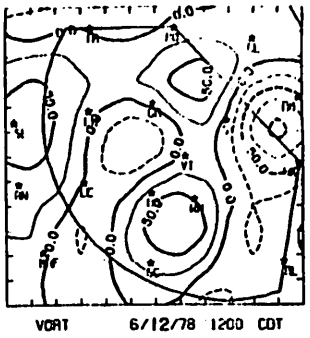

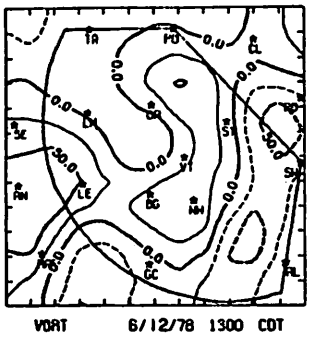

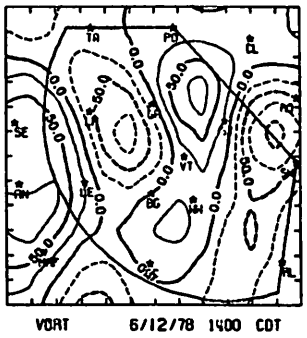

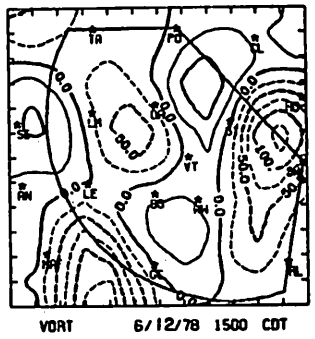

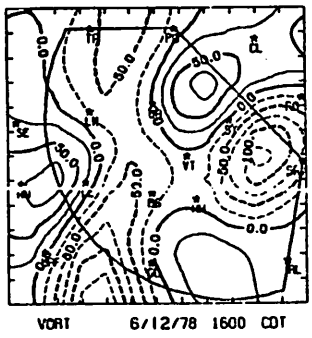

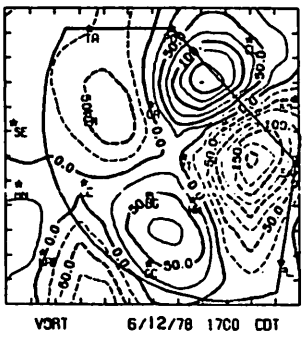

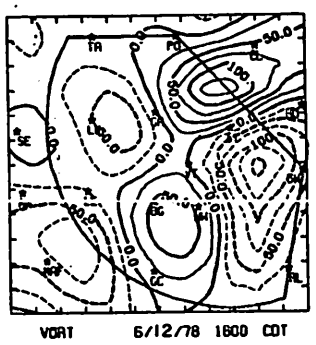

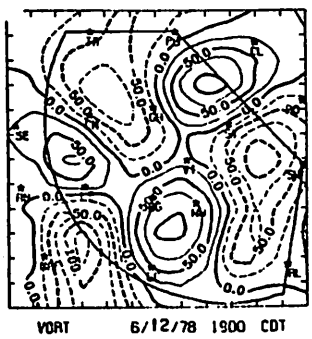

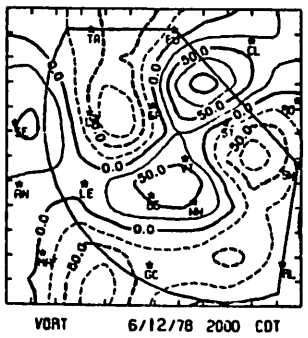

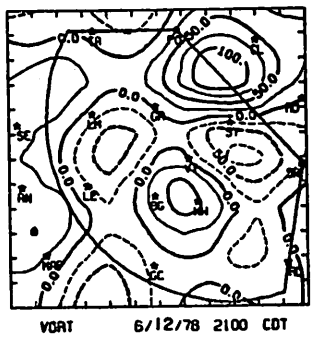

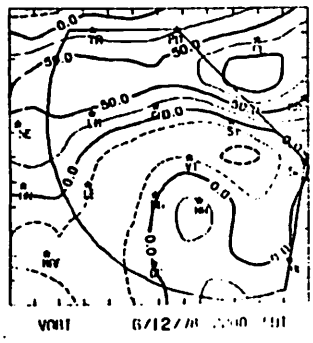

Fig. 5.7.2.10 Surface vorticity (s^{-1} x 10^{-6}) for 12 June 1978.

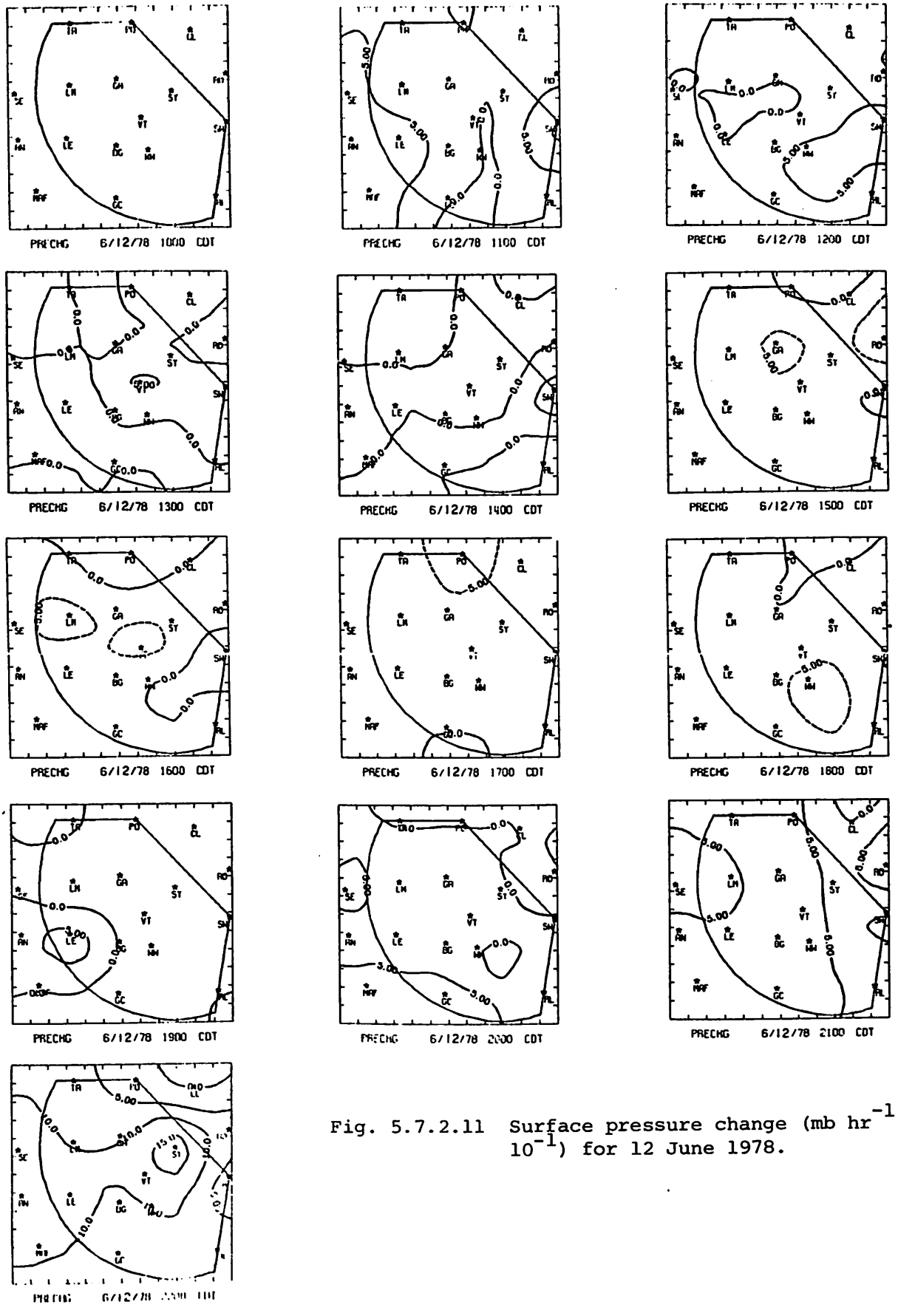

Fig. 5.7.2.11 Surface pressure change (mb hr^{-1} x 10^{-1}) for 12 June 1978.

The surface wind analysis (Fig. 5.7.2.12) shows high wind speeds in the western section of the network. Maximum wind speeds occurred between 2000 and 0100 GMT, and roughly correspond to the times during which thunderstorms were active to the west of the network.

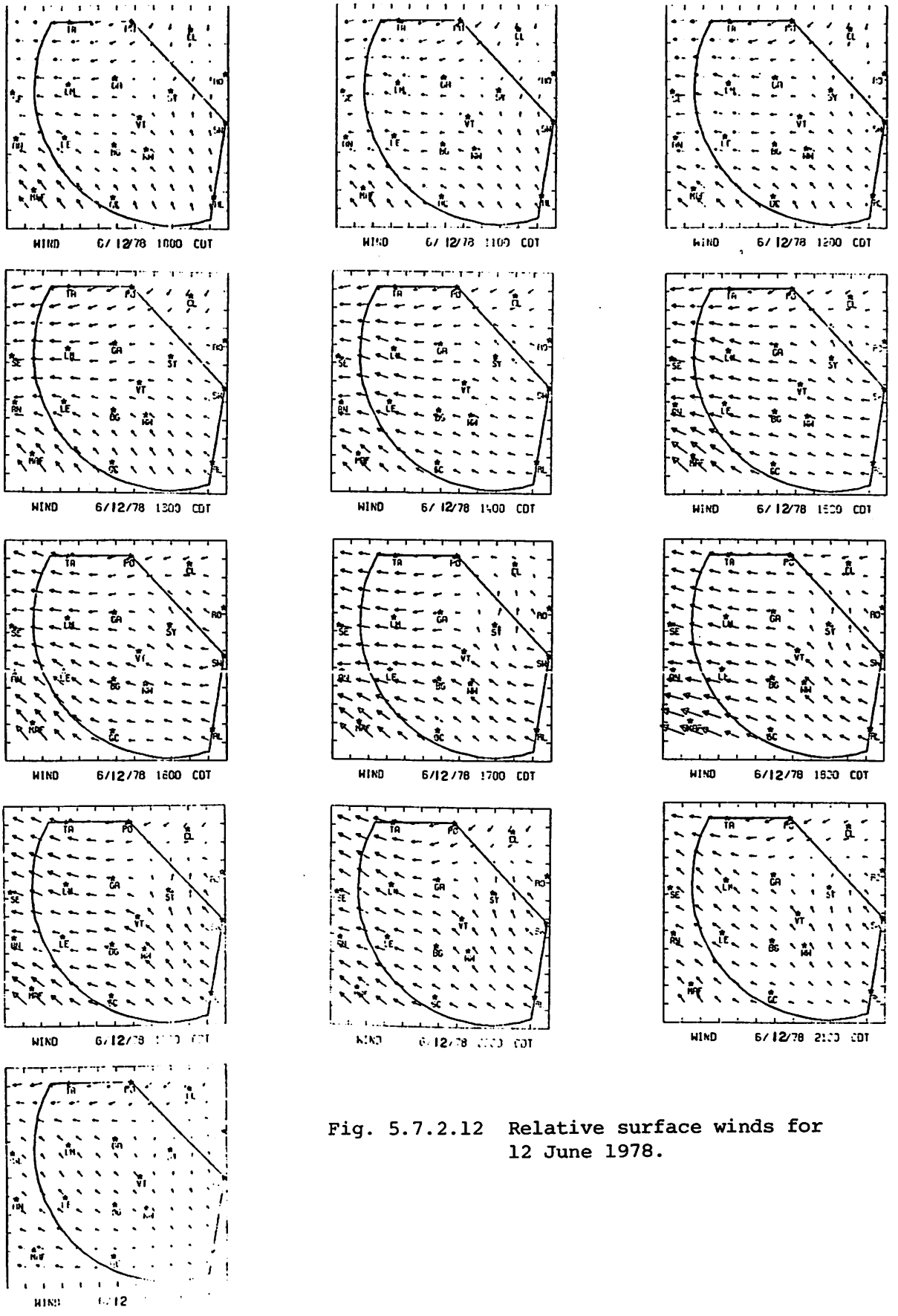

Fig. 5.7.2.12 Relative surface winds for 12 June 1978.

5.8 13 June 1978

5.8.1 Radar

No echoes were observed prior to 1900 GMT when a strong cell formed in the east near Snyder (Fig. 5.8.1.1). This cell moved eastward and at 2000 GMT shower activity began to develop in the west near Lamesa. Echo tops exceeded 15 km (50K ft) in the west between 2200 and 0000 GMT. After 0200 GMT no echo activity was present.

5.8.2 Surface

Surface temperature (fig. 5.8.2.1) showed a stable pattern early in the day with a maximum in the Big Spring area. At 2200 GMT, cooling occurred in the northeast at Tahoka and Gail in association with strong convective activity, and a minimum remained in that area through the remainder of the day.

Surface dewpoint depression (Fig. 5.8.2.2) increased early in the day but like the temperature fields the patterns remained stable until 2200 GMT. Minimum dewpoint depressions were present in the northeast at 2200 GMT and after 0000 GMT maximum depressions were centered at Lamesa throughout the day.

Surface mixing ratio (Fig. 5.8.2.3) was at a maximum at Big Spring during the first few hours. At 1900 GMT mixing ratios increased in the northeast with the onset of shower activity. Mixing ratios in the northwest were fairly low until 2200 GMT when they increased near Tahoka. Mixing ratios remained high in the north for the remainder of the day.

Equivalent potential temperature (Fig. 5.8.2.4) showed a maximum at Big Spring early in the day, corresponding to maximum mixing ratio in that area. Potential temperature increased in the northeast at 1800 GMT just prior to storm development, and remained high in that area for the remainder of the day. Potential temperature increased near Tahoka at 2200 GMT and at 0100 GMT due to moisture increases in that area.

Terrain-induced vertical motion (Fig. 5.8.2.5) was large at times. A center of downward motion persisted south of Walsh-Watts, and upward motion greater than 2.5 μbars s^{-1} was present at Gail between 2200 and 2300 GMT.

Patterns of surface divergence (Fig. 5.8.2.6) were variable through the day. Convergence increased in the east from 1800 to 2000 GMT as storms developed north of Snyder. Strong convergence also was present in the northwest at 2100 and 0000 GMT. The echo tops in the west exceeded 15 km (50K ft)

MISSING DATA

NO ECHOES

NO ECHOES

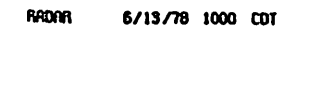

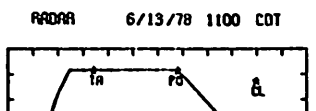

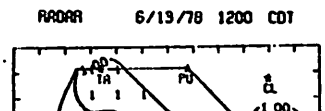

NO ECHOES

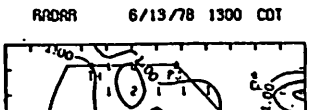

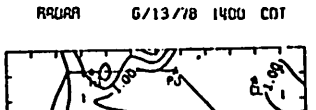

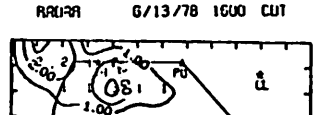

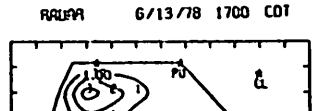

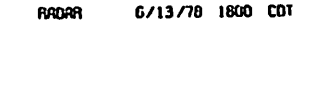

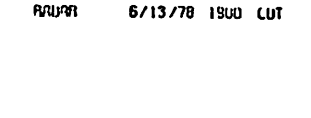

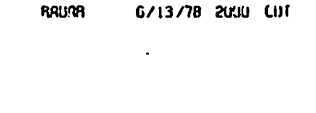

NO ECHOES

RADAR 6/13/78 2100 CDT

NO ECHOES

Fig. 5.8.1.1 Radar echoes for 13 June 1978.

RADAR 6/13/78 2200 CDT

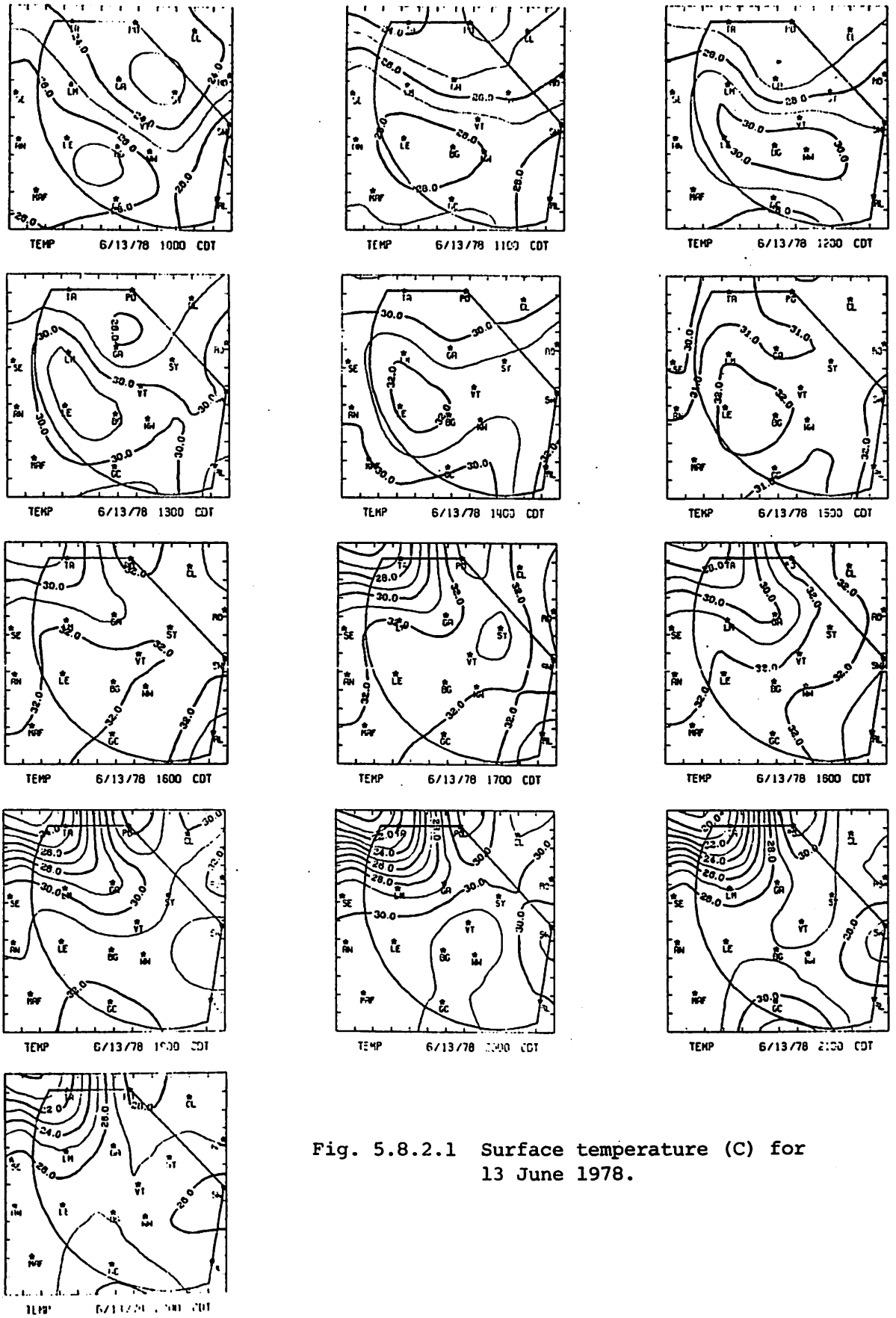

Fig. 5.8.2.1 Surface temperature (C) for 13 June 1978.

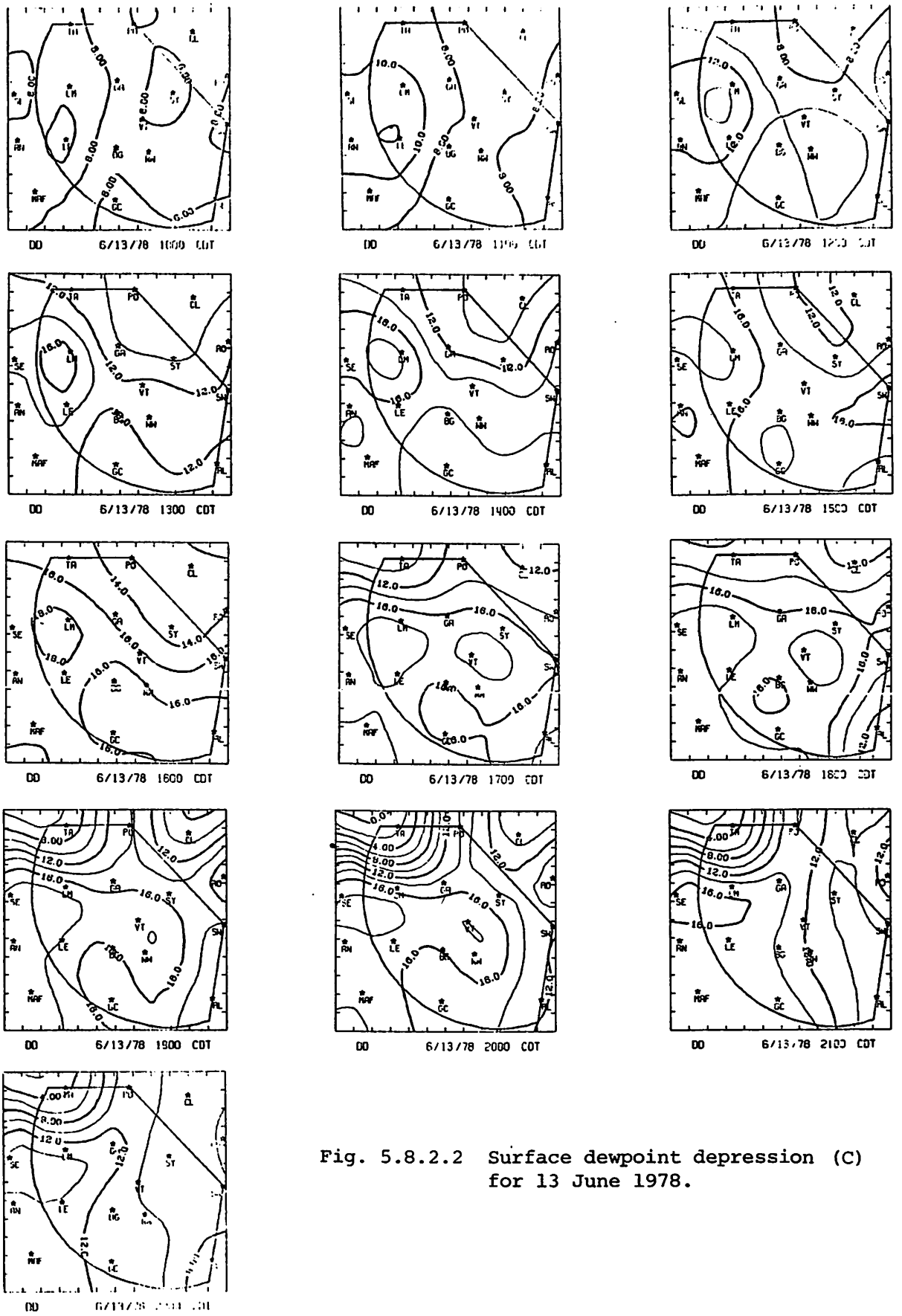

Fig. 5.8.2.2 Surface dewpoint depression (C) for 13 June 1978.

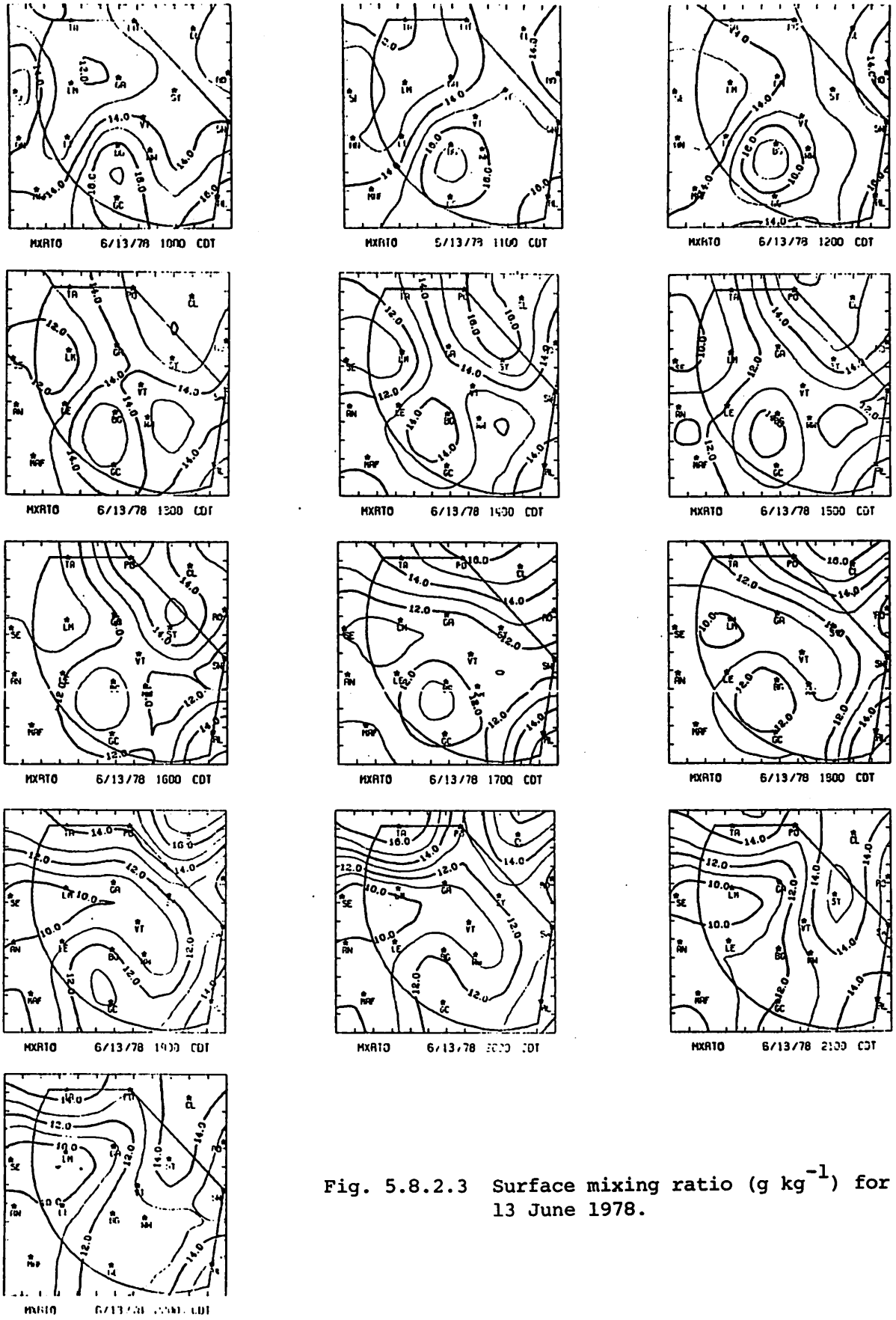

Fig. 5.8.2.3 Surface mixing ratio (g kg^{-1}) for 13 June 1978.

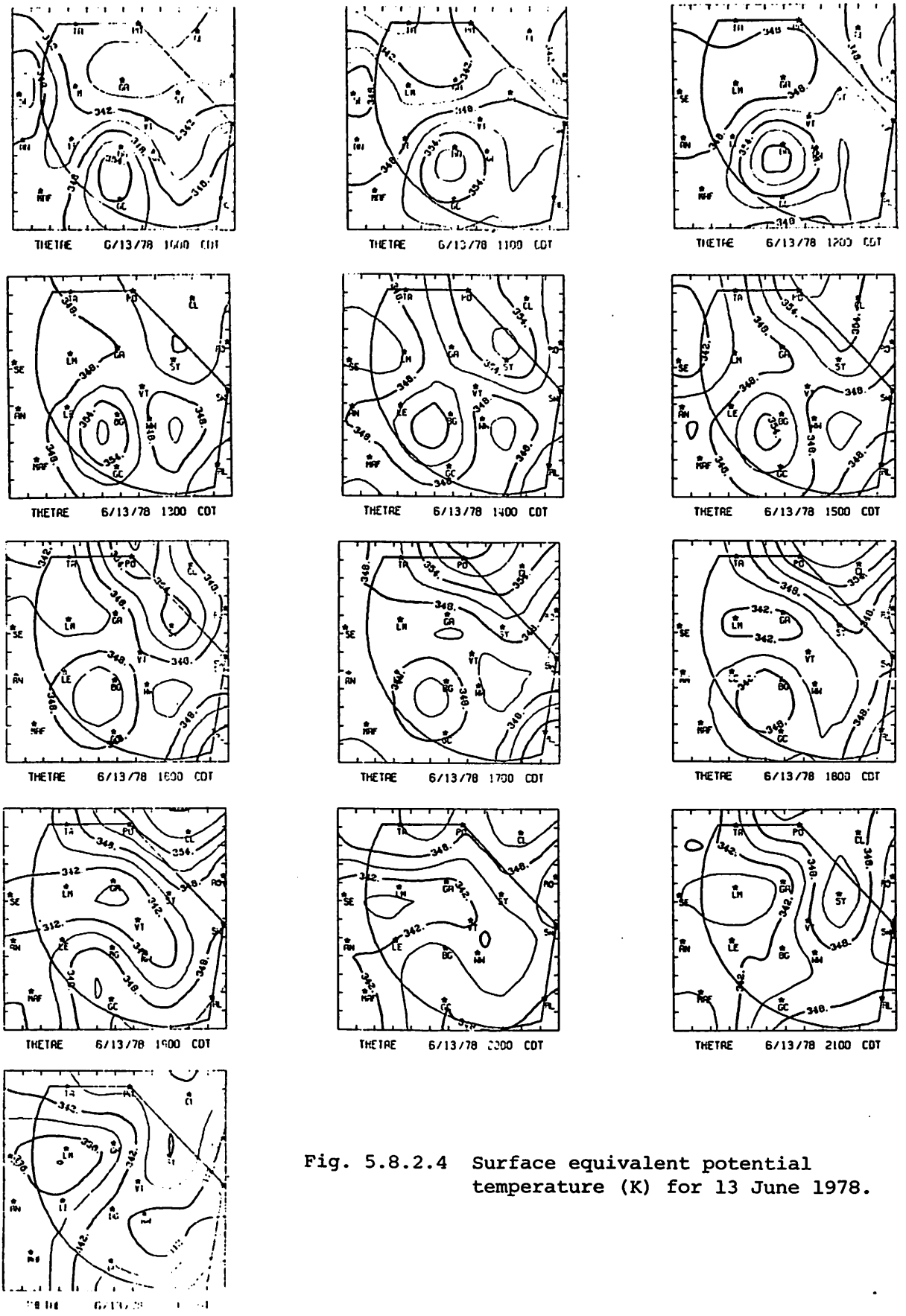

Fig. 5.8.2.4 Surface equivalent potential temperature (K) for 13 June 1978.

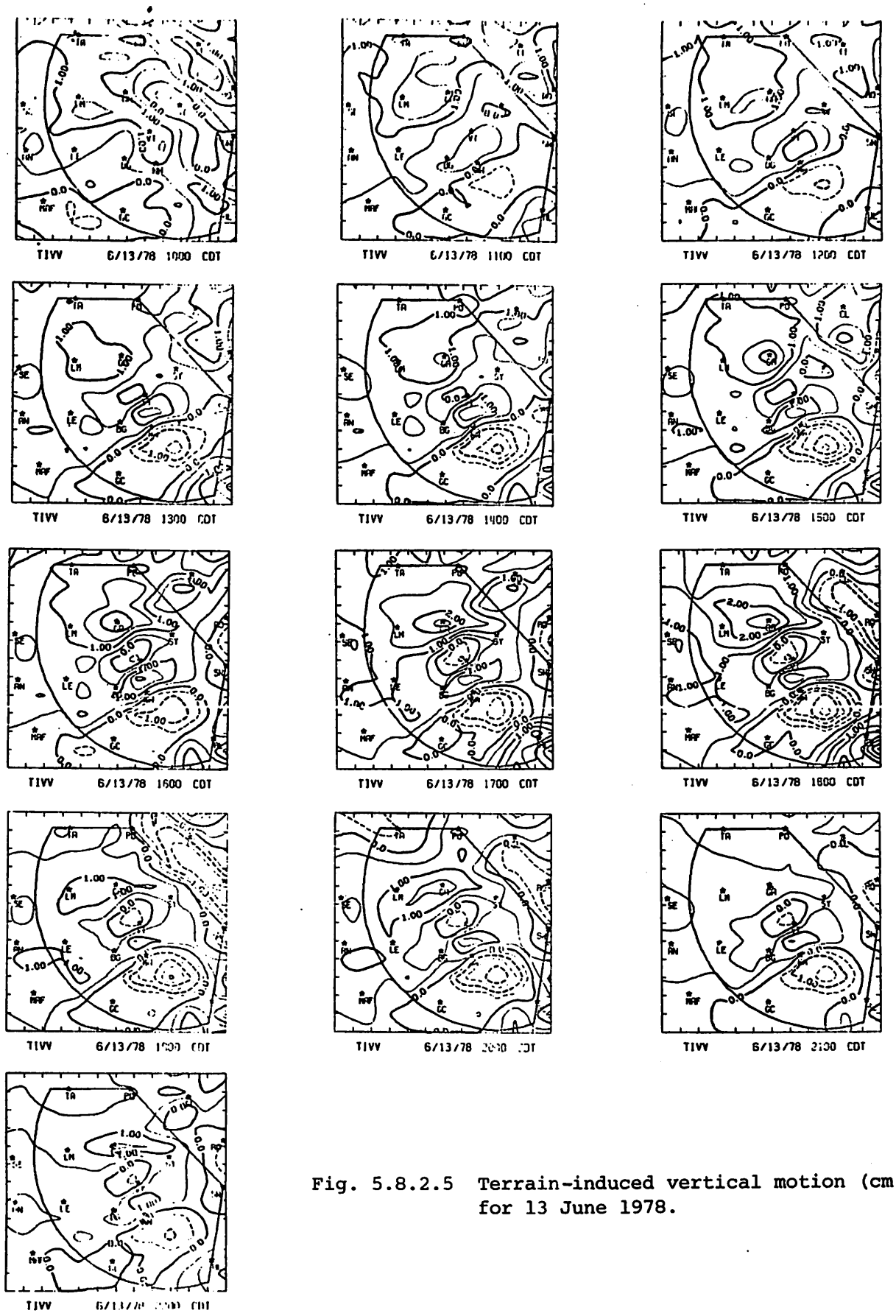

Fig. 5.8.2.5 Terrain-induced vertical motion (cm s^{-1}) for 13 June 1978.

Fig. 5.8.2.6 Surface velocity divergence (s^{-1} x 10^{-6}) for 13 June 1978.

at both 2200 and 0000 GMT. At 0200 GMT when all activity had ceased, the divergence decreased to small values.

The vertical motion 50 mb above the surface (Fig. 5.8.2.7), surface moisture divergence (Fig. 5.8.2.8), and vertical moisture flux (Fig. 5.8.2.9), showed patterns essentially similar to the divergence patterns. Moisture convergence and upward motion were associated with the storms in the east at 2000 GMT and with storms in the northwest at 2100 and 0000 GMT.

Surface vorticity (Fig. 5.8.2.10) also was variable during the day with the formation and dissipation of showers and resultant changes in surface winds. An axis of anticyclonic vorticity persisted throughout the day along a Post-to-Midland line. Strong vorticity centers formed in the northwest at 2000 GMT and in the west from 0000 to 0100 GMT at times of strong convective activity.

Surface pressure changes (Fig. 5.8.2.11) were generally negative before 0200 GMT. The largest drop was -1.7 mb at Sweetwater at 2300 GMT, when shower activity in that area dissipated.

Surface winds (Fig. 5.8.2.12) were mostly easterly at 1500 GMT, and shifted to the southeast by 1800 GMT. Wind speeds increased during the shower activity from 1900 to 2200 GMT. Light southerly winds were present after 0200 GMT when the storm activity had ceased.

5.8.3 Upper Level Kinematic Parameters

Several strong storm cells were present in the HIPLEX area between 1900 and 0100 GMT. Since most of these were located outside the MA-PO-RL computation triangle their effects did not show up well in the upper-level profiles.

Figure 5.8.3.1 shows that divergence was predominant in most layers, although some weak convergence was present. An exception to this occurred in the lowest layer at 1500 GMT, which exhibited moderately strong convergence.

The divergence is reflected in vertical motion profiles (Fig. 5.8.3.2), which show downward vertical motion except near the surface.

Profiles of moisture divergence (Fig. 5.8.3.3) show convergence in the lowest layer at 1500 GMT. Other profiles show divergence below 700 mb. This divergence was strong at 0300 GMT after all shower activity had dissipated.

5.8.4 Energetics

Figure 5.8.4.1 depicts horizontal transport of latent heat. Latent heat inflow was present in lower layers at 1500 GMT. The 1800 and 2100 GMT profiles

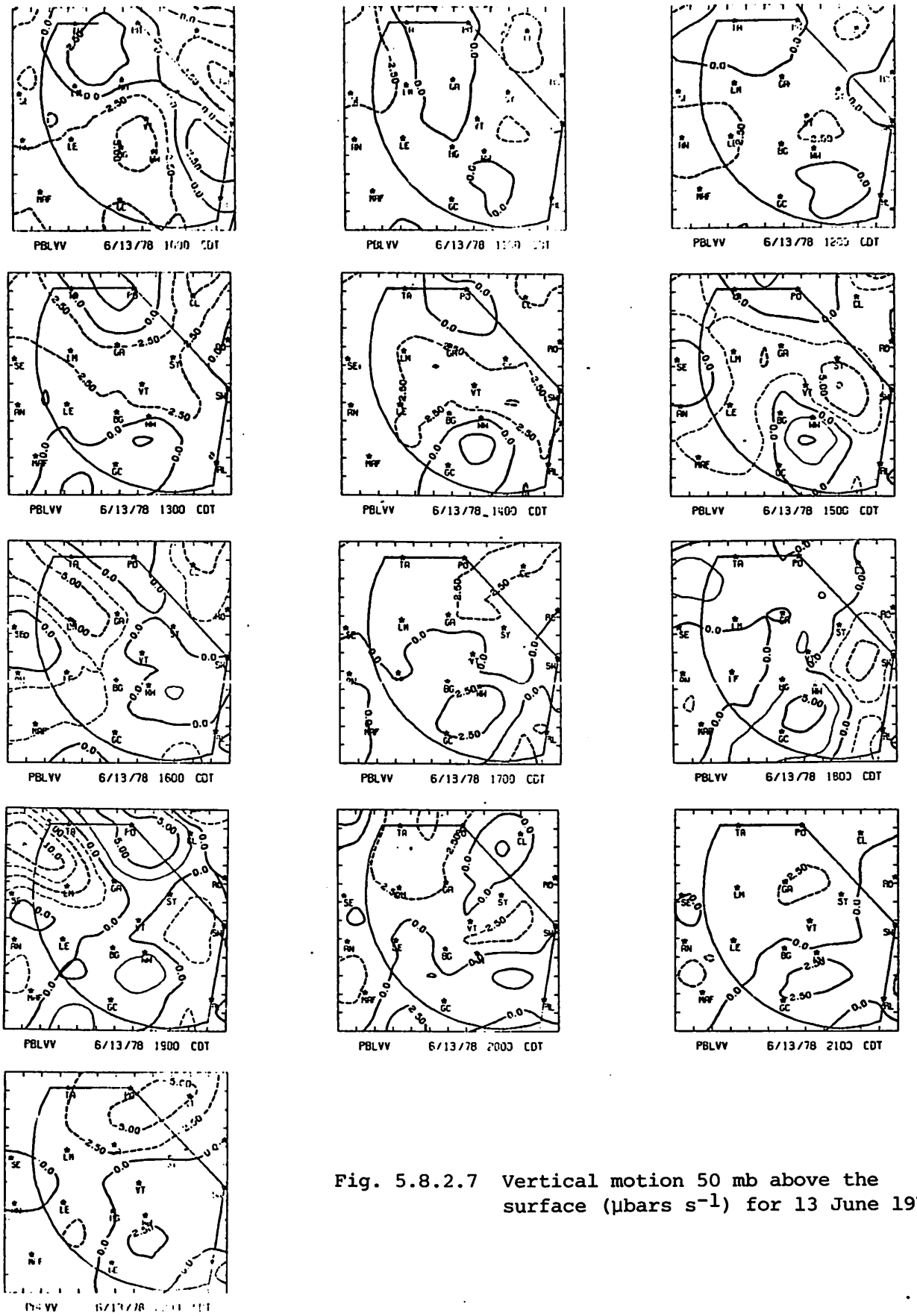

Fig. 5.8.2.7 Vertical motion 50 mb above the surface (μbars s^{-1}) for 13 June 1978.

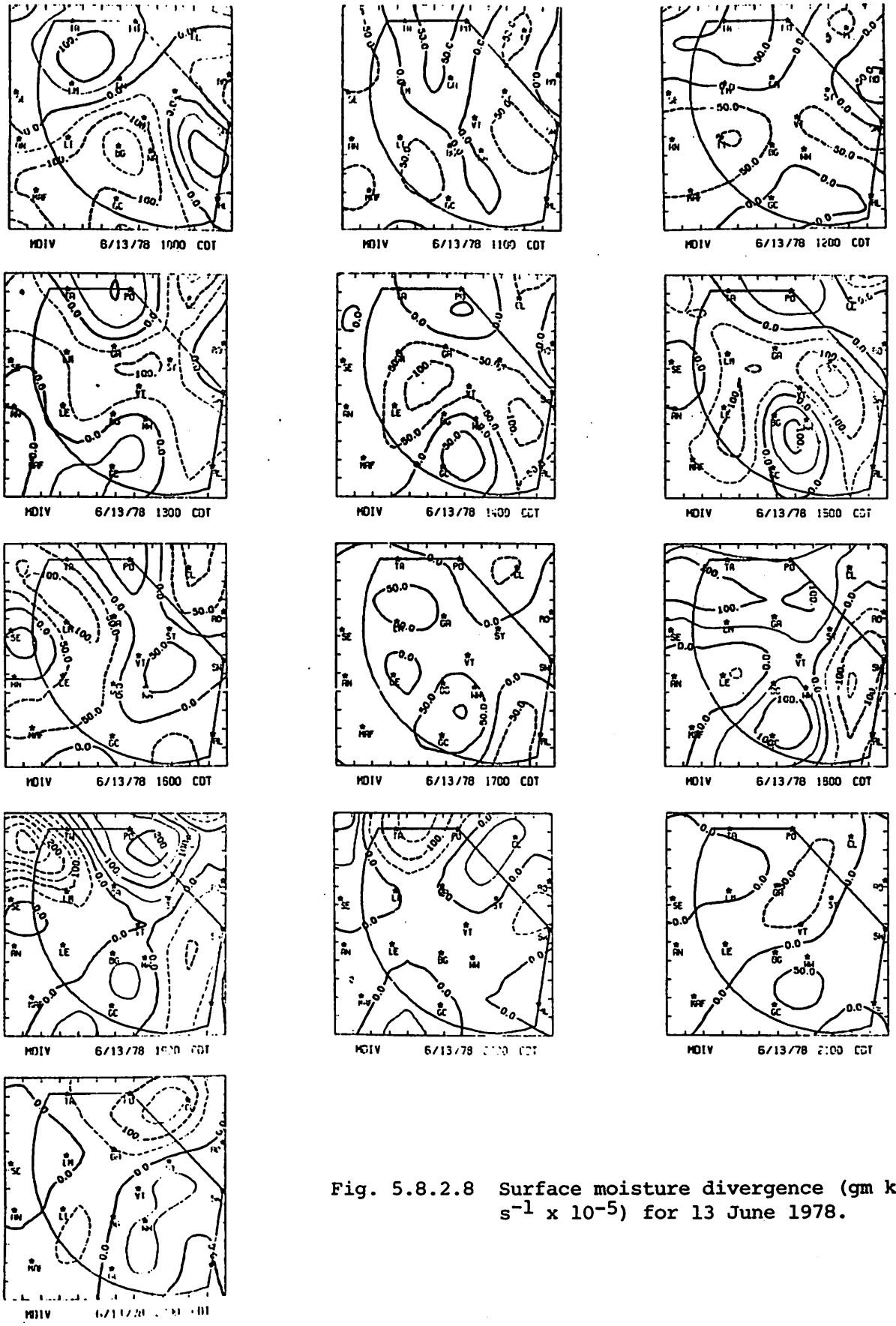

Fig. 5.8.2.8 Surface moisture divergence (gm kg^{-1} s^{-1} x 10^{-5}) for 13 June 1978.

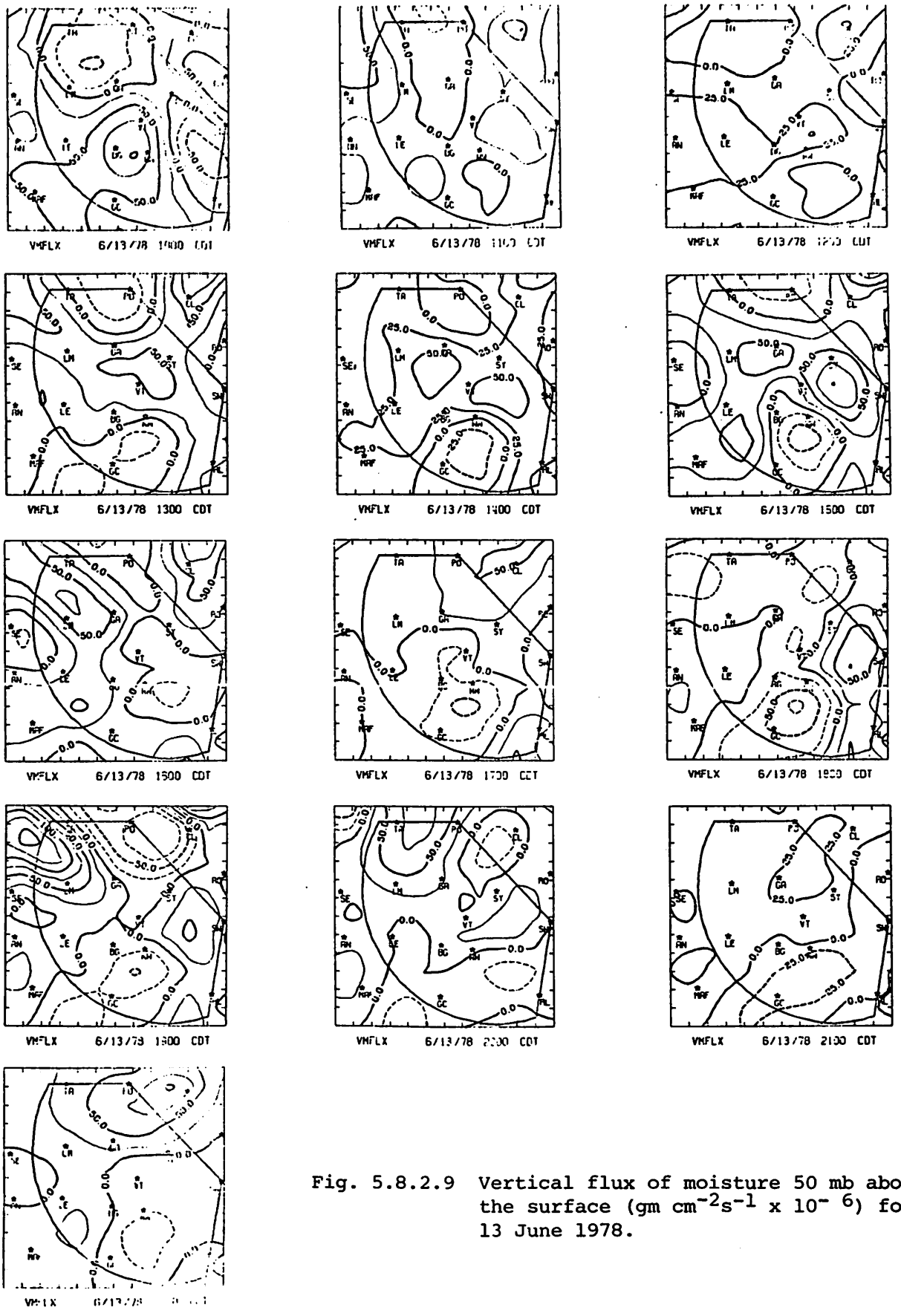

Fig. 5.8.2.9 Vertical flux of moisture 50 mb above the surface (gm $cm^{-2}s^{-1}$ x 10^{-6}) for 13 June 1978.

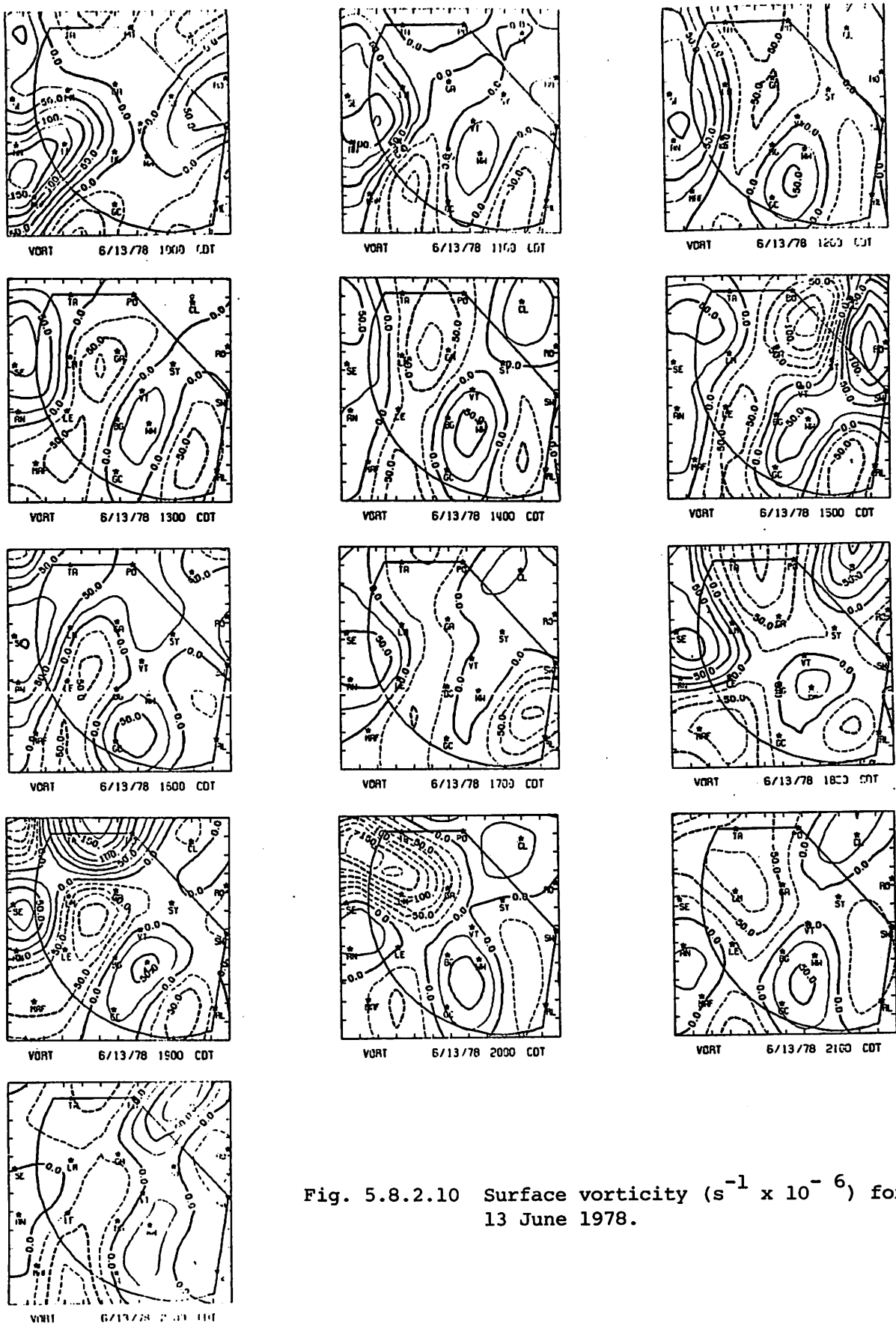

Fig. 5.8.2.10 Surface vorticity (s^{-1} x 10^{-6}) for 13 June 1978.

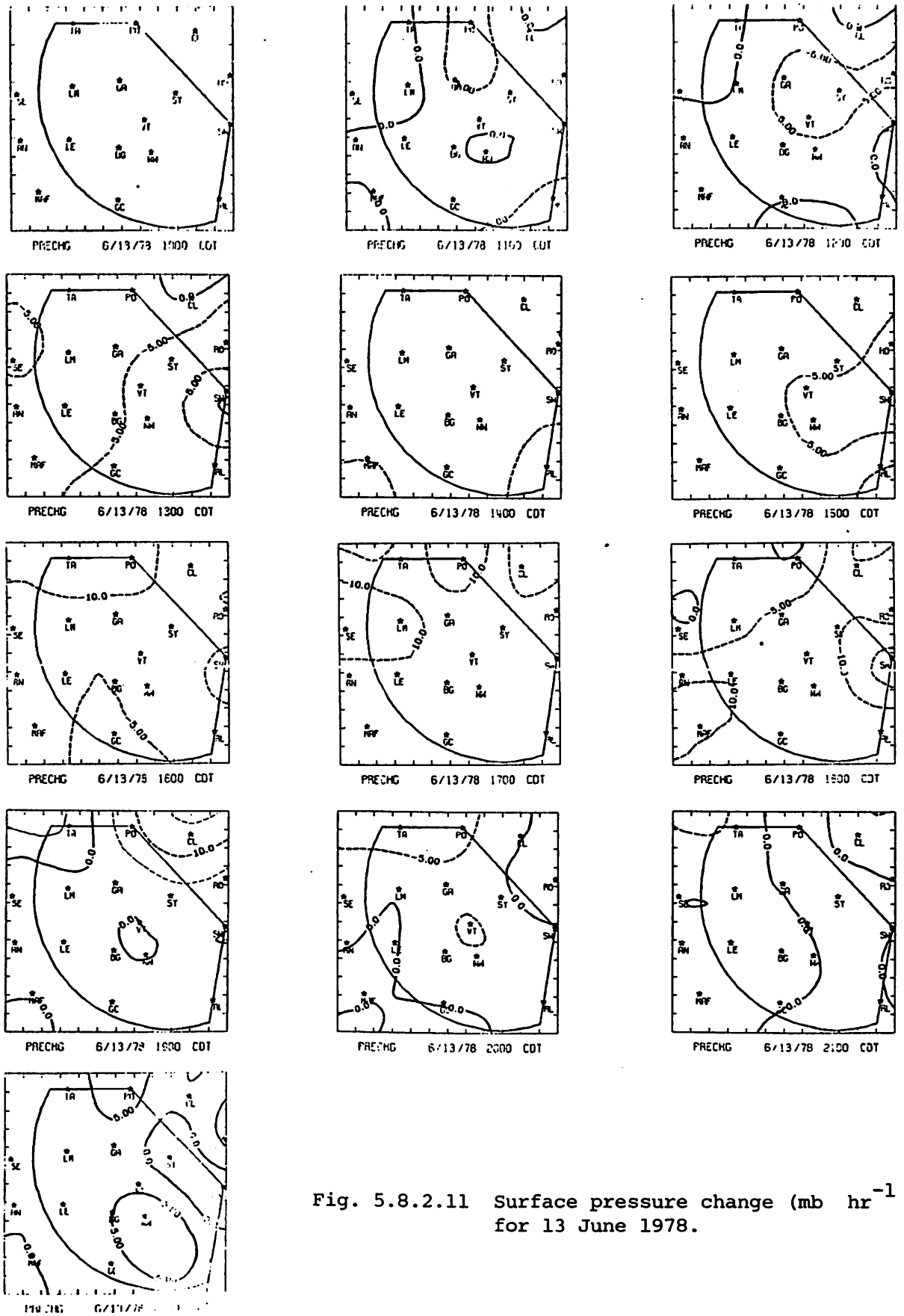

Fig. 5.8.2.11 Surface pressure change (mb hr^{-1} x 10^{-1}) for 13 June 1978.

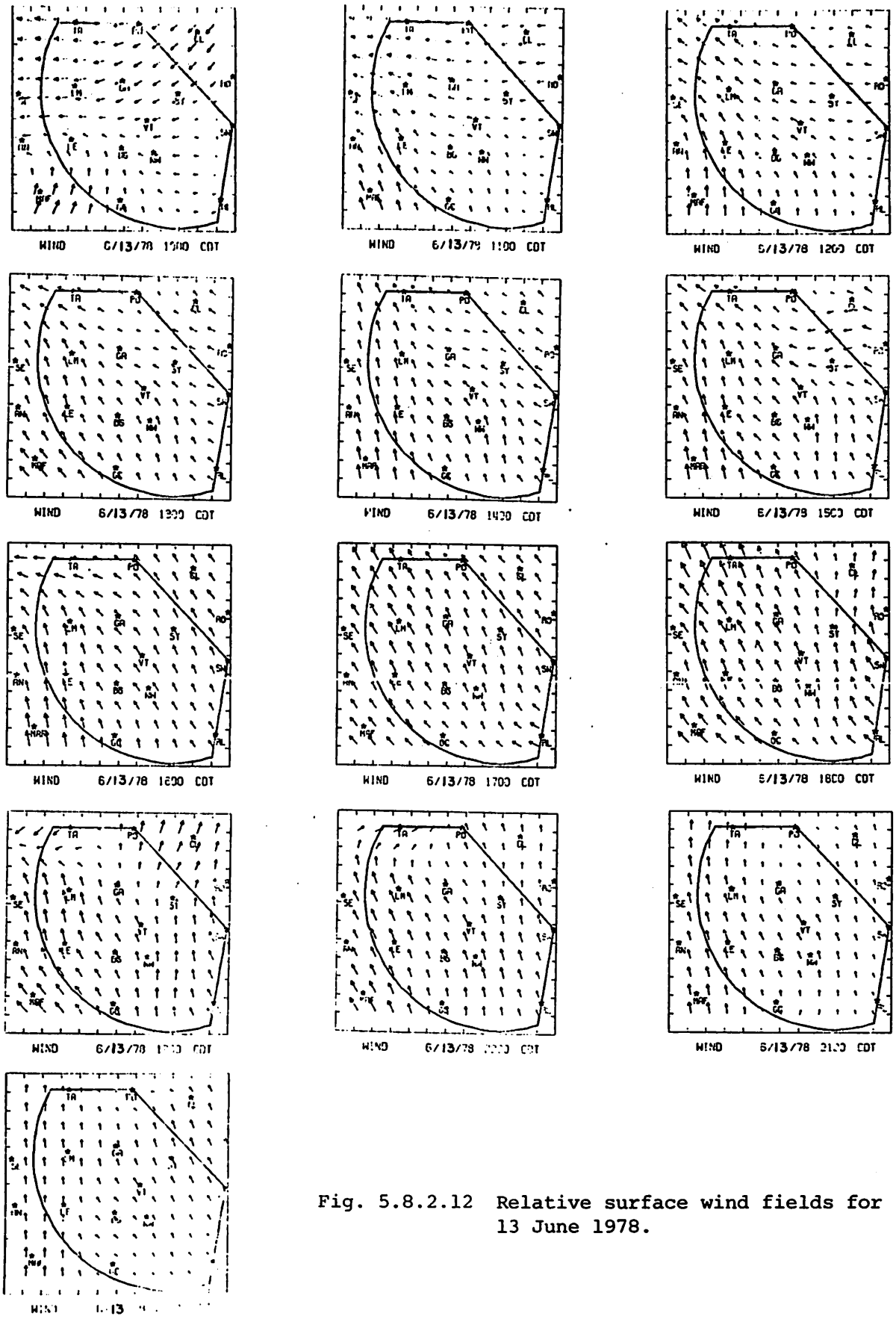

Fig. 5.8.2.12 Relative surface wind fields for 13 June 1978.

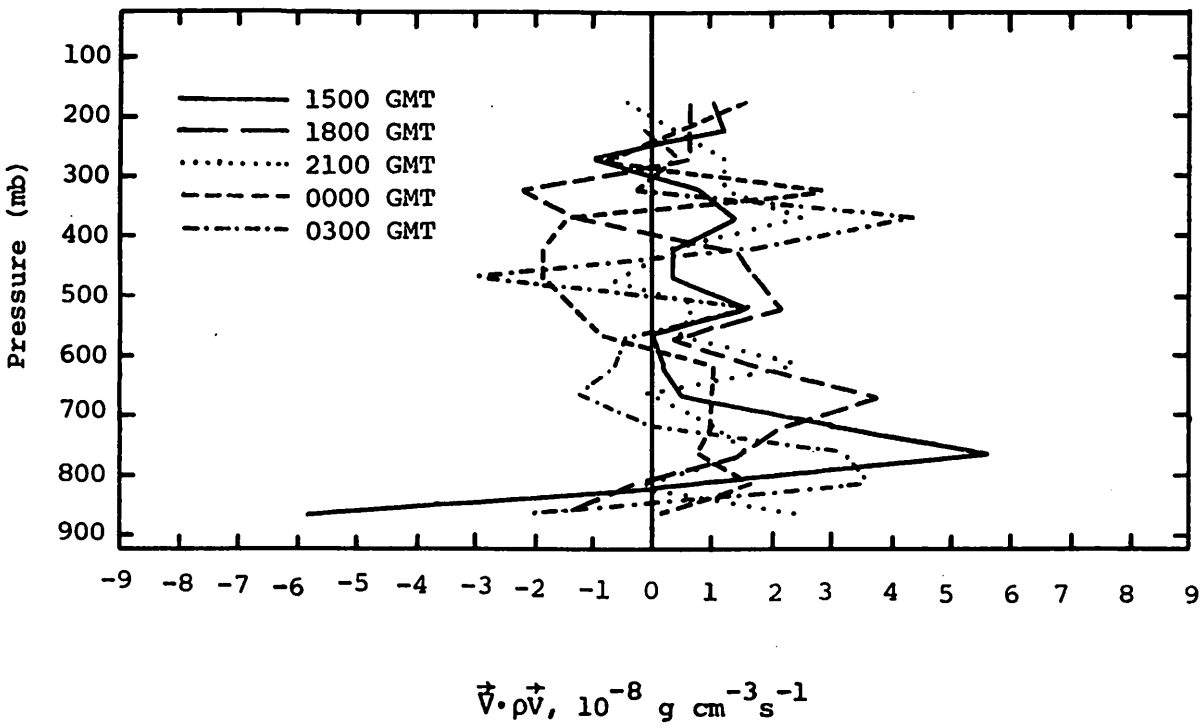

Fig. 5.8.3.1 Vertical profiles of mass divergence on 13 June 1978.

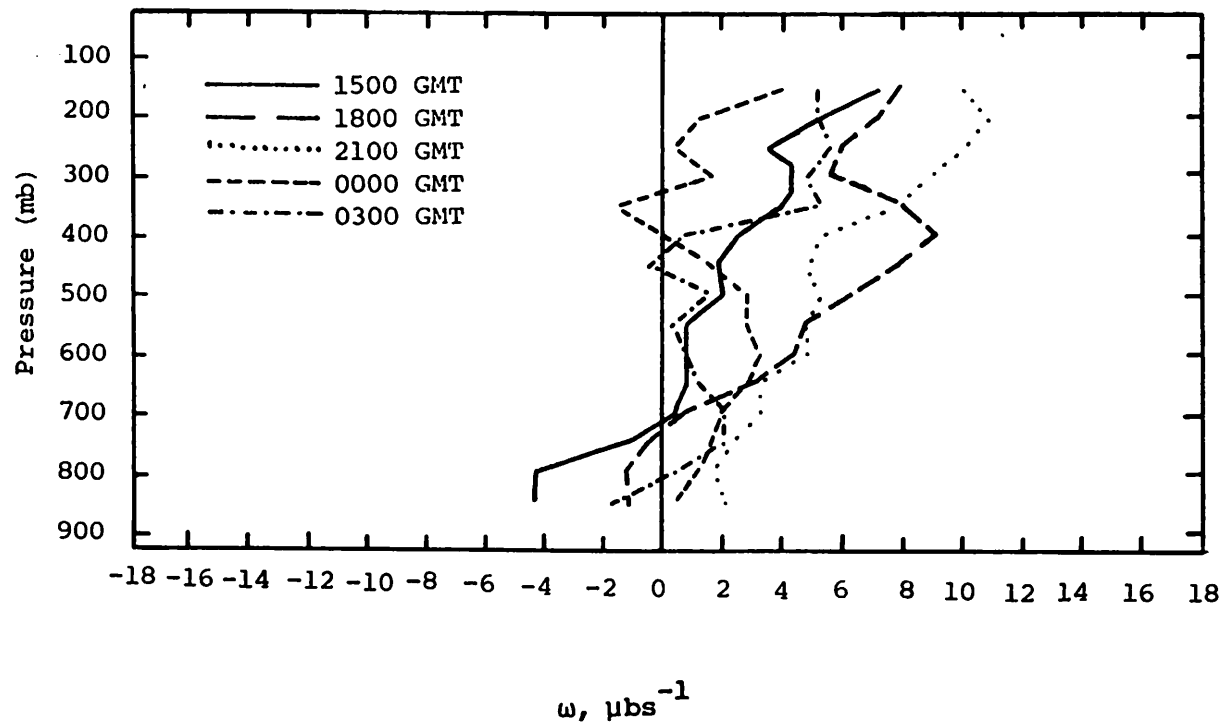

Fig. 5.8.3.2 Vertical profiles of vertical motion on 13 June 1978.

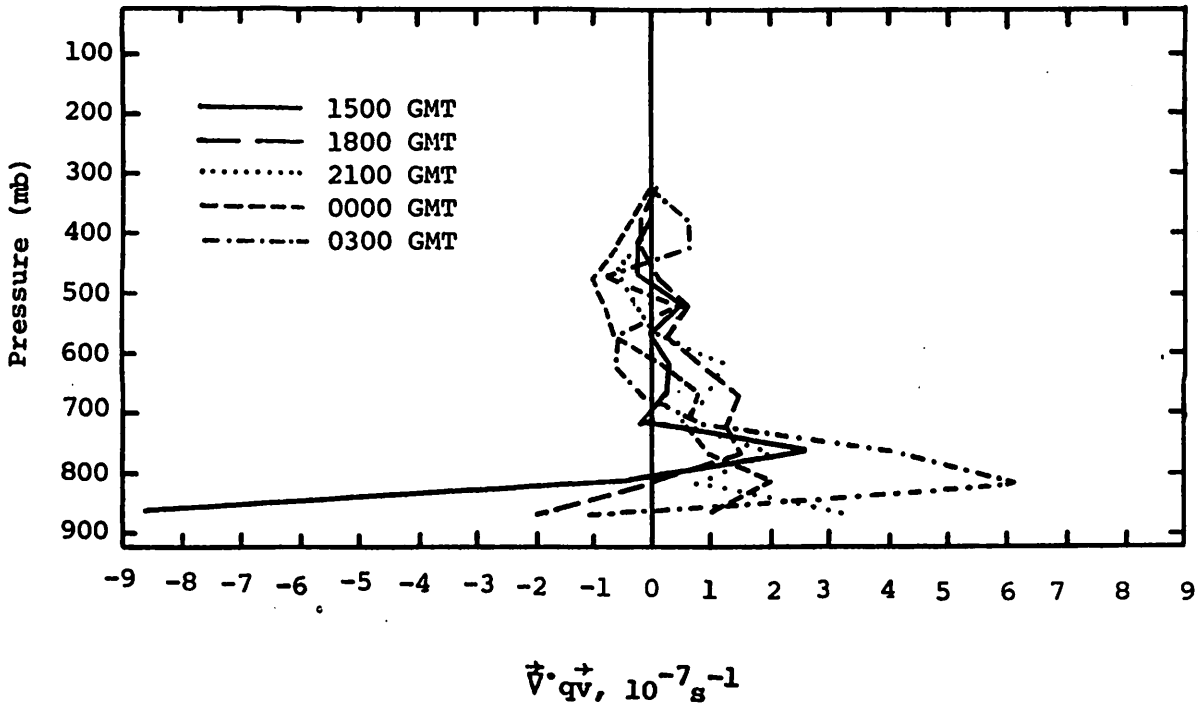

Fig. 5.8.3.3 Vertical profiles of moisture divergence on 13 June 1978.

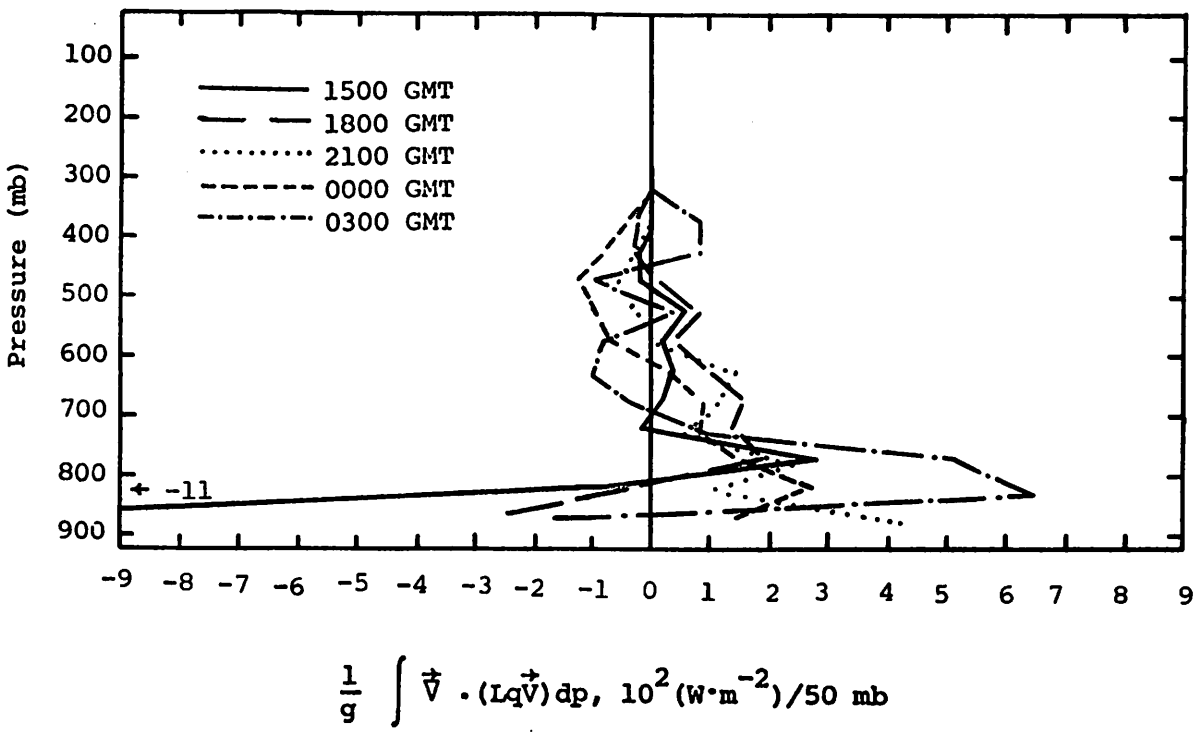

Fig. 5.8.4.1 Vertical profiles of the horizontal flux of latent heat energy on 13 June 1978.

show mostly outflow of latent heat in all layers. At 0000 GMT some inflow was present above 700 mb. This inflow decreased at 0300 GMT and strong outflow of latent heat developed in the lower layers.

Figure 5.8.4.2 shows vertical transport of latent heat. Latent heat losses occurred in all profiles in a layer near 800 mb. Small gains were present in upper layers throughout the day.

Profiles of the local change of latent heat (Fig. 5.8.4.3) show increases in latent heat above 800 mb at 1500 and 1800 GMT before the convective activity formed. Latent heat change was near zero at 2100 GMT, and decreased at 0000 and 0300 GMT as convective activity ended.

Profiles of the residual of the latent heat energy equation (Fig. 5.8.4.4) show generally negative values except at 1500 GMT. The positive values at 1500 GMT indicate condensation and cloud formation processes, while the shift to negative values later in the day indicates evaporation.

Figure 5.8.4.5 shows profiles of diabatic heating. Small increases in sensible heat occurred in the lowest layers. In middle layers decreases in sensible heat may have resulted from evaporative cooling, but the large values in upper layers suggest some other process such as radiation.

Light winds in lower layers produced low values of horizontal and vertical flux of kinetic energy (Figs. 5.8.4.6 and 5.8.4.7). Strong horizontal convergence of kinetic energy was present in upper layers later in the day. Vertical transport into layers near 200 and 400 mb also took place.

5.8.5 Water Vapor Budget

Profiles of net horizontal transport of water vapor (Fig. 5.8.5.1) show losses in most layers at 1500 and 1800 GMT. After shower activity began, most layers showed gains in water vapor from horizontal transport. There were losses near 700 mb at 0000 GMT and below 750 mb at 0300 GMT.

Profiles of net vertical transport of water vapor (Fig. 5.8.5.2) show that at 1500 and 1800 GMT layers below 500 mb experienced gains in water vapor. In later profiles losses due to vertical transport predominated except near the surface.

Vertical transport of water vapor through constant pressure surfaces (Fig. 5.8.5.3) was primarily downward as vertical motion was mostly downward. Upward transport of water vapor occurred below 700 mb at 1500 and 1800 GMT and near the surface at 0300 GMT.

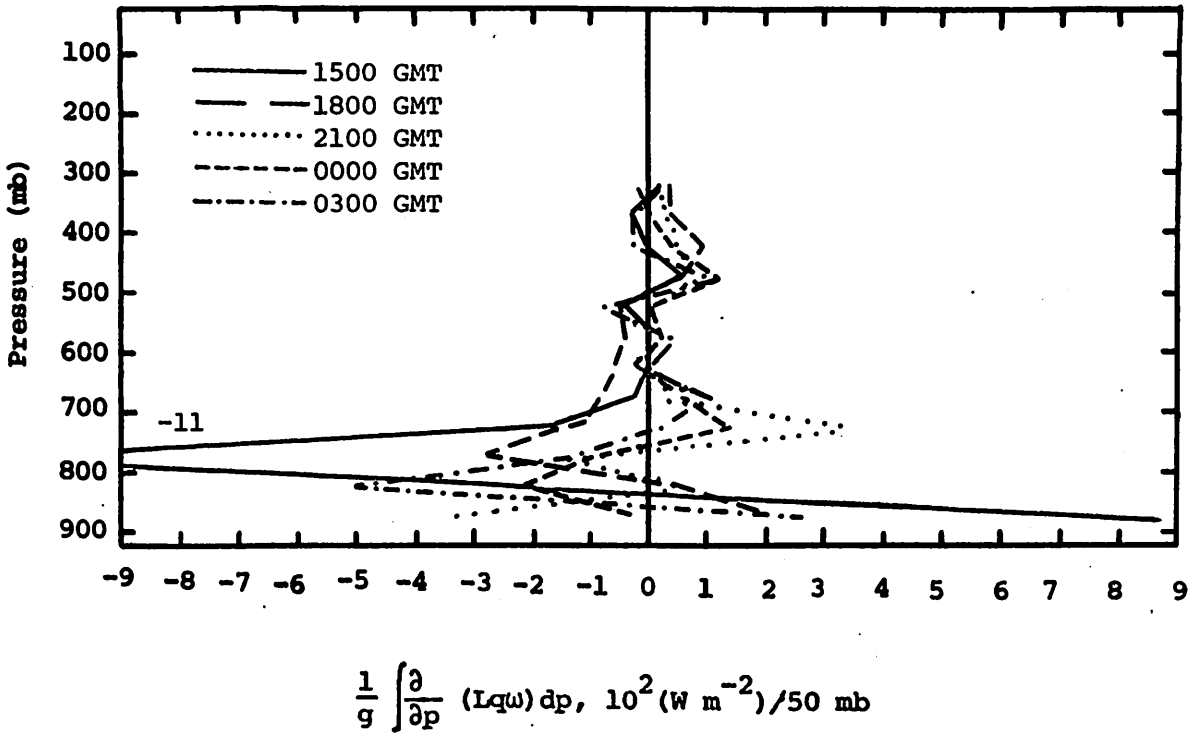

Fig. 5.8.4.2 Vertical profiles of the vertical flux of latent heat energy on 13 June 1978.

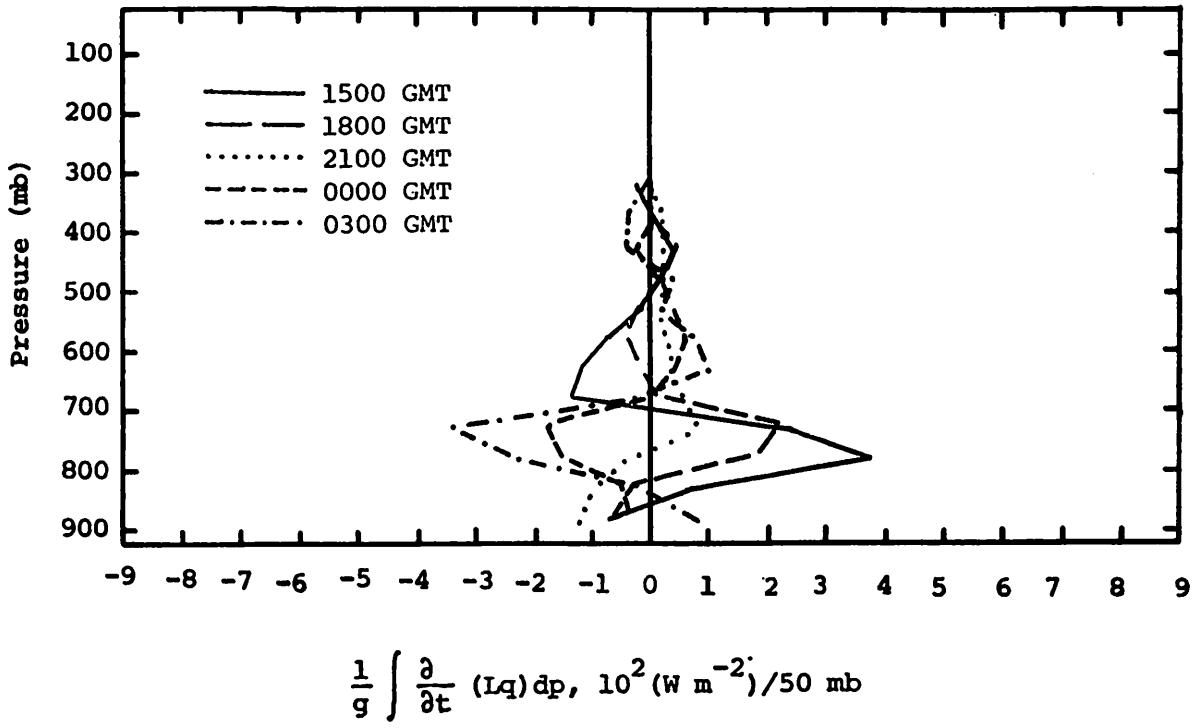

Fig. 5.8.4.3 Vertical profiles of the local change of latent heat energy on 13 June 1978.

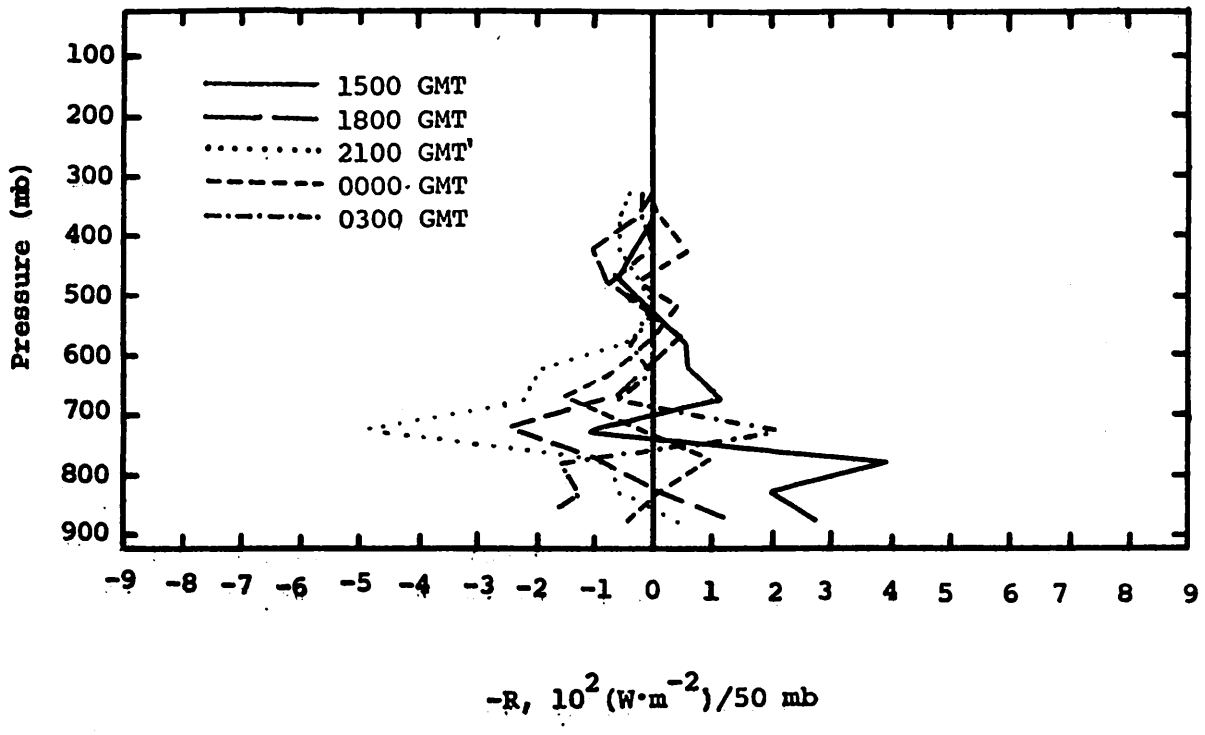

Fig. 5.8.4.4 Vertical profiles of the residual of the latent heat energy equation on 13 June 1978.

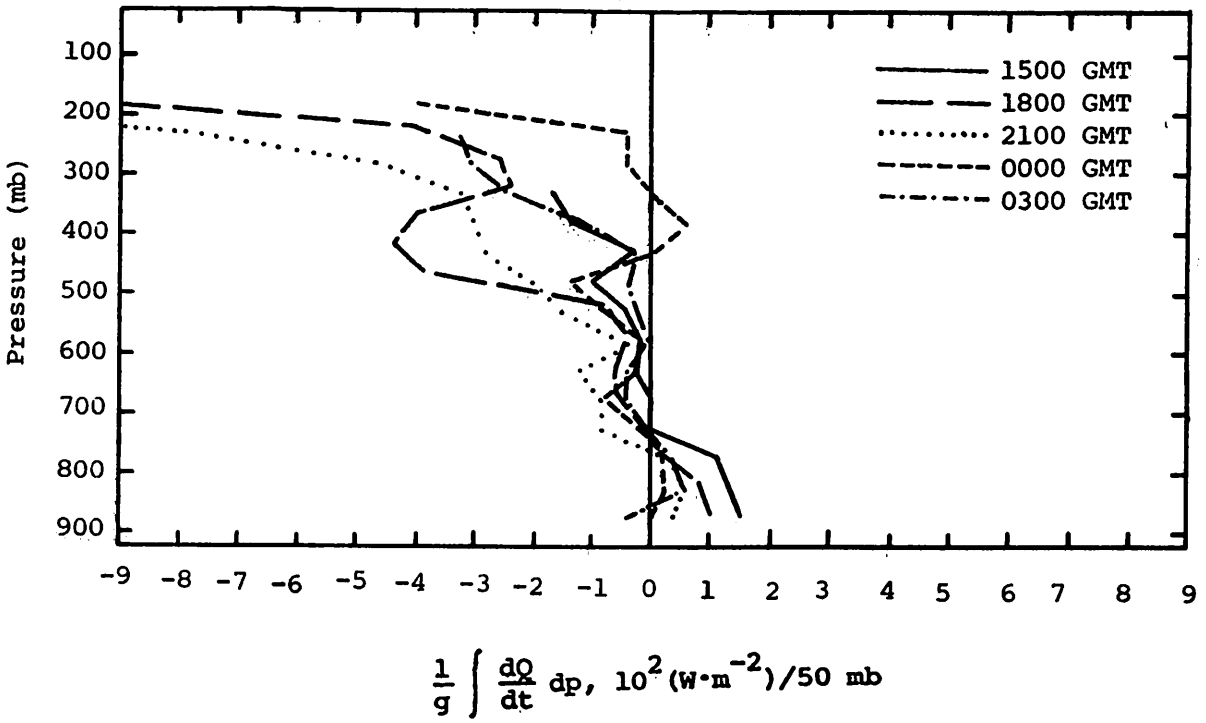

Fig. 5.8.4.5 Vertical profiles of diabatic heating computed from the first law of thermodynamics on 13 June 1978.

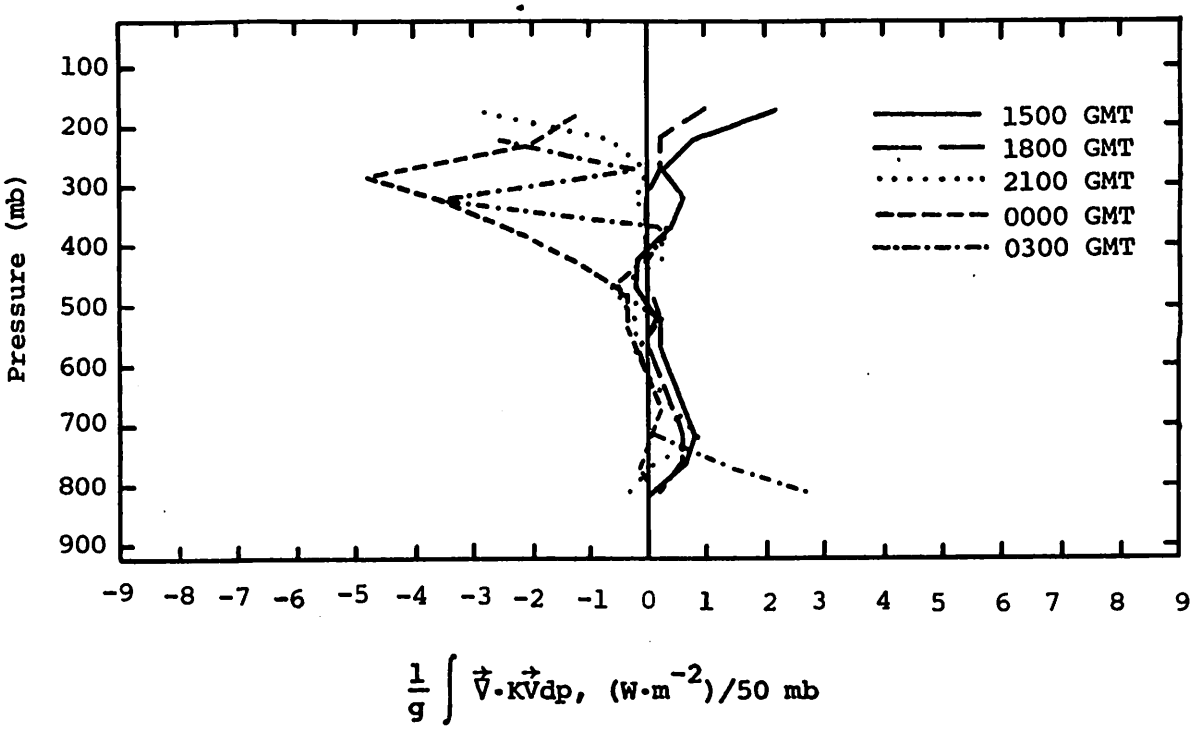

Fig. 5.8.4.6 Vertical profiles of the horizontal flux of kinetic energy on 13 June 1978.

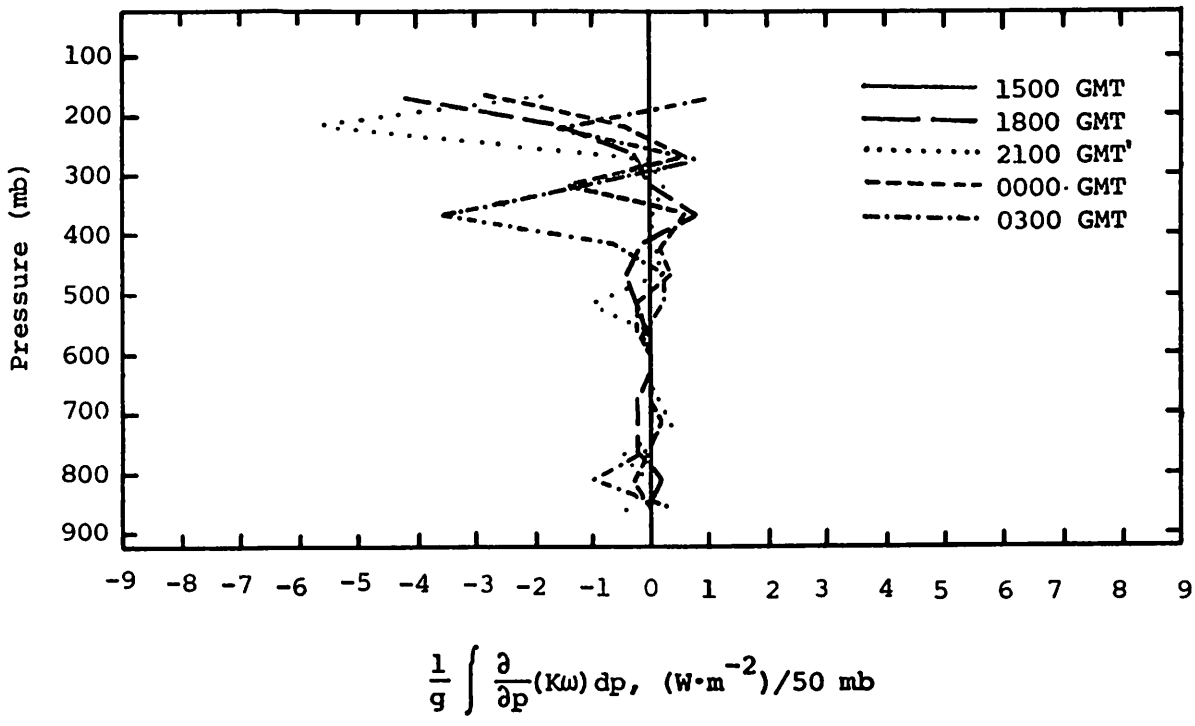

Fig. 5.8.4.7 Vertical profiles of the vertical flux of kinetic energy on 13 June 1978.

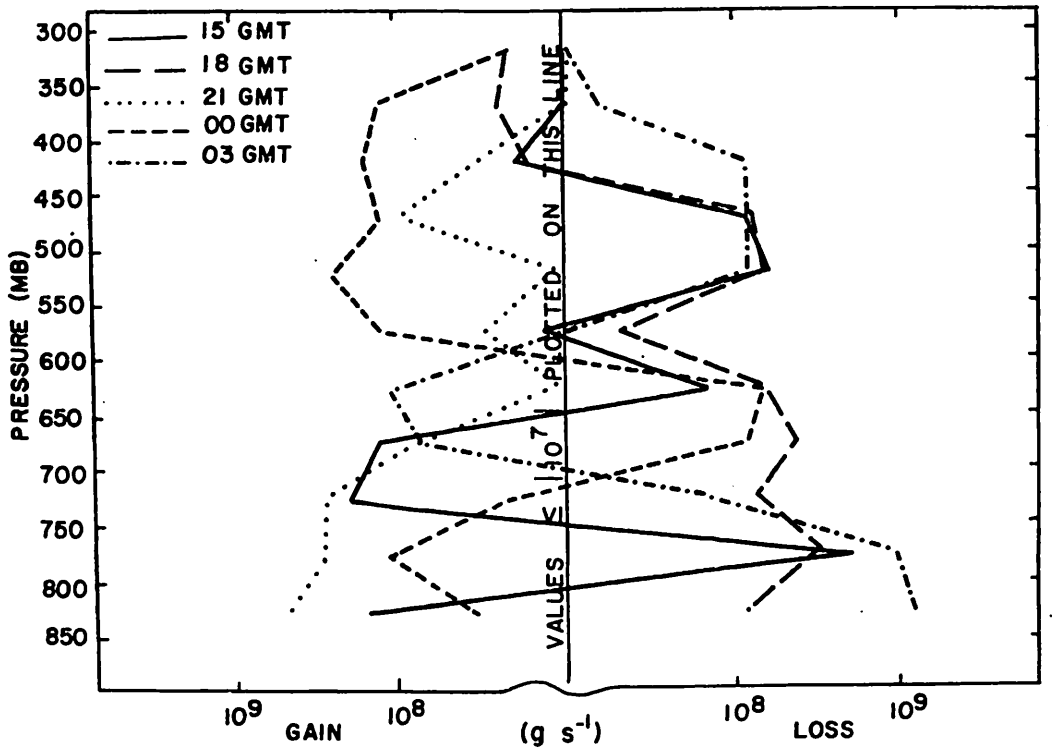

Fig. 5.8.5.1 Net horizontal transport of water vapor through boundaries of 50-mb layers (gm s^{-1}) over the Texas HIPLEX area for 13 June 1978.

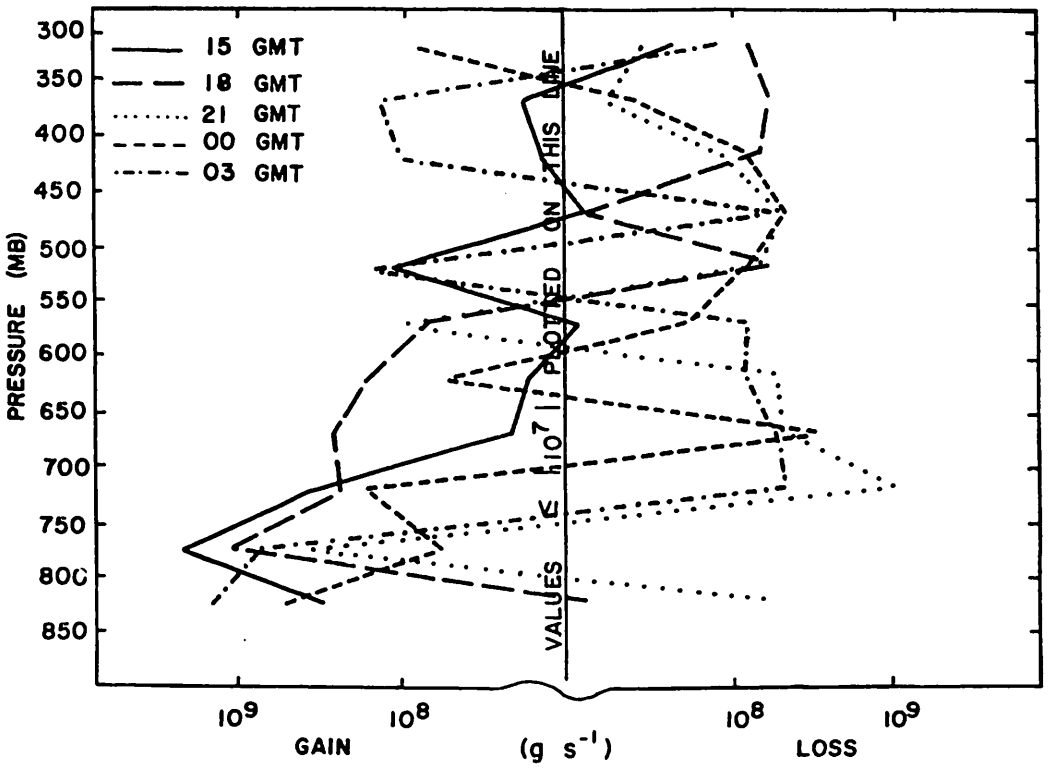

Fig. 5.8.5.2 Net vertical transport of water vapor through boundaries of 50-mb layers (gm s^{-1}) over the Texas HIPLEX area for 13 June 1978.

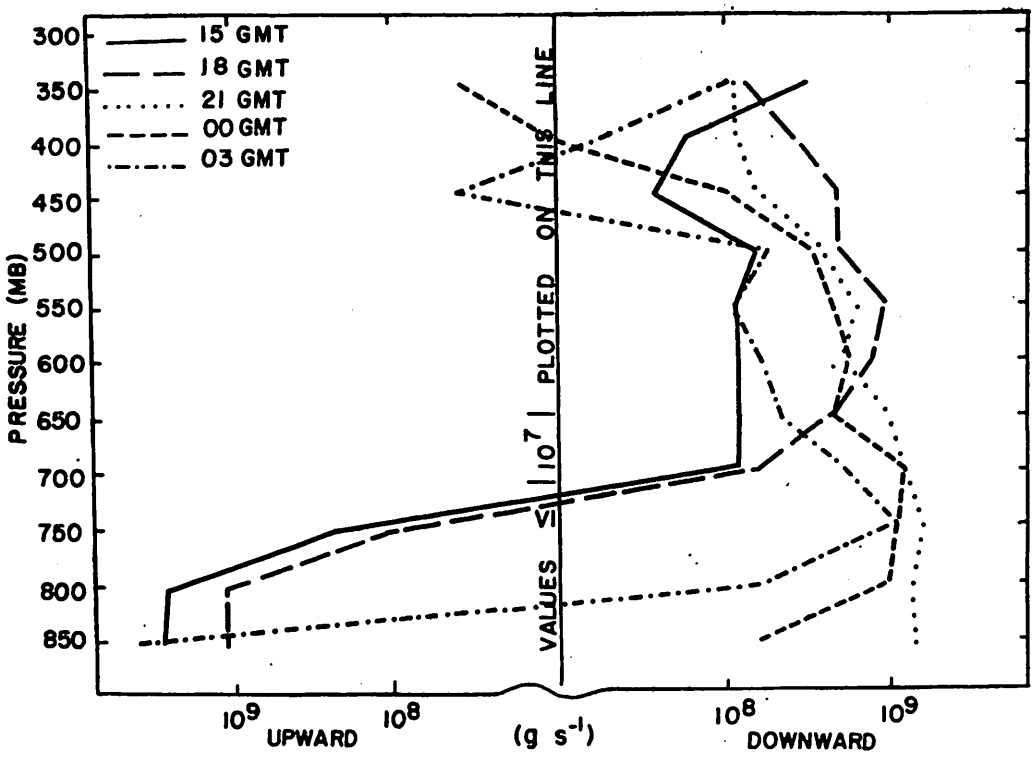

Fig. 5.8.5.3 Vertical transport of water vapor through constant pressure surfaces (gm s^{-1}) over the Texas HIPLEX area on 13 June 1978.

Combined net horizontal and vertical transport of water vapor is shown in Fig. 5.8.5.4. All profiles show gains below 700 mb, with mostly losses above, except near 600 mb.

Figures 5.8.5.5 and 5.8.5.6 depict total mass of water vapor in 50-mb layers, and local change of water vapor, respectively. Large changes in water vapor occurred during the day. Water vapor increased below 650 mb to a maximum at 2100 GMT and decreased afterwards. Above 650 mb the largest increases were between 2100 and 0000 GMT. The dry layer above 800 mb at 1500 and 1800 GMT represents the effects of a capping inversion which had dissipated at 2100 GMT.

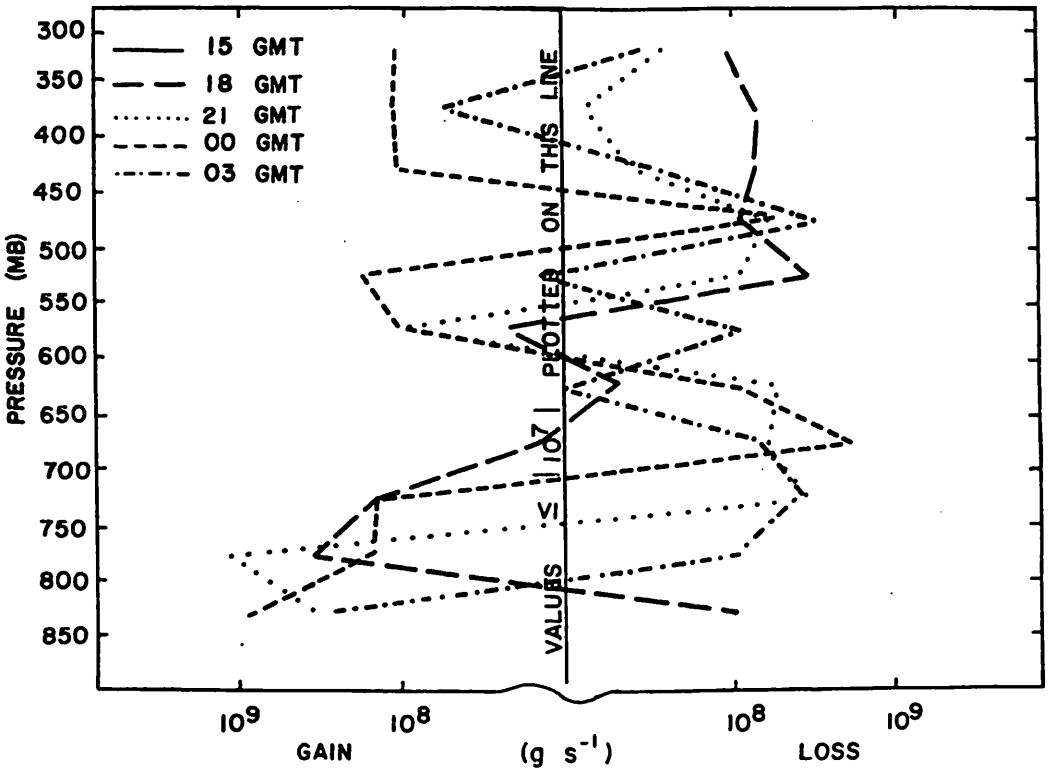

Fig. 5.8.5.4 Combined net horizontal and vertical transport of water vapor through boundaries of 50-mb layers (gm s^{-1}) over the Texas HIPLEX area on 13 June 1978.

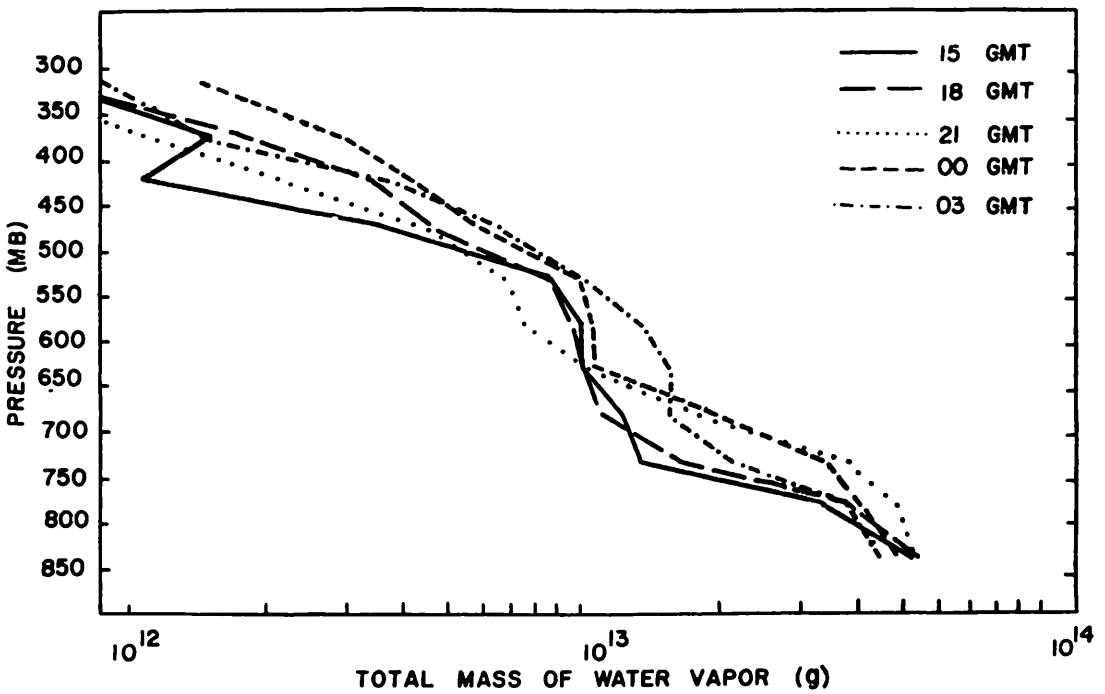

Fig. 5.8.5.5 Total mass of water vapor in layers 50 mb deep (gm) over the Texas HIPLEX area on 13 June 1978.

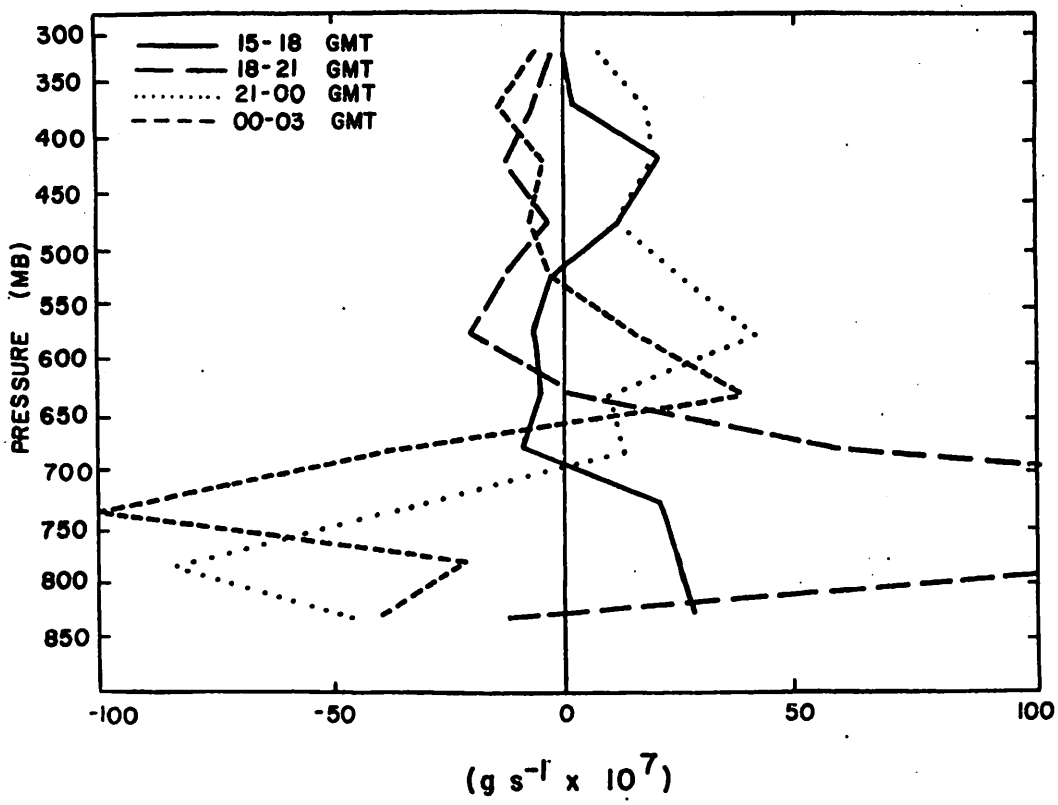

Fig. 5.8.5.6 Local rate-of-change in total mass of water vapor ($g\ s^{-1} \times 10^7$) for the Texas HIPLEX area for 13 June 1978.

5.9 14 June 1978

5.9.1 Radar

No radar echoes were observed in the Texas HIPLEX area on this day. A few thunderstorms with maximum tops of 13 km (42K ft) developed in New Mexico, approximately 175 km to the west, but dissipated before 0300 GMT on June 15.

5.9.2 Surface

Stations in and near the analysis area reported cumulus clouds from 1800 to 0000 GMT on this day, and skies were clear at 1500 and 0300 GMT.

The small number of clouds resulted in high temperatures across the network (Fig. 5.9.2.1). The highest temperature reported was 34°C from 2000 to 2200 GMT. The temperature gradient was generally small, though a slight ridge of maximum temperature was observed before 1800 GMT across the middle of the network.

High temperatures also resulted in large dewpoint depressions throughout the day (Fig. 5.9.2.2), although mixing ratio values were as high as 16 gm/kg at Big Spring before 1800 GMT (Fig. 5.9.2.3). Mixing ratio varied across the network and showed the largest gradient between 1800 and 0100 GMT when temperatures were highest. A ridge of mixing ratio extended from the southwest to the northeast corners of the network during most of the day. This ridge corresponded with high equivalent potential temperature (Fig. 5.9.2.4). The lowest amount of moisture was measured near Tahoka, in the northwest corner of the analysis area.

Sustained wind speeds as high as 8 m/sec at 1500 GMT created strong downward terrain-induced vertical motion near Walsh-Watts and Rotan (Fig. 5.9.2.5). Upward motions as large as 3 cm/sec also were calculated for an area near Gail from 2100 to 0000 GMT.

Fields of divergence (Fig. 5.9.2.6), boundary layer vertical velocity (Fig. 5.9.2.7), and moisture divergence (Fig. 5.9.2.8) show few significant features during the day. An exception is a convergent area near Big Spring where divergence reached -10^{-4} sec^{-1} at 2100 GMT. Vertical moisture flux was small due to small vertical motions (Fig. 5.9.2.9).

The largest value of vorticity (Fig. 5.9.2.10) was 1.5×10^{-4} sec^{-1} at 1800 GMT near Midland. A weak trough of negative vorticity persisted throughout most of the day from just east of Midland to Post.

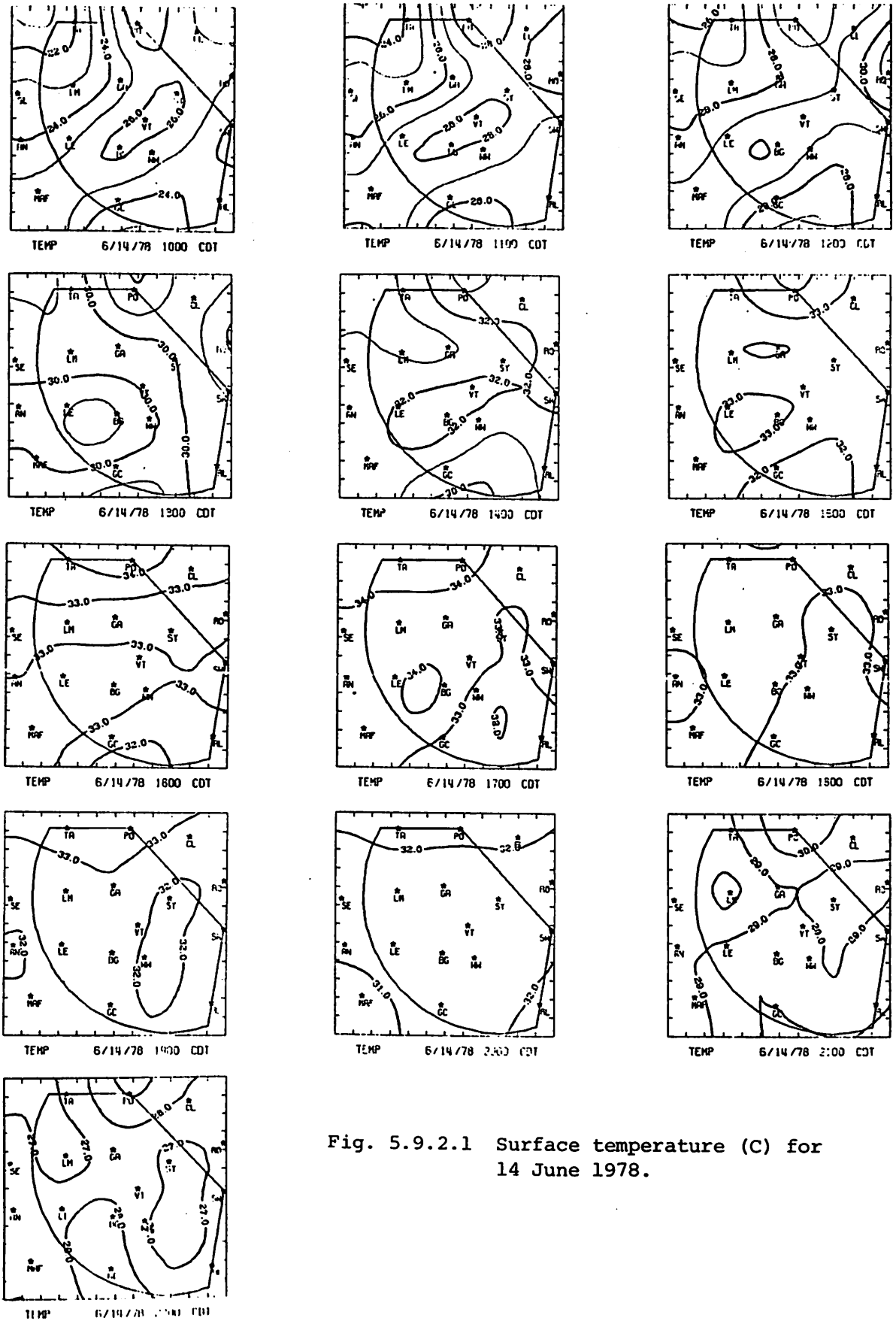

Fig. 5.9.2.1 Surface temperature (C) for 14 June 1978.

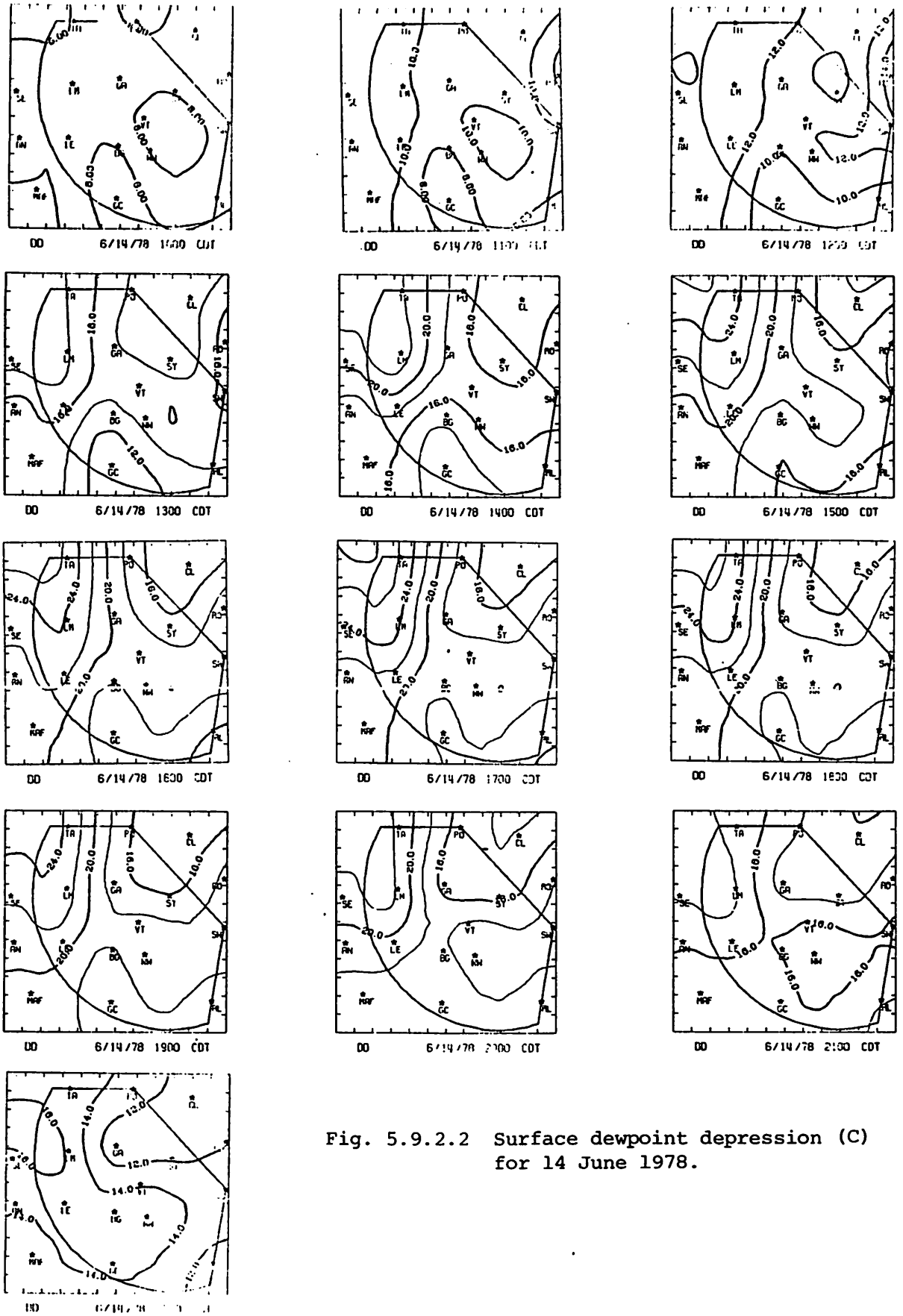

Fig. 5.9.2.2 Surface dewpoint depression (C) for 14 June 1978.

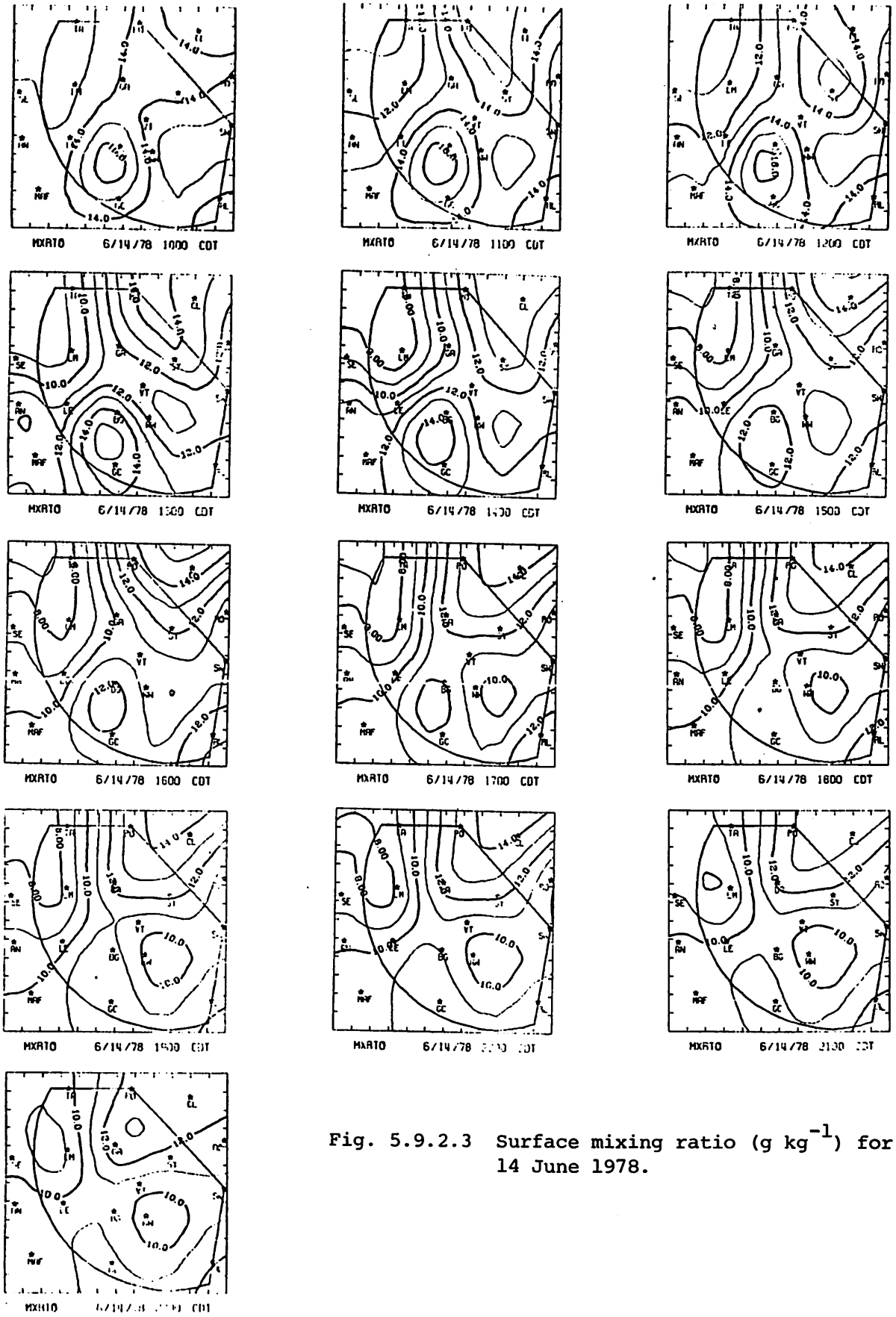

Fig. 5.9.2.3 Surface mixing ratio (g kg^{-1}) for 14 June 1978.

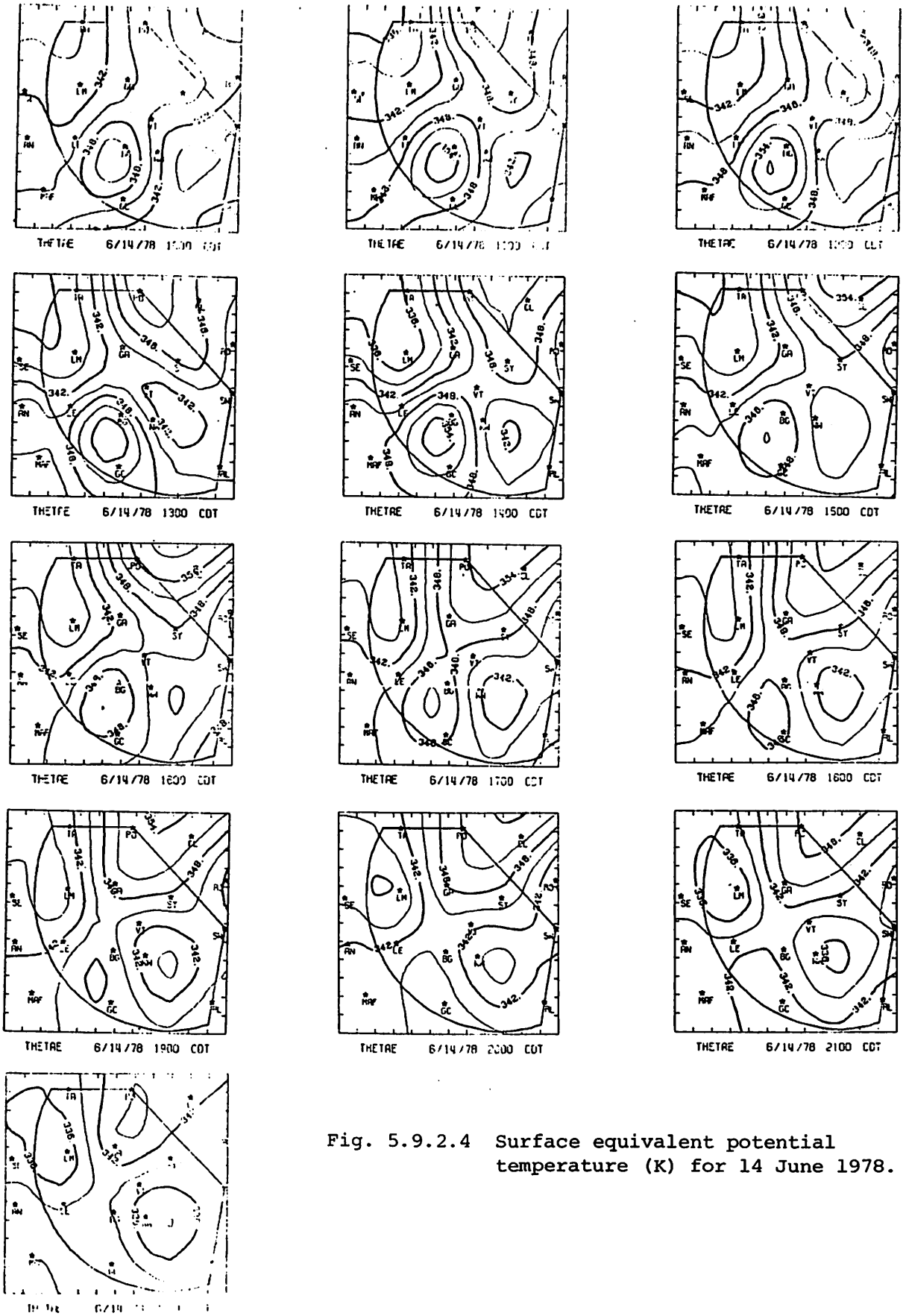

Fig. 5.9.2.4 Surface equivalent potential temperature (K) for 14 June 1978.

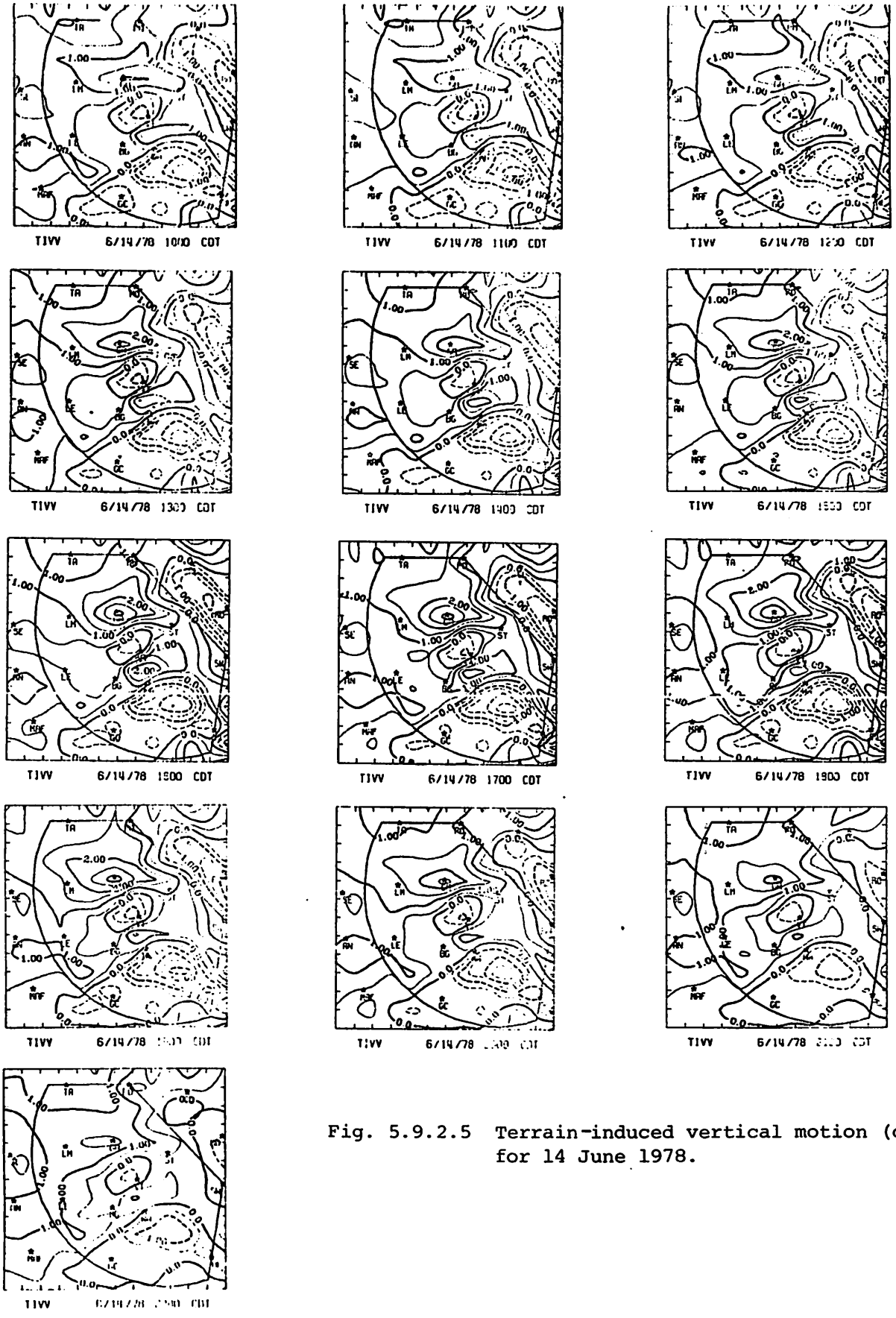

Fig. 5.9.2.5 Terrain-induced vertical motion (cm s^{-1}) for 14 June 1978.

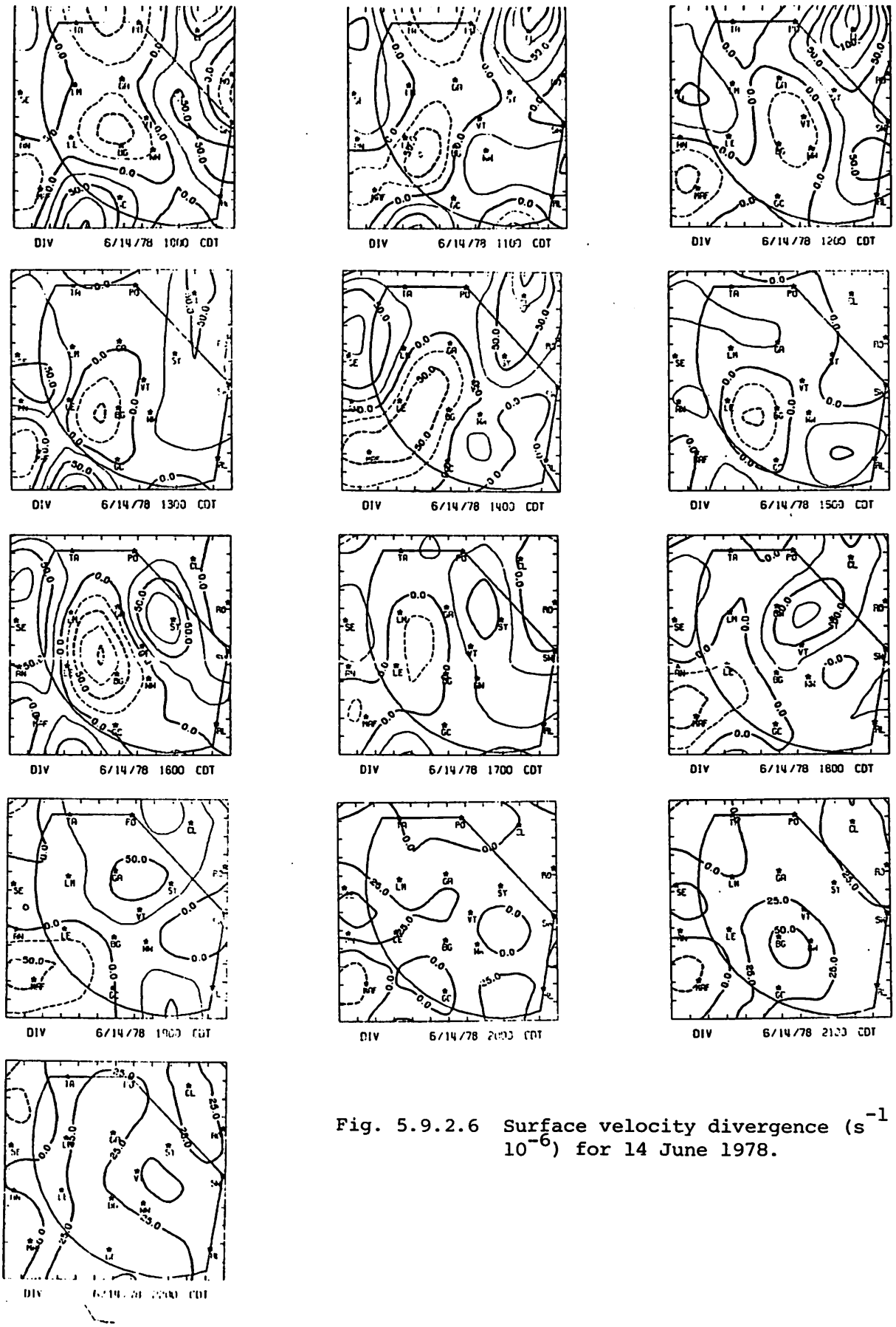

Fig. 5.9.2.6 Surface velocity divergence (s^{-1} x 10^{-6}) for 14 June 1978.

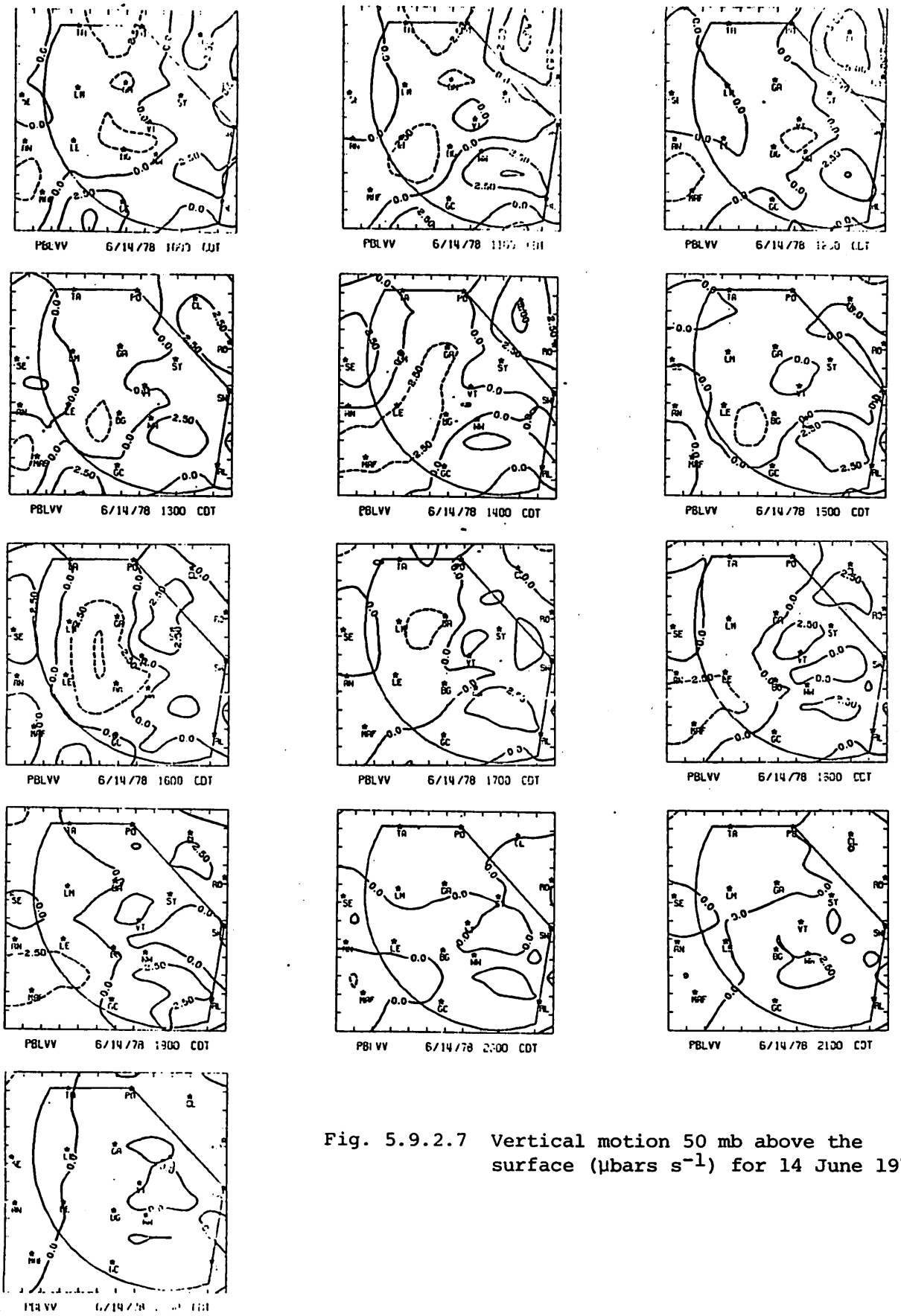

Fig. 5.9.2.7 Vertical motion 50 mb above the surface (μbars s^{-1}) for 14 June 1978.

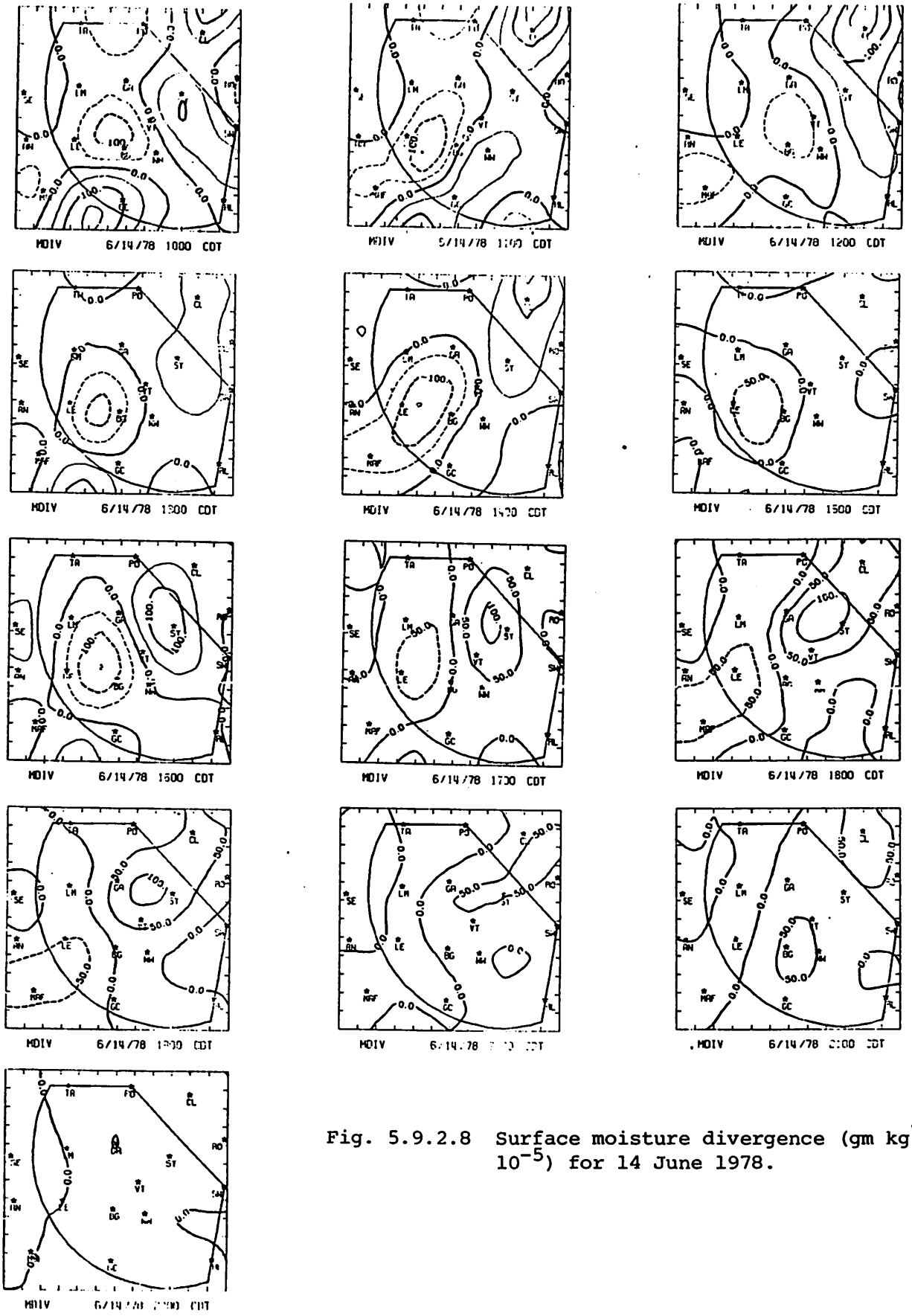

Fig. 5.9.2.8 Surface moisture divergence (gm kg^{-1} s^{-1} x 10^{-5}) for 14 June 1978.

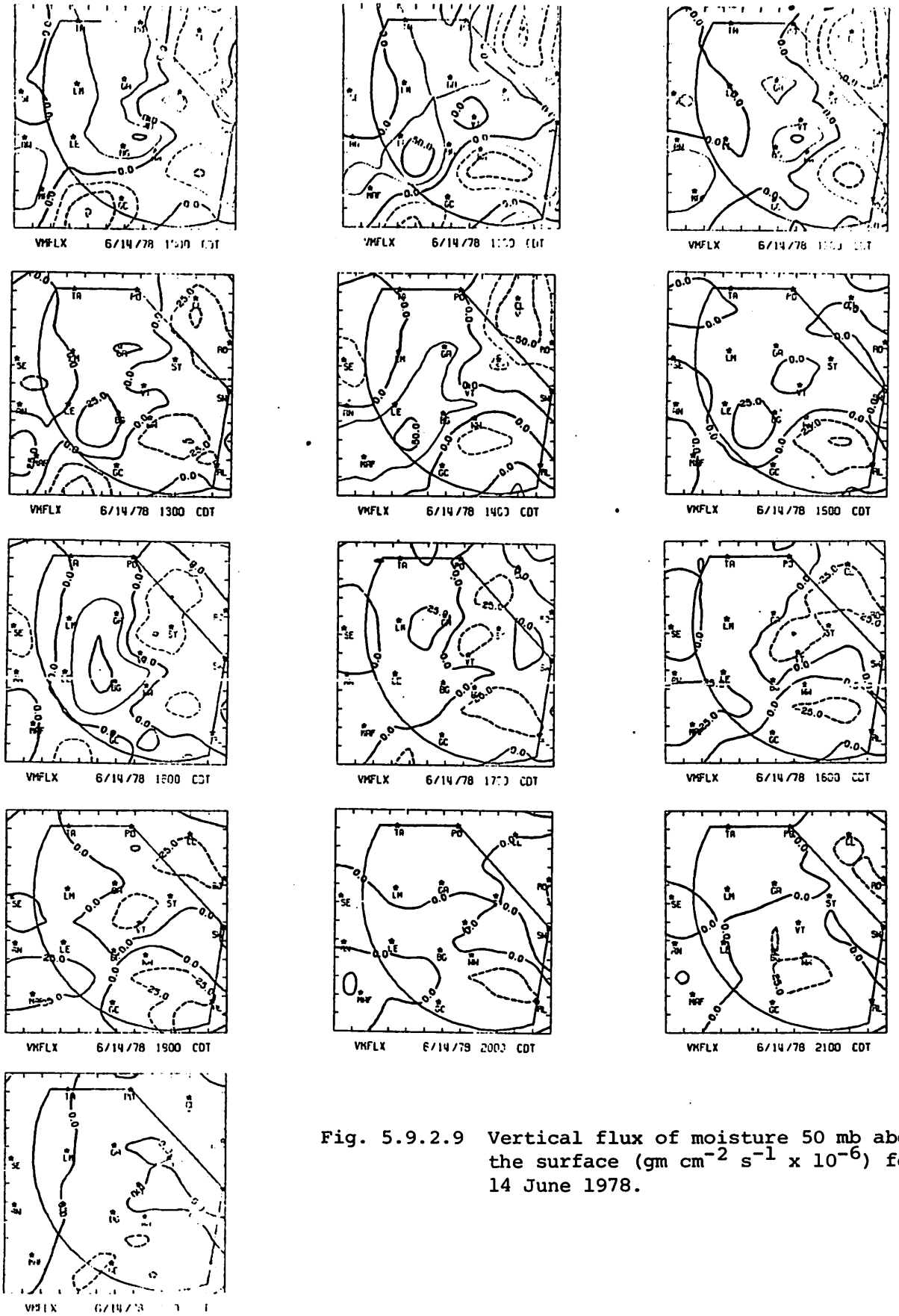

Fig. 5.9.2.9 Vertical flux of moisture 50 mb above the surface (gm cm^{-2} s^{-1} x 10^{-6}) for 14 June 1978.

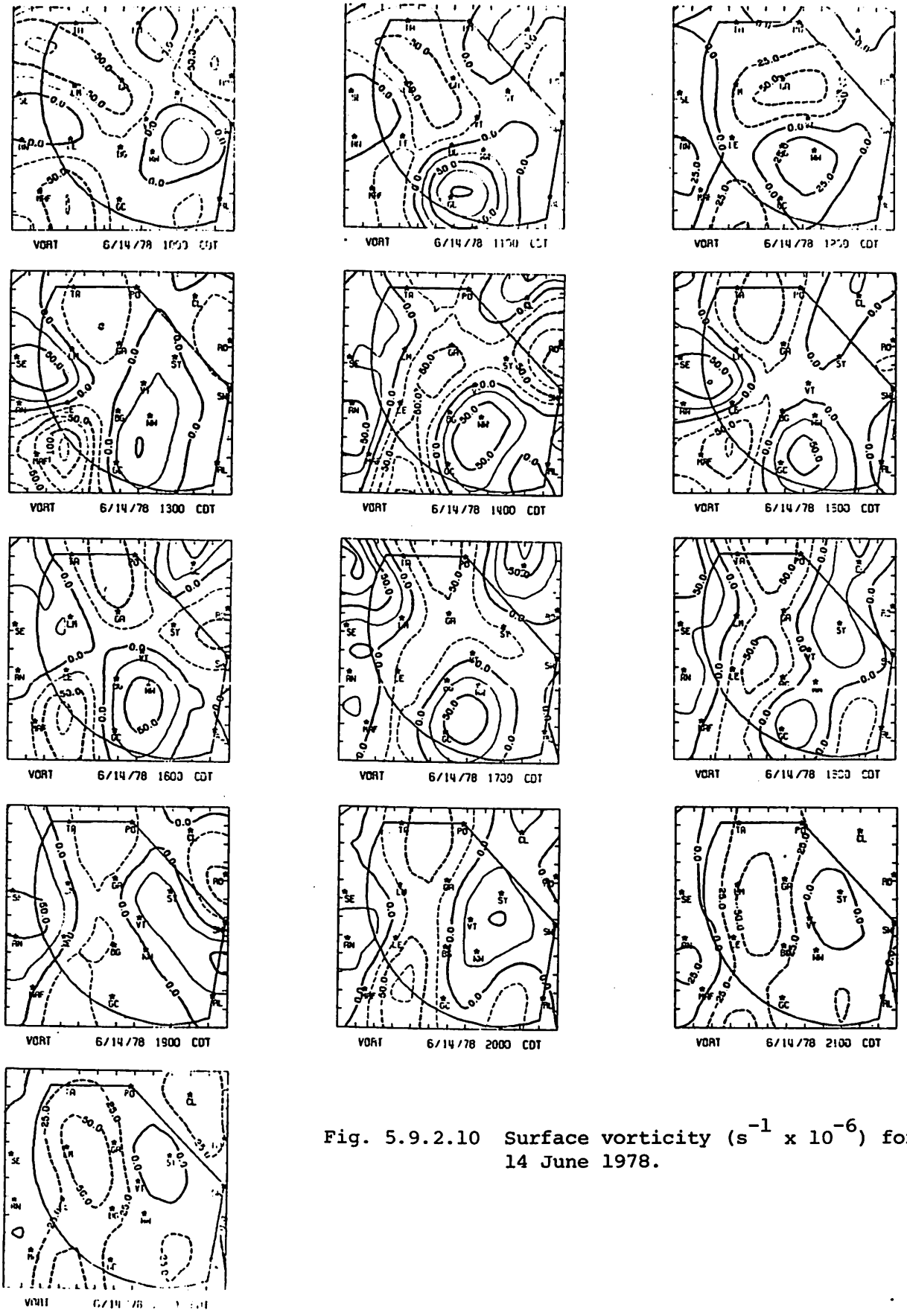

Fig. 5.9.2.10 Surface vorticity (s^{-1} x 10^{-6}) for 14 June 1978.

Pressure changes were also small on this day with 0.5 mb/hr being the largest change recorded (Fig. 5.9.2.11).

Surface wind speed (Fig. 5.9.2.12) was quite high on this day and southerly. These high wind speeds led to large terrain-induced vertical motion as noted above.

5.9.3 Upper Level Kinematic Parameters

June 14 is a good day to observe environmental conditions in the absence of any echo-producing convection. Although profiles of mass divergence fluctuated throughout the day, a layer of mass divergence between 500 mb and 350 mb was persistent (Fig. 5.9.3.1). The shapes of vertical velocity profiles (Fig. 5.9.3.2) were also consistent, although their sign varied from one time to the next. In general, vertical velocities become more negative higher in the atmosphere. A ridge centered over Texas at 500 and 300 mb was associated with the downward motions. Convergent layers between 800 and 500 mb at every time period (Fig. 5.9.3.1) are reflected in vertical velocity profiles as minima. Though they are not at the same height each time, these minima occur at each observation time and appear significant.

Profiles of moisture divergence fluctuate similarly to those of mass divergence (Fig. 5.9.3.3). Except for the 2100 GMT profile, moisture divergence occurred from 850 to 700 mb, and convergence from 700 to 600 mb throughout the day. Variation of the 2100 GMT profile is unexplained, but it occurred when the largest number of cumulus clouds were observed.

5.9.4 Energetics

Figure 5.9.4.1 shows the divergence of latent heat due to horizontal motions. The most predominant feature of these profiles is the convergence of latent heat at 775 mb at 2100 GMT. As mentioned before, this corresponds to the time of maximum cumulus development. The gain of latent heat due to horizontal convergence was opposed by a downward flux of latent heat (Fig. 5.9.4.2) at the same level. All other profiles of vertical flux of latent heat show a gain of latent heat at that level. The local change of latent heat (Fig. 5.9.4.3) was negative at 1800 and 2100 GMT between 850 and 700 mb. Therefore, latent heat energy was being removed faster than it was being concentrated in that layer. This produced a negative residual for 1800 and 2100 GMT (Fig. 5.9.4.4) which suggests that cloud moisture was being evaporated into the environment around 725 mb. This occurred at about 1.5 km (5K ft) above the surface, which soundings indicate is the top of the well-mixed surface layer.

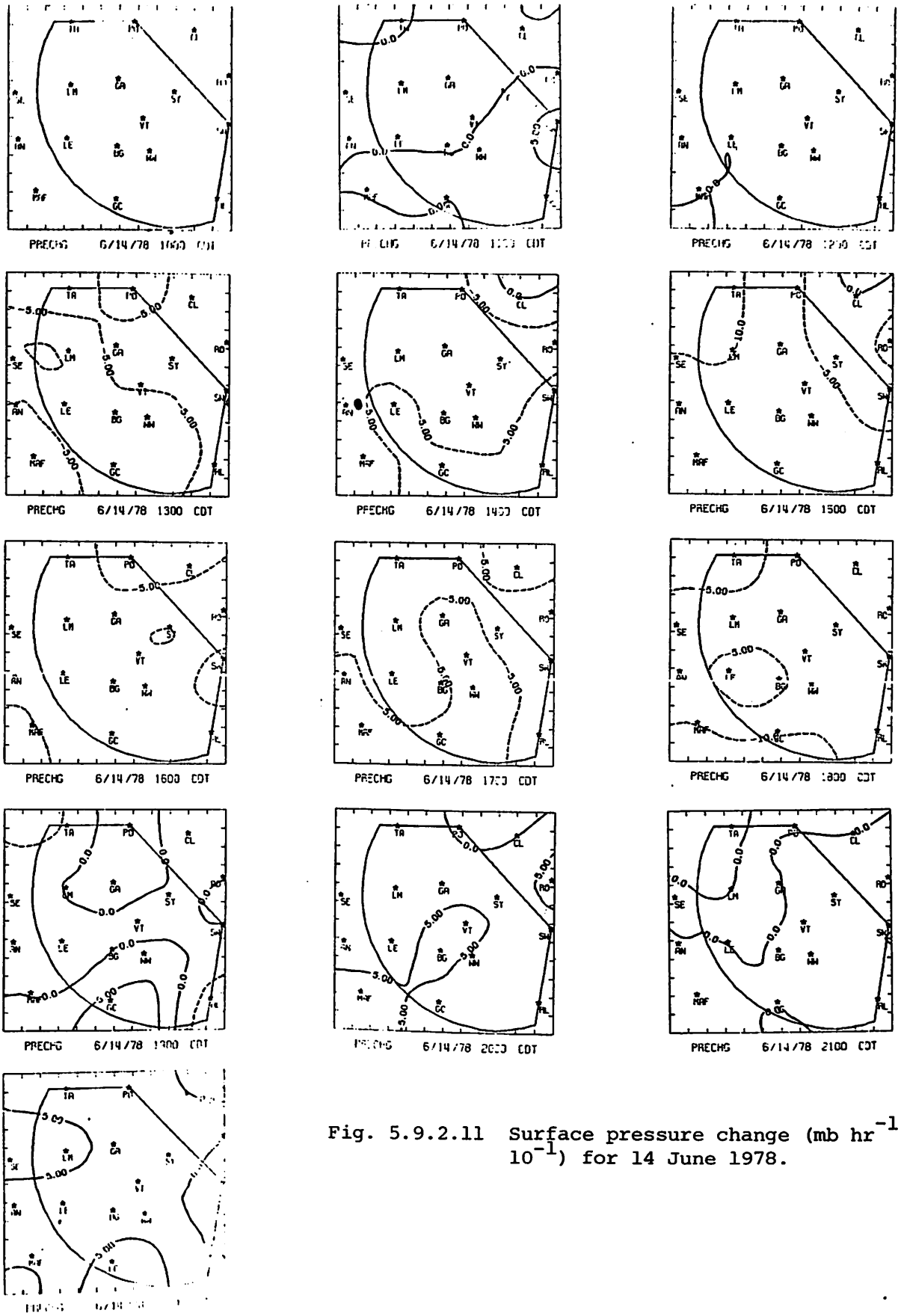

Fig. 5.9.2.11 Surface pressure change (mb hr^{-1} x 10^{-1}) for 14 June 1978.

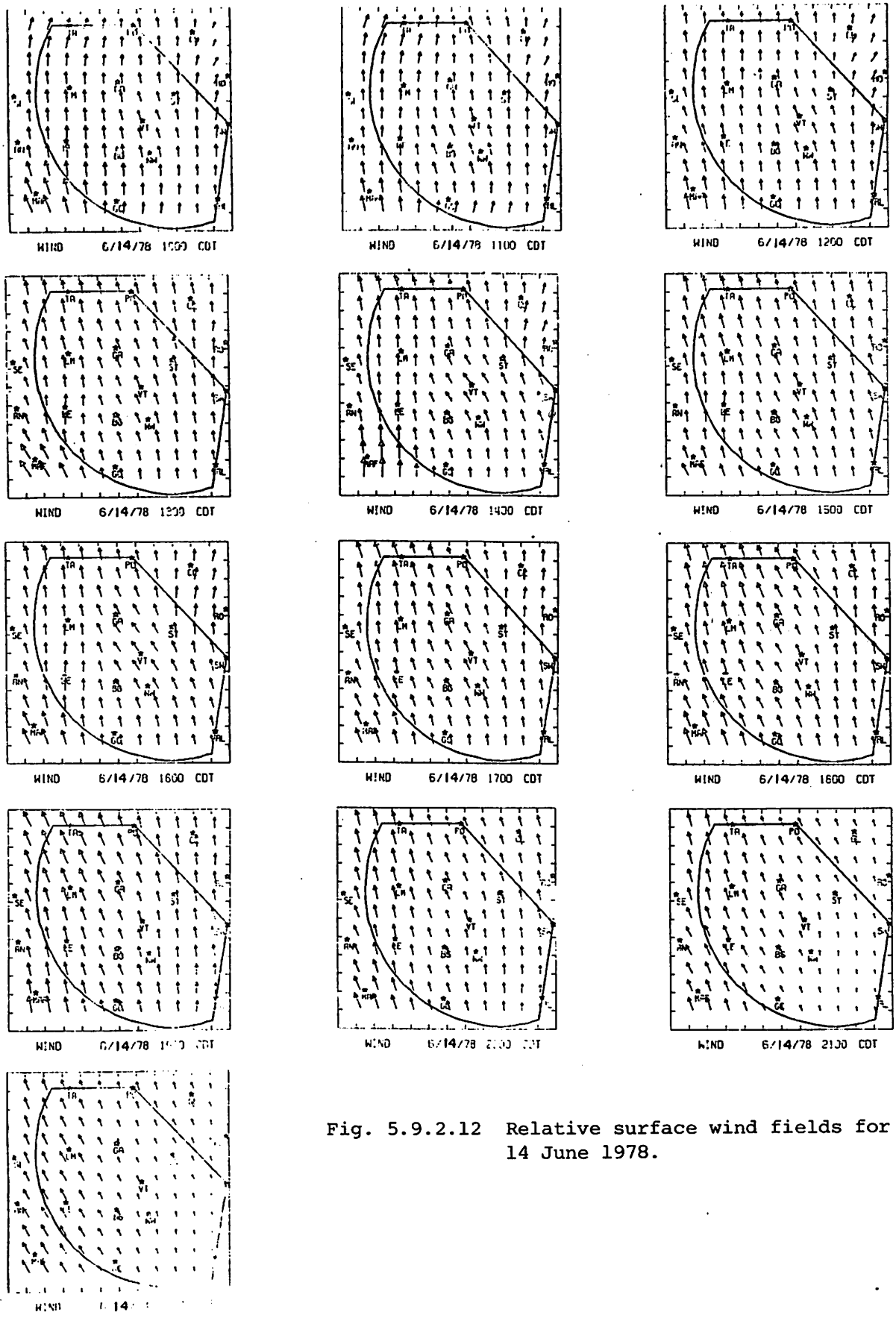

Fig. 5.9.2.12 Relative surface wind fields for 14 June 1978.

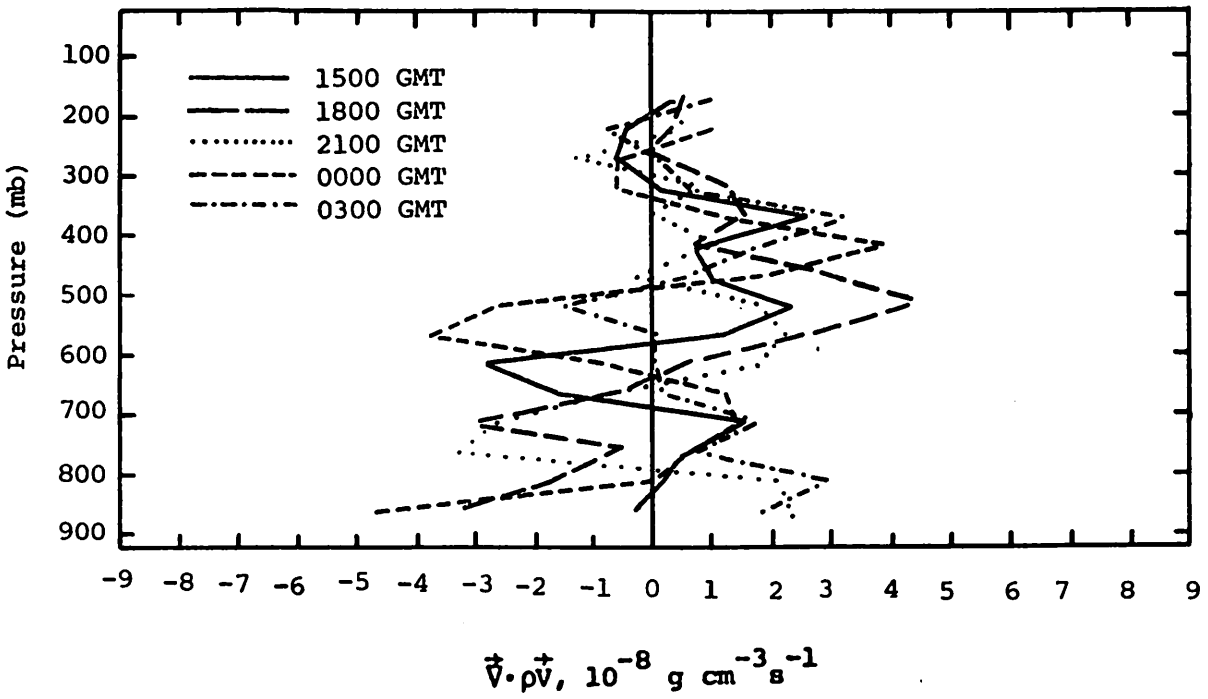

Fig. 5.9.3.1 Vertical profiles of mass divergence on 14 June 1978.

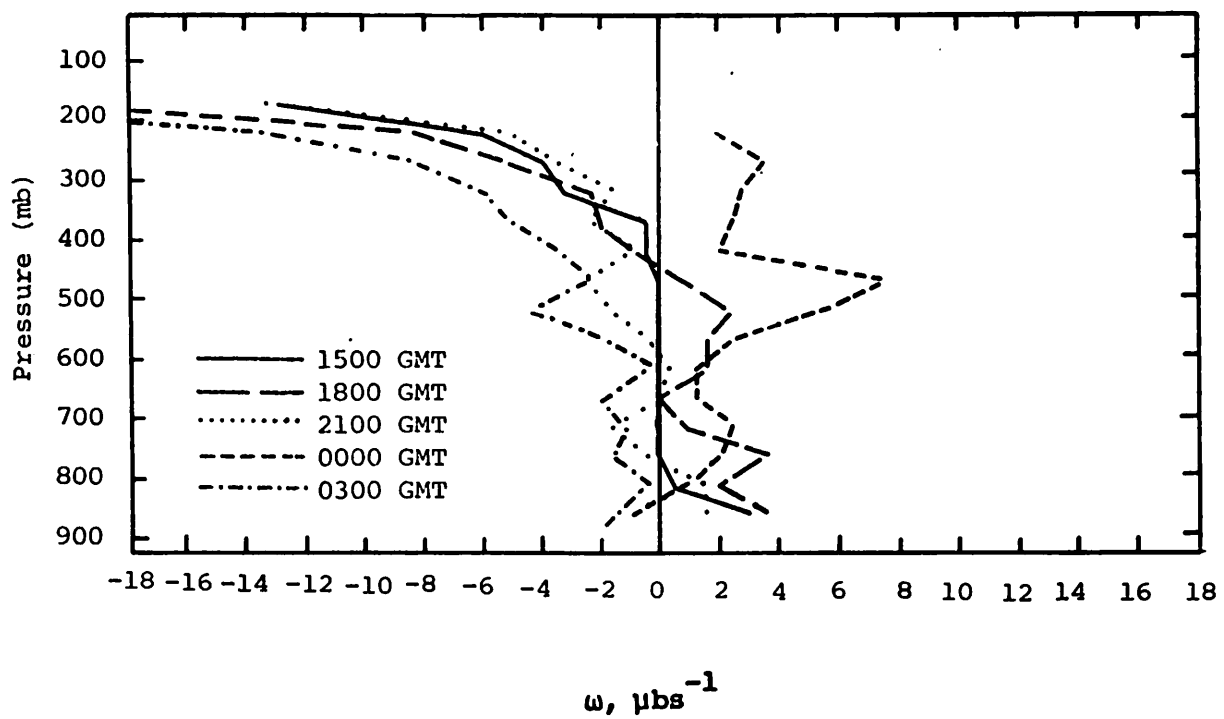

Fig. 5.9.3.2 Vertical profiles of vertical motion on 14 June 1978.

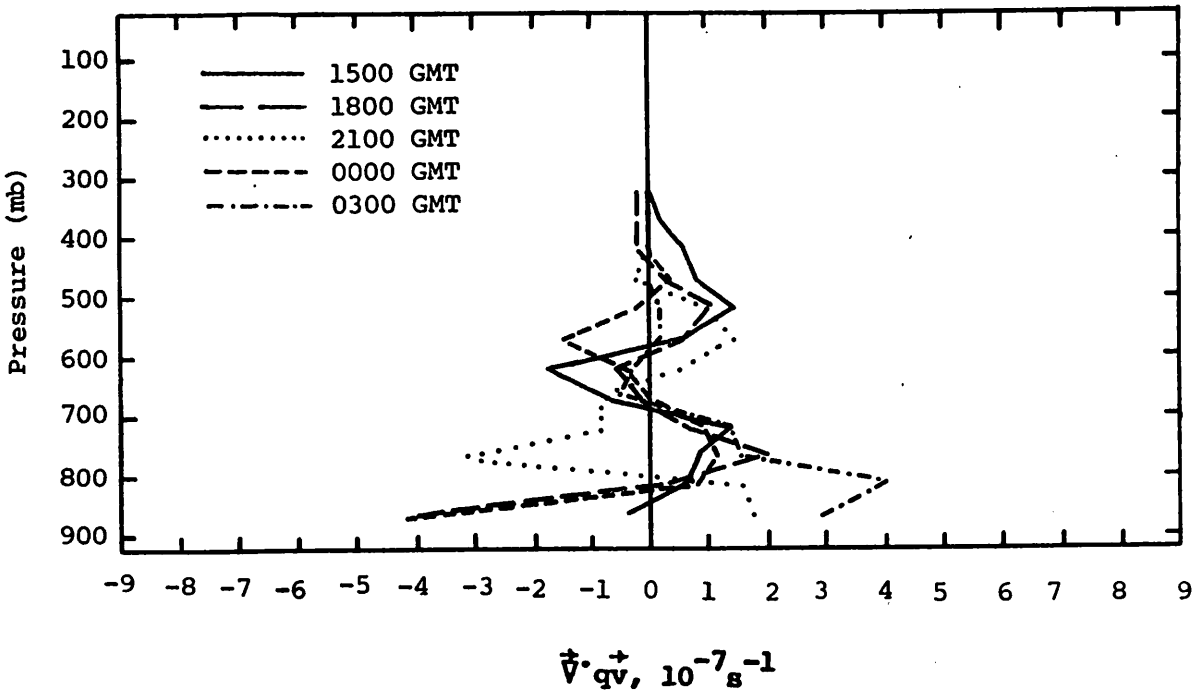

Fig. 5.9.3.3 Vertical profiles of moisture divergence on 14 June 1978.

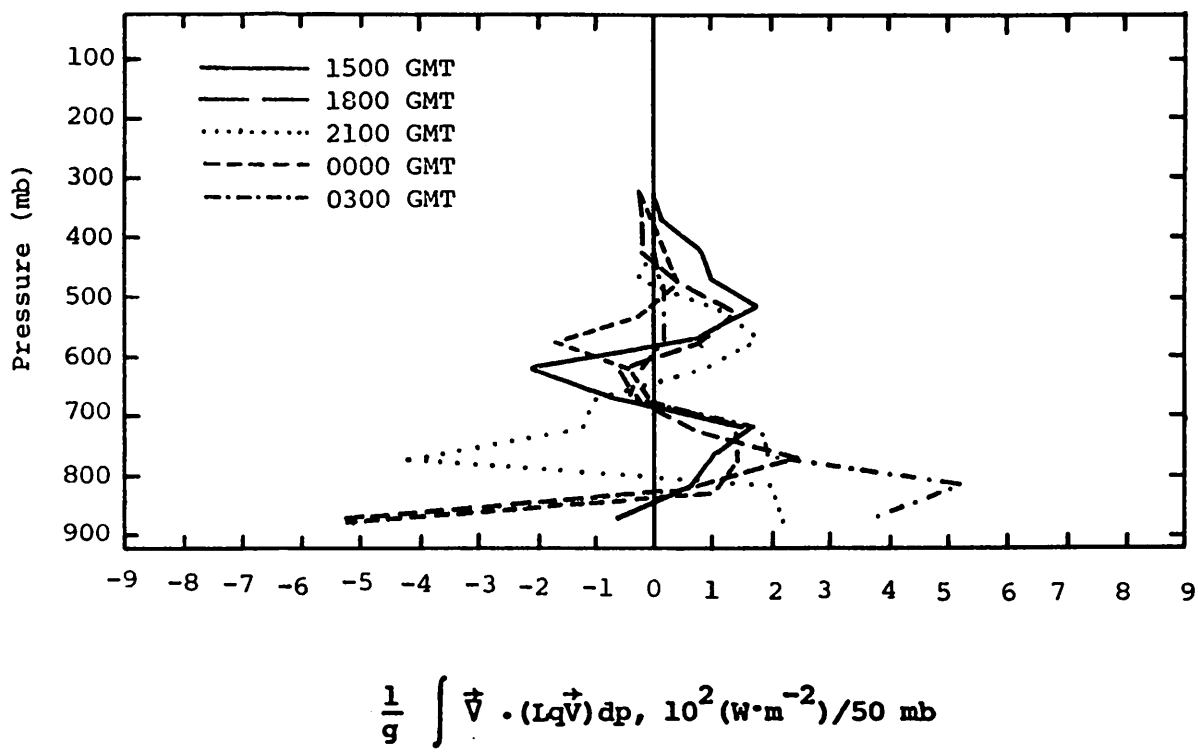

Fig. 5.9.4.1 Vertical profiles of the horizontal flux of latent heat energy on 14 June 1978.

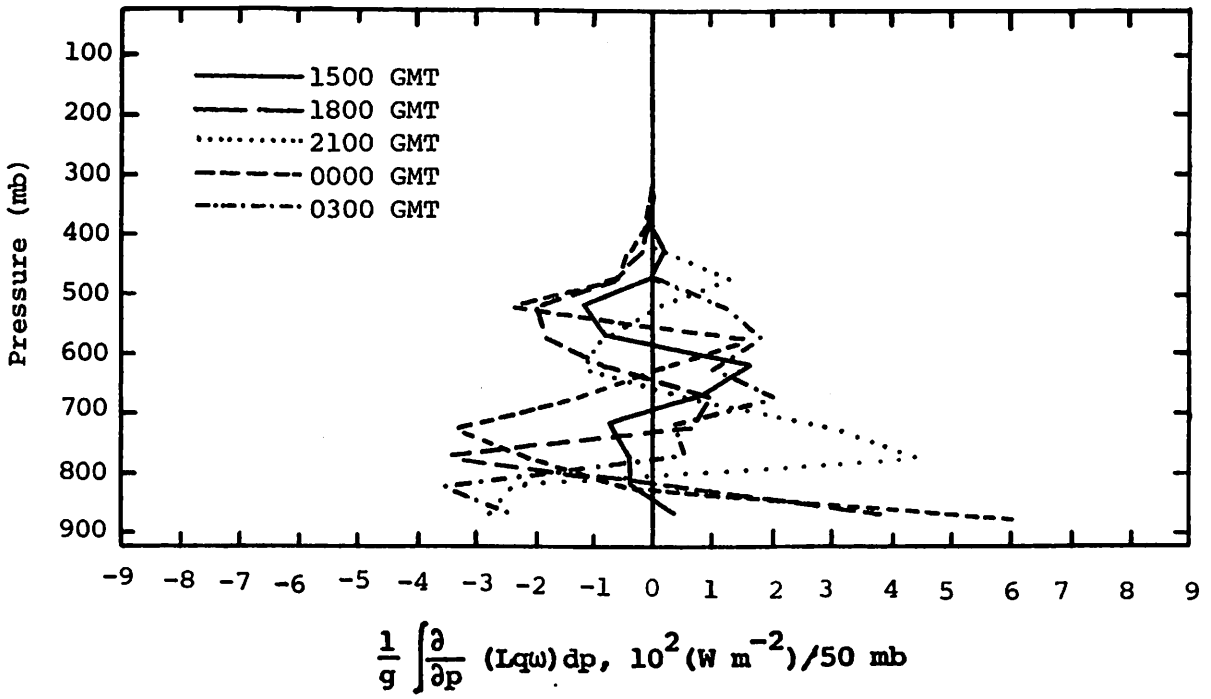

Fig. 5.9.4.2 Vertical profiles of the vertical flux of latent heat energy on 14 June 1978.

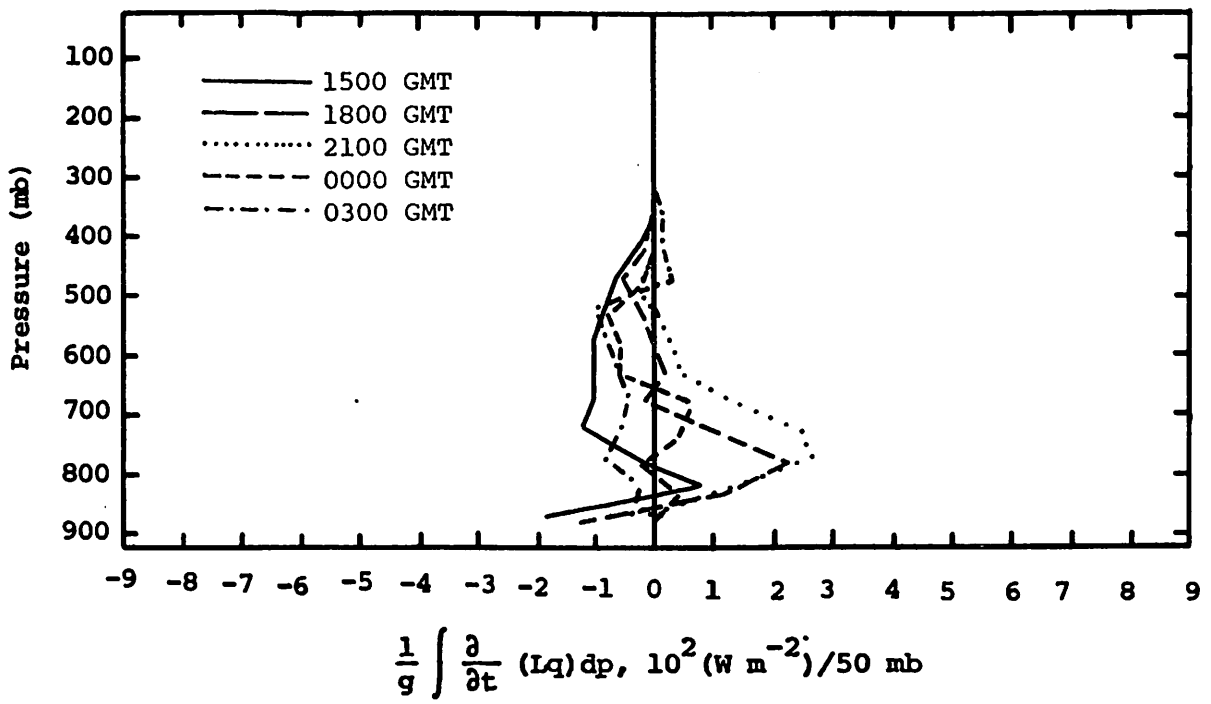

Fig. 5.9.4.3 Vertical profiles of the local change of latent heat energy on 14 June 1978.

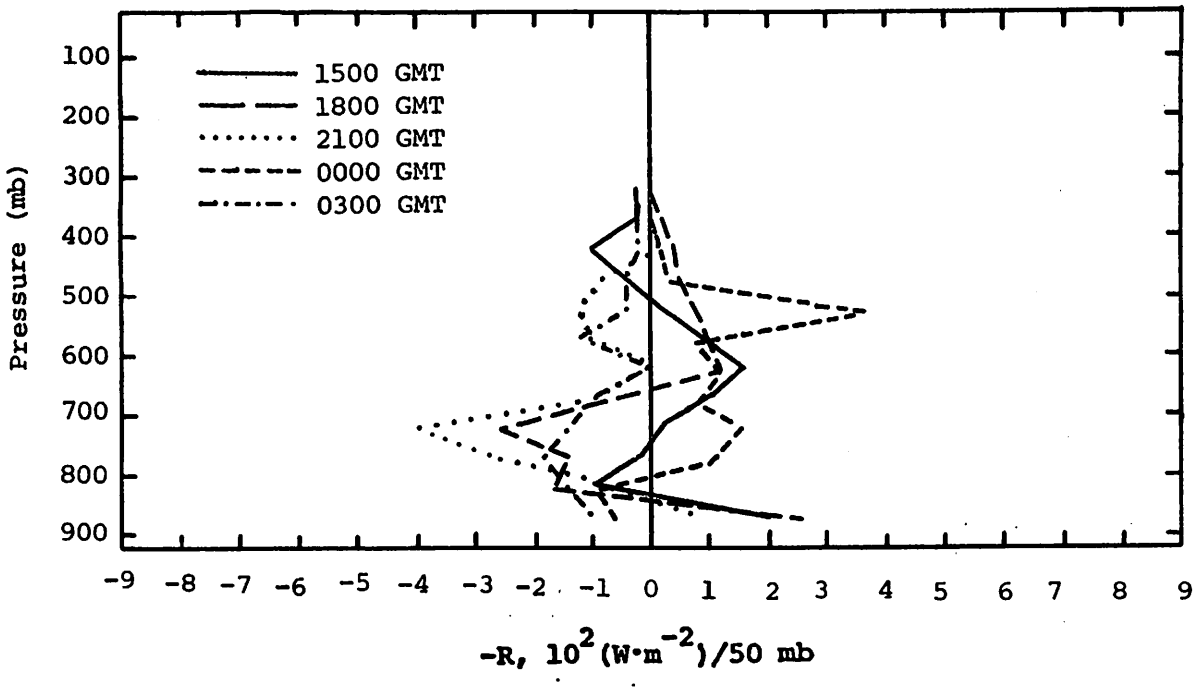

Fig. 5.9.4.4 Vertical profiles of the residual of the latent heat energy equation on 14 June 1978.

These results agree well with water vapor budget results for this day.

Diabatic heating profiles (Fig. 5.9.4.5) show that heat was being converged above 450 mb at all times except 0000 GMT. In contrast, the 0000 GMT profile shows a loss of sensible heat at all levels.

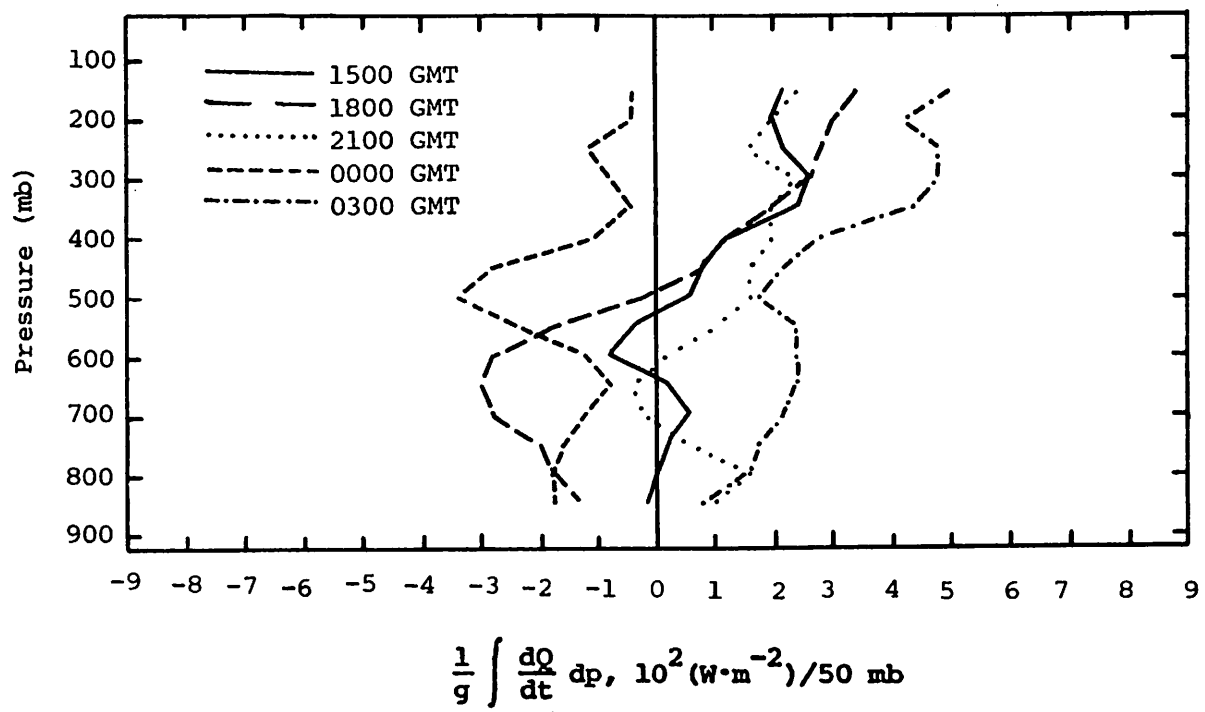

Fig. 5.9.4.5 Vertical profiles of diabatic heating computed from the first law of thermodynamics on 14 June 1978.

Figure 5.9.4.6 shows profiles of kinetic energy divergence. Profiles are consistent throughout the day with kinetic energy being converged above 325 mb and diverged from 475 to 325 mb at all times. Below 475 mb, values were small. The vertical flux of kinetic energy was not significantly large below 500 mb (Fig. 5.9.4.7). Above that level, values were fairly large, but do not vary systematically with time.

5.9.5 Water Vapor Budget

Profiles of the net horizontal transport of water vapor (Fig. 5.9.5.1) show a loss of water vapor between 600 and 450 mb at all times. Water vapor was being converged below 650 mb at 2100 GMT, and at 0300 GMT it was being diverged throughout all levels. Profiles of net vertical transport (Fig. 5.9.5.2) varied considerably from time to time, though features of the vertical transport through constant pressure surfaces (Fig. 5.9.5.3) were more definite. Vertical moisture transport at 1800 and 0000 GMT was upward and at 0300 GMT downward at all levels. No systematic changes during the day were observed.

The most prominent feature of the net combined transport (Fig. 5.9.5.4) is that a loss of water vapor occurred in all layers at 0300 GMT due to transport mechanisms. Profiles at 1800 and 2100 GMT show a loss at 725 mb, which is the height at which cloud growth was reported for those times.

Profiles of the total mass of water vapor (Fig. 5.9.5.5) show a relatively small amount of water vapor below 700 mb at 1500 and 1800 GMT, and an increase due to mixing at 2100 GMT.

Maximum values of the local rate-of-change of water vapor (Fig. 5.9.5.6) occurred at the top of the mixed surface layer in the 1500-1800, 1800-2100, and 2100-0000 GMT profiles. This layer became thicker as insolation heated the surface. The upward progression of the top of the mixed layer was relatively uninhibited due to the lack of clouds. The 0000-0300 GMT profile shows a decrease of water vapor, primarily at 800 mb, as surface cooling reduced vertical mixing.

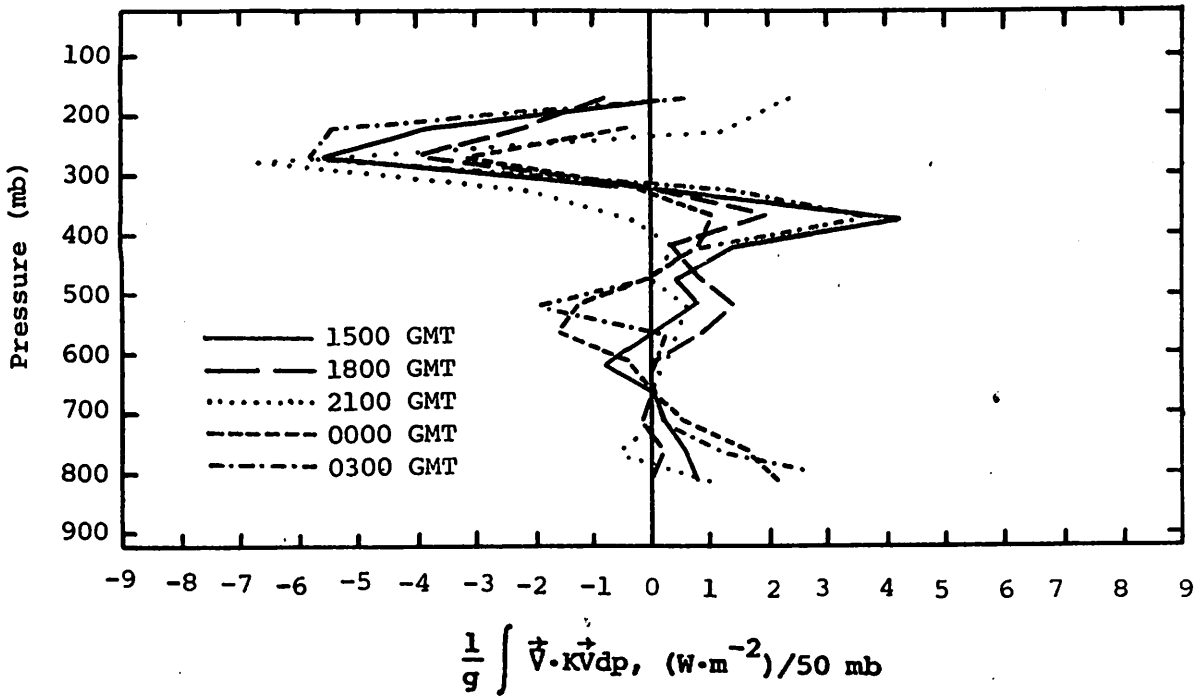

Fig. 5.9.4.6 Vertical profiles of the horizontal flux of kinetic energy on 14 June 1978.

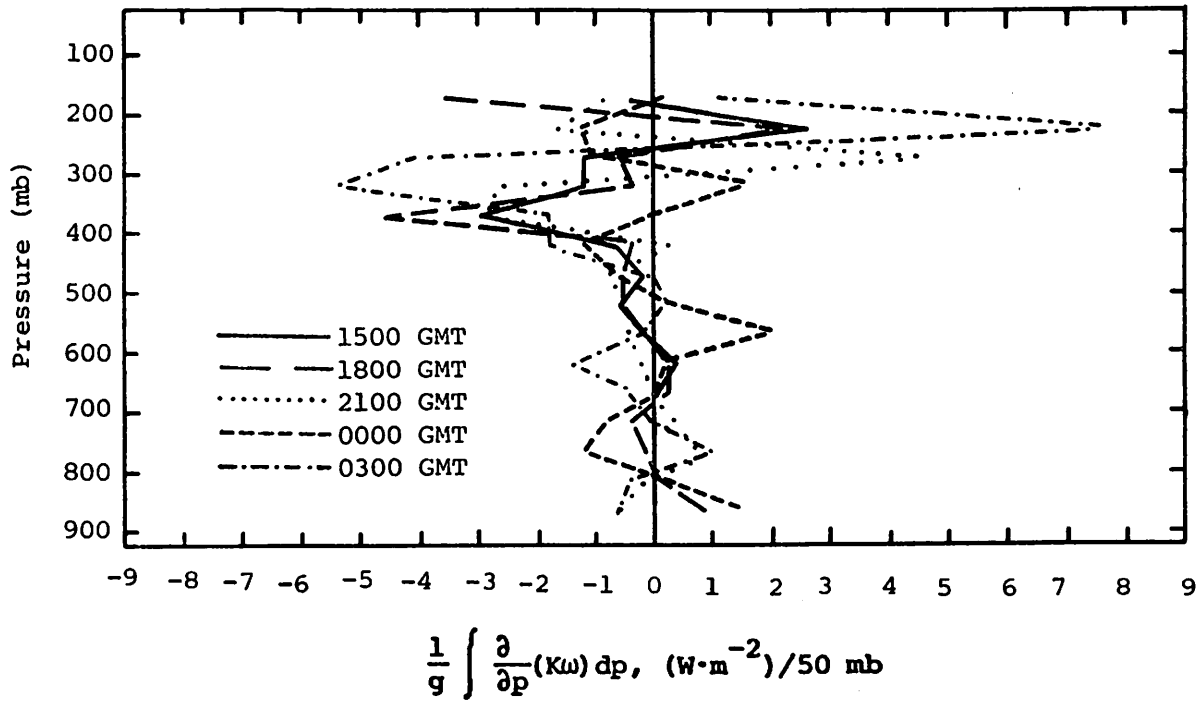

Fig. 5.9.4.7 Vertical profiles of the vertical flux of kinetic energy on 14 June 1978.

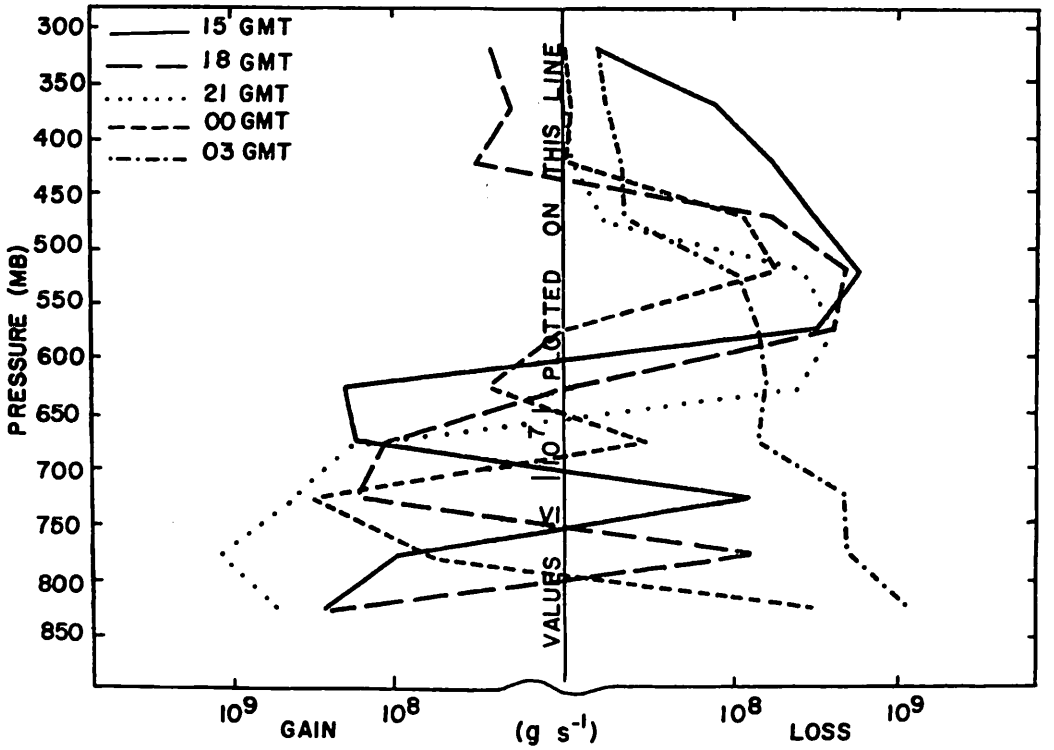

Fig. 5.9.5.1 Net horizontal transport of water vapor through boundaries of 50-mb layers (g s^{-1}) over the Texas HIPLEX area for 14 June 1978.

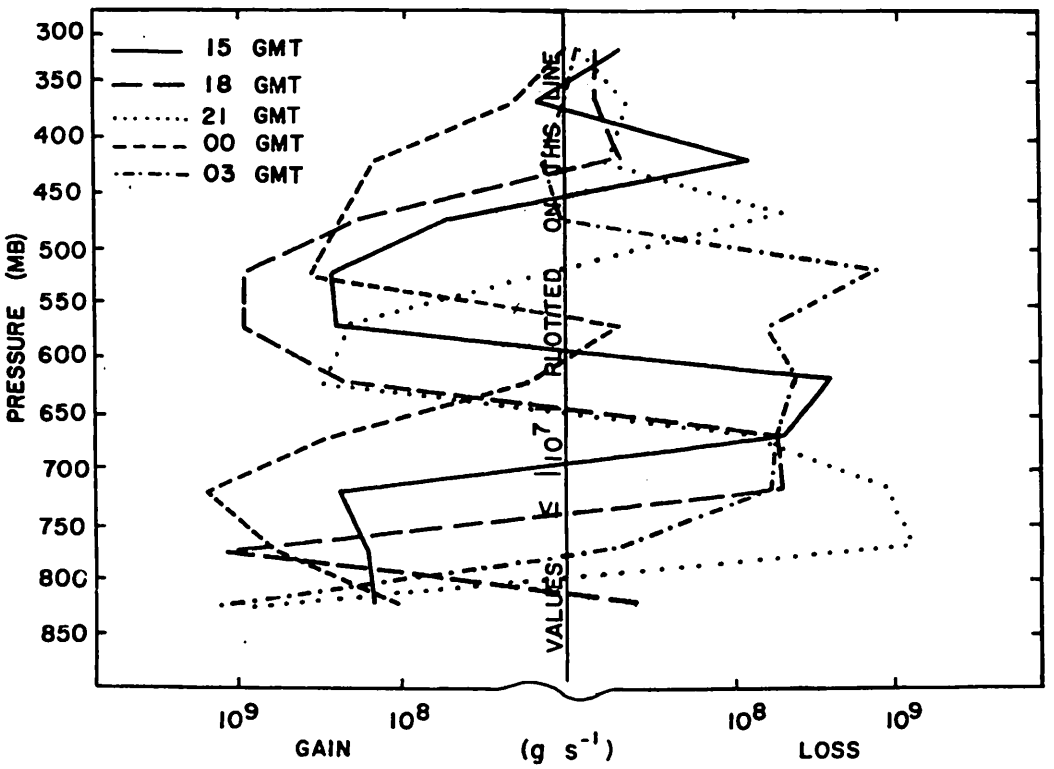

Fig. 5.9.5.2 Net vertical transport of water vapor through boundaries of 50-mb layers (g s^{-1}) over the Texas HIPLEX area for 14 June 1978.

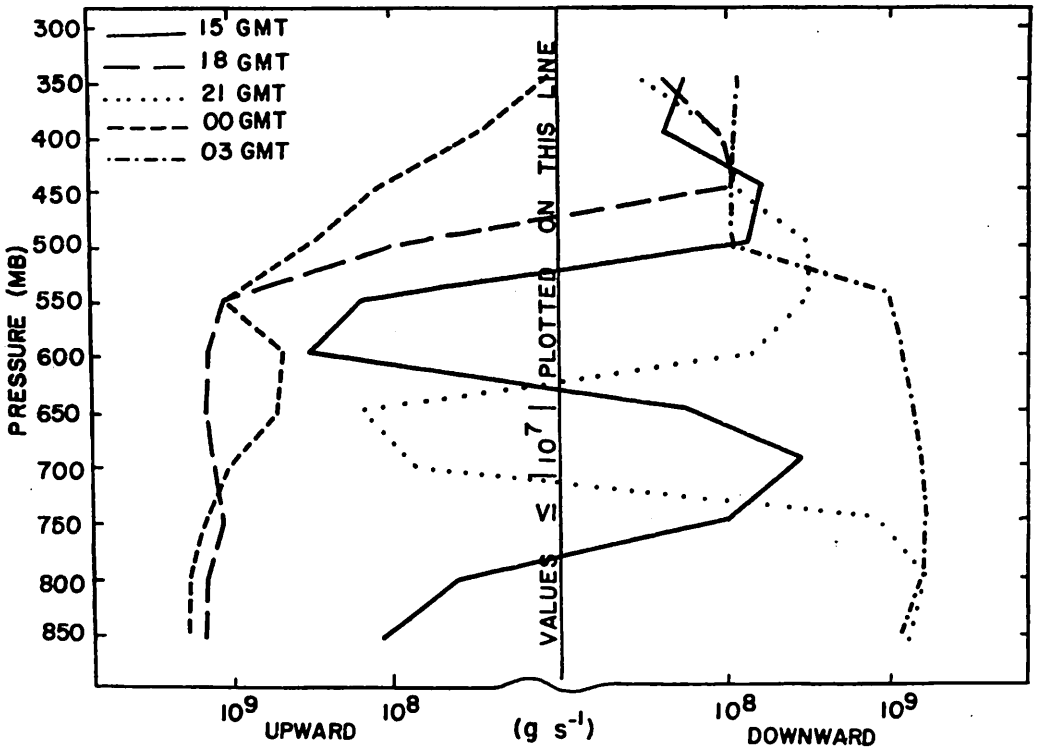

Fig. 5.9.5.3 Vertical transport of water vapor through constant pressure surfaces (g s^{-1}) over the Texas HIPLEX area on 14 June 1978.

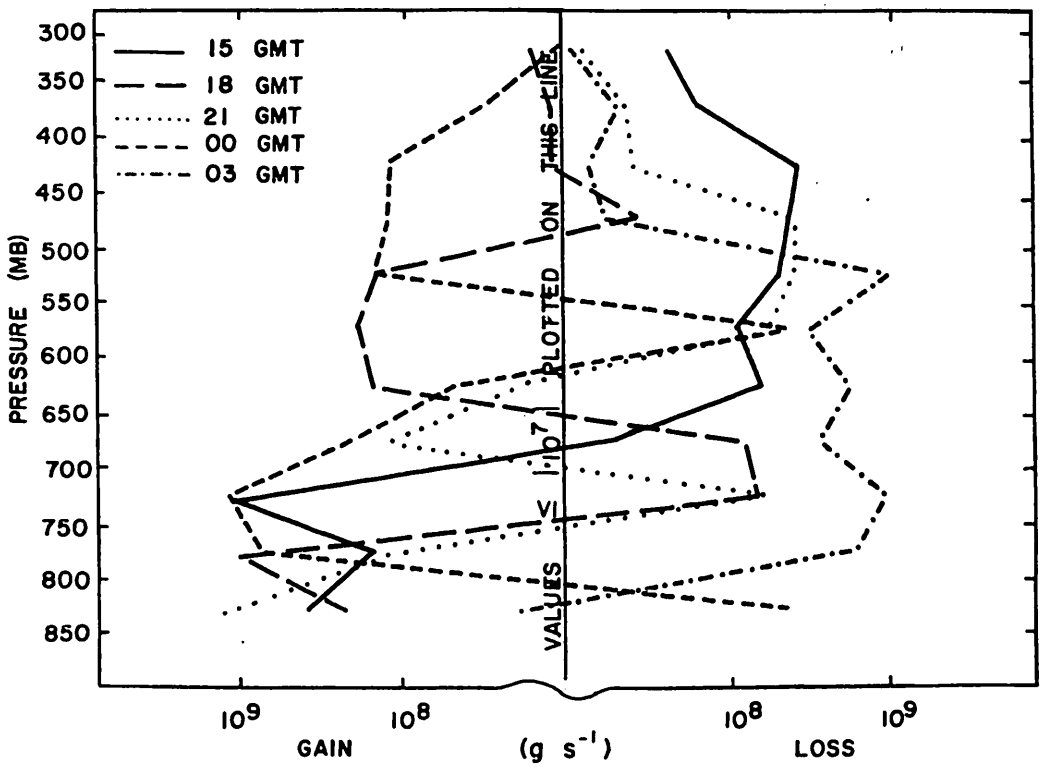

Fig. 5.9.5.4 Combined net horizontal and vertical transport of water vapor through boundaries of 50-mb layers (g s^{-1}) over the Texas HIPLEX area on 14 June 1978.

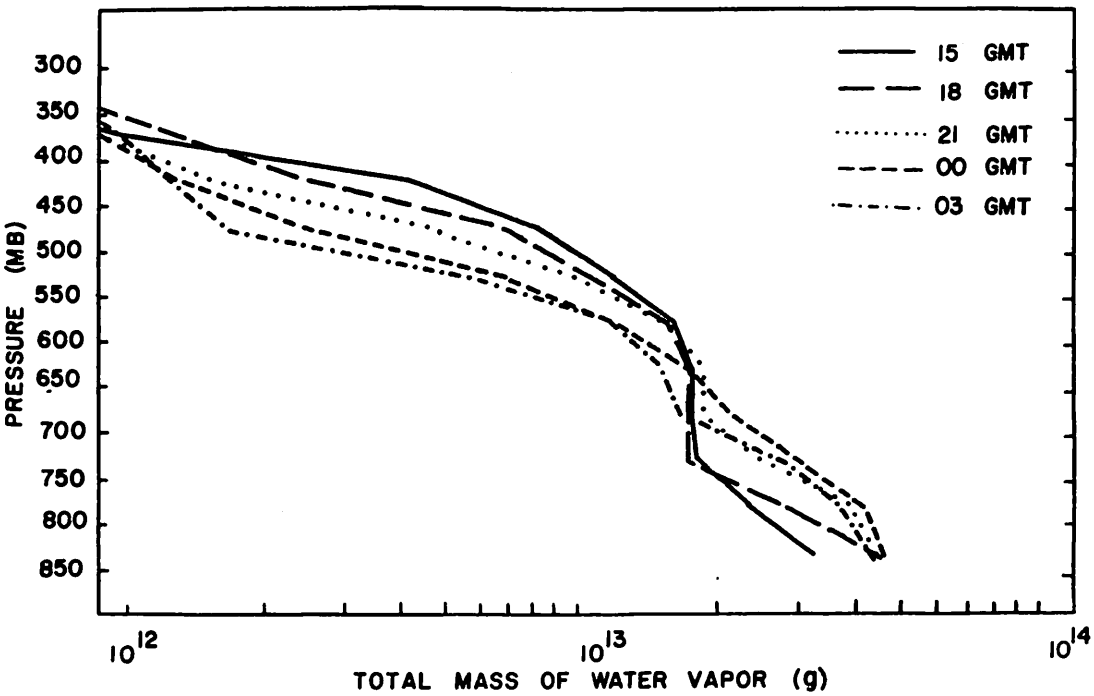

Fig. 5.9.5.5 Total mass of water vapor in layers 50 mb deep (gm) over the Texas HIPLEX area on 14 June 1978.

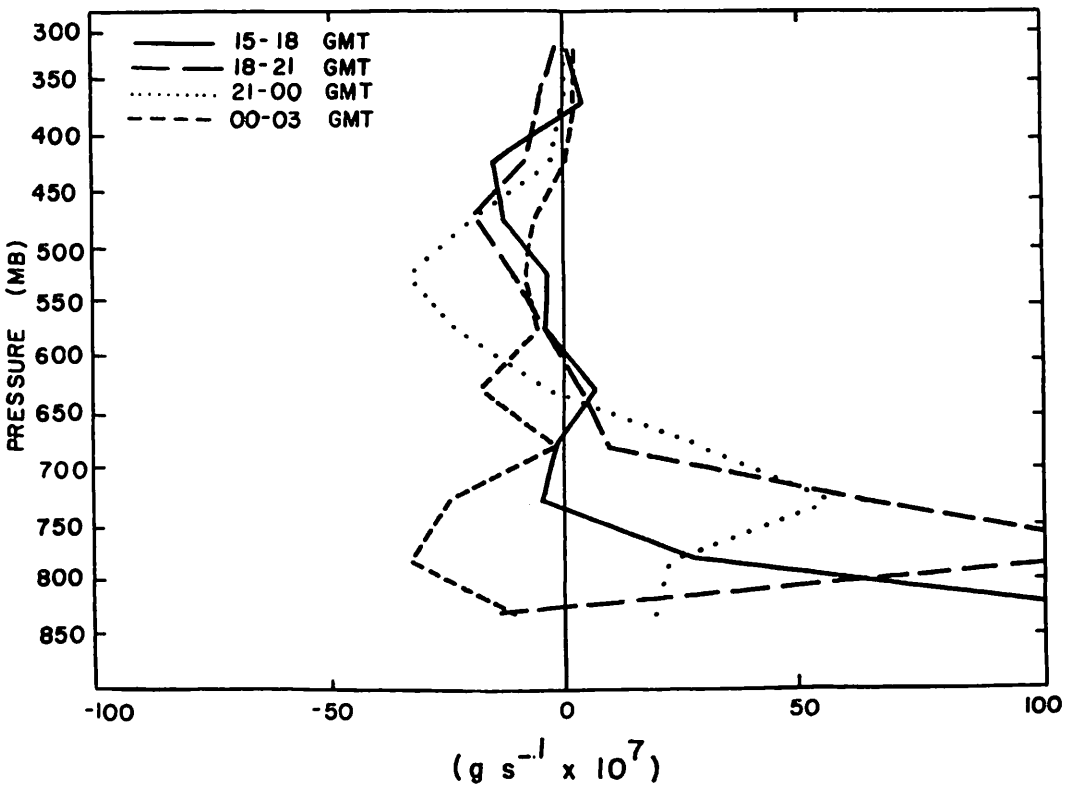

Fig. 5.9.5.6 Local rate-of-change in total mass of water vapor (g s^{-1} x 10^7) for the Texas HIPLEX area for 14 June 1978.

5.10 20 June 1978

5.10.1 Radar

No radar echoes were observed in or near the analysis area until 0000 GMT on June 21 (Fig. 5.10.1.1). At 0000 GMT, an echo with a maximum height of 7.3 km (24K ft) developed over Lamesa. At 0100 GMT, two tops were measured in the echo, one at 13.3 km (44K ft) and the other at 13.9 km (46K ft). At 0200 GMT, those tops were 13.3 km (44K ft) and 11.5 km (38K ft), respectively. No echoes were observed at 0300 GMT due to missing data.

5.10.2 Surface

The temperature field was fairly flat this day, though a slight maximum persisted near Lenorah (Fig. 5.10.2.1). Dewpoint depression (Fig. 5.10.2.2) and mixing ratio (Fig. 5.10.2.3) analyses show that Post and Big Spring were relatively moist throughout the day. Before echoes were observed at 0000 GMT, mixing ratio ranged from 9 to 16 g/kg. Equivalent potential temperature fields (Fig. 5.10.2.4) also reflected greater moisture at Post and Big Spring.

Terrain-induced vertical motion (Fig. 5.10.2.5) showed centers which are typical of days having wind from the south. Centers of downward motion near Walsh-Watts and Rotan persisted throughout the day.

A weak zone of convergence was observed at many times in the Gail-Lamesa area (Fig. 5.10.2.6). Values reached 2×10^{-4} sec^{-1} at 1900 GMT, and the orientation of the zone changed as the day progressed. This divergence produced vertical motions of -5 μbars/sec at several times (Fig. 5.10.2.7). Moisture divergence (Fig. 5.10.2.8) and vertical moisture flux (Fig. 5.10.2.9) also show these weak but persistent features.

The vorticity analysis shows centers which shift throughout the day (Fig. 5.10.2.10). Pressure changes were small and variable (Fig. 5.10.2.11) with the highest change being 1 mb/hr.

Characteristics of the wind field (Fig. 5.10.2.12) help explain characteristics of the divergence fields. The flow was generally from the south, except in the northwest corner of the area where the flow was from the east to northeast. The intersection of these two flow regimes caused the divergence pattern which remained in the same general location most of the day.

At 0200 GMT, changes in the surface moisture field indicate outflow from the echo over Lamesa. Mixing ratio rose to 19 g/kg and dewpoint depression and temperature fell, particularly at 0300 GMT. The echoes producing these changes were the only ones to develop within 200 km of the network on this

MISSING DATA

RADAR 6/20/78 1000 CDT

MISSING DATA

RADAR 6/20/78 1100 CDT

MISSING DATA

RADAR 6/20/78 1200 CDT

NO ECHOES

RADAR 6/20/78 1300 CDT

MISSING DATA

RADAR 6/20/78 1400 CDT

NO ECHOES

RADAR 6/20/78 1500 CDT

NO ECHOES

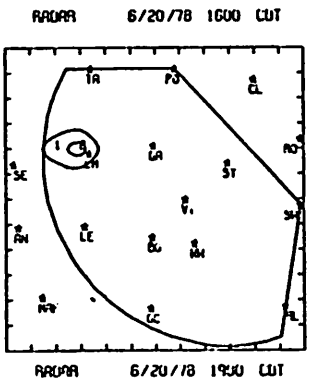

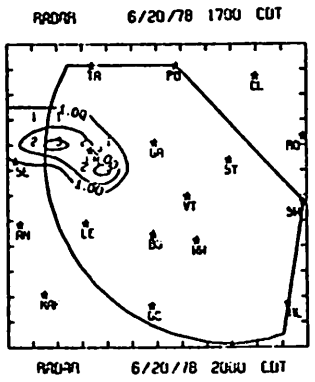

NO ECHOES

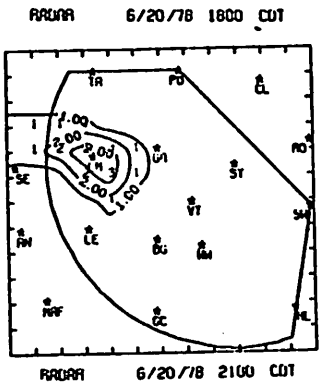

MISSING DATA

RADAR 6/20/78 2200 CDT

Fig. 5.10.1.1 Radar echoes for 20 June 1978.

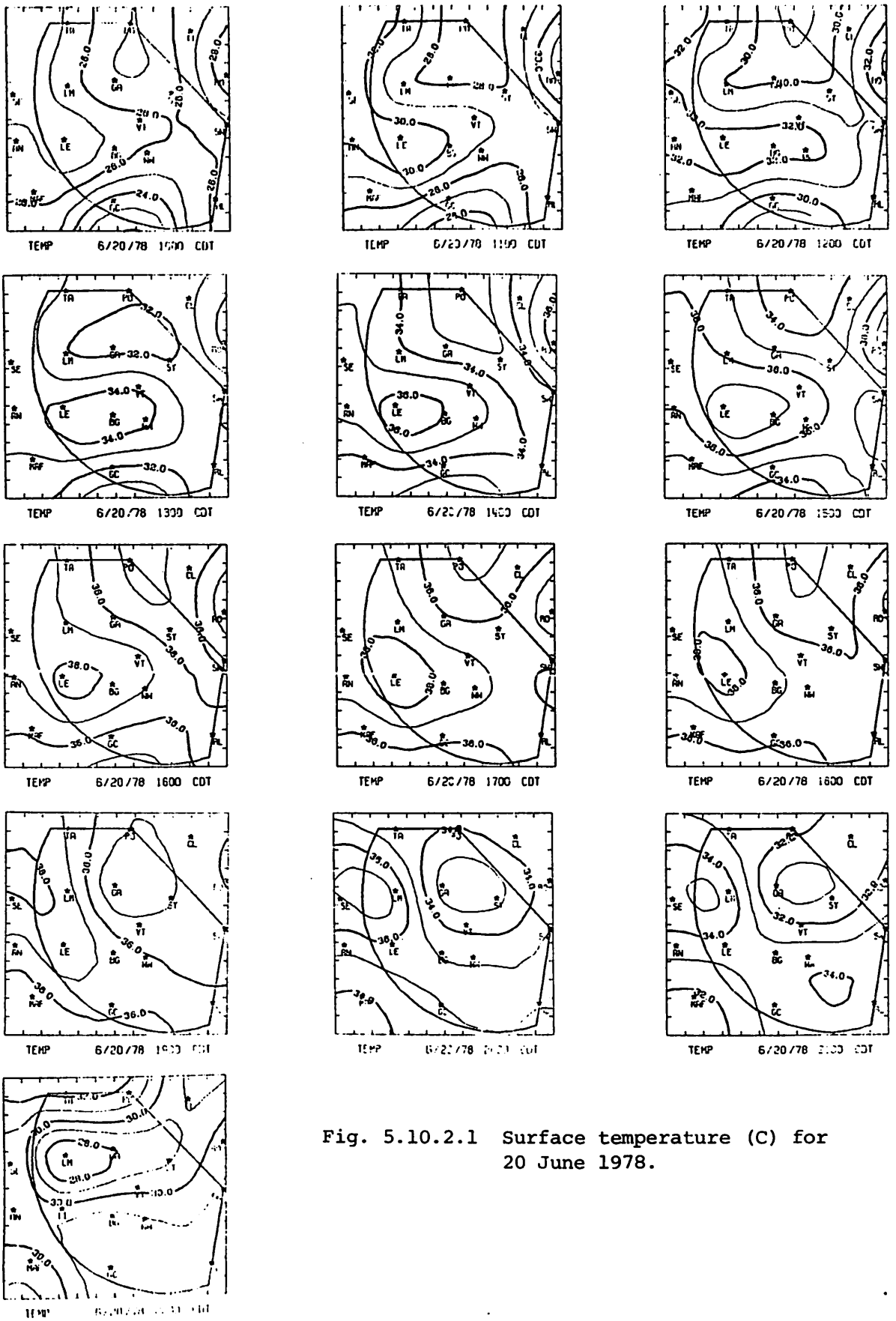

Fig. 5.10.2.1 Surface temperature (C) for 20 June 1978.

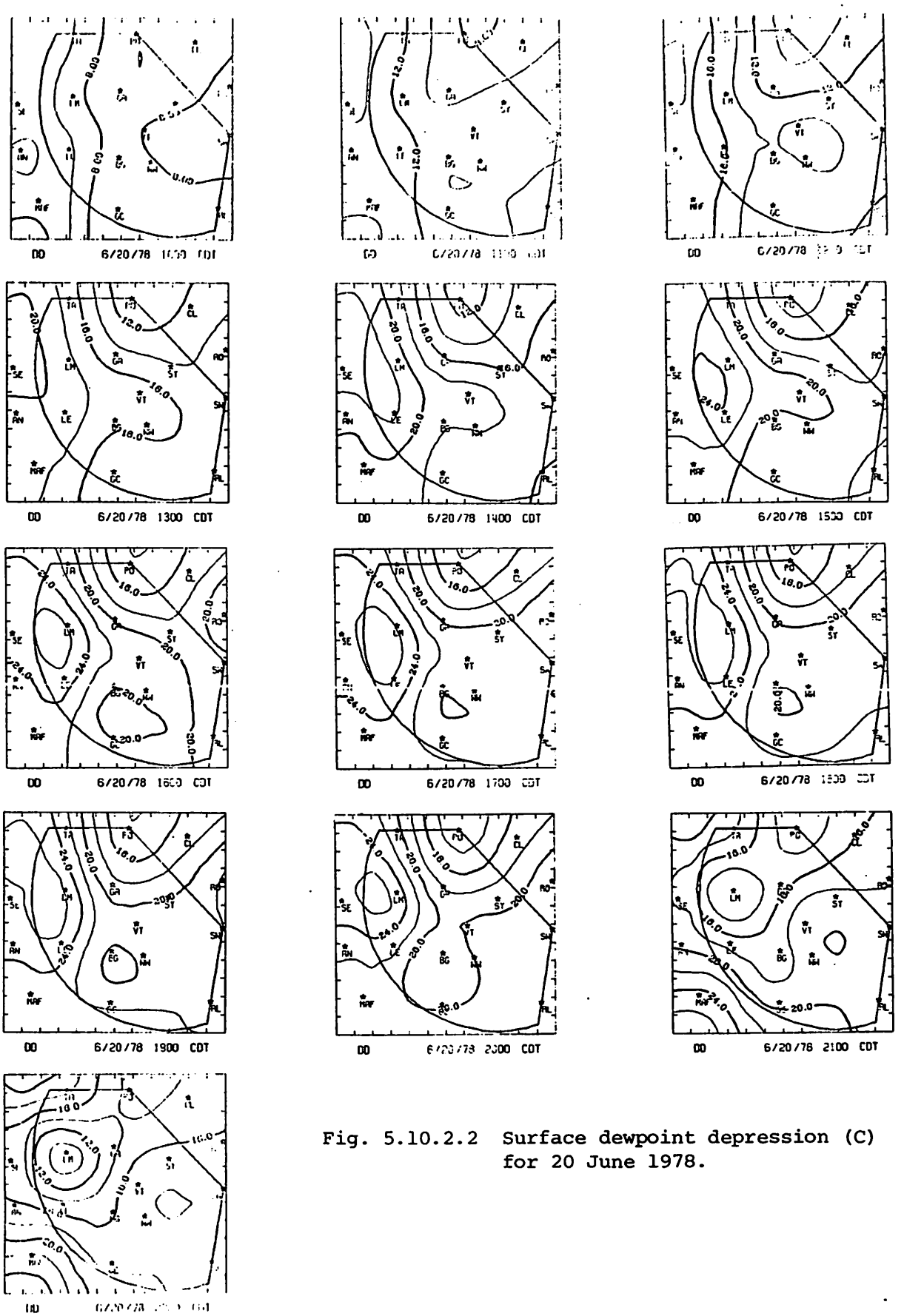

Fig. 5.10.2.2 Surface dewpoint depression (C) for 20 June 1978.

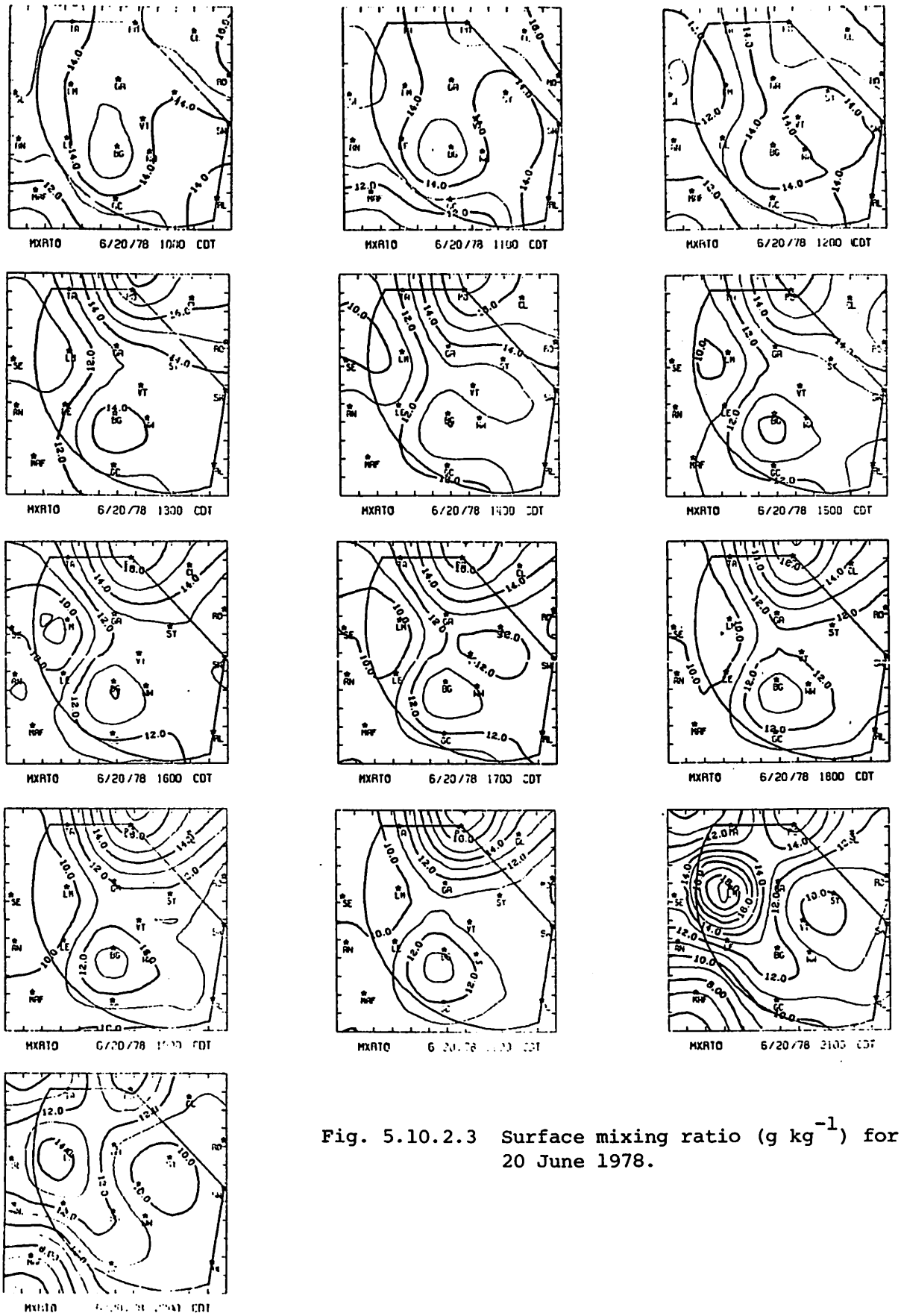

Fig. 5.10.2.3 Surface mixing ratio (g kg^{-1}) for 20 June 1978.

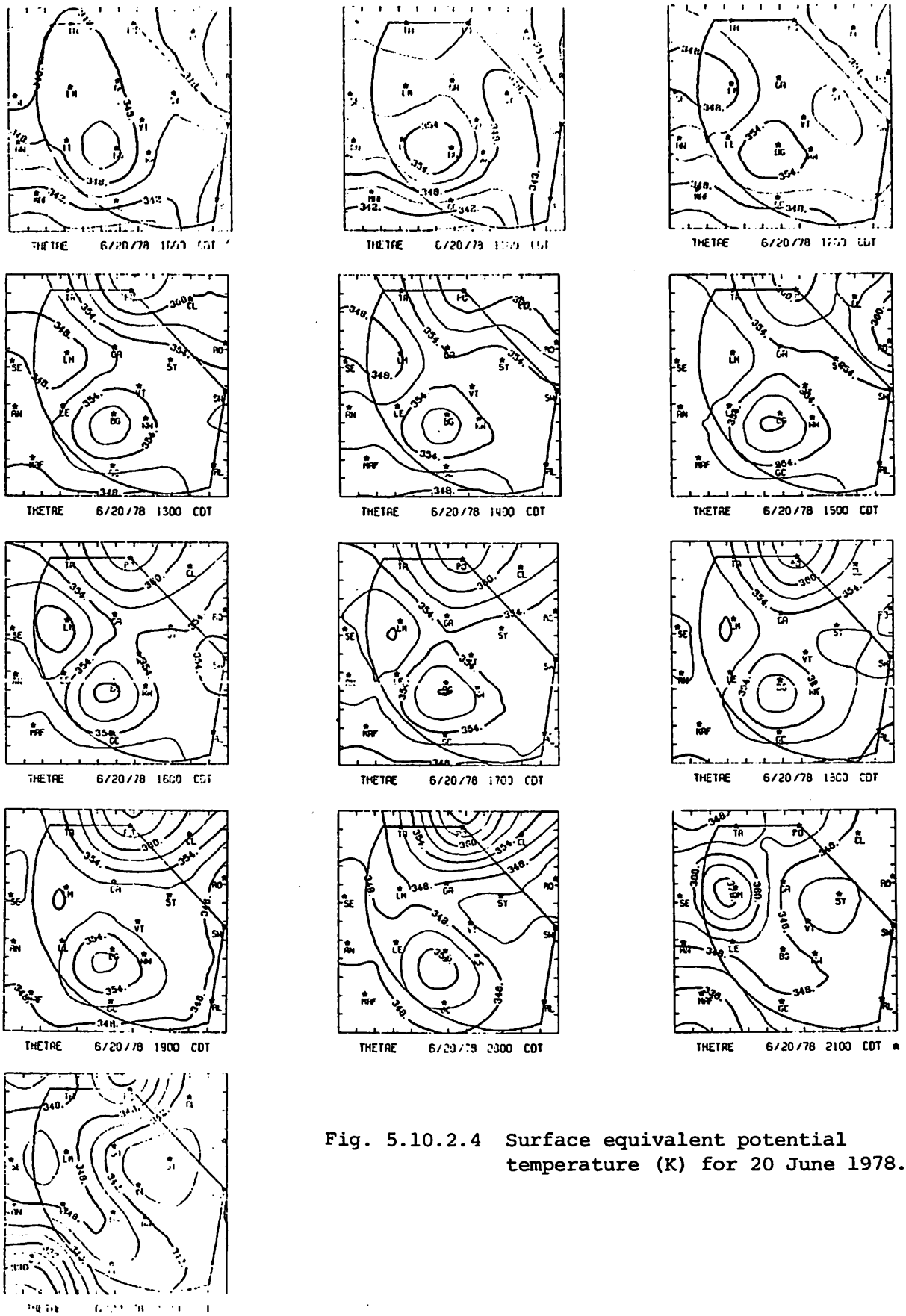

Fig. 5.10.2.4 Surface equivalent potential temperature (K) for 20 June 1978.

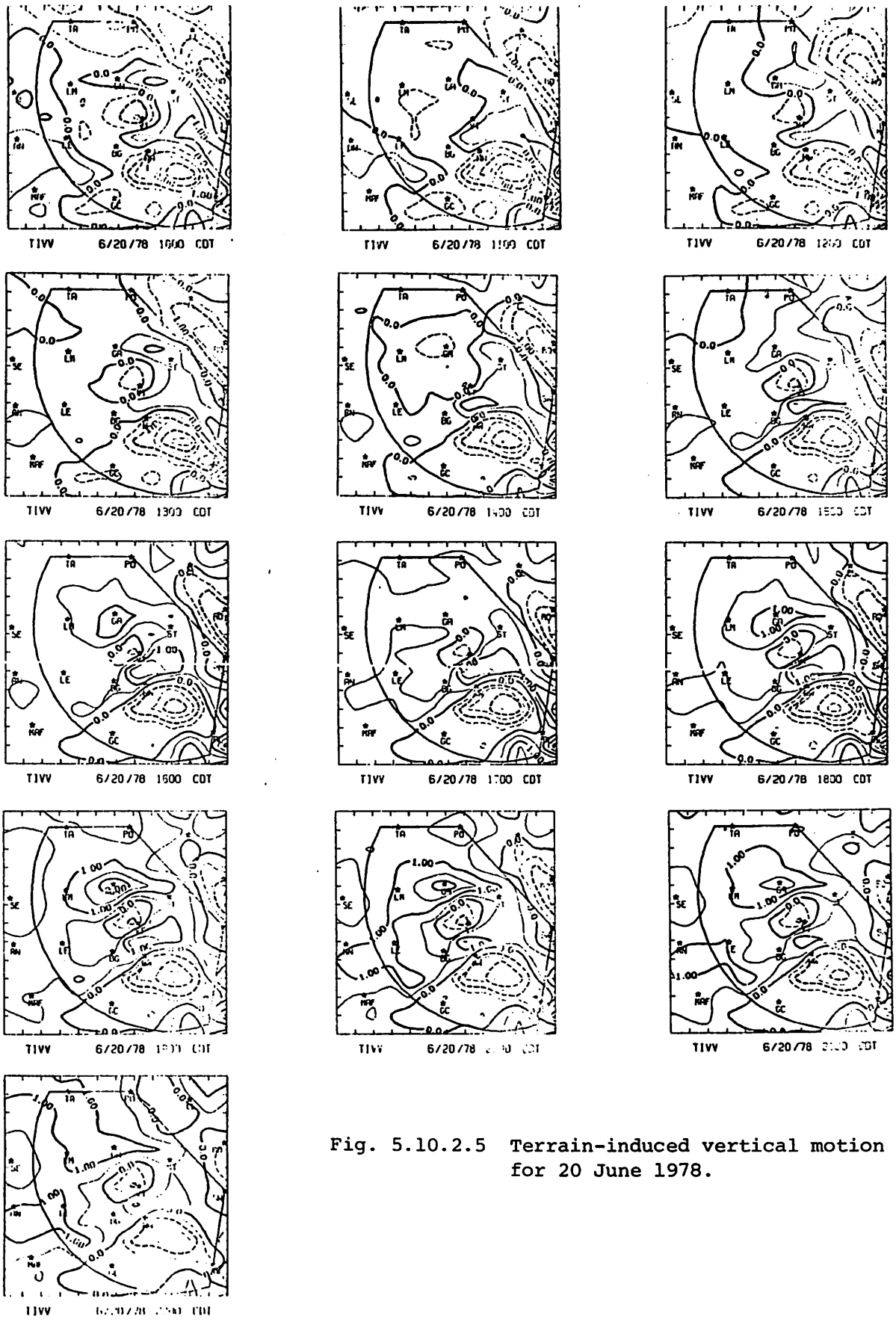

Fig. 5.10.2.5 Terrain-induced vertical motion (cm s^{-1}) for 20 June 1978.

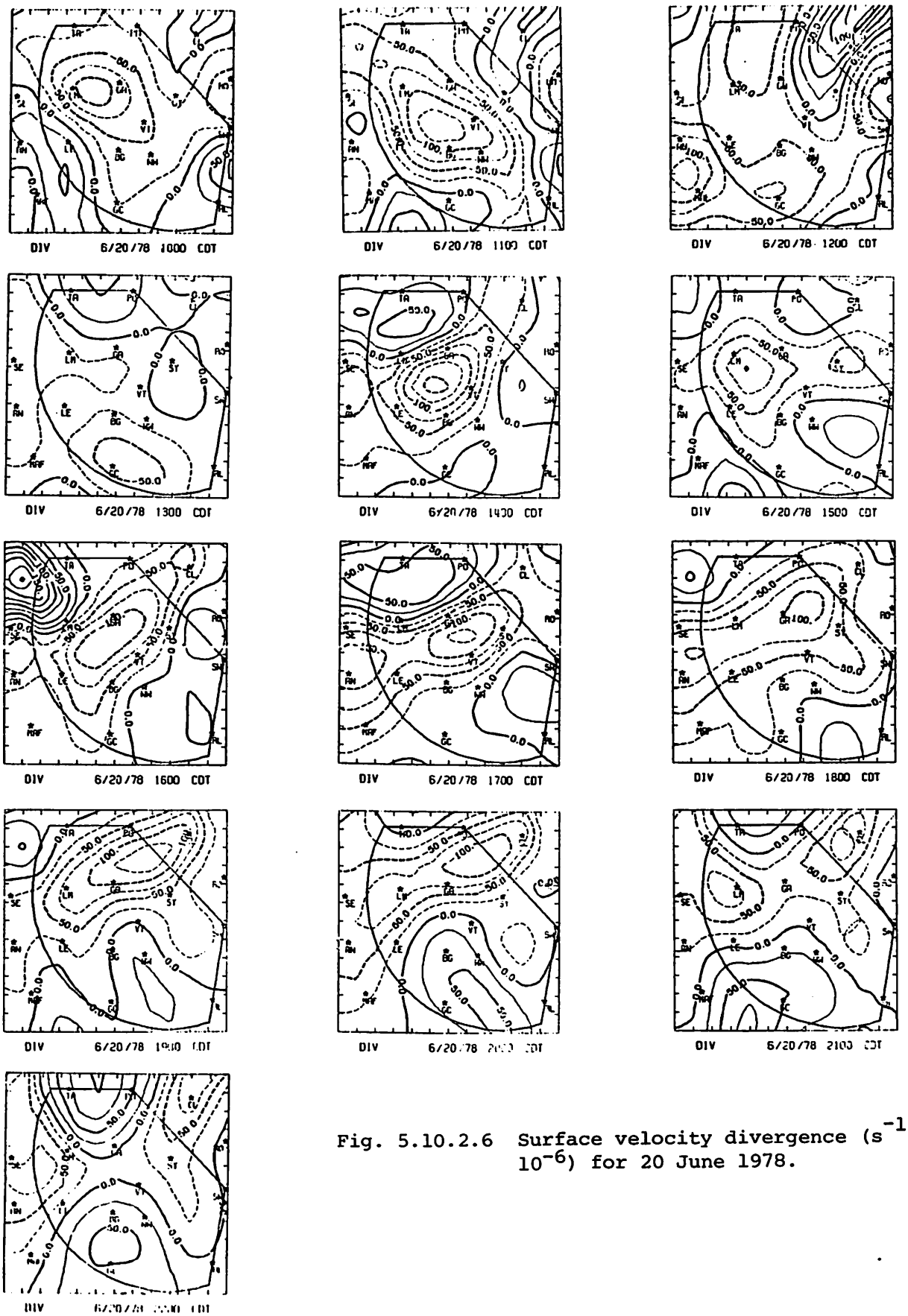

Fig. 5.10.2.6 Surface velocity divergence (s^{-1} x 10^{-6}) for 20 June 1978.

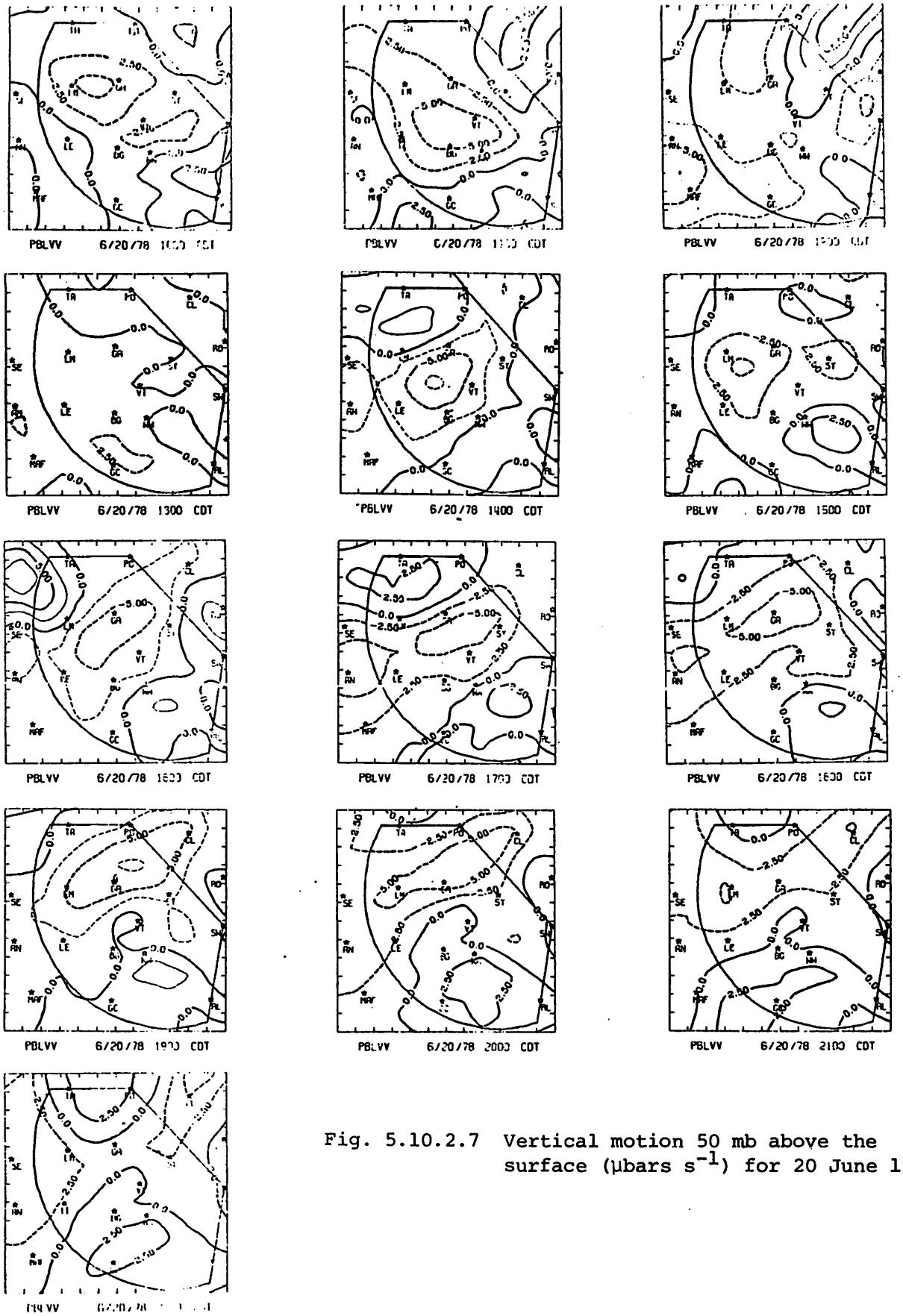

Fig. 5.10.2.7 Vertical motion 50 mb above the surface (μbars s^{-1}) for 20 June 1978.

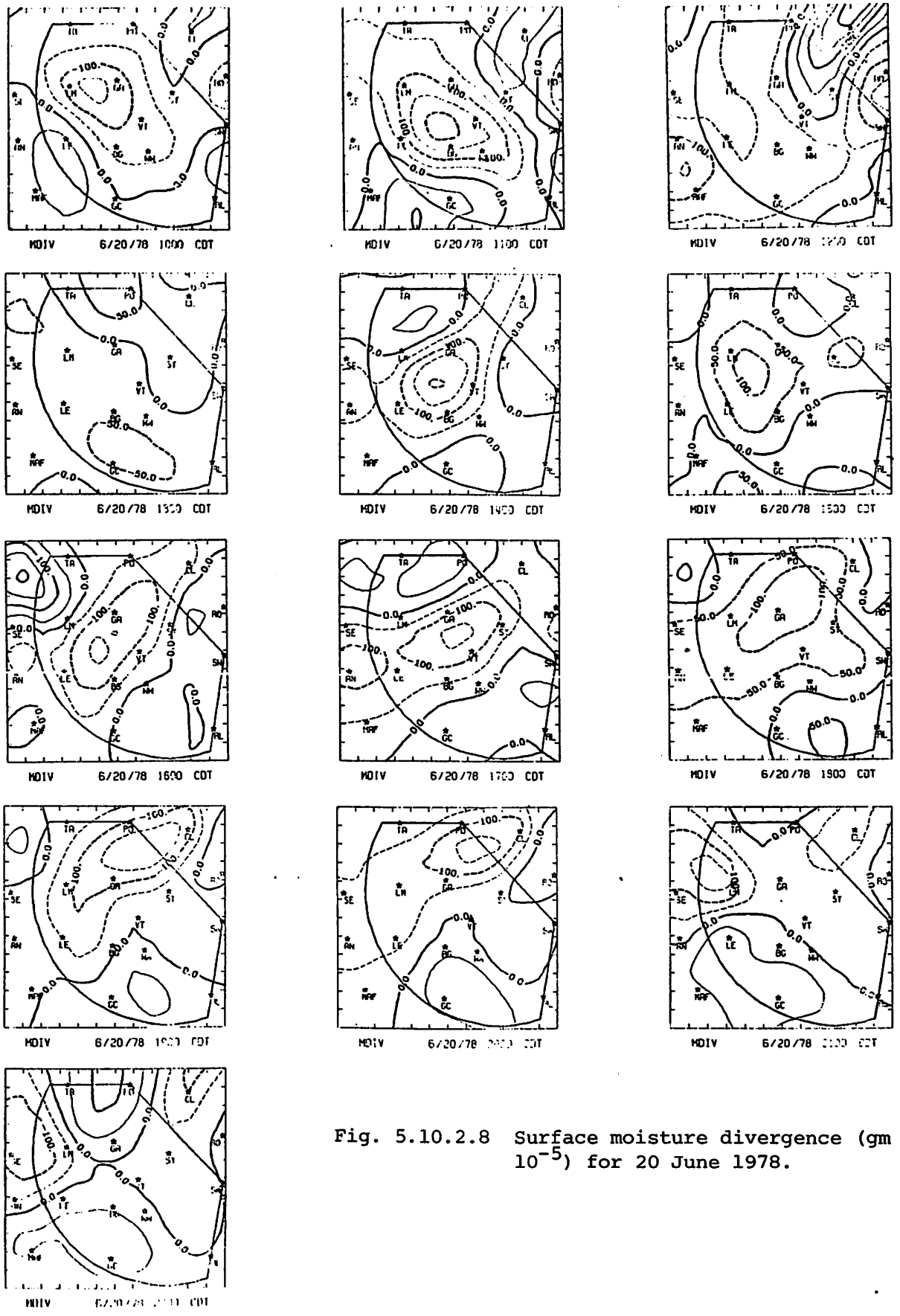

Fig. 5.10.2.8 Surface moisture divergence (gm kg^{-1} s^{-1} x 10^{-5}) for 20 June 1978.

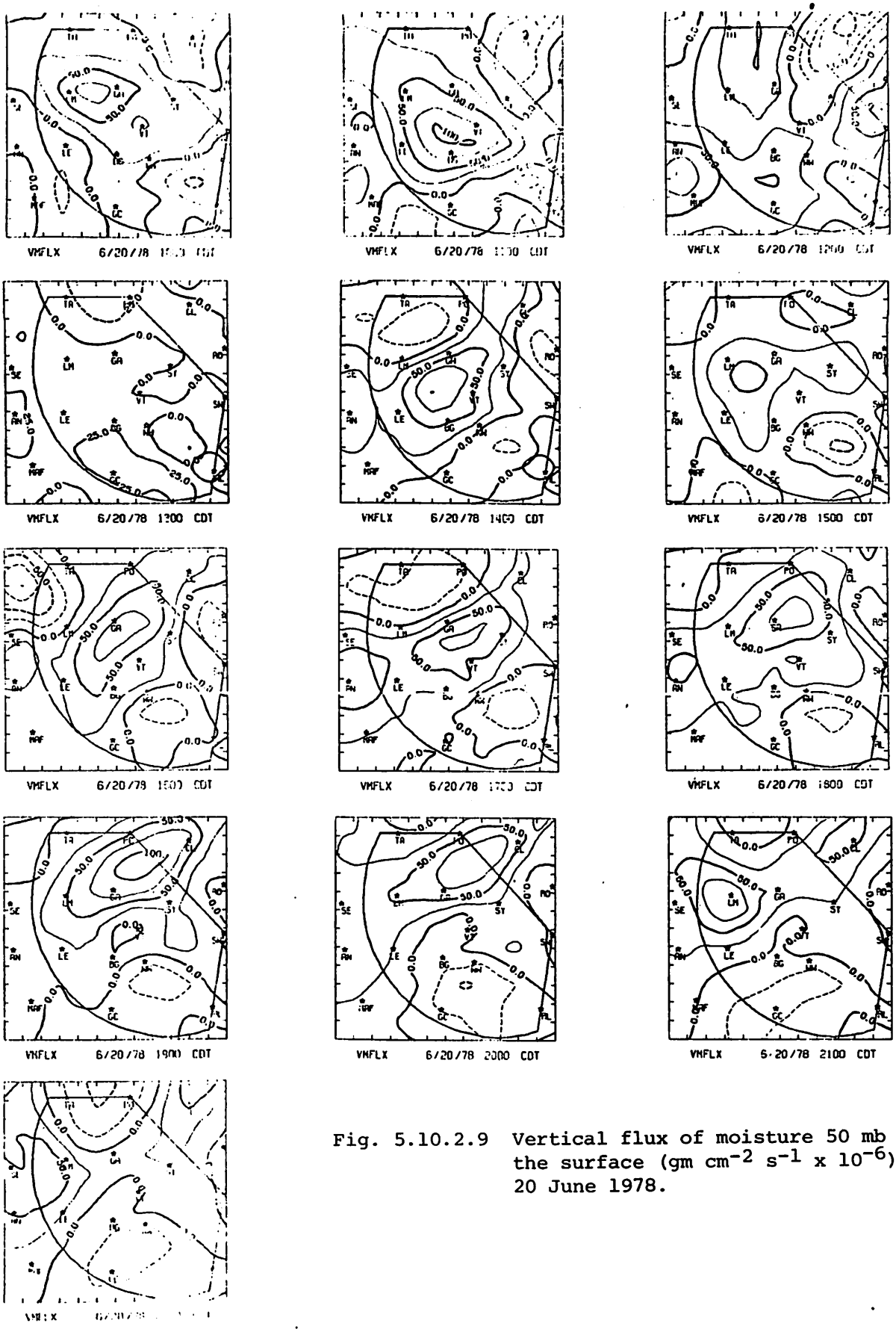

Fig. 5.10.2.9 Vertical flux of moisture 50 mb above the surface (gm cm^{-2} s^{-1} x 10^{-6}) for 20 June 1978.

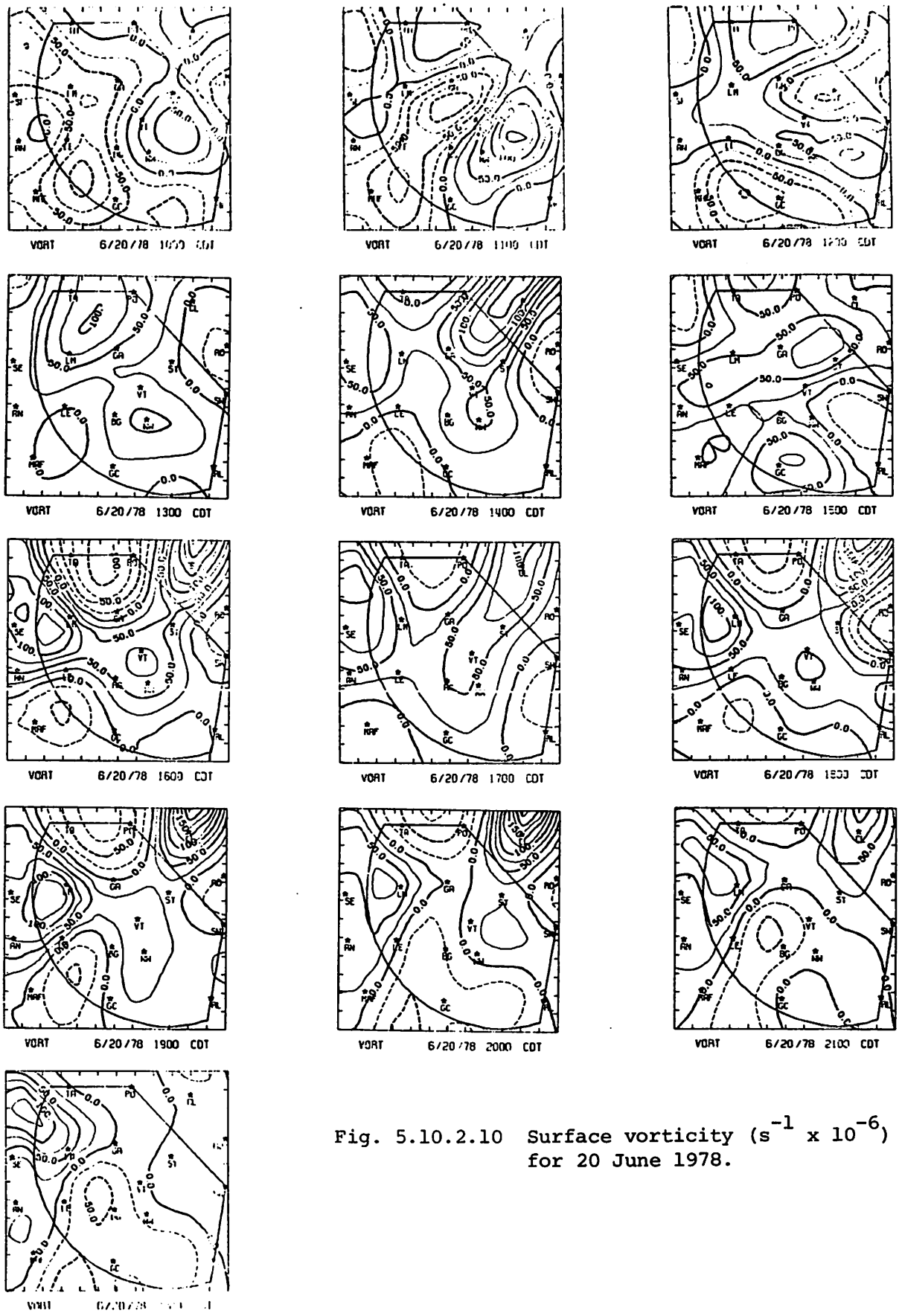

Fig. 5.10.2.10 Surface vorticity (s^{-1} x 10^{-6}) for 20 June 1978.

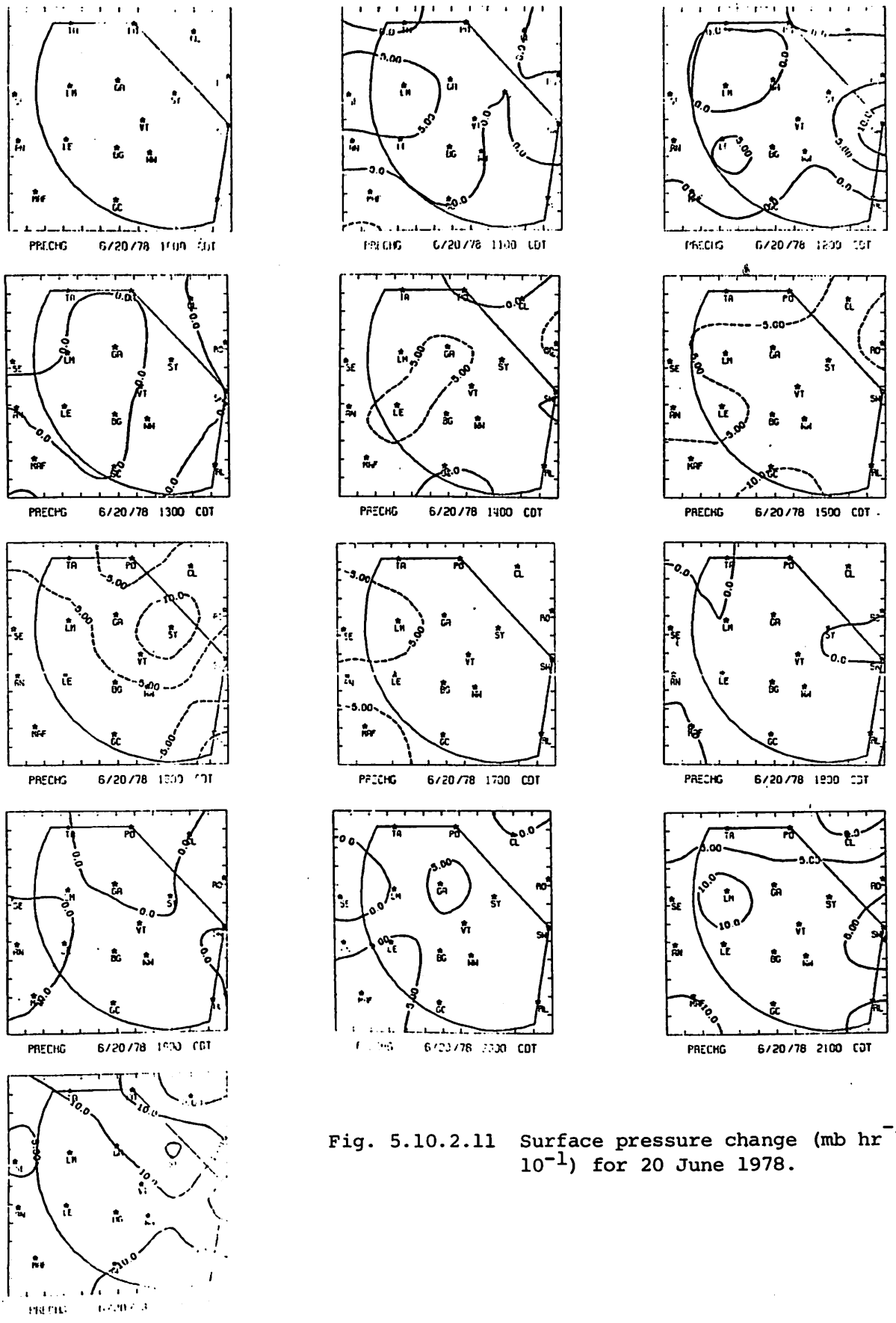

Fig. 5.10.2.11 Surface pressure change (mb hr^{-1} x 10^{-1}) for 20 June 1978.

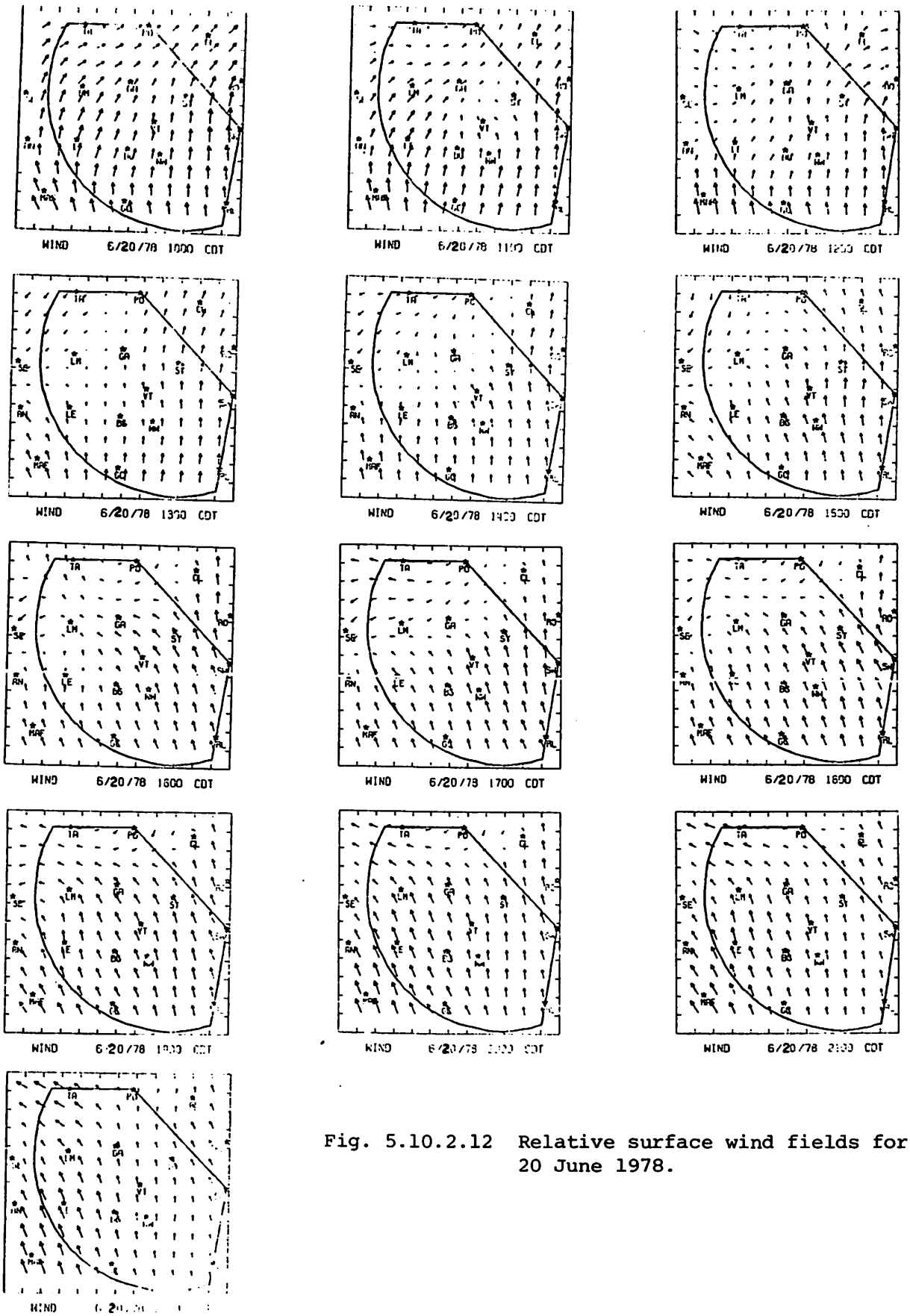

Fig. 5.10.2.12 Relative surface wind fields for 20 June 1978.

day. They formed in the corridor of weak surface convergence, which was persistent and aligned with the echo formation.

Wind data at Lamesa were missing for the entire day. If a small downdraft were associated with the moisture increase at Lamesa at 0200 GMT, it may have been detected only by wind observations at Lamesa. Because the data were missing, it is not clear whether or not the storm affected the surface kinematic fields.

5.11 27 June 1978

5.11.1 Radar

No echoes were observed in the HIPLEX area during this day.

5.11.2 Surface

Figure 5.11.2.1 shows surface temperature fields. Minimum temperatures were observed in the northwest near Tahoka and in the south near Garden City. Maximum values were observed in the northeast near Clairemont. A secondary maximum was situated near Big Spring and Walsh-Watts after 1800 GMT. A minimum formed near Gail at 0000 GMT.

Surface dewpoint depressions (Fig. 5.11.2.2), though moderate at 1500 GMT, became fairly large as daytime heating took place. Minimum dewpoint depressions were toward the southwest with a separate center near Big Spring at 1500 GMT and again at 0000 GMT.

Charts of surface mixing ratio (Fig. 5.11.2.3) show a maximum at Big Spring throughout the day. The largest values occurred before 1800 GMT and decreased over the area during the day.

Surface equivalent potential temperature charts (Fig. 5.11.2.4) show a maximum near Lenorah and Big Spring through the day with minimum values near Gail. Magnitudes were moderate to high but decreased over the area later in the day with the decrease in moisture.

Terrain-induced vertical motion (Fig. 5.11.2.5) was positive over most of the area. Centers of downward motion were near Vincent and southeast of Walsh-Watts. A center of positive motion was near Gail with values greater than 3 μbars/s at 0000 GMT.

Surface velocity divergence (Fig. 5.11.2.6), vertical motion 50 mb above the surface (Fig. 5.11.2.7), surface moisture divergence (Fig. 5.11.2.8), and vertical moisture flux 50 mb above the surface (Fig. 5.11.2.9) had similar patterns. An axis of velocity divergence extended north-south through the middle of the area throughout the day. Downward vertical motion, moisture divergence, and downward moisture flux were associated with this axis. Two major centers of convergence were present, one near Andrews and the other west of Garden City. The largest values of convergence and upward motion were near Andrews at 2200 GMT.

Surface vorticity patterns are shown in Fig. 5.11.2.10. A center of anticyclonic vorticity remained near Post through the day. Moderate positive (cyclonic) vorticity was observed over much of the remainder of the area.

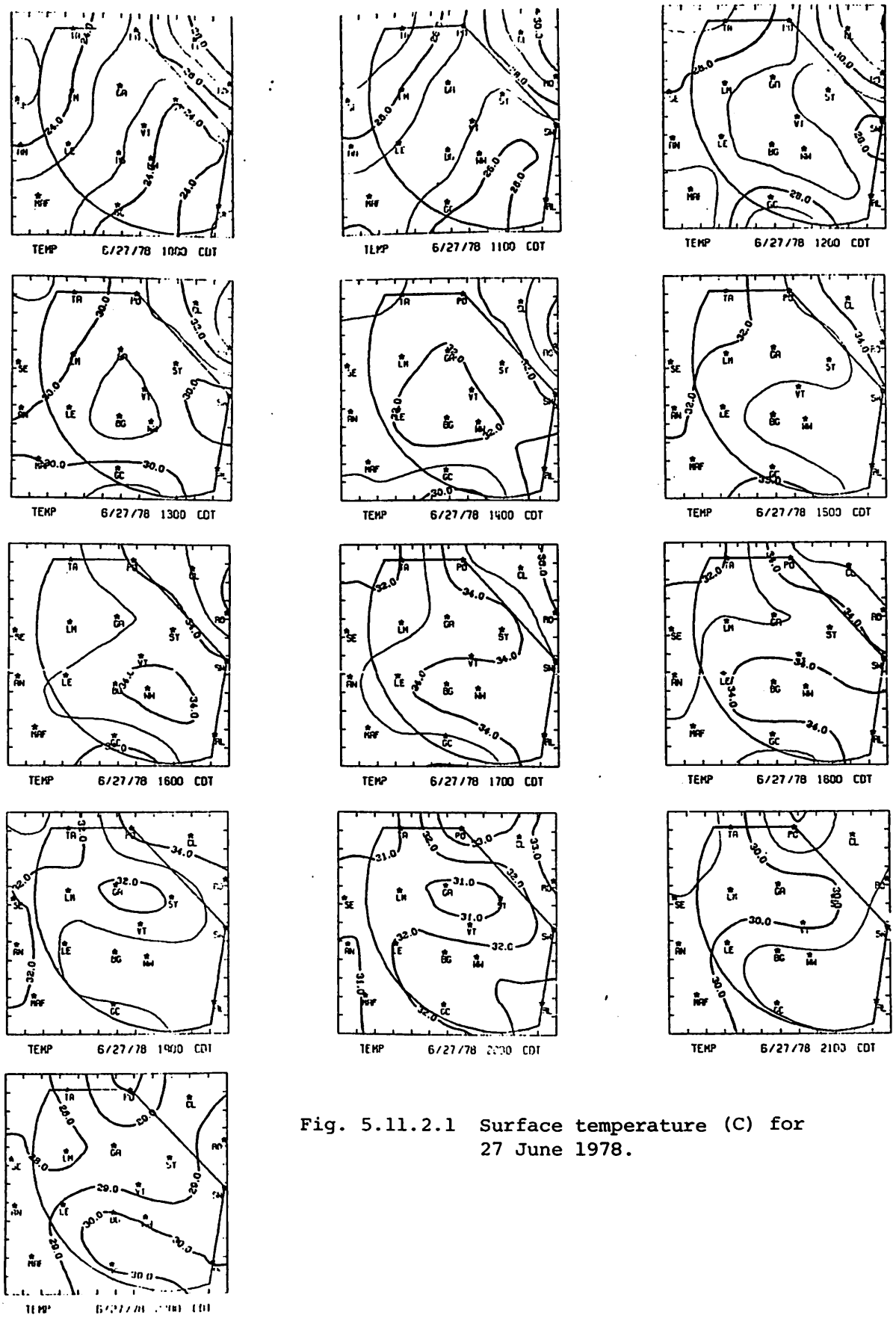

Fig. 5.11.2.1 Surface temperature (C) for 27 June 1978.

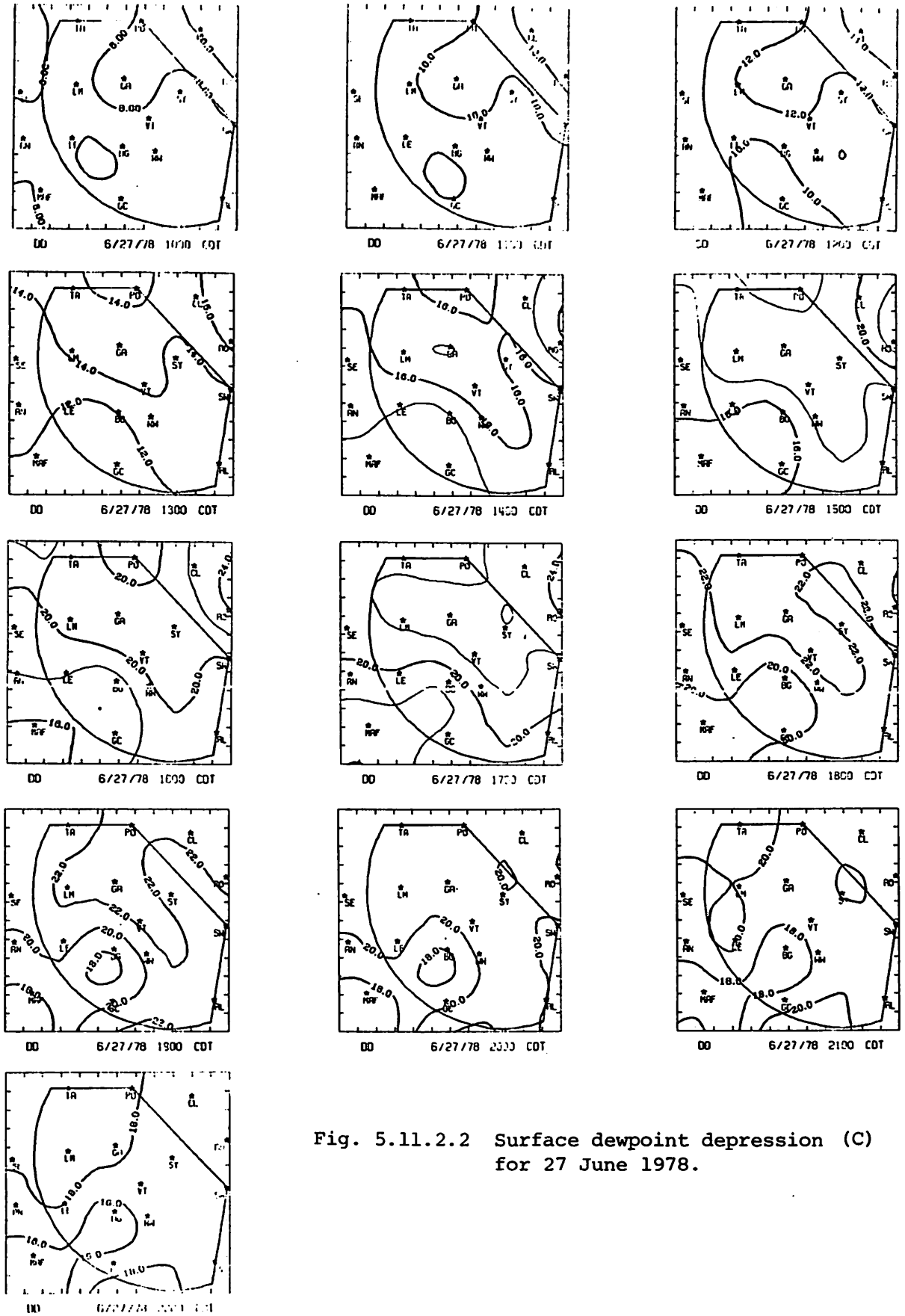

Fig. 5.11.2.2 Surface dewpoint depression (C) for 27 June 1978.

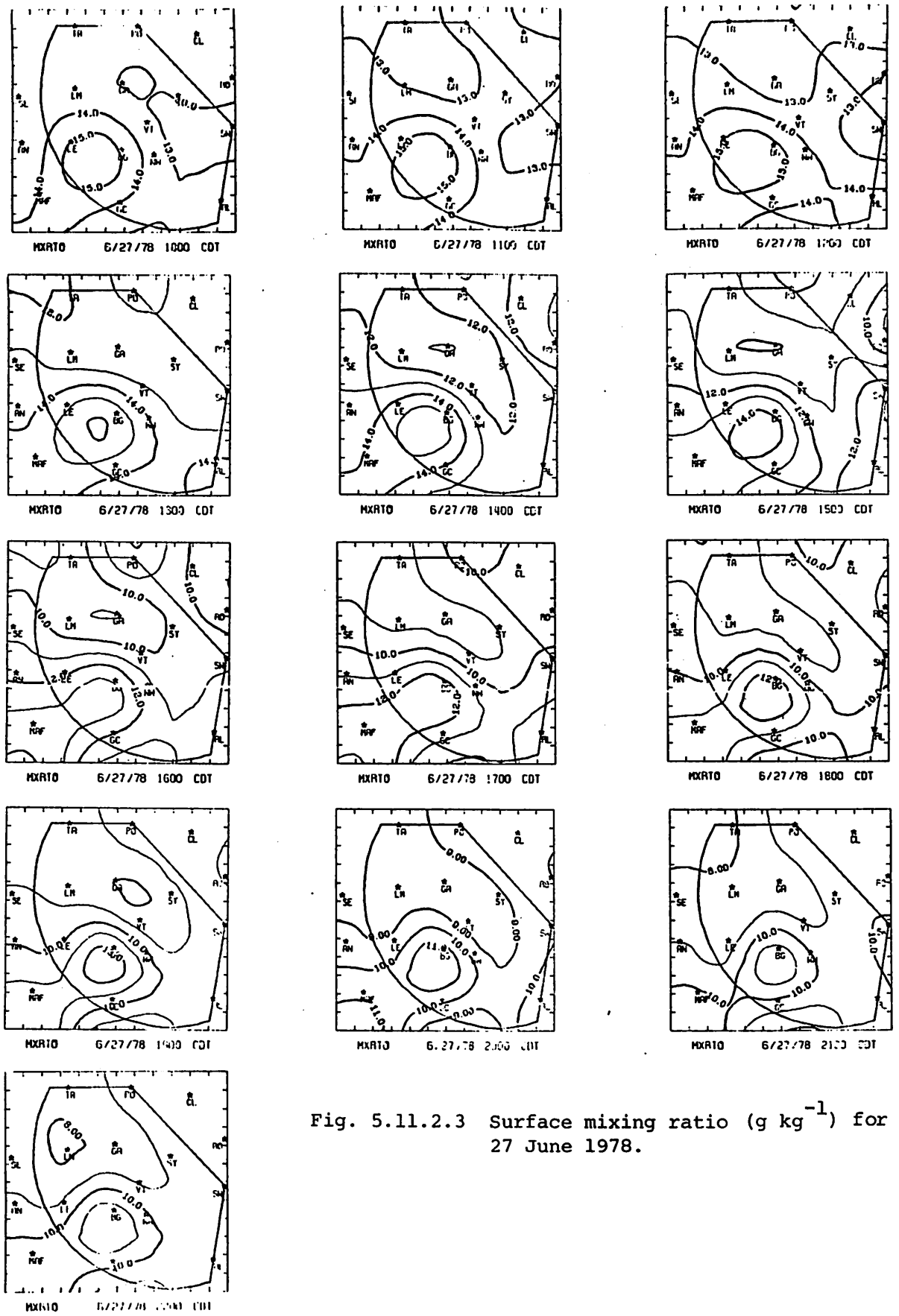

Fig. 5.11.2.3 Surface mixing ratio (g kg^{-1}) for 27 June 1978.

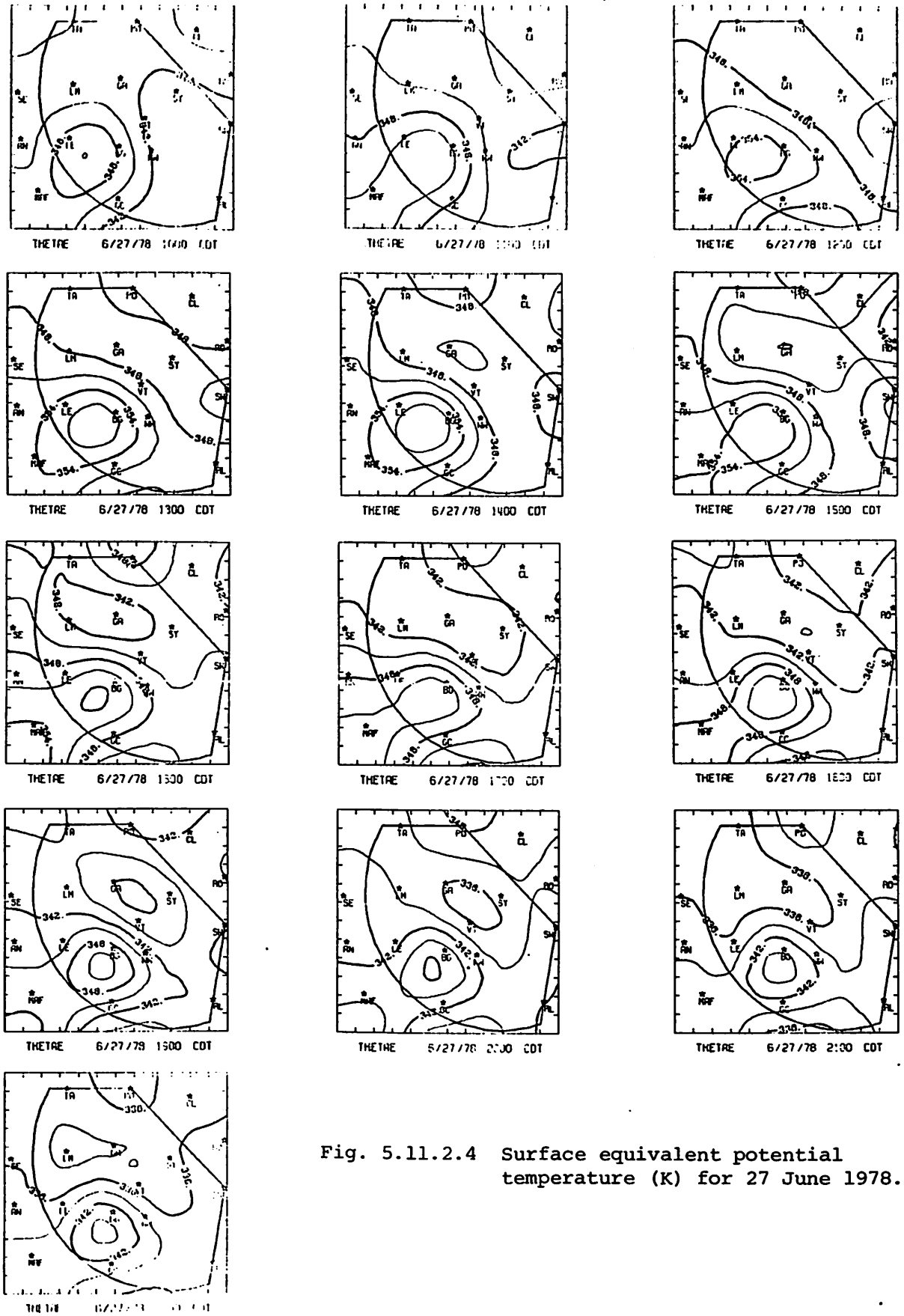

Fig. 5.11.2.4 Surface equivalent potential temperature (K) for 27 June 1978.

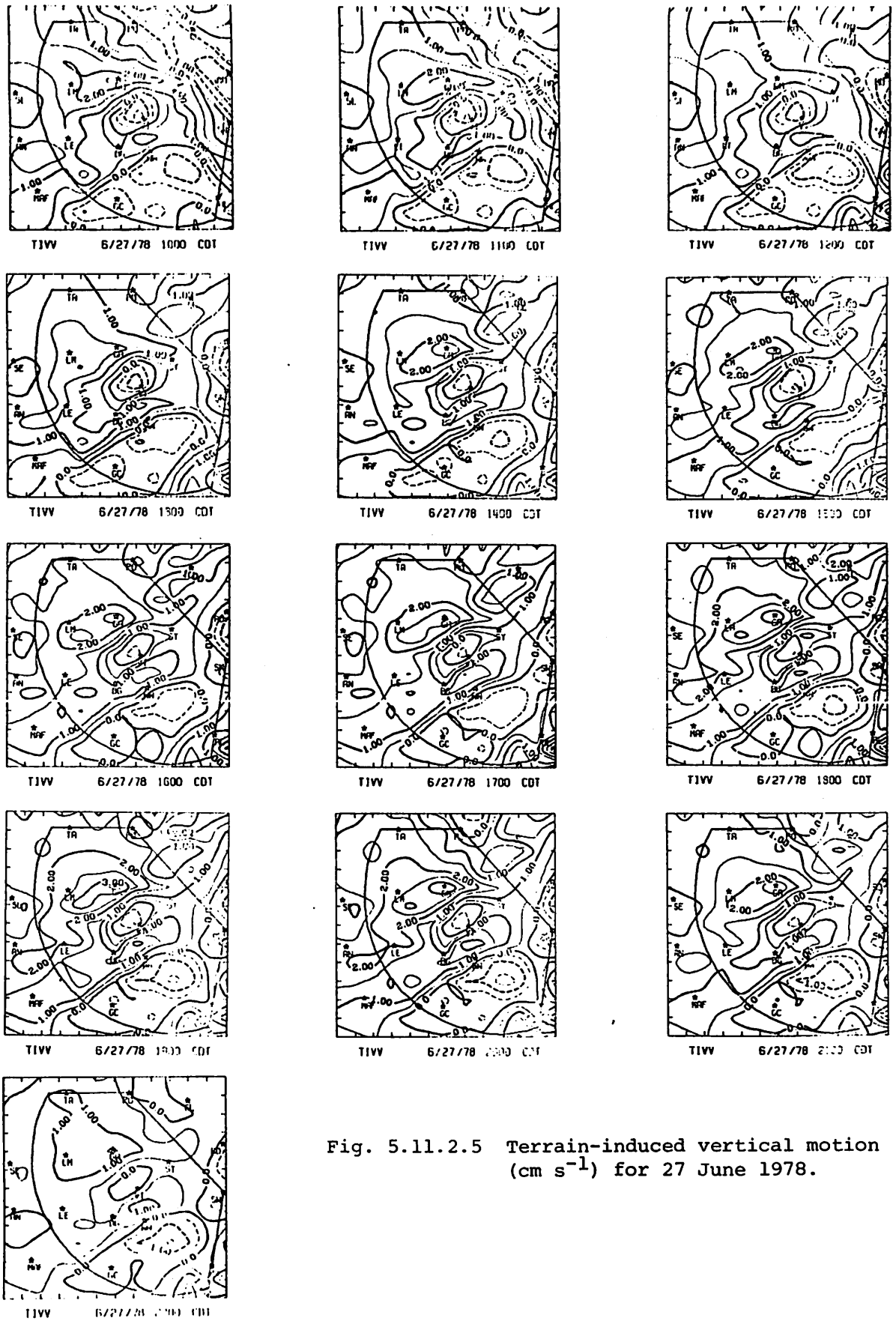

Fig. 5.11.2.5 Terrain-induced vertical motion (cm s^{-1}) for 27 June 1978.

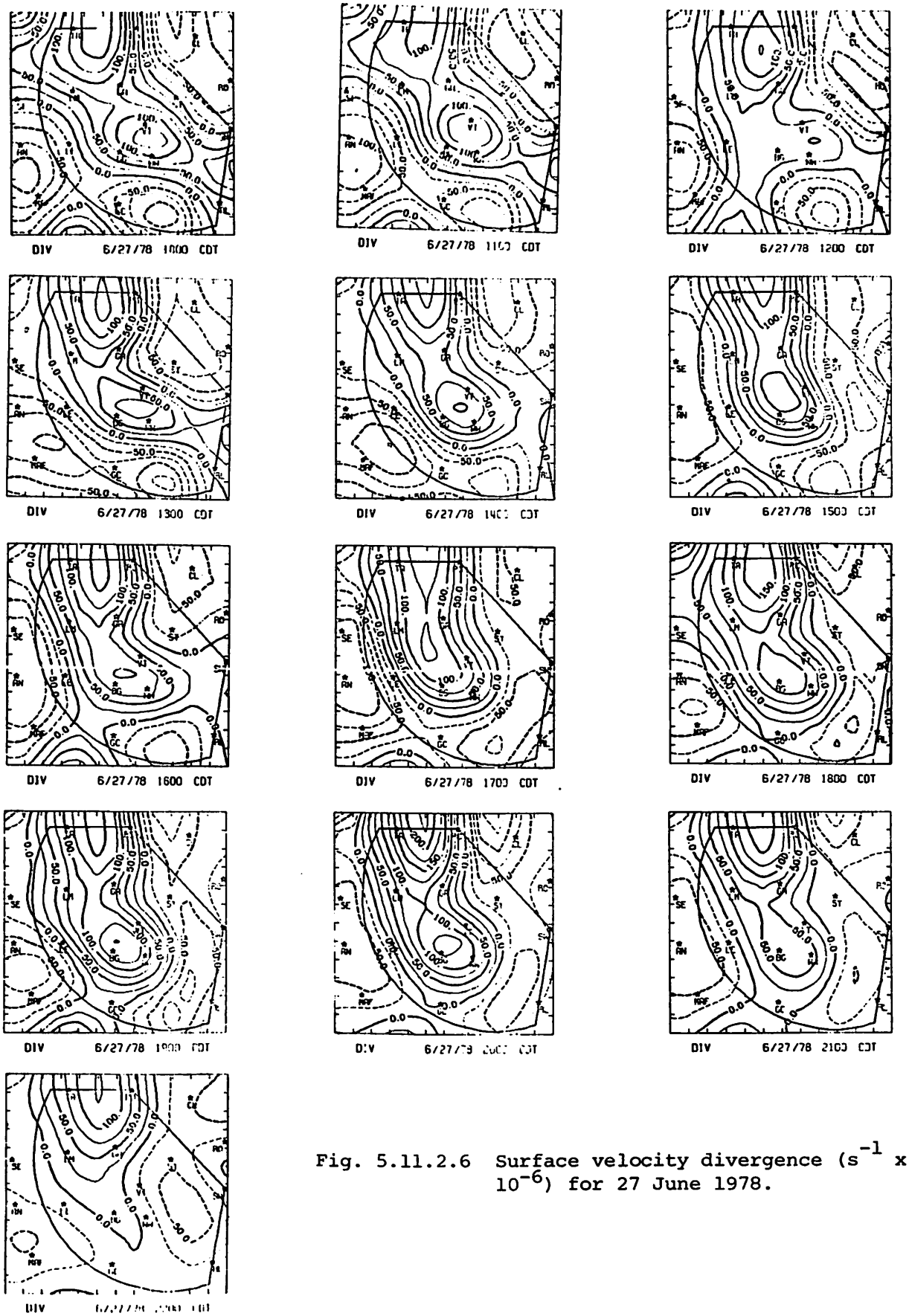

Fig. 5.11.2.6 Surface velocity divergence (s^{-1} x 10^{-6}) for 27 June 1978.

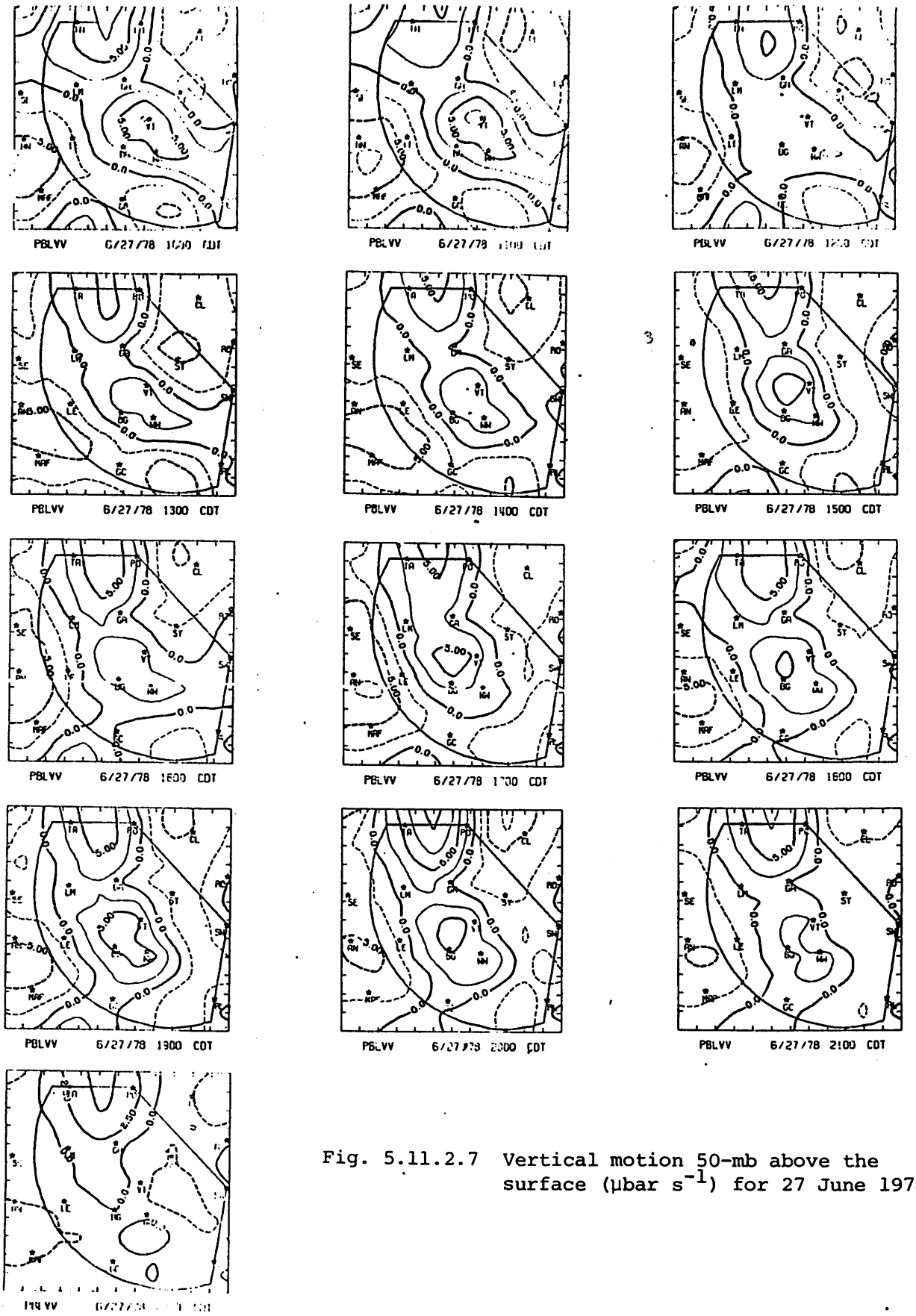

Fig. 5.11.2.7 Vertical motion 50-mb above the surface (μbar s^{-1}) for 27 June 1978.

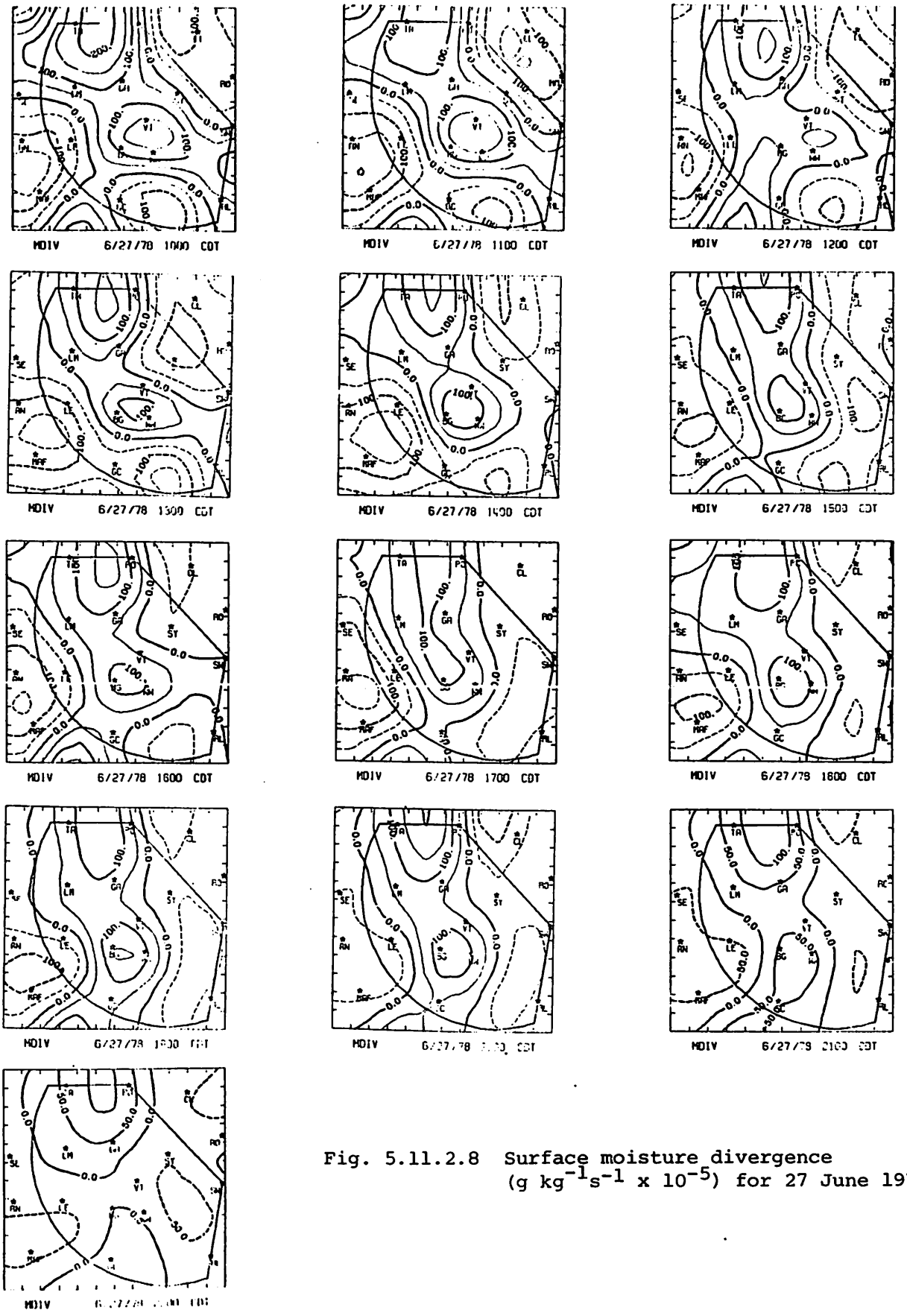

Fig. 5.11.2.8 Surface moisture divergence ($g\ kg^{-1}s^{-1} \times 10^{-5}$) for 27 June 1978.

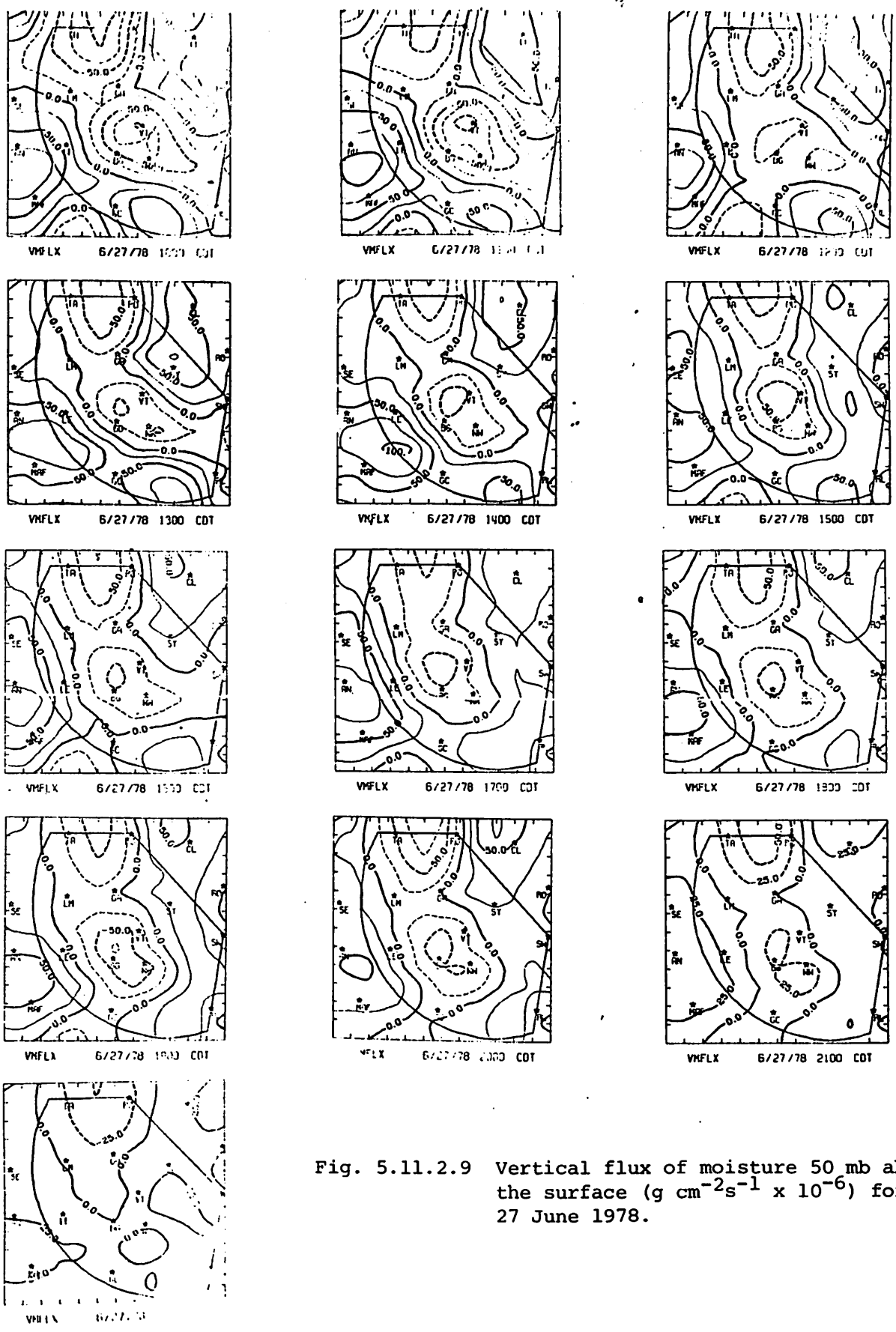

Fig. 5.11.2.9 Vertical flux of moisture 50 mb above the surface (g $cm^{-2}s^{-1}$ x 10^{-6}) for 27 June 1978.

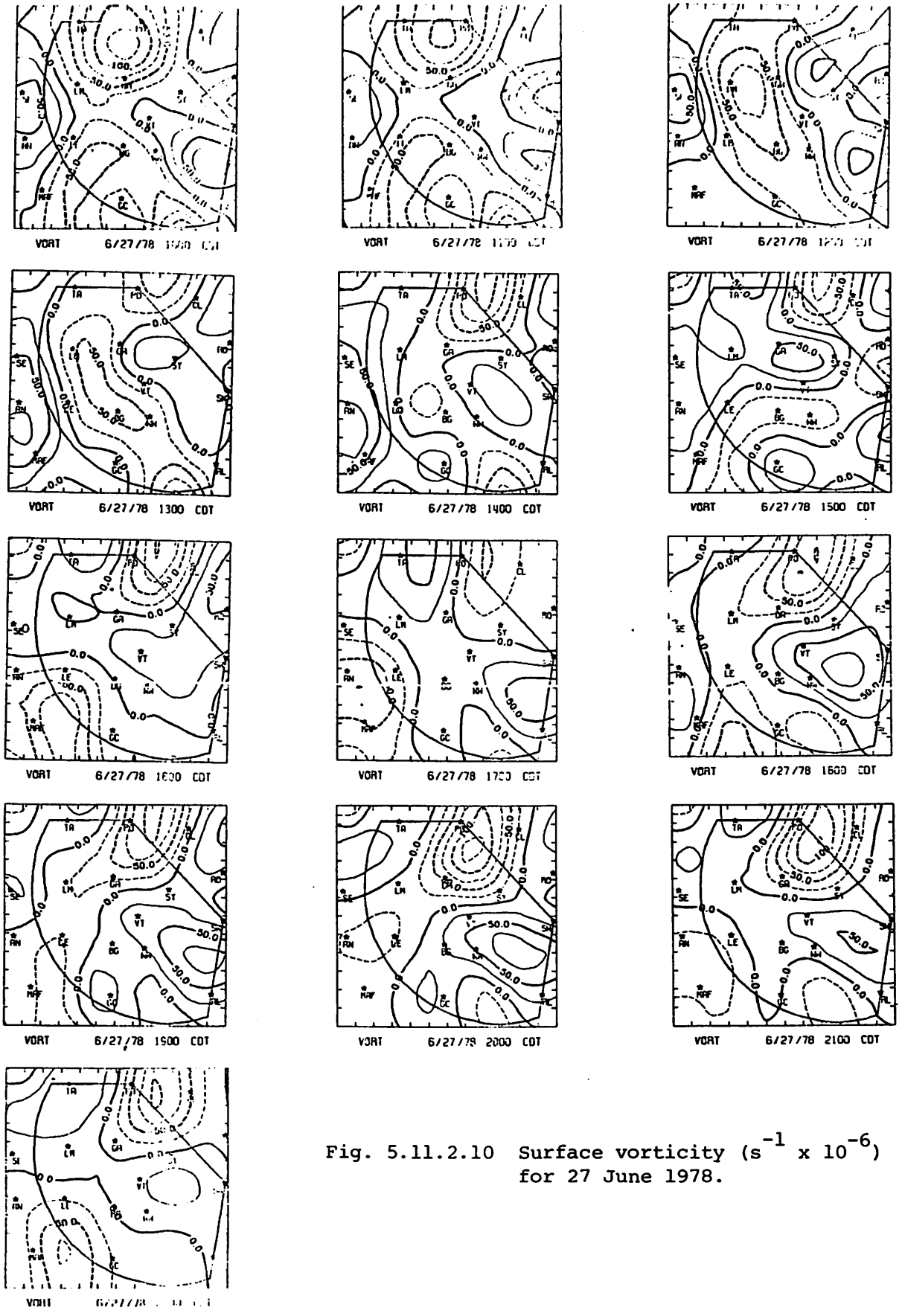

Fig. 5.11.2.10 Surface vorticity (s^{-1} x 10^{-6}) for 27 June 1978.

Surface pressure change (Fig. 5.11.2.11) was small prior to 0200 GMT. Between 0100 and 0300 GMT strong pressure rises took place over most of the area with the largest rise near Andrews (+2.1 mb) at 0200 GMT and at Midland at 0300 GMT.

Surface winds (Fig. 5.11.2.12) were southerly except in the northwest quarter at 1500 GMT where southeast winds were present. By 2100 GMT the wind had shifted to the southeast. Wind speeds were moderate.

5.11.3 Upper Level Kinematic Parameters

Profiles of horizontal mass divergence (Fig. 5.11.3.1) were generally similar. The lowest layers show mass convergence which increased between 0000 and 0300 GMT. Convergence also was present in middle layers and near 250 mb. This convergence was not strong, however. Divergence was present in layers near 700 and 350 mb.

Vertical motion profiles (Fig. 5.11.3.2) show upward vertical motion at all times. The maximum vertical motion was present at 0300 GMT.

Figure 5.11.3.3 shows profiles of horizontal moisture divergence. Moisture convergence was present in the lowest layers and was strong at 0300 GMT. Moisture divergence was present near 700 mb at 2100 and 0300 GMT. Moisture divergence was present near 700 mb at 2100 and 0300 GMT, and near 800 mb at 0000 GMT. Slight convergence took place above these levels, and above 500 mb the value of the term was near zero.

5.11.4 Energetics

Profiles of the horizontal flux of latent heat (Fig. 5.11.4.1) show inflow of latent heat below 800 mb. Strong outflow was present at 2100 GMT near 700 mb with weak inflow above. The outflow layer was near 800 mb at 0000 GMT and near 700 mb at 0300 GMT. Outflow at 0300 GMT was small, however.

Figure 5.11.4.2 shows profiles of the vertical flux of latent heat energy. There was a strong upward flux of latent heat out of the lowest layers into layers just above. The maximum inflow was near 700 mb at 2100 and 0300 GMT, and near 800 mb at 0000 GMT.

Profiles of the local change in latent heat energy (Fig. 5.11.4.3) are similar for all hours and show losses below 750 mb and gains above. Above 600 mb the value of this term was near zero.

The residual of the latent heat energy equation is shown in Fig. 5.11.4.4. The strong peak at 700 mb at 0300 GMT cannot be due entirely to condensation;

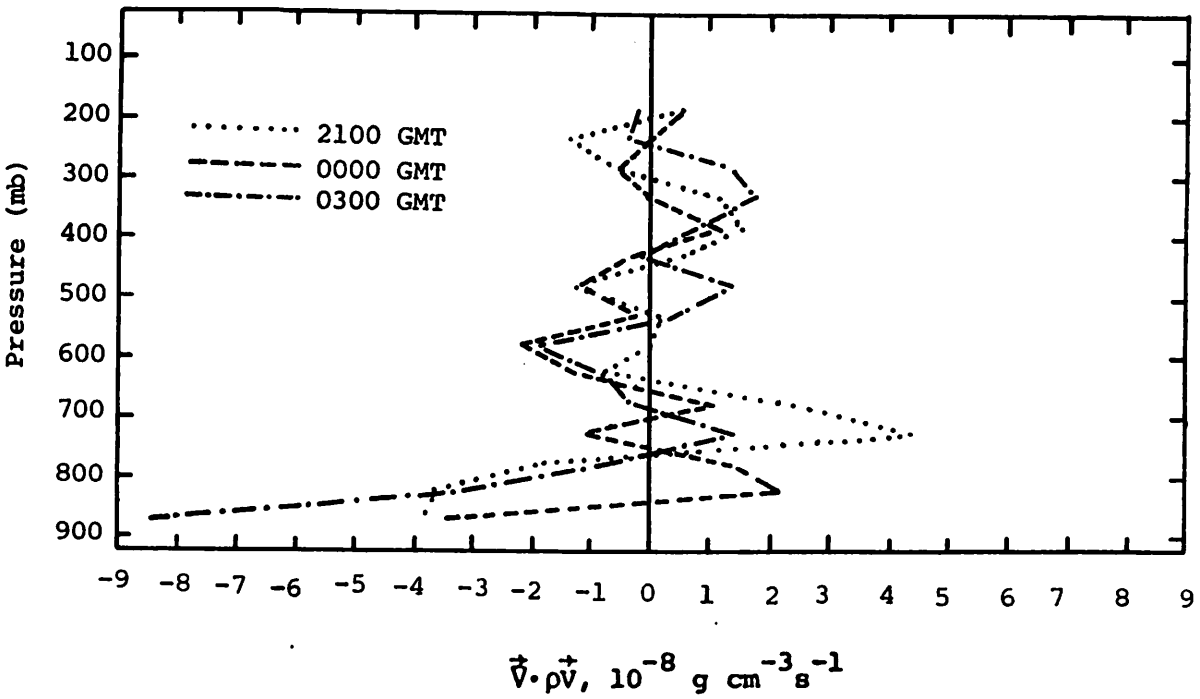

Fig. 5.11.3.1 Vertical profiles of mass divergence on 27 June 1978.

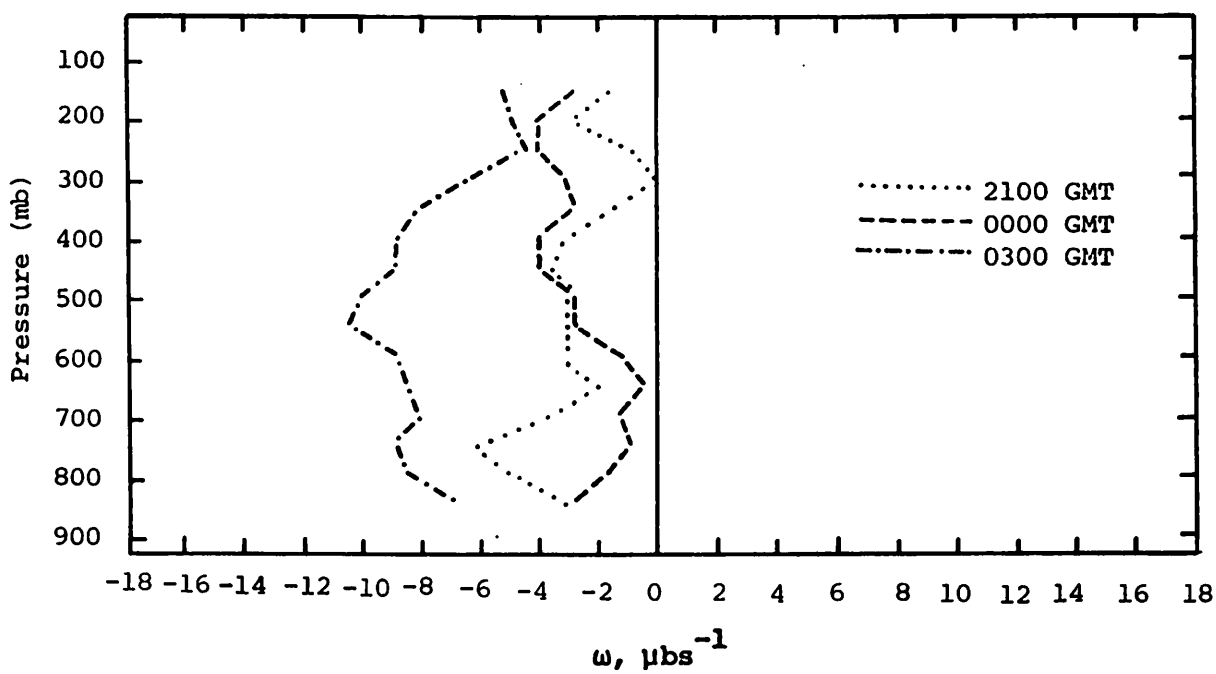

Fig. 5.11.3.2 Vertical profiles of vertical motion on 27 June 1978.

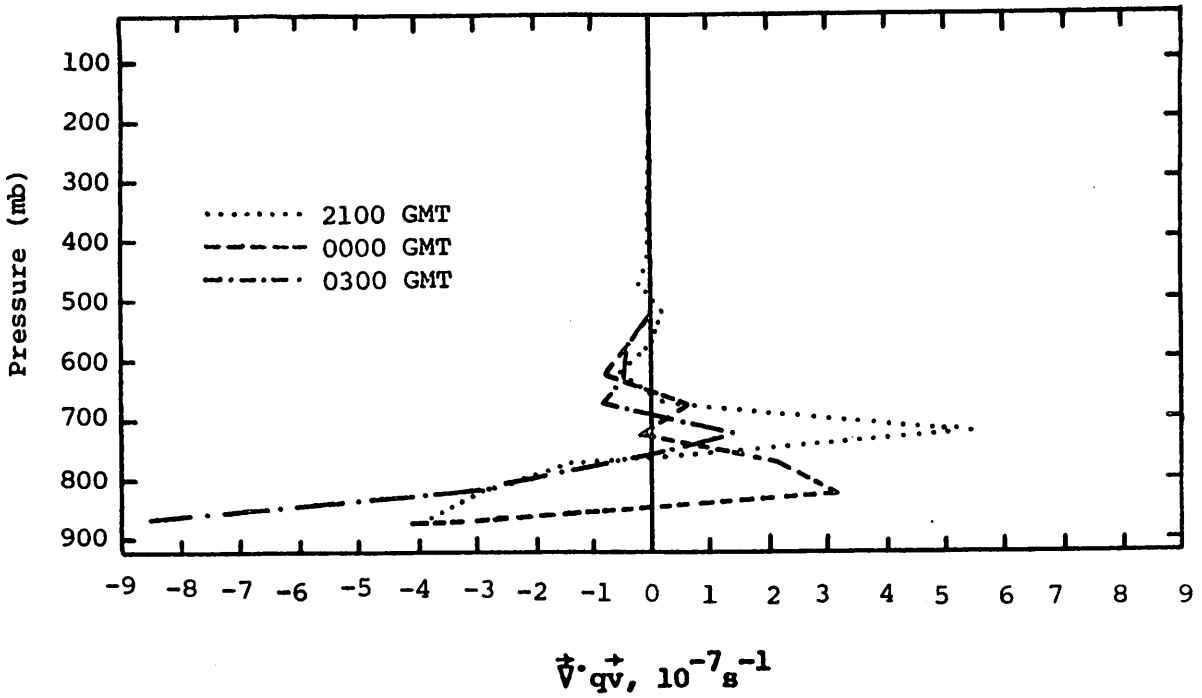

Fig. 5.11.3.3 Vertical profiles of horizontal moisture divergence on 27 June 1978.

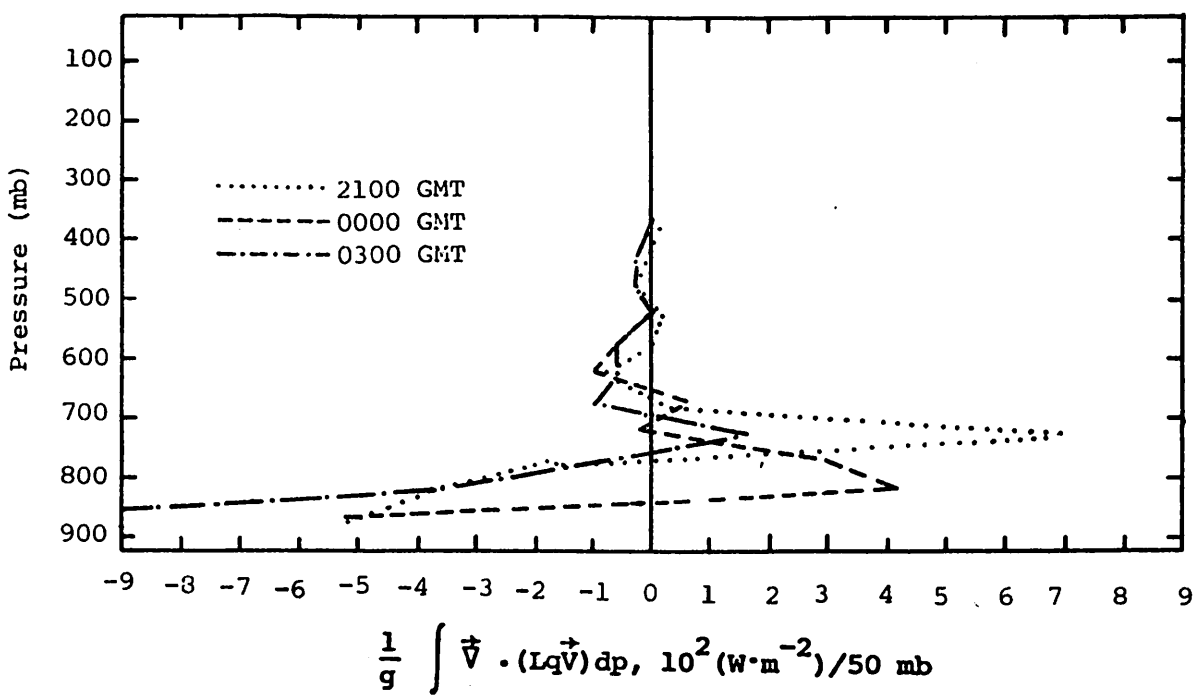

Fig. 5.11.4.1 Vertical profiles of the horizontal flux of latent heat energy on 27 June 1978.

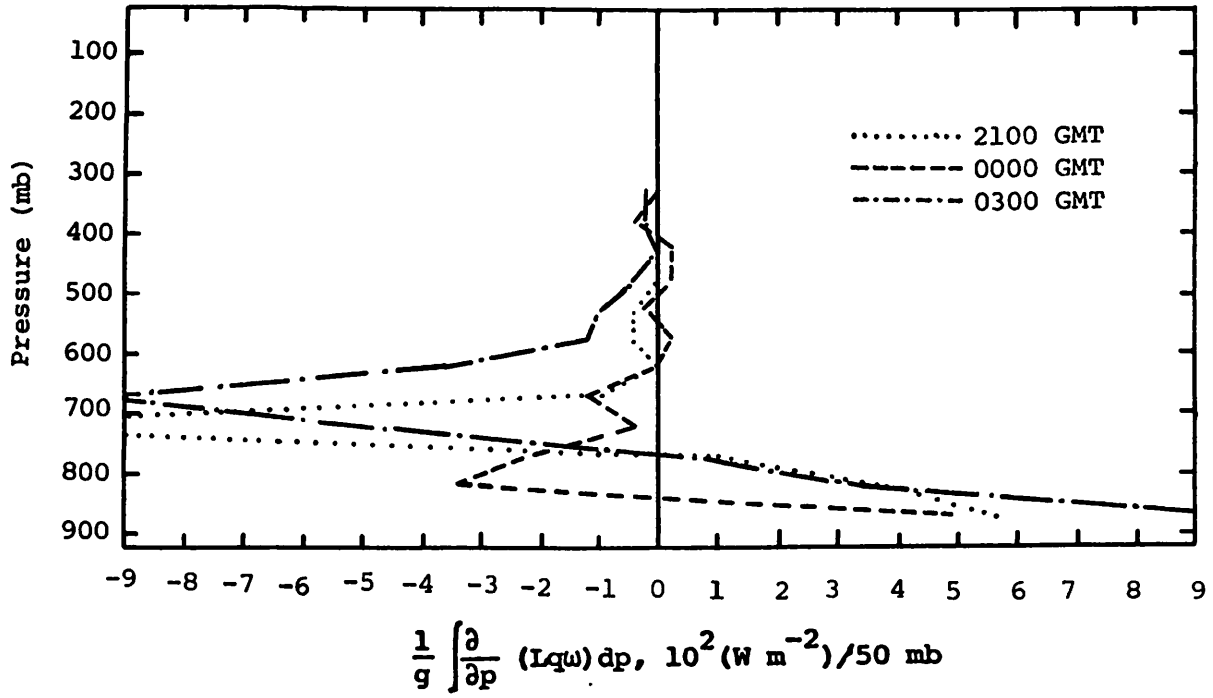

Fig. 5.11.4.2 Vertical profiles of the vertical flux of latent heat energy on 27 June 1978.

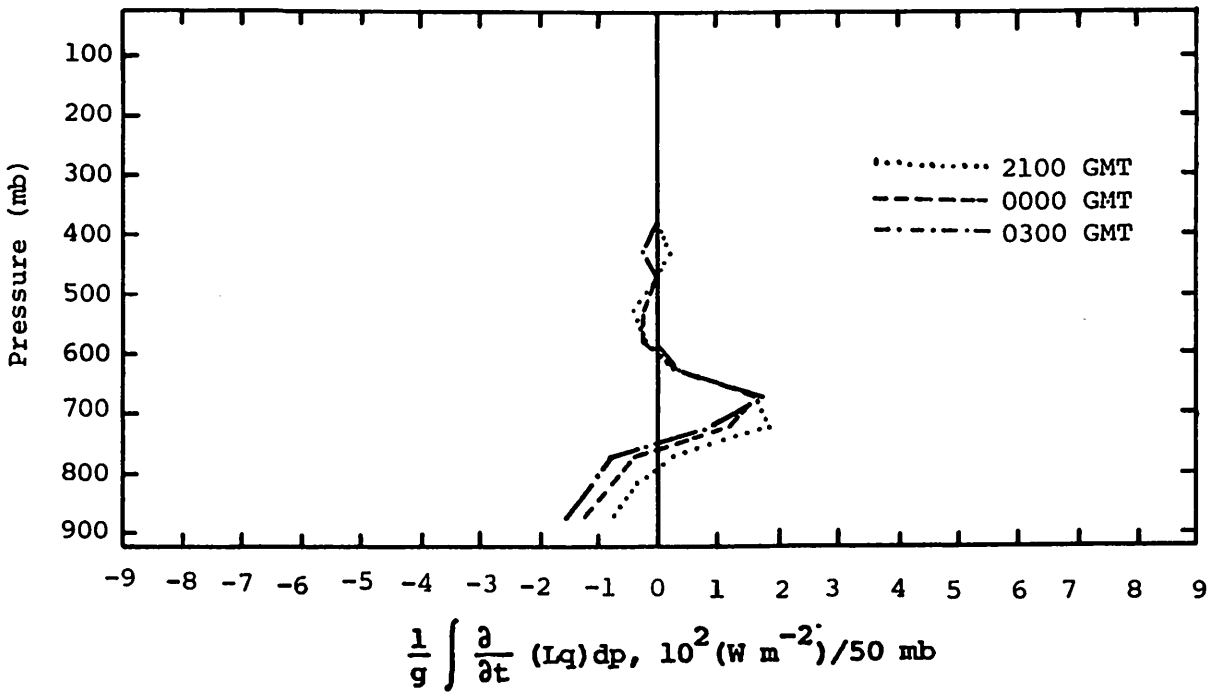

Fig. 5.11.4.3 Vertical profiles of the local change of latent heat energy on 27 June 1978.

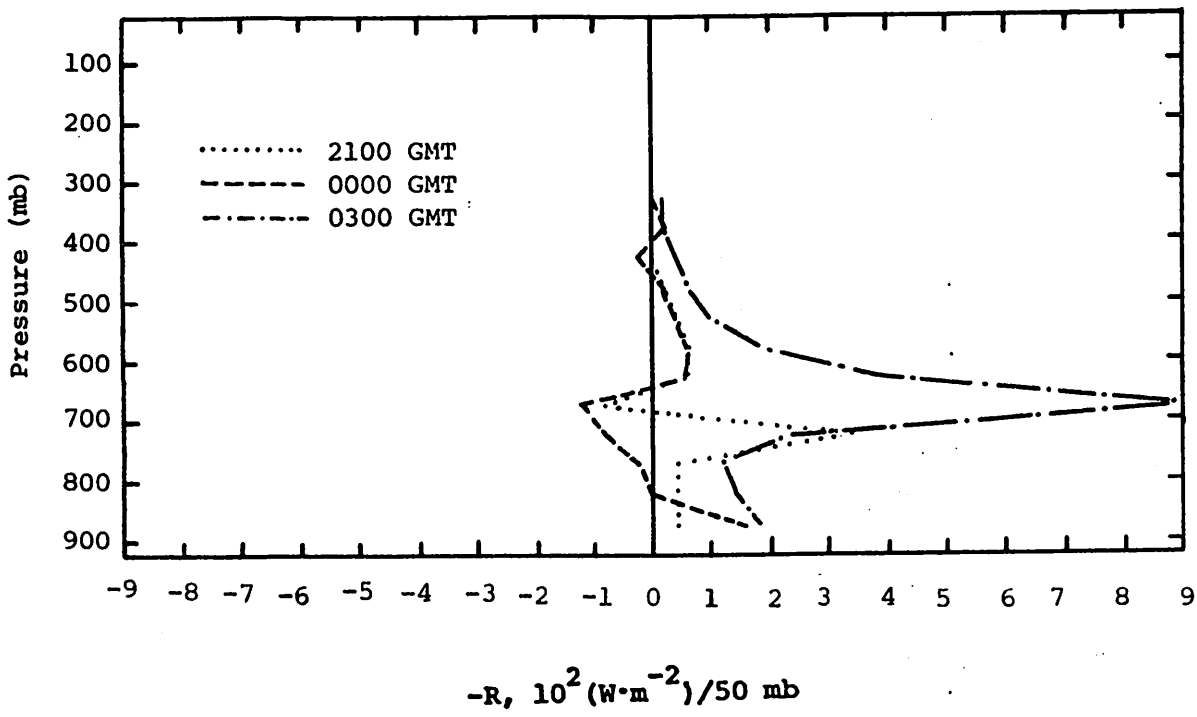

Fig. 5.11.4.4 Vertical profiles of the residual of the latent heat energy equation on 27 June 1978.

there were no showers on this day. The other profiles showed smaller positive and negative values that were more readily explained by condensation or evaporation or error from the other terms in the equation.

Figure 5.11.4.5 shows the profiles of diabatic heating. Mostly positive values were present. Some of the heating could have resulted from condensation as indicated in Fig. 5.11.4.4, but this does not account for all of the heating that occurred.

Profiles of horizontal flux of kinetic energy are shown in Fig. 5.11.4.6. Values were rather small. Kinetic energy outflow occurred in lower levels at 2100 and 0000 GMT. Inflow was present in lower levels at 0300 GMT. At all three time periods the transport above 600 mb was near zero.

Vertical flux of kinetic energy (Fig. 5.11.4.7) was fairly small. The flow was out of the lowest levels near the surface and into middle levels. Outflow also was present near 200 mb near the level of maximum wind speed. The kinetic energy was transported upward out of this layer.

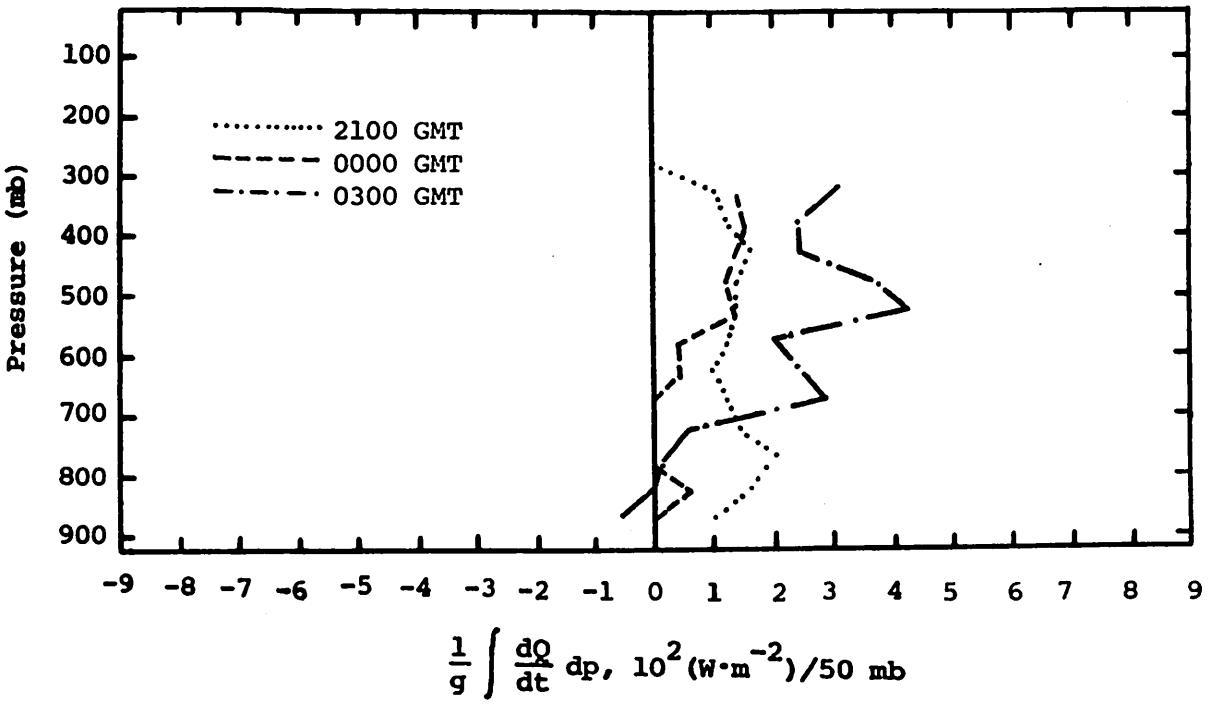

Fig. 5.11.4.5 Vertical profiles of diabatic heating computed from the first law of thermodynamics on 27 June 1978.

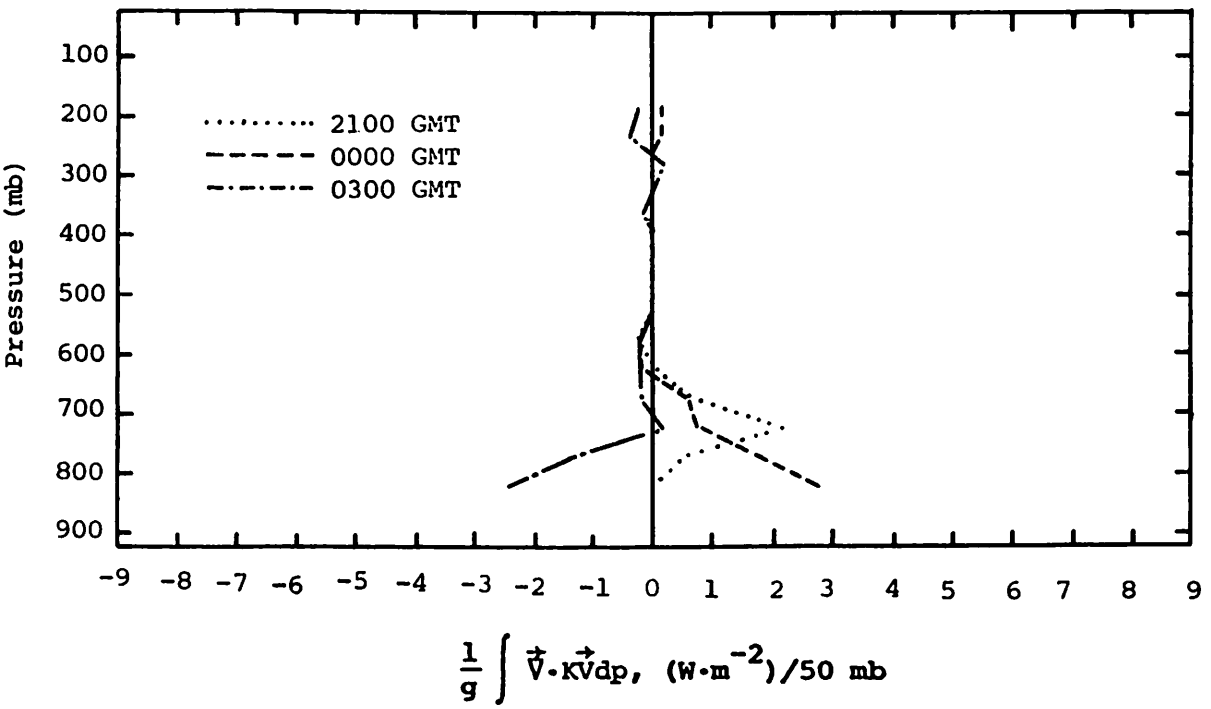

Fig. 5.11.4.6 Vertical profiles of the horizontal flux of kinetic energy on 27 June 1978.

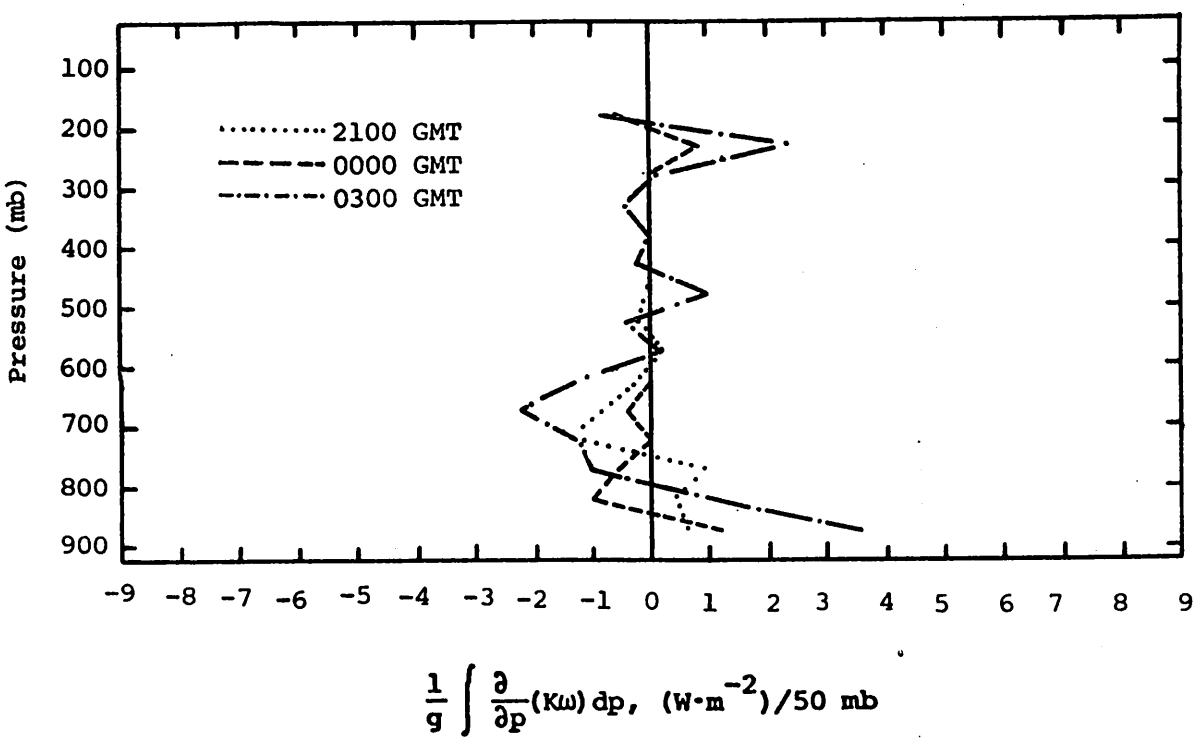

Fig. 5.11.4.7 Vertical profiles of the vertical flux of kinetic energy on 27 June 1978.

5.11.5 Water Vapor Budget

The profiles of net horizontal transport of water vapor (Fig. 5.11.5.1) show losses between 650 and 750 mb at 2100 GMT with moderate inflow below 750 mb and smaller inflow above 650 mb. By 0000 GMT the lower layer of inflow was replaced by a layer of outflow extending from the surface to 650 mb with inflow above. At 0300 GMT water vapor gains occurred at nearly all levels.

The profiles of net vertical transport of water vapor (Fig. 5.11.5.2) are similar for 2100 and 0300 GMT with losses in layers below 750 mb and gains above. At 0000 GMT the profile was somewhat different. There were gains in water vapor below 750 mb and a layered structure of alternating losses and gains suggesting an uneven distribution of water vapor.

Figure 5.11.5.3 shows vertical transport of water vapor through constant pressure surfaces. Transport was upward at all times and generally decreased with height. The largest values were at 0300 GMT. The profiles of combined net horizontal and vertical transport (Fig. 5.11.5.4) show gains at

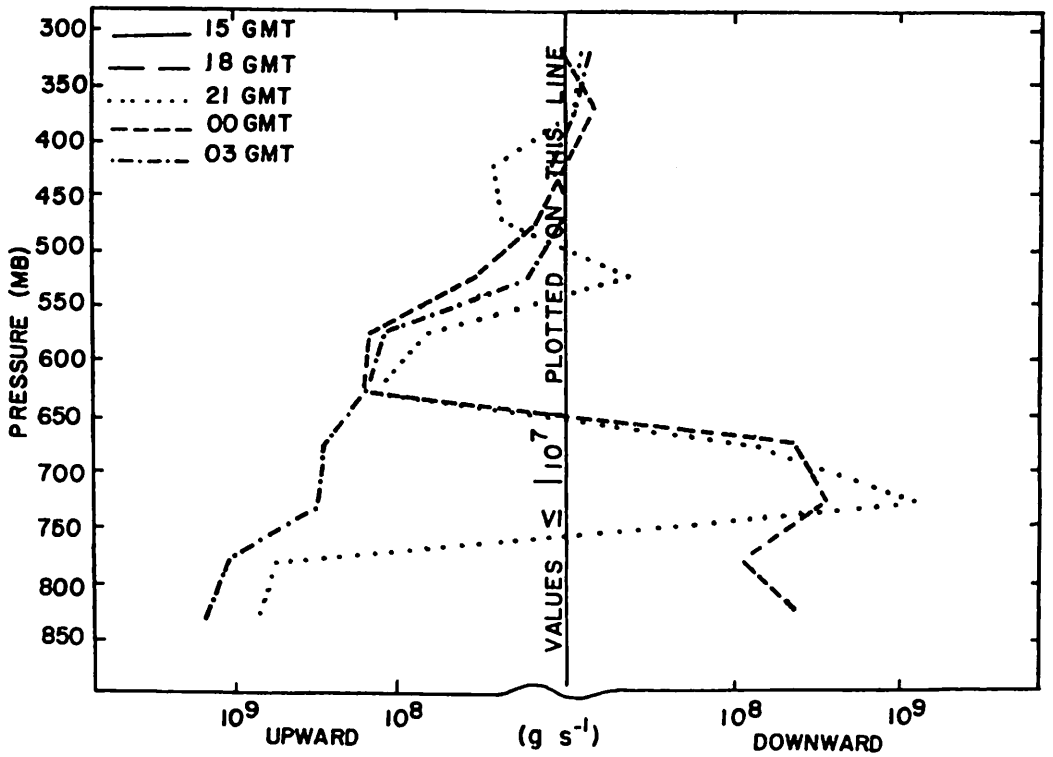

Fig. 5.11.5.1 Net horizontal transport of water vapor through boundaries of 50-mb layers (gm s^{-1}) over the Texas HIPLEX area for 27 June 1978.

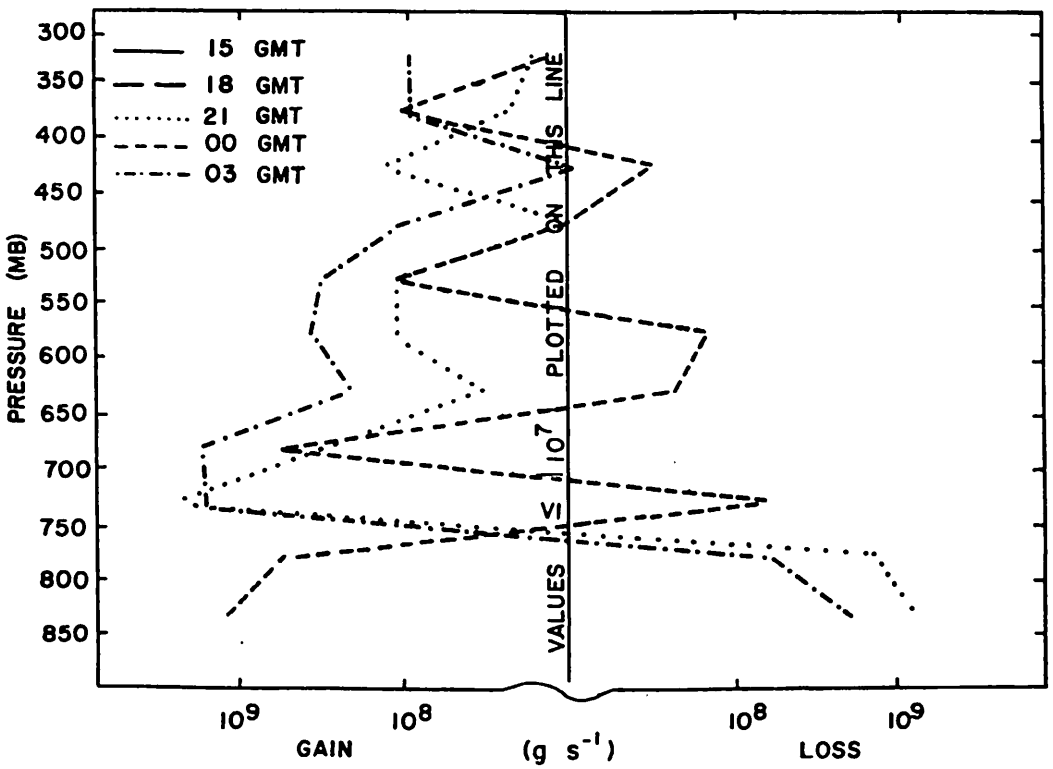

Fig. 5.11.5.2 Net vertical transport of water vapor through boundaries of 50-mb layers (gm s^{-1}) over the Texas HIPLEX area for 27 June 1978.

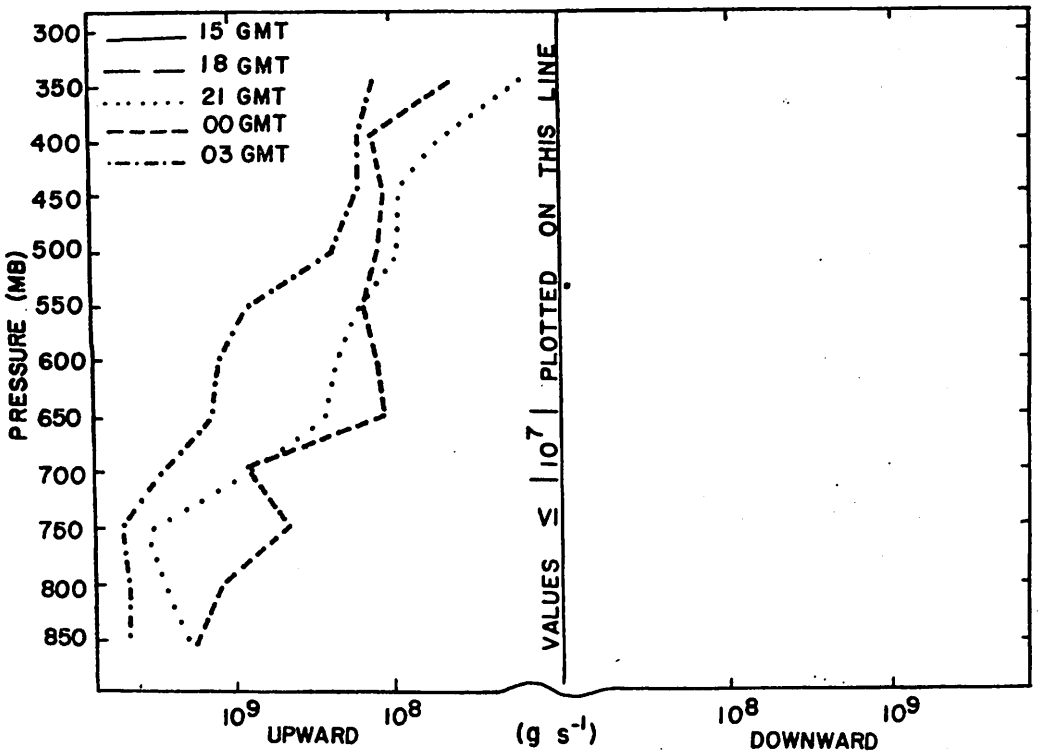

Fig. 5.11.5.3 Vertical transport of water vapor through constant pressure surfaces (gm s^{-1}) over the Texas HIPLEX area for 27 June 1978.

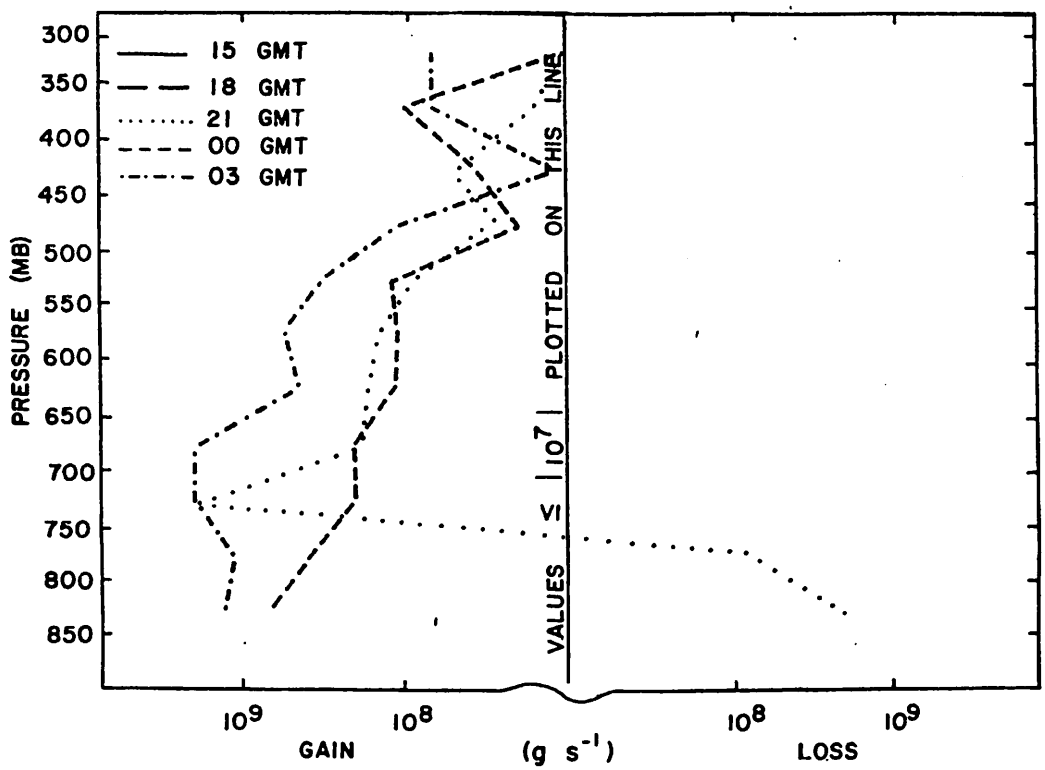

Fig. 5.11.5.4 Combined net horizontal and vertical transport of water vapor through boundaries of 50-mb layers (gm s^{-1}) over the Texas HIPLEX area for 27 June 1978.

all levels except below 750 mb at 1500 GMT. This resulted from large losses due to vertical transport that were not balanced by horizontal inflow of water vapor. The profiles for the other times showed gains at all levels, the magnitude of which decreased with height.

Profiles of total mass of water vapor (Fig. 5.11.5.5) show some rather dry layers at 2100 GMT. One of these was near 400 mb and the other was near 650 mb. These layers had been modified by 0000 GMT with the addition of moisture but there was some drying again at 0300 GMT.

Profiles of the local rate-of-change of total mass of water vapor (Fig. 5.11.5.6) show the moistening that took place between 2100 and 0000 GMT, and the drying between 0000 and 0300 GMT. The amount of water vapor added at 450 mb between 2100 and 0000 GMT was not as large as the amount added at the lower level, but it represented a larger fraction of the total mass of water vapor present at 0000 GMT. The losses between 0000 and 0300 GMT were fairly small at all levels.

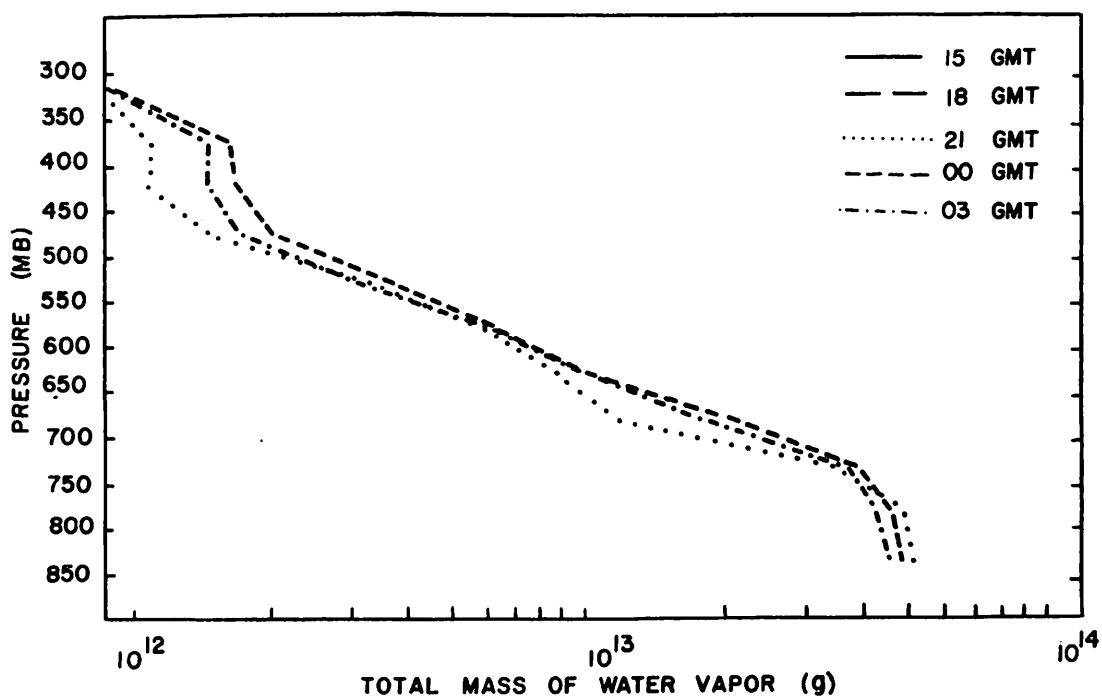

Fig. 5.11.5.5 Total mass of water vapor in layers 50 mb deep (gm) over the Texas HIPLEX area on 27 June 1978.

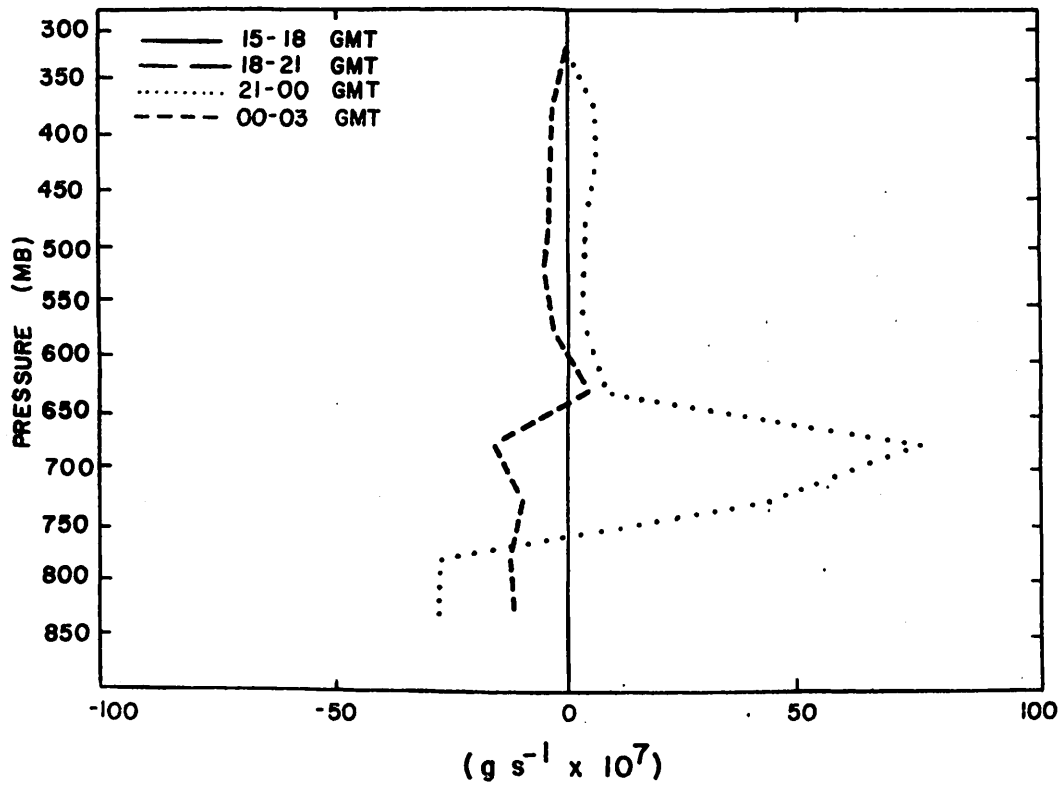

Fig. 5.11.5.6 Local rate of change in total mass of water vapor ($g\ s^{-1} \times 10^7$) for the Texas HIPLEX area for 27 June 1978.

5.12 28 June 1978

5.12.1 Radar

No echoes were reported until 2000 GMT when a few showers moved across the northwest part of the HIPLEX area (Fig. 5.12.1.1). Showers were present in the northwest during the remainder of the period. Another group of showers was present south of Walsh-Watts between 2300 and 0200 GMT. None of the echoes had tops above 9.1 km (30K ft.).

5.12.2 Surface

Surface temperature charts are shown in Fig. 5.12.2.1. Maximum temperatures were located in the northeast near Clairemont throughout the day, and minimum temperatures were in the south near Garden City until 2300 GMT. A second maximum in the temperature field was located in the northwest near Tahoka early in the day. After 2000 GMT, when showers moved into that area, temperatures decreased and a relative minimum formed in the northwest. Temperatures across the area dropped after 0000 GMT.

Surface dewpoint depression (Fig. 5.12.2.2) had moderate values at 1500 GMT but was fairly high through most of the day. Minimum depressions were generally in the south, and a closed center formed near Big Spring after 2000 GMT. Maximum depressions were in the northeast with the maximum temperatures and near Lamesa.

Surface mixing ratio was fairly low during much of the day (Fig. 5.12.2.3). Minima were near Lamesa and Gail, and a maximum was near Big Spring. The showers did not have much effect on these fields.

Surface equivalent potential temperature (Fig. 5.12.2.4) had moderate values. A maximum was located in the northwest at 1500 GMT but by 2000 GMT the highest values were near Big Spring. Potential temperature decreased in the northwest as showers moved into the area. Minimum potential temperature occurred near Gail after 1800 GMT.

Terrain-induced vertical motion (Fig. 5.12.2.5) had moderate values throughout the day. A center of negative values remained near Walsh-Watts through much of the day, but the downward motion decreased an hour prior to the formation of showers at 2300 GMT and remained small until 0200 GMT when the activity in that area decreased. Another center of downward motion was located near Vincent, and an upward motion center near Gail throughout the day.

Surface velocity divergence (Fig. 5.12.2.6) had primarily moderate values. Divergence extended along a north-south axis through the central part of the

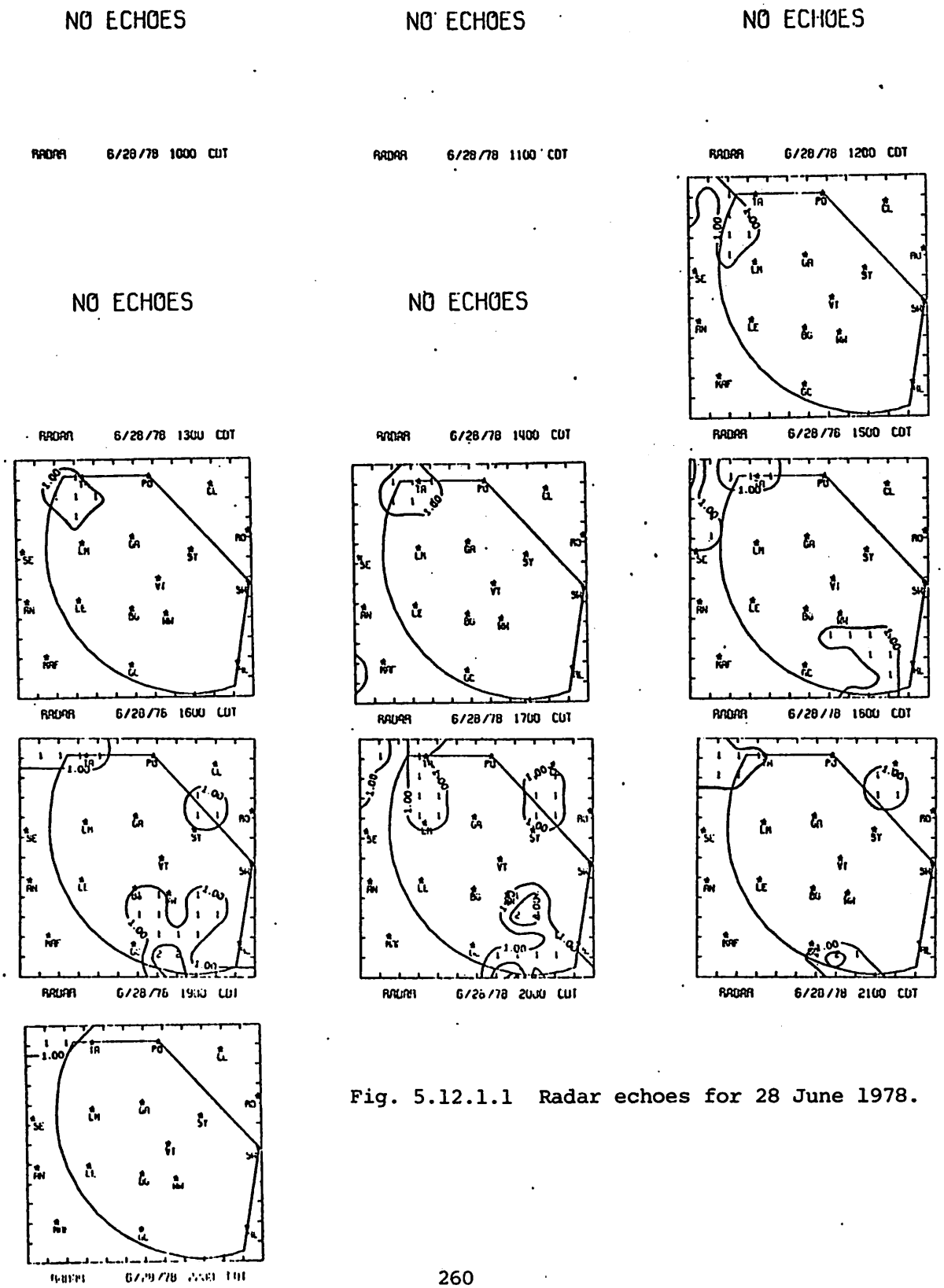

Fig. 5.12.1.1 Radar echoes for 28 June 1978.

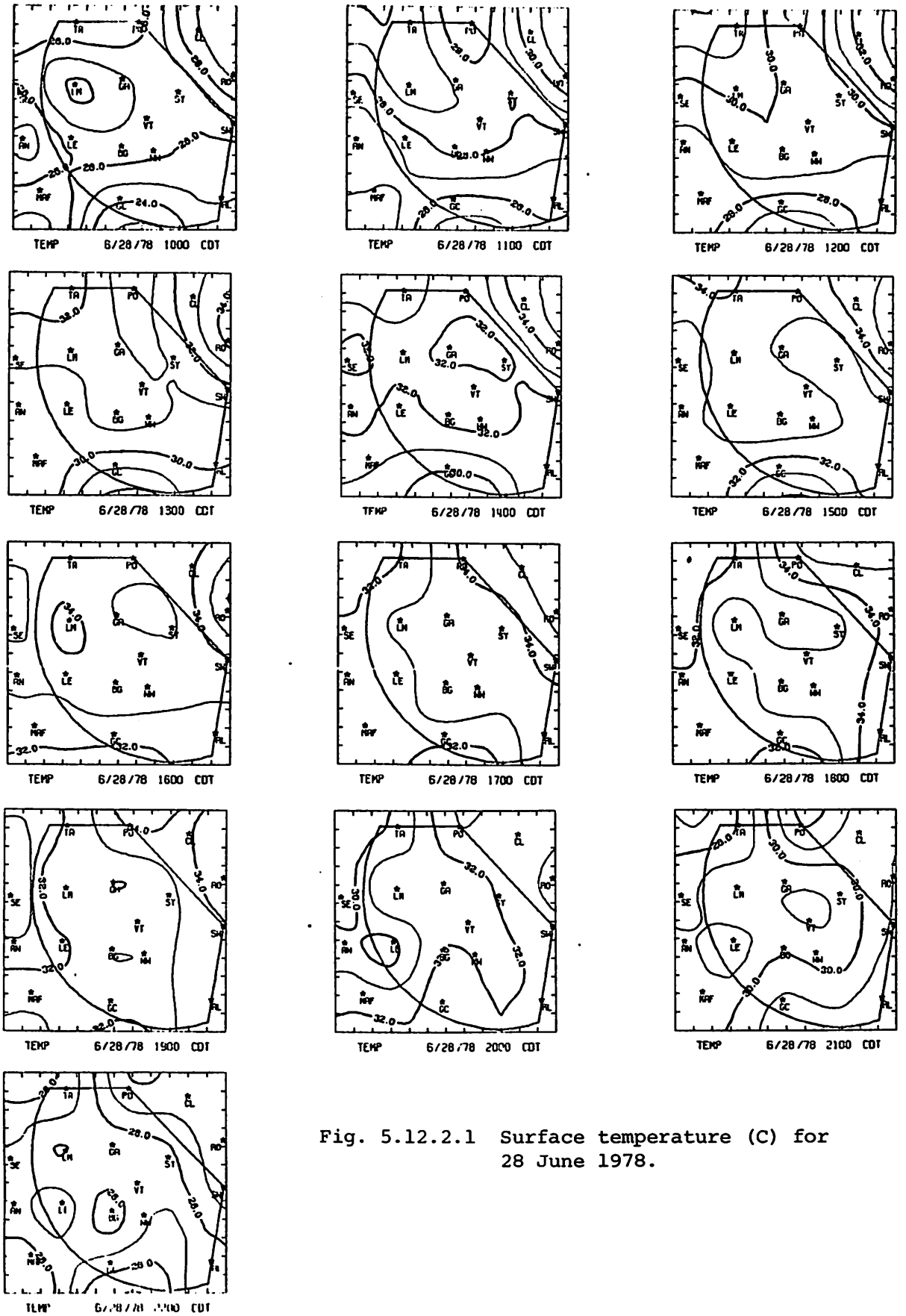

Fig. 5.12.2.1 Surface temperature (C) for 28 June 1978.

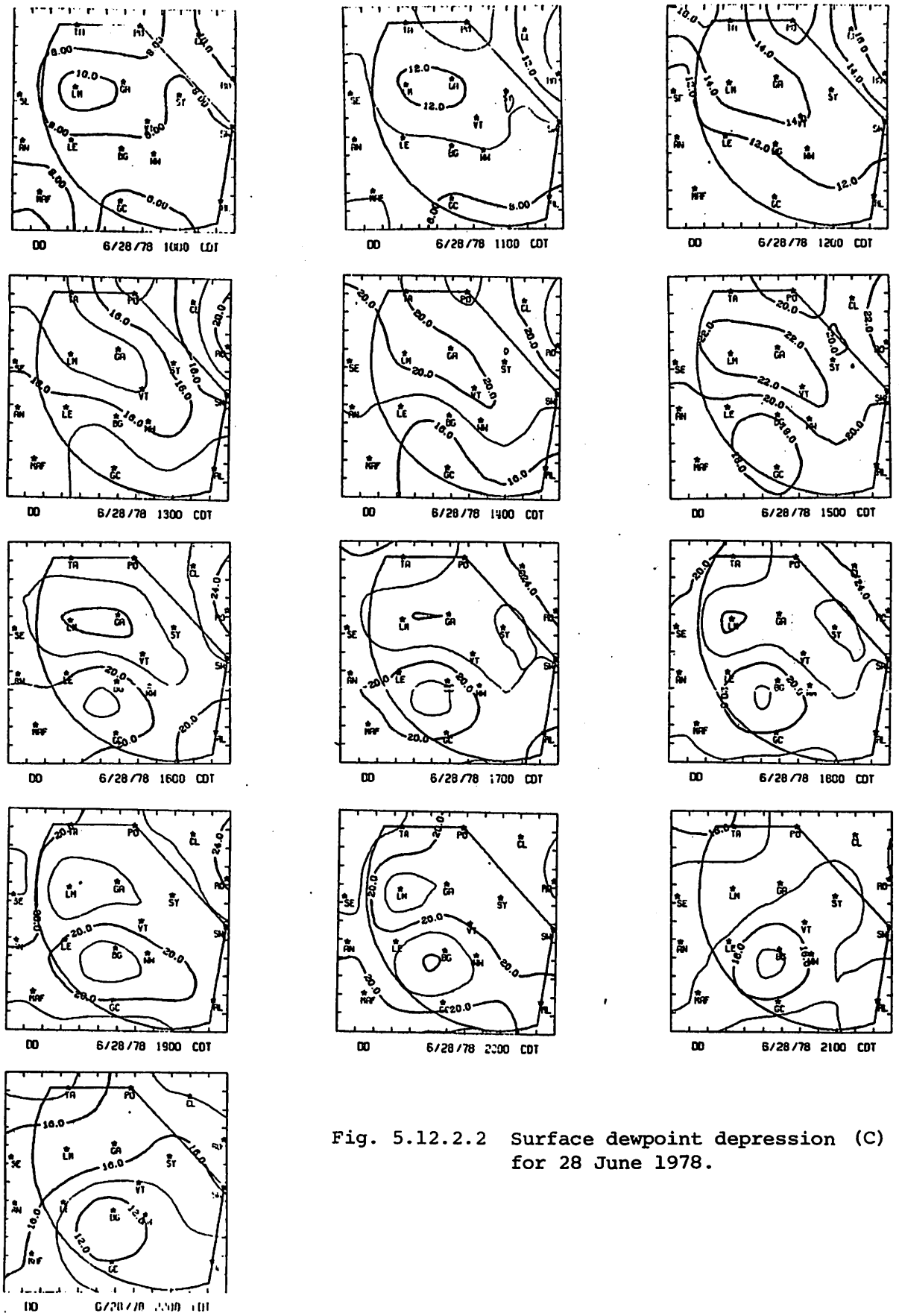

Fig. 5.12.2.2 Surface dewpoint depression (C) for 28 June 1978.

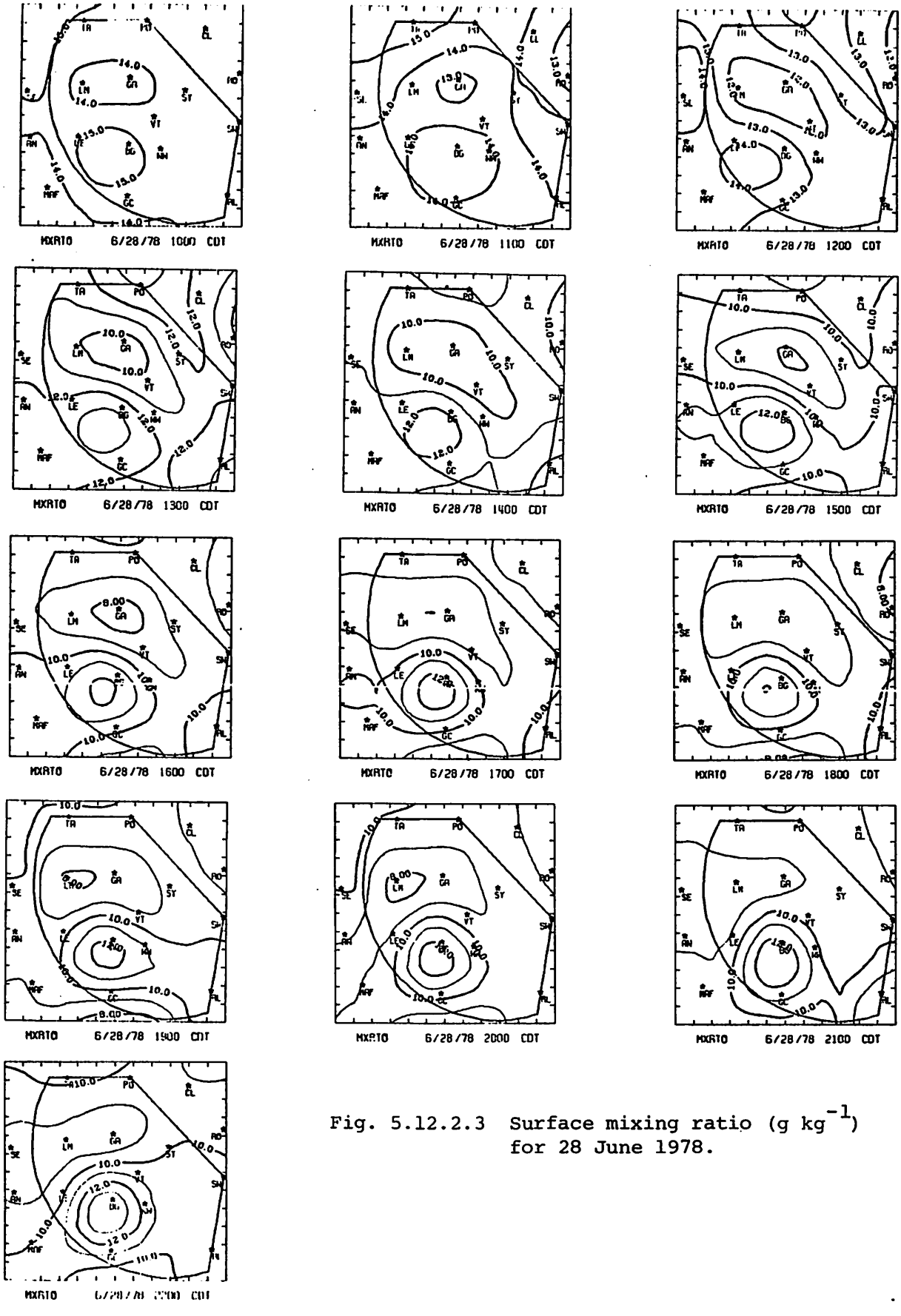

Fig. 5.12.2.3 Surface mixing ratio (g kg^{-1}) for 28 June 1978.

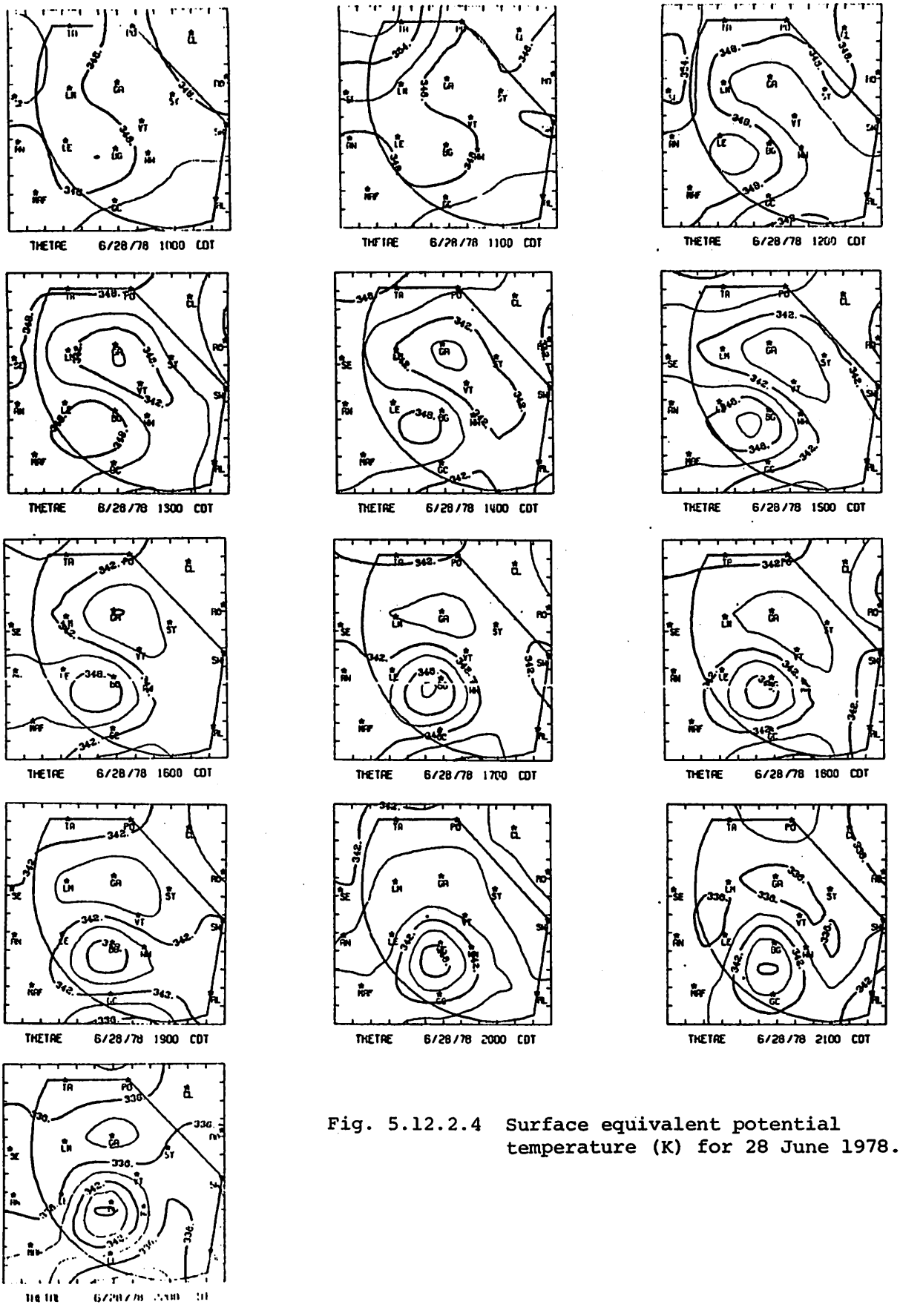

Fig. 5.12.2.4 Surface equivalent potential temperature (K) for 28 June 1978.

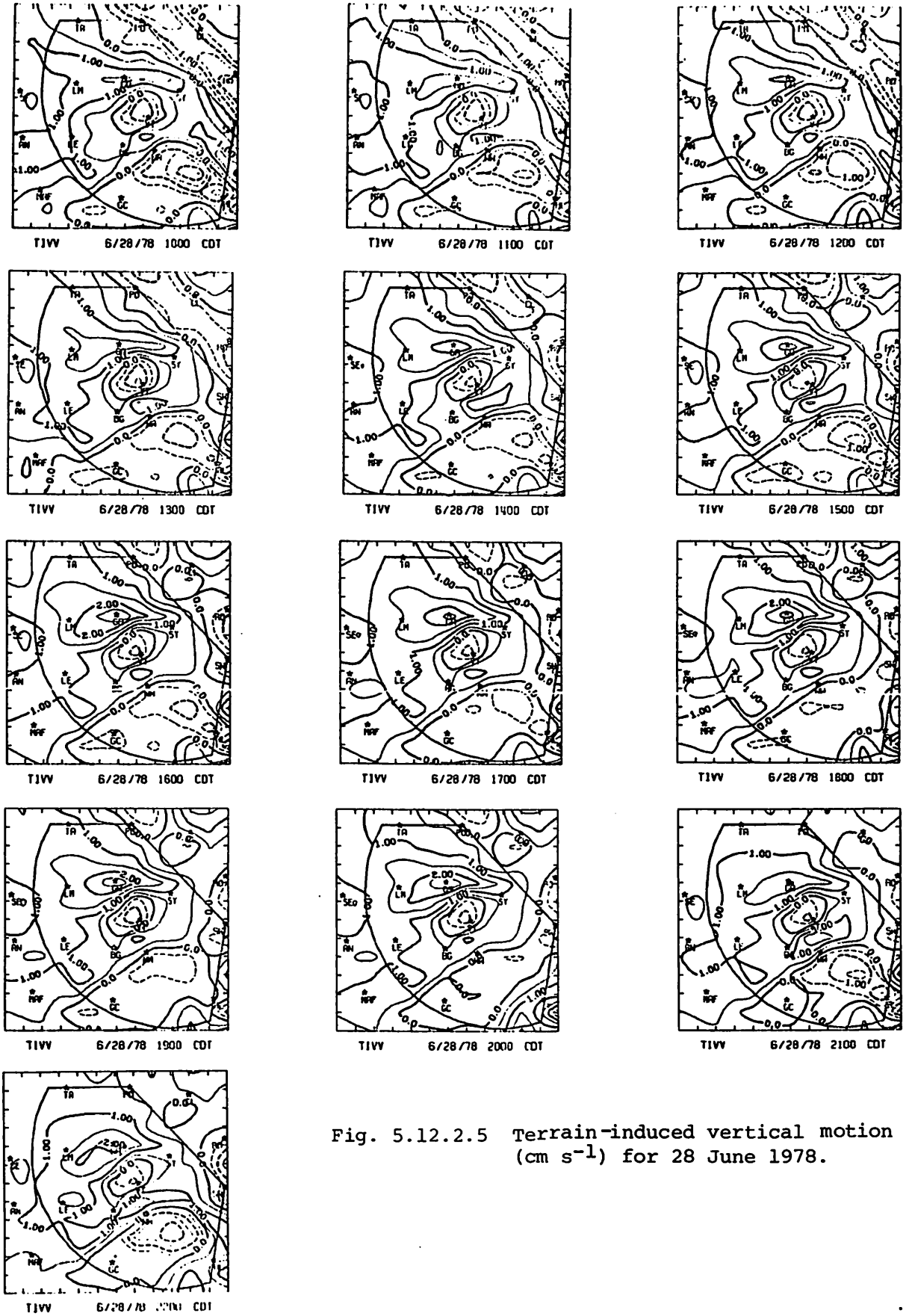

Fig. 5.12.2.5 Terrain-induced vertical motion (cm s^{-1}) for 28 June 1978.

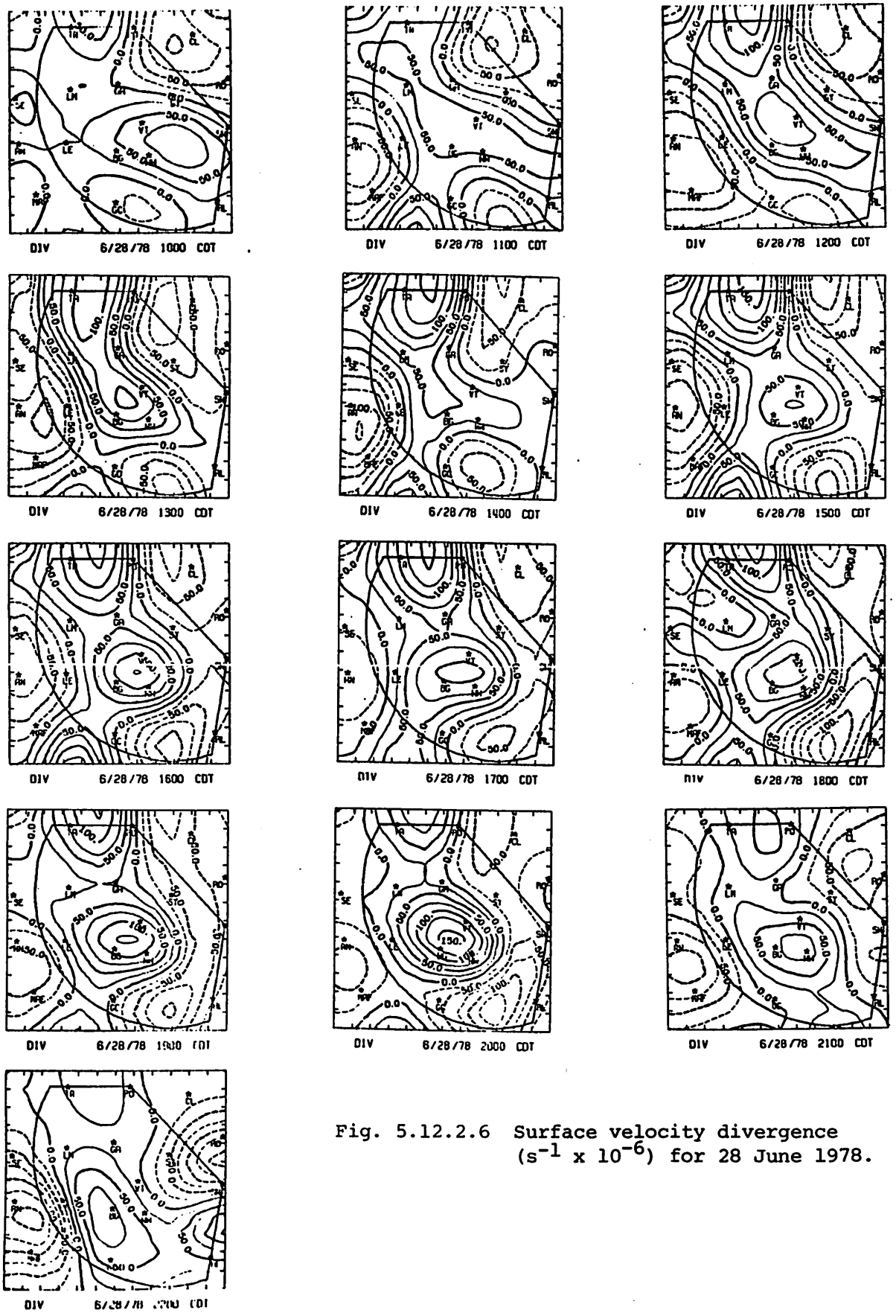

Fig. 5.12.2.6 Surface velocity divergence (s^{-1} x 10^{-6}) for 28 June 1978.

area throughout most of the day. Centers of convergence were located in the west near Andrews, in the southeast between Garden City and Robert Lee, and in the northeast near Clairemont. At 2000 GMT, as showers moved into the northwest part of the HIPLEX area, the center of divergence near Tahoka became fairly strong. The divergence also was rather strong north of Walsh-Watts at 0100 GMT when an echo with height greater than 5.1 km (20K ft) was present. There also was a rather strong center of convergence to the south of the storm at that time.

Figure 5.12.2.7 shows vertical motion 50 mb above the surface. Downward motion prevailed in the central part of the area near Vincent. Upward motion centers were located near Andrews and Clairemont. Strong upward motion was present between Garden City and Robert Lee at 0100 GMT when a storm of Code 2 was located near there. Strong upward motion also was present near Andrews at 0300 GMT but there was no associated activity.

Surface moisture divergence (Fig. 5.12.2.8) showed moderately large values throughout the day. Moisture divergence was present through the central part of the area with convergence in the east and west. There were no especially strong centers associated with the showers.

Vertical flux of moisture (Fig. 5.12.2.9) was moderately large. Downward flux was present in central areas near Vincent, and in the north between Tahoka and Post. Centers of downward flux were located near Andrews and Clairemont, and between Post and Robert Lee. Fairly strong downward moisture flux was present from 1900 to 2000 GMT near Tahoka as showers appeared just to the south of that area. Strong downward flux occurred near Big Spring at 0100 GMT in association with the storm south of Walsh-Watts.

Surface vorticity (Fig. 5.12.2.10) was moderate. A center of negative vorticity remained near Post during most of the day.

Surface pressure changes (Fig. 5.12.2.11) were generally small. The largest change was a 1-mb drop in the central part of the area at 2100 GMT.

Winds were southerly to southeasterly throughout the day with slight variations in direction and speed from hour to hour (Fig. 5.12.2.12).

5.12.3 Upper Level Kinematic Parameters

Figure 5.12.3.1 shows profiles of mass divergence. Convergence was present near the surface at all three times (2100, 0000, and 0300 GMT). A layer of divergence was present near 750 mb, and convergence alternated with layers of weak divergence above that level.

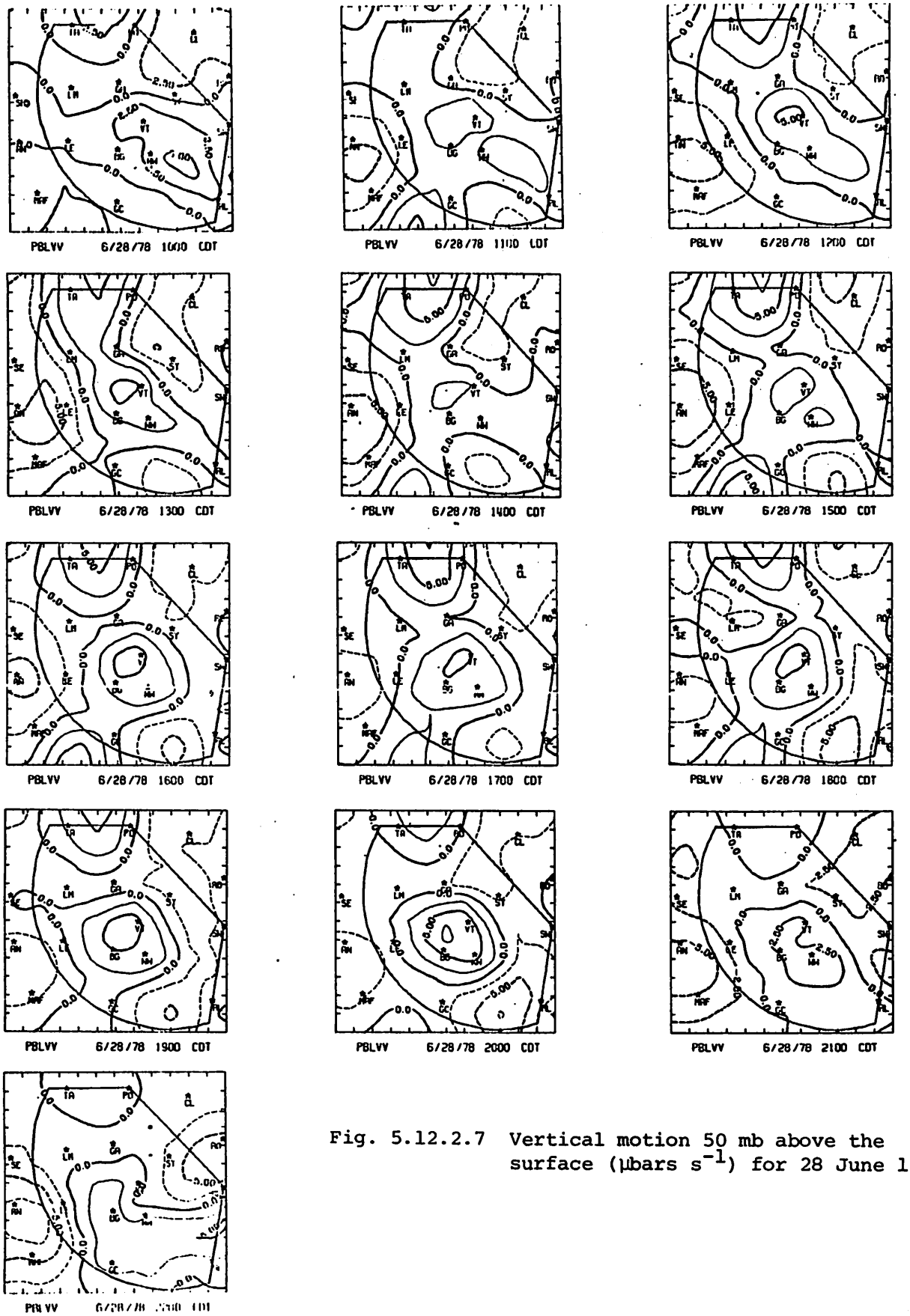

Fig. 5.12.2.7 Vertical motion 50 mb above the surface (μbars s^{-1}) for 28 June 1978.

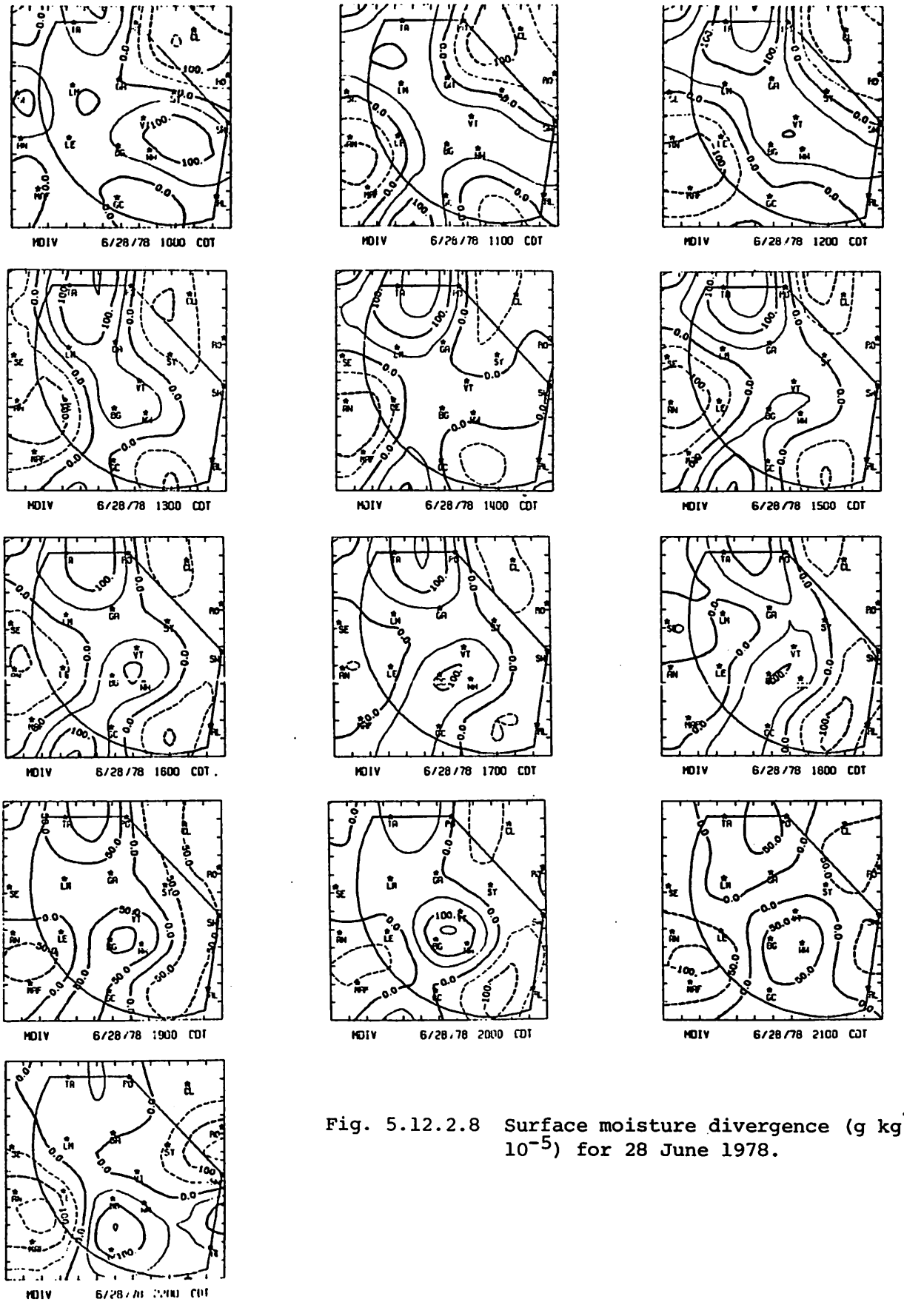

Fig. 5.12.2.8 Surface moisture divergence (g kg^{-1} s^{-1} x 10^{-5}) for 28 June 1978.

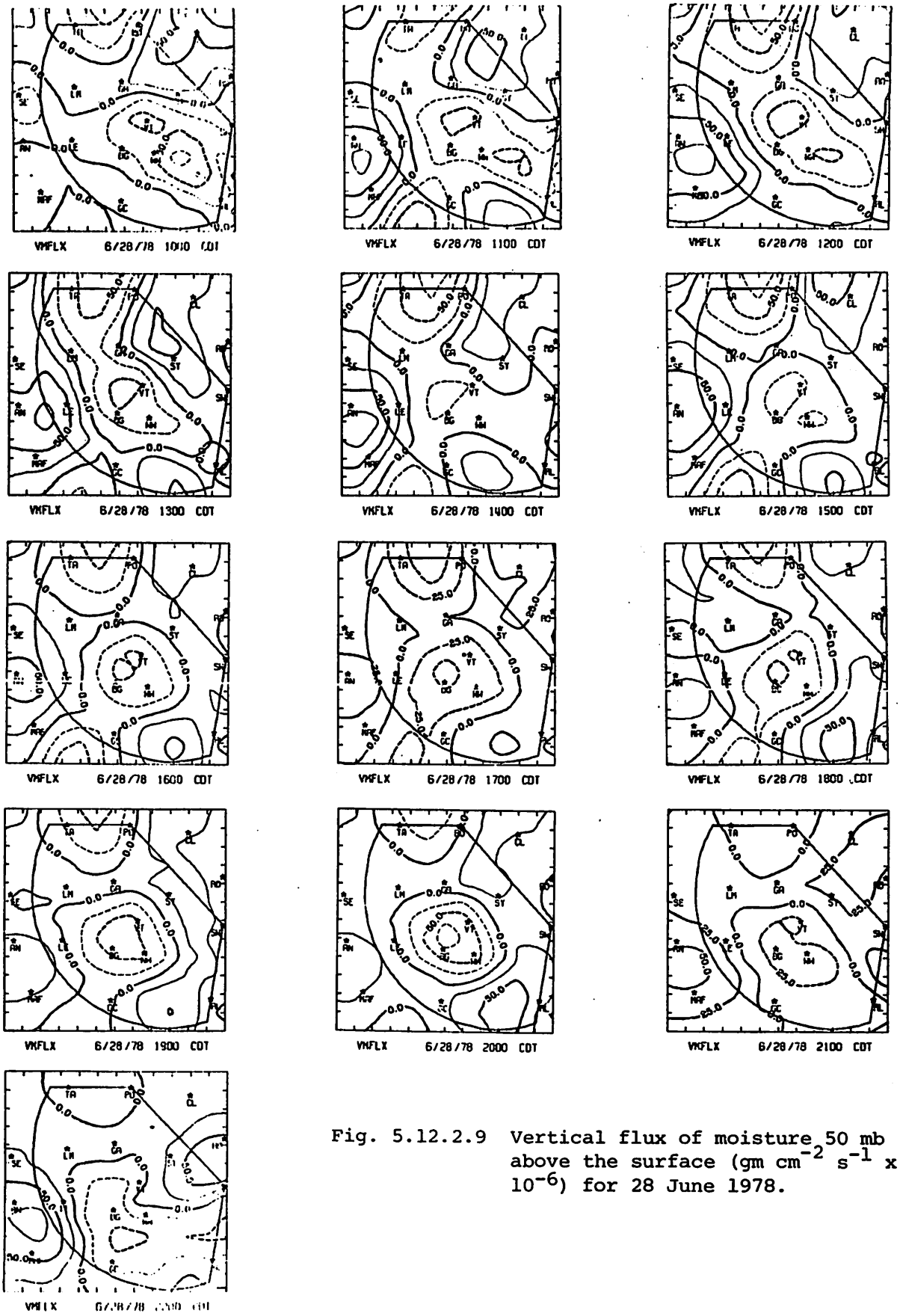

Fig. 5.12.2.9 Vertical flux of moisture 50 mb above the surface (gm cm^{-2} s^{-1} x 10^{-6}) for 28 June 1978.

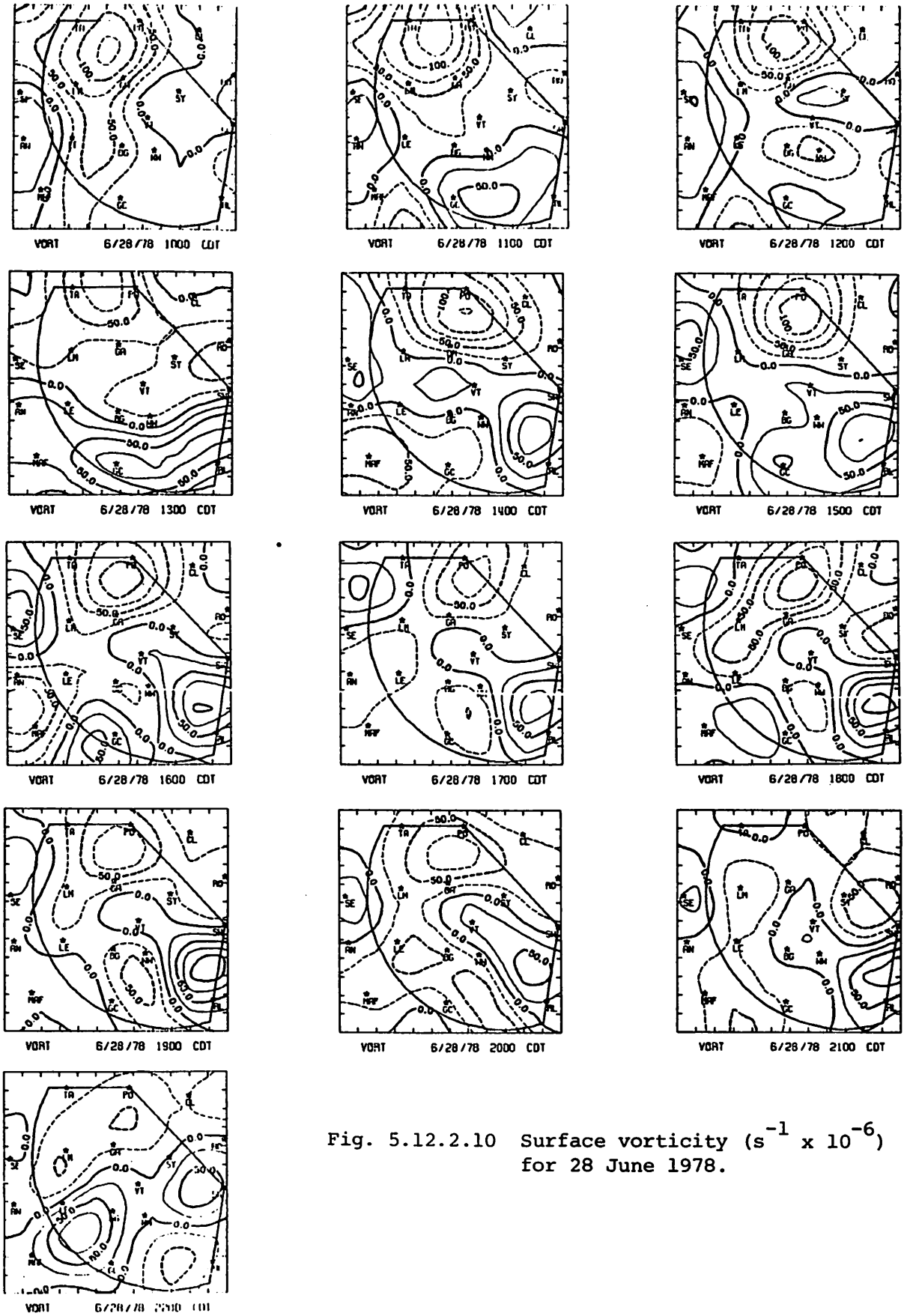

Fig. 5.12.2.10 Surface vorticity ($s^{-1} \times 10^{-6}$) for 28 June 1978.

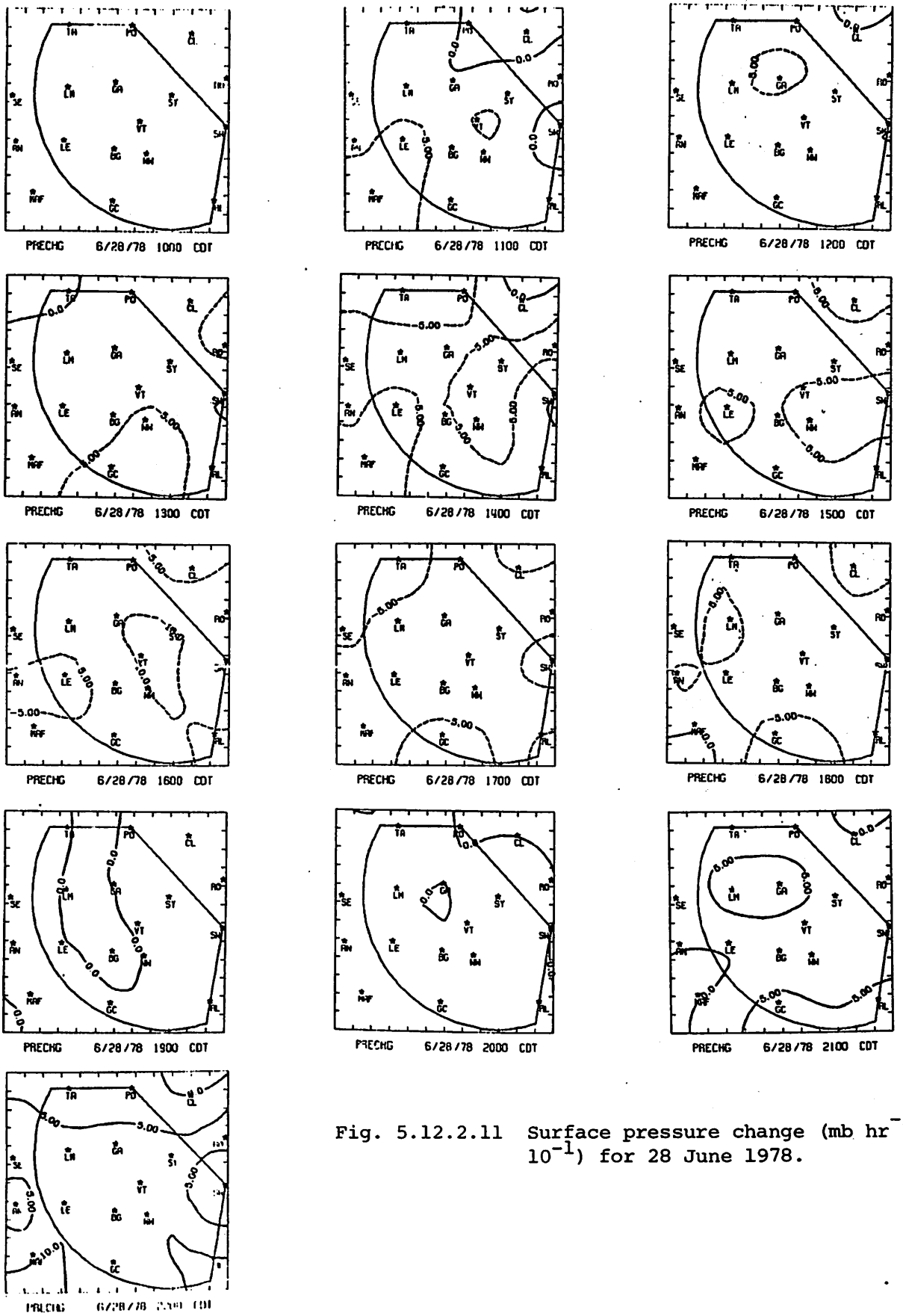

Fig. 5.12.2.11 Surface pressure change (mb hr^{-1} x 10^{-1}) for 28 June 1978.

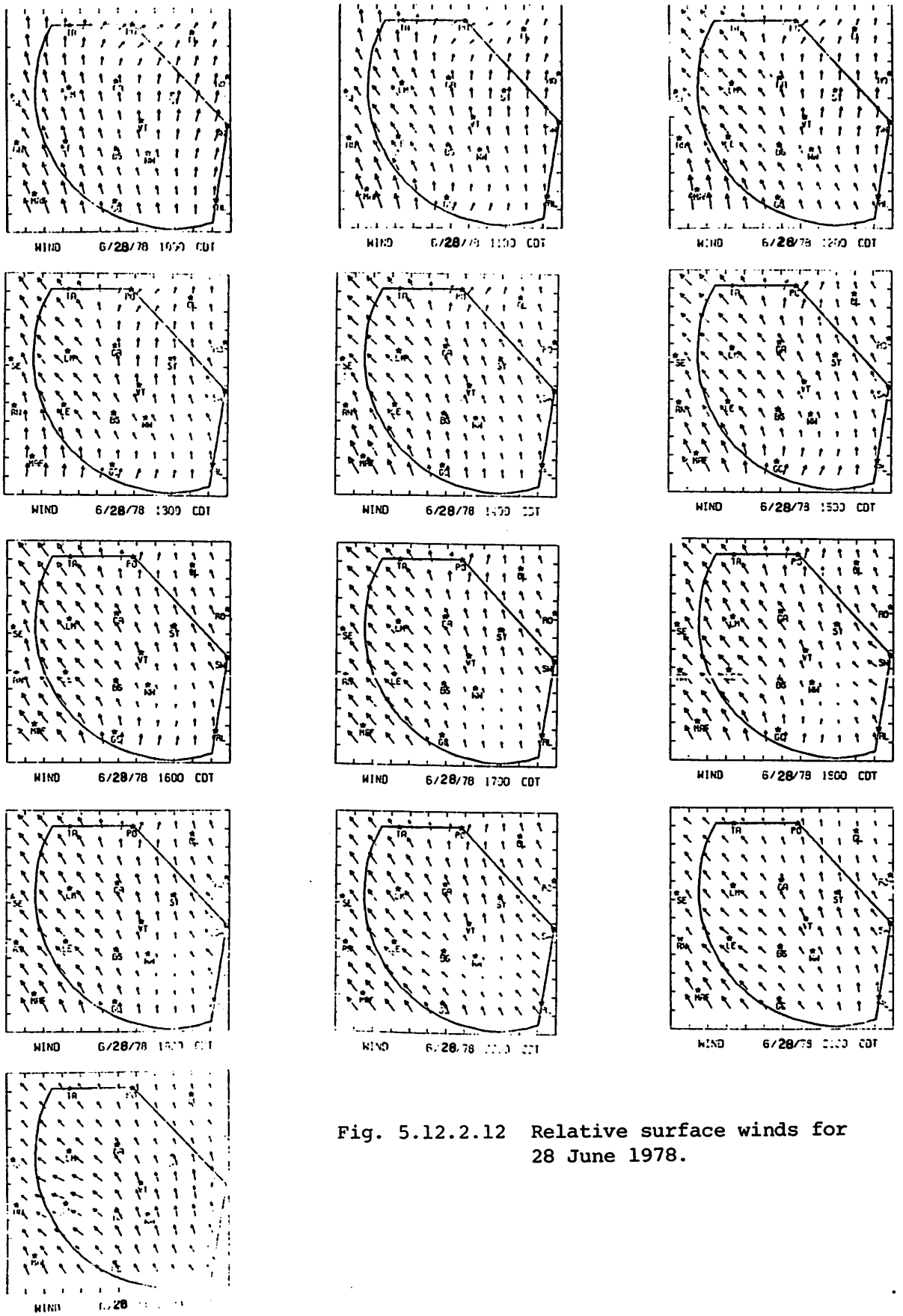

Fig. 5.12.2.12 Relative surface winds for 28 June 1978.

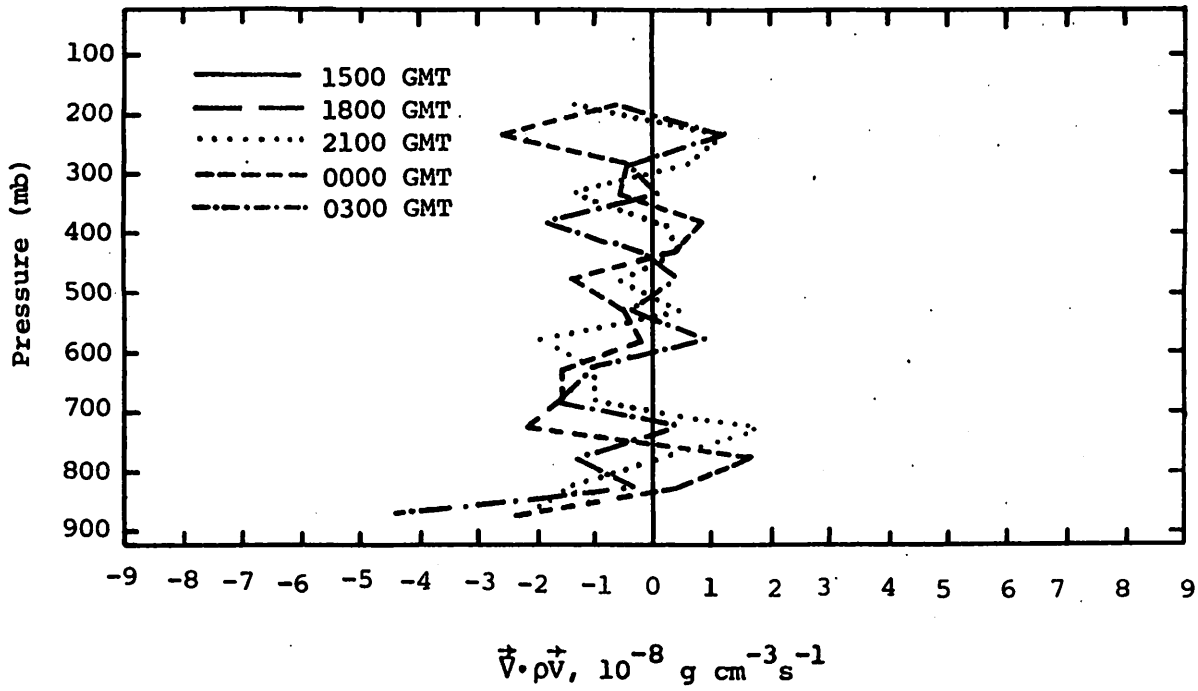

Fig. 5.12.3.1 Vertical profiles of mass divergence on 28 June 1978.

Vertical motion profiles (Fig. 5.12.3.2) show upward motion at all times which generally increased in magnitude with height.

Figure 5.12.3.3 shows profiles of horizontal moisture divergence. Like Fig. 5.12.3.1, convergence was present in the lowest layers with divergence near 750 mb. Convergence was present above 700 mb but in upper layers the value was near zero.

5.12.4 Energetics

Profiles of horizontal flux of latent heat (Fig. 5.12.4.1) show inflow in the lowest layers. Outflow occurred near 750 mb at 0000 GMT and near 700 mb at 2100 and 0300 GMT. Inflow was present above 700 mb but was weak above 600 mb.

Vertical flux of latent heat (Fig. 5.12.4.2) was upward out of the lowest layers into middle layers. The fluxes were small above 500 mb.

Local change of latent heat (Fig. 5.12.4.3) was negative at 2100 GMT as shower activity was starting in the area. At 0000 GMT the change was near zero and at 0300 GMT there were local gains in latent heat.

The residual term of the latent heat equation shows positive values at all levels at 2100 GMT, and above 700 mb at 0000 and 0300 GMT (Fig. 5.12.4.4). Negative values were present below 700 mb at 0000 and 0300 GMT. The positive

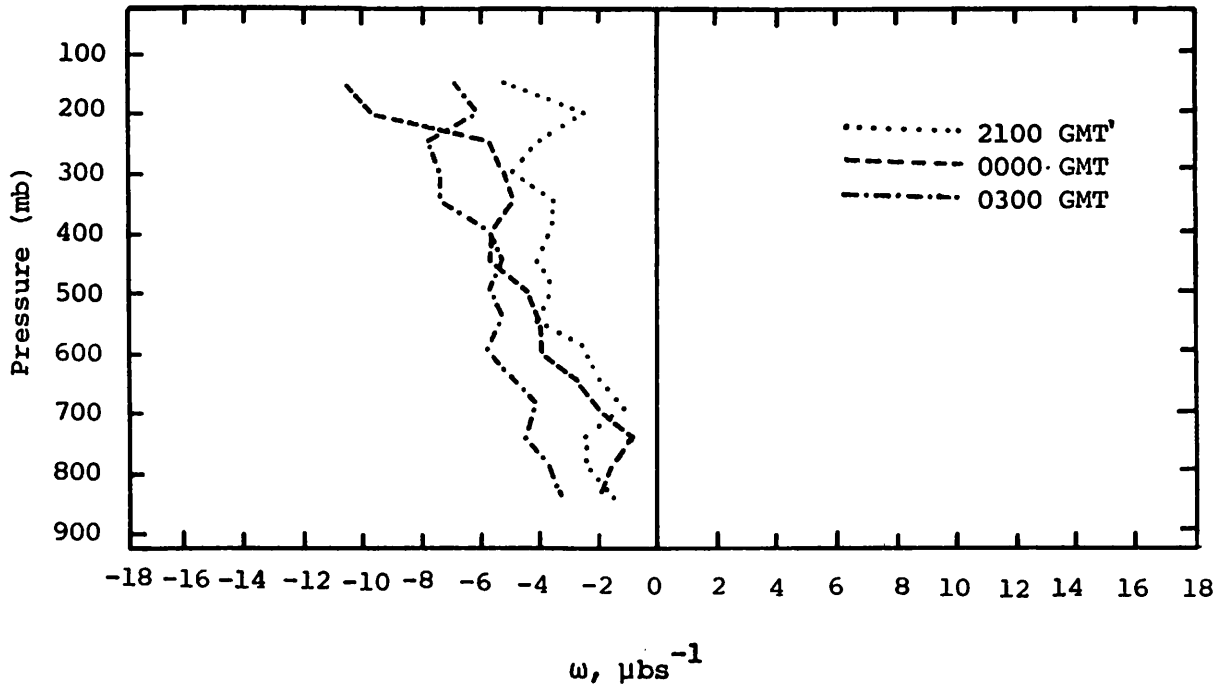

Fig. 5.12.3.2 Vertical profiles of vertical motion on 28 June 1978.

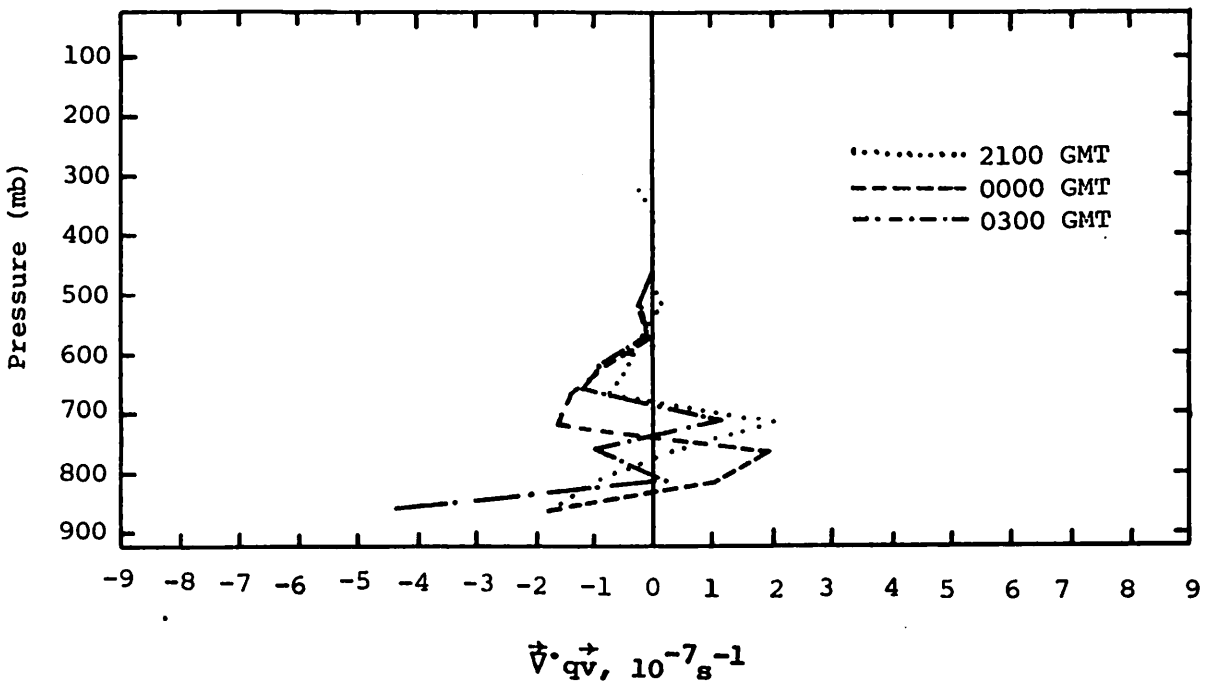

Fig. 5.12.3.3 Vertical profiles of moisture divergence on 28 June 1978.

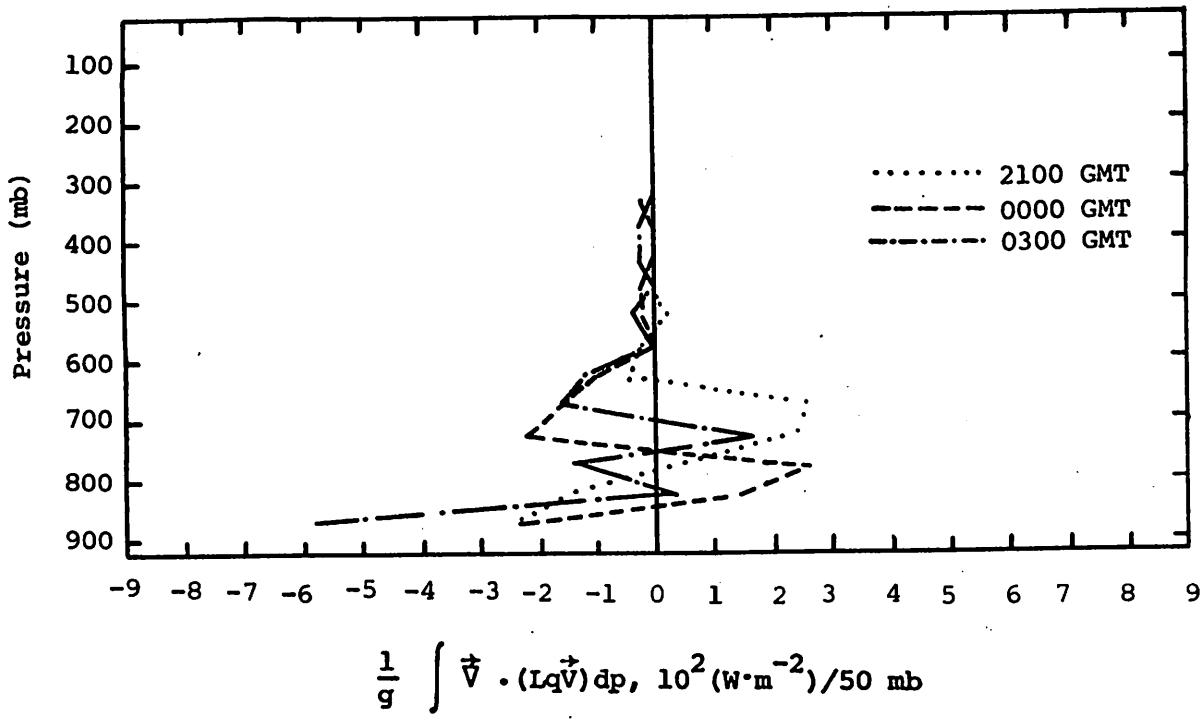

Fig. 5.12.4.1 Vertical profiles of the horizontal flux of latent heat on 28 June 1978.

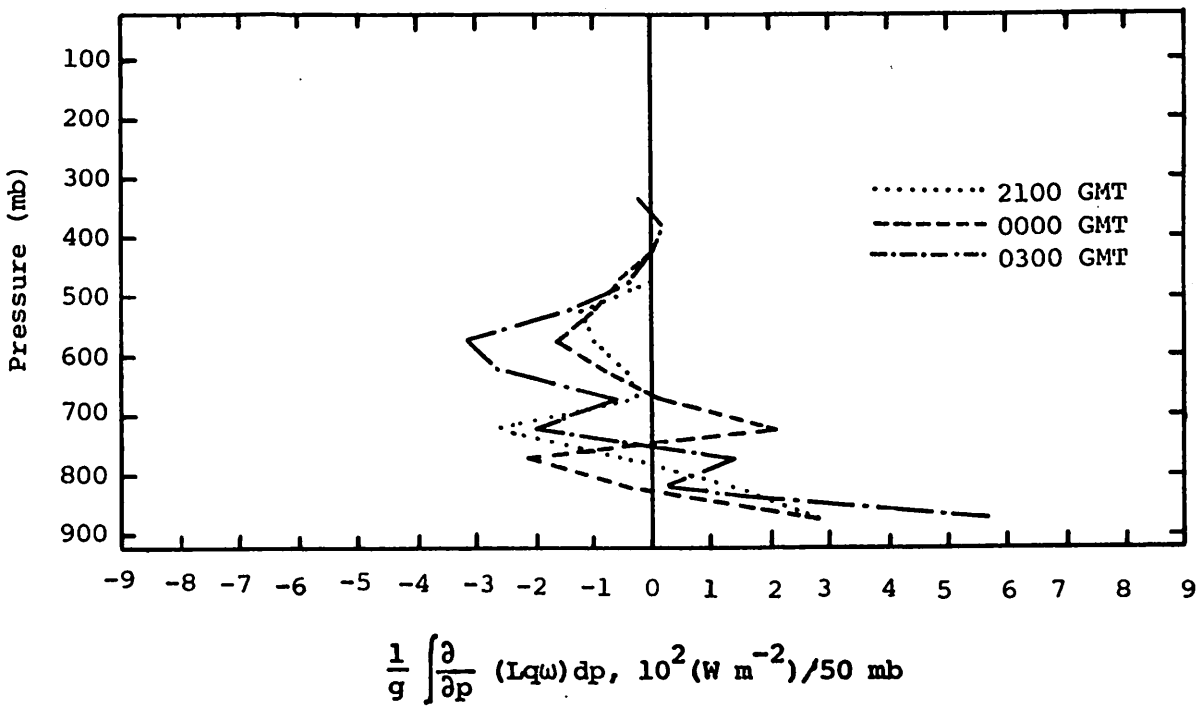

Fig. 5.12.4.2 Vertical profiles of the vertical flux of latent heat energy on 28 June 1978.

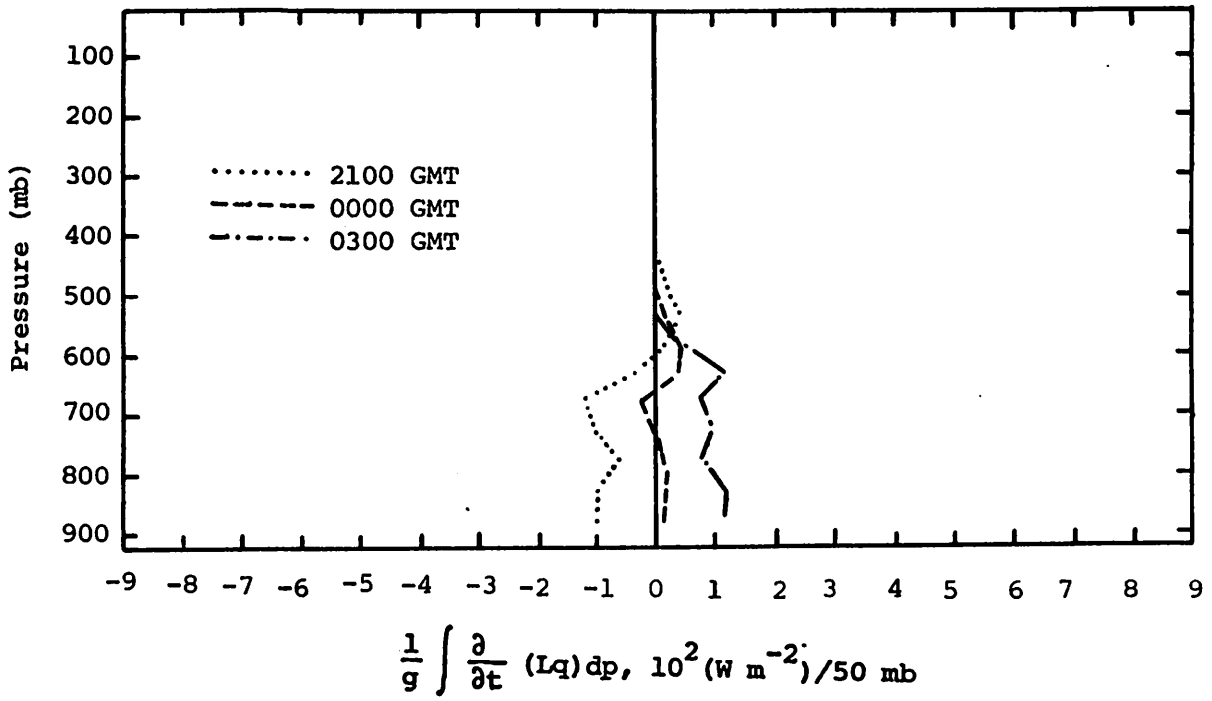

Fig. 5.12.4.3 Vertical profiles of the local change of latent heat energy on 28 June 1978.

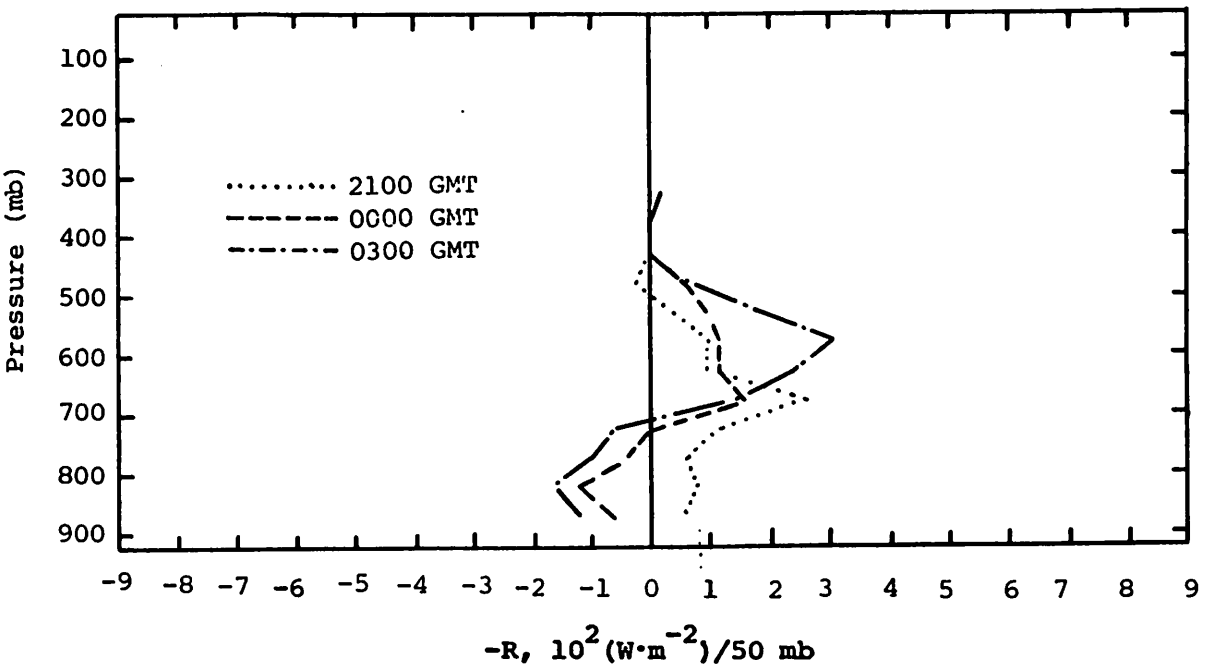

Fig. 5.12.4.4 Vertical profiles of the residual of the latent heat energy equation on 28 June 1978.

values could have resulted from condensation associated with the activity at those times.

Profiles of diabatic heating (Fig. 5.12.4.5) show increases at all levels at all three times. The heating above 700 mb coincides with the condensation taking place at those levels. Below 700 mb the heating was smaller and may have been due to some other diabatic process.

Figure 5.12.4.6 shows profiles of the horizontal flux of kinetic energy. This term was small in most levels as winds were light on this day. Near 200 mb, the level of maximum wind, there was moderate inflow of kinetic energy at 0000 GMT and outflow at 0300 GMT.

The vertical flux of kinetic energy (Fig. 5.12.4.7) was small at most levels. There was upward transport of kinetic energy from a layer near 300 mb into layers above.

5.12.5 Water Vapor Budget

Figure 5.12.5.1 shows the net horizontal transport of water vapor. At 2100 GMT gains were present at nearly all levels. At 0000 GMT there were losses only below 750 mb, and at 0300 GMT the losses were between 700 and 750 mb with increases at all other levels.

The profiles of net vertical transport of water vapor (Fig. 5.12.5.2) show losses near the surface and between 650 and 700 mb with gains in all other layers. By 0000 GMT gains occurred in the lowest layers but losses occurred between 600 and 750 mb through a much thicker layer than at 2100 GMT. At 0300 GMT there were losses in the lowest layers again, and gains at all levels above 750 mb.

The vertical transport of water vapor through constant pressure surfaces (Fig. 5.12.5.3) was upward at all three times. The largest transports occurred at 0300 GMT below 500 mb.

The profiles of combined net horizontal and vertical transport of water vapor (Fig. 5.12.5.4) show gains at nearly all levels. Losses were present below 800 mb at 2100 GMT and near 750 mb at 0000 GMT. Near zero transport occurred at 450 mb.

Profiles of total mass of water vapor (Fig. 5.12.5.5) show a dry layer near 400 mb at 2100 and 0000 GMT. At 0300 GMT the layer was modified somewhat by the addition of moisture, but the whole profile above 550 mb was still fairly dry.

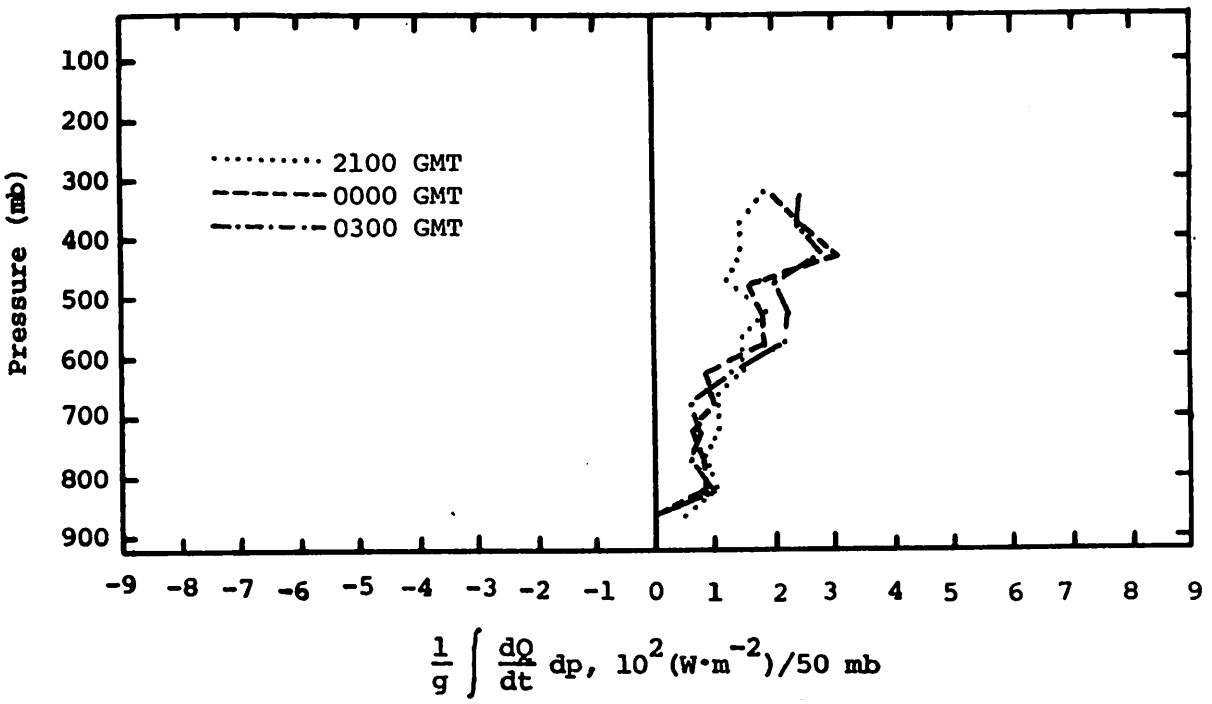

Fig. 5.12.4.5 Vertical profiles of diabatic heating computed from the first law of thermodynamics on 28 June 1978.

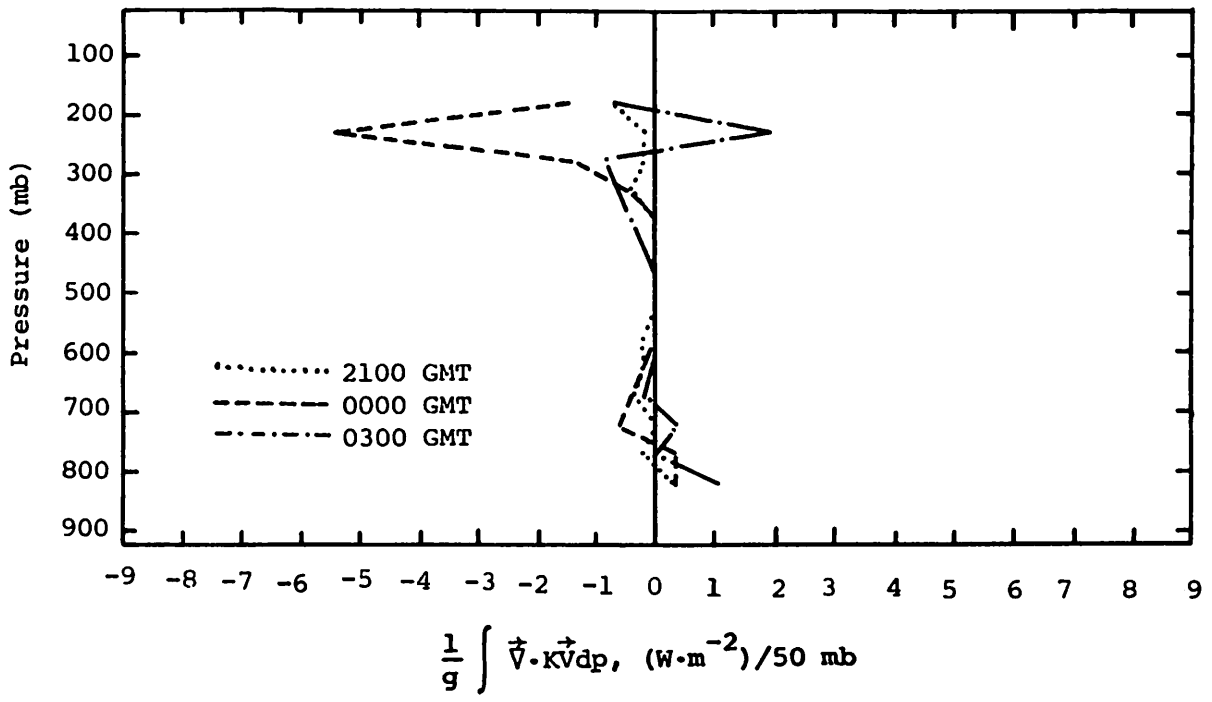

Fig. 5.12.4.6 Vertical profiles of the horizontal flux of kinetic energy on 28 June 1978.

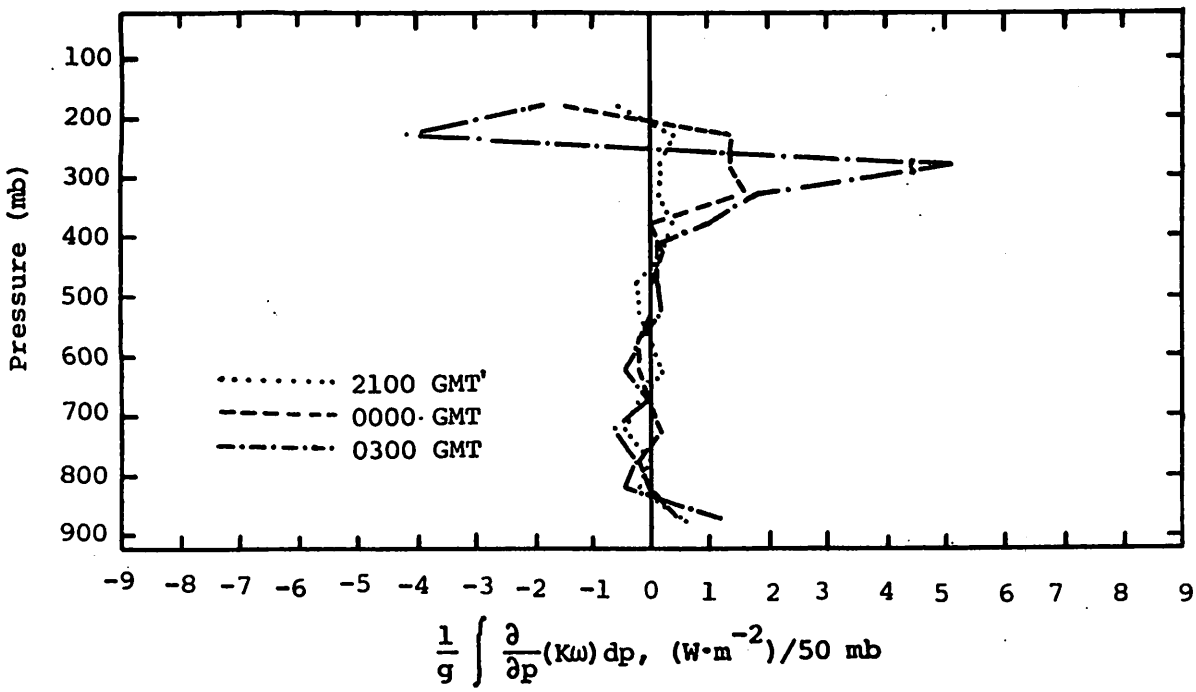

Fig. 5.12.4.7 Vertical profiles of the vertical flux of kinetic energy on 28 June 1978.

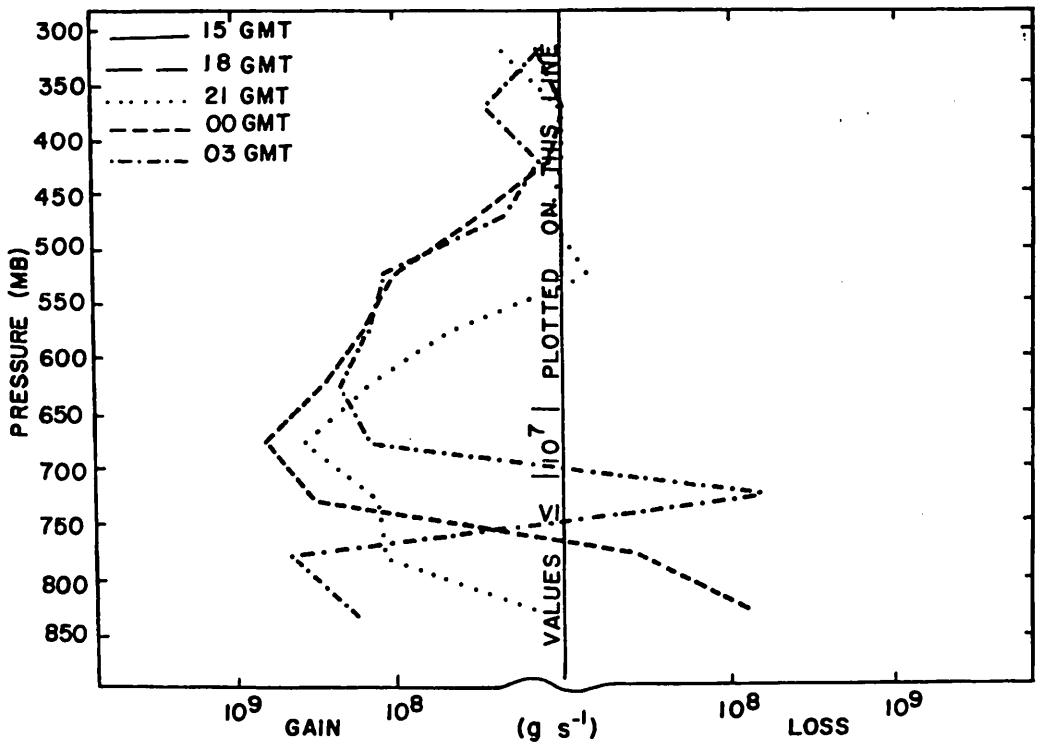

Fig. 5.12.5.1 Net horizontal transport of water vapor through boundaries of 50-mb layers (gm s^{-1}) over the Texas HIPLEX area for 28 June 1978.

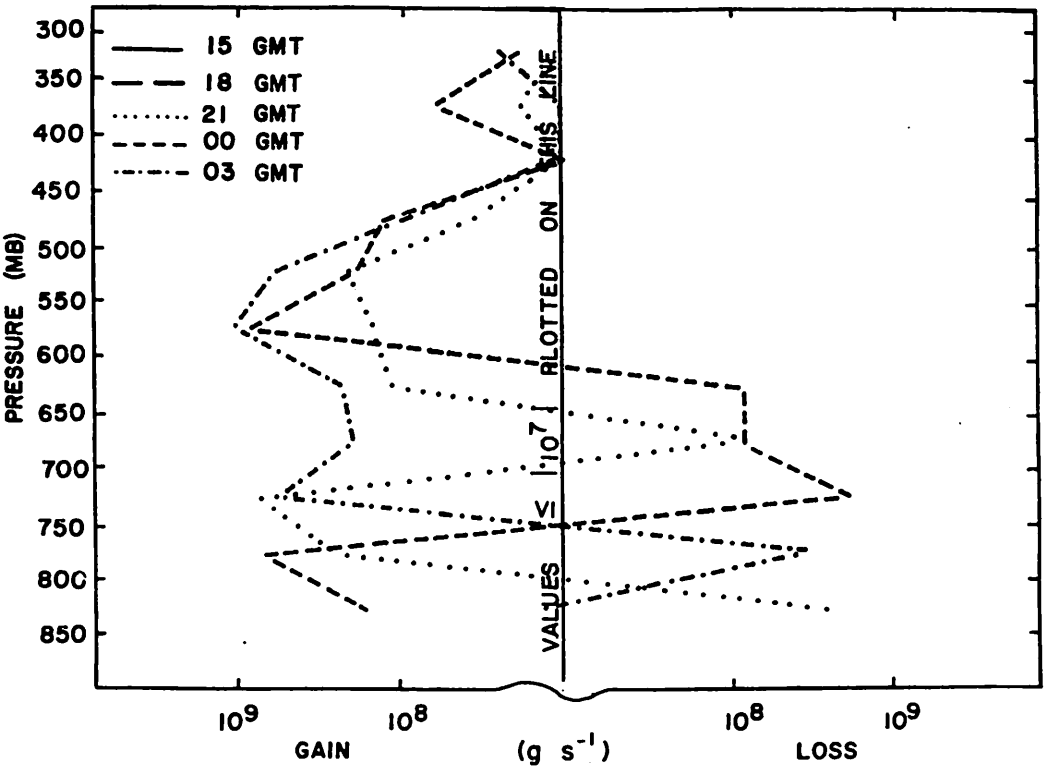

Fig. 5.12.5.2 Net vertical transport of water vapor through boundaries of 50-mb layers (gm s^{-1}) over the Texas HIPLEX area for 28 June 1978.

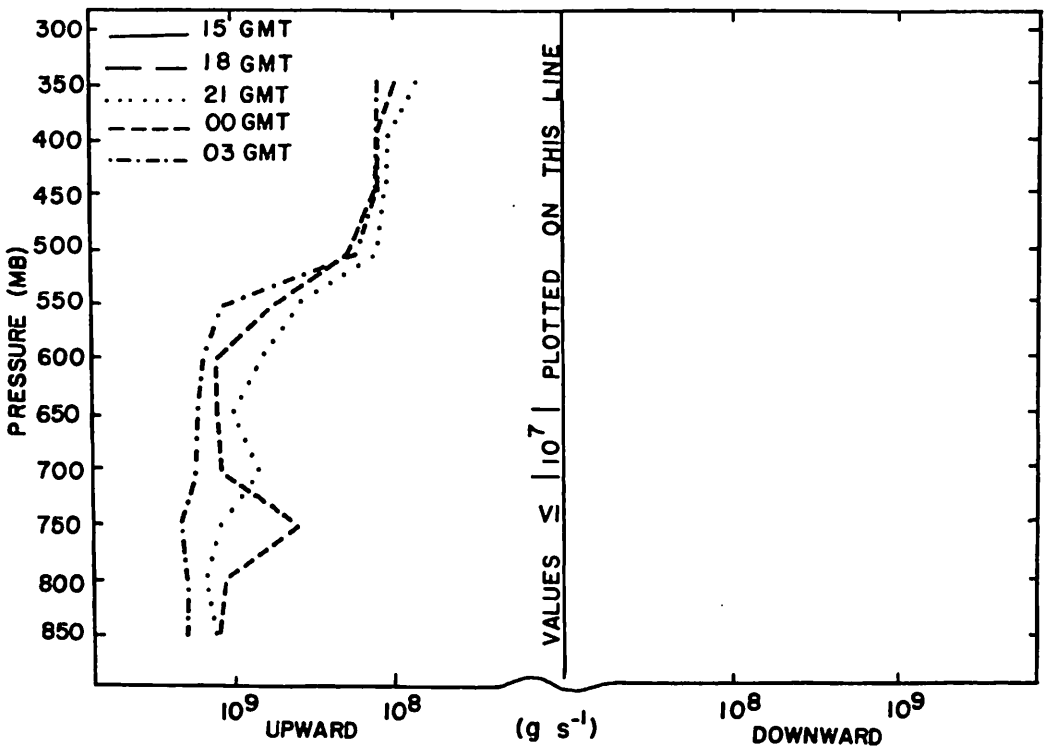

Fig. 5.12.5.3 Vertical transport of water vapor through constant pressure surfaces (gm s^{-1}) over the Texas HIPLEX area for 28 June 1978.

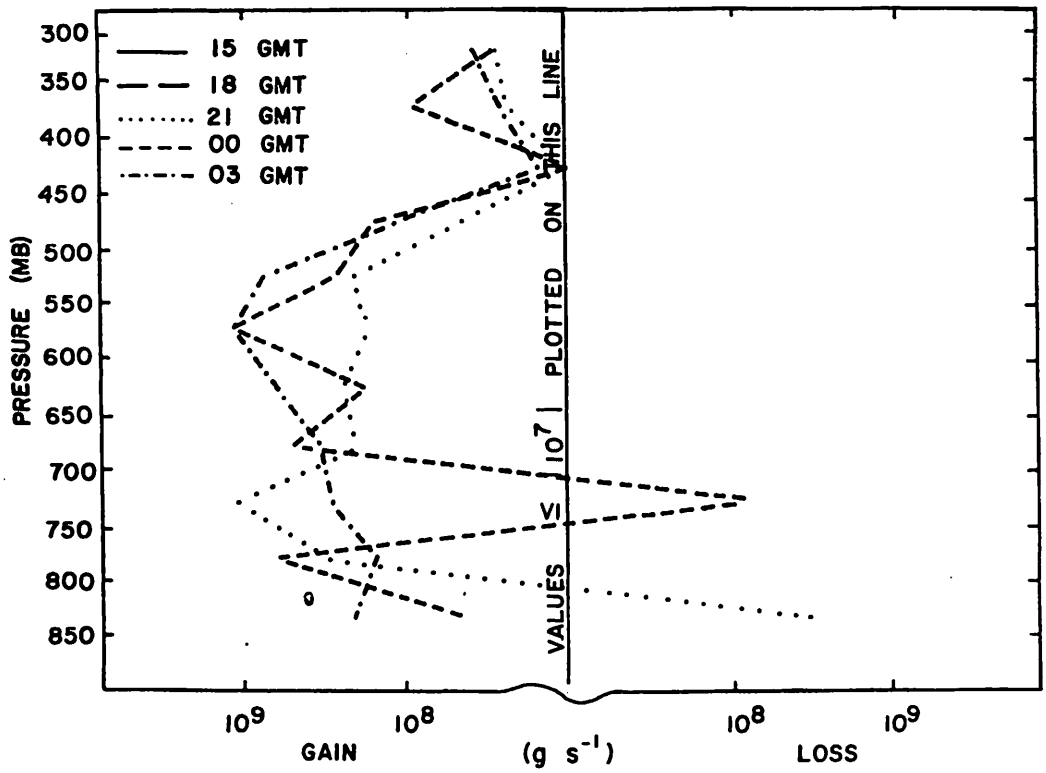

Fig. 5.12.5.4 Combined net horizontal and vertical transport of water vapor through boundaries of 50-mb layers (gm s^{-1}) over the Texas HIPLEX area for 28 June 1978.

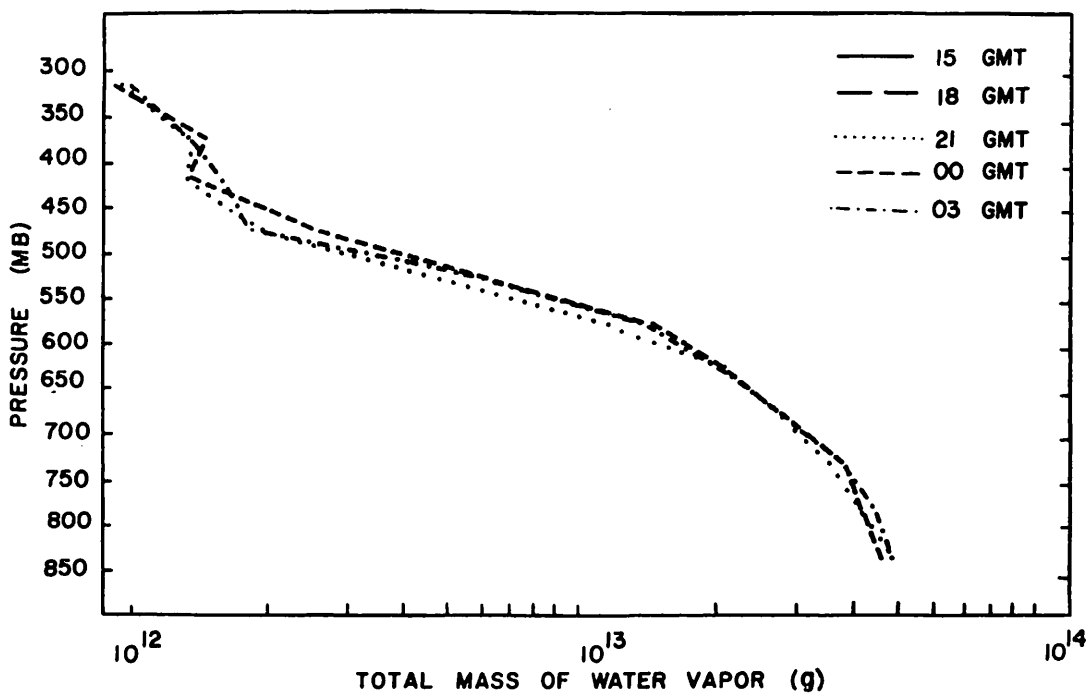

Fig. 5.12.5.5 Total mass of water vapor in layers 50 mb deep (gm) over the Texas HIPLEX area on 28 June 1978.

Figure 5.12.5.6 shows the local rate-of-change of the total mass of water vapor. Gains in water vapor at most levels occurred between 2100 and 0000 GMT, with losses below 800 mb. Between 0000 and 0300 GMT there were small losses in middle layers and larger gains below 650 mb. The small gain above 450 mb corresponds to the modification of the dry layer mentioned earlier.

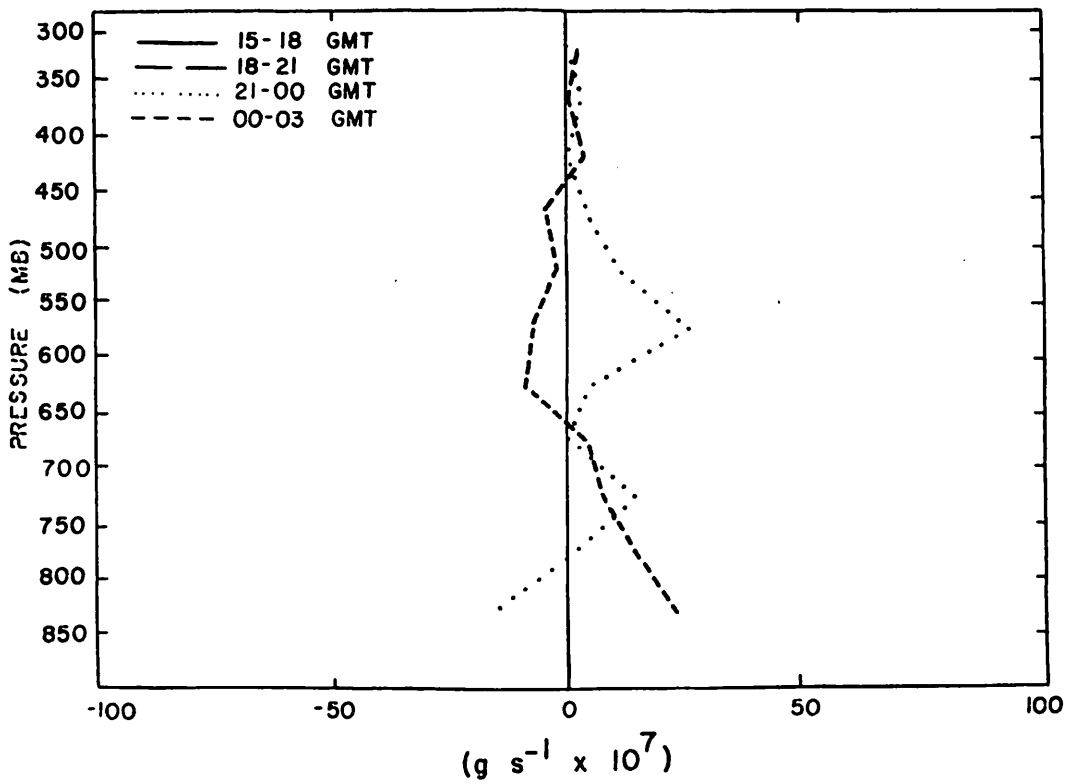

Fig. 5.12.5.6 Local rate-of-change in total mass of water vapor ($g\ s^{-1} \times 10^7$) for the Texas HIPLEX area for 28 June 1978.

5.13 29 June 1978

5.13.1 Radar

There were no echoes reported until 1800 GMT when showers began to move into the area from the west. A large cell with a height of 13.7 km (45K ft) moved into the northwest corner at 2000 GMT and another strong cell formed in the northwest at 2100 GMT. After 2200 GMT lighter showers were present until 0200 GMT. A moderately strong cell formed near Lamesa at that time and moved northward (Fig. 5.13.1.1).

5.13.2 Surface

Figure 5.13.2.1 shows fields of surface temperature. At 1500 GMT maximum temperatures were in the northwest near Tahoka and in the east near Rotan. A minimum was located near Garden City in the south. This pattern remained until 1900 GMT when cooling at Seminole occurred. This cooling was associated with a strong cell to the west of the area. As another storm moved through Tahoka at 2200 GMT the temperature dropped producing a temperature minimum that remained in the northwest through the remainder of the day. Temperatures dropped at Lamesa and Lenorah at 0200 GMT as a storm cell moved through those areas.

Surface dewpoint depressions (Fig. 5.13.2.2) were of moderate value at 1500 GMT, but increased in all areas, especially the northwest, by 1800 GMT. At 1900 GMT depressions decreased at Seminole as a result of the cooling. At the same time dewpoint depressions were still increasing in the central part of the area and a maximum formed near Gail and Vincent at 2000 GMT. At 2200 GMT dewpoint depressions remained low in the northwest for the remainder of the day. The area of minimum dewpoint depression was extended at 0200 GMT when cooling associated with a storm decreased dewpoint depressions at Lamesa and Lenorah.

Surface mixing ratios (Fig. 5.13.2.3) were moderate at 1500 GMT with a maximum near Post. A minimum formed near Gail at 1600 GMT and small mixing ratios persisted there to 0100 GMT. At 1900 GMT the mixing ratio increased at Seminole when that area was under the influence of a storm to the west of the HIPLEX area. At 2100 GMT the maximum at Seminole was not present as the first storm in the northwest had dissipated and a second storm north of Lamesa was just forming. Another maximum, near Big Spring, showed up at this hour, and mixing ratio remained higher near Big Spring than in surrounding areas for the remainder of the day. At 2200 GMT mixing ratio increased again

NO ECHOES

NO ECHOES

NO ECHOES

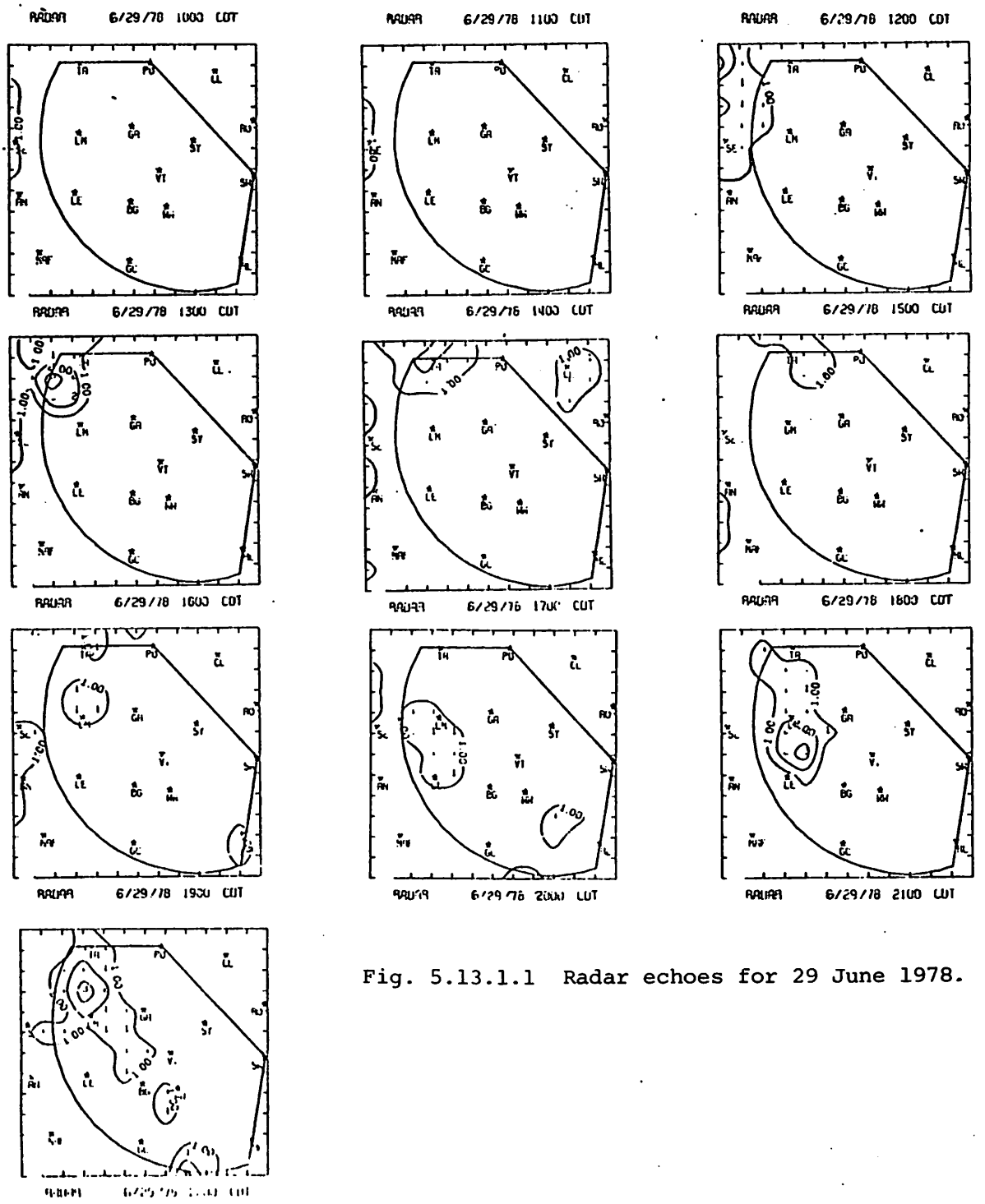

Fig. 5.13.1.1 Radar echoes for 29 June 1978.

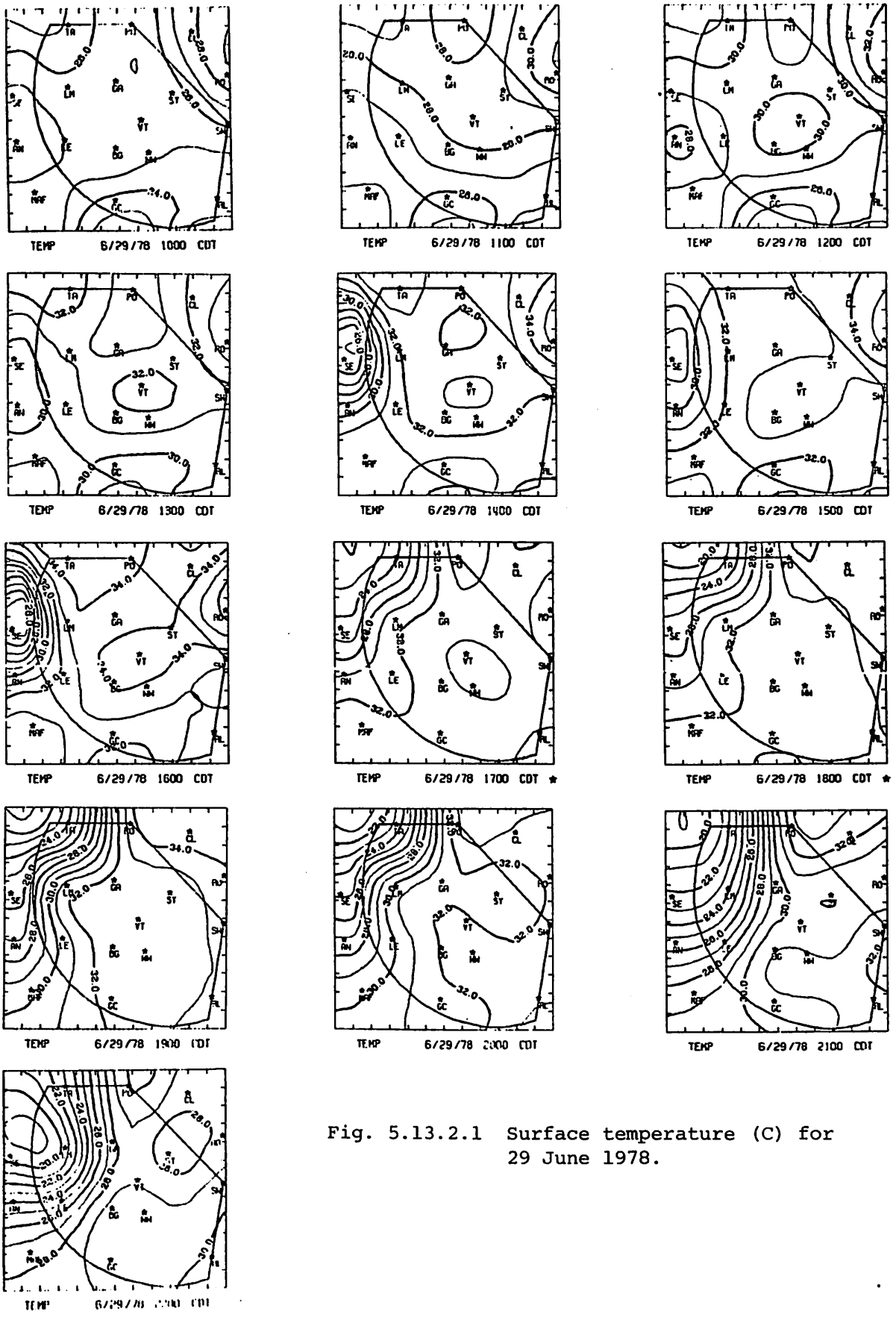

Fig. 5.13.2.1 Surface temperature (C) for 29 June 1978.

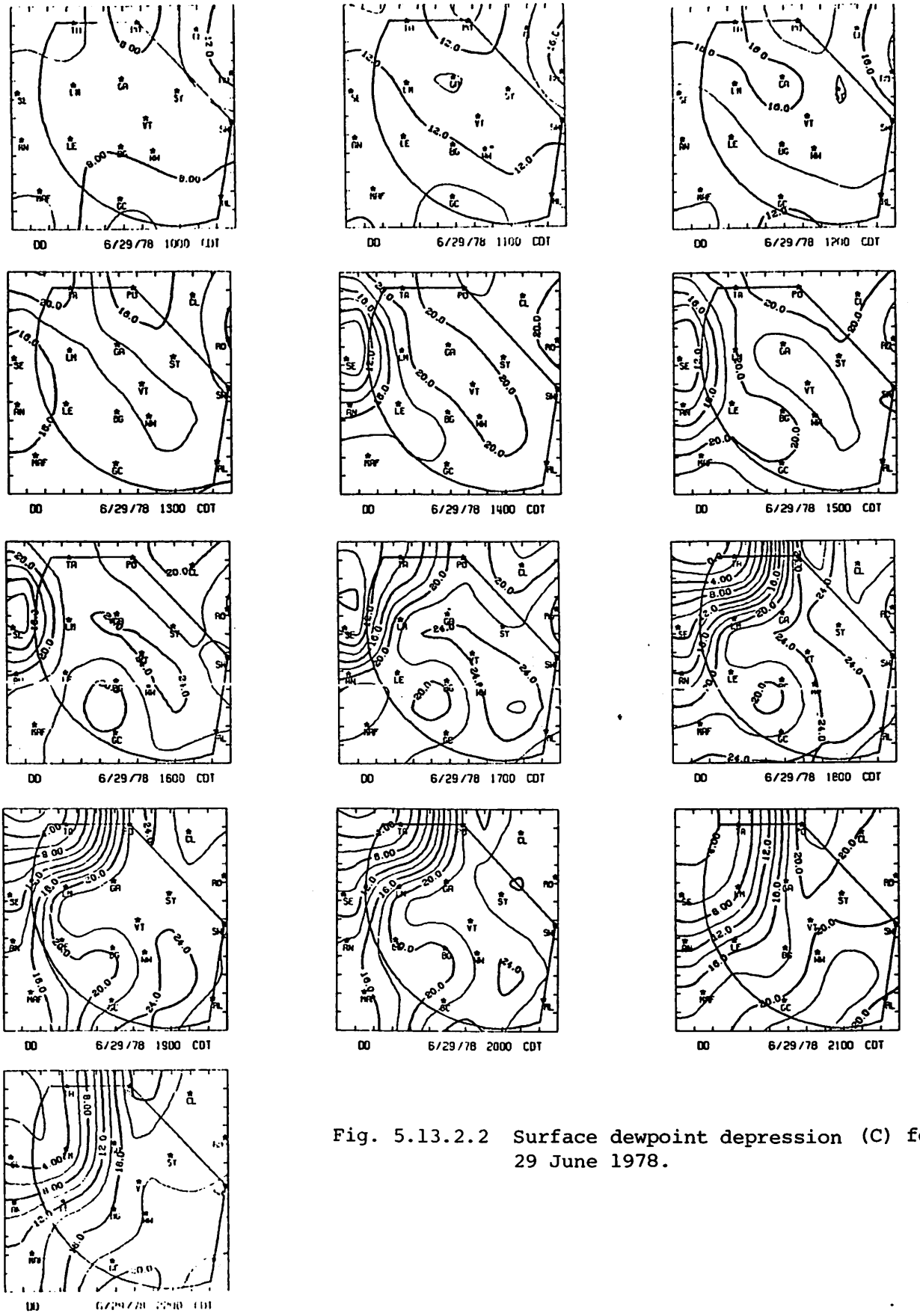

Fig. 5.13.2.2 Surface dewpoint depression (C) for 29 June 1978.

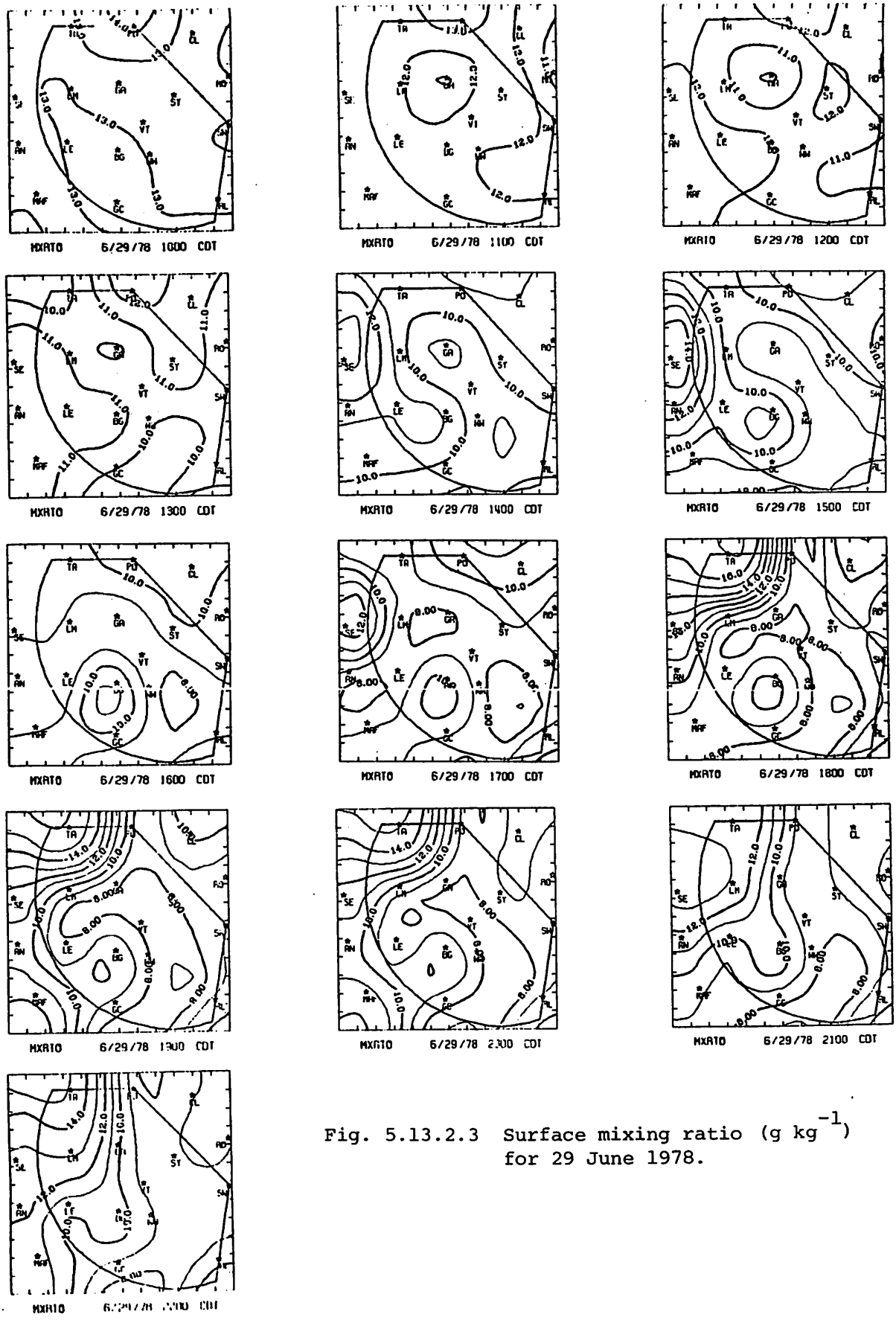

Fig. 5.13.2.3 Surface mixing ratio (g kg^{-1}) for 29 June 1978.

at Seminole and by 2300 GMT high values also were present near Tahoka. This area of maximum mixing ratio increased in size at 0200 GMT when values increased near Gail and Lamesa as a storm formed there.

Surface equivalent potential temperature (Fig. 5.13.2.4) at 1500 GMT showed a maximum in the northwest and a minimum in the southeast. At 1600 GMT a minimum began to form near Gail when mixing ratio decreased there. The potential temperature dropped at Seminole at 1900 GMT as a result of storm-induced cooling, but at 2000 GMT the potential temperature was high. This was when the large cell was passing to the north of Seminole. At 2100 GMT temperature and humidity dropped to produce low potential temperature but the temperature rose again at 2200 GMT. At that time the minimum potential temperature was at Tahoka in the vicinity of the dissipating cell. By 2300 GMT maximum potential temperatures were in the vicinity of Tahoka.

Terrain-induced vertical motion fields (Fig. 5.13.2.5) showed large negative values near Walsh-Watts throughout the day and a maximum was centered near Gail throughout the day.

Surface velocity divergence (Fig. 5.13.2.6) showed centers with moderate values at 1500 GMT. A center of convergence was located near Andrews which intensified at 1800 GMT as showers approached the HIPLEX area. The center remained strong through 2000 GMT but almost disappeared at 2100 GMT. This occurred when the strong thunderstorm cell that had been north of Seminole dissipated and the cell south of Tahoka had not yet become well organized. Also, since wind data from Seminole was missing, any strong convergence or divergence in that area may not have shown up in the field. At 2200 GMT strong convergence was again present and associated with the storm cell near Tahoka. Convergence also was present near Midland at this time. At 0200 GMT strong convergence was present near Lenorah where a thunderstorm cell had formed. This center remained there through 0300 GMT.

Vertical motion 50 mb above the surface is shown in Fig. 5.13.2.7. Upward motion was present through the center of the area with downward motion near both Andrews and Clairemont at 1500 GMT. The center of upward motion was strong at 1800 GMT as showers began to move into the west. At 2200 GMT the upward motion was strongest near Tahoka associated with the cell that formed near there in the preceding hour. At 0200 GMT the center of upward motion shifted southward to near Lenorah and showed upward motions associated with the cell that formed there at that time.

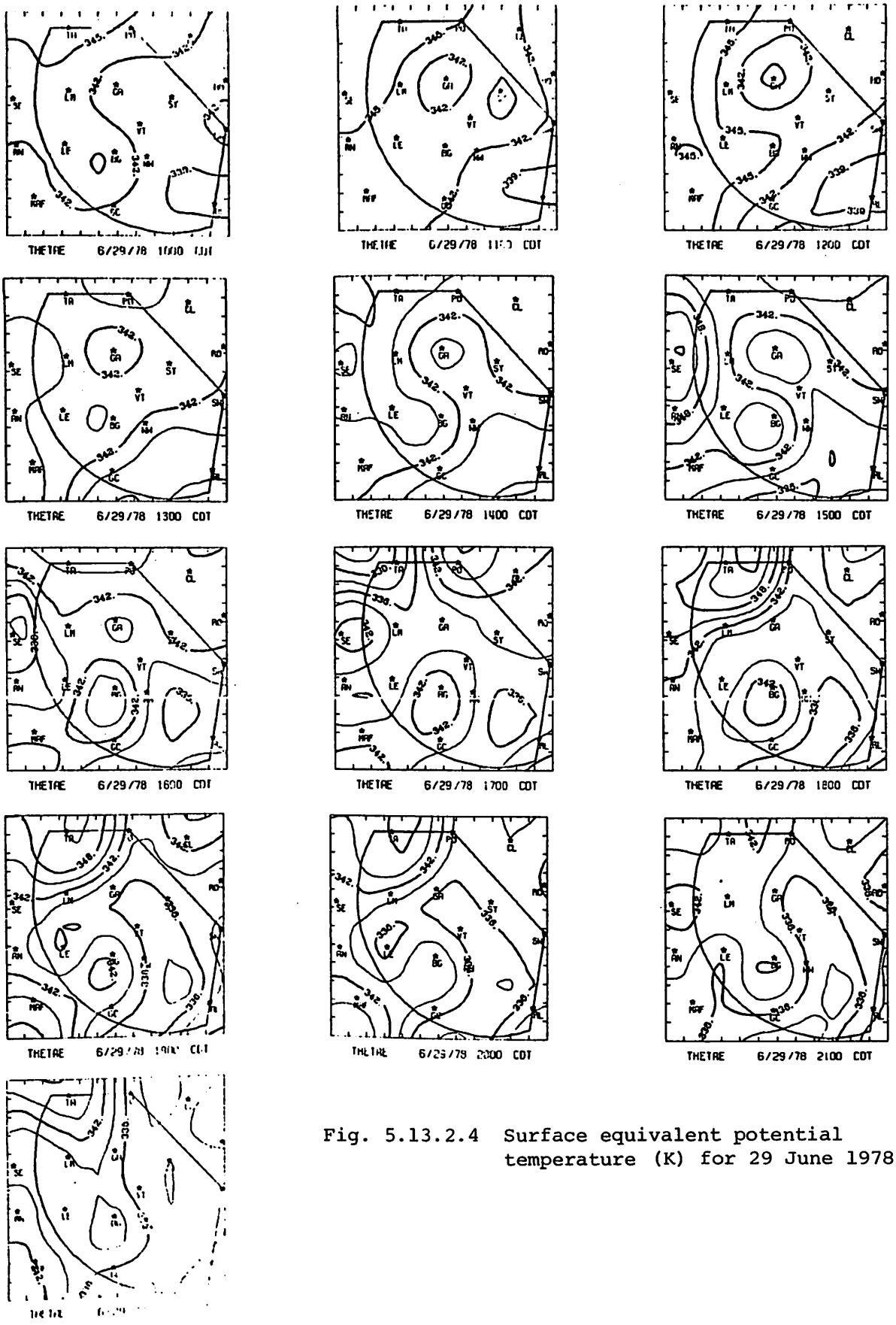

Fig. 5.13.2.4 Surface equivalent potential temperature (K) for 29 June 1978.

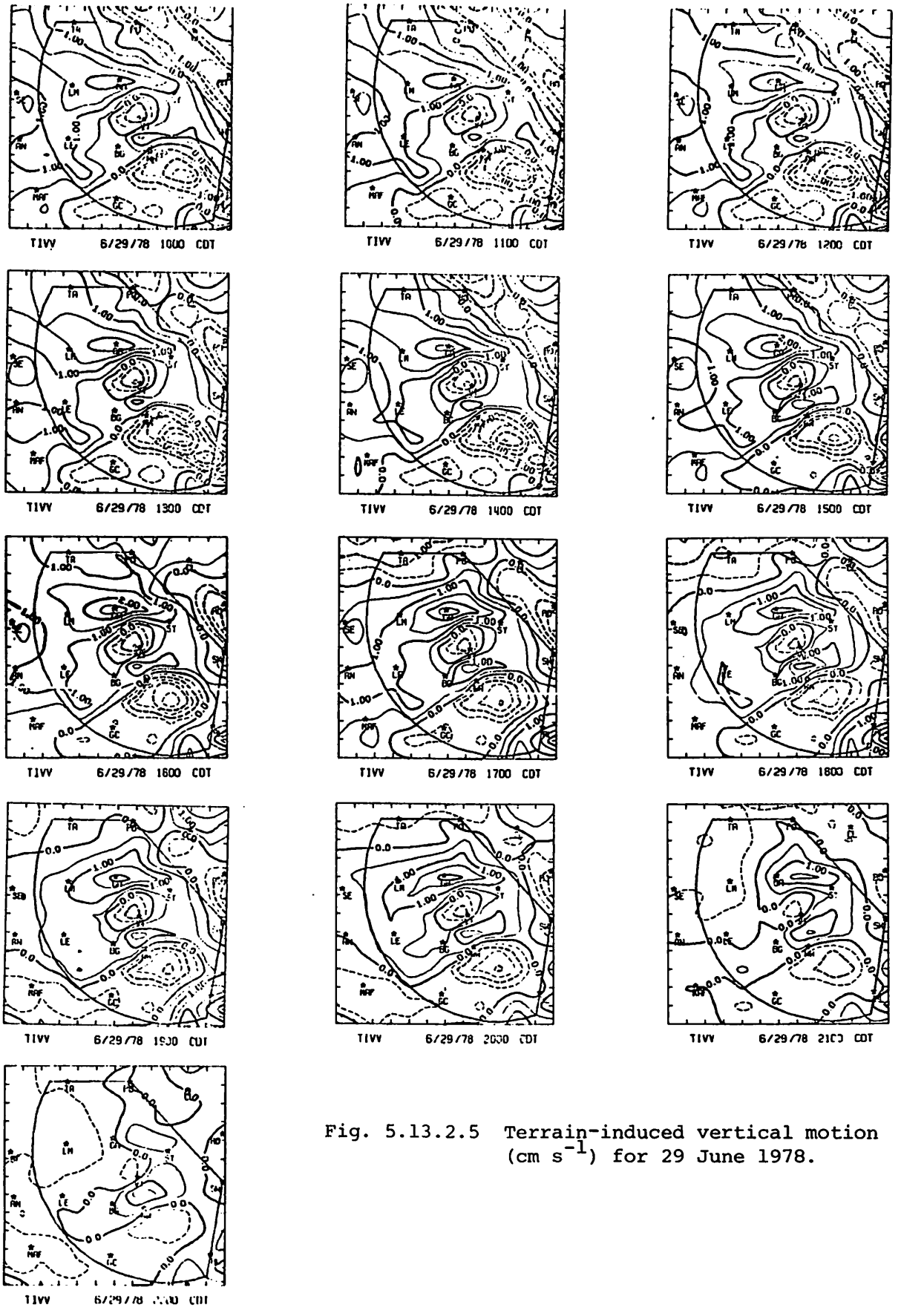

Fig. 5.13.2.5 Terrain-induced vertical motion (cm s^{-1}) for 29 June 1978.

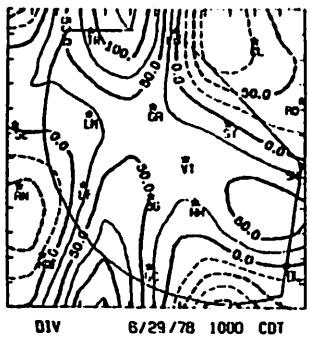

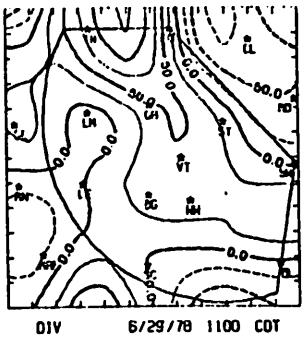

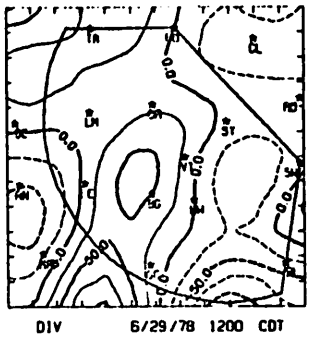

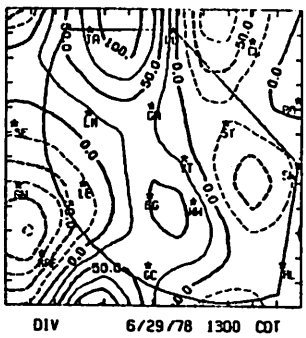

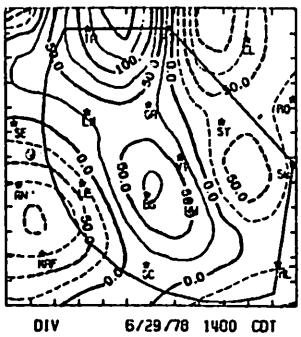

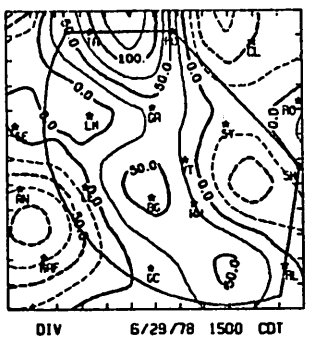

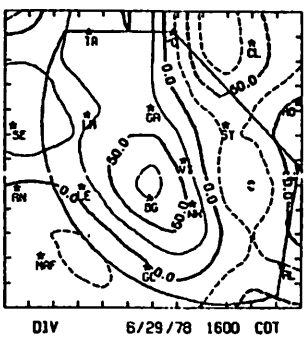

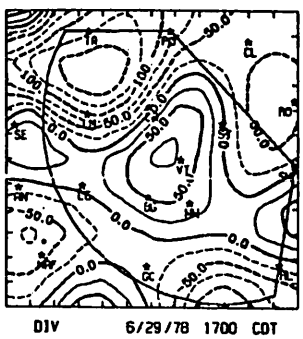

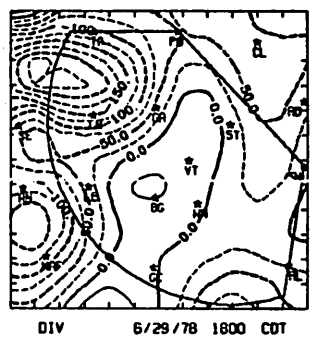

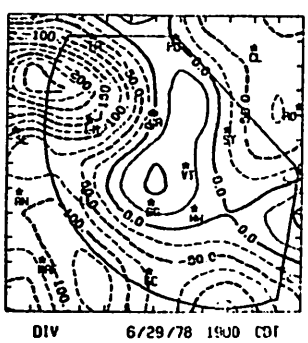

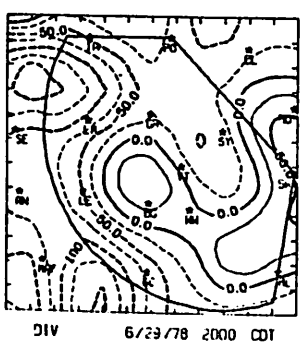

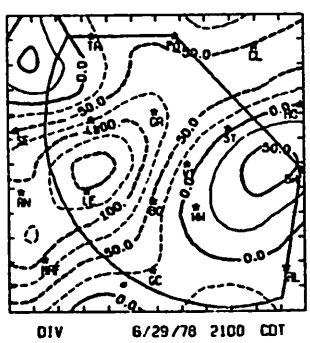

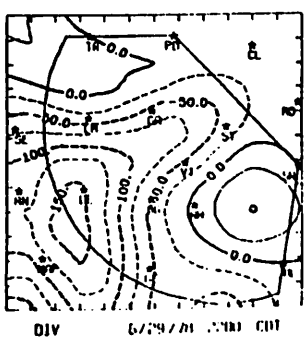

Fig. 5.13.2.6 Surface velocity divergence (s^{-1} x 10^{-6}) for 29 June 1978.

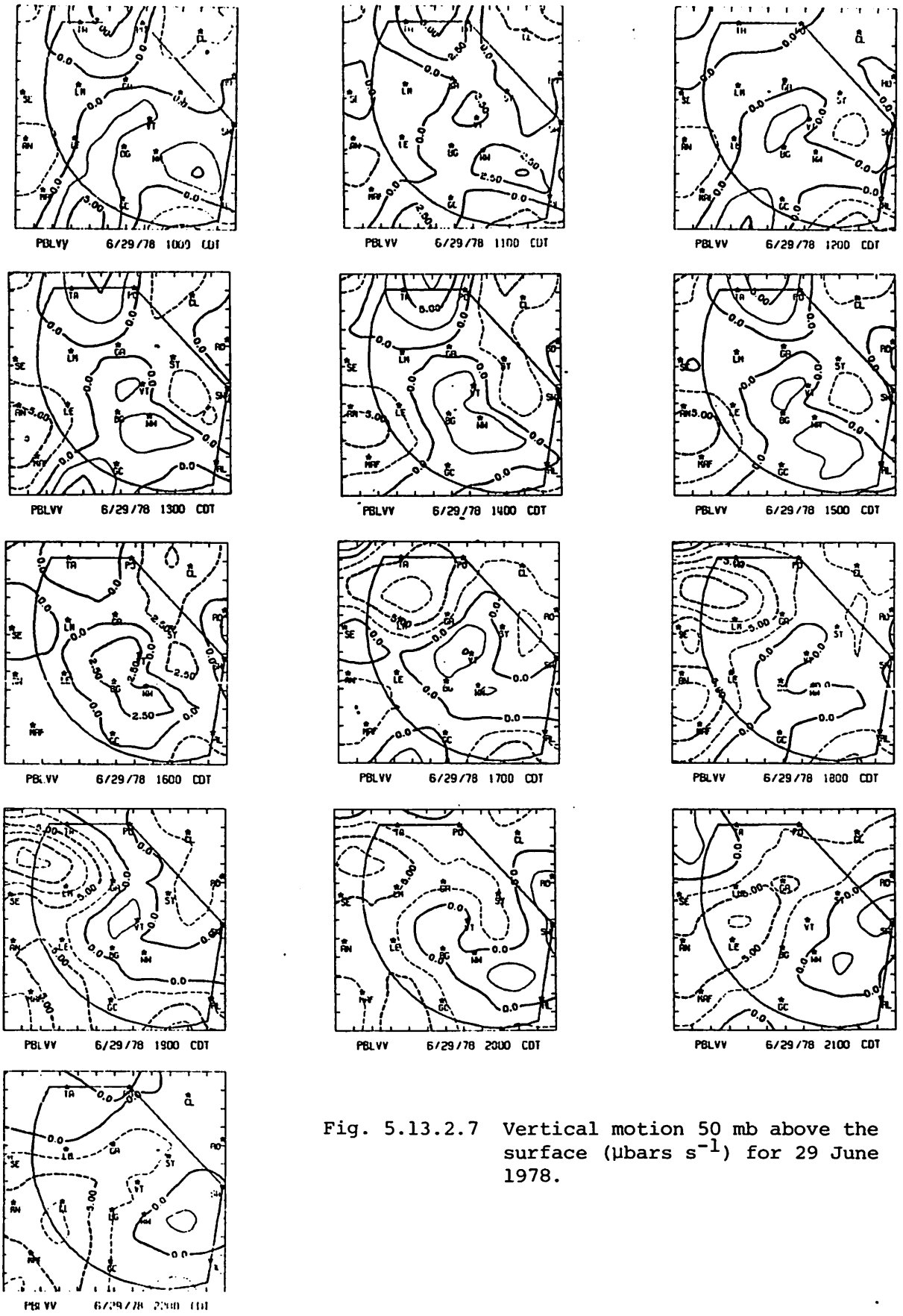

Fig. 5.13.2.7 Vertical motion 50 mb above the surface (μbars s^{-1}) for 29 June 1978.

Figure 5.13.2.8 shows surface moisture divergence. Moderate to strong divergence was present across the central part of the area with moisture convergence near Clairemont at 1500 GMT. A center of moisture convergence also was near Andrews. At 2200 GMT strong moisture convergence was present between Tahoka and Lamesa which persisted through 0100 GMT. At 0200 GMT the center of convergence was between Lenorah and Lamesa in association with the storm that formed there at that hour. The strong values persisted through 0300 GMT.

Plots of vertical flux of moisture 50 mb above the surface (Fig. 5.13.2.9) showed moderately strong upward flux of moisture near Andrews through 2000 GMT. Downward flux was primarily near Tahoka and Big Spring during that time period. At 2200 GMT strong upward flux began building between Tahoka and Lamesa. This center of upward flux of moisture remained until 0200 GMT. Maximum upward vertical flux of moisture was located near Lenorah after 0200 GMT when a storm cell formed in that area.

Surface vorticity (Fig. 5.13.2.10) showed fairly high values through the day. A center of negative vorticity remained southwest of Post until 2100 GMT, and positive vorticity centers were near Seminole and south of Walsh-Watts through most of that time period. Patterns of vorticity shifted after 2100 GMT when a new cell was forming north of Lamesa. Positive vorticity centers stayed near Andrews, Garden City, and Tahoka while negative vorticity persisted near Lamesa. Another large change in the vorticity pattern occurred at 0200 GMT when a storm cell built up north of Lenorah, leaving positive vorticity near Lenorah and negative vorticity near Clairemont.

Surface pressure changes (Fig. 5.13.2.11) were generally small. There were no large pressure rises through the day and the largest pressure drops were only 1 mb at 1900 GMT and 2000 GMT.

Surface winds (Fig. 5.13.2.12) were mostly from the south and southeast at 1500 GMT. Wind data from Seminole were missing, so any effects of the cell at 2100 GMT would not show up well. At 2200 GMT, however, a wind shift occurred at Tahoka with west winds in that part of the area. The winds shifted to southerly near Tahoka at 0000 GMT, and southwest winds were present near Midland at that time. By 0300 GMT the winds in the northwest were again from the northwest, with southwest winds in the southwest and south winds in the east.

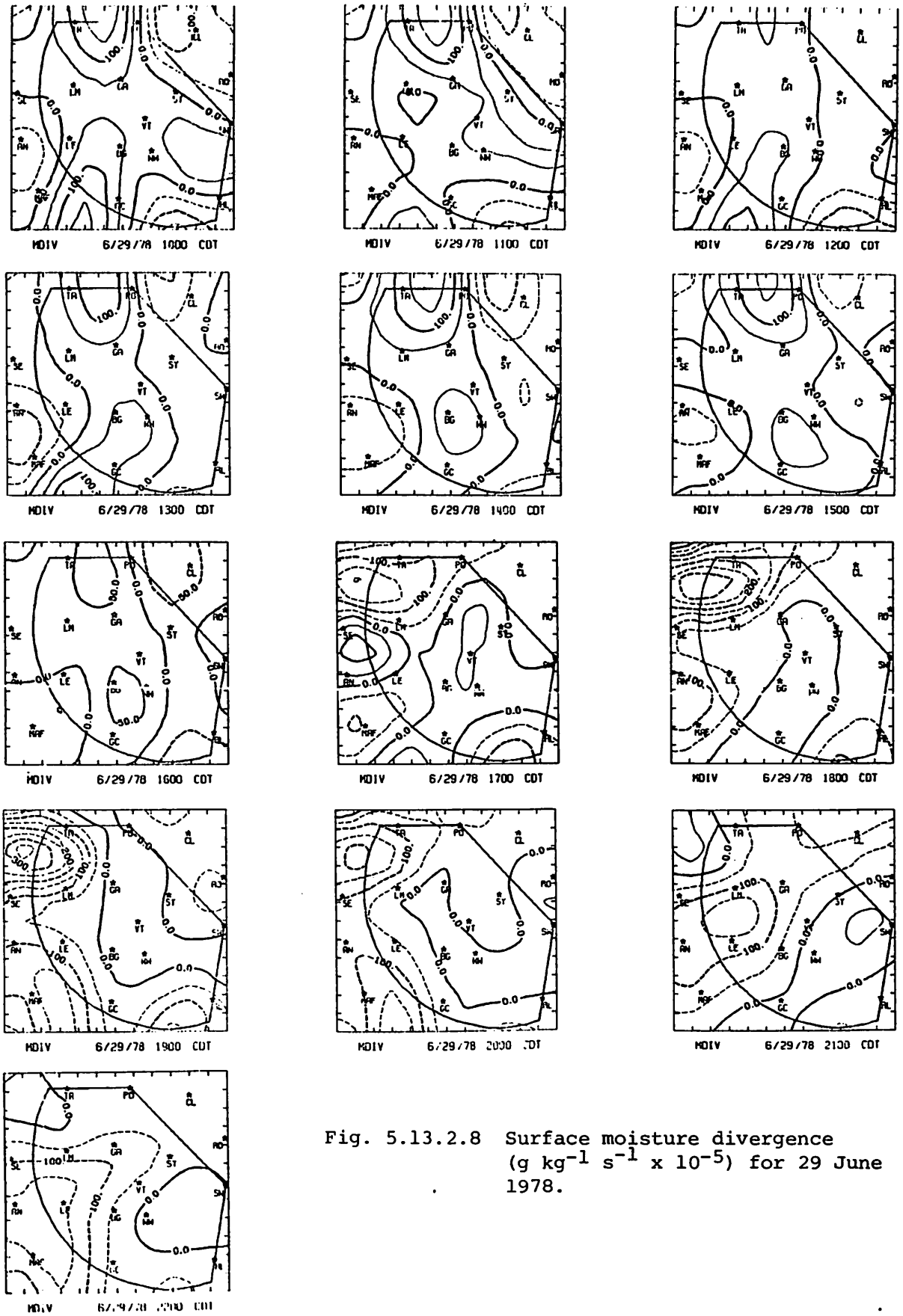

Fig. 5.13.2.8 Surface moisture divergence ($g\ kg^{-1}\ s^{-1} \times 10^{-5}$) for 29 June 1978.

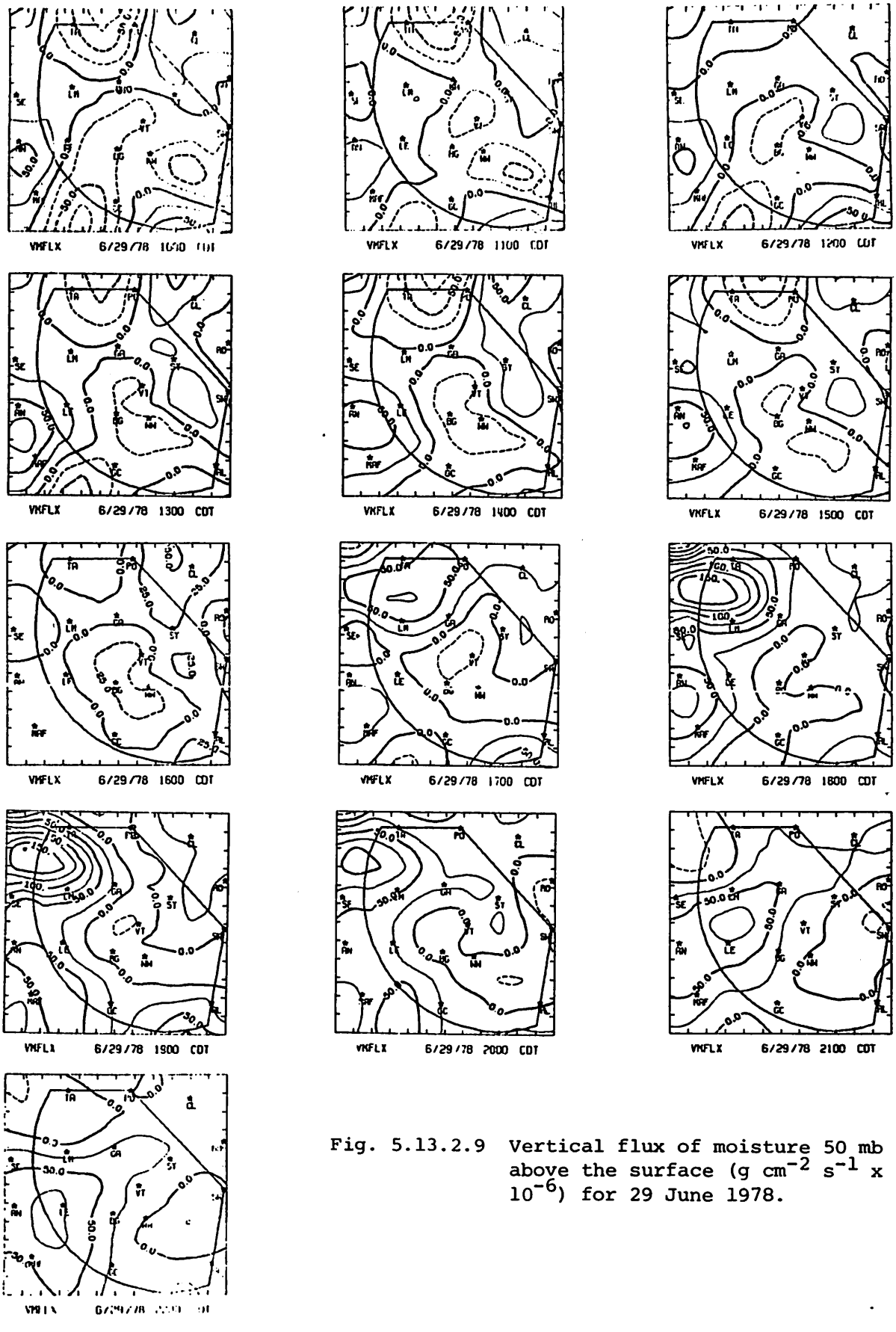

Fig. 5.13.2.9 Vertical flux of moisture 50 mb above the surface (g cm^{-2} s^{-1} x 10^{-6}) for 29 June 1978.

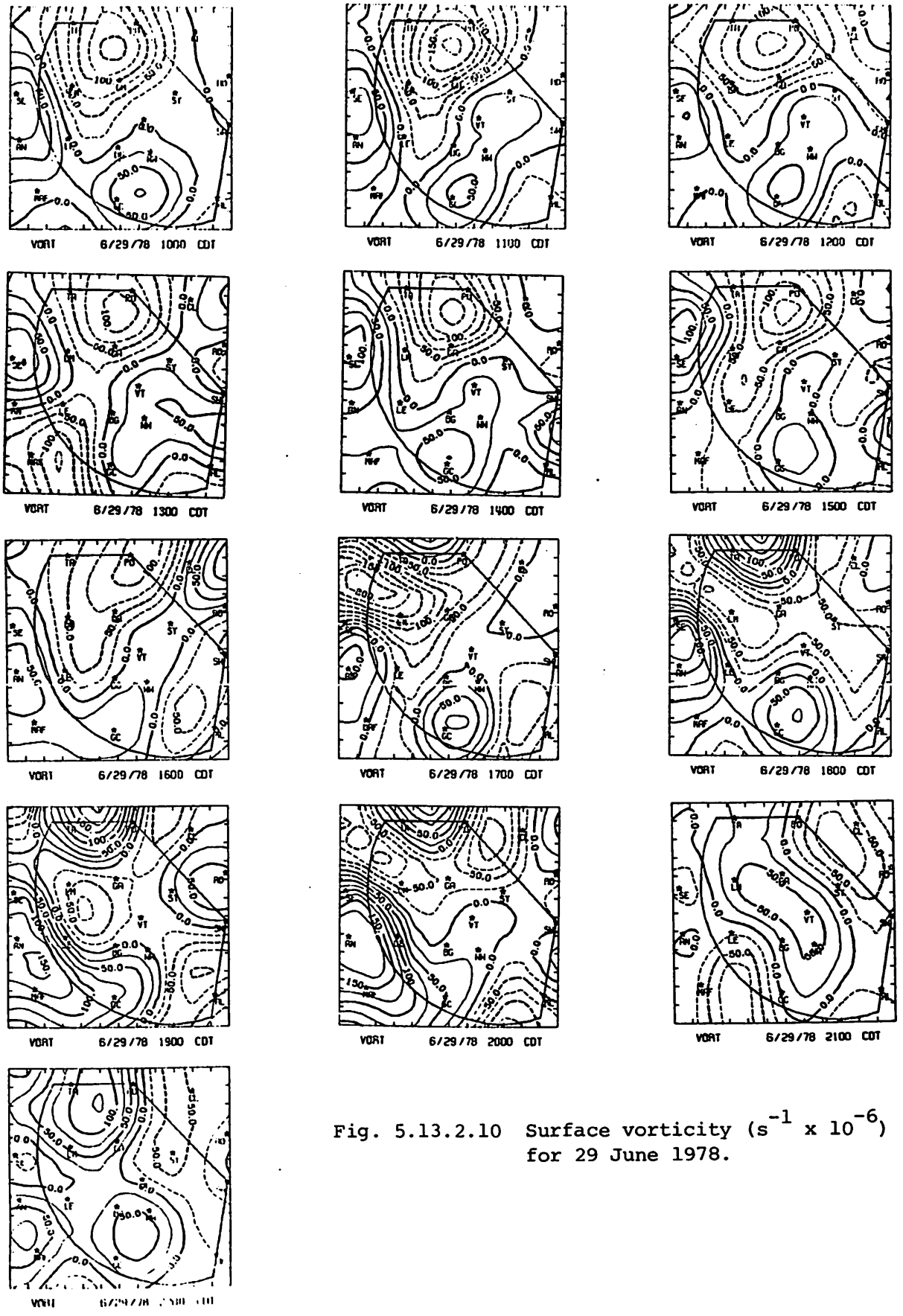

Fig. 5.13.2.10 Surface vorticity ($s^{-1} \times 10^{-6}$) for 29 June 1978.

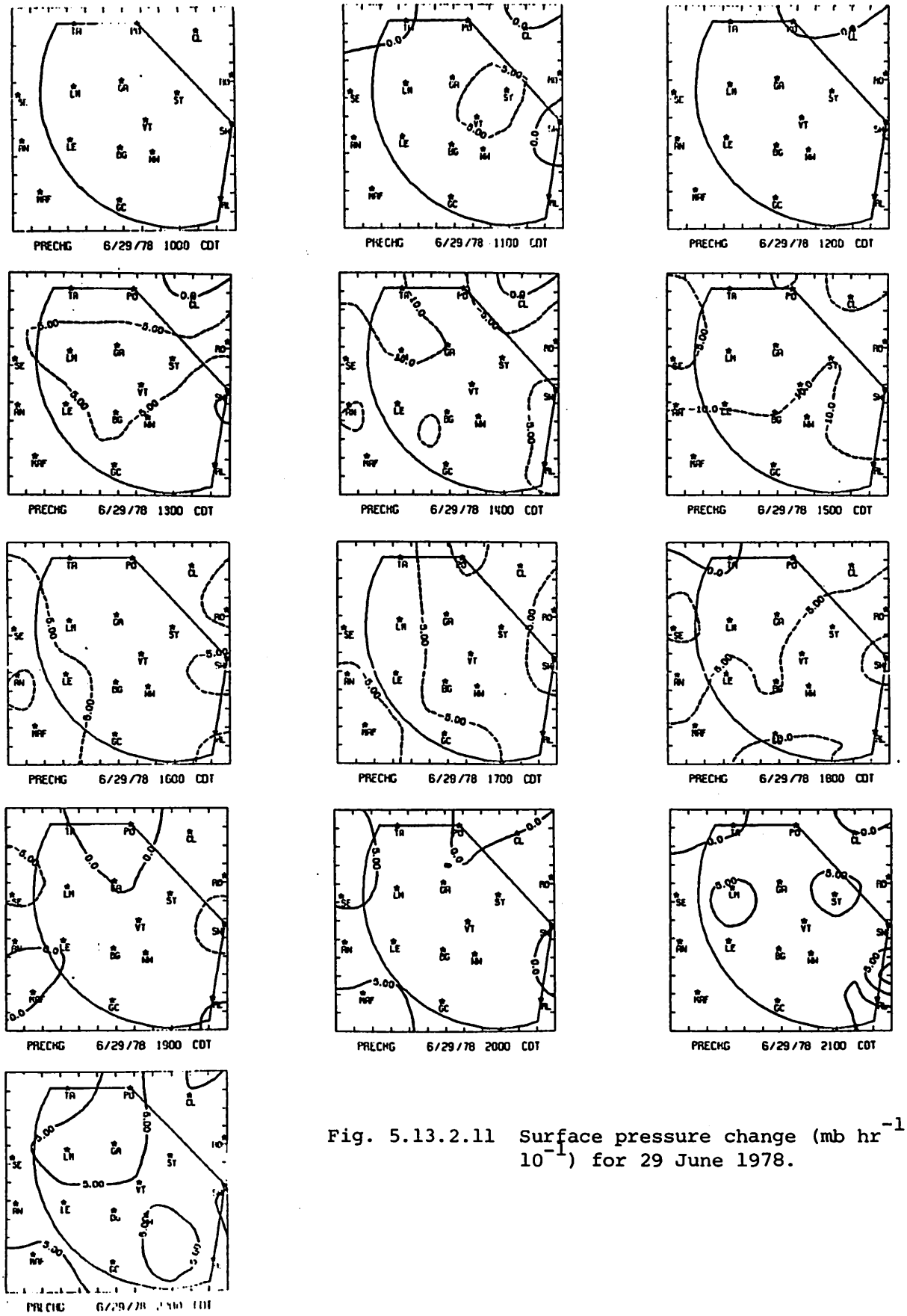

Fig. 5.13.2.11 Surface pressure change (mb hr^{-1} x 10^{-1}) for 29 June 1978.

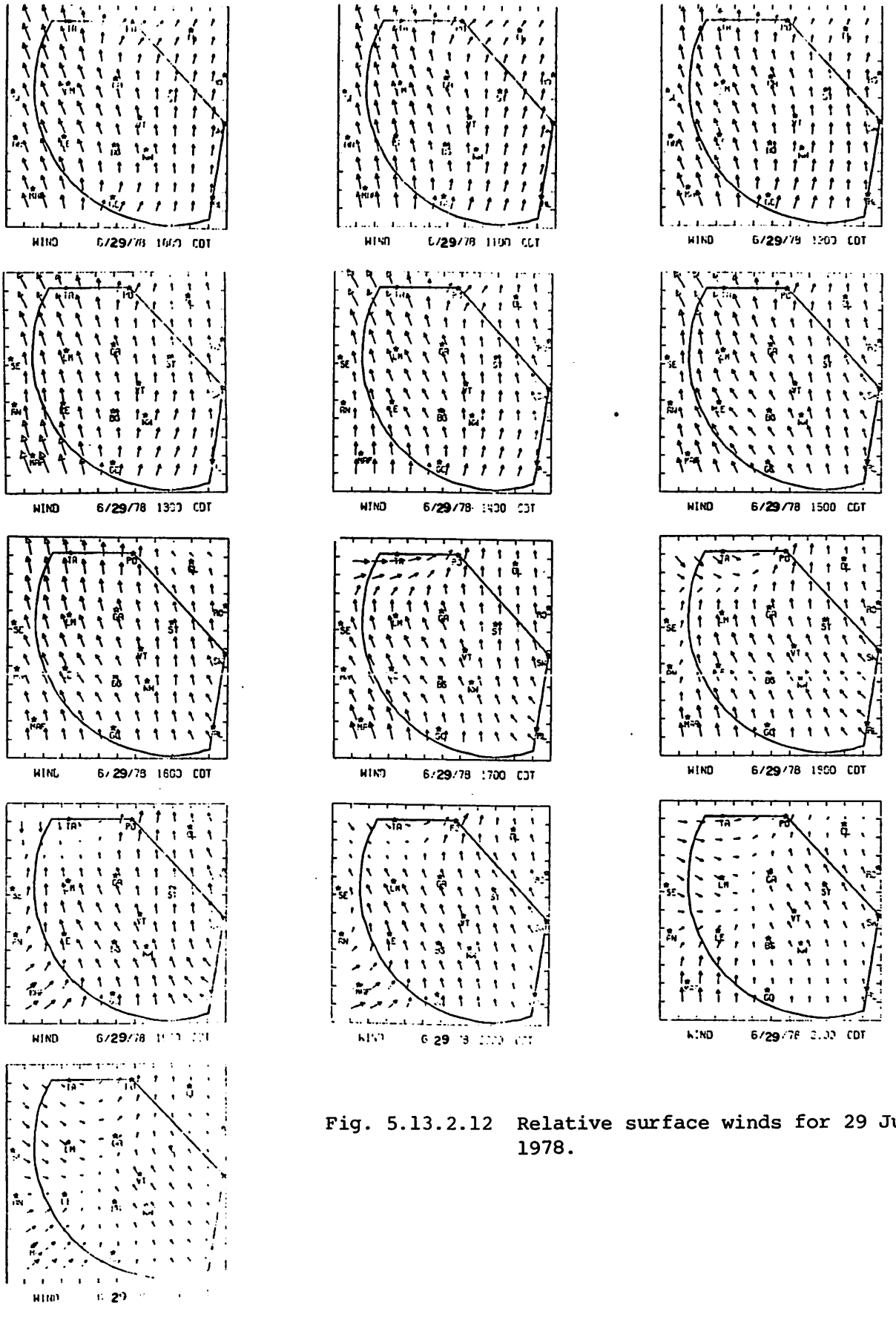

Fig. 5.13.2.12 Relative surface winds for 29 June 1978.

5.13.3 Upper Level Kinematic Parameters

Profiles of mass divergence (Fig. 5.13.3.1) show that, at 2100 GMT, convergence was present at almost all levels. Strong convergence was present near the surface and a layer of weak divergence was present near 500 mb. At 0000 GMT convergence was still present in the lowest layer. Most of the profile, however, showed weak divergence at a time when light shower activity was present. By 0300 GMT the low level convergence extended to 750 mb but the divergence above this layer was stronger that at 0000 GMT.

Vertical motions (Fig. 5.13.3.2) were predominantly upward at 2100 and 0000 GMT, with maximum vertical motions at 2100 GMT. At 0300 GMT, however, upward vertical motions were only present in layers below 600 mb with downward motion in layers above that level.

Profiles of moisture divergence (Fig. 5.13.3.3) showed strong convergence in the lower layers at 2100 GMT as shower activity was forming in the northwest part of the area. Weak moisture convergence also was present near 650 mb at that time. At 0000 GMT divergence was present at all levels above 850 mb. At 0300 GMT the layer of low level moisture convergence extended to 800 mb and moisture divergence above that layer was stronger that at 0000 GMT.

5.13.4 Energetics

Figure 5.13.4.1 shows profiles of the horizontal flux of latent heat energy. At 2100 GMT there was latent heat inflow in most layers. This inflow was particulatly strong in low levels. By 0000 GMT the low-level inflow had decreased and outflow of latent heat began to take place above 850 mb. This was when shower activity over the area was light. At 0200 GMT a new storm cell formed over the HIPLEX area but it had already begun to decrease at 0300 GMT. Low-level inflow of latent heat extended to 850 mb with strong outflow near 650 mb at 0300 GMT.

Profiles of vertical flux of latent heat (Fig. 5.13.4.2) show outflow in low levels and inflow in middle levels. The largest inflow at 2100 GMT was between 500 and 550 mb. At 0000 GMT inflow was moderate at most levels between 800 and 500 mb. At 0300 GMT the flow out of the lower levels was not as strong as at earlier hours but the inflow near 650 mb was rather strong.

The local change of latent heat energy (Fig. 5.13.4.3) was negative at 2100 and 0000 GMT, although the value was near zero at the latter time. At 0300 GMT the local change of latent heat was positive in layers with

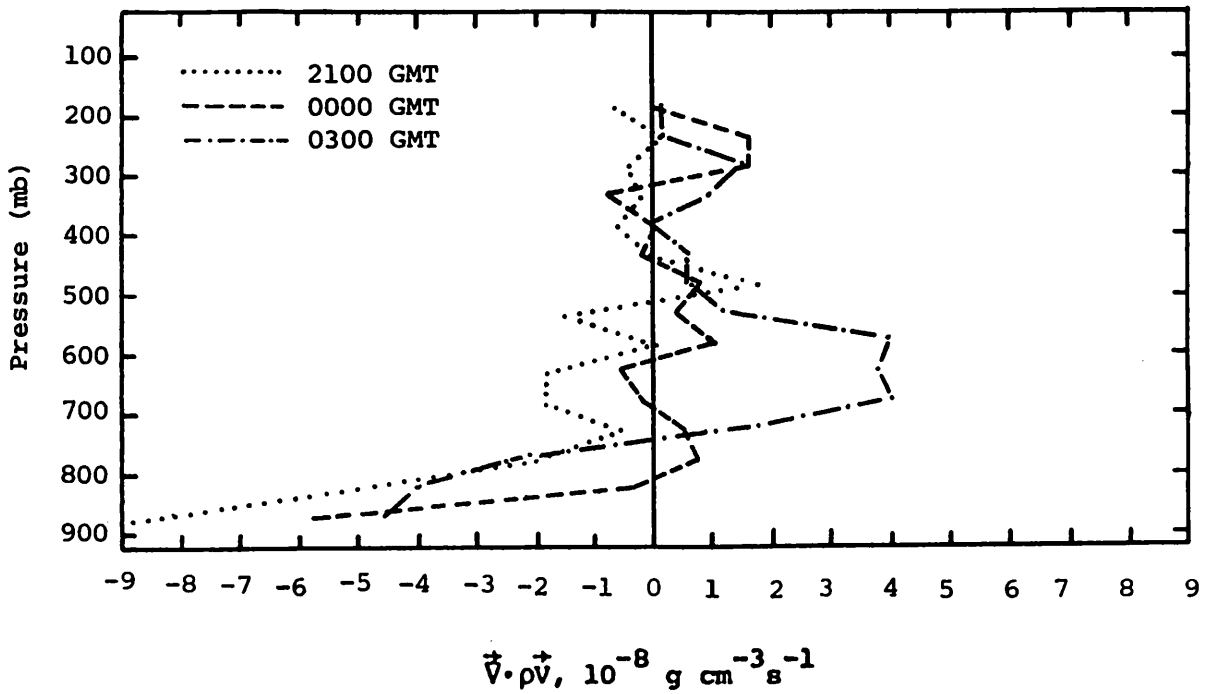

Fig. 5.13.3.1 Vertical profiles of mass divergence on 29 June 1978.

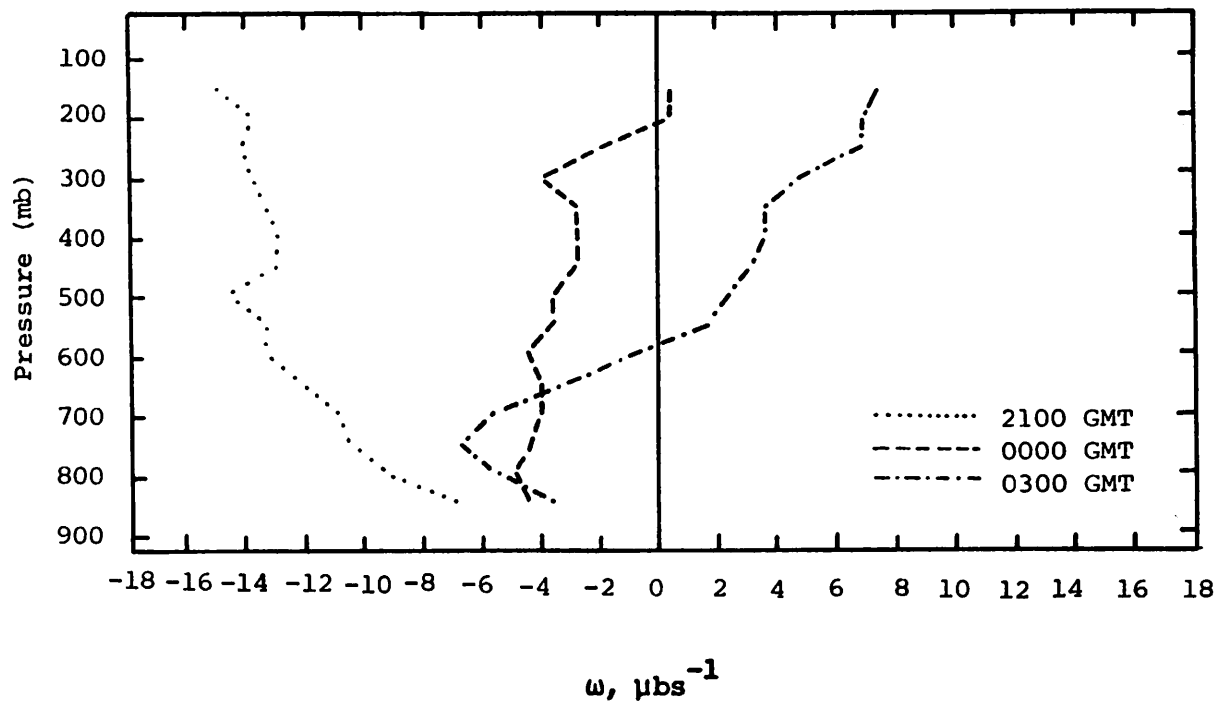

Fig. 5.13.3.2 Vertical profiles of vertical motion on 29 June 1978.

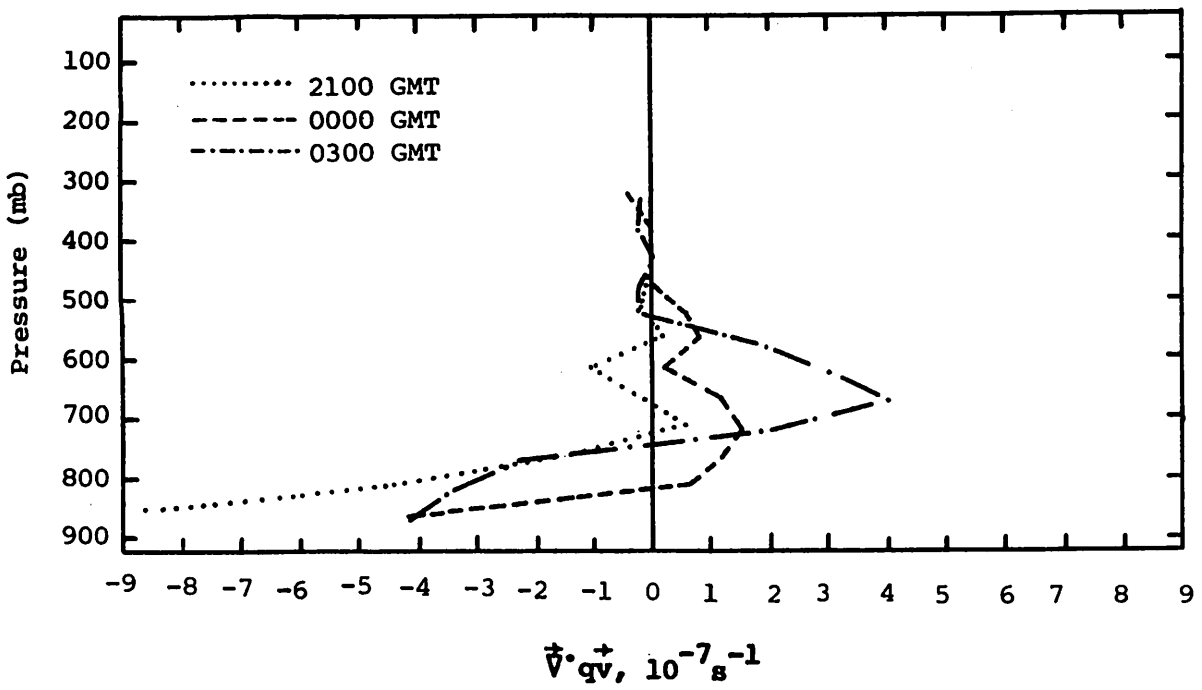

Fig. 5.13.3.3 Vertical profiles of moisture divergence on 29 June 1978.

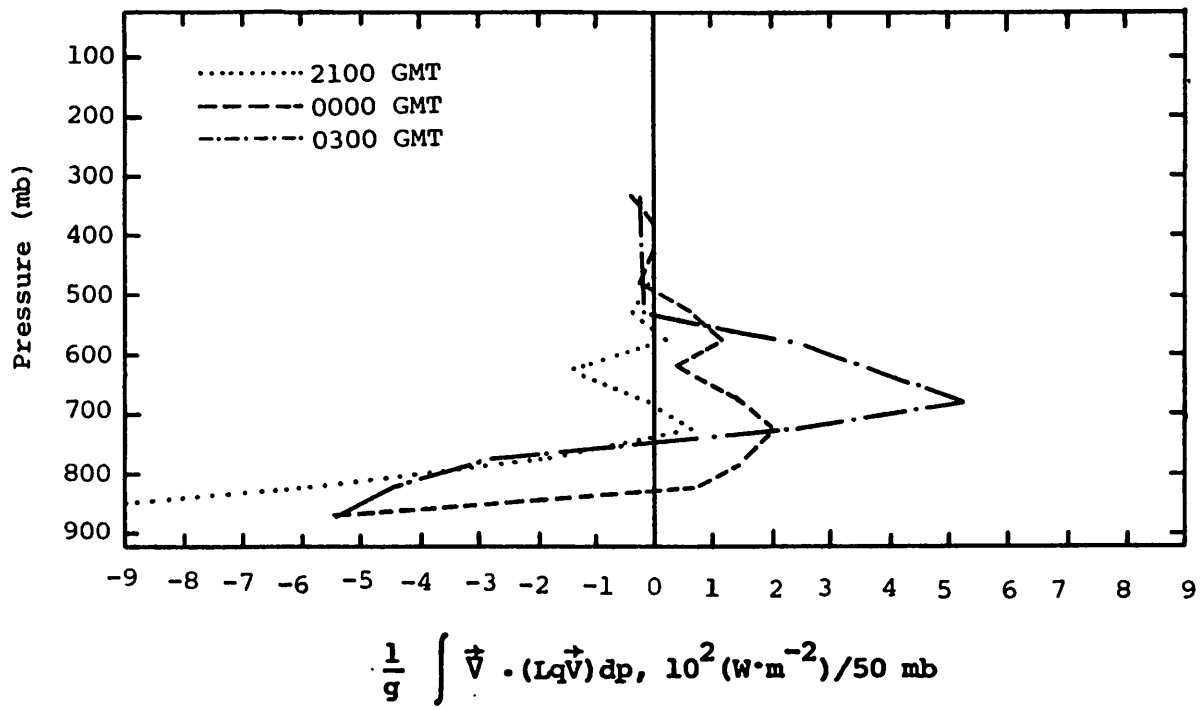

Fig. 5.13.4.1 Vertical profiles of the horizontal flux of latent heat energy on 29 June 1978.

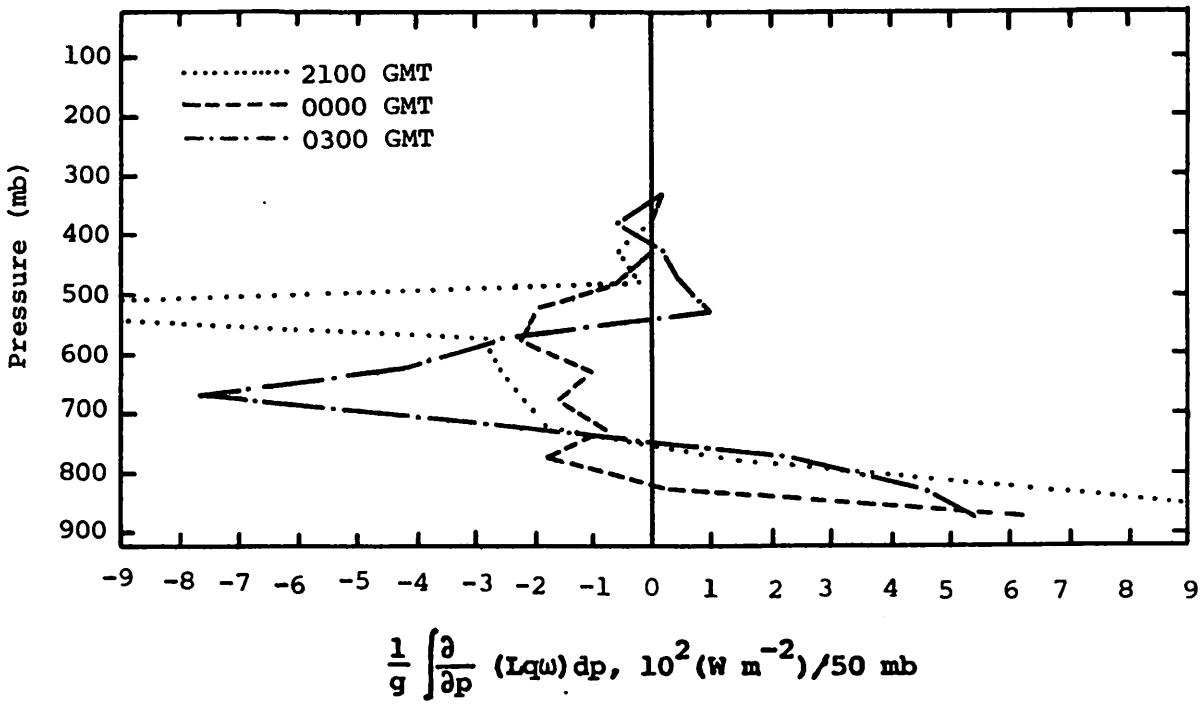

Fig. 5.13.4.2 Vertical profiles of the vertical flux of latent heat energy on 29 June 1978.

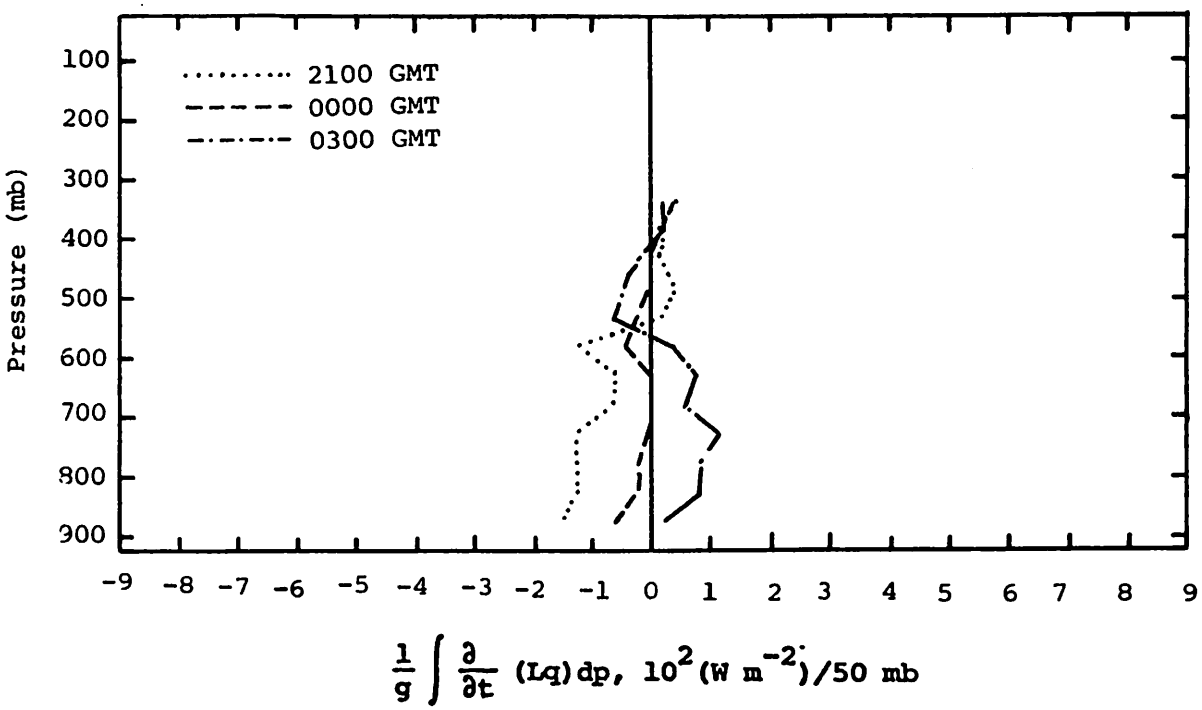

Fig. 5.13.4.3 Vertical profiles of the local change of latent heat energy on 29 June 1978.

negative values only above 500 mb.

The residual of the latent heat energy equation (Fig. 5.13.4.4) shows large positive values at 2100 GMT. This was when a strong storm was just forming in the northwest corner of the area. The positive values were due to condensation. At 0000 GMT negative values were present below 700 mb with mostly positive or near zero values above. The 0300 GMT profile also shows negative values in low levels. These values could have resulted from evaporation at those levels.

Figure 5.13.4.5 shows profiles of diabatic heating. Large positive values were present in the 2100 GMT profile. Below 600 mb these values fit well with the residual of the latent heat energy equation (Fig. 5.13.4.4) and resulted from heat released by condensation. At 0000 GMT the values are somewhat smaller, and some of the heating at this time could have been from other diabatic sources. The negative values above 650 mb may have resulted from evaporative cooling.

Profiles of the horizontal flux of kinetic energy show mostly weak inflow of kinetic energy (Fig. 5.13.4.6) at 2100 GMT. By 0000 GMT there was slight outflow near the surface and around 600 mb, and strong outflow near 200 mb. At 0300 GMT the upper-level outflow had decreased in strength and there was slight inflow in the lowest layers.

Figure 5.13.4.7 shows profiles of vertical flux of kinetic energy. At 2100 GMT there was flux of kinetic energy out of the lowest layer into middle layers. Another layer with outward flux was located between 400 and 200 mb. Kinetic energy was transferred out of this layer into higher layers. The 0000 GMT profile was similar to the 2100 GMT profile except that values of the flux were generally higher. The flux of kinetic energy was still out of lower layers and into middle layers. There also was transport of kinetic energy out of the layer near 350 mb into the layer just above. At 0300 GMT the situation was different since vertical motion was downward above 600 mb. Kinetic energy was transported out of the lower layers and upper layers and into middle layers. Values were moderate.

5.13.5 Water Vapor Budget

Figure 5.13.5.1 shows the net horizontal transport of water vapor. At 2100 GMT there were gains in water vapor in the lowest layer and above 650 mb. At 0000 GMT the profile was similar except there was an additional layer of

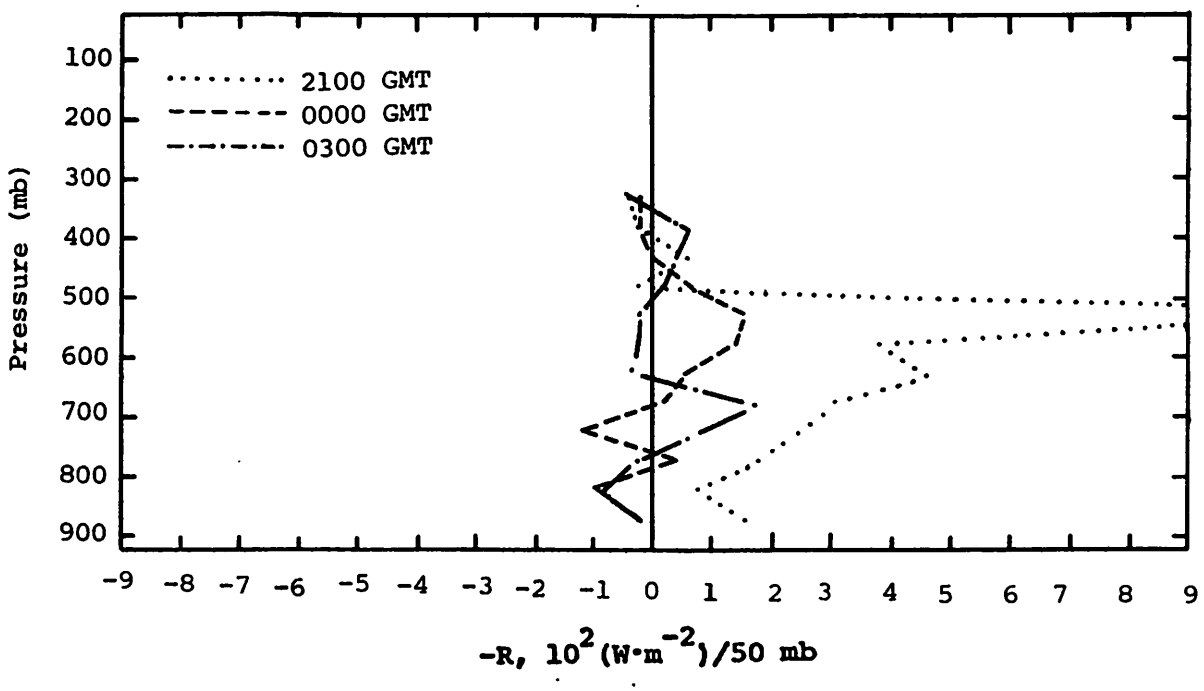

Fig. 5.13.4.4 Vertical profiles of the residual of the latent heat energy equation on 29 June 1978.

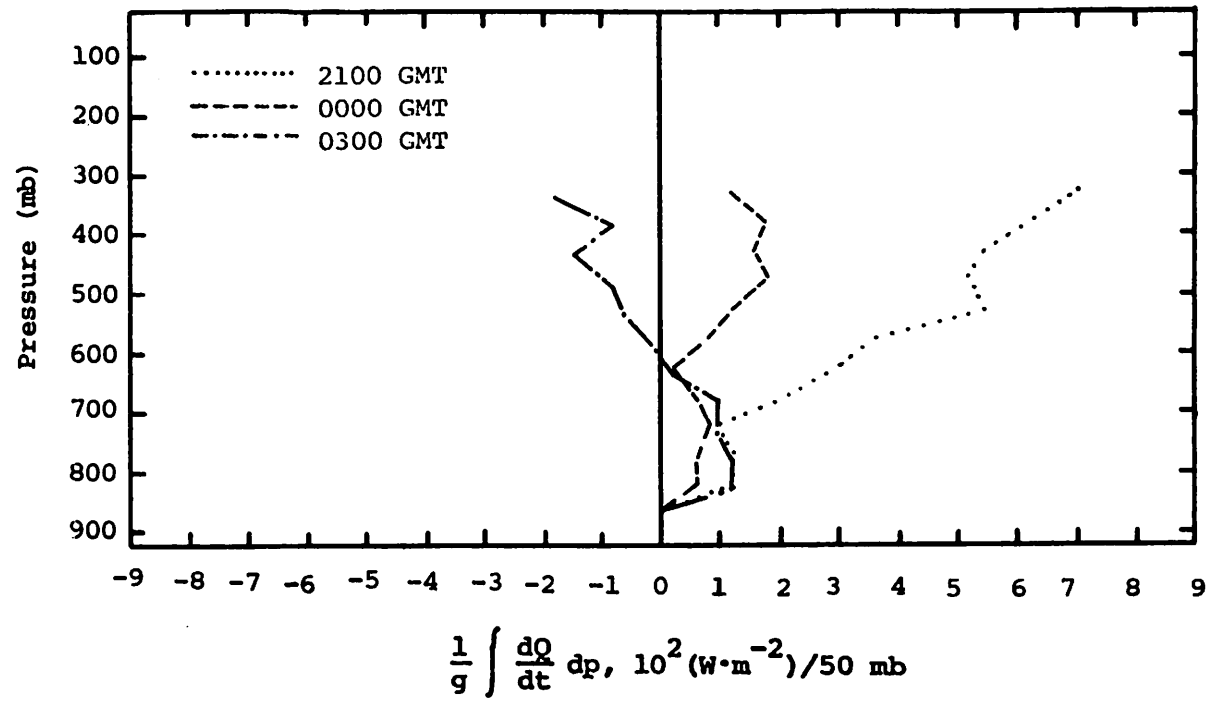

Fig. 5.13.4.5 Vertical profiles of diabatic heating computed from the first law of thermodynamics on 29 June 1978.

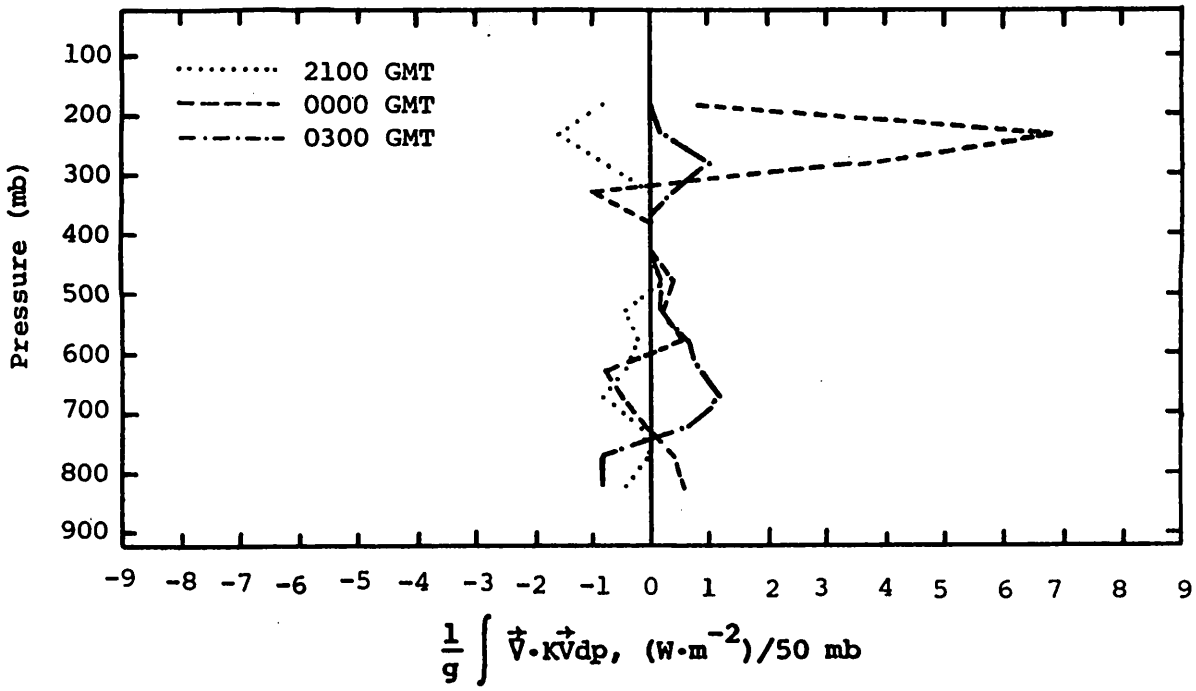

Fig. 5.13.4.6 Vertical profiles of the horizontal flux of kinetic energy on 29 June 1978.

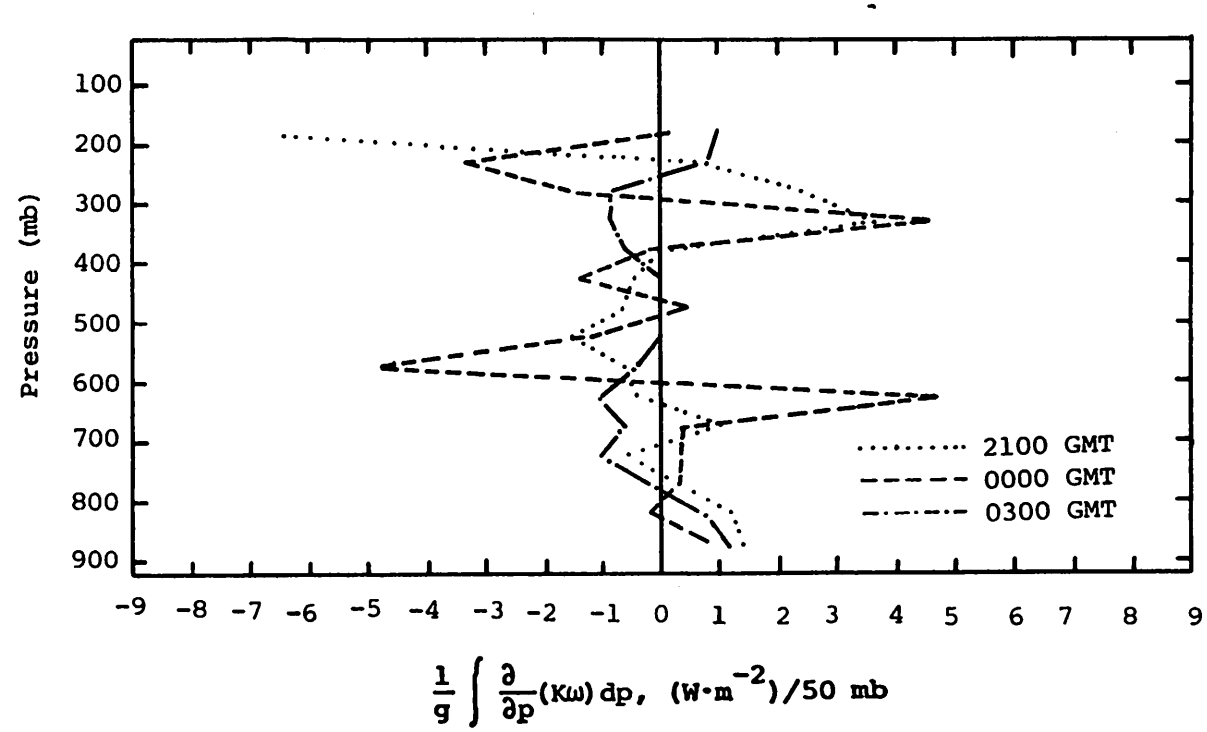

Fig. 5.13.4.7 Vertical profiles of the vertical flux of kinetic energy on 29 June 1978.

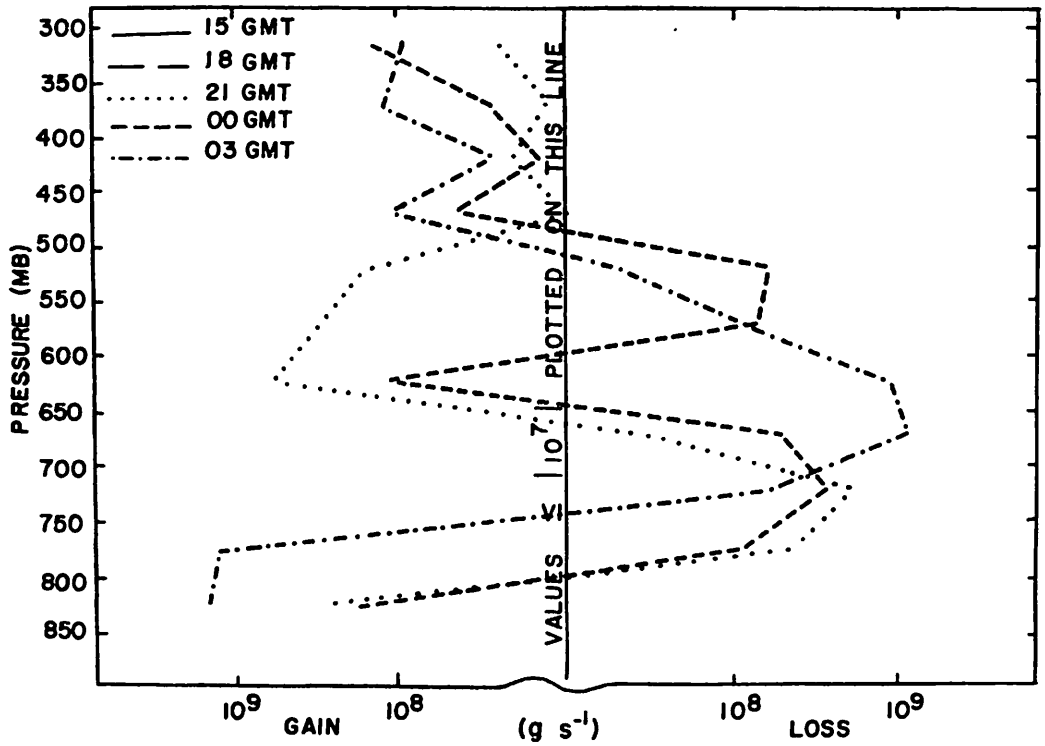

Fig. 5.13.5.1 Net horizontal transport of water vapor through boundaries of 50-mb layers (g s^{-1}) over the Texas HIPLEX area for 29 June 1978.

water vapor loss between 600 and 500 mb. At 0300 GMT the layer of water vapor losses through horizontal transport was fairly deep (from 750 mb to 500 mb). The inflow in the lowest layers is much larger than at the other times, however.

Profiles of net vertical transport of water vapor (Fig. 5.13.5.2) show gains in most layers. At 2100 GMT when a strong cell was forming in the northwest there were losses in the lowest layers and near 350 mb. By 0000 GMT there were gains in all layers below 400 mb. At 0300 GMT the losses resumed in the lowest layer when another storm cell was present over the area. There also was a layer of losses between 550 and 450 mb where transport was downward into middle layers.

Figure 5.13.5.3 shows vertical transport of water vapor through constant pressure surfaces. Transport was upward at 2100 and 0000 GMT at all levels. At 0300 GMT there was downward transport of water vapor above 600 mb. The upward transport was largest at 2100 GMT as a strong storm cell formed in the northwest.

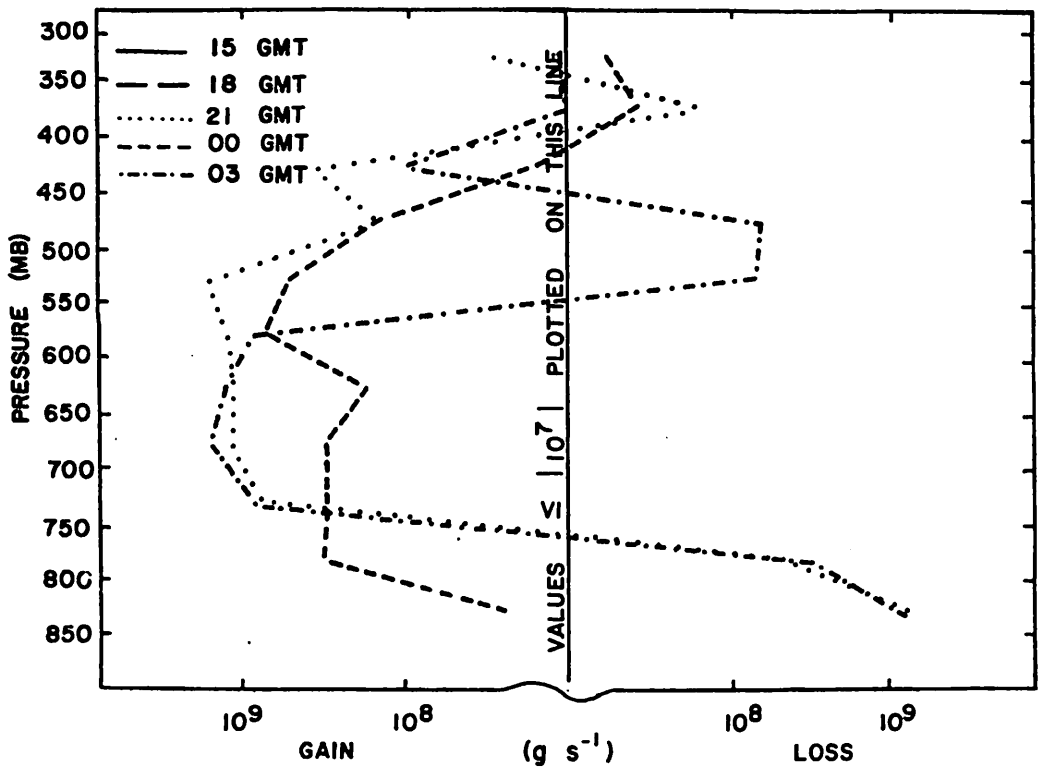

Fig. 5.13.5.2 Net vertical transport of water vapor through boundaries of 50-mb layers (gm s^{-1}) over the Texas HIPLEX area for 29 June 1978.

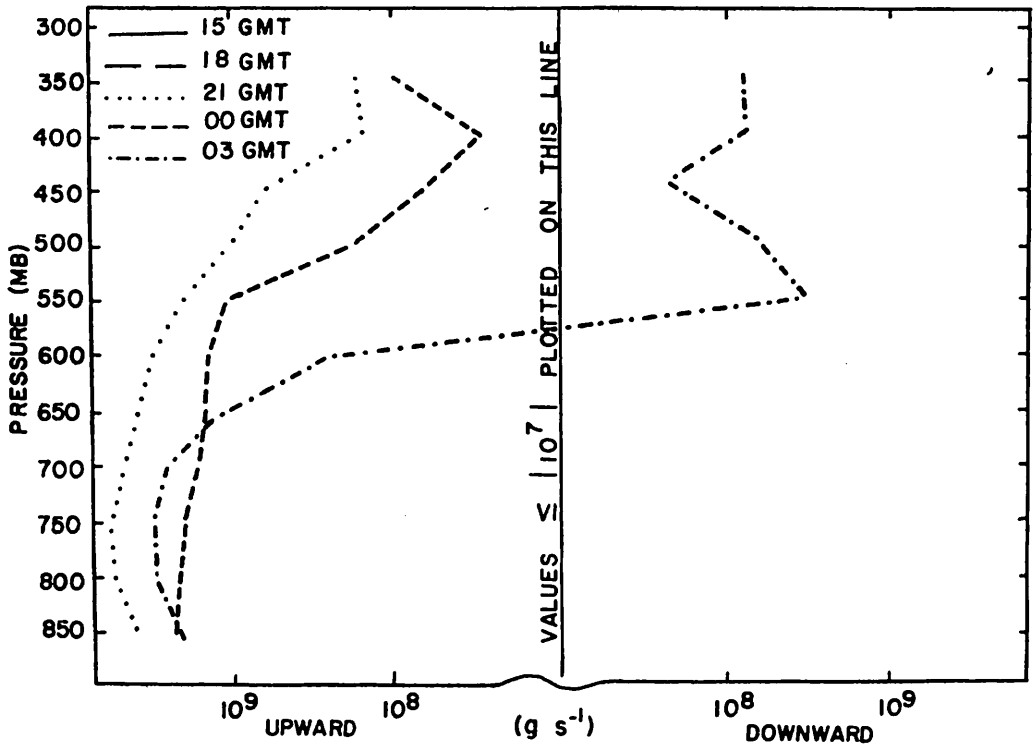

Fig. 5.13.5.3 Vertical transport of water vapor through constant pressure surfaces (gm s^{-1}) over the Texas HIPLEX area for 29 June 1978.

The profiles of combined net horizontal and vertical transport (Fig. 5.13.5.4) show gains in nearly all layers for the time periods shown. At 2100 GMT there were losses below 750 mb and near 350 mb. The 0300 GMT profile had losses only between 550 and 450 mb.

Profiles of total mass of water vapor (Fig. 5.13.5.5) show a fairly continuous decrease in water vapor with height below 450 mb. There was a dry layer near 400 mb, and the mass of water vapor increased with height above this. The water vapor content of this layer was small, but increased with time.

Figure 5.13.5.6 shows the local rate-of-change of the total mass of water vapor. The moistening of the layer near 400 mb is shown, as is the increase of water vapor below 500 mb between 2100 and 0000 GMT. The profile for 2100 to 0000 GMT showed losses between 400 and 500 mb, and below 700 mb. The profile for 0000 to 0300 GMT showed small gains at most levels.

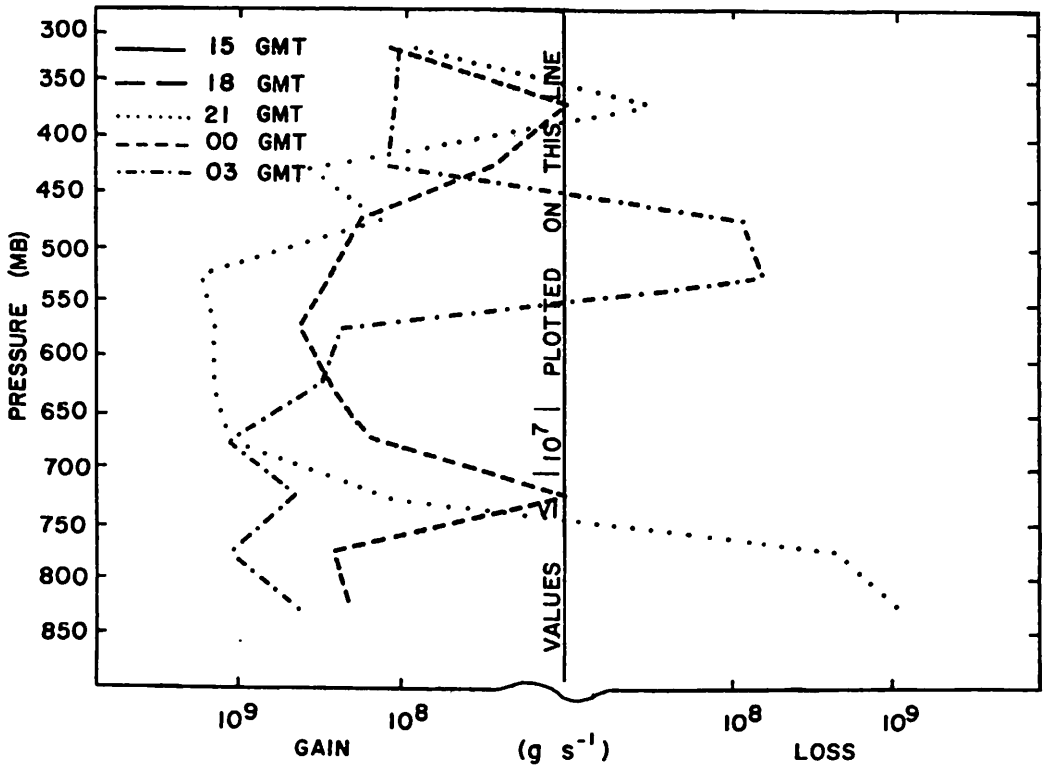

Fig. 5.13.5.4 Combined net horizontal and vertical transport of water vapor through boundaries of 50-mb layers (gm s^{-1}) over the Texas HIPLEX area for 29 June 1978.

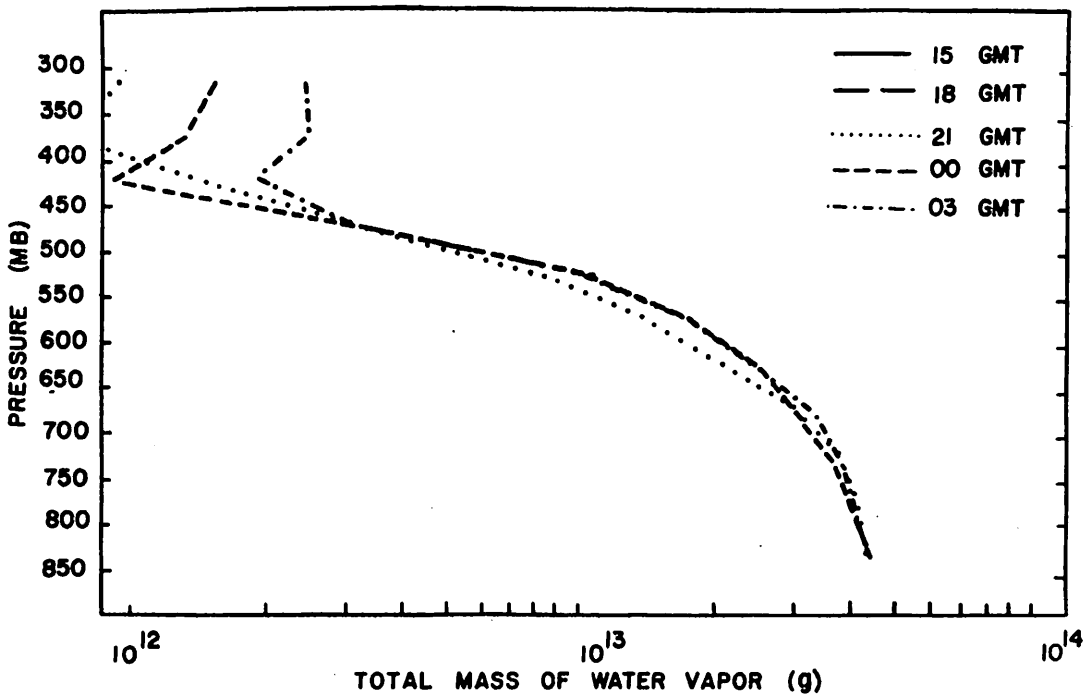

Fig. 5.13.5.5 Total mass of water vapor in layers 50 mb deep (gm) over the Texas HIPLEX area on 29 June 1978.

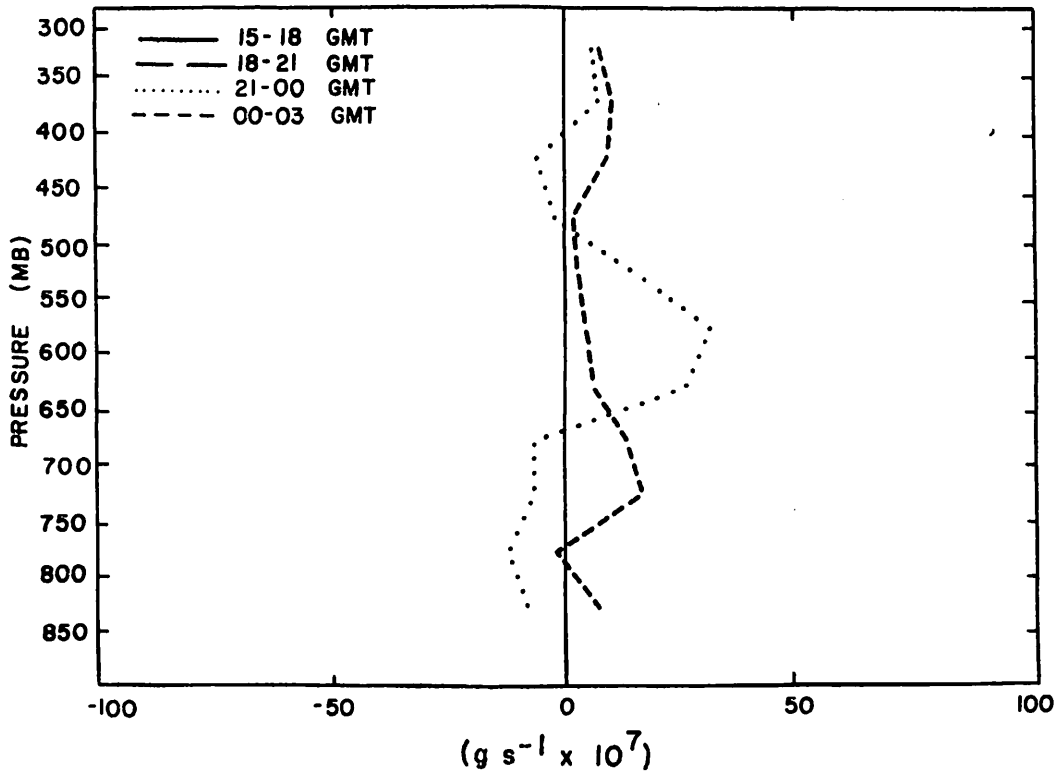

Fig. 5.13.5.6 Local rate-of-change in total mass of water vapor (g s^{-1} x 10^7) for the Texas HIPLEX area for 29 June 1978.

5.14 30 June 1978

5.14.1 Radar

Showers over the HIPLEX area were light until 1700 GMT when a strong cell formed northeast of Lamesa (Fig. 5.14.1.1). Between 1700 and 2200 GMT other strong cells formed in the west and moved across the area. The strongest cell was west of Post at 2000 GMT with a height of 15.8 km (52K ft). After 0000 GMT shower activity decreased.

5.14.2 Surface

Surface temperature (Fig. 5.14.2.1) displayed a minimum in the west near Seminole and a maximum at Rotan in the east. Temperature in the east rose during the next three hours but did not change much in the west until 1800 GMT. A few storms formed near Gail at 1700 GMT and by 1800 GMT the temperature there dropped 5.9°C. Temperatures also dropped near Andrews at 1900 GMT. At 2000 GMT temperatures had decreased across the northwest and, as shower activity spread across the area, temperature dropped in nearly all parts of the area. There was no shower activity near Robert Lee before 0000 GMT, and temperature did not decrease there until 0100 GMT.

Surface dewpoint depressions (Fig. 5.14.2.2) were moderate at 1500 GMT, and increased in the east between 1500 and 2000 GMT. Meanwhile, the dewpoint depression decreased near Gail at 1800 GMT and near Andrews at 1900 GMT as a result of the storm activity near those locations. Dewpoint depression decreased across the entire area as storm activity increased in size between 1900 and 0000 GMT. Increases in dewpoint depression occurred in the west at 0000 GMT. By 0300 GMT, however, dewpoint depressions were low all through the HIPLEX area.

Surface mixing ratio (Fig. 5.14.2.3) was variable during the first few hours but by 1900 GMT the lowest mixing ratio was in the southwest. At 2100 GMT a maximum formed near Big Spring that remained there for the remainder of the day. This maximum occurred when a moderately strong storm was in that area, and it corresponded to a minimum in the dewpoint depression field at the same time. Mixing ratio at Robert Lee increased at 0100 GMT as showers moved into that area, and after 0100 GMT values were fairly high across the area.

Surface equivalent potential temperature fields are shown in Fig. 5.14.2.4. A minimum was present near Lenorah at 1500 GMT, and potential temperature

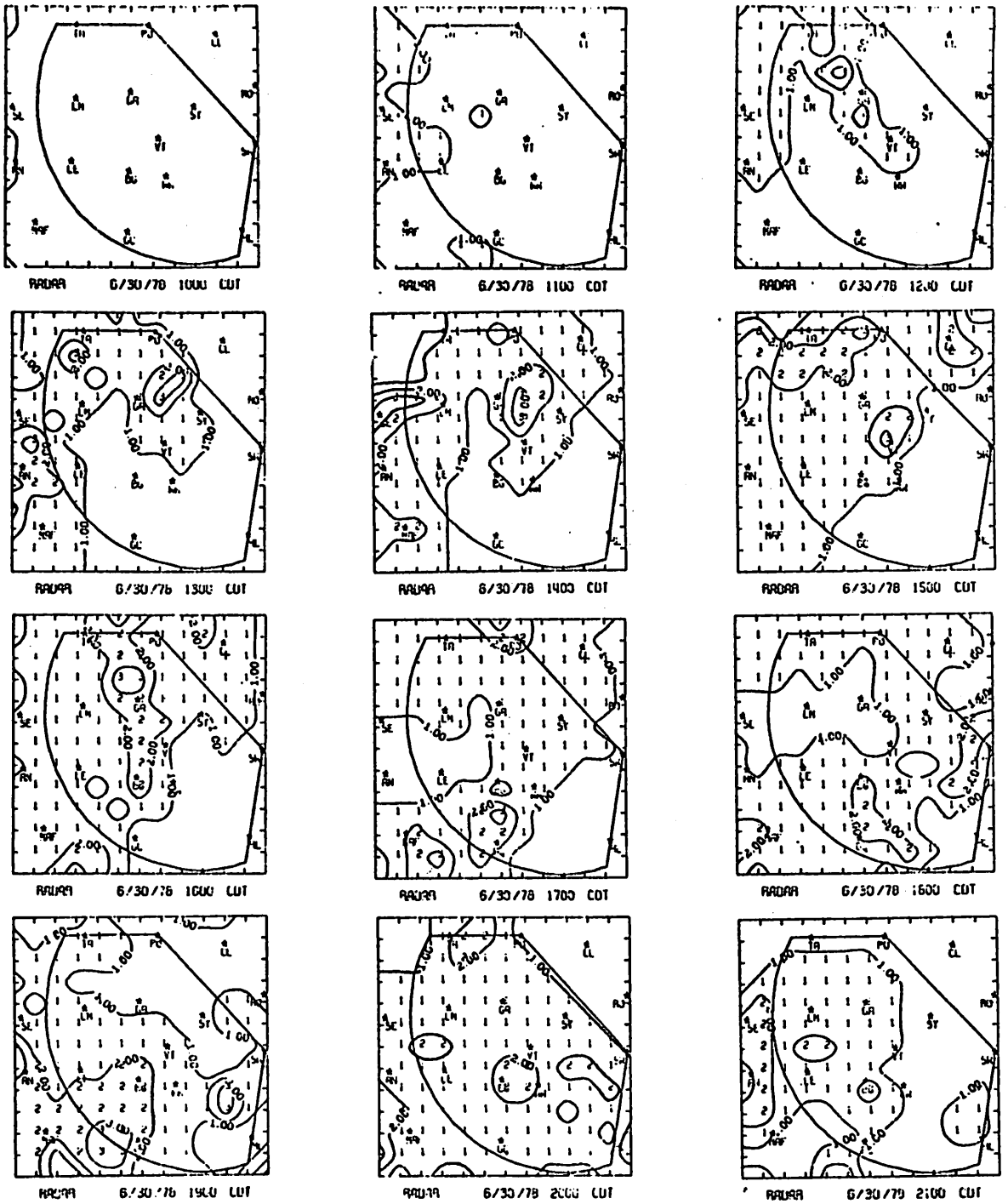

MISSING DATA

Fig. 5.14.1.1 Radar echoes for 30 June 1978.

RADAR 6/31/78 0400 CDT

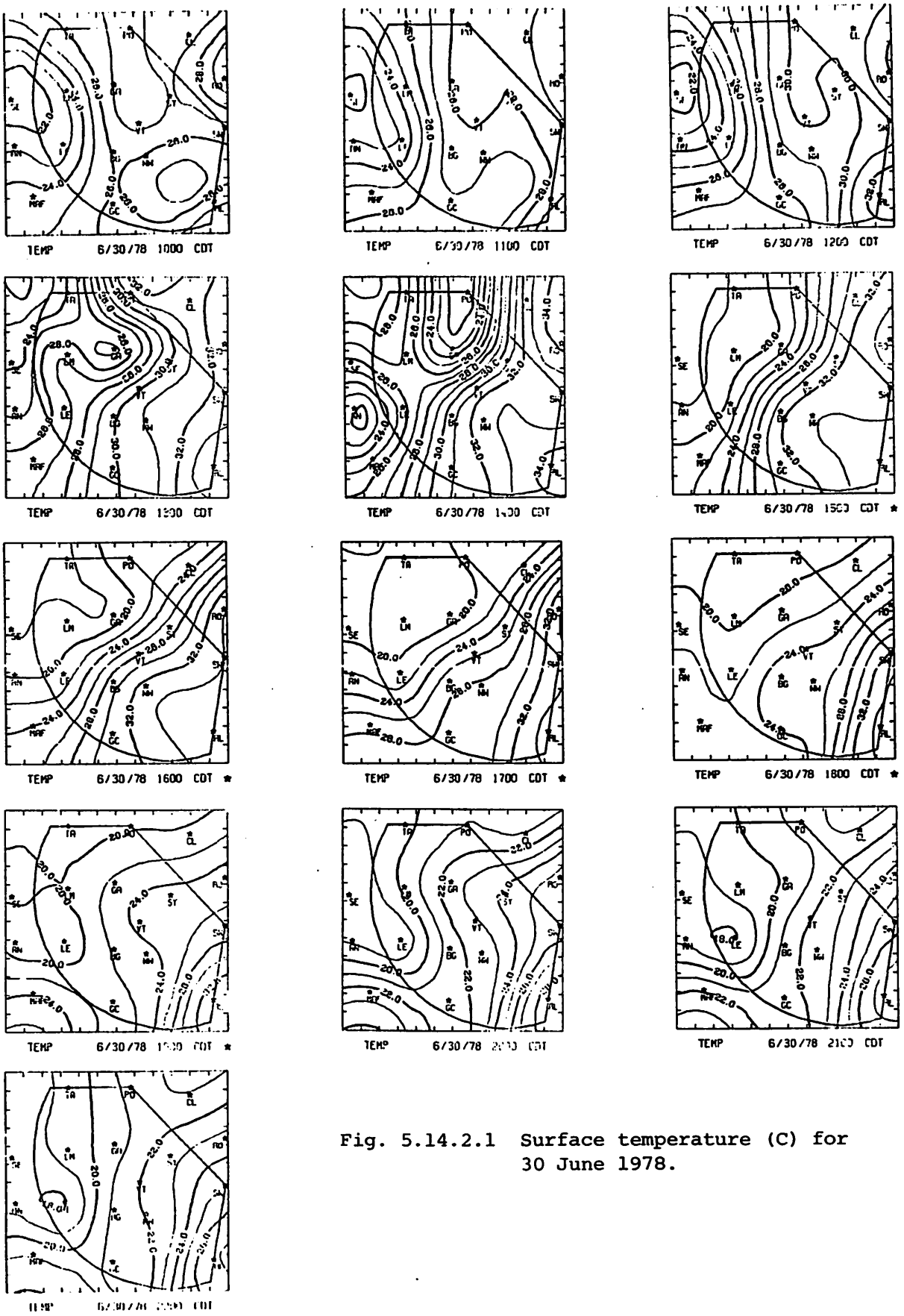

Fig. 5.14.2.1 Surface temperature (C) for 30 June 1978.

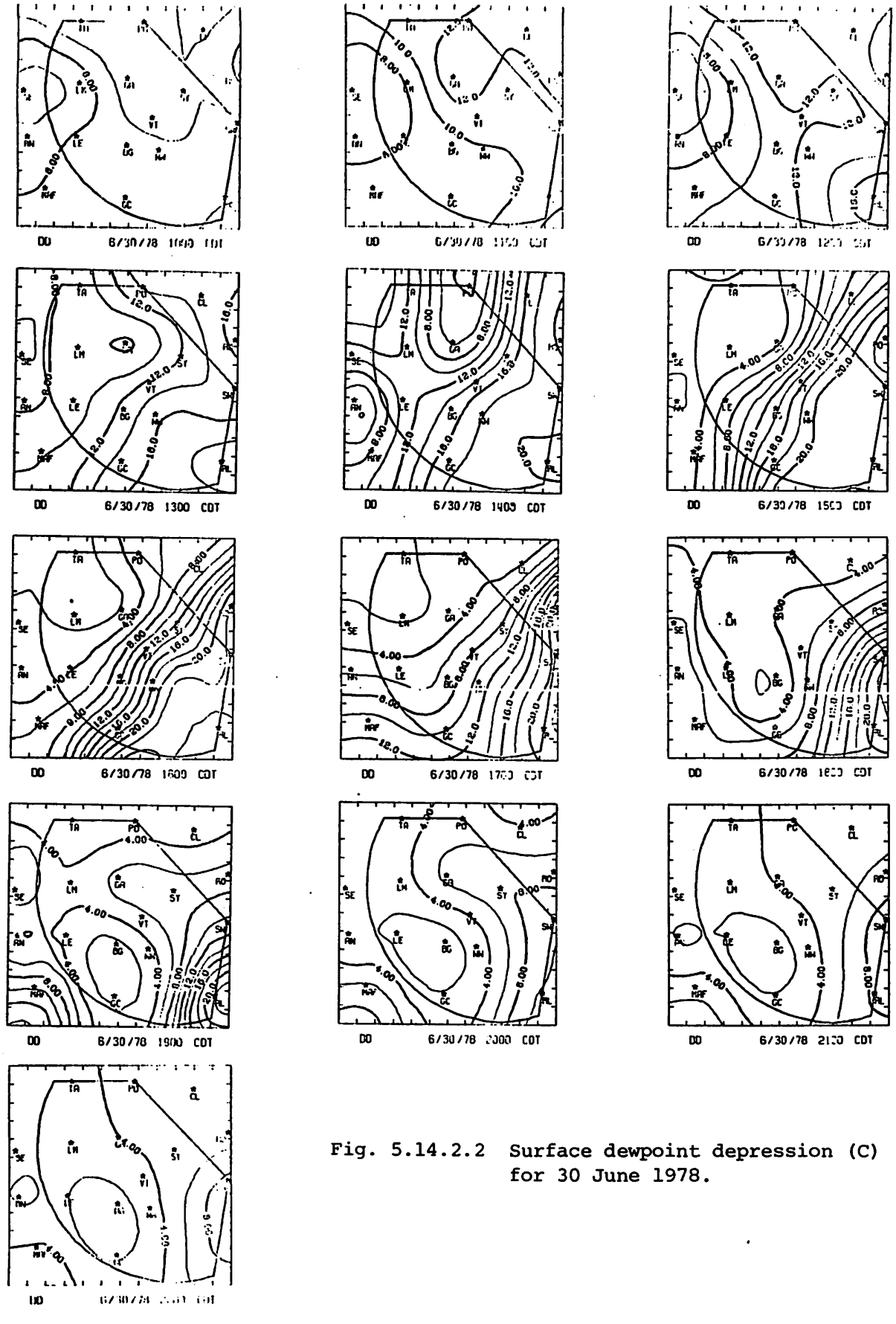

Fig. 5.14.2.2 Surface dewpoint depression (C) for 30 June 1978.

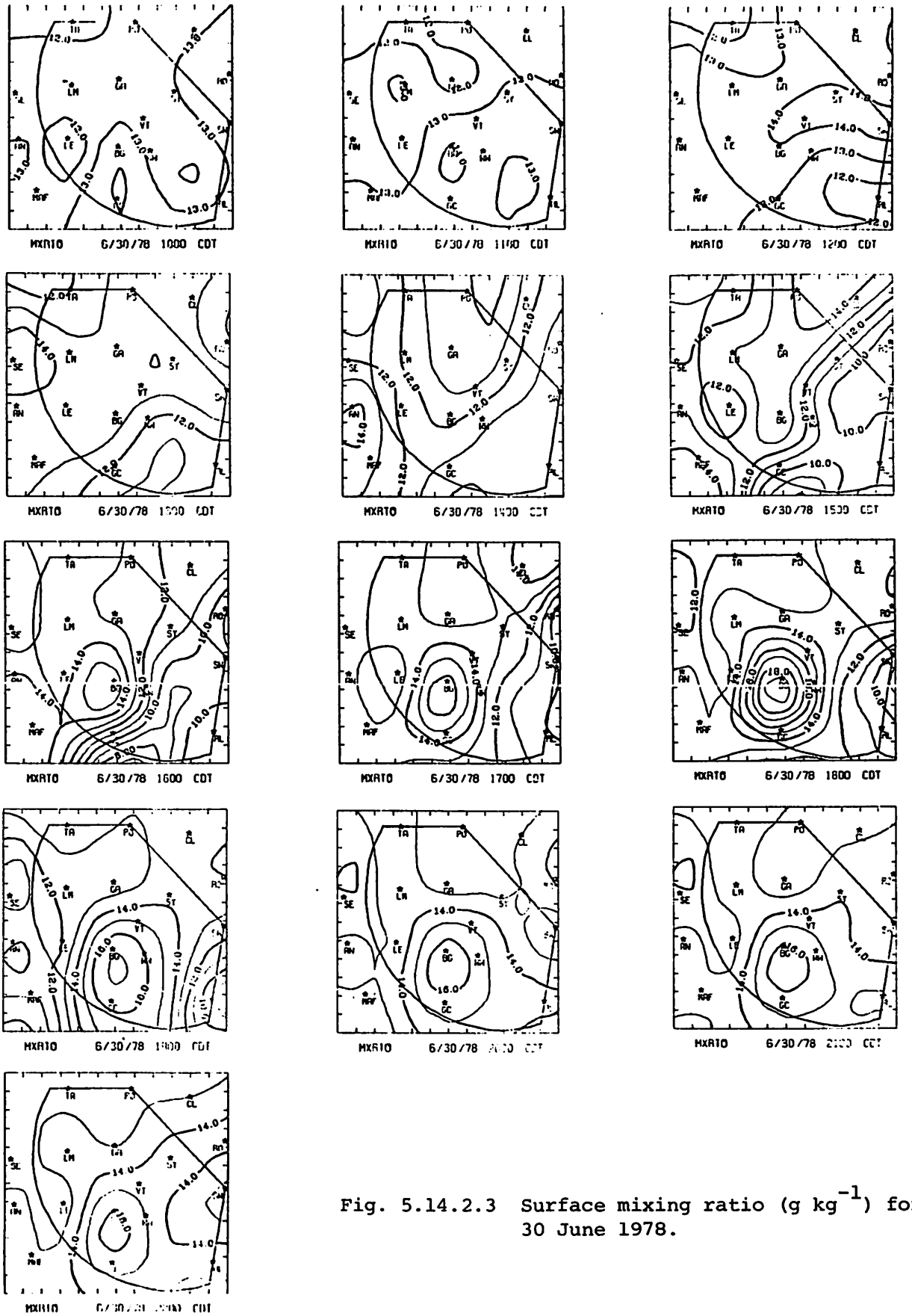

Fig. 5.14.2.3 Surface mixing ratio (g kg^{-1}) for 30 June 1978.

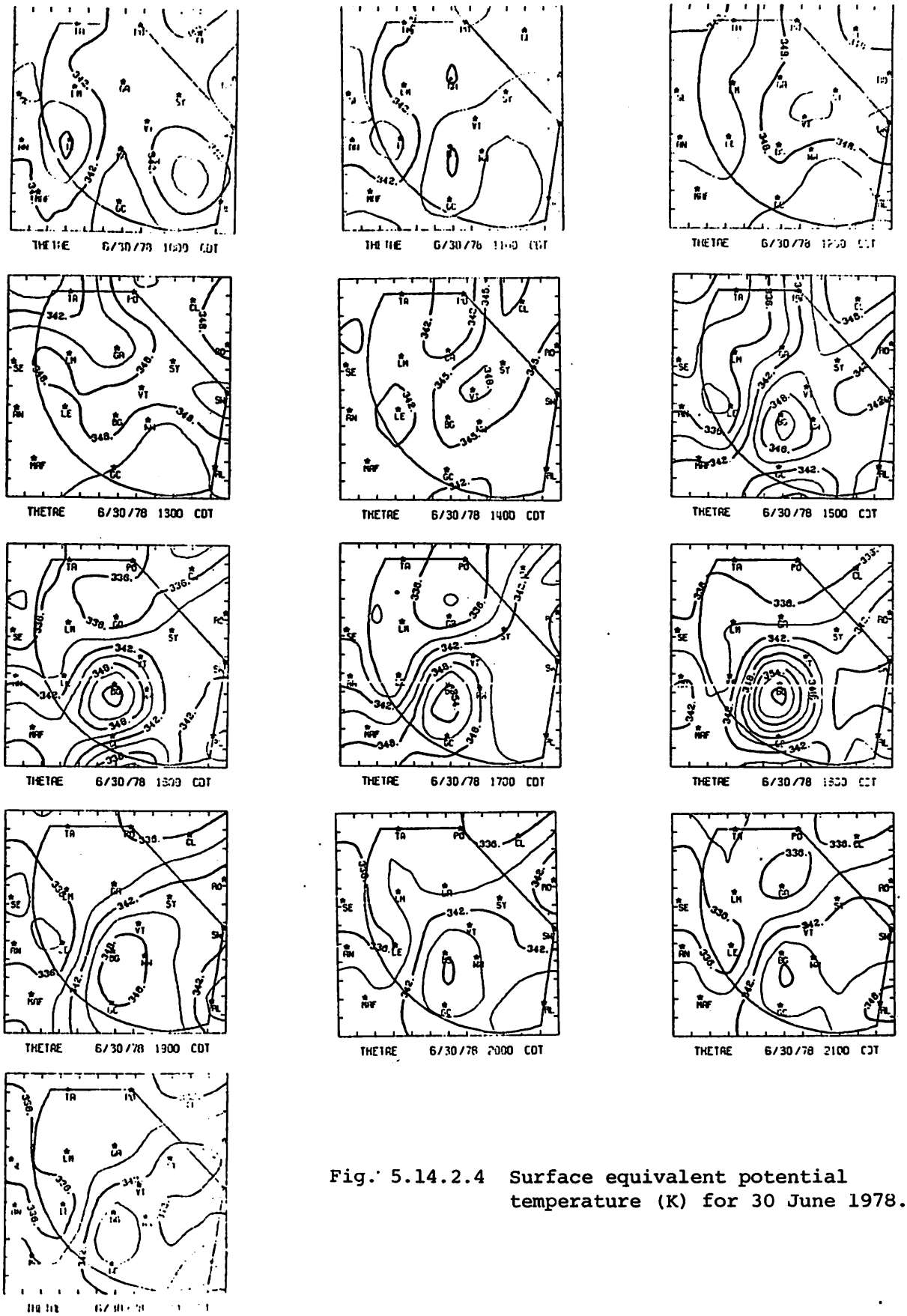

Fig. 5.14.2.4 Surface equivalent potential temperature (K) for 30 June 1978.

was relatively low there throughout the day. At 2000 GMT a maximum formed near Big Spring that persisted for the remainder of the day. The onset of showers produced some decreases in potential temperature in the northwest but did not have much effect in the east.

Terrain-induced vertical motion (Fig. 5.14.2.5) was generally small. There were no strong centers but a center of downward motion was southeast of Walsh-Watts and Vincent at 2200 GMT and remained through 0100 GMT.

Surface velocity divergence (Fig. 5.14.2.6) was moderate at 1500 GMT. A center of convergence formed between Big Spring and Gail at 1800 GMT which was associated with a storm cell just west of Lamesa. Convergence was strong in that area at 2000 GMT when an echo with height of 15.8 km (52K ft) was located north of Gail near Post. Strong convergence continued in the area through 0000 GMT. The axis along which the strongest convergence was present was oriented along the leading edge of the shower activity and moved westward as shower activity spread across the area. At 0100 GMT, as shower activity began to diminish, the convergence was replaced by divergence over most of the area which persisted through 0300 GMT.

Vertical motion 50 mb above the surface (Fig. 5.14.2.7) also showed moderate values at 1500 GMT. Strong downward motion was present in the northwest at 1800 GMT. Upward motion began to appear in the central part of the area at this time, and became quite strong at 2000 GMT. This area of strong upward motion moved toward the east as time progressed and as the storm activity in the area moved eastward. By 2300 GMT the strongest upward motion was along a line from Roscoe to Garden City and was associated with some moderate storm cells in that area. By 0100 GMT primarily downward motion was present in the area and the shower activity was diminishing.

Surface moisture divergence is shown in Fig. 5.14.2.8. Primarily divergence was present at 1500 GMT, a time of little shower activity. As showers began to build in the area moisture convergence developed and intensified in the central part of the area. This convergence became strong at 2000 GMT when a strong cell was located near Post. The centers of strong convergence moved eastward during the next few hours as the storm activity moved eastward. The moisture convergence remained generally east and south of the strong activity. Strong divergence also was present near Lamesa and Gail after 2200 GMT. At 0100 GMT shower activity was

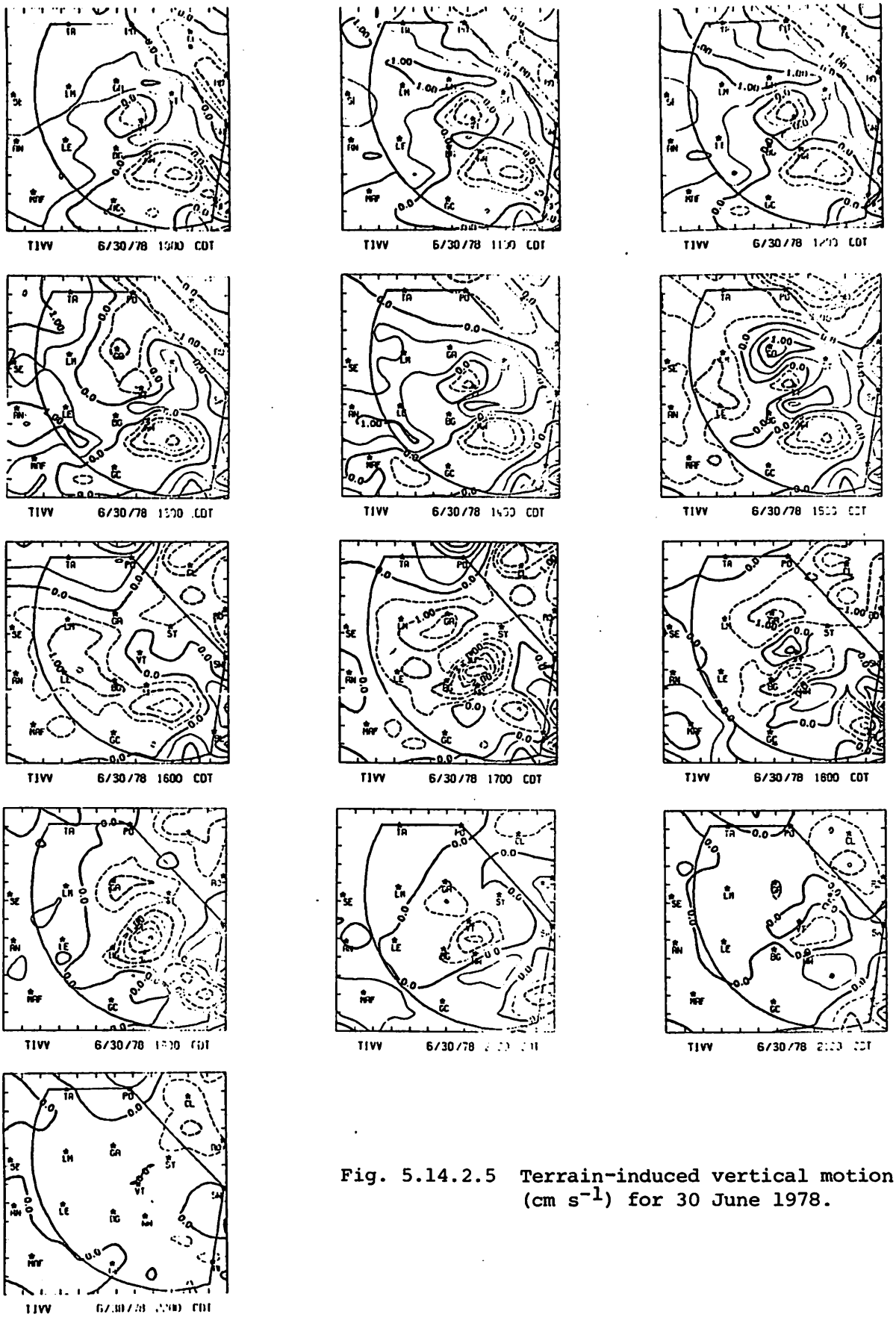

Fig. 5.14.2.5 Terrain-induced vertical motion (cm s^{-1}) for 30 June 1978.

Fig. 5.14.2.6 Surface velocity divergence ($s^{-1} \times 10^{-6}$) for 30 June 1978.

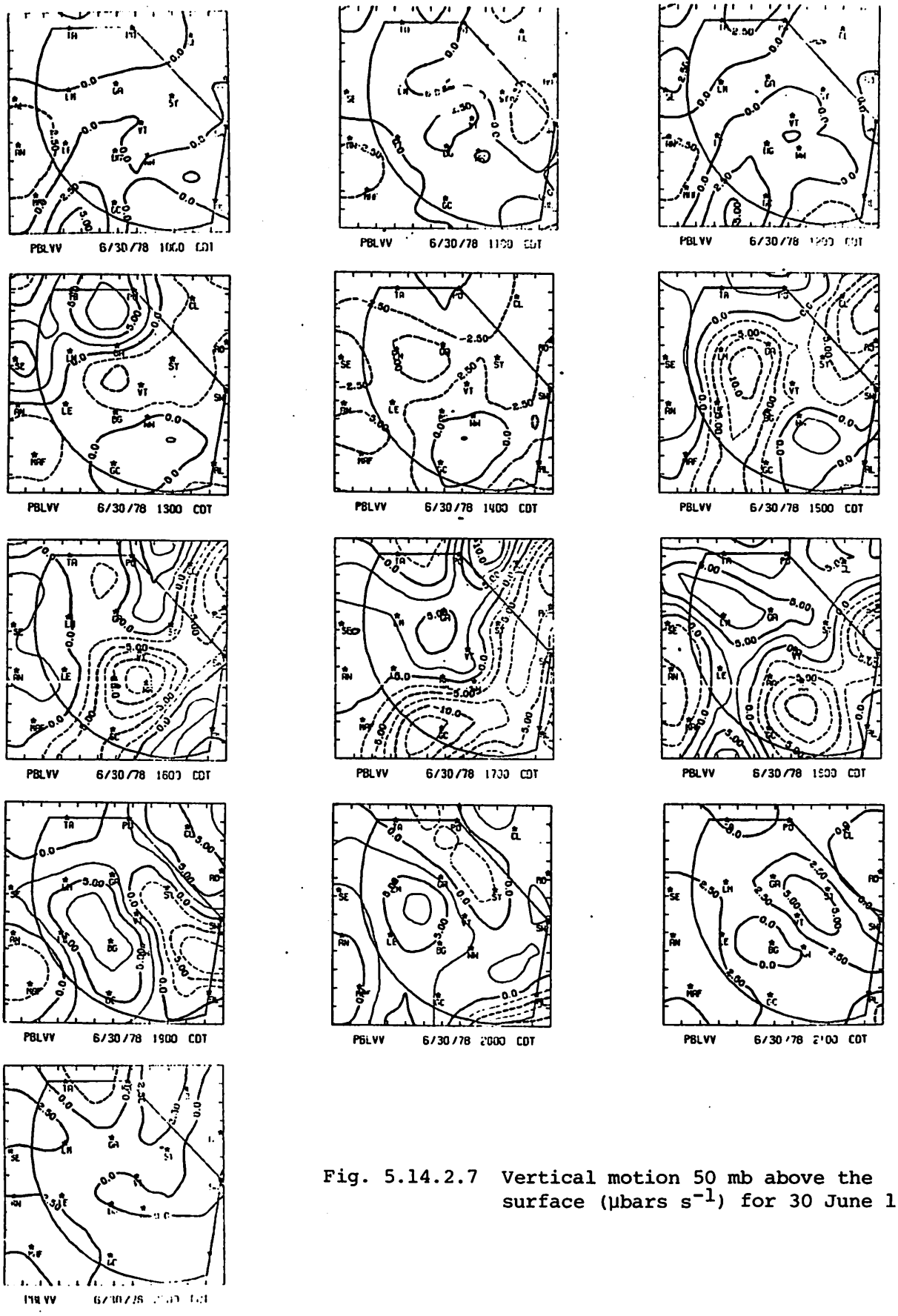

Fig. 5.14.2.7 Vertical motion 50 mb above the surface (μbars s^{-1}) for 30 June 1978.

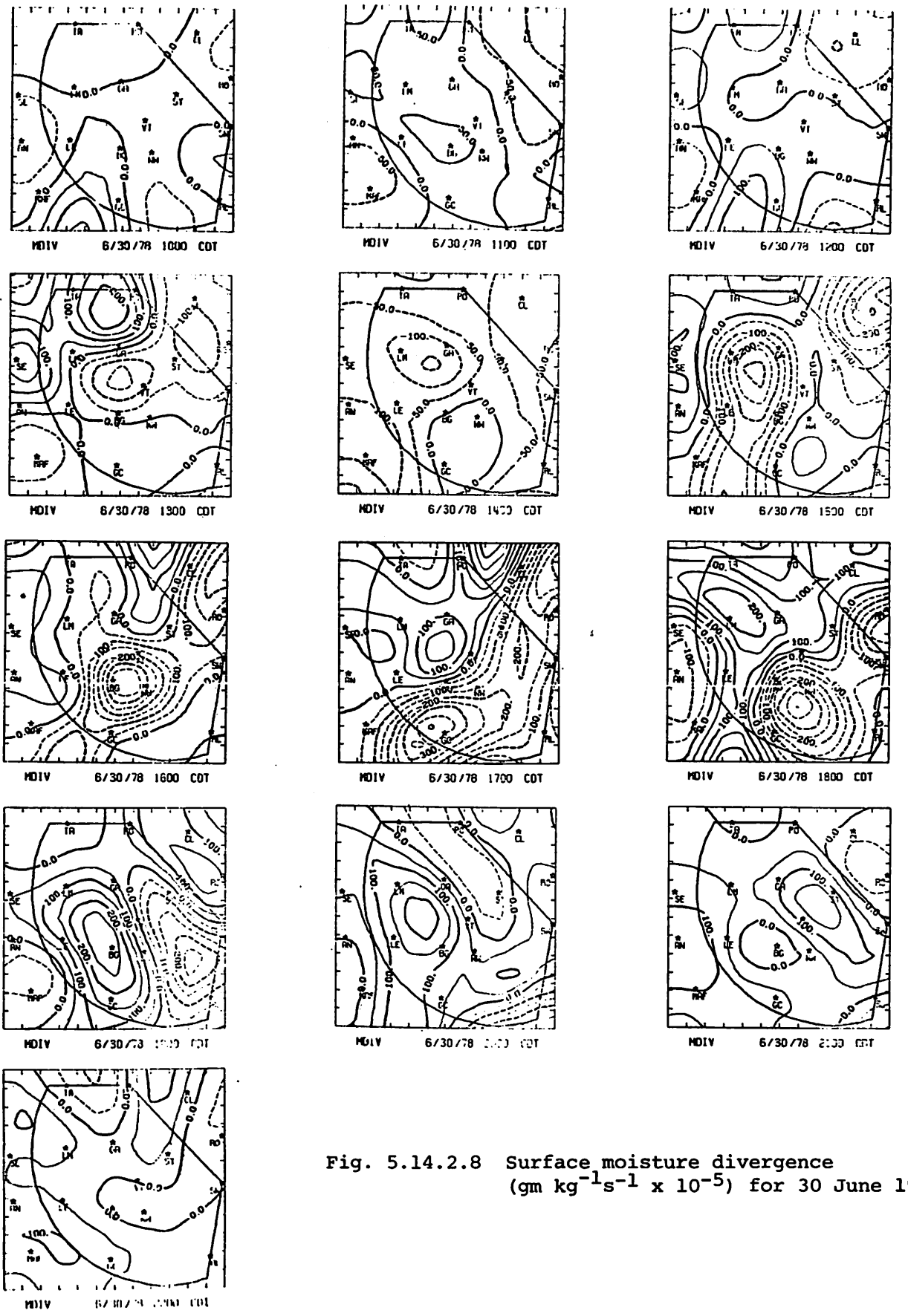

Fig. 5.14.2.8 Surface moisture divergence (gm $kg^{-1}s^{-1}$ x 10^{-5}) for 30 June 1978.

decreasing and the strong moisture convergence was no longer present except for a small area in the southeast. Moisture divergence predominated during the remainder of the day.

Vertical flux of moisture (Fig. 5.14.2.9) did not show any really strong values until 1800 GMT when shower activity was developing across the area. Strong downward moisture flux occurred in the northwest at 1800 GMT with moderate upward flux in the central areas. The upward flux increased in the next few hours as shower activity increased. Also, the centers of upward moisture flux moved eastward with time, as did centers of convergence and upward motion. This movement of the centers followed the movement of the eastern edge of the strong storm activity. As the storms moved eastward, downward moisture flux built up in the western areas. Shower activity was decreasing between 0000 and 0300 GMT and the strong upward moisture flux was replaced by weak downward flux at 0300 GMT.

Surface vorticity (Fig. 5.14.2.10) also showed moderate values at 1500 GMT which also increased with the onset of shower activity. Strong centers of positive and negative vorticity were present between 1800 and 0000 GMT when the storm activity was the strongest and most widespread. Most of the stronger storm cells were located in areas of positive vorticity. After 0000 GMT when storm activity decreased the values at the centers also decreased.

Surface pressure change (Fig. 5.14.2.11) was generally small until 1800 GMT when pressure dropped 1 mb or more in the east. These decreases were in areas where little or no shower activity was taking place. At 2100 GMT there was a 1 mb pressure rise at Tahoka after a strong storm had moved into the area an hour before. After 0100 GMT pressure changes were small.

Surface winds (Fig. 5.14.2.12) were southerly early in the day but showed variations due to the influence of shower activity after 1800 GMT. As shower activity spread eastward across the area, there were shifts to westerly and northwesterly winds in the west. Wind speeds decreased after 0000 GMT and by 0300 GMT the winds were very light.

5.14.3 Upper Level Kinematic Parameters

Profiles of mass divergence (Fig. 5.14.3.1) show that, at 1500 GMT, before shower activity had built up, there was convergence in the lowest

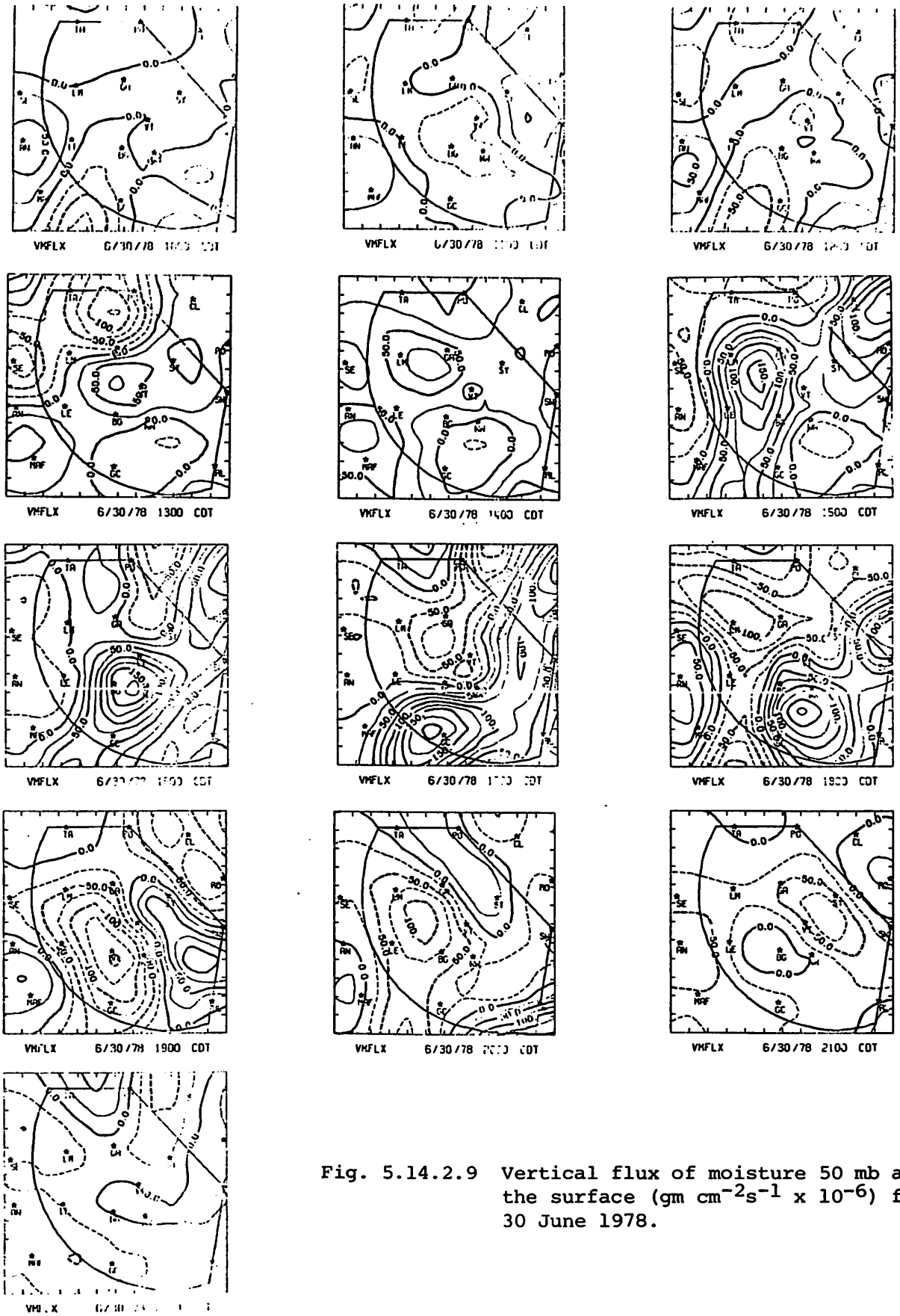

Fig. 5.14.2.9 Vertical flux of moisture 50 mb above the surface (gm $cm^{-2}s^{-1}$ x 10^{-6}) for 30 June 1978.

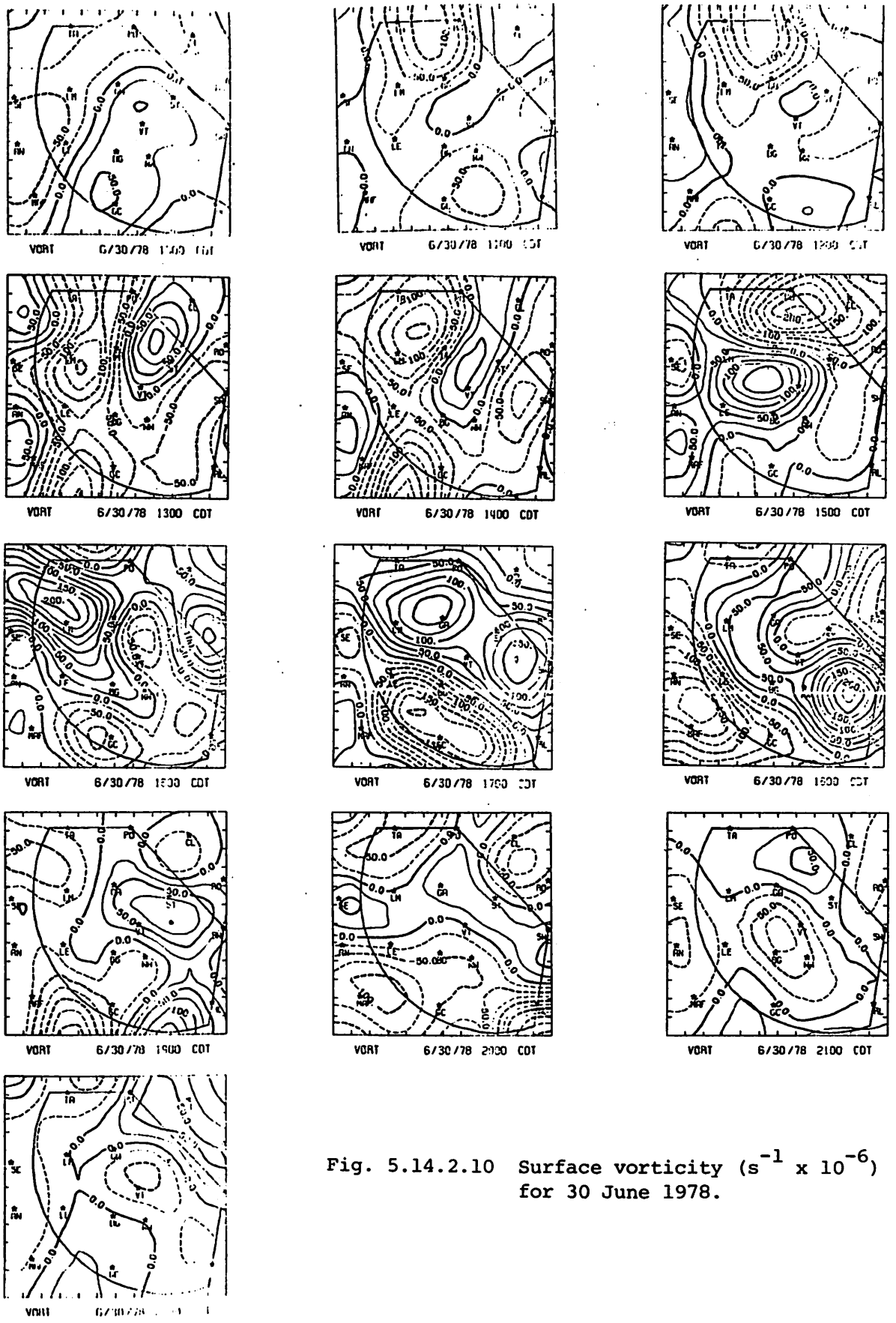

Fig. 5.14.2.10 Surface vorticity ($s^{-1} \times 10^{-6}$) for 30 June 1978.

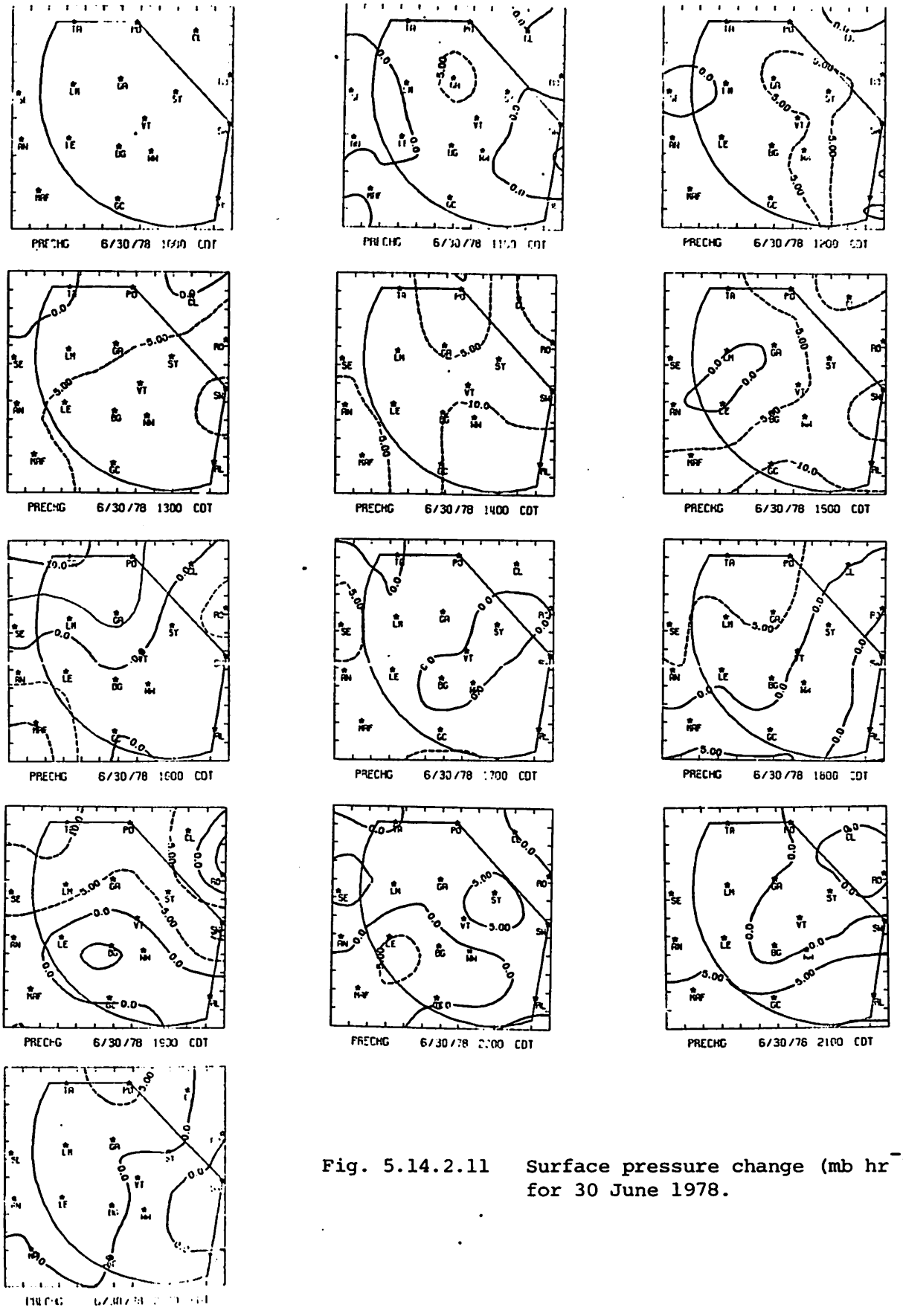

Fig. 5.14.2.11 Surface pressure change (mb hr^{-1} x 10^{-1}) for 30 June 1978.

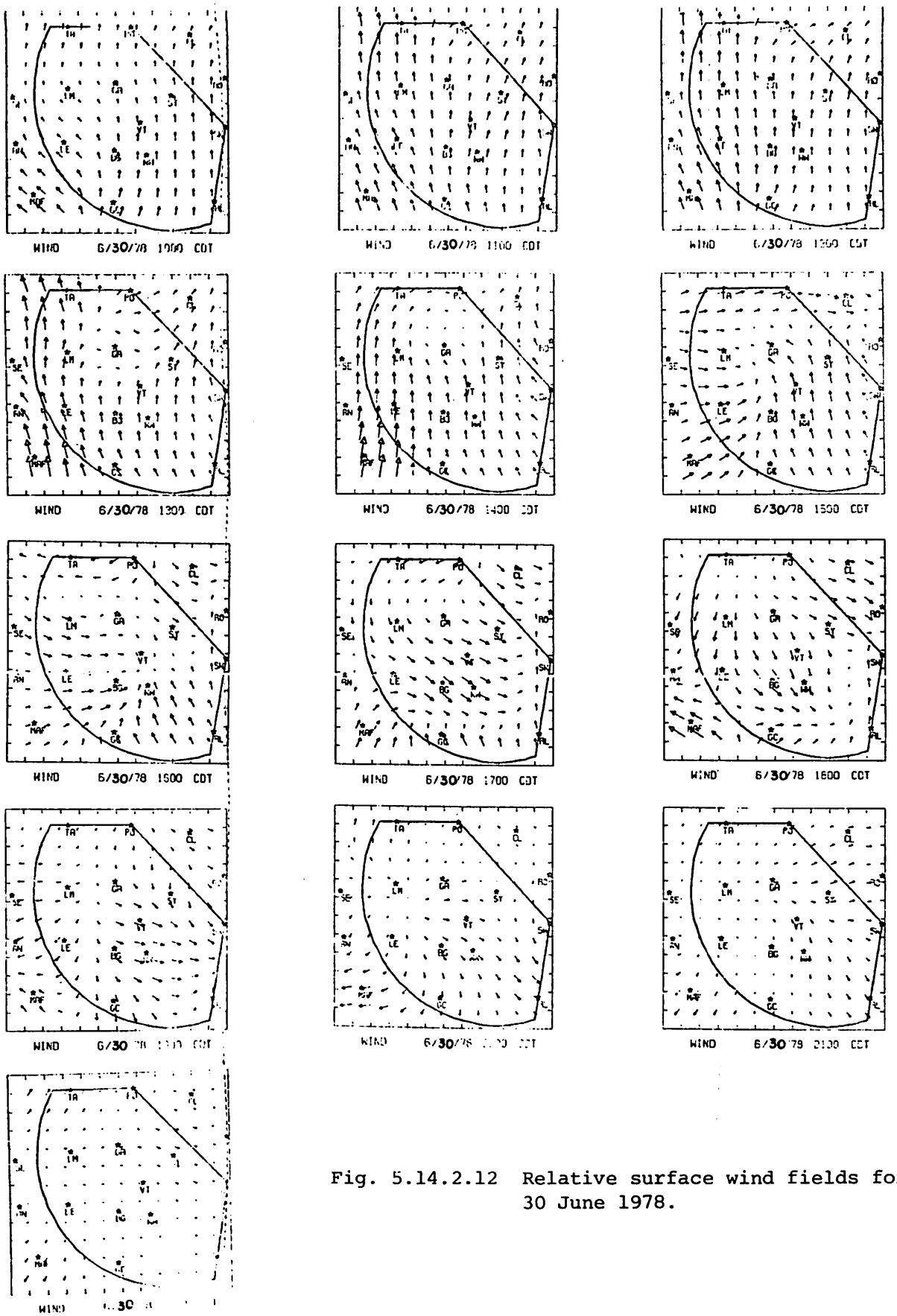

Fig. 5.14.2.12 Relative surface wind fields for 30 June 1978.

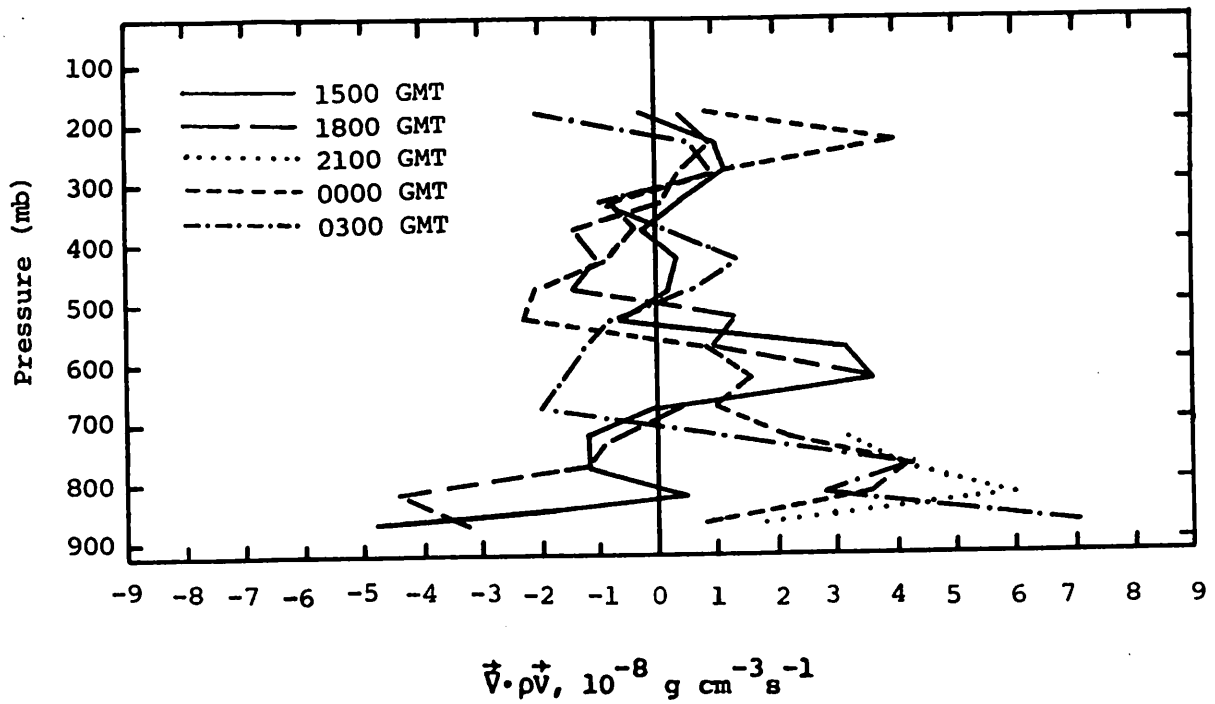

Fig. 5.14.3.1 Vertical profiles of mass divergence on 30 June 1978.

layers and divergence above 700 mb. As showers began to build at 1800 GMT convergence began in another layer, between 350 and 500 mb. At 2100 GMT a full profile was not available. When shower activity was decreasing, at 0000 GMT divergence was present in lower layers below 600 mb. There was mass convergence between 600 and 300 mb at 0000 GMT with divergence above. The profile at 0300 GMT was similar, although the low-level divergence was stronger and extended only to 700 mb.

Vertical motion at 1500 GMT (Fig. 5.14.3.2) was predominantly upward except above 300 mb. At 1800 GMT when shower activity was increasing, vertical motion was upward in all levels. No profile is shown for 2100 GMT when activity was at a maximum. At 0000 and 0300 GMT when shower activity decreased, downward motion was present at all levels.

Figure 5.14.3.3 shows profiles of moisture divergence. Convergence was present in the lowest layers at 1500 and 1800 GMT. Moisture divergence was present in middle layers with convergence above 550 mb. At 2100 GMT moisture divergence was present at low levels although most of the profile is missing. The 0000 and 0300 GMT profiles were similar in that they both

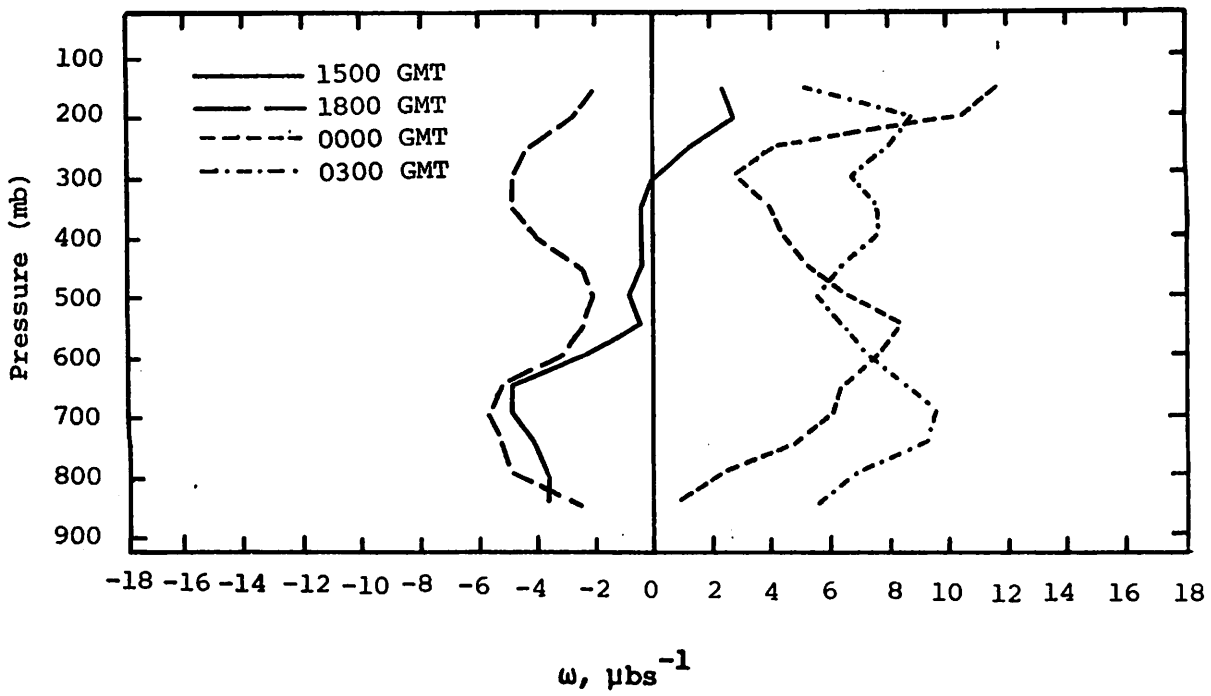

Fig. 5.14.3.2 Vertical profiles of vertical motion on 30 June 1978.

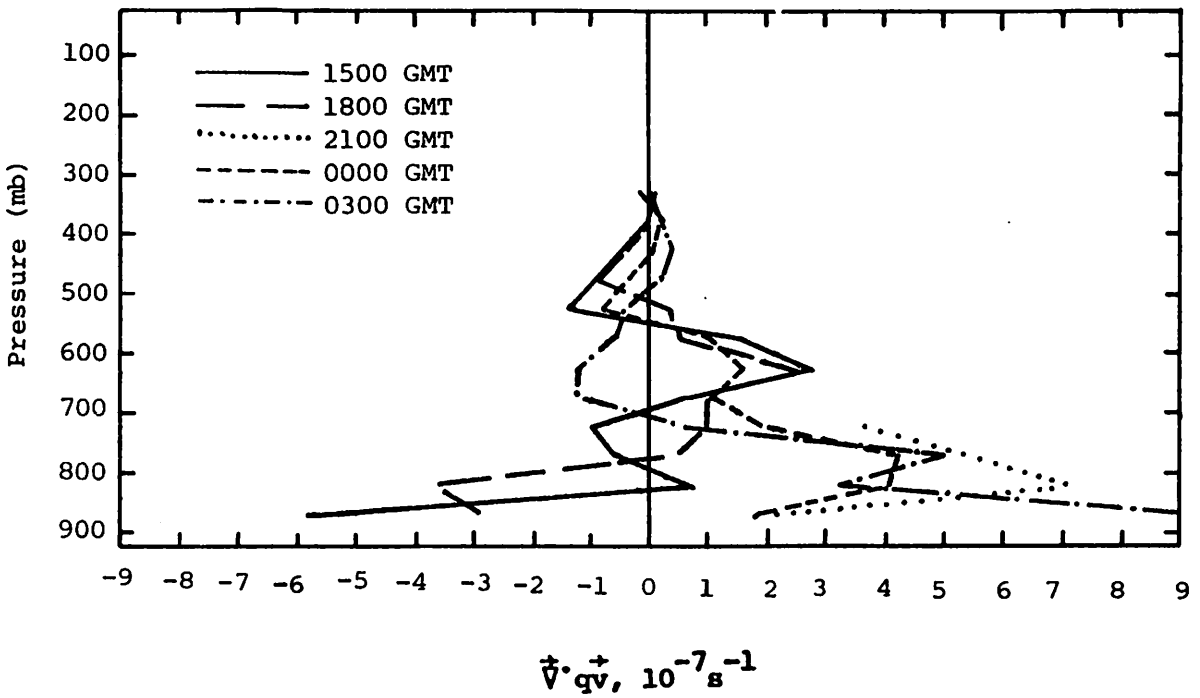

Fig. 5.14.3.3 Vertical profiles of moisture divergence on 30 June 1978.

exhibited low-level moisture divergence with some convergence above. Although the low-level moisture divergence was of larger magnitude at 0300 GMT it did not extend through as deep a layer as at 0000 GMT.

5.14.4 Energetics

Shower activity was slight at 1500 GMT but increased throughout the day until 2100 GMT. After 0000 GMT shower activity decreased.

Profiles of horizontal flux of latent heat (Fig. 5.14.4.1) were similar at 1500 and 1800 GMT. Both profiles show inflow of latent heat at low levels and outflow between 700 and 500 mb. Inflow was present at these times above 500 mb. The 2100 GMT profile was incomplete but indicated outflow of latent heat at low levels. At 0000 GMT the outflow of latent heat extended up to 550 mb with slight inflow above as shower activity was decreasing. At 0300 GMT there was also low-level outflow of latent heat but this extended only to 700 mb.

Figure 5.14.4.2 shows profiles of vertical flux of latent heat. At 1500 and 1800 GMT, as shower activity was increasing over the area, there was flow of latent heat out of the lowest layers and into middle layers. At 0000 and 0300 GMT, the flow was just opposite. Latent heat flux was out of upper and middle layers into the lower layers.

Local change of latent heat (Fig. 5.14.4.3) was generally negative in the low layers throughout the day, except at 0000 GMT when it was near zero. Above 600 mb small positive values were present.

Profiles of the residual of the latent heat energy equation (Fig. 5.14.4.4) were similar at 1500 and 1800 GMT. Both showed positive values for the most part with a layer of negative values near 650 mb. These positive values are consistent with the condensation taking place at those times as indicated by the formation of convective activity. Profiles at 0000 and 0300 GMT were generally negative, indicating evaporation and a decrease in shower activity.

Profiles of diabatic heating (Fig. 5.14.4.5) were generally in agreement with the profiles of the residual of the latent heat energy equation. The profiles showed warming at 1500 and 1800 GMT from the condensation that took place. Evaporative cooling occurred at 0000 and 0300 GMT as shower activity decreased.

Profiles of the horizontal flux of kinetic energy are shown in Fig. 5.14.4.6. Inflow of kinetic energy was present below 550 mb and primarily outflow

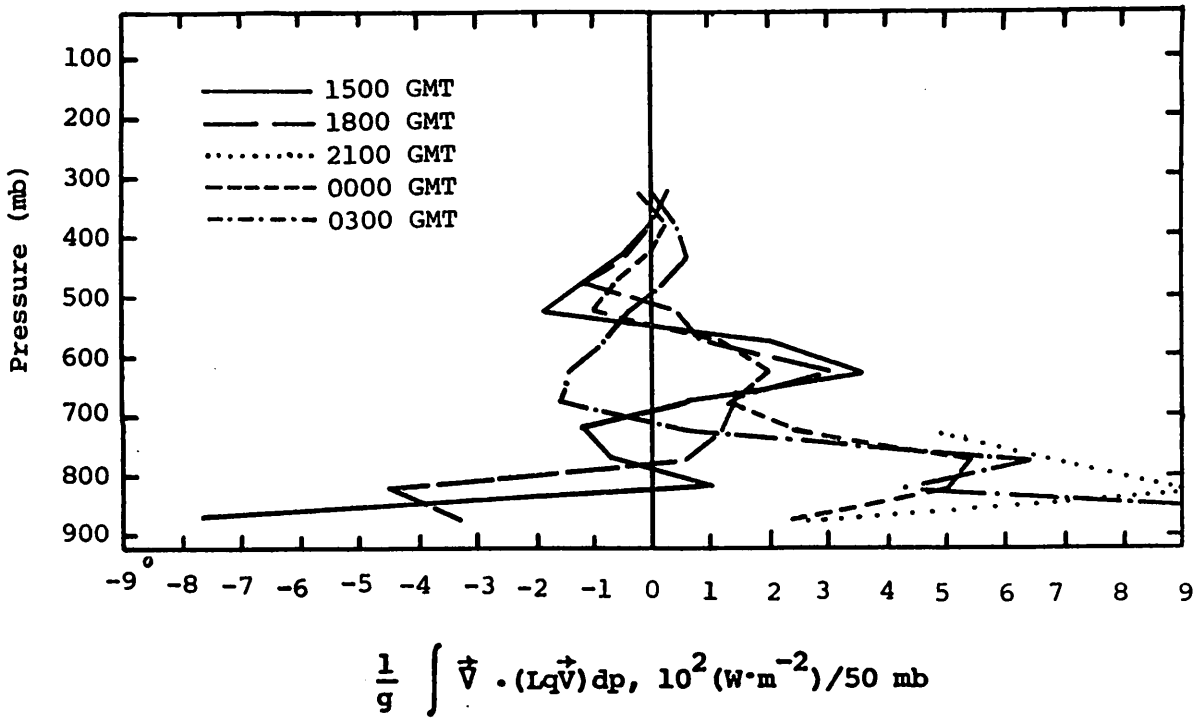

Fig. 5.14.4.1 Vertical profiles of the horizontal flux of latent heat energy on 30 June 1978.

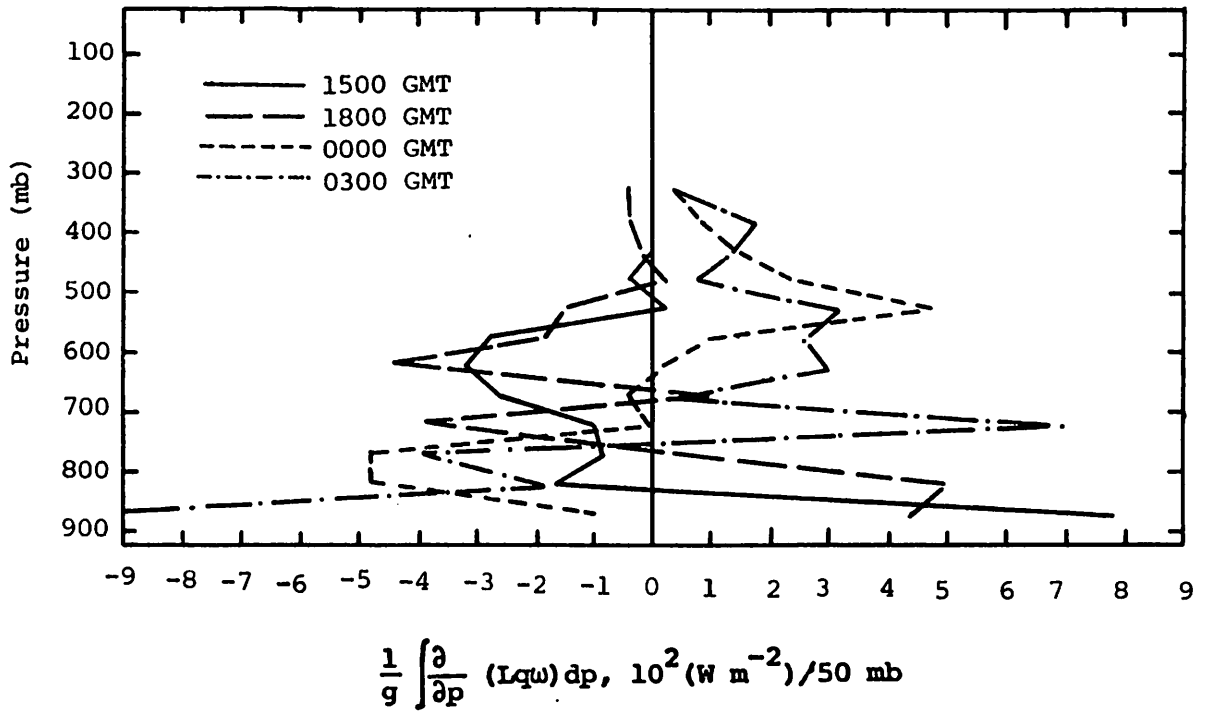

Fig. 5.14.4.2 Vertical profiles of the vertical flux of latent heat energy on 30 June 1978.

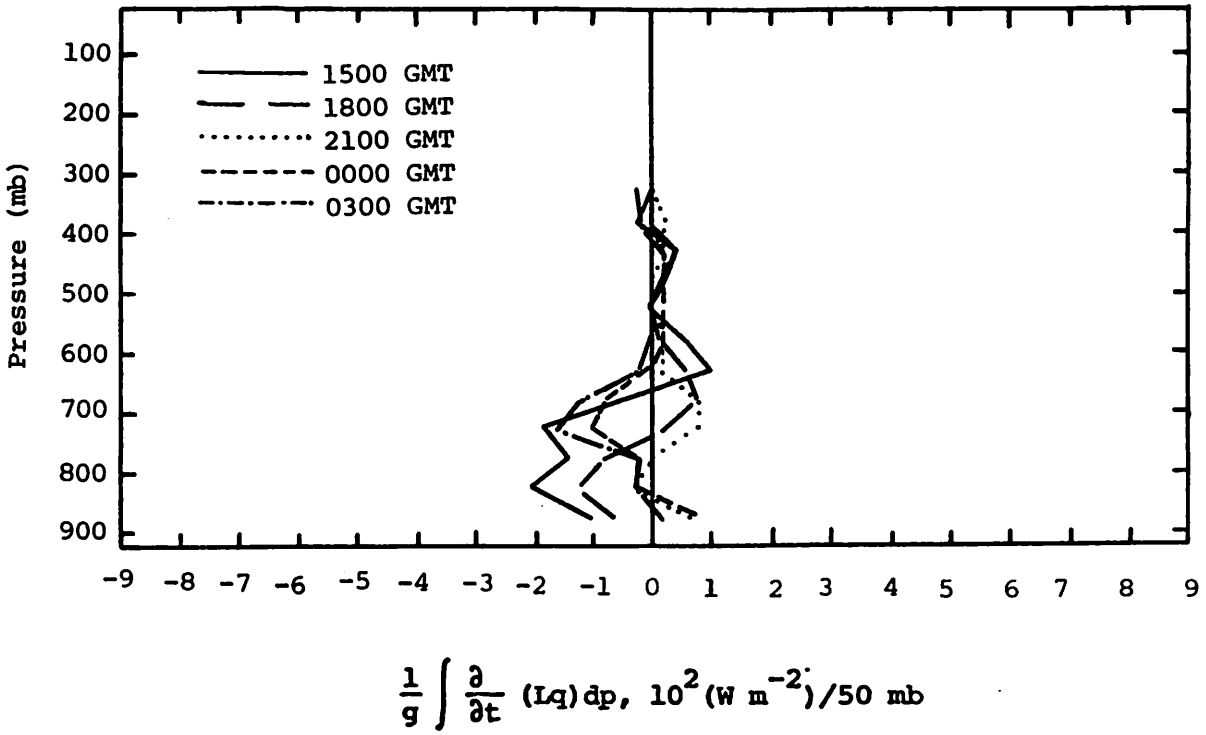

Fig. 5.14.4.3 Vertical profiles of the local change of latent heat energy on 30 June 1978.

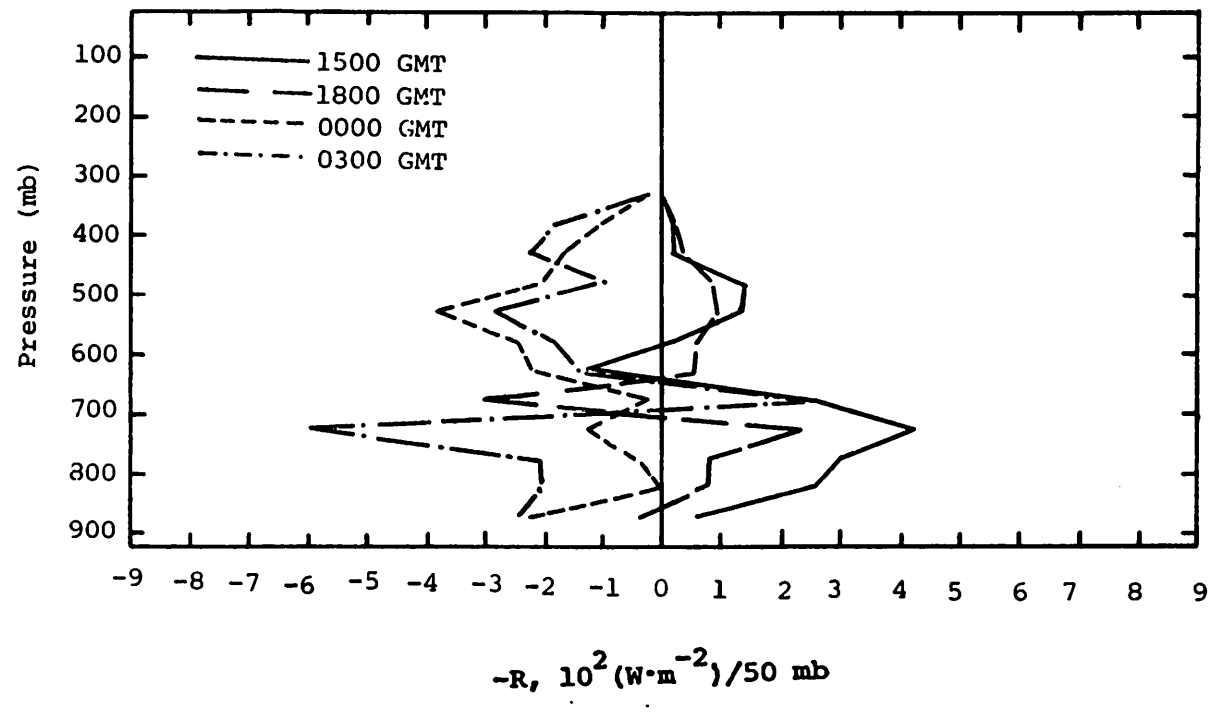

Fig. 5.14.4.4 Vertical profiles of the residual of the latent heat energy equation on 30 June 1978.

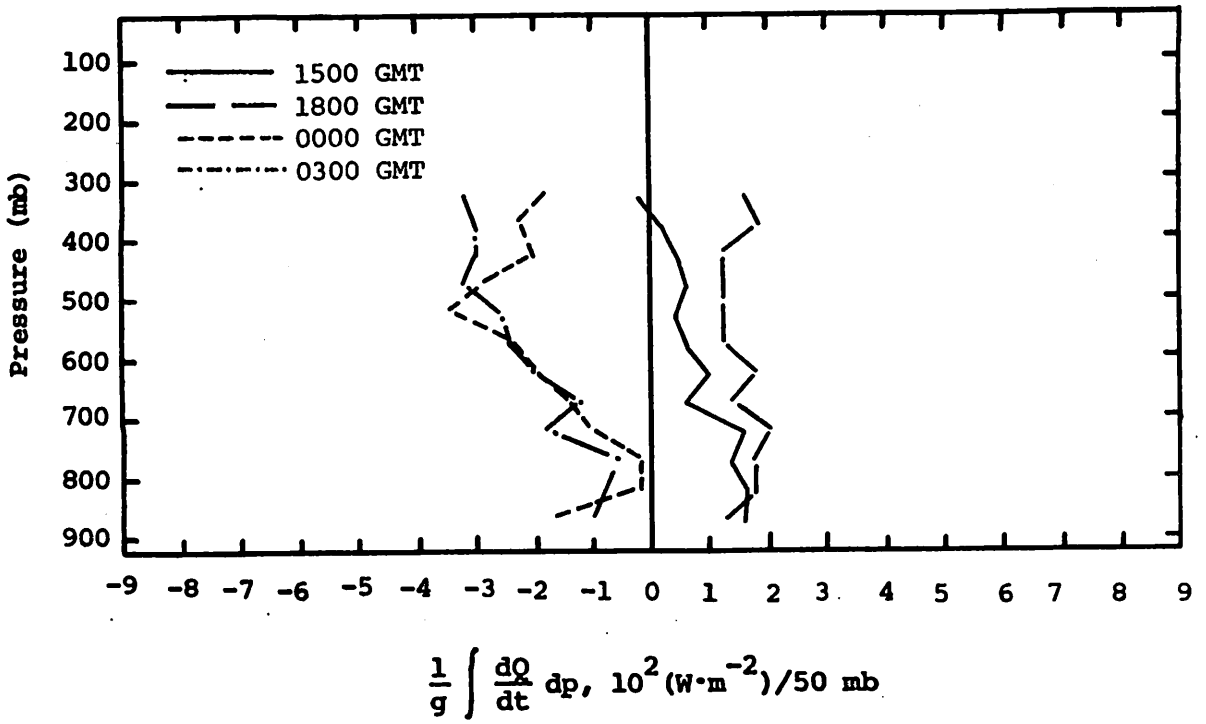

Fig. 5.14.4.5 Vertical profiles of diabatic heating computed from the first law of thermodynamics on 30 June 1978.

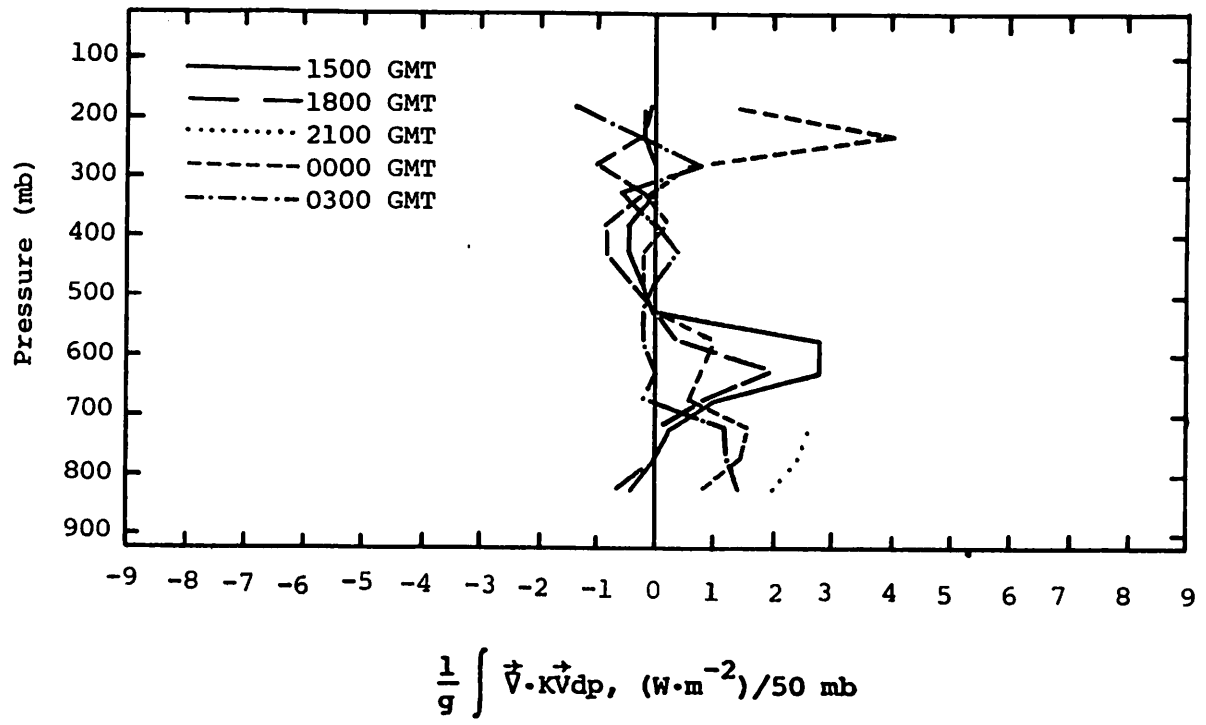

Fig. 5.14.4.6 Vertical profiles of the horizontal flux of kinetic energy on 30 June 1978.

above. At 0000 GMT there was a layer of strong inflow near 200 mb, however.

Vertical flux of kinetic energy (Fig. 5.14.4.7) was upward out of the lowest levels into middle layers at 1500 and 1800 GMT. There also was transport from a layer near 300 mb into layers above that level. At 0000 and 0300 GMT transport was downward from the highest layers into a layer near 200 mb, and there was transport of kinetic energy from middle layers into the lowest layers.

5.14.5 Water Vapor Budget

At 1500 GMT only a small amount of shower activity was present in the west. This activity increased during the next six hours and eventually showers spread across the entire area. After 0000 GMT shower activity decreased.

Profiles of net horizontal transport of water vapor are shown in Fig. 5.14.5.1. At 1500 and 1800 GMT there were gains in water vapor in the lowest levels and also in upper levels above 550 mb. Middle layers showed losses due to outflow of water vapor. At 0000 and 0300 GMT there were losses in the lowest layers and layers above 500 mb, and gains in middle layers.

Profiles of net vertical transport of water vapor (Fig. 5.14.5.2) show mainly gains at 1500 GMT except near 500 mb. At 1800 GMT there were gains in most layers except below 800 mb. The profiles at 0000 and 0300 GMT show gains in low levels with losses above 750 mb.

The vertical transport of water vapor through constant pressure surfaces (Fig. 5.14.5.3) was upward at both 1500 and 1800 GMT when shower activity was increasing. Transport was downward at 0000 and 0300 GMT as showers were diminishing.

The combined net horizontal and vertical transport of water vapor (Fig. 5.14.5.4) showed gains at all levels at 1500 and 1800 GMT. The gains were smaller in low levels at 1800 GMT, however. This was when shower activity was building. After 0000 GMT the shower activity was decreasing although there still was quite a lot of shower activity present. The profile for 0000 GMT shows gains below 600 mb and losses above. At 0300 GMT net losses were present at all levels.

The profiles of total mass of water vapor (Fig. 5.14.5.5) show no extremely dry or moist layers. The water vapor content was fairly high

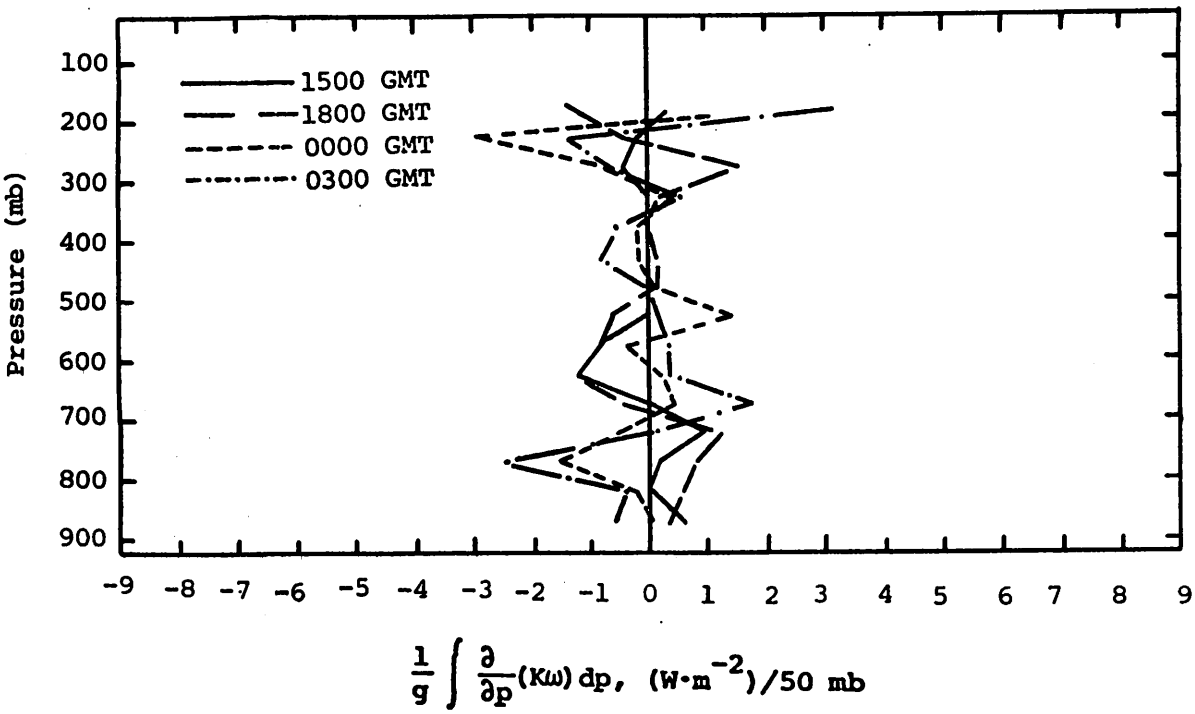

Fig. 5.14.4.7 Vertical profiles of the vertical flux of kinetic energy on 30 June 1978.

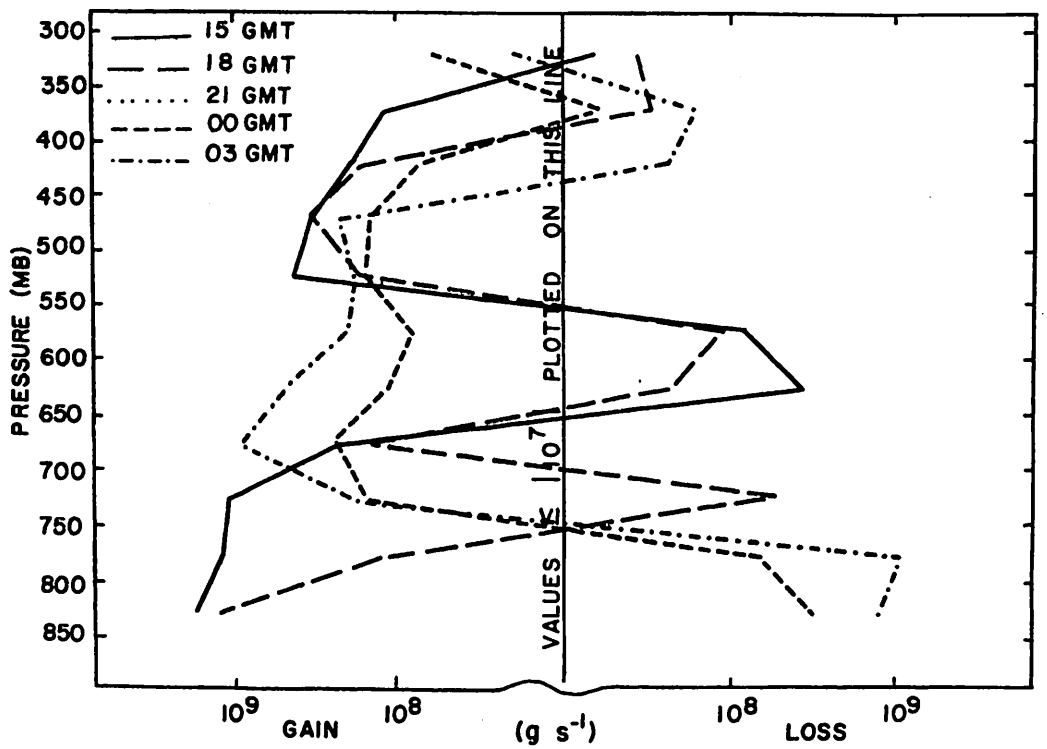

Fig. 5.14.5.1 Net horizontal transport of water vapor through boundaries of 50-mb layers (gm s^{-1}) over the Texas HIPLEX area for 30 June 1978.

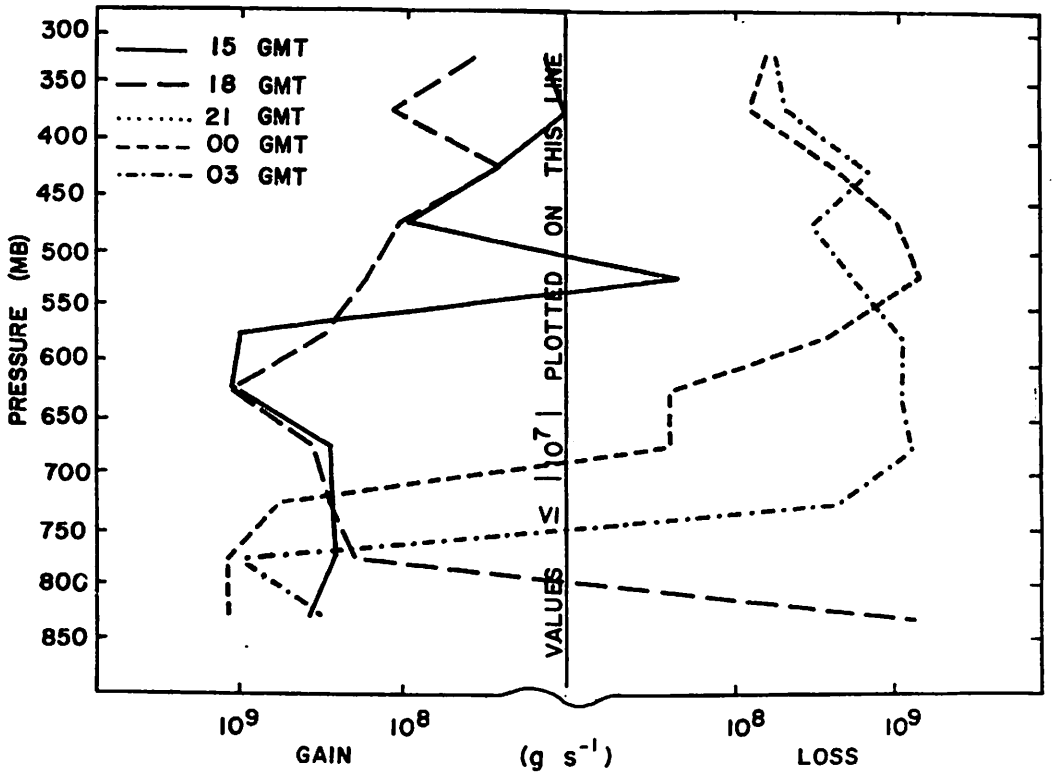

Fig. 5.14.5.2 Net vertical transport of water vapor through boundaries of 50-mb layers (gm s^{-1}) over the Texas HIPLEX area for 30 June 1978.

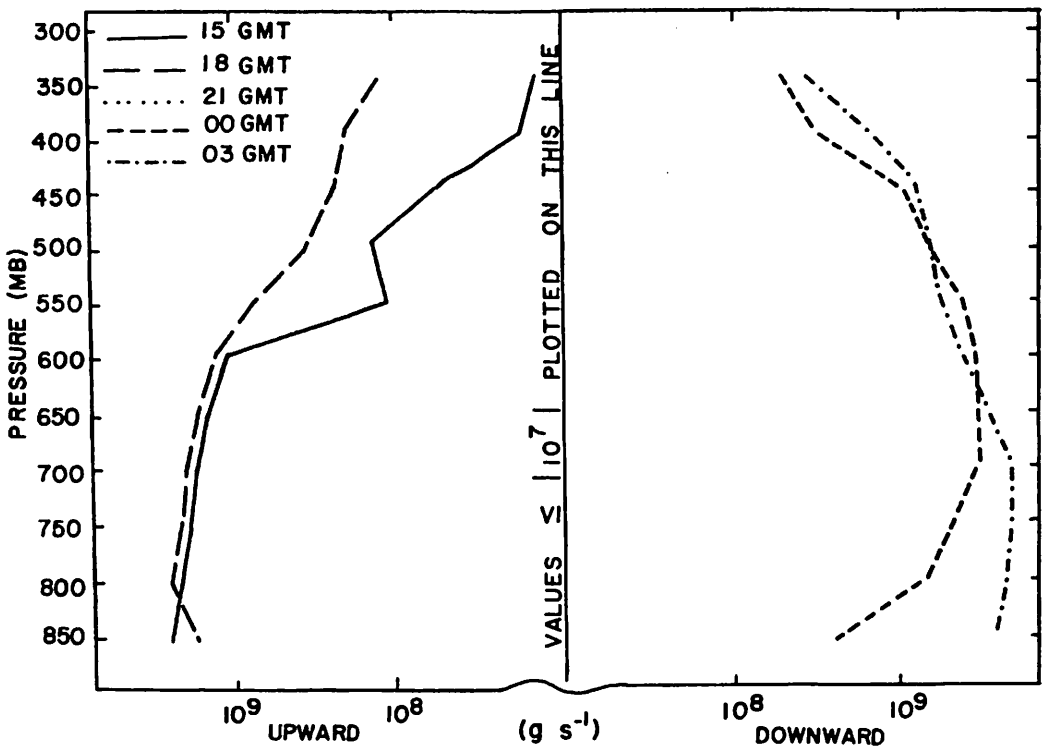

Fig. 5.14.5.3 Vertical transport of water vapor through constant pressure surfaces (gm s^{-1}) over the Texas HIPLEX area for 30 June 1978.

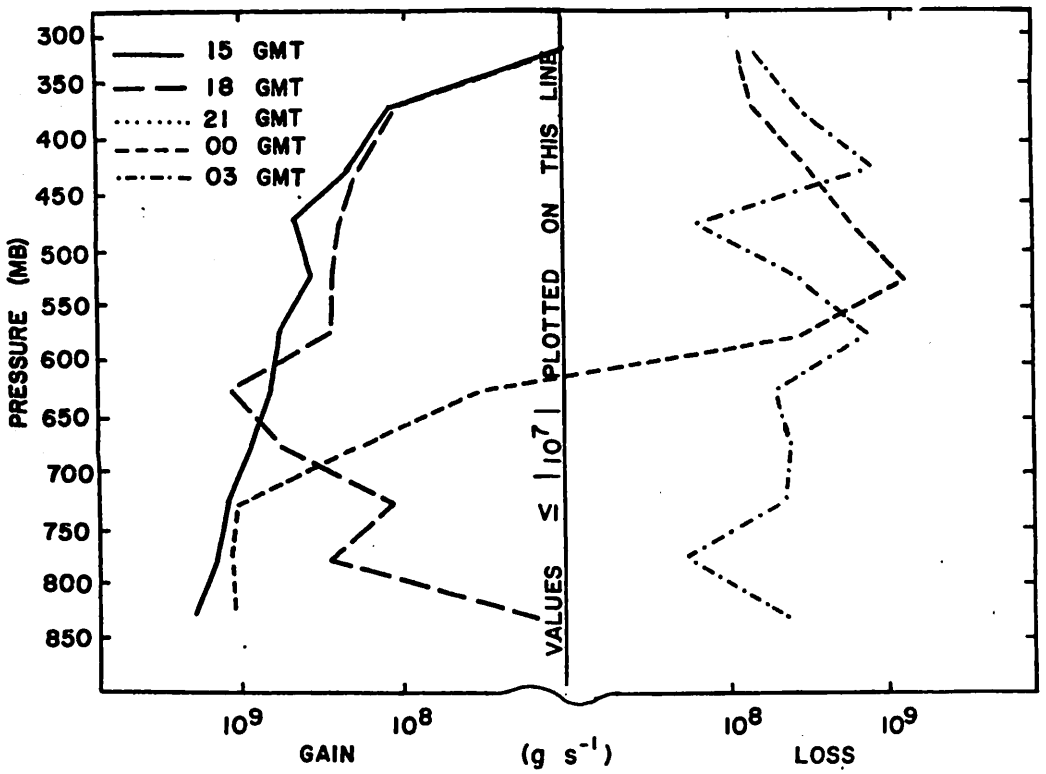

Fig. 5.14.5.4 Combined net horizontal and vertical transport of water vapor through boundaries of 50-mb layers (gm s^{-1}) over the Texas HIPLEX area for 30 June 1978.

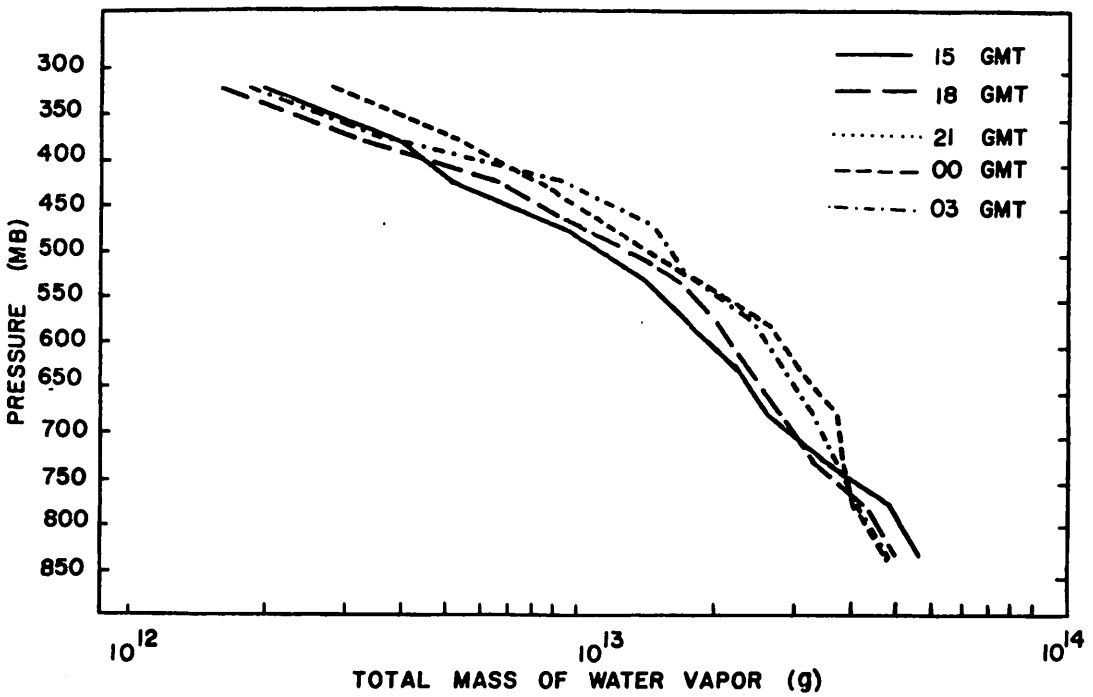

Fig. 5.14.5.5 Total mass of water vapor in layers 50 mb deep (gm) over the Texas HIPLEX area on 30 June 1978.

in most layers throughout the day. The water vapor decreased in lower layers all through the day but increased in middle layers.

The profiles of the local rate-of-change of water vapor (Fig. 5.14.5.6) showed the increases in middle layers between 1500 and 1800 GMT. Also, fairly large losses below 750 mb occurred. This is consistent with the large vertical transport of water vapor shown at 1800 GMT in Fig. 5.14.5.2. Between 0000 and 0300 GMT there were losses in water vapor below 500 mb. A moderate gain in water vapor occurred between 500 and 400 mb at that time, with losses above 400 mb.

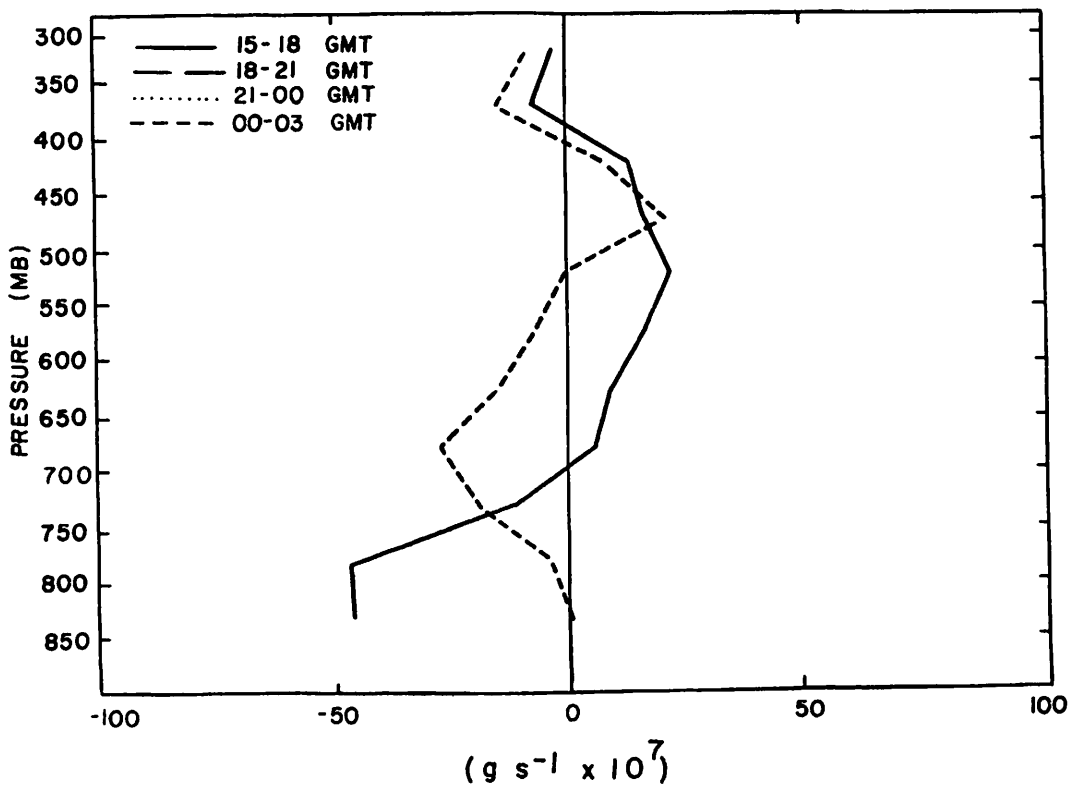

Fig. 5.14.5.6 Local rate-of-change in total mass of water vapor ($g\ s^{-1} \times 10^7$) for the Texas HIPLEX area for 30 June 1978.

5.15 1 July 1978

5.15.1 Radar

At 1700 GMT strong echoes with heights in excess of 9.1 km (30K ft) were present in the central part of the area between Lenorah and Walsh-Watts (Fig. 5.15.1.1). The echoes increased in intensity in the next three hours and moved south and east of Big Spring at 2000 GMT. At 2200 GMT other strong echoes had formed near Midland which persisted until 0000 GMT. At 0000 GMT a strong cell formed near Big Spring but was gone by the next hour. Shower activity decreased over the area between 0000 GMT and 0300 GMT.

5.15.2 Surface

The effect of the storms on the pattern of surface temperature was not pronounced prior to 1900 GMT (Fig. 5.15.2.1). A temperature gradient oriented generally northwest-southeast was present until 1900 GMT when a minimum formed near Walsh-Watts associated with the strong storm cell. This center intensified at 2000 GMT and remained strong through 2300 GMT. At that time thunderstorm activity had diminished near Walsh-Watts. Between 0000 GMT and 0300 GMT the minimum temperatures were generally in the south where most shower activity was taking place.

Dewpoint depressions (Fig. 5.15.2.2) were moderate at the beginning of the day and increased through the area until 1900 GMT. A center of minimum dewpoint depression associated with thunderstorm-induced cooling was located near Walsh-Watts between 1900 and 2300 GMT. Large dewpoint depressions were located near Lenorah between 1900 and 2300 GMT. The depressions decreased there at 2200 GMT as storms formed in that area. After 0000 GMT minimum depressions were in the south and in the northwest.

Surface mixing ratios (Fig. 5.15.2.3) were high in the northwest until 1900 GMT. A minimum persisted near Lenorah all through the day. At 1900 GMT mixing ratio increased at Big Spring in association with the shower activity. The maximum that formed there persisted until 0100 GMT when storm activity diminished. High mixing ratios also were present near Midland after a strong storm formed there at 2300 GMT.

Equivalent potential temperature (Fig. 5.15.2.4) exhibited minimum values in the northeast and maximum values generally in the west and northwest through the day. Relatively low potential temperatures were present at Lenorah and Walsh-Watts at 1900 and 2000 GMT, when two strong storm cells were located in that area. Clairemont's potential temperature was low at 2100 GMT as the

MISSING DATA

MISSING DATA

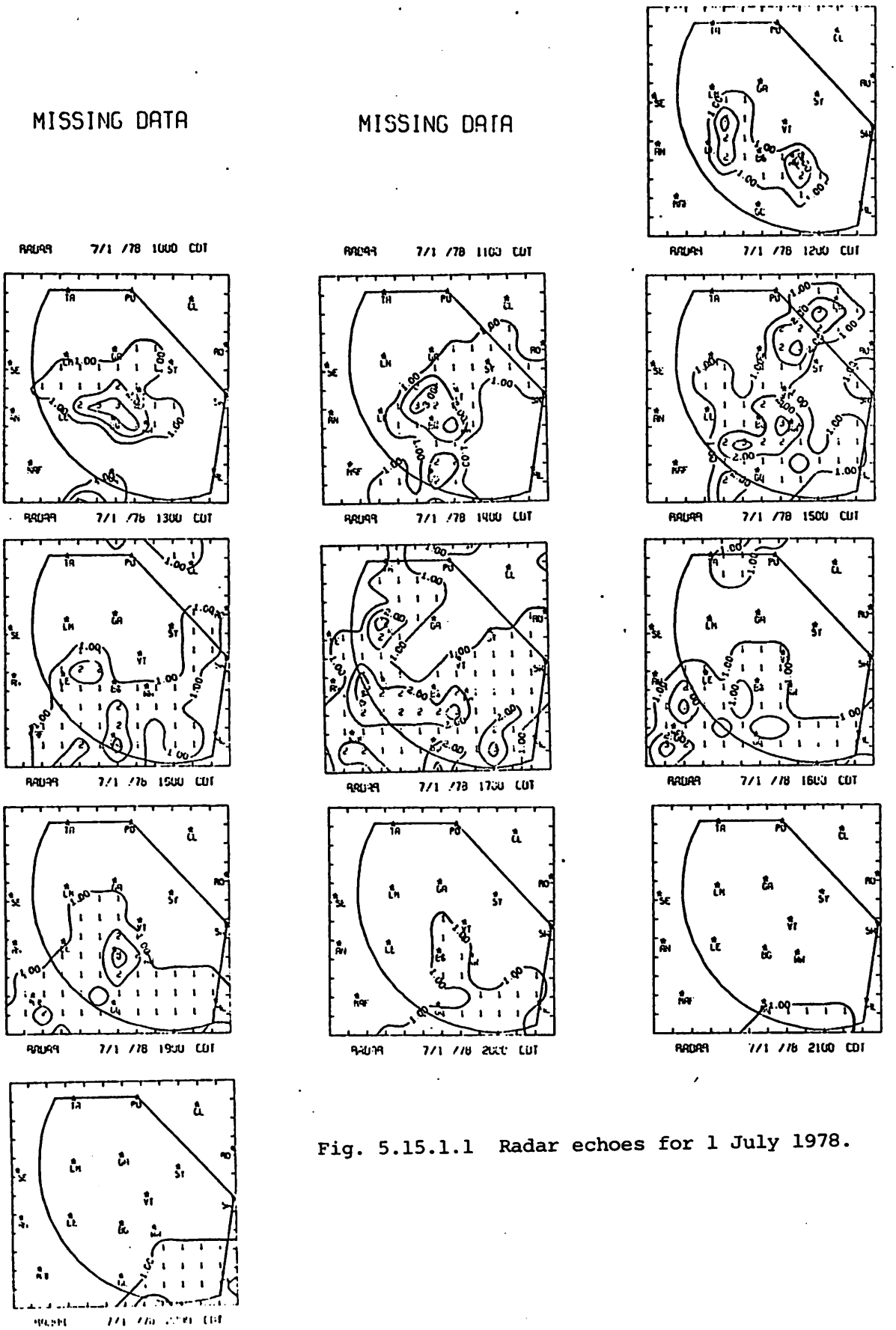

Fig. 5.15.1.1 Radar echoes for 1 July 1978.

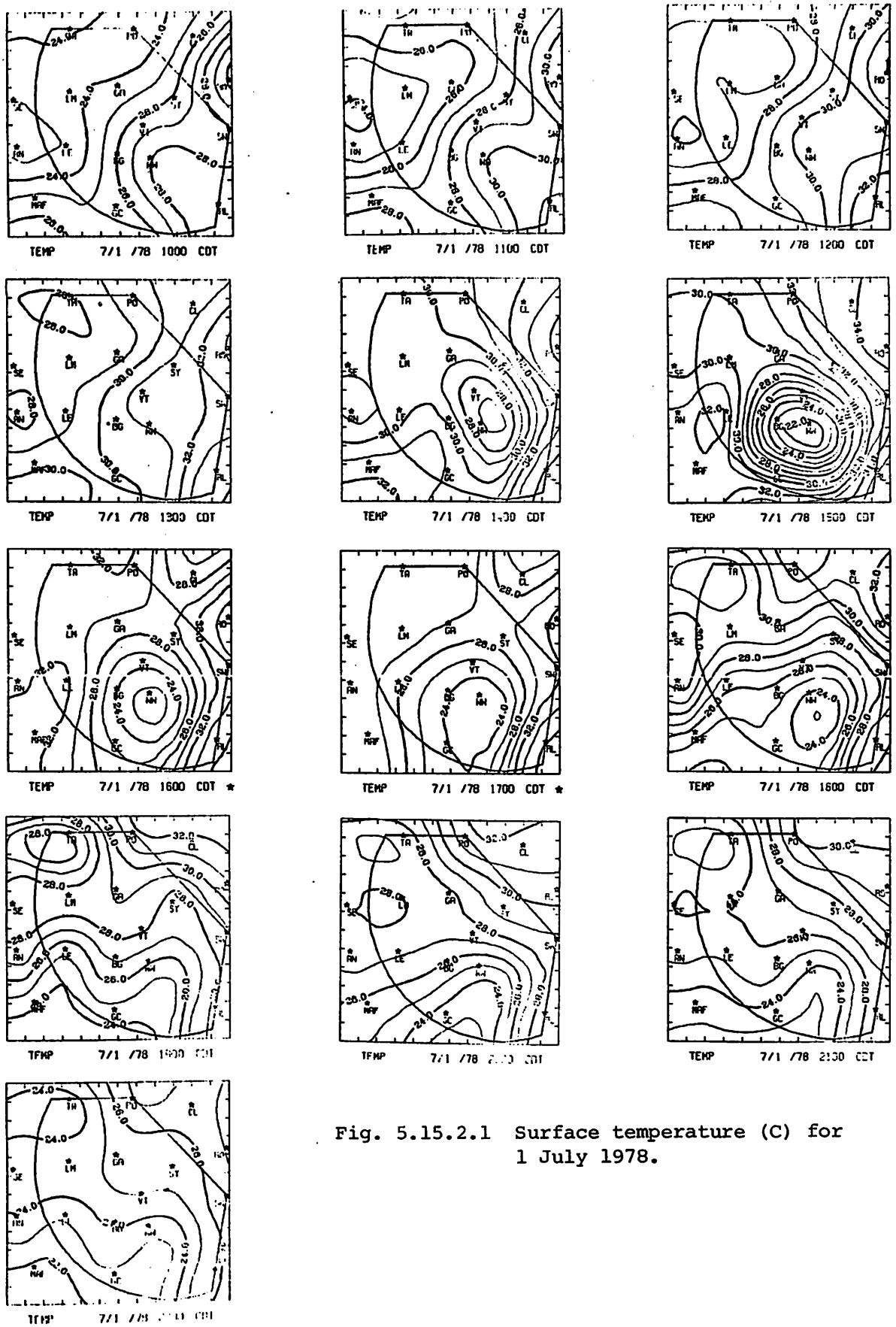

Fig. 5.15.2.1 Surface temperature (C) for 1 July 1978.

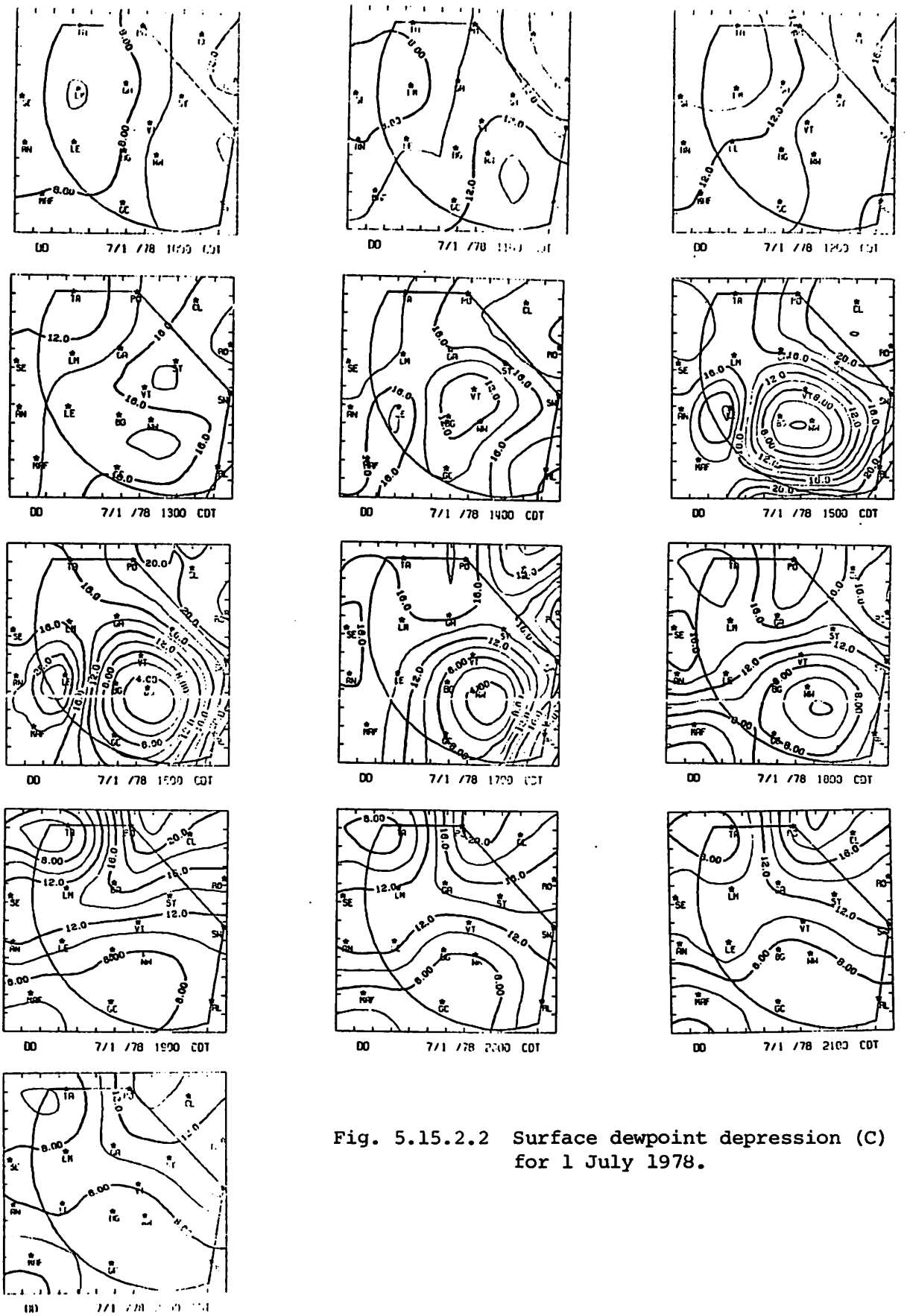

Fig. 5.15.2.2 Surface dewpoint depression (C) for 1 July 1978.

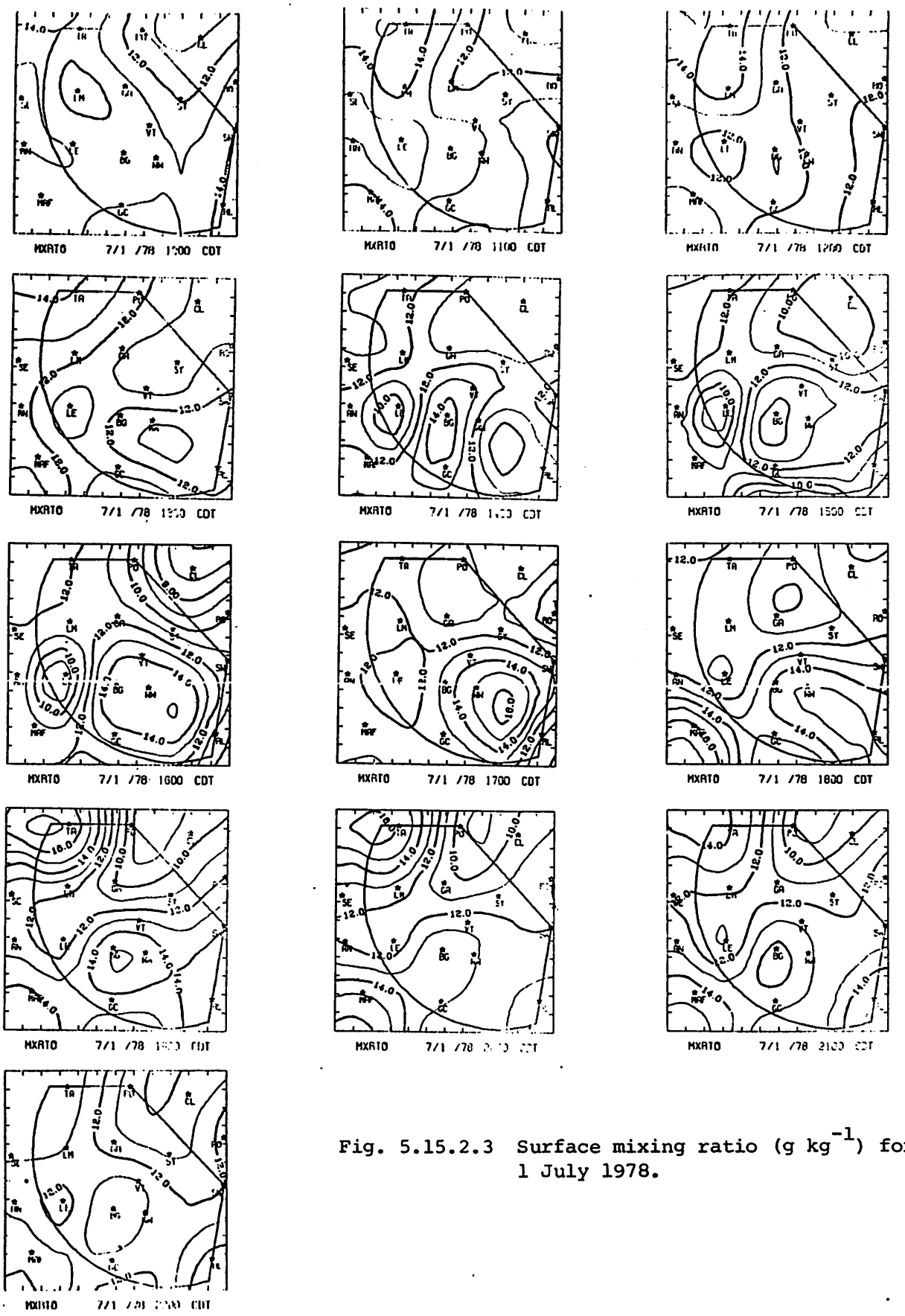

Fig. 5.15.2.3 Surface mixing ratio (g kg^{-1}) for 1 July 1978.

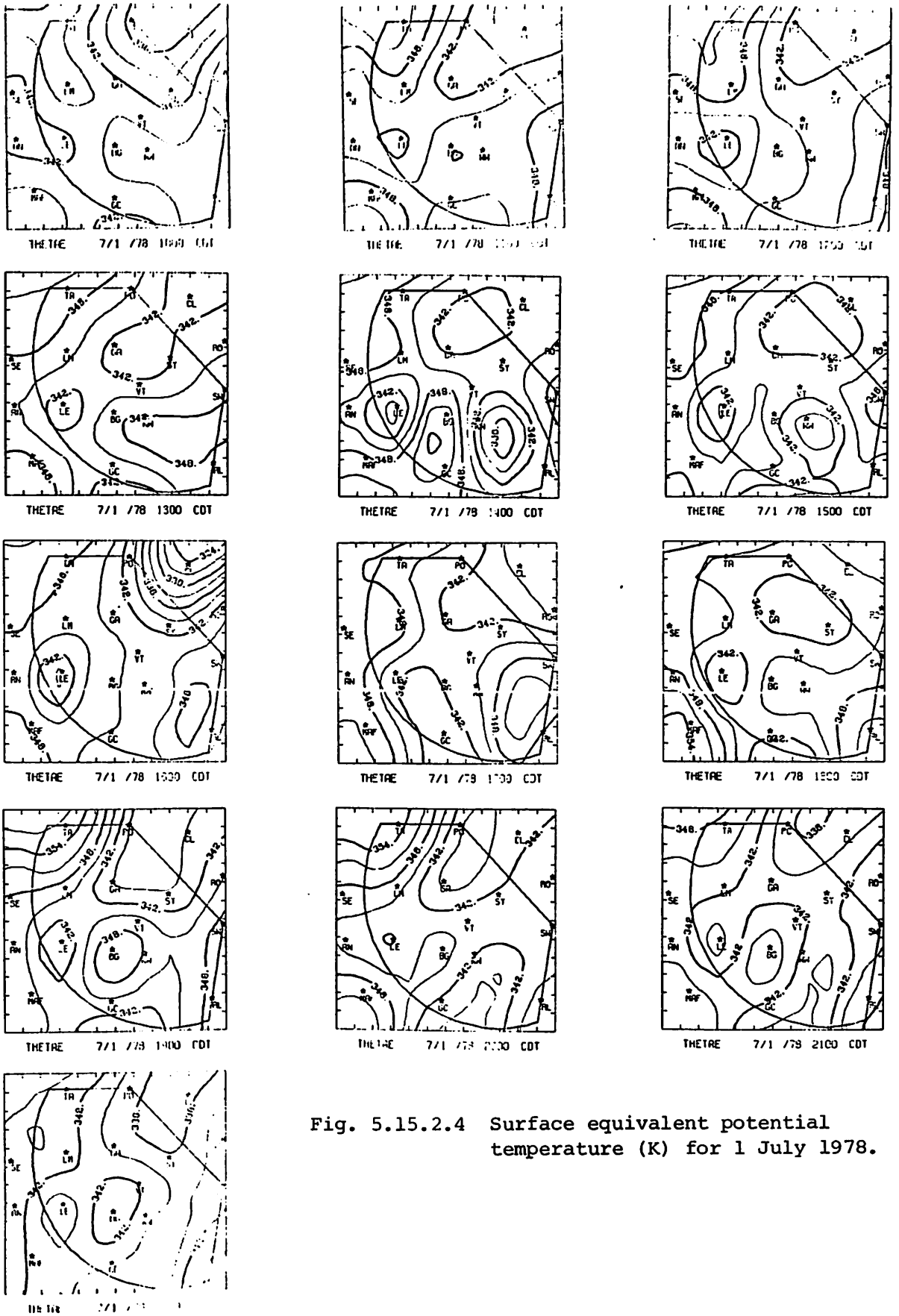

Fig. 5.15.2.4 Surface equivalent potential temperature (K) for 1 July 1978.

temperature and mixing ratio decreased in that area. A strong storm cell dissipated near Clairemont at that time. Increases in potential temperature took place at Midland at 2300 GMT, and near Big Spring at 0000 GMT as strong cells formed in those areas. Potential temperatures decreased across the area after 0000 GMT as temperatures decreased and storm activity diminished.

Terrain-induced vertical motion (Fig. 5.15.2.5) was generally small over the area. A few centers of downward motion were indicated but these did not have a significant effect on storm activity.

Surface divergence (Fig. 5.15.2.6) showed only moderate values until 1800 GMT. Strong convergence formed in the south at 1800 GMT as strong thunderstorm cells were building in the central part of the area. Convergence also was present in the northeast between 1900 and 2000 GMT when storm cells were forming in that area. Divergence developed near Vincent at 2000 GMT, and shower activity decreased there in the next hour. Meanwhile, convergence formed in the southwest near Midland between 2100 and 2300 GMT concurrent with storm formation in that area. Divergence prevailed over the area after 0000 GMT as shower activity decreased.

Vertical motion 50 mb above the surface is shown in Fig. 5.15.2.7. Strong vertical motion was not present until 1800 GMT when a center of strong upward motion formed in the south. Strong downward motion associated with the storms was present in the central area after 2000 GMT, generally in the area of storm-induced cooling (see Fig. 5.15.2.1). Strong upward motion was present near Midland after 2100 GMT associated with storm formation there. Generally weak downward motion occurred over the area after 0000 GMT.

Surface moisture divergence (Fig. 5.15.2.8) showed only moderate values before 1800 GMT. Strong centers of convergence and divergence formed in the south after 1800 GMT associated with storm formation in the center of the region. Strong moisture divergence developed in the central area at 2000 GMT north of some well developed storms with heights of 13.7 km (45K ft). Convergence developed near Midland at 2100 GMT and was strong in that area through 2300 GMT as storms developed near there. Strong moisture divergence replaced the convergence at 0000 GMT. As the storms near Midland dissipated, weak divergence prevailed after 0000 GMT.

Vertical flux of moisture 50 mb above the surface (Fig. 5.15.2.9) also shows moderate values until 1800 GMT. Strong centers of upward and downward flux developed at 1800 GMT in the south with the increase in shower activity

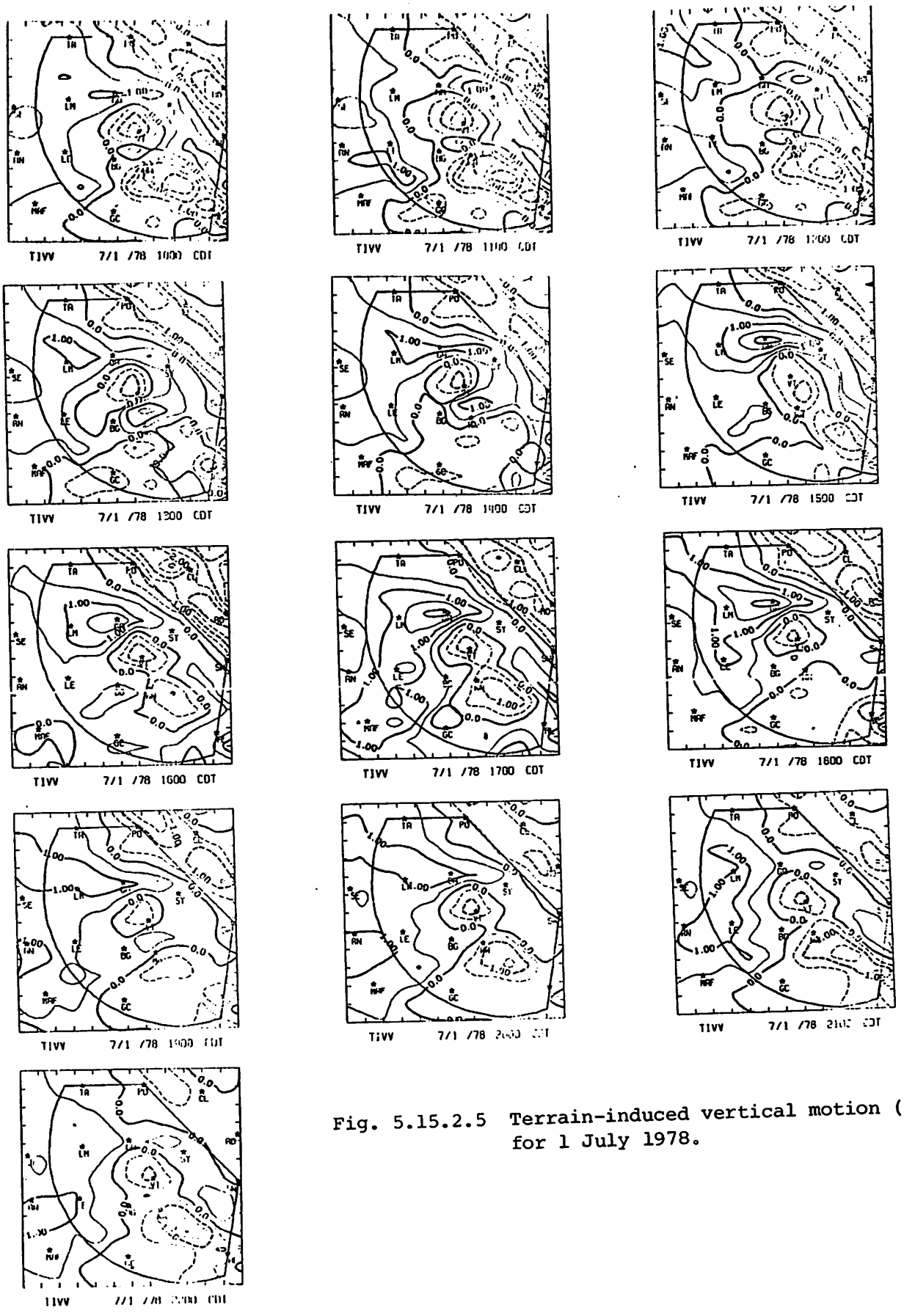

Fig. 5.15.2.5 Terrain-induced vertical motion (cm s^{-1}) for 1 July 1978.

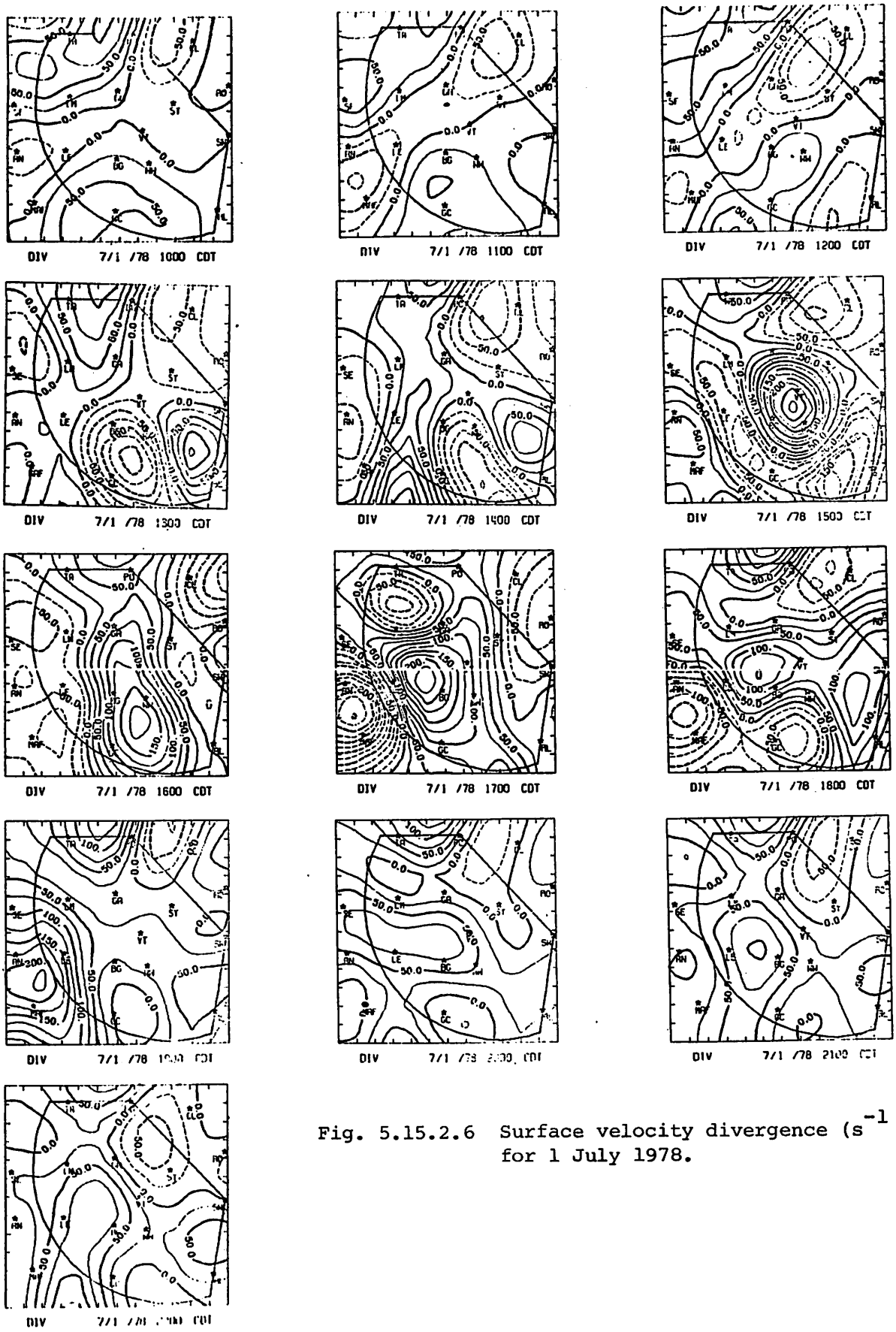

Fig. 5.15.2.6 Surface velocity divergence ($s^{-1} \times 10^{-6}$) for 1 July 1978.

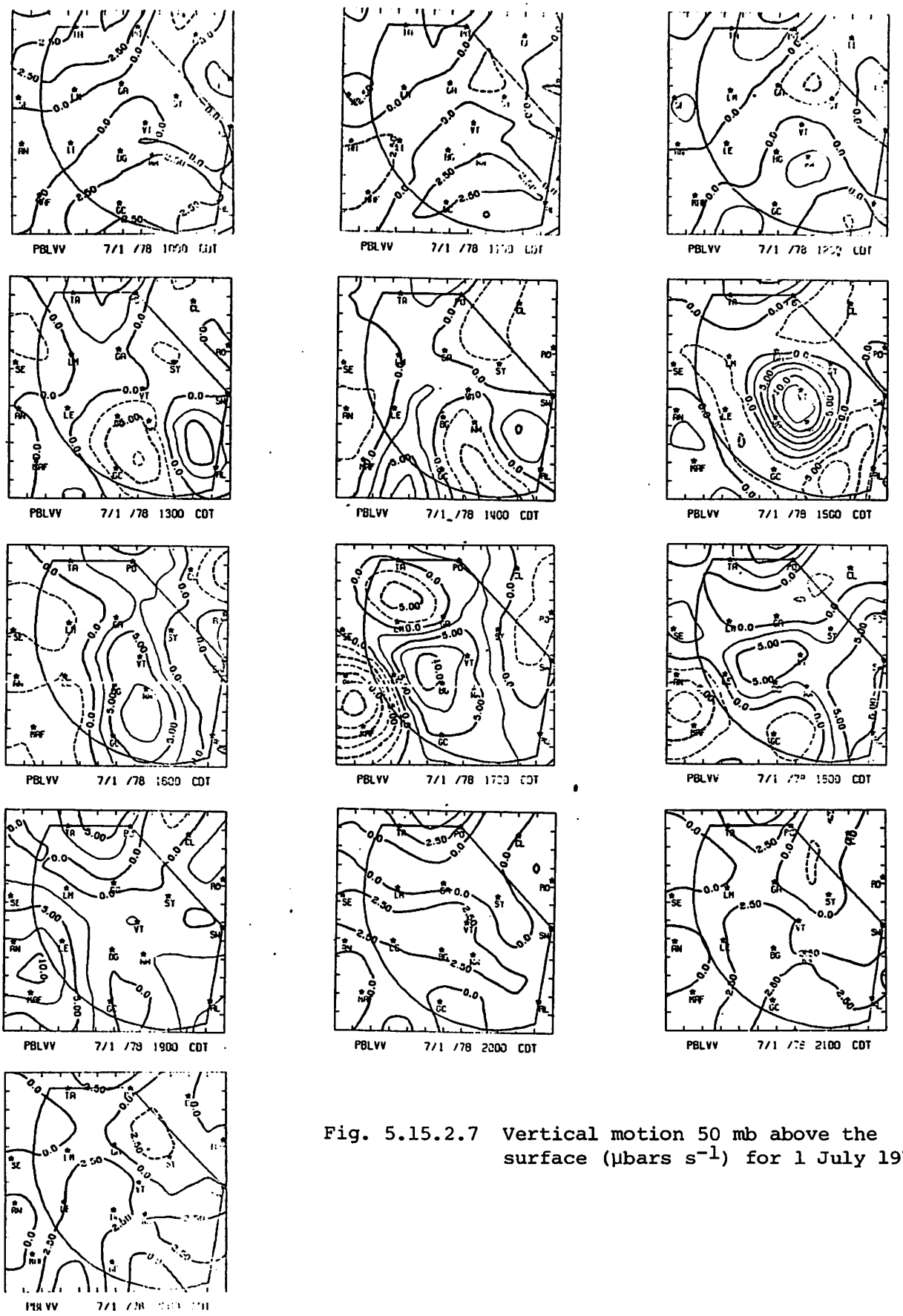

Fig. 5.15.2.7 Vertical motion 50 mb above the surface (μbars s^{-1}) for 1 July 1978.

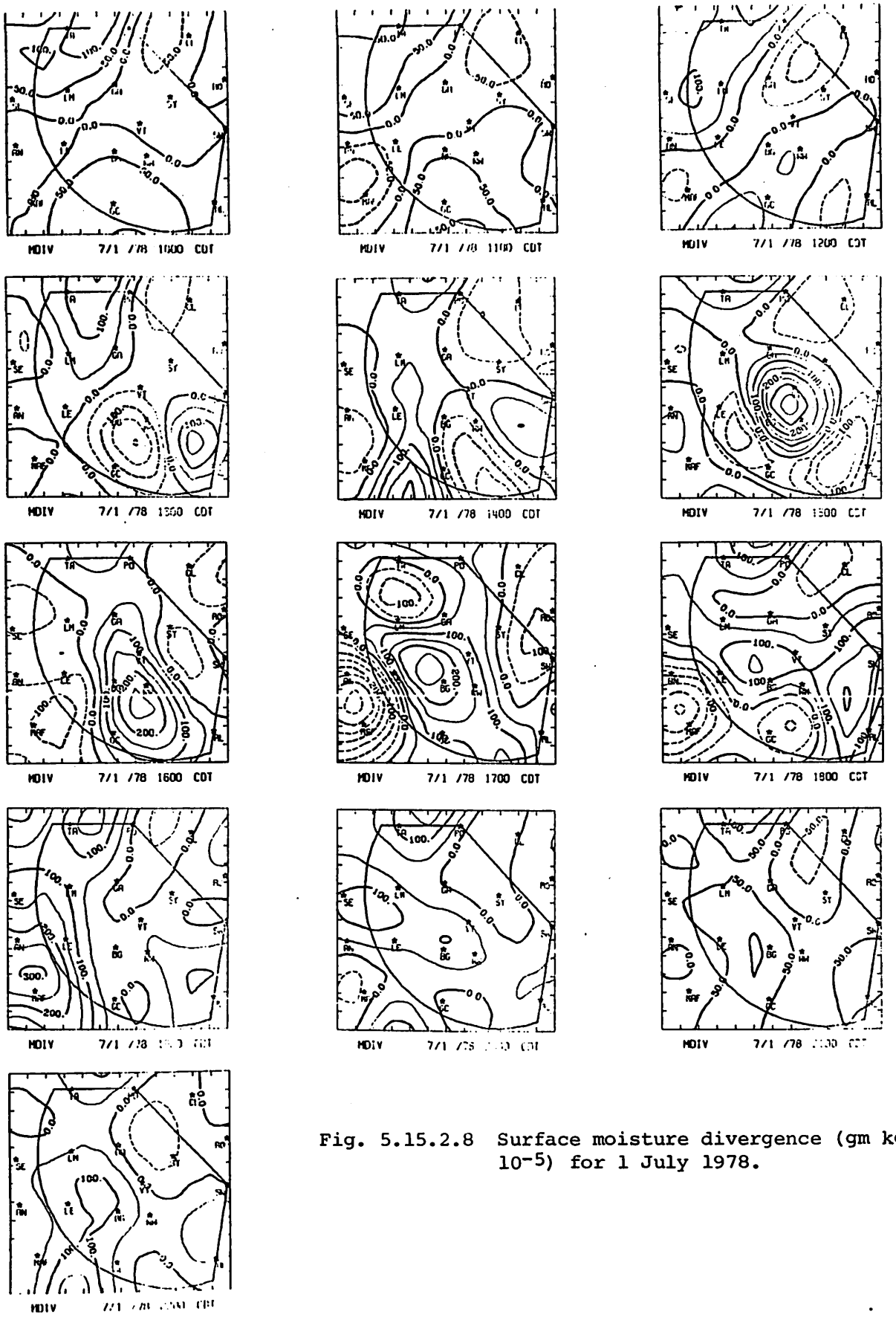

Fig. 5.15.2.8 Surface moisture divergence (gm kg^{-1} s^{-1} x 10^{-5}) for 1 July 1978.

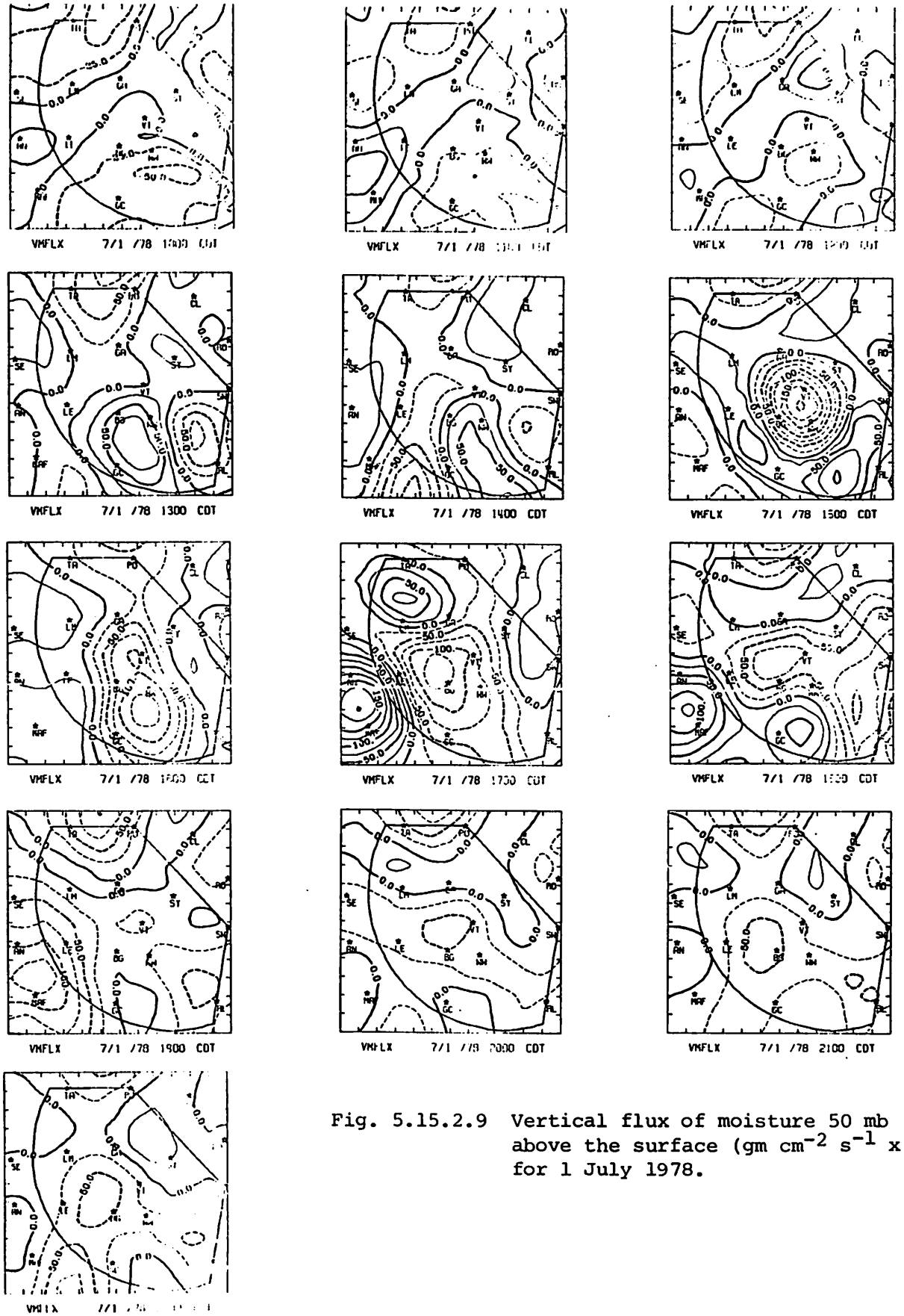

Fig. 5.15.2.9 Vertical flux of moisture 50 mb above the surface (gm cm^{-2} s^{-1} x 10^{-6}) for 1 July 1978.

in the HIPLEX area. Strong downward flux of moisture was present in the downdraft near Vincent at 2000 GMT and near Walsh-Watts at 2100 GMT. Strong upward fluxes of moisture were present in the southwest at 2200 and 2300 GMT as strong storm cells developed there. This was replaced by strong downward flux at 0000 GMT as the storms in the southwest dissipated. Generally moderate values of moisture flux were present after 0000 GMT.

Surface vorticity (Fig. 5.15.2.10) showed small to moderate values at the centers until 1800 GMT. Strong centers of both positive and negative vorticity formed and dissipated over the next six hours as storm activity moved through the area. After 0000 GMT, as storm acitvity decreased across the area, moderate values again prevailed.

Surface pressure changes (Fig. 5.15.2.11) were not large from hour to hour. Pressure data from Tahoka were missing from 1700 GMT and following so the pressure drop shown at that time may not be valid. The pressure rise of 0.5 mb at Walsh-Watts at 2000 GMT is interesting to note since it occurred when pressures at other stations were dropping. This rise is connected with the thunderstorm activity and coincides with the area of downward vertical motion and downdraft-induced cooling. At 2200 GMT the pressure dropped 1 mb at Lamesa as a strong storm cell formed in that area and then dissipated. Small pressure changes were present after 0000 GMT.

Surface winds (Fig. 5.15.2.12) were generally southerly at 1500 GMT. At 1800 GMT winds shifted near Walsh-Watts as shower activity increased. Changes in the wind pattern occurred in the next few hours which produced changes in both divergence and vorticity. By 0100 GMT, however, the winds were generally southerly again as storm activity decreased.

5.15.3 Upper Level Kinematic Parameters

Figure 5.15.3.1 shows vertical profiles of mass divergence. At 1500 GMT convergence was present in the lowest levels with some middle-level divergence. As shower activity increased, the layer of middle-level divergence decreased until 2100 GMT when convergence was present to 400 mb. This was just before the time of maximum storm coverage in the area. By 0000 GMT storm activity had begun to diminish and low-level divergence was present. By 0300 GMT convergence in middle layers had decreased in magnitude as shower activity decreased.

Profiles of vertical motion (Fig. 5.15.3.2) show mostly upward motion at 1500 GMT. At 1800 and 2100 GMT, when moderate to strong activity developed

Fig. 5.15.2.10 Surface vorticity (s^{-1} x 10^{-6}) for 1 July 1978.

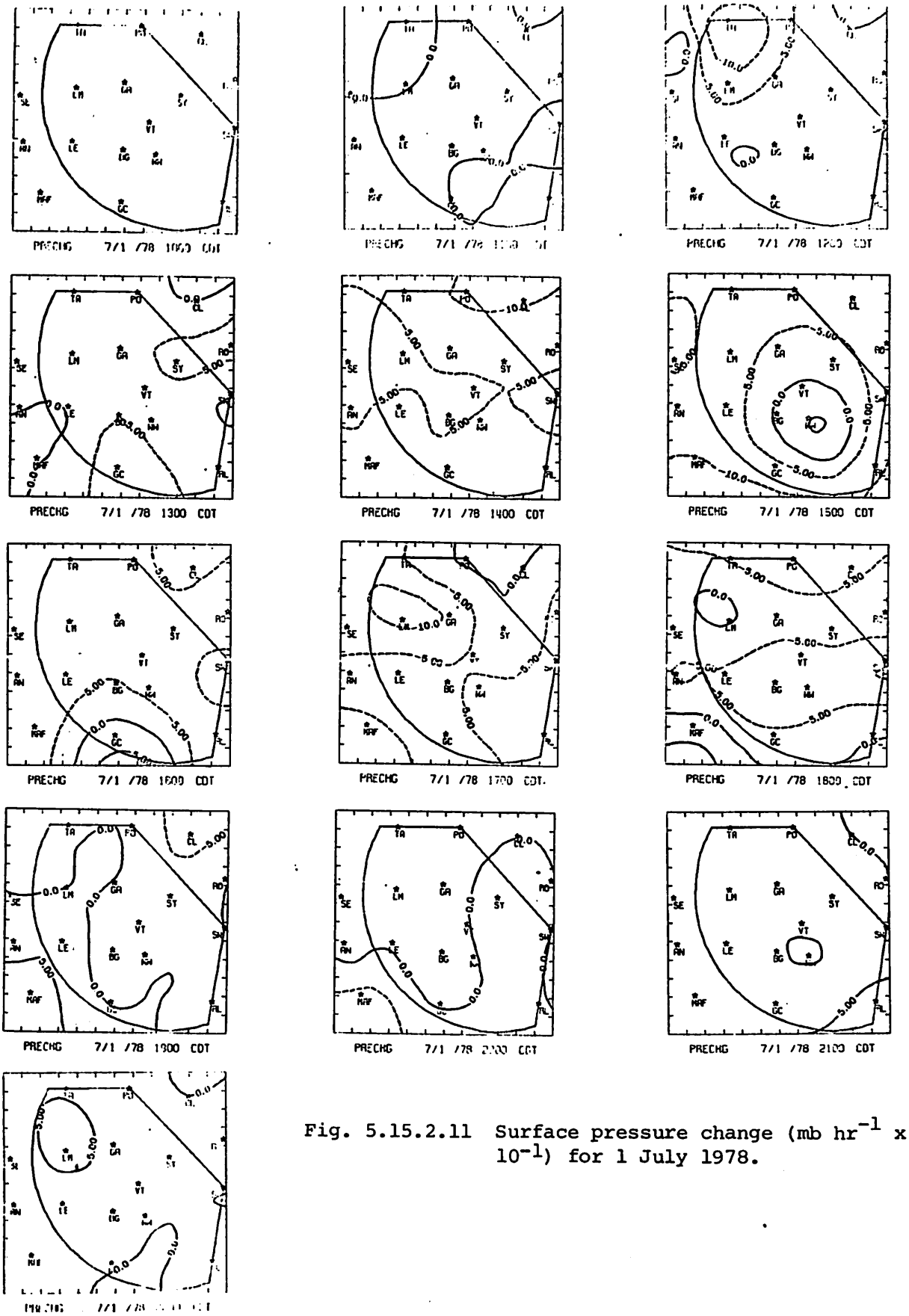

Fig. 5.15.2.11 Surface pressure change (mb hr^{-1} x 10^{-1}) for 1 July 1978.

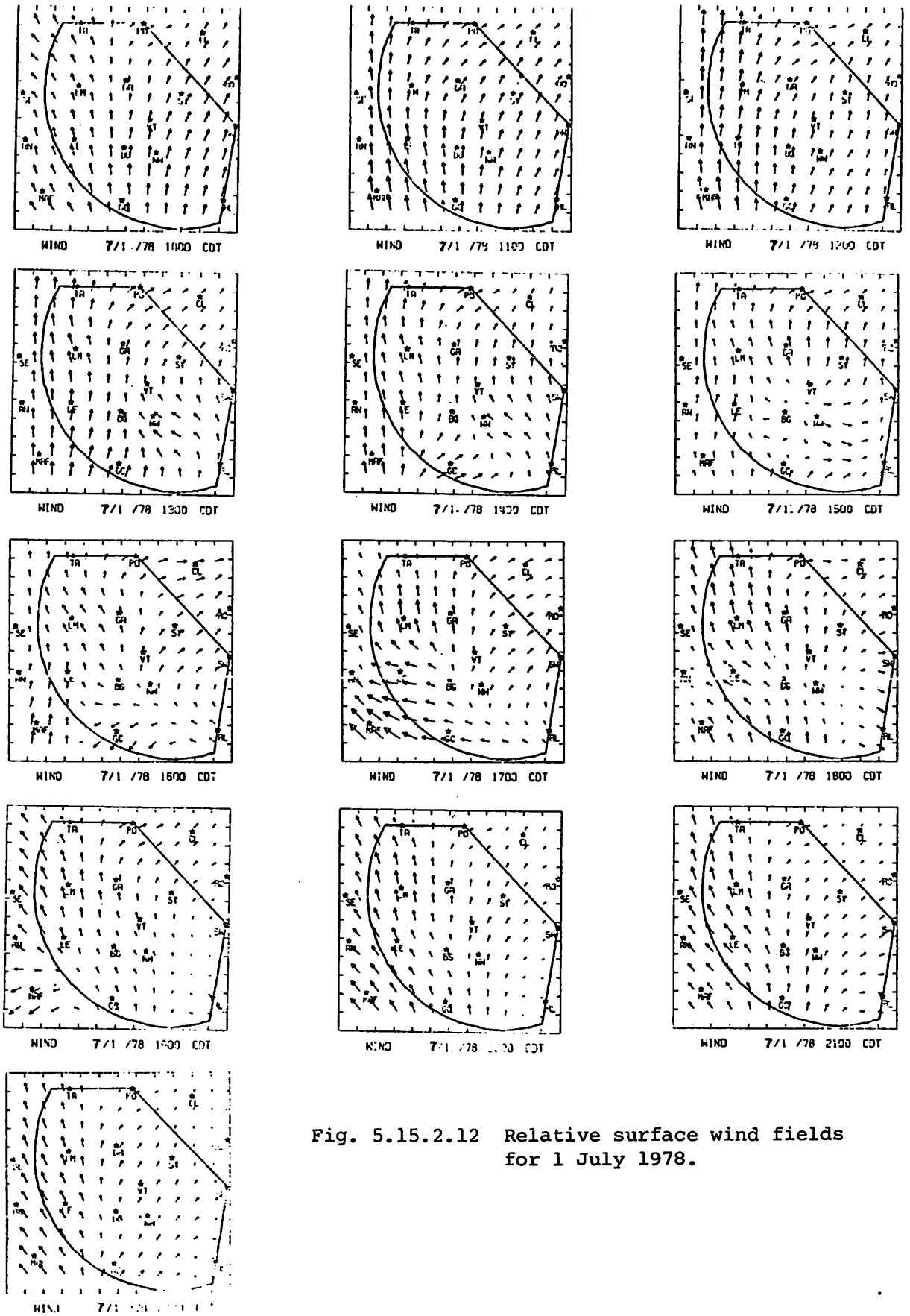

Fig. 5.15.2.12 Relative surface wind fields for 1 July 1978.

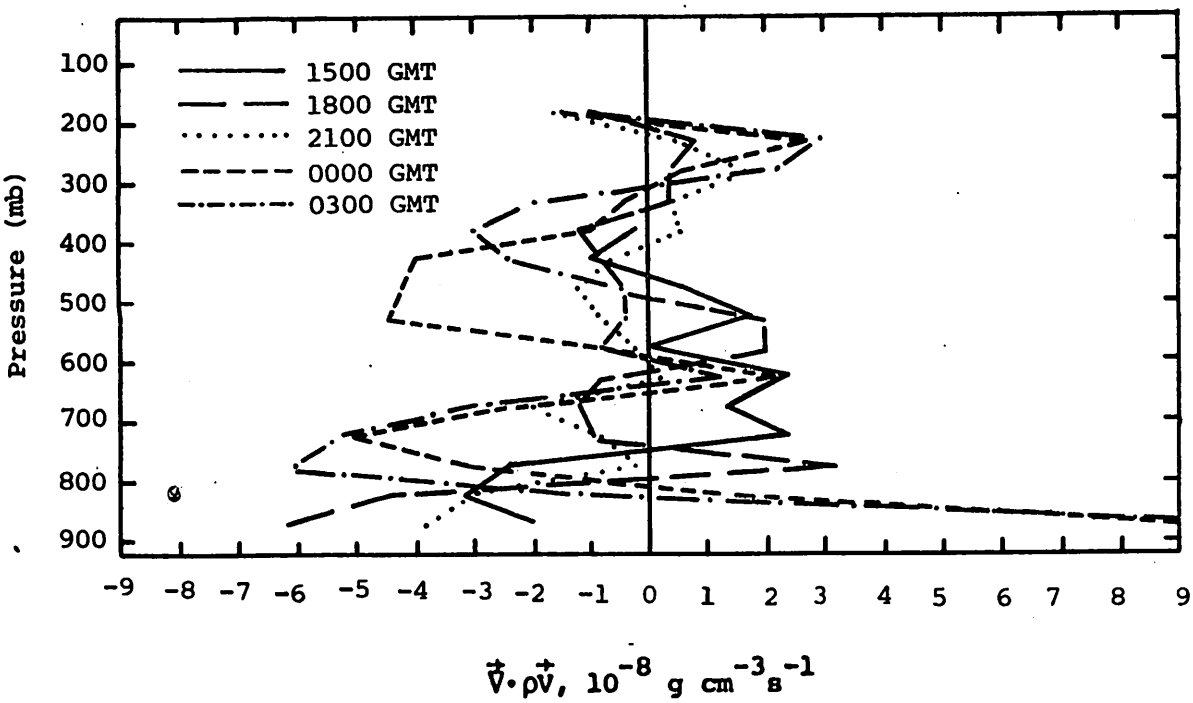

Fig. 5.15.3.1 Vertical profiles of mass divergence on 1 July 1978.

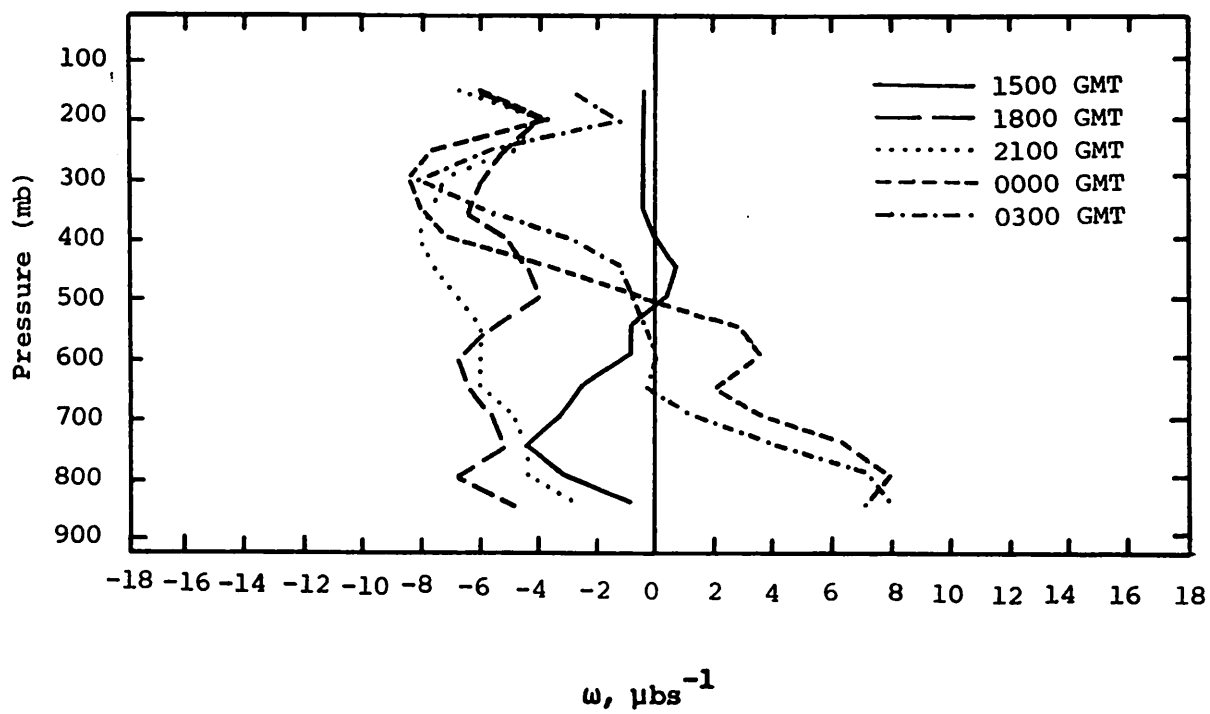

Fig. 5.15.3.2 Vertical profiles of vertical motion on 1 July 1978.

in the area, the magnitude of the upward motion increased. At 0000 and 0300 GMT, as shower activity was decreasing, downward motion was present below 500 mb. Above 500 mb there was not much change in vertical motion, however.

Profiles of moisture divergence (Fig. 5.15.3.3) show convergence in low levels at 1500 GMT with divergence above 750 mb. As showers developed at 1800 GMT, low-level moisture convergence increased. By 2100 GMT moisture convergence was present to 500 mb. After 0000 GMT, however, divergence was present in the lowest layers and convergence in middle layers.

5.15.4 Energetics

At 1500 GMT, inflow of latent heat energy was present below 750 mb with outflow above that level. The low-level inflow increased at 1800 GMT as shower activity developed over the HIPLEX area. By 2100 GMT latent heat inflow was present at all levels below 500 mb although the inflow was small at some levels. Strong outflow of latent heat energy occurred in the lowest layer at 0000 and 0300 GMT as storms were decreasing. Strong inflow of latent heat was present in the 700-800-mb layer at that time (See Fig. 5.15.4.1).

Profiles of vertical flux of latent heat (Fig. 5.15.4.2) show transport upward out of the lowest layers into middle layers between 1500 and 2100 GMT. At 0000 and 0300 GMT the situation was reversed. Latent heat was transported downward from middle layers into lower layers as showers were decreasing.

Profiles of local change of latent heat (Fig. 5.15.4.3) showed gains in layers between 700 and 800 mb and losses above and below this layer. The gains in latent heat had increased through the area at 1800 GMT, and by 2100 GMT the local change of latent heat was positive in all layers. This was when the storm activity was increasing through the area. At 0000 GMT the local change was negative or near zero through all the layers. The profile at 0300 GMT was similar, though the 650-750-mb layer showed larger positive local change in latent heat.

Figure 5.15.4.4 shows profiles of the residual of the latent heat energy equation. The profiles show mainly positive values between 1500 and 1800 GMT which would correspond to losses in latent heat as a result of condensation. This occurred just prior to and during storm formation. The storm activity decreased after 0000 GMT which shows up in the 0000 and 0300 GMT profiles as predominantly negative values.

Profiles of diabatic heating are shown in Fig. 5.15.4.5. These profiles agree in a general way with the profiles in Fig. 5.15.4.4. Loss of latent

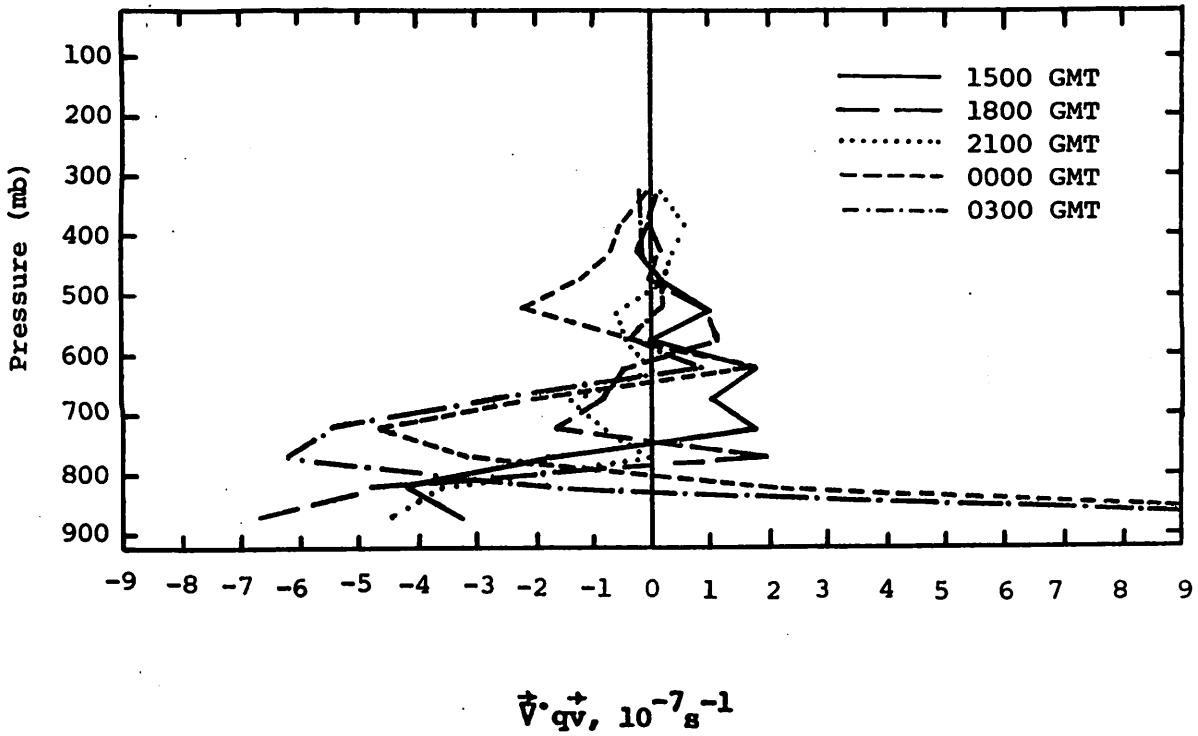

Fig. 5.15.3.3 Vertical profiles of moisture divergence on 1 July 1978.

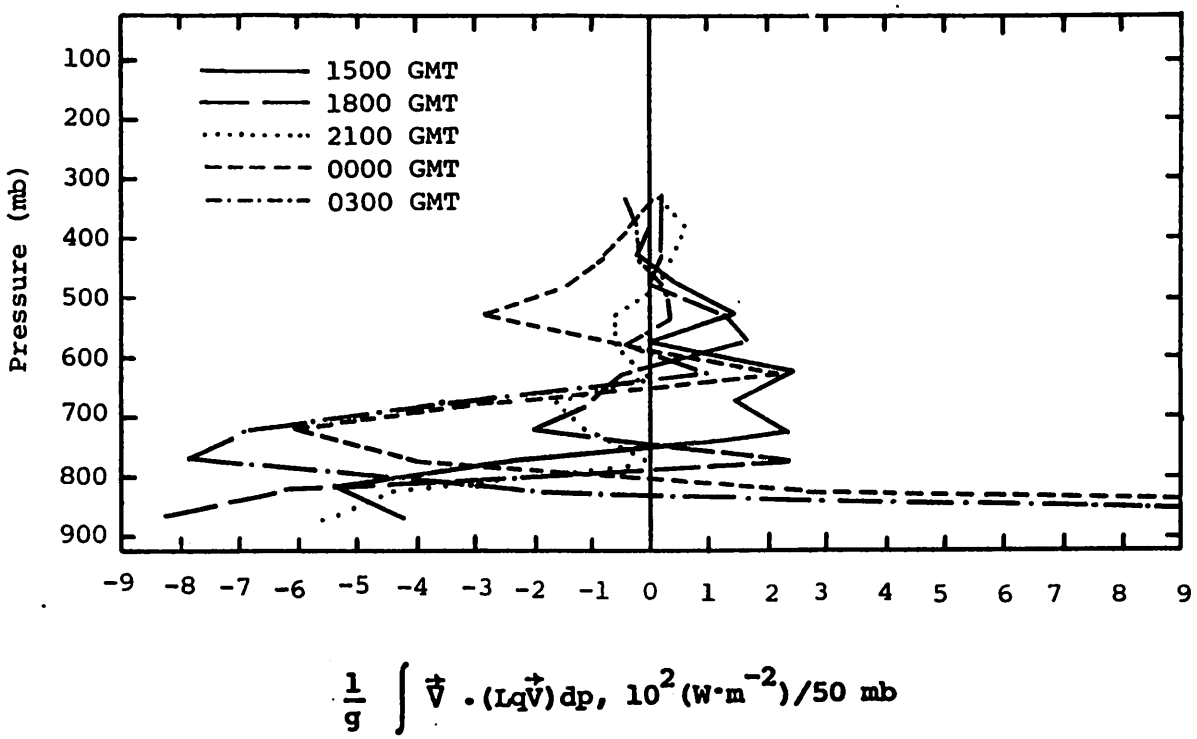

Fig. 5.15.4.1 Vertical profiles of the horizontal flux of latent heat energy on 1 July 1978.

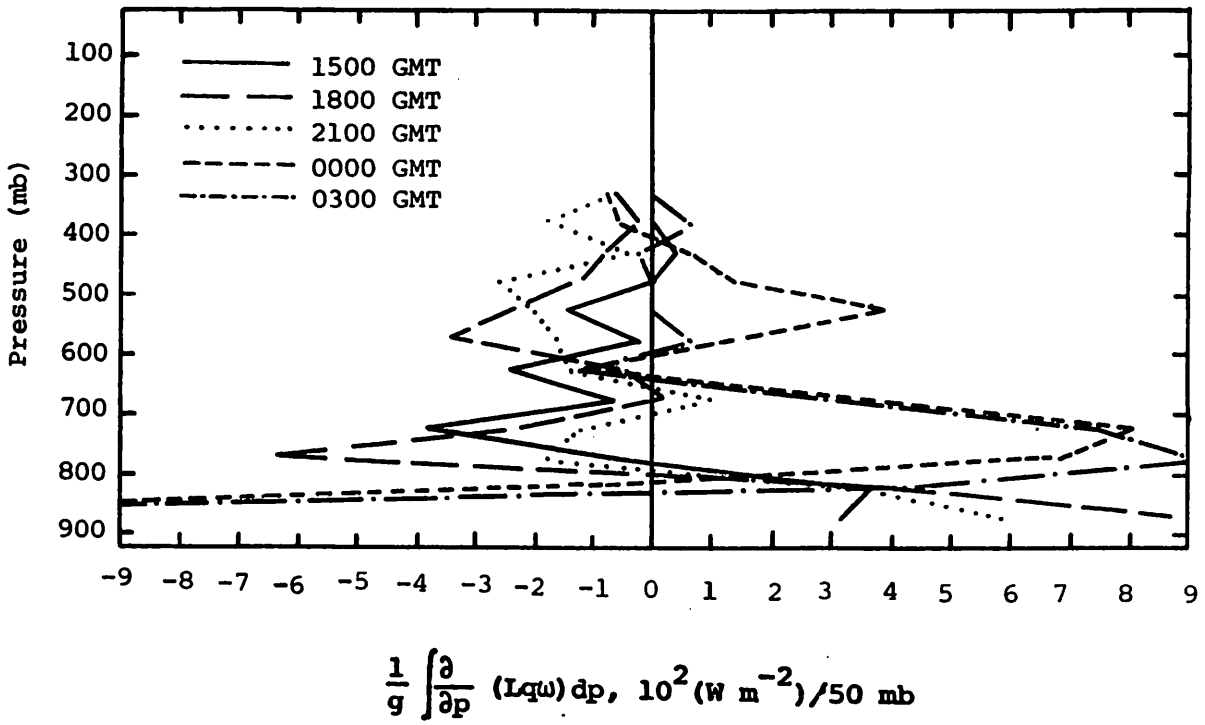

Fig. 5.15.4.2 Vertical profiles of the vertical flux of latent heat on 1 July 1978.

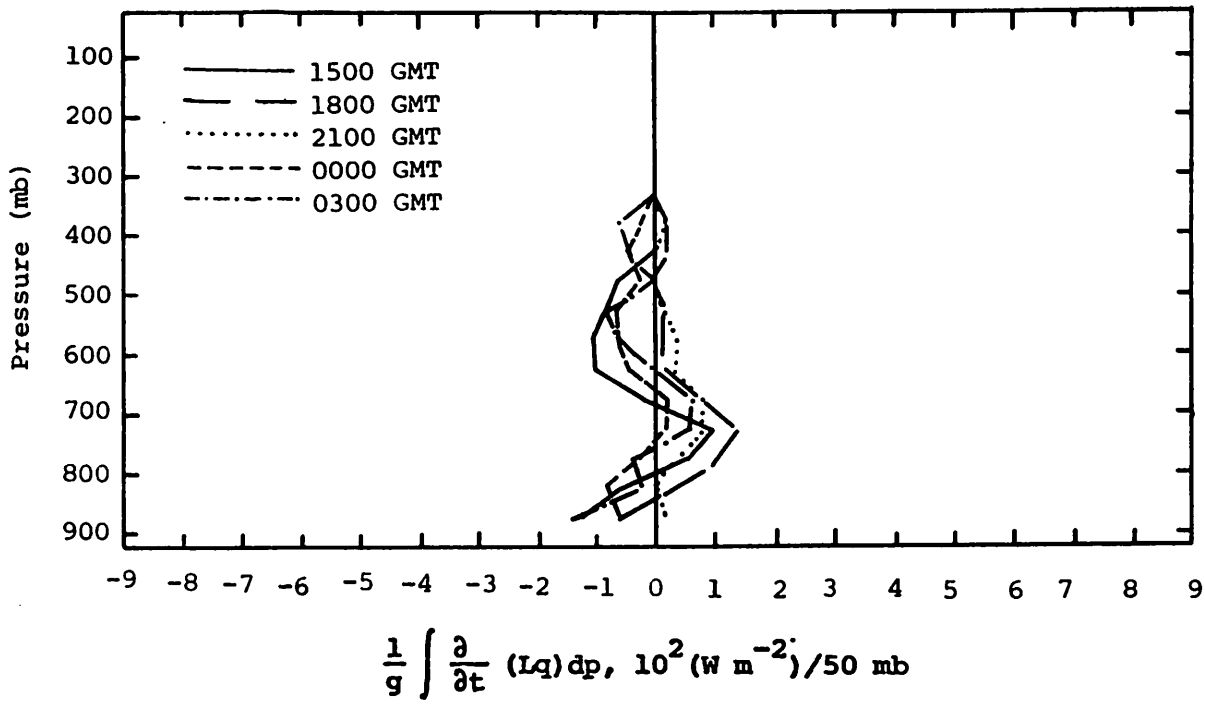

Fig. 5.15.4.3 Vertical profiles of the local change of latent heat energy on 1 July 1978.

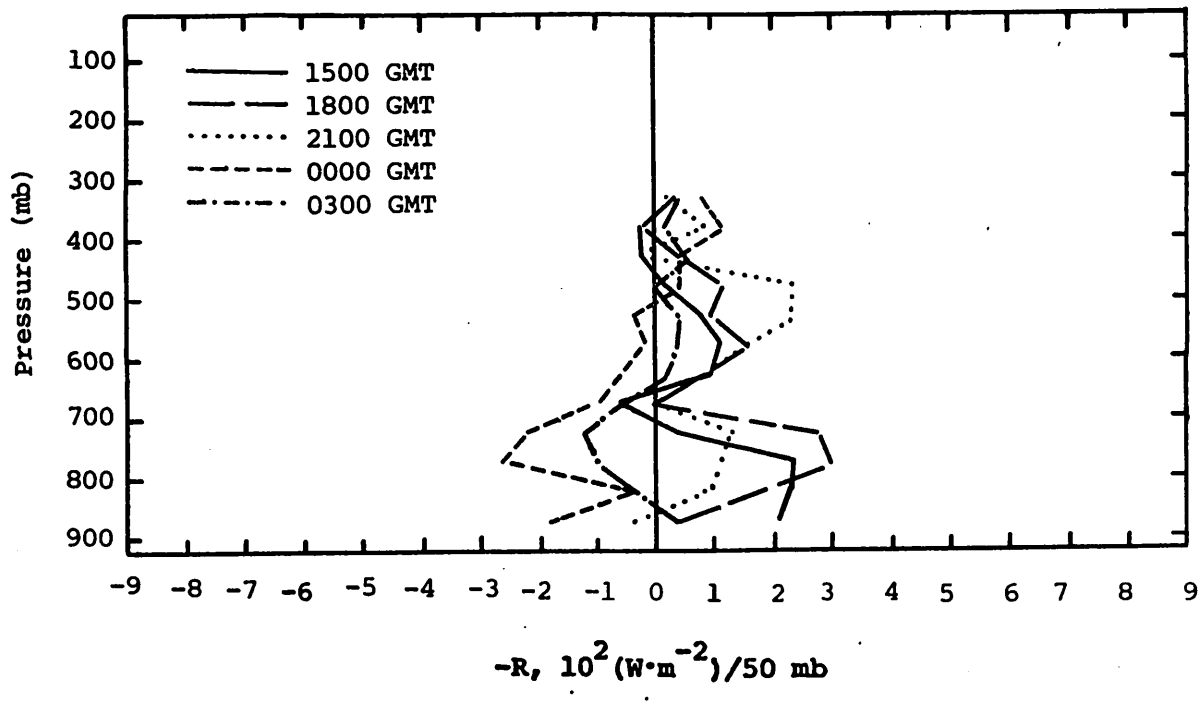

Fig. 5.15.4.4 Vertical profiles of the residual of the latent heat energy equation on 1 July 1978.

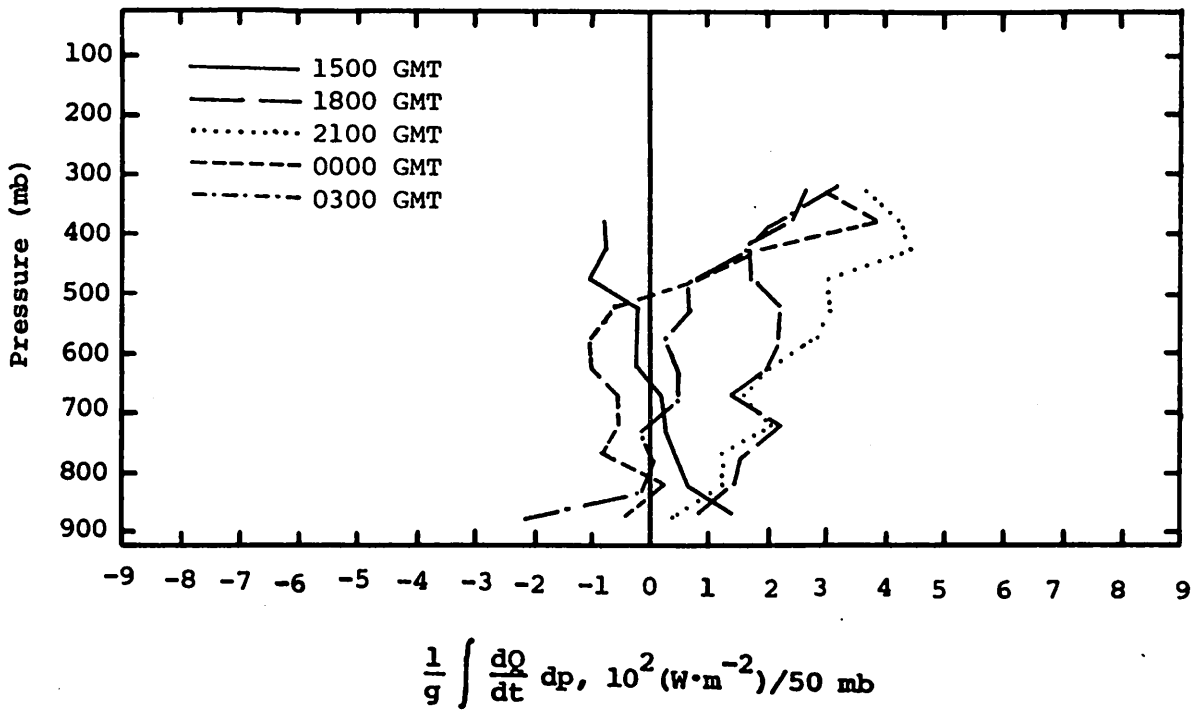

Fig. 5.15.4.5 Vertical profiles of diabatic heating computed from the first law of thermodynamics on 1 July 1978.

heat by condensation corresponds to increases in sensible heat and this is exhibited in the 1800 and 2100 GMT profiles. The profiles of the other time periods show less similarity to the corresponding profiles of the residual of the latent heat energy equation. This could have resulted from the effect of some other form of diabatic heating or the incorporation of a residual error in either of the sets of profiles.

The horizontal flux of kinetic energy (Fig. 5.15.4.6) was generally small in layers below 300 mb. Horizontal outflow of kinetic energy was present in layers below 300 mb at 1500 and 1800 GMT. Inflow of kinetic energy predominated in layers below 300 mb after 2100 GMT. In the layer between 200 and 300 mb, moderate to strong horizontal outflow was present at all time periods.

Vertical fluxes of kinetic energy (Fig. 5.15.4.7) were also generally small in the lower layers. All time periods showed vertical flux of kinetic energy upward out of a layer between 300 and 400 mb to layers above this level. At 0000 GMT there was also moderate flux of kinetic energy downward below 700 mb.

5.15.5 Water Vapor Budget

Figure 5.15.5.1 shows profiles of net horizontal transport of water vapor. At 1500 GMT the profile shows outflow in middle layers between 750 and 450 mb with inflow above and below. At 1800 GMT, as shower activity was building, inflow of water vapor began between 650 and 750 mb. The water vapor outflow at 1800 GMT was not as extensive as in the earlier profile. At 2100 GMT inflow was present at all layers below 500 mb, and the shower activity was well developed. At 0000 GMT some outflow was present in the lowest layer and from 600 to 650 mb but water vapor gains prevailed. The shower activity decreased after 0000 GMT, and in the 0300 GMT profiles there were losses of water vapor between 450 and 650 mb. However, strong inflow of water vapor was present below 650 mb.

The net vertical transport of water vapor is shown in Fig. 5.15.5.2. The 1500 GMT profile shows losses in the lowest layer with gains in middle layers. Above 500 mb losses were present at that time. At 1800 and 2100 GMT, when showers developed and increased in the area, the profiles were similar. Losses were present only in the lowest layer and water vapor was transported into the middle and upper layers. After 0000 GMT the shower activity decreased, and the profiles showed predominantly losses of water

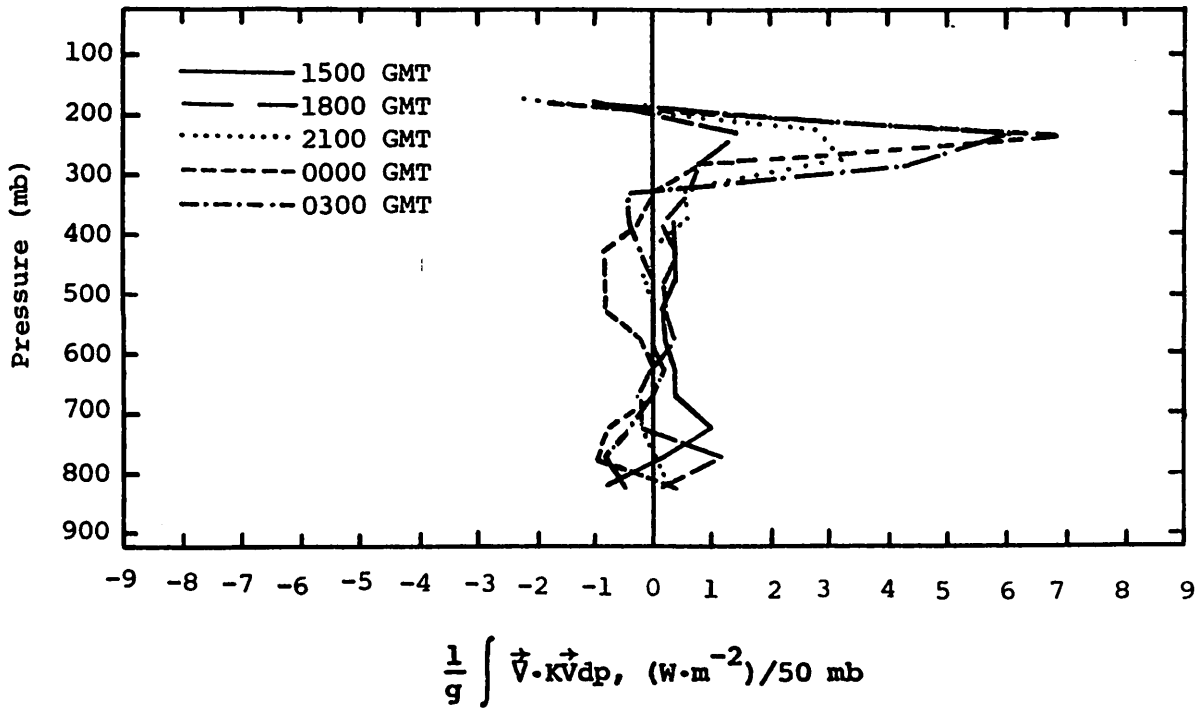

Fig. 5.15.4.6 Vertical profiles of the horizontal flux of kinetic energy on 1 July 1978.

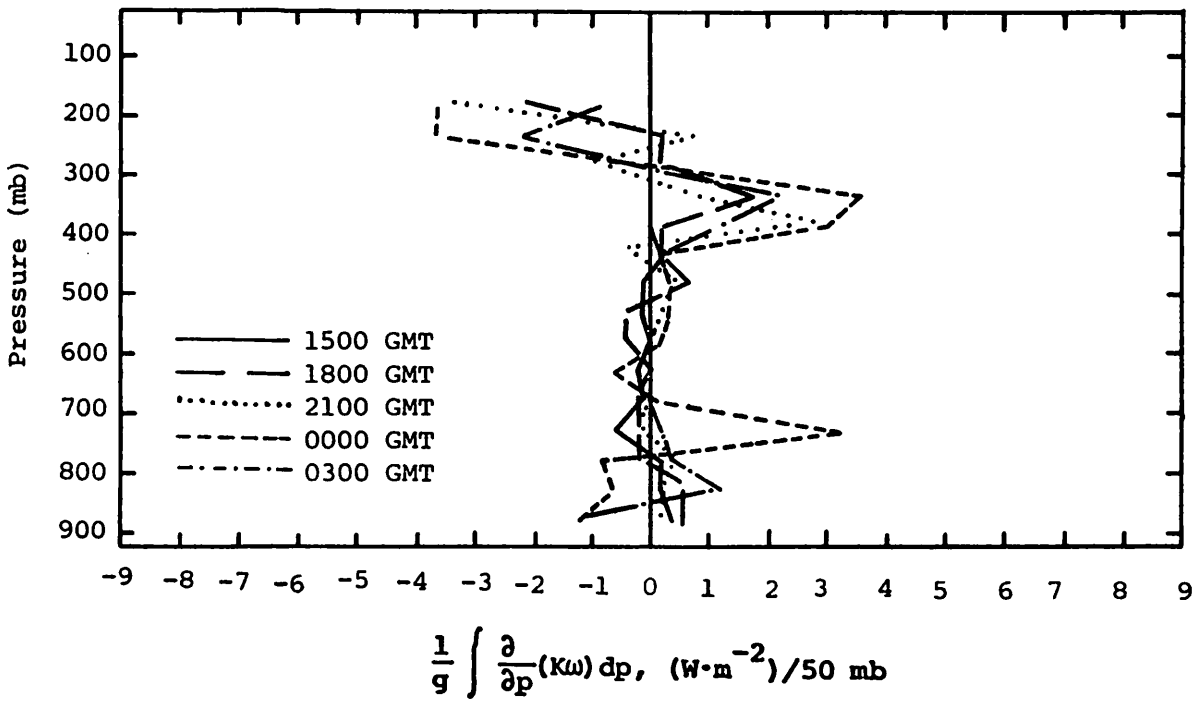

Fig. 5.15.4.7 Vertical profiles of the vertical flux of kinetic energy on 1 July 1978.

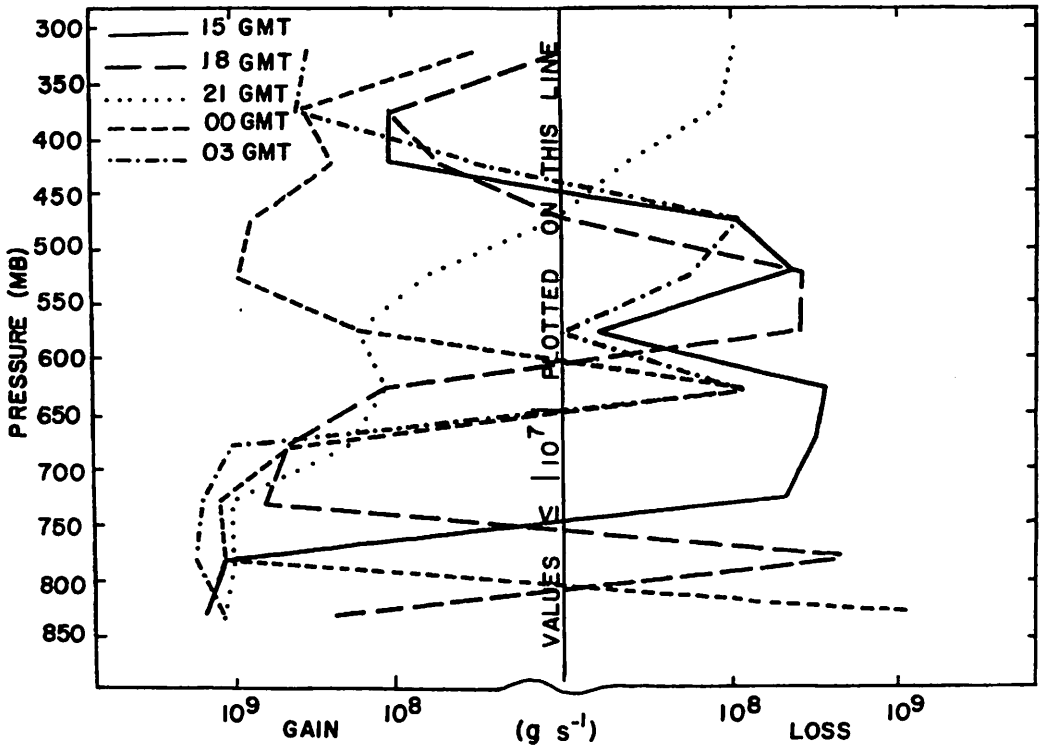

Fig. 5.15.5.1 Net horizontal transport of water vapor through boundaries of 50-mb layers (g s^{-1}) over the Texas HIPLEX area for 1 July 1978.

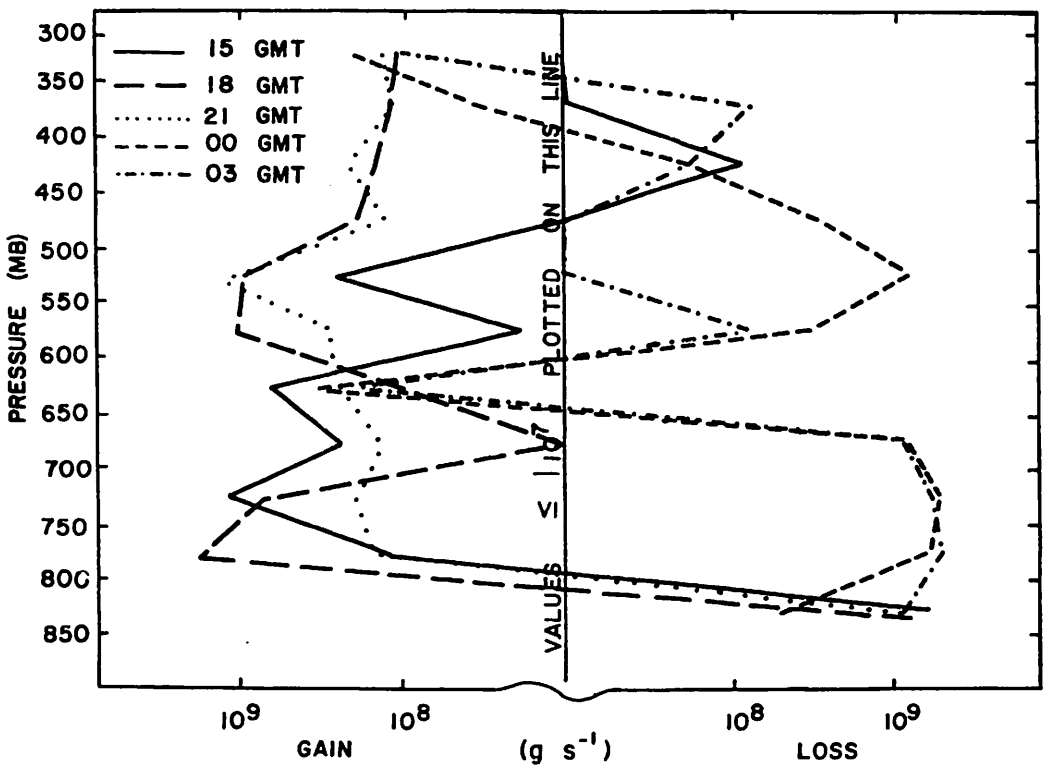

Fig. 5.15.5.2 Net vertical transport of water vapor through boundaries of 50-mb layers (g s^{-1}) over the Texas HIPLEX area for 1 July 1978.

vapor by vertical transport. The 600-650-mb layer showed increases at these times, however.

Profiles of vertical transport through constant pressure surfaces (Fig. 5.15.5.3) show upward transport below 500 mb at 1500 GMT. Upward transport of water vapor was present at all levels at 1800 and 2100 GMT as shower activity formed and increased over the HIPLEX area. At 0000 GMT shower activity began to decrease and downward transport of water vapor prevailed below 500 mb. At 0300 GMT downward transport of water vapor was present below 700 mb but there was upward transport at 650 mb and above 550 mb. The upward transport at 650 mb contributed to the gains due to vertical transport at that level shown in Fig. 5.15.5.2.

Figure 5.15.5.4 shows combined net horizontal and vertical transport of water vapor. At 1500 GMT the transport of water vapor resulted in gains in most layers. There were losses between 400 and 500 mb at that time, however. At 1800 GMT there were losses only in the lowest layer, and at 2100 GMT the combined net transport resulted in gains at all levels. The transport at 2100 GMT also was fairly large. At 0000 GMT, the combined profiles show losses below 650 mb due to the strong vertical transport out of those layers and the outflow of water vapor near the surface. There also were losses between 500 and 600 mb, and water vapor gains were present in the upper layers. At 0300 GMT activity had decreased in the HIPLEX area. The 600-650-mb layer showed gains in water vapor but most other layers at this time showed losses.

Profiles of total mass of water vapor (Fig. 5.15.5.5) show a fairly high water vapor content through the atmosphere. There was a rapid decrease in water vapor above 750 mb which created a relatively "dry" layer from 650 to 750 mb at 1500 GMT. This layer was modified by 0000 GMT so that it was no longer dry. Layers above 600 mb show decreases in water vapor at that time. At 0000 GMT water vapor content was fairly high through all the layers. At 0300 GMT, after shower activity decreased, there were decreases in water vapor above 500 mb.

The profiles in Fig. 5.15.5.6 show the local rate-of-change of water vapor. These profiles expand on what was shown in Fig. 5.15.5.5. The addition of moisture in the 650-800-mb layer at nearly all time periods is shown. There was a small decrease near 750 mb between 2100 and 0000 GMT.

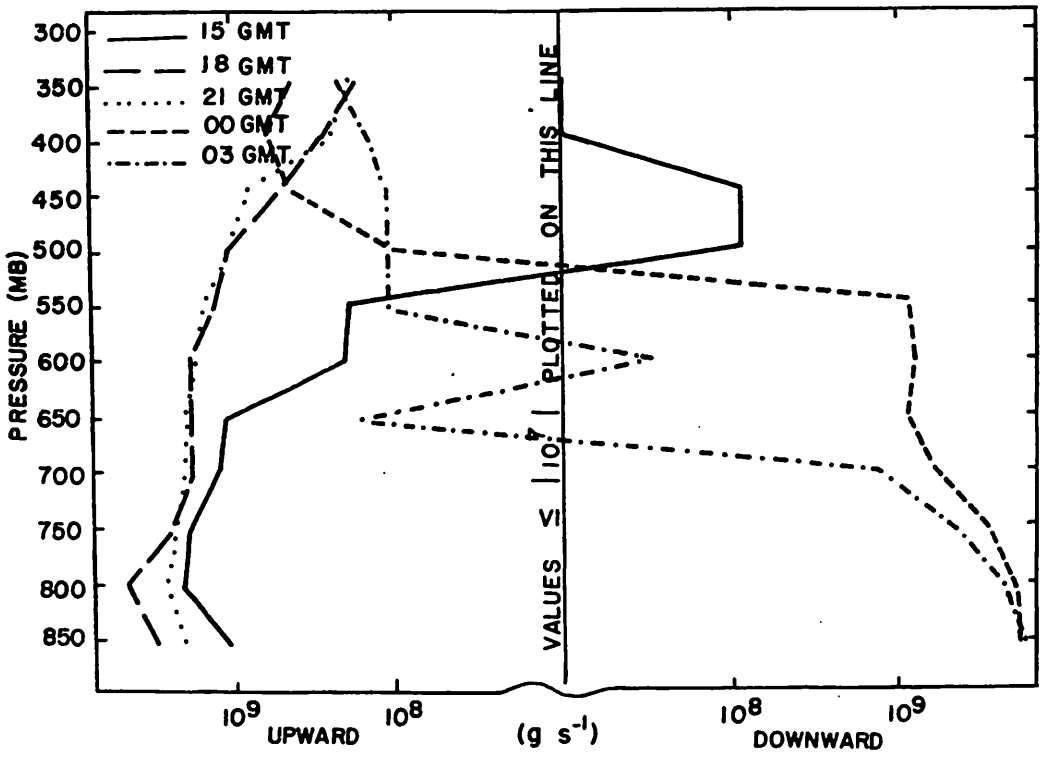

Fig. 5.15.5.3 Vertical transport of water vapor through constant pressure surfaces (gm s^{-1}) over the Texas HIPLEX area for 1 July 1978.

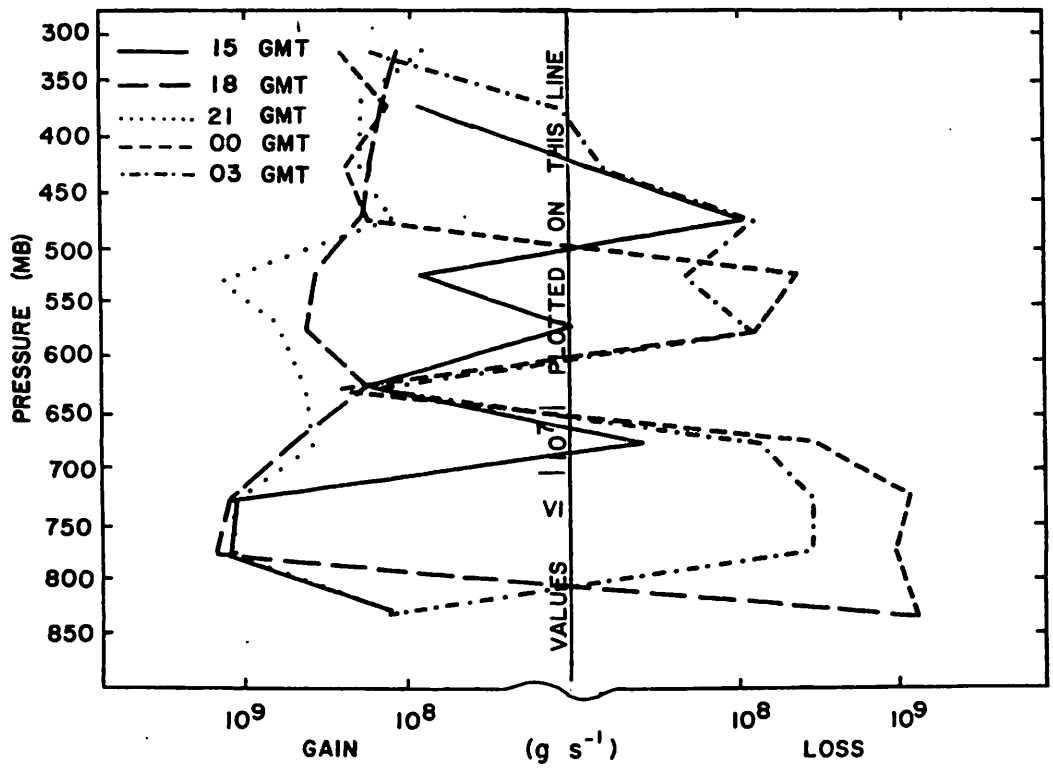

Fig. 5.15.5.4 Combined net horizontal and vertical transport of water vapor through boundaries of 50-mb layers (gm s^{-1}) over the Texas HIPLEX area for 1 July 1978.

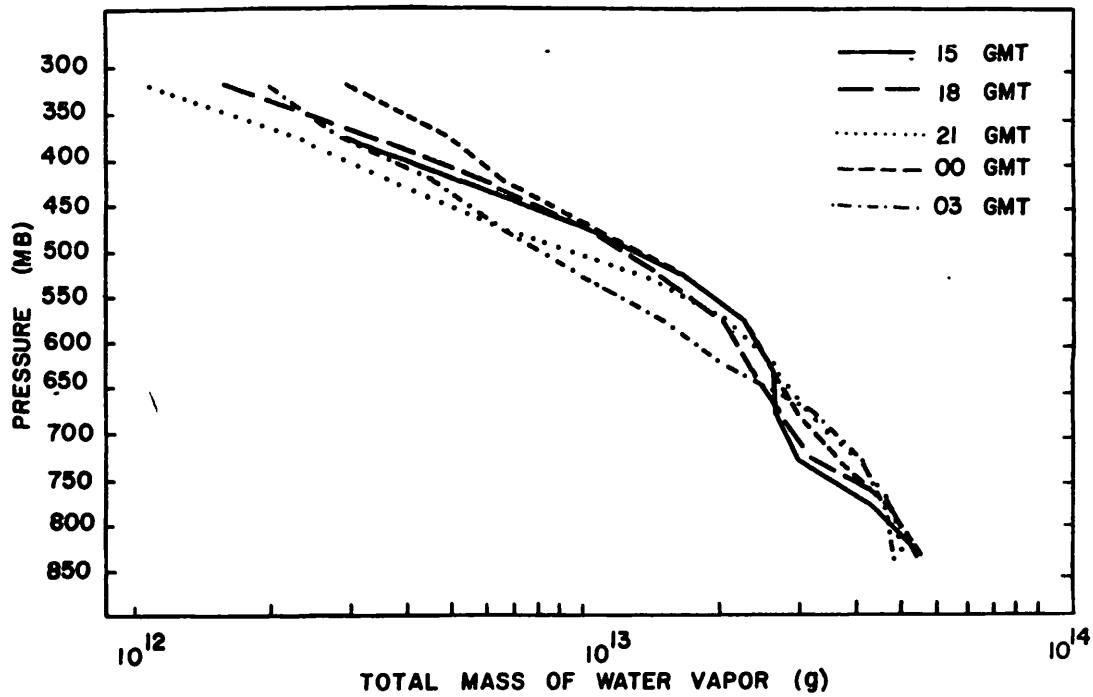

Fig. 5.15.5.5 Total mass of water vapor in layers 50 mb deep (gm) over the Texas HIPLEX area on 1 July 1978.

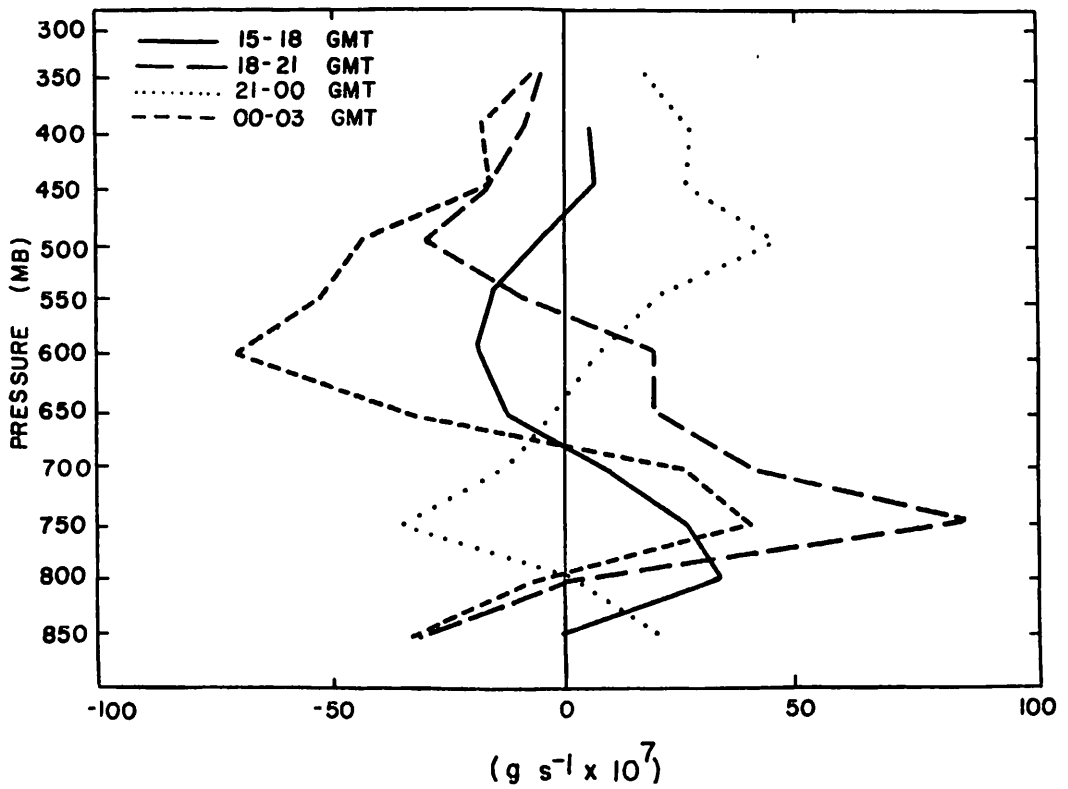

Fig. 5.15.5.6 Local rate-of-change in total mass of water vapor (g s^{-1} x 10^7) for the Texas HIPLEX area for 1 July 1978.

Decreases in higher levels were the general rule, except for the profile of change between 2100 and 0000 GMT. The gains in water vapor above 650 mb coincided with the times of strongest shower activity.

5.16 2 July 1978

5.16.1 Radar

No radar data were available before 1900 GMT (Fig. 5.16.1.1). At 1900 GMT showers were present in the south and southeast. A storm cell with height of 10.6 km (35K ft) was located between Midland and Garden City at 1900 GMT, but decreased in strength at 2000 GMT. Activity spread across the area at 2100 GMT and strong cells formed near Vincent and between Snyder and Roscoe. These cells decreased in strength at 2200 GMT. At 2300 GMT showers were building in the northwest corner, and by 0000 GMT strong cells with heights greater than 9.1 km (30K ft) were between Seminole and Post. Another strong cell was southeast of Roscoe just outside of the HIPLEX area. At 0100 GMT most of the activity had dissipated, leaving only the strong cell near Post, and a weaker cell in the southeast between Walsh-Watts and Roscoe. The latter cell increased in strength at 0200 GMT while another cell developed in the northeast near Clairemont. All activity had ceased by 0300 GMT.

5.16.2 Surface

Surface temperatures are shown in Fig. 5.16.2.1. Early in the day, from 1500 to 2000 GMT, a general east-west temperature gradient prevailed and temperatures increased in all parts of the area with the daytime heating. Decreases in temperature associated with the shower activity occurred successively at Lenorah, Rotan, Lamesa, Roscoe, and Post between 2100 and 0100 GMT. At 0200 GMT decreases occurred at both Clairemont and Walsh-Watts due to the shower activity. Temperature decreased across the area between 0200 and 0300 GMT with nocturnal cooling.

Surface dewpoint depression (Fig. 5.16.2.2) was small at 1500 GMT, but increased during the day. The lowest dewpoint depressions were in the southwest until 2100 GMT. The dewpoint depression decreased at Rotan at 2100 GMT and again at 2200 GMT when temperature dropped. At 0000 GMT dewpoint depression was low at Roscoe as shower activity took place there. The effects of the storm at Post at 0100 GMT produced minimum dewpoint depressions that lasted through the remainder of the day.

Surface mixing ratio (Fig. 5.16.2.3) showed continuous change and a general decrease across the area before 2100 GMT. The storms near Rotan caused mixing ratio increases at 2100 and 2200 GMT. At 0000 GMT the area of maximum mixing ratio extended to Roscoe as a result of shower activity

MISSING DATA

MISSING DATA

MISSING DATA

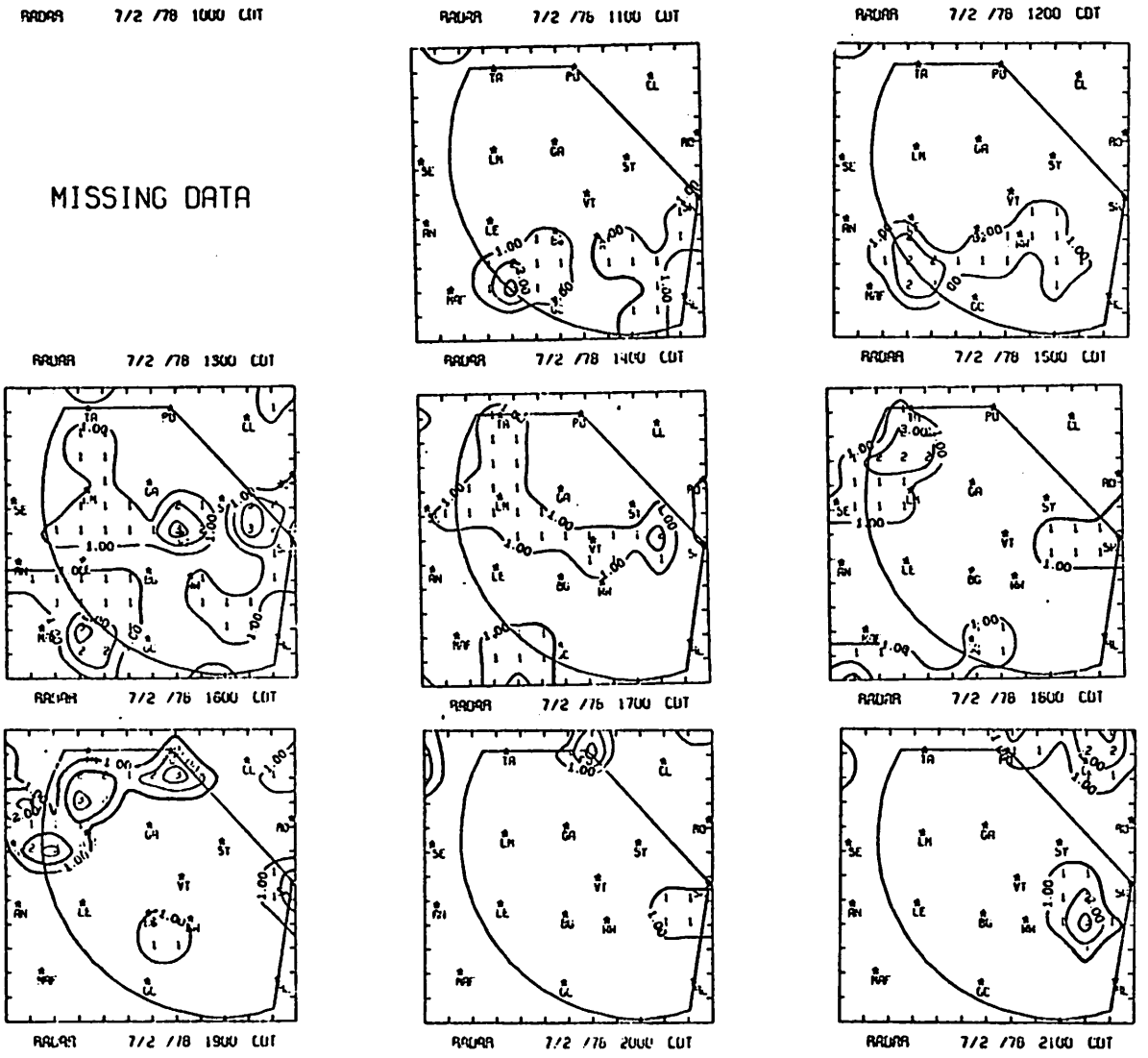

NO ECHOES

Fig. 5.16.1.1 Radar echoes for 2 July 1978.

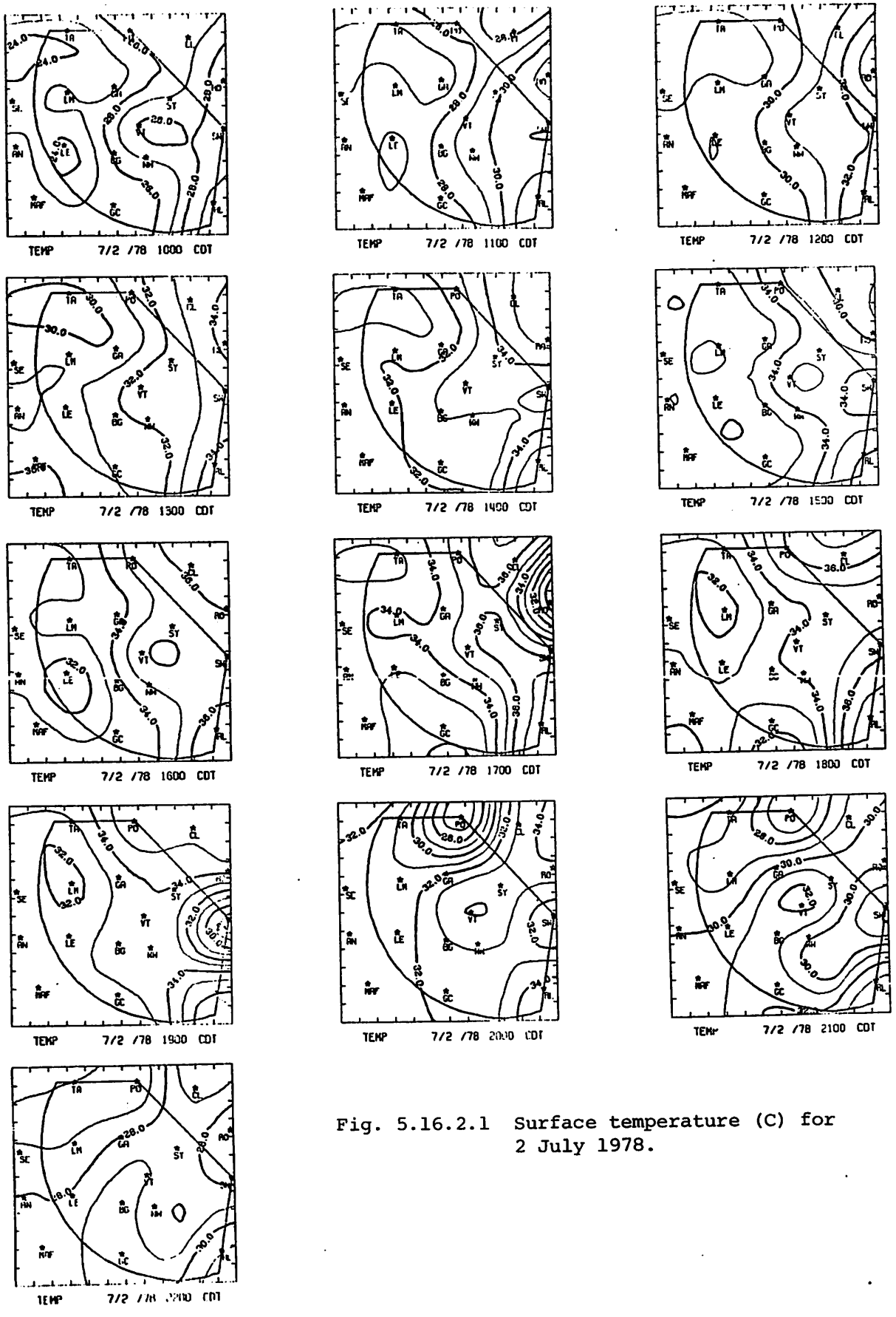

Fig. 5.16.2.1 Surface temperature (C) for 2 July 1978.

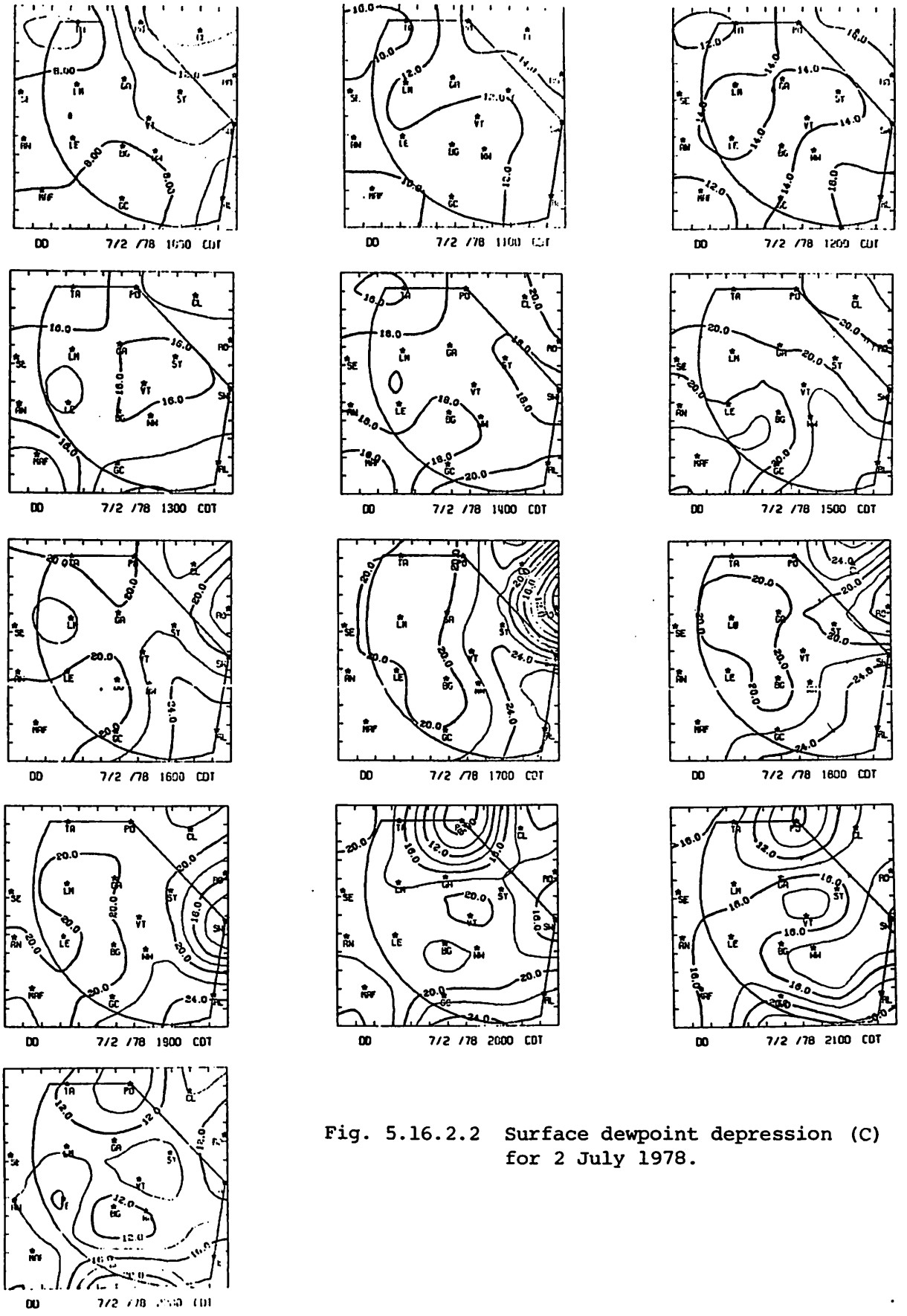

Fig. 5.16.2.2 Surface dewpoint depression (C) for 2 July 1978.

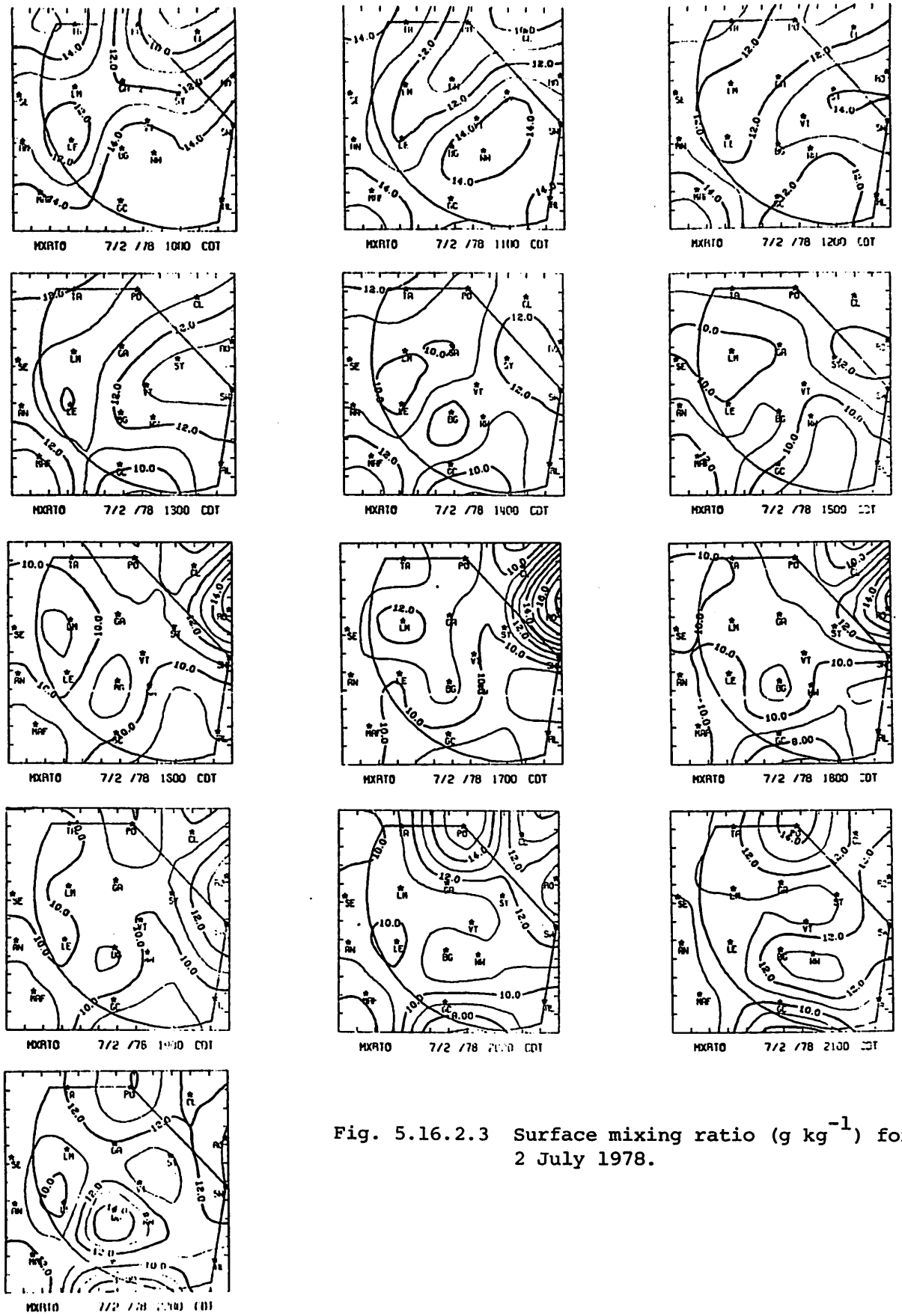

Fig. 5.16.2.3 Surface mixing ratio (g kg^{-1}) for 2 July 1978.

there. At 0100 GMT Post showed a large increase in connection with the shower there. The increase at Big Spring from 0100 to 0300 GMT did not seem to be related to any shower activity, however.

Surface equivalent potential temperature (Fig. 5.16.2.4) varied in a similar way as the mixing ratio. High potential temperature was present at Rotan from 2100 to 2300 GMT because of the addition of moisture by storm activity. The potential temperature did not show a large increase at Post or Roscoe, however, because the increase in latent heat in those areas was offset by the decrease in temperature. Again, the maximum at Big Spring at 0300 GMT was not directly connected with shower activity.

Terrain-induced vertical motion (Fig. 5.16.2.5) was not large during the day as surface winds were moderate. It did not appear to influence the convective activity.

Surface velocity divergence (Fig. 5.16.2.6) was moderate at 1500 GMT. Convergence was present in the south and divergence was in the north central part of the area. The convergence in the southeast increased at 1800 GMT, and radar reports showed showers in that area an hour later. Convergence remained in the south at 2000 GMT but was replaced by divergence. At 2100 GMT convergence was centered in the Gail area where new activity was forming. Convergence also was present at Roscoe at 0000 GMT, near Post at 0100 GMT, and east of Walsh-Watts at 0200 GMT in association with the strong echoes in those areas.

Vertical motion 50 mb above the surface (Fig. 5.16.2.7) was generally small before 1900 GMT. Upward motion developed in the southeast at 1900 GMT, and showers were present in that area one hour later. Upward motion also was present in the Midland area at 1800 GMT and radar indicated a strong cell west of Midland at 1900 GMT. Upward motion was not very strong between 2000 and 2300 GMT although it generally occurred in shower areas. At 0000 GMT stronger upward motions occurred in the east, just west of the Roscoe area. The upward motion at 0100 GMT was stronger and associated with a cell near Post. At 0200 GMT the strong upward motion was in the east again where another storm formed east of Walsh-Watts. By 0300 GMT the echoes had disappeared but moderately strong upward motion was still present in the northeast.

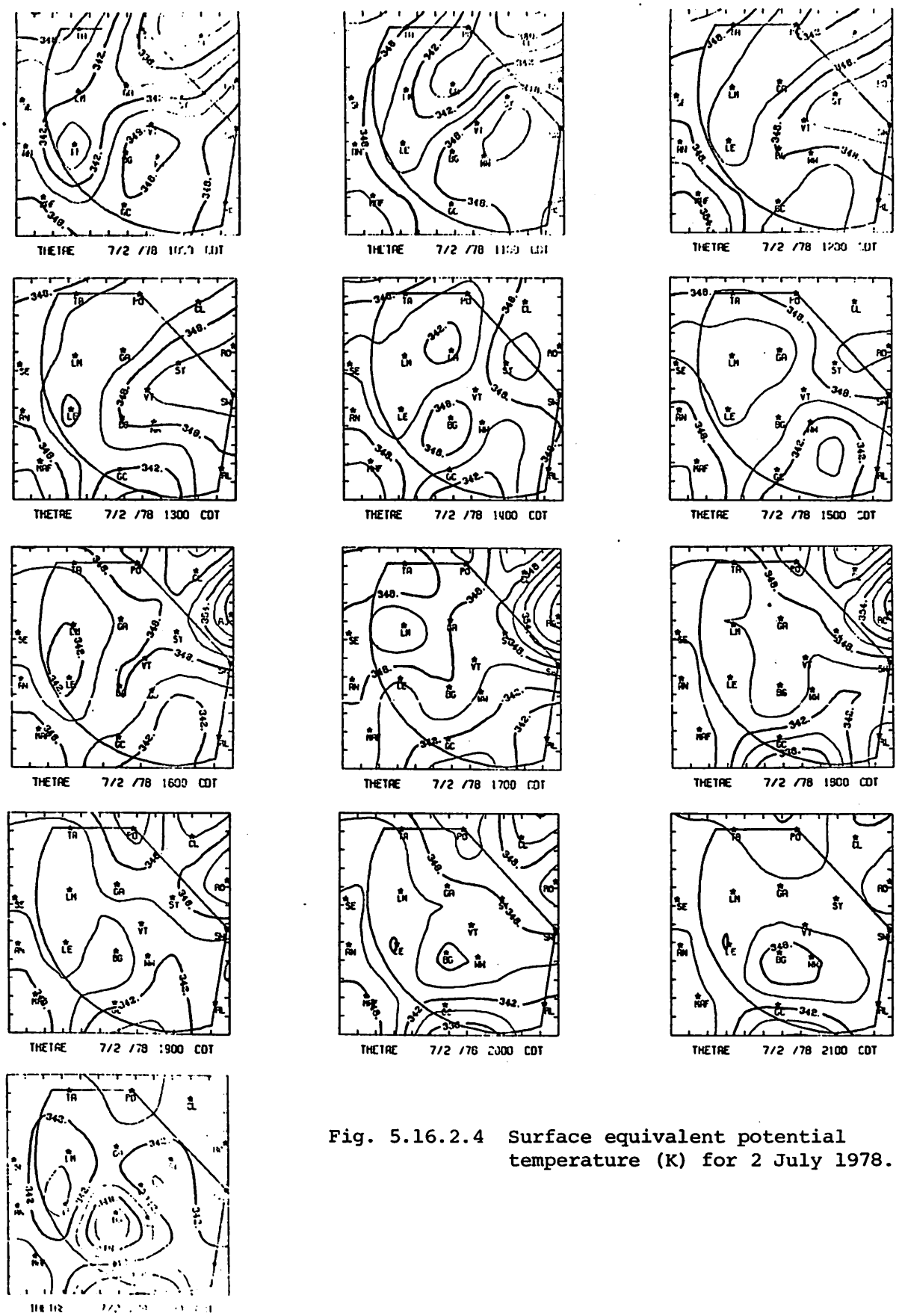

Fig. 5.16.2.4 Surface equivalent potential temperature (K) for 2 July 1978.

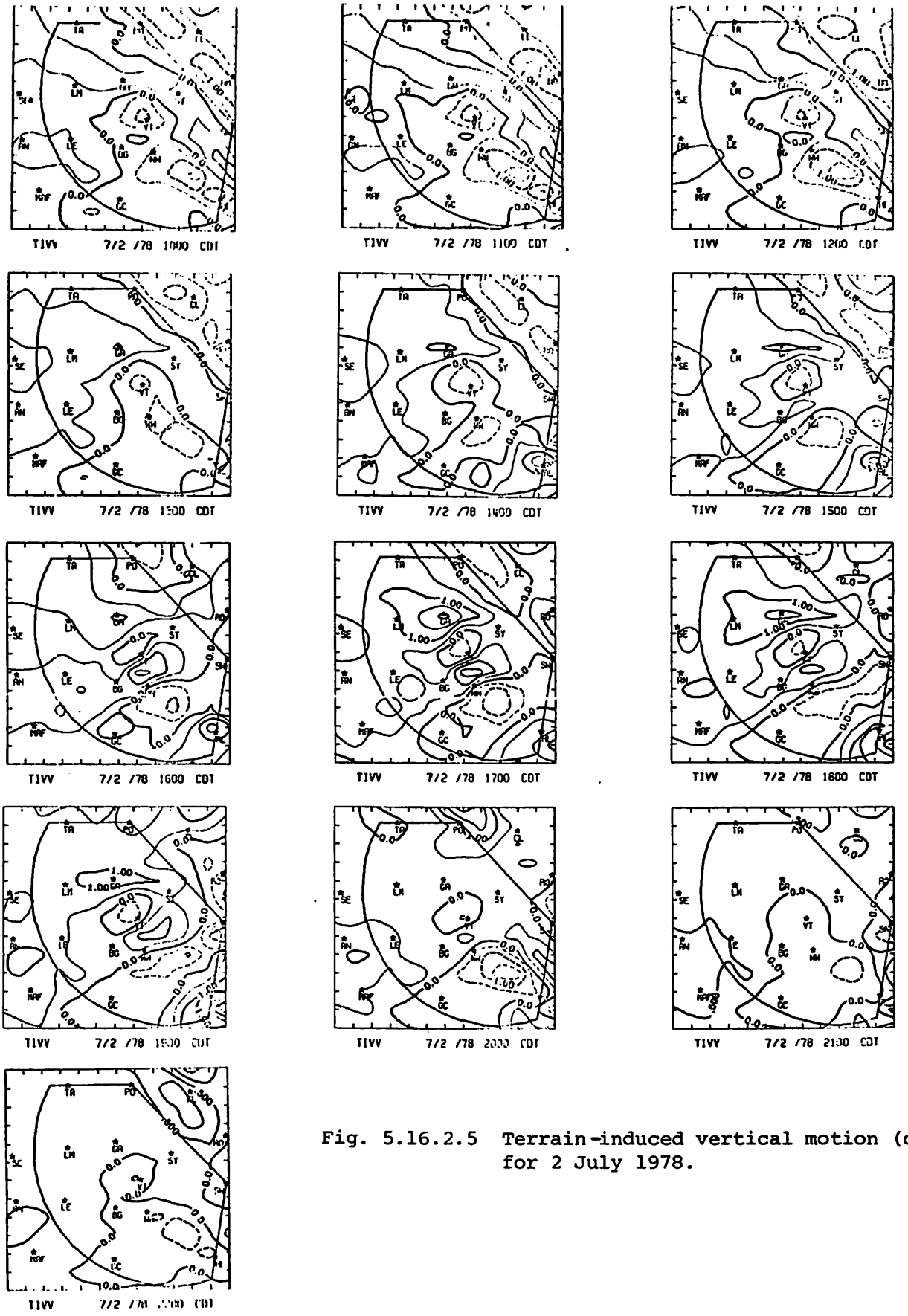

Fig. 5.16.2.5 Terrain-induced vertical motion (cm s^{-1}) for 2 July 1978.

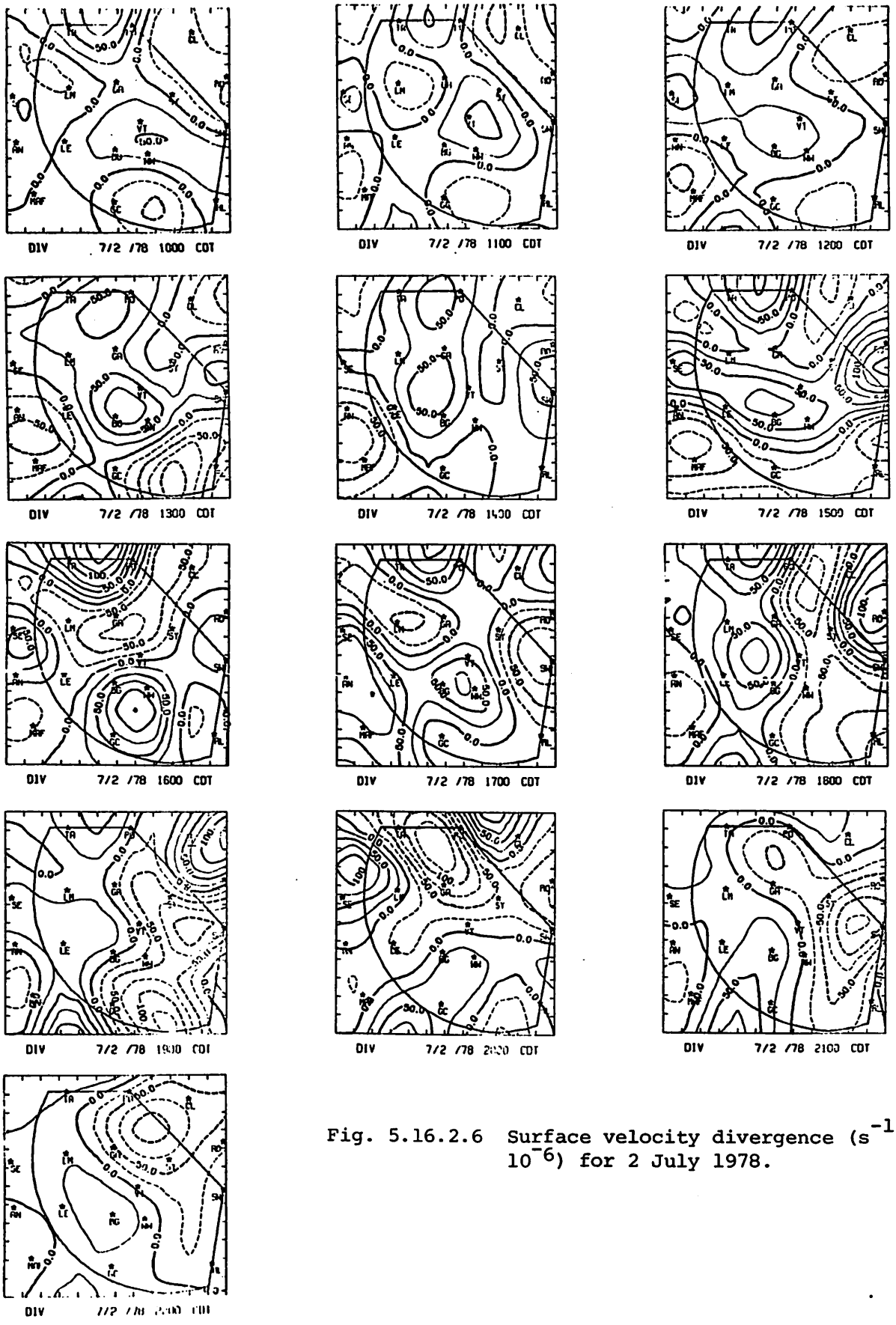

Fig. 5.16.2.6 Surface velocity divergence (s^{-1} x 10^{-6}) for 2 July 1978.

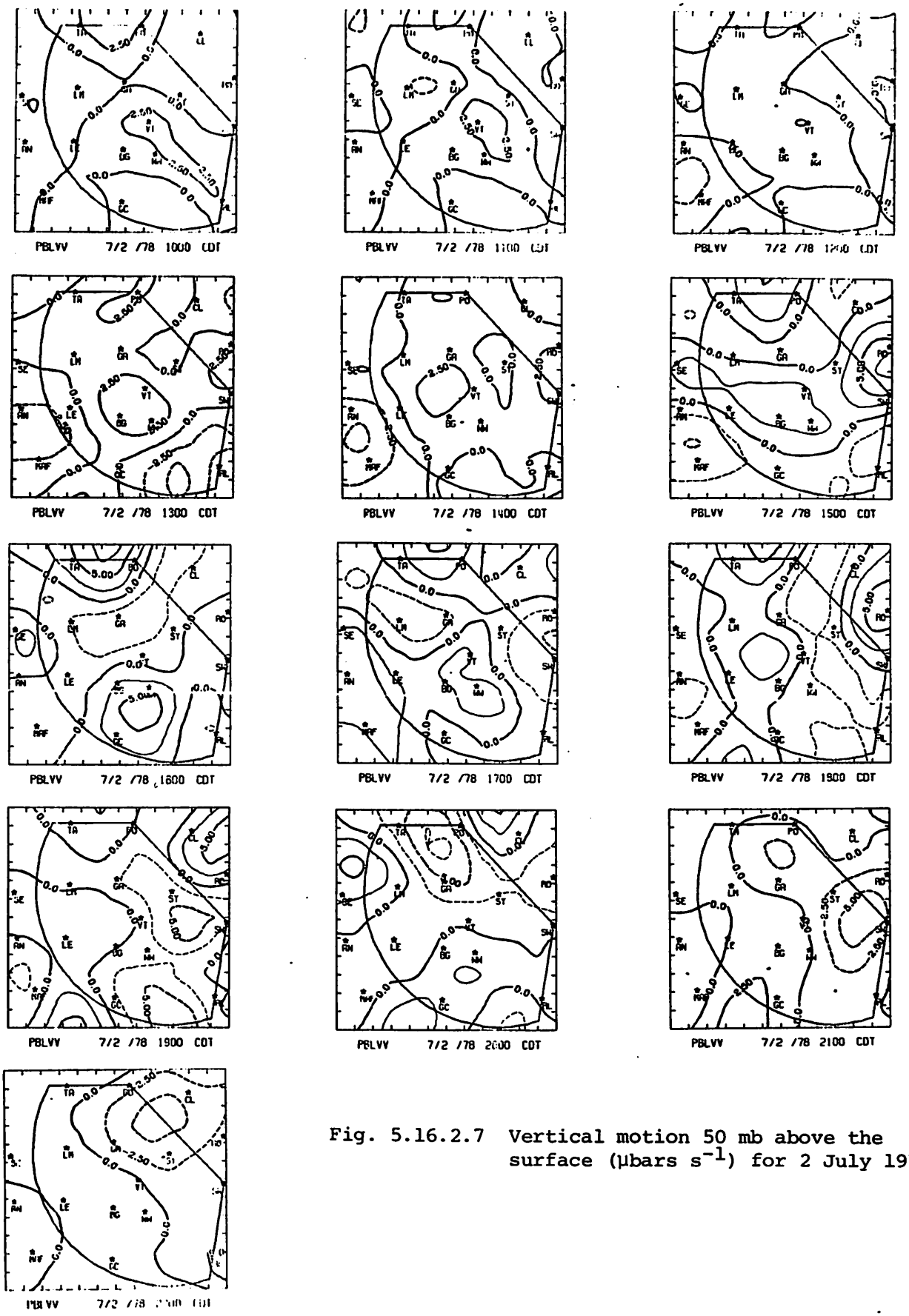

Fig. 5.16.2.7 Vertical motion 50 mb above the surface (μbars s^{-1}) for 2 July 1978.

Surface moisture divergence is shown in Fig. 5.16.2.8. Larger values of moisture convergence did not appear until 1800 GMT in the south. At 1900 and 2000 GMT echoes were present in the south where moisture convergence had been taking place. Echoes began to form in the north at 2100 GMT, and moisture convergence developed near Gail and Clairemont. Strong moisture convergence was present near Roscoe, Post, and west of Walsh-Watts as strong echoes developed in those areas between 0000 and 0200 GMT.

Patterns of vertical flux of moisture (Fig. 5.16.2.9) were similar to the vertical motion patterns. Both showed weak upward motion before 1800 GMT with stronger upward flux of moisture in the south from 1800 to 2000 GMT. Between 2100 and 2300 GMT the largest values of upward flux were in the north where new activity formed. Upward moisture flux was located near Roscoe at 0000 GMT and near Post at 0100 GMT where strong storms were located. At 0200 GMT upward flux was strongest east of Walsh-Watts. By 0300 GMT echoes had dissipated but strong upward flux was still present in the northwest.

Surface vorticity (Fig. 5.16.2.10) was moderate at the beginning of the day but increased as shower activity formed in the area. Anticyclonic vorticity increased in the south at 1900 GMT when radar indicated echoes in that area. Strong centers of both cyclonic and anticyclonic vorticity were associated with the echoes near Vincent at 2100 GMT and east of Snyder at 2200 GMT. The echoes at Roscoe at 0000 GMT and at Post at 0100 GMT also had strong centers of vorticity associated with them. Vorticity values decreased at 0300 GMT when showers had dissipated.

Surface pressure change is shown in Fig. 5.16.2.11. Most of the pressure changes were small. Pressures generally decreased after 1700 GMT but began to increase again at 0100 GMT.

Surface winds (Fig. 5.16.2.12) were southerly early in the day and did not change too much as the day progressed. The shower activity altered the wind field to mostly southeasterly after 2100 GMT. Wind speeds decreased after 0200 GMT when shower activity dissipated.

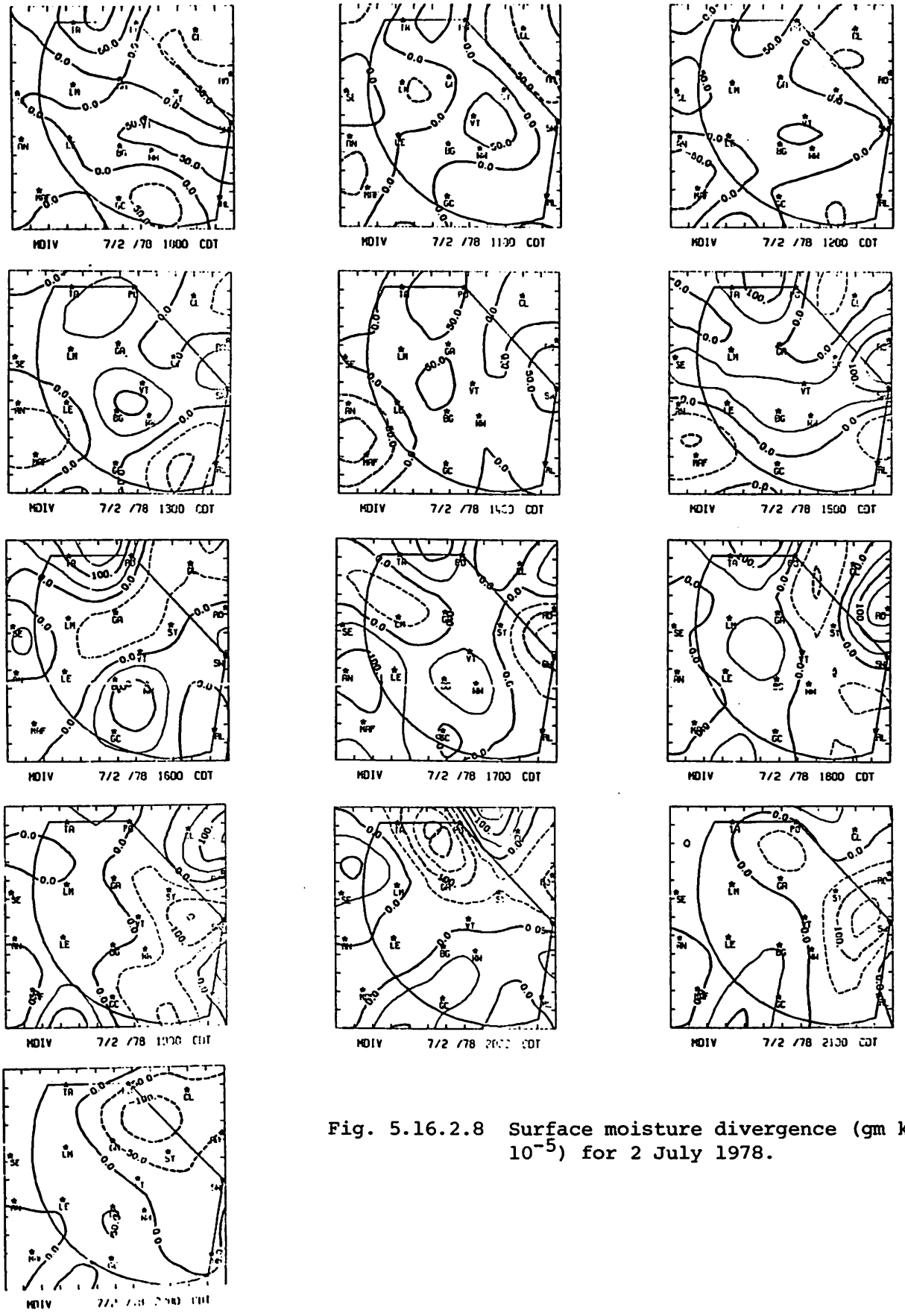

Fig. 5.16.2.8 Surface moisture divergence (gm kg^{-1} s^{-1} x 10^{-5}) for 2 July 1978.

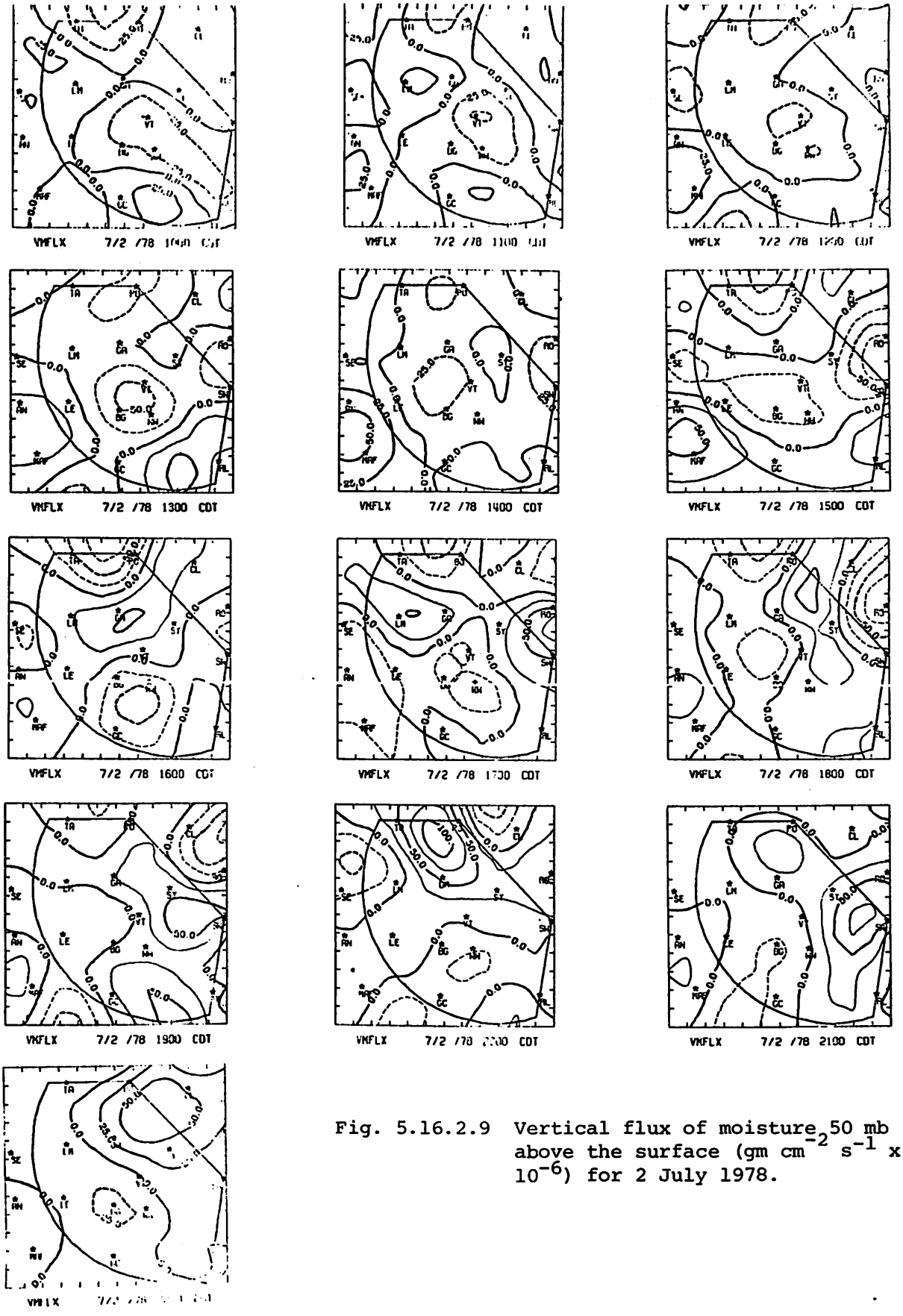

Fig. 5.16.2.9 Vertical flux of moisture 50 mb above the surface (gm cm^{-2} s^{-1} x 10^{-6}) for 2 July 1978.

Fig. 5.16.2.10 Surface vorticity (s^{-1} x 10^{-6}) for 2 July 1978.

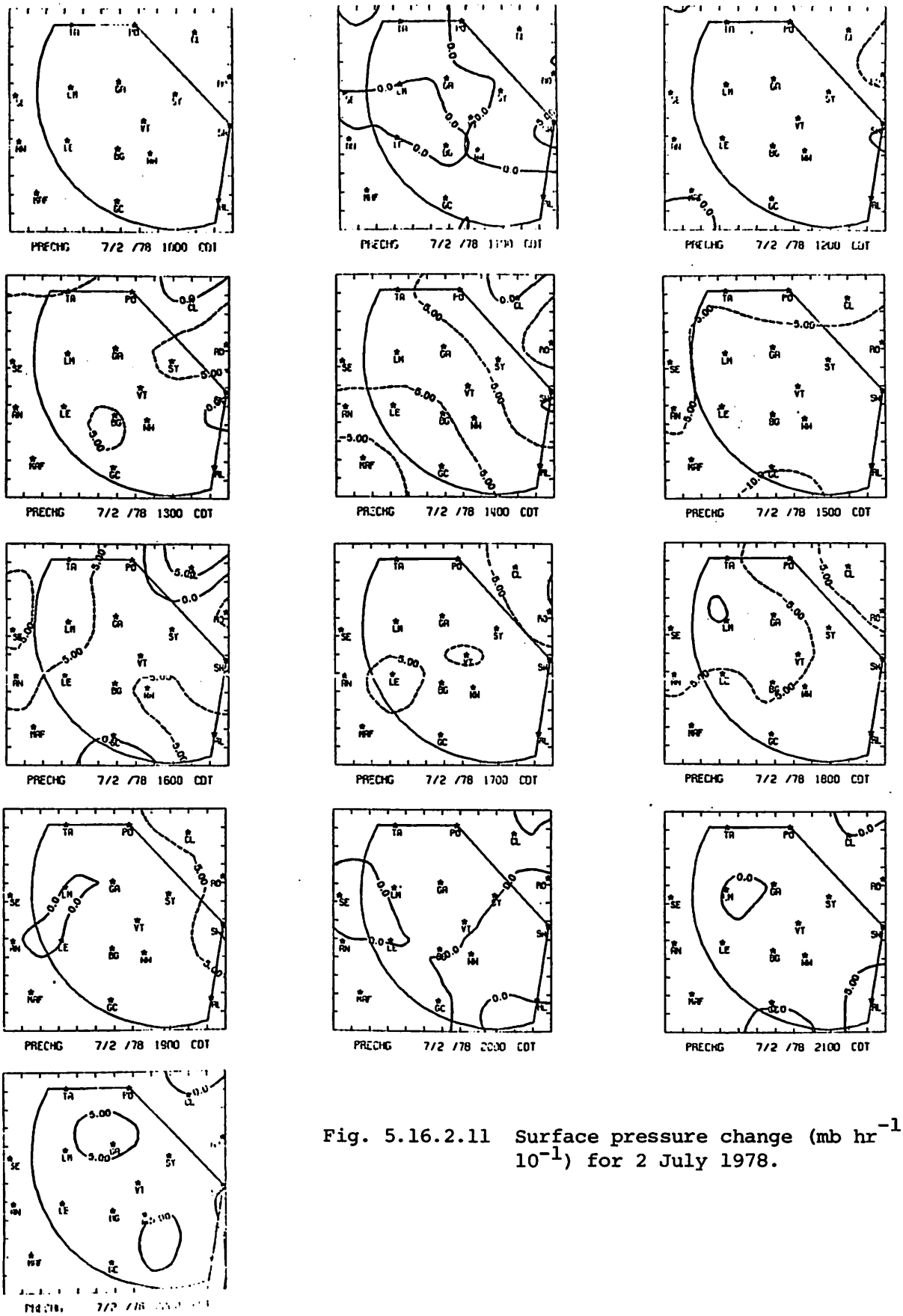

Fig. 5.16.2.11 Surface pressure change (mb hr^{-1} x 10^{-1}) for 2 July 1978.

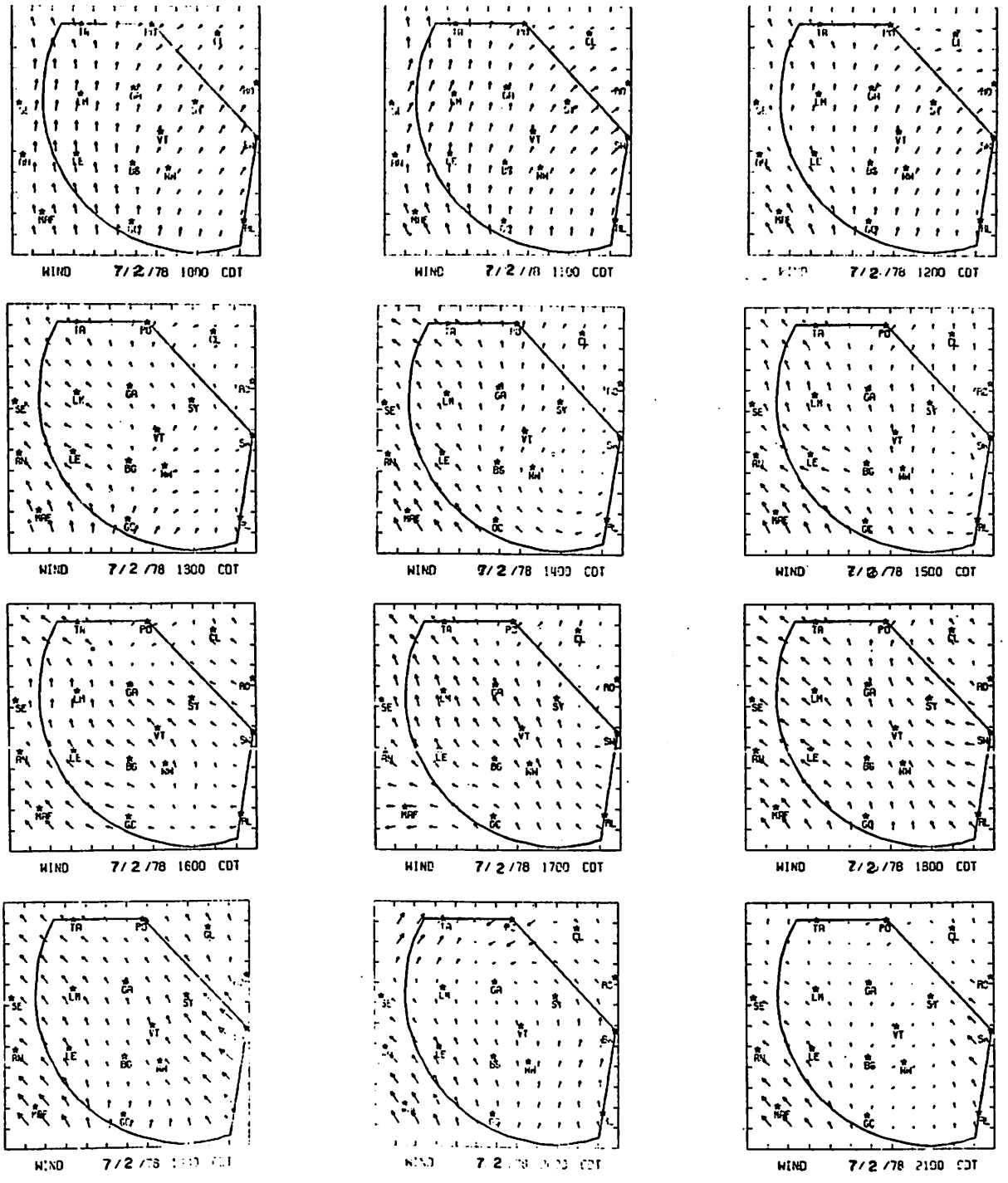

Fig. 5.16.2.12 Relative surface wind fields for 2 July 1978.

5.17 3 July 1978

5.17.1 Radar

No radar data were available for 1500-1600 GMT (Fig. 5.17.1.1). At 1700 GMT no echoes were recorded. Shower activity began at 1800 GMT and spread across the northern part of the area by 1900 GMT. This area of showers moved slowly to the southwest, and numerous strong echoes with heights above 9.1 km (30K ft) developed between 2000 and 0300 GMT. The strongest activity was between 2300 and 0000 GMT, and east of Andrews at 0000 GMT where echoes reached 15.2 km (50K ft).

5.17.2 Surface

Surface temperature (Fig. 5.17.2.1) at 1500 GMT showed an east-west temperature gradient with cool centers at Lenorah and Gail. By 1800 GMT the daytime heating had eliminated the cool centers and temperatures across the area had increased. At 2000 GMT the effects of the shower activity began to show up as a cold center developed at Rotan. Strong cooling occurred at several places where strong convective activity was located during the next few hours. By 0000 GMT a large cold center was located in the central part of the area where the strongest activity had taken place. Temperatures increased slightly in the north where shower activity had ceased. In the south, where no activity had taken place, temperatures remained fairly high until 0200 GMT when the showers' influence finally reached this area.

Surface dewpoint depressions (Fig. 5.17.2.2) were fairly even across the area at 1500 GMT, but increased irregularly across the area as temperatures increased. The dewpoint depressions were fairly large at 2000 GMT, but by 2100 GMT the effects of the shower activity reduced the dewpoint depressions across the northern part of the area. Dewpoint depressions remained high in the southwest until 0200 GMT.

Surface mixing ratio (Fig. 5.17.2.3) was moderately high at 1500 GMT, with maximum values in the northeast and near Big Spring. The mixing ratio decreased across the area until 2000 GMT, but then showed increases in some areas due to shower activity. These increases were limited in some areas where temperature, and thus saturation mixing ratio, decreased. Mixing ratios in the southwest, where no shower activity took place, did not increase until after 0100 GMT, when the showers' influence spread to that area. Equivalent potential temperature (Fig. 5.17.2.4) behaved in a similar fashion to the surface mixing ratio, showing increases in shower areas where the temperature decrease was not too large.

MISSING DATA

MISSING DATA

NO ECHOES

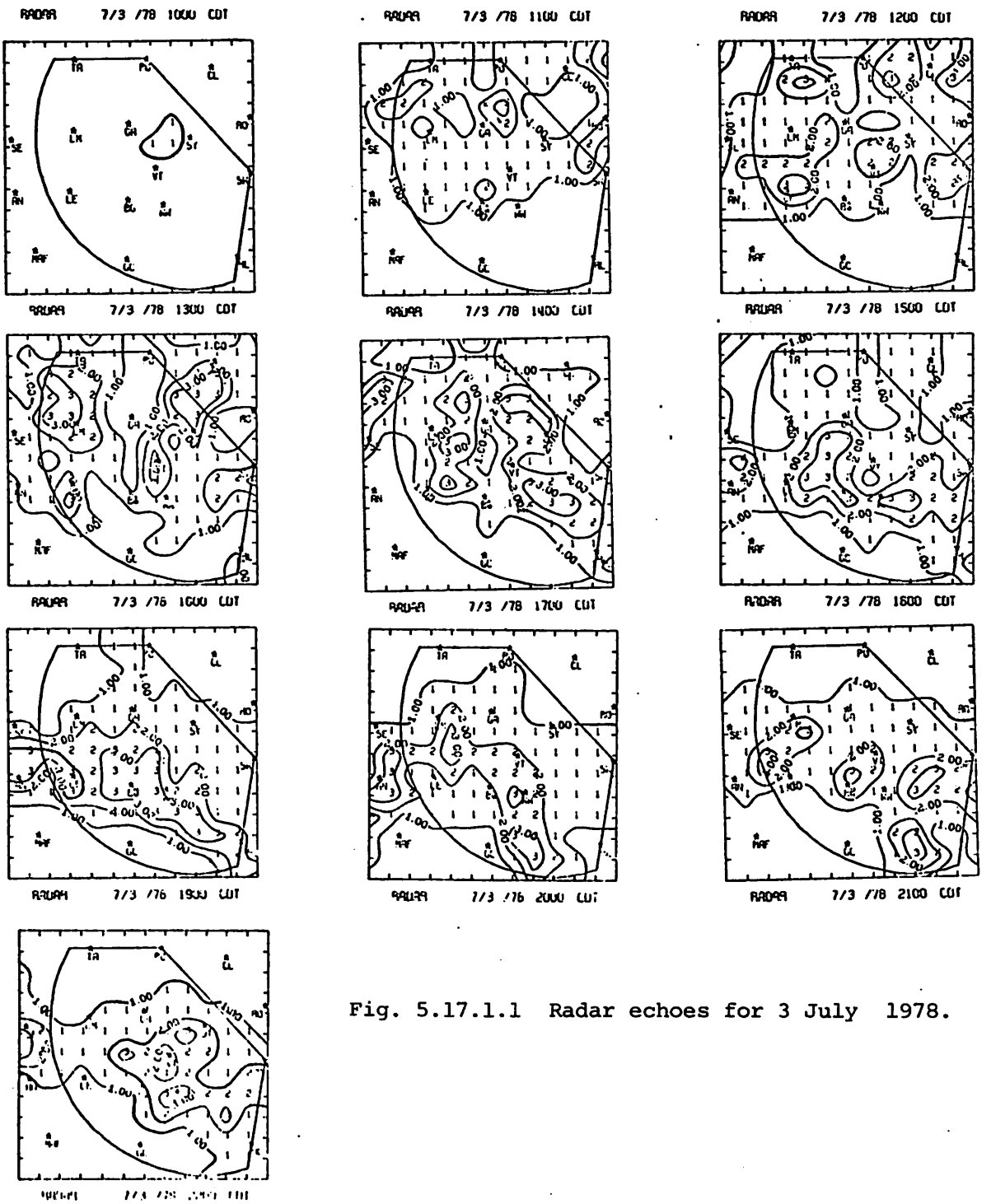

Fig. 5.17.1.1 Radar echoes for 3 July 1978.

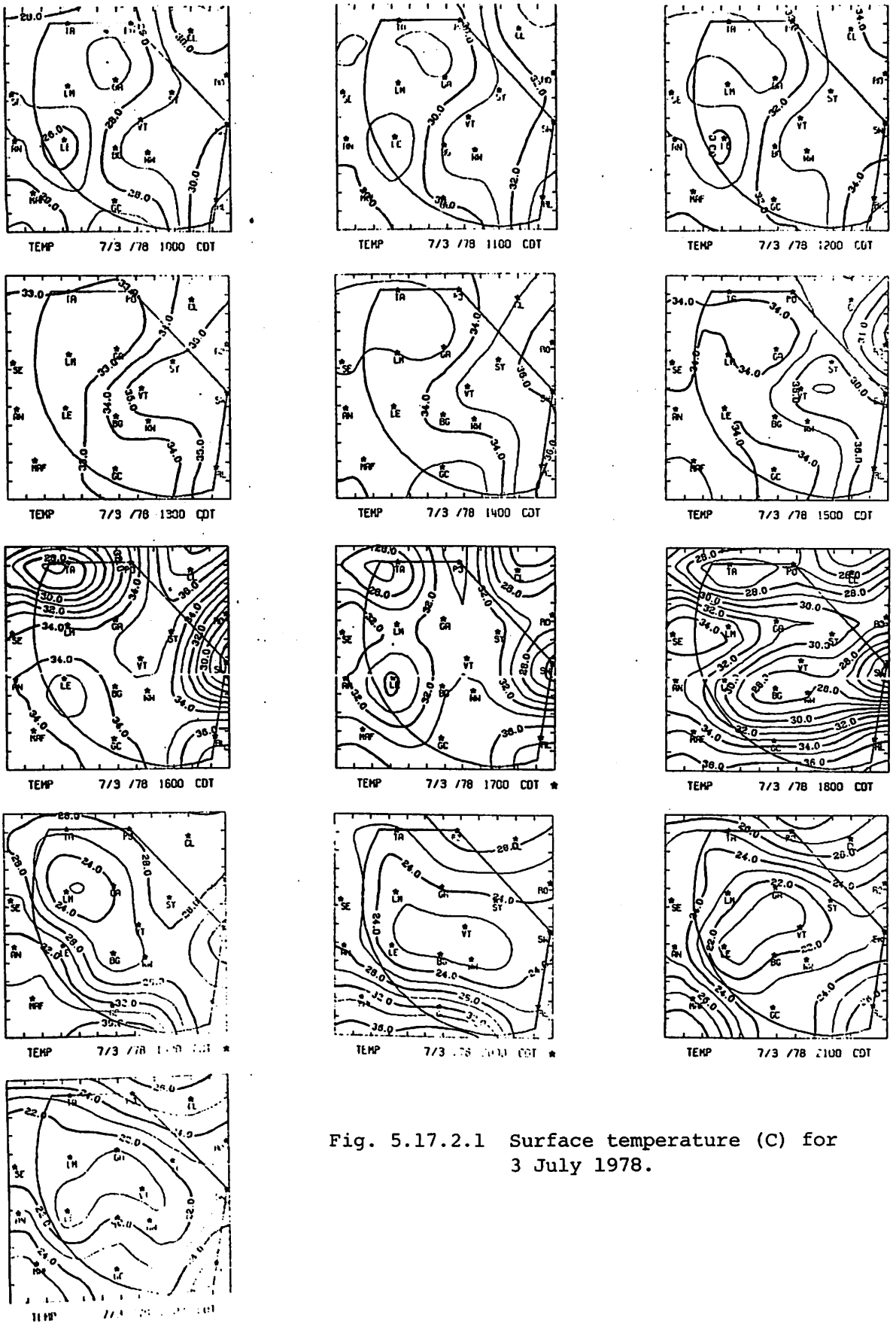

Fig. 5.17.2.1 Surface temperature (C) for 3 July 1978.

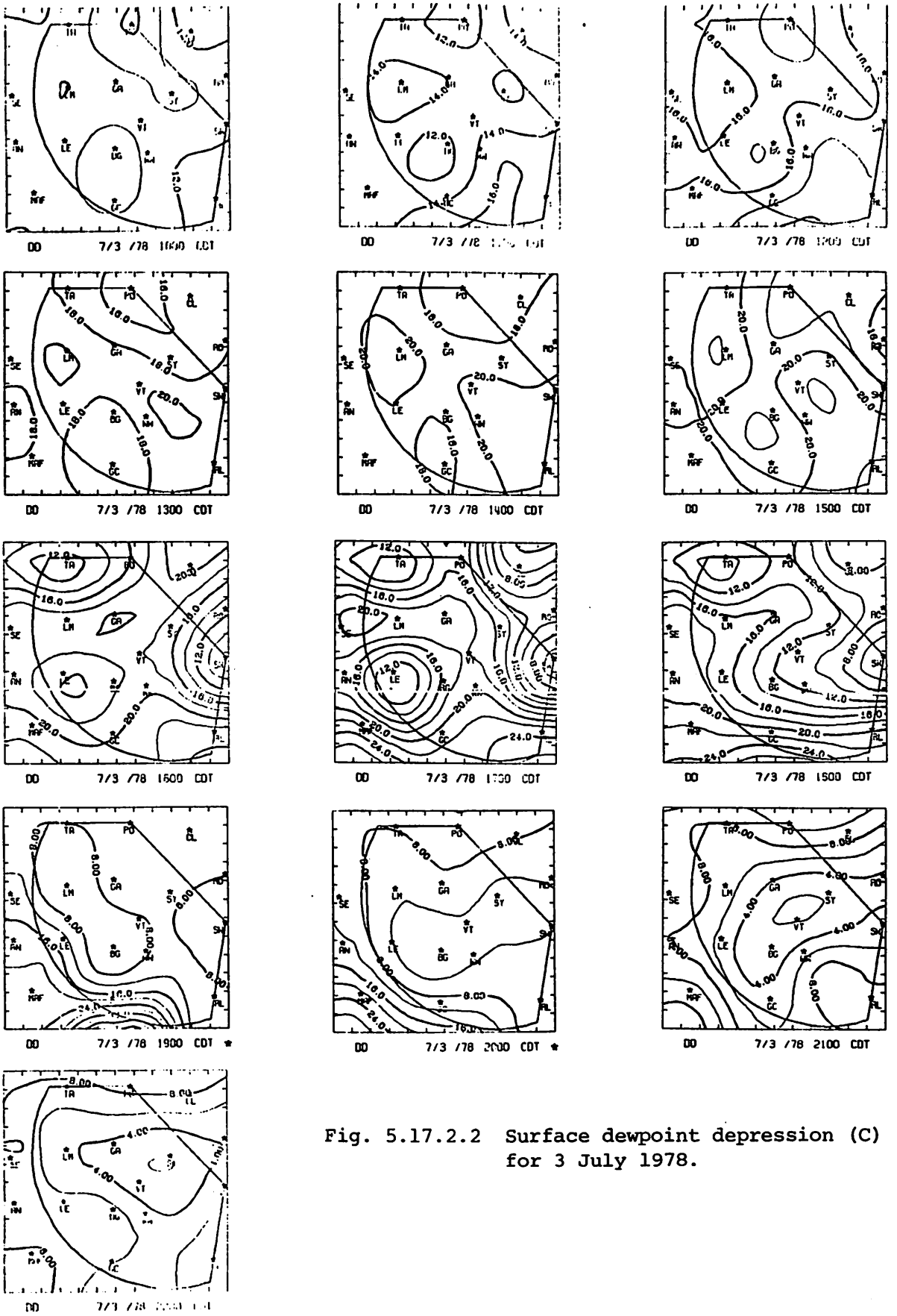

Fig. 5.17.2.2 Surface dewpoint depression (C) for 3 July 1978.

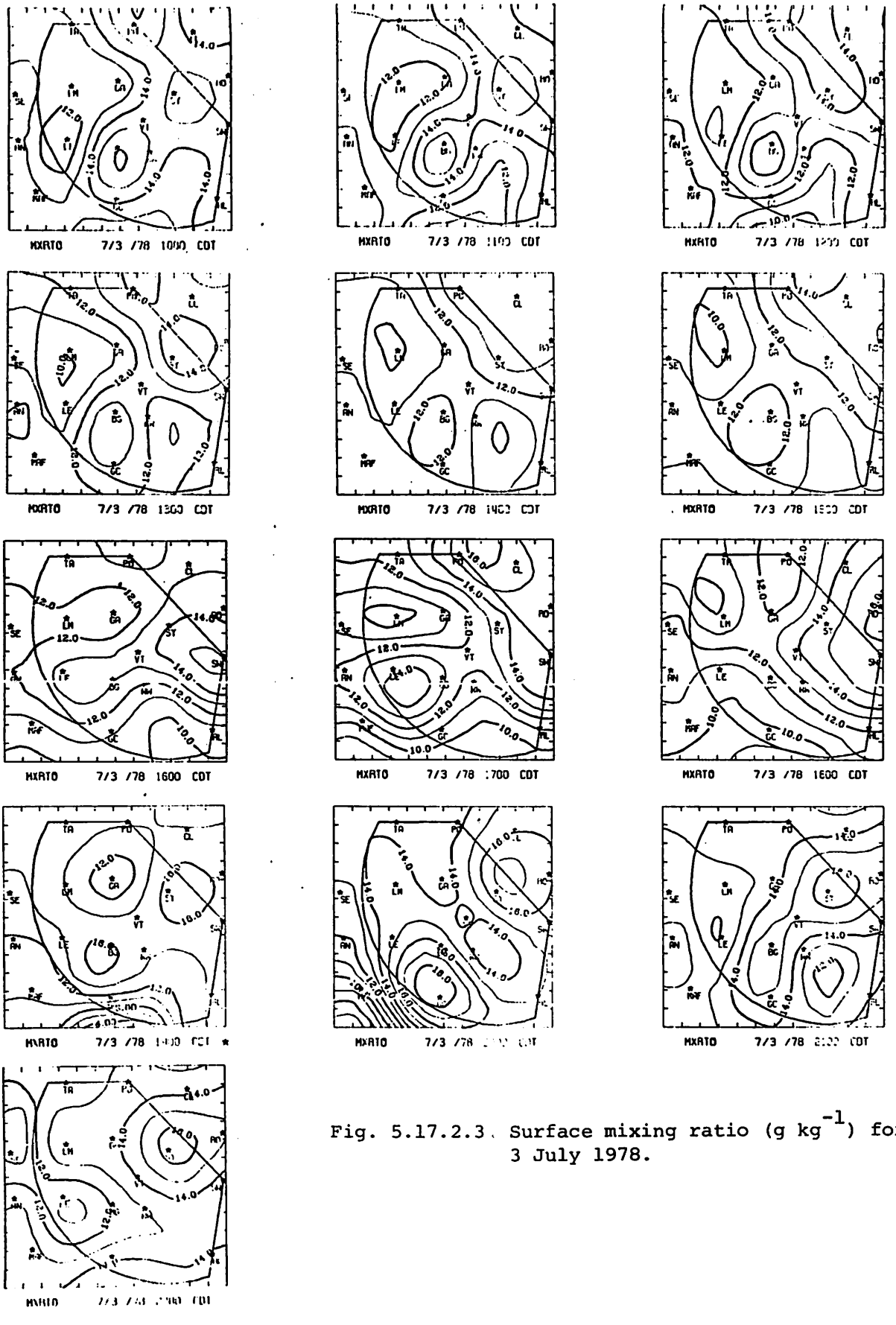

Fig. 5.17.2.3. Surface mixing ratio (g kg^{-1}) for 3 July 1978.

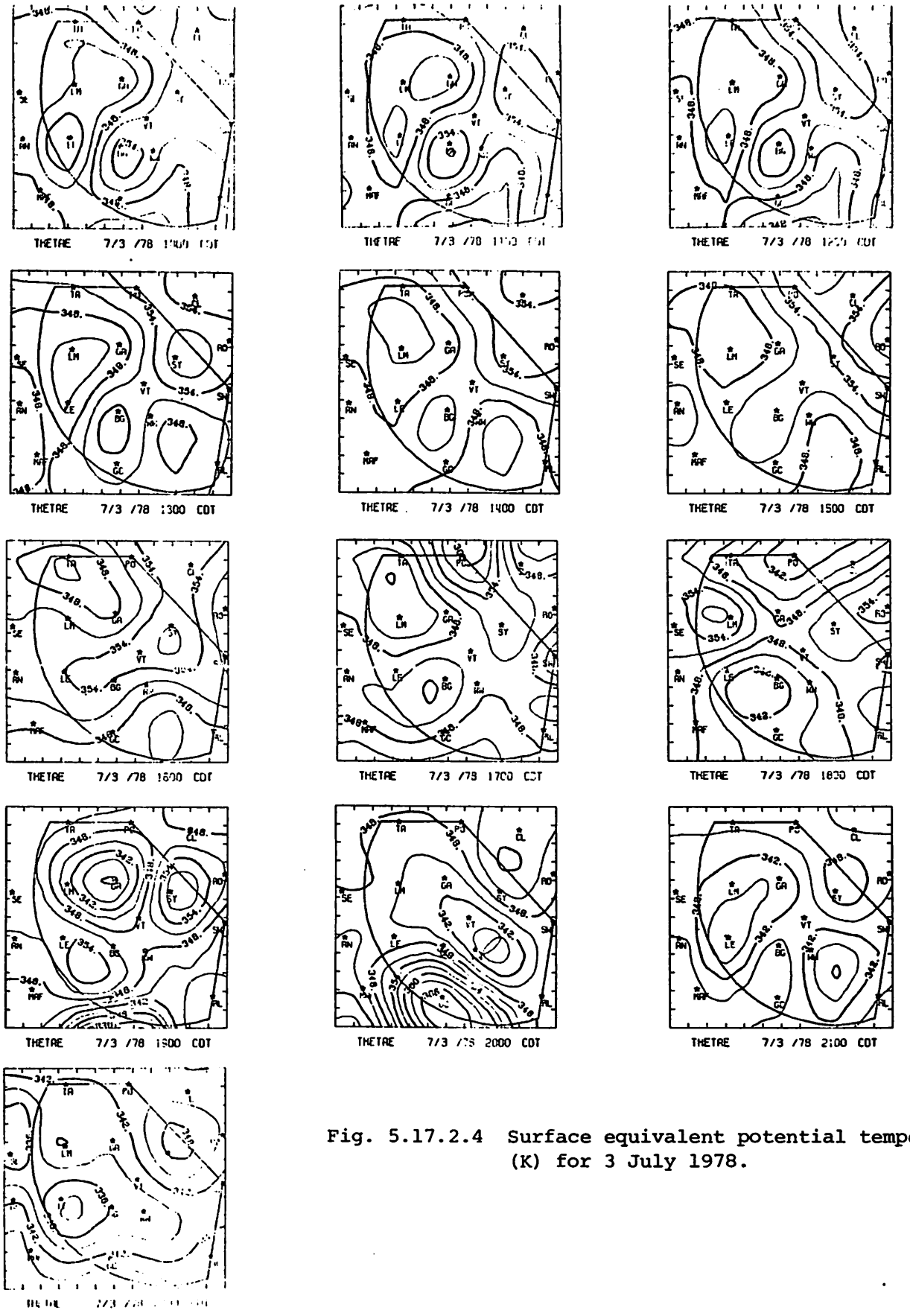

Fig. 5.17.2.4 Surface equivalent potential temperature (K) for 3 July 1978.

Terrain-induced vertical motion (Fig. 5.17.2.5) became large when wind speeds increased during the storm activity. At 2200 GMT strong downward motion occurred at Walsh-Watts, and strong upward terrain-induced motion was in the same area at 2300 GMT.

Surface velocity divergence (Fig. 5.17.2.6) showed small to moderate values of divergence early in the day. The values increased after 2000 GMT as convective activity increased. Strong convergence was present in the central part of the shower area between 2100-2200 GMT. At 2300 GMT convergence was located on the south side of the shower area where the strongest cells were located. Velocity divergence was just to the north of the strongest cells and increased considerably at 0000 GMT. By 0200 GMT divergence had spread over almost the entire area, except in the northwest, where only weak convergence was present.

Vertical motion 50 mb above the surface (Fig. 5.17.2.7), surface moisture divergence (Fig. 5.17.2.8), and vertical flux of moisture 50 mb above the surface (Fig. 5.17.2.9), showed patterns similar to the surface velocity divergence. These variables also had small to moderate values early in the day and increased as shower activity increased at 2000 GMT. Strong upward motion, moisture convergence, and upward flux of moisture occurred through the center of the storm area at 2100-2200 GMT and on the south side of the area from 2300-0000 GMT. Large values of downward motion, moisture divergence, and downward moisture flux developed at 0000 GMT; this was when the storm activity was at its peak. After 0100 GMT downward motion, moisture divergence, and downward moisture flux were dominant as the storm activity decreased in strength.

Surface vorticity (Fig. 5.17.2.10) was primarily anticyclonic between 1500 and 2000 GMT. As shower activity increased at 2100 GMT, wind speed increased and surface vorticity increased. Strong centers of positive and negative vorticity shifted from hour to hour with the movement of the storms. Values remained strong through 0300 GMT.

Surface pressure changes (Fig. 5.17.2.11) were mostly small early in the day. Pressure drops occurred after 1700 GMT and continued over most of the area until 2300 GMT. Large pressure rises occurred at Gail at 2300 GMT, at Big Spring at 0000 GMT, and at Walsh-Watts at 0100 GMT. Pressure dropped in the Walsh-Watts area at 0200 GMT, otherwise pressure rises were dominant after 0100 GMT.

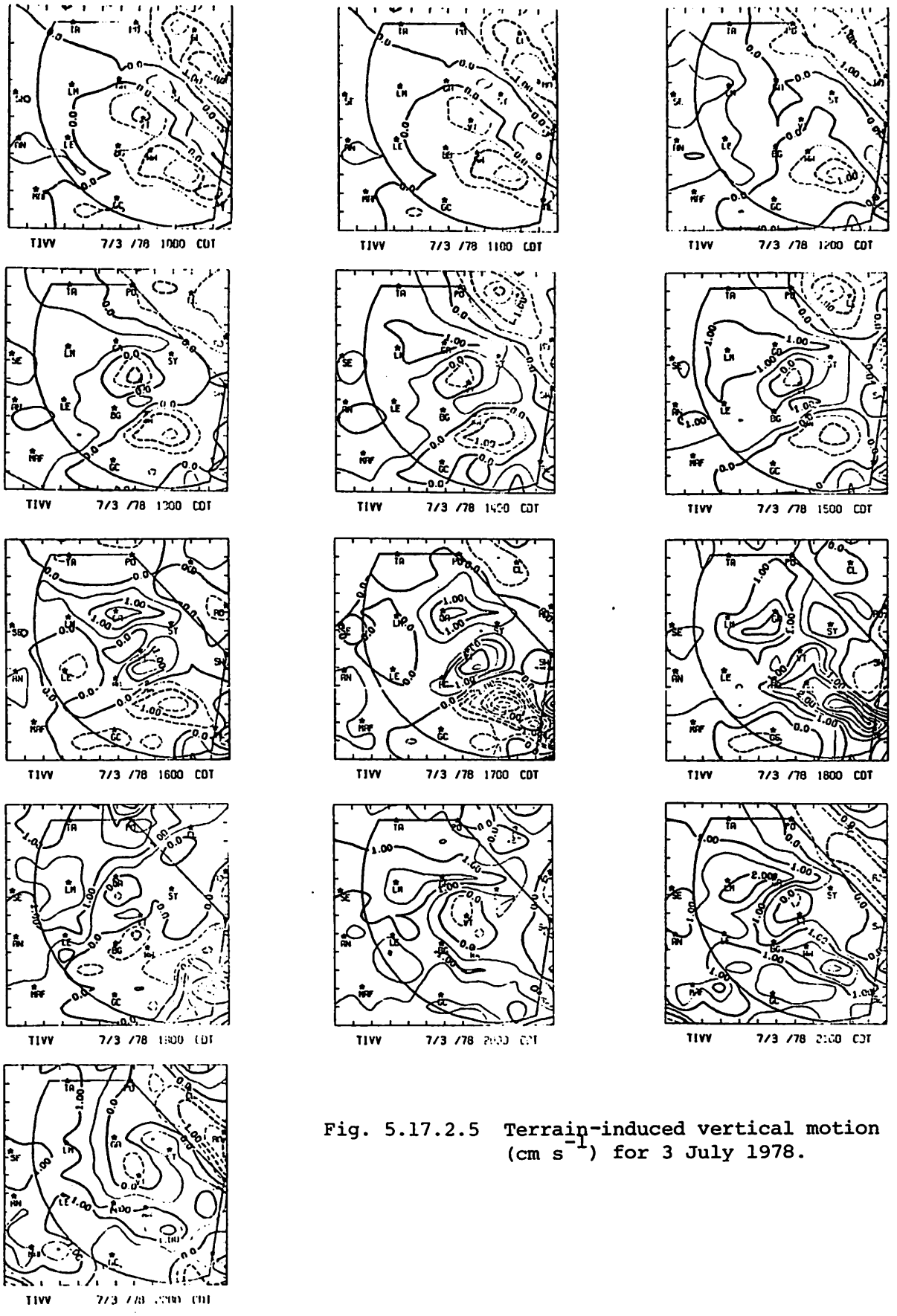

Fig. 5.17.2.5 Terrain-induced vertical motion (cm s^{-1}) for 3 July 1978.

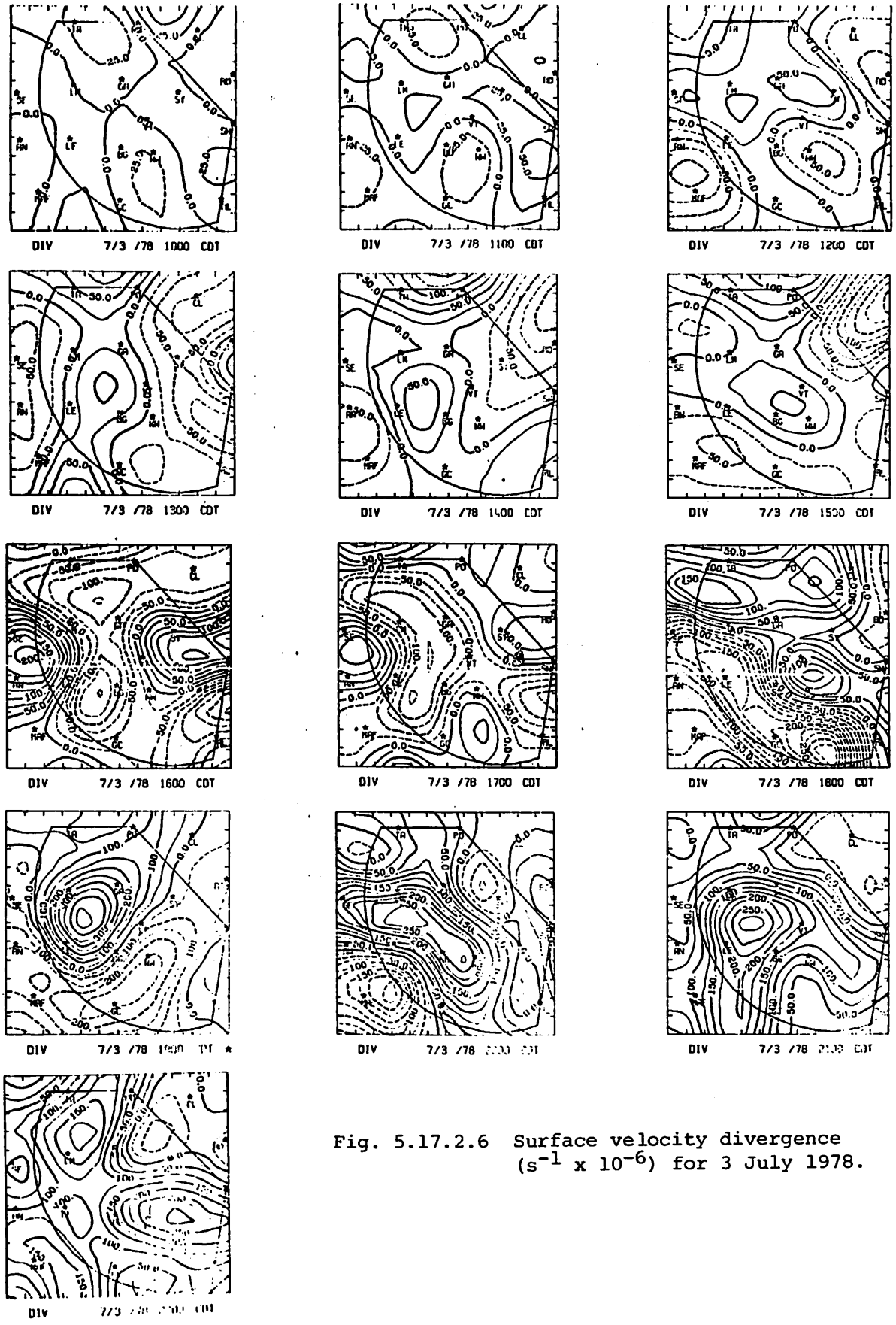

Fig. 5.17.2.6 Surface velocity divergence (s^{-1} x 10^{-6}) for 3 July 1978.

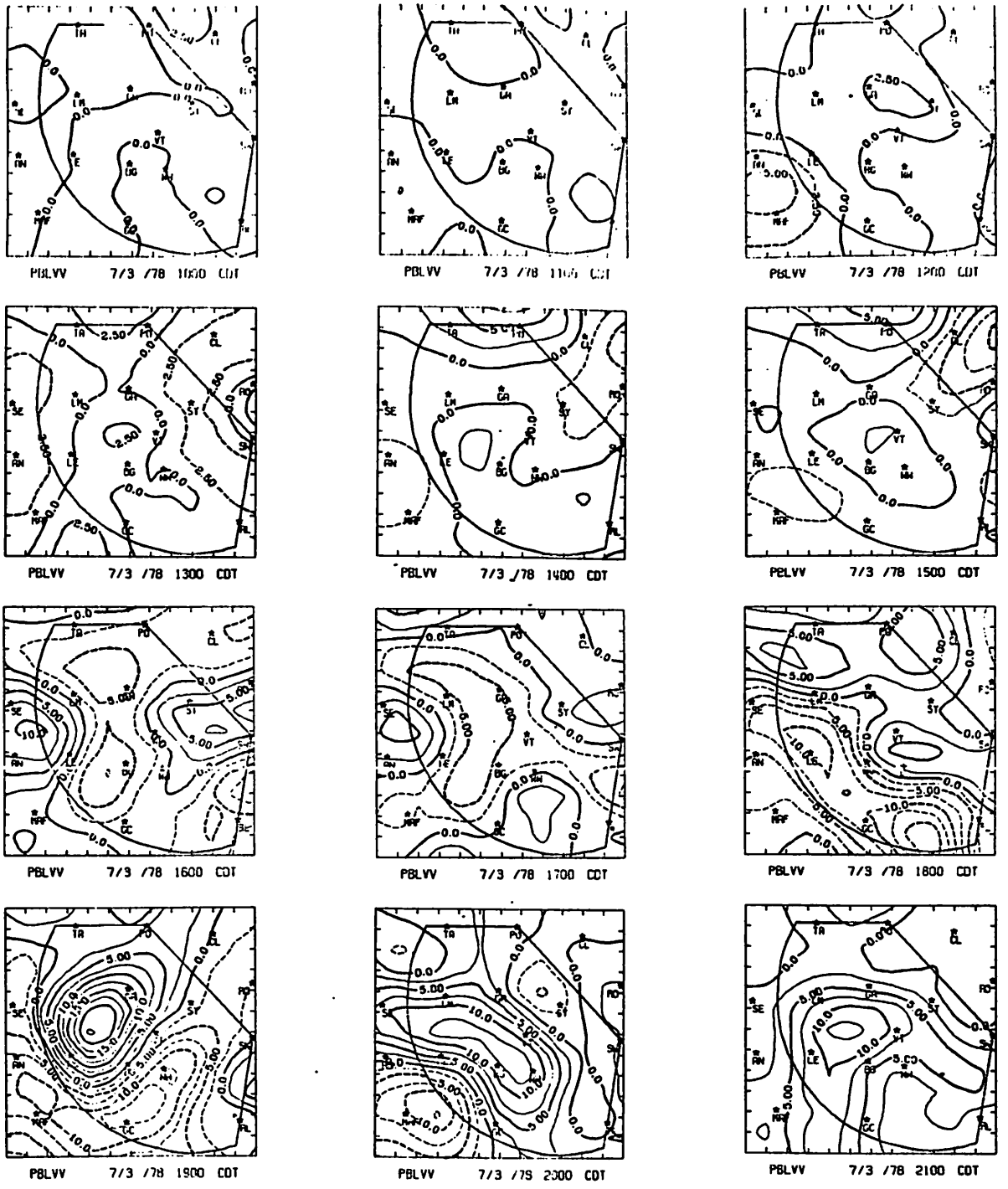

Fig. 5.17.2.7 Vertical motion 50 mb above the surface (μbars s^{-1}) for 3 July 1978.

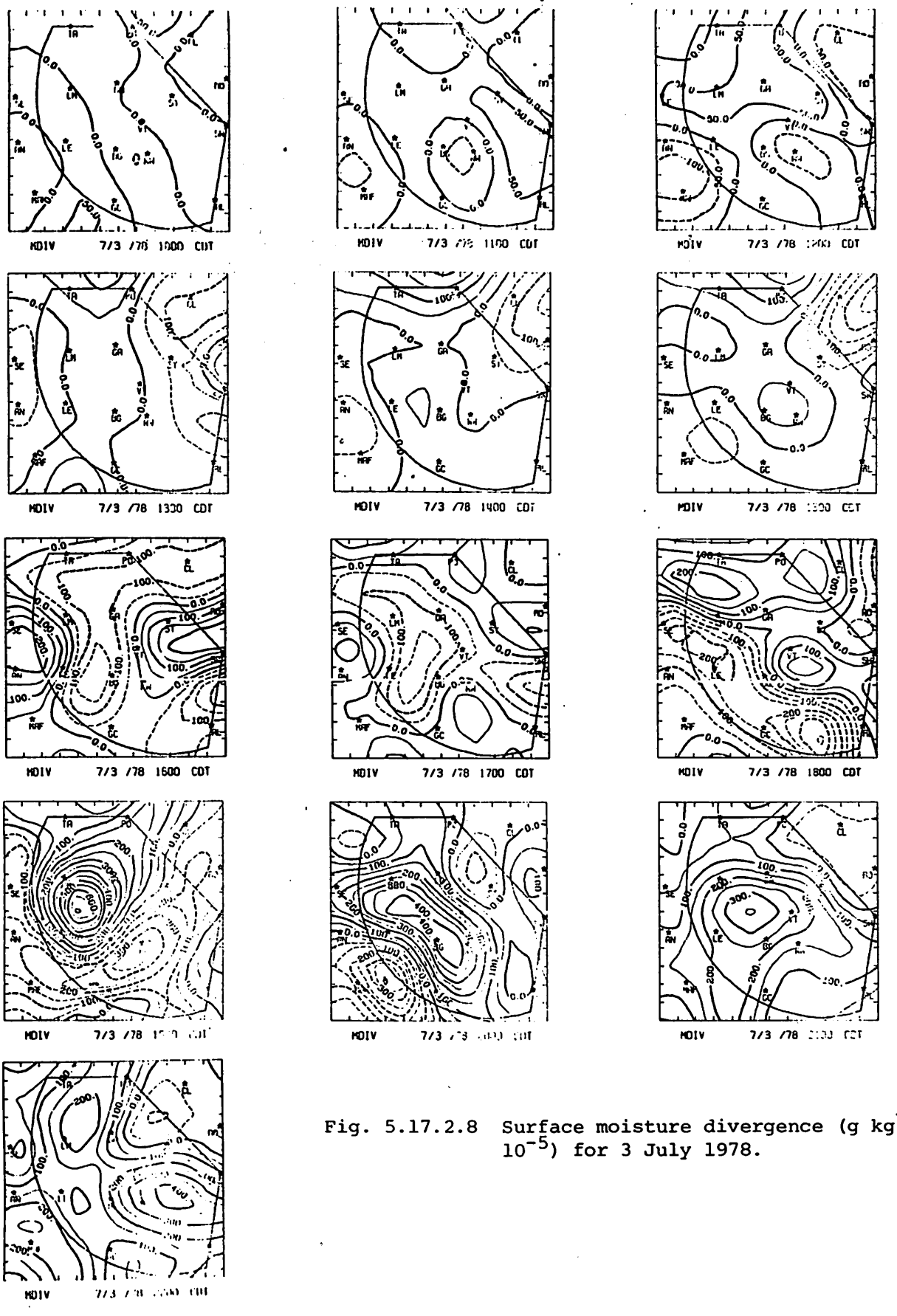

Fig. 5.17.2.8 Surface moisture divergence (g kg^{-1} s^{-1} x 10^{-5}) for 3 July 1978.

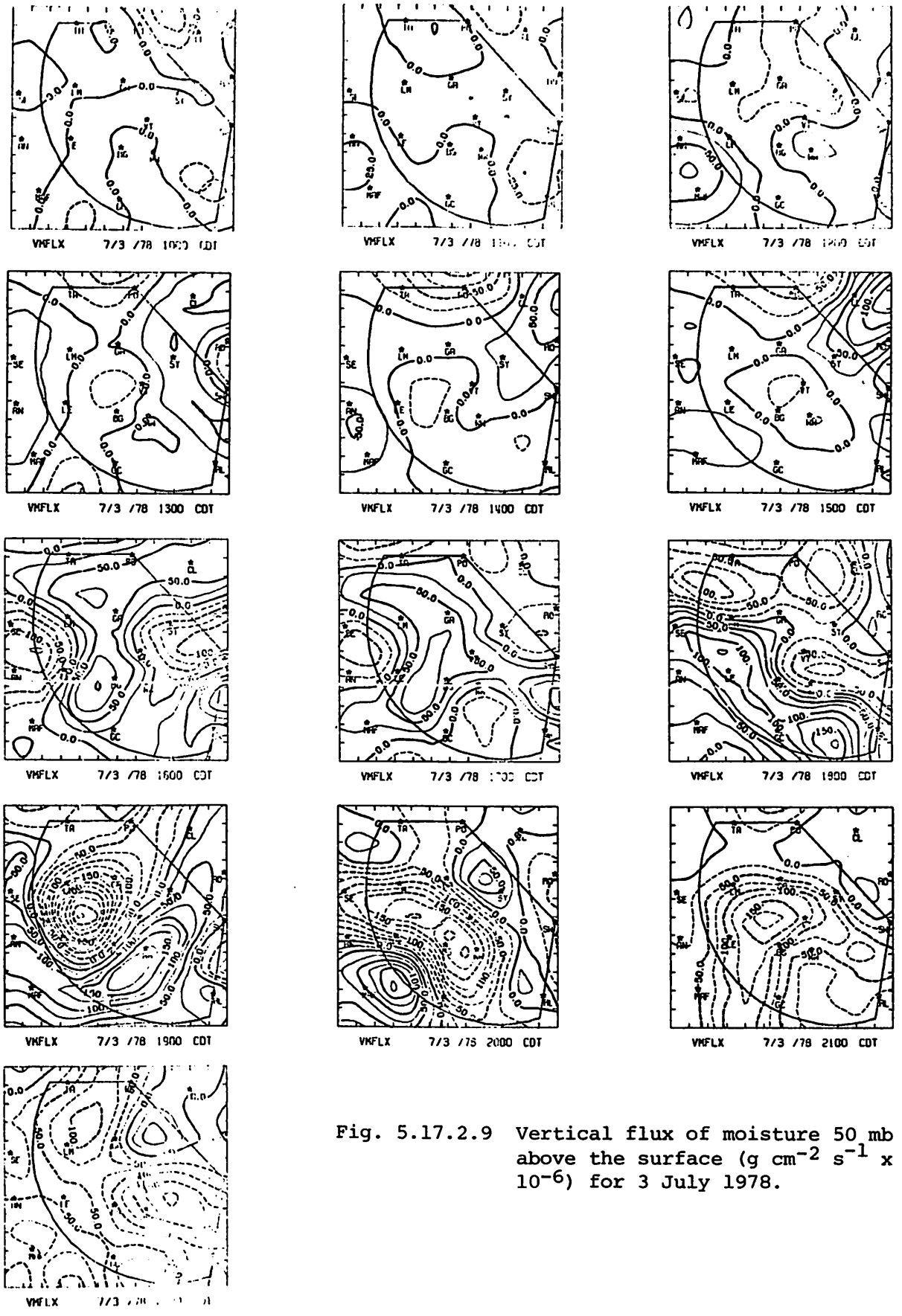

Fig. 5.17.2.9 Vertical flux of moisture 50 mb above the surface (g cm^{-2} s^{-1} x 10^{-6}) for 3 July 1978.

Fig. 5.17.2.10 Surface vorticity (s^{-1} x 10^{-6}) for 3 July 1978.

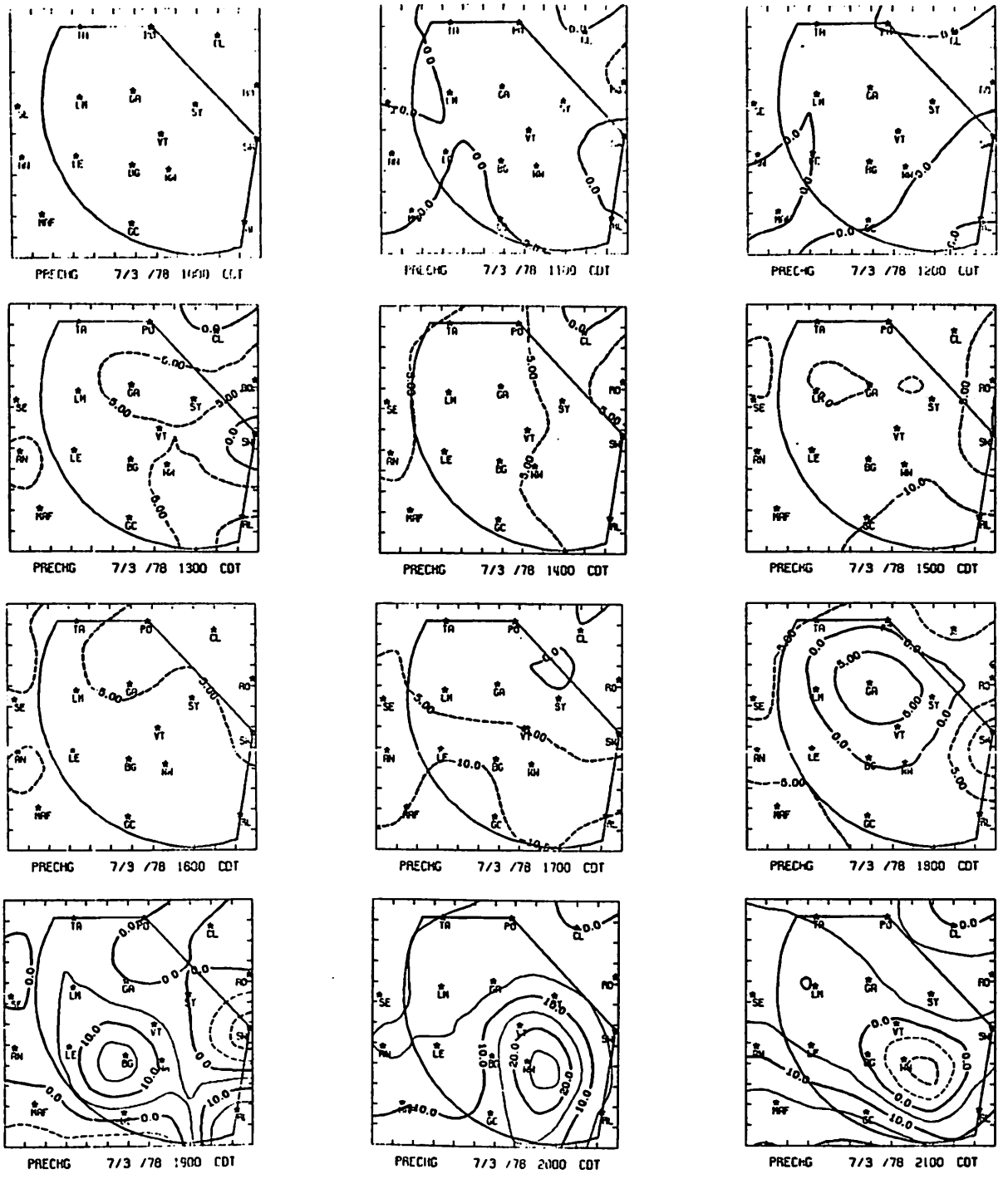

Fig. 5.17.2.11 Surface pressure change (mb hr^{-1} x 10^{-1}) for 3 July 1978.

Relative surface winds (Fig. 5.17.2.12) were mostly south and southwesterly early in the day. As showers formed and increased in strength their influence on the wind pattern showed up as convergence and divergence. The wind flow was generally into the storm area from 2000 to 0000 GMT. After 0100 GMT winds were generally directed out of the storm area and divergence dominated.

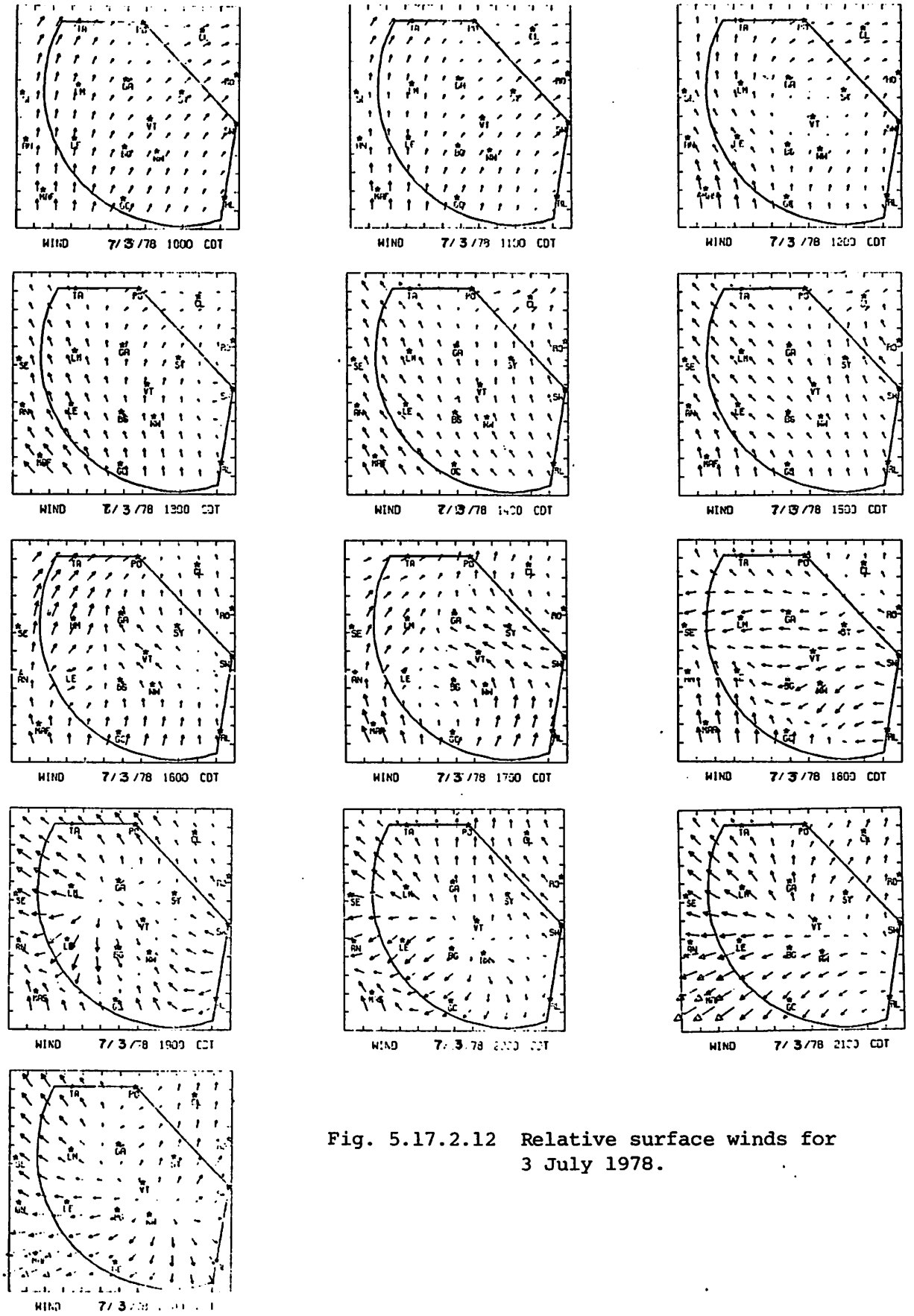

Fig. 5.17.2.12 Relative surface winds for 3 July 1978.

5.18 15 July 1978

5.18.1 Radar

No data were recorded for the first five hours of this day (Fig. 5.18.1.1). Showers appeared near Clairemont at 2000 GMT, with one fairly strong cell just to the south of there. The activity spread across the HIPLEX area in the next hour and the cells moved toward the southwest. Several strong cells formed and moved across the HIPLEX area during the next four hours. At 2100 GMT the cells were along a line between Tahoka and Rotan. The cells had moved southwest at 2200 GMT and were generally between Lamesa and Roscoe. A strong cell with height of 13.7 km (45K ft) was located north of Vincent at that time. At 2300 GMT the cells continued to move south and west. The strongest cell was just southeast of Lamesa with a top of 14.9 km (49K ft). At 0000 GMT the storms' intensity had decreased and the storms continued to move south and west. The strongest cells were northwest of Lenorah and Lamesa. The storms continued to diminish until, at 0200 GMT, there was no significant activity over the HIPLEX area.

5.18.2 Surface

Surface temperature (Fig. 5.18.2.1) showed a generally stable pattern from 1500 to 2000 GMT, with a general temperature increase across the area. The highest temperatures were in the northeast and the lowest in the south and southwest. Locally high temperatures were present near Vincent and Big Spring. At 2100 GMT the temperature had dropped 5.5°C just after a storm moved through Clairemont. No cool center was evident at 2200 GMT, but the cooling could have taken place between stations at that time. Between 2200 and 2300 GMT, temperature near Gail decreased by over 10°C, and Snyder and Vincent also showed lower temperatures. This occurred as a strong cell moved between these stations. This cool center remained through the remainder of the day. At 0100 GMT, another cool center appeared at Seminole after showers moved through that area. Temperatures decreased across the area after 0100 GMT.

Dewpoint depressions (Fig. 5.18.2.2) were highest in the northwest at 1500 GMT. The minimum shown at Big Spring through most of the day was probably not valid; relative humidities at Big Spring were rather high. The dewpoint depressions increased across the area until 2000 GMT. At 2100 GMT the dewpoint depression at Clairemont decreased because of the storm-induced

MISSING DATA

MISSING DATA

MISSING DATA

RADAR 7/15/78 1000 CDT

RADAR 7/15/78 1100 CDT

RADAR 7/15/78 1200 CDT

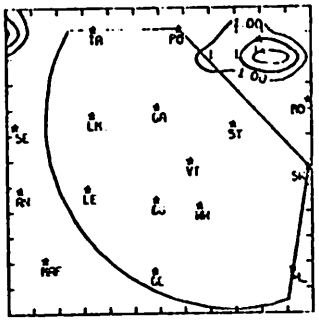

MISSING DATA

MISSING DATA

RADAR 7/15/78 1300 CDT

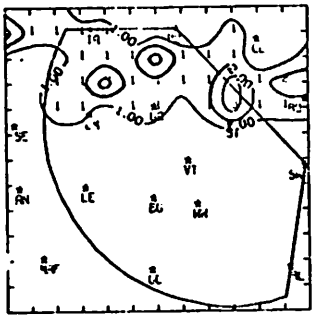

RADAR 7/15/78 1400 CDT

RADAR 7/15/78 1500 CDT

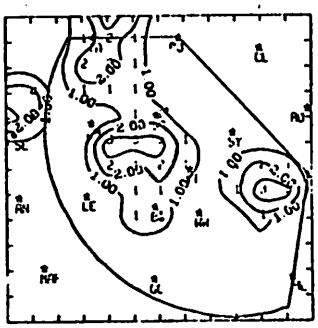

RADAR 7/15/78 1600 CDT

RADAR 7/15/78 1700 CDT

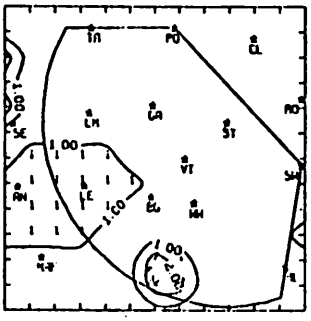

RADAR 7/15/78 1800 CDT

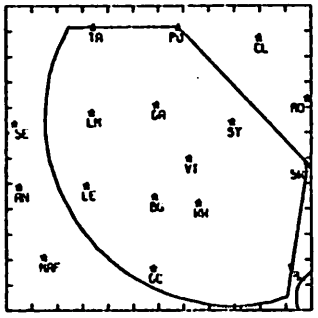

RADAR 7/15/78 1900 CDT

RADAR 7/15/78 2000 CDT

RADAR 7/15/78 2100 CDT

MISSING DATA

Fig. 5.18.1.1 Radar echoes for 15 July 1978.

RADAR 7/15/78 2200 CDT

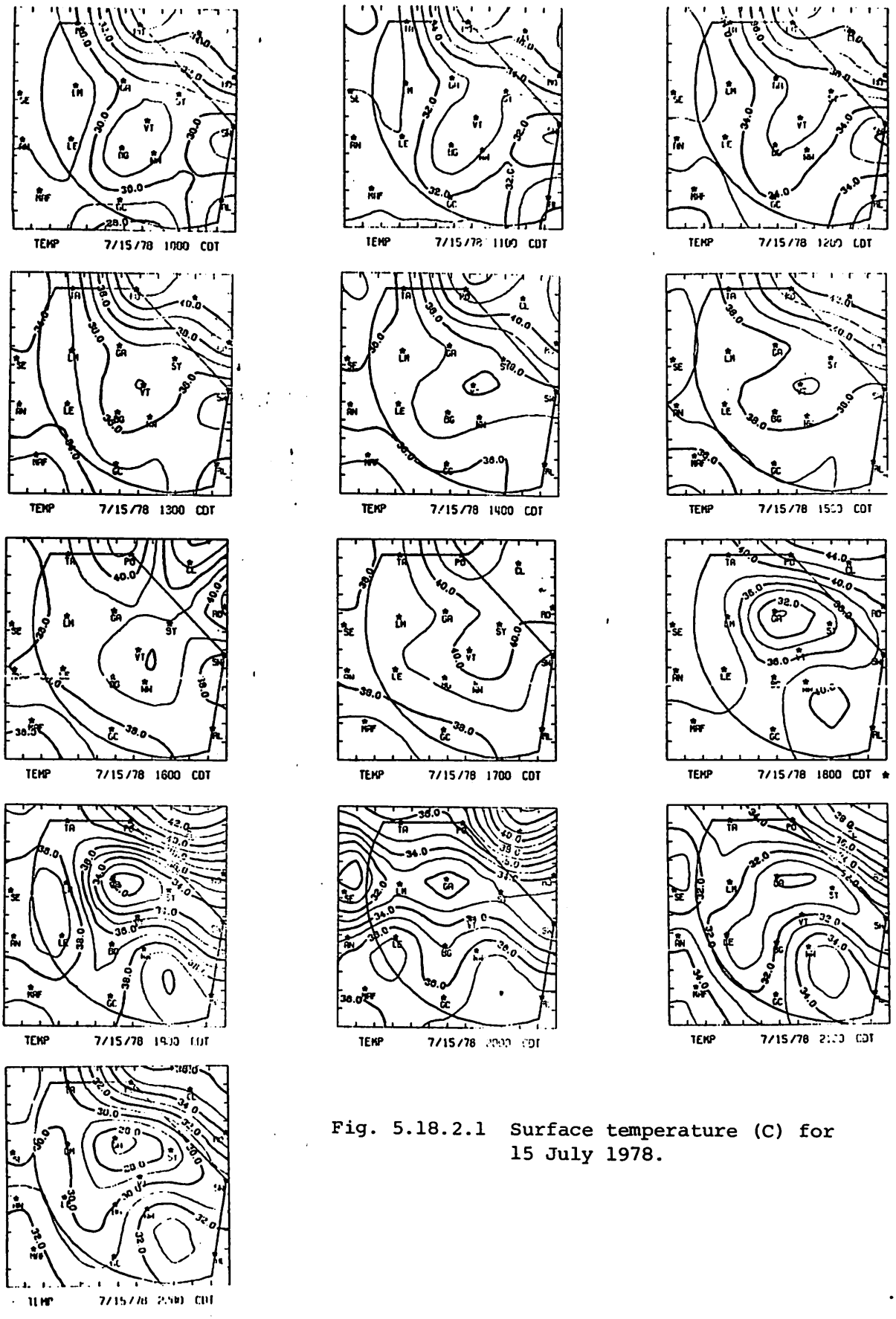

Fig. 5.18.2.1 Surface temperature (C) for 15 July 1978.

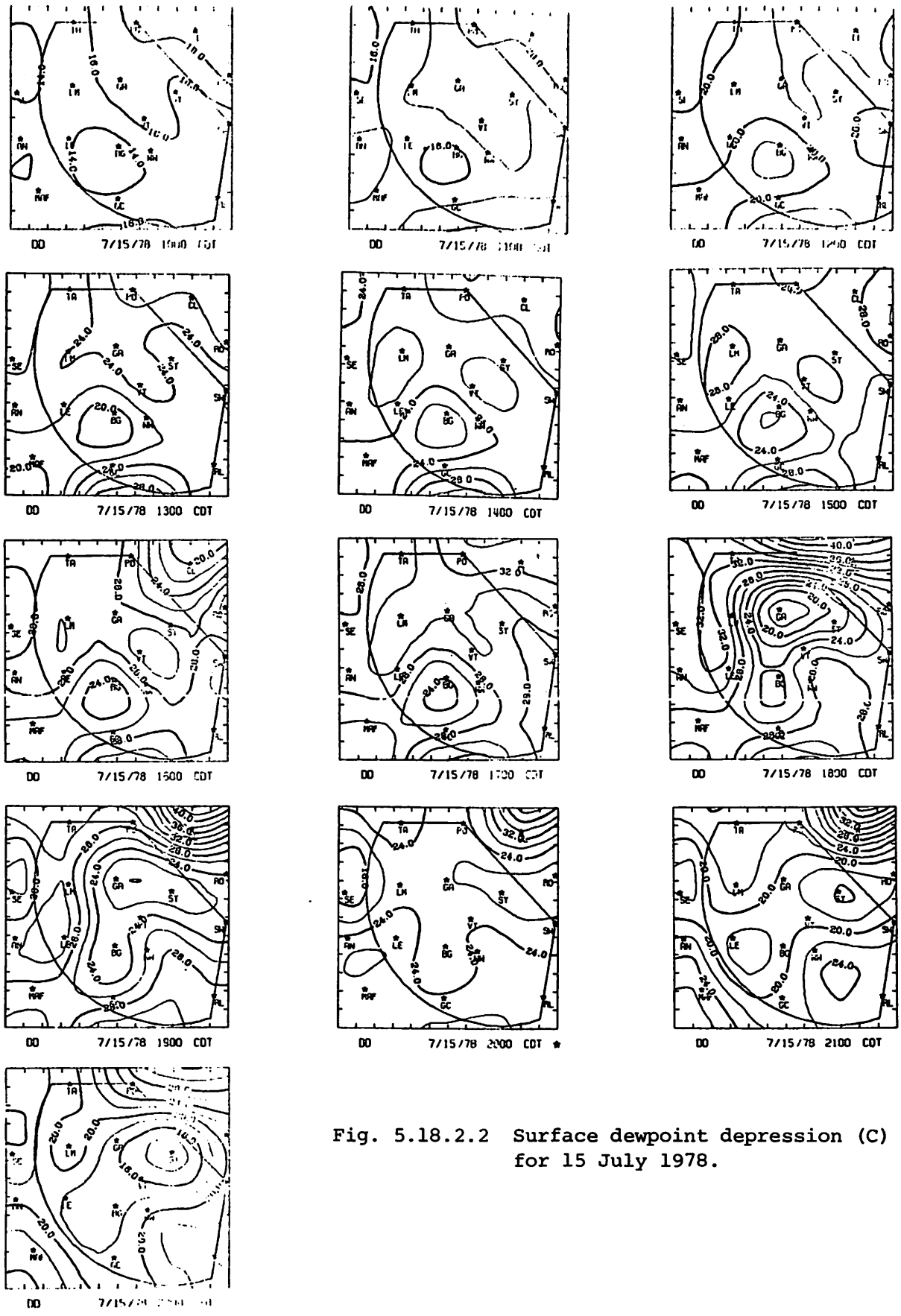

Fig. 5.18.2.2 Surface dewpoint depression (C) for 15 July 1978.

cooling. However, dewpoint depressions increased in that area in the next hour. At 2300 GMT the dewpoint depression decreased at Gail because of storm-induced cooling and because of an increase in dewpoint due to the addition of moisture. Dewpoint depressions decreased across the area after 0000 GMT when temperatures decreased. Another center of low dewpoint depression formed at Seminole at 0100 GMT because of the cooling and addition of moisture when a storm passed through that area.

Surface mixing ratios (Fig. 5.18.2.3) are shown as too high at Big Spring because of the overly high relative humidity. There was, nonetheless, a maximum located near there until at least 2000 GMT, although the maximum was not as strong as shown. At 2100 GMT mixing ratio was high at Clariemont with the passage of a storm during the last hour. The mixing ratio was low again in the Clairemont area by 2200 GMT. At 2300 GMT mixing ratio increased in the Gail area as storms passed south of there. This took place at the same time as the cooling in that area. At 0000 GMT mixing ratio increased at Seminole just after showers moved into that area. The mixing ratio increased at Seminole at 0100 GMT as the showers moved through that area.

Equivalent potential temperatures (Fig. 5.18.2.4) also were influenced by high recorded humidities at Big Spring. The maximum center that persisted near Big Spring throughout the day was probably real, although not as strong as depicted. Equivalent potential temperatures also were high in the north and northeast (near Post and Clairemont) from 1500 GMT until after 2100 GMT. Shower activity was present in that area from 2000 to 2100 GMT, and the potential temperature decreased after the showers had left that area. A minimum formed near Gail at 2300 GMT as a storm moved to the south of that area. This minimum persisted for the remainder of the day. High potential temperature showed up at Seminole at 0000 GMT as a result of showers, but the potential temperature there decreased in the next hour.

Terrain-induced vertical motion (Fig. 5.18.2.5) at 1500 GMT was primarily downward. By 1900 GMT mainly small upward and downward motions were present across the area. Stronger upward motions did not develop until 2300 GMT in the northwest, after showers had already left that area.

Surface divergence (Fig. 5.18.2.6) showed mainly small values at 1500 GMT. Convergence increased between Gail and Snyder at 1700 GMT, and

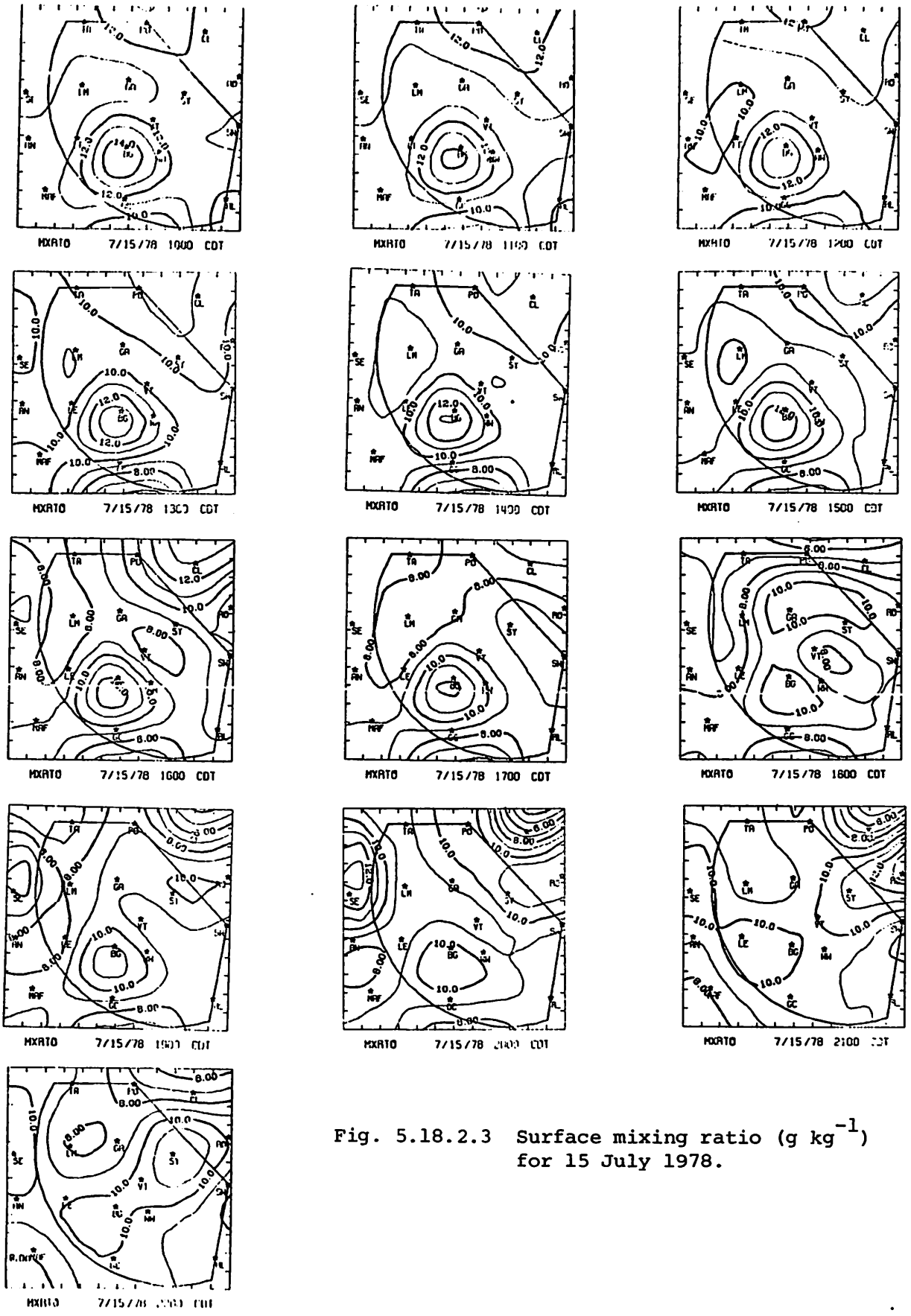

Fig. 5.18.2.3 Surface mixing ratio (g kg^{-1}) for 15 July 1978.

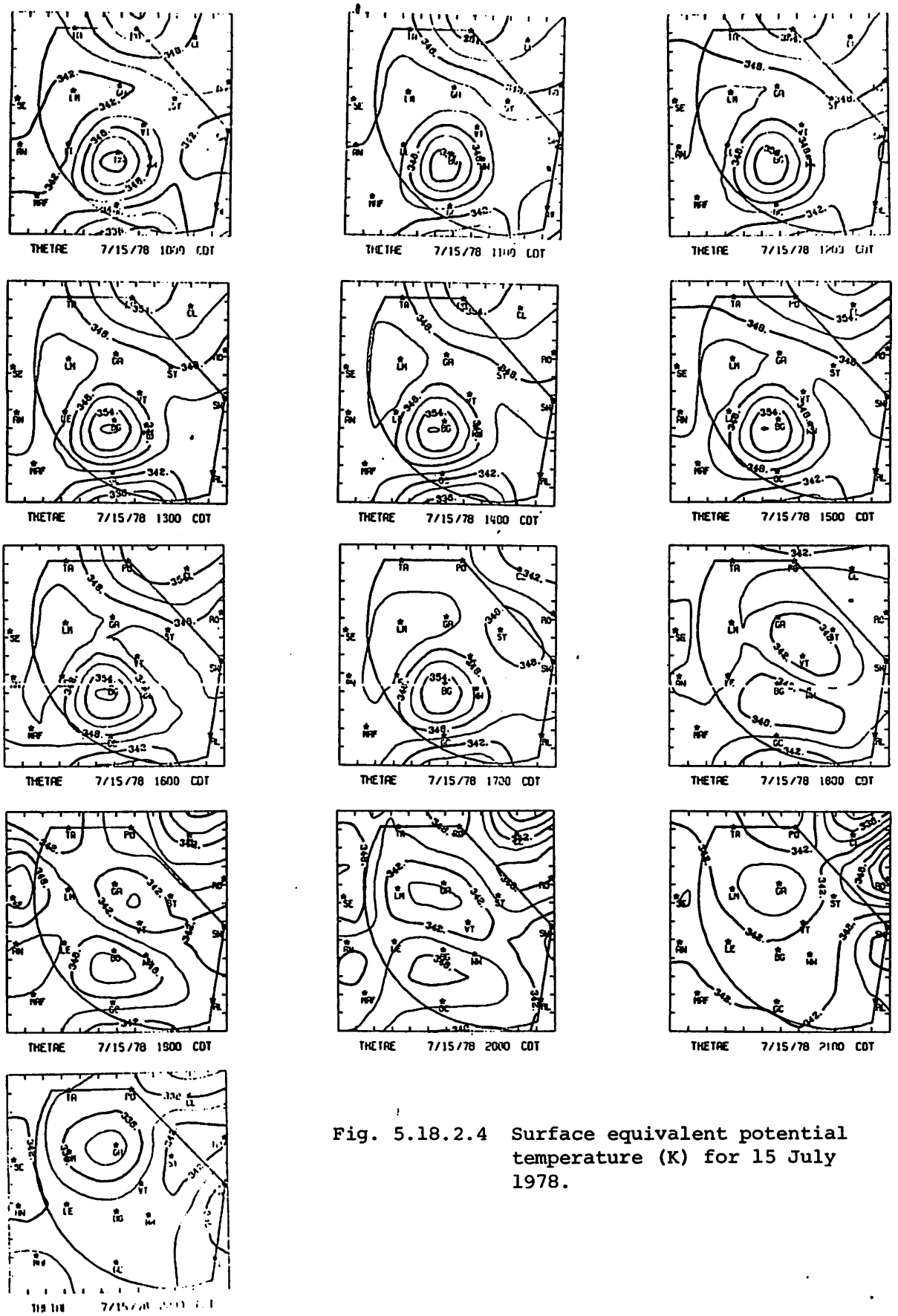

Fig. 5.18.2.4 Surface equivalent potential temperature (K) for 15 July 1978.

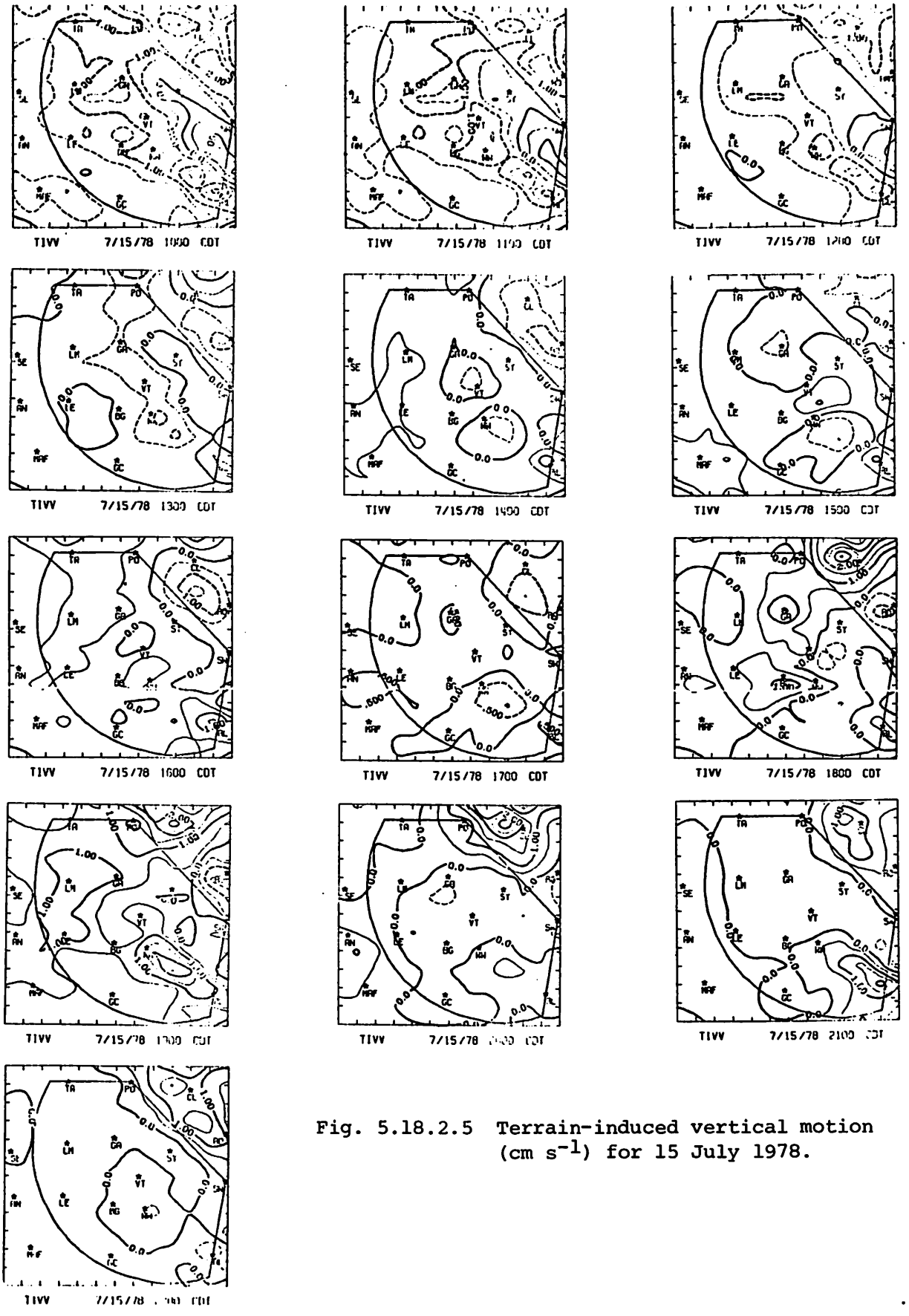

Fig. 5.18.2.5 Terrain-induced vertical motion (cm s^{-1}) for 15 July 1978.

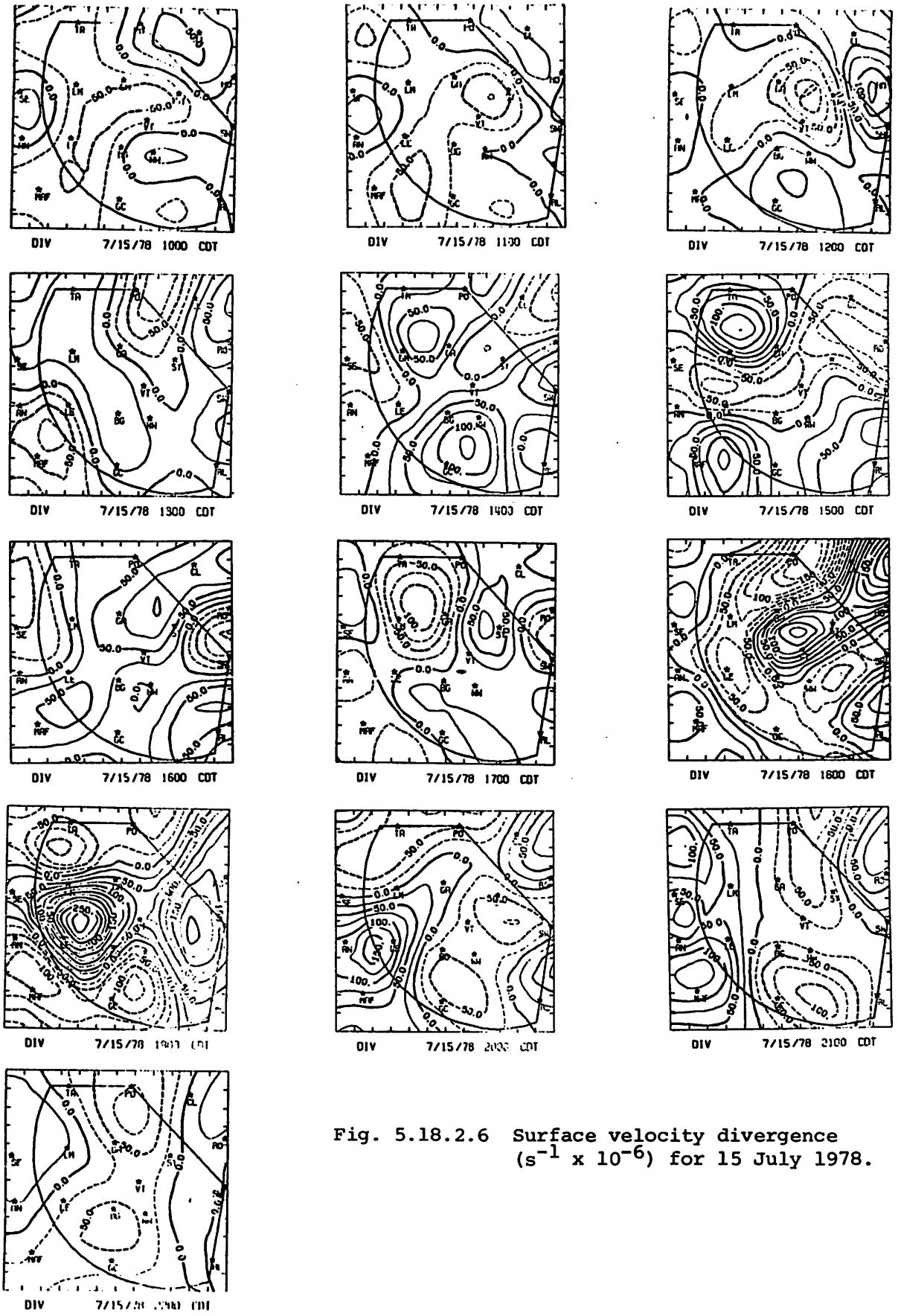

Fig. 5.18.2.6 Surface velocity divergence (s^{-1} x 10^{-6}) for 15 July 1978.

was present between Post and Clairemont at 1800 GMT. Convergence remained in the Clairemont area until 2100 GMT when showers moved out. At 2200 GMT the strongest convergence was between Gail and Lamesa. Strong divergence was southwest of Gail at 2300 GMT as shower activity moved out of that area. Convergence was present from Lenorah to Lamesa and between Lamesa and Post. This was in areas where shower activity was taking place. Another area of convergence was between Roscoe and Walsh-Watts associated with the shower in that area. At 0000 GMT the strongest divergence was between Gail, Lamesa, and Lenorah in the central part of the area. This was associated with the shower activity north and east of Lenorah. The intensity of the divergence and convergence decreased at 0100 GMT as showers moved out of the area and dissipated. The central part of the area showed moderate convergence by 0300 GMT with weak divergence in the east and west.

Vertical motion 50 mb above the surface is shown in Fig. 5.18.2.7. Moderate downward motion was present in the northwest at 1500 GMT, with some upward motion in the Snyder area. The upward motion increased at Gail and Snyder at 1700 GMT but decreased again at 1800 GMT. At 1900 and 2000 GMT there were small values of upward motion in the northeast where storm activity took place at 2000 GMT. This upward motion was gone at 2100 GMT. At 2200 GMT upward motion was present in the west, and strongest between Lamesa and Gail. A strong downdraft was shown at 2300 GMT at Gail where substantial cooling had taken place. Upward motion at 2300 GMT was located from Post to Lamesa and southward to Lenorah in an area where most of the shower activity was taking place. At 0000 GMT strong downward motions were centered to the east of Lenorah and Lamesa on the northeast side of the strongest storm activity. Upward motion was strongest just south of Andrews to the south of the strongest activity, and south of Walsh-Watts. At 0100 GMT the magnitudes of the vertical motions decreased as the storm activity dissipated. Motions were still small at 0300 GMT.

Surface moisture divergence (Fig. 5.18.2.8) showed patterns similar to the velocity divergence (Fig. 5.18.2.6). There was moisture convergence near Vincent from 1500 to 1800 GMT, and in the northeast from 1800 to 2000 GMT. Moisture divergence occurred in the northeast after 2100 GMT when the storms

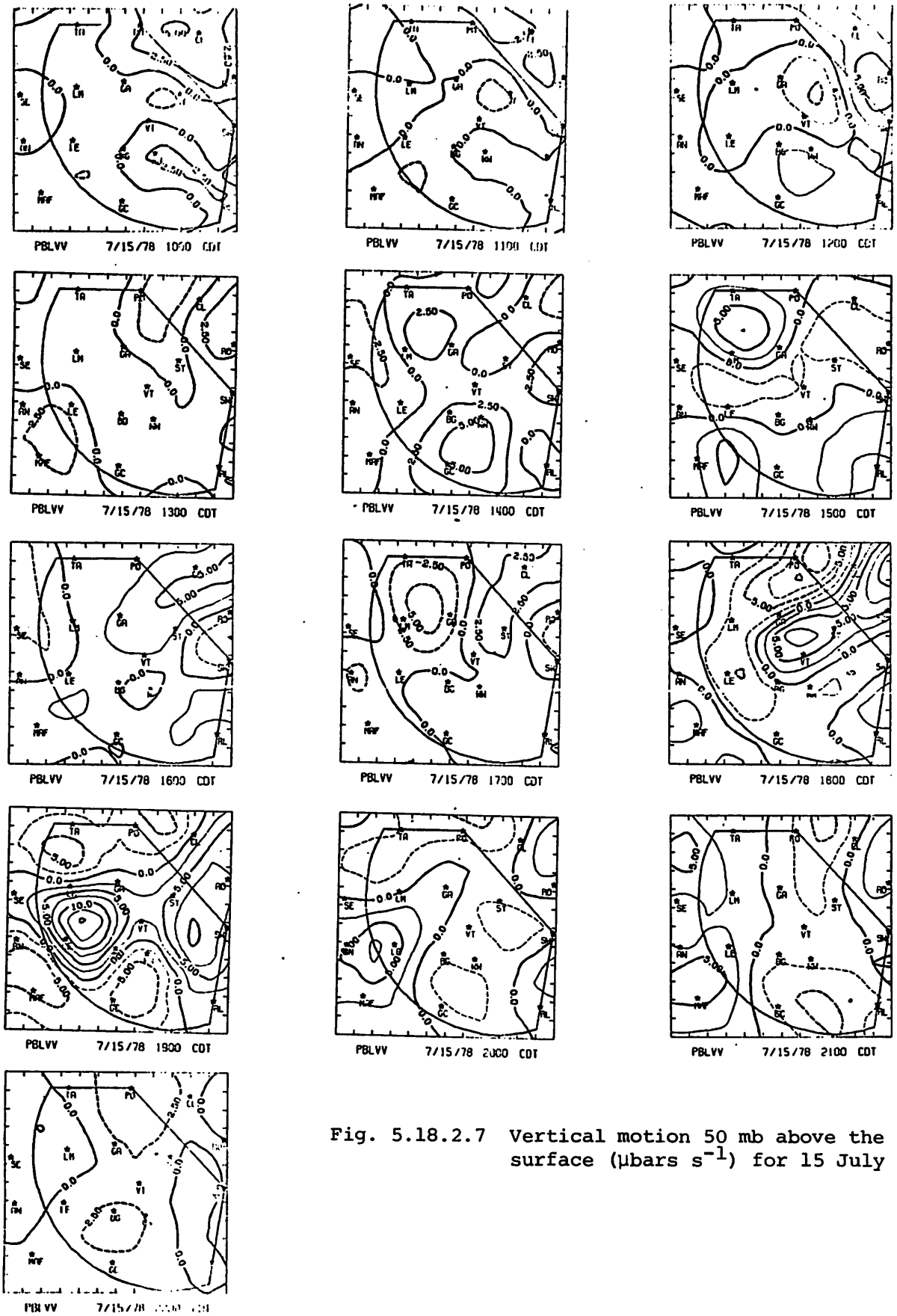

Fig. 5.18.2.7 Vertical motion 50 mb above the surface (μbars s^{-1}) for 15 July 1978.

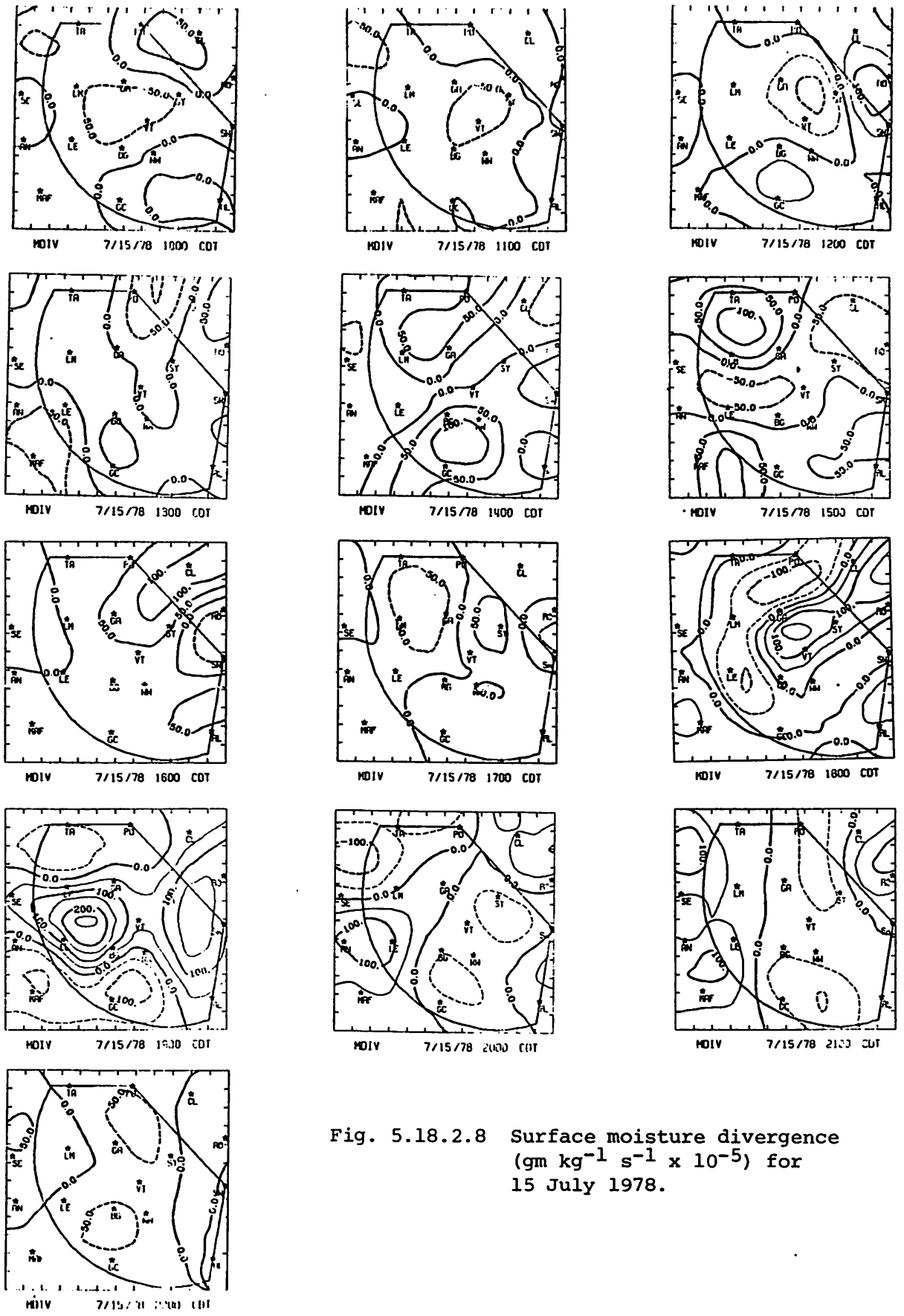

Fig. 5.18.2.8 Surface moisture divergence (gm kg^{-1} s^{-1} x 10^{-5}) for 15 July 1978.

moved out of that area. Moisture convergence occurred near Lamesa and Gail at 2200 GMT, and extended from Post to Lamesa to south of Lenorah at 2300 GMT. Moisture divergence occurred at Gail at 2300 GMT, and northeast of Lenorah at 0000 GMT to the east of the storm activity. Centers of convergence and divergence moved westward from 0100 to 0300 GMT but decreased in value as shower activity diminished.

The vertical flux of moisture 50 mb above the surface is shown in Fig. 5.18.2.9. Downward moisture flux was present in the northeast from 1500 to 1800 GMT while upward moisture flux was centered near Vincent. From 1800 to 2000 GMT upward moisture flux was present in the northeast where shower activity was present at 2000 GMT. Downward flux of moisture occurred after the showers were moving out of the Clairemont area at 2100 GMT. Upward flux began in the Lamesa-Gail area at 2200 GMT and increased at 2300 GMT as shower activity moved through the area. Downward moisture flux was present near the Gail area at 2300 GMT where mixing ratio had increased. The downward moisture flux was strongest to the northeast of Lenorah at 0000 GMT, with upward flux to the south and west of the storm activity. The magnitudes of the moisture flux decreased at 0100 GMT, and generally small upward moisture fluxes were present by 0300 GMT when storm activity had ceased.

Surface vorticity (Fig. 5.18.2.10) showed moderate values through the first few hours. Centers of negative vorticity were located in the northeast and northwest from 1500 to 1700 GMT, and in the west and southeast from 1800 to 2000 GMT. As the storms moved through the area the centers of positive and negative vorticity shifted in position and increased in magnitude. The strongest centers were at 2300 and 0000 GMT when the strongest activity took place. At 2300 GMT a negative vorticity center was located just north of Big Spring in the area of the strongest activity. At 0000 GMT the center intensified and moved west along with the shower activity. At 0100 GMT the vorticity decreased across the area and by 0300 GMT the values were small.

Surface pressure changes (Fig. 5.18.2.11) were small at 1600 GMT. After 1700 GMT surface pressure was falling over most of the area. At 2300 GMT there was a pressure rise of 0.8 mb at Gail when the pressure was falling over most of the area. This occurred near the area of maximum cooling and downward motion and was clearly associated with the storm's downdraft area.

Fig. 5.18.2.9 Vertical flux of moisture 50 mb above the surface (gm cm^{-2} s^{-1} x 10^{-6}) for 15 July 1978.

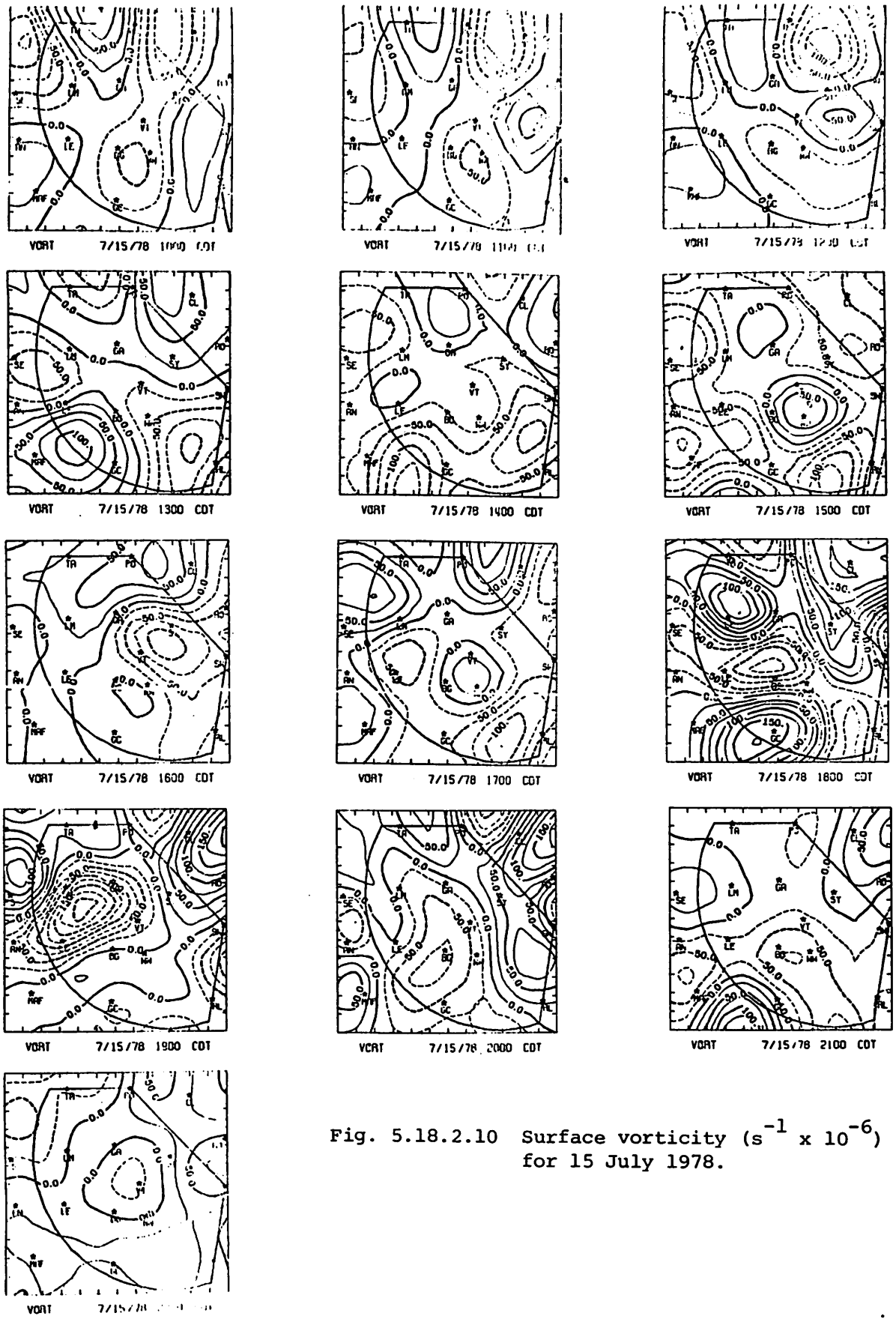

Fig. 5.18.2.10 Surface vorticity ($s^{-1} \times 10^{-6}$) for 15 July 1978.

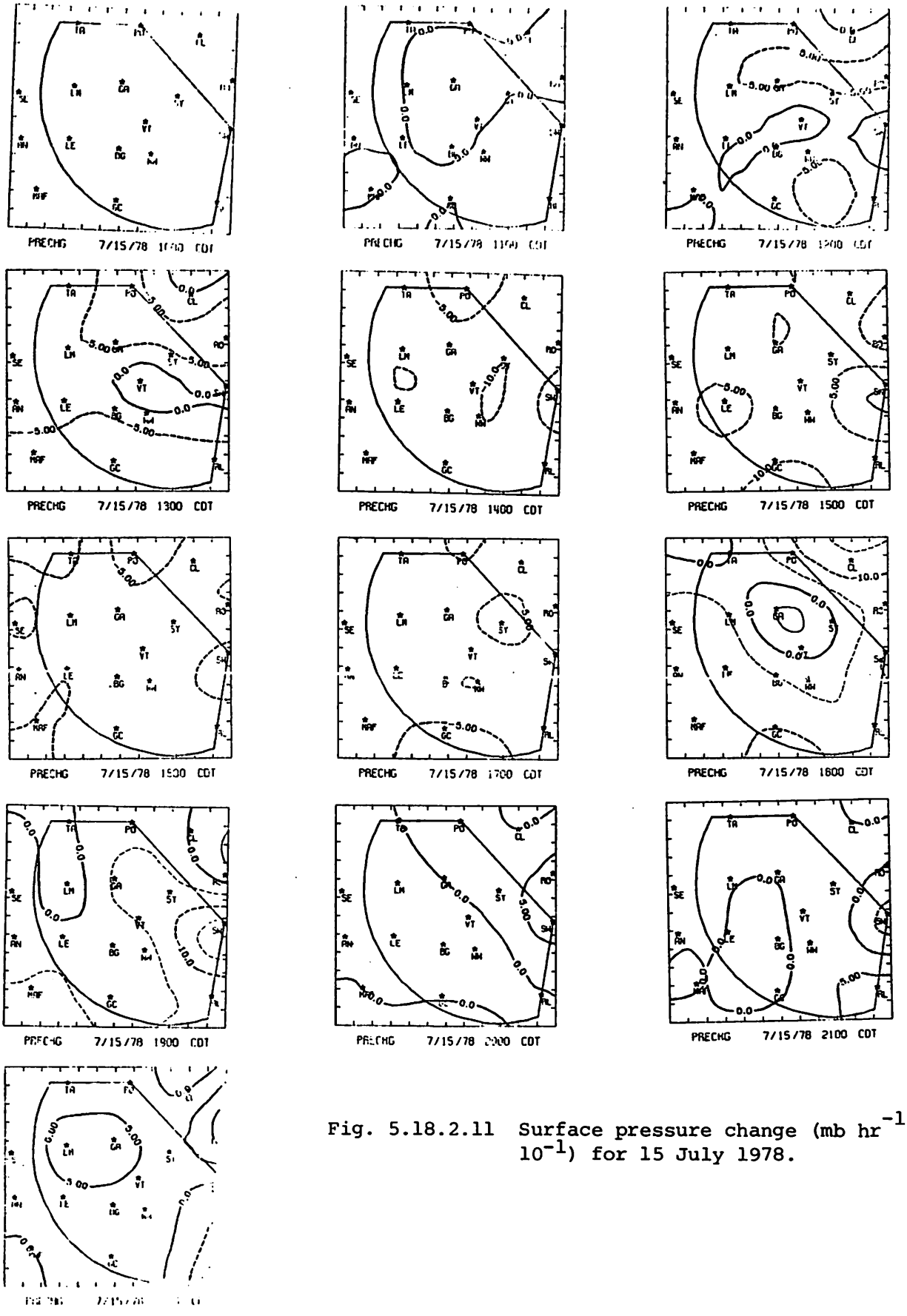

Fig. 5.18.2.11 Surface pressure change (mb hr^{-1} x 10^{-1}) for 15 July 1978.

After 0100 GMT the pressure falls were very small and pressure rises began to occur across the area.

Relative surface winds (Fig. 5.18.2.12) were easterly and northeasterly at 1500 GMT. By 1800 GMT the winds had become light and variable. In the southwest the winds shifted to a westerly direction while in other sections the winds were more northerly. After 2000 GMT winds shifted with the movement of showers across the area. During this period the winds mainly were directed into and around the storms. At 0000 GMT wind speeds increased in the west with strong northerlies in the northwest and strong westerlies in the southwest. This produced the large divergence shown in Fig. 5.18.2.6 at that time. As the storms dissipated at 0100 GMT the wind speeds decreased and by 0300 GMT the winds were very light.

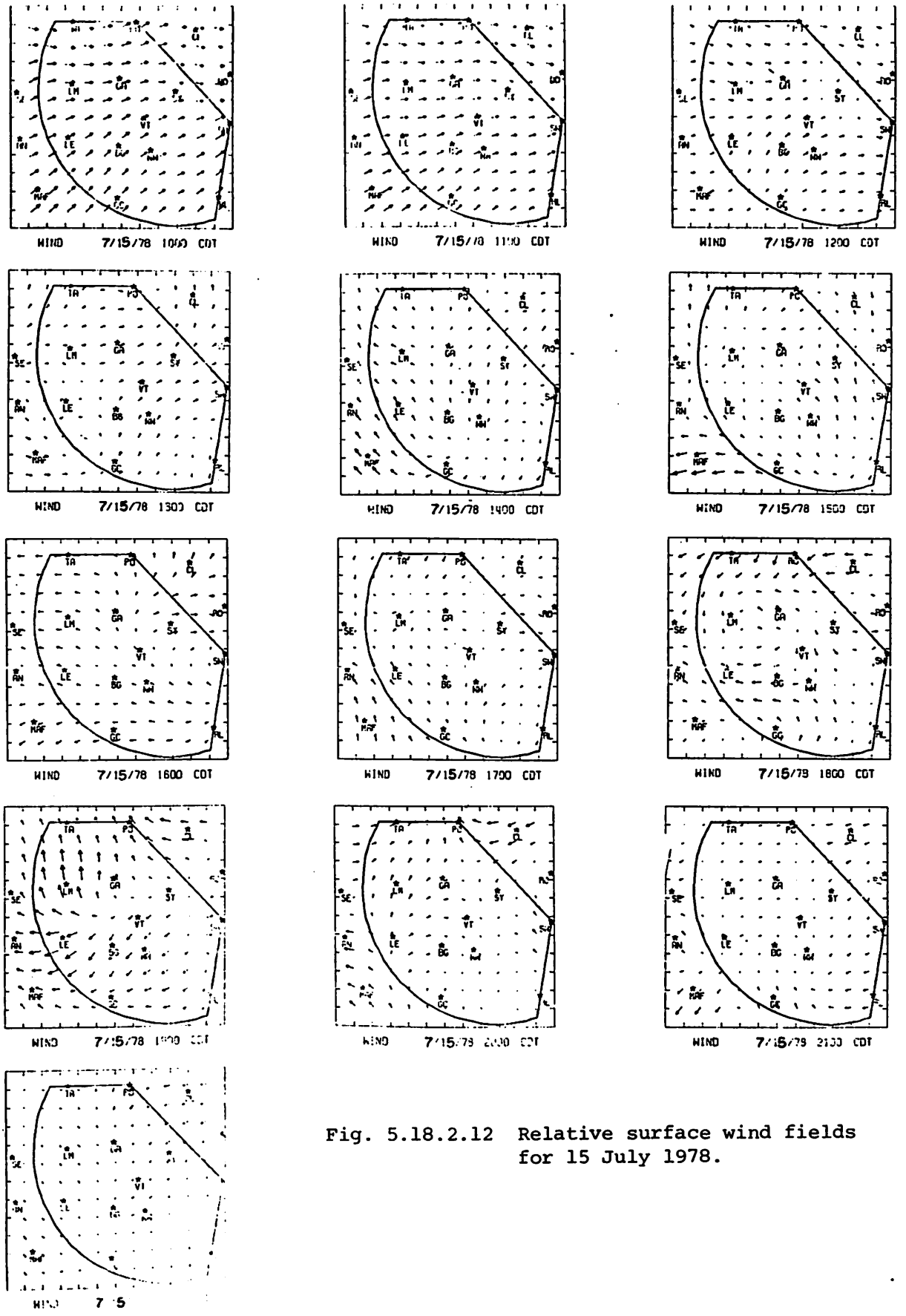

Fig. 5.18.2.12 Relative surface wind fields for 15 July 1978.

5.19 17 July 1978

5.19.1 Radar

There were no radar echoes recorded over the HIPLEX area on this day.

5.19.2 Surface

Surface temperature (Fig. 5.19.2.1) increased over the area until 2100 GMT and decreased after 2300 GMT. The patterns of temperature were similar from hour to hour, with lowest temperatures in the south and also in the central part of the area along a line from Gail to Roscoe. The highest temperatures were in the northeast and also along a line from Seminole to Walsh-Watts.

Surface dewpoint depression(Fig. 5.19.2.2), mixing ratio (Fig. 5.19.2.3) and equivalent potential temperature (Fig. 5.19.2.4) show similar patterns from hour to hour through the day with an extreme value (minimum dewpoint depression and maximum mixing ratio) at Big Spring. The humidity at Big Spring was higher than it should have been, so these fields should have been nearly flat with little variation across the area. Terrain-induced vertical motion (Fig. 5.19.2.5) was small through the day and there were no centers of vertical motion that persisted for more than a short time.

Surface divergence (Fig. 5.19.2.6) showed patterns that were quite variable throughout the day. The winds were generally light and variable, and values of divergence were generally small. Convergence was present in the north-central part of the area between 1500 and 1700 GMT. Convergence occurred in the south from 1800 to 2000 GMT, and was present over the entire central section at 2200 GMT. It increased in magnitude at 2300 GMT between Post and Clairemont and at 0000 GMT near Rotan. Mostly weak divergence and convergence was present between 0100 and 0200 GMT, with moderately strong convergence developing in the southwest at 0300 GMT. For the most part, the values shown were typical of a day with no activity.

Vertical motion 50 mb above the surface (Fig. 5.19.2.7) varied in much the same way as the divergence. Upward motion generally occurred in the central part of the area prior to 2200 GMT. At 2300 GMT the strongest upward motion was in the northeast near Post, and this center moved east to near Rotan at 0000 GMT. From 0100 to 0200 GMT the motion was generally small. At 0300 GMT another center of upward motion developed; it was in the southwest near Midland.

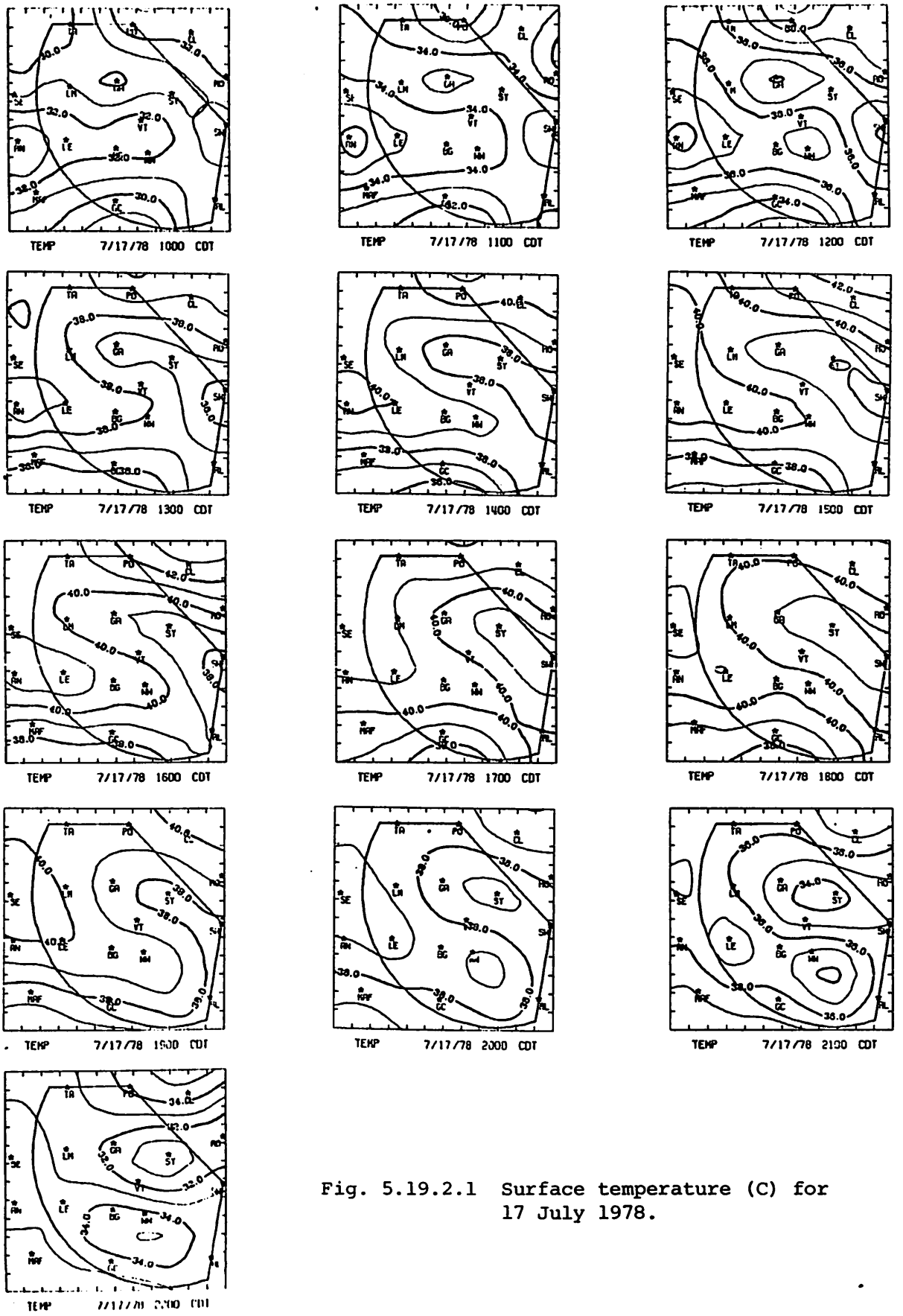

Fig. 5.19.2.1 Surface temperature (C) for 17 July 1978.

Fig. 5.19.2.2 Surface dewpoint depression (C) for 17 July 1978.

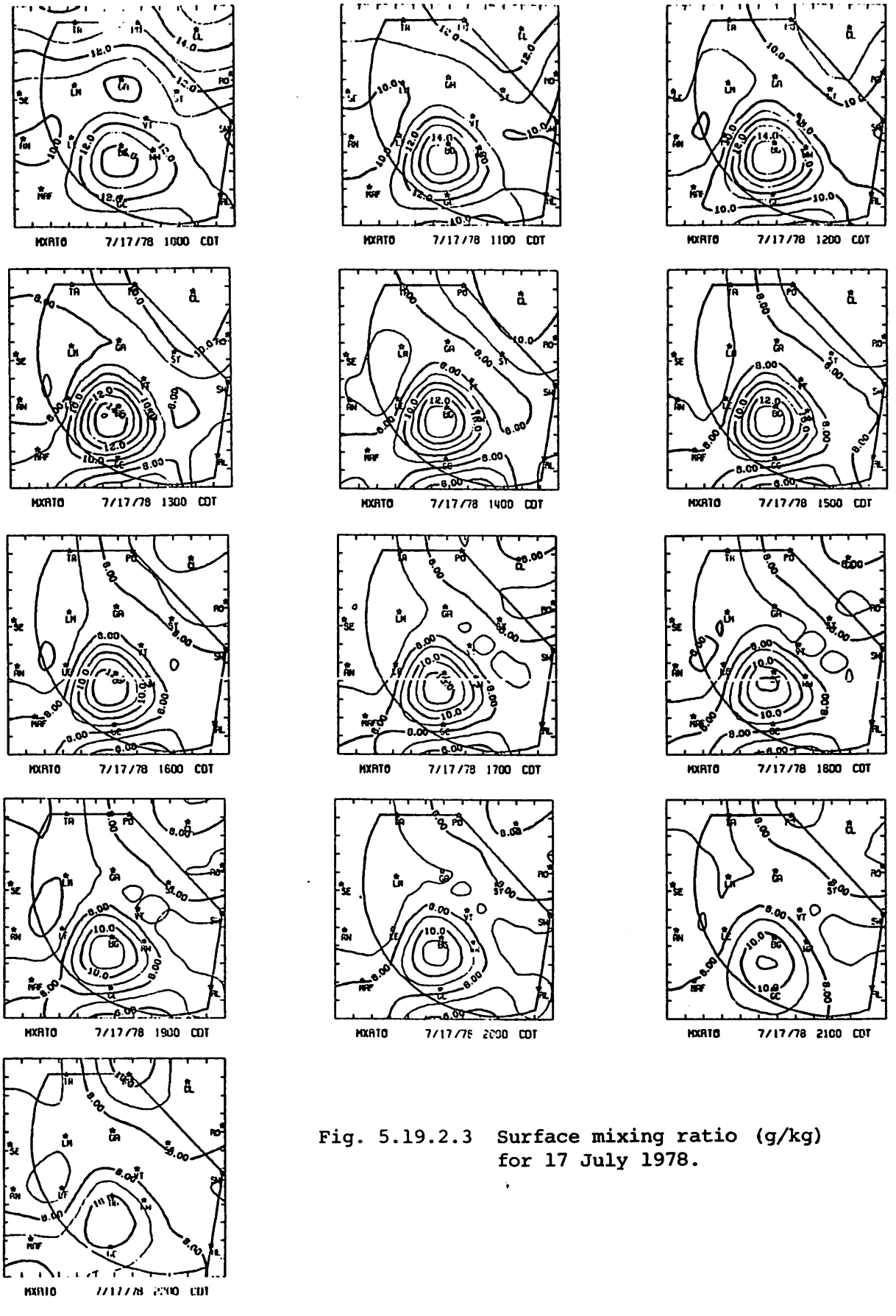

Fig. 5.19.2.3 Surface mixing ratio (g/kg) for 17 July 1978.

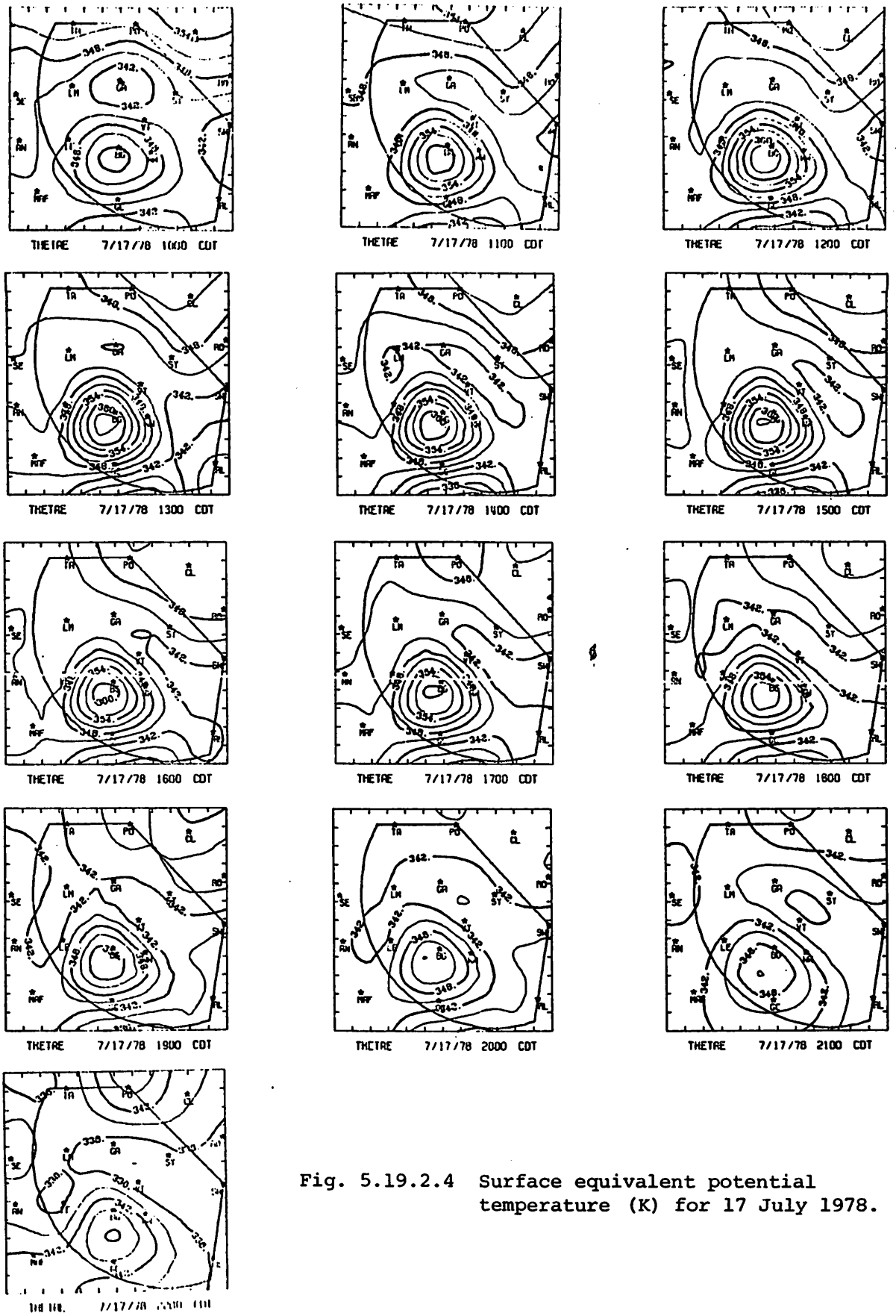

Fig. 5.19.2.4 Surface equivalent potential temperature (K) for 17 July 1978.

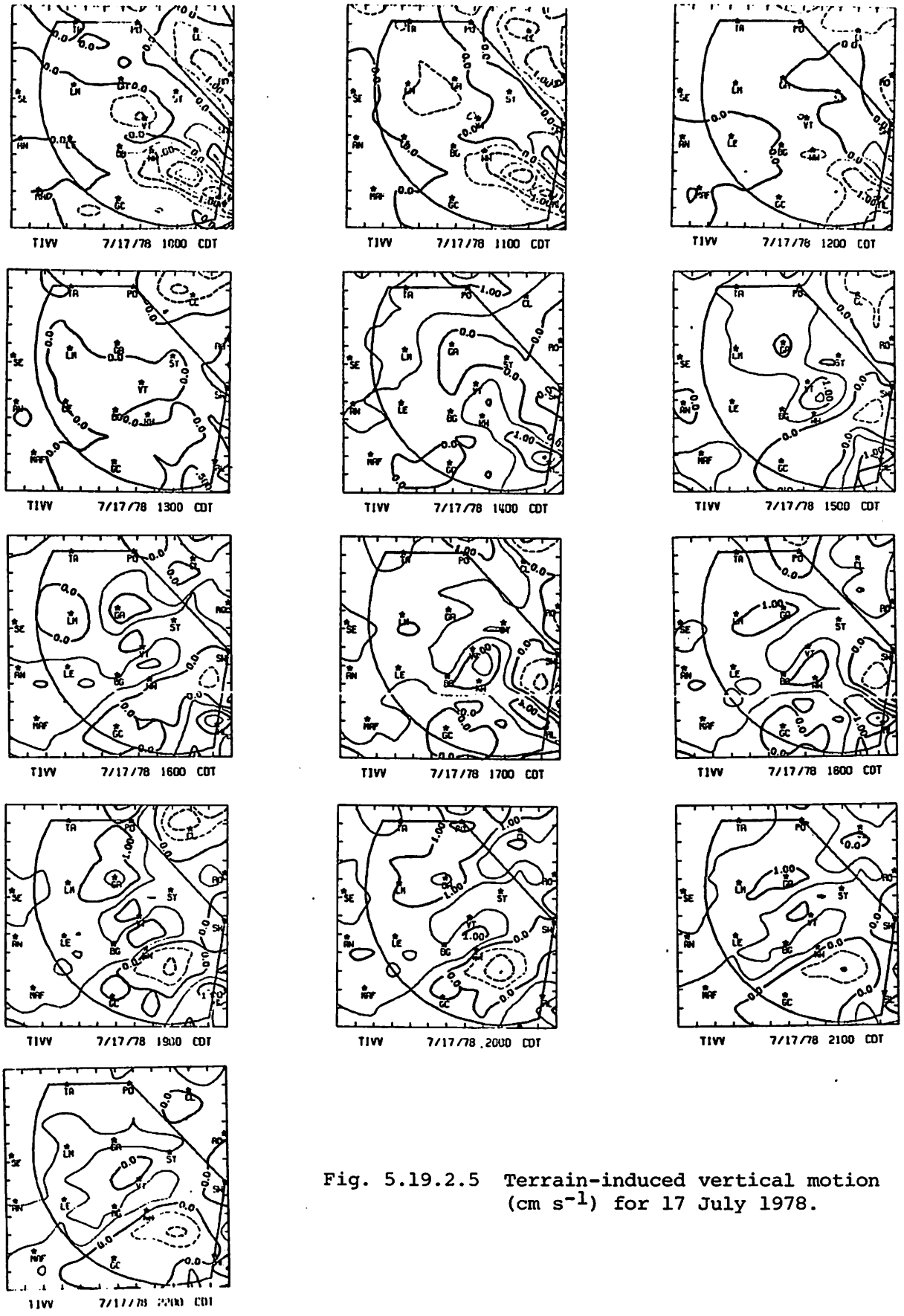

Fig. 5.19.2.5 Terrain-induced vertical motion (cm s^{-1}) for 17 July 1978.

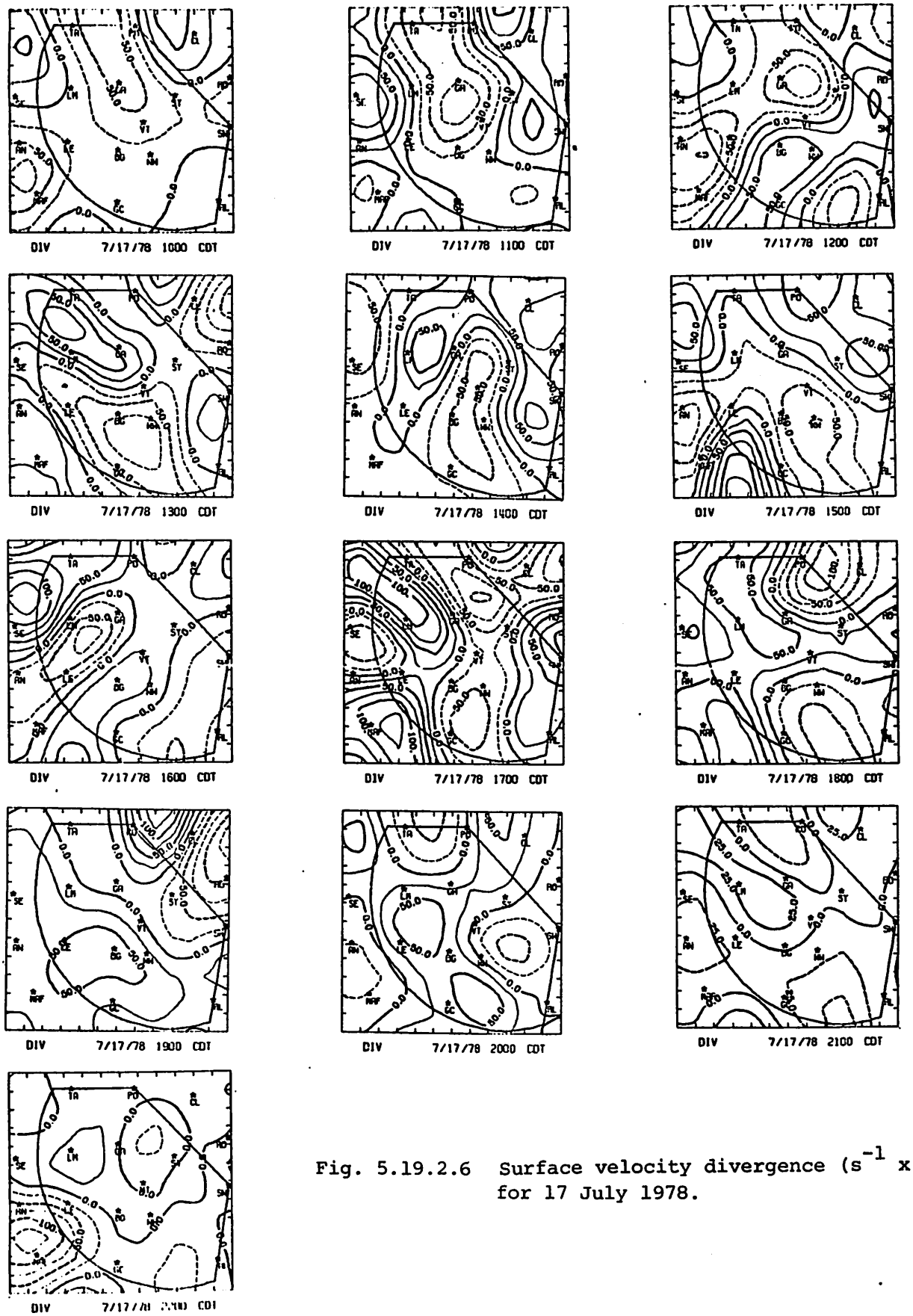

Fig. 5.19.2.6 Surface velocity divergence ($s^{-1} \times 10^{-6}$) for 17 July 1978.

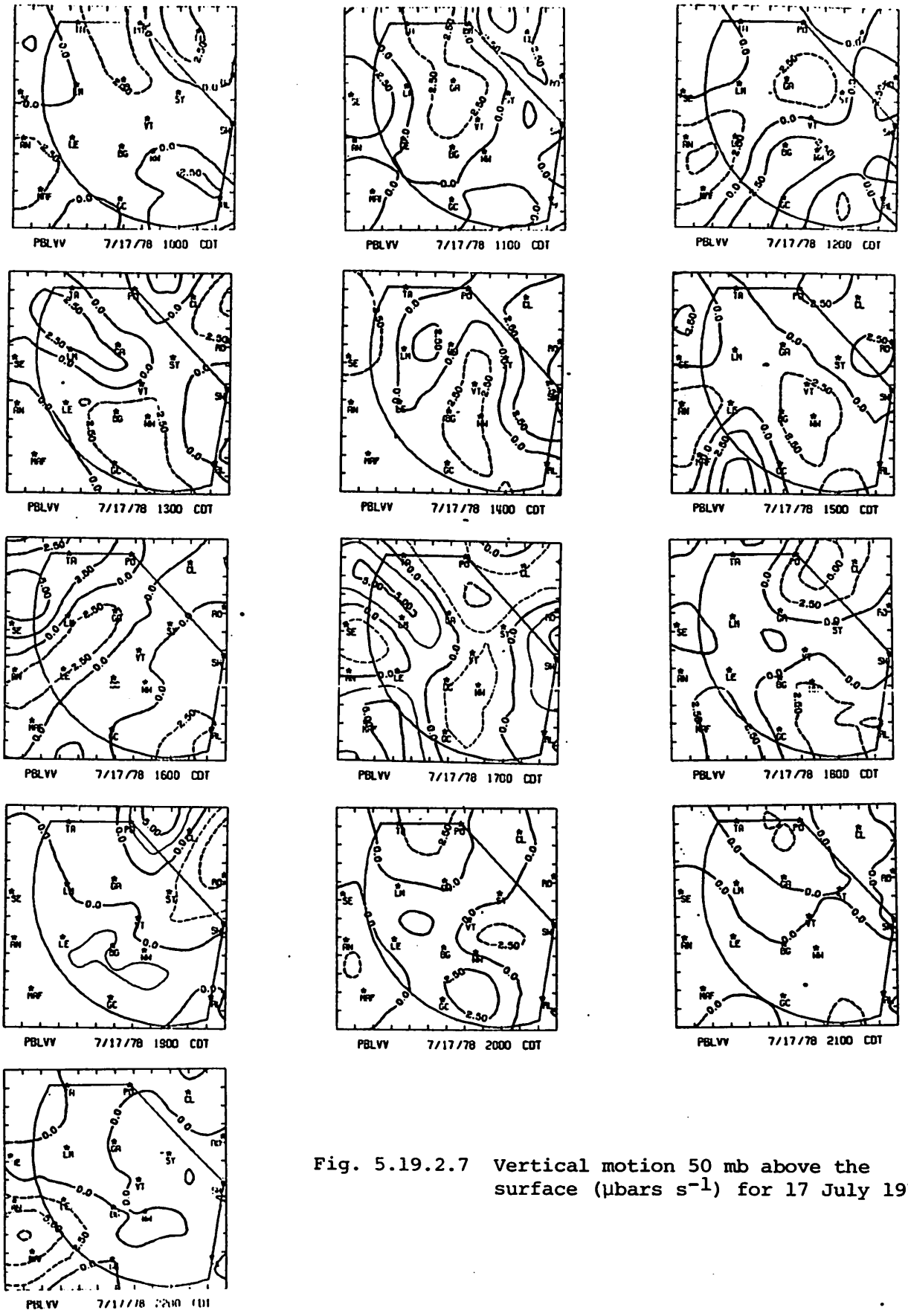

Fig. 5.19.2.7 Vertical motion 50 mb above the surface (μbars s^{-1}) for 17 July 1978.

Moisture divergence (Fig. 5.19.2.8) was mostly small over the area. Strong convergence indicated near Big Spring at 1600 and 1800 GMT was influenced by the high moisture value reported by Big Spring. Moisture divergence generally prevailed at other times prior to 0200 GMT. At 0300 GMT a center of moisture convergence was indicated in the southwest. This center was strong for a day with no activity.

Vertical flux of moisture (Fig. 5.19.2.9) was small. The large humidity at Big Spring influenced this variable, also. A large downward flux at 1700 GMT and an upward flux at 1800 GMT shown near Big Spring may have been thus influenced. The only other strong upward fluxes were shown at Rotan at 0000 GMT and at Midland at 0300 GMT but these values were not large.

Surface vorticity (Fig. 5.19.2.10) was generally small throughout the day. The patterns changed from hour to hour as surface winds changed, and there were no persistent centers of positive or negative vorticity.

Pressure changes (Fig. 5.19.2.11) also were small. Pressure dropped across the area from 1900 to 2300 GMT and near zero changes or small rises occurred after 0000 GMT.

Surface winds (Fig. 5.19.2.12) were mostly light and variable. They shifted from south and southwest at 1500 GMT to mainly east at 2000 GMT. Southeast winds prevailed between 0000 and 0300 GMT.

5.19.3 Upper-Level Kinematic Parameters

Figure 5.19.3.1 shows vertical profiles of mass divergence. Divergence was dominant in the 1500 and 1800 GMT profiles. In the 2100 and 0000 GMT profiles a few layers in the middle levels (between 700 and 400 mb) had convergence, and at 0300 GMT convergence was present in most of the middle layers.

Vertical motion profiles appear in Fig. 5.19.3.2. Most of the profiles show downward motion at all levels above 750 mb. The 0300 GMT profile shows upward motion above 600 mb, however.

Profiles of moisture divergence are shown in Fig. 5.19.3.3. Most times showed some convergence in the lowest layer although divergence dominated. At 2100 GMT moisture convergence occurred between 700 and 750 mb. At 0000 GMT there was moisture convergence above 650 mb. The moisture convergence increased at 0300 GMT and was between the 400 and 600 mb levels. None of the values were especially high, however.

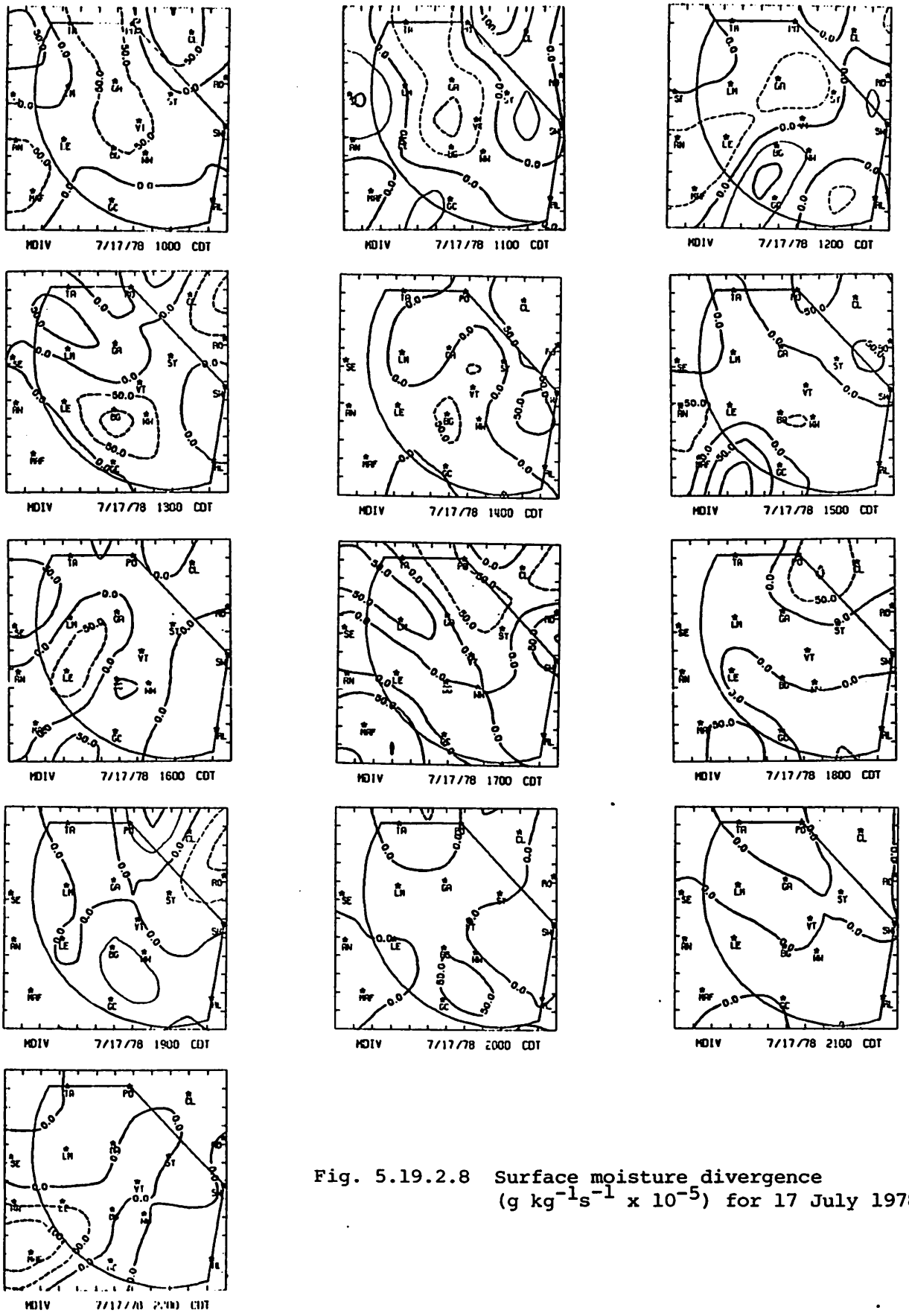

Fig. 5.19.2.8 Surface moisture divergence ($g\ kg^{-1}s^{-1} \times 10^{-5}$) for 17 July 1978.

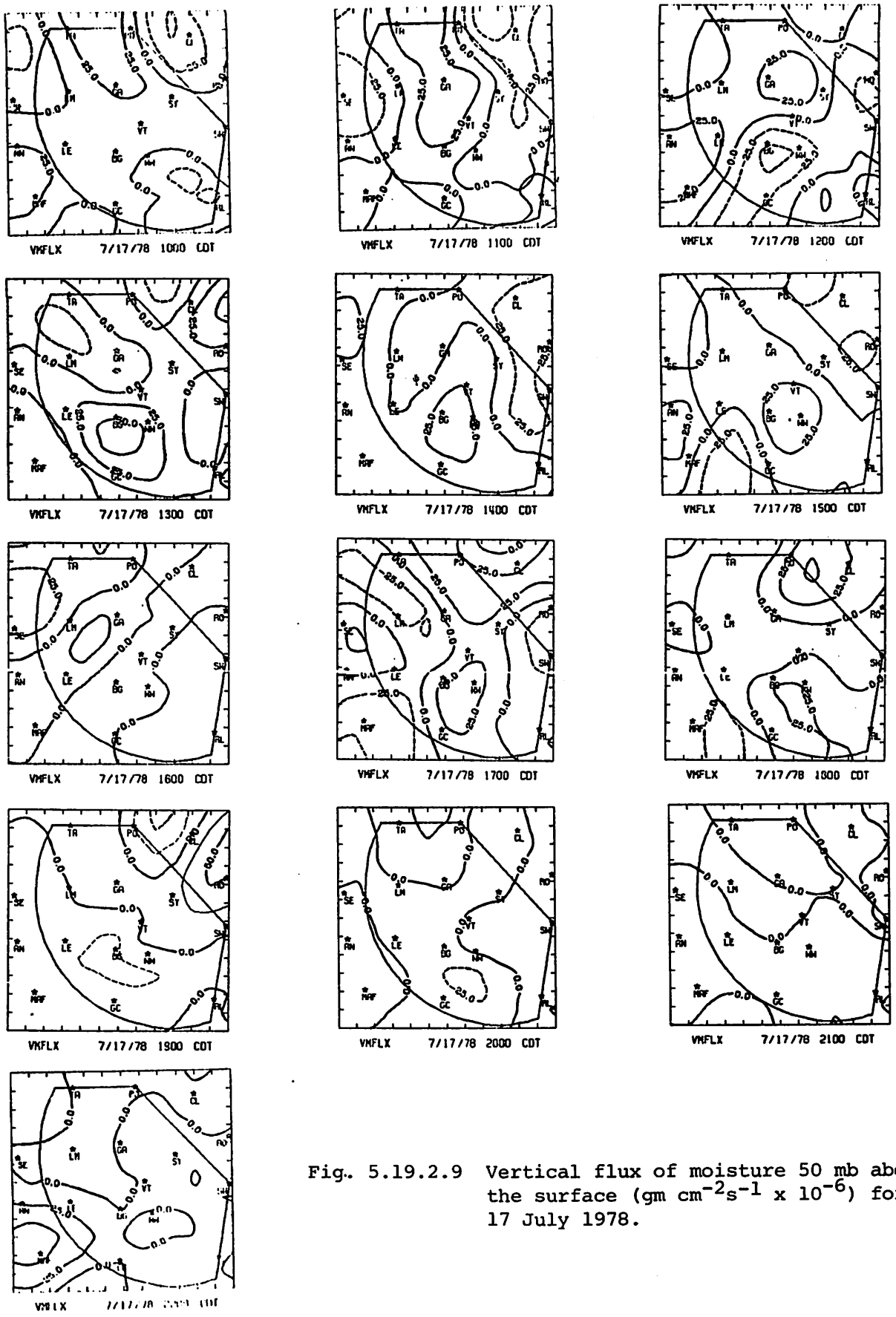

Fig. 5.19.2.9 Vertical flux of moisture 50 mb above the surface (gm $cm^{-2}s^{-1}$ x 10^{-6}) for 17 July 1978.

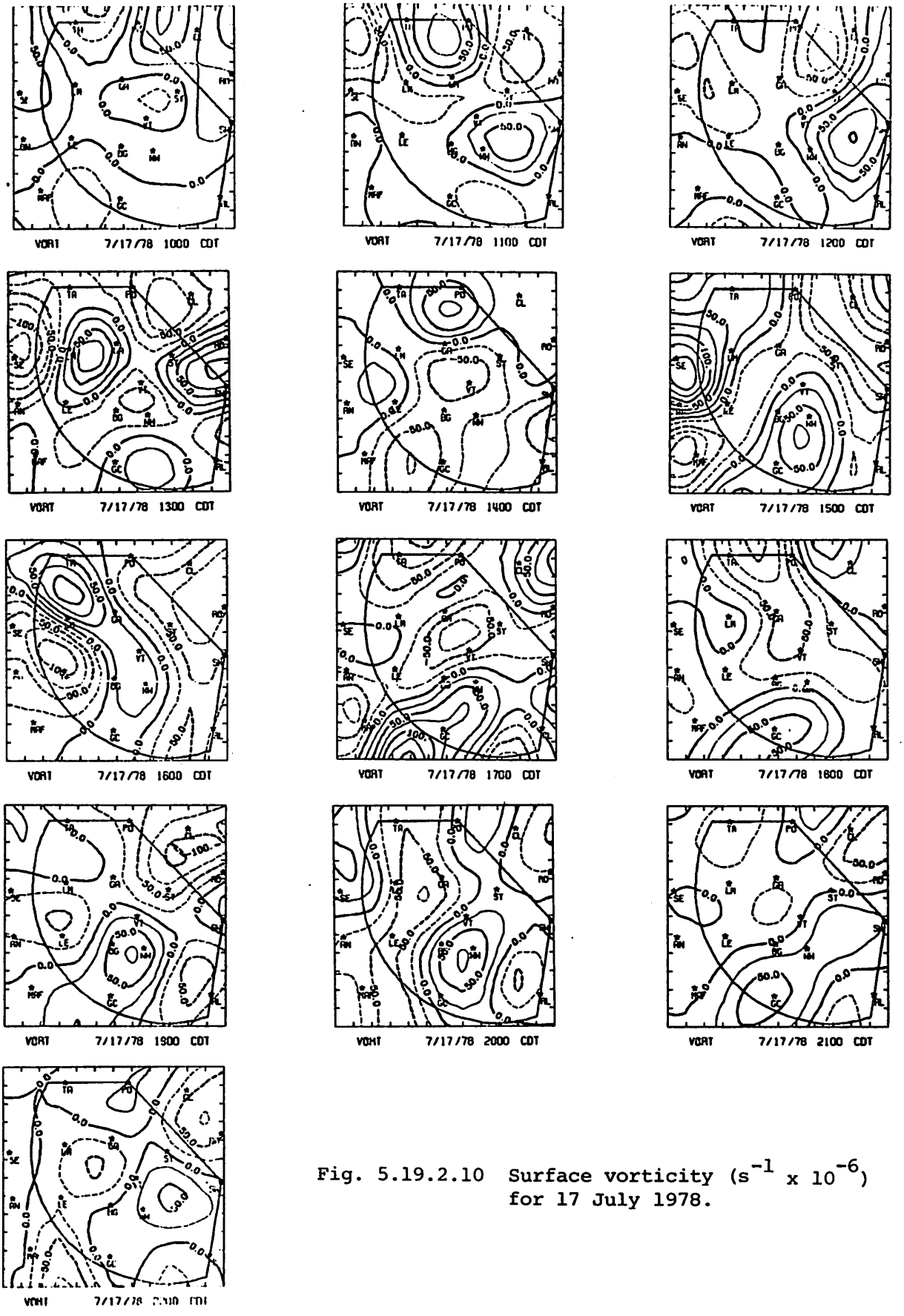

Fig. 5.19.2.10 Surface vorticity (s^{-1} x 10^{-6}) for 17 July 1978.

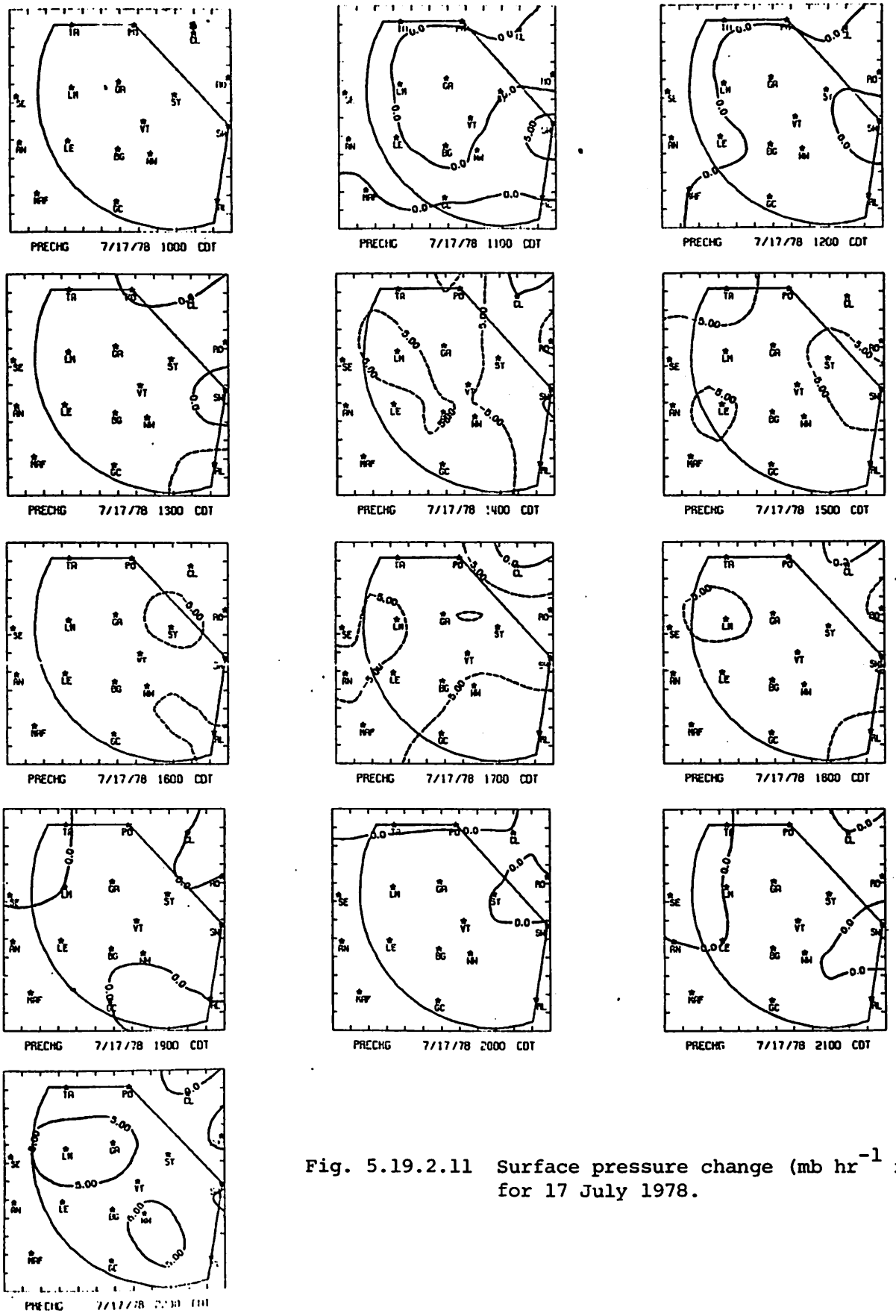

Fig. 5.19.2.11 Surface pressure change (mb hr^{-1} x 10^{-1}) for 17 July 1978.

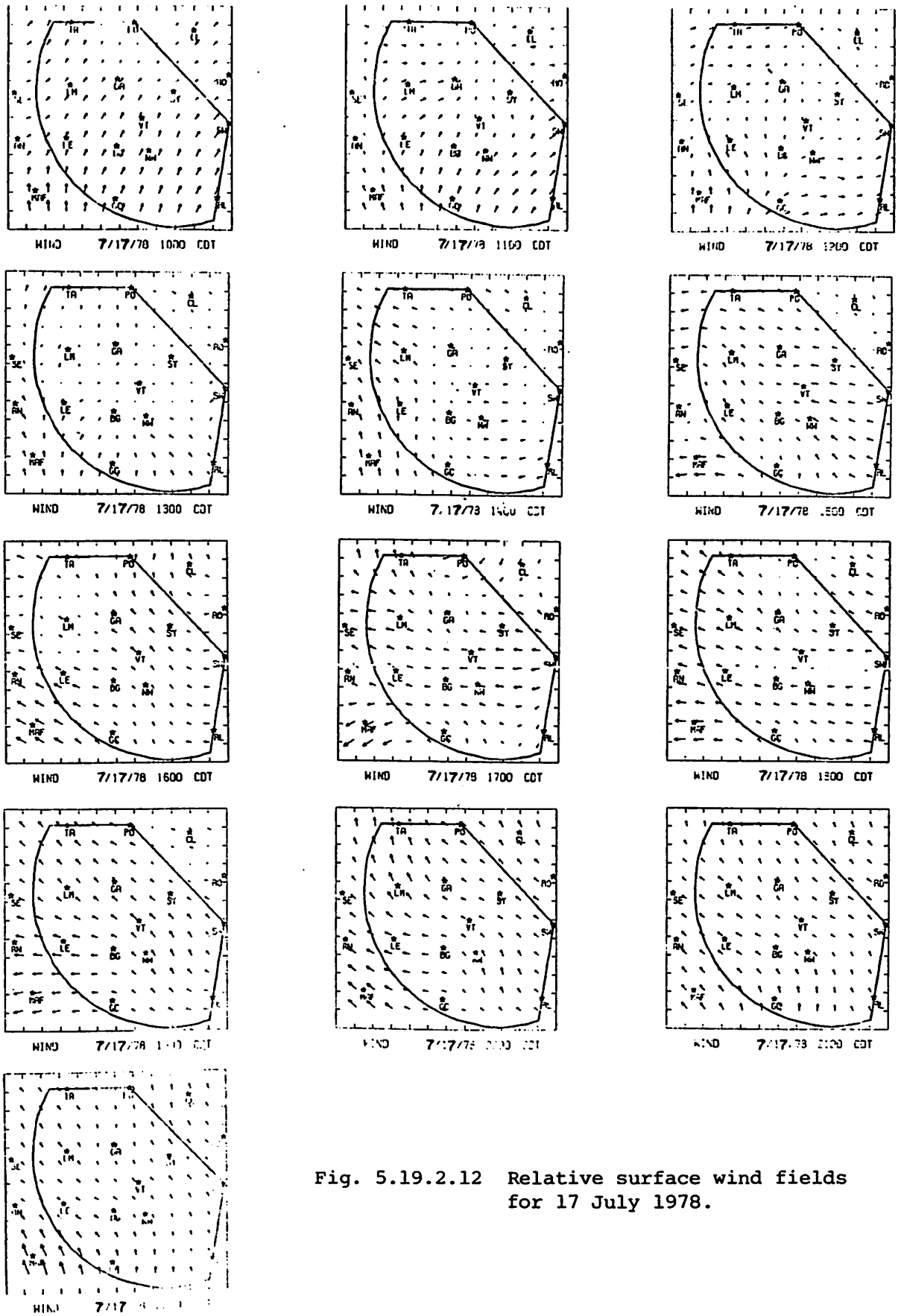

Fig. 5.19.2.12 Relative surface wind fields for 17 July 1978.

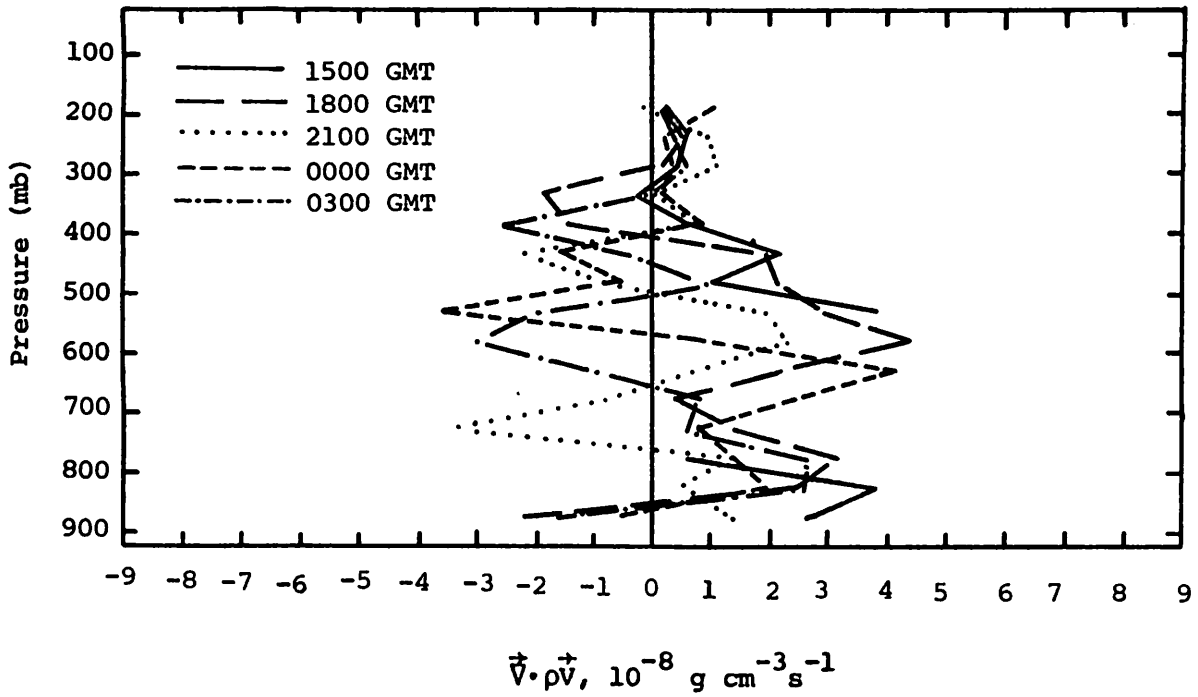

Fig. 5.19.3.1 Vertical profiles of mass divergence on 17 July 1978.

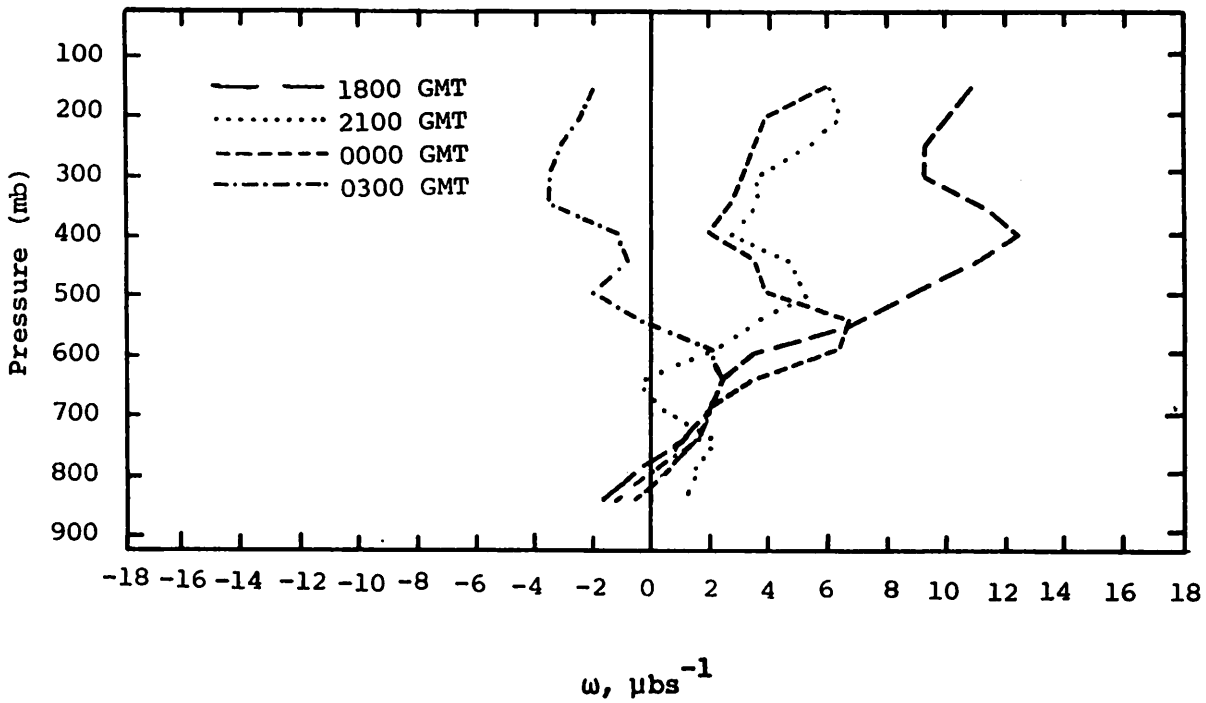

Fig. 5.19.3.2 Vertical profiles of vertical motion on 17 July 1978.

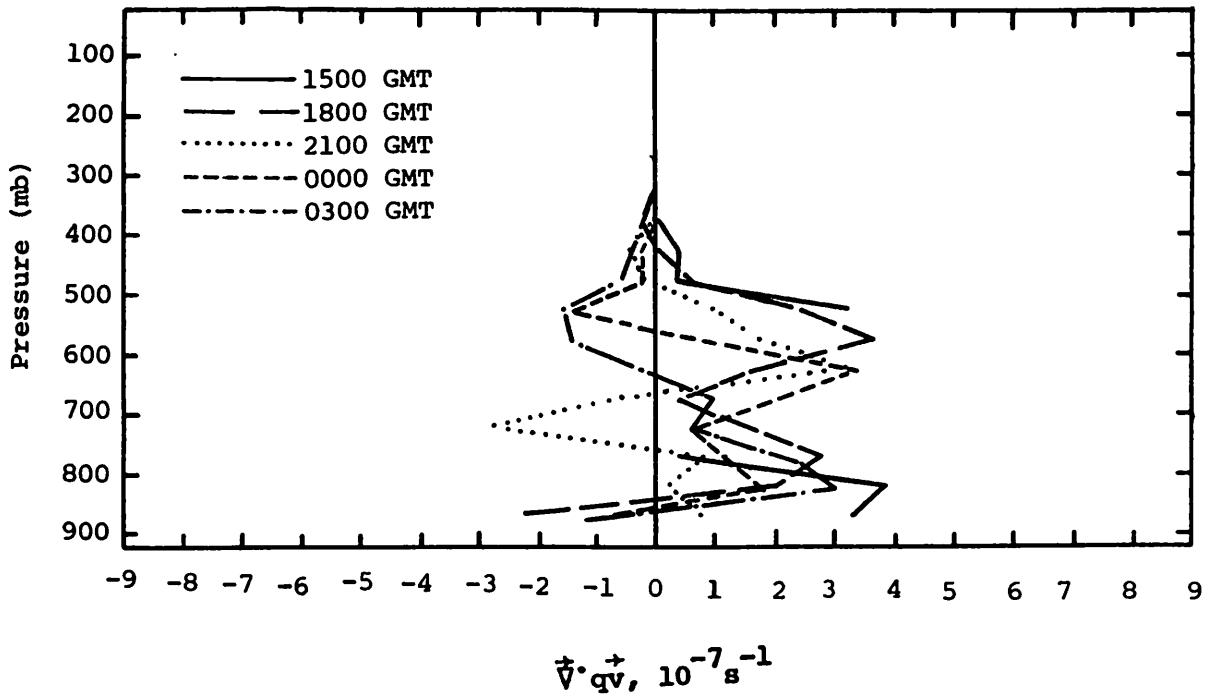

Fig. 5.19.3.3 Vertical profiles of moisture divergence on 17 July 1978.

5.19.4 Energetics

Figure 5.19.4.1 shows profiles of the horizontal flux of latent heat. Latent heat outflow is dominant in these profiles except in the lowest 50-mb layer. There was some inflow in middle layers; this occurred after 2100 GMT.

Profiles of vertical flux of latent heat (Fig. 5.19.4.2) show losses of latent heat in upper layers and gains in middle layers. This is consistent with the downward vertical motion shown in Fig. 5.19.3.2. Latent heat is thus transported downward from upper layers to middle layers.

The local change of latent heat (Fig. 5.19.4.3) was primarily negative at 1500 and 1800 GMT. The 2100 GMT profile shows some small positive values above 750 mb. At 0000 and 0300 GMT positive values were located below 700 mb with negative values above.

The profiles of the residual of the latent heat energy equation show predominantly negative values (fig. 5.19.4.4). This would indicate that evaporative processes were taking place. A large negative value was indicated at 1800 GMT in the 500 to 550-mb layer indicating large amounts of evaporation. At 0300 GMT the same level shows positive values which suggests condensation

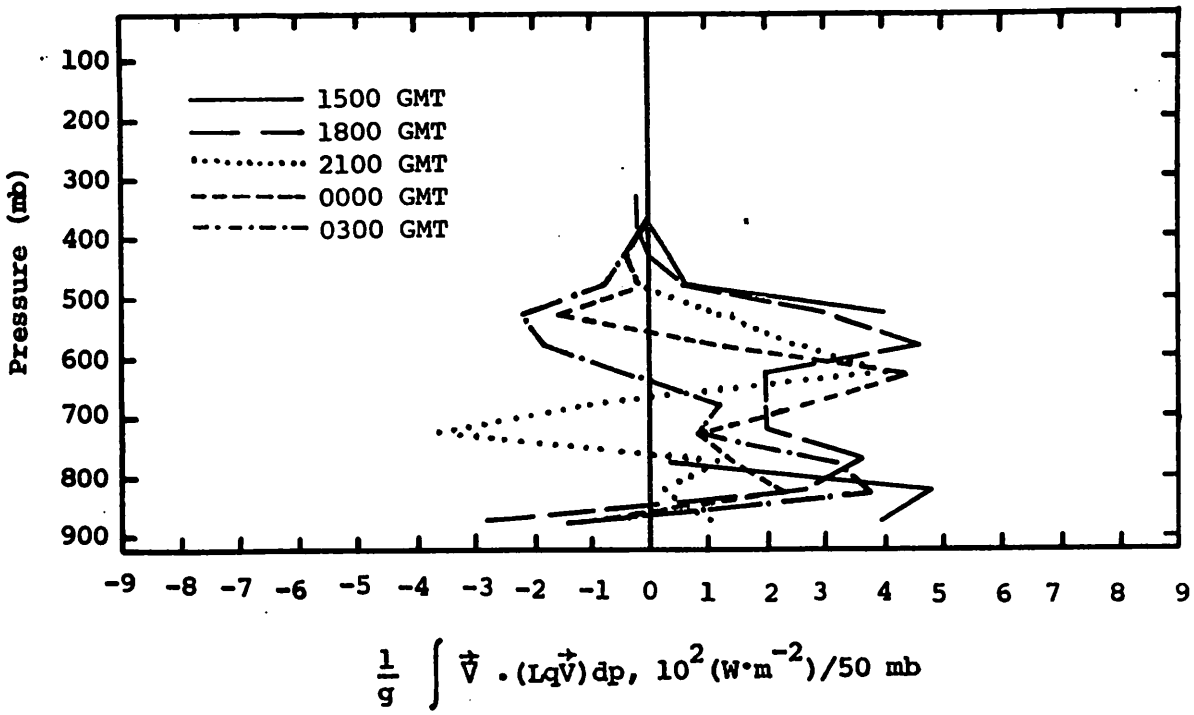

Fig. 5.19.4.1 Vertical profiles of the horizontal flux of latent heat energy on 17 July 1978.

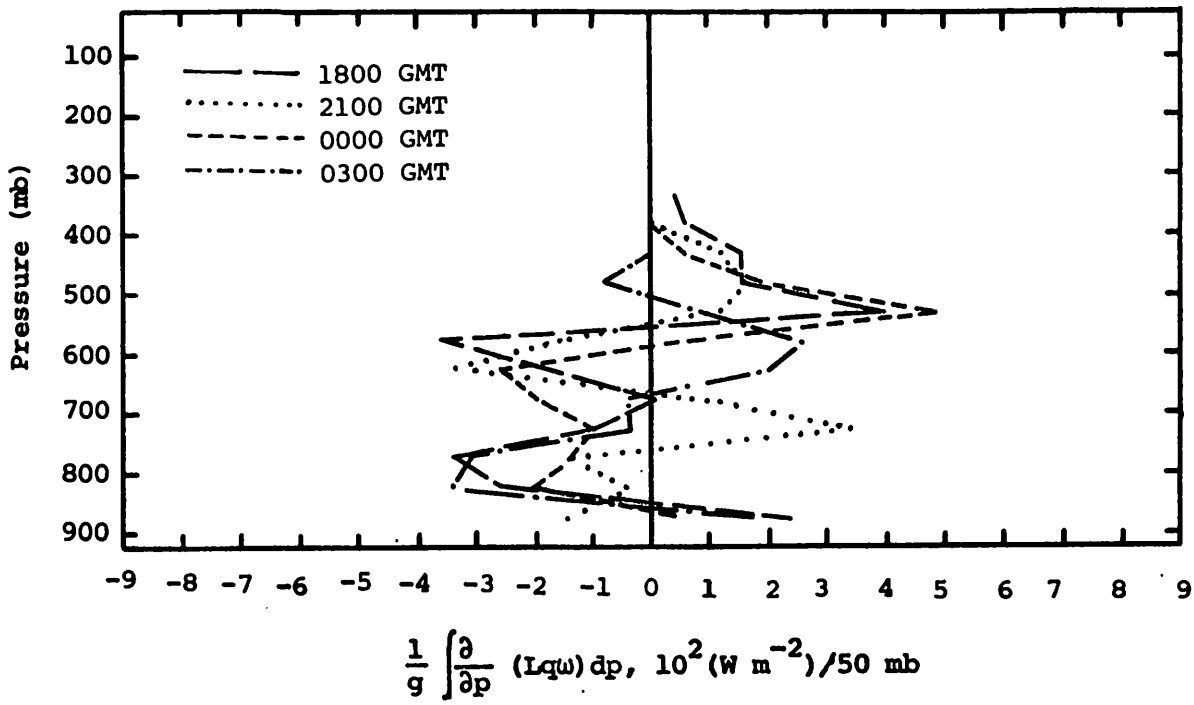

Fig. 5.19.4.2 Vertical profiles of the vertical flux of latent heat energy on 17 July 1978.

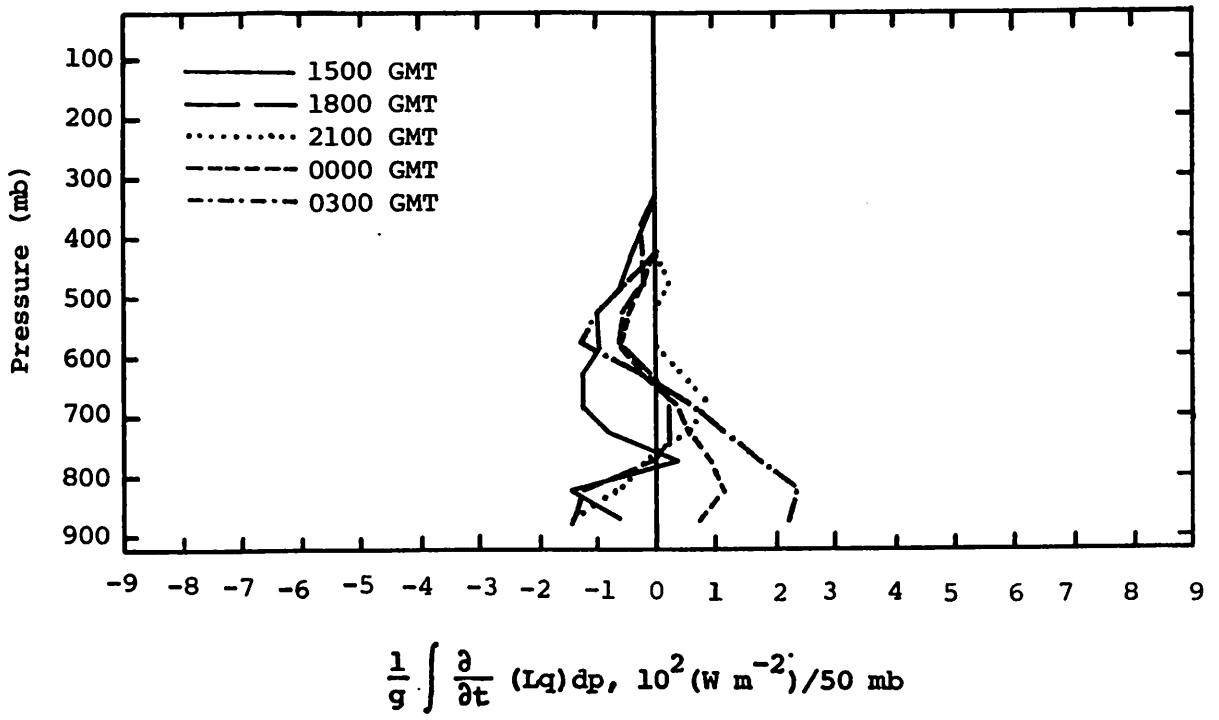

Fig. 5.19.4.3 Vertical profiles of the local change of latent heat energy on 17 July 1978.

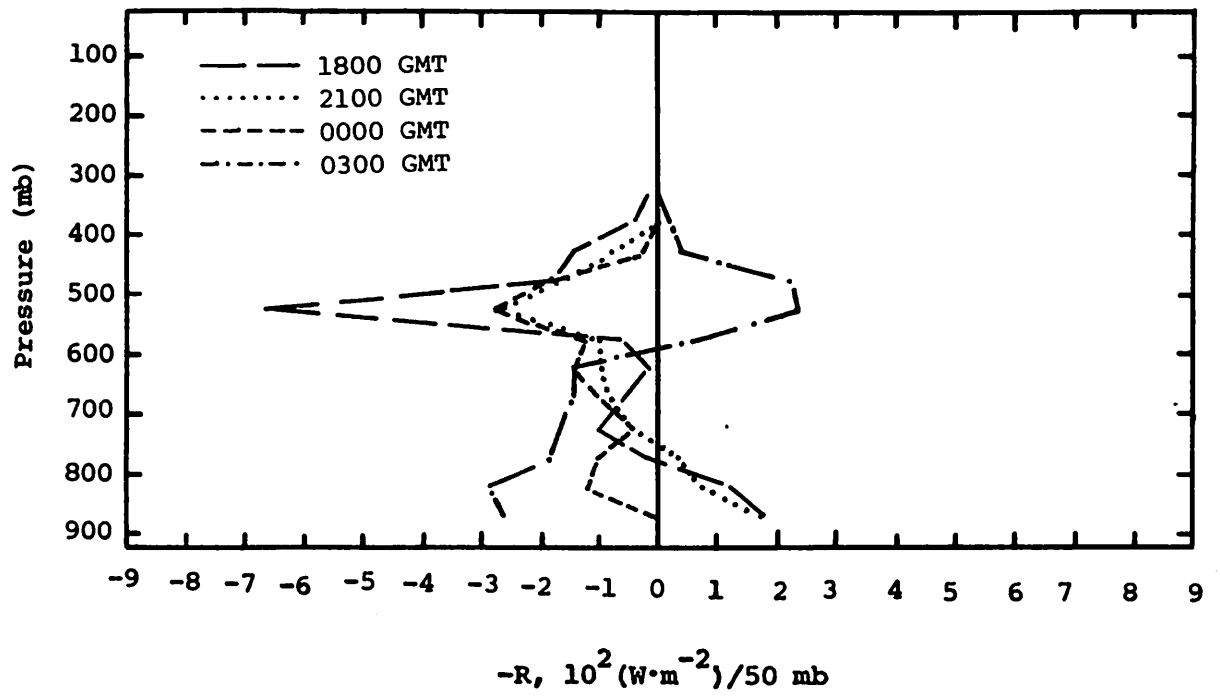

Fig. 5.19.4.4 Vertical profiles of the residual of the latent heat energy equation on 17 July 1978.

of water vapor. This could have resulted from clouds evaporating at 1800 GMT and reforming at 0300 GMT.

Profiles of diabatic heating (Fig. 5.19.4.5) also show mainly negative values as a result of the evaporative cooling. The small positive values in some of the profiles below 600 mb could be a result of other diabatic heating processes.

Figure 5.19.4.6 shows profiles of the horizontal flux of kinetic energy. Positive values, indicating horizontal outflow of kinetic energy, predominated. At 1500 and 1800 GMT the largest values of outflow were in middle levels. At 0000 and 0300 GMT there was a shift to kinetic energy inflow in middle levels.

Profiles of the vertical flux of kinetic energy (Fig. 5.19.4.7) show only small values in upper levels. The highest wind speeds were in middle layers between 700 and 500 mb, so the largest amounts of vertical transport of kinetic energy appear in these layers. Kinetic energy was transported downward from this higher energy layer into layers just below 500 mb. The lowest layers showed little vertical transport of kinetic energy.

5.19.5 Water Vapor Budget

The profiles of net horizontal transport of water vapor (Fig. 5.19.5.1) show, for 1800 GMT, primarily losses, with gains only in the highest and lowest levels. Losses dominated the other profiles, also. The 2100 GMT profile showed a layer of net gains due to horizontal transport between 650 and 750 mb. This layer decreased at 0000 GMT. Inflow in upper levels increased at 0300 GMT; it extended upward from 550 mb.

Profiles of net vertical transport of water vapor are shown in Fig. 5.19.5.2. The higher levels generally show losses while the lower levels show mainly gains in water vapor. The 0300 GMT profile shows gains in upper levels above 500 mb; this agrees with the upward motion indicated at that time in Fig. 5.19.3.2.

Figure 5.19.5.3 shows vertical transport of water vapor through constant pressure surfaces. Most of the transport is downward. The 2100 GMT profile shows upward transport through the 650-mb surface. At 0300 GMT, there was upward transport at and above 550 mb.

Profiles of the combined net horizontal and vertical transport of water vapor show losses through all but the lowest layers (Fig. 5.19.5.4). The gains in the lowest layers were the result of downward transport of water

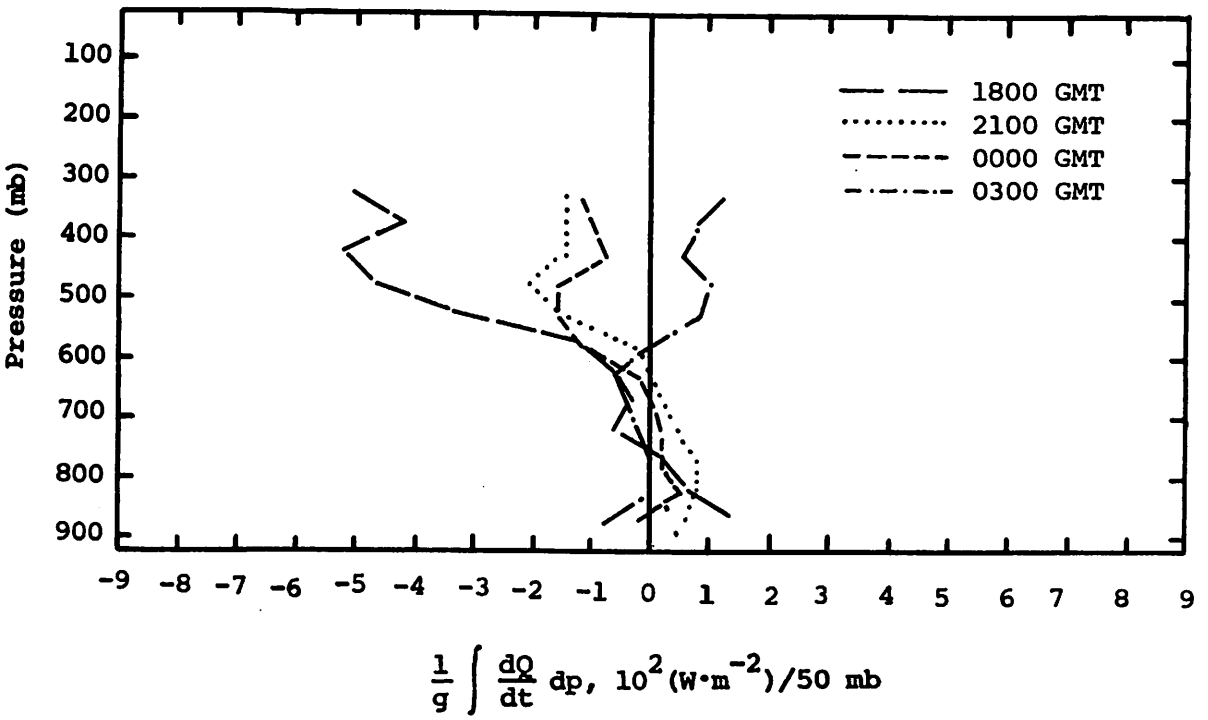

Fig. 5.19:4.5 Vertical profiles of diabatic heating computed from the first law of thermodynamics on 17 July 1978.

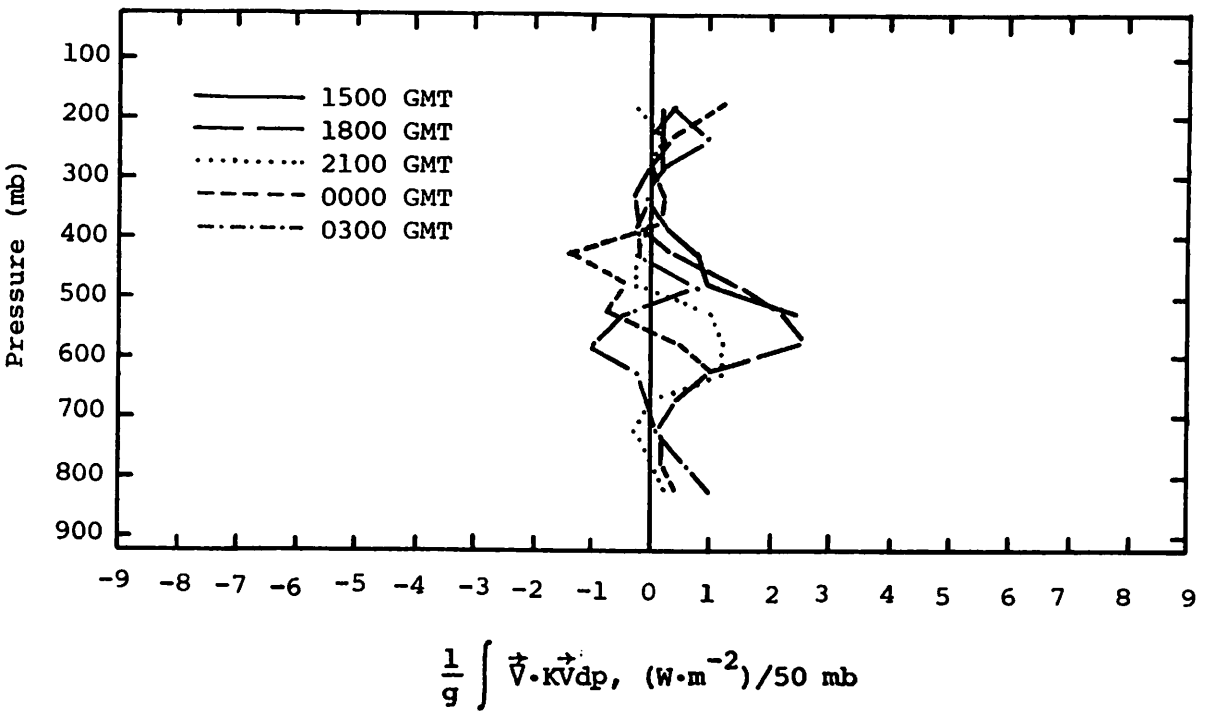

Fig. 5.19.4.6 Vertical profiles of the horizontal flux of kinetic energy on 17 July 1978.

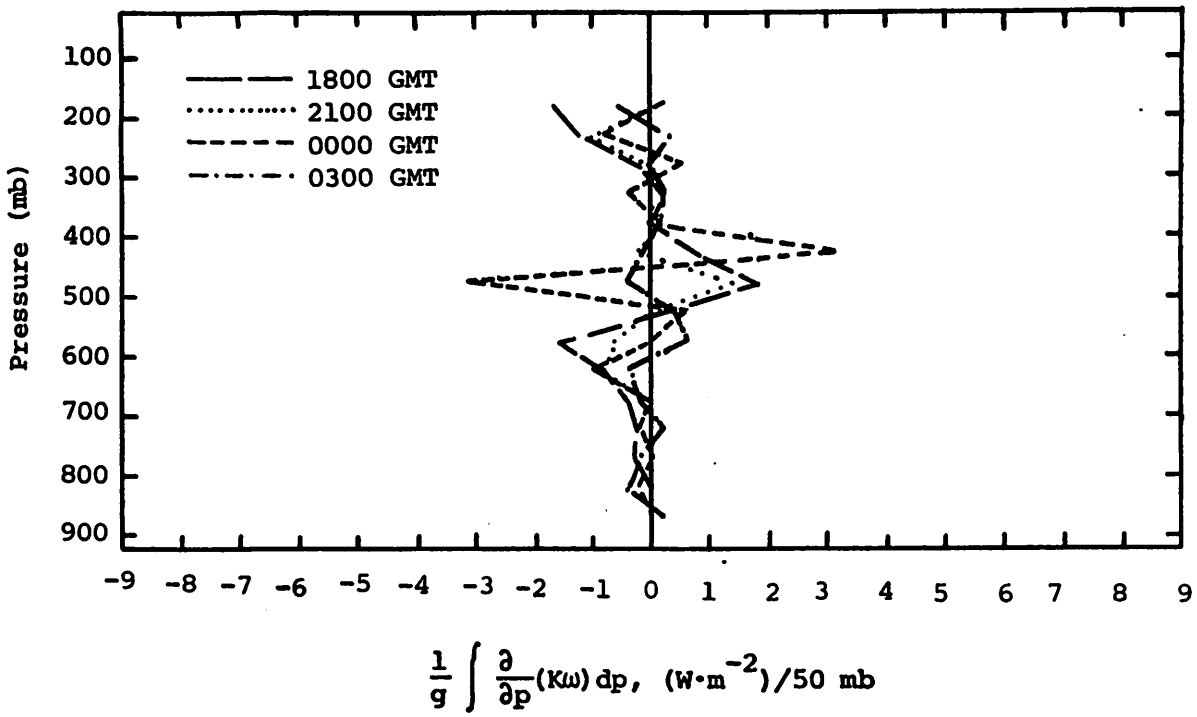

Fig. 5.19.4.7 Vertical profiles of the vertical flux of kinetic energy on 17 July 1978.

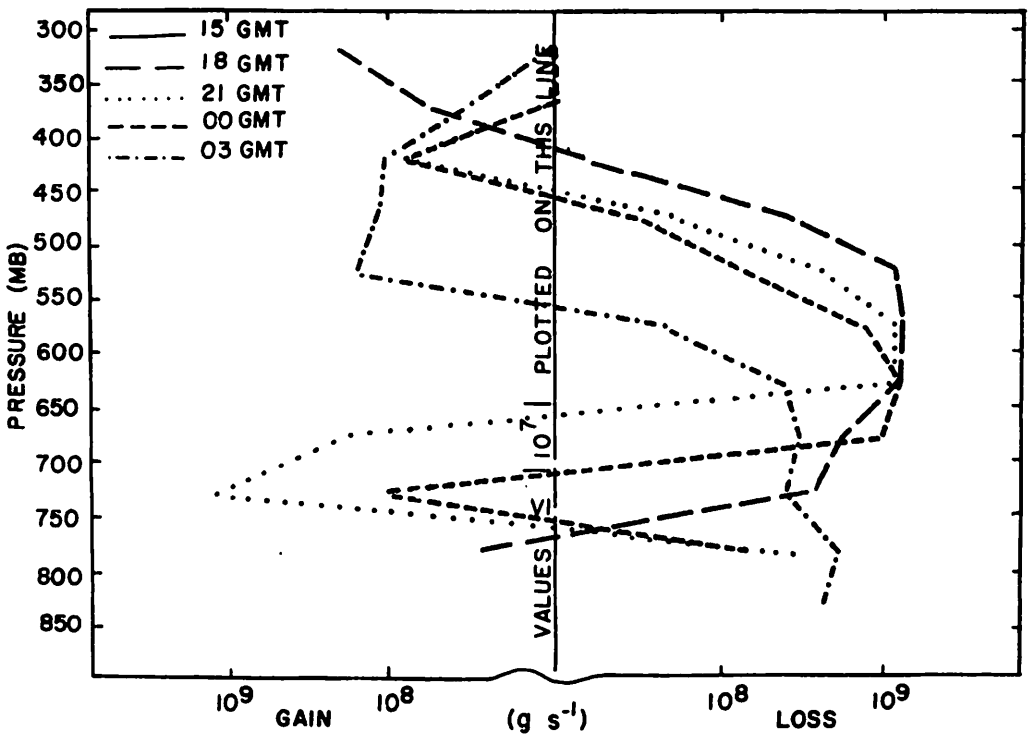

Fig. 5.19.5.1 Net horizontal transport of water vapor through boundaries of 50-mb layers (gm s^{-1}) over the Texas HIPLEX area for 17 July 1978.

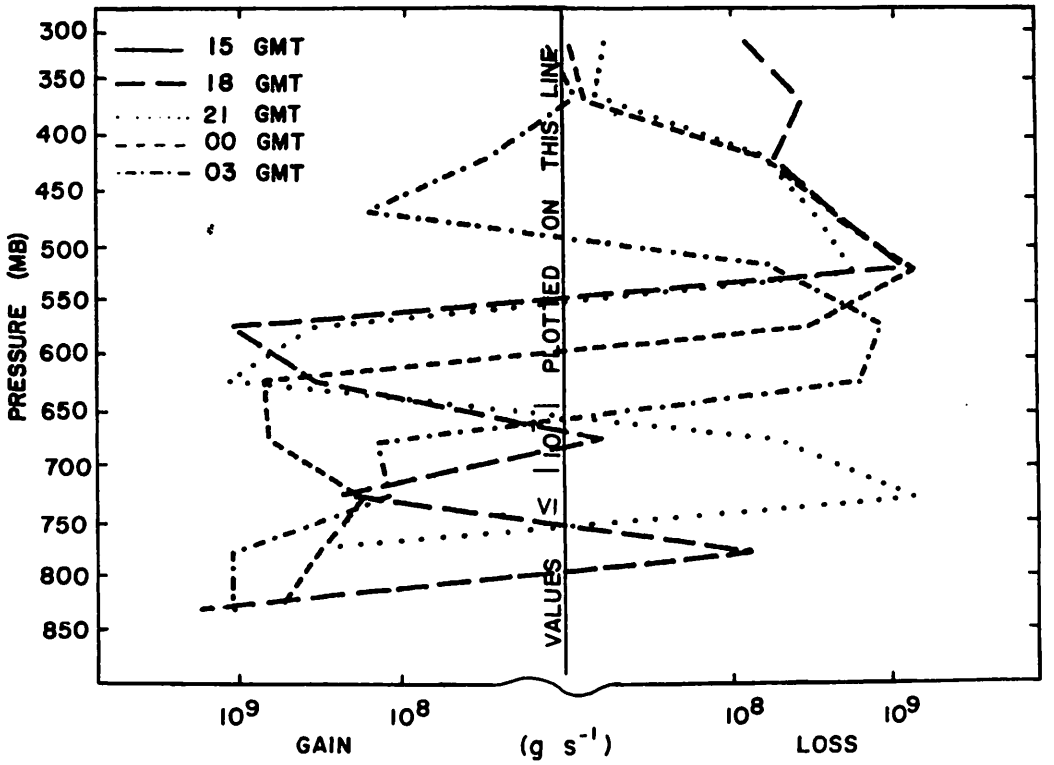

Fig. 5.19.5.2 Net vertical transport of water vapor through boundaries of 50-mb layers (gm s^{-1}) over the Texas HIPLEX area for 17 July 1978.

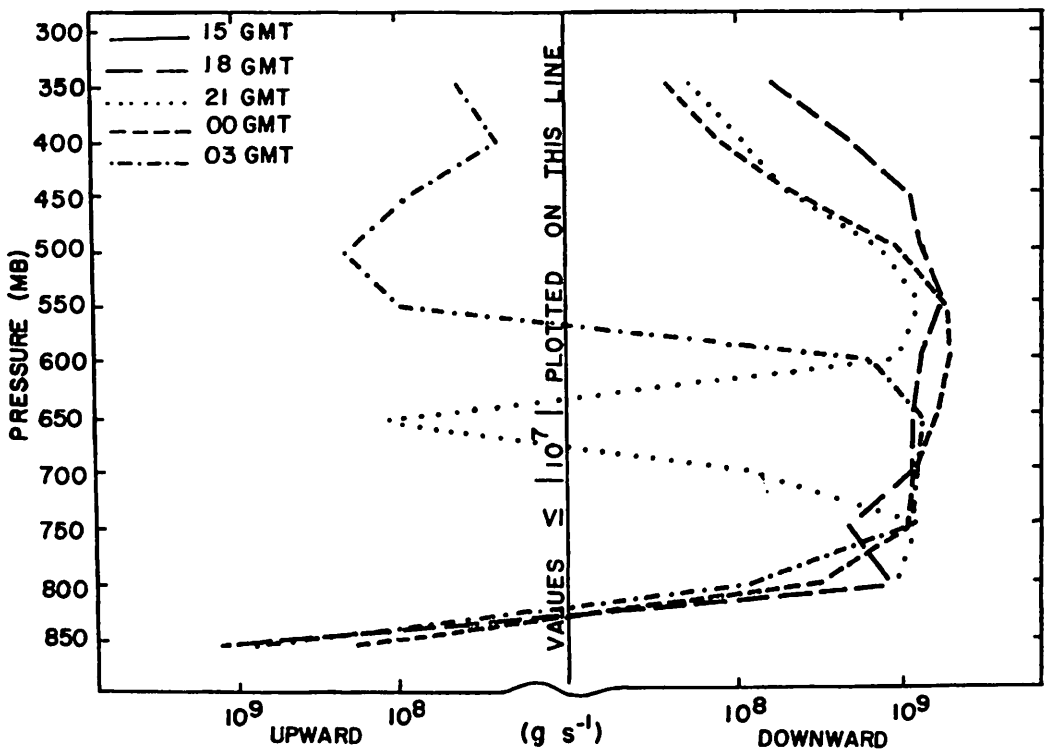

Fig. 5.19.5.3 Vertical transport of water vapor through constant pressure surfaces (gm s^{-1}) over the Texas HIPLEX area for 17 July 1978.

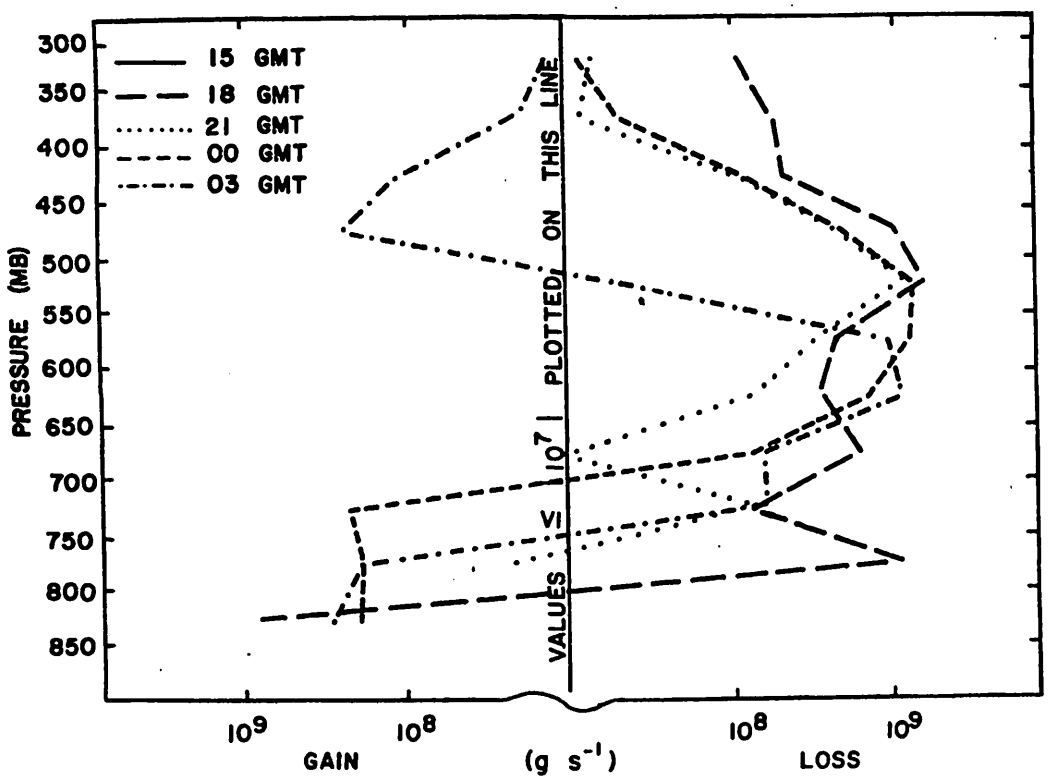

Fig. 5.19.5.4 Combined net horizontal and vertical transport of water vapor through boundaries of 50-mb layers (gm s^{-1}) over the Texas HIPLEX area for 17 July 1978.

vapor from higher levels. The 0300 GMT profile also shows gains above 550 mb. These gains resulted from both vertical and horizontal transport.

Profiles of the total mass of water vapor (Fig. 5.19.5.5) did not show any layers that were exceptionally dry or moist. The water vapor content was moderate and so was not really a contributing factor to the lack of convective activity on this day.

The local rate-of-change of water vapor profiles (Fig. 5.19.5.6) show that the changes in water vapor content between soundings were small. The lower layers below 600 mb showed generally small increases but upper layers showed decreases in some time periods.

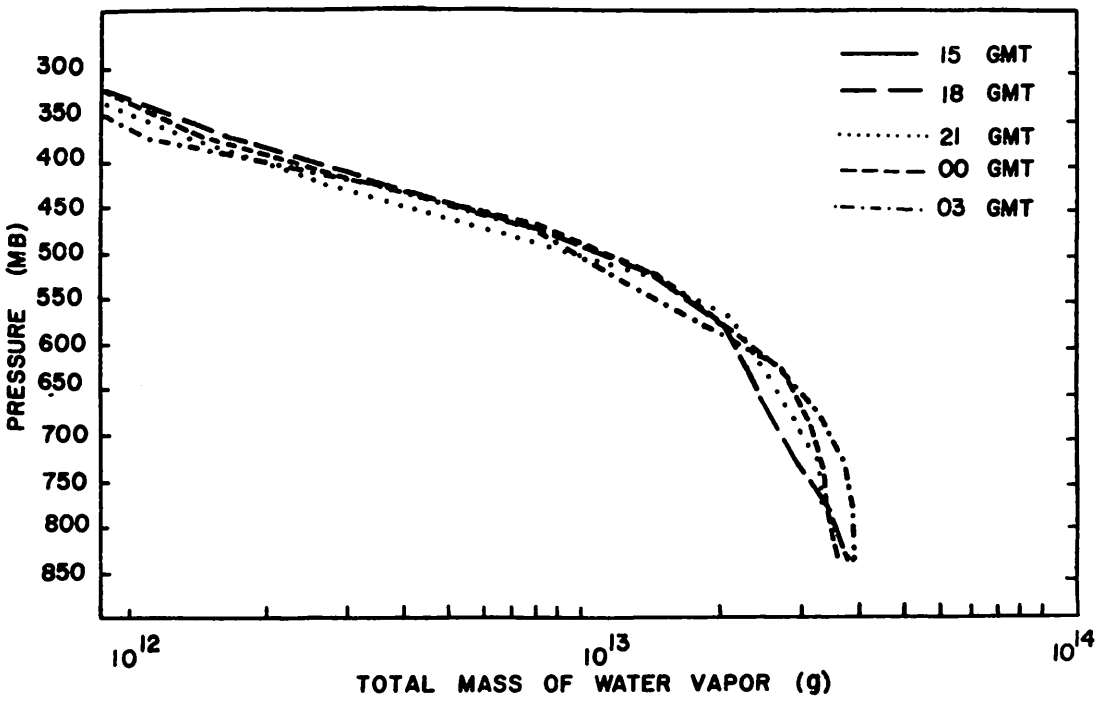

Fig. 5.19.5.5 Total mass of water vapor in layers 50 mb deep (gm) over the Texas HIPLEX area on 17 July 1978.

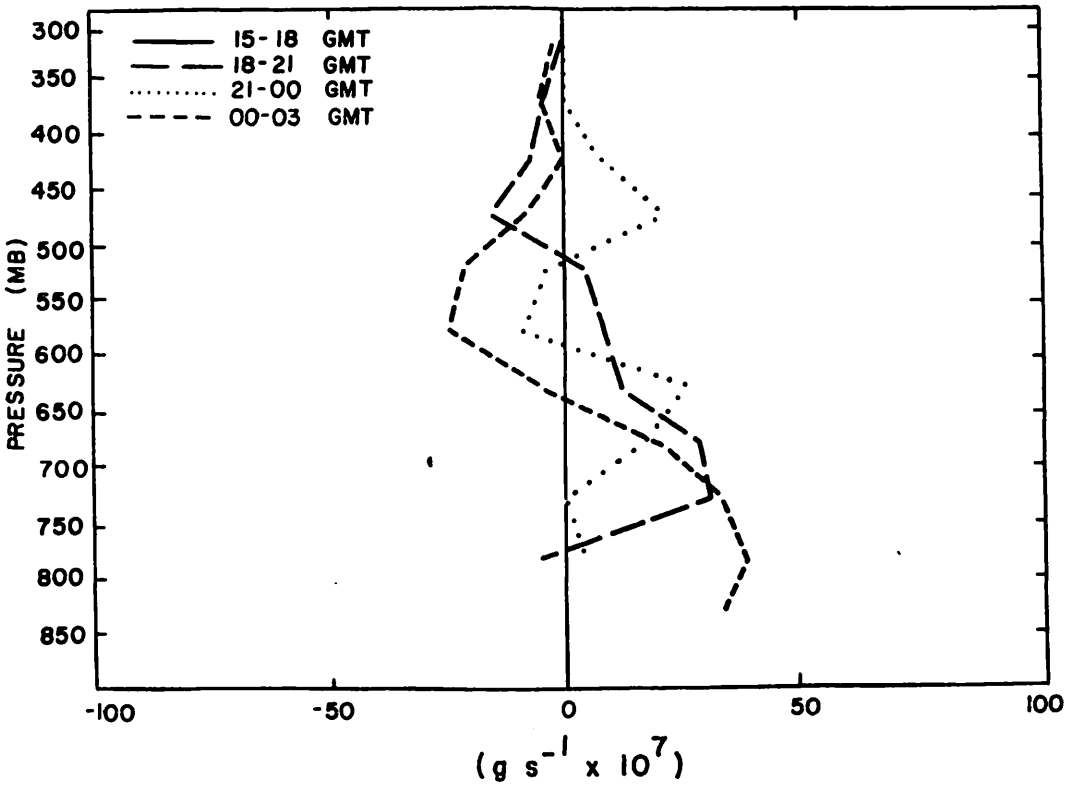

Fig. 5.19.5.6 Local rate-of-change in total mass of water vapor ($g\ s^{-1} \times 10^{7}$) for the Texas HIPLEX area for 17 July 1978.

5.20 20 July 1978

5.20.1 Radar

Radar echoes formed in the analysis area at 1800 GMT (Fig. 5.20.1.1). Maximum tops were measured between 11.6 km (35K ft) and 14 km (42K ft). Echoes were generally isolated and randomly spaced. They began to dissipate at 2300 GMT, the last being observed at 0100 GMT near Post. The echoes observed on this day formed and dissipated quickly, and experienced little systematic movement.

5.20.2 Surface

Several of the observed thunderstorms affected values of surface parameters. Echoes observed between 1800 and 2000 GMT, many of which extended above 10 km (30K ft), did not noticeably affect surface temperature fields. However, temperatures fell at Tahoka at 2100 GMT and again at Clairemont and Post at 2200 and 2300 GMT (Fig. 5.20.2.1). Minimum temperature at these times was 26°C, while values across the network during these times were between 34 and 36°C. The temperature fields did not show any prominent features during other time periods. Values ranged from a minimum of 26°C at 1500 GMT to a maximum of 37°C at 2300 GMT.

Dewpoint depression (Fig. 5.20.2.2) and mixing ratio (Fig. 5.20.2.3) also reflect the influence of thunderstorms from 2100 to 2300 GMT. Moisture deviations occurred at the same stations as temperature changes except at Tahoka at 2100 GMT. Mixing ratio at Tahoka increased from 10 g/kg at 1900 GMT to 15 g/kg at 2000 GMT, reflecting the presence of an echo over that station at 2000 GMT. Temperature did not decrease there until 2100 GMT after the echo had begun to dissipate and move away. The largest mixing ratio observed on this day was 20 g/kg at Clairemont at 2100 GMT. Values across parts of the network not affected by thunderstorms were 8 to 12 g/kg. Errors in mixing ratio apparently occurred at Big Spring throughout the day.

Equivalent potential temperature (Fig. 5.20.2.4) also reflects the discrepancy at Big Spring throughout the day, and results in large gradients between Big Spring and Gail. Thunderstorm effects occurred from 2000 to 2300 GMT at Tahoka, Post, and Clairemont. Equivalent potential temperature associated with the thunderstorms were as much as 25°K higher than those for the remainder of the network.

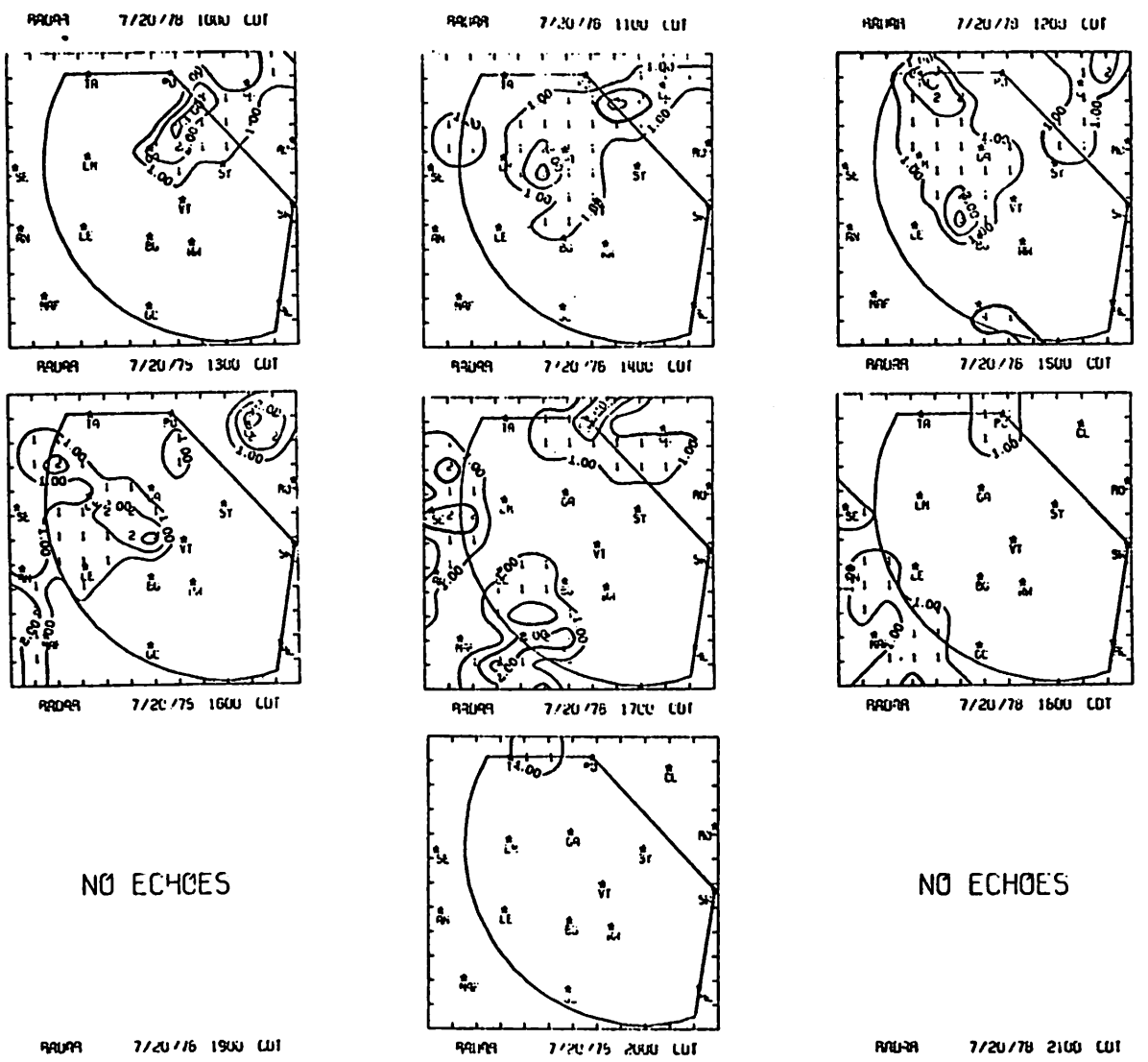

Fig. 5.20.1.1 Radar echoes for 20 July 1978.

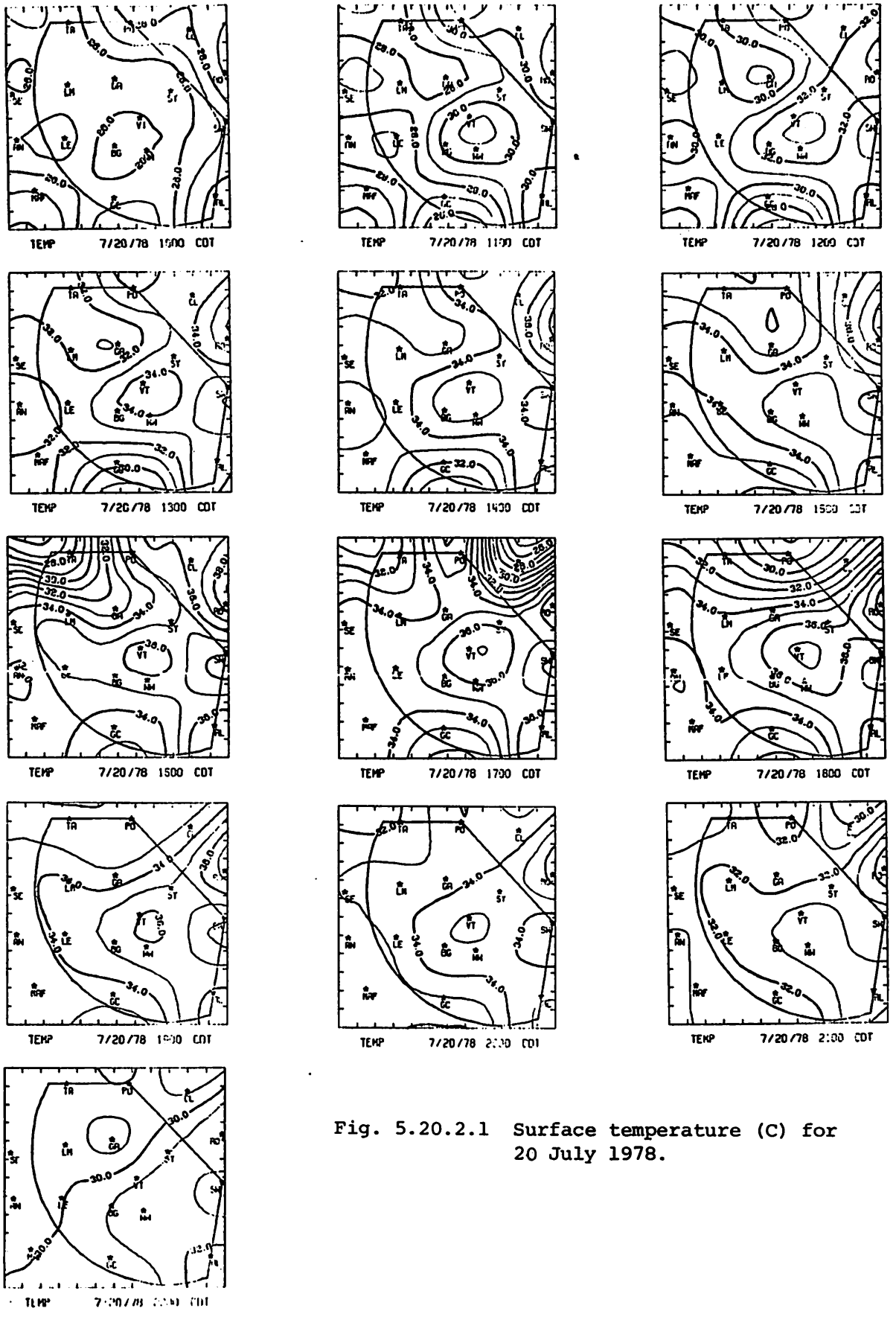

Fig. 5.20.2.1 Surface temperature (C) for 20 July 1978.

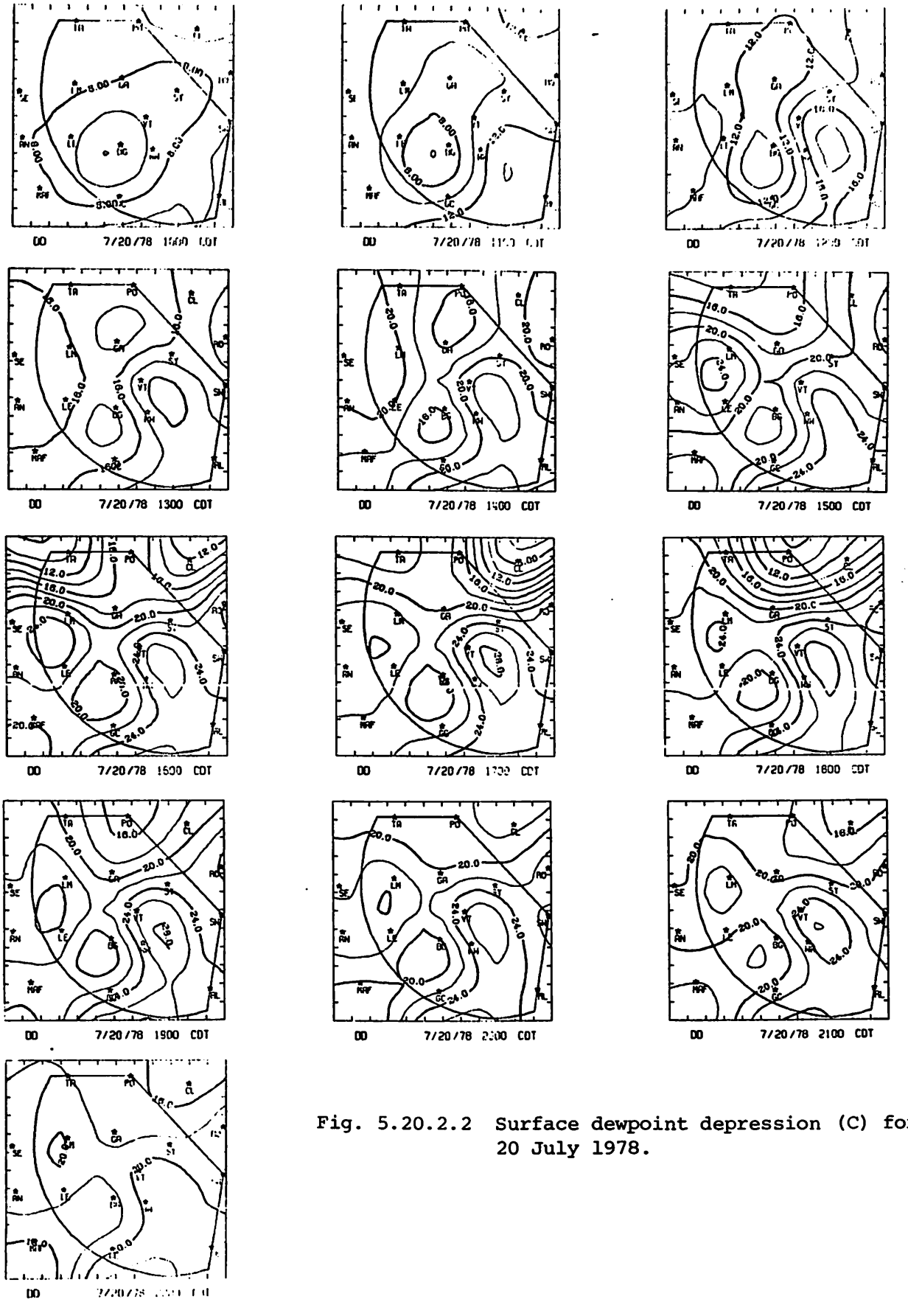

Fig. 5.20.2.2 Surface dewpoint depression (C) for 20 July 1978.

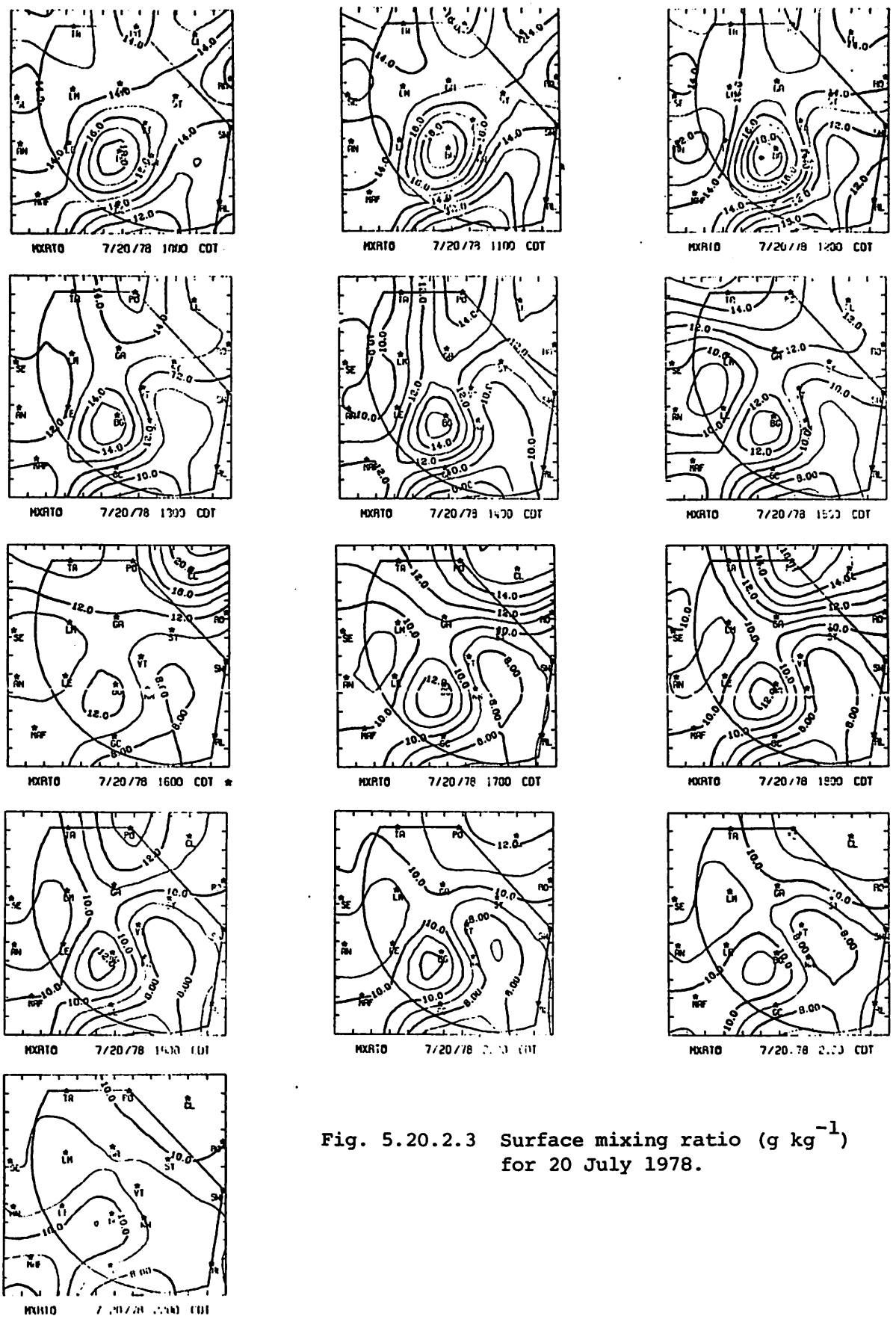

Fig. 5.20.2.3 Surface mixing ratio (g kg^{-1}) for 20 July 1978.

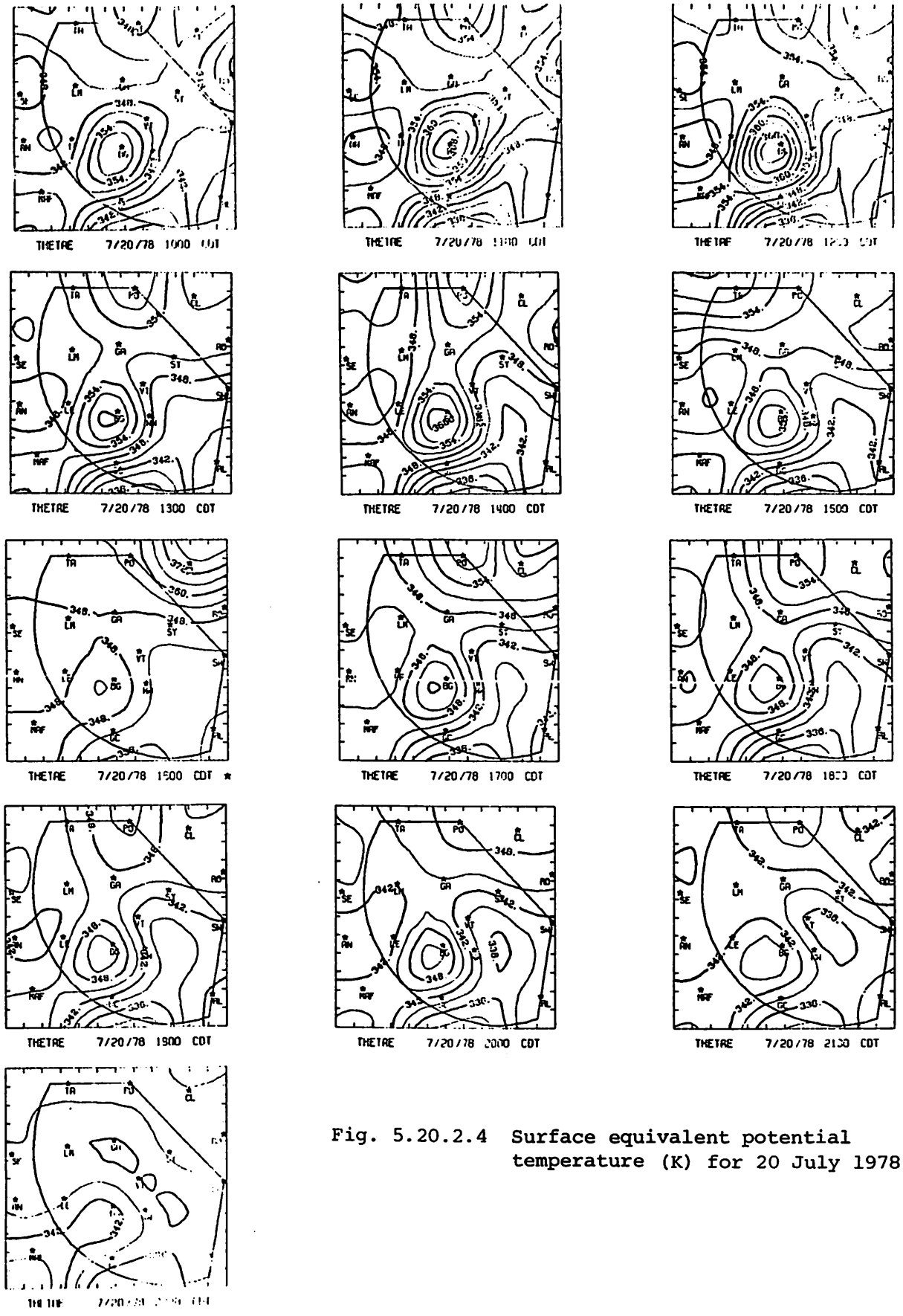

Fig. 5.20.2.4 Surface equivalent potential temperature (K) for 20 July 1978.

Terrain-induced vertical motion (Fig. 5.20.2.5) was generally downward throughout the day. Maximum downward values were observed between 1500 and 1700 GMT along the eastern edge of the network, and some reached -2.5 cm/sec.

Patterns of velocity divergence (Fig. 5.20.2.6), boundary layer vertical velocity (Fig. 5.20.2.7), moisture divergence (Fig. 5.20.2.8), and vertical moisture flux (Fig. 5.20.2.9) responded to thunderstorms which occurred from 1900 to 0000 GMT. A convergence area located near Lamesa, Lenorah, and Gail was replaced at 1900 GMT with divergence associated with an echo near Post. Most of the network was convergent again at 2100 GMT, but at 2200 GMT three small areas of divergence appeared at the same locations as strong radar echoes. Values in these areas remained below 10^{-4} sec^{-1}, and weak convergence existed in non-echo areas. Divergence associated with the echo between Midland and Garden City increased to 1.5×10^{-4} sec^{-1} and continued until 0000 GMT, which coincided with the time of the echo dissipation. A divergence maximum and temperature minimum were observed at 2200 GMT near Post. Boundary layer vertical motion indicated that downdrafts resulting from thunderstorms were not intense on this day.

Vorticity centers with values to 1.5×10^{-4} sec^{-1} were observed in the vicinity of radar echoes (Fig. 5.20.2.10). Pressure changes do not exceed 0.5 mb/hr and have no apparent correlation with thunderstorm activity (Fig. 5.20.2.11). At 1900 and 2000 GMT, relatively small-scale centers of vorticity occurred near Post and Lamesa, which is an area of small surface wind speed (Fig. 5.20.2.12) and large surface velocity divergence. An area of negative vorticity also occurred between Tahoka and Post at 2300 and 0000 GMT and was associated with the dissipation of the echo observed over Post at 2300 GMT. Values of vorticity at other times rarely exceed 0.75×10^{-4} sec^{-1}.

Surface winds were predominantly from the south on this day and speeds averaged close to 4 m/sec (Fig. 5.20.2.12). Speeds are at a maximum at 2100 GMT and decreased to between 1 and 2 m/sec at 0300 GMT.

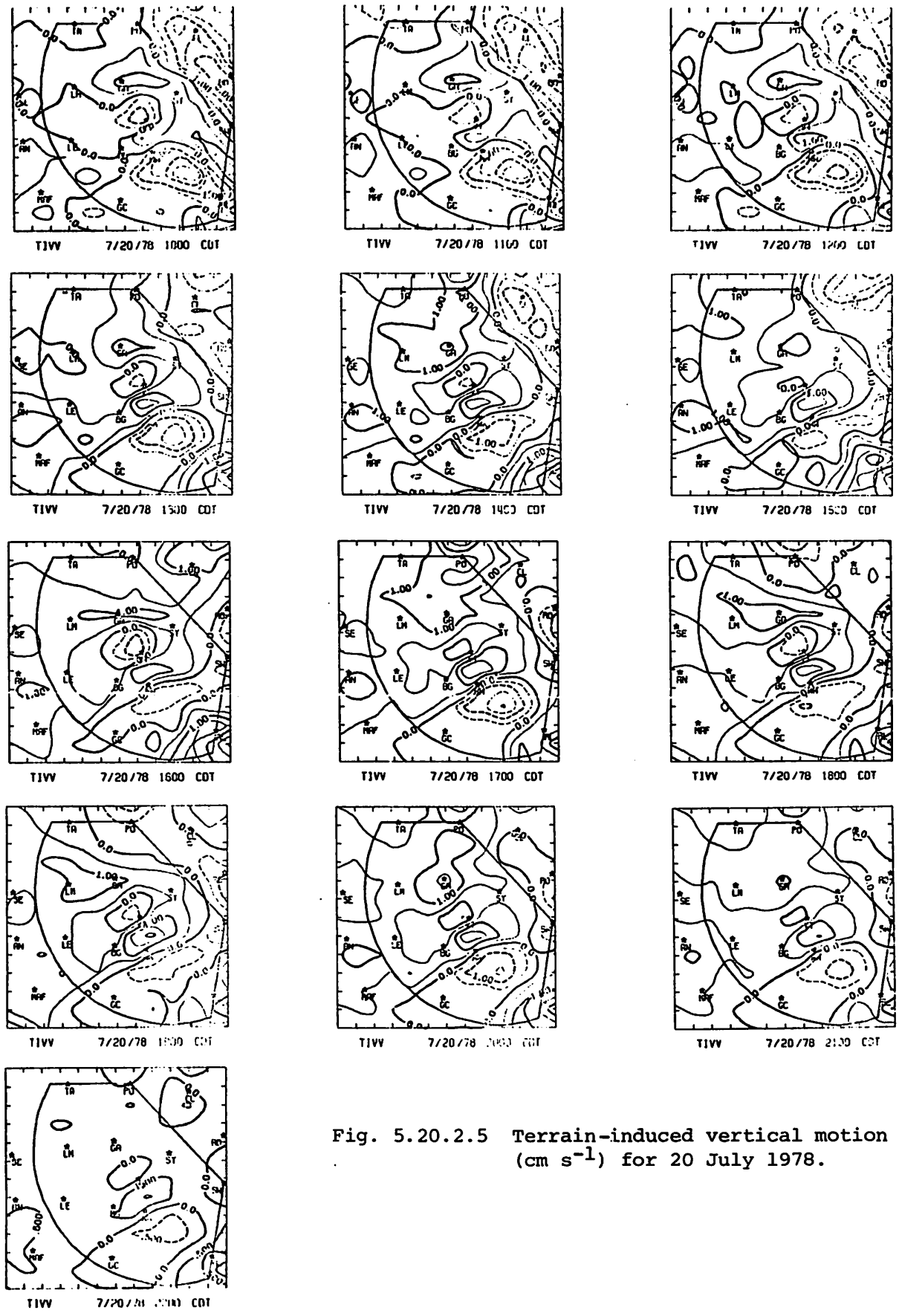

Fig. 5.20.2.5 Terrain-induced vertical motion (cm s^{-1}) for 20 July 1978.

Fig. 5.20.2.6 Surface velocity divergence (s^{-1} x 10^{-6}) for 20 July 1978.

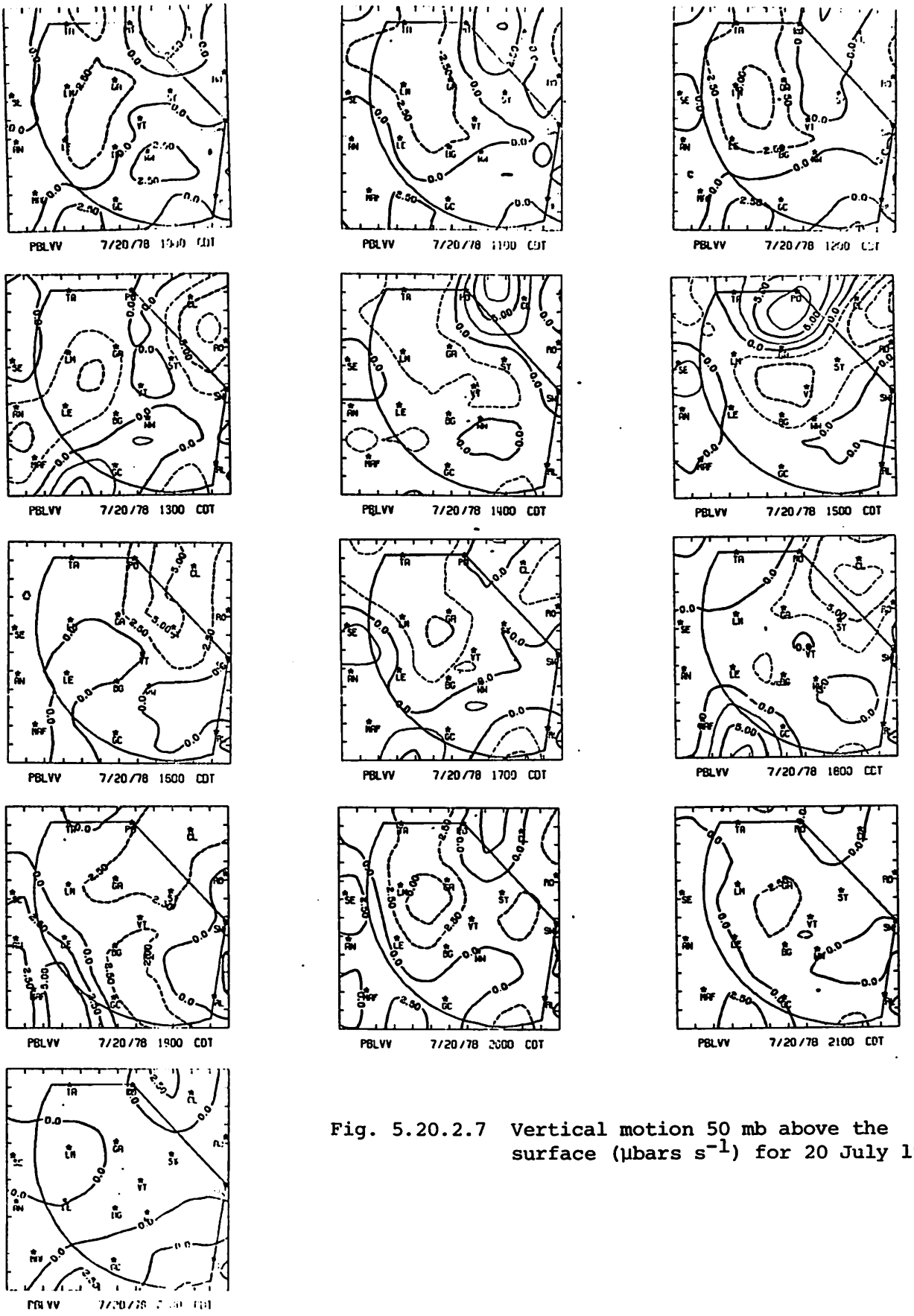

Fig. 5.20.2.7 Vertical motion 50 mb above the surface (μbars s^{-1}) for 20 July 1978.

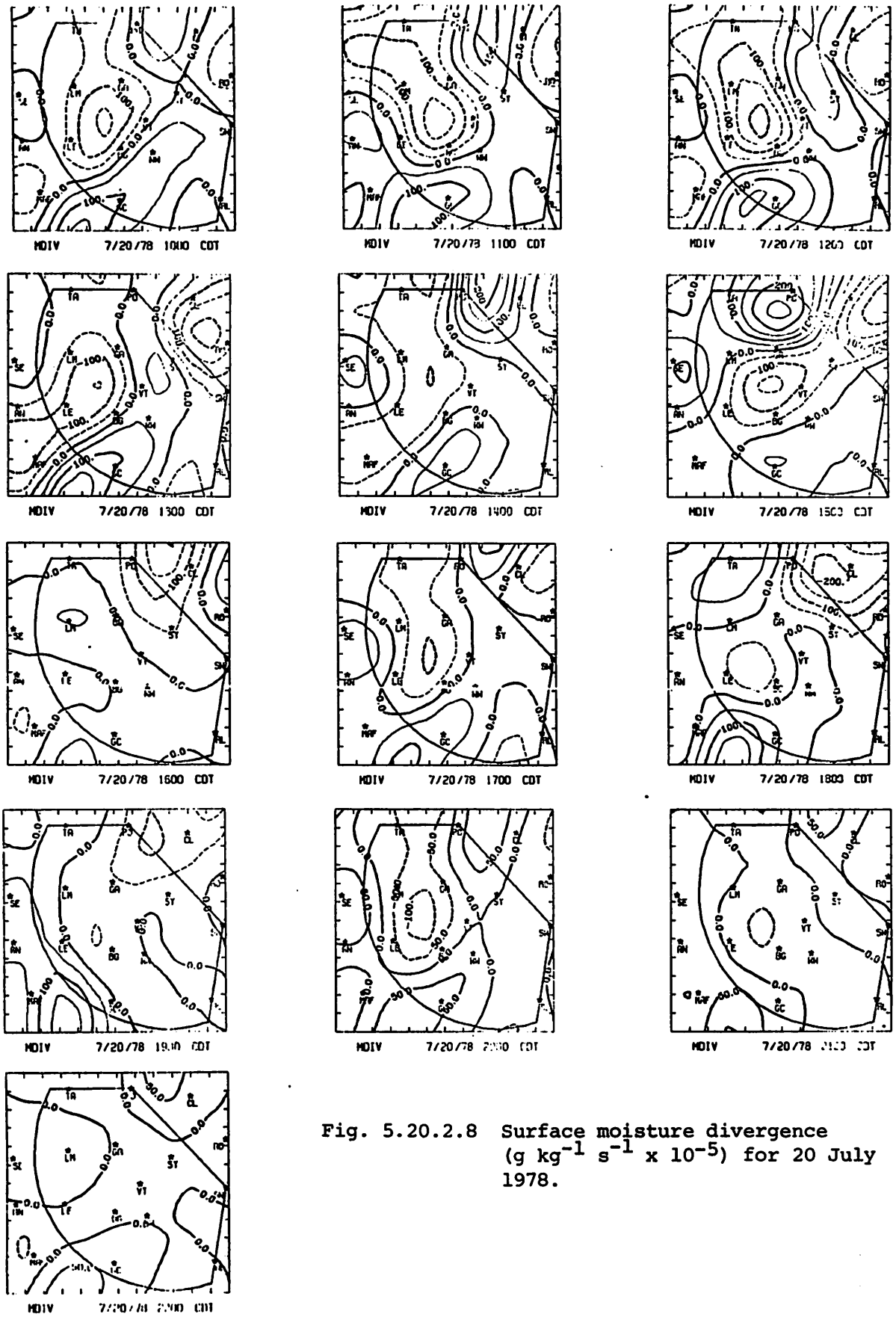

Fig. 5.20.2.8 Surface moisture divergence ($g\ kg^{-1}\ s^{-1} \times 10^{-5}$) for 20 July 1978.

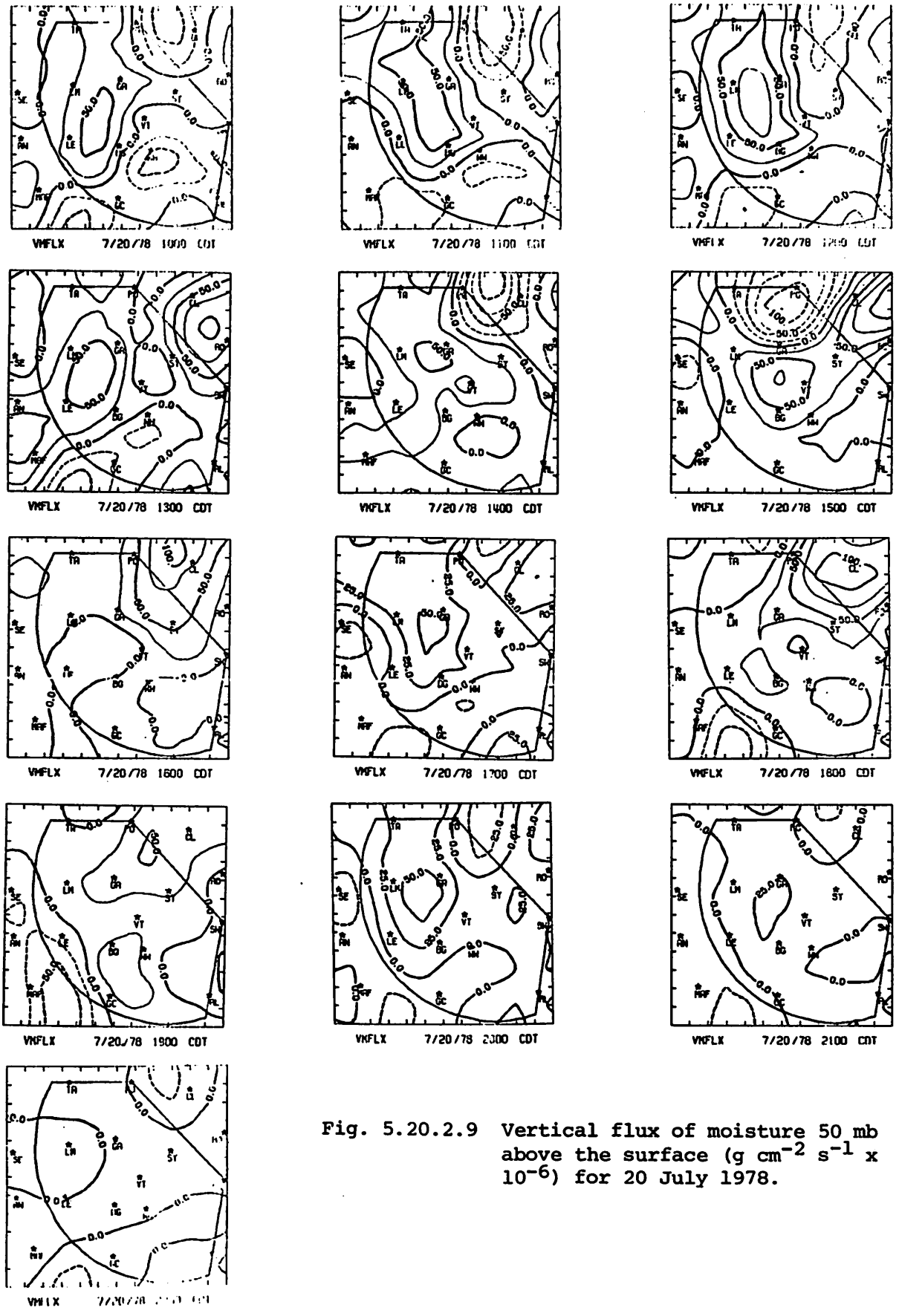

Fig. 5.20.2.9 Vertical flux of moisture 50 mb above the surface (g cm^{-2} s^{-1} x 10^{-6}) for 20 July 1978.

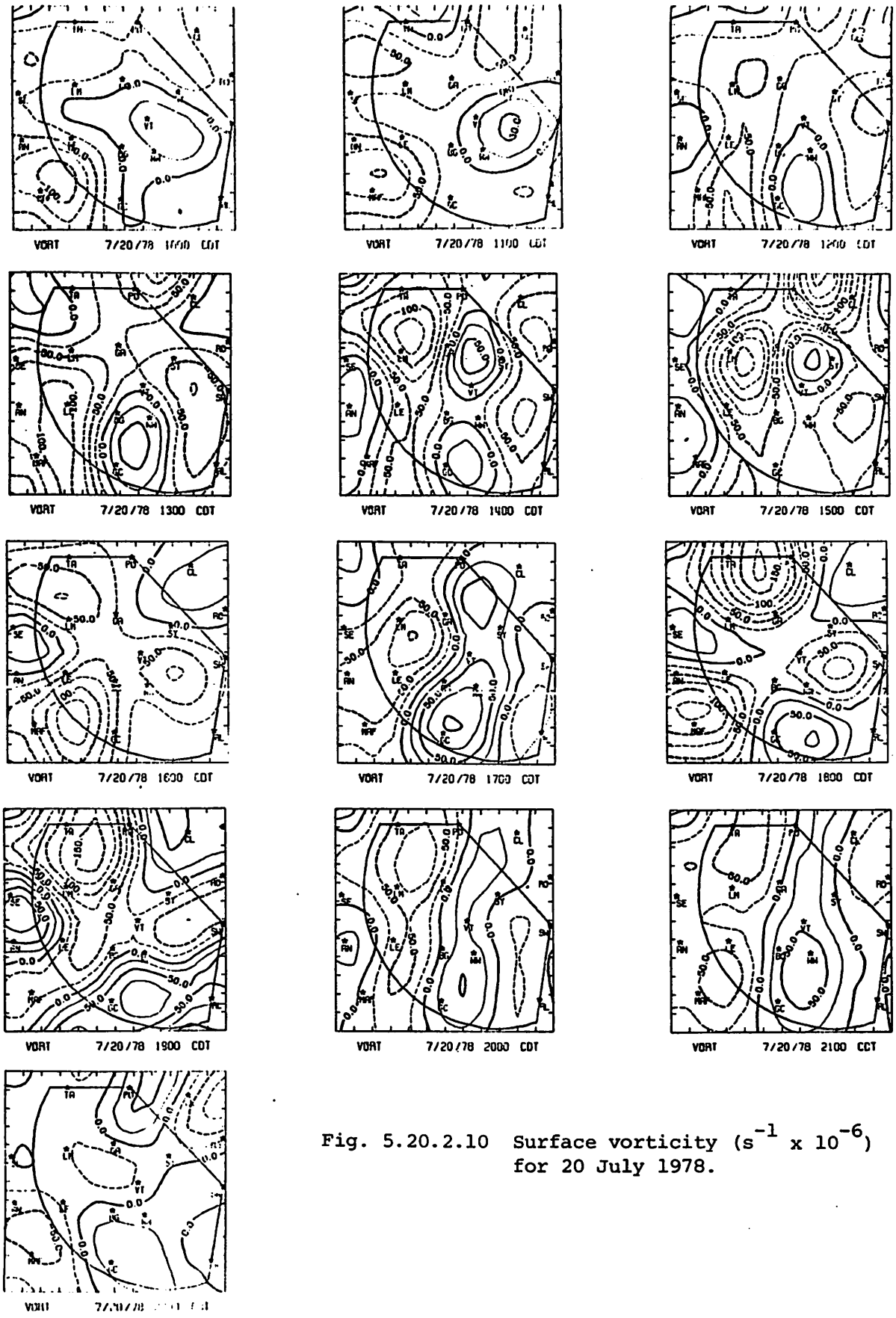

Fig. 5.20.2.10 Surface vorticity (s^{-1} x 10^{-6}) for 20 July 1978.

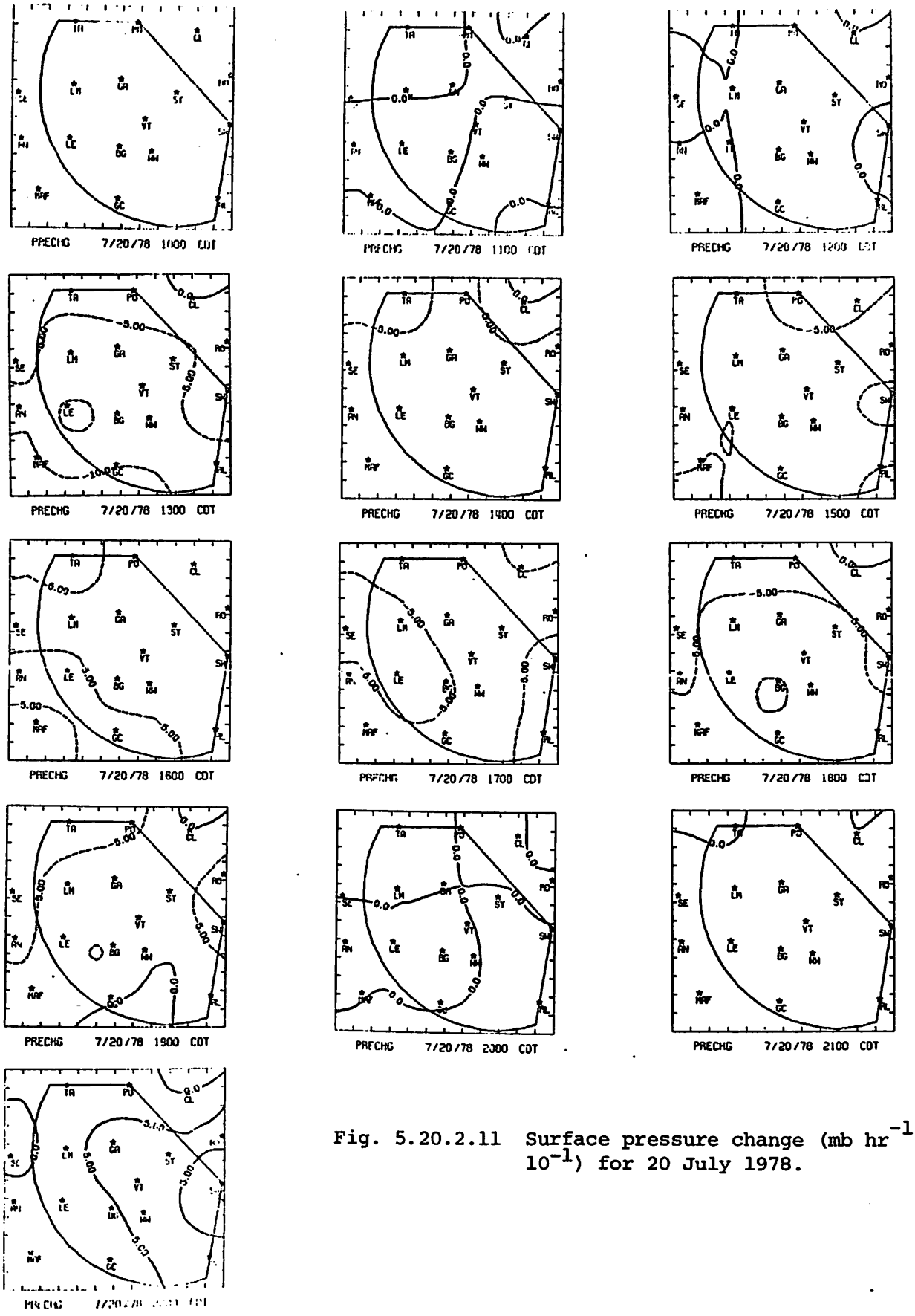

Fig. 5.20.2.11 Surface pressure change (mb hr^{-1} x 10^{-1}) for 20 July 1978.

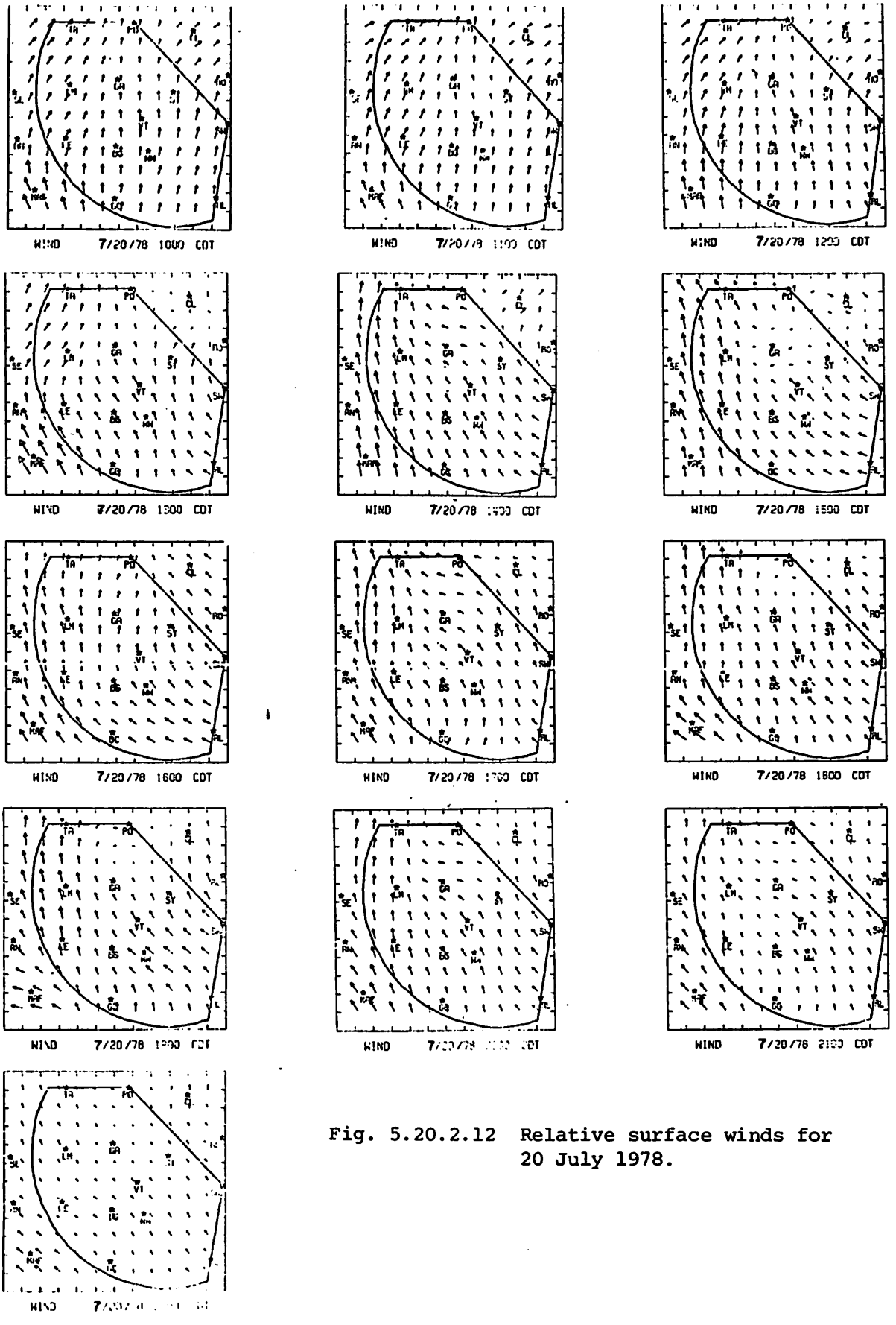

Fig. 5.20.2.12 Relative surface winds for 20 July 1978.

5.21 21 July 1978

5.21.1 Radar

No significant echoes developed in the HIPLEX area on this day. However, two small isolated echoes formed at 2200 GMT near Tahoka and Post (Fig. 5.21.1.1). The echo over Tahoka was also observed at 2300 GMT. Thunderstorms formed to the west of the analysis area, but they never moved closer than 96 km (60 mi) to Midland.

5.21.2 Surface

National Weather Service stations around the HIPLEX area reported cirrus clouds until 0300 GMT and some cumulus in the afternoon hours. As a result, insolation was large and temperatures rose to 37°C at 2200 GMT (Fig. 5.21.2.1). The lowest temperature observed was 27°C at 1500 GMT. A warm ridge extended from Clairemont to Lamesa most of the day, but temperature in that ridge averaged only 2°C above other stations.

A humidity anomaly at Big Spring biased the dewpoint-depression (Fig. 5.21.2.2), mixing ratio (Fig. 5.21.2.3), and equivalent potential temperature (Fig. 5.21.2.4) fields throughout the day. The relative humidity did not vary more than 11% across the network at any one time, if Big Spring is ignored. Also, the absolute amount of moisture, as determined from mixing ratio, decreased from 1500 to 2000 GMT and then remained constant through 0300 GMT. This was probably due to mixing within the surface layer. At 2000 GMT, the mixing ratio varied from 8 to 10 g/kg, except for Big Spring.

The largest value of terrain-induced vertical velocity was 3.0 cm/sec (Fig. 5.21.2.5). It occurred at 1500 GMT between Robert Lee and Walsh-Watts. Negative values persisted at that location throughout the day. Elsewhere, centers with values from +2.5 to -1.5 cm/sec occurred primarily in the center of the network near Big Spring, Gail, and Vincent.

Persistent divergence features occurred near the edge of the analysis area (Fig. 5.21.2.6). Maximum values of divergence and convergence were 10^{-4} and 2×10^{-4} sec^{-1}, respectively. Boundary layer vertical motion (Fig. 5.21.2.7) was generally small but reached -7.5 μbars sec^{-1} at 2000 GMT. Moisture divergence (Fig. 5.21.2.8) also shows features similar to velocity divergence. Values were largest before 2100 GMT due to the drop in mixing ratio at that time. The vertical moisture flux (Fig. 5.21.2.9) had the same patterns, reflecting the lack of moisture gradients across the network. Vorticity fields (Fig. 5.21.2.10) contained some definite positive and negative centers throughout the day. A positive center was located between Walsh-Watts and Garden City throughout the day. Other centers were more variable.

NO ECHOES

RADAR 7/21/78 1000 CDT

NO ECHOES

RADAR 7/21/78 1100 CDT

NO ECHOES

RADAR 7/21/78 1200 CDT

NO ECHOES

RADAR 7/21/78 1300 CDT

NO ECHOES

RADAR 7/21/78 1400 CDT

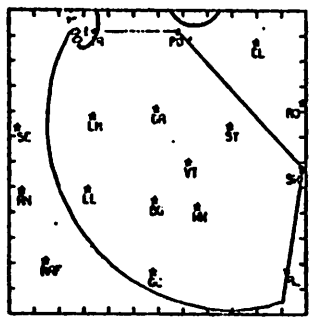

RADAR 7/21/78 1500 CDT

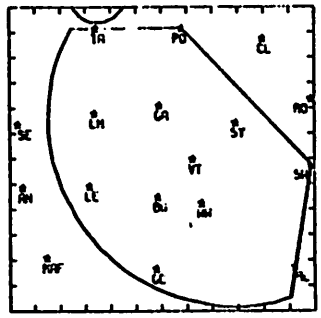

RADAR 7/21/78 1600 CDT

NO ECHOES

RADAR 7/21/78 1700 CDT

NO ECHOES

RADAR 7/21/78 1800 CDT

NO ECHOES

RADAR 7/21/78 1900 CDT

NO ECHOES

RADAR 7/21/78 2000 CDT

NO ECHOES

RADAR 7/21/78 2100 CDT

NO ECHOES

RADAR 7/21/78 2200 CDT

Fig. 5.21.1.1 Radar echoes for 21 July 1978.

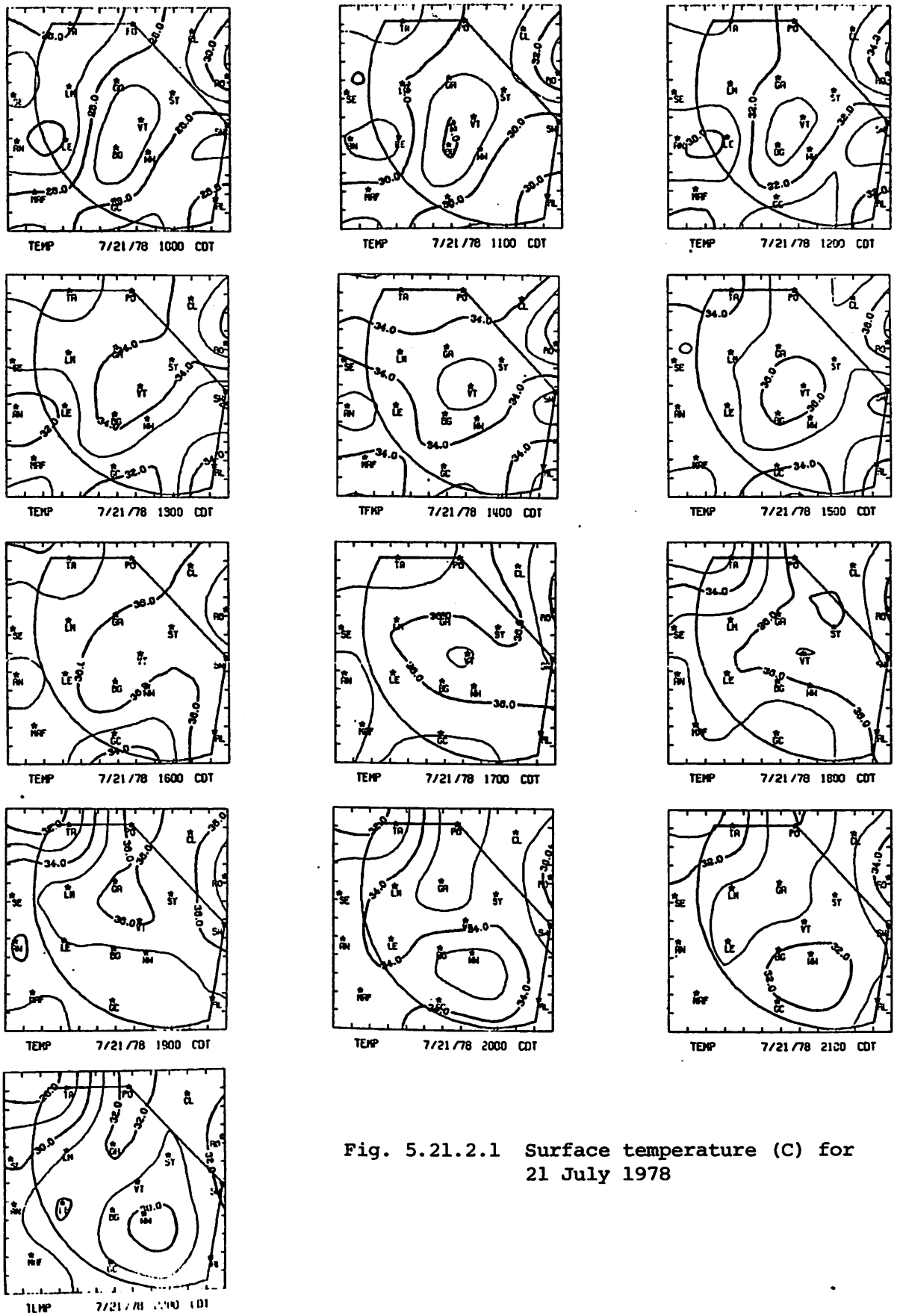

Fig. 5.21.2.1 Surface temperature (C) for 21 July 1978

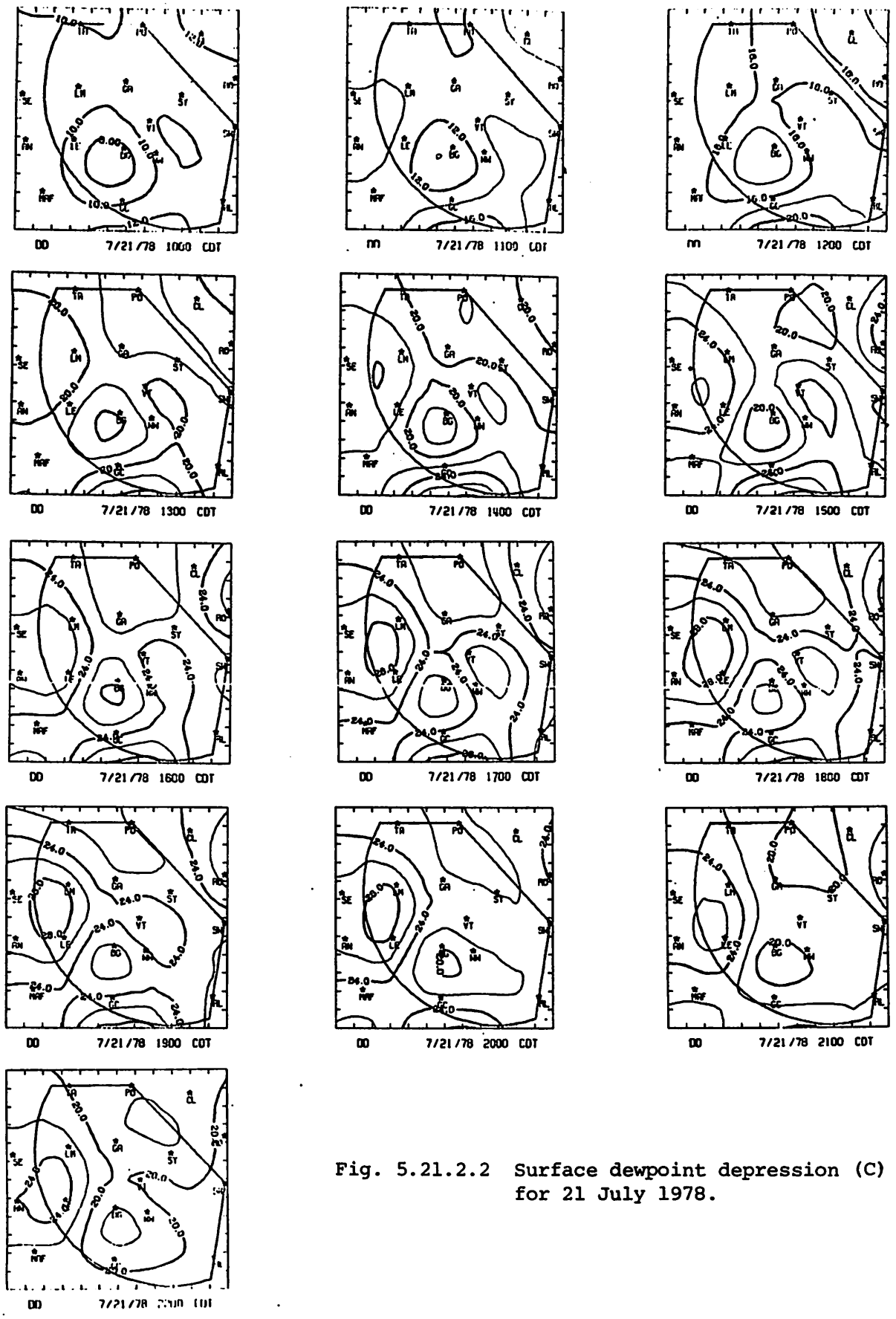

Fig. 5.21.2.2 Surface dewpoint depression (C) for 21 July 1978.

Fig. 5.21.2.3 Surface mixing ratio (g kg^{-1}) for 21 July 1978.

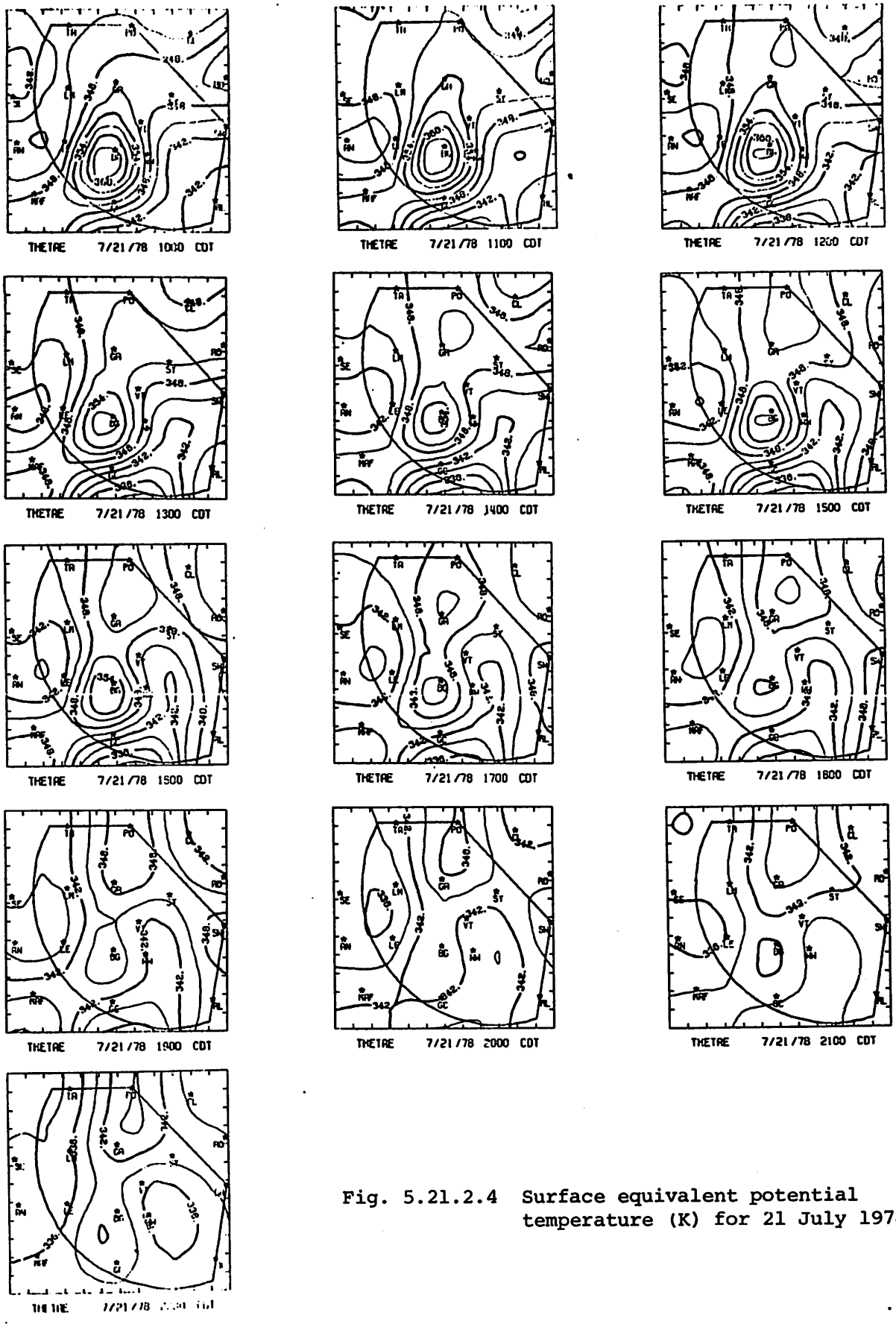

Fig. 5.21.2.4 Surface equivalent potential temperature (K) for 21 July 1978.

Fig. 5.21.2.5 Terrain-induced vertical motion (cm s^{-1}) for 21 July 1978.

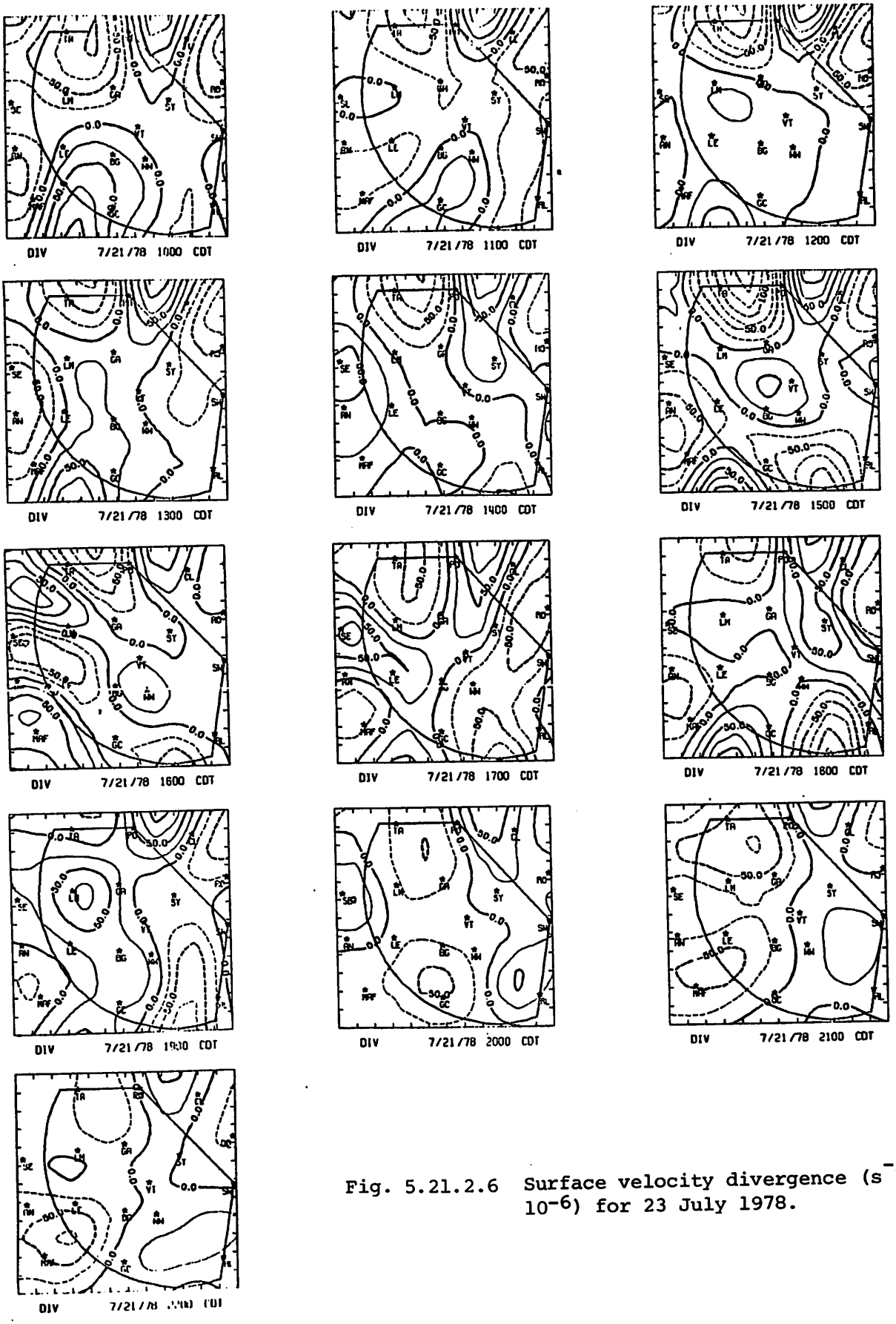

Fig. 5.21.2.6 Surface velocity divergence (s^{-1} x 10^{-6}) for 23 July 1978.

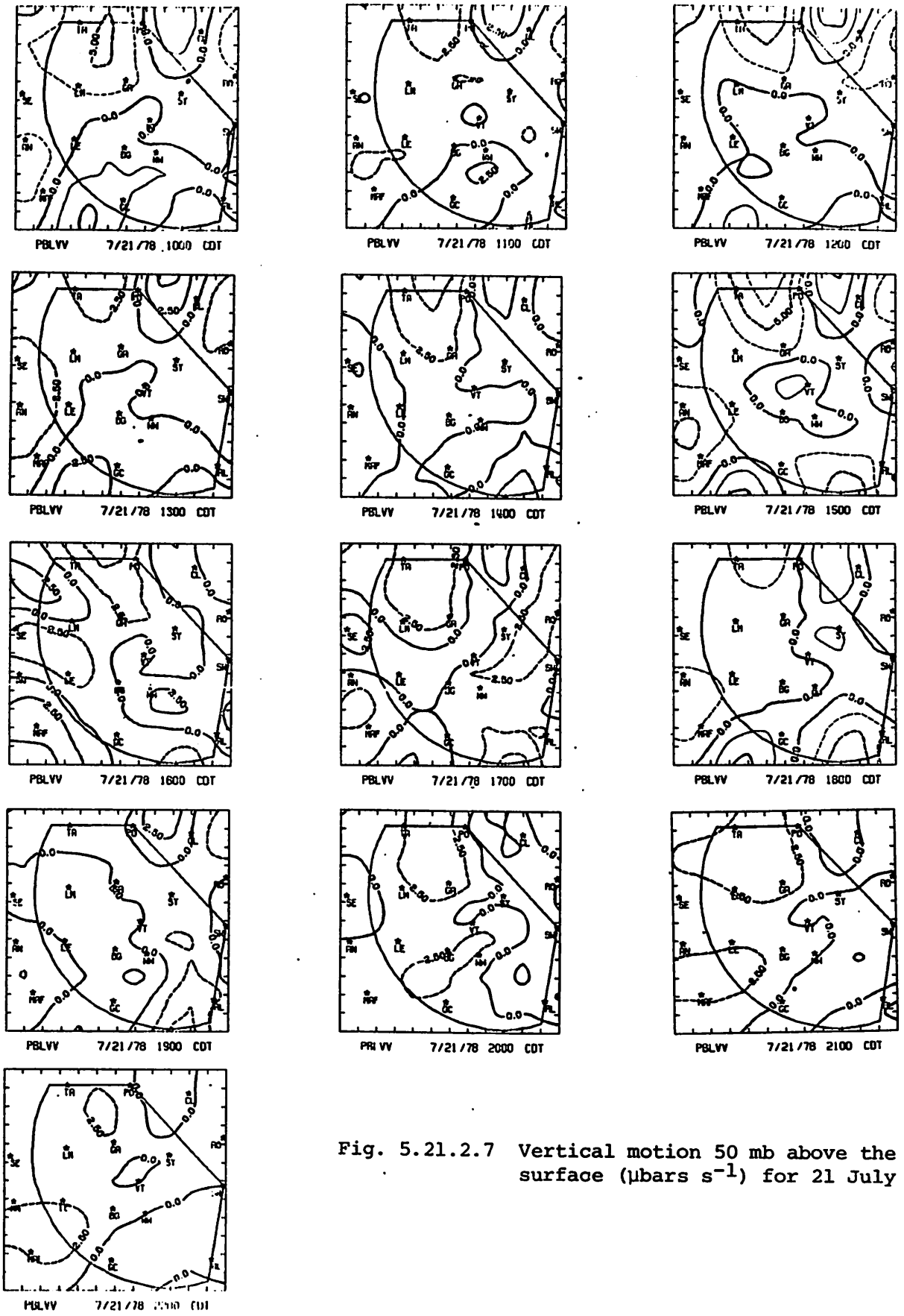

Fig. 5.21.2.7 Vertical motion 50 mb above the surface (μbars s^{-1}) for 21 July 1978.

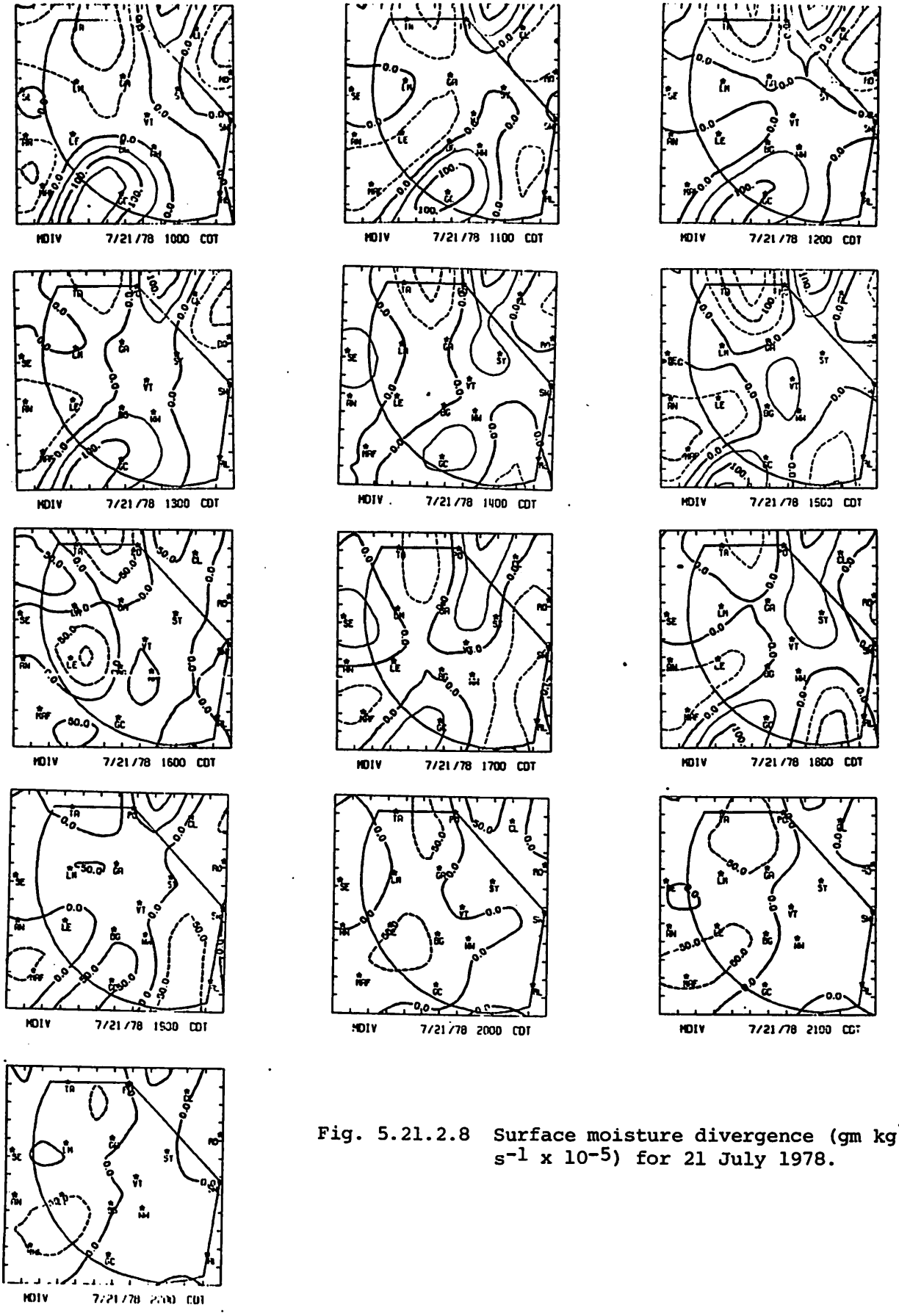

Fig. 5.21.2.8 Surface moisture divergence (gm kg^{-1} s^{-1} x 10^{-5}) for 21 July 1978.

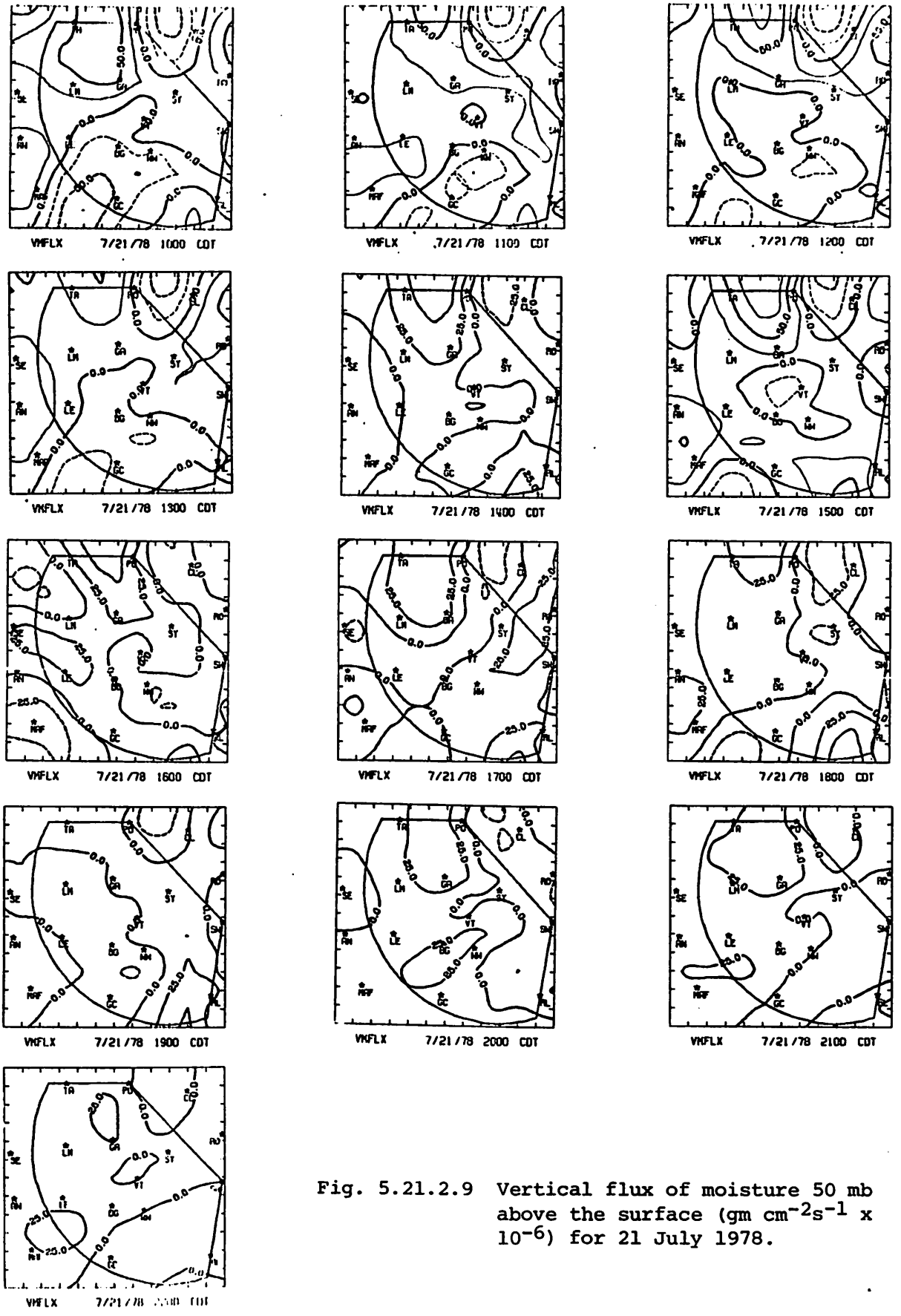

Fig. 5.21.2.9 Vertical flux of moisture 50 mb above the surface (gm $cm^{-2}s^{-1}$ x 10^{-6}) for 21 July 1978.

Fig. 5.21.2.10 Surface vorticity ($s^{-1} \times 10^{-6}$) for 21 July 1978.

Pressure changes were inconsistent and small (Fig. 5.21.2.11). A pressure change of 1.0 mb hr^{-1} was observed at Clairemont at 2100 GMT, but most changes were equal to or less than 0.5 mb hr^{-1}.

The surface wind fields were persistent throughout the day (Fig. 5.21.2.12) and speeds were moderate. The flow was from the south to southeast throughout the day over the entire area.

5.21.3 Upper Level Kinematic Parameters

Mass convergence occurred below 800 mb at all times, and mass divergence occurred at 700 mb at 1500, 1800, and 0300 GMT (Fig. 5.21.3.1). Large values of convergence near the surface led to upward vertical motion at all times with the exception of 0300 GMT (Fig. 5.21.3.2). At that time, strong divergence between 750 and 550 mb resulted in downward motion above 450 mb. Except for 0300 GMT, values of vertical motion did not vary significantly with height. The greatest upward motion occurred at 2100 GMT.

Moisture divergence profiles reflect the dryness of air above 550 mb (Fig. 5.21.3.3). They show similar patterns to mass divergence below 550 mb.

5.21.4 Energetics

Figure 5.21.4.1 shows the horizontal flux divergence of latent heat energy. Latent heat energy was being concentrated near the surface at all times. It was being diverged at 700 mb at 1500, 1800, and 0300 GMT. The profiles show no systematic tendencies with respect to time.

The vertical flux divergence of latent heat energy opposed the horizontal flux term (Fig. 5.21.4.2). Latent heat energy was removed in the region below 800 mb and concentrated from 700 to 450 mb at all times.

Profiles in Figure 5.21.4.3 show a tendency to concentrate latent heat energy below 600 mb as the day progressed. The 1500 GMT profile shows a decrease of latent heat energy in all layers. The 1800 GMT profile is similar, except a slight gain occurred at 650 mb. At 2100 GMT the trend continued, and energy was being increased from 725 to 550 mb. Finally, at 0000 and 0300 GMT, latent heat energy was being gained below 600 mb, but decreased slightly between 550 and 475 mb. The tendency toward increasing water vapor between 600 and 700 mb corresponded to the increase in cumulus at that level, and may have resulted from cloud evaporation.

The residual of the latent heat energy budget is positive, with the exception of the layer below 700 mb at 0300 GMT (Fig. 5.21.4.4). Values

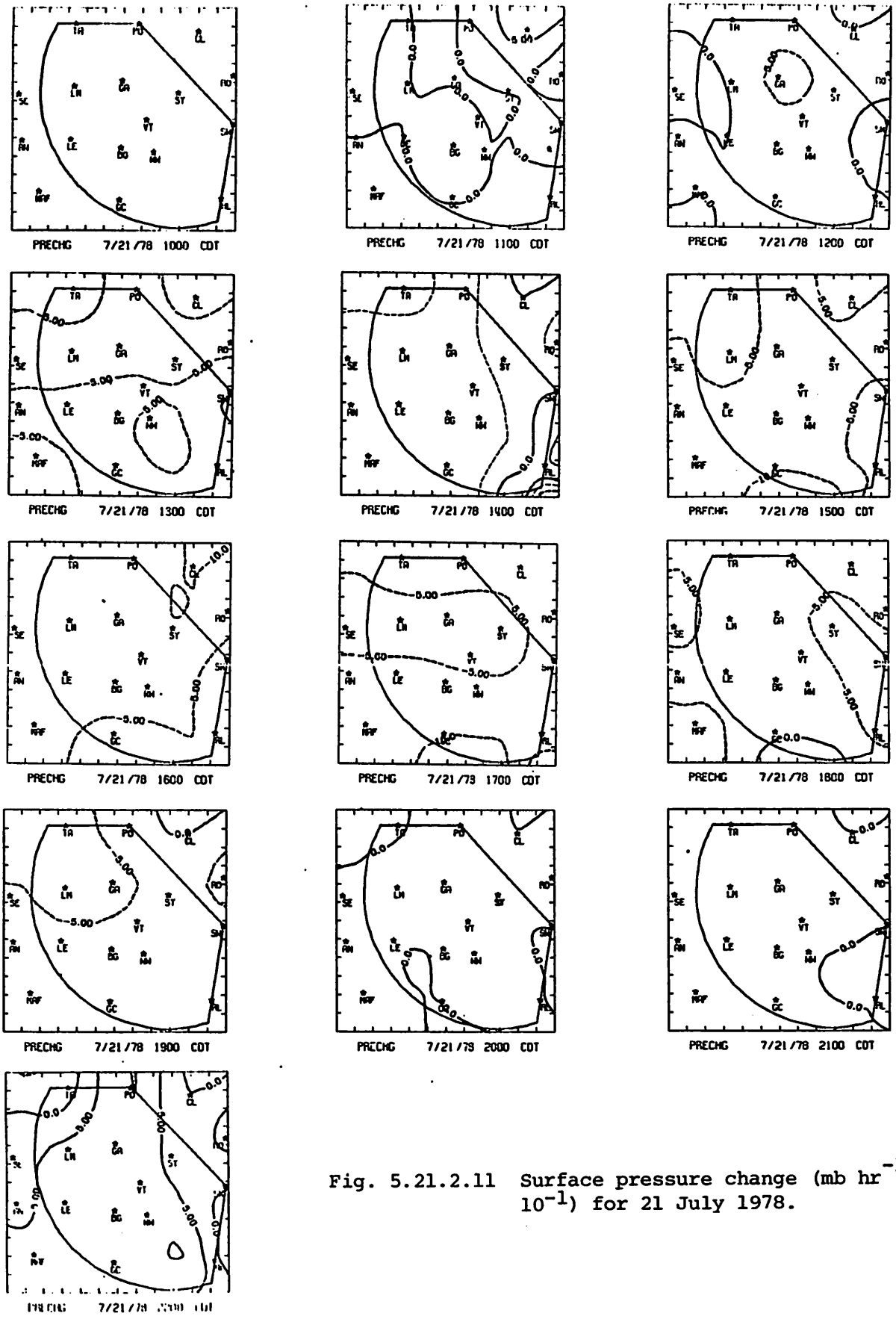

Fig. 5.21.2.11 Surface pressure change (mb hr^{-1} x 10^{-1}) for 21 July 1978.

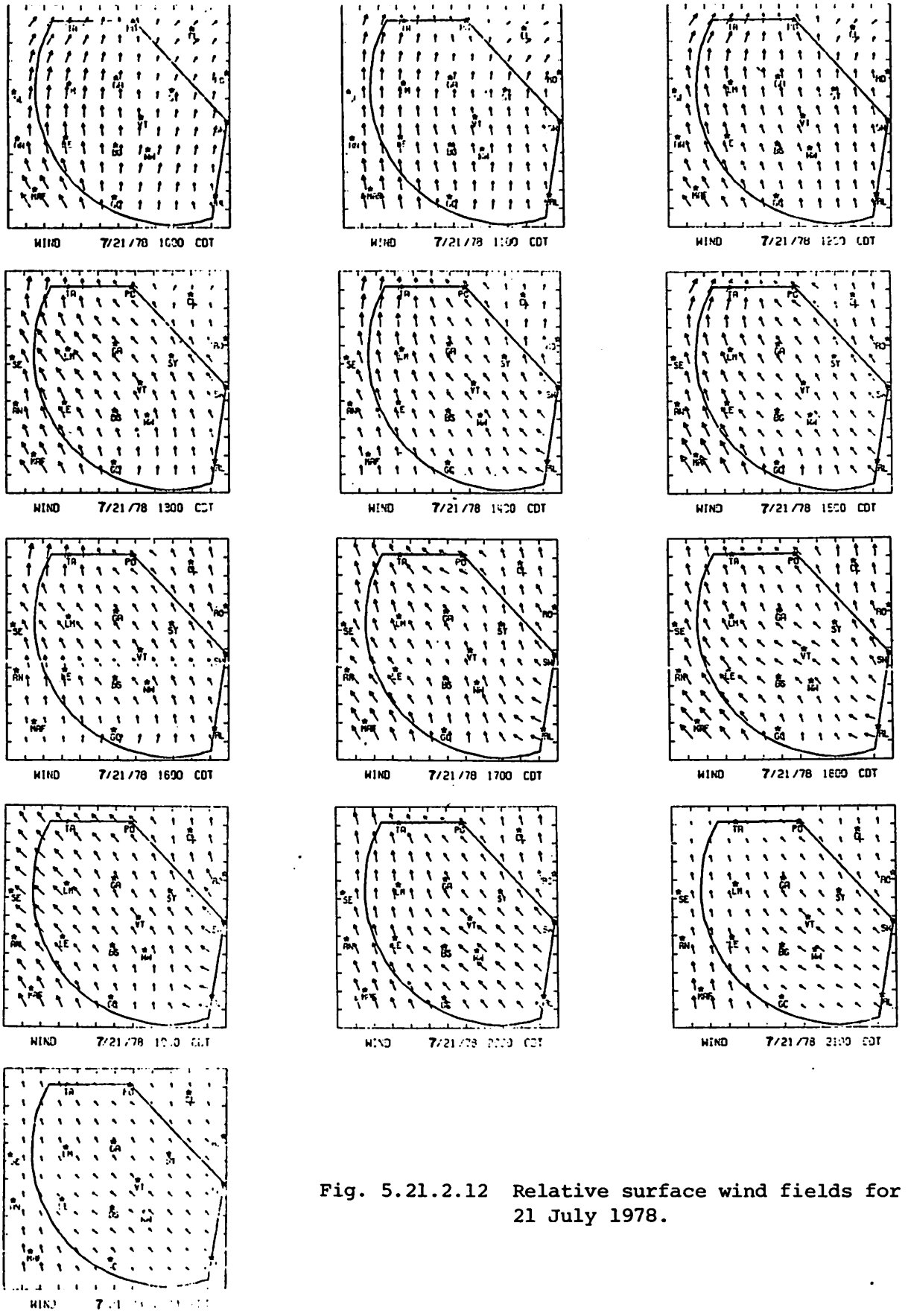

Fig. 5.21.2.12 Relative surface wind fields for 21 July 1978.

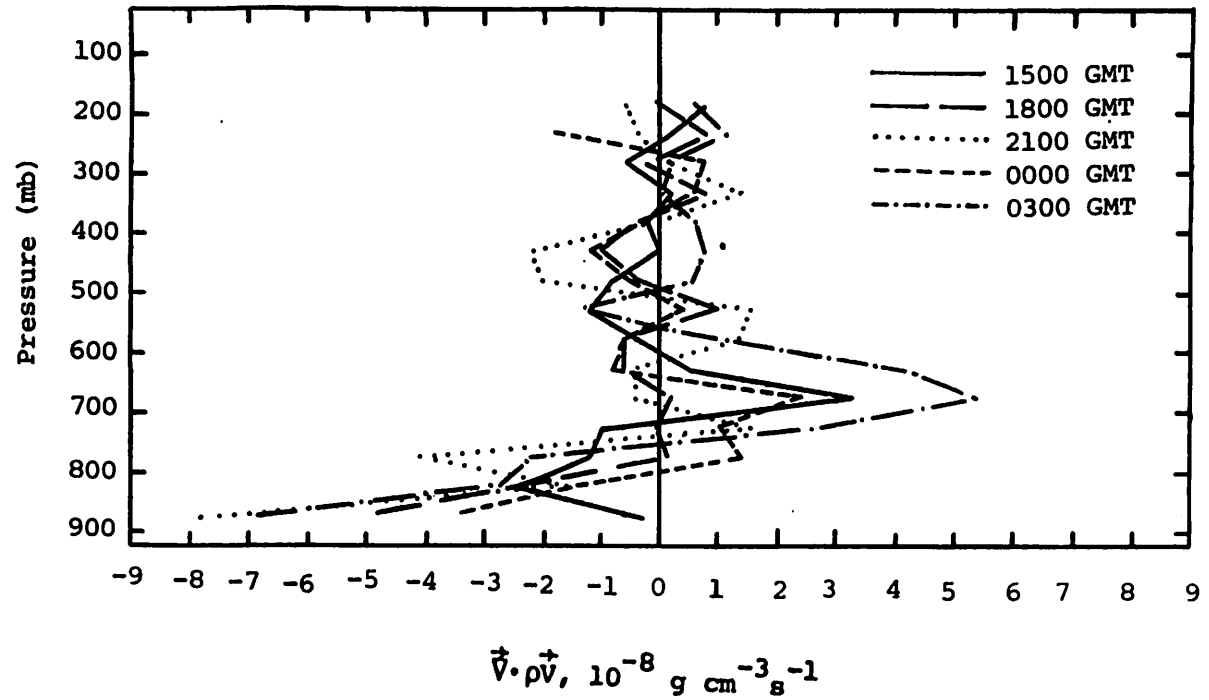

Fig. 5.21.3.1 Vertical profiles of mass divergence on 21 July 1978.

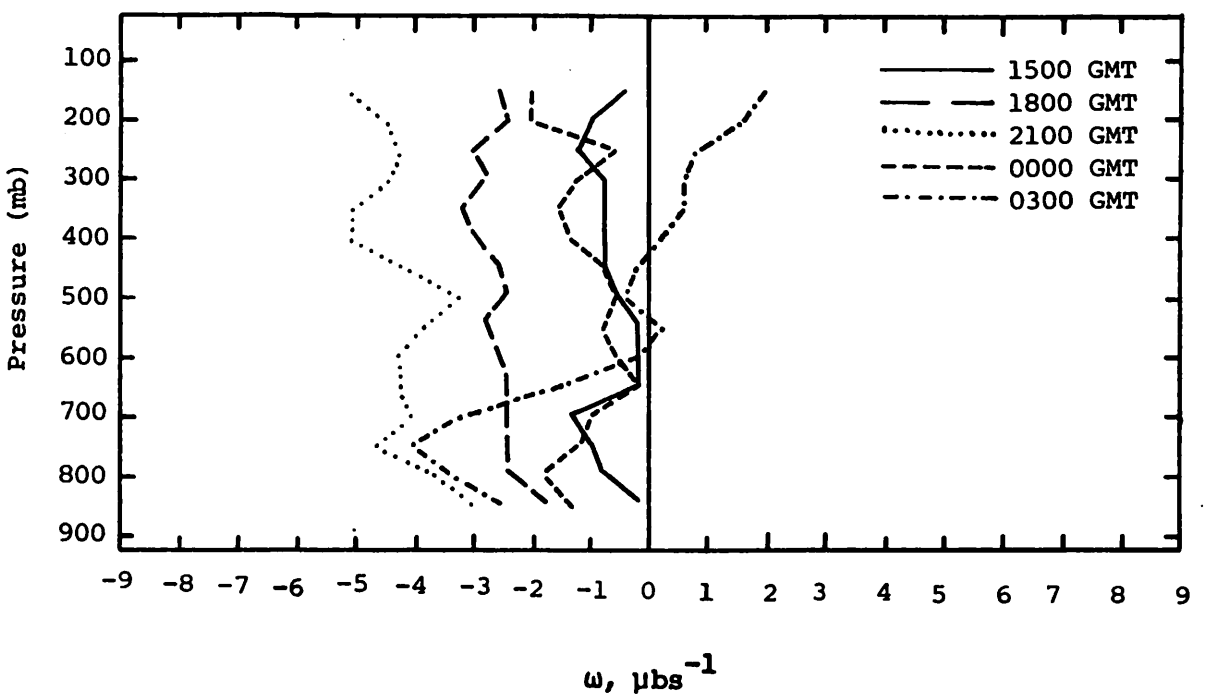

Fig. 5.21.3.2 Vertical profiles of vertical motion on 21 July 1978.

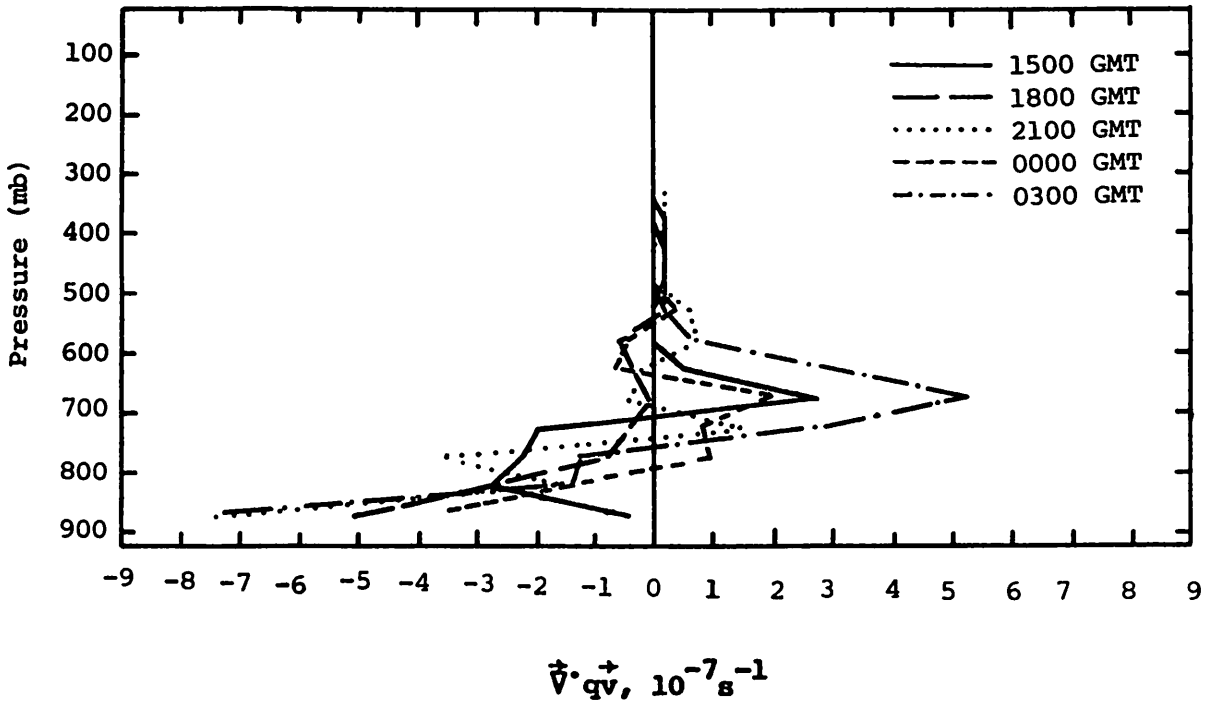

Fig. 5.21.3.3 Vertical profiles of moisture divergence on 21 July 1978.

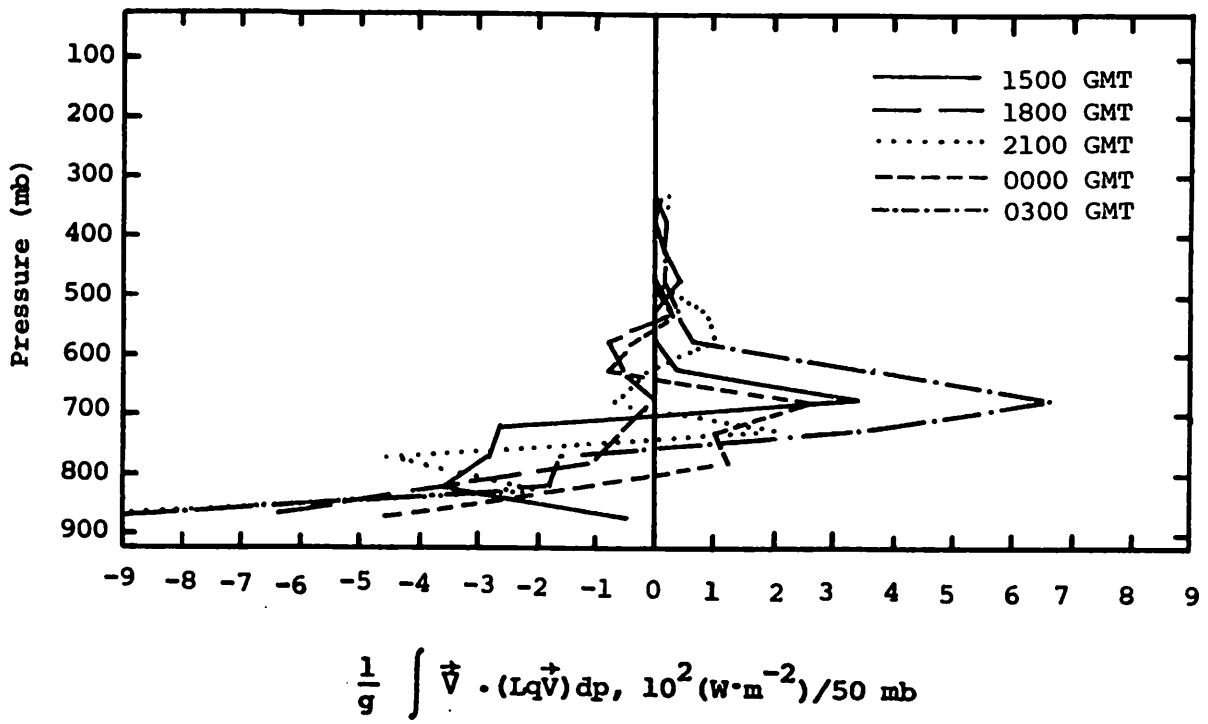

Fig. 5.21.4.1 Vertical profiles of the horizontal flux of latent heat energy on 21 July 1978.

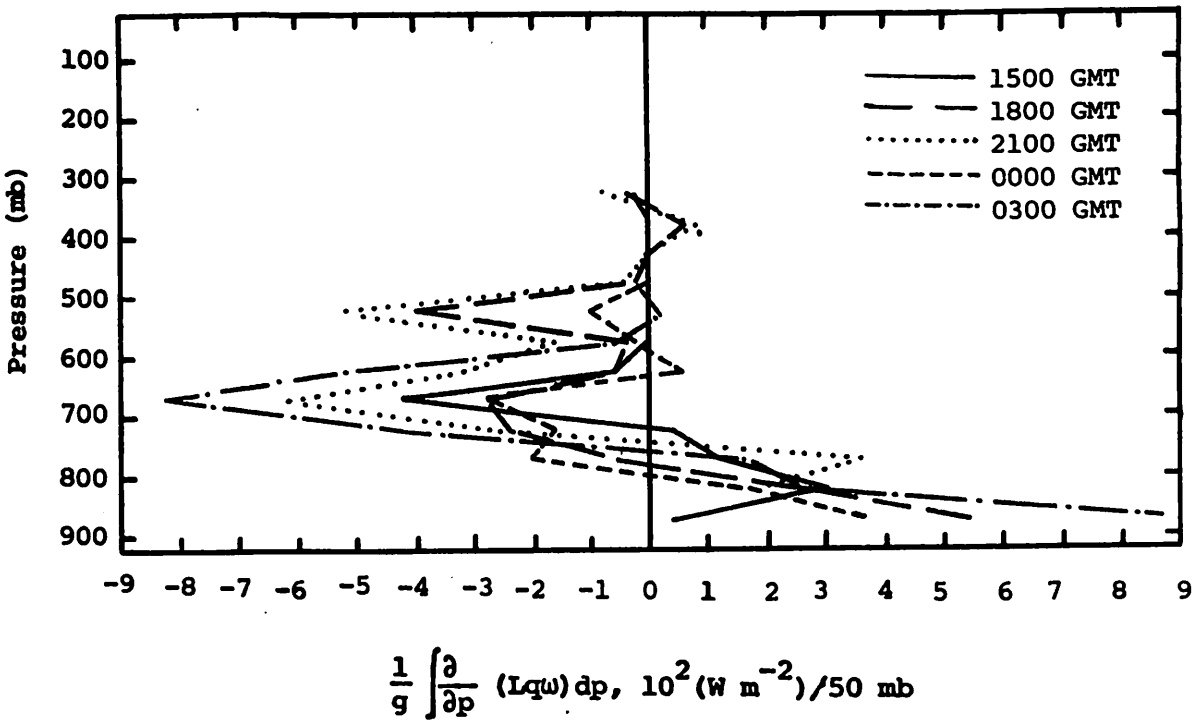

Fig. 5.21.4.2 Vertical profiles of the vertical flux of latent heat energy on 21 July 1978.

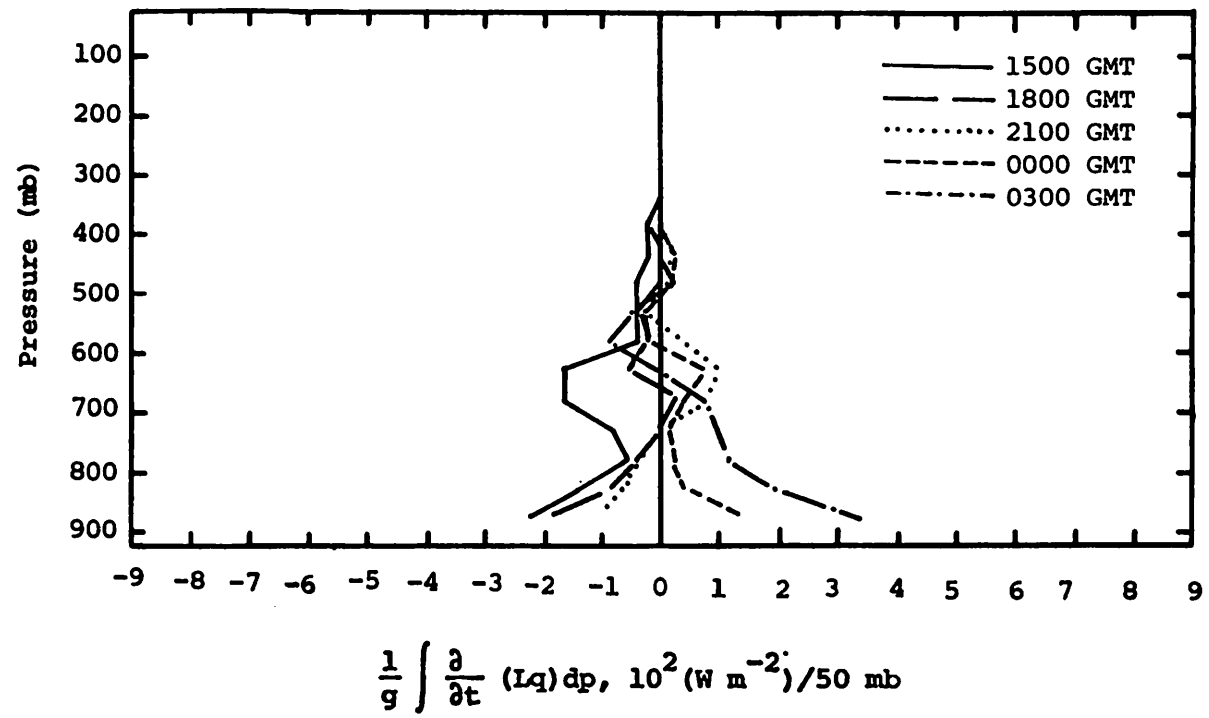

Fig. 5.21.4.3 Vertical profiles of the local change of latent heat energy on 21 July 1978.

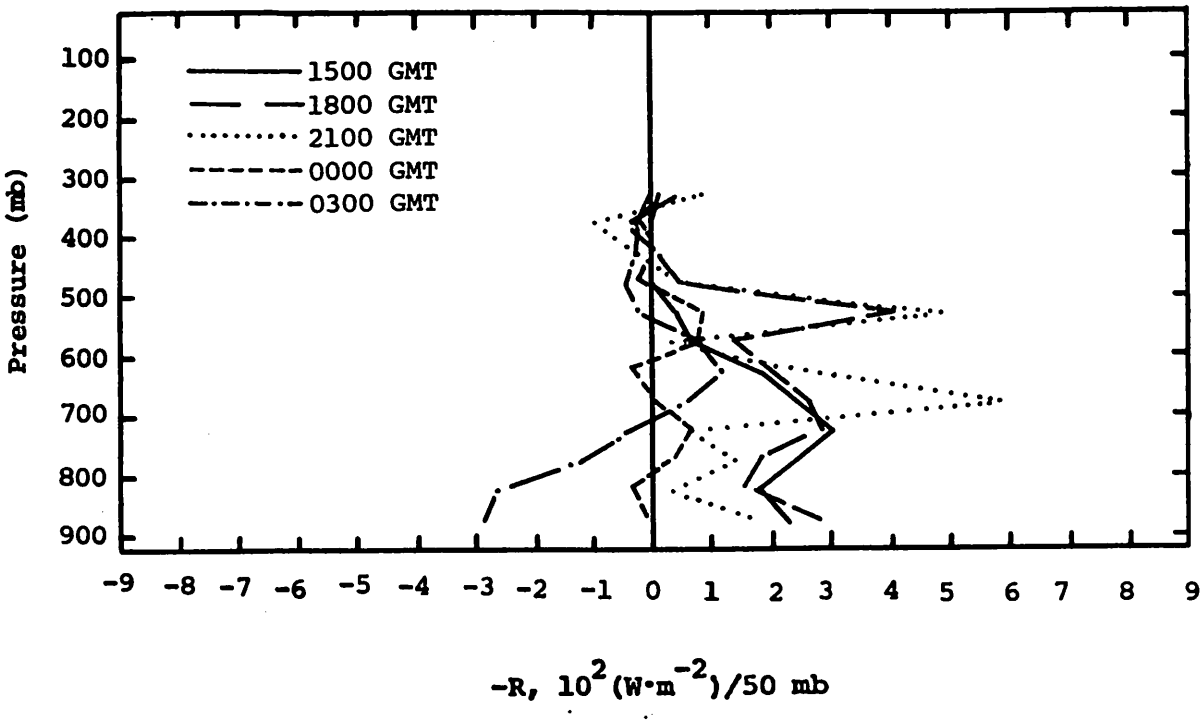

Fig. 5.21.4.4 Vertical profiles of the residual of the latent heat energy equation on 21 July 1978.

were fairly large from 1500 to 2100 GMT and represent a loss of energy due to condensation or sub-scale processes.

Profiles of diabatic heating (Fig. 5.21.4.5) show that sensible heat was being gained at virtually every level and every time. This is consistent with large insolation due to modest cloud amounts throughout the day. Diabatic heating was greatest at 1800 and 2100 GMT, the period of greatest insolation.

Low wind speeds (largest wind speed measured was 13 m sec^{-1}) resulted in small kinetic energy values and virtually featureless profiles of kinetic energy transport (Figs. 5.21.4.6 and 5.21.4.7). Most wind speeds observed on this day were well below 10 m sec^{-1}.

5.21.5 Water Vapor Budget

Profiles of the net horizontal transport of water vapor (Fig. 5.21.5.1) show gains at most levels at 1500 and 1800 GMT and losses at other times.

There was upward transport of water vapor at all times (Fig. 5.21.5.2). Water vapor was being concentrated in most layers by vertical transport (Fig. 5.21.5.3), however, the surface layer experienced a loss at all times, especially at 1500, 2100, and 0300 GMT due to the vertical stretching of that layer. The horizontal transport was more variable, except at 2100 and

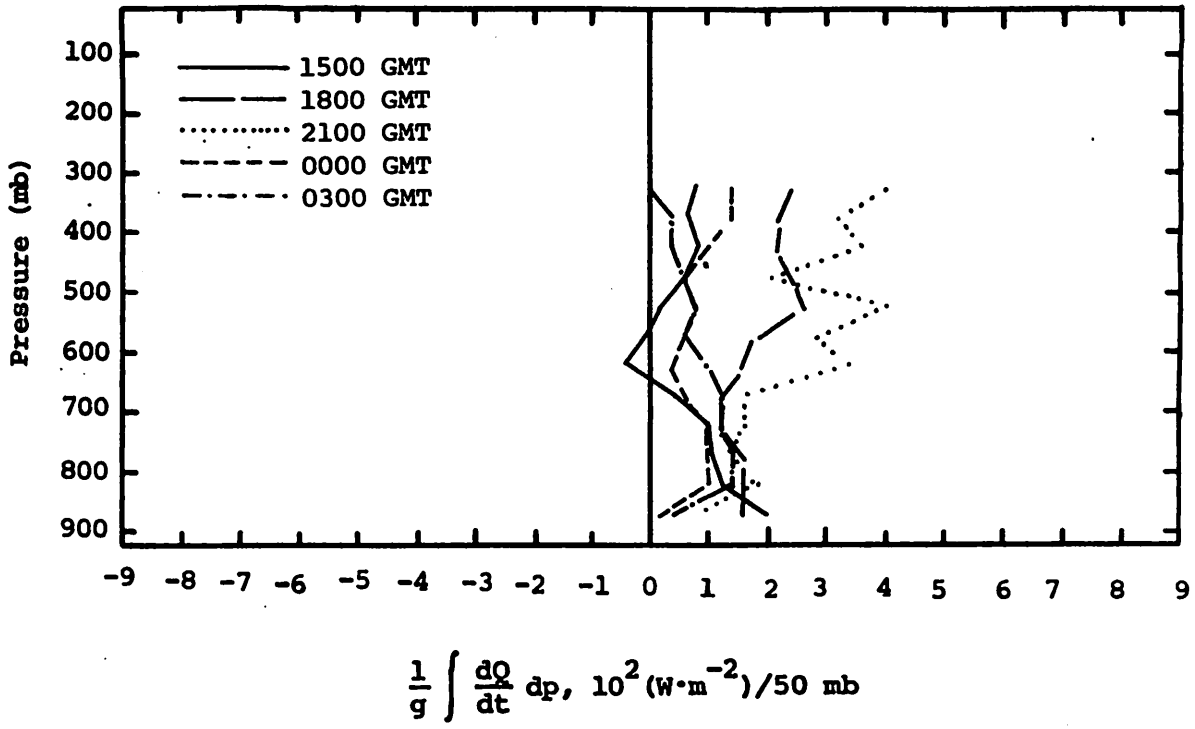

Fig. 5.21.4.5 Vertical profiles of diabatic heating computed from the first law of thermodynamics on 21 July 1978.

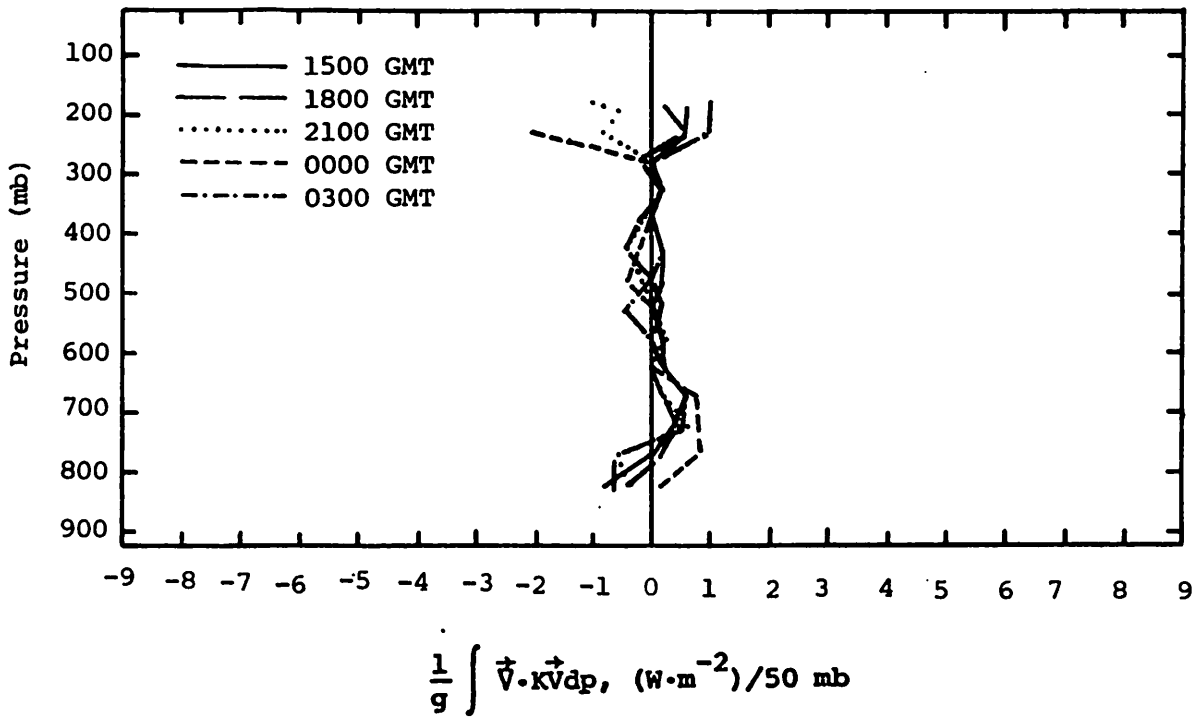

Fig. 5.21.4.6 Vertical profiles of the horizontal flux of kinetic energy on 21 July 1978.

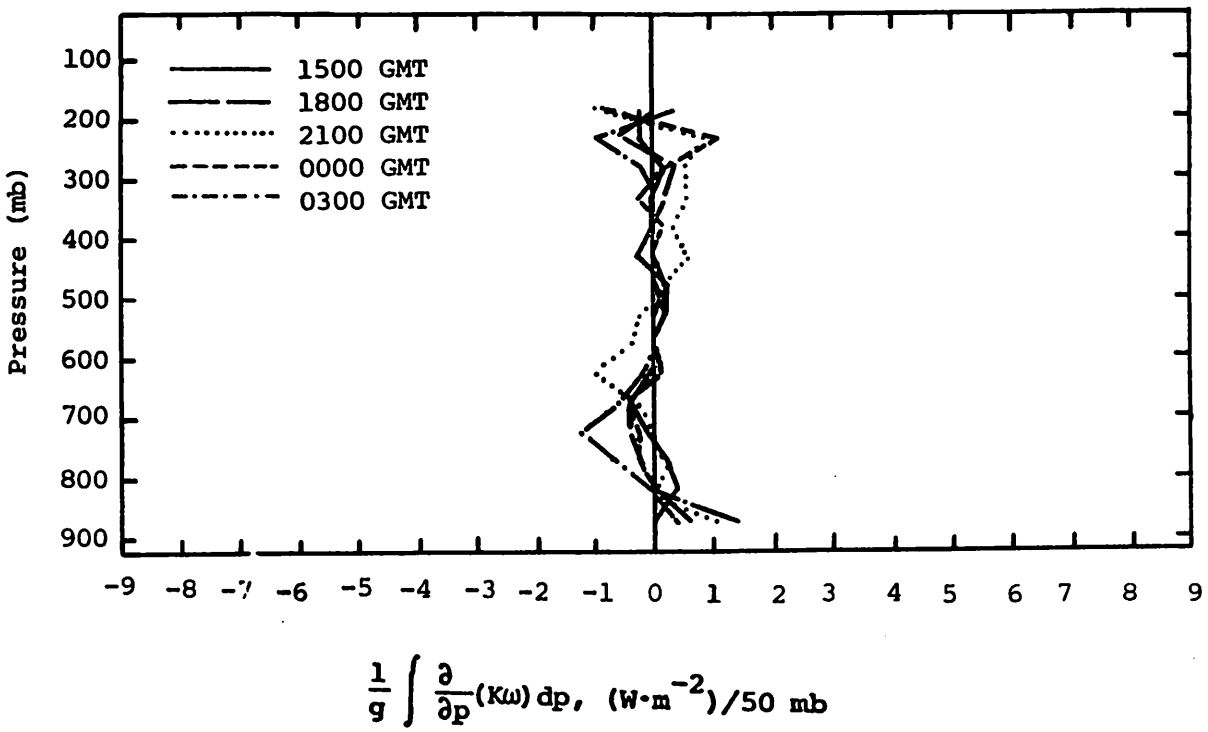

Fig. 5.21.4.7 Vertical profiles of the vertical flux of kinetic energy on 21 July 1978.

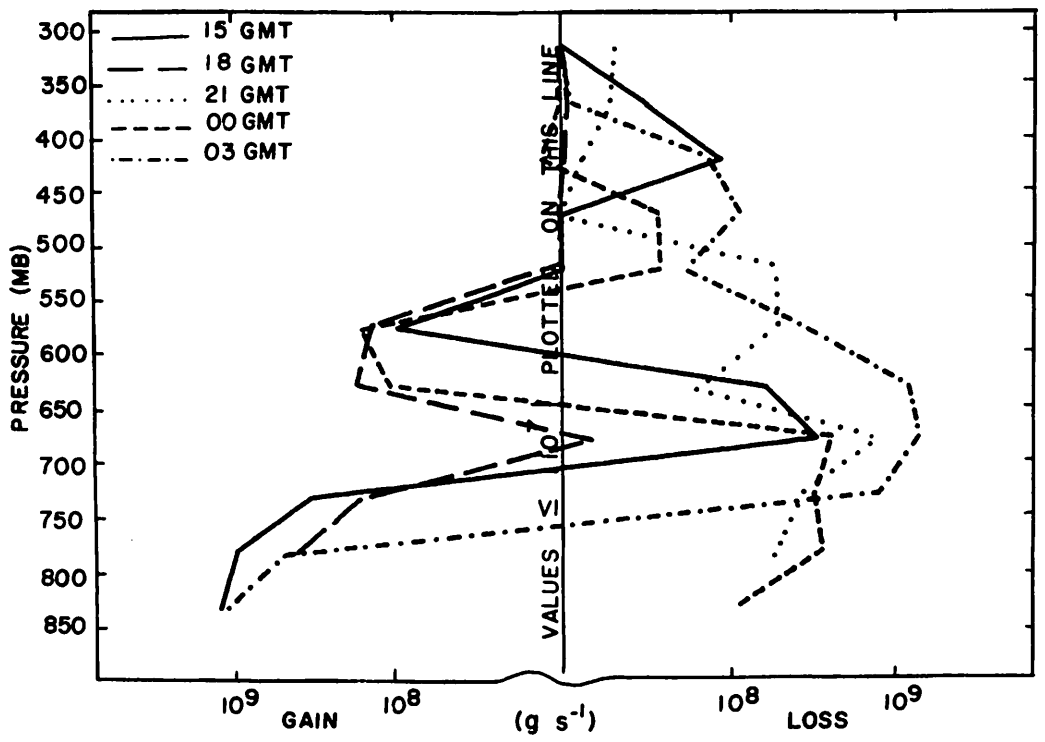

Fig. 5.21.5.1 Net horizontal transport of water vapor through boundaries of 50-mb layers (gm s^{-1}) over the Texas HIPLEX area for 21 July 1978.

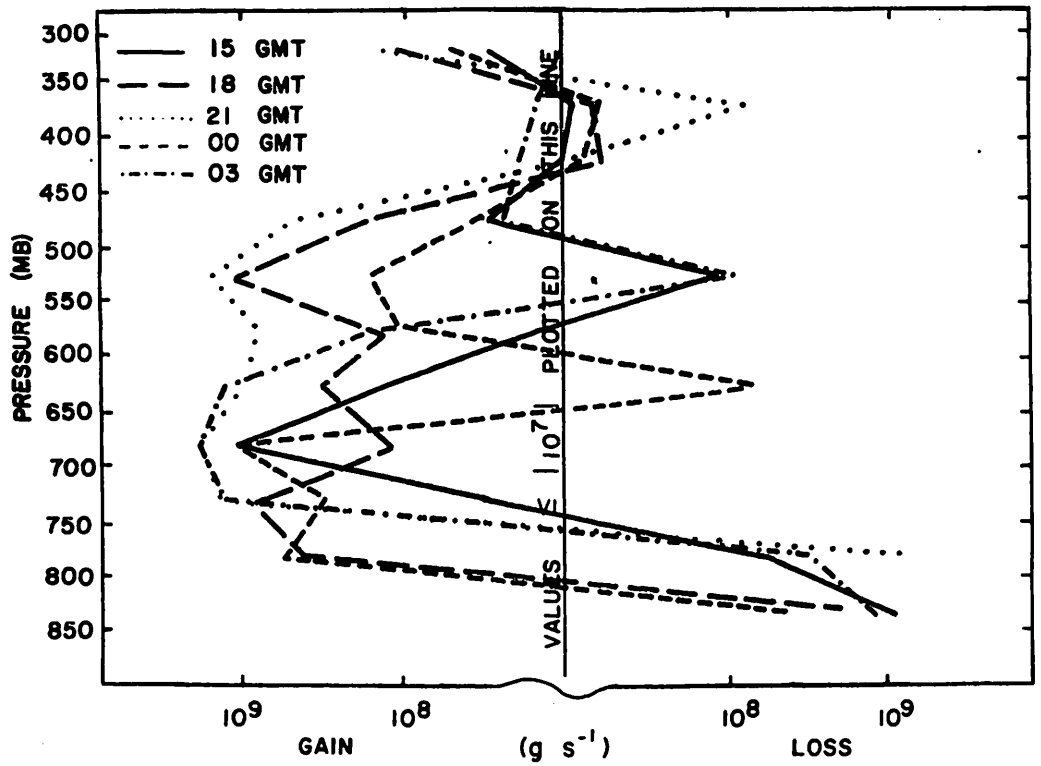

Fig. 5.21.5.2 Net vertical transport of water vapor through boundaries of 50-mb layers (gm s^{-1}) over the Texas HIPLEX area for 21 July 1978.

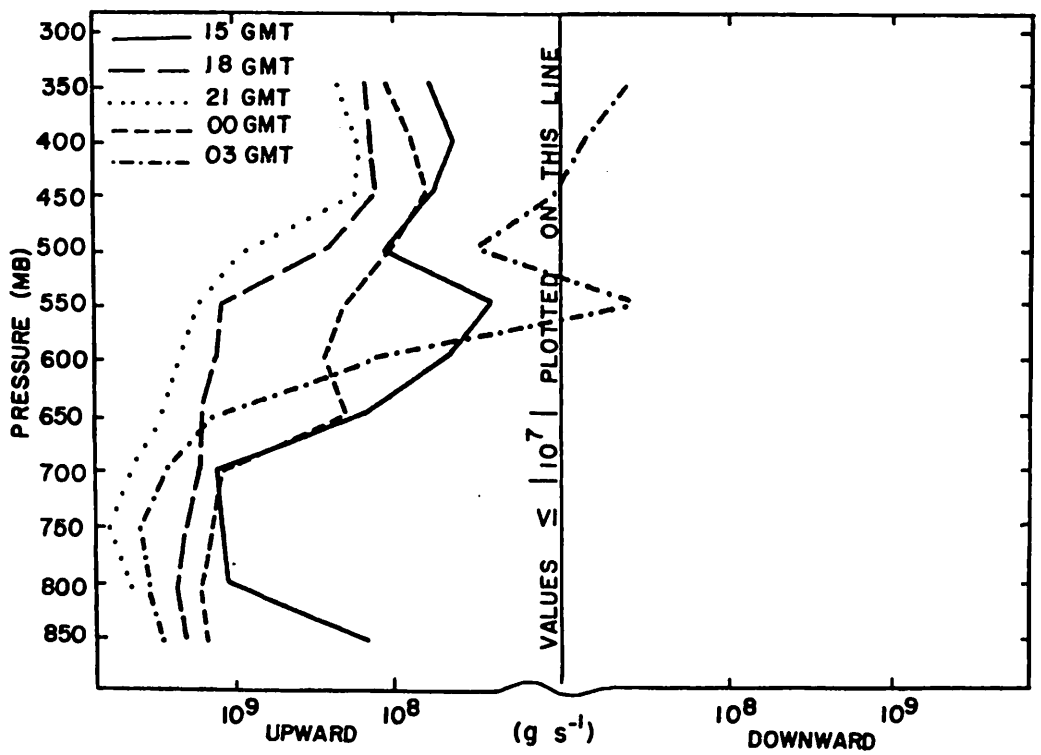

Fig. 5.21.5.3 Vertical transport of water vapor through constant pressure surfaces (gm s^{-1}) over the Texas HIPLEX area for 21 July 1978.

0300 GMT. At those times, horizontal motions removed water vapor at most levels.

Profiles of the combined net horizontal and vertical transport of water vapor (Fig. 5.21.5.4) show that, in general, water vapor was being concentrated below 450 mb throughout the day. The 1500 GMT profile indicates a loss of water vapor below 650 mb. However, maximum values at 725 mb for the 1800 to 2100 GMT period and at 625 mb for the 2100 to 0000 GMT period corresponded well with the location of the top of the mixed layer, thus indicating an upward transport of surface-layer moisture. From 0000 to 0300 GMT, when surface temperature dropped, the vertical transport of moisture decreased.

The total mass of water vapor (Fig. 5.21.5.5) increased due to the upward transport between 775 and 600 mb from 1800 to 0000 GMT. Also, above 450 mb, the amount of water vapor decreased from 1500 to 2100 GMT, then increased again until 0300 GMT. Reports of high-level clouds, most of which were observed from 1800 to 0000 GMT, correlated well with these changes.

The local rate-of-change of water vapor (Fig. 5.21.5.6) was generally small except below 700 mb between 0000 and 0300 GMT. During this period a significant gain occurred in that layer.

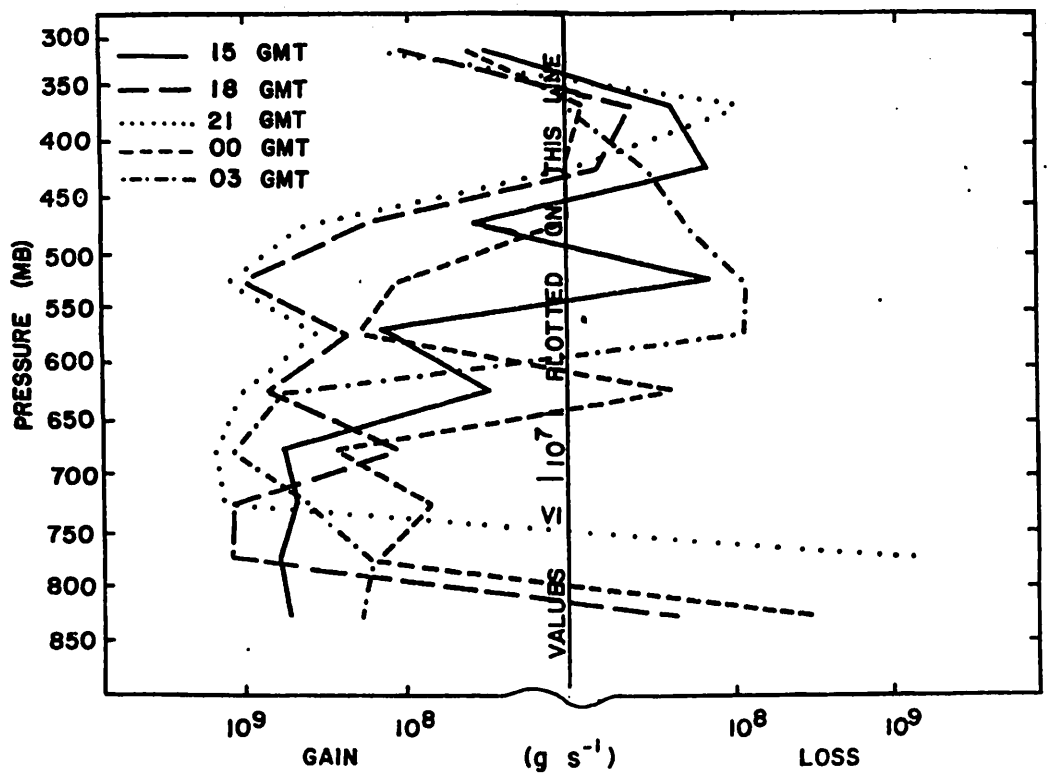

Fig. 5.21.5.4 Combined net horizontal and vertical transport of water vapor through boundaries of 50-mb layers (gm s^{-1}) over the Texas HIPLEX area for 21 July 1978.

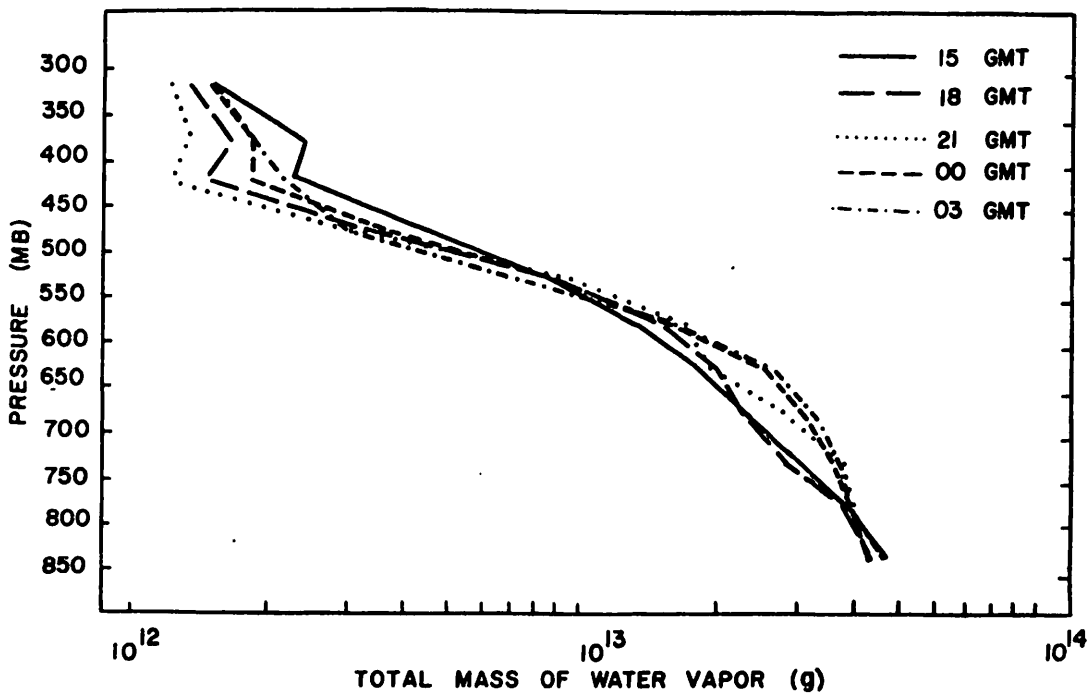

Fig. 5.21.5.5 Total mass of water vapor in layers 50 mb deep (gm) over the Texas HIPLEX area on 21 July 1978.

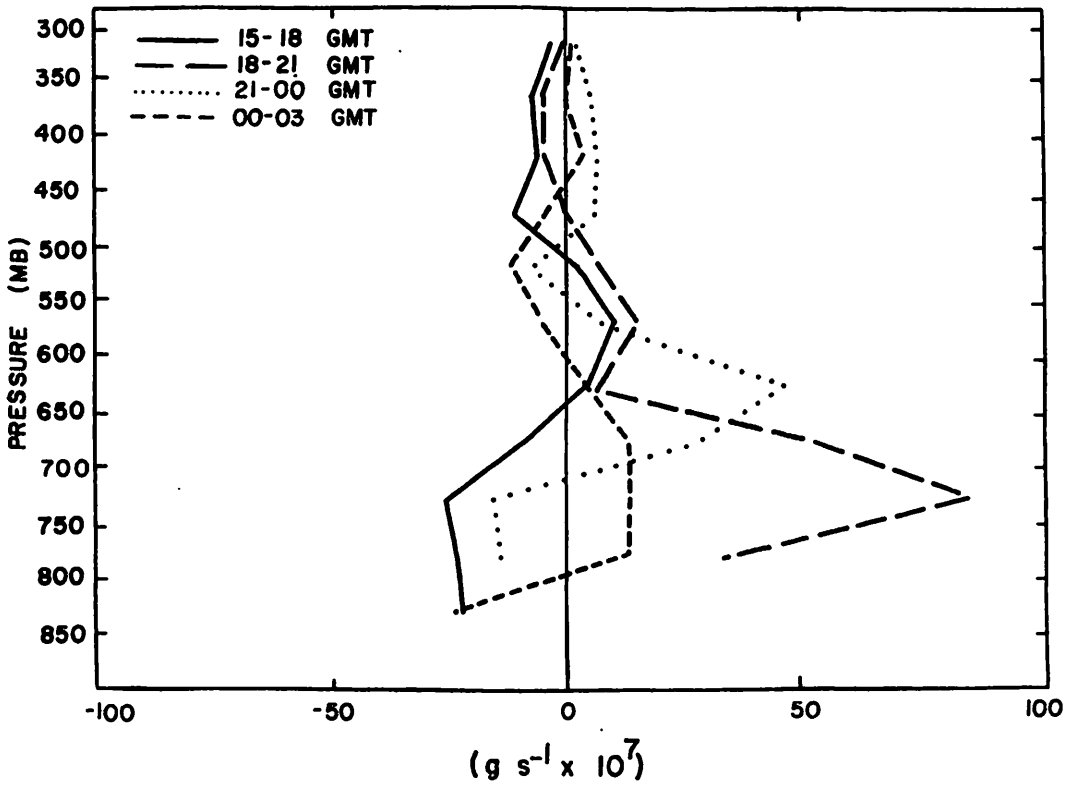

Fig. 5.21.5.6 Local rate-of-change in total mass of water vapor ($g\ s^{-1} \times 10^7$) for the Texas HIPLEX area for 21 July 1978.

5.22 22 July 1978

5.22.1 Radar

Radar echoes formed rapidly in the network between 1800 and 1900 GMT and continued until 0300 GMT (Fig. 5.22.1.1). The greatest activity was between 1900 and 0000 GMT and several echo tops were measured over 16 km (50K ft). Storm clusters usually persisted for about two hours, formed rapidly, and appeared to move to the west or southwest.

5.22.2 Surface

Surface fields were highly affected by thunderstorms. Temperature dropped as much as 7°C as the first downdraft occurred near Snyder and Walsh-Watts at 2000 GMT (Fig. 5.22.2.1). Temperatures dropped in many parts of the network from downdraft effects. Pre-development temperatures were near 34°C at 1900 GMT, but at 2200 GMT which is normally the warmest time of the day, temperatures varied from 22 to 36°C.

Temperature minima corresponded fairly well with thunderstorm locations. Particularly evident was the persistence of temperature minima after downdraft influence. The dissipation of a thunderstorm echo at Snyder at 2200 GMT (see surface wind in Fig. 5.22.2.12 and velocity divergence in Fig. 5.22.2.6) led to a relative temperature minimum between Snyder, Gail, and Vincent which continued through 0000 GMT. In addition, surface winds indicated the location of a downdraft which resulted from an echo over Gail at 2100 GMT and led to a relative temperature minimum near that station. That temperature minimum was distinct until 0200 GMT, when temperature decreased throughout the network.

Temperature minima were more strongly associated with the dissipation of radar echoes in the network than with the existence of strong echoes. Category 3 echoes which occurred from 2000 to 2300 GMT fail to produce large temperature minima until they reduced into Category 2 echoes.

Dewpoint-depression fields (Fig. 5.22.2.2) delineate a large area which is very near saturation and is coincident with the low-temperature, high-mixing ratio area associated with downdrafts. Near saturation is not achieved, however, until several hours after downdrafts begin. This suggests that persistent, near-saturation conditions at the surface are a product of the interaction between several precipitation areas rather than effects from a single storm.

NO ECHOES

NO ECHOES

NO ECHOES

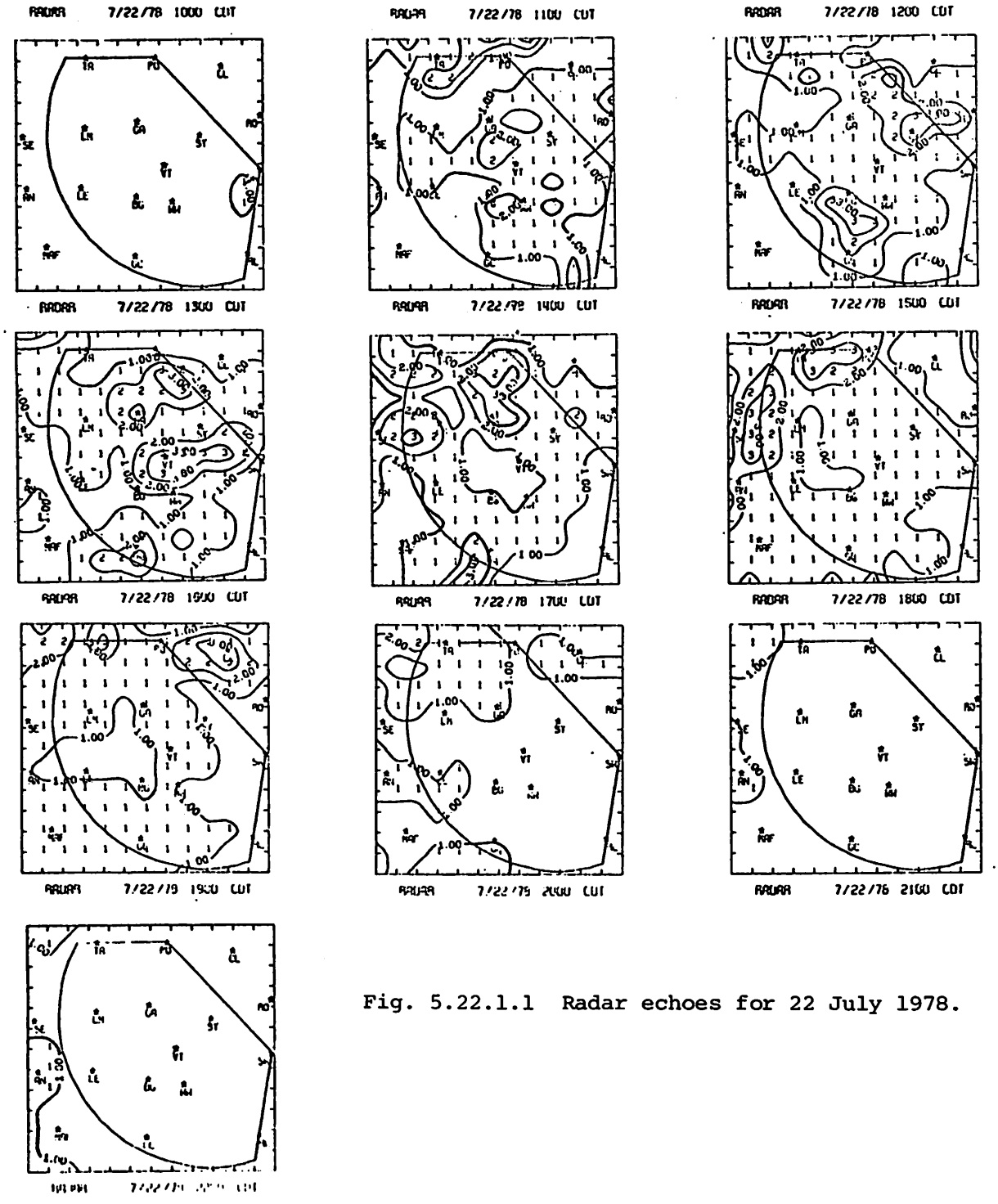

Fig. 5.22.1.1 Radar echoes for 22 July 1978.

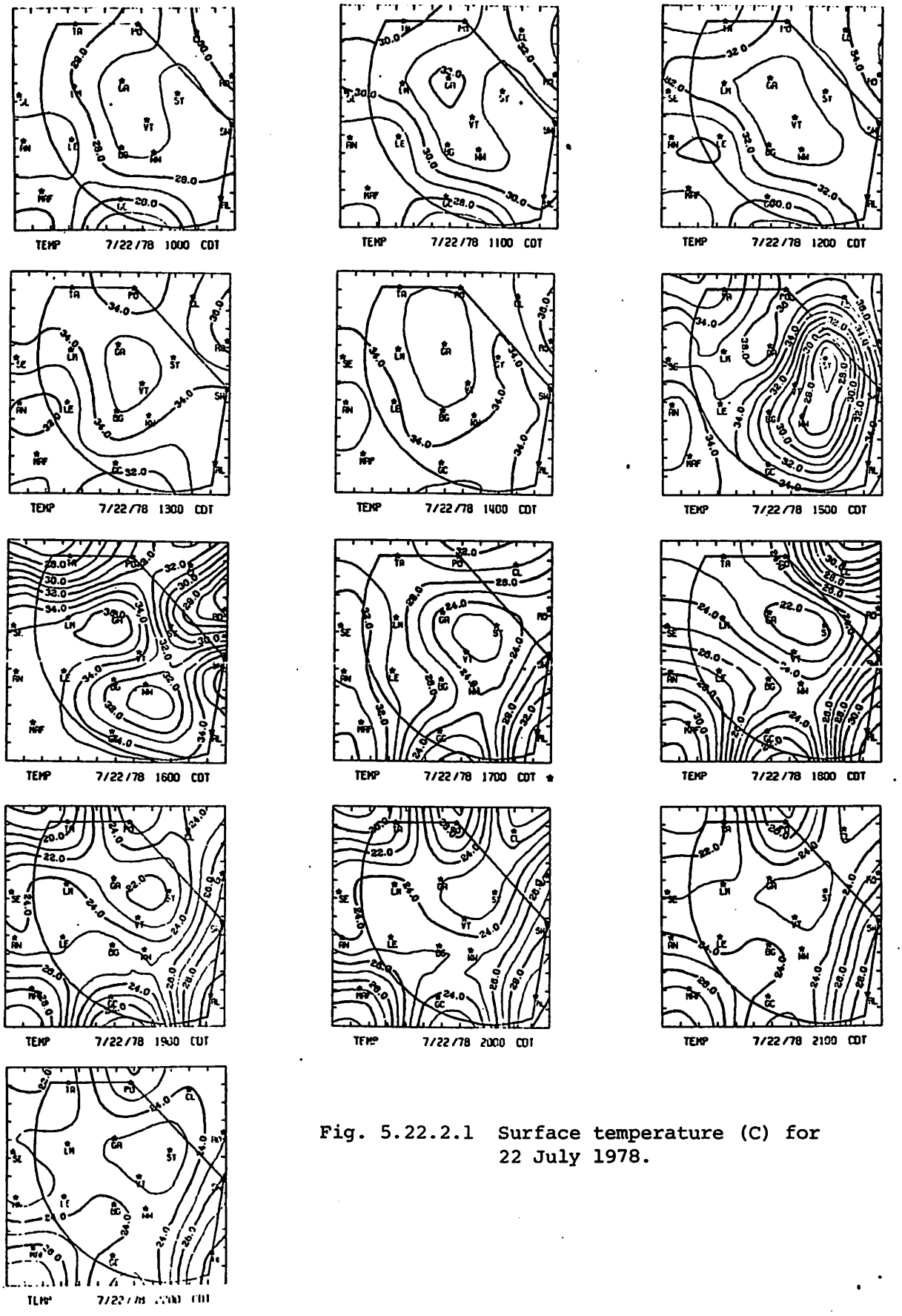

Fig. 5.22.2.1 Surface temperature (C) for 22 July 1978.

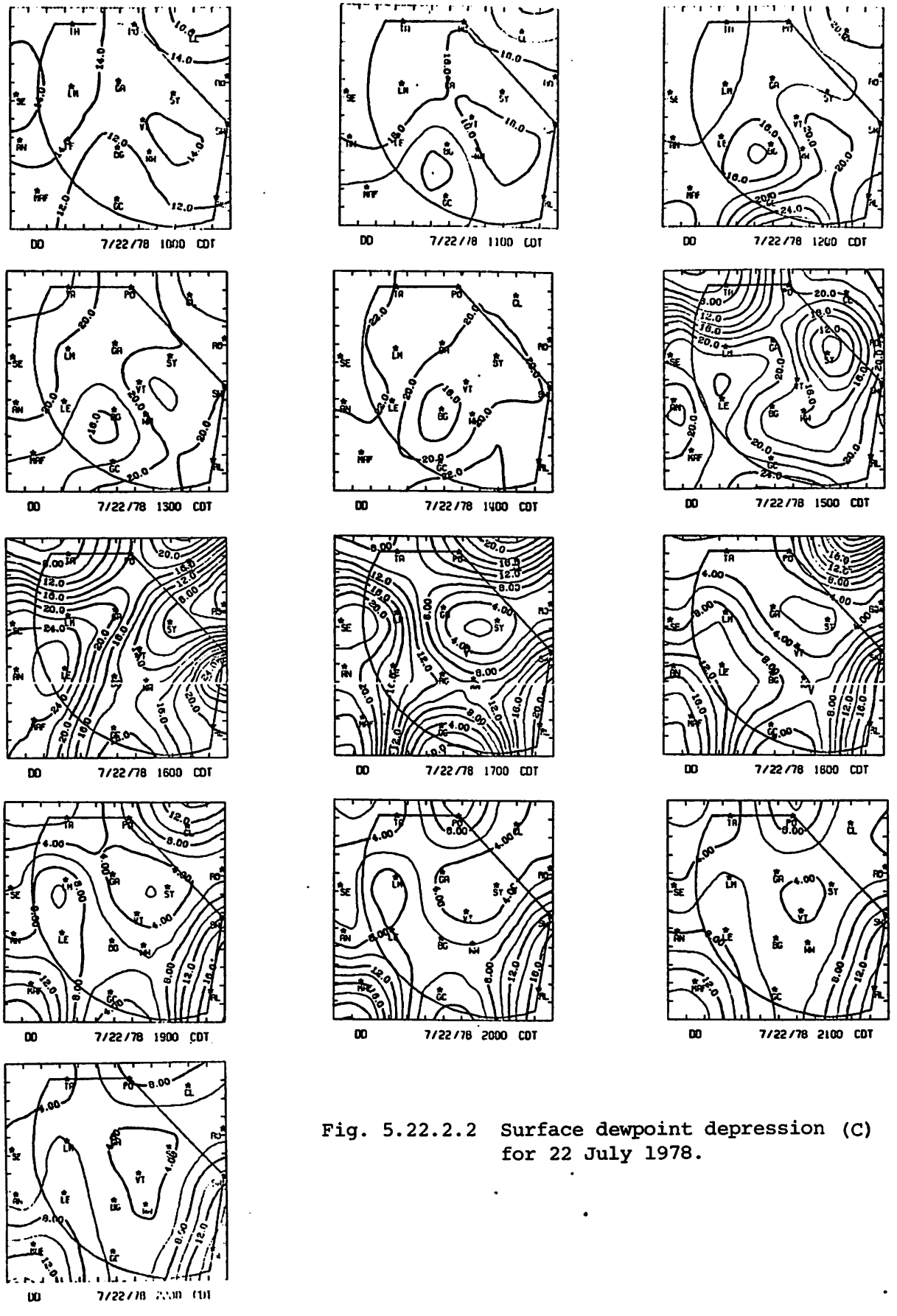

Fig. 5.22.2.2 Surface dewpoint depression (C) for 22 July 1978.

A humidity anomaly at Big Spring was observed until 1900 GMT. Moisture increases at other stations were well correlated with echo location, and usually well correlated with temperature minima. At 2000 GMT a large mixing ratio maximum at Tahoka reflects the dissipation of an echo which is barely inside the network at 1900 GMT (Fig. 5.22.2.3). The mixing ratio did not change in the low-temperature area from Snyder to Walsh-Watts, however, until the next hour. With the exception of these two cases, the location of temperature and mixing ratio fields coincide.

High equivalent potential temperature occurred in areas where mixing ratio and temperature were high. These regions exist predominantly where moisture increases were observed before temperature decreased due to cool downdrafts. Values above 370°K are calculated for three such regions--one over Tahoka at 2000 GMT, one over Gail at 2100 GMT, and another near Vincent at 2100 GMT (Fig. 5.22.2.4). Regions such as these fail to occur after 2100 GMT as moisture and temperature fields become more uniform.

Centers of terrain-induced vertical velocities with large magnitudes were formed primarily from winds which result from thunderstorm proximity in areas of large terrain-height gradients (Fig. 5.22.2.5). An area of downward motion occurred between Walsh-Watts and Robert Lee until 2100 GMT, and attained a maximum value of -3 cm sec^{-1} at 2000 GMT. A center of upward motion occurred adjacent to Robert Lee during most of the day, and reached 4 cm sec^{-1} at 2100 GMT. Large wind speeds on the western side of the network from 2100 to 0000 GMT failed to produce significant vertical velocities due to small terrain-height gradients.

Regions of divergence were persistent in location and large in magnitude (Fig. 5.22.2.6). Weak convergence preceded the initiation of echoes at 1900 GMT. Upon the development of Code 3 radar echoes at 2000 GMT, convergence and divergence patterns of large magnitudes become juxtaposed. Features of the surface wind field (Fig. 5.22.2.12) make apparent the interaction of several thunderstorm downdrafts at every time period between 2000 and 2300 GMT. Particularly after 2000 GMT, widespread regions of positive divergence and minimum temperatures (Fig. 5.22.2.1) appear coincident. This lends strong support to the idea that settling of cool downdraft air leads to large areas of surface divergence. Profiles of upper-level mass divergence (Fig. 5.22.3.1) support this explanation by showing that layers immediately above the surface layer are strongly convergent at 2100, 0000, and 0300 GMT.

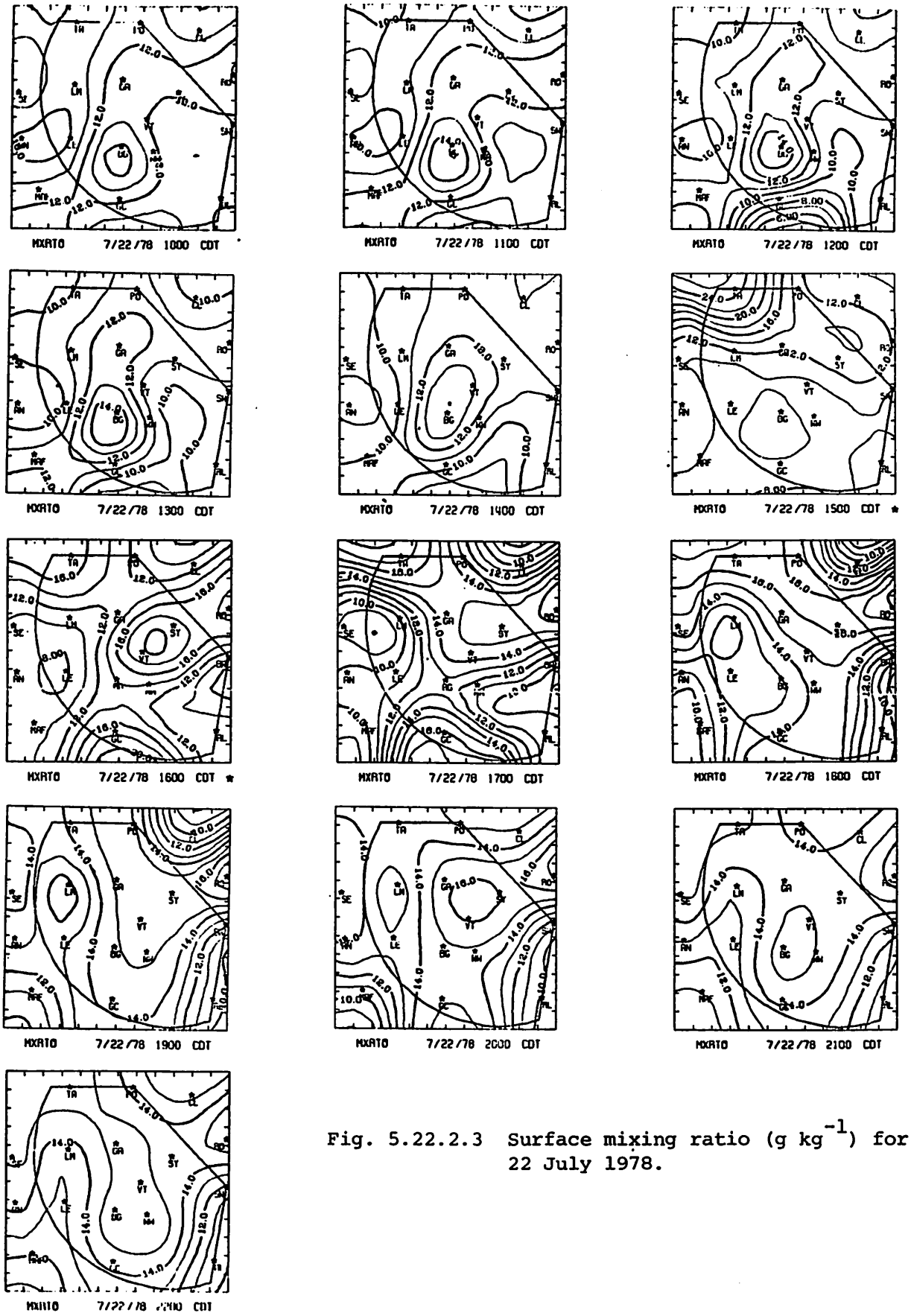

Fig. 5.22.2.3 Surface mixing ratio (g kg^{-1}) for 22 July 1978.

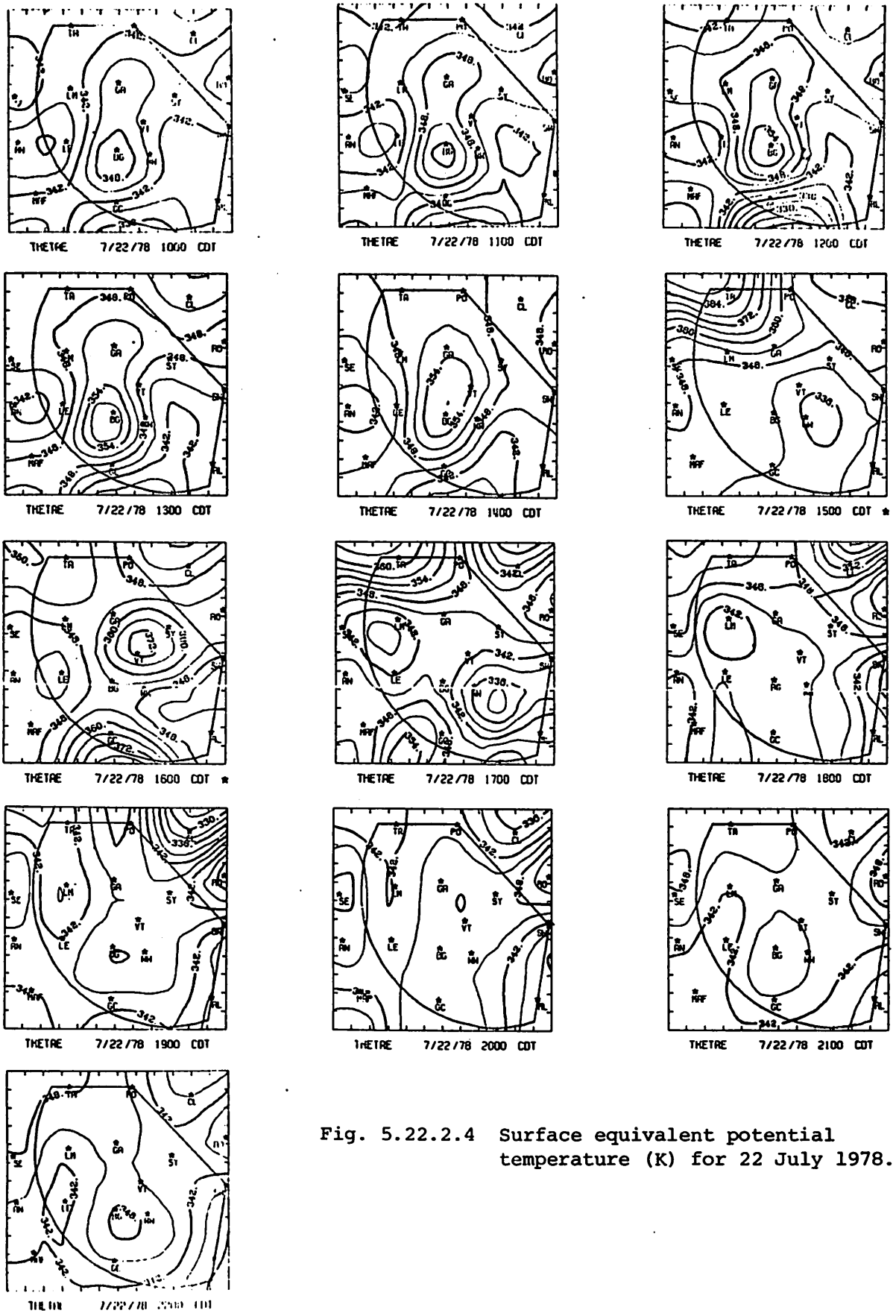

Fig. 5.22.2.4 Surface equivalent potential temperature (K) for 22 July 1978.

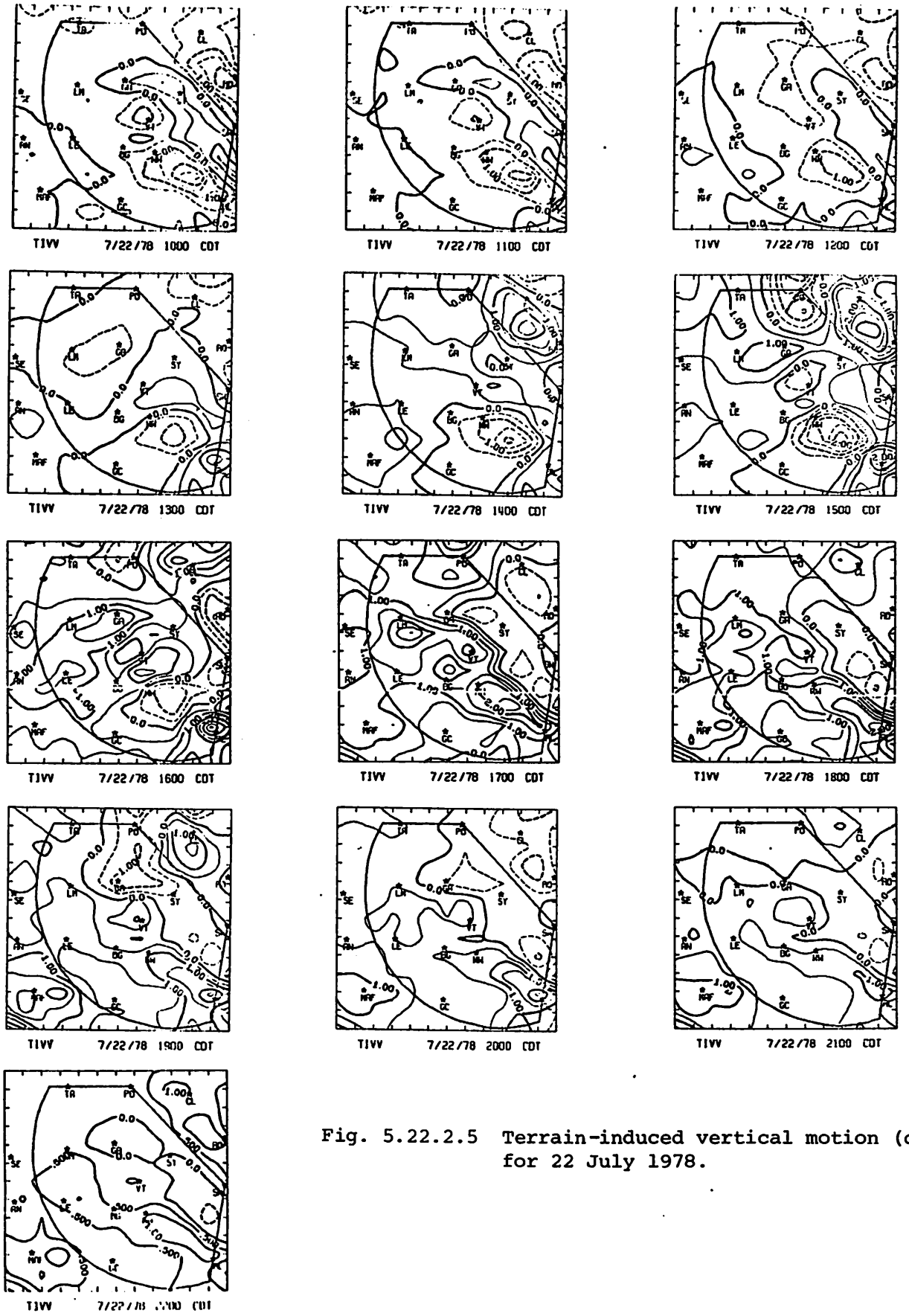

Fig. 5.22.2.5 Terrain-induced vertical motion (cm s^{-1}) for 22 July 1978.

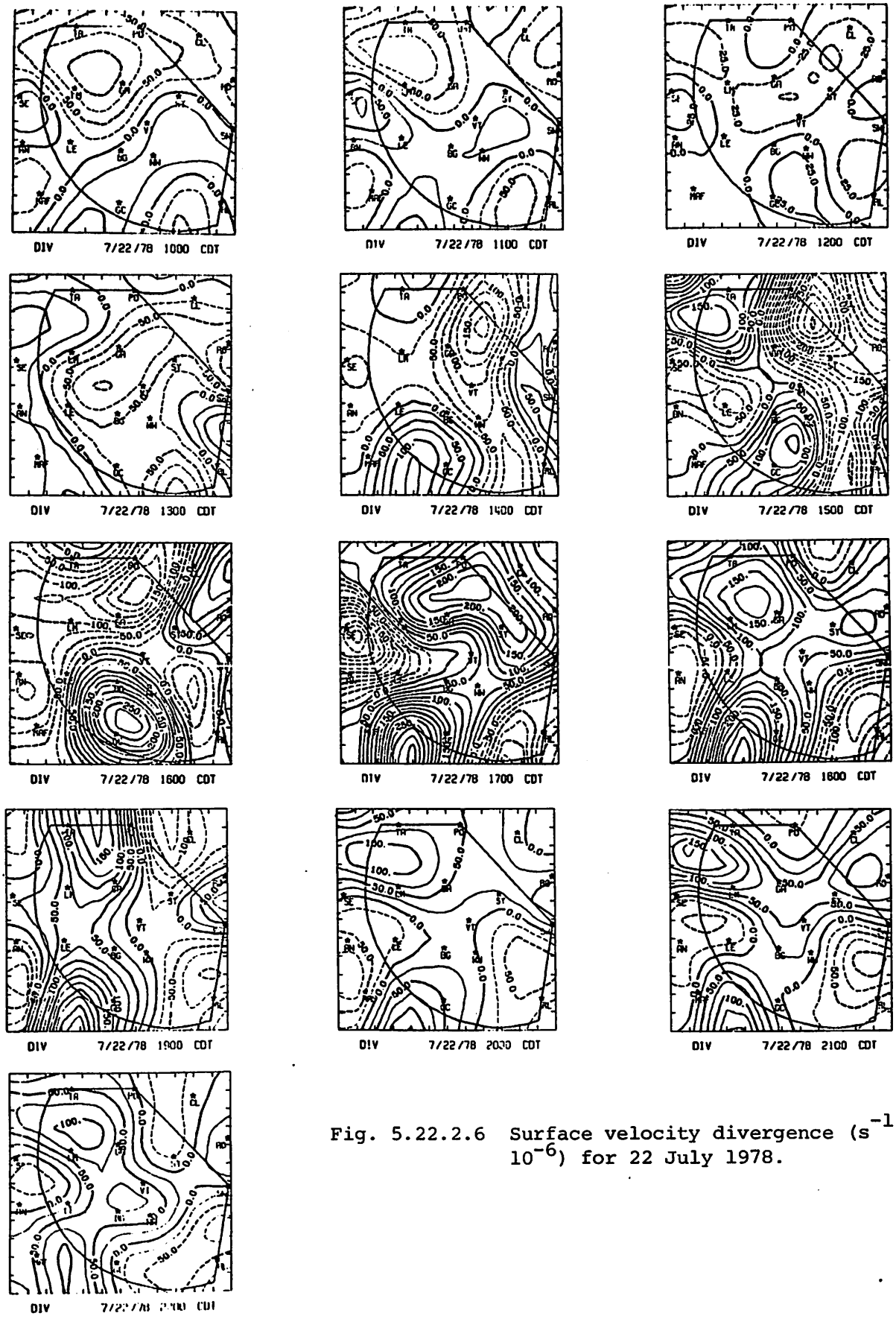

Fig. 5.22.2.6 Surface velocity divergence (s^{-1} x 10^{-6}) for 22 July 1978.

Therefore, the mean surface wind field appears to be thermally induced after 2100 GMT while thunderstorm downdrafts cause perturbations to that flow.

Because regions of positive divergence coincide with areas of cool, moist air, and convergent areas coincide with regions of dry air, areas of surface moisture divergence are much stronger than areas of surface moisture convergence (Fig. 5.22.2.8). This is evident in patterns of moisture divergence which occur from 2100 to 0000 GMT. After 2300 GMT relatively small values of moisture divergence occurred throughout the network.

Planetary boundary layer vertical velocities (Fig. 5.22.2.7) and vertical moisture flux (Fig. 5.22.2.9) reflect the tendencies of divergence and moisture divergence, respectively. Vertical velocities of ± 10 μbars sec^{-1} were generated in strongly divergent or convergent areas. Similarly, strong centers of vertical moisture flux occurred where moisture and divergence were large.

Vorticity centers (Fig. 5.22.2.10) with large magnitudes were generated by the interaction of thunderstorm downdrafts and with the environmental surface wind field. The strongest centers occurred between 1900 and 0000 GMT, when the most downdrafts occurred. Some of the vorticity centers persisted up to 5 hr.

Pressure changes over a 1-hr period (Fig. 5.22.2.11) correlate well with large drops in temperature (Fig. 5.22.2.1). Pressure falls were recorded over most of the network at 2000 GMT, except that Snyder and Walsh-Watts experienced large temperature decreases. The pressure field reacted over the following hour, however, and at 2100 GMT Snyder and Rotan recorded a pressure rise of 1.0 mb.

Then, at 2200 GMT, along with a temperature drop of 12°C, the pressure at Gail rose 2.5 mb. Pressure also rose 1.5 mb at Seminole from 2200 to 2300 GMT in response to a temperature decrease of 7°C. Pressure rises of more than 1 mb hr^{-1} also occurred at Clairemont at 0100 GMT and at Midland at 0200 GMT. However, temperature falls at those stations were only on the order of 2-3°C hr^{-1}.

The surface wind field (Fig. 5.22.2.12) has already been related to changes in values of other surface parameters. Early in the day the flow was

Fig. 5.22.2.7 Vertical motion 50 mb above the surface (μbars s^{-1}) for 22 July 1978.

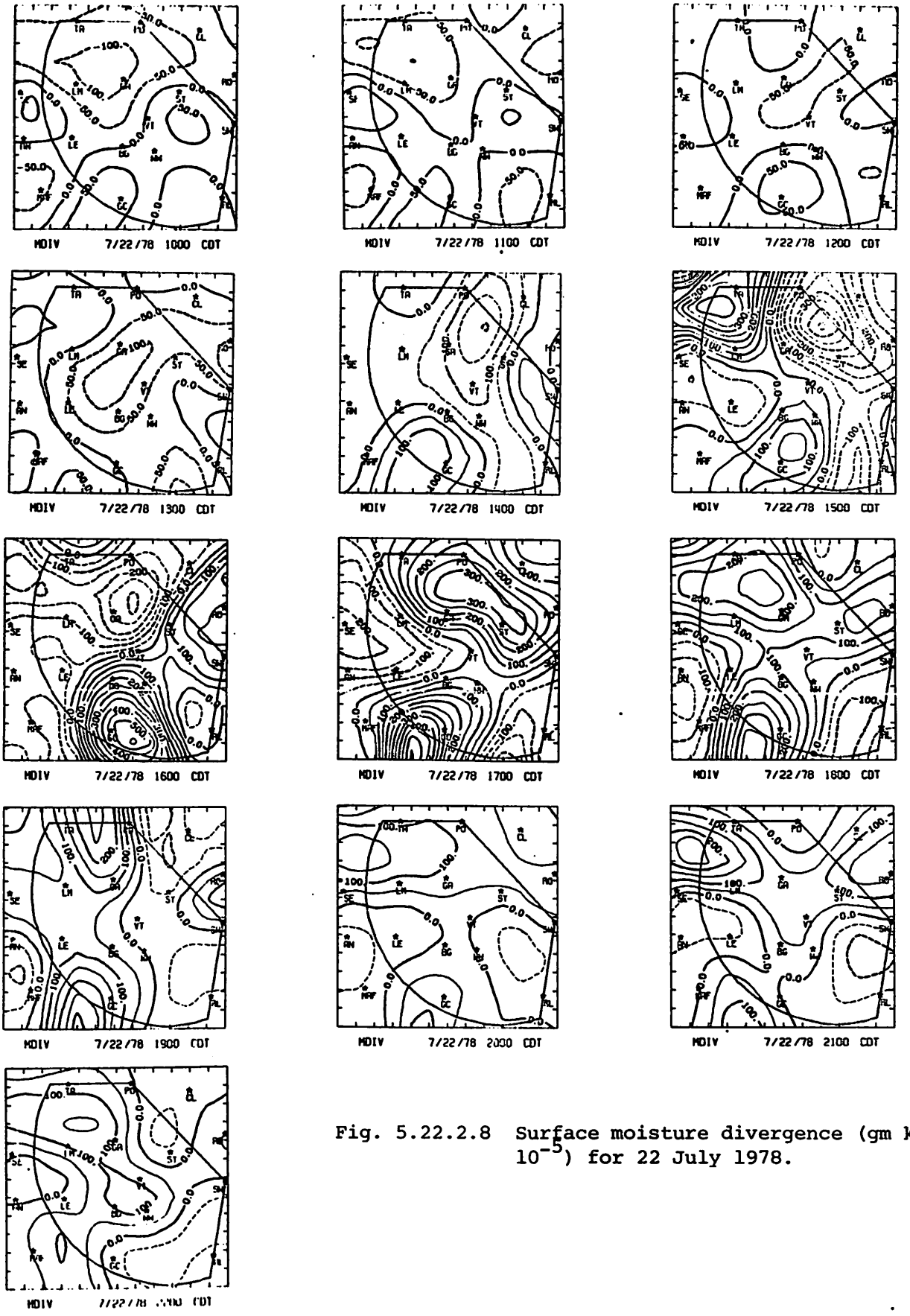

Fig. 5.22.2.8 Surface moisture divergence (gm kg^{-1} s^{-1} x 10^{-5}) for 22 July 1978.

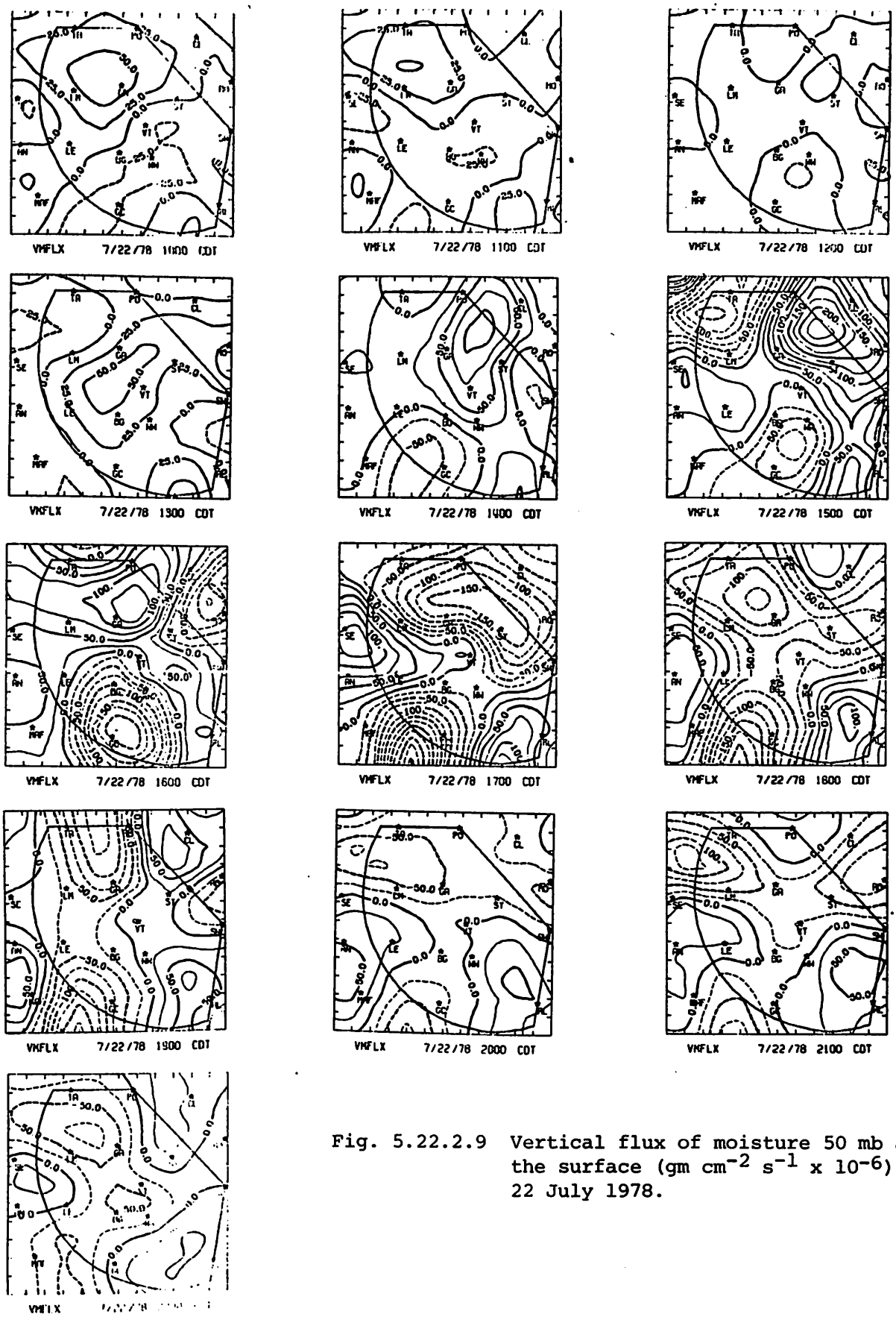

Fig. 5.22.2.9 Vertical flux of moisture 50 mb above the surface (gm cm^{-2} s^{-1} x 10^{-6}) for 22 July 1978.

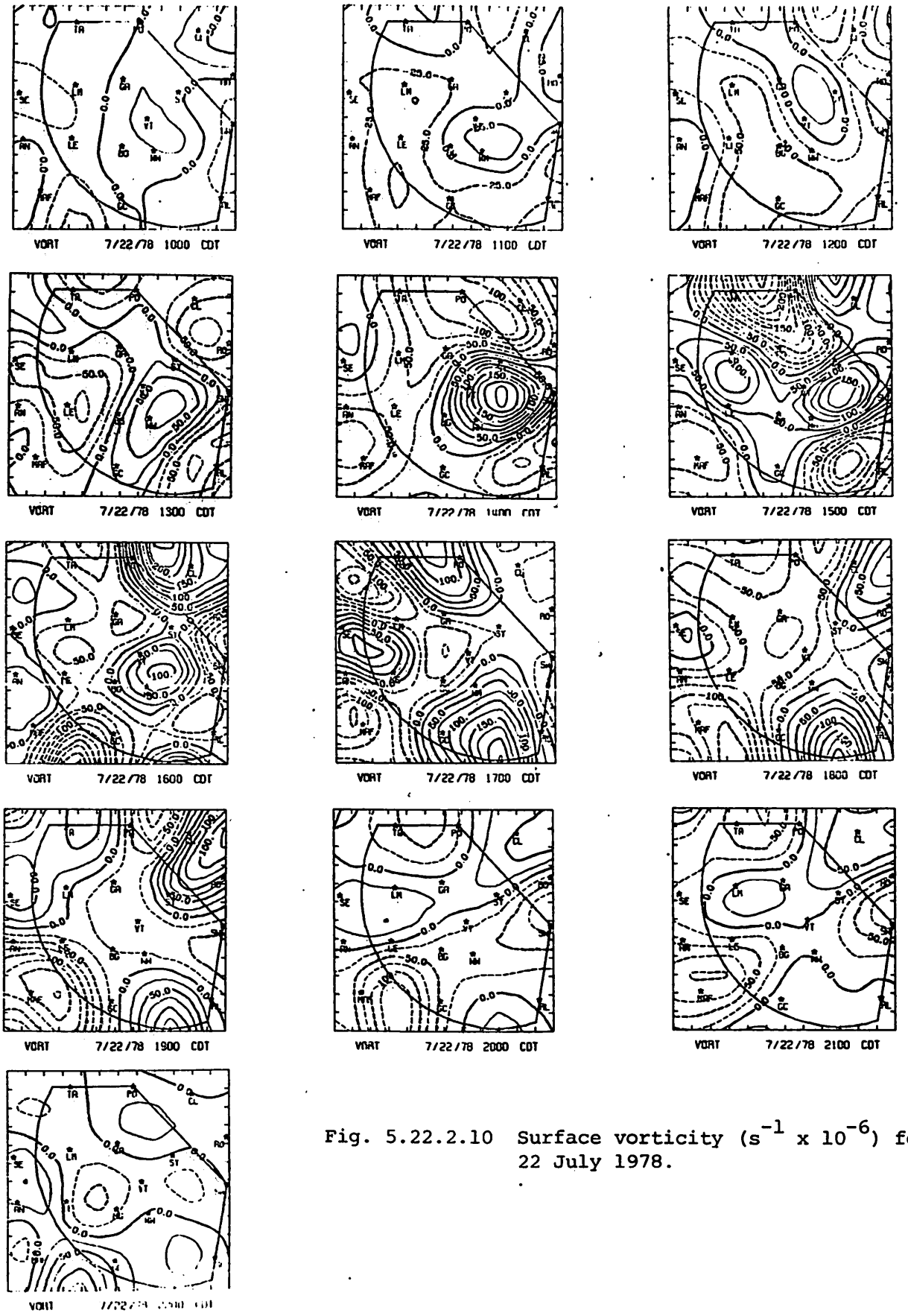

Fig. 5.22.2.10 Surface vorticity ($s^{-1} \times 10^{-6}$) for 22 July 1978.

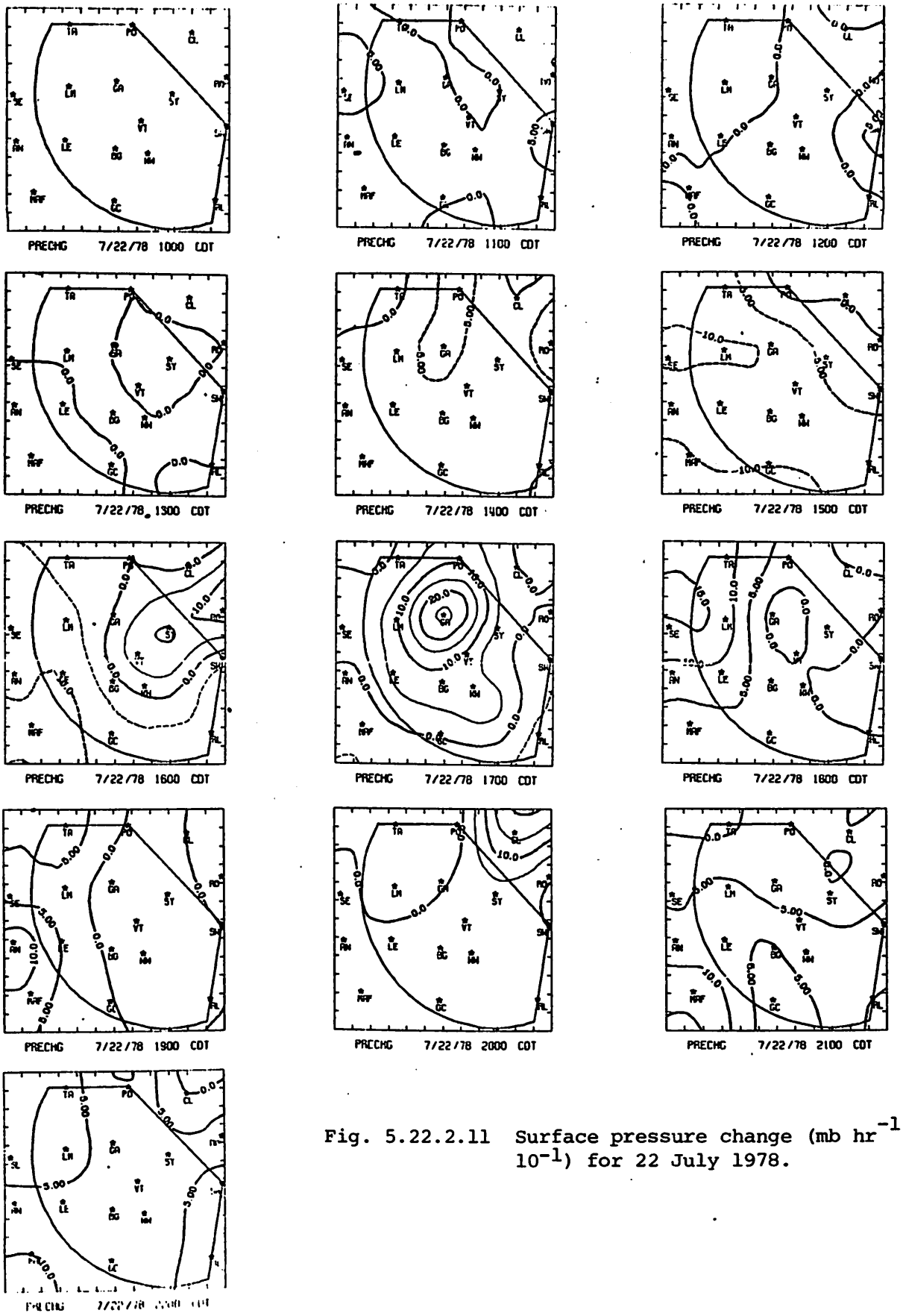

Fig. 5.22.2.11 Surface pressure change (mb hr^{-1} x 10^{-1}) for 22 July 1978.

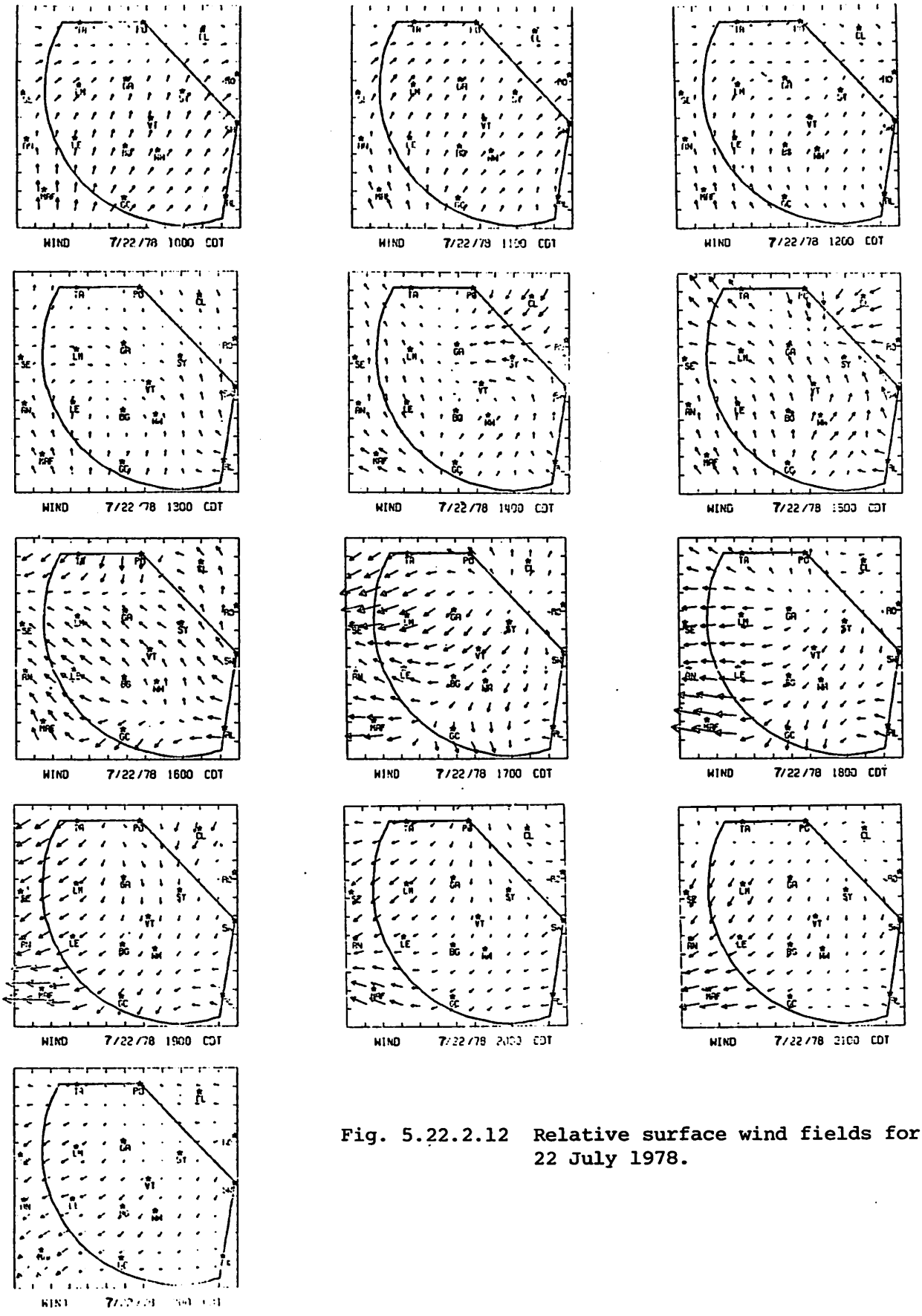

Fig. 5.22.2.12 Relative surface wind fields for 22 July 1978.

from the south, but thunderstorm influences produced strong changes in the flow during the afternoon. After most echoes had dissipated, the flow was generally from the east or northeast, and speeds had dropped to pre-development levels. Maximum wind speeds recorded were 12.8 m sec^{-1} at Lamesa at 2200 GMT, and close to 14 m sec^{-1} at Midland at 0000 GMT.

Missing wind data should be considered when interpreting fields such as divergence or vorticity, although missing data were sparse on this day. Wind data at Seminole were missing all day, and wind data at Snyder were missing from 2000 to 0300 GMT.

5.22.3 Upper-Level Kinematic Parameters

Soundings were taken at 2100, 0000, and 0300 GMT on this day.

Thunderstorm development at 2100 GMT resulted in large mass convergence below 700 mb and mass divergence above (Fig. 5.22.3.1). At 0000 GMT only Code 1 echoes remained in the computational area and mass convergence occurred throughout most of the atmosphere. No echoes were observed in the area at 0300 GMT. Magnitudes of mass divergence were not large at that time, but significant mass convergence below 800 mb was indicated.

Large values of mass convergence in the lowest layers resulted in strong upward vertical motion at 2100 and 0000 GMT, followed by moderate upward motion at 0300 GMT (Fig. 5.22.3.2). Vertical motion was greatest when strong echoes occurred in the computational area, and smallest when no echoes occurred.

Profiles of moisture divergence are similar to those of mass divergence except above 600 mb (Fig. 5.22.3.3). The magnitude of moisture divergence above that level is smaller than below 600 mb, due primarily to the decrease of water vapor with height.

5.22.4 Energetics

The horizontal flux divergence term of the latent heat energy budget shows that latent heat energy is being concentrated in the lowest layers at 2100, 0000, and 0300 GMT (Fig. 5.22.4.1). The profile at 2100 GMT shows the greatest concentration, and the 0300 GMT profile shows the least. At 2100 GMT, when the greatest thunderstorm activity was in progress, a loss of latent heat energy occurred from 700 to 500 mb.

The net change of latent heat energy due to vertical motion reflects the large vertical velocities calculated for this day (Fig. 5.22.4.2). All profiles show a loss in the lowest layers, which implies a decrease of

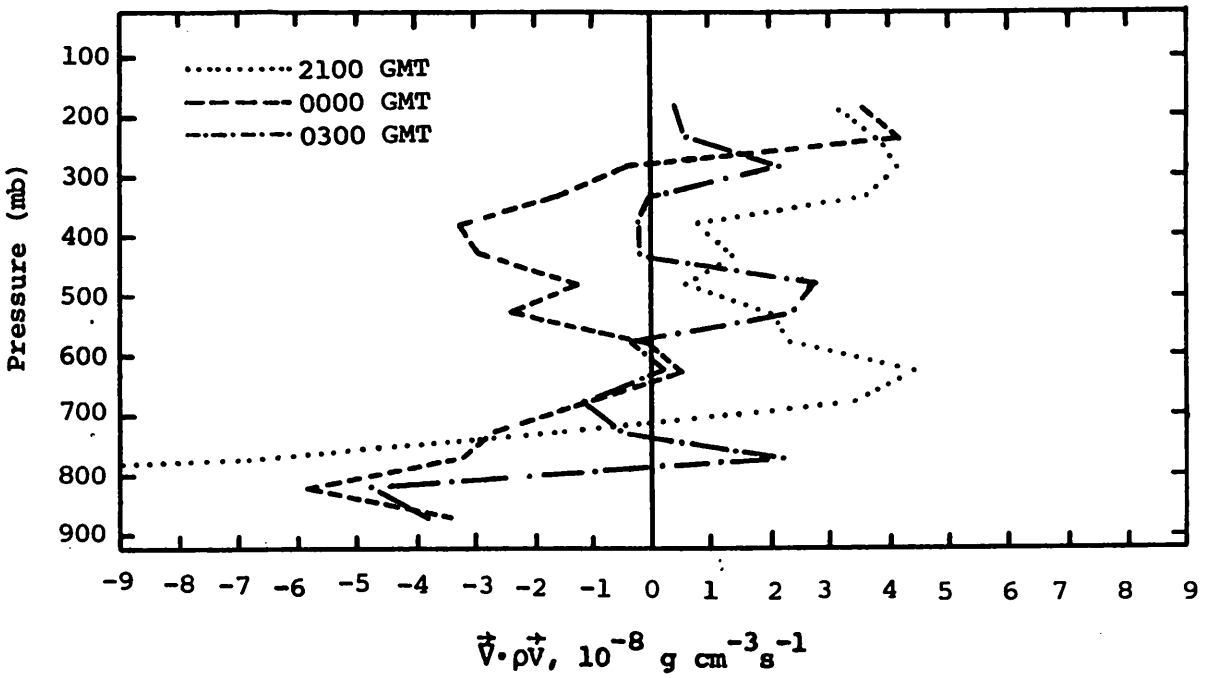

Fig. 5.22.3.1 Vertical profiles of mass divergence on 22 July 1978.

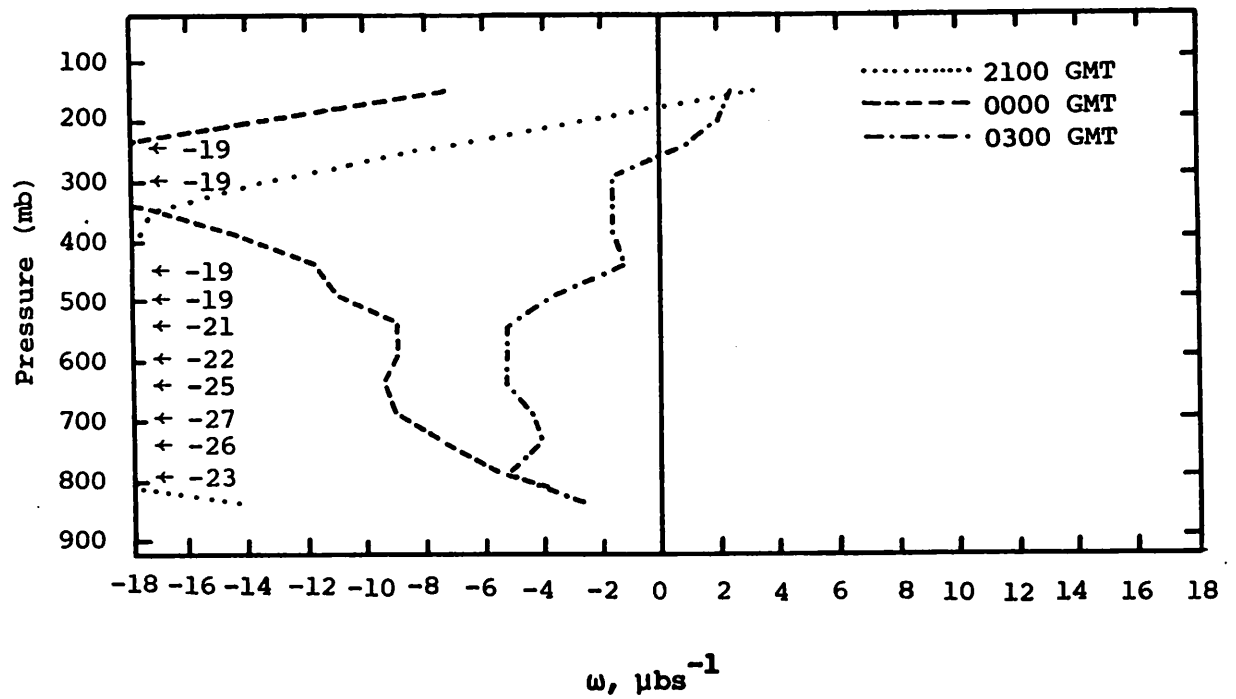

Fig. 5.22.3.2 Vertical profiles of vertical motion on 22 July 1978.

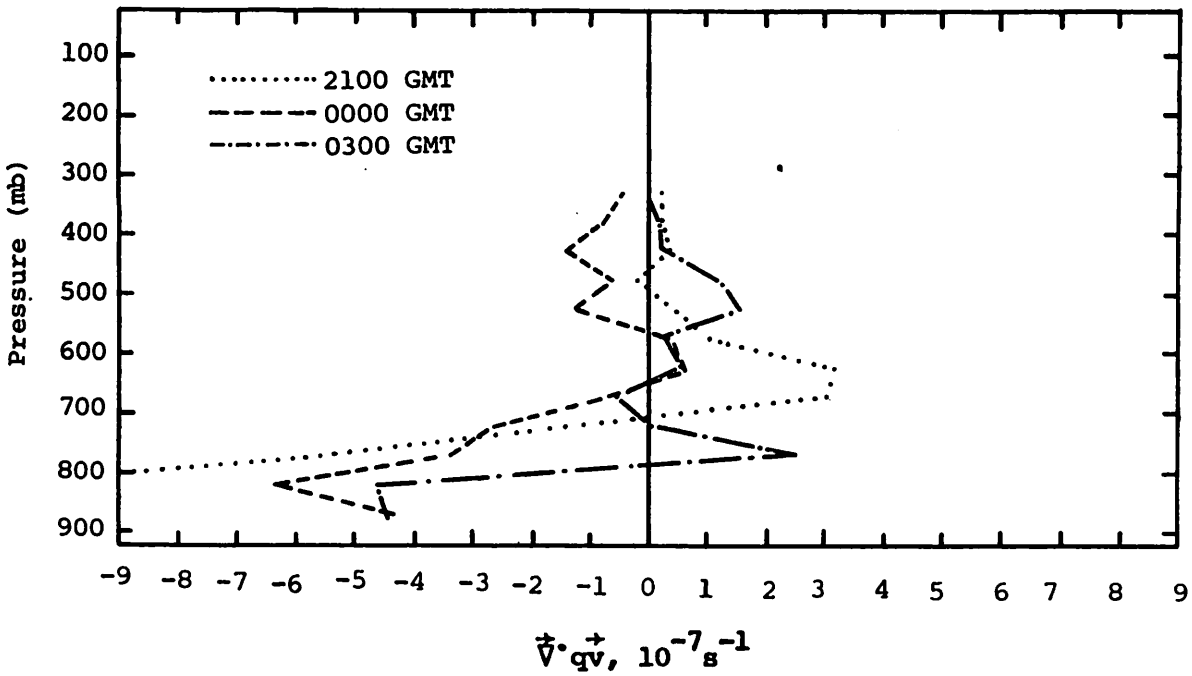

Fig. 5.22.3.3 Vertical profiles of moisture divergence on 22 July 1978.

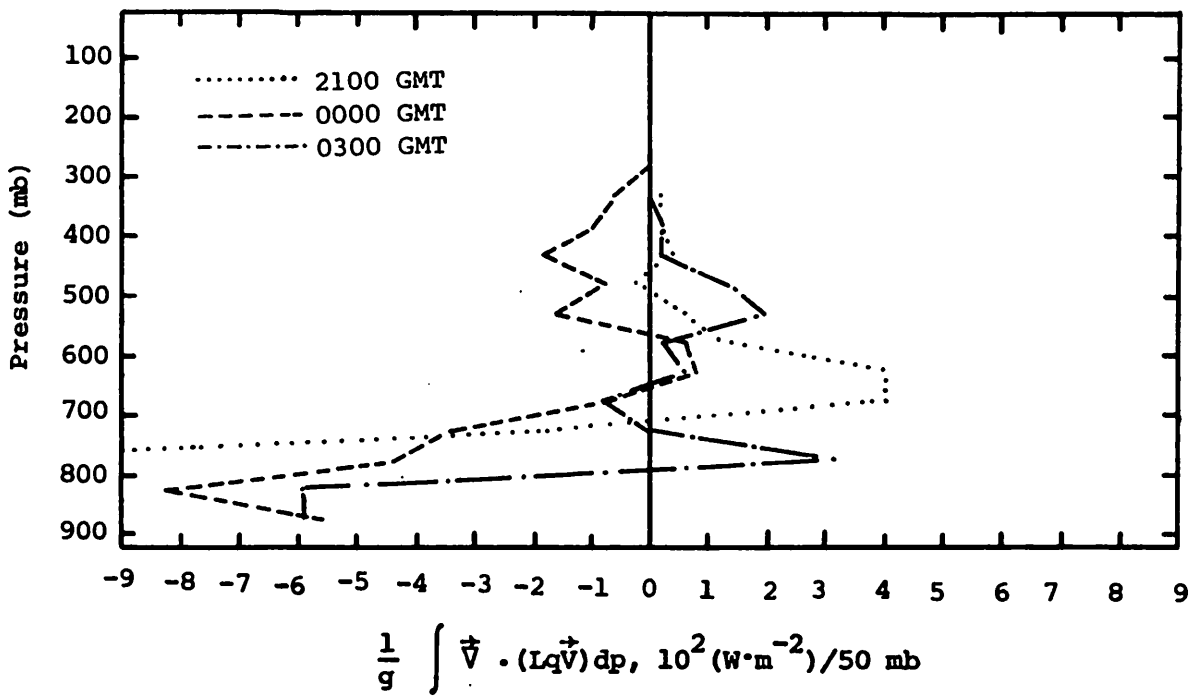

Fig. 5.22.4.1 Vertical profiles of the horizontal flux of latent heat energy on 22 July 1978.

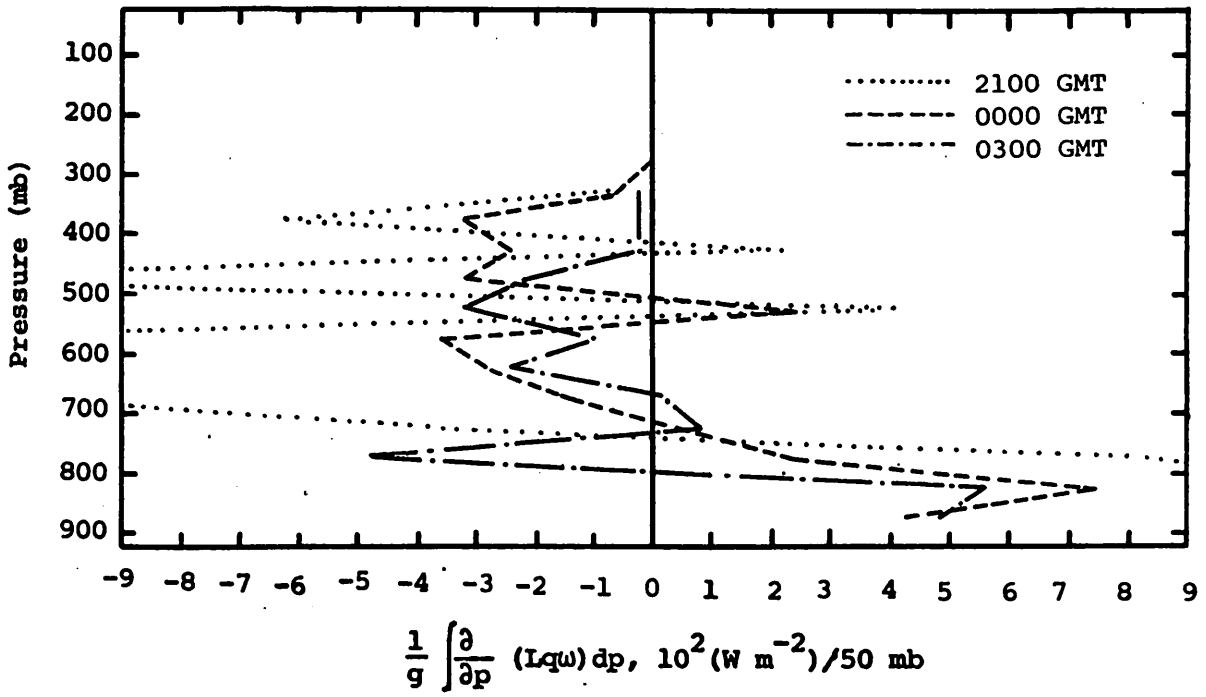

Fig. 5.22.4.2 Vertical profiles of the vertical flux of latent heat energy on 22 July 1978.

latent heat energy with height. The 2100 GMT profile has large fluctuations, but above 750 mb a concentration is observed. Profiles of 0000 and 0300 GMT conditions also show gains above 700 mb, but of a lesser magnitude.

The local rate-of-change of latent heat energy appears to be a function of the amount and strength of echoes in or around the analysis network (Fig. 5.22.4.3). A significant gain occurred in all layers at 2100 GMT, followed by a smaller gain at 0000 GMT. At 0300 GMT, small losses occurred at 800 and 500 mb, with equally small gains at other levels. Sounding profiles show saturation in thick layers of the atmosphere at 0000 and 0300 GMT, which attests to the increase of water vapor, and therefore latent heat energy, after 2100 GMT.

Figure 5.22.4.4 shows that in most layers and at most times, latent heat energy was being lost by condensation, convection, or turbulent motions. The 2100 GMT profile shows the largest loss, as large increases due to local change and vertical motion are not compensated by horizontal divergence.

The diabatic heating profile shows large heating at times with thunderstorm activity (Fig. 5.22.4.5). The 2100 GMT profile is the most extreme, with significant heating occurring above 700 mb. As thunderstorm activity

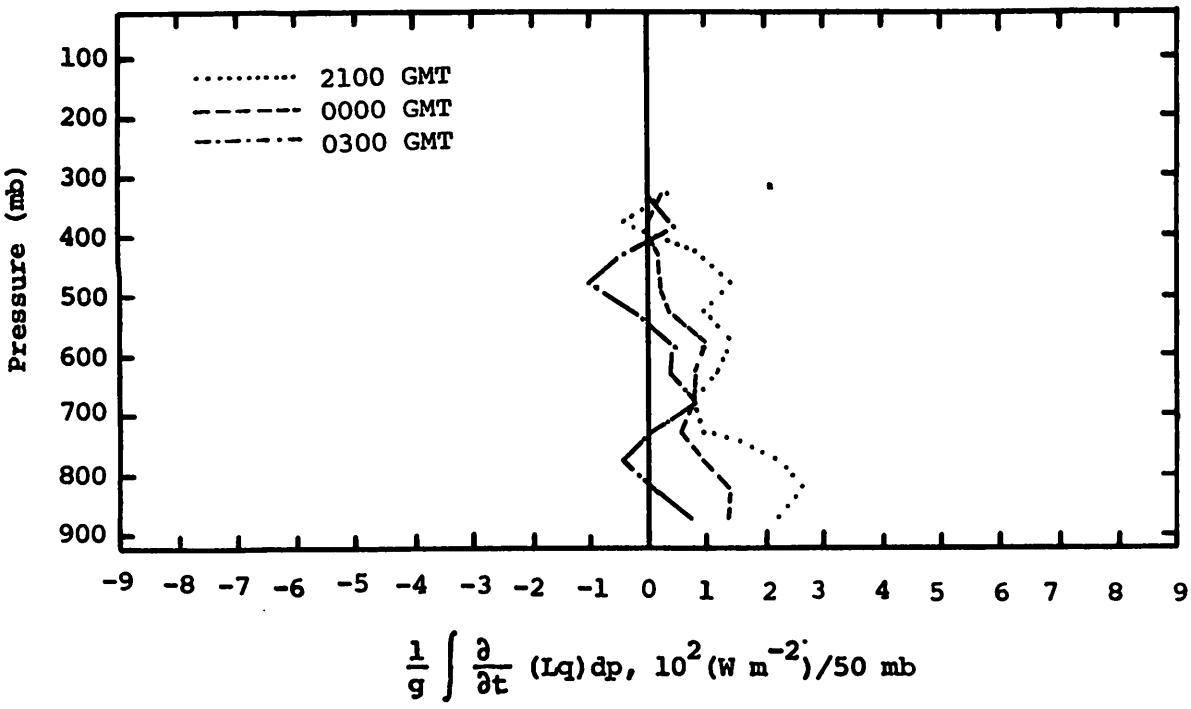

Fig. 5.22.4.3 Vertical profiles of the local change of latent heat energy on 22 July 1978.

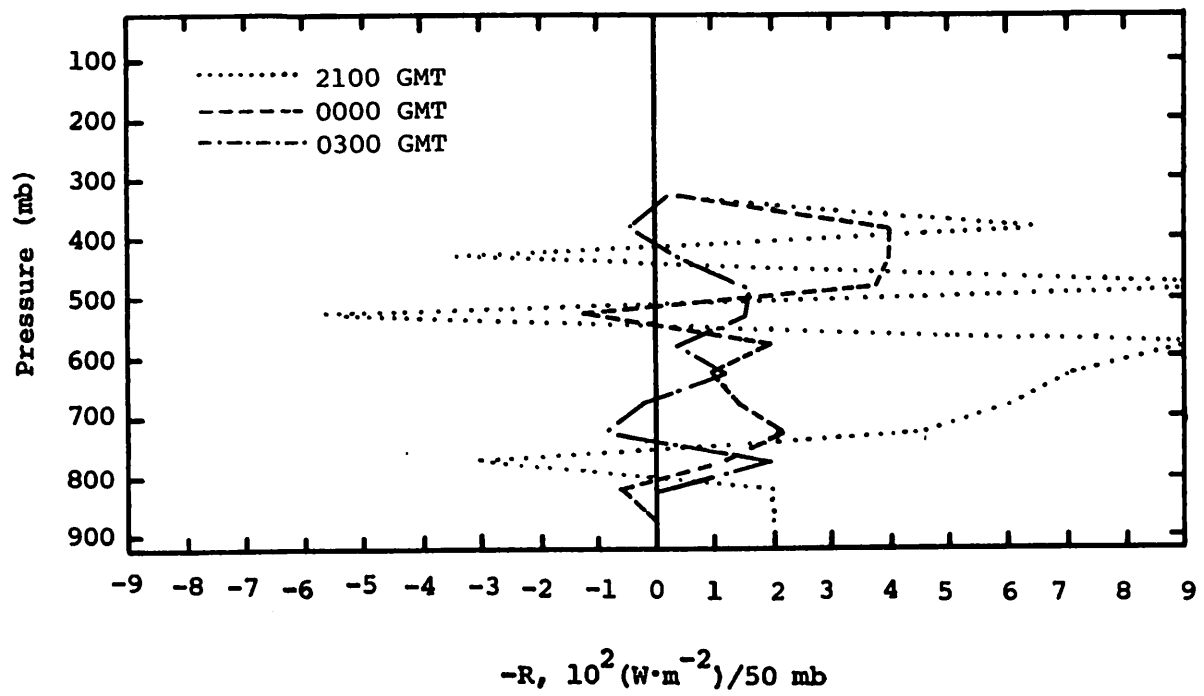

Fig. 5.22.4.4 Vertical profiles of the residual of the latent heat energy equation on 22 July 1978.

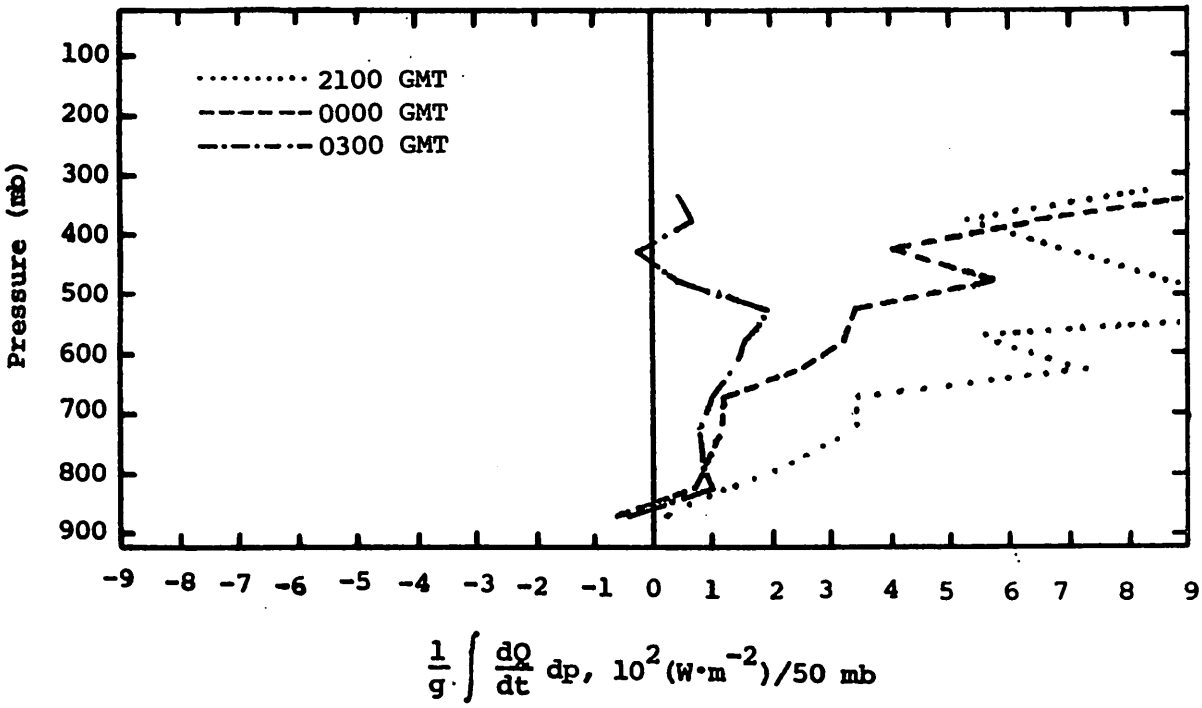

Fig. 5.22.4.5 Vertical profiles of diabatic heating computed from the first law of thermodynamics on 22 July 1978.

decreased at 0000 GMT and vanished at 0300 GMT, diabatic heating decreased significantly. The transfer of released latent heat from the thunderstorm into the environment resulted in large diabatic heating.

As on the previous day, wind speeds were small throughout most of the area. This led to small values of kinetic energy below 300 mb. The horizontal and vertical flux of kinetic energy are shown in Figs. 5.22.4.6 and 5.22.4.7, respectively. The horizontal flux term shows an export of kinetic energy above 300 mb at 2100 and 0300 GMT, which corresponds well with thunderstorm activity at those times.

5.22.5 Water Vapor Budget

Results of the water vapor budget agree with those of the latent heat energy budget by showing a net increase of water vapor in most layers from 2100 to 0300 GMT. Although profiles of net horizontal transport of water vapor (Fig. 5.22.5.1) show losses at 2100 and 0300 GMT, the net vertical transport (Fig. 5.22.5.2) more than compensates and results in a generally

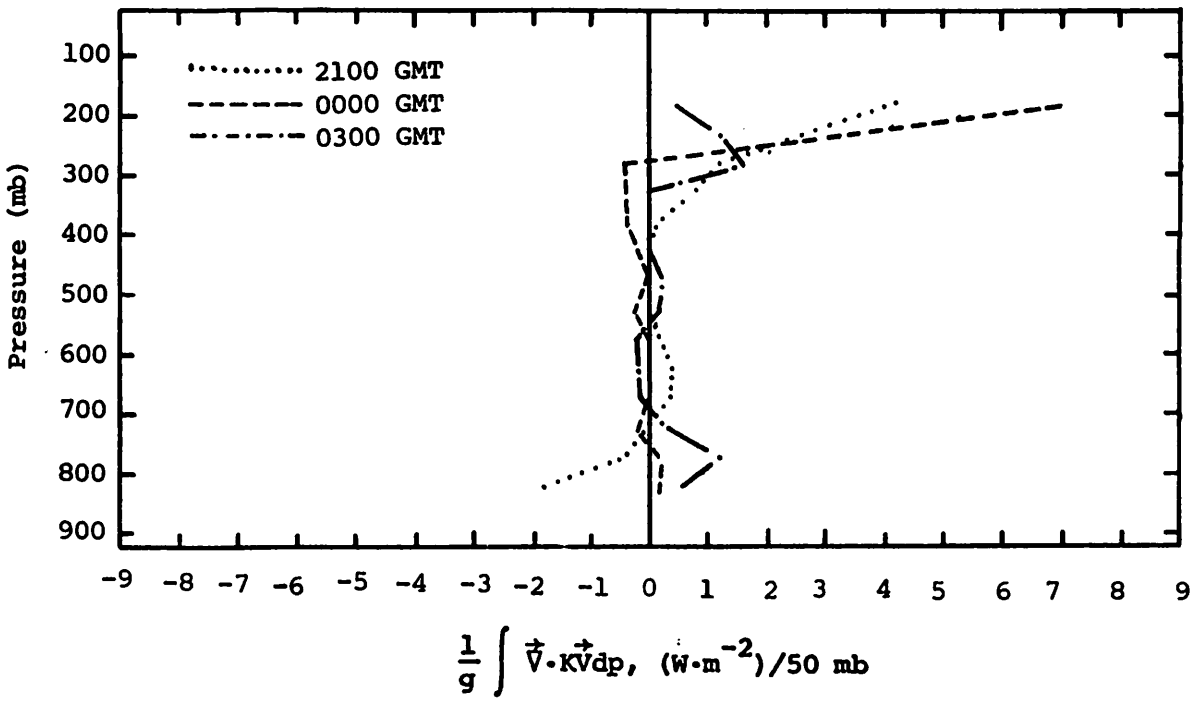

Fig. 5.22.4.6 Vertical profiles of the horizontal flux of kinetic energy on 22 July 1978.

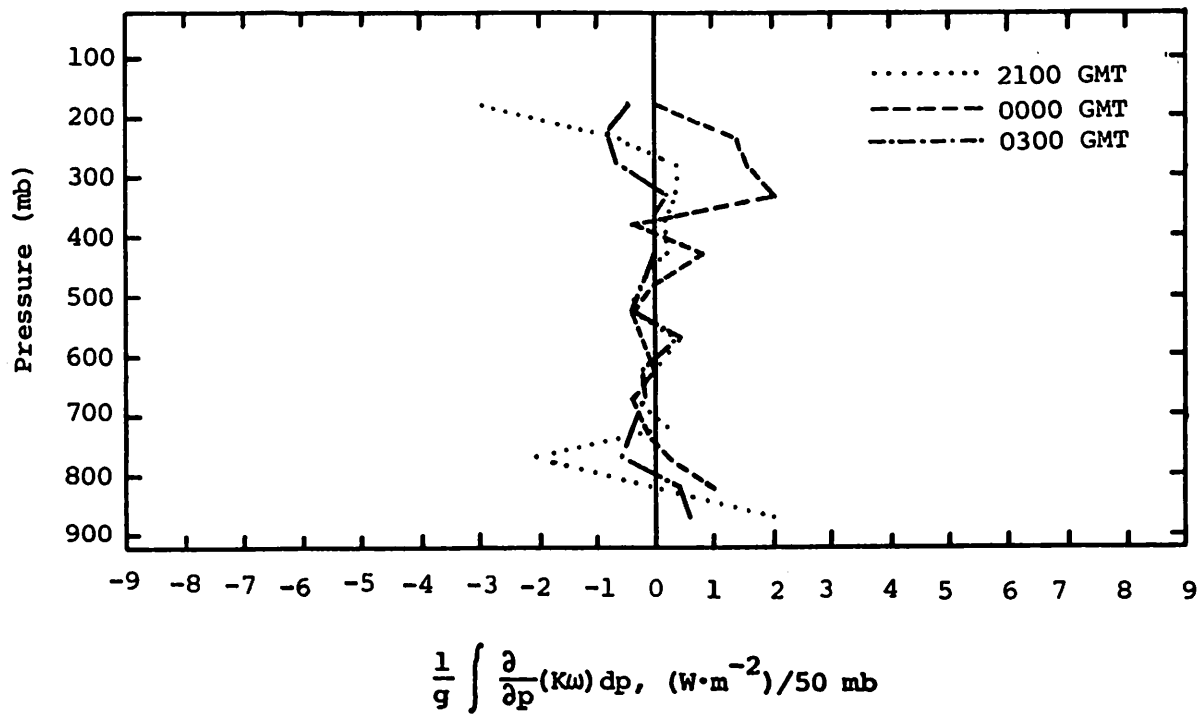

Fig. 5.22.4.7 Vertical profiles of the vertical flux of kinetic energy on 22 July 1978.

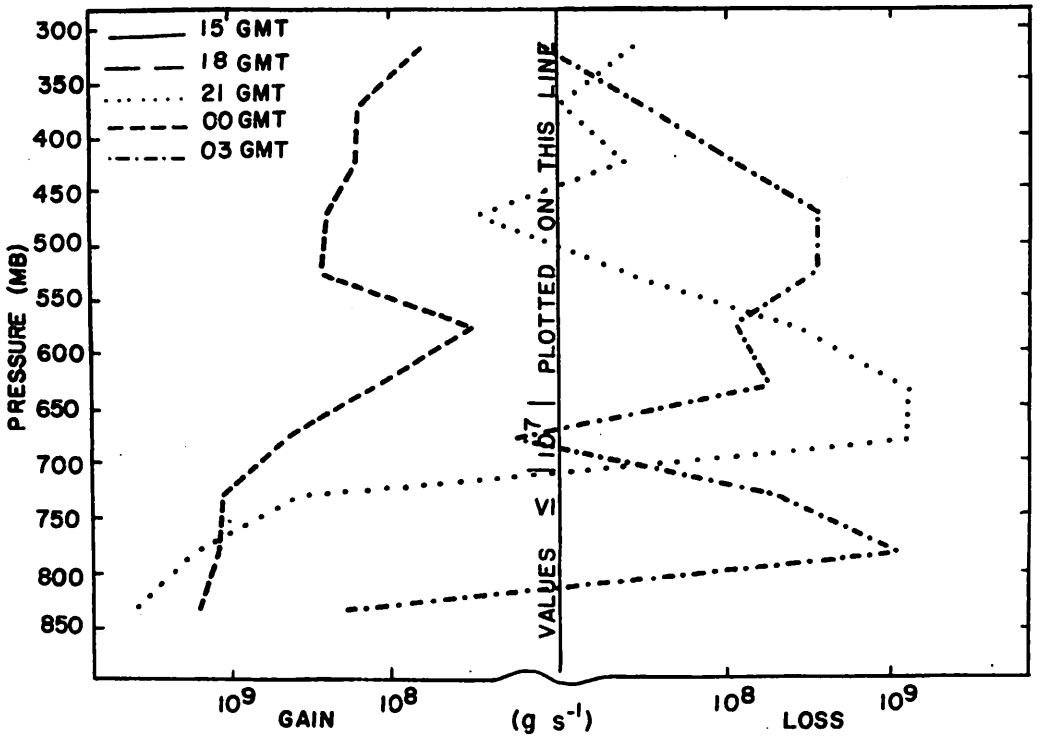

Fig. 5.22.5.1 Net horizontal transport of water vapor through boundaries of 50-mb layers (gm s^{-1}) over the Texas HIPLEX area for 22 July 1978.

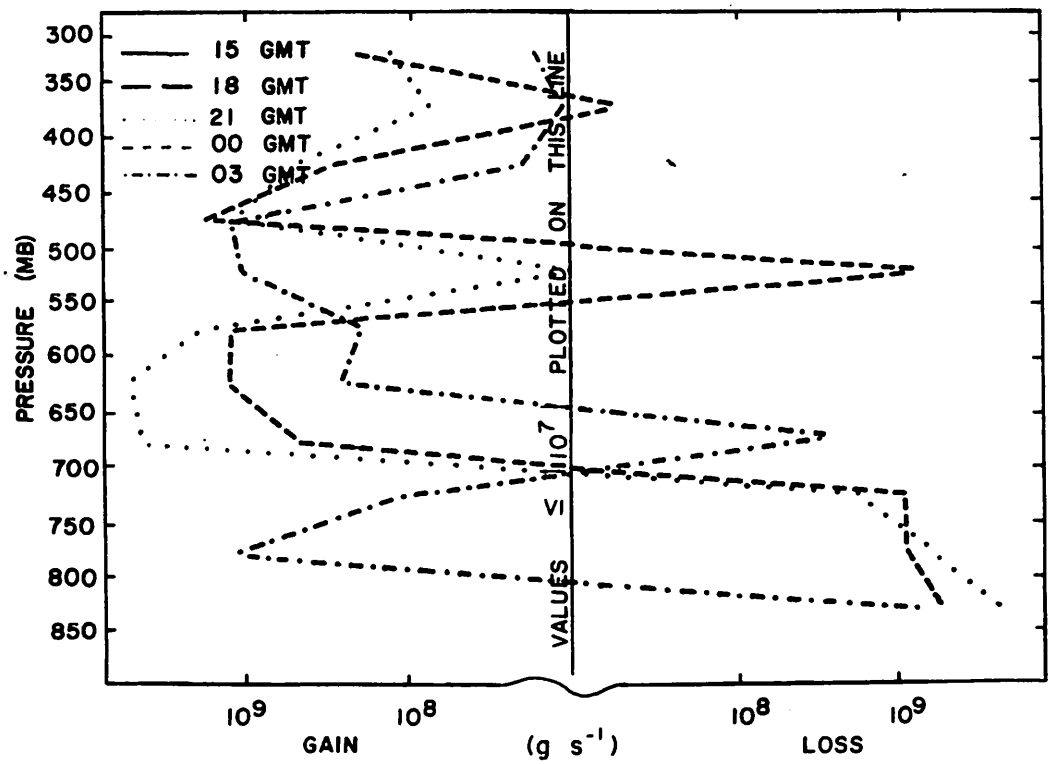

Fig. 5.22.5.2 Net vertical transport of water vapor through boundaries of 50-mb layers (gm s^{-1}) over the Texas HIPLEX area for 22 July 1978.

positive net combined transport (Fig. 5.22.5.4).

Figure 5.22.5.3 shows that water vapor is being transported upwards at all times and all levels, and results from strong vertical motion throughout the day (Fig. 5.22.3.2).

As noted earlier, saturation of substantial portions of the troposphere occurred after 2100 GMT. This is reflected in Fig. 5.22.5.5, which shows the total mass of water vapor in the HIPLEX area. Large increases occurred above 650 mb between 2100 and 0000 GMT.

The local rate-of-change of water vapor (Fig. 5.22.5.6) also supports this observation. Changes are positive at all levels from 2100 to 0000 GMT as thunderstorms dissipated. From 0000 to 0300 GMT, changes were negative from 775 to 625 mb, but positive below 775 mb and between 625 and 475 mb. At 0000 GMT, the cloud base in most soundings was generally at 700 mb, and by 0300 GMT it had risen to 650. The associated drying of the immediate subcloud layer accounts for the water vapor decrease centered at 700 mb.

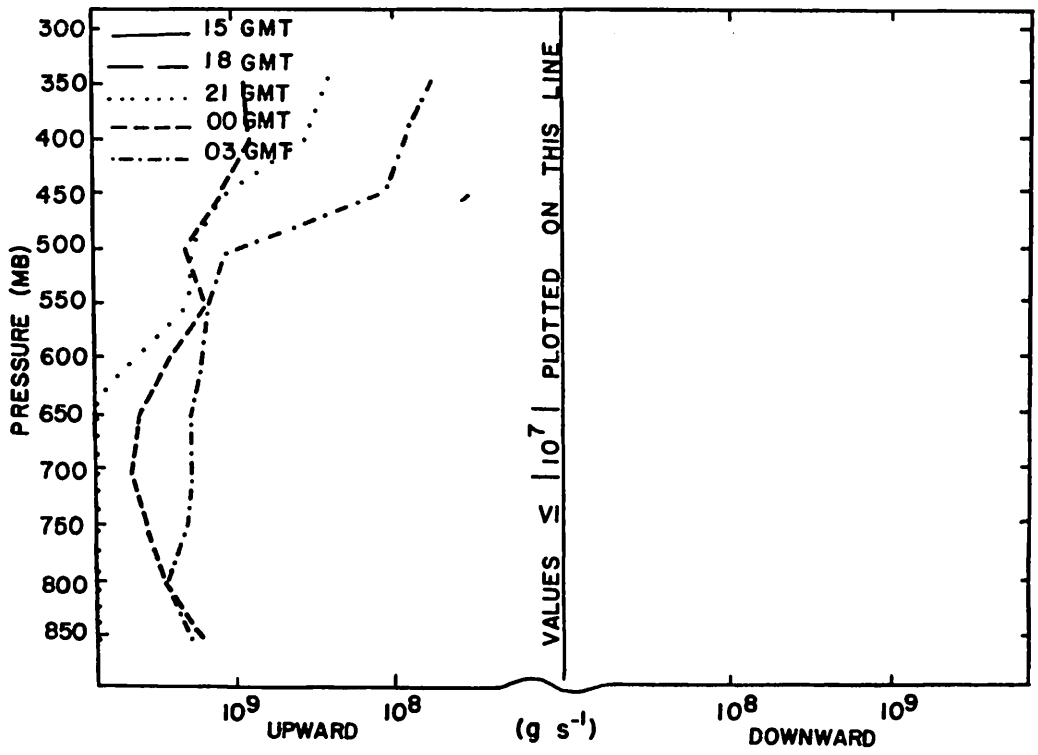

Fig. 5.22.5.3 Vertical transport of water vapor through constant pressure surfaces (gm s^{-1}) over the Texas HIPLEX area for 22 July 1978.

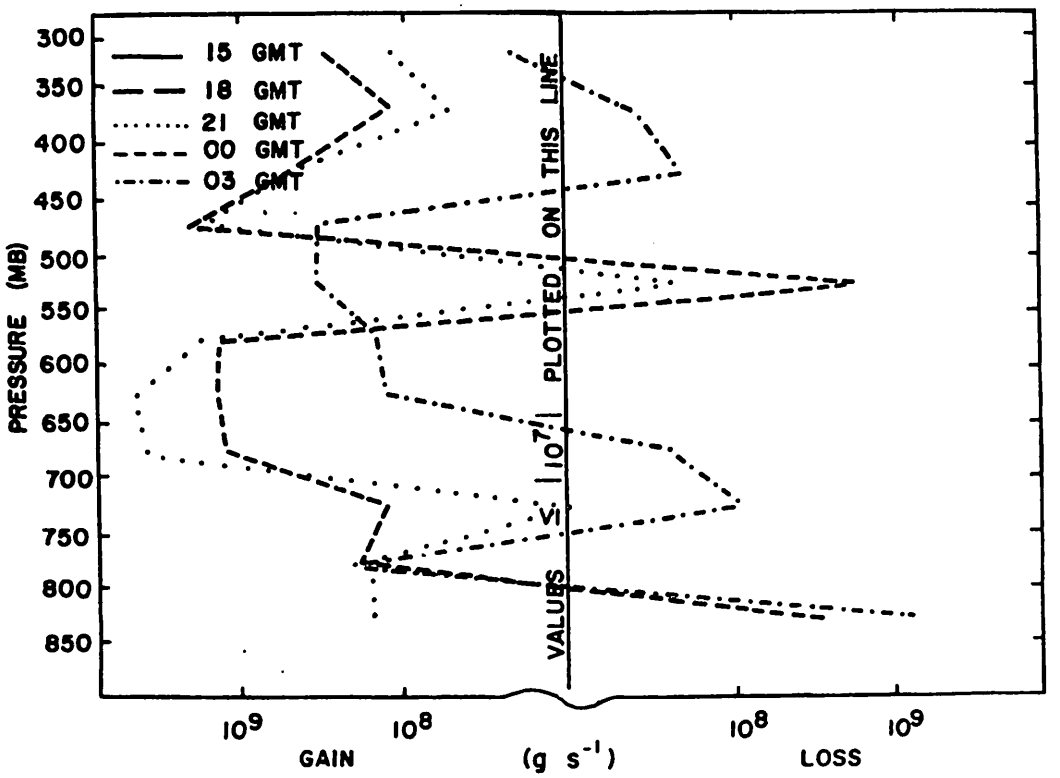

Fig. 5.22.5.4 Combined net horizontal and vertical transport of water vapor through boundaries of 50-mb layers (gm s^{-1}) over the Texas HIPLEX area for 22 July 1978.

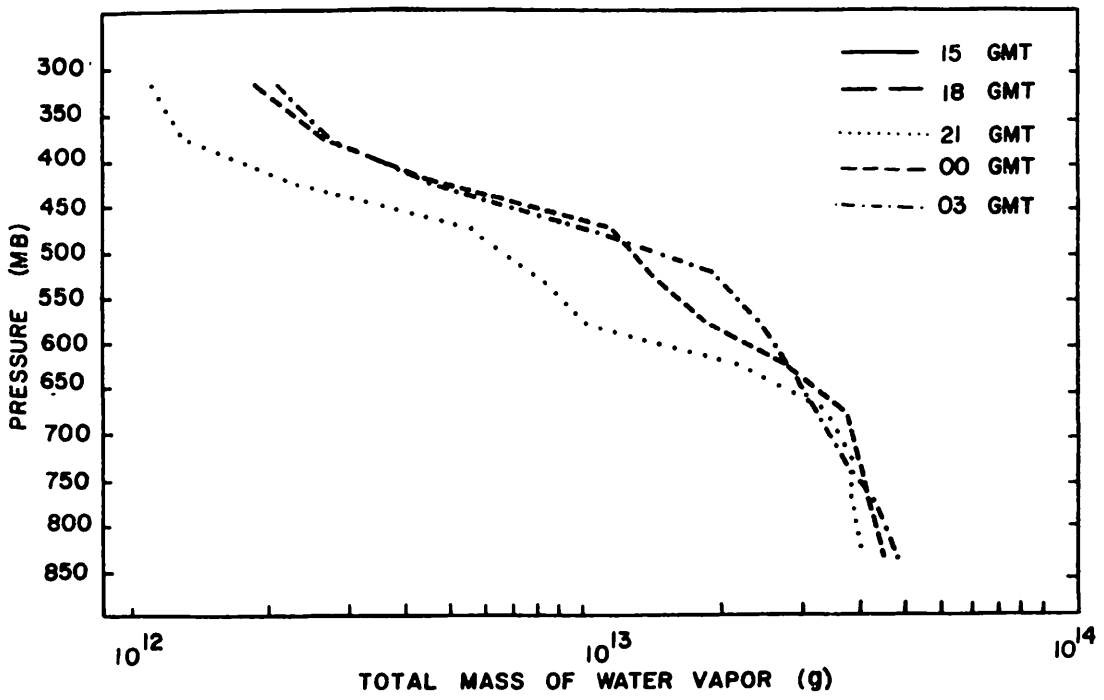

Fig. 5.22.5.5 Total mass of water vapor in layers 50 mb deep (gm) over the Texas HIPLEX area on 22 July 1978.

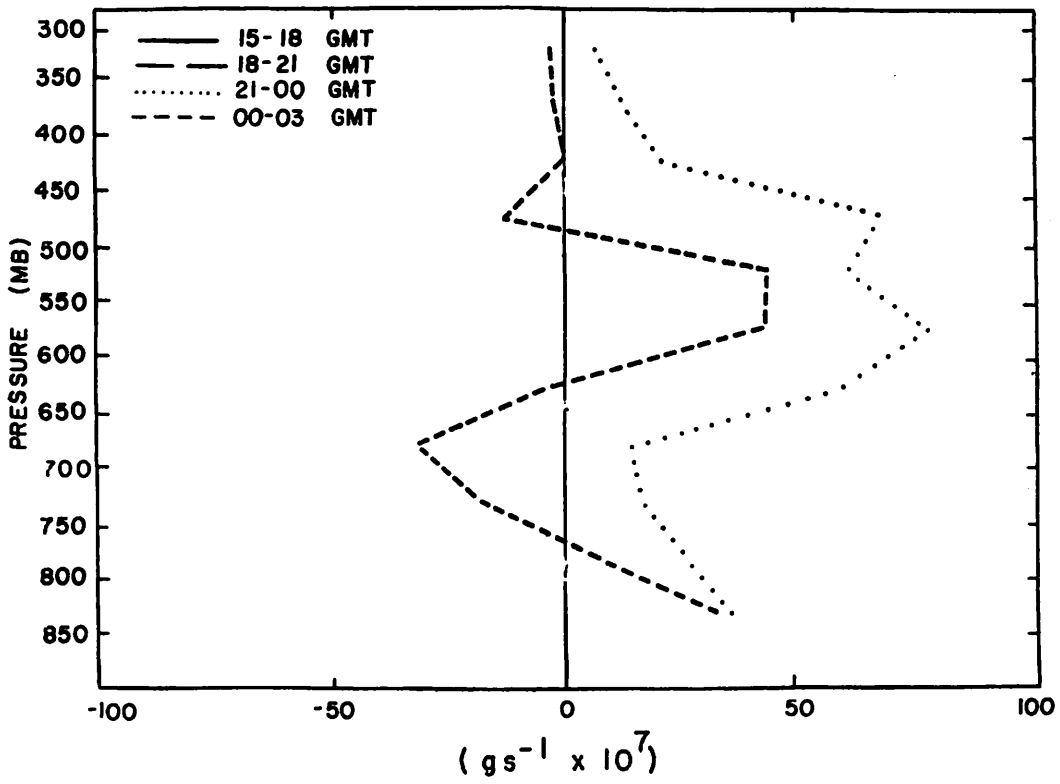

Fig. 5.22.5.6 Local rate-of-change in total mass of water vapor ($g\ s^{-1} \times 10^7$) for the Texas HIPLEX area for 22 July 1978.

5.23 23 July 1978

5.23.1 Radar

Radar echoes were observed at all times except 0300 GMT (Fig. 5.23.1.1). Echo tops were below 9.1 km (30K ft) before 1700 GMT, but exceeded 12 km (40K ft) by 1900 GMT. Cells were usually organized into clusters and dissipated after 0000 GMT.

5.23.2 Surface

Temperature changes across the network were small until an echo located approximately 20 miles west of Post dissipated between 1800 and 1900 GMT (Fig. 5.23.2.1). The top of the echo was measured at 11.2 km (37K ft) at 1800 GMT, and the cool temperature associated with its downdraft was evident until after 2100 GMT. Dewpoint depression fell to 4°C at Tahoka at 1900 GMT, then rose slowly until 2100 GMT (Fig. 5.23.2.2). Mixing ratio was not noticeably affected by the downdraft (Fig. 5.23.2.3).

At 2100 GMT a cluster of cells with tops at 13.6 km (45K ft) greatly affected surface parameters near Snyder and Vincent. Temperature fell 8°C and dewpoint depression lowered to 2°C. Mixing ratio was not affected in this area and remained near 14 gm kg^{-1}. In general, thunderstorms on this day affected surface temperature, but did not significantly alter mixing ratio.

The temperature minimum near Snyder at 2100 GMT slowly spread as the day progressed and was enhanced by temperature falls at Midland at 2300 GMT and Clairemont at 0000 GMT. These falls occurred where Code 3 echoes were dissipating (Fig. 5.23.1.1). Dewpoint depression decreased to 2°C, but mixing ratio remained only slightly lower than during non-convective conditions. The mixing ratio maximum at Big Spring, evident throughout most of the day was not correlated with convective activity. This may have been due to erroneous data. Fields of equivalent potential temperature (Fig. 5.23.2.4) were similar to those of mixing ratio throughout the day.

Terrain-induced vertical motion was small and not persistent (Fig. 5.23.2.5). Fields of divergence (Fig. 5.23.2.6) and boundary layer vertical motion (Fig. 5.23.2.7) reflected downdraft influences at several times. The convergent area at Tahoka at 1900 GMT resulted from outflow from the thunderstorm between Tahoka and Post at 1800 GMT. Similarly, other moderate to strong centers were generated through 2200 GMT. At that

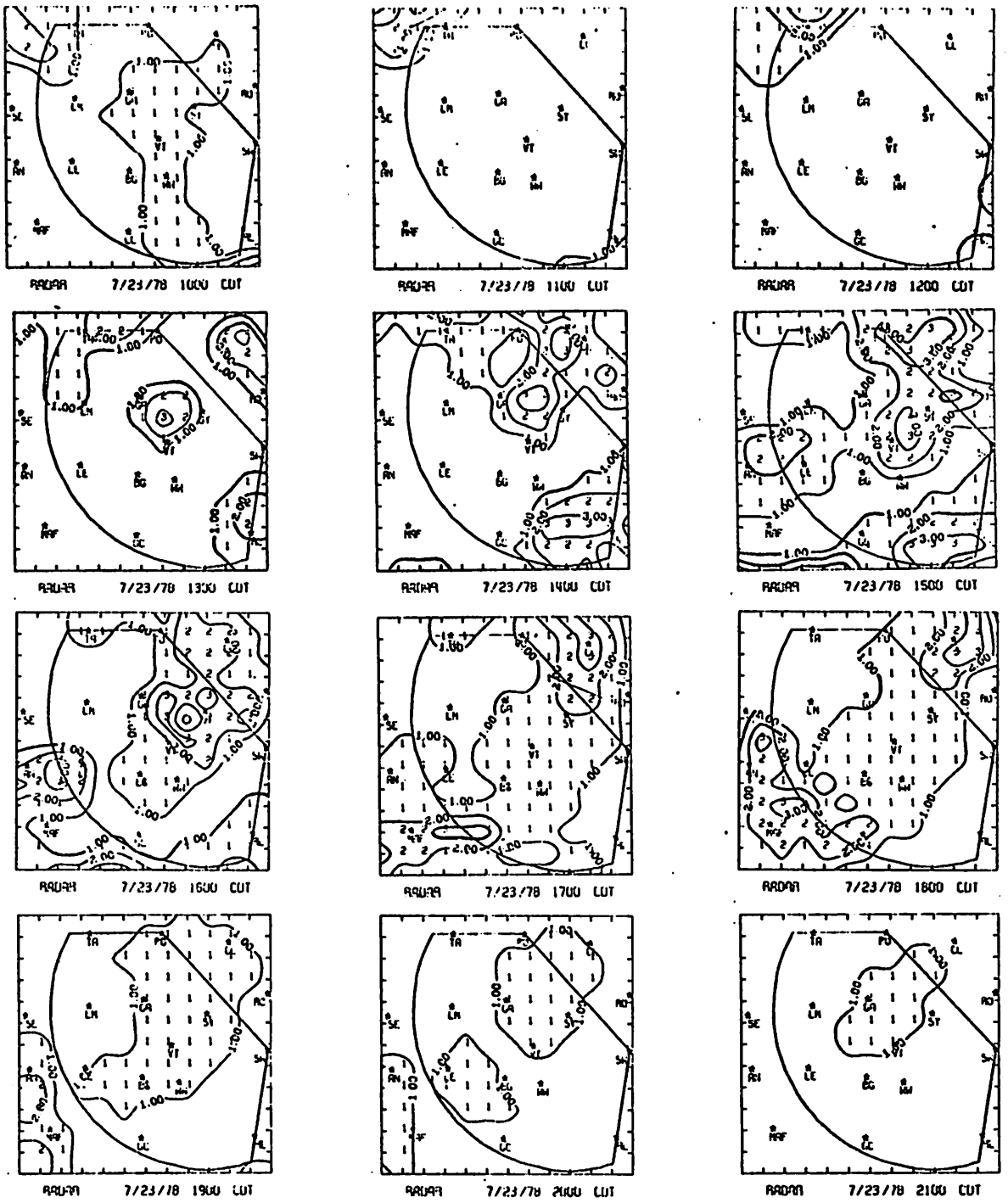

NO ECHOES

Fig. 5.23.1.1 Radar echoes for 23 July 1978.

RADAR 7/23/78 2200 CUT

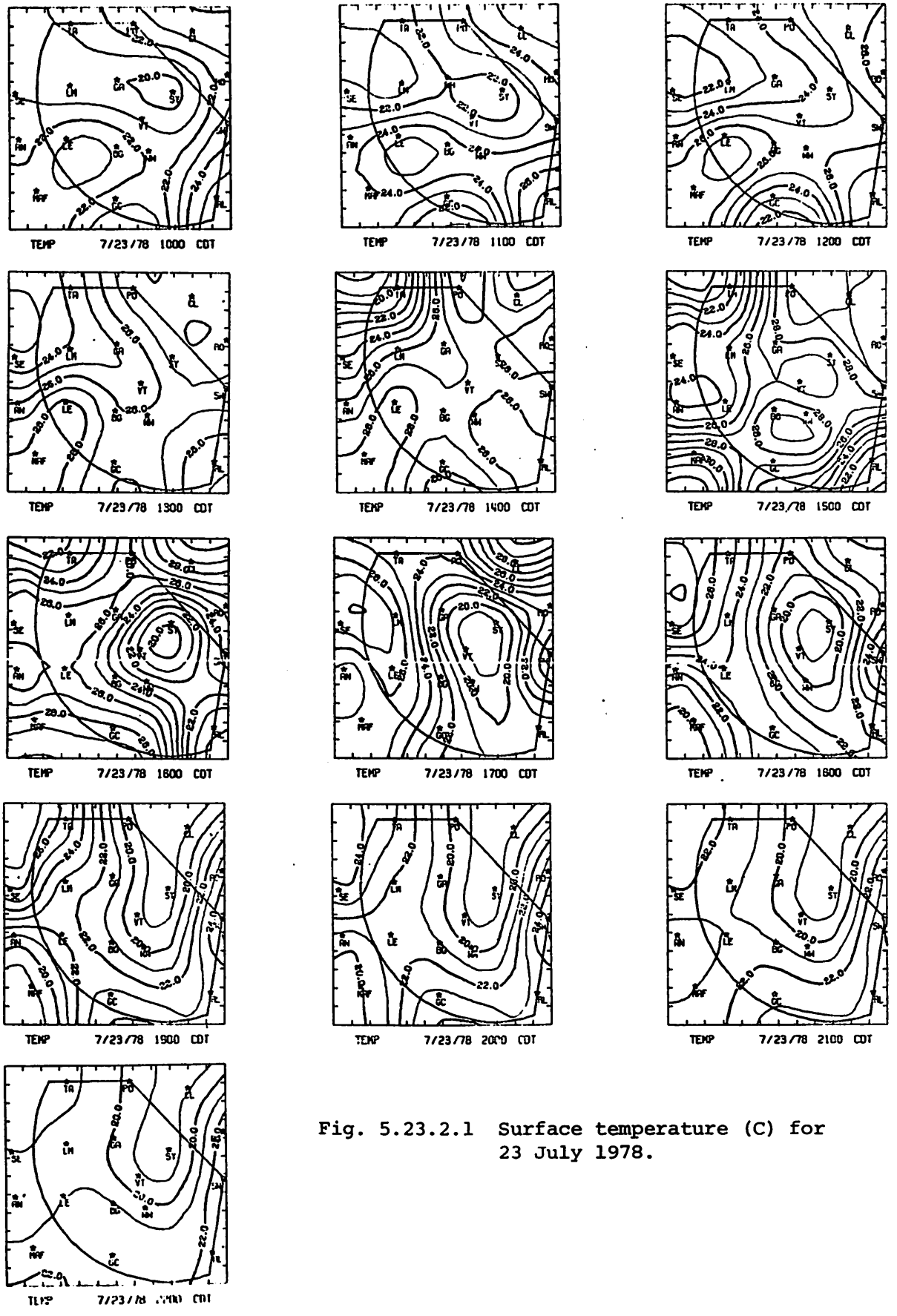

Fig. 5.23.2.1 Surface temperature (C) for 23 July 1978.

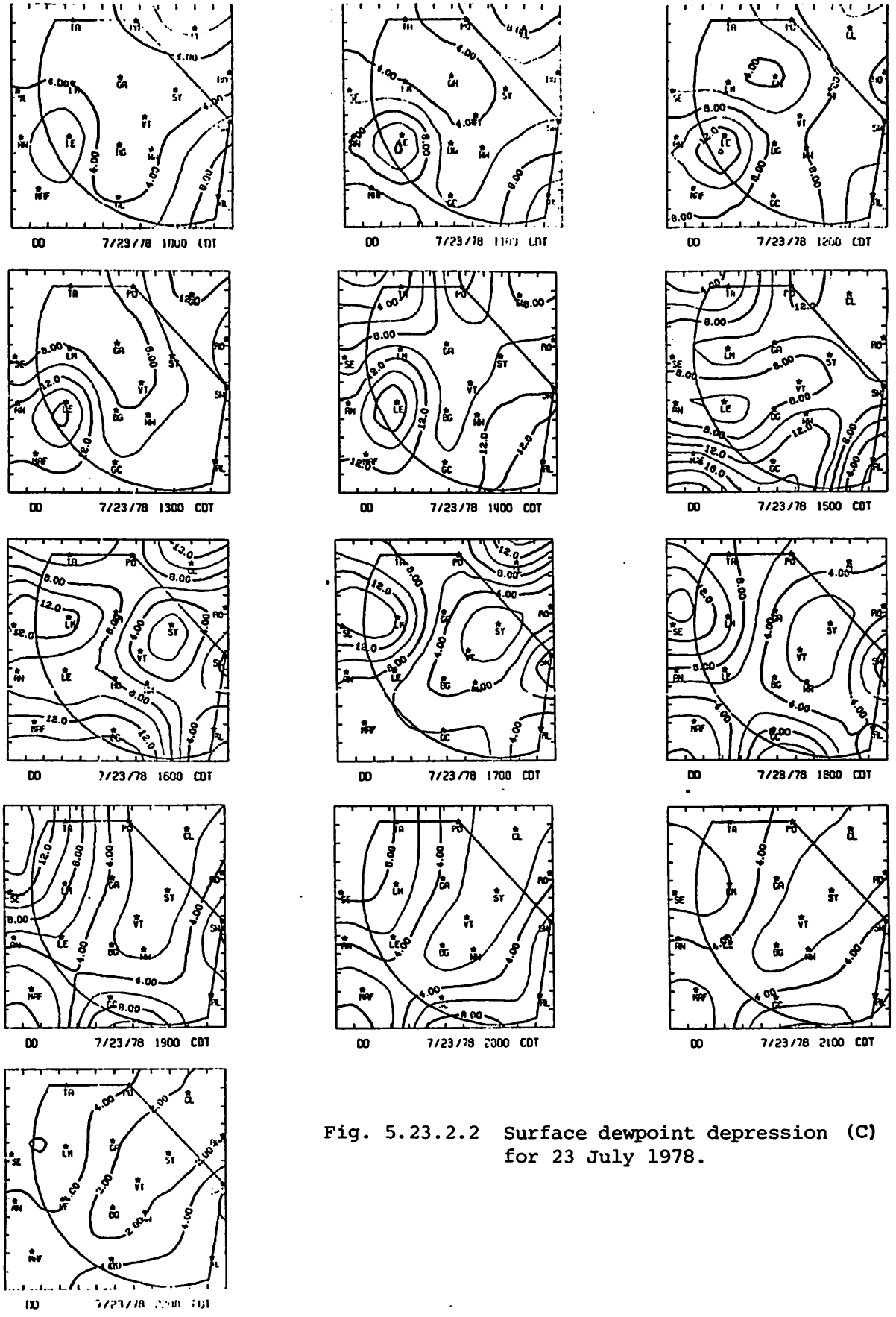

Fig. 5.23.2.2 Surface dewpoint depression (C) for 23 July 1978.

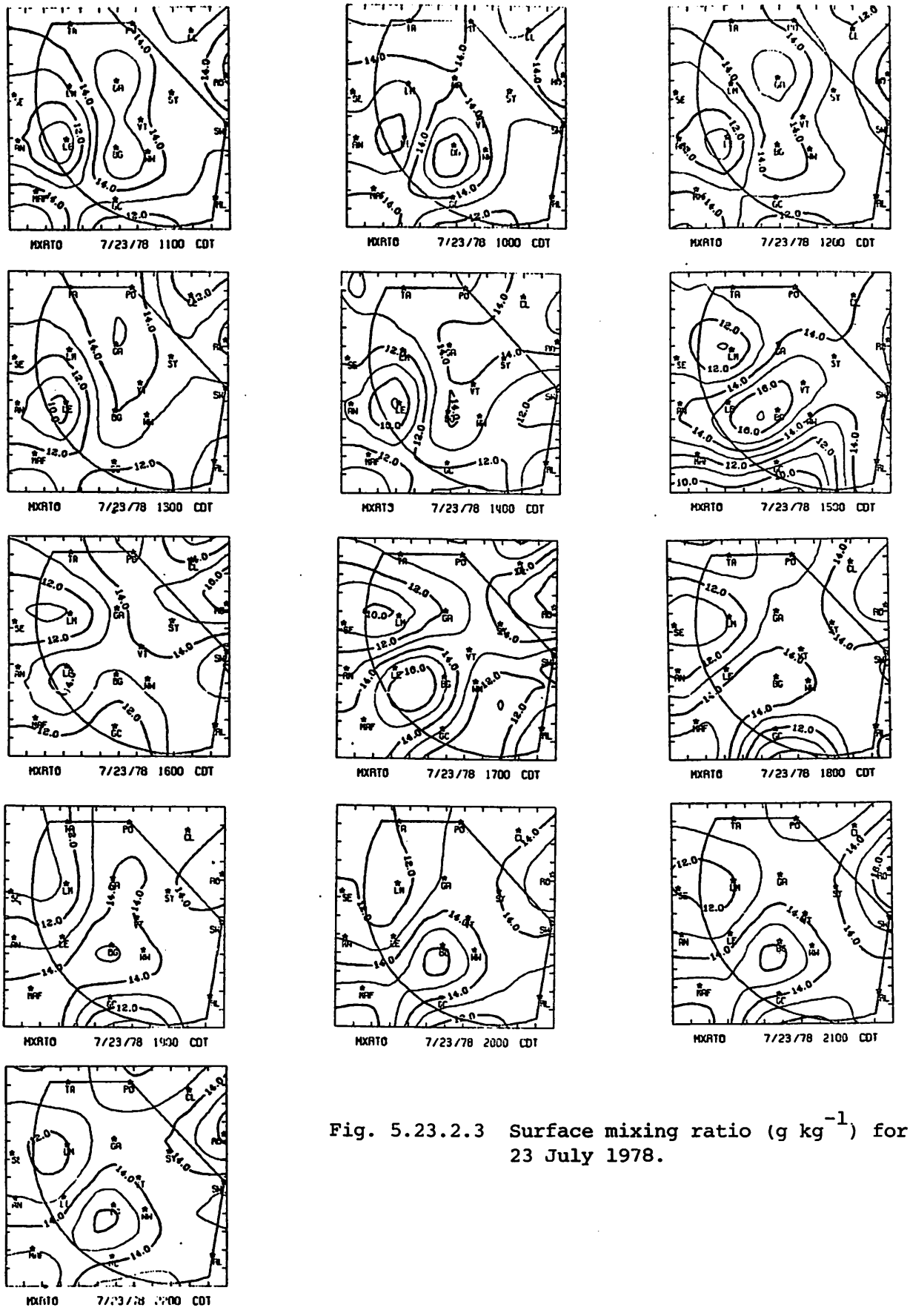

Fig. 5.23.2.3 Surface mixing ratio (g kg^{-1}) for 23 July 1978.

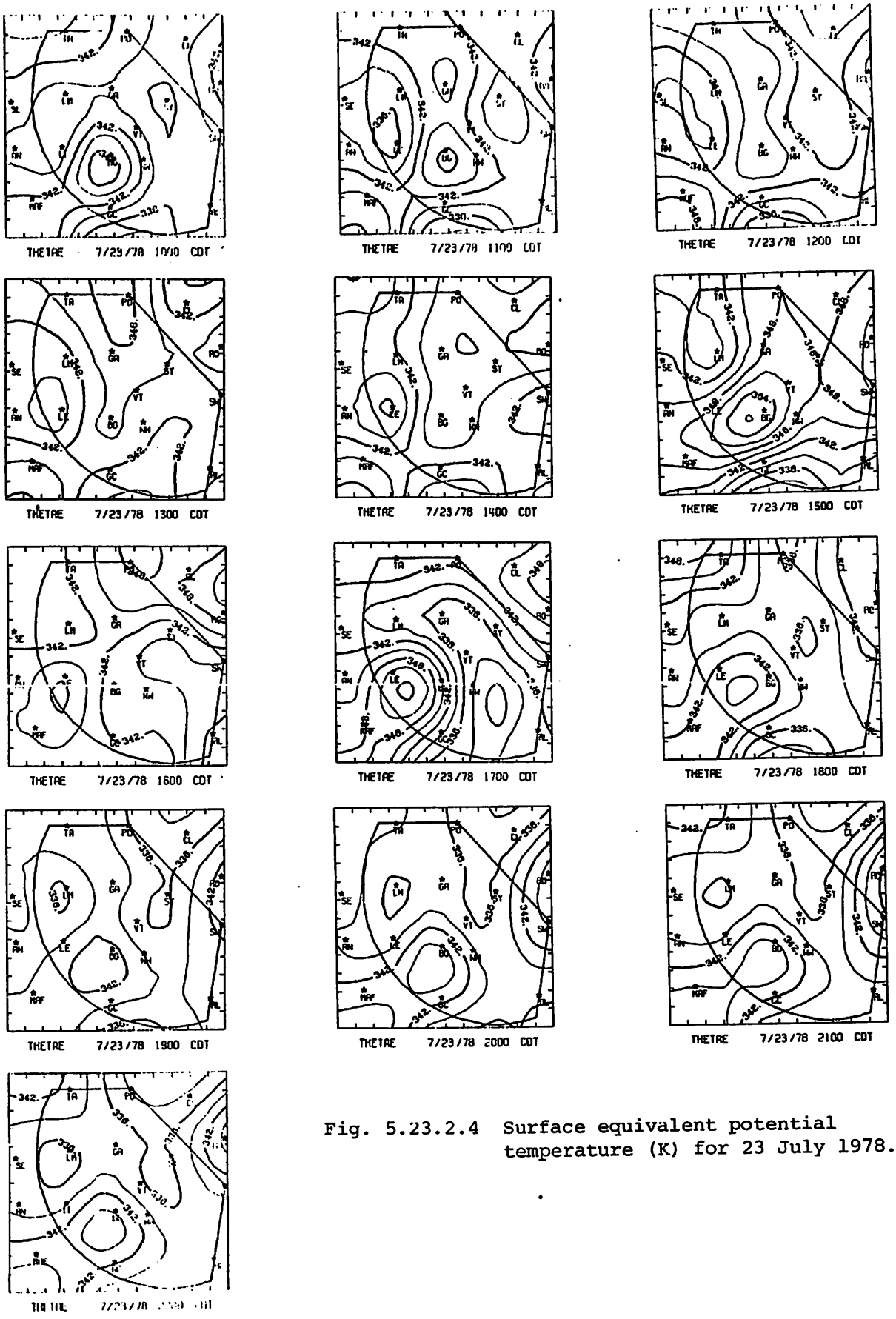

Fig. 5.23.2.4 Surface equivalent potential temperature (K) for 23 July 1978.

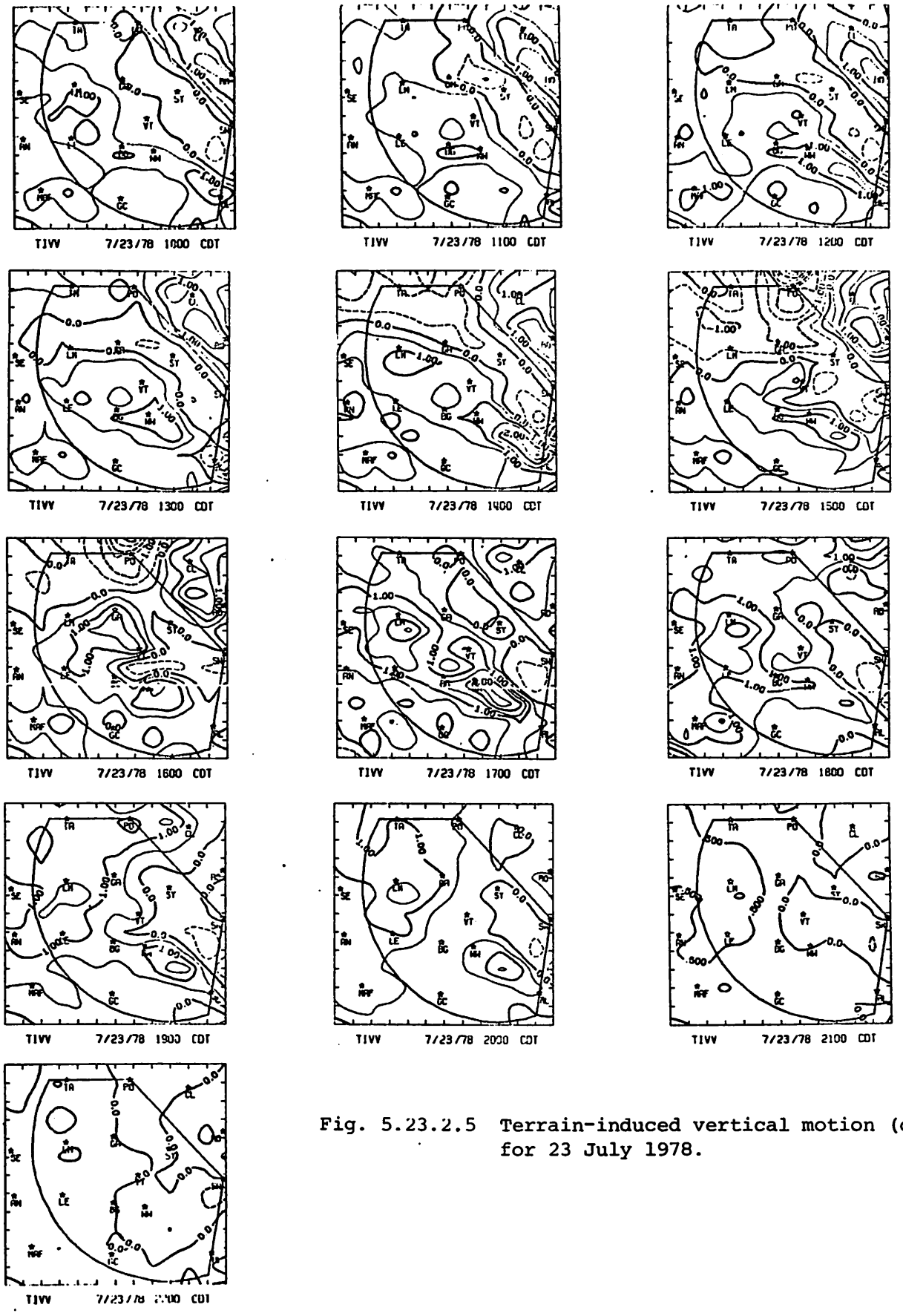

Fig. 5.23.2.5 Terrain-induced vertical motion (cm s^{-1}) for 23 July 1978.

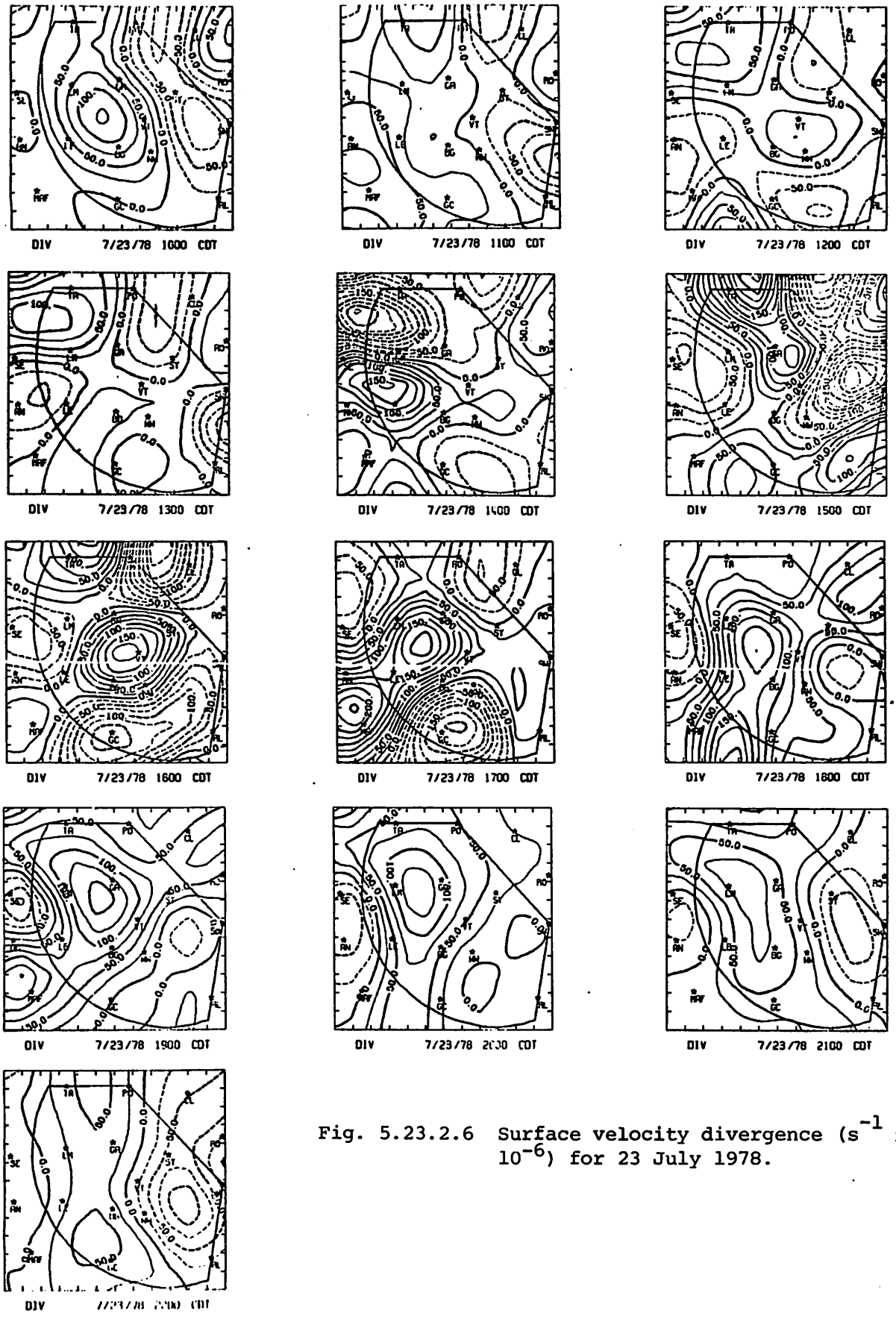

Fig. 5.23.2.6 Surface velocity divergence (s^{-1} x 10^{-6}) for 23 July 1978.

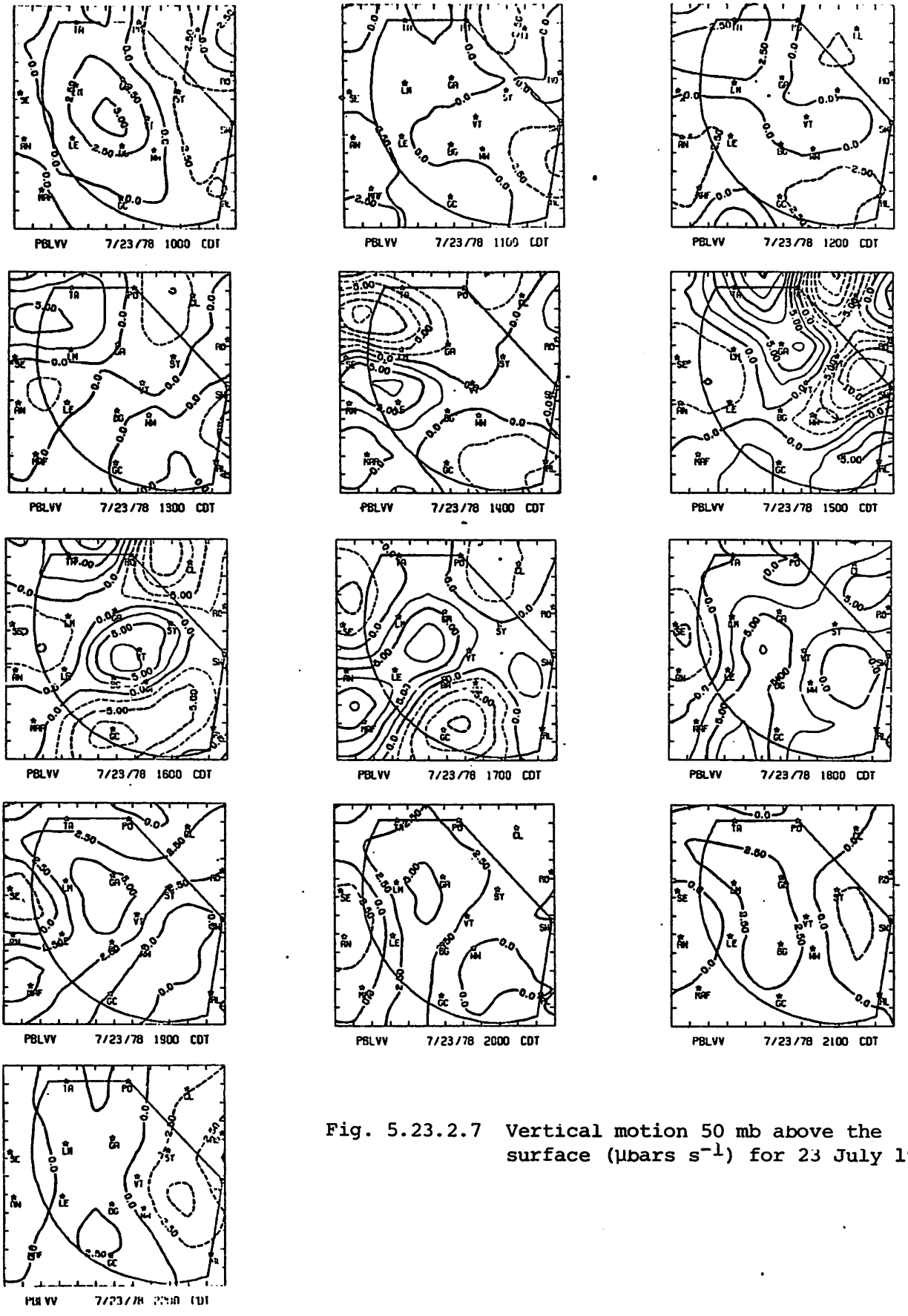

Fig. 5.23.2.7 Vertical motion 50 mb above the surface (μbars s^{-1}) for 23 July 1978.

time, small values of divergence predominated throughout the network as thunderstorm activity dissipated. Widespread, but small, divergence was typical of time periods experiencing weak echo dissipation.

Moisture divergence patterns were similar in areas with and without convective activity (Fig. 5.23.2.8). Also, patterns of vertical moisture flux (Fig. 5.23.2.9) were much like those of boundary layer vertical motion.

Vorticity centers were generated from thunderstorm influences at the same times that divergence centers were present (Fig. 5.23.2.10). They occurred due to thunderstorm downdrafts and usually changed location from hour-to-hour.

The surface pressure dropped 1 mb at Clairemont before effects from a thunderstorm were observed at 2300 GMT, which corresponds to measured downdraft effects at that station. Pressure changes at other times were small (Fig. 5.23.2.11).

The surface wind field showed significant changes in response to the convective activity (Fig. 5.23.2.12). Except in the proximity of echoes, winds were generally from the east during the day.

5.23.3 Upper-Level Kinematic Parameters

Only 1500 and 1800 GMT upper-level results were available for this day.

Profiles of horizontal mass divergence at 1500 and 1800 GMT were nearly identical (Fig. 5.23.3.1). Mass divergence occurred below 550 mb with a significant peak at 825 mb. Above 550 mb divergence was small, although both profiles show convergence at 450 mb and divergence at 350 mb.

Divergence in the lower layers led to downward motion at all levels (Fig. 5.23.3.2). Profiles of moisture divergence (Fig. 5.23.3.3) were similar to those of mass divergence, except that above 500 mb the lack of water vapor reduced values to near zero.

5.23.4 Energetics

Horizontal flux divergence of latent heat energy resulted in a loss in layers below 550 mb (Fig. 5.23.4.1). This was compensated by a concentration of latent heat energy due to vertical transport shown in Fig. 5.23.4.2. The gain below 700 mb shown in the latter profile, indicates transport from a saturated layer which may be observed above 800 mb in soundings taken at 1500 and 1800 GMT. This downward transport is atypical, as water vapor

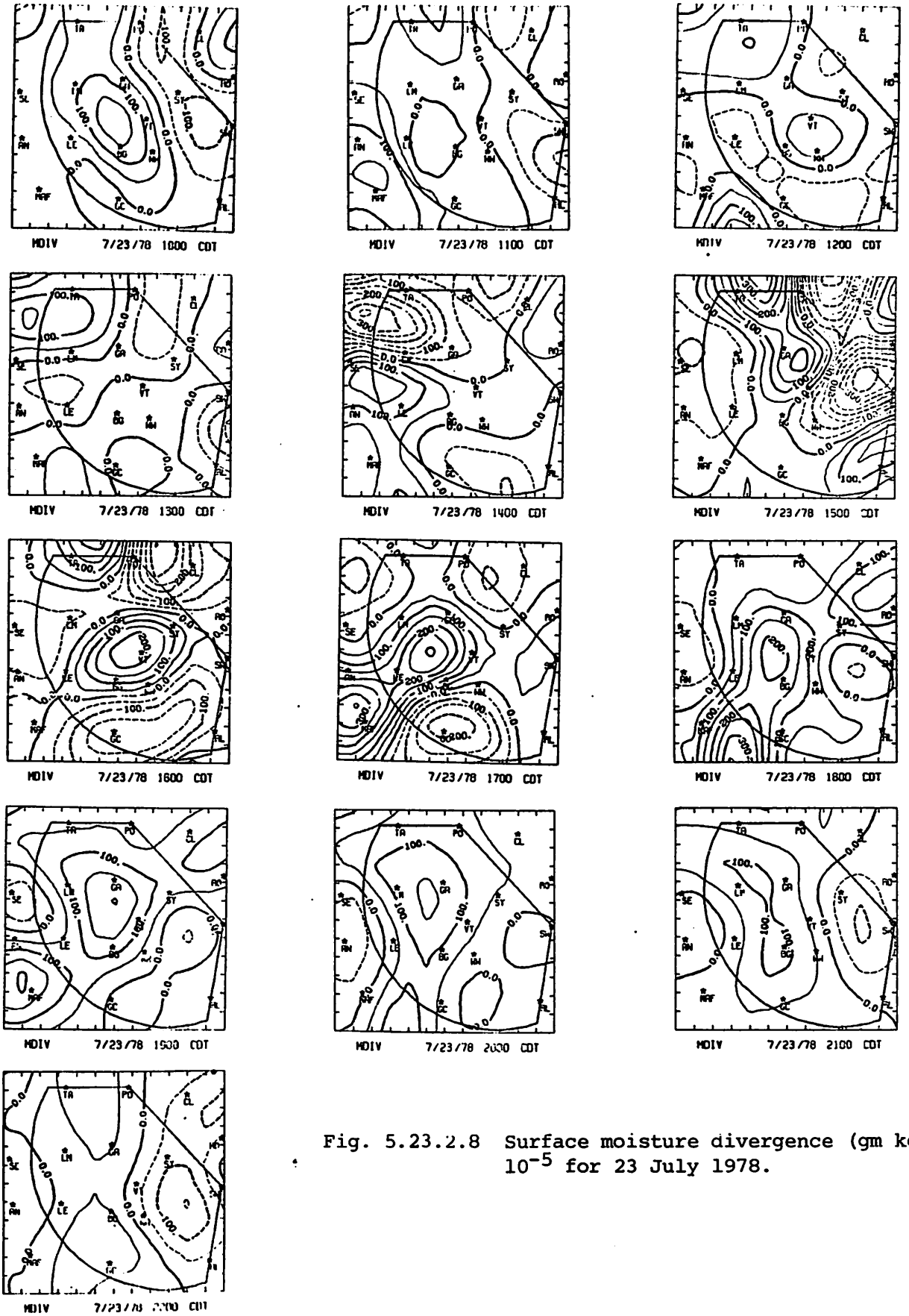

Fig. 5.23.2.8 Surface moisture divergence (gm kg^{-1} s^{-1} x 10^{-5} for 23 July 1978.

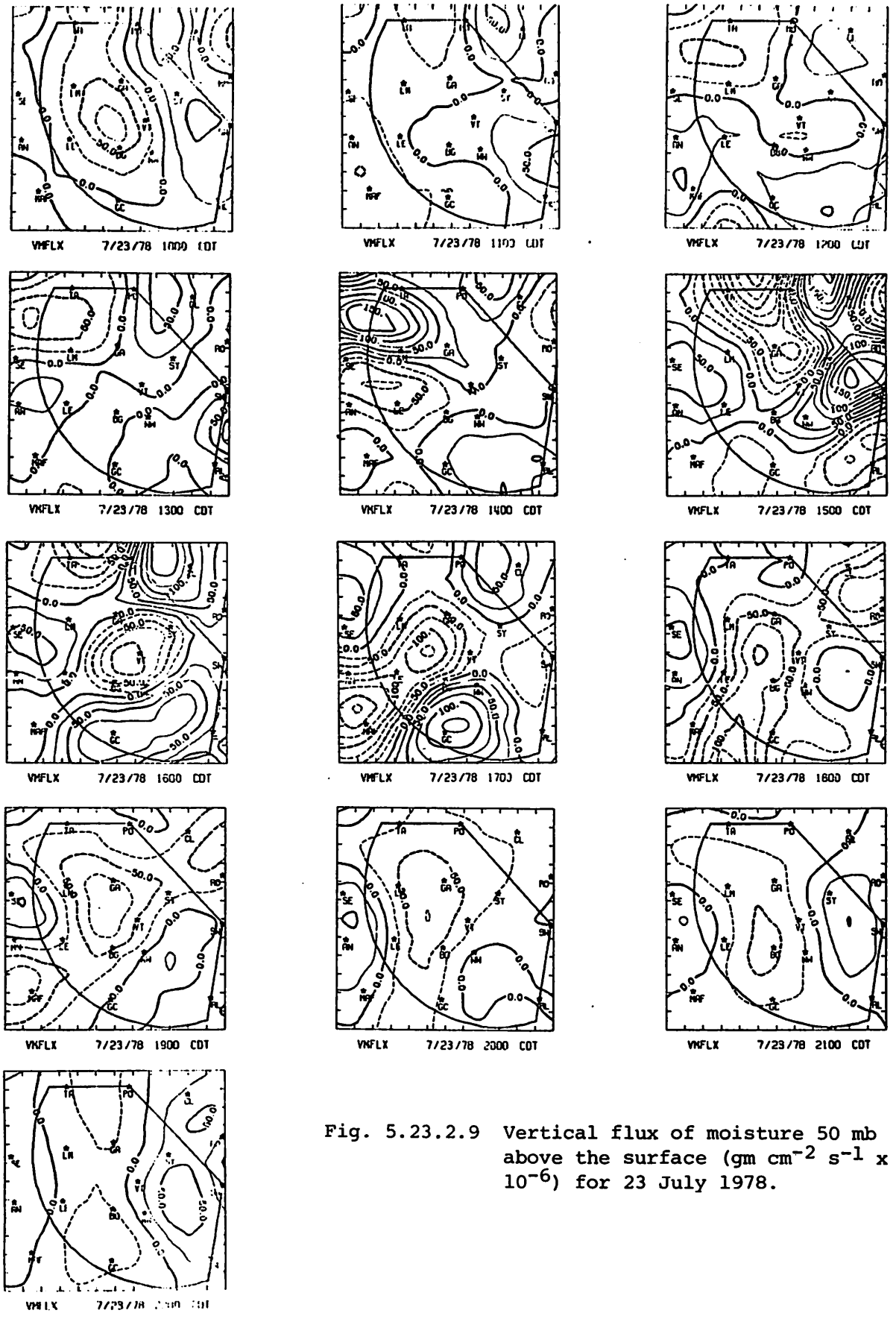

Fig. 5.23.2.9 Vertical flux of moisture 50 mb above the surface (gm cm^{-2} s^{-1} x 10^{-6}) for 23 July 1978.

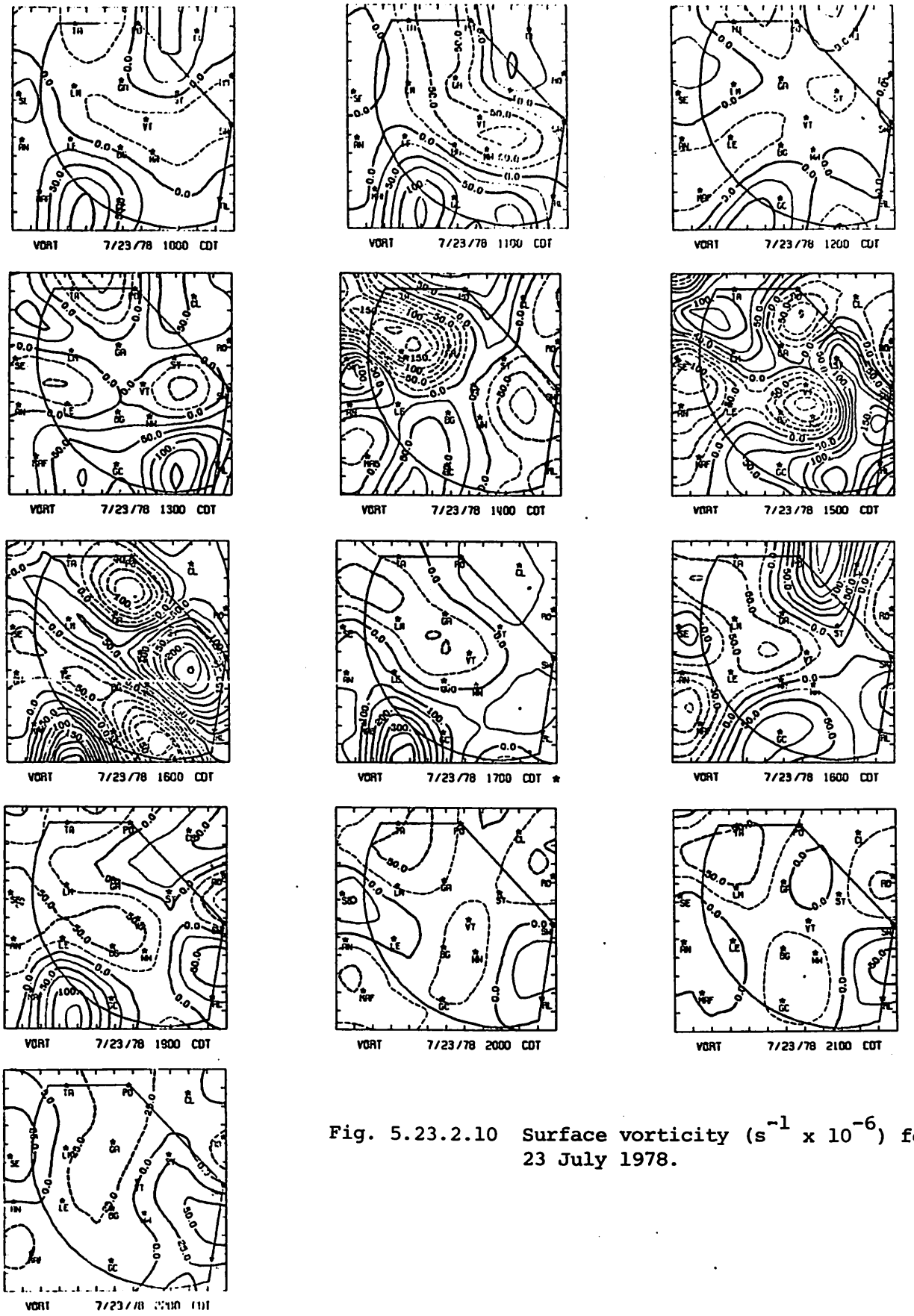

Fig. 5.23.2.10 Surface vorticity ($s^{-1} \times 10^{-6}$) for 23 July 1978.

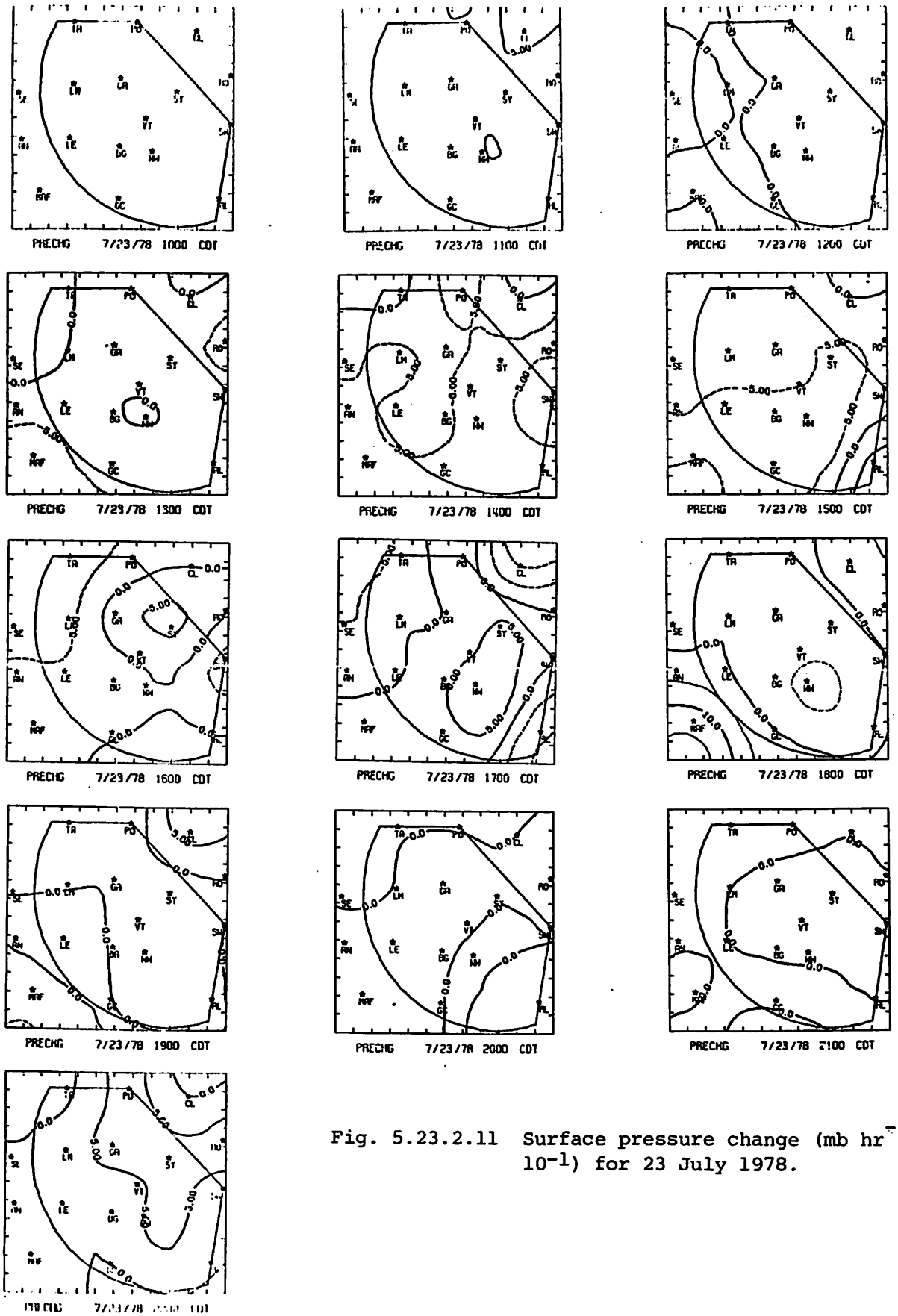

Fig. 5.23.2.11 Surface pressure change (mb hr^{-1} x 10^{-1}) for 23 July 1978.

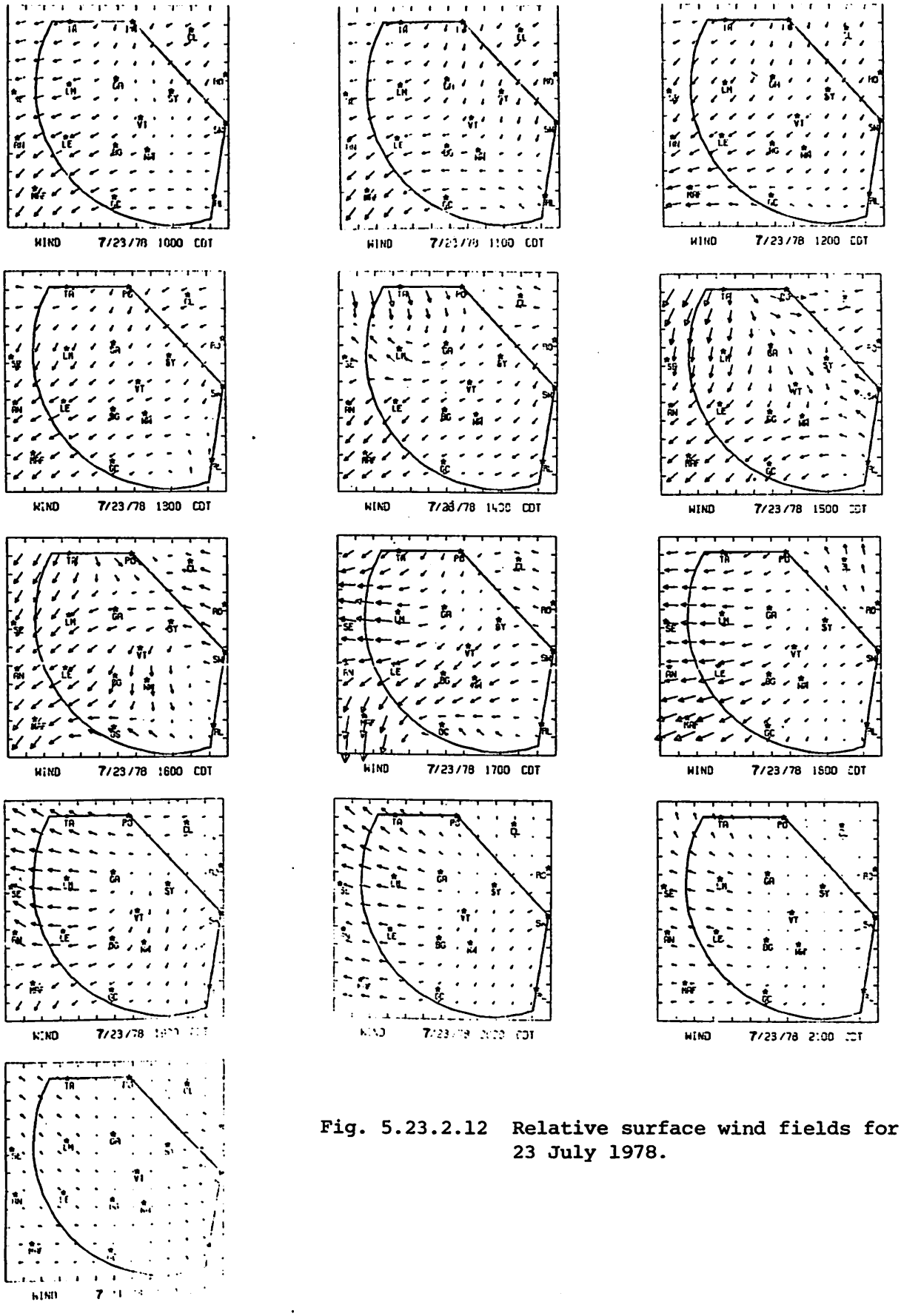

Fig. 5.23.2.12 Relative surface wind fields for 23 July 1978.

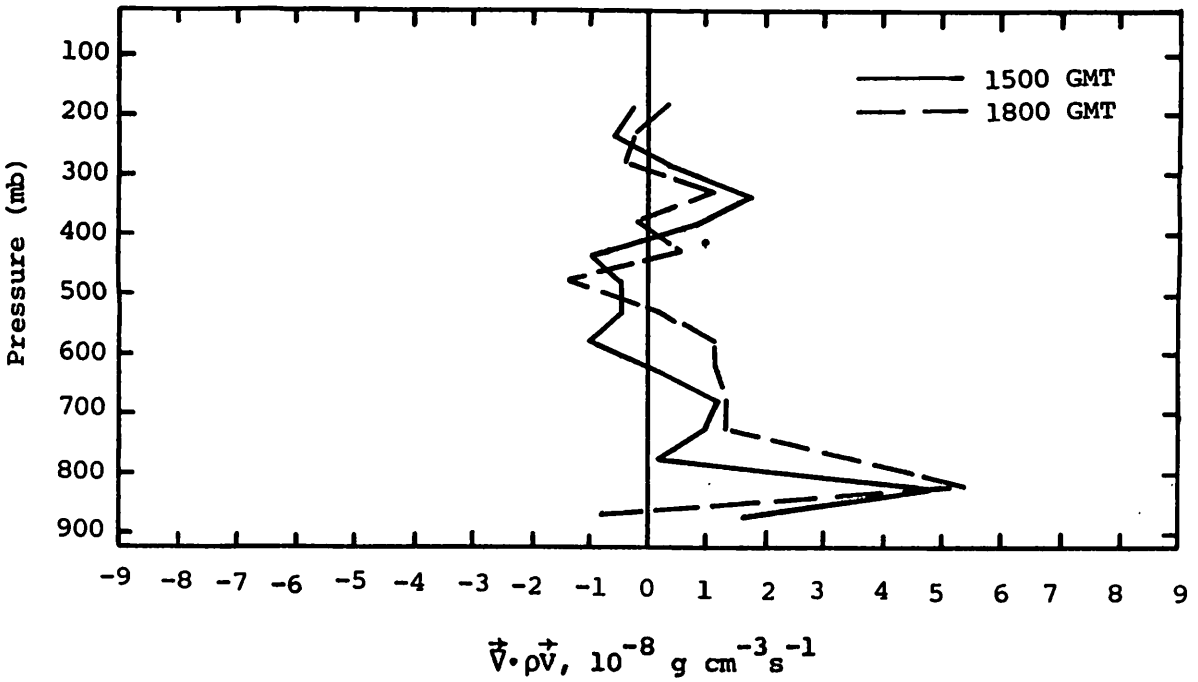

Fig. 5.23.3.1 Vertical profiles of mass divergence on 23 July 1978.

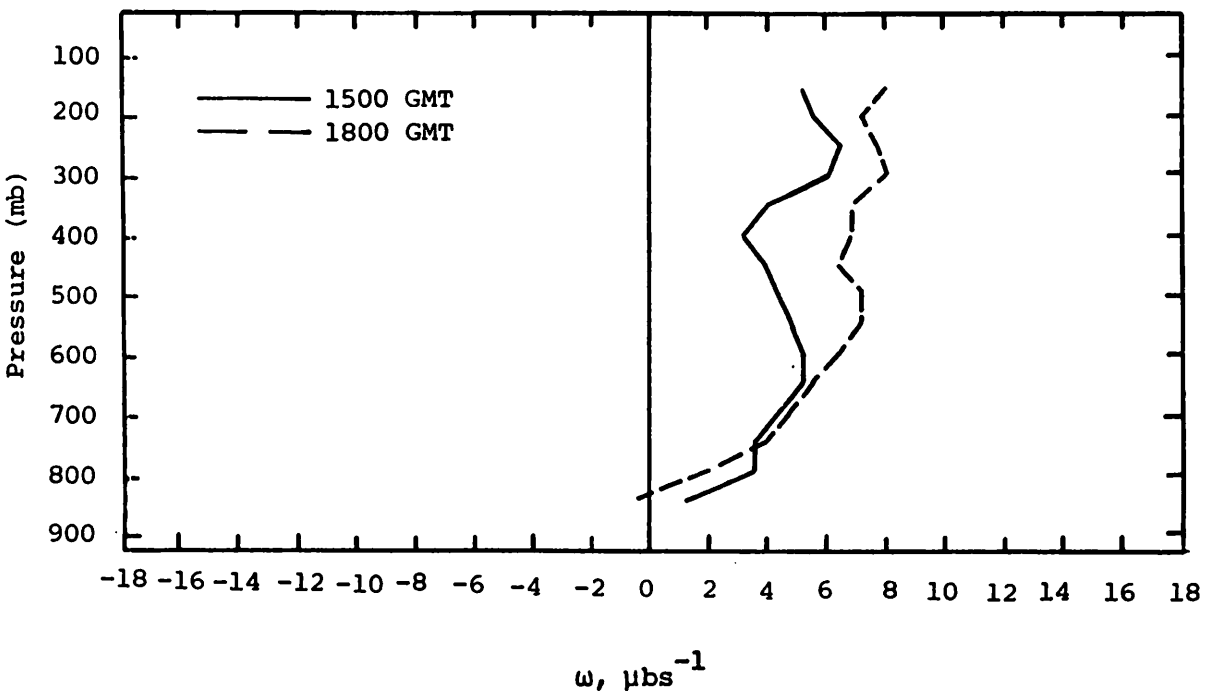

Fig. 5.23.3.2 Vertical profiles of vertical motion on 23 July 1978.

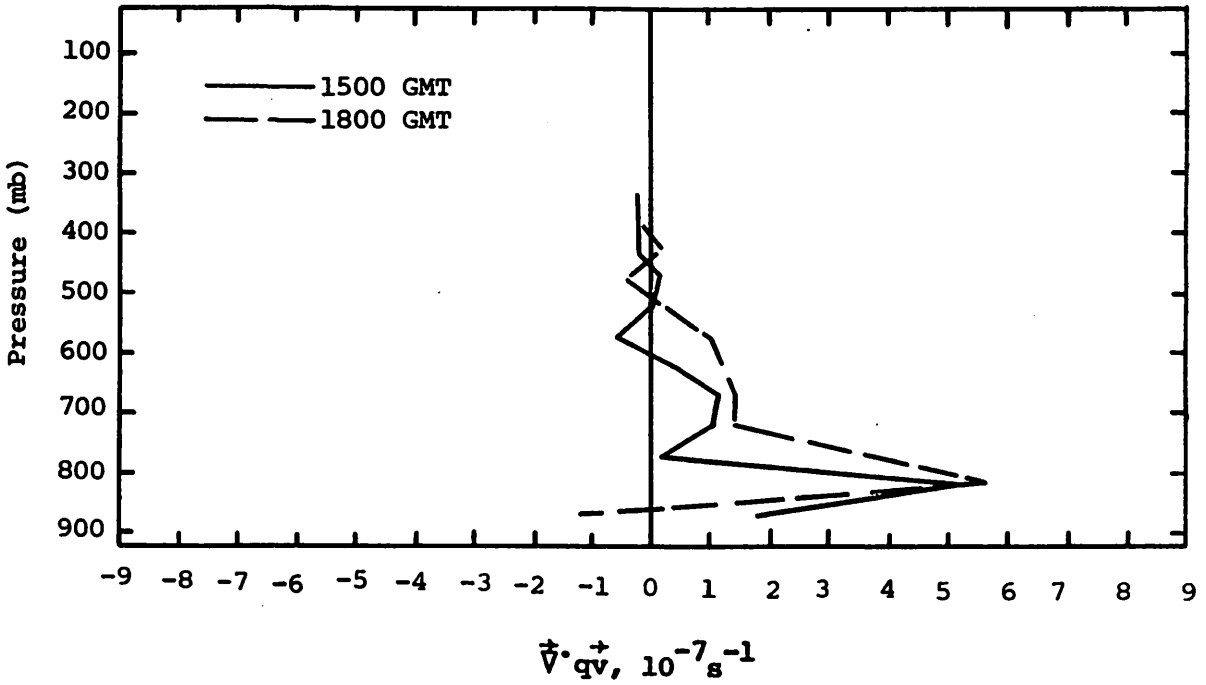

Fig. 5.23.3.3 Vertical profiles of moisture divergence on 23 July 1978.

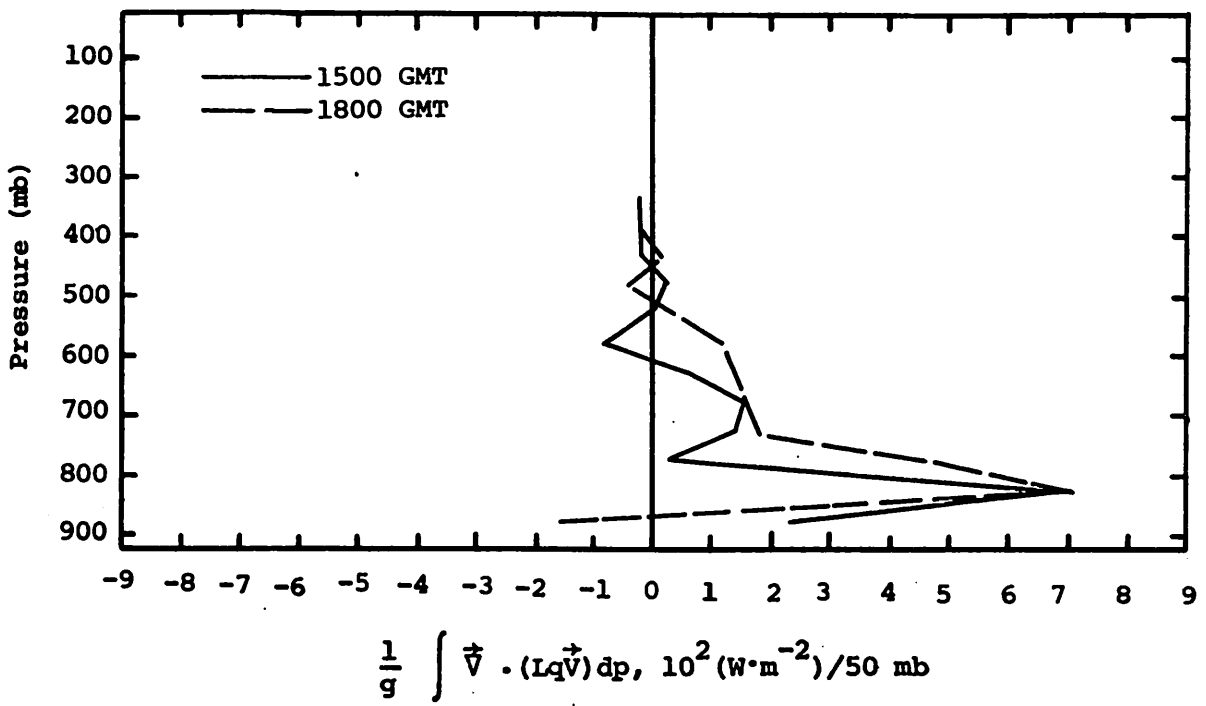

Fig. 5.23.4.1 Vertical profiles of the horizontal flux of latent heat energy on 23 July 1978.

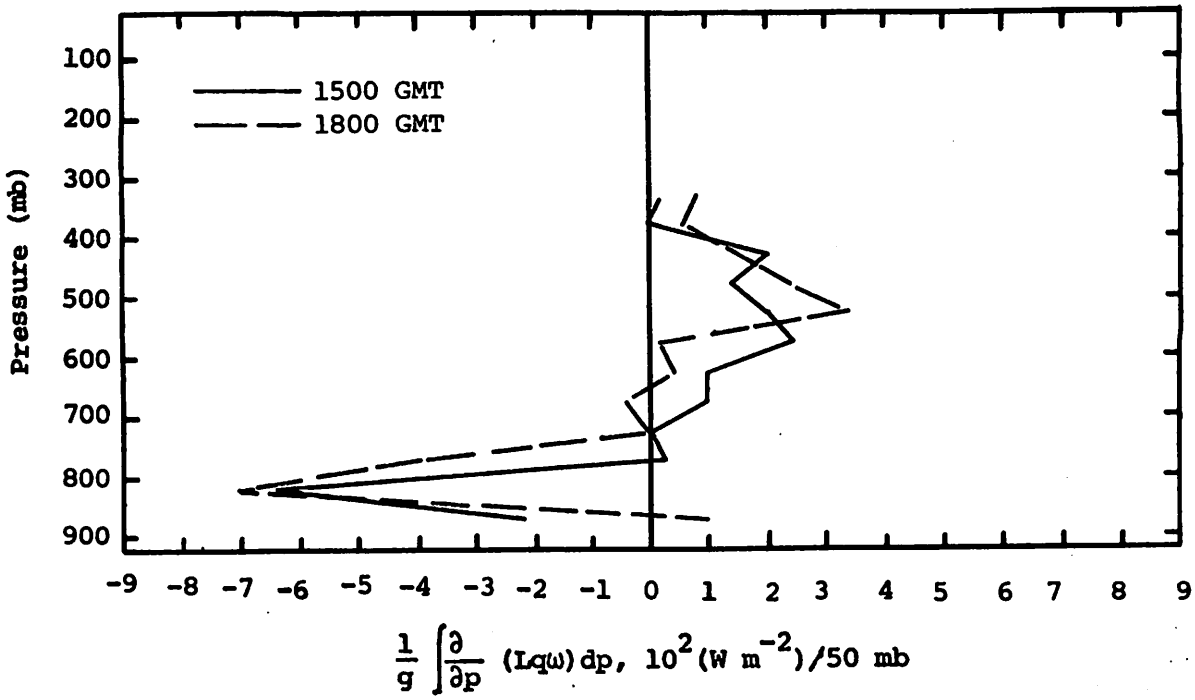

Fig. 5.23.4.2 Vertical profiles of the vertical flux of latent heat energy on 23 July 1978.

content usually decreases with height. Figure 5.23.4.2 also shows a loss of latent heat energy from 700 to 300 mb at both times.

The local change of latent heat energy shows a loss below 600 mb and a slight gain above 450 mb (Fig. 5.23.4.3). The loss resulted from horizontal flux divergence since the vertical flux was small and the residual showed gain in the same layers (Fig. 5.23.4.4). In fact, the residual indicated a gain of latent energy in all layers above 700 mb. This may have been due to evaporation of cloud water.

The 1500 GMT profile of diabatic heating shows a loss of sensible heat at all layers except 850-900 mb (Fig. 5.23.4.5). Evaporation of cloud water, as was indicated in the residual of the latent heat energy budget, may have contributed to the loss of sensible heat.

Profiles of the horizontal and vertical flux divergence of kinetic energy (Figs. 5.23.4.6 and 5.23.4.7) show few features and with negligible values below 400 mb.

5.23.5 Water Vapor Budget

Profiles of the net horizontal transport of water vapor for 1500 and 1800 GMT show a loss of water vapor below 600 mb (Fig. 5.23.5.1). This is

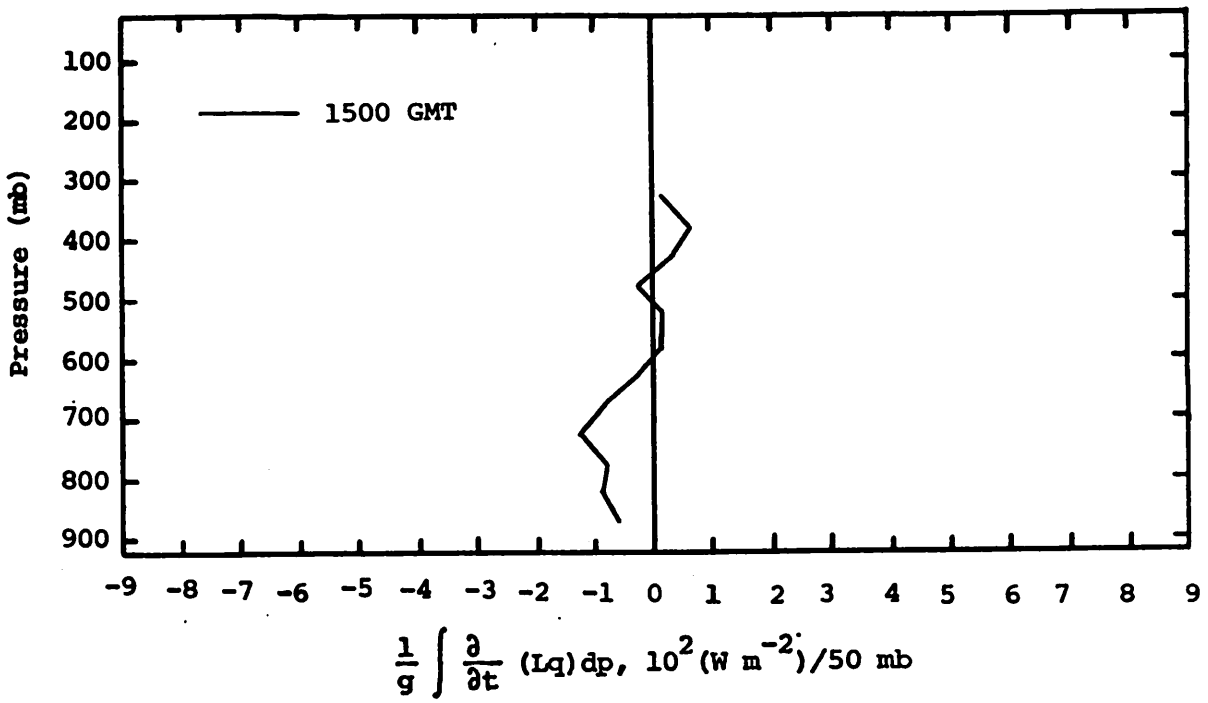

Fig. 5.23.4.3 Vertical profiles of the local change of latent heat energy on 23 July 1978.

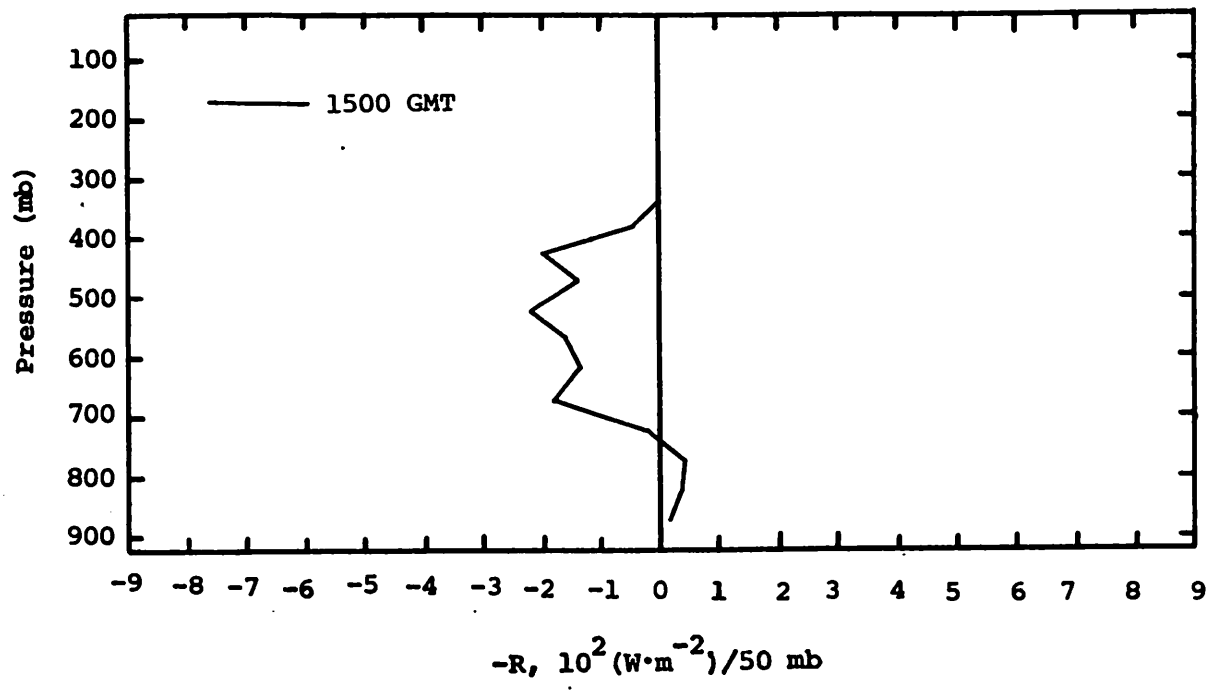

Fig. 5.23.4.4 Vertical profiles of the residual of the latent heat energy equation on 23 July 1978.

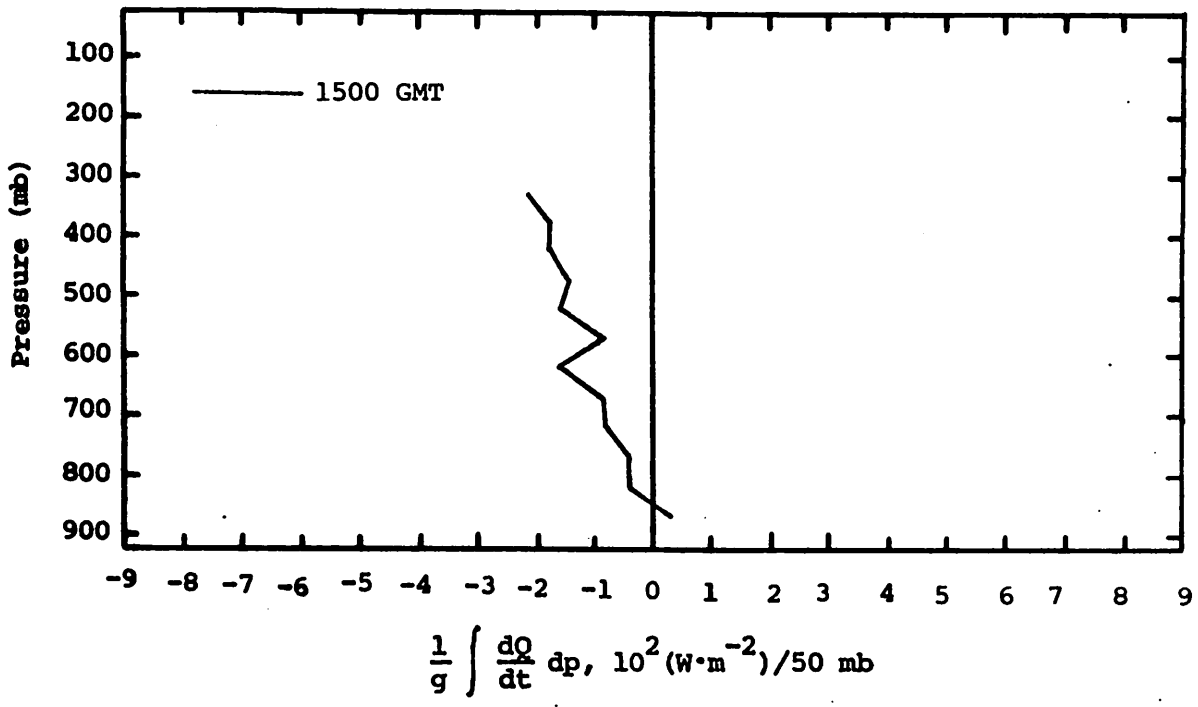

Fig. 5.23.4.5 Vertical profiles of diabatic heating computed from the first law of thermodynamics on 23 July 1978.

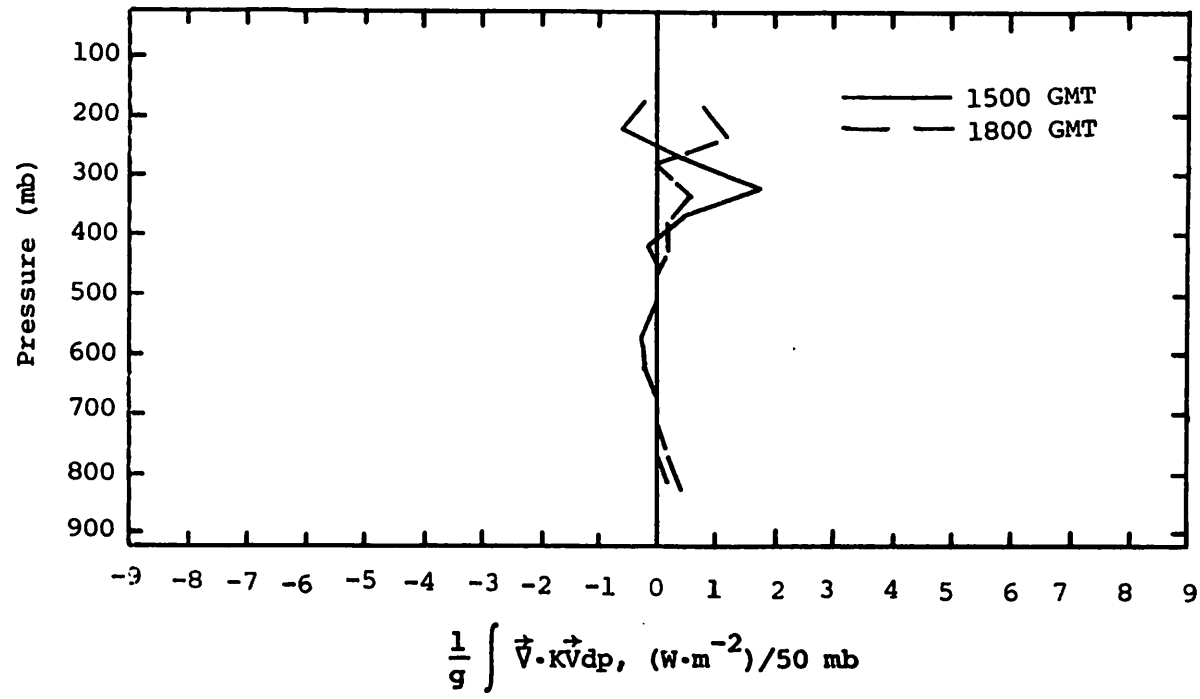

Fig. 5.23.4.6 Vertical profiles of the horizontal flux of kinetic energy on 23 July 1978.

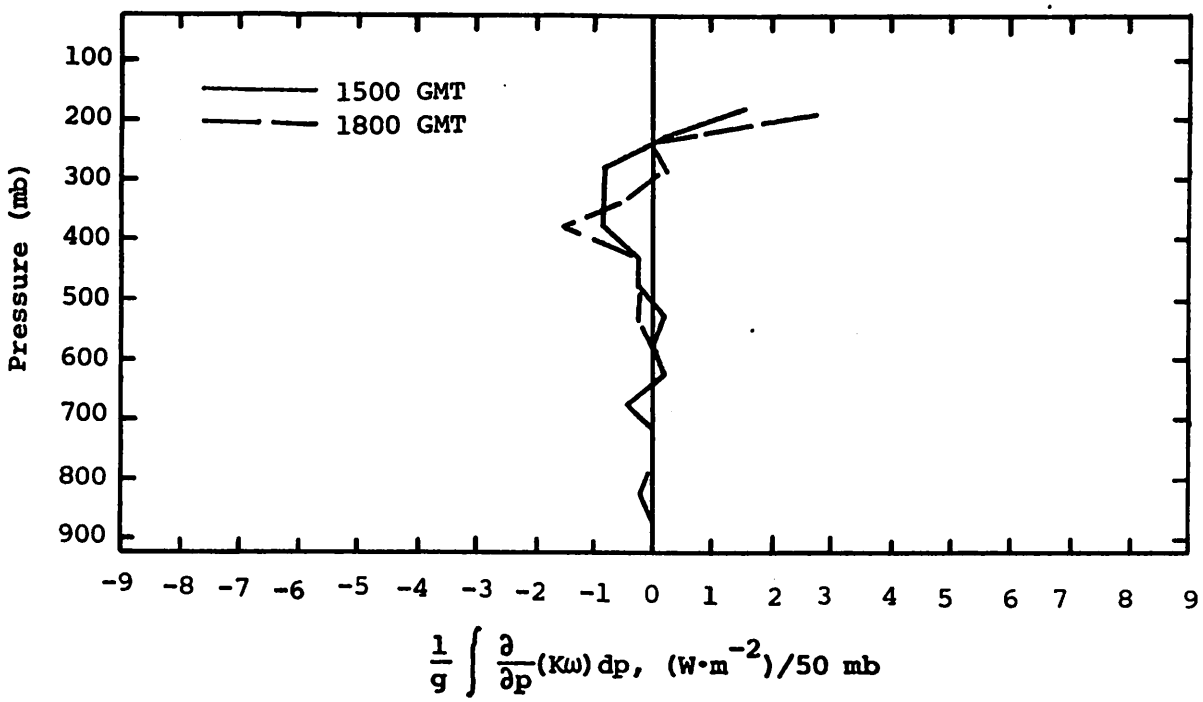

Fig. 5.23.4.7 Vertical profiles of the vertical flux of kinetic energy on 23 July 1978.

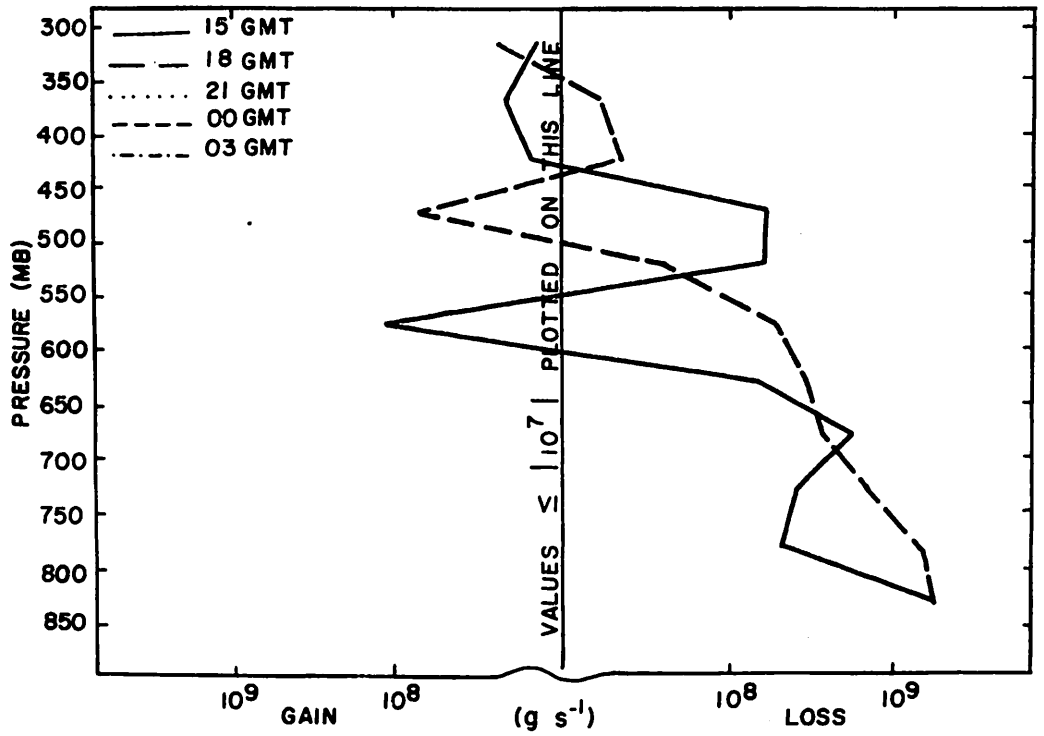

Fig. 5.23.5.1 Net horizontal transport of water vapor through boundaries of 50-mb layers (gm s^{-1}) over the Texas HIPLEX area for 23 July 1978.

consistent with results of the latent heat energy budget.

The net vertical transport indicated a loss of water vapor above 800 mb at 1500 GMT, and a loss above 700 mb at 1800 GMT (Fig. 5.23.5.2). The concentration of water vapor below 800 and 700 mb at 1500 and 1800 GMT, respectively, was due to downward transport through the cloud region observed in soundings. That the transport was downward at both times is evident from Fig. 5.23.5.3 which shows the vertical transport through constant pressure surfaces.

Calculations of net combined transport (Fig. 5.23.5.4) show that water vapor flux was diverged at all levels for both time periods. The total mass of water vapor in 50-mb layers (Fig. 5.23.5.5) shows changes that are indicated by the local rate-of-change profile (Fig. 5.23.5.6). Between 1500 and 1800 GMT, water vapor concentration was increased below 700 mb and from 600 to 500 mb, and decreased above 500 mb. The local rate-of-change of water vapor for the period 1500 to 1800 GMT shows a loss below 475 mb but a gain above that level. The loss below 700 mb may be attributed to horizontal and vertical flux divergence. The smaller losses above 700 mb, and the gain above 475 mb, may have resulted from evaporation of the cloud or turbulent transport.

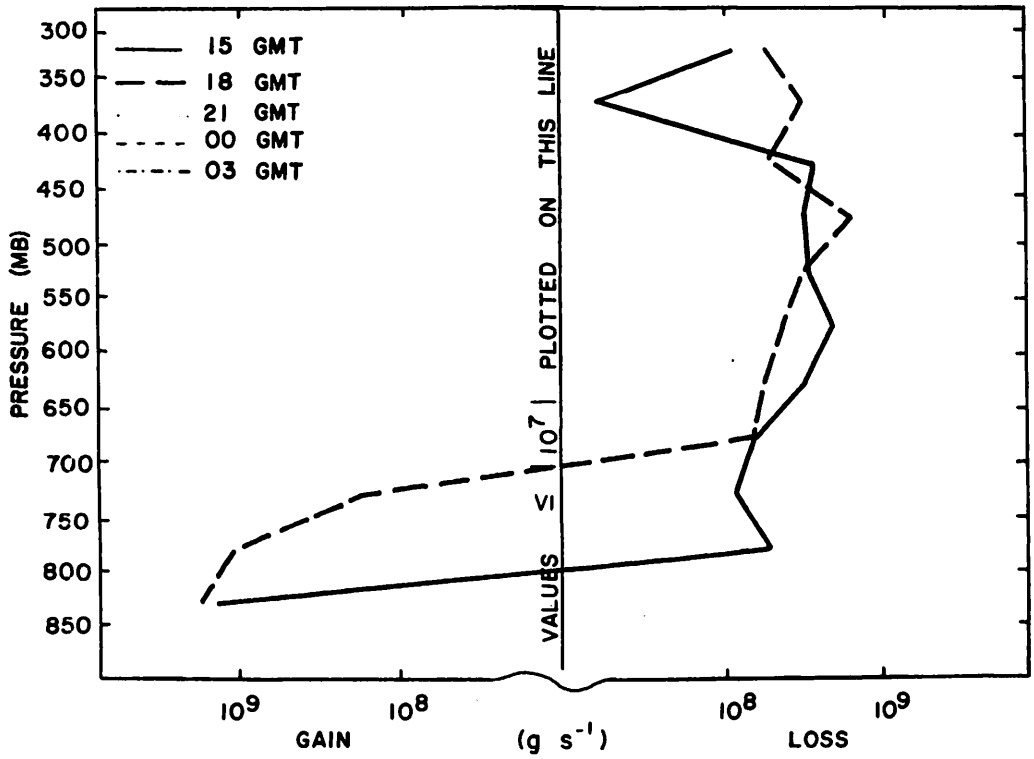

Fig. 5.23.5.2 Net vertical transport of water vapor through boundaries of 50-mb layers (gm s^{-1}) over the Texas HIPLEX area for 23 July 1978.

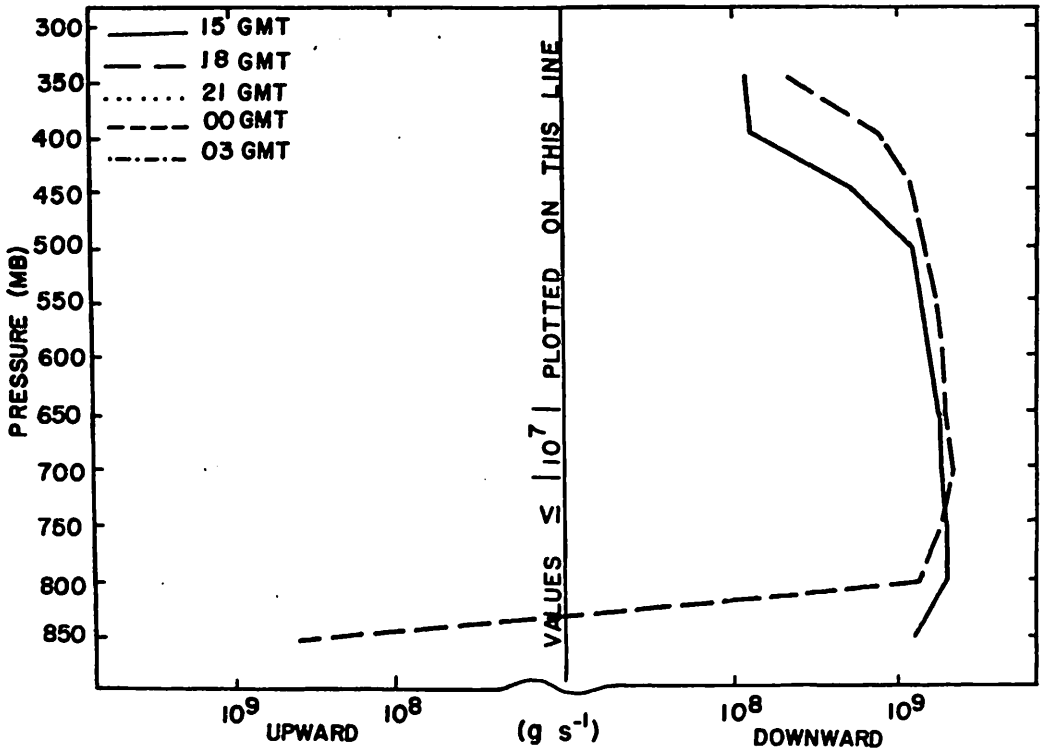

Fig. 5.23.5.3 Vertical transport of water vapor through constant pressure surfaces (gm s^{-1}) over the Texas HIPLEX area for 23 July 1978.

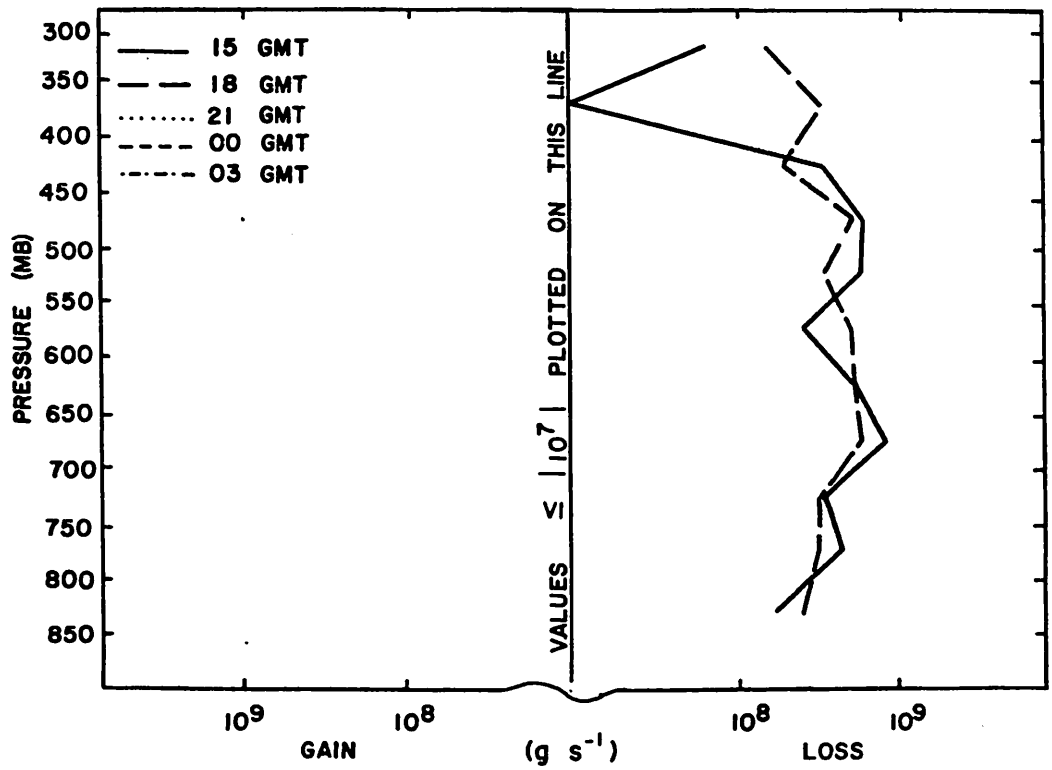

Fig. 5.23.5.4 Combined net horizontal and vertical transport of water vapor through boundaries of 50-mb layers (gm s^{-1}) over the Texas HIPLEX area for 23 July 1978.

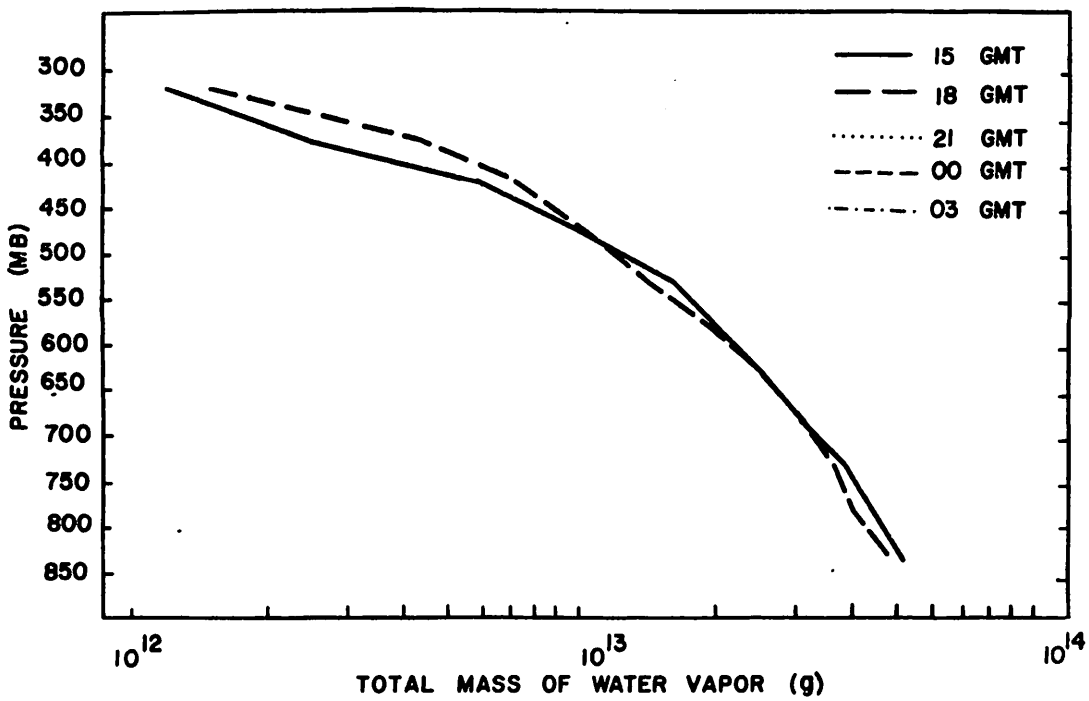

Fig. 5.23.5.5 Total mass of water vapor in layers 50 mb deep (gm) over the Texas HIPLEX area on 23 July 1978.

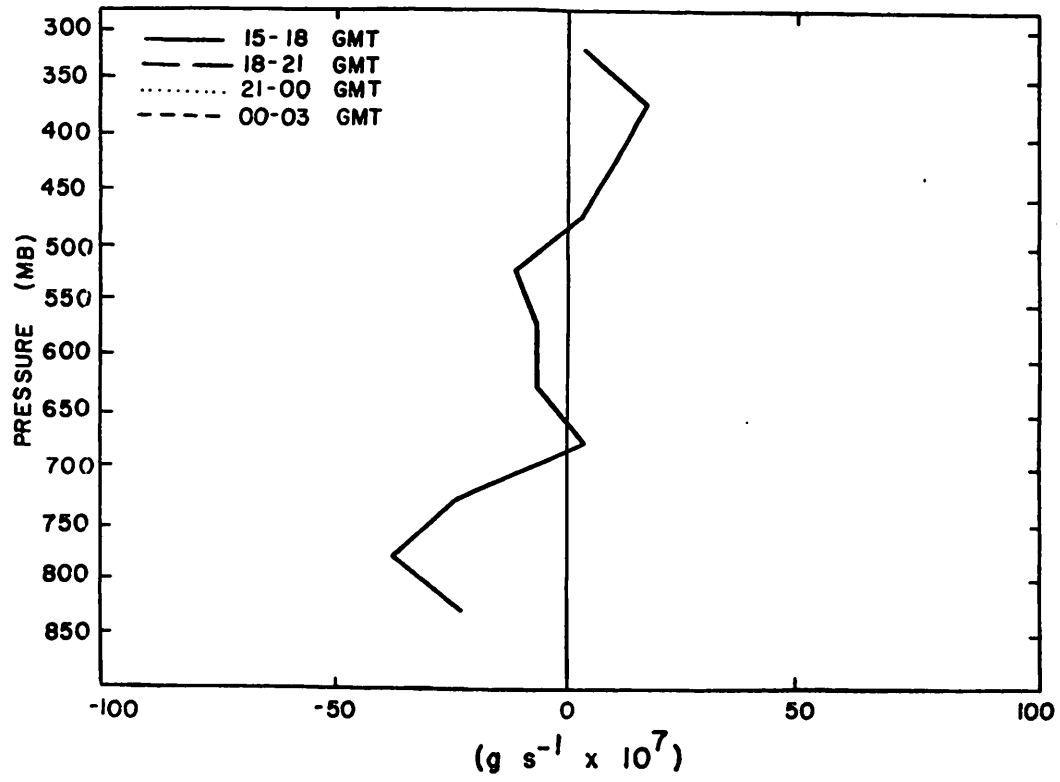

Fig. 5.23.5.6 Local rate-of-change in total mass of water vapor (g s^{-1} x 10^7) for the Texas HIPLEX area for 23 July 1978.

5.24 24 July 1978

5.24.1 Radar

The first radar echoes observed in the HIPLEX area formed at 1800 GMT, and echoes were observed after 0000 GMT (Fig. 5.24.1.1). Most echo tops were between 7.6 and 10.6 km (25 and 35K ft), but at 2200 and 2300 GMT, echoes to the north of Midland were measured at 12.5 km (41K ft). Echoes were isolated except at 2100 and 2200 GMT when the most convective activity was observed.

5.24.2 Surface

The occurrence of temperature minima (Fig. 5.24.2.1) were highly correlated with the dissipation of radar echoes. Temperature dropped from 4 to 8°C at Tahoka, Clairemont, Lenorah, and Garden City after 2000 GMT. All decreases except that at Lenorah at 2100 GMT were associated with the dissipation of echoes.

Relative humidity was more affected that absolute humidity from storm influences as is evident from charts of dewpoint-depression (Fig. 5.24.2.2). Pre-storm dewpoint-depression values of 12 to 16°C were reduced to 4 to 8°C at stations which recorded temperature drops. The humidity anomaly at Lamesa appeared to be unrelated to any convective activity and may be an error.

Changes in mixing ratio at stations which recorded temperature drops were small (Fig. 5.24.2.3). Tahoka, Lenorah, and Garden City recorded mixing ratio increases of 2 to 3 gm kg^{-1} between 2100 and 0000 GMT.

Temperature and humidity effects from thunderstorms usually lasted 2 to 3 hours after initial storm dissipation and at least one hour after echoes were no longer observed. Thunderstorms which moved through, but did not dissipate in, the network fail to produce significant thermodynamic effects at the ground. Examples on this day are echoes near Lamesa and Sweetwater at 2200 GMT.

Equivalent potential temperature showed little response to thunderstorm influences, since mixing ratio values were only slightly altered (Fig. 5.24.2.4). Anomalous centers at Lamesa probably resulted from erroneous data.

Terrain-induced vertical velocities reached values of -2.5 cm sec^{-1} near Robert Lee at 2000 GMT, but showed little continuity in other areas (Fig. 5.24.2.5).

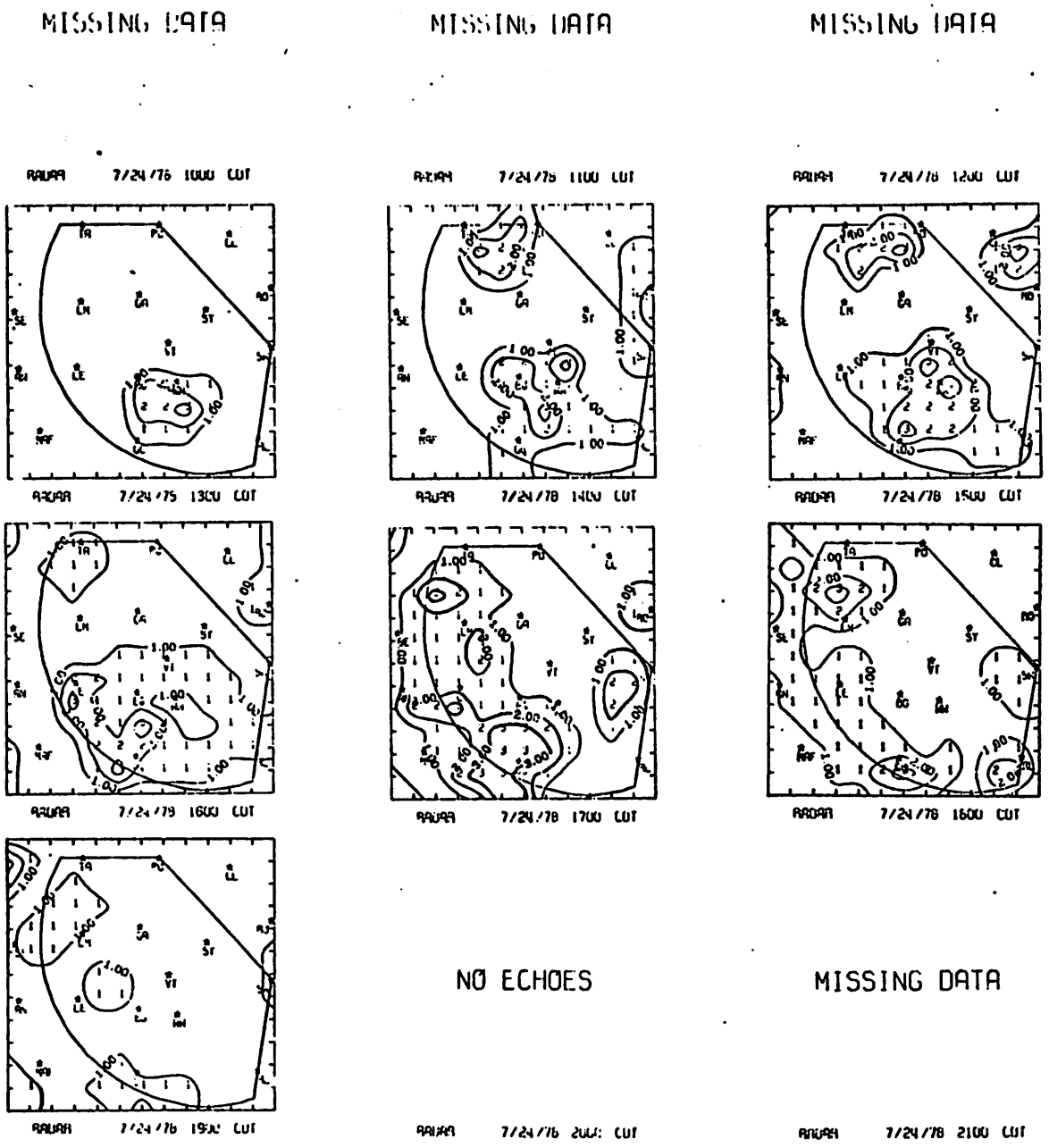

Fig. 5.24.1.1 Radar echoes for 24 July 1978.

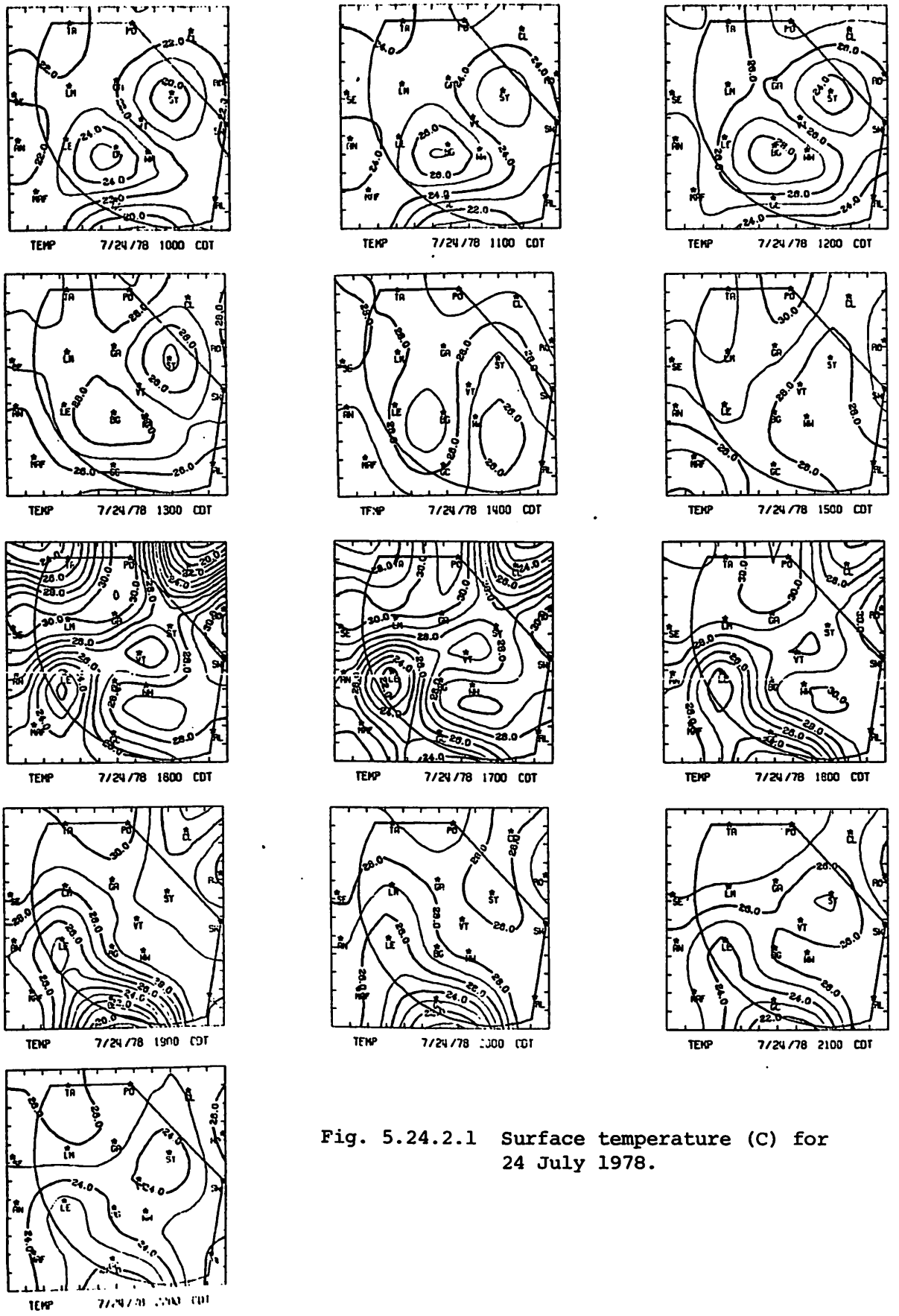

Fig. 5.24.2.1 Surface temperature (C) for 24 July 1978.

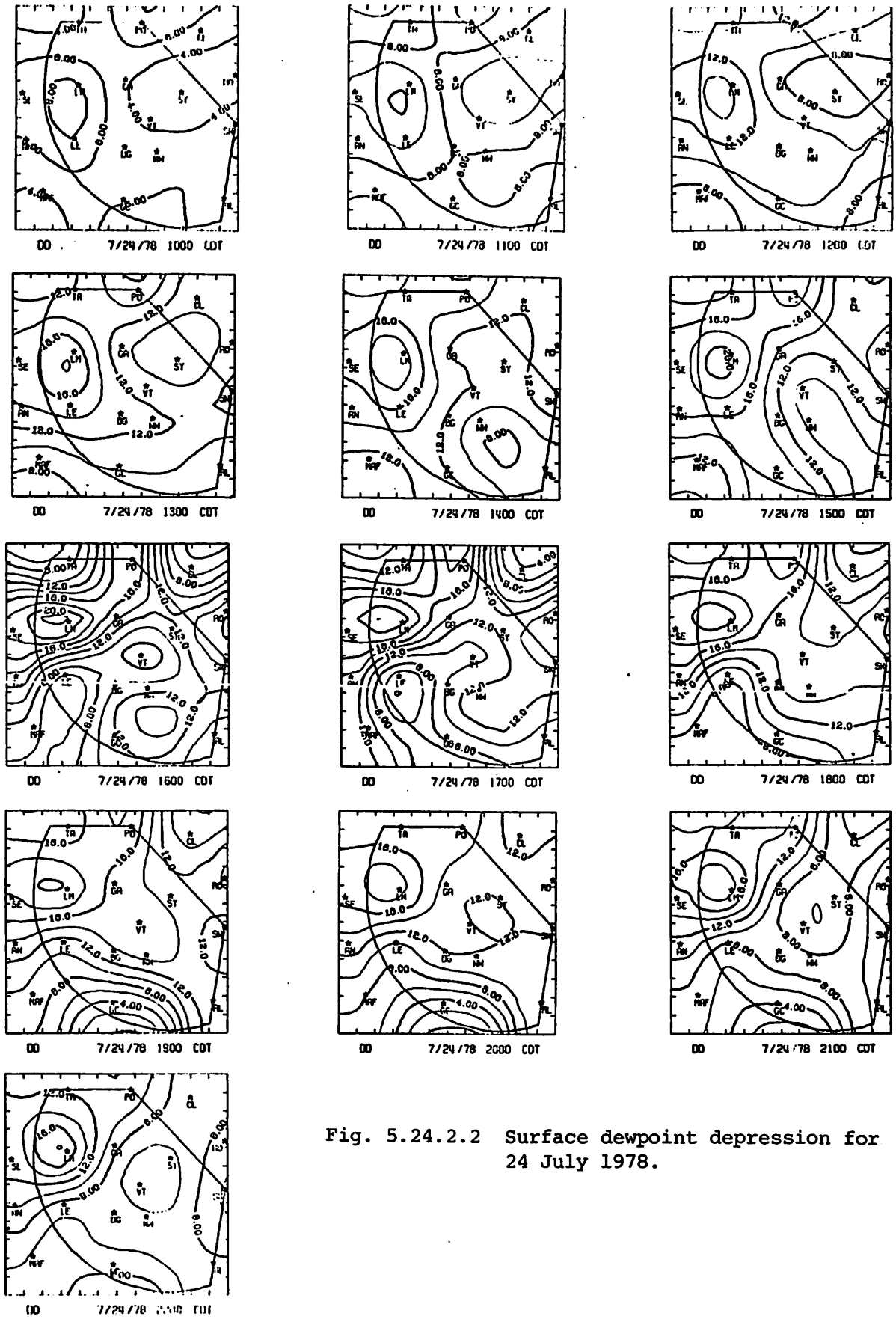

Fig. 5.24.2.2 Surface dewpoint depression for 24 July 1978.

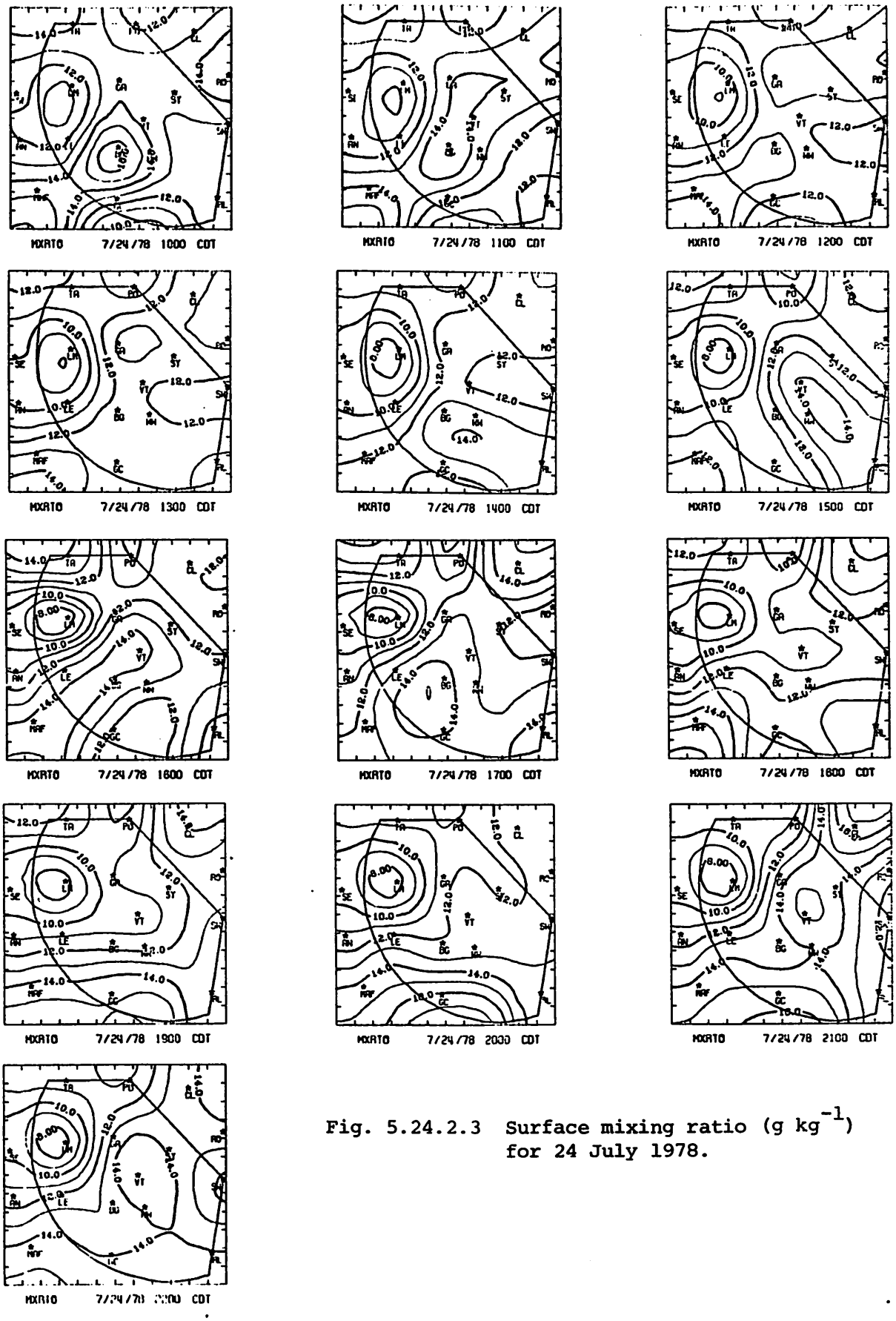

Fig. 5.24.2.3 Surface mixing ratio (g kg^{-1}) for 24 July 1978.

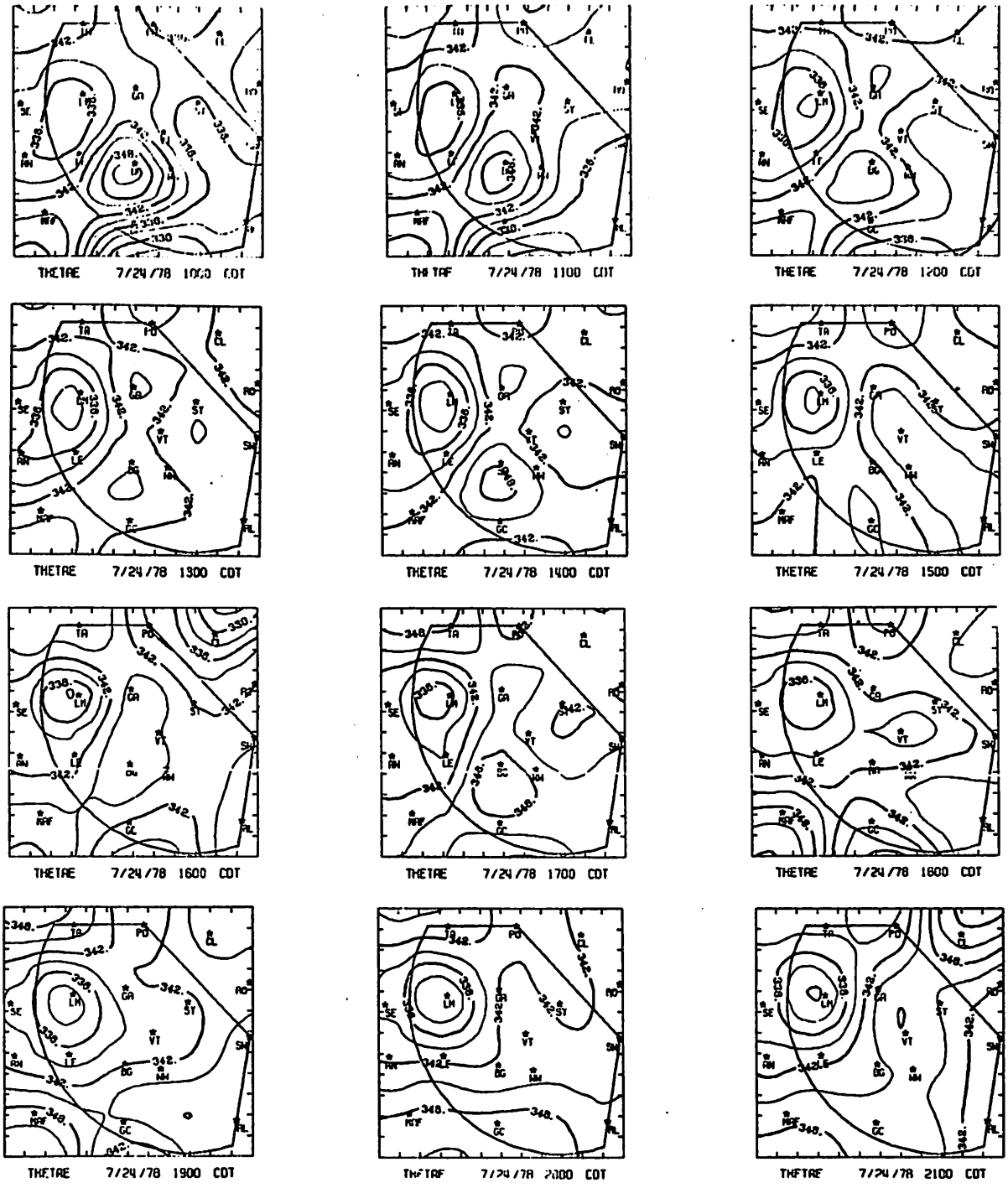

Fig. 5.24.2.4 Surface equivalent potential temperature (K) for 24 July 1978.

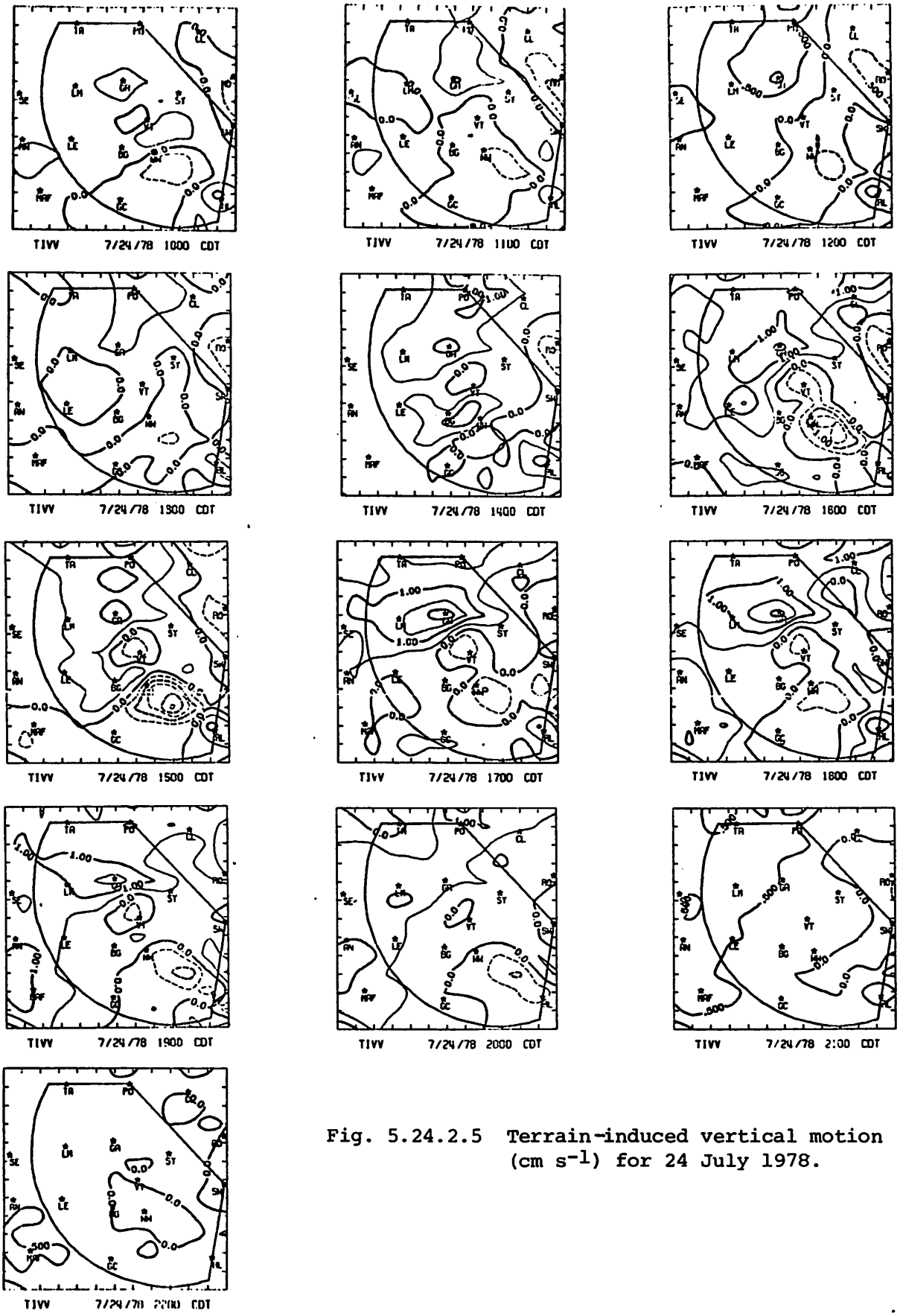

Fig. 5.24.2.5 Terrain-induced vertical motion (cm s^{-1}) for 24 July 1978.

Centers of velocity divergence were particularly responsive to clusters of thunderstorm cells (Fig. 5.24.2.6), though they often were not co-located with centers in fields of thermodynamic variables.

Boundary layer vertical velocities were calculated from surface divergence fields and show maximum values of 12.5 and -10.0 μbars sec^{-1} in strongly divergent and convergent areas, respectively (Fig. 5.24.2.7).

Moisture divergence (Fig. 5.24.2.8) was largest at 2100 GMT near Big Spring, where large velocity divergence and mixing ratio existed. Values there reached 3.5×10^{-4} sec^{-1}. Fields of vertical moisture flux (Fig. 5.24.2.9) followed the same pattern as that of moisture divergence.

Vorticity fields which resulted from thunderstorm effects on this day are shown in Fig. 5.24.2.10. Small, but strong, centers of vorticity occurred when thunderstorm activity was greatest. These centers usually were observed for less that two hours.

Pressure changes were negligible during the day (Fig. 5.24.2.11). Pressures across the network generally decreased until 0000 GMT and increased after that time.

Surface wind speeds were small when thunderstorm echoes were not nearby (Fig. 5.24.2.12). Effects from downdrafts, particularly at 2100 GMT, were reflected in the wind fields. The largest wind speed was 7.8 m sec^{-1} at Lenorah at 2100 GMT. Wind data were missing at Seminole throughout the day.

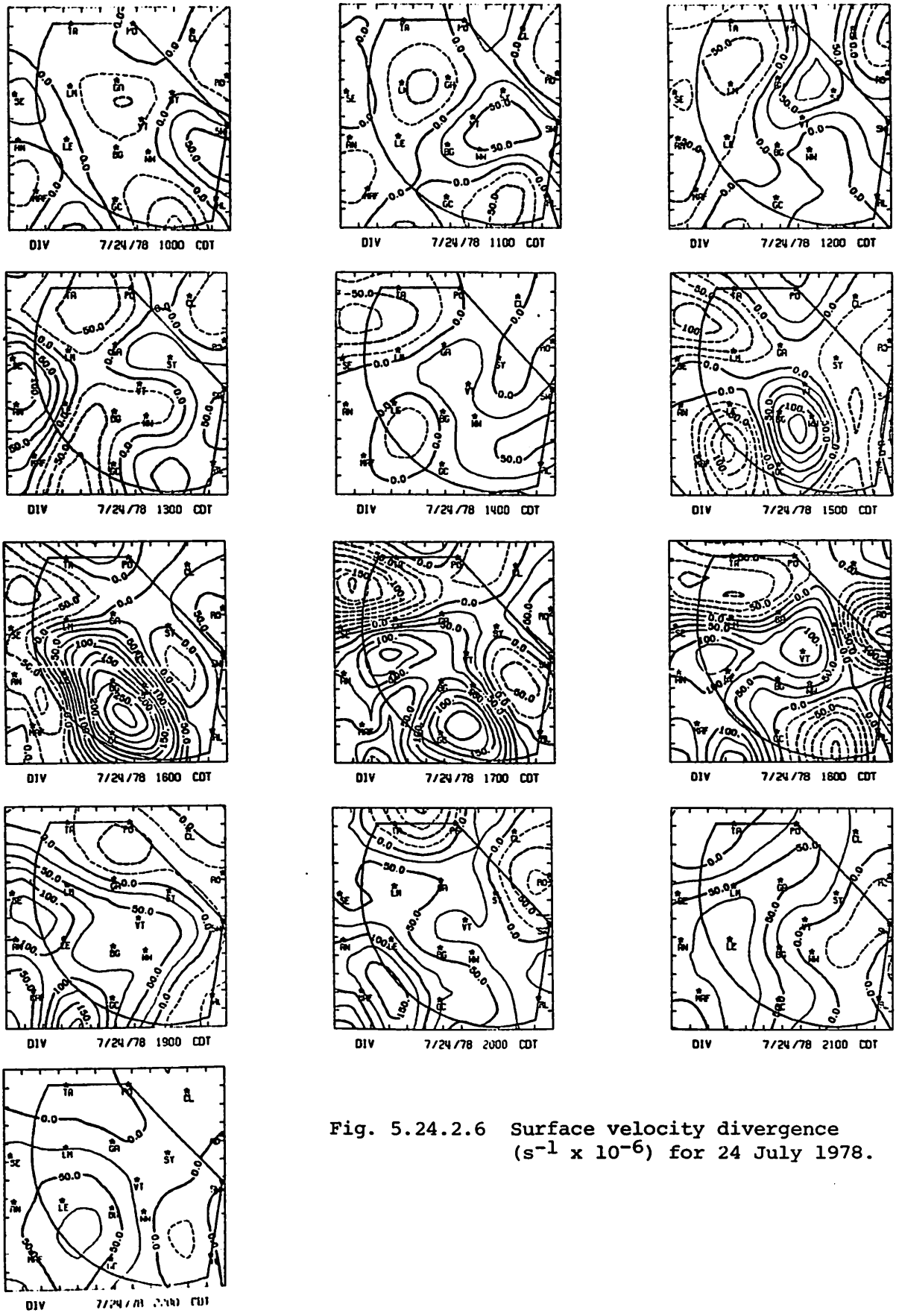

Fig. 5.24.2.6 Surface velocity divergence (s^{-1} x 10^{-6}) for 24 July 1978.

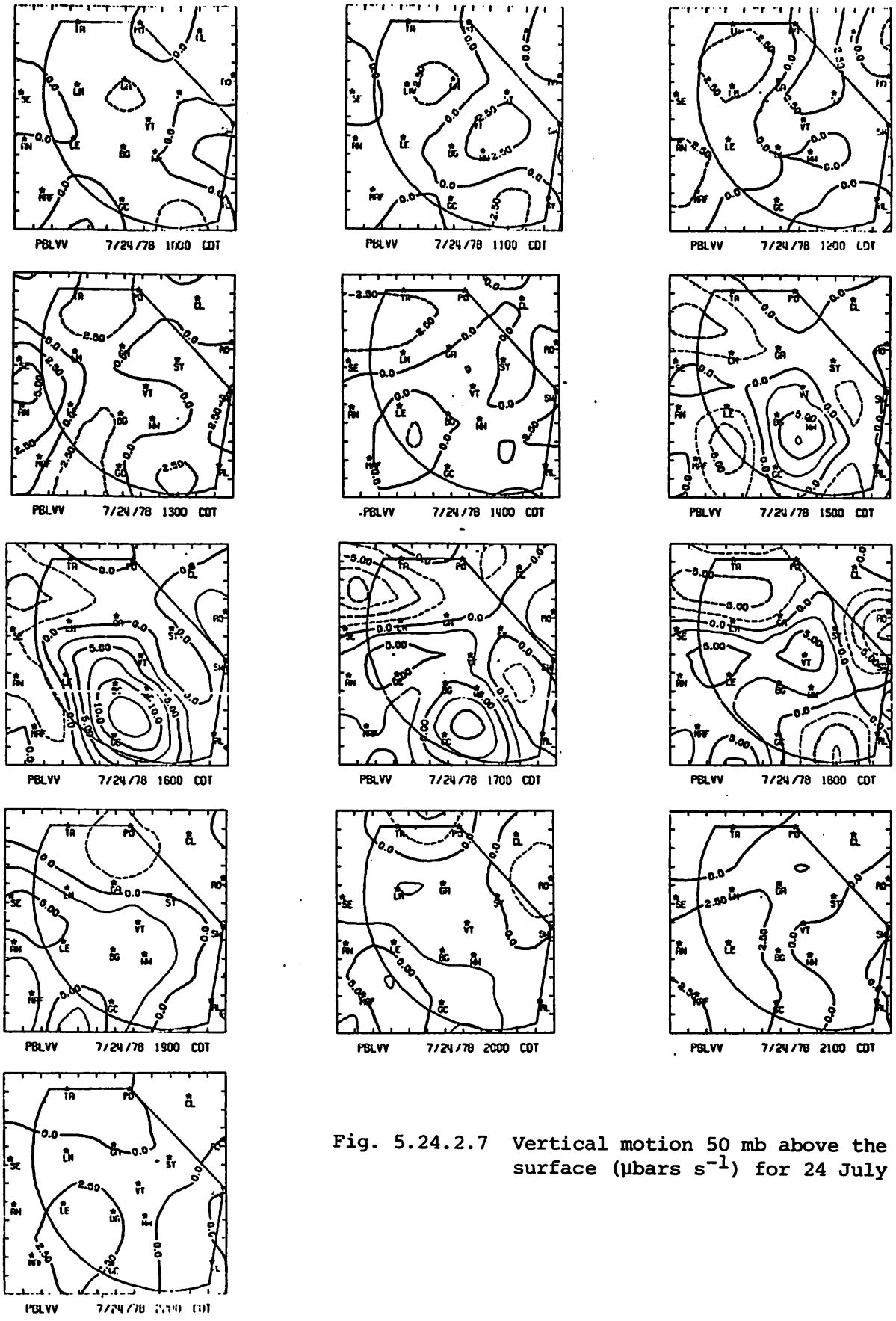

Fig. 5.24.2.7 Vertical motion 50 mb above the surface (μbars s^{-1}) for 24 July 1978.

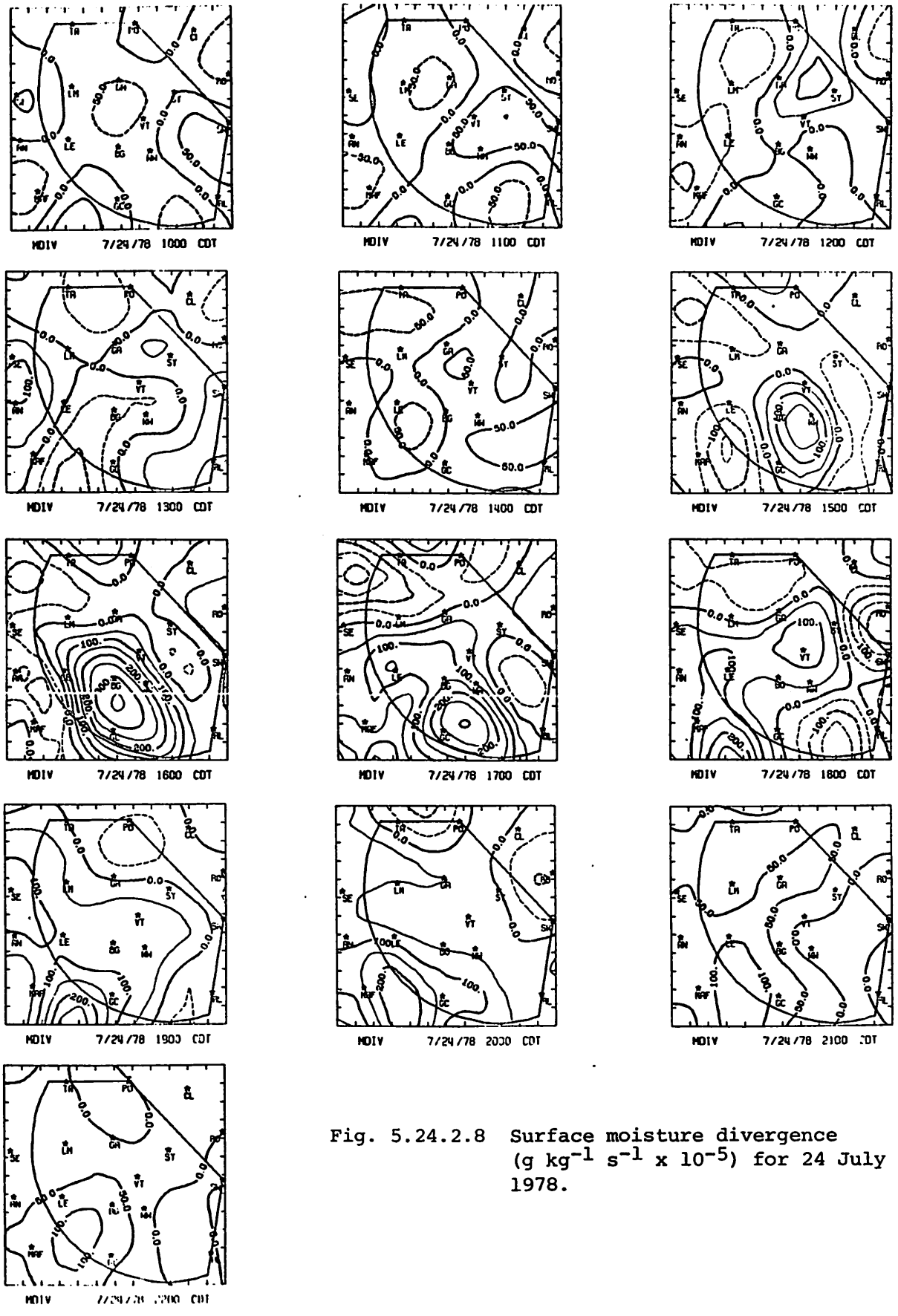

Fig. 5.24.2.8 Surface moisture divergence ($g\ kg^{-1}\ s^{-1} \times 10^{-5}$) for 24 July 1978.

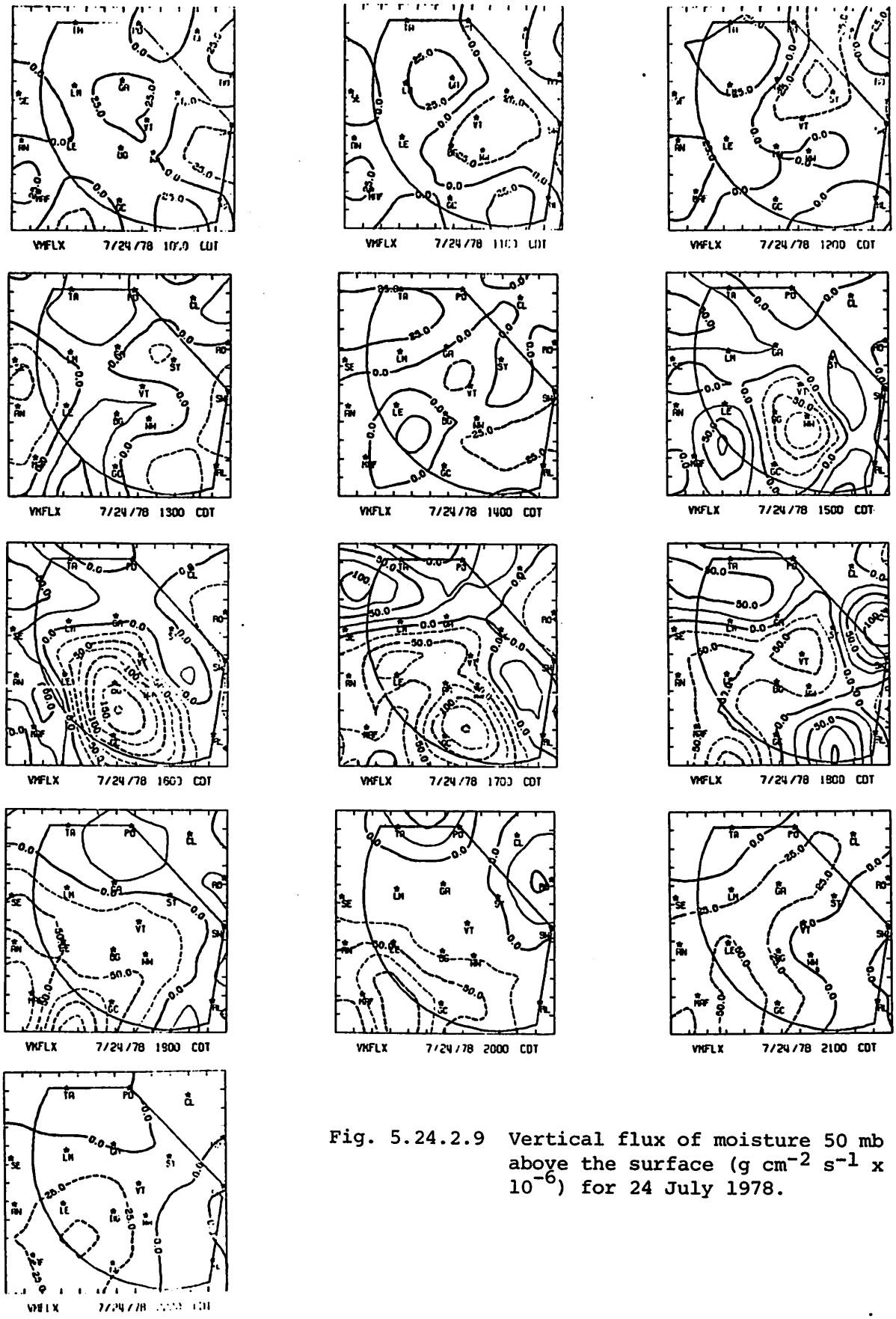

Fig. 5.24.2.9 Vertical flux of moisture 50 mb above the surface (g cm^{-2} s^{-1} x 10^{-6}) for 24 July 1978.

Fig. 5.24.2.10 Surface vorticity ($s^{-1} \times 10^{-6}$) for 24 July 1978.

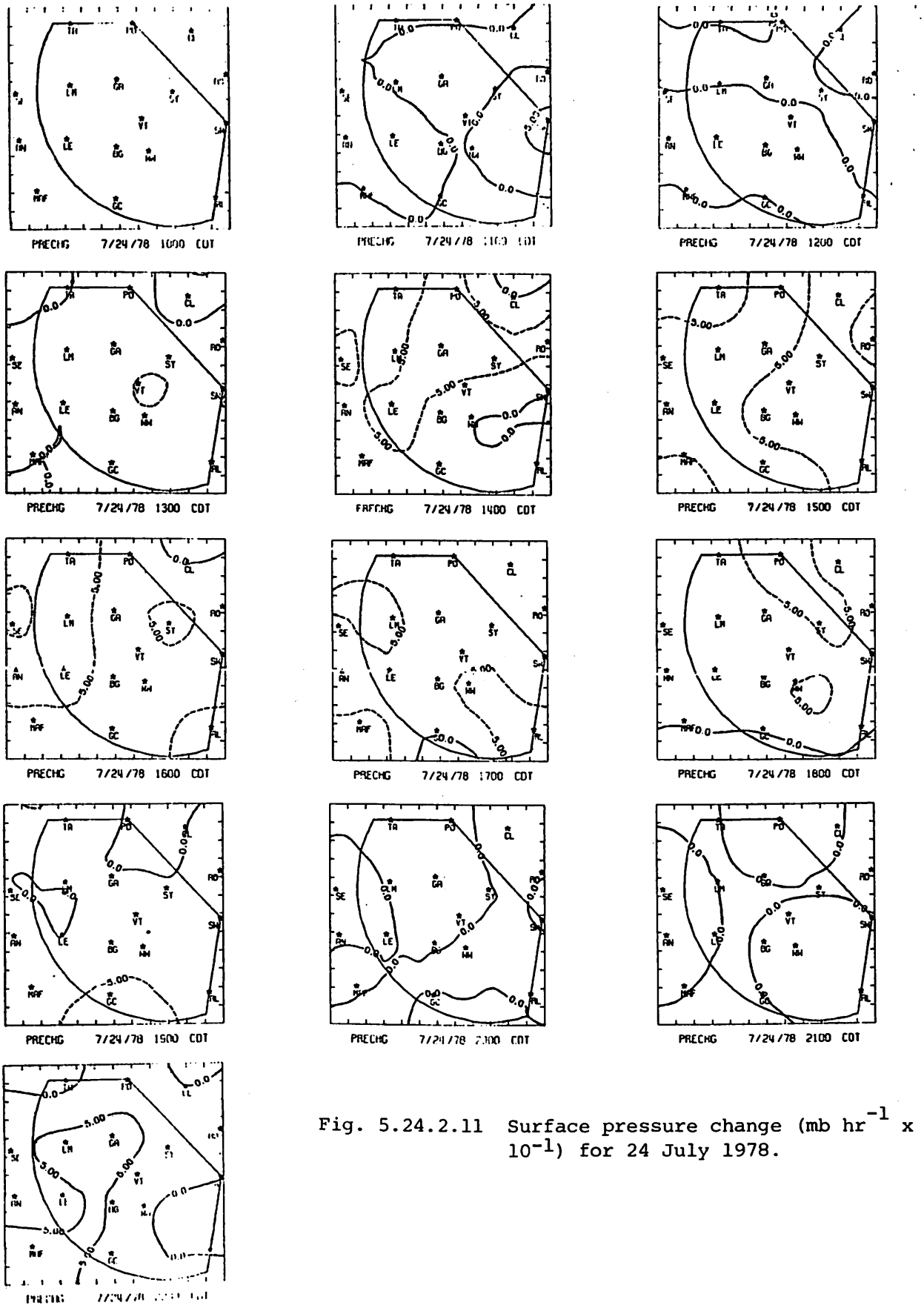

Fig. 5.24.2.11 Surface pressure change (mb hr^{-1} x 10^{-1}) for 24 July 1978.

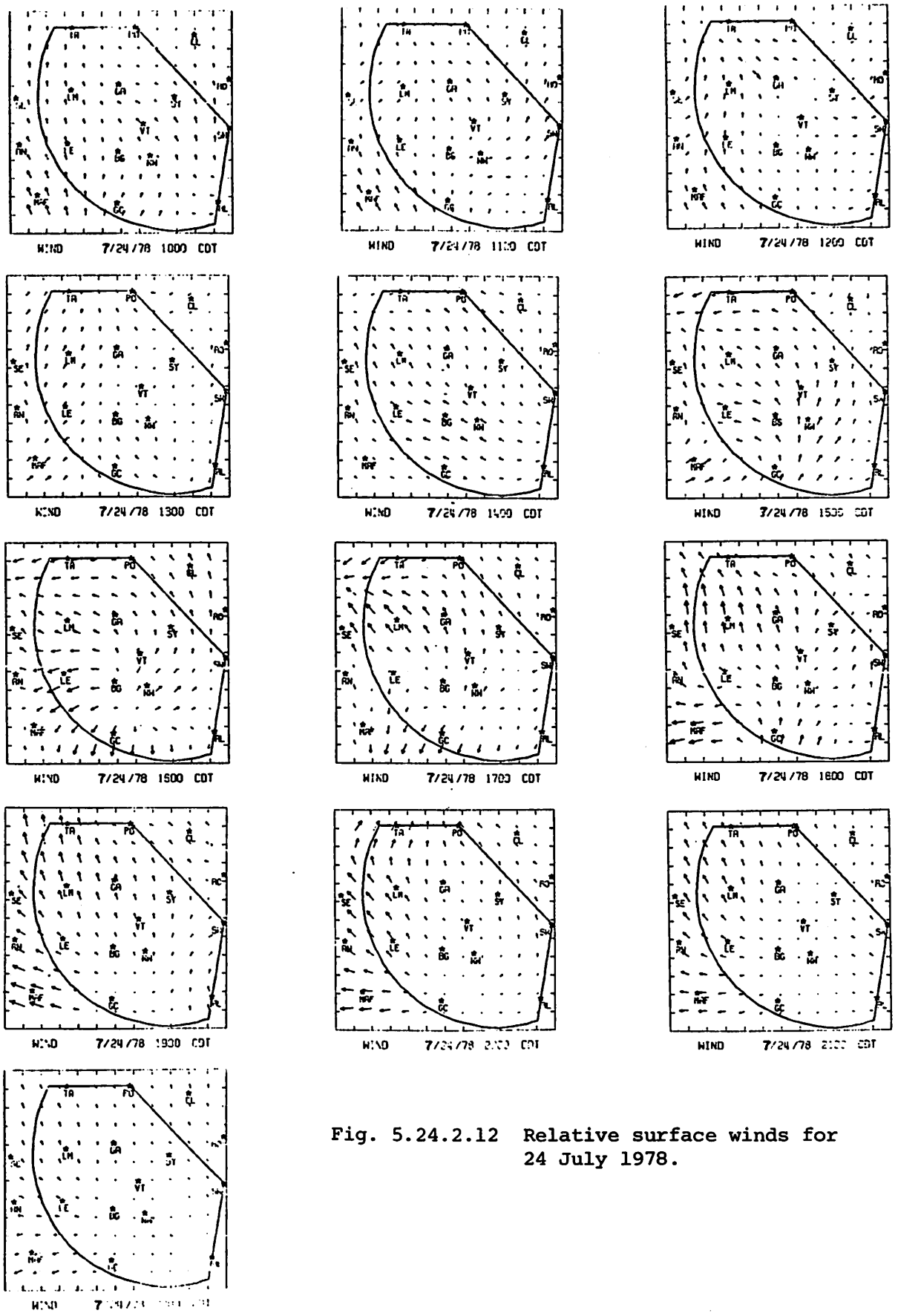

Fig. 5.24.2.12 Relative surface winds for 24 July 1978.

5.25 25 July 1978

5.25.1 Radar

No radar echoes were observed over the HIPLEX area on this day. Cumulus, and some towering cumulus, were reported at surrounding locations.

5.25.2 Surface

Features of the surface temperature field varied only slightly during the day (Fig. 5.25.2.1). Temperatures across the network never varied by more than 4°C. The maximum temperature recorded was 35°C.

Dewpoint depression (Fig. 5.25.2.2), mixing ratio (Fig. 5.25.2.3), and equivalent potential temperature (Fig. 5.25.2.4) also varied little across the network due to the absence of significant convective activity. Features of those fields were consistent throughout the day. Mixing ratios were moderately low, as 15 gm kg^{-1} was the largest value measured. Most stations recorded values of 10 to 12 gm kg^{-1}.

Steady wind velocities produced persistent terrain-induced vertical velocity fields (Fig. 5.25.2.5). Largest value calculated was -3.0 cm sec^{-1} near Robert Lee at 1600 GMT.

Divergence fields failed to show any significant centers (Fig. 5.25.2.6). Those that did occur were fairly persistent and represent a surface flow field which is unaffected by convective activity. Boundary layer vertical velocities are also small (Fig. 5.25.2.7), the largest values being ±5.0 cm sec^{-1}.

Moisture divergence (Fig. 5.25.2.8) and vertical moisture flux (Fig. 5.25.2.9) fields were similar to those of velocity divergence in that features are small and persistent. These features are typical of days having no convective activity.

Surface vorticity fields show no significant features except the negative vorticity center near Lamesa (Fig. 5.25.2.10). This center was caused by wind directions near Tahoka, which differ from those of surrounding stations. Values in that vorticity center are small.

Pressure changes were small (Fig. 5.25.2.11) and showed patterns similar to the previous day. Pressures decreased until 0100 GMT, at which time they were fairly steady.

Surface wind speeds were small (Fig. 5.25.2.12), and wind directions were mainly from the south and were persistent throughout the day.

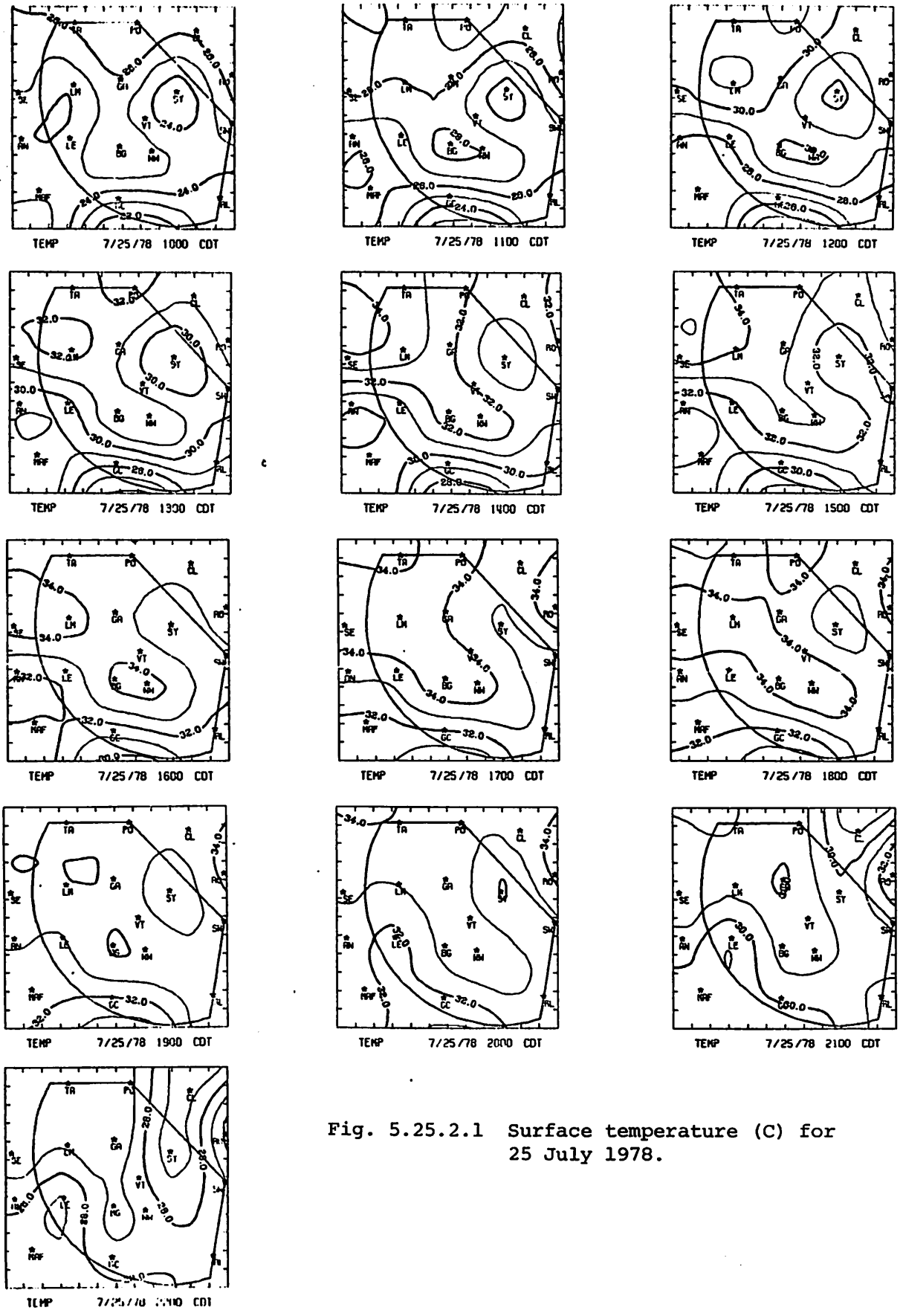

Fig. 5.25.2.1 Surface temperature (C) for 25 July 1978.

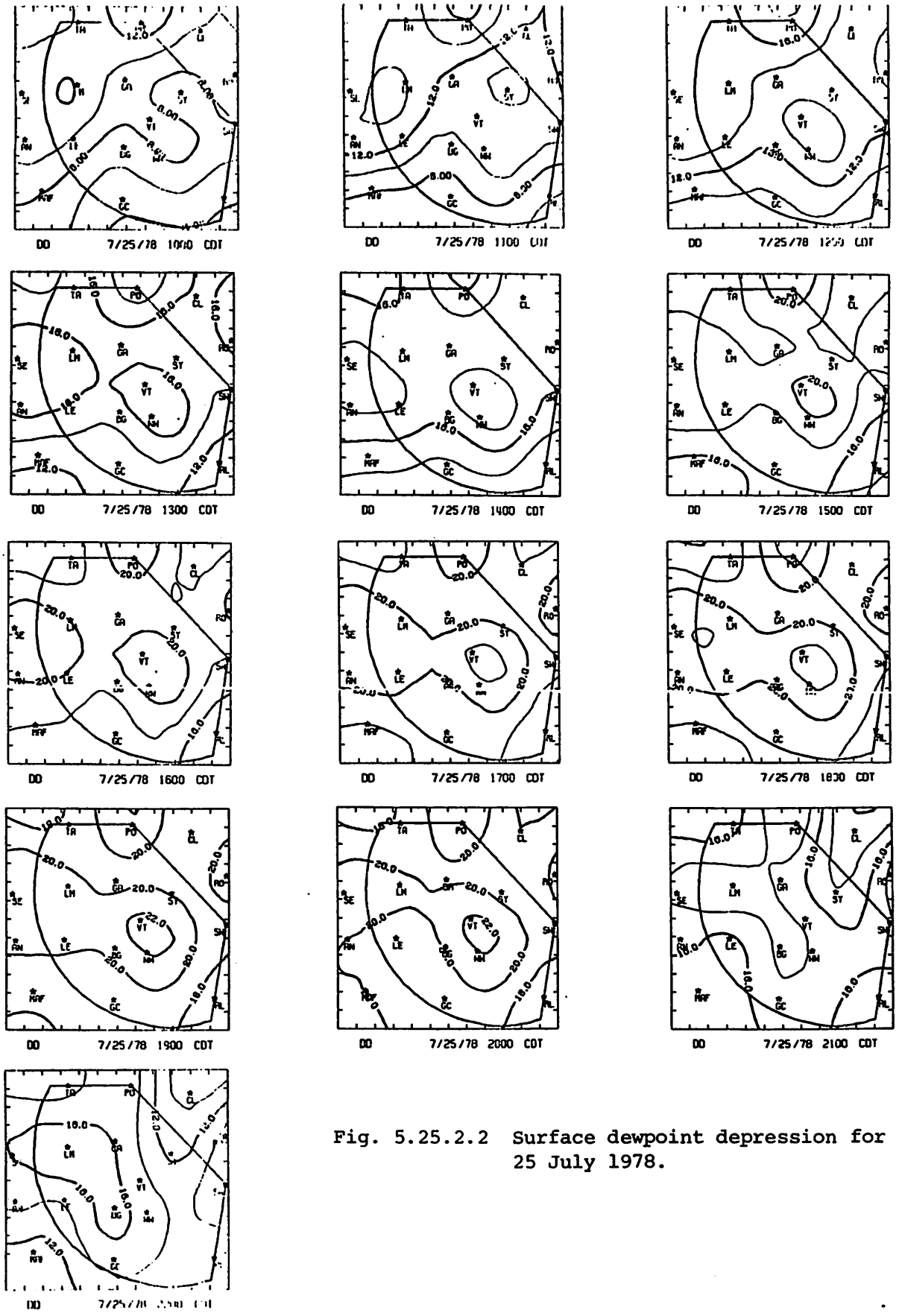

Fig. 5.25.2.2 Surface dewpoint depression for 25 July 1978.

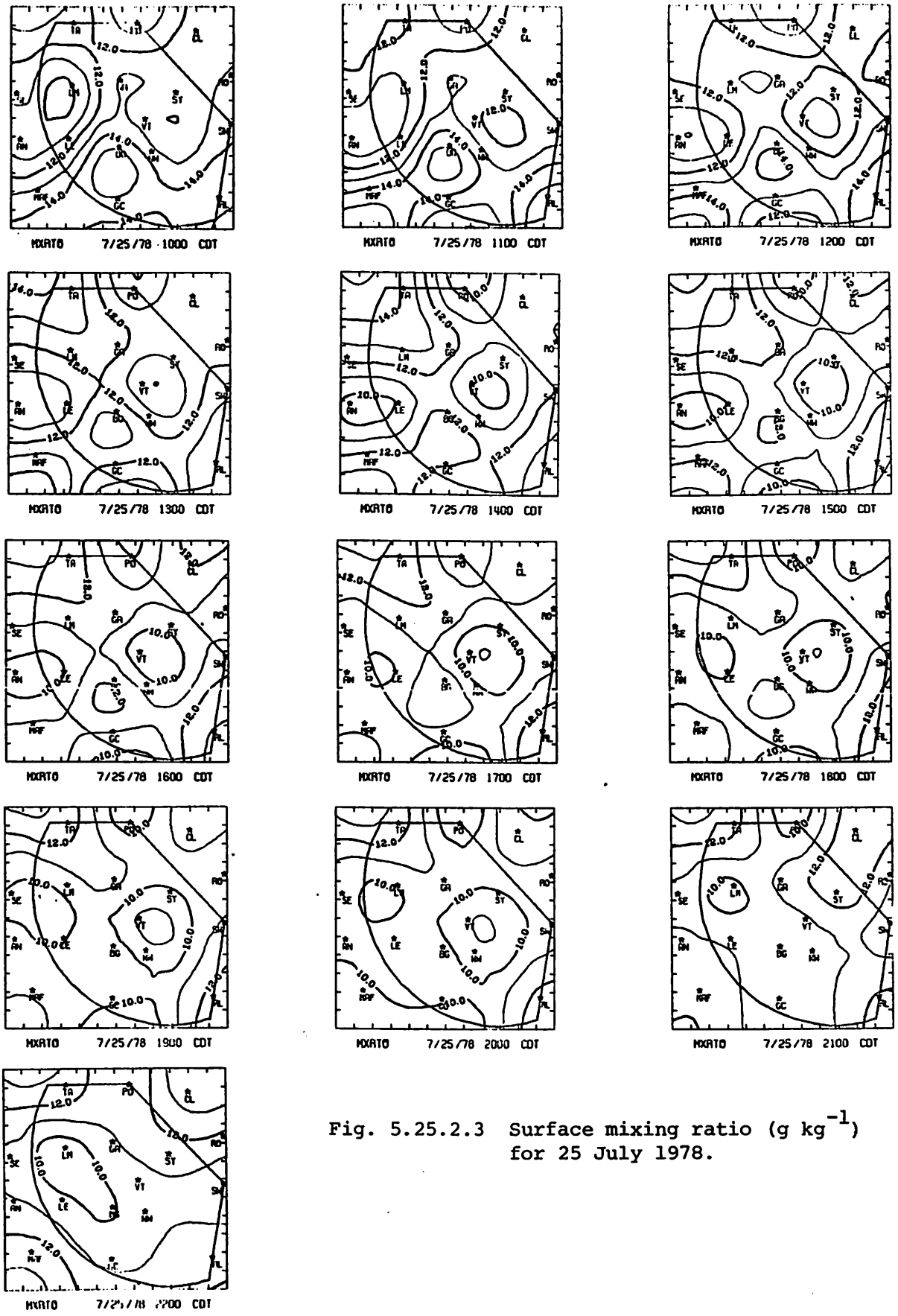

Fig. 5.25.2.3 Surface mixing ratio (g kg^{-1}) for 25 July 1978.

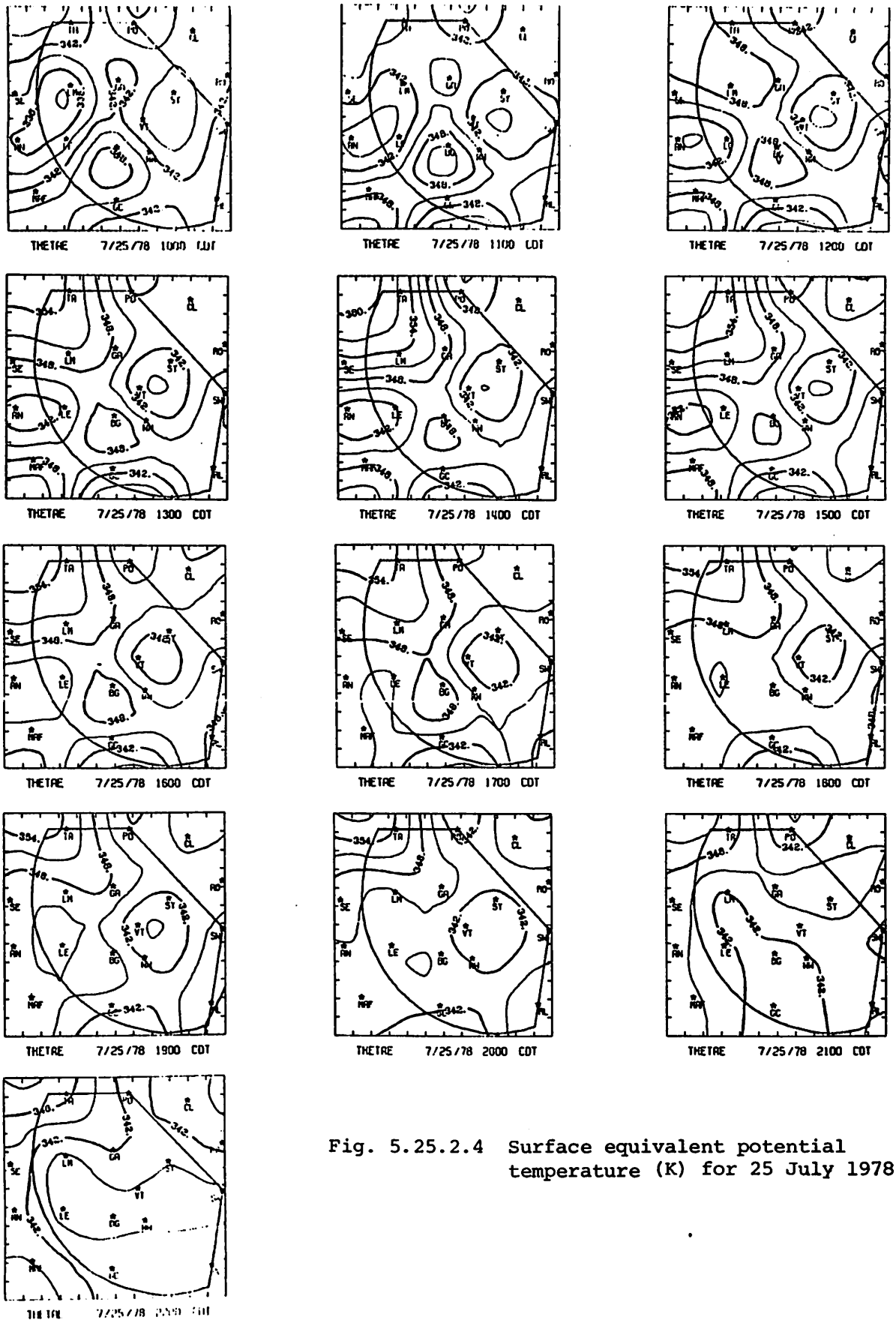

Fig. 5.25.2.4 Surface equivalent potential temperature (K) for 25 July 1978.

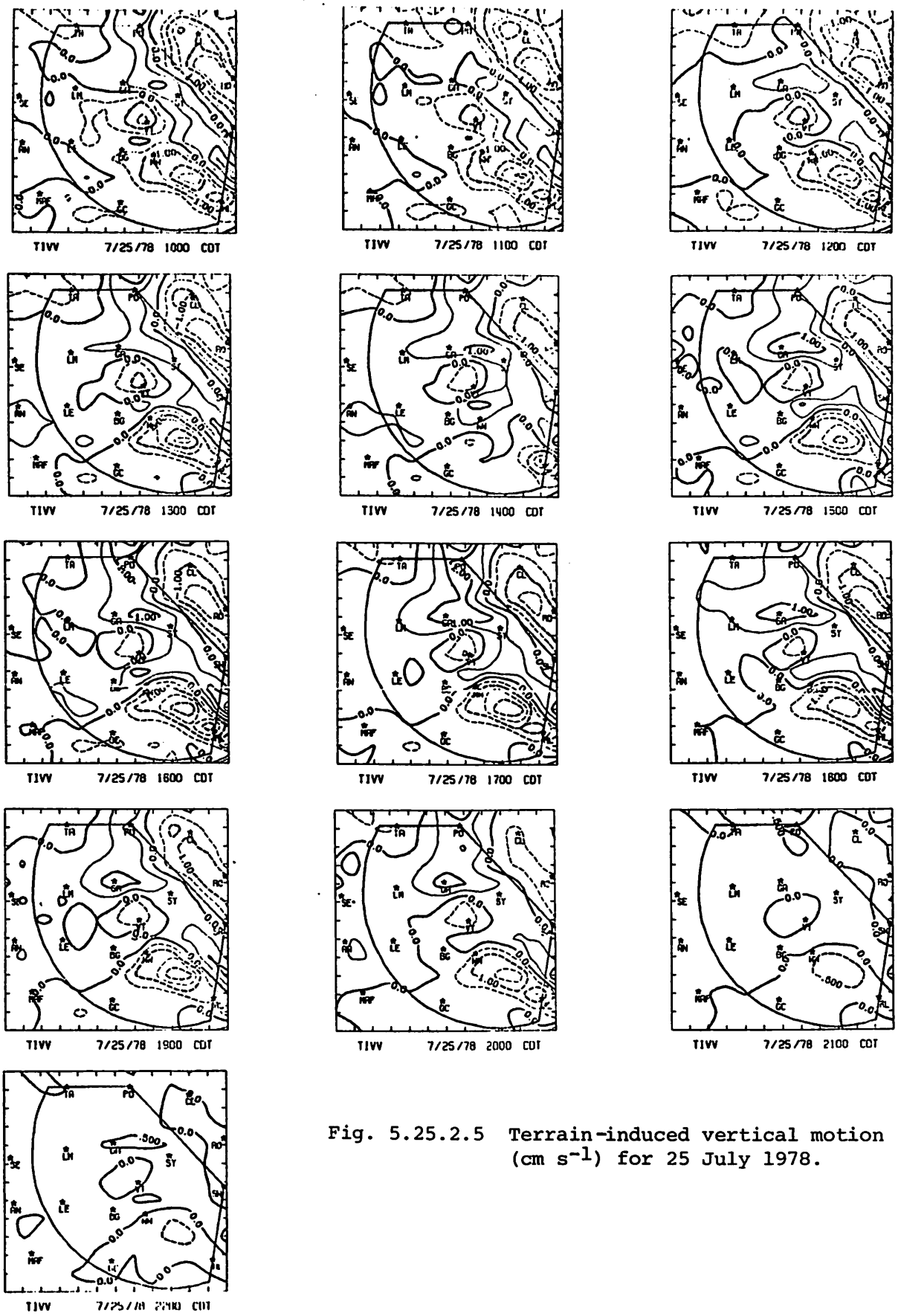

Fig. 5.25.2.5 Terrain-induced vertical motion (cm s^{-1}) for 25 July 1978.

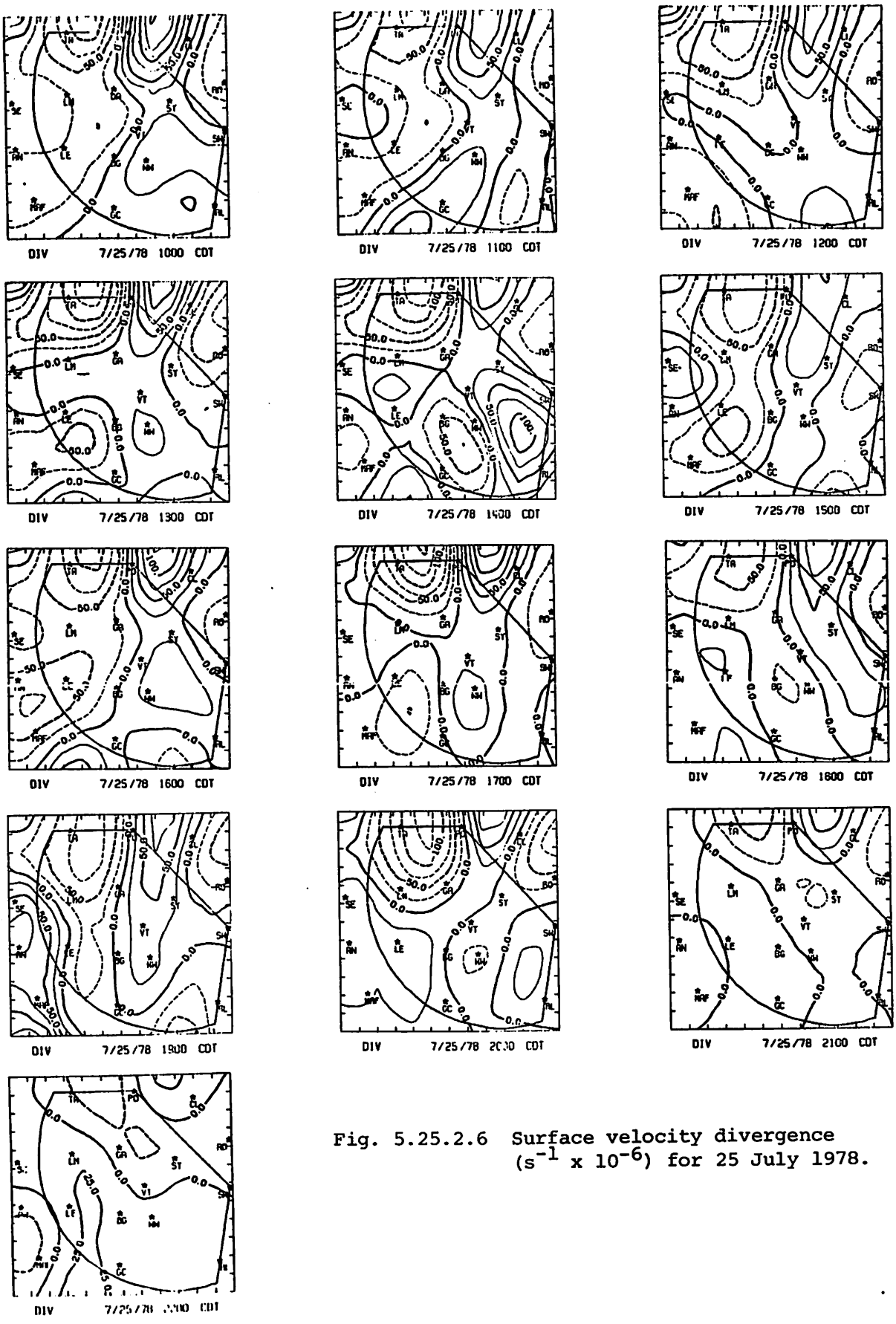

Fig. 5.25.2.6 Surface velocity divergence (s^{-1} x 10^{-6}) for 25 July 1978.

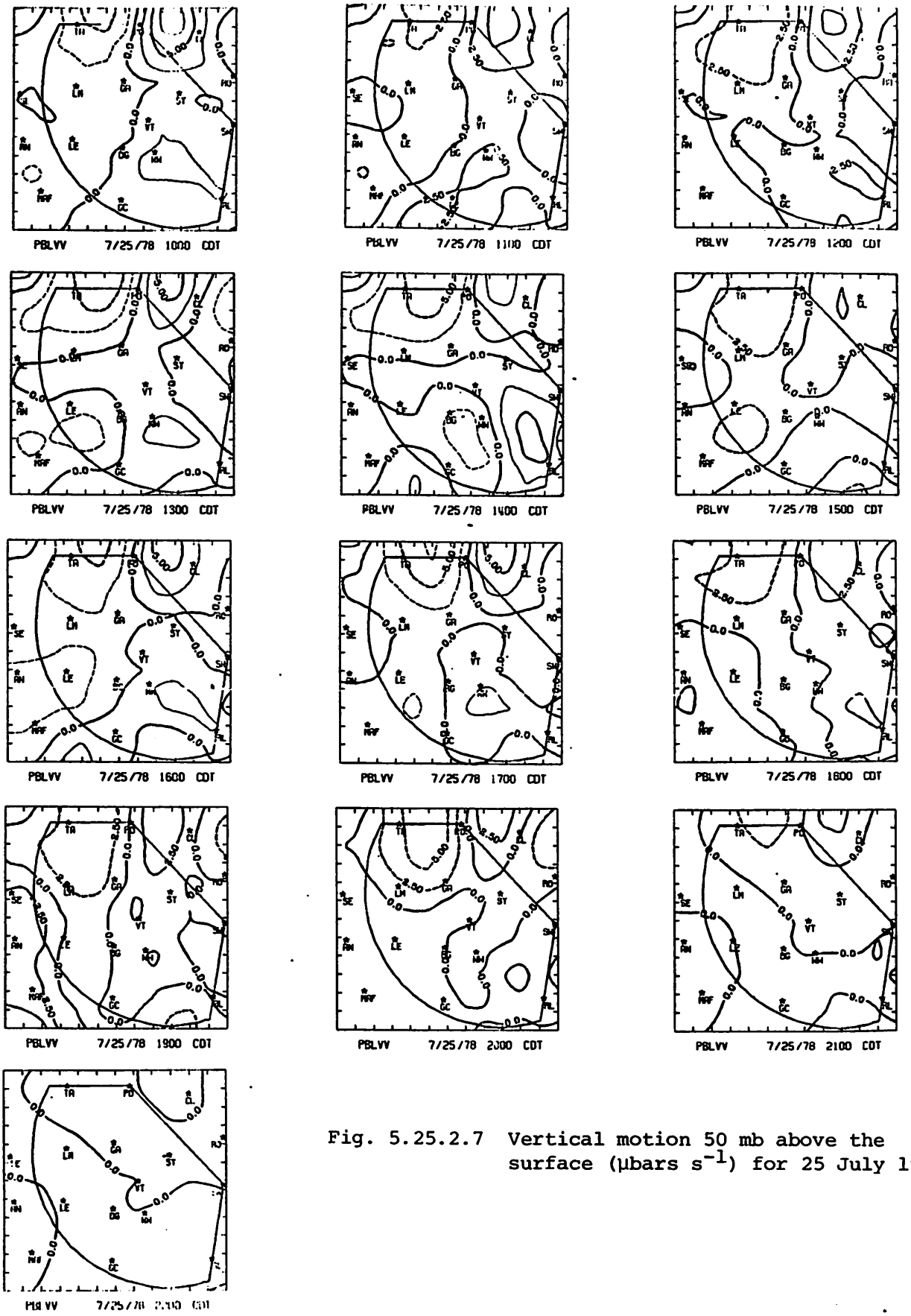

Fig. 5.25.2.7 Vertical motion 50 mb above the surface (μbars s^{-1}) for 25 July 1978.

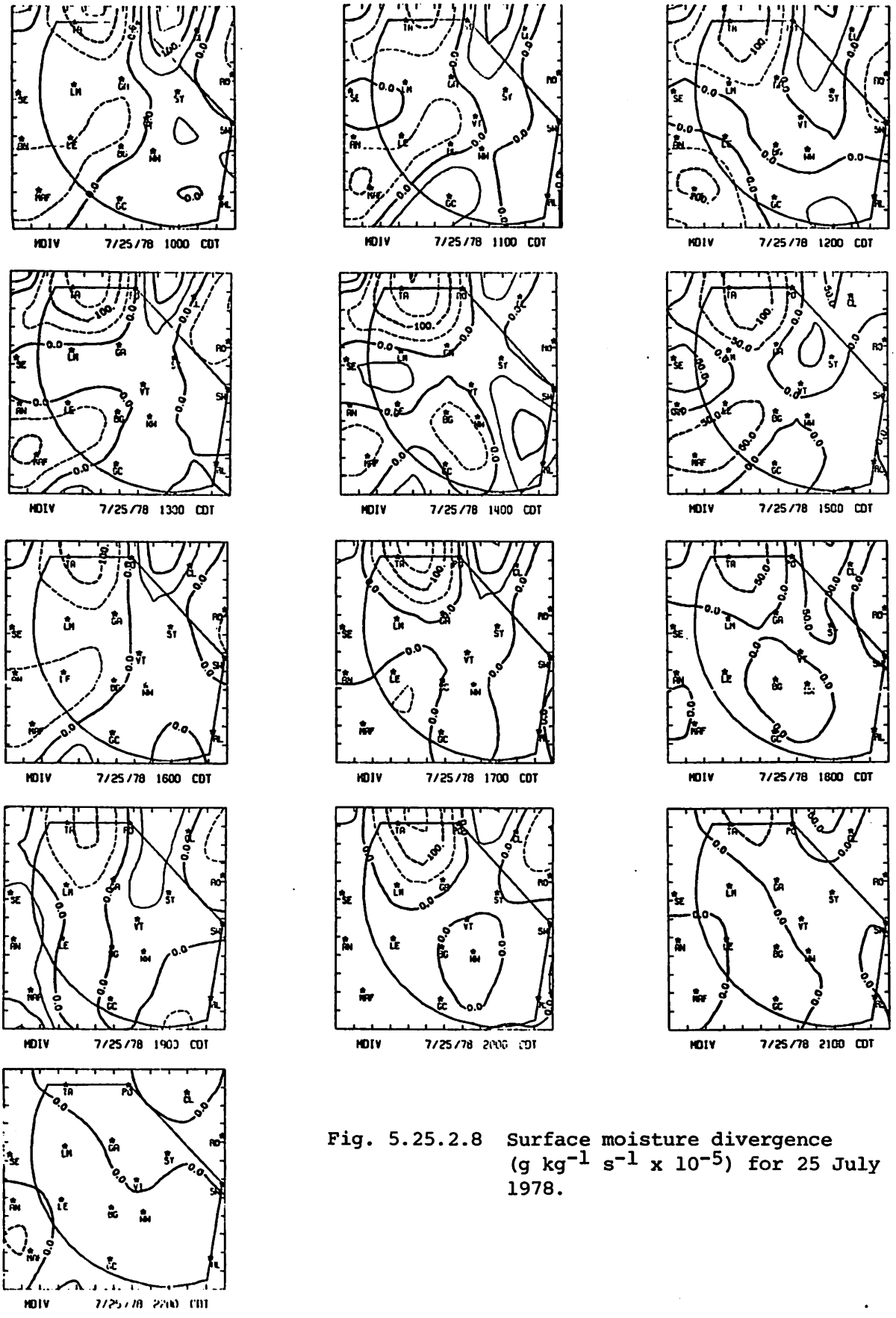

Fig. 5.25.2.8 Surface moisture divergence ($g\ kg^{-1}\ s^{-1} \times 10^{-5}$) for 25 July 1978.

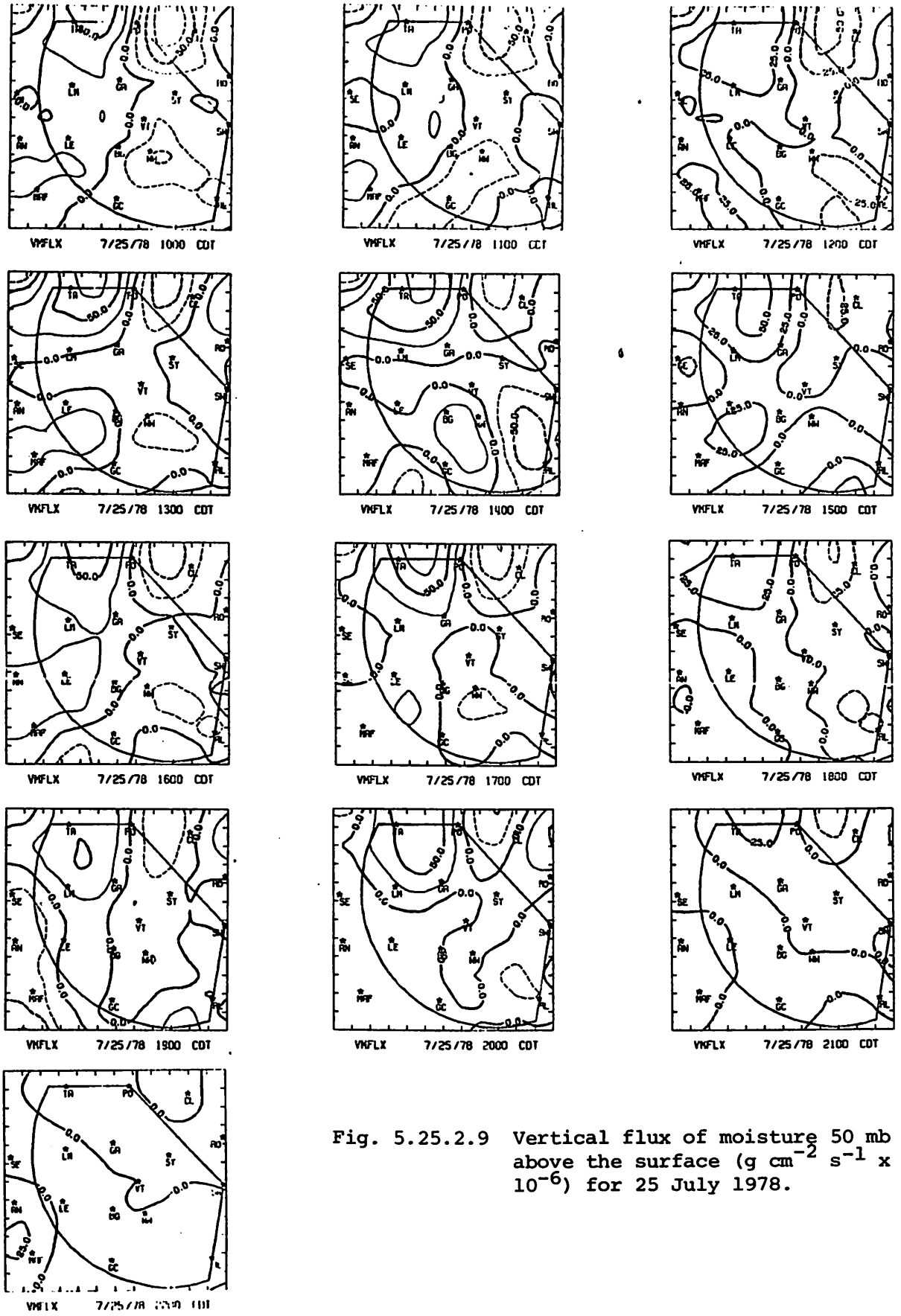

Fig. 5.25.2.9 Vertical flux of moisture 50 mb above the surface (g cm^{-2} s^{-1} x 10^{-6}) for 25 July 1978.

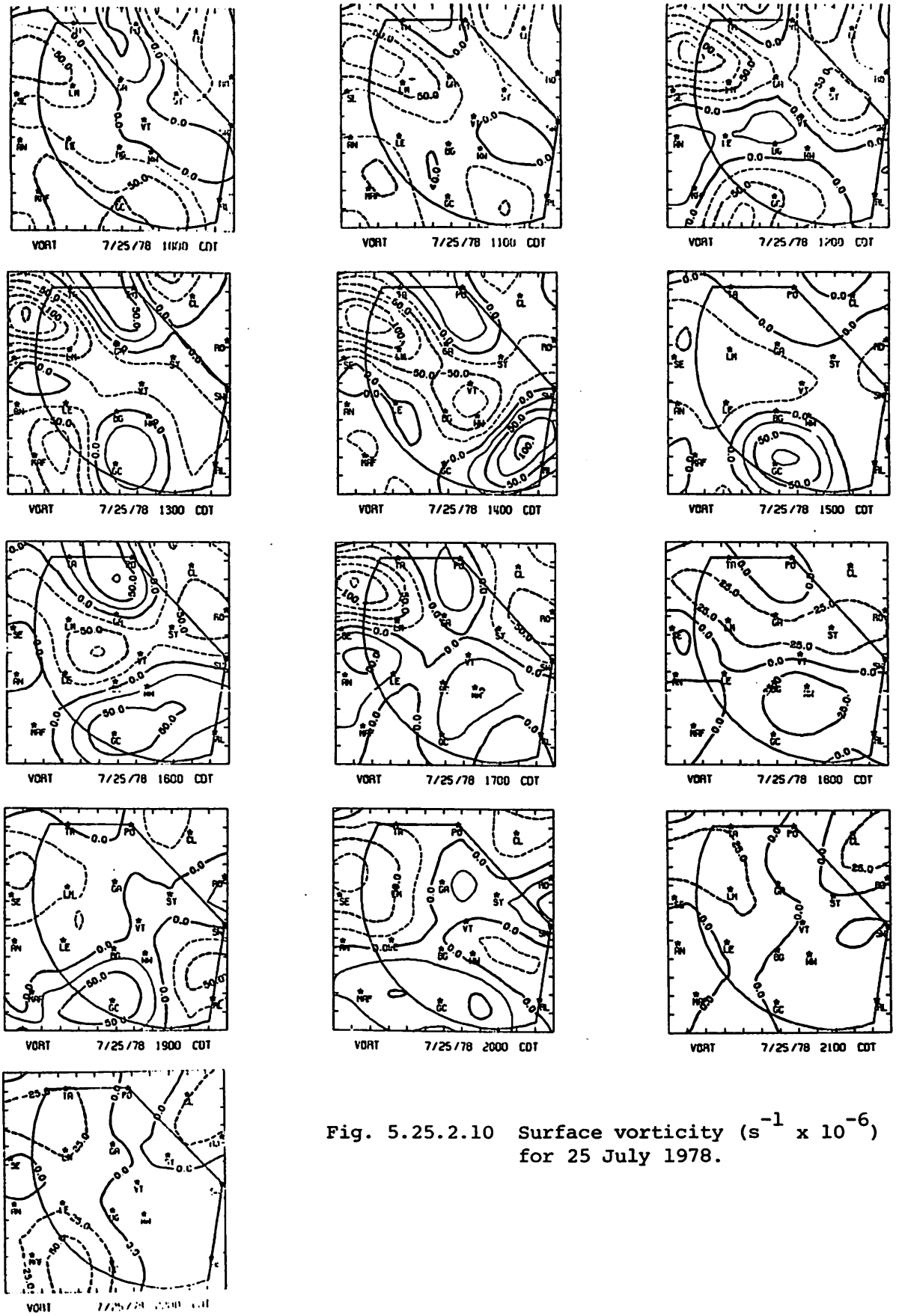

Fig. 5.25.2.10 Surface vorticity (s^{-1} x 10^{-6}) for 25 July 1978.

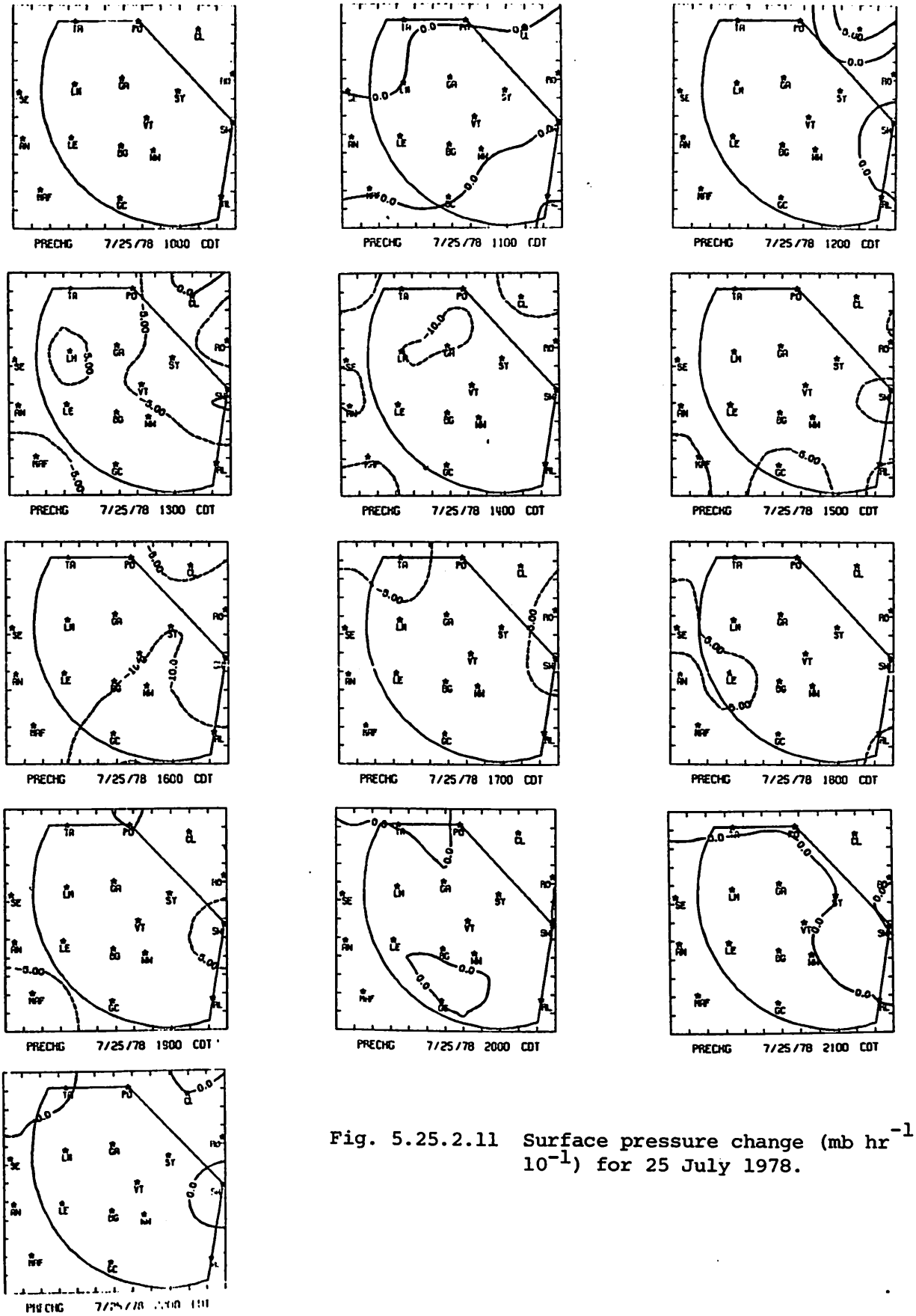

Fig. 5.25.2.11 Surface pressure change (mb hr^{-1} x 10^{-1}) for 25 July 1978.

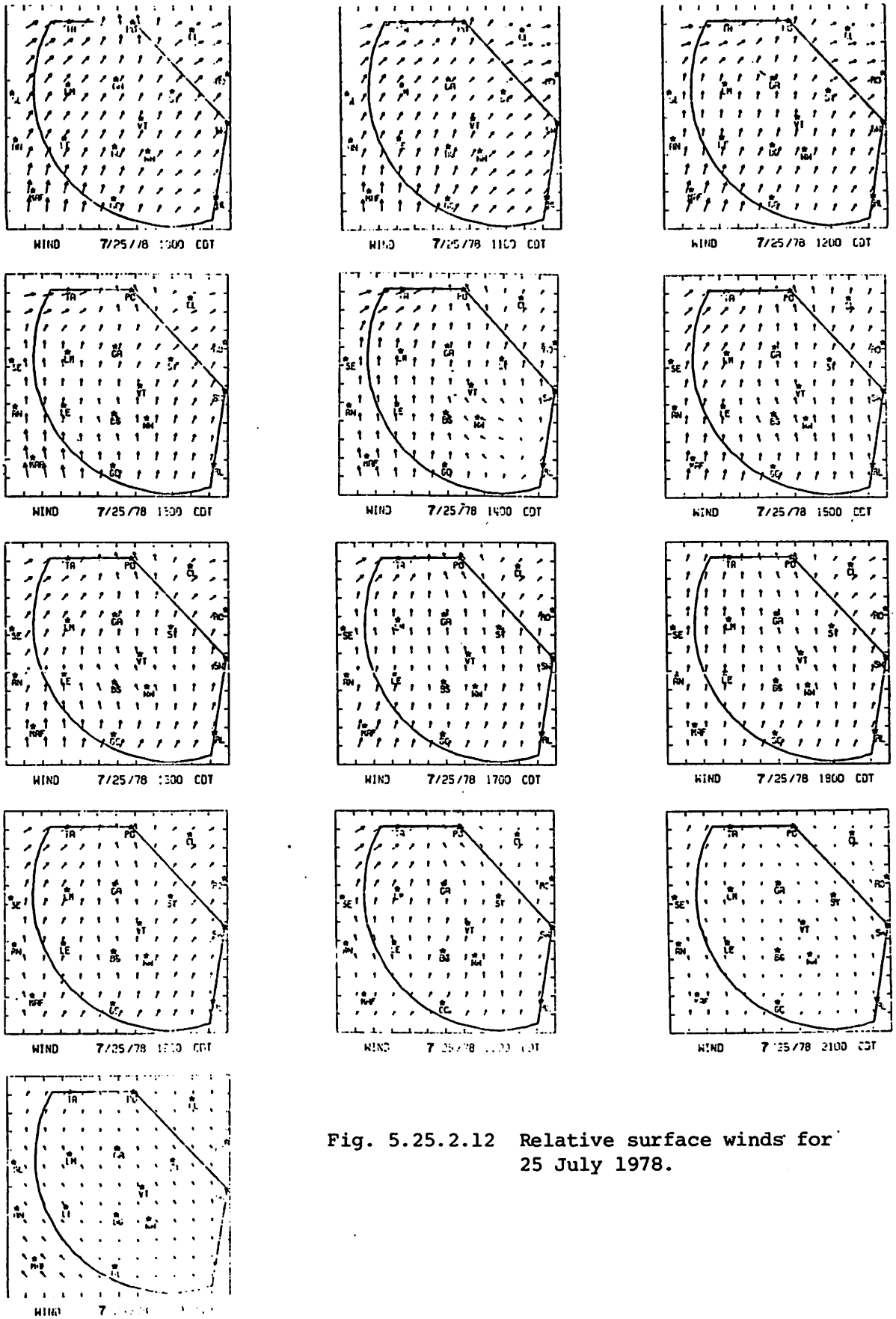

Fig. 5.25.2.12 Relative surface winds for 25 July 1978.

5.25.3 Upper Level Kinematic Parameters

Upper level parameters were calculated only for 2100, 0000, and 0300 GMT sounding times. Profiles for the three times are similar and fail to show large changes from one time to the next.

Horizontal mass divergence was positive in the lowest 100 mb at 2100 GMT (Fig. 5.25.3.1). Profiles for 0000 and 0300 GMT show a trend toward less divergence and greater convergence in the surface-550-mb layer. This trend caused vertical velocities to change from negative at 2100 and 0000 GMT to positive between 700 and 200 mb at 0300 GMT (Fig. 5.25.3.2). Profiles for 0000 and 0300 GMT show small mass divergence above 500 mb, and vertical velocities reflect that tendency by decreasing slightly with height above that level.

Profiles of moisture divergence are similar to those of mass divergence (Fig. 5.25.3.3).

5.25.4 Energetics

Effects of the horizontal (Fig. 5.25.4.1) and vertical (Fig. 5.25.4.2) flux terms of the latent heat energy budget tend to oppose each other. Horizontal motions diverge latent heat energy in the lowest layers at all times, but vertical motions (downward) tend to concentrate it there. Similarly, in a region centered at 700 mb, horizontal motions progressively converged more latent heat energy at each consecutive sounding time, but vertical motion transported that energy downward.

The local change term of the latent heat energy budget is small at 0000 and 0300 GMT (Fig. 5.25.4.3), so that the residual term balanced differences between horizontal and vertical flux divergence (Fig. 5.25.4.4). At 0000 GMT this led to negative values of -R, implying that evaporation or small-scale fluxes were increasing latent heat energy content. At 0300 GMT, energy was being decreased above 800 mb, particularly at 600 mb. None of the terms of the budget were significantly large above 500 mb.

Diabatic heating occurred in most layers of the area at 0000 GMT, while heating and cooling occurred below and above 600 mb, respectively, at 0300 GMT (Fig. 5.25.4.5). Values, however, were small.

Horizontal and vertical flux divergence of kinetic energy were negligible below 300 mb due to very small wind speed (Figs. 5.25.4.6 and 5.25.4.7).

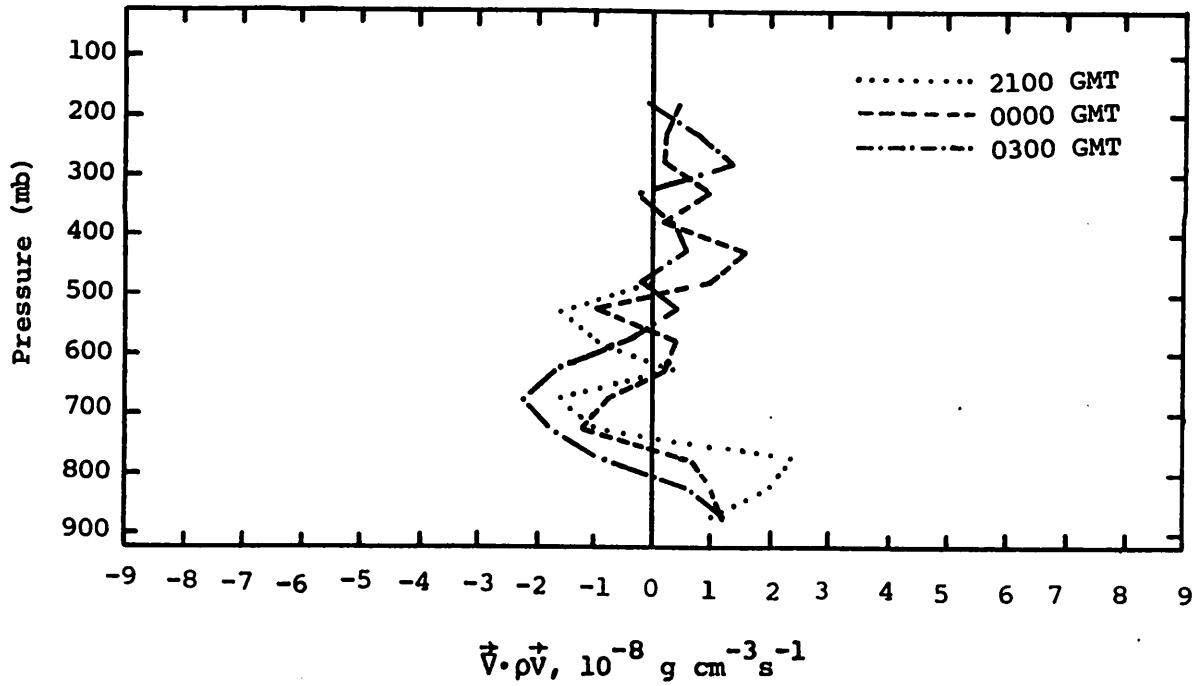

Fig. 5.25.3.1 Vertical profiles of mass divergence on 25 July 1978.

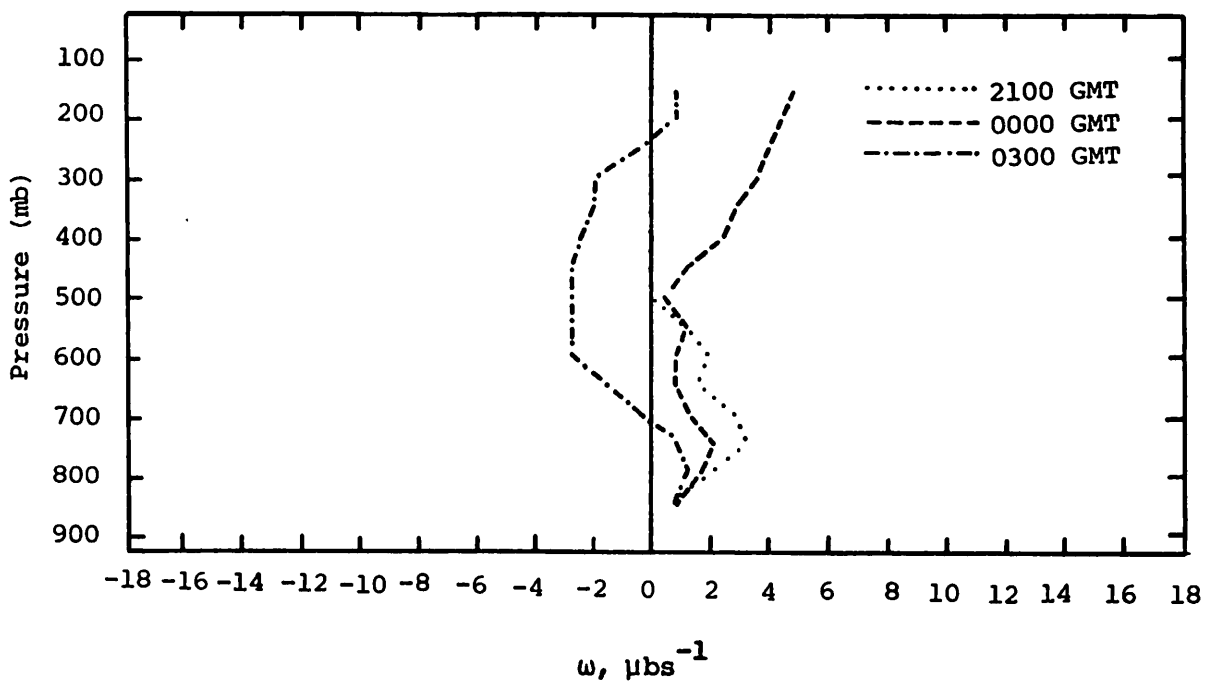

Fig. 5.25.3.2 Vertical profiles of vertical motion on 25 July 1978.

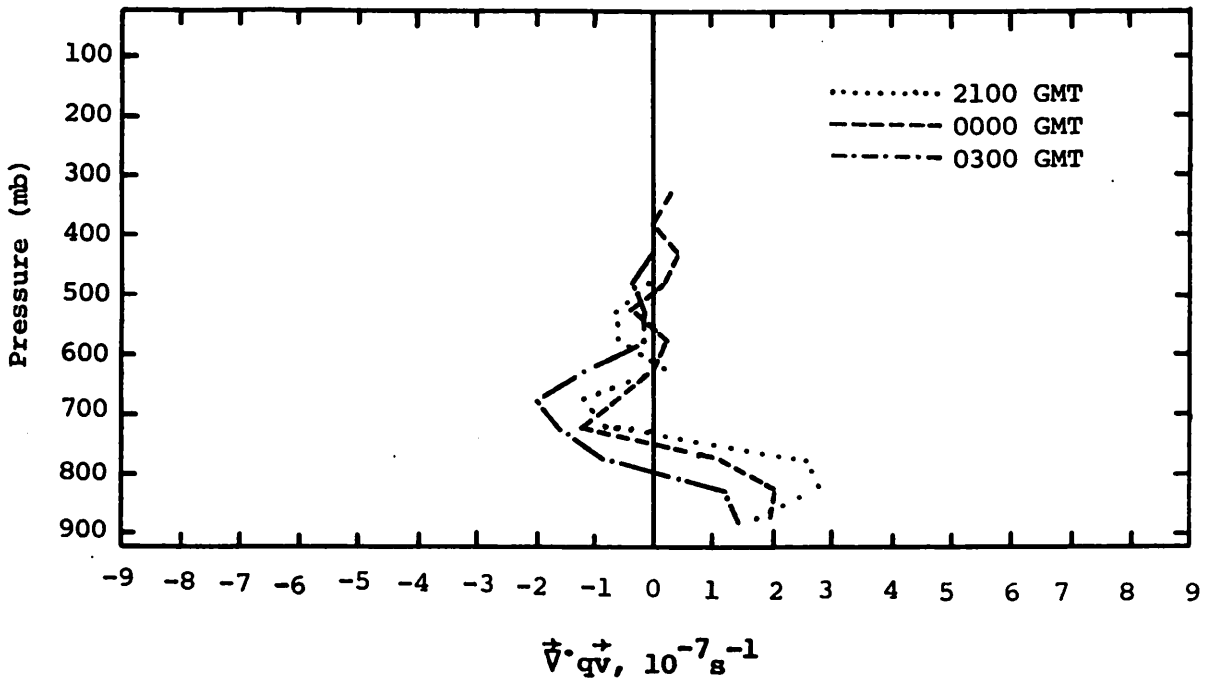

Fig. 5.25.3.3 Vertical profiles of moisture divergence on 25 July 1978.

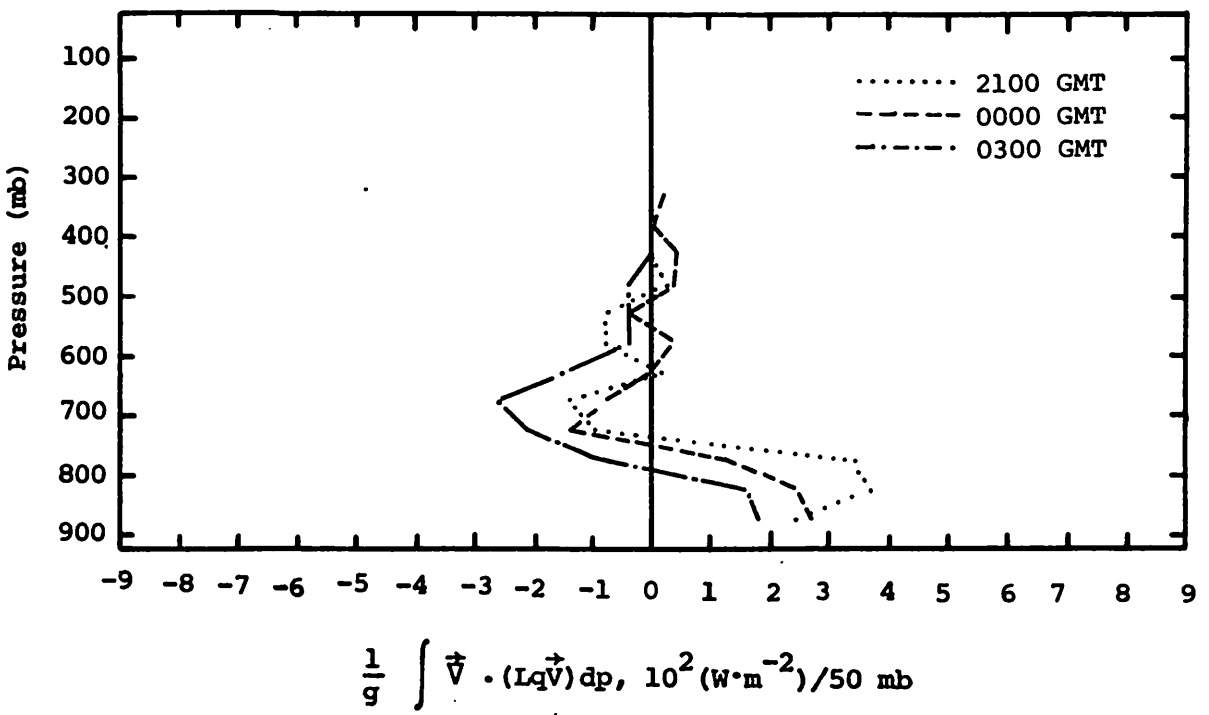

Fig. 5.25.4.1 Vertical profiles of the horizontal flux of latent heat energy on 25 July 1978.

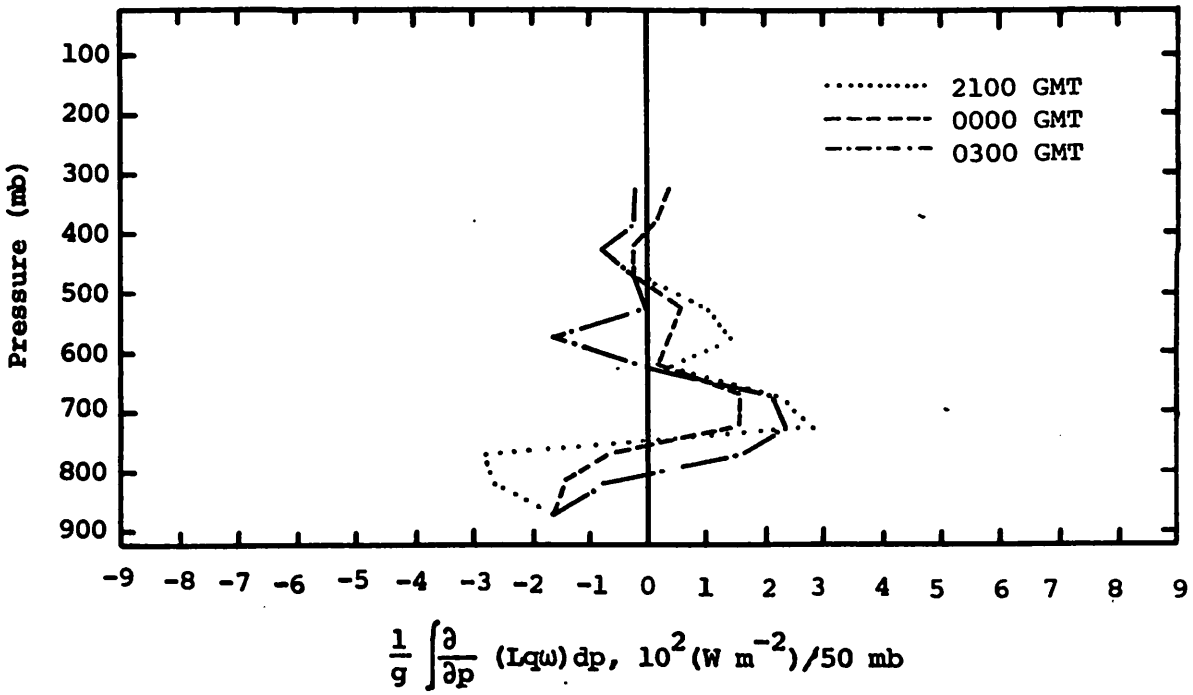

Fig. 5.25.4.2 Vertical profiles of the vertical flux of latent heat energy on 25 July 1978.

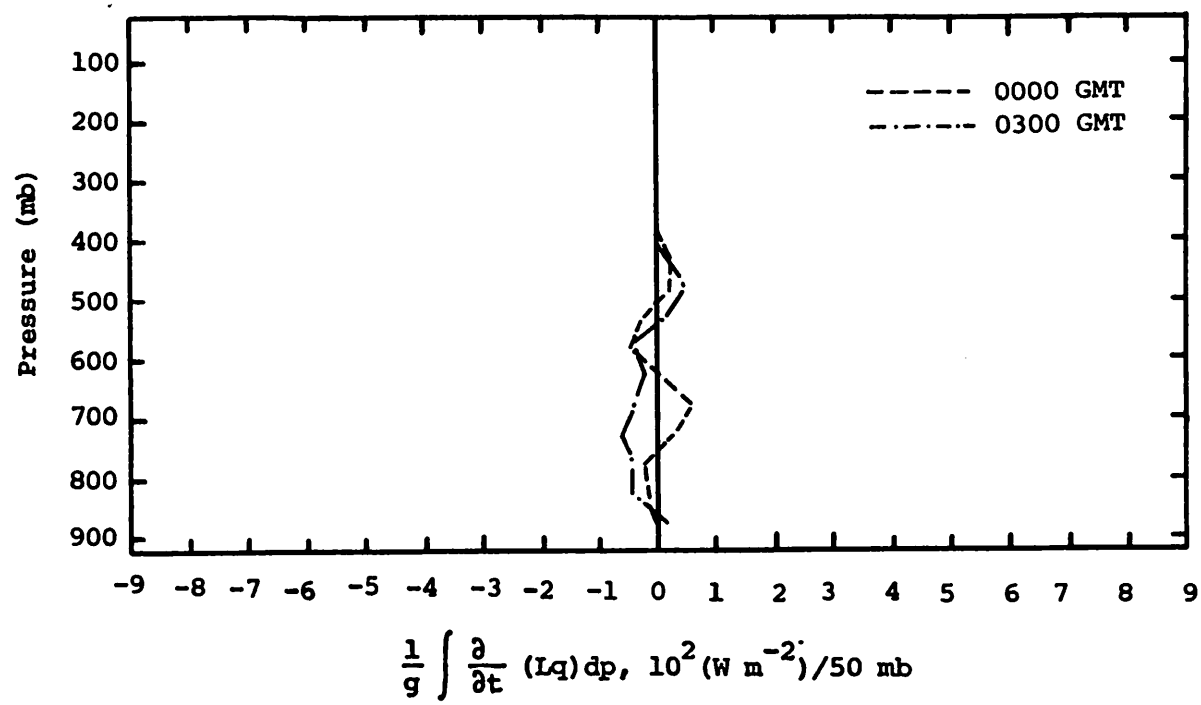

Fig. 5.25.4.3 Vertical profiles of the local change of latent heat energy on 25 July 1978.

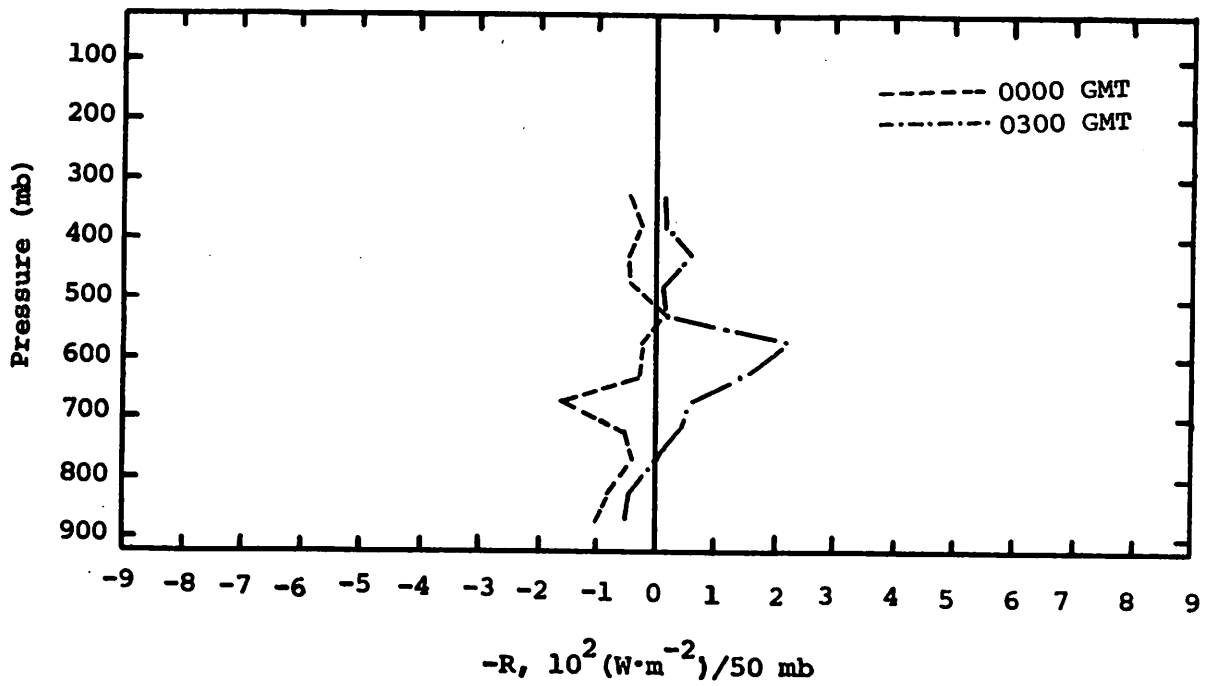

Fig. 5.25.4.4 Vertical profiles of the residual of the latent heat energy equation on 25 July 1978.

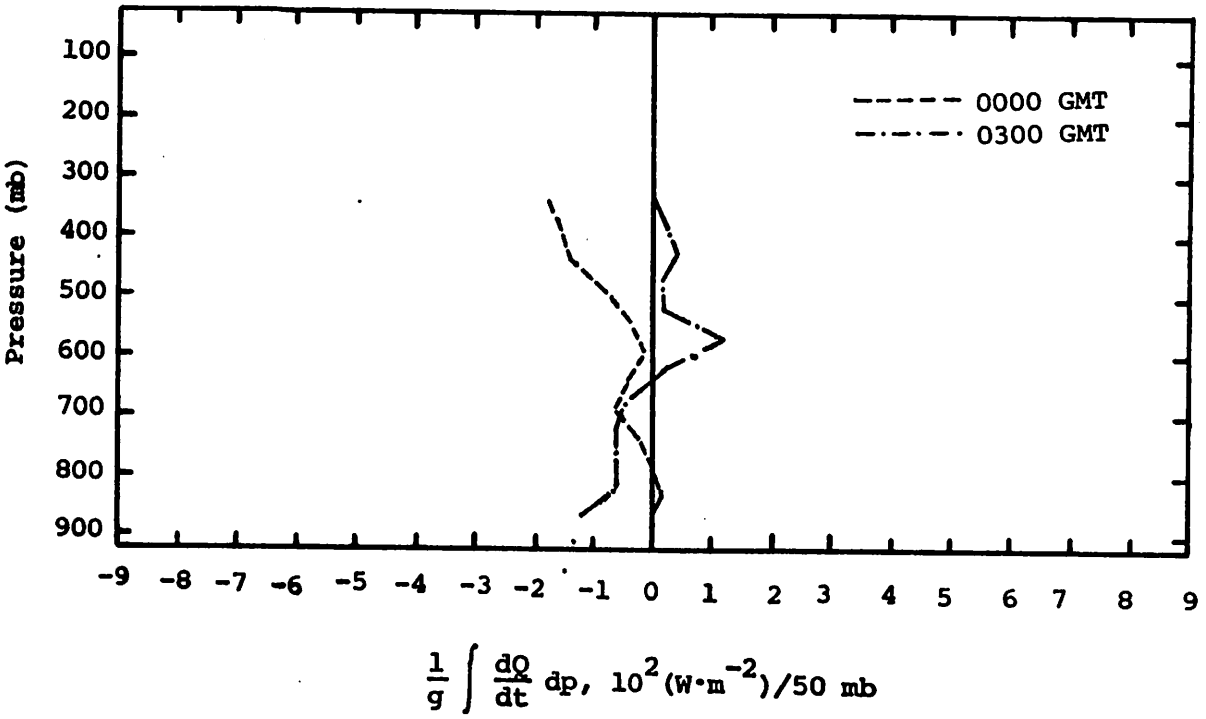

Fig. 5.25.4.5 Vertical profiles of diabatic heating computed from the first law of thermodynamics on 25 July 1978.

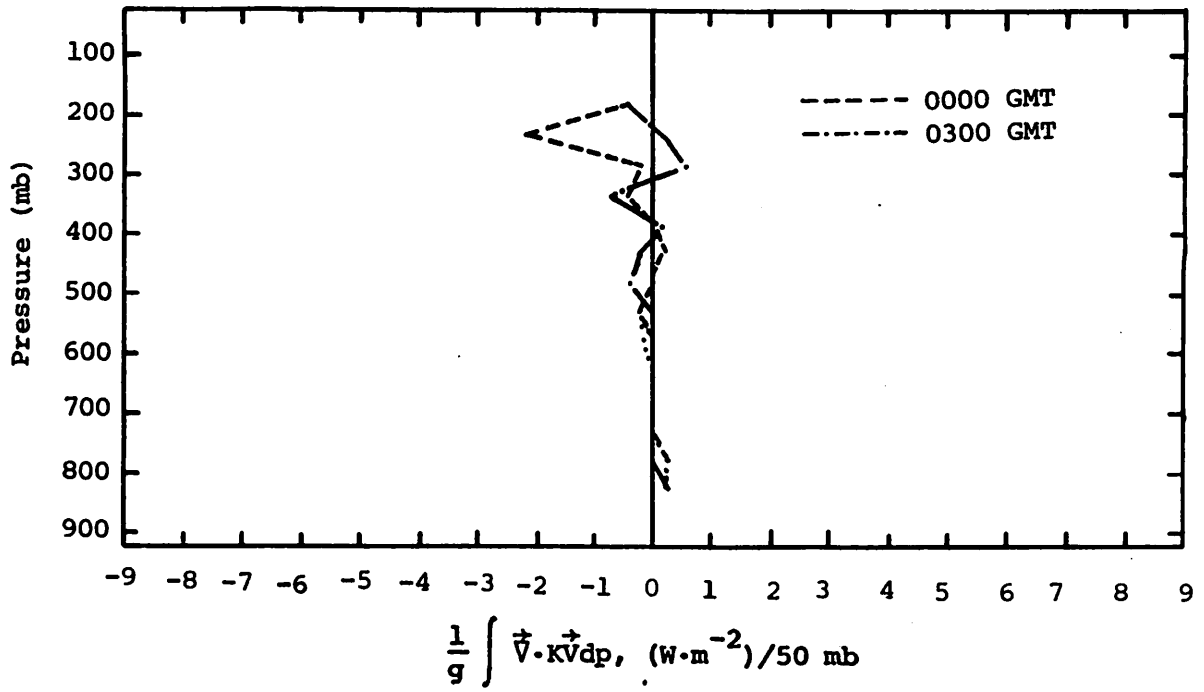

Fig. 5.25.4.6 Vertical profiles of the horizontal flux of kinetic energy on 25 July 1978.

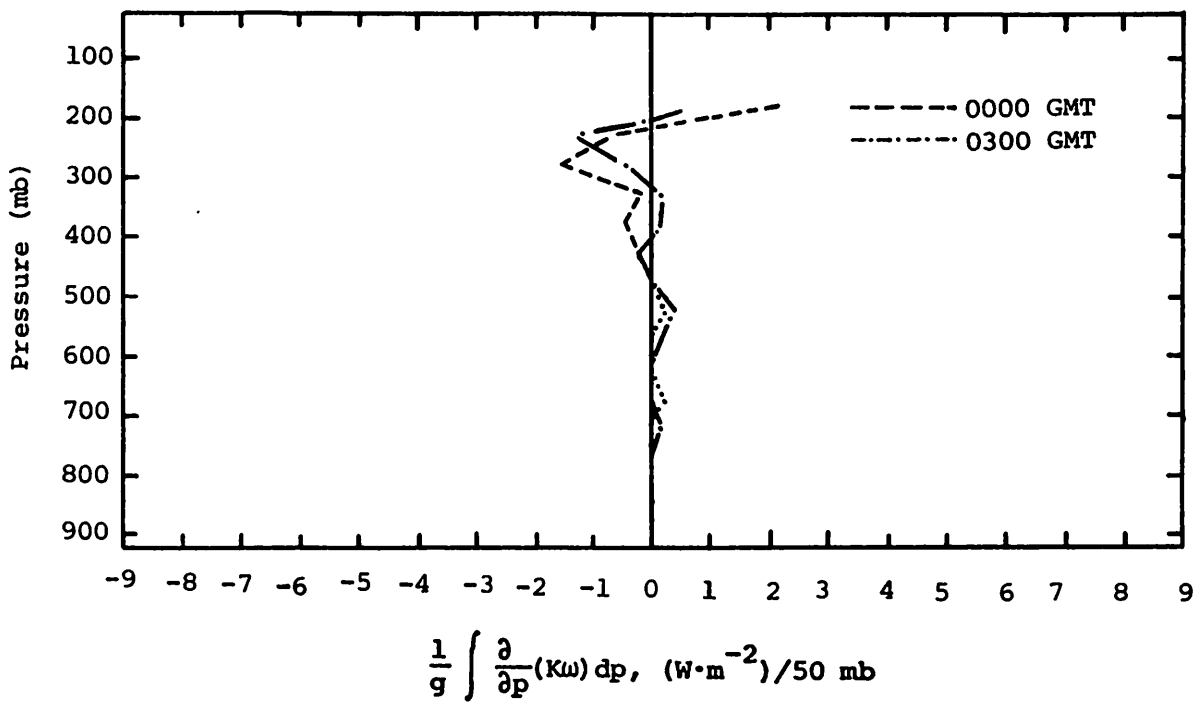

Fig. 5.25.4.7 Vertical profiles of the vertical flux of kinetic energy on 25 July 1978.

Values above 300 mb also were small, though a slight gain of kinetic energy was indicated at 0000 GMT due to horizontal and vertical motions.

5.25.5 Water Vapor Budget

Profiles from the water vapor budget fluctuated above 600 mb but indicated some persistent features below that level. The primary feature of the net horizontal transport was the concentration of water vapor in the 750-650-mb region at 2100 and 0300 GMT, and at virtually all levels at 0300 GMT (Fig. 5.25.5.1). These tendencies were somewhat cancelled by losses of water vapor resulting from vertical transport (Figs. 5.25.5.2 and 5.25.5.3). Figure 5.25.5.4 shows the resulting net combined transport. The tendency above 750 mb was toward more concentration of water vapor at each successive sounding period. This resulted in increases of water vapor content at some levels, as Fig. 5.25.5.5 shows. The total mass of water vapor increased around 700 and 450 mb, though it decreased slightly at 600 mb. Profiles of the local rate-of-change of water vapor also indicate these changes (Fig. 5.25.5.6).

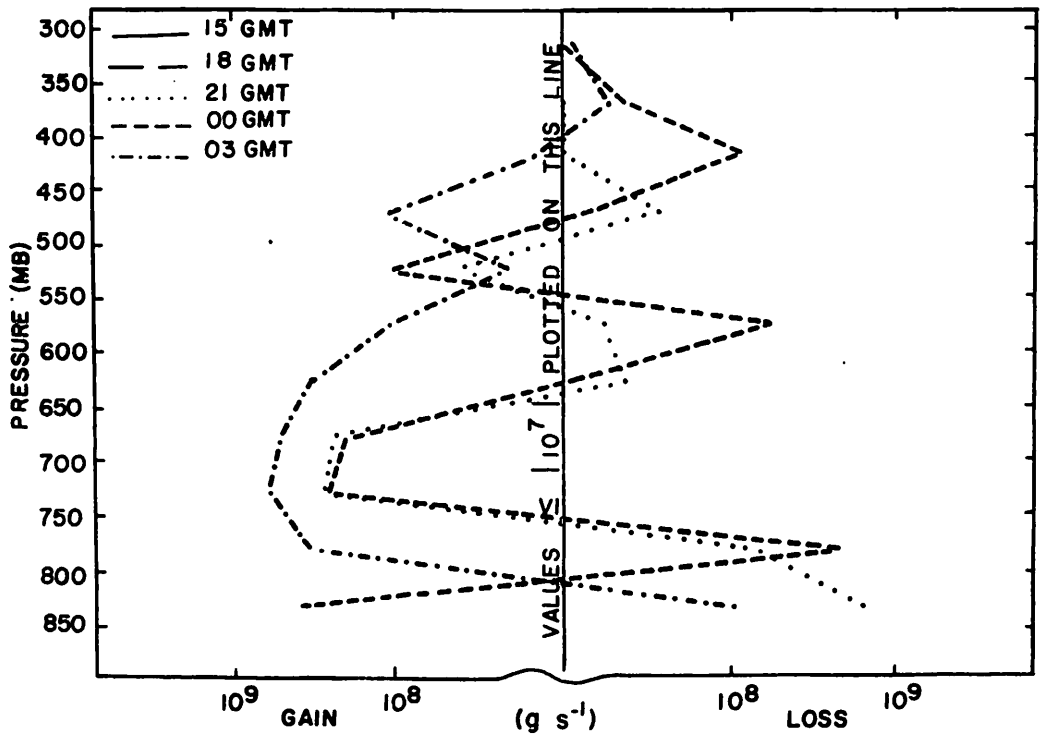

Fig. 5.25.5.1 Net horizontal transport of water vapor through boundaries of 50-mb layers (g s^{-1}) over the Texas HIPLEX area for 25 July 1978.

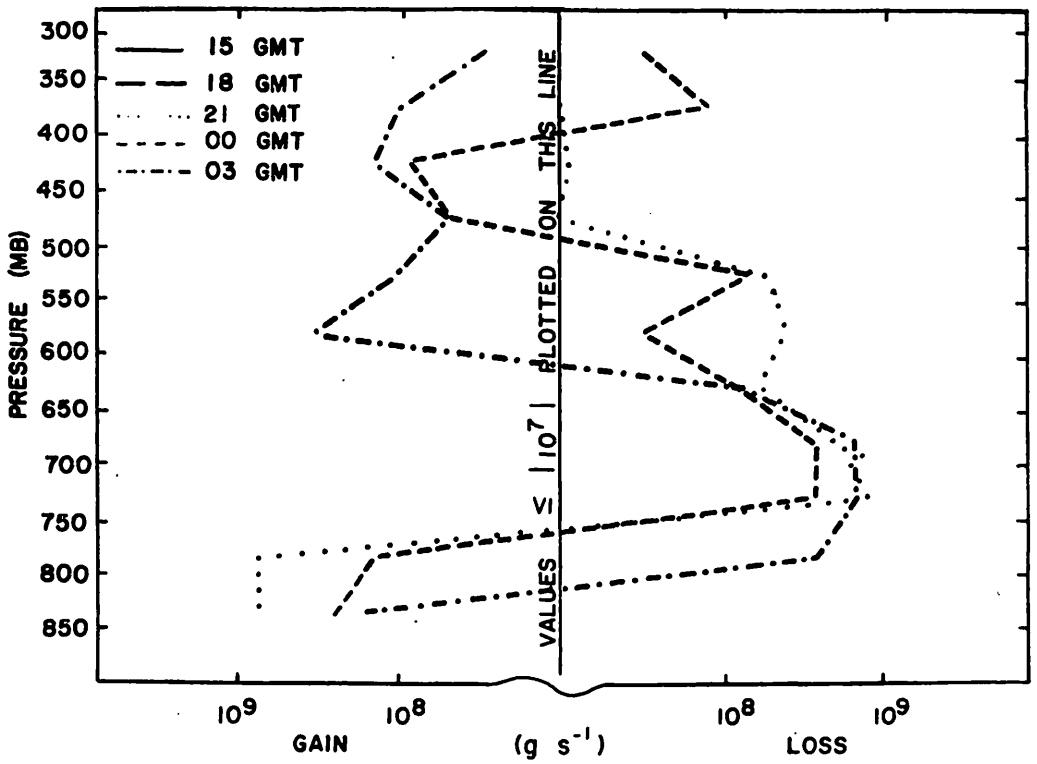

Fig. 5.25.5.2 Net vertical transport of water vapor through boundaries of 50-mb layers (gm s^{-1}) over the Texas HIPLEX area for 25 July 1978.

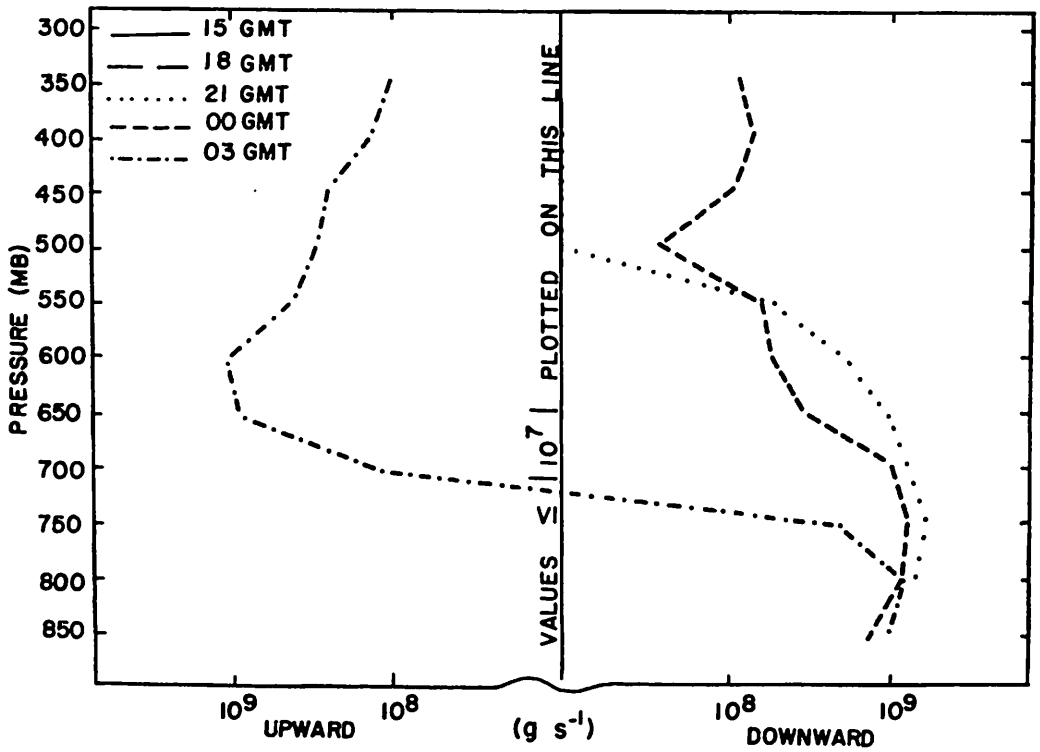

Fig. 5.25.5.3 Vertical transport of water vapor through constant pressure surfaces (gm s^{-1}) over the Texas HIPLEX area for 25 July 1978.

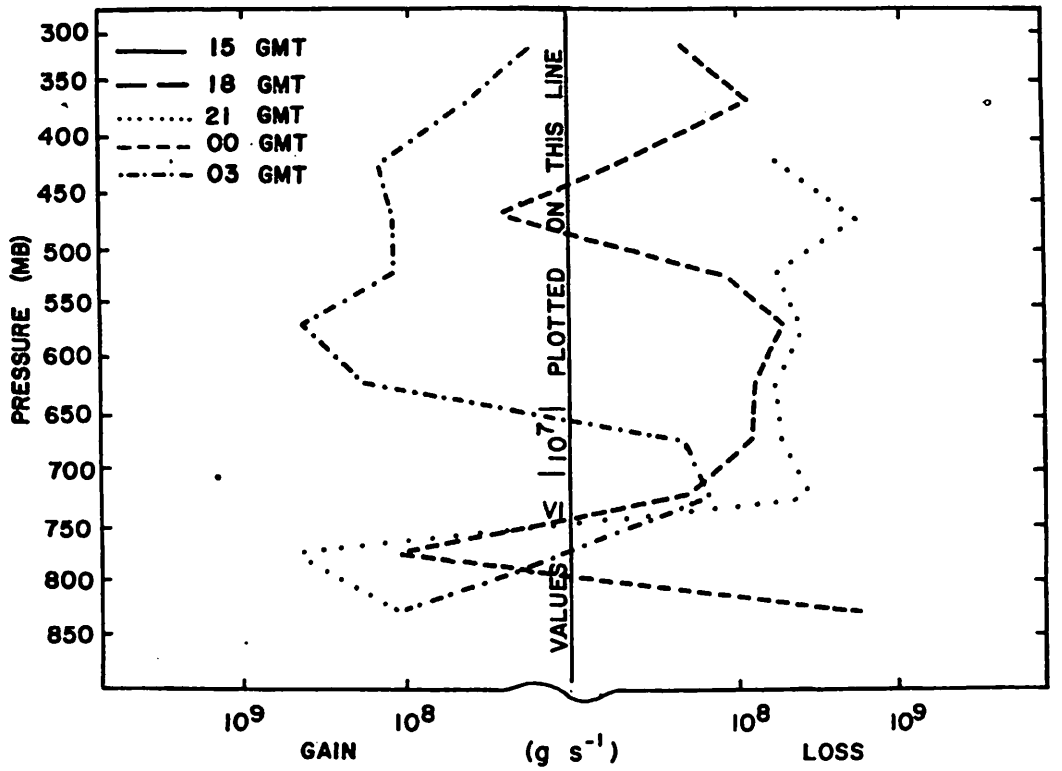

Fig. 5.25.5.4 Combined net horizontal and vertical transport of water vapor through boundaries of 50-mb layers (gm s^{-1}) over the Texas HIPLEX area for 25 July 1978.

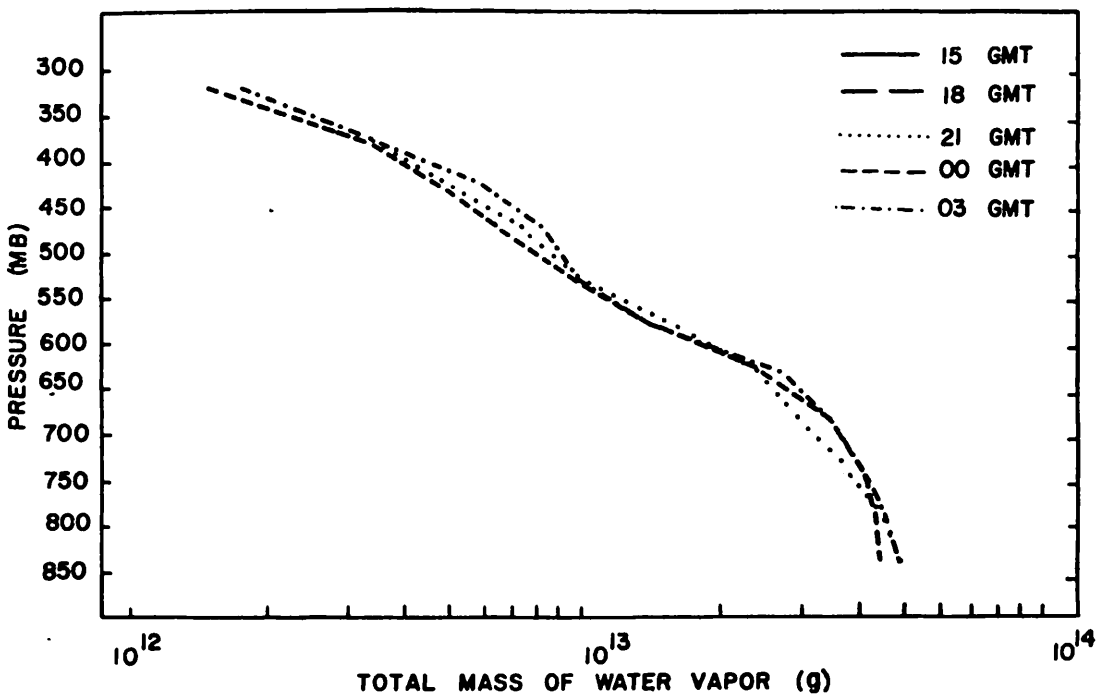

Fig. 5.25.5.5 Total mass of water vapor in layers 50 mb deep (gm) over the Texas HIPLEX area on 25 July 1978.

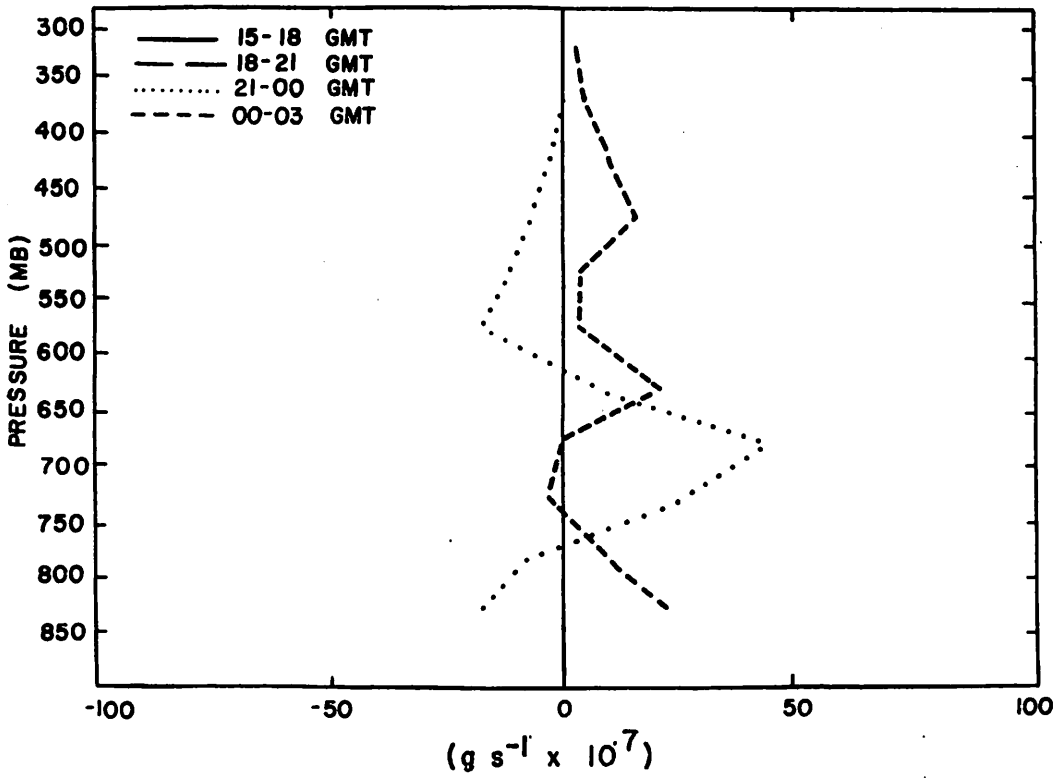

Fig. 5.25.5.6 Local rate-of-change in total mass of water vapor ($g\ s^{-1} \times 10^7$) for the Texas HIPLEX area for 25 July 1978.

5.26 26 July 1978

5.26.1 Radar

Isolated thunderstorm cells and clusters of cells were observed prior to 0100 GMT (Fig. 5.26.1.1). Maximum echo tops exceeded 12.1 km (40K ft) from 2000 to 2200 GMT, and echoes moved from the north-northeast at 6 m/sec (12 knots).

At 0100 GMT a line of thunderstorms with tops to 14.8 km (49K ft) formed north of the network, and was partially visible on the 0100 GMT radar chart in Fig. 5.26.1.1. By 0200 GMT the line had moved into the analysis area, and by 0300 GMT it had begun to dissipate. Echo tops were 12.7 km (42K ft) near Clairemont and Seminole at 0300 GMT.

Radar charts at 0300 and 0400 GMT (0400 GMT chart not shown) indicated a line of anomalous propagation associated with the line of echoes observed at 0200 GMT. This line is not represented in Fig. 5.26.1.1 because it was not a precipitation echo. Nevertheless, it appears to have had an effect on some surface parameters. At 0330 GMT the line was observed from Big Spring to Andrews and continued movement to the northwest. It moved from the north-northeast at 13 m/sec (26 kts), which is the same direction of movement as the line but somewhat faster. The line was last observed at 0430 GMT as it extended from Garden City to Midland and then out of the analysis area.

5.26.2 Surface

Temperatures were steady across the network until 2100 GMT, when a temperature drop of 2.5°C occurred at Sweetwater in the vicinity of a thunderstorm (Fig. 5.26.2.1). That temperature change was likely due to decreased insolation rather than downdraft effects, as moisture (Figs. 5.26.2.2 and 5.26.2.3) and other fields were not greatly affected.

Temperatures were again steady until 2300 GMT when a temperature drop of 9°C at Robert Lee occurred in conjunction with the partial dissipation of the radar echo located over that station (measured top decreased from 11.8 km (39K ft) at 2200 GMT to 9.4 km (31K ft) at 2300 GMT. No thermodynamic effects were evident from the dissipation of another echo (measured top 12.4 km (41K ft)) near Big Spring at 2300 GMT.

Low temperature at Robert Lee at 2300 GMT decreased further at 0000 GMT, and represented a temperature change of 12°C in two hours. Note that the contour interval was doubled at 0000 and 0200 GMT due to the large temperature

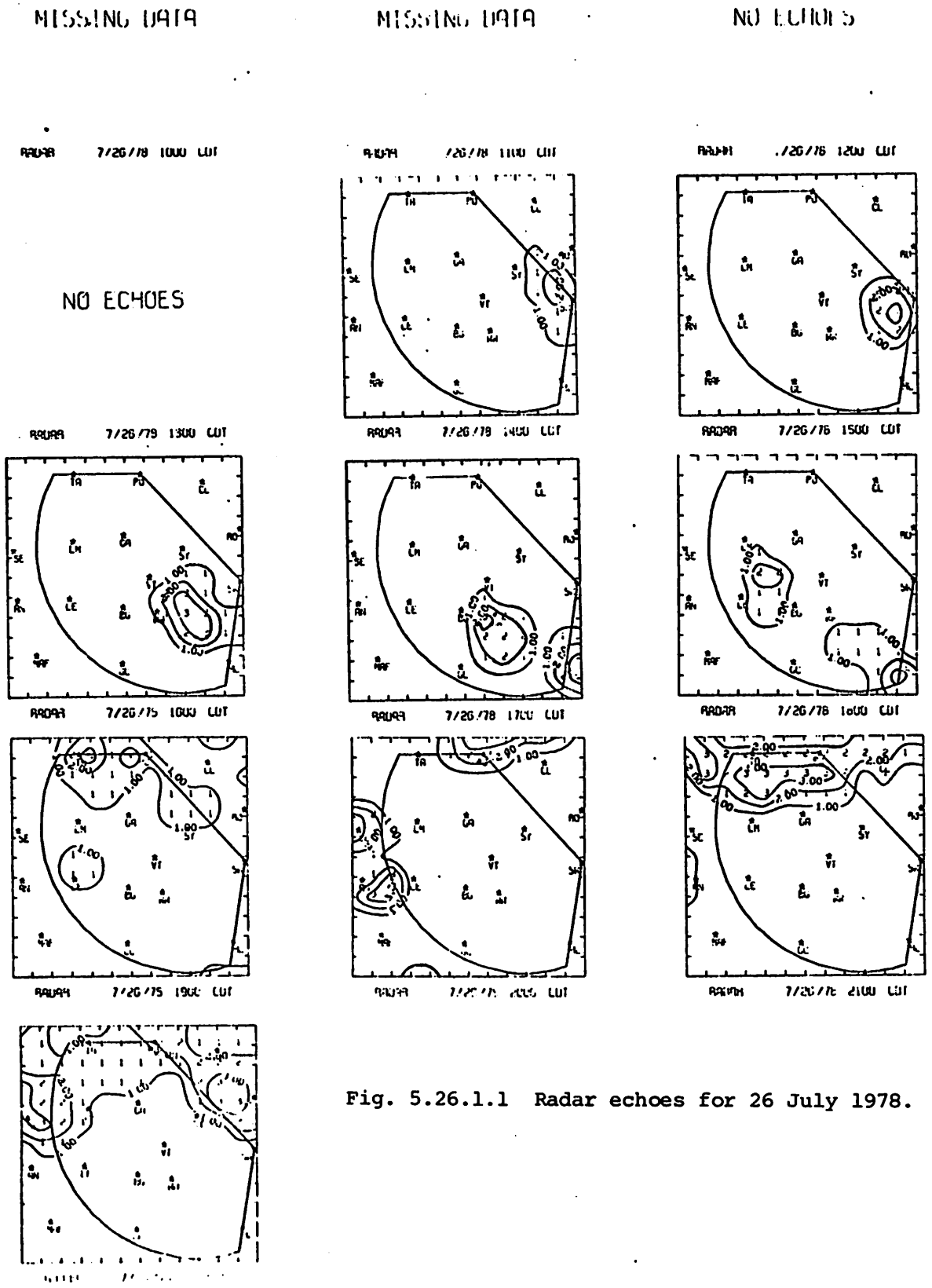

Fig. 5.26.1.1 Radar echoes for 26 July 1978.

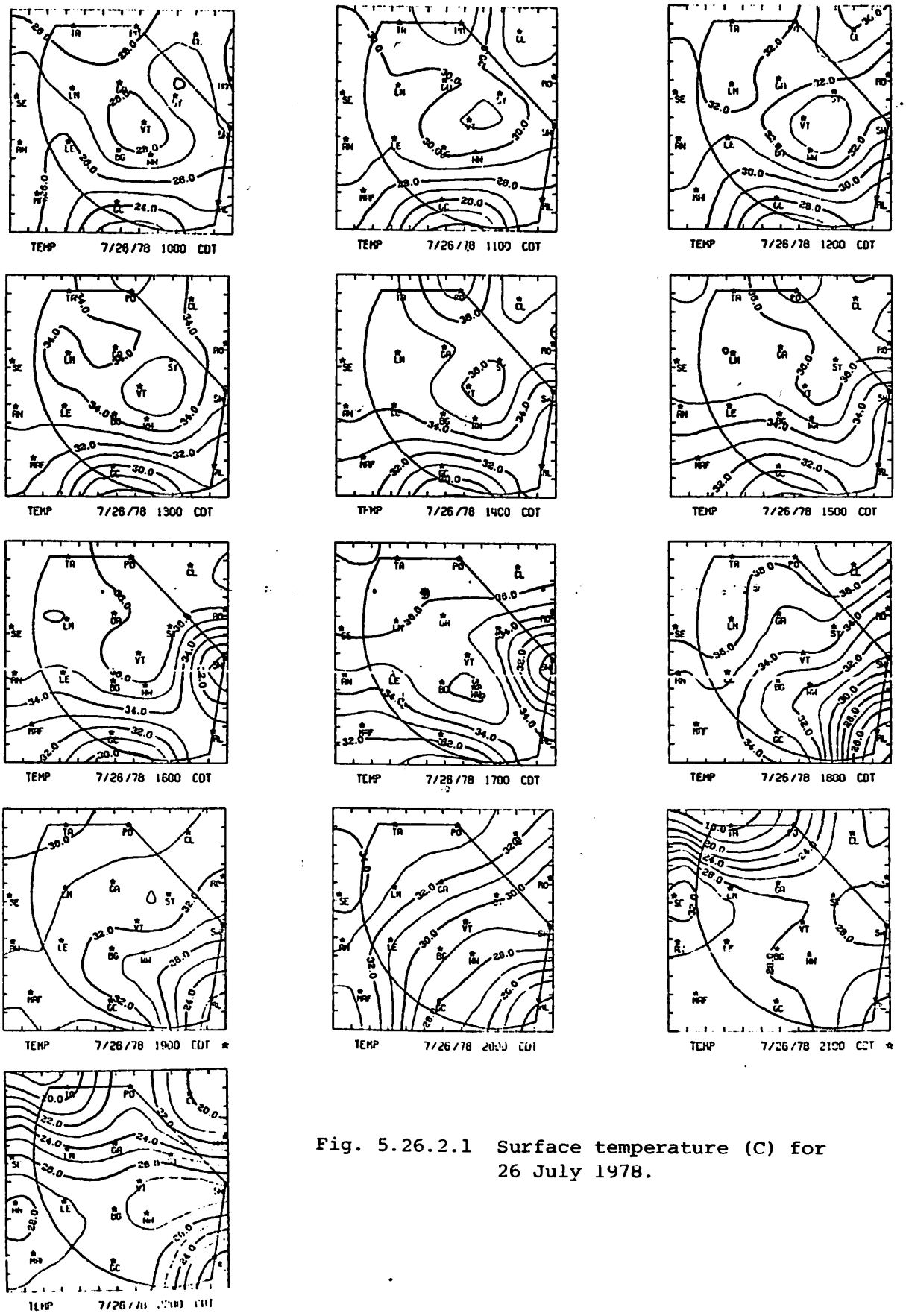

Fig. 5.26.2.1 Surface temperature (C) for 26 July 1978.

gradient. At 0100 GMT a large temperature gradient existed across the network, with values in the northwest section representing non-convective conditions. At 0200 and 0300 GMT a temperature drop occurred in response to the line of thunderstorms to the north. Tahoka experienced an 18°C drop of temperature and at 0200 GMT Clairemont measured an 8°C change.

Dewpoint-depression drops were virtually co-located with temperature drops throughout the day (Fig. 5.26.2.2). Dewpoint-depressions less than 4°C were common near thunderstorms after 2300 GMT. Mixing ratios (Fig. 5.26.2.3) responded less abruptly until effects from the line of thunderstorms were indicated at 0200 GMT. Large centers of equivalent potential temperature occurred where mixing ratio was high and thunderstorms cause rapid changes in surface variables (Fig. 5.26.2.4).

Large values in terrain-induced vertical velocity (Fig. 5.26.2.5) occurred where thunderstorms caused large surface wind speeds. Values up to 4 cm sec^{-1} are observed at several times during the day.

Centers of surface velocity divergence (Fig. 5.26.2.6) were generated in the vicinity of isolated echoes before 0200 GMT but were not co-located with the echoes. The centers of divergence exhibited continuity from 2100 to 0100 GMT. When the line of thunderstorms entered the network at 0200 GMT positive divergence resulting from downdrafts reached 3.5×10^{-4} sec^{-1}. Convergence ahead of the downdrafts was observed at 0200 and 0300 GMT.

Boundary layer vertical motion was large at 0200 and 0300 GMT (Fig. 5.26.2.7). Values of 15 µbars sec^{-1} occurred near strong thunderstorm outflow regions. In convergent areas ahead of the outflow, values of -10 µbars sec^{-1} were computed.

Moisture divergence (Fig. 5.26.2.8) and vertical moisture flux (Fig. 5.26.2.9) also were large near thunderstorm outflow regions, particularly at 0200 and 0300 GMT. The centers were similar to those observed in velocity divergence.

Vorticity was largest when thunderstorms influenced the surface wind field (Fig. 5.26.2.10). Centers with values of $1.25 \times 10^{-4} sec^{-1}$ were common prior to 0200 GMT. At that time, values of $3 \times 10^{-4} sec^{-1}$ were calculated as the line of thunderstorms entered the network. Values were smaller at 0200 GMT as outflow from the thunderstorms spread over a greater area.

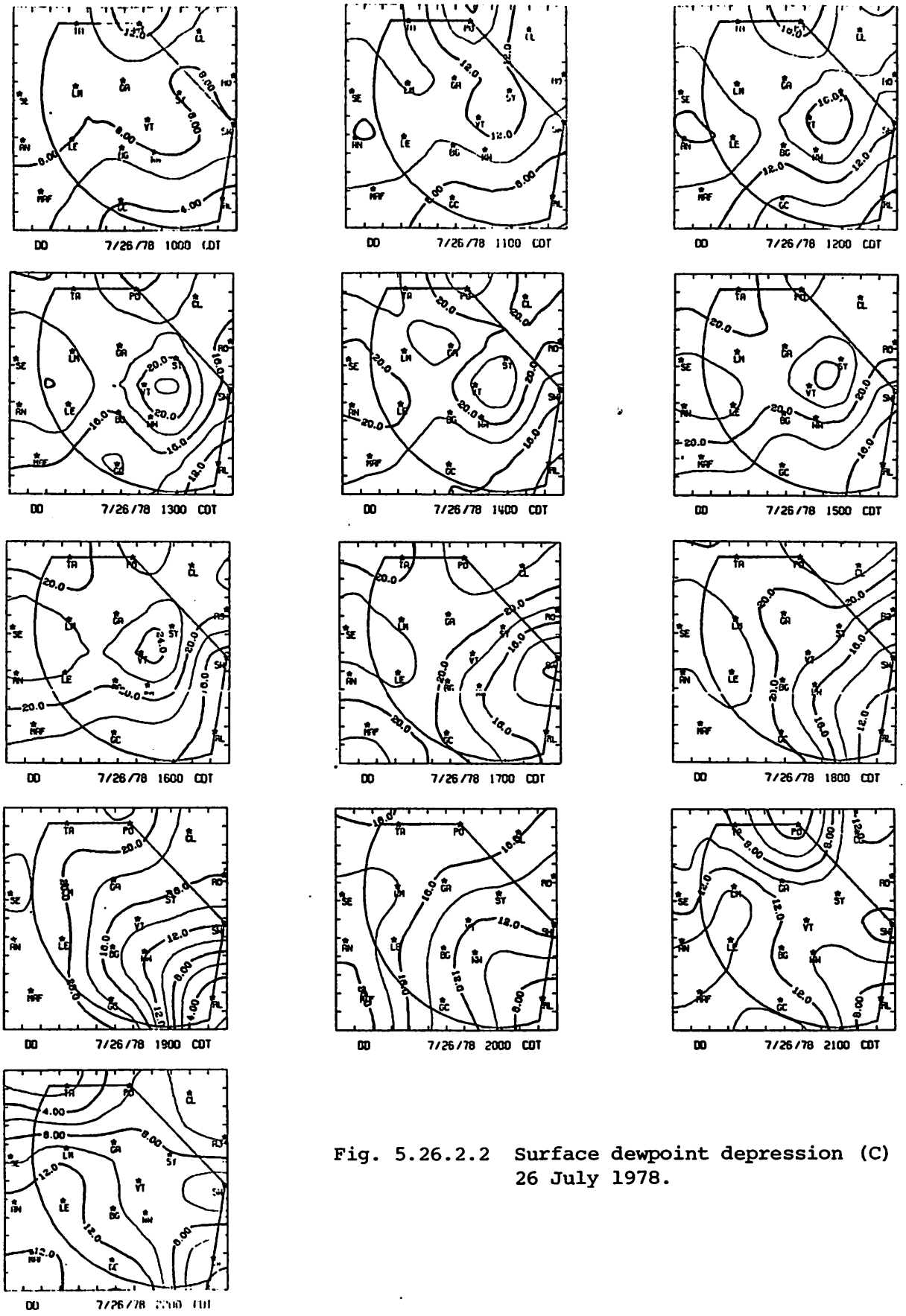

Fig. 5.26.2.2 Surface dewpoint depression (C) for 26 July 1978.

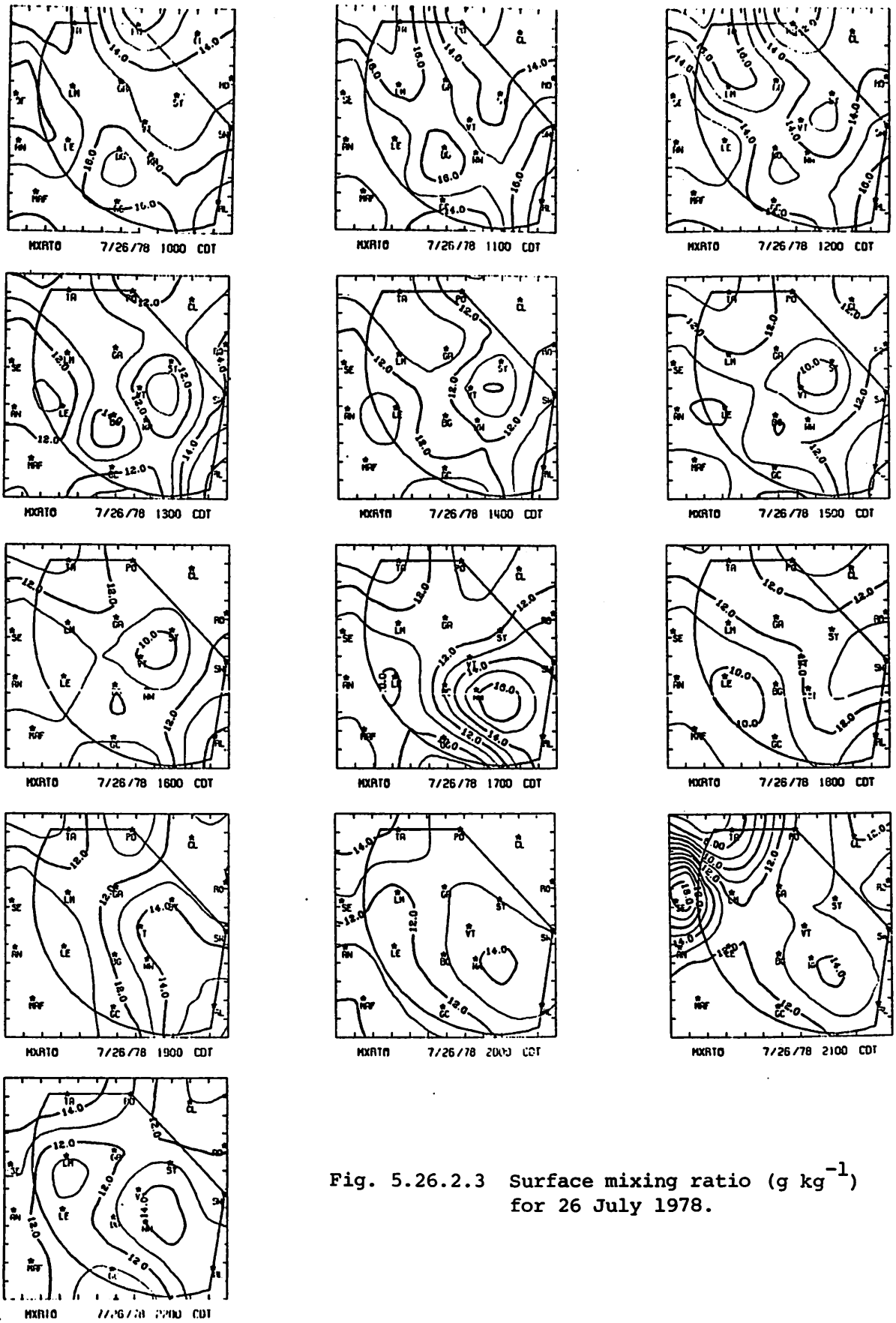

Fig. 5.26.2.3 Surface mixing ratio (g kg^{-1}) for 26 July 1978.

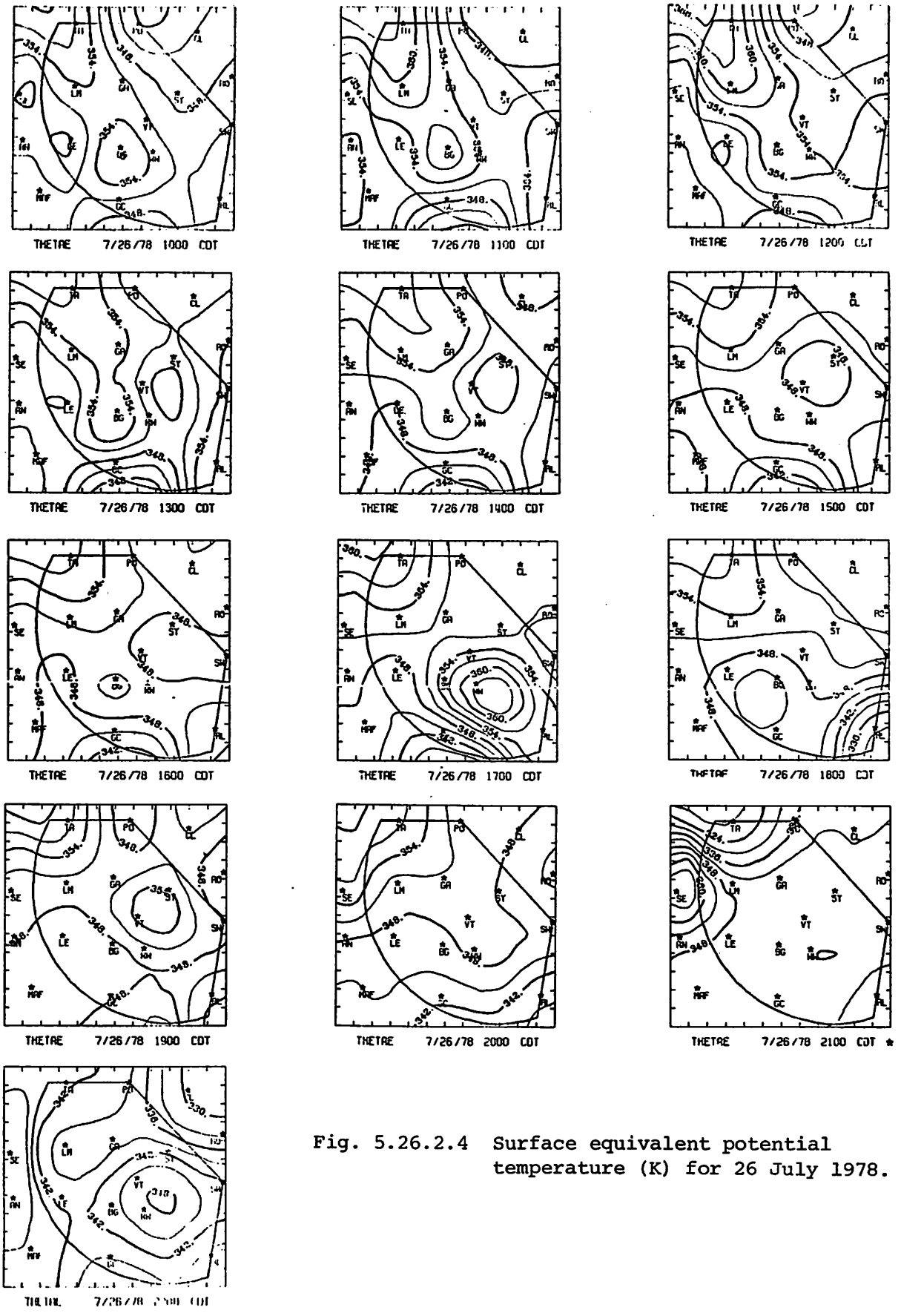

Fig. 5.26.2.4 Surface equivalent potential temperature (K) for 26 July 1978.

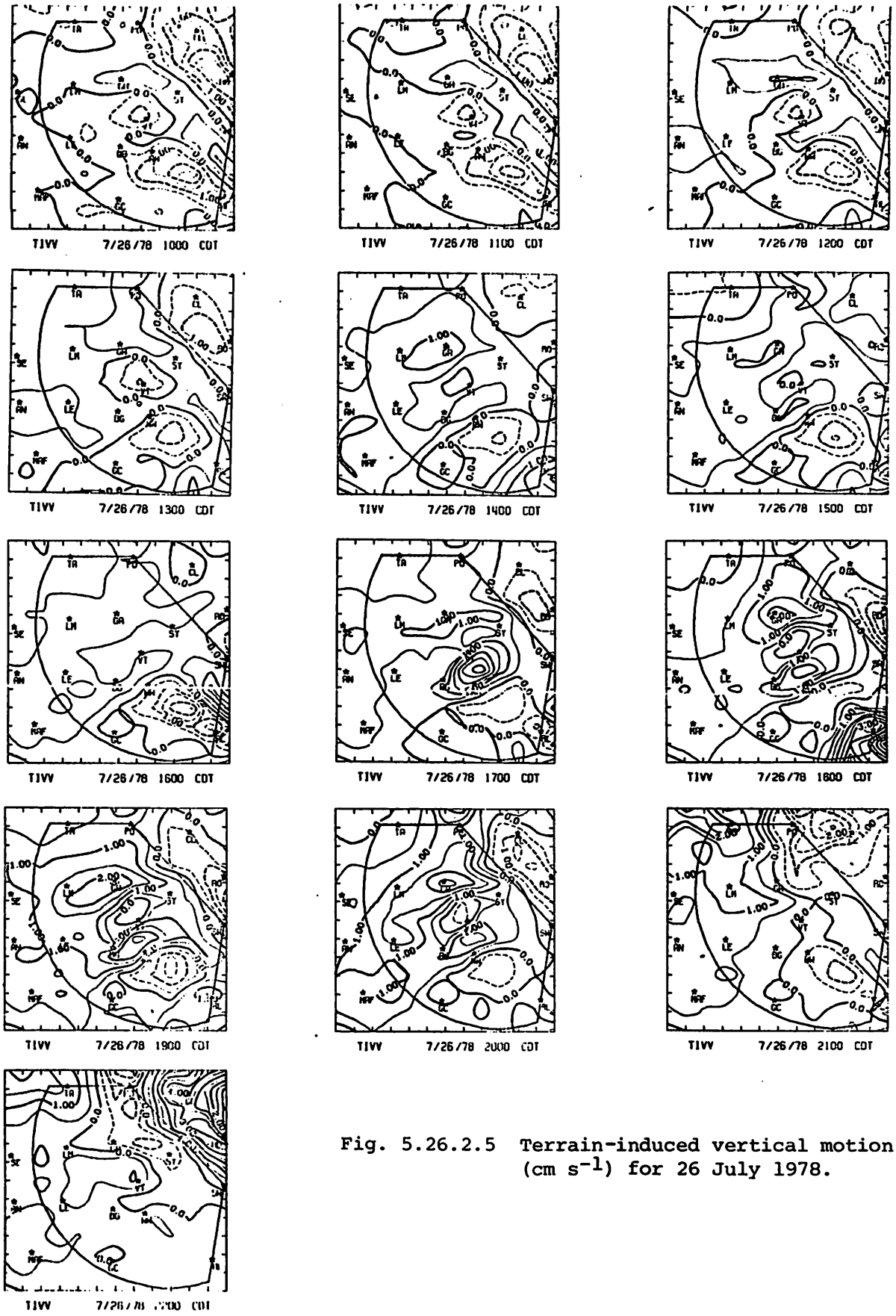

Fig. 5.26.2.5 Terrain-induced vertical motion (cm s^{-1}) for 26 July 1978.

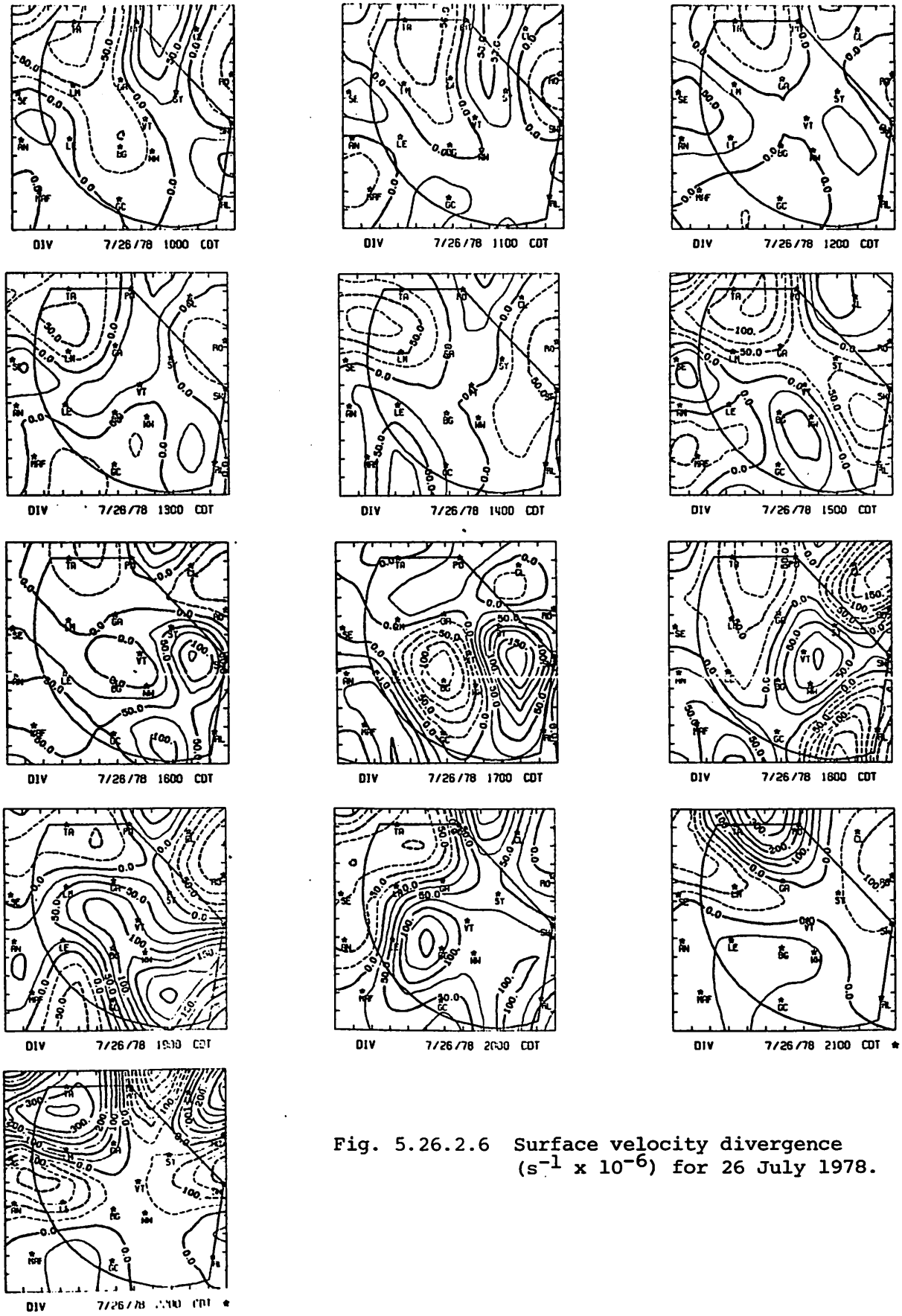

Fig. 5.26.2.6 Surface velocity divergence (s^{-1} x 10^{-6}) for 26 July 1978.

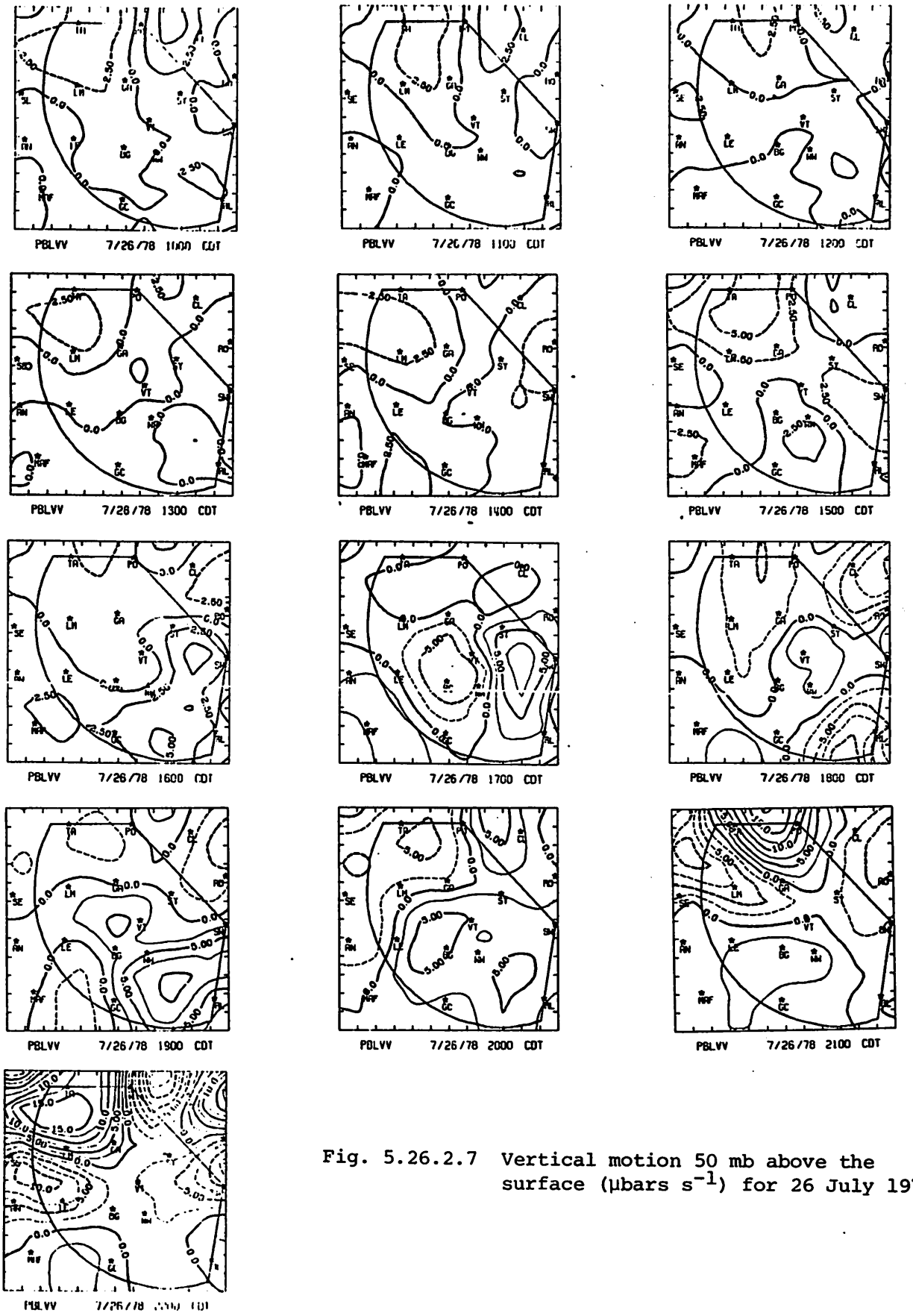

Fig. 5.26.2.7 Vertical motion 50 mb above the surface (μbars s^{-1}) for 26 July 1978.

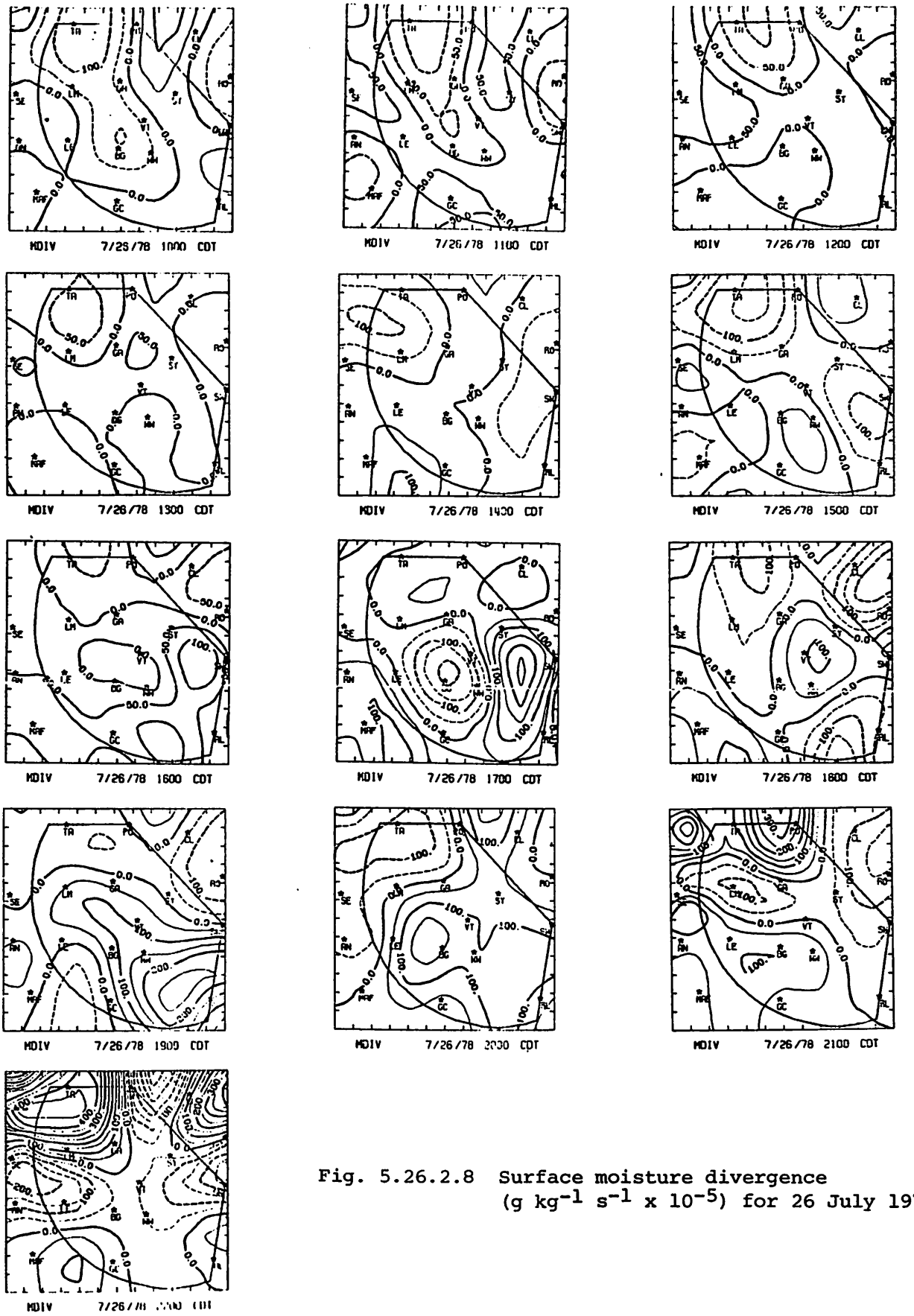

Fig. 5.26.2.8 Surface moisture divergence ($g\ kg^{-1}\ s^{-1} \times 10^{-5}$) for 26 July 1978.

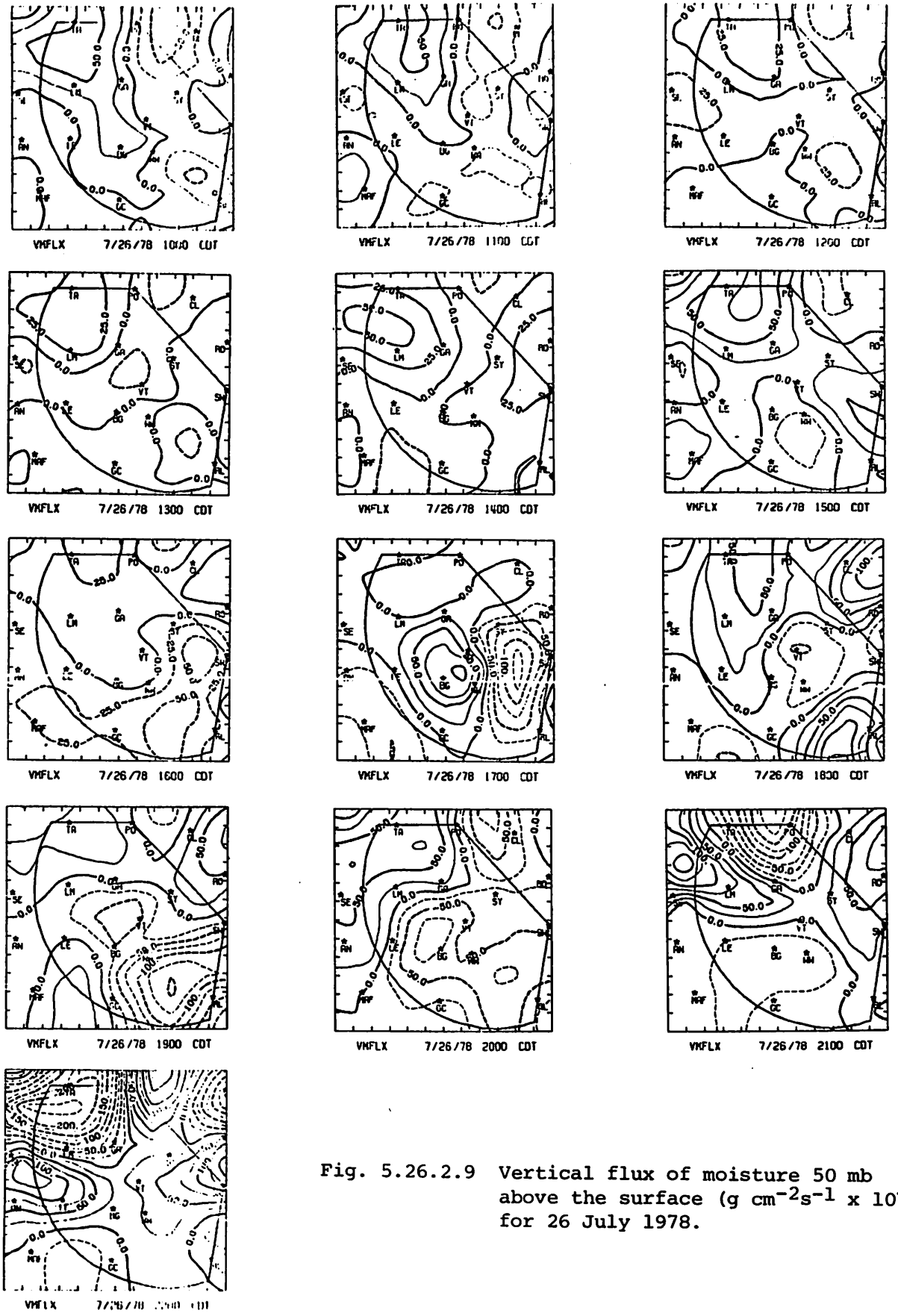

Fig. 5.26.2.9 Vertical flux of moisture 50 mb above the surface (g $cm^{-2}s^{-1}$ x 10^{-6}) for 26 July 1978.

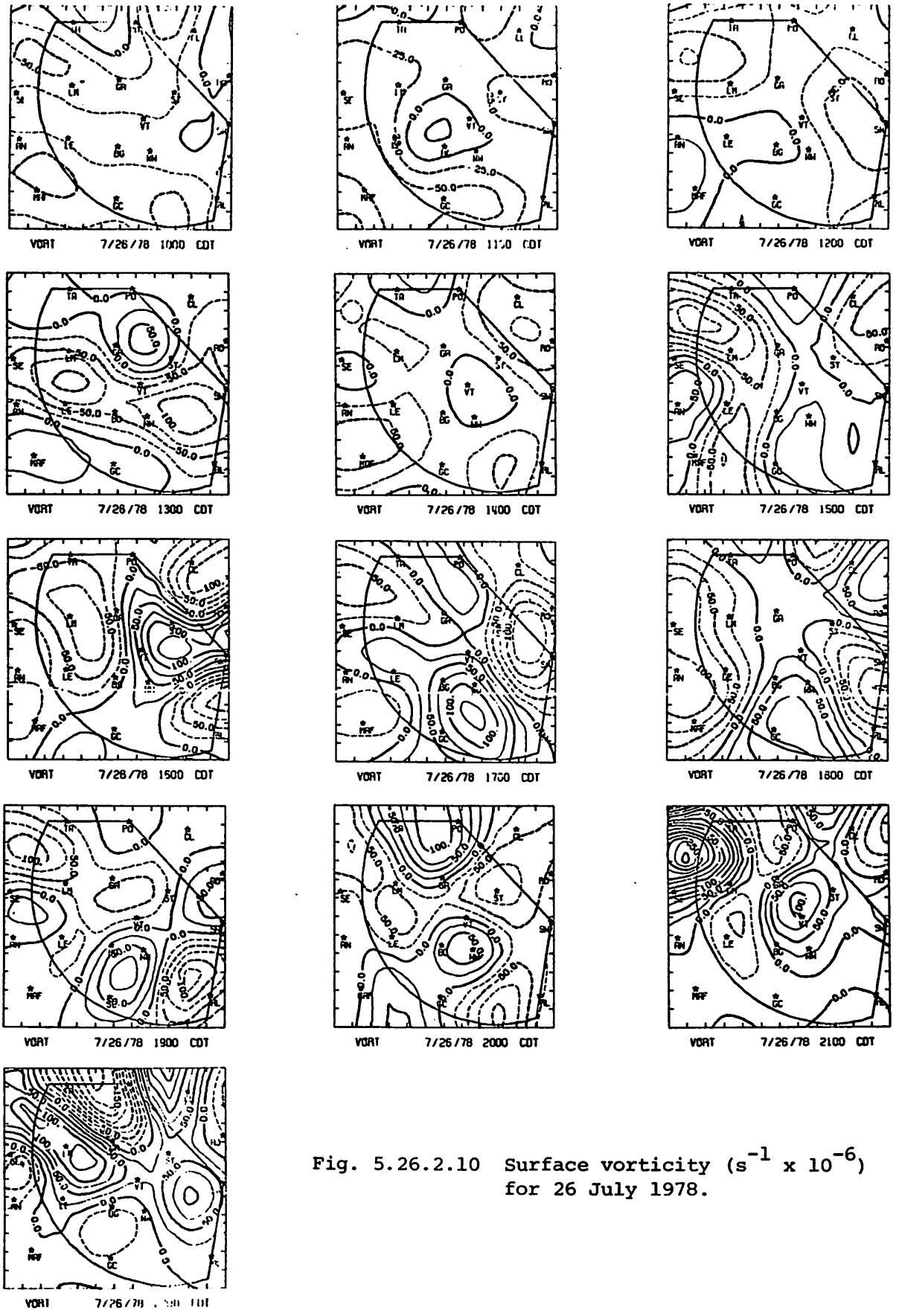

Fig. 5.26.2.10 Surface vorticity (s^{-1} x 10^{-6}) for 26 July 1978.

The line of thunderstorms at 0200 and 0300 GMT caused extreme changes in the surface pressure field (Fig. 5.26.2.11). The exact relationship between the anomalous radar echo which was observed as a line (see Section 5.26.1) and the pressure changes is unknown. However, because the anomalous echo was due to a sharp air density discontinuity, it follows that a relationship may have existed. Surface pressures rose at all stations on the north side of the network from 0100 to 0200 GMT, and at all stations in the network except Tahoka from 0200 to 0300 GMT.

The surface wind fields (Fig. 5.26.2.12) experienced large variations in response to the convective activity. These changes are associated with fields of other variables discussed above.

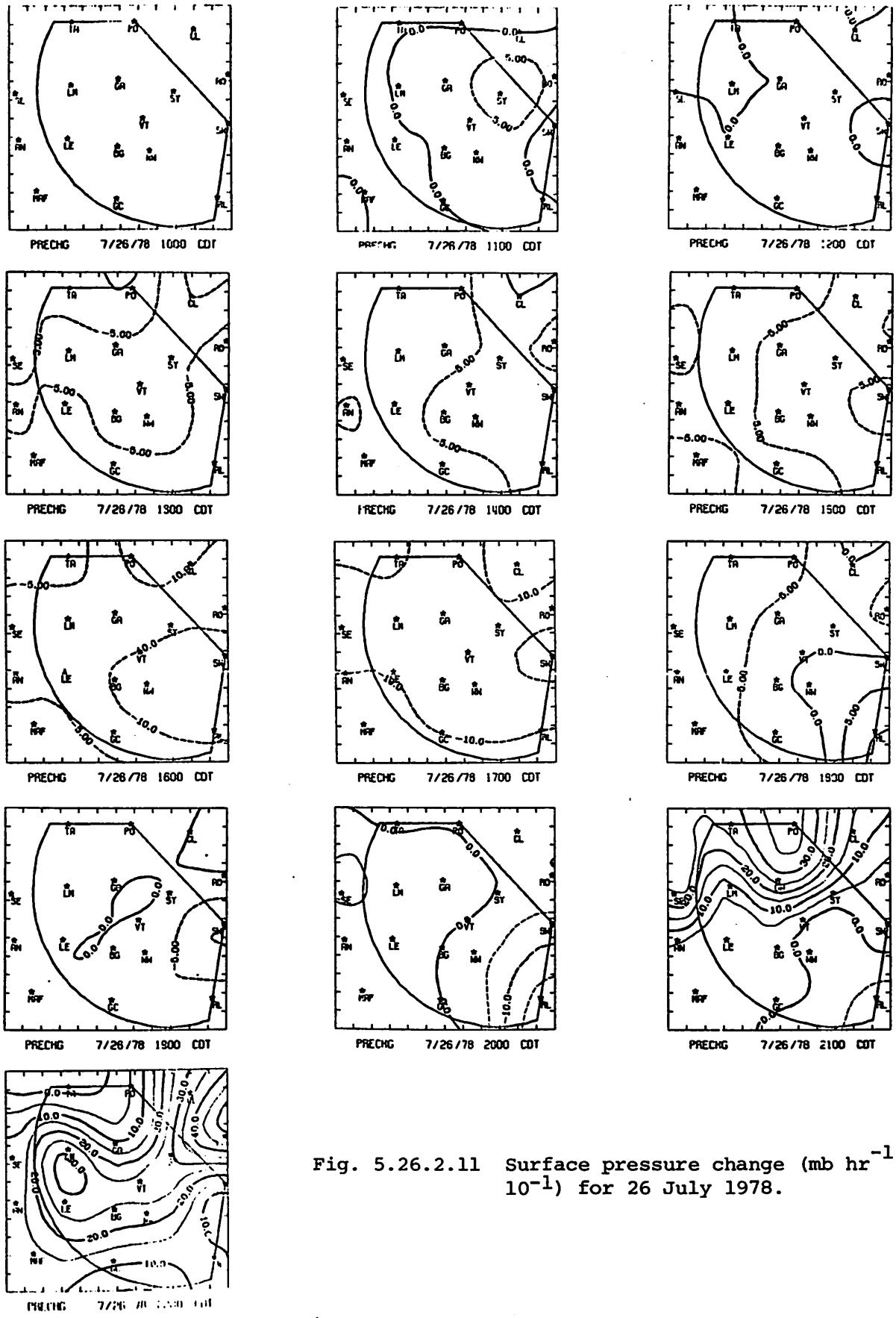

Fig. 5.26.2.11 Surface pressure change (mb hr^{-1} x 10^{-1}) for 26 July 1978.

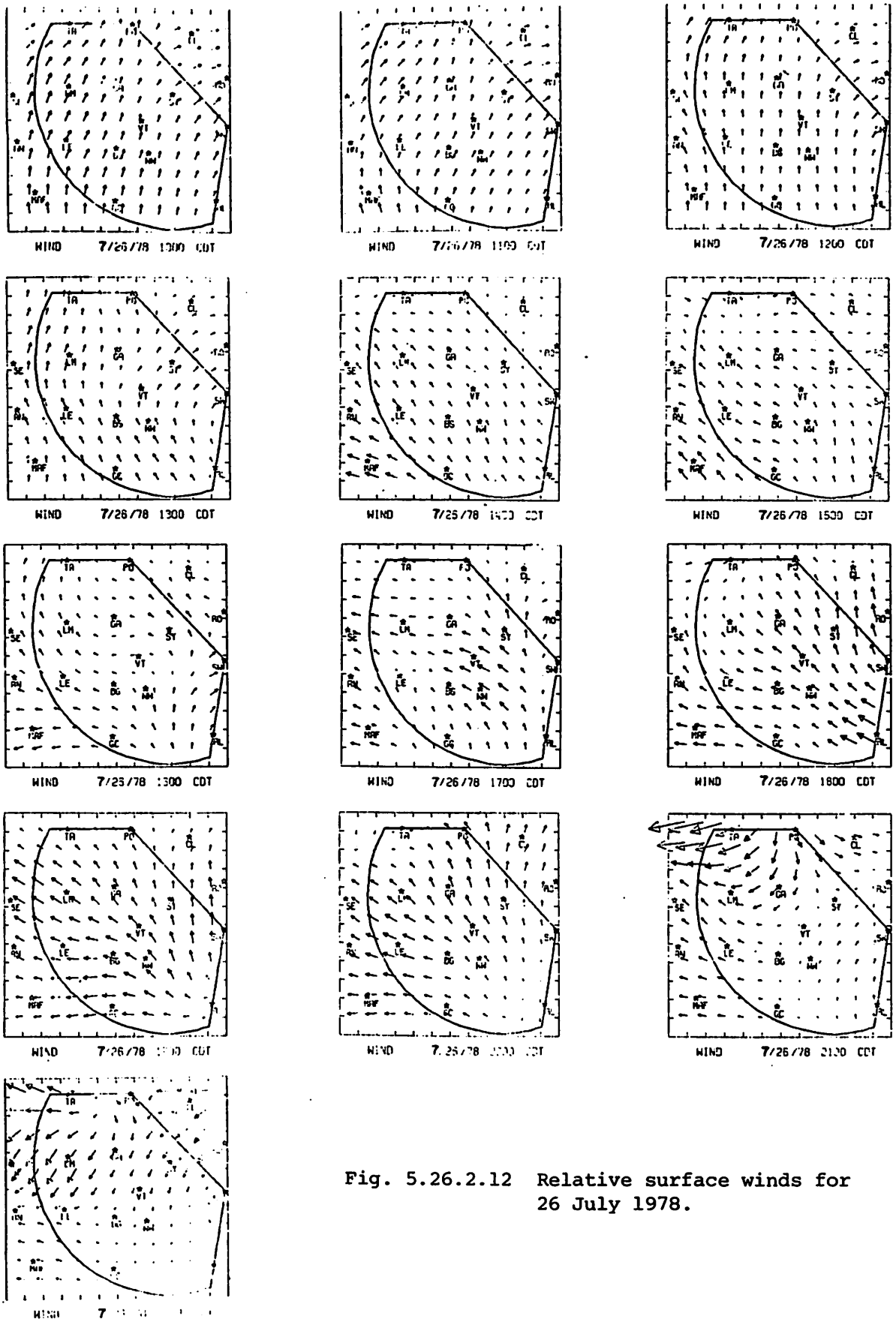

Fig. 5.26.2.12 Relative surface winds for 26 July 1978.

5.27 Composite Surface Analysis

Maximum values of velocity and moisture convergence (negative divergence), upward vertical motion ($-\omega$) 50 mb above the surface, and upward flux of moisture ($-\rho q\omega$) 50 mb above the surface observed anywhere in the Texas HIPLEX area were obtained from computer charts each hour between 1500 and 0300 GMT inclusive. The data were grouped for echoes and no echoes. There were 170 observation times when echoes were present, and 129 times when they were not present. Percentage frequency distributions were prepared for each parameter and are shown in Figs. 5.27.1 through 5.27.4. The value of a parameter at the cross-over point represents the value that best distinguishes between the occurrence or nonoccurrence of a radar echo. These values are: velocity divergence, $-10^{-4}s^{-1}$; moisture divergence, -1.5×10^{-3} g kg^{-1} s^{-1}; vertical motion 50 mb above the surface (ω), -7.5 μbars s^{-1}; and vertical flux of moisture 50 mb above the surface ($-\rho q\omega$), -5×10^{-5} g cm^{-2} s^{-1}. It is clear from these figures that when the magnitudes of these parameters are smaller than the cross-over values, there is a higher percentage of no echoes than when the values are exceeded. Also, the figures show that for each variable the extreme magnitudes are larger when echoes are present than when they are absent.

To aid further in the interpretation of the frequency distributions, contingency tables were prepared using the cross-over values as criteria for distinguishing between echoes and no echoes. The tables are shown in Fig. 5.27.5. When values of all parameters exceed the cross-over values, there is only a slightly more than 1:1 probability that echoes will be observed than not. This probability is less than for 1977 results (Scoggins *et al.*, 1979). However, ratios for values below the cross-over values vary between 10:1 and 3:1. It should be noted here that the values of the parameters chosen at a given time are not necessarily associated with an echo if one was observed.

To gain some idea of how the cross-over values are related to echoes of various types, the echoes were classified as follows.

Lines: Cells organized into a line which exhibits movement.

Clusters: Organized group of three or more echoes.

Unorganized (A): One or more individual cells the tops of which are under 10 km (Codes 1 and 2), and none of which are organized into a line or cluster as defined above.

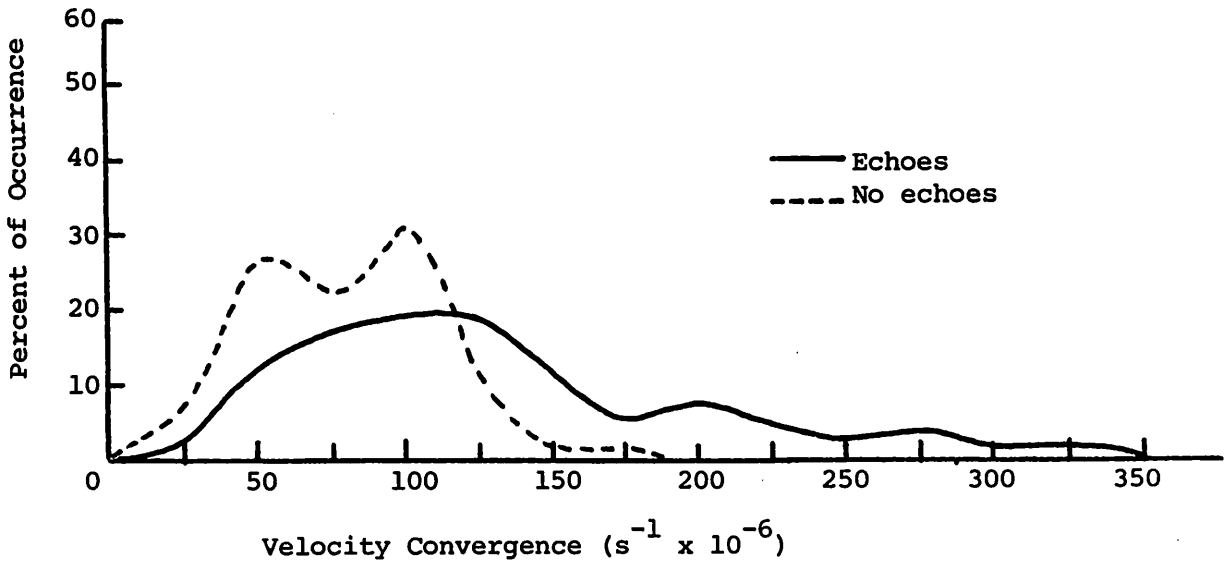

Fig. 5.27.1 Percentage frequency distributions of maximum negative velocity divergence (i.e., convergence) observed anywhere in the mesonetwork when echoes were and were not observed.

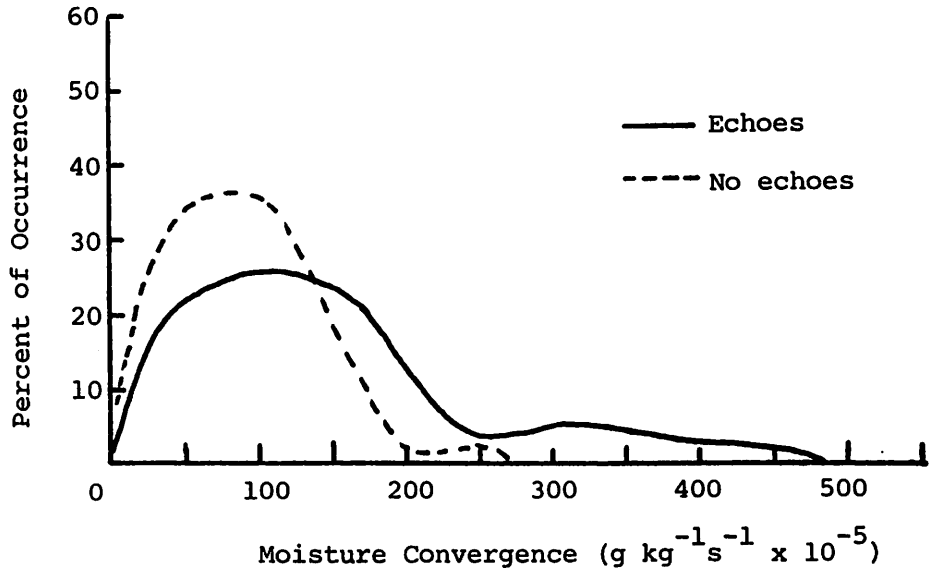

Fig. 5.27.2 Percentage frequency distributions of maximum negative moisture divergence (i.e., convergence) observed anywhere in the mesonetwork when echoes were and were not observed.

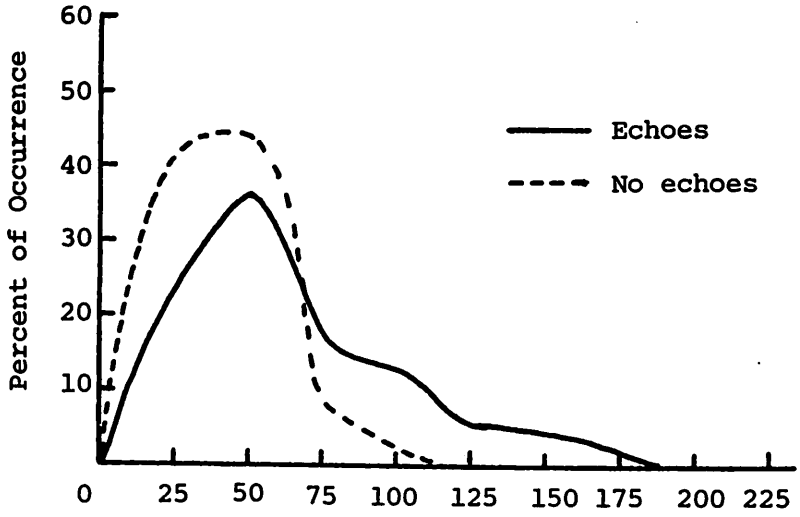

Fig. 5.27.3 Percentage frequency distributions of maximum $-\omega$ 50 mb above surface observed anywhere in the mesonetwork when echoes were and were not observed.

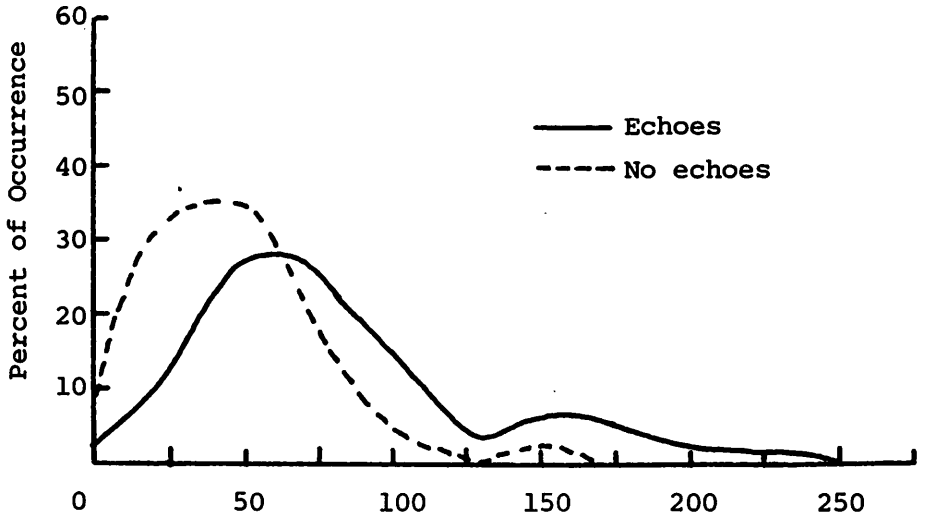

Fig. 5.27.4 Percentage frequency distributions of maximum upward vertical flux of moisture 50 mb above surface observed anywhere in mesonetwork when echoes were and were not observed.

$\vec{\nabla}\cdot\vec{v} < -10^{-4}s^{-1}$

Radar echoes	no	yes
no	111	18
yes	81	89

a. Velocity convergence

$\vec{\nabla}\cdot q\vec{v} < -1.5 \times 10^{-3}$ g kg^{-1}s^{-1}

Radar echoes	no	yes
no	100	29
yes	78	92

b. Moisture convergence

$\omega_{50} < -7.5$ µbars s^{-1}

Radar echoes	no	yes
no	118	11
yes	103	67

c. Vertical motion

$\rho q\omega > 5 \times 10^{-5}$ gm cm^{-2}s^{-1}

Radar echoes	no	yes
no	98	31
yes	72	98

d. Vertical flux of moisture

Fig. 5.27.5 Contingency tables for velocity and moisture convergence, vertical motion 50 mb above the surface, and vertical flux of moisture 50 mb above the surface versus radar echoes.

Unorganized (B): Same as above except tops exceed 10 km (Code 3).

Echo(es) approaching or receding from the area: Edge of echo(es) on the edge of grid area and there is no complete cell present in the gridded area. In other words, this does not include cases in which there is a complete echo in the grid area at the same time.

No echoes: No echoes, partial or complete, observed anywhere in the grid area.

The number of occurrences when the magnitudes of the parameters were less than or greater than the cross-over values are shown in Table 5.27.1 for each echo classification and when no echoes were present. For most cases there is a greater probability for echoes when the cross-over values are exceeded than when they are not. This is especially true for cases of lines and clusters of cells, similar to results obtained using 1977 data.

Table 5.27.1 Occurrences of echoes as function of echo characteristics and cross-over values for velocity and moisture divergence, vertical motion 50 mb above the surface, and vertical flux of moisture 50 mb above the surface.

Echo Classification	Divergence (s^{-1})		Moisture Divergence ($gm\ kg^{-1}s^{-1}$)		Vert. Moist. Flux ($gm\ cm^{-2}s^{-1}$)		Vertical Motion ($\mu bars\ s^{-1}$)	
	$\geq -10^{-4}$	$< -10^{-4}$	$> -1.5 \times 10^{-3}$	$\leq -1.5 \times 10^{-3}$	$> -5 \times 10^{-5}$	$< -5 \times 10^{-5}$	> -7.5	< -7.5
Lines	17	17	12	22	13	21	17	17
Clusters	7	17	5	19	5	19	9	15
Unorganized (A)	20	17	22	15	21	16	25	12
Unorganized (B)	17	25	15	27	12	30	25	17
Receding or Approaching	20	13	24	9	21	12	27	6
No Echoes	111	18	100	29	98	31	118	11

5.28 Average Conditions of Upper-Level Kinematics and Atmospheric Energetics During Times With and Without Convective Activity

Profiles of mass divergence for convective and non-convective conditions (Fig. 5.28.1) show little difference below 750 mb. Mass convergence near the surface has been shown to be associated with convection in the analysis of the 1976 and 1977 data (Scoggins et al., 1978, and Scoggins et al., 1979). A second layer of mass convergence exists at 450 mb for convective cases. The primary difference between these profiles indicate that larger magnitudes of mass divergence and convergence occur for convective cases rather than non-convective cases.

Nearly similar profiles for convective and non-convective cases of vertical velocity (Fig. 5.28.2) were observed. Upward vertical velocities occurred in all layers for times of convection, and in all layers below 200 mb for times of no convection. However, upward vertical velocities in most layers were slightly larger for convective cases than for non-convective cases.

Profiles of moisture divergence (Fig. 5.28.3) resemble those of mass divergence for both convective and non-convective cases. Horizontal moisture convergence in low layers was larger than for non-convective cases, and moisture divergence occurred above 800 mb for non-convective conditions. This same pattern is reflected in profiles of horizontal flux divergence of latent heat (Fig. 5.28.4) where a strong net inflow in layers near the surface supplies latent heat for storm development. A smaller net horizontal flux convergence occurs in these layers for non-convective conditions which might accompany the development and maintenance of small "fair weather" cumulus.

Profiles of the vertical flux divergence of latent heat (Fig. 5.28.5) for convective and non-convective conditions show flux divergence in low layers near the surface and flux convergence aloft. This corresponds to a net vertical transport of latent heat consistent with the upward vertical motion field from low levels to mid levels where cooling and condensation produce convective cloud formation and the release of latent heat. For non-convective conditions a similar profile in shape and sign to convective conditions is shown but smaller in magnitude. These similarities are basically due to a similar vertical velocity field.

Profiles of the local change of latent heat (Fig. 5.28.6) for both

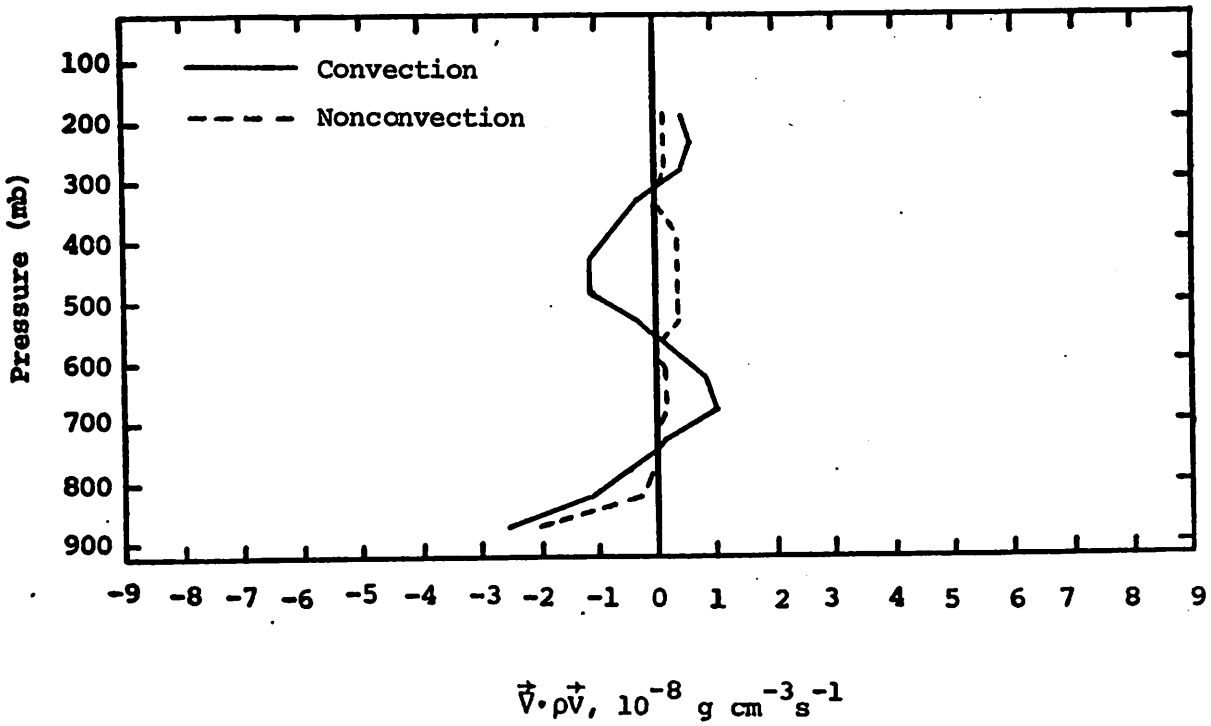

Fig. 5.28.1 Vertical profiles of mass divergence averaged for times of convection and nonconvection.

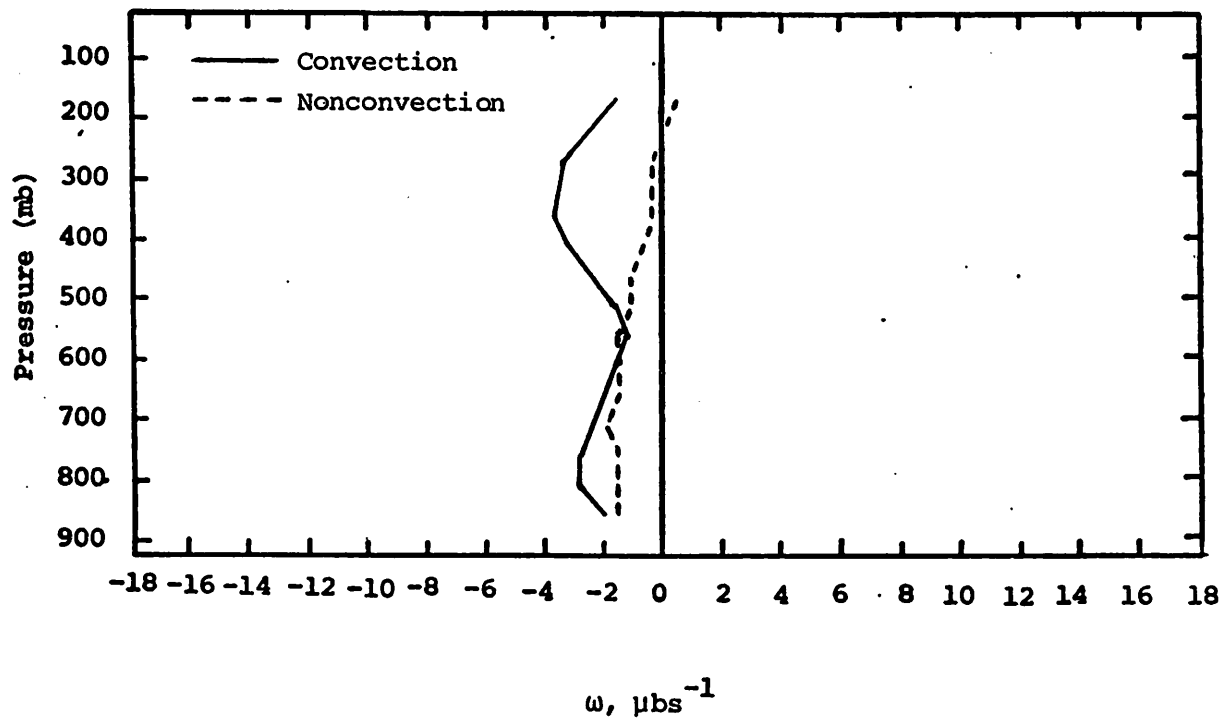

Fig. 5.28.2 Vertical profiles of vertical motion averaged for times of convection and nonconvection.

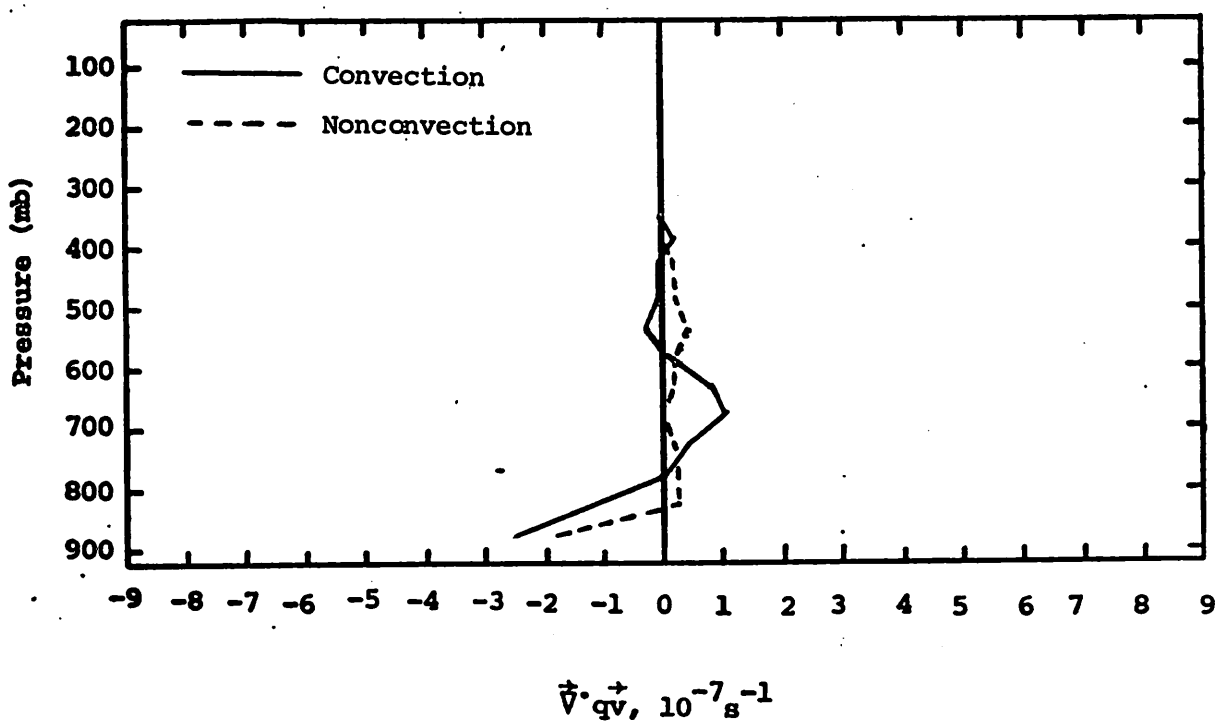

Fig. 5.28.3 Vertical profiles of moisture divergence averaged for times of convection and nonconvection.

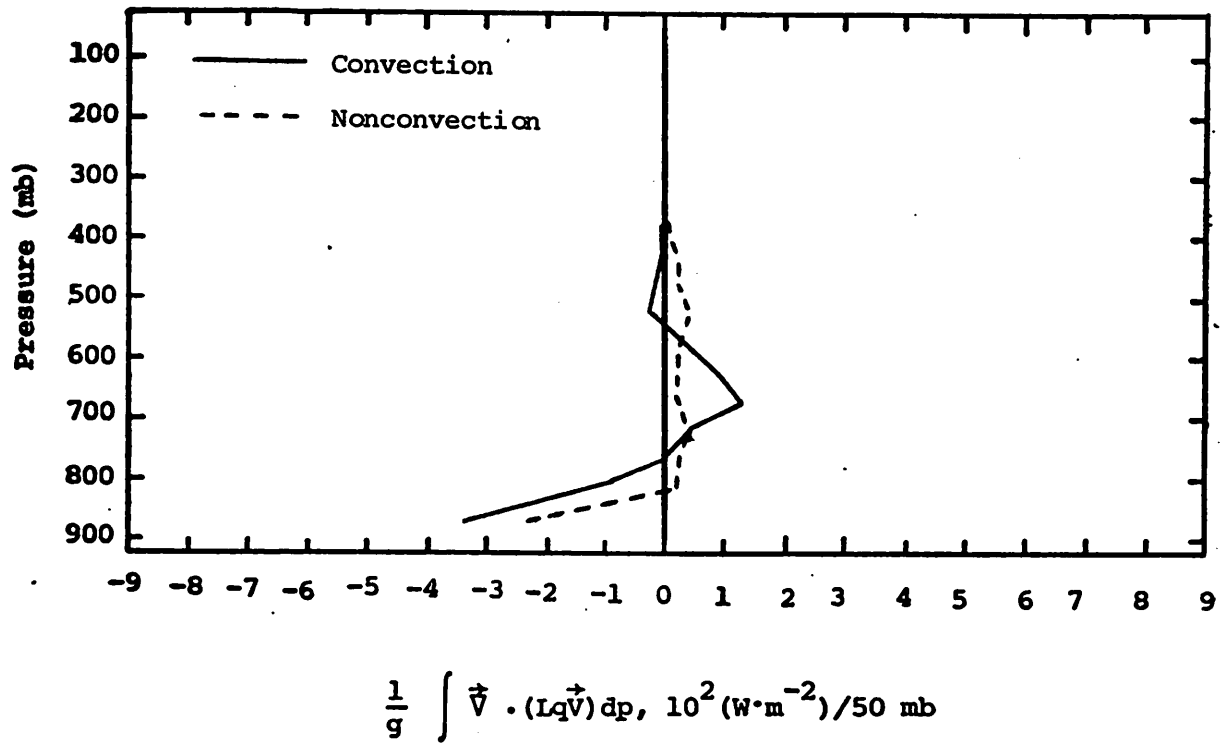

Fig. 5.28.4 Vertical profiles of horizontal flux divergence of latent heat energy averaged for times of convection and nonconvection.

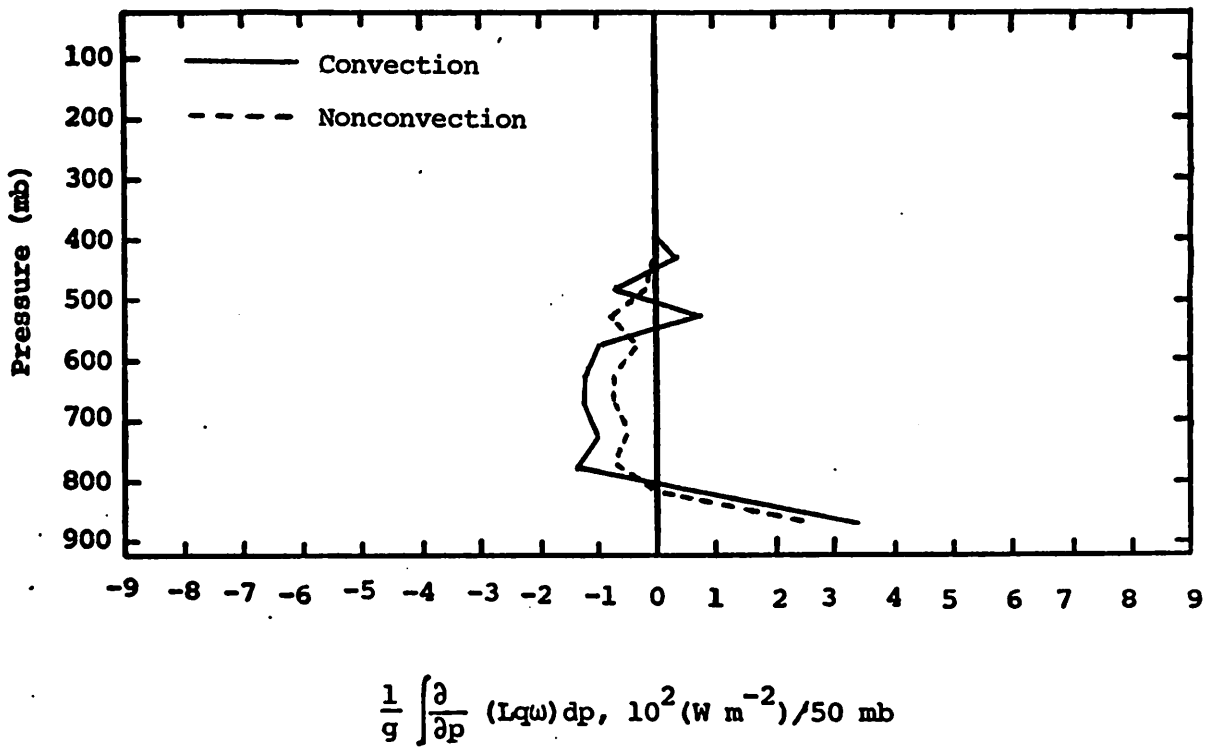

Fig. 5.28.5 Vertical profiles of vertical flux divergence of latent heat energy averaged for times of convection and nonconvection.

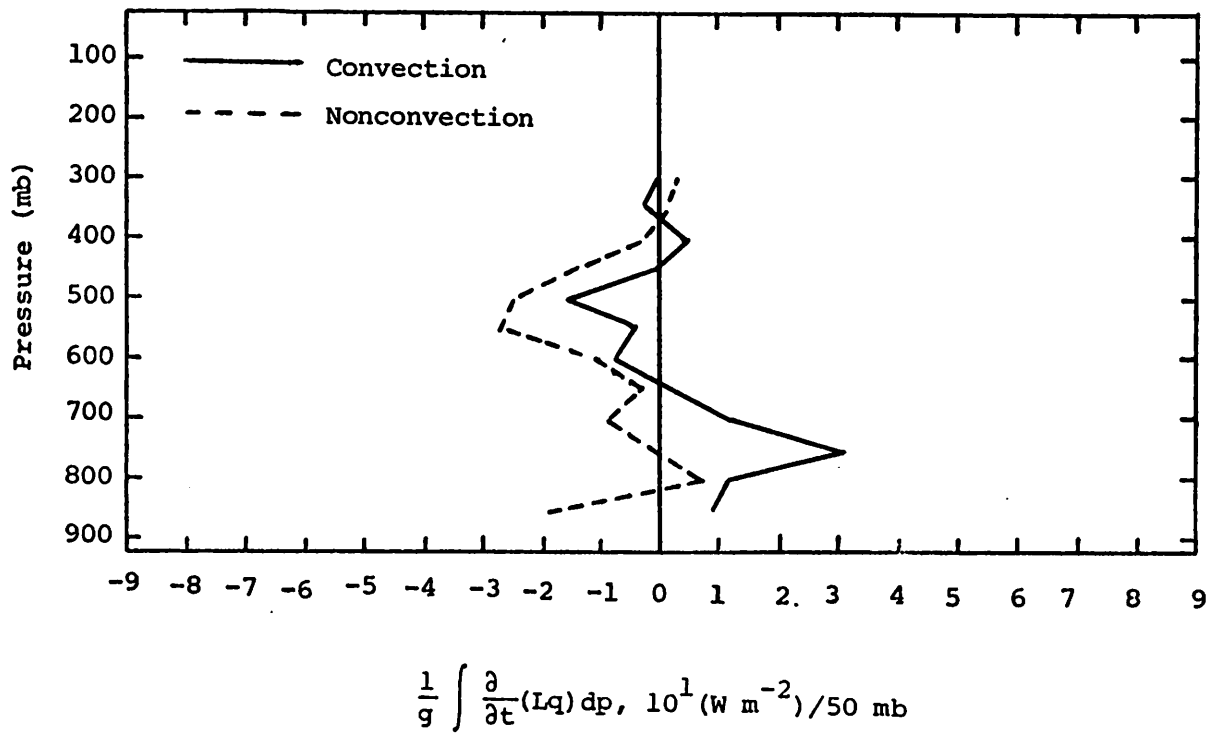

Fig. 5.28.6 Vertical profiles of the local change of latent heat energy averaged for times of convection and nonconvection.

convective and non-convective cases remain small in comparison to other terms in the latent energy budget. For the convective case, positive values in low levels and negative values at mid levels might reflect losses of water vapor that occur during condensation. Values seem to be large for the non-convective case which might be attributed to the importance of turbulent flux of latent heat when activity is absent.

Similar to other terms in the latent energy budget, profiles of the residual (Fig. 5.28.7) show little difference between convective and non-convective cases. The release of latent heat is due to condensation and the result is environmental heating. This same pattern is closely resembled by profiles of diabatic heating (Fig. 5.28.8) below 400 mb. Sensible heating is shown for both convective and non-convective profiles which is strongly related to condensation within an upward vertical velocity field. The heating shown in both profiles is partially due to diabatic effects, but unresolved adiabatic processes also might be a factor. This suggests that perhaps net radiation and the turbulent flux divergence of water vapor may be responsible.

Profiles of horizontal and vertical flux of kinetic energy (Figs. 5.28.9 and 5.28.10) for non-convective cases are near zero but show a slight outflow at all levels except above 400 mb where a net inflow of kinetic energy occurred. The opposite is seen for times with convection where kinetic energy flows inward at low levels, is transported vertically to the upper troposphere, and is horizontally exported. This result is shown in the local change of kinetic energy (Fig. 5.28.11). During non-convective periods little or no change in kinetic energy occur below 400 mb with a slight loss in layers above. However, for convective periods a large gain is observed in the upper troposphere mainly due to a strong upward flux of kinetic energy from lower layers.

Horizontal flux convergence of sensible heat (Fig. 5.28.12) occurs in layers near the surface for both convective and non-convective cases which increase low level temperatures and decrease static stability. For non-convective times divergence aloft contributes to an increase in static stability. The convective and non-convective profiles are consistent with storm formation and suppression, respectively.

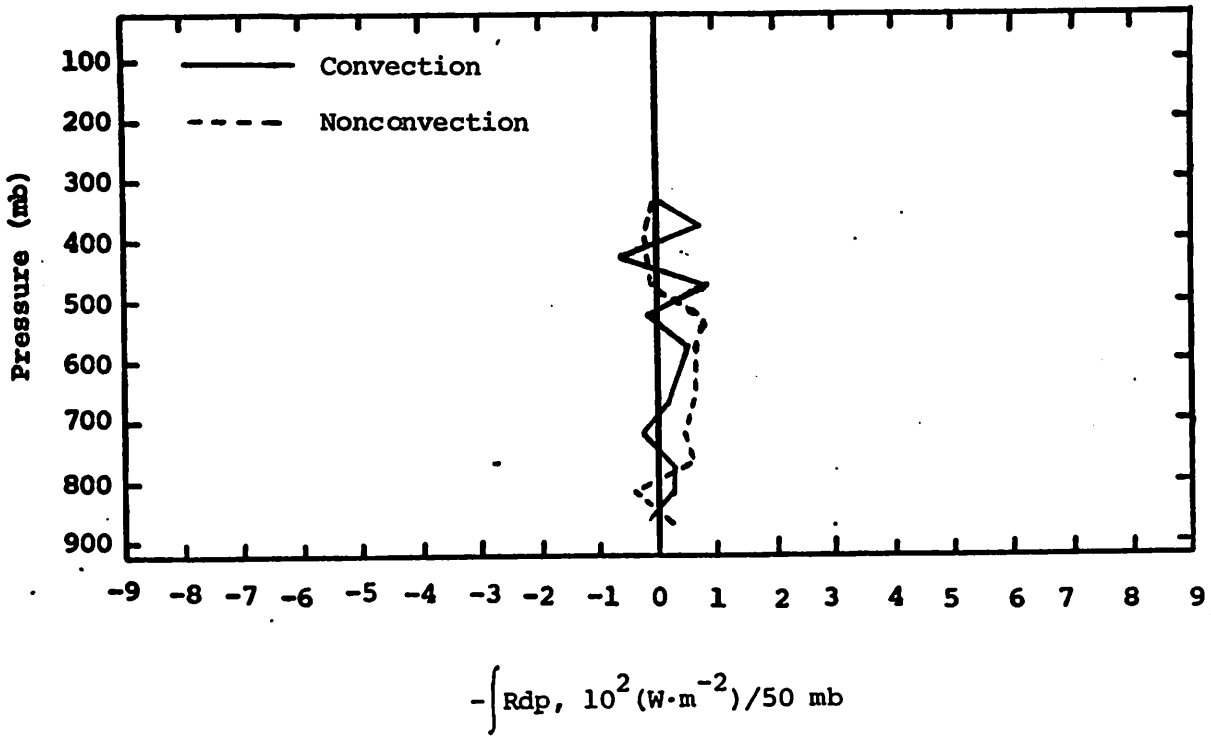

Fig. 5.28.7 Vertical profiles of the residual of the latent heat energy equation averaged for times of convection and nonconvection.

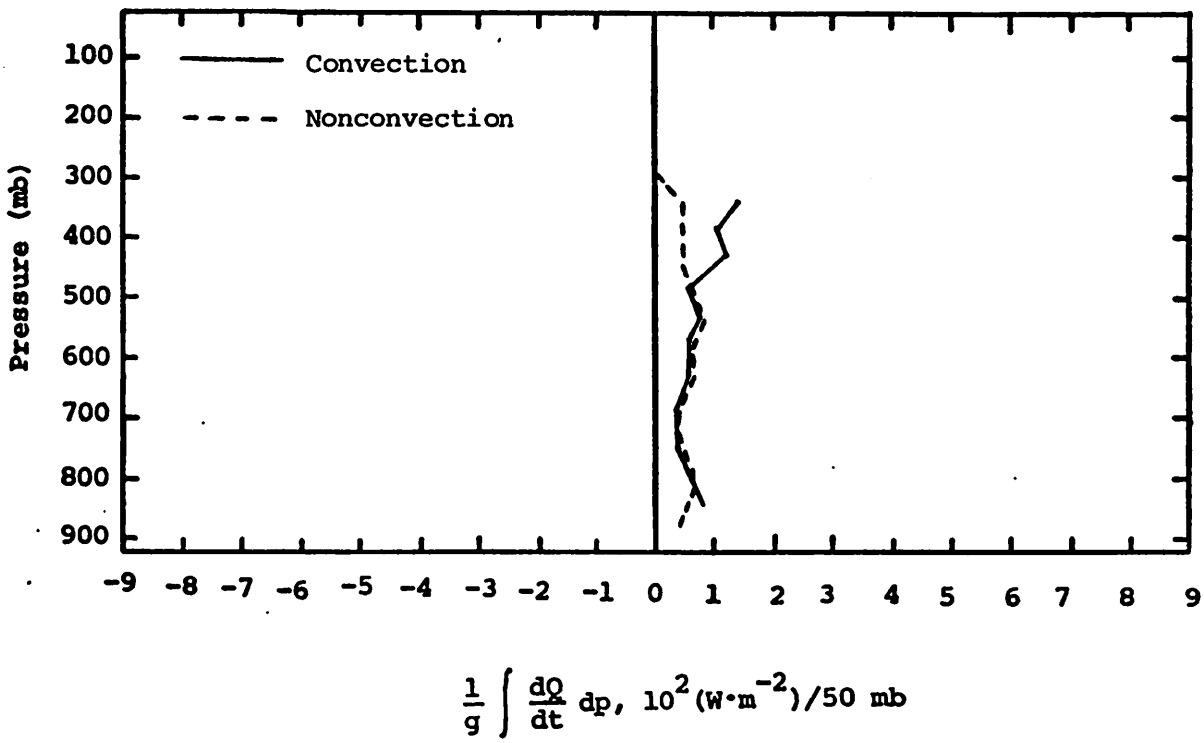

Fig. 5.28.8 Vertical profiles of diabatic heating computed from the first law of thermodynamics averaged for times of convection and nonconvection.

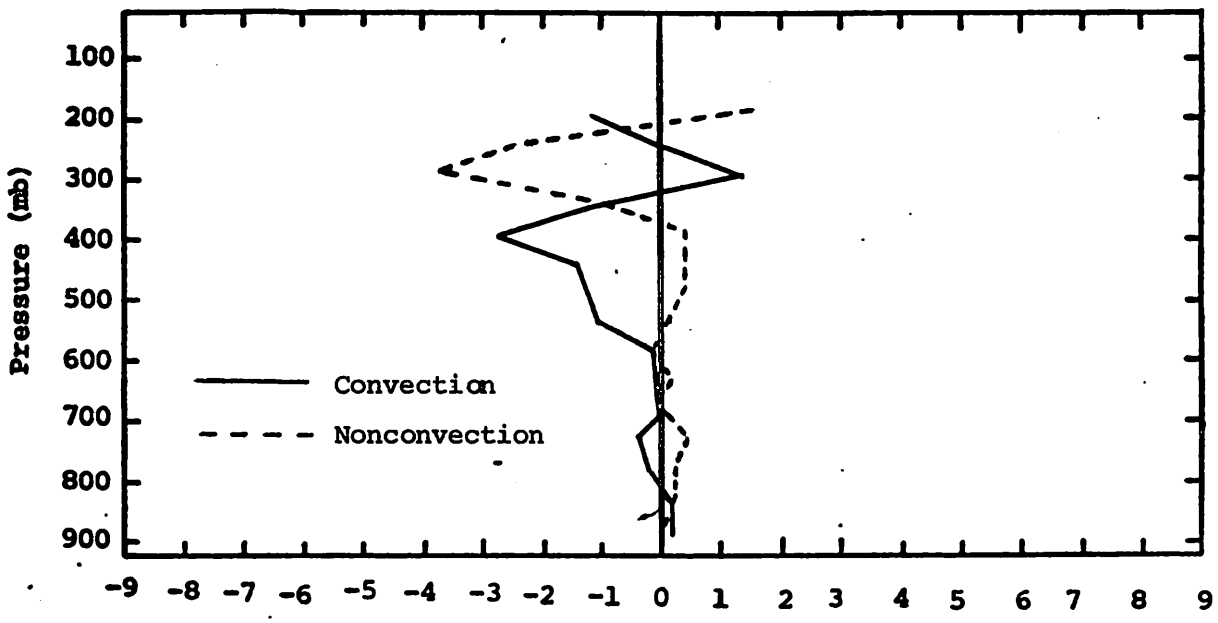

Fig. 5.28.9 Vertical profiles of horizontal flux divergence of kinetic energy averaged for times of convection and nonconvection.

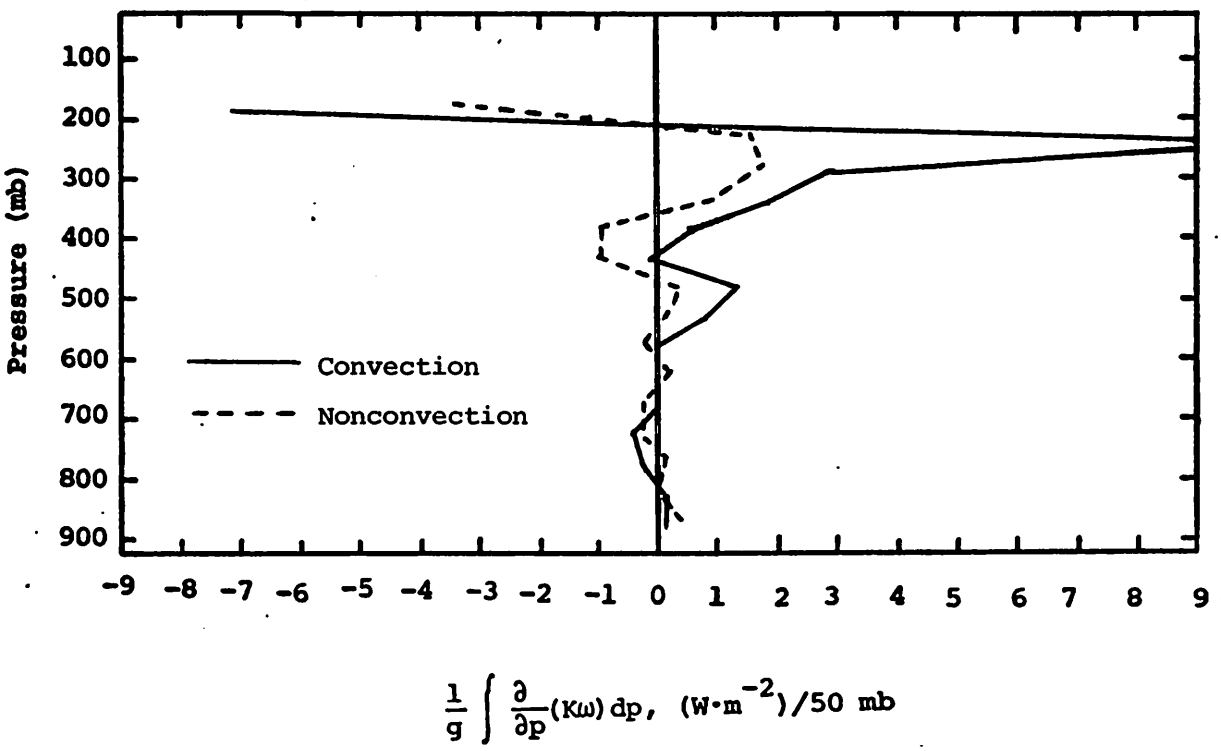

Fig. 5.28.10 Vertical profiles of vertical flux divergence of kinetic energy averaged for times of convection and nonconvection.

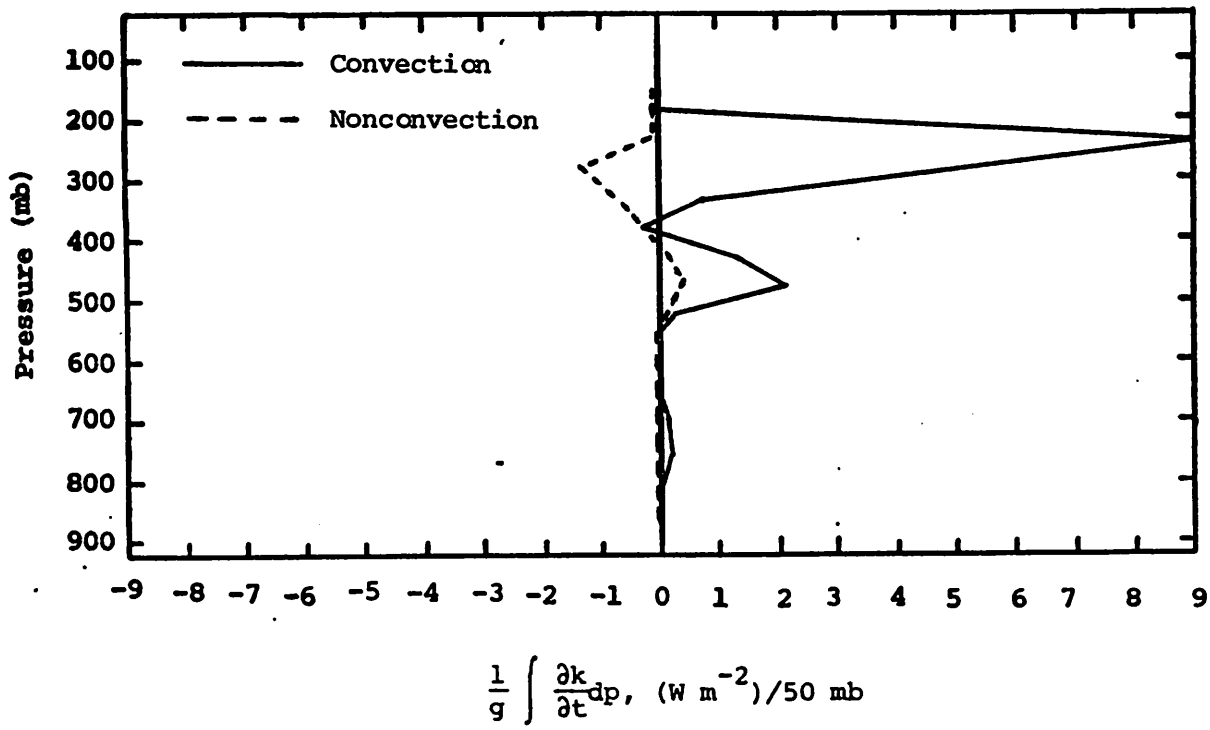

Fig. 5.28.11 Vertical profiles of the local change of kinetic energy averaged for times of convection and nonconvection.

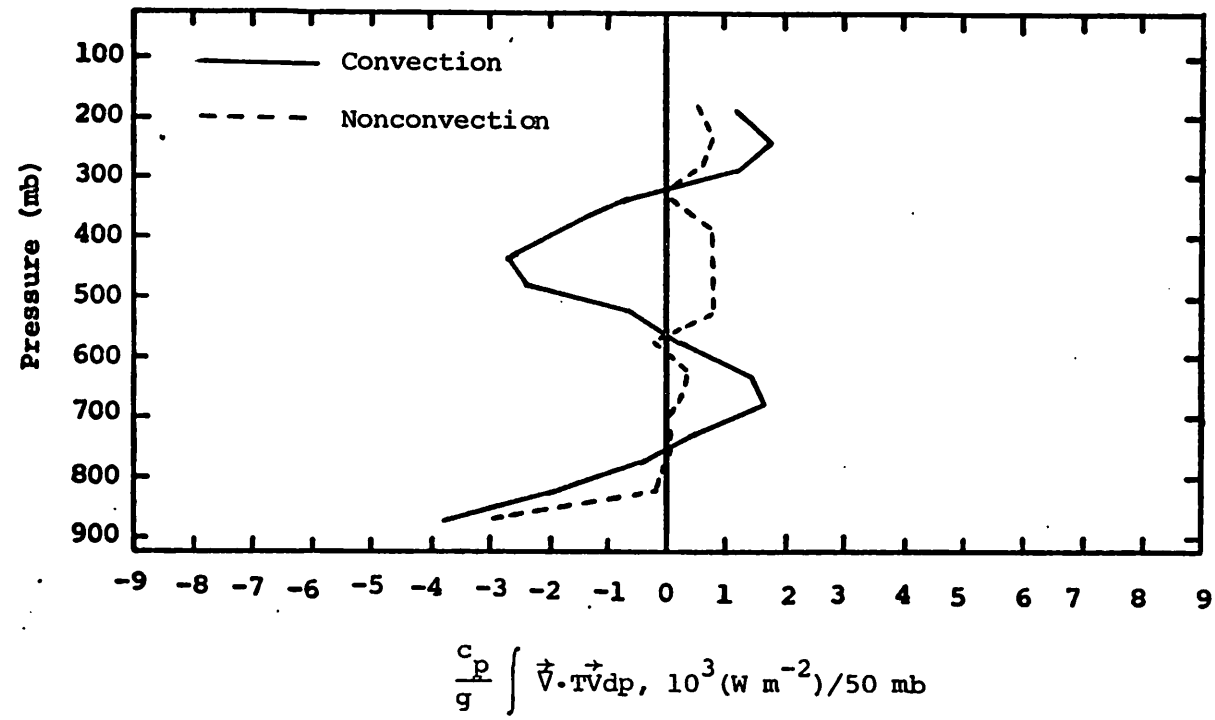

Fig. 5.28.12 Vertical profiles of horizontal flux divergence of sensible heat averaged for times of convection and nonconvection.

Profiles of the vertical flux divergence of sensible heat (Fig. 5.28.13) for convective and non-convective cases show divergence in layers below 800 mb and convergence aloft. This upward transport of sensible heat is consistent with the low level horizontal convergence of sensible heat and the observed upward environmental vertical velocities. These similar processes for convective and non-convective cases are further shown in the profiles for local rate-of-change of internal energy (Fig. 5.28.14). Small negative values were observed near the ground with positive values aloft. However, it should be noted that these changes remain smaller by over two orders of magnitude than horizontal and vertical flux divergence terms.

Profiles of horizontal and vertical flux divergence of potential energy are shown in Figs. 5.28.15 and 5.28.16, respectively. These profiles for convective and non-convective cases remain nearly similar in shape and sign, showing a net horizontal inflow near the surface, vertical transport to the upper troposphere, and net horizontal export aloft. When activity was present net horizontal outflow of potential energy was large in upper layers. However, values of the flux terms tend to increase with height because potential energy increases with height. At 400 mb, strong horizontal flux convergence and strong vertical divergence of potential energy occur for convective cases. This same pattern was found in profiles of horizontal and vertical flux divergence of sensible heat and kinetic energy. The similarity in these profiles indicates an important energy source at 400 mb as well as near the surface for convective cases.

Local changes for geopotential energy (Fig. 5.28.17) are small and negative for convective and non-convective cases. As was observed for the local changes of internal and kinetic energy, the local change of geopotential energy are several orders of magnitude smaller than the corresponding flux terms.

In summary, substantial differences occur in energy budget terms when averages over times of convection are compared to averages over times of non-convection. Low-level inflow, upward transport, and upper-level export of internal, kinetic, and potential energy are enhanced during periods of convection. Strong horizontal inflow of latent heat energy in the lower atmosphere is nearly balanced by latent heat release during times of

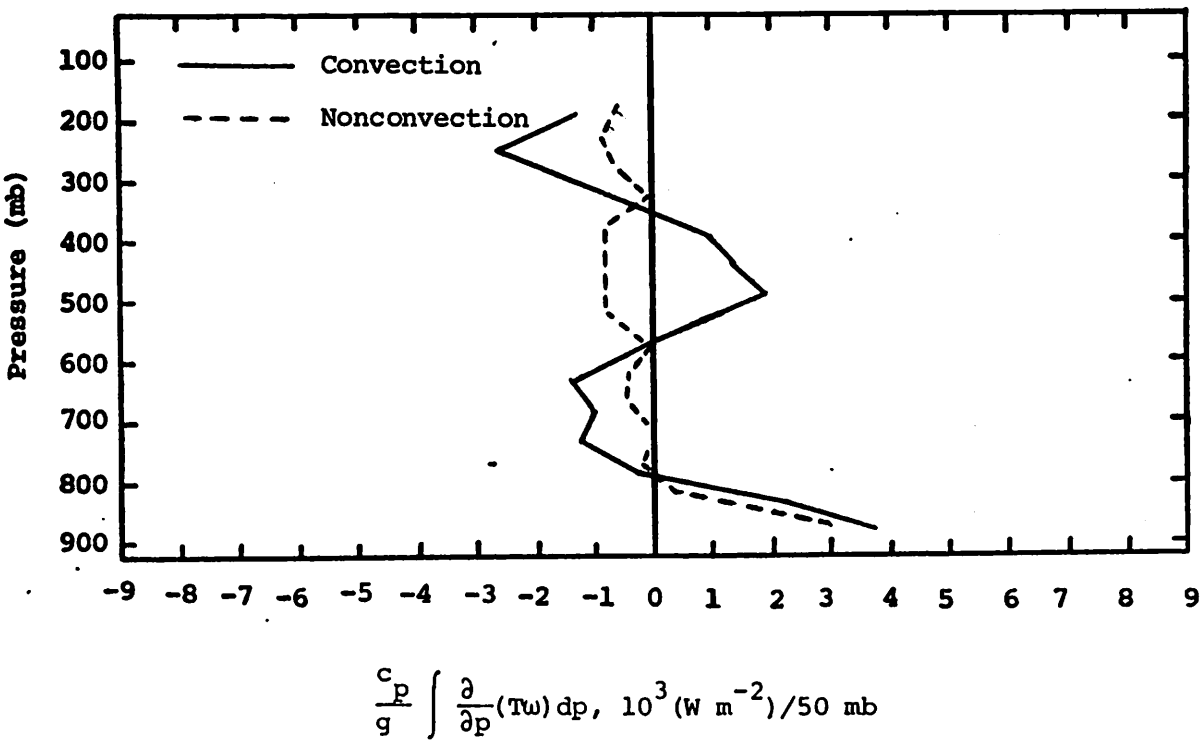

Fig. 5.28.13 Vertical profiles of vertical flux divergence of sensible heat averaged for times of convection and nonconvection.

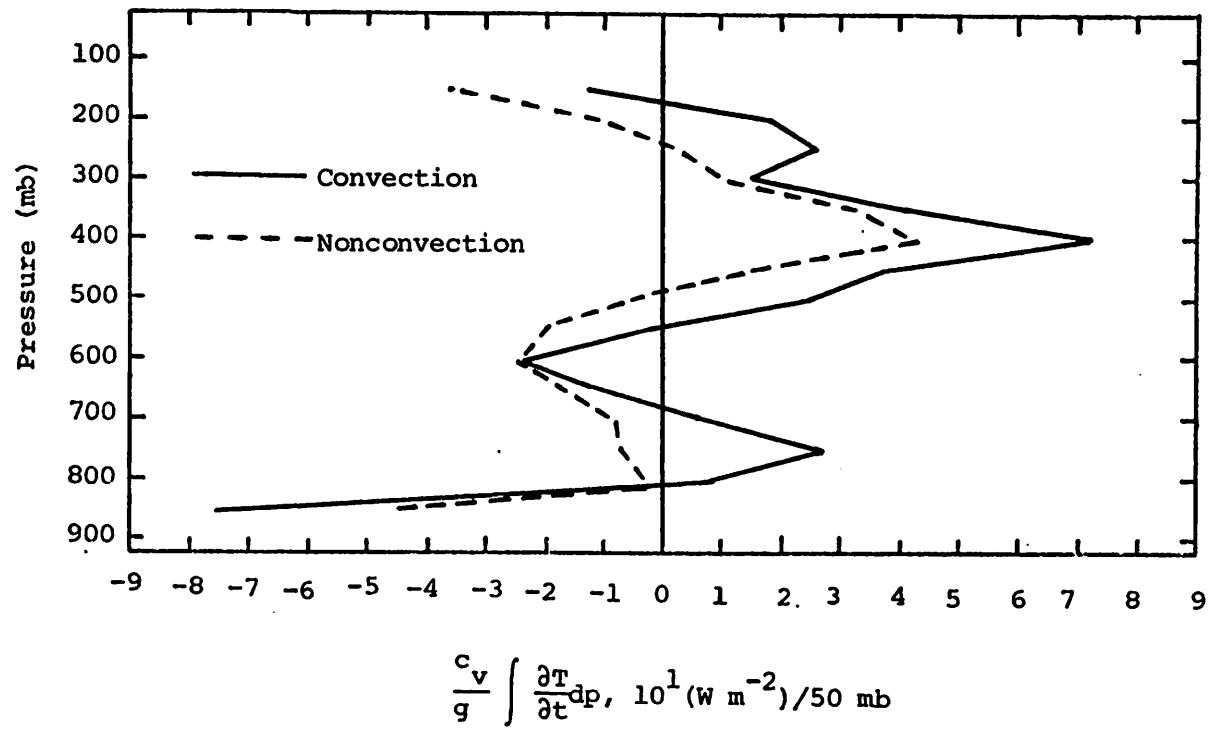

Fig. 5.28.14 Vertical profiles of local change of internal energy averaged for times of convection and nonconvection.

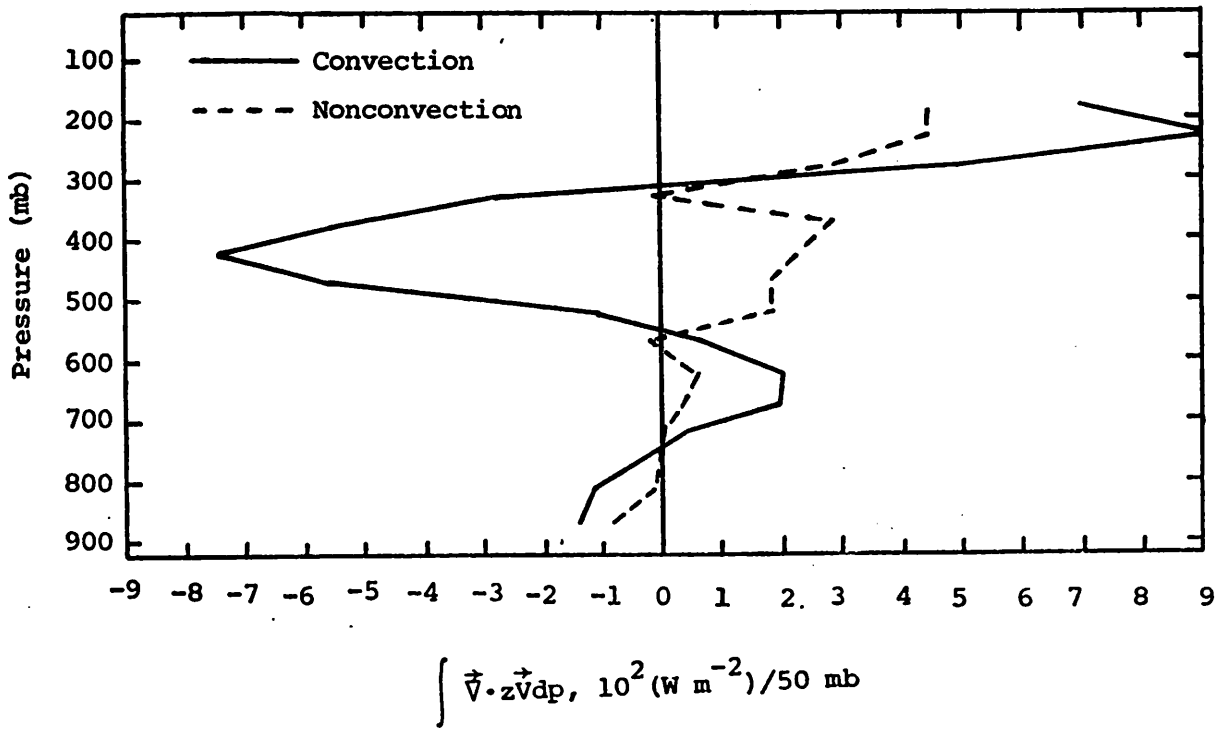

Fig. 5.28.15 Vertical profiles of horizontal flux divergence of potential energy averaged for times of convection and nonconvection.

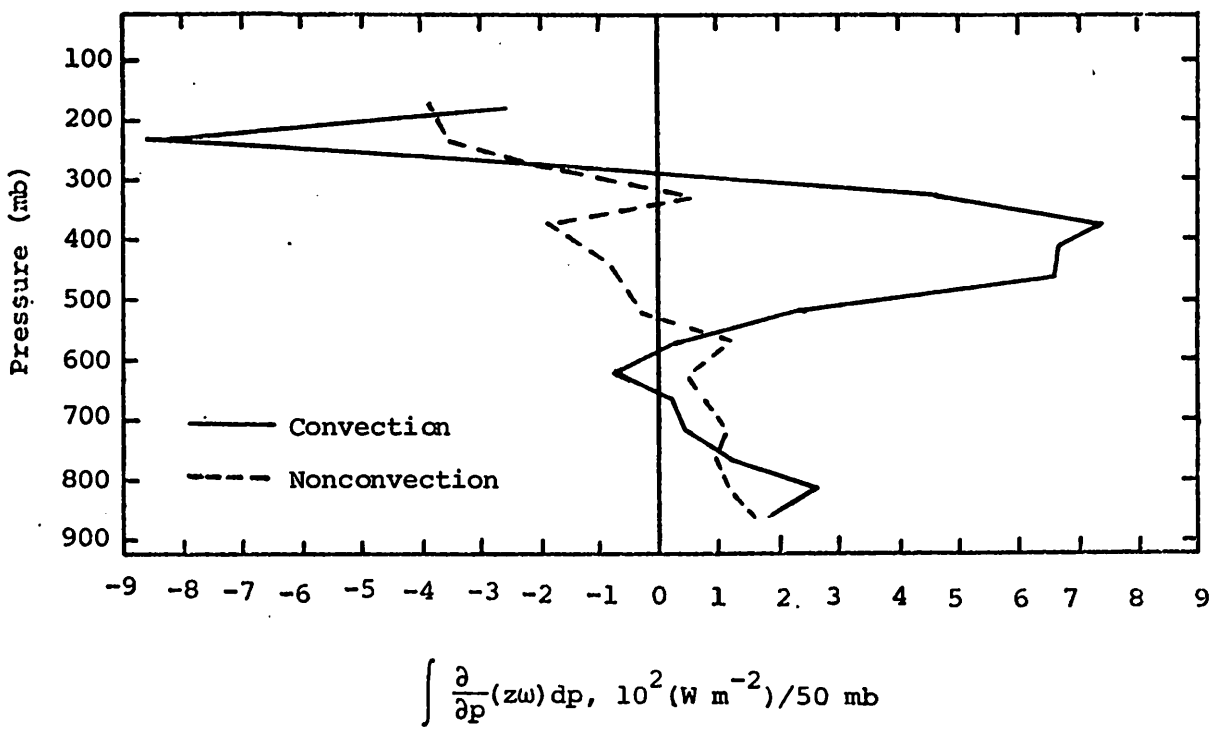

Fig. 5.28.16 Vertical profiles of vertical flux divergence of potential energy averaged for times of convection and nonconvection.

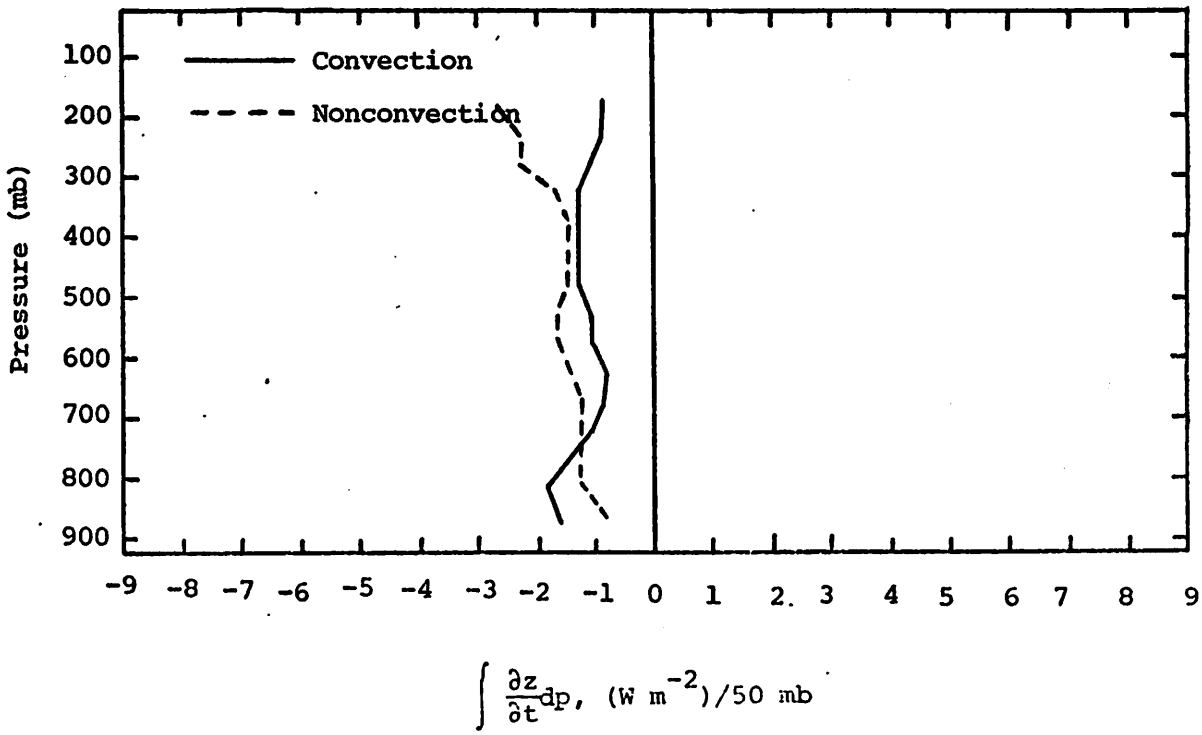

Fig. 5.28.17 Vertical profiles of the local change of potential energy averaged for times of convection and nonconvection.

convection and, therefore, plays an important role in the formation and maintenance of convective activity. Particularly strong energy sources for convective activity were shown to occur near the surface and at approximately 450 mb.

5.29 Average Moisture Processes as a Function of Convective Activity

Profiles of the net horizontal transport of water vapor (Fig. 5.29.1) show large differences between convective and non-convective cases. During times of non-convection, a net loss of water vapor is observed in all layers except near the surface where a slight gain of water vapor might be associated with the development and maintenance of small "fair weather" cumulus clouds. However, for times of convection a net gain of water vapor is seen in all layers especially near the surface where water vapor transports are over one order of magnitude larger than for non-convective cases. Two distinct layers of maximum net gain of water vapor are shown for convective cases: (1) near the surface to approximately cloud base (i.e. 700 mb) and; (2) 550 to 450 mb. These two layers of maximum net gain in the transport of water vapor correspond to a maximum net horizontal convergence of kinetic, potential, and internal energy. These two layers have been shown to be principal energy sources for convective activity.

Similarity in profiles of the net vertical transport of water vapor (Fig. 5.29.2) exists between convective and non-convective cases. For non-convective cases a net loss occurs in all layers with the maximum transport at approximately 700 mb. A large net gain of water vapor is seen near the surface for times of convection. The loss of water vapor in lower layers is shown by a strong upward transport of water vapor through constant pressure surfaces (Fig. 5.29.3). These profiles remain nearly similar with strong upward transports of water vapor at every level. The transport of water vapor through constant pressure levels is due to the amount of water vapor present and the environmental vertical velocities. From Fig. 5.28.2, vertical velocities remain nearly the same up to 500 mb, so that the increased water vapor transport for convective cases is due mainly to the increased water vapor associated with convection.

Profiles of the combined net horizontal and vertical transport of water vapor (Fig. 5.29.4) resemble those of the net horizontal transport of water vapor which indicates the dominance of the net horizontal transport term. During non-convective cases, a strong net loss of water vapor is shown for most layers. For convective cases, a net loss of water vapor occurs between 700 and 550 mb, but two layers of strong net gain of water vapor emerge especially near the surface.

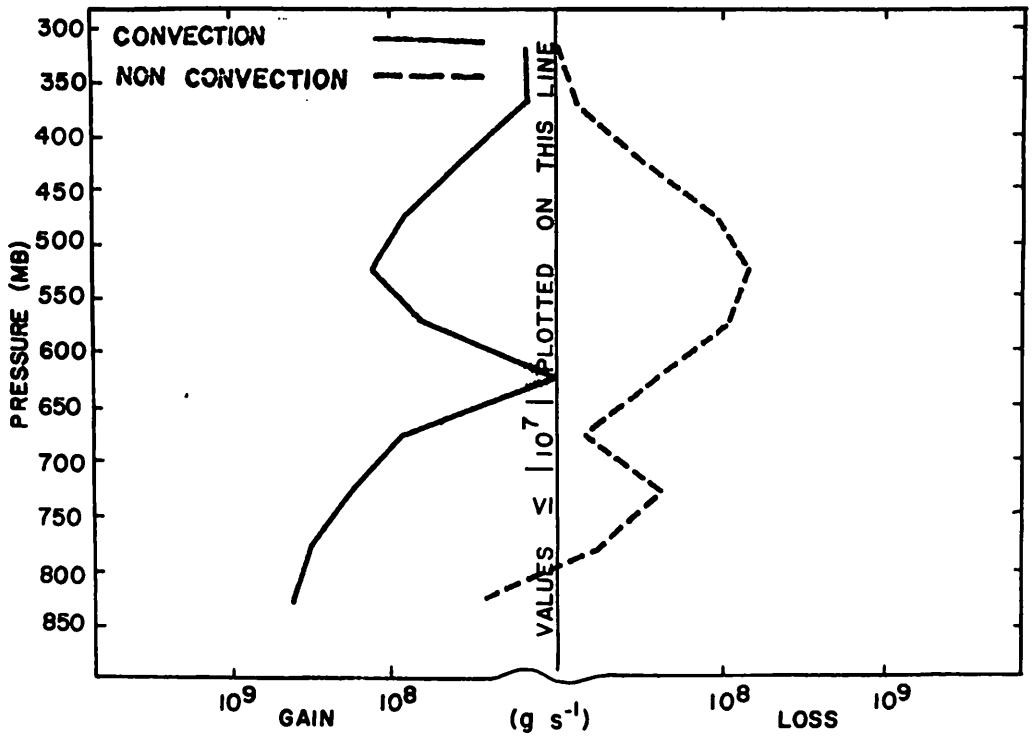

Fig. 5.29.1 Vertical profiles of net horizontal transport of water vapor through boundaries of 50-mb layers averaged for times of convection and nonconvection.

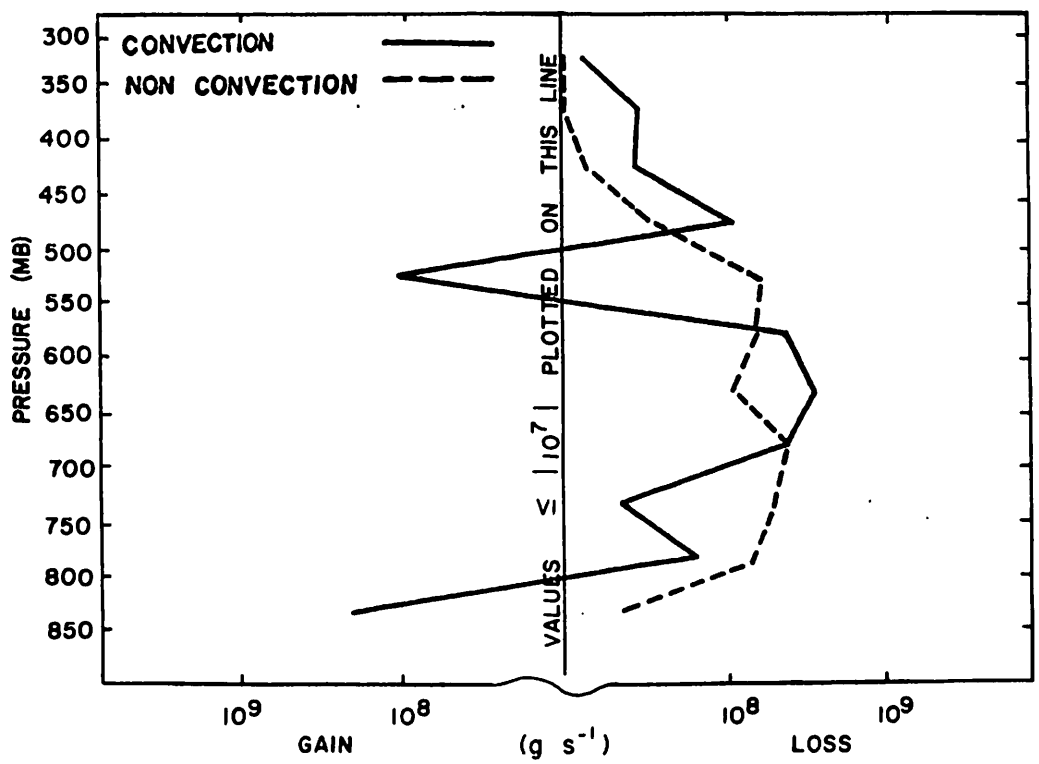

Fig. 5.29.2 Vertical profiles of net vertical transport of water vapor through boundaries of 50-mb layers averaged for times of convection and nonconvection.

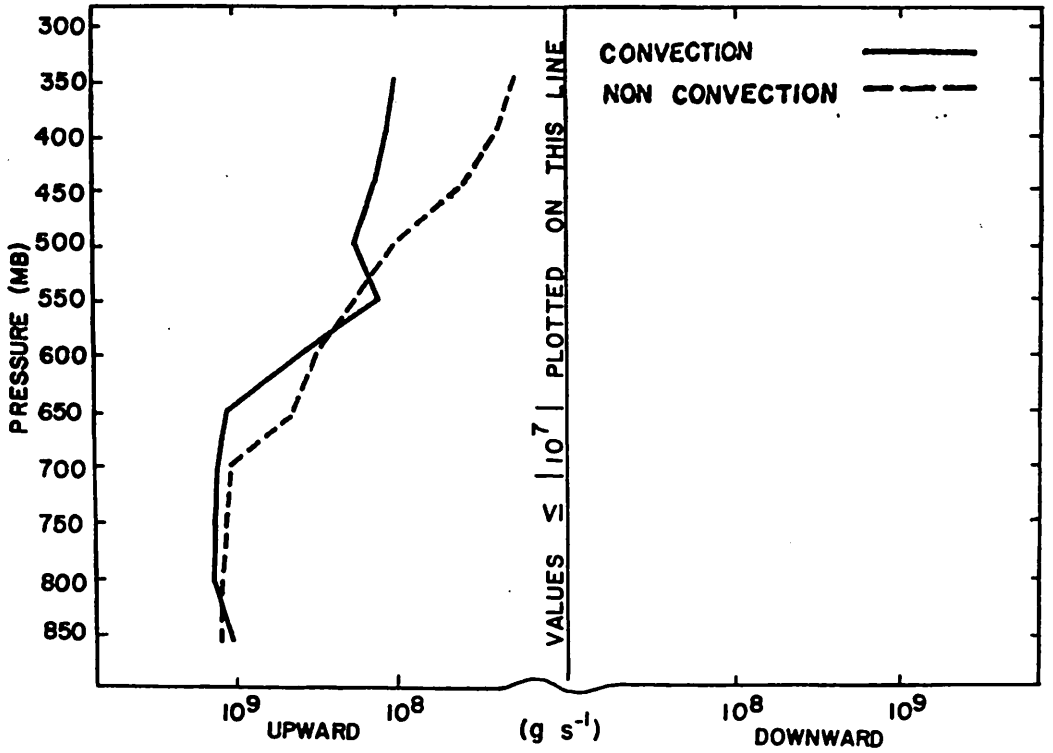

Fig. 5.29.3 Vertical profiles of the vertical transport of water vapor through constant pressure surfaces averaged for times of convection and nonconvection.

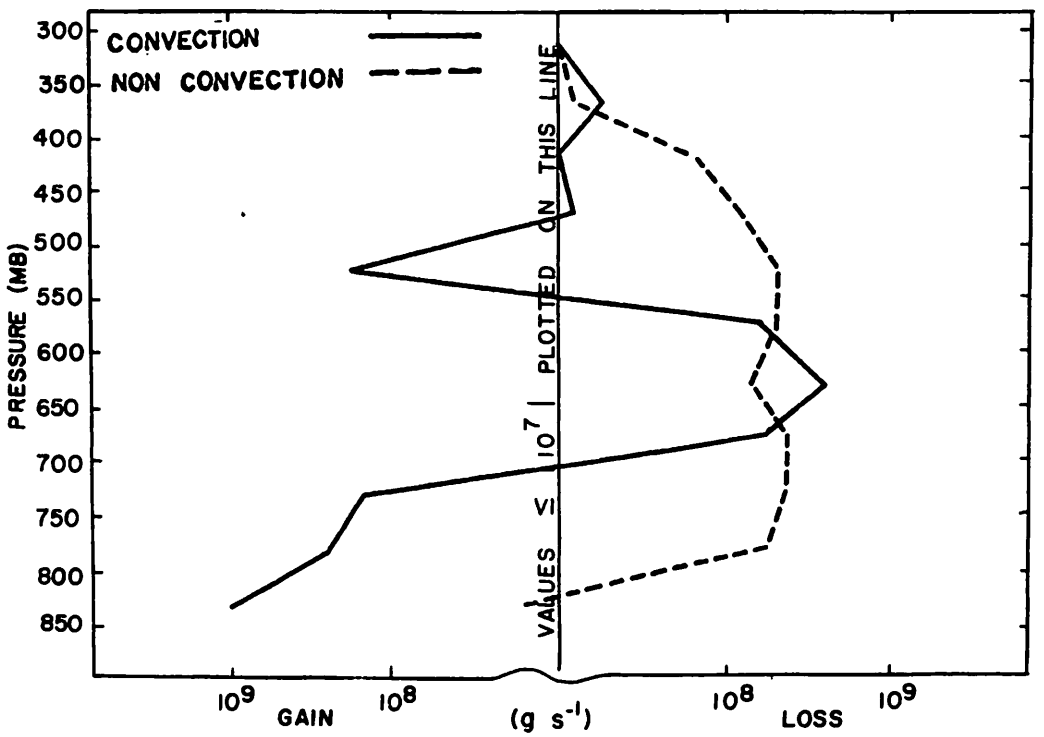

Fig. 5.29.4 Vertical profiles of combined net horizontal and vertical transport of water vapor through boundaries of 50-mb layers averaged for times of convection and nonconvection.

The local rate-of-change in the total mass of water vapor (Fig. 5.29.5) shows a net gain of water vapor in all layers below 550 mb for non-convective cases. A net gain in every layer is seen for convective cases except near the surface. The largest gain of water vapor occurs at 725 mb, approximately just below cloud base. However, these local changes similar to the local rate-of-change terms of other energy budgets are one to two orders of magnitude smaller than the corresponding flux divergence terms.

The residual term of the water vapor budget (Fig. 5.29.6) shows two layers of difference between convective and non-convective cases. Large net losses are seen below cloud base (700 mb to the surface) and above 550 mb for times of convection. These layers corresponding to a strong net gain of water vapor by horizontal transport indicate a water vapor source for condensation and perhaps leads to precipitation. The largest loss in the residual occurs near the surface where greater amounts of water vapor exist and are processed by convection. A net gain of water vapor in all layers except near the surface occurs for non-convective cases which may be attributed to evaporation and the turbulent flux of water vapor aloft.

In summary, the evaluation of individual water vapor budget terms averaged over times of convection and non-convection show distinct differences. The amounts of water vapor are greater for convective cases than non-convective cases, resulting in increased water vapor transports. Maximum water vapor transport occurs in two layers, near the surface and approximately 450 mb and corresponds to layers of maximum flux convergence of the total energy budget which indicates important energy sources for convective activity. Comparisons of individual water vapor budget terms have shown the net horizontal transport term to be the dominant term during convective activity.

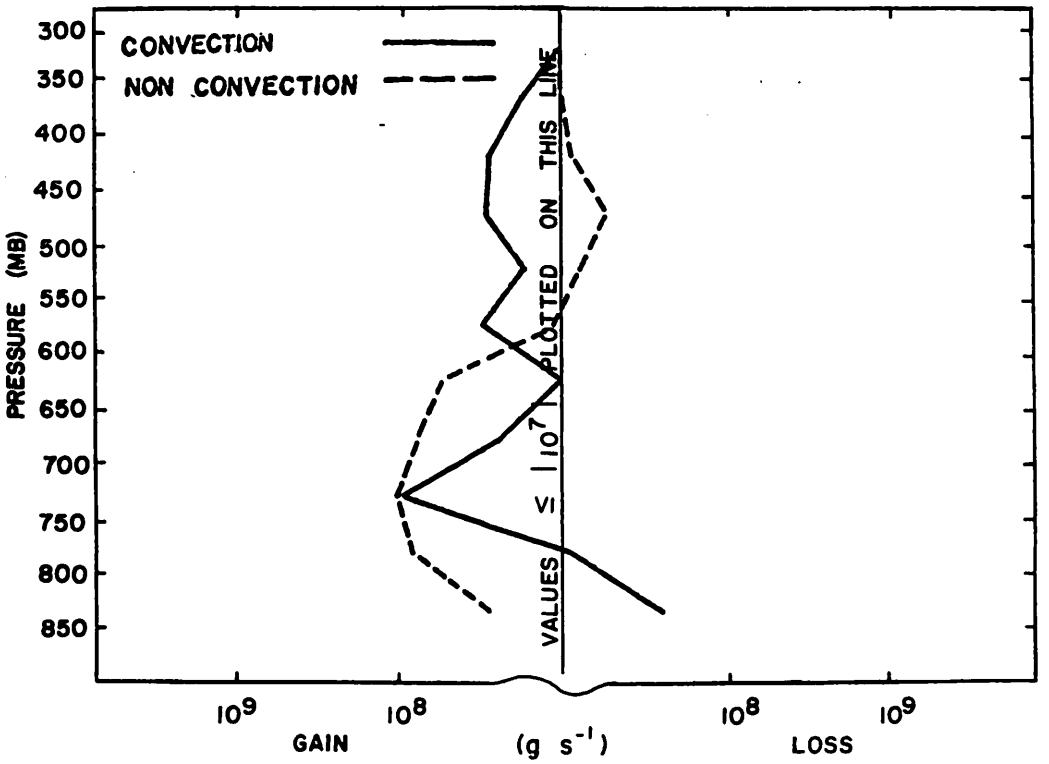

Fig. 5.29.5 Vertical profiles of the local rate-of-change in total mass of water vapor averaged for times of convection and nonconvection.

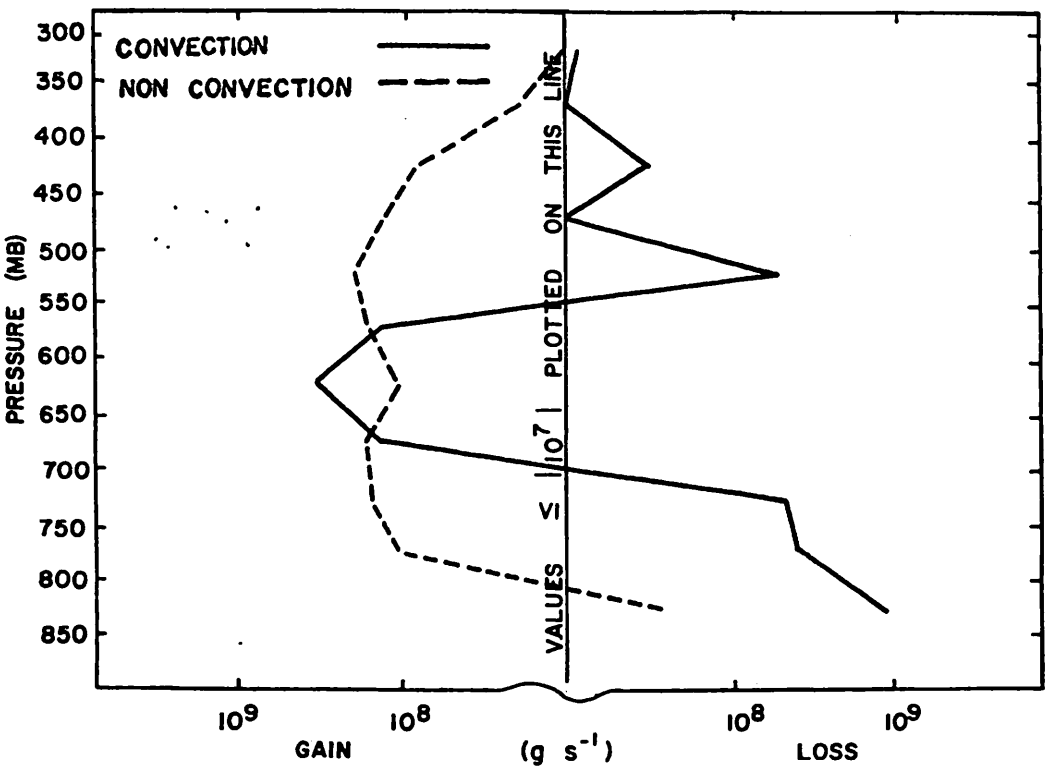

Fig. 5.29.6 Vertical profiles of the residual in the water vapor budget equation averaged for times of convection and nonconvection.

6. SUMMARY AND COMMENTS

This report contains an analysis of Texas HIPLEX mesoscale data for 1978. The approach was to treat each day as a case study, analyze selected surface variables in a composite sense, and establish average conditions of atmospheric kinematics, energetics, and moisture processes during times with and without convective activity.

A total of 26 days is included in this study. Nine of these days consist of surface analyses only, while 17 of the days consist of both surface and upper-air analyses. The surface analyses include radar echoes, temperature, mixing ratio, equivalent potential temperature, terrain-induced vertical motion, velocity divergence, vertical motion 50 mb above the surface, moisture divergence, vertical flux of moisture 50 mb above the surface, vorticity, pressure change, and relative wind fields. The upper-air analyses include mass divergence, vertical motion, moisture divergence, and various terms in budgets of latent heat, total energy, and moisture.

The results confirm those reported for 1976 (Scoggins, et al., 1978) and 1977 (Scoggins, et al., 1979), and show that, in most cases, both surface and upper air conditions were altered significantly by convective activity and vice versa. In some cases, pronounced changes in variables such as moisture divergence at all levels including the surface, and vertical motion aloft were associated with the occurrence and extent of convective activity.

Even though the number of days considered in this report is small, the results together with those for 1976 and 1977, demonstrate conclusively the value and, indeed, the necessity of mesoscale data in the assessment of environmental conditions associated with convective activity, and for determining the interactions of convective clouds with their environment. This type of research is essential in the development of the technology required for rainfall enhancement.

One significant aspect of this research is that it confirms the general results obtained for 1976 and 1977 data. Also, the importance of horizontal moisture convergence below 3 km and the vertical transport of moisture from the lower to the mid atmosphere and above is shown to be the principal energy source for the convective activity. In addition, these results, combined with those for 1976 and 1977, form a data set large enough to begin to draw definitive conclusions.

REFERENCES

Barnes, S. L., 1964: A technique for maximizing detail in numerical weather map analysis. J. Appl. Meteor., 3, 396-409.

Kornegay, F. C., and D. G. Vincent, 1976: Kinetic energy budget analysis during interaction of tropical storm Candy (1968) with an extratropical frontal system. Mon. Wea. Rev., 104, 849-859.

Kung, E. C., and T. L. Tsui, 1975: Subsynoptic-scale kinetic energy balance in the storm area. J. Atmos. Sci., 32, 729-740.

Reynolds, P. G., M. L. Gerhard, G. S. Wilson, and J. R. Scoggins, 1979: Texas HIPLEX Mesoscale Experiment-Summer 1978. Mesoscale Data Report, TDWR Contract No. 14-80039, 9 pp. plus 4 appendices.

Scoggins, J. R., H. E. Fuelberg, S. F. Williams, and M. E. Humbert, 1978: Mesoscale Characteristics of the Texas HIPLEX Area during summer 1976. Final Report, TWDB Contract No. 14-70020, 343 pp.

Scoggins, J. R., G. S. Wilson, and S. F. Williams, 1979: Mesoscale Characteristics of the Texas HIPLEX Area During Summer 1977. Final Report, TWDB Contract Nos. 14-80002 and 14-80039, 433 pp.

Vincent, D. G., and L. N. Chang, 1975: Kinetic energy budgets of moving systems: Case studies for an extratropical cyclone and hurricane Celia, 1970, Mon. Wea. Rev., 102, 35-47.